TN
1
A5
Vol. 189
N/C

TRANSACTIONS

of the

American Institute of Mining and Metallurgical Engineers

(Incorporated)

American Institute of Mining, Metallurgical, and Petroleum Engineers.,

VOLUME 189

PETROLEUM DEVELOPMENT AND TECHNOLOGY

1950

PETROLEUM BRANCH

PAPERS AND DISCUSSIONS PRESENTED BEFORE THE BRANCH AT MEETINGS HELD AT SAN ANTONIO, OCTOBER 5-7, 1949, LOS ANGELES, OCTOBER 20-21, 1949; NEW YORK, FEBRUARY 11-15, 1950; TULSA, MAY 12-13, 1950, AND NEW ORLEANS, OCTOBER 4-6, 1950

PUBLISHED BY THE INSTITUTE
AT THE OFFICE OF THE PETROLEUM BRANCH
601 CONTINENTAL BUILDING
DALLAS, TEXAS

Headquarters of the Institute are at 29 West 39th Street, New York, N. Y.

COPYRIGHT, 1950, BY THE
AMERICAN INSTITUTE OF MINING AND METALLURGICAL ENGINEERS
(INCORPORATED)

PRINTED IN THE UNITED STATES OF AMERICA

STORM PRINTING COMPANY, DALLAS, TEXAS

FOREWORD

DURING 1950 the Petroleum Branch of AIME continued its steps toward relative autonomy begun in 1944, at the same time confirming and strengthening those ties of professional fellowship by which AIME now balances the functional interests and scope of our Branch with those of the Mining and Metals Branches. As a result of consistent gains in Petroleum Branch membership each month, our active membership, including students, grew to 4,969 members, or 23 per cent of the Institute total.

Further evidence of continued progress was provided by formation of two new and important petroleum groups; namely, the Wyoming Petroleum Chapter in Casper and the San Antonio-Austin Sub-section of the Southwest Texas Section. Since "oil is where you find it" and oil men follow the discoveries, this formation of active AIME groups, whatever we may call them organizationally, is one of the best symptoms of membership participation and interest. It points the way to further gains through more flexible organization of Branch membership compared with the old method of local sections embracing all divisions.

Paralleling the new Branch-Institute understanding and acceptance, we saw the JOURNAL OF PETROLEUM TECHNOLOGY rapidly developing new and broader values. In format, in technical material, in advertising material and in revenue it surpassed former issues and we have only seen the beginning. Enthusiasm stirred by prompt publication of timely technical papers has proved stimulating to other authors, with the result that these transactions continue their trend toward increased variety and number of excellent papers. With this support the Technology Committee, Program Chairmen and Publications Committee have provided forty technical papers published in JOURNAL OF PETROLEUM TECHNOLOGY during 1950 and ten technical notes for binding in Volume 189 of our *Transactions.*

As it must be, financial accountability is now vested in the Branch, maintaining however, justifiable and proper support of the Institute, comparable with the Metals and Mining Branches. Your officers have stayed within the budget, even though its evolutionary state has caused some difficulties. There is no reason why all the Branches as well as the Institute as a whole should not set up satisfactory budget control during the coming year, thus eliminating many of the awkward problems of the past.

Although the Branch Certificate of Service was not awarded during 1950, the Charles F. Rand Medal was awarded posthumously in 1949 to Mr. Harry C. Weiss, president of Humble Oil and Refining Company.

Departing from traditional reluctance to engage in any public statement or expression beyond technology, members of the Petroleum Branch have—despite considerable warm discussion—taken a firm stand, apparently accepted by membership at large, for speaking out on larger issues of social, economic and political affairs. This acceptance of responsibilities above and beyond technological ones is encouraging evidence of a new concern with "outside" affairs.

Although war possibilities and eventualities may seriously affect the training and indoctrination of young Engineers and Geologists into our membership, every effort will be made during 1951 to renew the means and application of earliest contact with students, student associates and younger Engineers in introducing them personally, technically, and socially into the Petroleum Branch.

According to consensus, the annual meetings of the Branch held last fall in New Orleans and Los Angeles were unsurpassed. Under the aggressive leadership of John E. Sherborne, ably supported by our new secretary, Joe B. Alford, and his assistant, Jess E. Adkins, the Branch has more than fulfilled the expectations of the Executive Committee in building a constantly improved organization.

The unexpected death of Charles B. Carpenter in the spring of the year was a blow to the Branch and all of its members. Remembering his years of service and loyal support of the Branch, your officers for 1951 will strive to achieve as he would have, the full measure of progress and satisfaction for the membership.

R. W. FRENCH, *Chairman*
Petroleum Branch, 1951

CLEVELAND, OHIO
January 2, 1951

AIME OFFICERS AND DIRECTORS

For the Year Ending February, 1951

PRESIDENT

Donald H. McLaughlin, San Francisco, California

PAST PRESIDENTS

W. E. Wrather, Washington, D. C.
L. E. Young, Pittsburgh, Pennsylvania

VICE-PRESIDENTS

C. Harry Benedict, Lake Linden, Michigan
Philip Kraft, New York, N. Y.
A. B. Kinzel, New York, N. Y.
C. V. Millikan, Tulsa, Oklahoma
Robert W. Thomas, Roy, Arizona

VICE-PRESIDENT AND TREASURER

Andrew Fletcher, New York, N. Y.

DIRECTORS

Newell G. Alford, Pittsburgh, Pennsylvania
Richard J. Ennis, Schumacher, Ontario
J. B. Haffner, Kellogg, Idaho
Albert J. Phillips, Barber, New Jersey
Earle E. Schumacher, Murray Hill, New Jersey
Cresap P. Watson, Los Angeles, California
Clyde E. Weed, New York N. Y.
William J. Coulter, Denver, Colorado
Erle V. Daveler, New York, N. Y.
James L. Head, New York, N. Y.
Hjalmar W. Johnson, Chicago, Illinois
W. M. Peirce, Palmerton, Pennsylvania
George P. Swift, Watertown, Massachusetts
Harold Decker, Houston, Texas
Francis B. Foley, Bayonne, New Jersey
E. C. Meagher, New York, N. Y.
Gail F. Moulton, New York, N. Y.
Howard I. Young, St. Louis, Missouri

DIVISION CHAIRMEN—DIRECTORS EX OFFICIIS

Charles H. Behre (*Mineral Economics*), New York, N. Y.
Allison Butts (*Mineral Industry Education*), Bethlehem, Pennsylvania
Richard M. Foose (*Industrial Minerals*), Lancaster, Pennsylvania
Maxwell Gensamer (*Institute of Metals*), Pittsburgh, Pennsylvania
Carroll F. Hardy (*Coal*), Cincinnati, Ohio
Grover J. Holt (*Minerals Beneficiation*), Ishpeming, Michigan
Carleton C. Long (*Extractive Metallurgy*), Monaca, Pennsylvania
Philip J. Shenon (*Mining, Geology, and Geophysics*), Salt Lake City, Utah
John E. Sherborne (*Petroleum*), Whittier, California
Harold K. Work (*Iron and Steel*), New York, N. Y.

SECRETARY

Edward H. Robie, 29 West 39th Street, New York 18, N. Y.

ASSISTANT SECRETARIES

E. J. Kennedy, Jr.
Ernest Kirkendall

ASSISTANT TO THE SECRETARY

H. Newell Appleton

PUBLICATIONS MANAGER

Thomas E. Lloyd

ASSISTANT TREASURER

H. A. Maloney

CONTROLLER

George I. Brigden

CONTENTS

Foreword, *by* R. W. French . . . iii

AIME Officers and Directors . . . iv

Petroleum Branch Officers . . . vii

Petroleum Branch Past Chairmen . . . viii

The Anthony F. Lucas Fund and Medal . . . ix

Petroleum Branch Certificate of Service . . . x

PAPERS

OFFSHORE OPERATION

The Force Exerted by Surface Waves on Piles. By J. R. Morison, M. P. O'Brien, J. W. Johnson, *and* S. A. Schaaf . . . 149

CORE ANALYSIS

(See also Technical Note 55, page 359; Technical Note 57, page 364; Technical Note 60, page 369)

Relative Permeability to Gas. By W. J. Leas, L. H. Jenks, and Charles D. Russell . . . 65

Liquid-Liquid Displacement in Porous Media as Affected by the Liquid-Liquid Viscosity Ratio and Liquid-Liquid Miscibilty. By J. P. Everett, F. W. Gooch, Jr., and John C. Calhoun, Jr. 215

The Kobe Porosimeter and the Oilwell Research Porosimeter. By Carrol M. Beeson . . . 313

Analysis of Fractured Limestone Cores. By Frank C. Kelton . . . 225

The Effect of Permeability Stratification in Complete Water-Drive Systems. By Morris Muskat 349

DRILLING AND PRODUCTION—EQUIPMENT, METHODS AND MATERIALS

(See also Technical Note 56, page 363; Technical Note 58, page 366; Technical Note 59, page 367; Technical Note 62, page 372; Technical Note 64, page 374)

Ability of Drilling Mud to Lift Bit Cuttings: By H. N. Hall, Howard Thompson, and Frank Nuss . . . 35

Squeeze Cementing Operations. By George C. Howard and C. R. Fast . . . 53

Determining Friction Factors for Measuring Productivity of Gas Wells. By R. V. Smith . . . 73

Dynamometer Charts and Well Weighing. By L. W. Fagg . . . 165

Corrosion Mitigation Within Dehydrating Tanks. By Ernest O. Kartinen . . . 175

Relative Productivity of Perforated Casing—I. By Robert A. Howard and Marsh S. Watson, Jr. 179

The Effect on Well Productivity of Formation Penetration Beyond Perforated Casing. By James M. McDowell and Morris Muskat . . . 309

Relative Productivity of Perforated Casing—II. By Robert A. Howard and Marsh S. Watson, Jr. . . . 323

LOGGING

Some Preliminary Investigations of Quantitative Interpretations of Radioactivity Logs. By Robert E. Bush and E. S. Mardock . . . 19

The Presence of Conductive Solids in Reservoir Rocks as a Factor in Electric Log Interpretation. By H. W. Patnode and M. R. J. Wyllie . . . 47

Some Theoretical Considerations Related to the Quantitative Evaluation of the Physical Characteristics of Reservoir Rock from Electrical Log Data. By M. R. J. Wyllie and Walter D. Rose . . . 105

Selective SP Logging. By H. G. Doll . . . 129

The MicroLog—A New Electrical Logging Method for Detailed Determination of Permeable Beds. By H. G. Doll . . . 155

The SP Log in Shaly Sands. By H. G. Doll . . . 205

Estimation of Interstitial Water from the Electric Log. By Milton Williams . . . 295

PHASE RELATIONSHIPS

Phase Equilibria in Hydrocarbon-Water Systems. By O. L. Culberson, Albert B. Horn and J. J. McKetta, Jr. . . . 1

The Coexistence of Liquid and Vapor Phases at Pressure Above 10,000 Psi. By Michael J. Rzasa and Donald L. Katz . . . 119

An Electronic Analog Computer for Solving the Flash Vaporization Equilibrium Equation. By F. W. Bubb, R. G. Nisle and P. G. Carpenter . . . 143
Vapor-Liquid Equilibrium Data on the System Natural Gas-Water-Triethylene Glycol at Various Temperatures and Pressures. By Joe A. Porter and Laurance S. Reid . . . 235
The Water Vapor Content of Essentially Nitrogen-Free Natural Gas Saturated at Various Conditions of Temperature and Pressure. By Eugene L. McCarthy, William L. Boyd and Laurance S. Reid . . . 241
Phase Equilibria in Hydrocarbon-Water Systems—II. The Solubility of Ethane in Water at Pressures to 10,000 Psi. By O. L. Culberson and J. J. McKetta, Jr. . . . 319

PVT DATA

Volumetric Behavior of Oil and Gas from a Louisiana Field—I. By H. H. Reamer and B. H. Sage 261
Correlation of Bottom Hole Sample Data. By Guy Borden, Jr., and Michael J. Rzasa . . . 345

RESERVOIR ENGINEERING

(See also Technical Note 61, page 371; Technical Note 63, page 373)

The Estimation of Permeability and Reservoir Pressure from Bottom Hole Pressure Build-Up Characteristics. By C. C. Miller, A. B. Dyes and C. A. Hutchinson, Jr. . . . 91
Improvements in the X-Ray Saturation Technique of Studying Fluid Flow. By F. Morgan, J. M. McDowell and E. C. Doty . . . 183

RESERVOIR PERFORMANCE

Lakeview Pool, Midway-Sunset Field. By W. P. Sims and W. G. Frailing . . . 7
Performance Characteristics of a Volumetric Condensate Reservoir. By F. H. Allen and R. P. Roe 83
Pore Size Distribution of Petroleum Reservoir Rocks. By N. T. Burdine, L. S. Gournay and P. P. Reichertz . . . 195
A Study of Reservoir Performance of the First Grubb Pool, San Miguelito Field, Ventura County, California. By Wayne E. Glenn . . . 243
Critical Analysis of the Effect of Well Density on Recovery Efficiency. By W. O. Keller and F. H. Callaway . . . 269
Review of Cycling Operations in the La Gloria Field. By W. H. Justice . . . 281
Performance of Limestone Reservoirs. By R. C. Craze . . . 287
High Pressure Water Injection for Maintaining Reservoir Pressures, New Hope Field, Franklin County, Texas. By Albert S. Trube, Jr., and Sam N. DeWitt . . . 325
Performance of the Lower Pawelek Reservoir, Falls City Field, Karnes County, Texas. By John W. Crutchfield and Emil F. Bowers . . . 335

TECHNICAL NOTES

Attainment of Connate Water in Long Cores by Dynamic Displacement. By Robert L. Slobod 359
Stainless Steel Containers for Laboratory Drilling Mud Test Work. By W. B. Lilienthal . . . 363
Anomalies in the Measurement of Wetting Liquid Pressure Gradients. By Walter Rose and Bernard Greifer . . . 364
Lime Content of Drilling Mud—Calculation Method. By M. D. Nelson and T. E. Watkins . . 366
Influence of Different Types of Formation Waters on Disintegration of Cements. By Roscoe C. Clark, Jr. . . . 367
Interpretation of Capillary Pressure Data. By W. R. Purcell . . . 369
Pressure Distribution in Unsaturated Oil Reservoirs. By E. R. Brownscombe and Francis Collins . . . 371
High Pressure Mercury Pump. By J. R. Spencer . . . 372
Carter Reservoir Analyzer Timing Circuit. By W. F. Baldwin . . . 373
Some Controlling Factors Regarding Variable Weighting of Cement Slurries. By M. A. Mallinger 374

PETROLEUM BRANCH OFFICERS AND COMMITTEE CHAIRMEN

For the Year Ending February, 1951

CHAIRMAN

John E. Sherborne
Union Oil Company of California
Wilmington, California

VICE-CHAIRMEN

Paul Andrews
Signal Oil & Gas Company
Los Angeles, Calilfornia

Richard W. French
Sohio Petroleum Company
Cleveland, Ohio

EXECUTIVE COMMITTEE

Paul Andrews
John E. Sherborne
Richard W. French

Benjamin C. Craft
Louisiana State University
Baton Rouge, Louisiana

John R. McMillan
Fullerton Oil Company
Los Angeles, California

Harold Decker
Houston Oil Company of Texas
Houston, Texas

Lloyd E. Elkins
Stanolind Oil & Gas Company
Tulsa, Oklahoma

R. C. Earlougher
Earlougher Engineering
Tulsa, Oklahoma

MEMBERSHIP COMMITTEE

Burton Atkinson, *Chairman*
Humble Oil and Refining Company
Midland, Texas

Vice-Chairmen

Jack M. Moore
Dowell Incorporated
Midland, Texas

J. N. McGirl
Tide Water Associated Oil Company
Tulsa, Oklahoma

H. C. Peterson
Freeport Sulphur Company
New Orleans, Louisiana

E. A. Rassinier
Phillips Petroleum Company
Houston, Texas

C. T. McClure
Youngstown Steel Products Company
Los Angeles, California

PRODUCTION REVIEW COMMITTEE

E. W. Berlin
Socony-Vacuum Company
New York, New York

Vice-Chairmen

R. B. Gilmore, *Domestic*
DeGolyer and MacNaughton
Dallas, Texas

A. H. Chapman, *Foreign*
Arabian American Oil Company
New York, New York

John H. Murrell
DeGolyer & McNaughton
Dallas, Texas

Dean H. Sheldon
Consulting Engineer
Los Angeles, California

Harry H. Power
University of Texas
Austin, Texas

H. J. Struth
Petroleum Consultant
Dallas, Texas

TREASURER

R. B. Gilmore
DeGolyer & McNaughton
Dallas, Texas

PRODUCTION TECHNOLOGY COMMITTEE

Morris Muskat, *Chairman*
Gulf Research & Development Company
Pittsburgh, Pennsylvania

Vice-Chairmen

Lincoln Elkins
Sohio Petroleum Company
Oklahoma City, Oklahoma

Earl Kipp
The California Company
New Orleans, Louisiana

R. L. Parsons
California Research Corporation
Los Agelens, California

Frank H. Dotterweich
Texas College of Arts & Industries
Kingsville, Texas

ECONOMICS COMMITTEE

Paul Schultz, *Chairman*
Stanolind Oil & Gas Company
Tulsa, Oklahoma

Minor S. Jameson, Jr.
Independent Petroleum Association of America
Washington, D. C.

PUBLICATIONS COMMITTEE

J. M. Bugbee
Shell Oil Company
Houston, Texas

John P. Hammond, *Vice-Chairman*
Amerada Petroleum Corporation
Tulsa, Oklahoma

STAFF OF THE PETROLEUM BRANCH IN DALLAS

Executive Secretary
Joe B. Alford

Editor, Journal of Petroleum Technology
Jess E. Adkins

PEROLEUM BRANCH, AIME

Established as a Division March 24, 1922
Established as a Branch in 1948

PAST CHAIRMEN

RALPH ARNOLD, 1922
E. DEGOLYER, 1923, 1924
F. JULIUS FOHS, 1925, 1926
JOHN M. LOVEJOY, 1927
A. W. AMBROSE, 1928
JOSEPH B. UMPLEBY, 1929
C. V. MILLIKAN, 1930
C. E. BEECHER, 1931
EARL OLIVER, 1932
W. E. WRATHER, 1933
H. D. WILDE, JR., 1934
HARRY H. POWER, 1935
HALLAN N. MARSH, 1936
M. ALBERTSON, 1937
GEORGE B. CORLESS, 1938
W. H. GEIS, 1939
T. V. MOORE, 1940
EUGENE A. STEPHENSON, 1941
HARRY P. STOLTZ, 1942
C. A. WARNER, 1943
W. S. MORRIS, 1944
M. L. HAIDER, 1945
H. F. BEARDMORE, 1946
HOWARD C. PYLE, 1947
IRWIN W. ALCORN, 1948
LLOYD E. ELKINS, 1949
JOHN E. SHERBORNE, 1950

THE ANTHONY F. LUCAS FUND AND MEDAL

In 1936 the Institute established the Anthony F. Lucas Gold Medal, to be awarded from time to time "for distinguished achievement in improving the technique and practice of finding and producing petroleum." These awards are sponsored by the Petroleum Branch.

Captain Lucas was a pioneer in the oil industry, one of the early wildcatters and a leading mining and petroleum engineer. He was famous as the discoverer of Spindletop. He became a member of the Institute in 1895 and in 1913 was the first Chairman of the Petroleum and Gas Committee of the Institute, the forerunner of the present Petroleum Branch. He also headed the Committee in 1914, 1917 and 1918.

Medals Awarded

J. Edgar Pew, February 1937
Henry L. Doherty, February 1938
E. DeGolyer, February 1940
Conrad (posthumously) and Marcel Schlumberger, February 1941
John Robert Suman, February 1943
Charles Van Ormer Millikan, February 1944
James Ogier Lewis, 1946
William Noble Lacey, 1947
Wallace Everette Pratt, 1948
William Embry Wrather, 1950

Committee on Awards

Herbert F. Beardmore, *Chairman*

Until Feb. 1951	*Until Feb. 1952*	*Until Feb. 1953*	*Until Feb. 1954*
Herbert F. Beardmore	A. R. Denison	J. E. Brantly	Lloyd E. Elkins
W. N. Lacey	M. Gordon Gulley	Fred M. Nelson	W. H. Geis
Theodore E. Swigart	Howard C. Pyle	Wallace E. Pratt	John H. Murrell

Members Ex Officiis

C. L. Moody	Frank M. Porter	D. H. McLaughlin	James Boyd
President AAPG	President API	President AIME	Director, B. of M.

PETROLEUM BRANCH CERTIFICATE OF SERVICE

Established in 1948, the Petroleum Branch CERTIFICATE OF SERVICE is awarded to recognize and show appreciation for exceptional services of Members to the Branch.

CERTIFICATES AWARDED

EUGENE A. STEPHENSON, 1948

FRED B. PLUMMER, 1948
(posthumously)

EARL OLIVER, 1948

E. JULIUS FOHS, 1949

JOSEPH B. UMPLEBY, 1949

The basic data for T. P. 2931, "Correlation of Bottom Hole Sample Data," page 345, can be secured from Document 3139, American Documentation Institute, Science Service Building, 1719 North Street Northwest, Washington, D. C.

T.P. 2778

PHASE EQUILIBRIA IN HYDROCARBON-WATER SYSTEMS

The Solubility of Ethane in Water at Pressures to 1200 Pounds Per Square Inch

O. L. CULBERSON, THE UNIVERSITY OF TEXAS, AUSTIN, **ALBERT B. HORN,** ETHYL CORP., BATON ROUGE, LOUISIANA, AND **J. J. McKETTA, JR.,** THE UNIVERSITY OF TEXAS, AUSTIN, MEMBER AIME

ABSTRACT

Since water is present in natural gas and petroleum reservoirs, it is of engineering value to have accurate experimental data regarding the behavior of water in hydro-carbon systems. Since experimental data of this nature are so scarce in literature, a program is under way at the University of Texas to obtain experimental data regarding the distribution of water in petroleum hydrocarbons.

This initial paper is subdivided into three parts:

A. The apparatus and analytical procedure are discussed.

B. The equipment has been checked by comparing the experimental data with data of literature on the solubility of methane in water at 77°F and pressures to 10,000 psia.

C. Experimental data are presented at 100, 160, 220, 280, and 340°F on the solubility of ethane in water at pressures to 1200 psia. As the temperature is increased the solubility of ethane in water first exhibits a minimum and then a maximum solubility. The range of applicability of Henry's Law is discussed.

INTRODUCTION

Although considerable experimental data have been published on water-hydrocarbon systems in the hydrate region, the information on these systems in the vapor-liquid and the vapor-liquid-liquid regions at elevated pressures is extremely scarce. A survey of the literature on hydrocarbon-water systems at elevated pressures was presented by McKetta and Katz[12,13,14] showing the systems and phases investigated. In addition to these existing published data, Poettman and Dean[17] have reported the water content of propane in the three-phase region (only the propane-rich liquid and the vapor phases were studied) and Michels, et al.[15] have reported the solubility of methane in water at pressures to 6800 pounds per square inch at 77°F and at pressures to 1500 psia at temperatures to 300°F.

It has been shown[12,14] that the presence of water will materially affect the phase equilibrium of hydrocarbon systems. In order to make experimental studies on the quantitative effect of the presence of water in naturally-occurring hydrocarbon systems, it is desirable to have data available on binary hydrocarbon-water systems.

A program is underway at this laboratory to determine the phase relations of the hydrocarbon-water systems. Initially the investigation will be limited to binary systems with water as one of the components. Later ternary and complex systems will be investigated and reported.

EQUIPMENT AND ANALYTICAL PROCEDURE

Apparatus

In order to avoid a description of the methods employed in each subsequent paper, a description of the apparatus and the analytical procedure will be given here. The apparatus is shown schematically in Fig. 1. The numbered items in Fig. 1 represent the high pressure valves.

The equilibrium cell is of the totally enclosed type, with a volume of 550 cubic centimeters. The cell is mounted in an air bath which in turn is mounted on pillow blocks and connected to a rocking mechanism so that the cell and bath will oscillate approximately 30 degrees above and below the horizontal at 35 oscillations per minute.

The air bath is heated by two resistance heaters. The first or primary heater is 250 watts and is controlled by a thermoregulator; the second heater is of 500-watt size and is manually controlled to aid in bringing the cell to equilibrium temperature. Air circulation in the bath is accomplished by means of a fan, the shaft of which is concentric to the heaters. The walls of the bath are insulated with 2-in. thick blocks of 85 per cent magnesia. Temperature observations are made with three calibrated thermocouples. One couple is sealed in a well provided within the equilibrium cell, and is used as the criterion of the cell being at the equilibrium temperature. The other two thermocouples are located on opposite sides of the cell to indicate temperature uniformity within the air bath. The thermoregulator, used in conjunction with a relay, gives a variation in the temperature of the air in the bath of plus or minus one degree Fahrenheit. However, since the equilibrium cell weighs approximately 55 pounds, the

---

[1] References are given at end of paper.

Manuscript received at the office of the Petroleum Branch August 31, 1949.

temperature sine curve which exists in the bath is so dampened by the cell that no temperature fluctuations in the cell can be detected with the semi-precision type potentiometer used.

The tubing used in the equipment is 18-8 stainless tubing with an outside diameter of ¼ in. and an inside diameter of 3/32 in. Valves and tees are of the super-pressure type.

Three pressure gauges are connected to the equilibrium cell to determine the pressure conditions within the cell. These gauges (Ashcroft Duragauge) have 12-in. dials and are of the pressure ranges 0-1000, 0-5000 and 0-10,000 psia. Only one gauge is used at one time depending upon the pressure within the equilibrium cell. These gauges are calibrated at intervals with a dead weight gauge and at no time have these gauges deviated from the preceding calibrations.

A stainless steel bomb of 365 cubic centimeters capacity is used as the water surge and a low carbon steel bomb of 710 cubic centimeters capacity is used as the hydrocarbon surge bomb. Each surge bomb is equipped with a pressure gauge to indicate the pressure within the bombs. Within the system, material is pumped to the desired places by means of a converted 20-ton hydraulic jack of the Walker type. The fluid used in the pump is additive-free heavy mineral oil which is pumped to a mercury-oil surge where the oil displaces mercury into the system. The mercury-oil surge is equipped with an electric contact mechanism which causes a bell to ring when the mercury interface is within three inches of the bottom of the mercury-oil surge bomb. There is no indication that the oil is leaking with the mercury from the bottom of the mercury-oil surge.

In making a solubility determination, the cell is first charged with the hydrocarbon vapor to a pressure about one-half of that desired for the equilibrium pressure. Water is then pumped into the cell from the liquid surge until the pressure is approximately the equilibrium pressure. The liquid volume is then approximately one-half of the total volume of the equilibrium cell. All tubing leading to the cell is then pumped full of mercury. The heaters are turned on and the rocking mechanism is started. After the contents of the cell reach the desired temperature, the oscillations are continued for a minimum of three hours. Some preliminary time-concentration experiments indicated that less than one hour of oscillation is required to attain equilibrium within the cell.

At the end of three hours of rocking, the cell is placed in a vertical position and the liquid portion of the cell is sampled and analyzed. Valves (8) and (10) are opened slowly until all of the mercury is removed from the tubing. At the same time, mercury is pumped into the cell to maintain the equilibrium pressure. As soon as all of the mercury is removed from the tubing, valve (10) is closed and valve (9), which leads to the analytical train, is opened.

Analytical Procedure

The analytical train is shown in Fig. 2 and is composed of a trap for collecting the liquid water, three drying tubes containing magnesium perchlorate

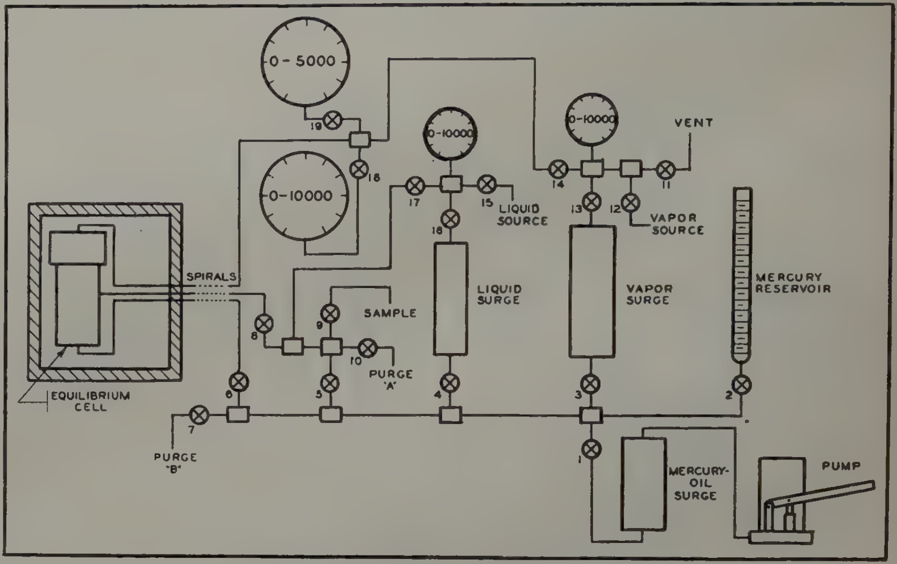

FIG. 1 — DIAGRAM OF APPARATUS

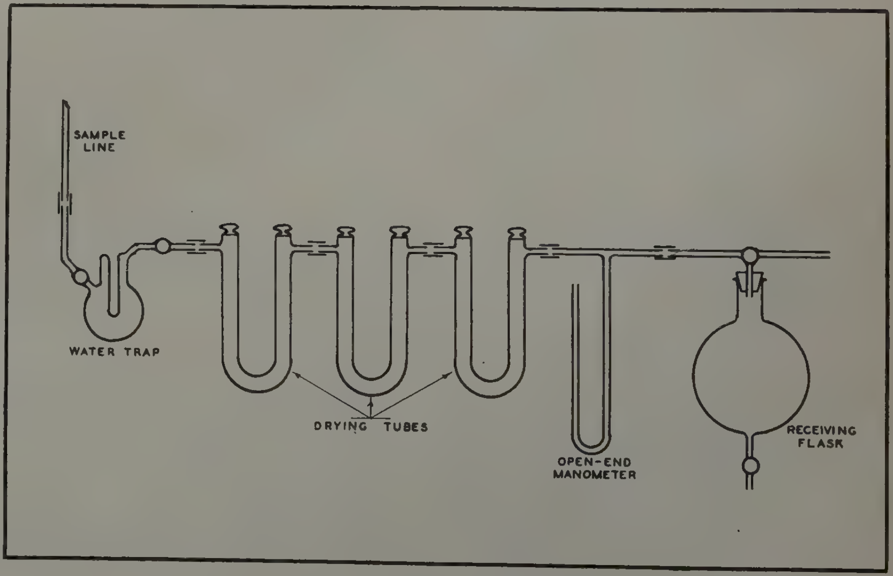

FIG. 2 — ANALYTICAL APPARATUS

to collect water vapor leaving the trap, and a receiving flask in which the dry hydrocarbon vapor is collected over mercury. A manometer and thermometer are also part of the train.

Before the train receives the sample, the water trap and drying tubes are weighed on an analytical balance while they are filled with hydrocarbon vapor at a known temperature and pressure. The receiving flask is filled with mercury up to the three-way stopcock. The train is then reassembled and connected to the equilibrium apparatus. It may be added here that it was necessary initially to pass considerable predried pure hydrocarbon through the drying tubes until they attained a constant weight. This indicated that some hydrocarbon vapor was adsorbed by the drying agent.

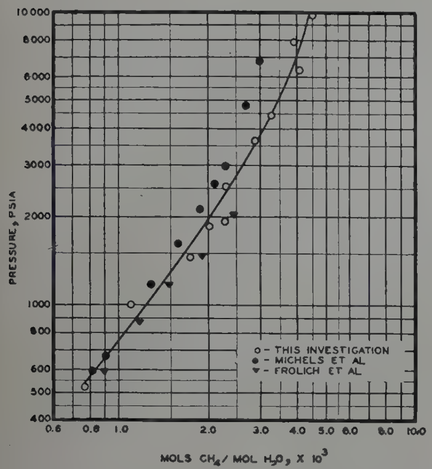

FIG. 3—SOLUBILITY OF METHANE IN WATER AT 77°F AT PRESSURES TO 10,000 PSIA

The sample is passed from the equilibrium cell through valve (9) to the train and at the same time mercury is pumped into the cell to maintain the equilibrium pressure. As the sample passes valve (9), it flashes to atmospheric pressure and this pressure reduction causes most of the hydrocarbon vapor to flash out of solution. The water, saturated with hydrocarbon vapor at this low pressure, is collected in the trap and the wet gas passes through to the drying tubes, and from there the dry gas passes to the receiving flask. By gradually removing some mercury from the receiving flask, the pressure in the train is maintained at the predetermined near-atmospheric pressure. When the trap is filled (approximately 50 cc of the water-rich liquid) the sampling is stopped. The analytical train is then brought to the initial temperature and pressure conditions.

The weight of the vapor hydrocarbon in the sample is that weight which would occupy a volume at the train pressure and temperature equal to that of the volume of the mercury displaced from the receiving flask less the volume of the water-rich liquid which entered the train. The total weight of the hydrocarbon is the weight of the vapor hydrocarbon plus the weight of the hydrocarbon remaining in solution in the water-rich liquid in the trap. This latter weight of hydrocarbon can be calculated from the solubility data of Winkler[19] at atmospheric pressure. The weight of the water in the sample is the weight of the water in the trap plus the water-gain of the drying tubes.

Accuracy

The weighings are made on an analytical balance with perfect tares using weights which were calibrated against the National Bureau of Standards weights. The temperature of the material within the cell is determined with a calibrated thermocouple and no fluctuation of the temperature is indicated with a semi-precision potentiometer. The pressures are read from the calibrated bourdon gauges and it is believed that the pressures are within the following accuracy on the individual gauges: Below 1000 psia, ±3 psia; between 1000 and 5000 psia, ±10 psia and between 5000 and 10,000 psia, ±20 psia.

SOLUBILITY OF METHANE IN WATER AT 77°F AND PRESSURES TO 10,000 PSIA

In order to check the apparatus, operating procedure and analytical technique it was decided to determine the solubility of methane in water at 77°F, since these data have been reported by Michels, et al.[15] for pressures to 6800 psia and by Hogan[7] and Frolich, et al.[3] for pressures to 2060 psia.

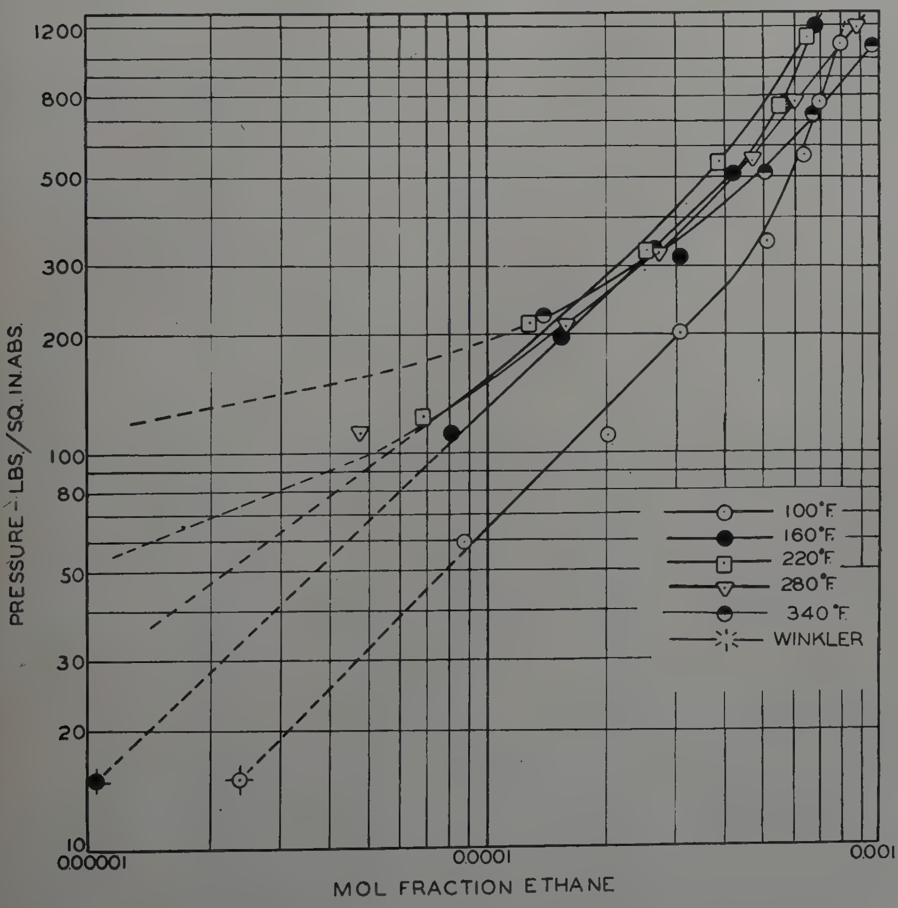

FIG. 4 — EFFECT OF PRESSURE ON THE SOLUBILITY OF ETHANE IN WATER

The data obtained in this investigation are shown in Table I along with the data of the investigators mentioned above. The data of Hogan are included in the paper of Frolich et al. These data of Table I are shown graphically in Fig. 3 and it may be seen in this figure that there is substantial agreement in all three investigations. The data of this investigation lie between those of Frolich and Michels. Hogan indicates in his thesis that he was interested in practical results and also states that he made no attempt to obtain precise data. Therefore little concern arises from the deviation of the data obtained in this investigation from those data of Hogan. Michels and his coworkers obtained their results by using a method which they class as a "synthetic" one. The liquid is brought into contact with the gas, shaken until equilibrium has been attained and calculating the amount of gas dissolved by noting the decrease in pressure. The method of calculating the solubility was that suggested by Krichevsky and Kasarnovsky[9]. Since Michels and his co-workers started at a low pressure, attained equilibrium, calculated the solubility, added more gas to attain a higher pressure, again attained equilibrium and again calculated the solubility at the new pressure, it seems very likely that any error resulting from the original set of equations[9] because of the assumptions made for low pressure conditions would be cumulative. Therefore it is not at all surprising that there is over 20 per cent deviation of Michels data when compared to the data of this investigation. It is remarkable, however, that the data agree as well as they do, especially at these concentrations.

SOLUBILITY OF ETHANE IN WATER

There are no data in the literature on the solubility of ethane in water at elevated pressures. The data of Winkler[19] are universally accepted as being accurate; however, these data, while at various temperatures, are only for atmospheric pressure.

The work reported here consists of an experimental investigation of the water-rich liquid phase of the ethane-water system at 100, 160, 220, 280, and 340°F and pressures to 1200 pounds per square inch absolute (psia). Since the lowest temperature of this investigation is above the critical temperature of ethane and above the hydrate forming temperatures at these pressures, only two phases were present at any time during this investigation.

Experimental Results

Upon investigation of the compressibility factors for ethane, it is readily seen that ethane departs from ideality at pressures lower than 1200 psia.[1] This, coupled with the fact that water is a highly polar compound, indicated that the system would depart from ideality and would deviate considerably from Henry's law.[4,5]

The experimental data obtained in this investigation are given in Table II.

Table I
Solubility of Methane in Water at 77°F (25°C)
(Moles Methane Per Mole Water)

Pressure psia	This Investigation Experimental	Smoothed	Michels[15]	Frolich[3]
296				0.000665
525	0.000770	0.000750		
589		0.000825	0.00081	0.000887
666		0.000910	0.00090	
880		0.00112		0.00118
1000	0.00110	0.00123		
1175		0.00139		0.00148
1180		0.00140	0.00128	
1450	0.00180	0.00162		
1465		0.00163		0.00192
1623		0.00175	0.00158	
1845	0.00202	0.00191		
1930	0.00227	0.00198		
2115		0.00210	0.00187	
2060		0.00206		0.00244
2535	0.00231	0.00235		
2560		0.00237	0.00210	
2970		0.00260	0.00229	
3615	0.00288	0.00293		
4435	0.00328	0.00325		
4800		0.00337	0.00269	
6342	0.00407	0.00380		
6800		0.00391	0.00298	
7935	0.00391	0.00412		
9680	0.00451	0.00434		

Table II
Solubility of Ethane in Water

Temp. °F	Pressure psia	Mole Fraction Experimental	Ethane x 10^4 Smoothed	Per Cent Deviation
100	59	0.893	0.930	+4.15
100	110	2.04	1.730	−5.20
100	200	3.11	3.11	0.00
100	340	5.21	5.00	−4.01
100	568	6.47	6.39	−1.23
100	767	7.09	7.20	+1.55
100	1080	8.01	8.01	0.00
160	113	0.812	0.850	+4.69
160	196	1.54	1.54	0.00
160	315	3.09	2.55	−17.55
160	512	4.17	4.21	+0.96
160	785	5.70	5.64	−1.05
160	1215	6.79	6.79	0.00
220	123	0.698	0.750	+7.45
220	212	1.30	1.47	+13.1
220	322	2.56	2.42	−5.47
220	548	3.91	3.91	0.00
220	752	5.60	5.20	+7.14
220	1120	6.61	6.70	+1.36
280	113	0.475	0.530	+25.00
280	210	1.58	1.56	−1.27
280	320	2.72	2.72	0.00
280	557	4.64	4.64	0.00
280	785	6.00	6.10	+1.67
280	1215	8.65	8.65	0.00
340	226	1.40	1.42	+1.43
340	334	2.61	2.75	+5.36
340	529	5.03	4.90	−2.58
340	742	6.71	6.82	+1.64
340	1140	9.70	9.70	0.00

Fig. 4 shows the effect of pressure on the solubility of ethane at 100, 160, 220, 280, and 340°F, and plotted as mole fraction of ethane versus total pressure of the system. Since ethane exhibits a minimum and maximum solubility in water at the temperatures and pressure covered by this investigation, it is difficult to visualize the trend of solubility from Fig. 4. For this reason these data are cross-plotted in Fig. 5 which shows the effect of temperature on the solubility of ethane in water and clearly indicates the minimum and maximum trends. The data for Fig. 5 were obtained by interpolating values from the smoothed curves of Fig. 4. The minimum and maximum in solubility illustrated here is not uncommon; these phenomena have been reported in various systems[2,6,8,10,14,18] and have been explained by Winkler[19] and Kuenen[10] as a neutralization effect of the opposing factors of viscosity and the thermal expansion of the liquid. Winkler showed that the solubility of a gas in water is zero at a total pressure equal to the vapor pressure of water.

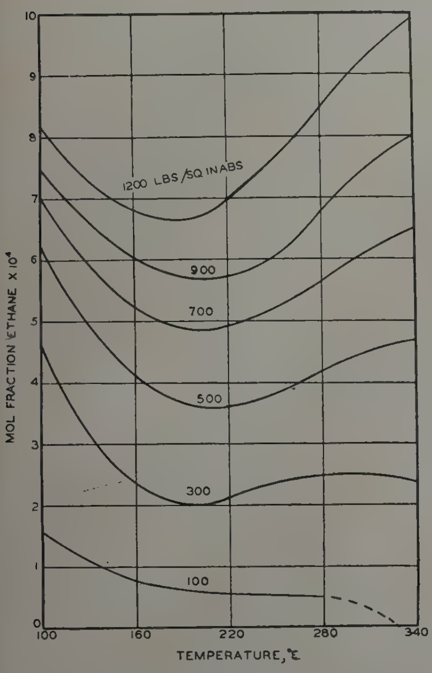

FIG. 5 — SOLUBILITY OF ETHANE IN WATER EXHIBITING MINIMUM SOLUBILITY

Fig. 6 shows the solubility of ethane in water, plotted as volume of ethane per unit volume of water, both components referred to 32°F and a pressure of 760 mmHg[11,16]. Fig. 6 demonstrates the range of applicability of Henry's law to this system. It is seen that temperature has considerable effect on the maximum pressure to which Henry's law may be applied. The maximum pressure at which Henry's law would apply for the various isotherms is as follows: 100°F, 300 psia; 160°F, 600 psia; 280°F, 600 psia; 280°F, 400 psia; 340°F, 400 psia. The relatively high pressure at which Henry's law is applicable for the 160 and 220°F isotherms can possibly be explained as the effect of the factors previously mentioned; viscosity and thermal expansion of the liquid. Above 220°F the maximum pressure limit for the application of Henry's law is seen to decrease. This agrees in part with the data of McKetta and Katz[14]; however, the effect of temperature in their system was not so marked as in this investigation.

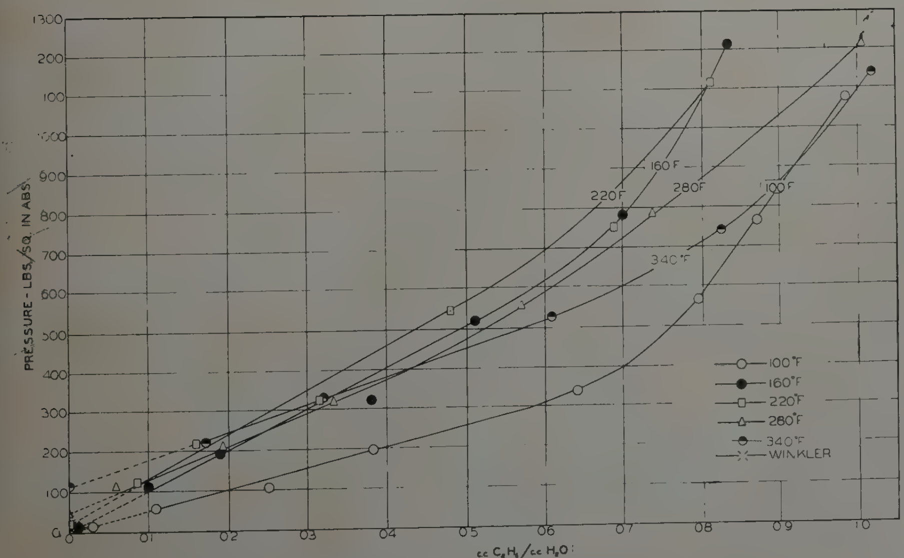

FIG. 6 — VOLUMETRIC SOLUBILITY OF ETHANE IN WATER

Fig. 7 is a comparison of the data of this investigation with similar systems at 100°F[3,14,20]. The data of Frolich[3] are for the solubility of methane in water at 77°F, and are included here rather than the data of Michels[15], although the latter data are available at 100°F, because only two (of Michel's) experimental points fell within the range of this investigation.

It is interesting to note that the solubilities of the hydrocarbons tend to converge at a pressure of 200 psia. The solubility of methane-n-butane[14], however, is essentially the same as that of methane in water[3]. It is also interesting to note that the solubility of hydrogen in water is in the same order of magnitude.

Although the data presented here are expressed in terms of mole fraction ethane, there is no essential difference between mole fraction and mole ratio for the data determined in this investigation. This is due to the fact that the difference between mole ratio and mole fraction for this low solubility lies outside the accuracy of the data.

Materials

The methane used in this investigation was donated by the Phillips Petroleum Co. and has a purity of 99.0 mole per cent minimum. No attempt was made to purify the methane further.

The ethane was also donated by the Phillips Petroleum Co. and was certified by the National Bureau of Standards to have a minimum purity of 99.99 mole per cent.

The water used in this work was obtained from the distilled water supply of the chemical engineering department. This distilled water was boiled to remove dissolved air from solution.

ACKNOWLEDGMENT

The writers gratefully acknowledge the assistance and interest of the following:

1. The Gulf Oil Corp., for the fellowship granted to O. L. Culberson for this work.

2. The Phillips Petroleum Co. for furnishing the methane and ethane.

3. The president of the University of Texas for furnishing a special research grant to initiate this investigation.

REFERENCES

1. Brown, Katz, Oberfell and Alden. "Natural Gasoline and the Volatile Hydrocarbons," Tulsa, Okla., Nat. Gas Assn., p. 26, (1948).
2. Dodson and Standing. Proc. Am. Petroleum Inst., Drill. and Prod. Practice, p. 173, (1944).
3. Frolich, Tauch, Hogan and Peer. *Ind. Eng. Chem.*, 23, 543-50 (1931).
4. Gibbs, *Collected Works.* New York, Longmanns, Green and Co. (1931).
5. Gladstone, S. *Textbook of Physical Chemistry.* New York, D. Van Nostrand Co. 2nd Ed. (1946), pp. 693-8.
6. Goodman and Krase. *Ind. Eng. Chem.* 23, 401 (1931).
7. Hogan. Master of Science Dissertation, M.I.T., (1931).
8. Kay. Chem. Revs., 29, 501 (1943).
9. Krichevsky and Kasarnovsky. *J. Amer. Chem. Soc.*, 57, 2169 (1935).
10. Kuenen. Proc. Roy. Soc. Edinburgh, 23, 312 (1901).
11. Lange. *Handbook of Chemistry.* Sandusky, Ohio, Handbook Publishing Co., 7th Ed. (1946), pp. 1358-60.
12. McKetta, Ph.D. Dissertation, University of Michigan (1946).
13. McKetta and Katz, *Trans.* AIME Petr. Div., 170, 34-43 (1947).
14. McKetta and Katz, *Ind. Eng. Chem.*, 40, 853-863 (1948).
15. Michels, Gerver and Bijl. Physics 3, 797-808 (1936).
16. Pickering, *International Critical Tables.* New York, McGraw-Hill Book Co., III, 3, (1928).
17. Poettman and Dean, *Petr. Ref.*, 25, 635 (1946).
18. Saddington and Krase, *J. Am. Chem. Soc.*, 56, 353 (1934).
19. Winkler, Ztsch. physik. chem., 9, 171 (1899).
20. Anonymous. *Hydrogen Bulletin,* Girdler Corporation, p. 37 (1946).

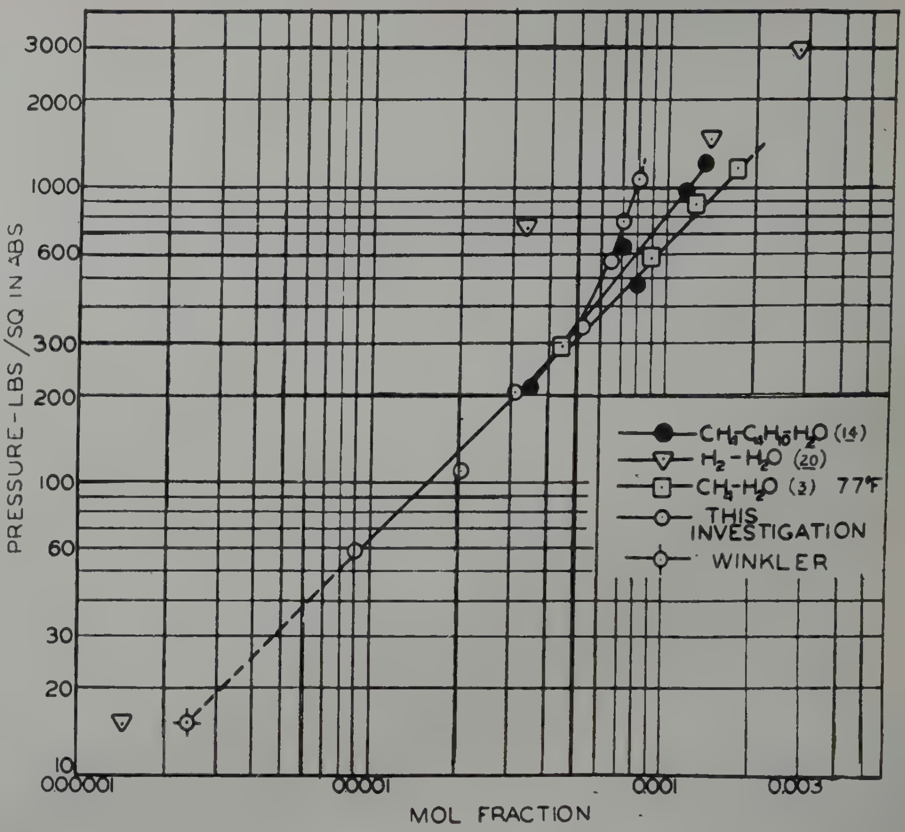

FIG. 7 — COMPARISON OF LABORATORY DATA WITH LITERATURE AT 100°F

★ ★ ★

T.P. 2779

LAKEVIEW POOL, MIDWAY-SUNSET FIELD

W. P. SIMS AND **W. G. FRAILING,** STANDARD OIL CO. OF CALIFORNIA, TAFT, CALIFORNIA

ABSTRACT

The Lakeview Pool of Kern County, California, was discovered in 1910 with the drilling of Lakeview No. 1 which blew out and produced an estimated 8,250,000 bbl of oil in 544 days of uncontrolled flow. The well has since been known as the Lakeview Gusher. Full exploitation of the pool did not take place until about 25 years later. A total of 112 producing wells were completed in the Lakeview sand through April 30, 1949. As of that date, about 30 per cent of the total wells drilled were still producing, with an average pool production rate of approximately 2000 bbl per day. The cumulative oil production was about 41 million bbl of oil, or 55.3 per cent of the tank oil originally in place.

The pool is bordered on its downstructure side by a body of inactive edgewater and water production where present has been principally the result of coning.

Since the depletion of the greater portion of the gas energy by the Lakeview Gusher, the pool has operated under gravity drive. Relatively high angle dips, good permeabilities and favorable fluid characteristics have made gravity drainage particularly effective. Since January, 1942, the oil recovery has been relatively constant at about 53,000 bbl per ft drop in fluid level. Correlations between the volume of reservoir space drained and the cumulative oil produced indicate that an ultimate recovery of 63.3 per cent of the tank oil originally in place is attainable.

INTRODUCTION

The Lakeview Pool is an outstanding example of gravity drainage. It is one of many productive reservoirs of the Midway-Sunset Field, and is located in Kern County, approximately five miles southeast of Taft and two miles north of Maricopa, California. Its position relative to surrounding pools and to the Thirty-Five anticline is shown on Fig. 1. The northern portion of the pool lies in sections 32 and 33, Township 32 South, Range 24 East, Mt. Diablo Base and Meridian, while the southern portion lies in sections 25, 26, 35 and 36, Township 12 North, Range 24 West, San Bernardino Base and Meridian. As no two sections bear the same number, they will hereafter be referred to by section number alone.

The purpose of this paper is to review the performance of the Lakeview Pool in an effort to evaluate the effectiveness of gravity drive as a recovery mechanism.

REGIONAL STRATIGRAPHY AND STRUCTURE

The oustanding structural feature in this area is the Thirty-Five anticline, the axis of which plunges South 75° East through the center of Section 35. As shown on Fig. 2, the following zones are oil and gas bearing in the Thirty-Five anticline area:

Pleistocene
  Basal Tulare
    Tar Sands
Pliocene
  San Joaquin
    Mya Sands
    Top Oil or Scalez Zone
  Etchegoin
    Kinsey Sand
    Wilhelm Zone
    Gusher Sand
    Calitroleum Sand
Miocene
  Reef Ridge
    Lakeview Sand
    Sub-Lakeview Miocene Sands
    Monarch Sands or fractured shale equivalent
  Maricopa
    Webster Sand or fractured shale equivalent
    Fractured Shale-Uvigerina Zone C
    Obispo Sand and fractured shale equivalent
    Pacific Shale Zone

The productive interval of the Lakeview Pool is limited to Upper Miocene and Lower Pliocene deposition. In this general area, the most prevalent type of accumulation results from stratigraphic traps or permeability pinchouts. As is the case of the Lakeview Pool, stratigraphic traps resulting from angular unconformities are present. The structure within the Miocene does not parallel that of the Etchegoin (Pliocene), as the Miocene beds were folded, and in places faulted, and subjected to erosion prior to Pliocene deposition.

The Lakeview horizon consists of truncated sands which occur on the northeast flank of the Thirty-Five anticline. The direction of strike is west and northwesterly through sections 25 and 36 and continues northwesterly through sections 26 and 33, to the approximate center of section 32. At this point the strike swings to the northeast and the horizon re-enters section 33, in the northwest corner. The change in strike in section 32 affords synclinal accumulation at that point. The Lakeview sand is truncated updip by the Etchegoin overlap. To the southeast, the sand shales out, while to the northwest, the productive interval appears to be limited by a combination of stratigraphic pinchout and permeability barrier.

Structurally, the Lakeview reservoir presents three areas of interest, as shown on Fig. 3. Area I in section 32 is a region in which a productive Sub-Lakeview Miocene sand is present. It occurs from 10 feet to 30 feet below the base of the Lakeview sand and attains a maximum thickness of 25 feet in Well No. 21, section 32. The producing characteristics of the Sub-Lakeview Miocene sand differ radically from those of the Lakeview sand. Water production at high structural locations and abnormally high fluid levels indicate that there was no communication with the Lakeview sand. Wells in Area I penetrated this sand and produced it in conjunction with the Lakeview sand.

In Area II, the Lakeview sand is a

---

[1] References are given at end of paper.

Manuscript received at the office of the Petroleum Branch September 10, 1949. Paper presented at the Petroleum Branch meeting in Los Angeles, October 20-21, 1949.

relatively continuous Miocene sand body unconformably overlain by Etchegoin (Pliocene) sediments. It is overlapped upstructure and apparently shales out downstructure, although downstructure production is limited by an inactive edgewater.

In Area III, the Lakeview sand is broken into two fingers by an intermediate Miocene shale body. In addition, a productive Etchegoin sand, the Calitroleum, overlies the Miocene Lakeview sand, being separated from it by an intermediate Etchegoin shale. This structural relationship is shown in Fig. 4. In this area all wells exposed to the Lakeview sand also include the Calitroleum sand. The Calitroleum sand lenses out along the west boundary of this third area as a result of an unconformity at the top of the Lakeview sand. Downstructure production is limited by inactive edgewater in both the Lakeview and Calitroleum sands. To the east these sands feather into shales. Due to the similar production characteristics of both the Calitroleum and Lakeview sand fingers, these productive sands, for the purpose of this report, have been designated as Lakeview sand and will hereafter be referred to as the first, second and third fingers of Lakeview sand.

Fig. 5 is a subsurface structure map contoured on the top of the Lakeview sand. The productive limits of the pool are delineated by a line of zero net productive sand thickness. The change in strike direction in section 32 is accompanied by a change in dip. The dip varies from 7.3° along the synclinal axis in section 32 to a maximum of 31.0° in section 33. An average of individual dips at 250′ intervals along strike is 24°.

DEVELOPMENT

The discovery well, Lakeview No. 1, section 25, generally known as the Lakeview Gusher, was spudded by the Lakeview Oil Company on January 1, 1909. At a depth of 1655 ft, the well was acquired by the Union Oil Company through purchase of the controlling stock of the Lakeview Oil Company. Drilling was then continued to 2225 ft where the Lakeview sand was encountered.[1] The well blew in on March

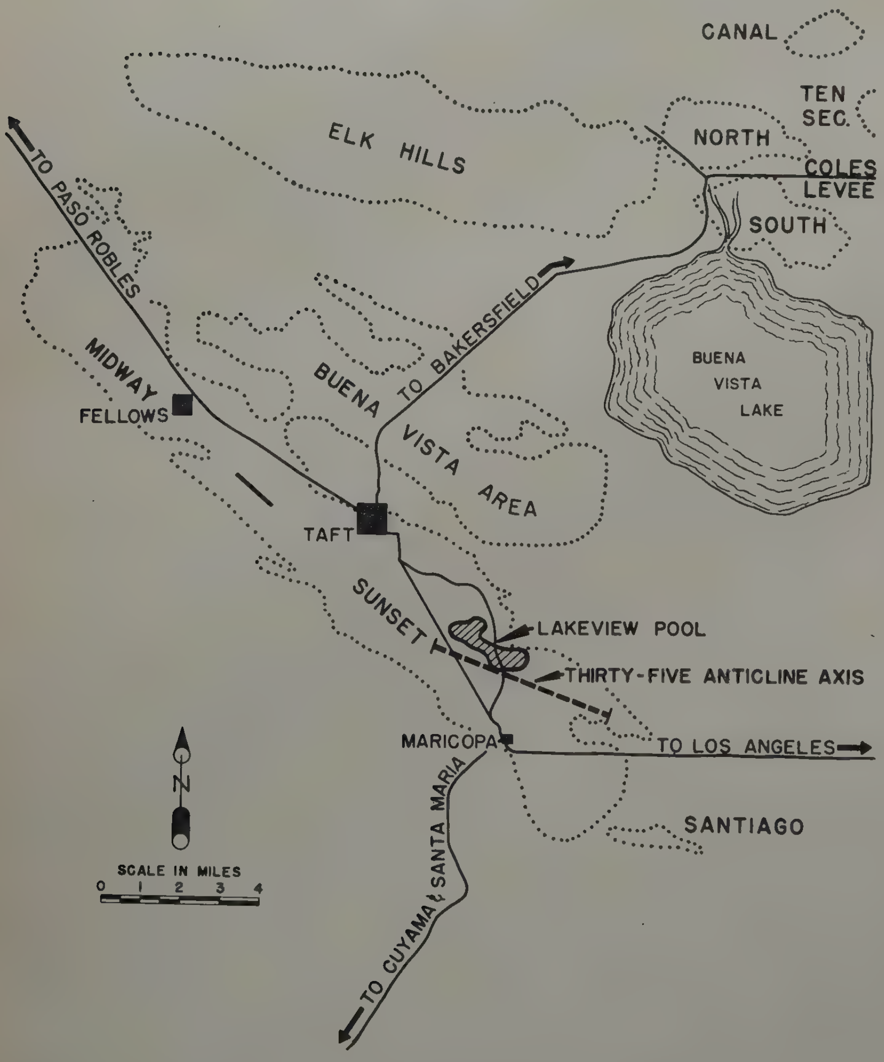

FIG. 1 — REGIONAL MAP OF THE TAFT-MARICOPA AREA

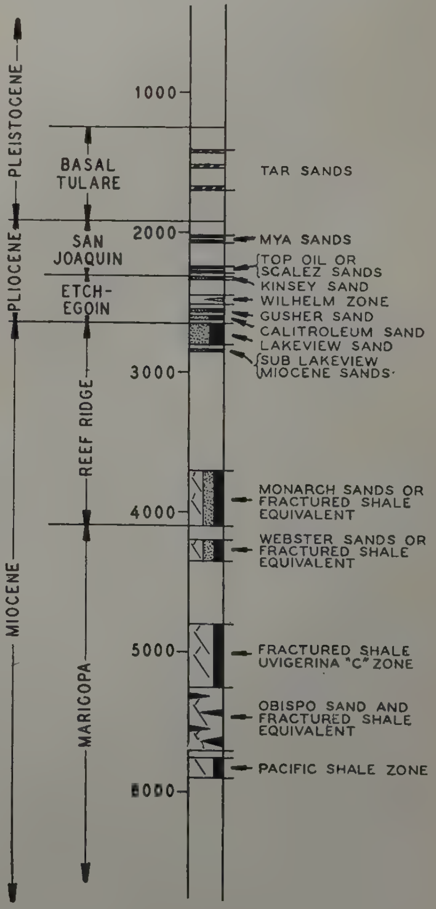

FIG. 2 — COLUMNAR SECTION THIRTY-FIVE ANTICLINE

15, 1910, and flowed uncontrolled for 544 days until September 9, 1911, at which time it died, apparently due to bottom hole caving. It was estimated that at its peak blow, the Lakeview Gusher produced in excess of 68,000 bbl of oil per day, and it was conservatively estimated that the total production approximated eight and one-quarter million barrels. At that time existing storage and shipping facilities in the Midway-Maricopa area were entirely inadequate to handle this uncontrolled production. As a result, twenty sumps or earthen reservoirs were built, covering an area of sixty acres and having a capacity of approximately seven million barrels. Remnants of the levees can be seen today, the largest of which is located approximately one and one-half miles from the well location. It was reported that the oil produced during the uncontrolled flow had a temperature of 92°F and tested 21.2° Baumé gravity at 60°F. The gravity dropped to 18.5° Bé after standing in open reservoirs for seven days and to 17.5° Bé after standing for one year. Based upon subsequent gravity determinations, it appears that the accuracy of the above gravities is questionable. In addition to possibly two hundred and fifty thousand barrels which disappeared through cracks in five of the earthen reservoirs, the loss of approximately three and one-half million barrels of oil is attributed to evaporation and seepage.[2] Subsequent to the blowout, this well was redrilled and deepened five times without establishing satisfactory production.

The development of the Lakeview Pool can be broken into three periods. The first, from the discovery of Lakeview No. 1 in March, 1910, through December, 1934, saw the drilling of seven additional wells. Four of these wells were grouped in sections 33 and 26 while the remaining three were in the immediate vicinity of the discovery well. During the intervening years, it was thought that these two groups were producing from separate horizons.[3] The productive characteristics of these seven wells were sufficiently dissimilar to those of the discovery well that it was not realized the wells were all producing from the same reservoir. After cessation of the gusher, none of the wells completed exclusively in the Lakeview sand were capable of flowing. The sec-

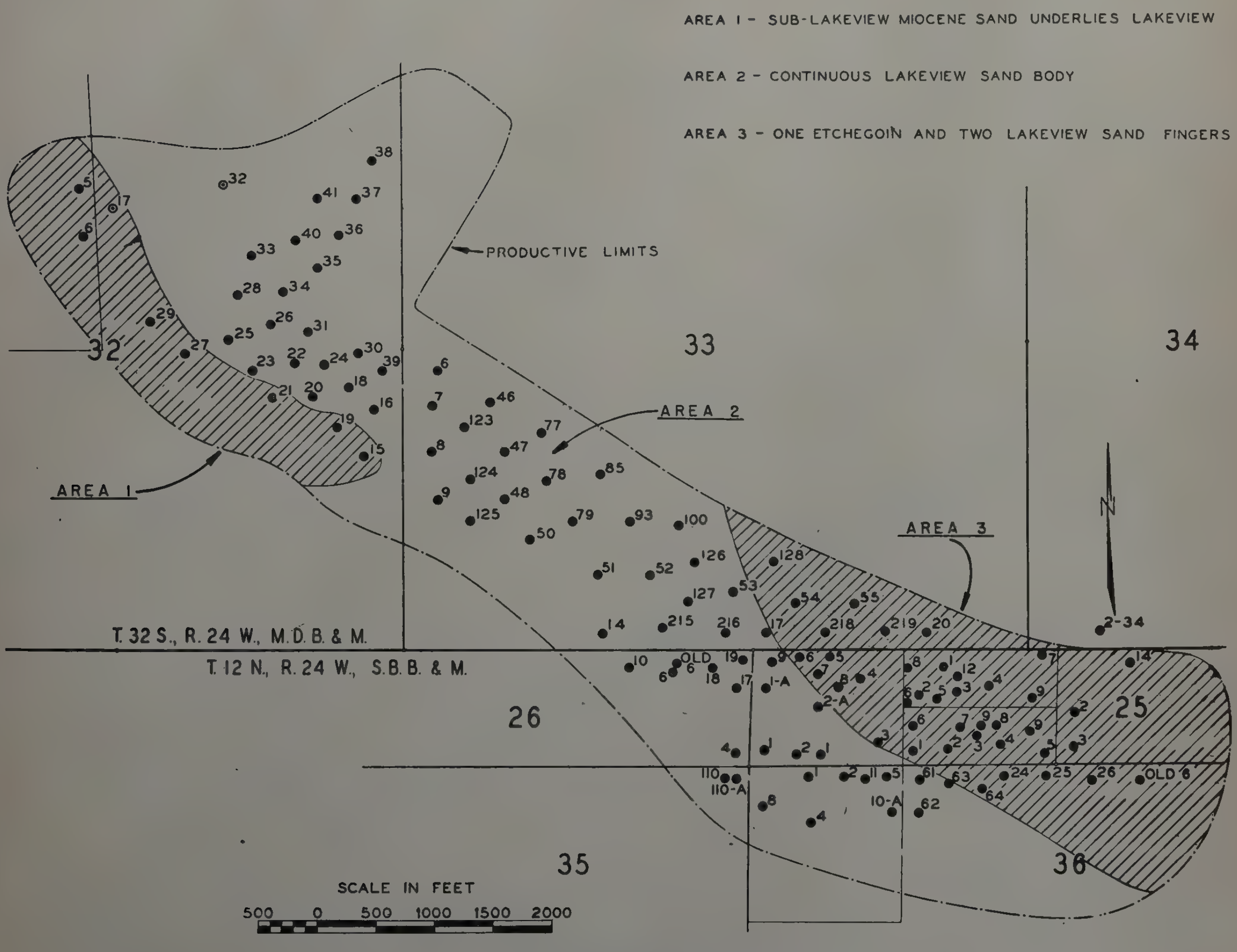
AREA 1 - SUB-LAKEVIEW MIOCENE SAND UNDERLIES LAKEVIEW
AREA 2 - CONTINUOUS LAKEVIEW SAND BODY
AREA 3 - ONE ETCHEGOIN AND TWO LAKEVIEW SAND FINGERS
PRODUCTIVE LIMITS
AREA 1
AREA 2
AREA 3
32
33
34
26
25
35
36
N
T. 32 S., R. 24 W., M.D.B. & M.
T. 12 N., R. 24 W., S.B.B. & M.
SCALE IN FEET
500 0 500 1000 1500 2000

FIG. 3 — AREAS OF DEPOSITIONAL VARIATION

ond period was initiated in January, 1935, by the drilling of the rediscovery well, Hallmark 1-A, section 25. A period of intensive development continued through December, 1940, during which time nearly all the existing wells were drilled. During the third period, from January, 1941, to the present date, five additional wells were drilled in an attempt to more accurately establish the downstructure limits of production. This unusual development history is graphically depicted in Fig. 6. In all, 121 wells were drilled to the Lakeview sand by April 30, 1949, and, of these, 112 were productive.

Operators involved in the development of the Lakeview Pool were the Alford Oil Co., General Petroleum Corp., Hallmark Oil Co., Lakeview Oil Co., Maricopa 36 Oil Co., Merritt-Annex Oil Co., Petroleum Drilling and Exploration Co., Richfield Oil Corp., Sage Oil Co., Standard Oil Co. of California, The Sunset Monarch Oil Co., The Interstate Oil Corp., The Pacific Oil Co., The Texas Co., The United Oil Co., and Union Oil Co. of California.

DRILLING AND COMPLETION PRACTICES

The long development period and the many different companies involved in developing the Lakeview Pool have resulted in a wide variation in drilling practices and completion methods. Most of the wells in the pool were drilled with rotary equipment, but a few were drilled with cable tools. A number of the Lakeview wells were originally shallower zone wells, which were deepened to the Lakeview sands.

It has been the recent practice of some companies to drill to the top of the sand, where the water string was cemented and a water shut-off obtained. A reduced hole was then drilled through the Lakeview zone, the hole underreamed and a slotted liner hung. Other companies favored drilling to total depth before cementing the water string. After obtaining a water shutoff, the cement was drilled out, the hole underreamed and a slotted liner hung.

The time required to drill Lakeview wells has varied from 7 to 91 days. Water string sizes vary somewhat but

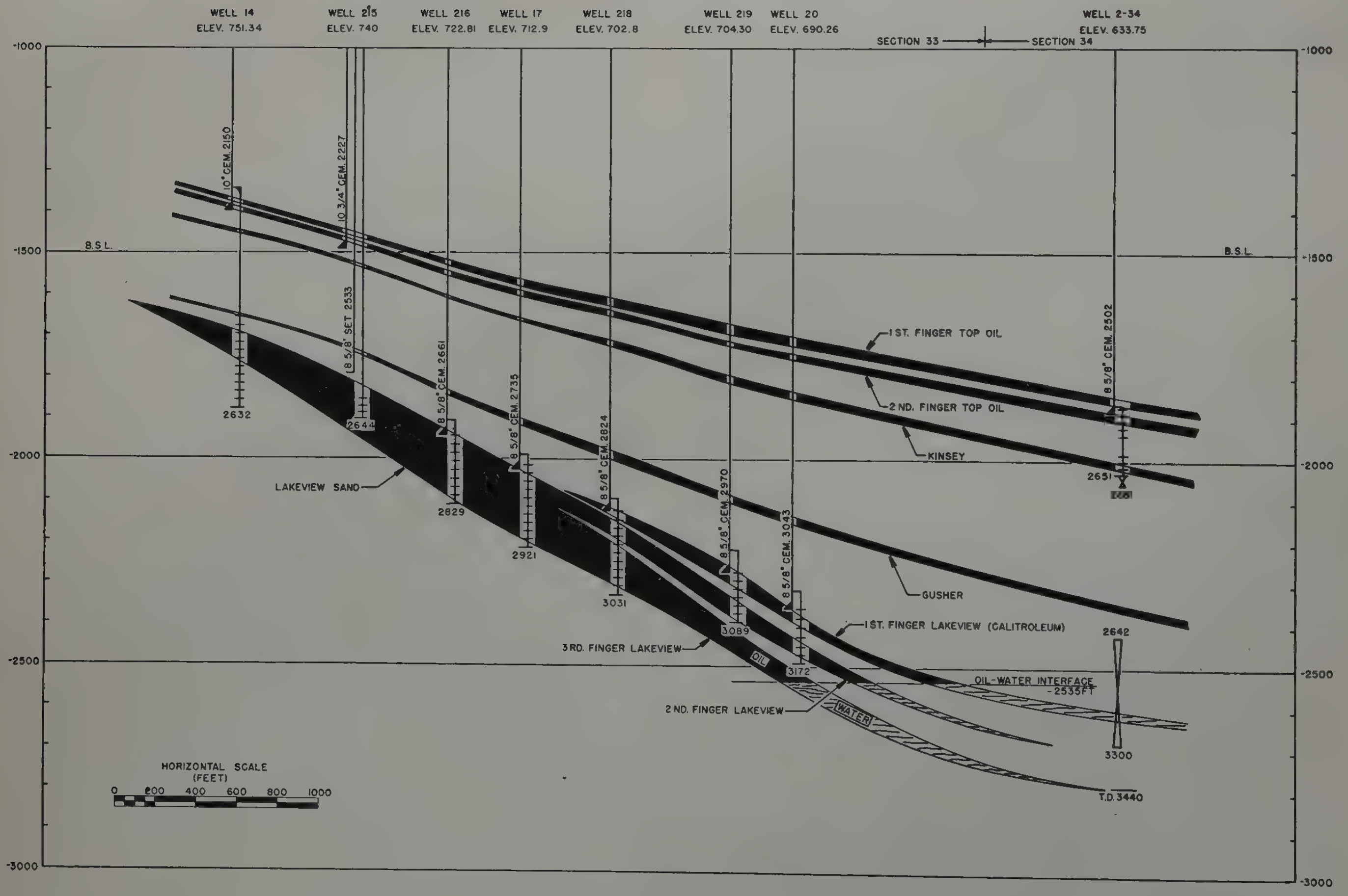

FIG. 4 — WEST-EAST CROSS SECTION NEAR CENTER OF THE LAKEVIEW POOL

are predominantly $8\frac{5}{8}$ in. casing. Liners range in size from about $4\frac{3}{4}$ in. to 7 in. and perforations vary from 60 mesh to 250 mesh.

The majority of the wells were drilled with water base mud, though some of the more recent completions have been with oil or oil base mud.

WELL SPACING

The well spacing in the Lakeview Pool is extremely irregular, varying from about one to seven acres per well. Within this density range there appears to be no correlation between well spacing and cumulative production, even for wells at comparable structural elevations. It is probable that the effect of variable well spacing is obscured by the influence of other factors which, in this pool, have a more pronounced bearing on production. These factors include the number of producing days per month, the downdip rate of gravity drainage, size and efficiency of producing equipment, degree of sand trouble, and extent of sand penetration.

SAND CHARACTERISTICS

The Lakeview sands vary considerably in their characteristics both vertically and laterally over the extent of the field. Core descriptions indicate that the producing medium varies from compact, poorly sorted, tight, silty, poorly saturated oil sand to loose, friable, well sorted, permeable, well saturated oil sand, with the latter predominating. The presence of streaks of kaolin and limestone is common.

Although the sand grains vary in size from very fine to very coarse, medium to coarse grains predominate. Screen analyses of several core samples show a varation from 0.0190 in. to 0.0355 in. at the ten percentile cumulative point on the screen analysis curve.

Core analysis information on the Lakeview sand is meager. Obtaining core data which is representative is difficult due to poor core recovery and to the inability to satisfactorily measure the characteristics of some of the friable, unconsolidated samples. Though few in number, the samples analyzed appear to cover the range of sand characteristics encountered.

Table I is a recapitulation of the available core data. Included are analyses on four laboratory compacted samples which gave data that appear rea-

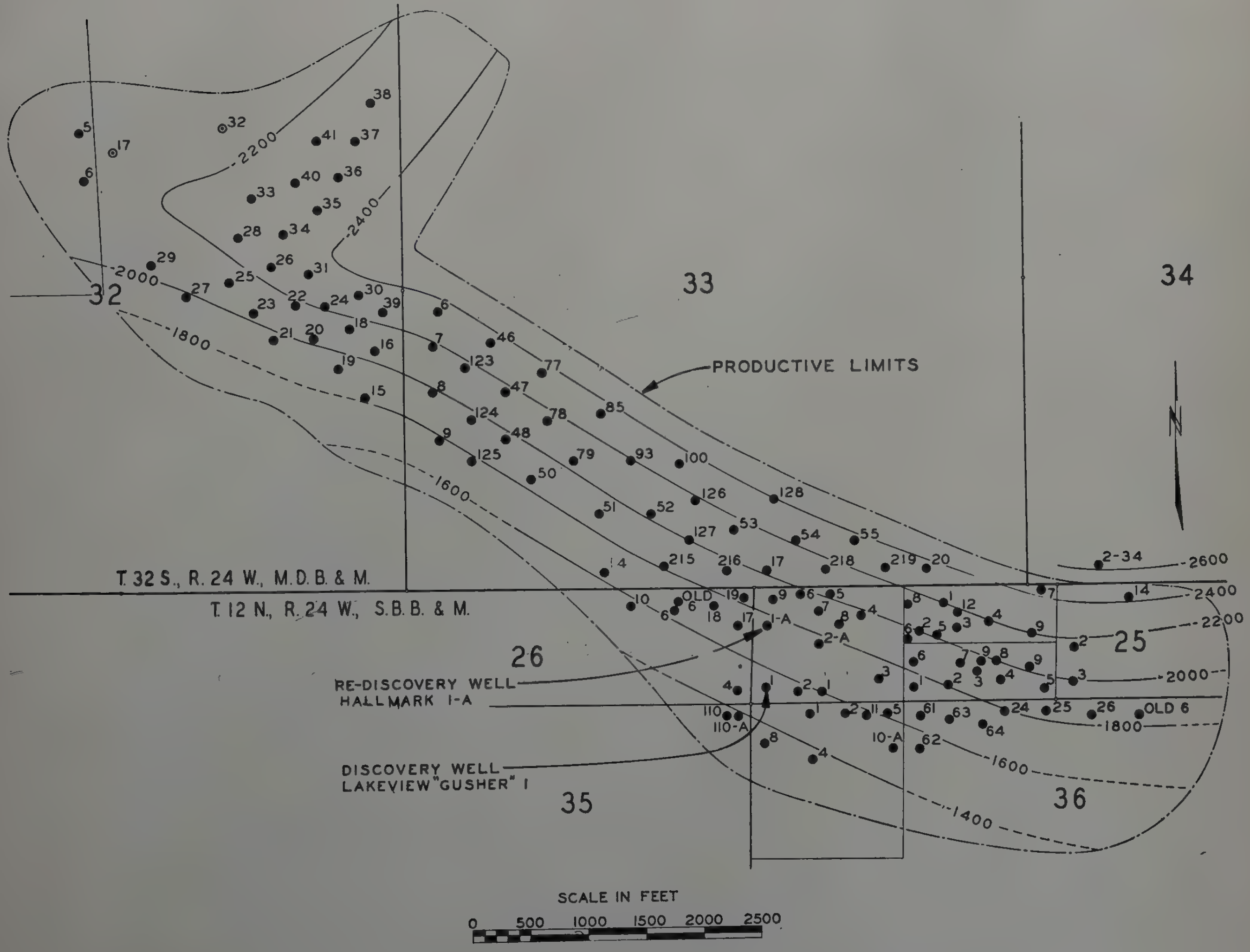

FIG. 5 — SUBSURFACE STRUCTURE MAP — CONTOURS ON TOP OF LAKEVIEW SAND

sonable. These data were included on the basis that a considerable portion of the Lakeview sand is loose and unconsolidated. Incorporation of these analyses on laboratory compacted samples is a conservative measure since it results in larger estimates of the tank oil originally in place and smaller estimates of recovery percentages.

Tests on 11 samples indicated that permeabilities to formation water are about 80 per cent as large as air permeabilities, while permeabilities to fresh water are only about 46 per cent as great as air permeabilities.

FLUID CHARACTERISTICS

The oil obtained from the Lakeview Pool is a naphthenic type crude averaging about 22.5° API gravity. Both initial pool pressures and original saturation conditions in the pool are unknown. Therefore, it has been assumed

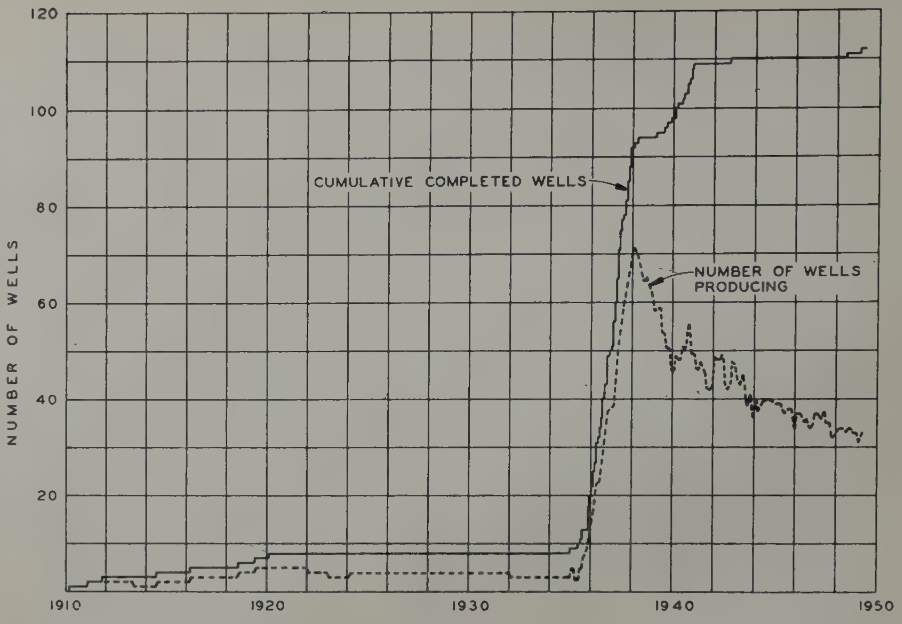

FIG. 6 — NUMBER OF PRODUCING WELLS

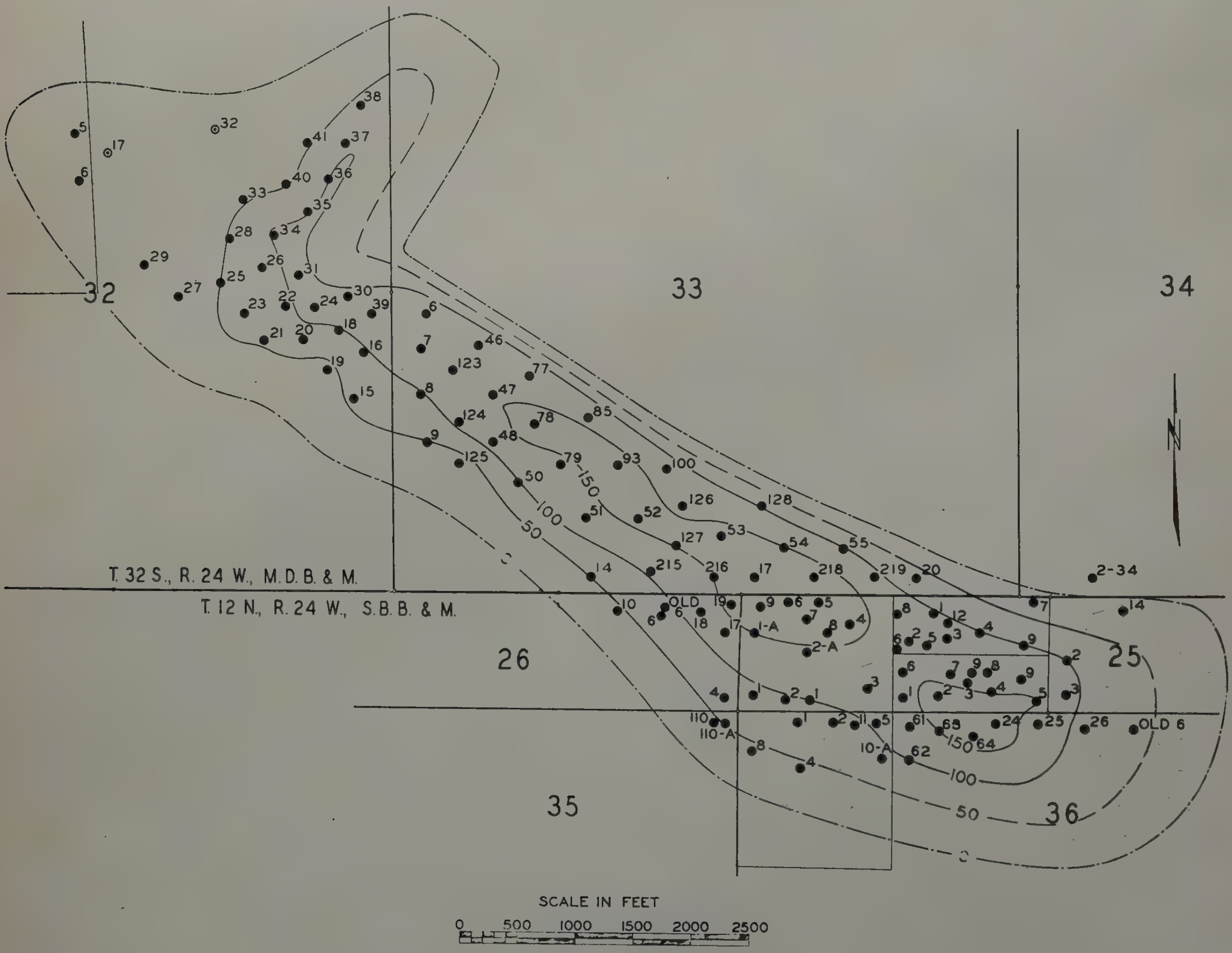
32
33
34
26
25
35
36
T. 32 S., R. 24 W., M.D.B. & M.
T. 12 N., R. 24 W., S.B.B. & M.
N
150
100
50
0
SCALE IN FEET
0 500 1000 1500 2000 2500

FIG. 7 — ISOPACHOUS MAP, NET PRODUCTIVE LAKEVIEW SAND

that initially the pool was saturated and had no free gas cap. It has also been assumed that the initial pressure was equal to a hydrostatic column of salt water equal in height to the average depth of the pool. In most California oil fields, original reservoir pressures can be approximated in this manner.[4] Neither subsurface nor recombined samples of Lakeview hydrocarbon have been analyzed, so it is necessary to rely upon generalized pressure-volume-temperature data for estimates of fluid behavior at reservoir conditions. Using these assumptions and for an average pool depth of 2875 ft the initial pressure would be about 1300 psia, the initial solution gas-oil ratio about 200 cu ft per bbl and the initial formation volume factor about 1.106 bbl of reservoir space per barrel of tank oil.[5,6]

Table I — Lakeview Sand Characteristics

Porosity, Per Cent of Bulk Volume

No. of Samples	Porosity Range, Per Cent	No. of Samples Laboratory Compacted
3	40.0 to 41.6	2
7	35.0 to 39.9	2
15	30.0 to 34.9	0
6	25.0 to 29.9	0
1	24.0 to 24.9	0
Total 32	Average 33.1 Per Cent	Total 4

Air Permeability, Millidarcys

No. of Samples	Permeability Range, md	No. of Samples Laboratory Compacted
3	10,000 to 10,500	2
4	5,000 to 9,999	0
12	1,000 to 4,999	2
5	495 to 999	0
Total 24	Average 3655 md	Total 4

Capillary Pressure Interstitial Water Saturation, Per Cent of Porosity

Interstitial Water corresponding to Permeability of 3655 md equals 23.5 per cent

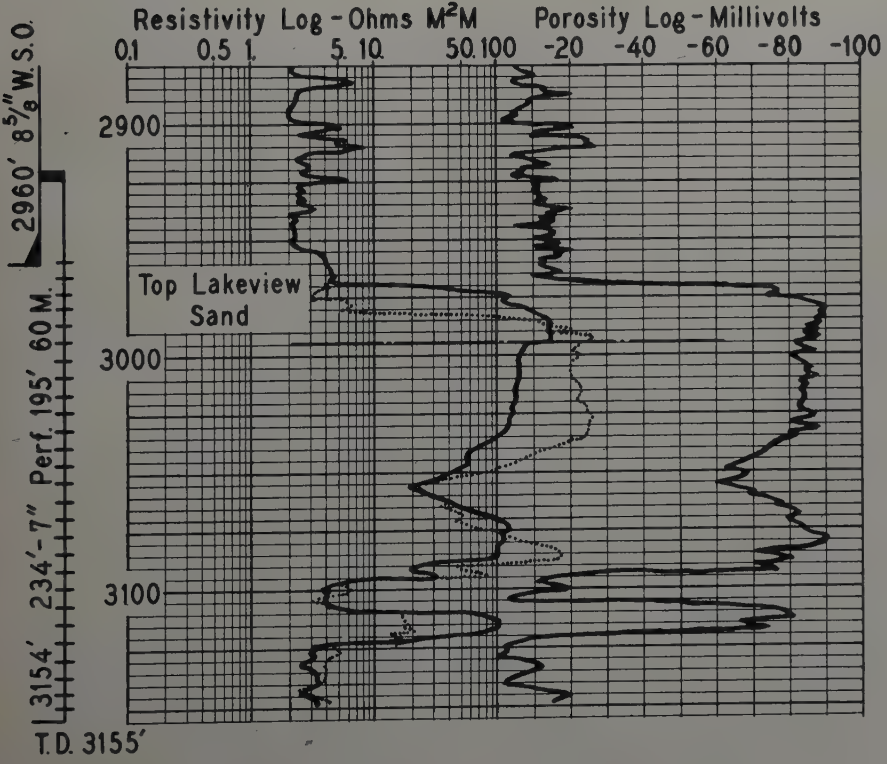

FIG. 8 — TYPICAL ELECTRIC WELL LOG AND COMPLETION METHOD

TANK OIL IN PLACE

In view of the inactivity of the edgewater, it has been assumed that the net productive reservoir volume in 1935 was identical to the productive volume at the time of the pool's discovery. The reservoir volume was determined by the volumetric-porosity method from an isopachous map contoured on 10 ft sand thickness. A similar isopachous map contoured on 50 ft sand thickness is shown on Fig. 7. The sand count was based upon a consideration of core data and electric logs. Of the 121 wells which penetrated the Lakeview sand, 85 were wholly or partially cored, while 92 have electric logs. A typical electric log of the Lakeview zone is shown on Fig. 8. The sand pinchouts upstructure and along strike were determined from cross-sectional analysis by assuming that the sand continued to thin uniformly beyond points of control. The lower limits of production were established by determining the oil-water contact on the basis of sands which were wet at the time of drilling.

The net productive sand volume was calculated to be 41,798 acre-ft. The productive sand encompasses an area of 588 acres and has an average thickness of 71 ft. Fig. 9 shows the approximate structural distribution of the net productive sand volume as determined by superimposing the isopachous map upon the structure map and computing the sand volume between structure contours.[7]

The tank oil originally in place was calculated to be 74,240,276 bbl, using the core data of Table I and a formation volume factor of 1.106 bbl of reservoir space per barrel of tank oil.

RESERVOIR PERFORMANCE

The production history of the pool is shown graphically in Fig. 6 and 10. As of April 30, 1949, the average pool production rate was about 2000 B/D.

At that time a total of 33 wells were still producing.

It is significant to point out that about 20 per cent of the cumulative oil production was estimated. However, it is believed that the estimates were conservative. The estimates were made principally on oil produced during the interval of 1910 to 1917, and about 90 per cent of the estimate was for oil presumably produced by the "Lakeview Gusher". For those wells where Sub-Lakeview Miocene or Gusher production was commingled with Lakeview production, a reasonable amount was deducted in an effort to obtain only Lakeview production.

Accurate water production statistics are not available for certain relatively small properties within the pool. However, the water production accumulated for those properties on which it was reported has been used in determining the water cut shown on Fig. 10. Accurate gas production data are not available for the pool and have, therefore, not been included.

In the Lakeview Pool, it has been the practice to utilize static fluid level data in place of bottom hole pressures as a basis for studying reservoir behavior. Depth pressure data are so meager, consisting of only nine surveys taken during 1937, as to be inadequate for purposes of reservoir analysis. Fluid level determinations suggest that the fluid surface is not level, but tends to slope downdip with the structure. Because sufficient data are not available for the preparation of iso-fluid level maps, arithmetically averaged fluid levels have been used. The excellent agreement between these averaged fluid levels and fluid levels determined from well performance is shown on Fig. 11. Curve A represents the average of actual fluid level measurements while Curve B designates time-depth depletion fluid levels. The latter was determined by plotting the subsea depth of the bottom of the well, providing it is not deeper than the base of the sand, versus the date that the well ceased to produce from lack of fluid.

The principal production problem experienced in Lakeview zone wells has been sand trouble. Prior to 1936, most wells were completed with liners having wide slots generally ranging from 120 to 250 mesh. Excessive sand difficulties, which necessitated frequent bailing, perforation cleaning and equipment repair and replacement, resulted from these completions. The extent of the sand difficulties prompted some of the operators to conduct experiments on the bridging characteristics of the sands, which in turn resulted in a trend towards gravel packed liners of the circulated type and towards conventional liners with 60 mesh slots. Although the effects of these changes in completion technique have not been studied in detail, it appears that they have been instrumental in practically eliminating sand trouble.

The Lakeview Pool is apparently bordered on its downstructure side by a comparatively inactive edgewater. However, as shown on Fig. 12, there are three general areas in the pool that have produced appreciable quantities of water. Areas 1 and 2 are regions in which edgewater has been coned into wells. These areas generally exist along competitive property lines. In Area 1, the first significant appearance of water

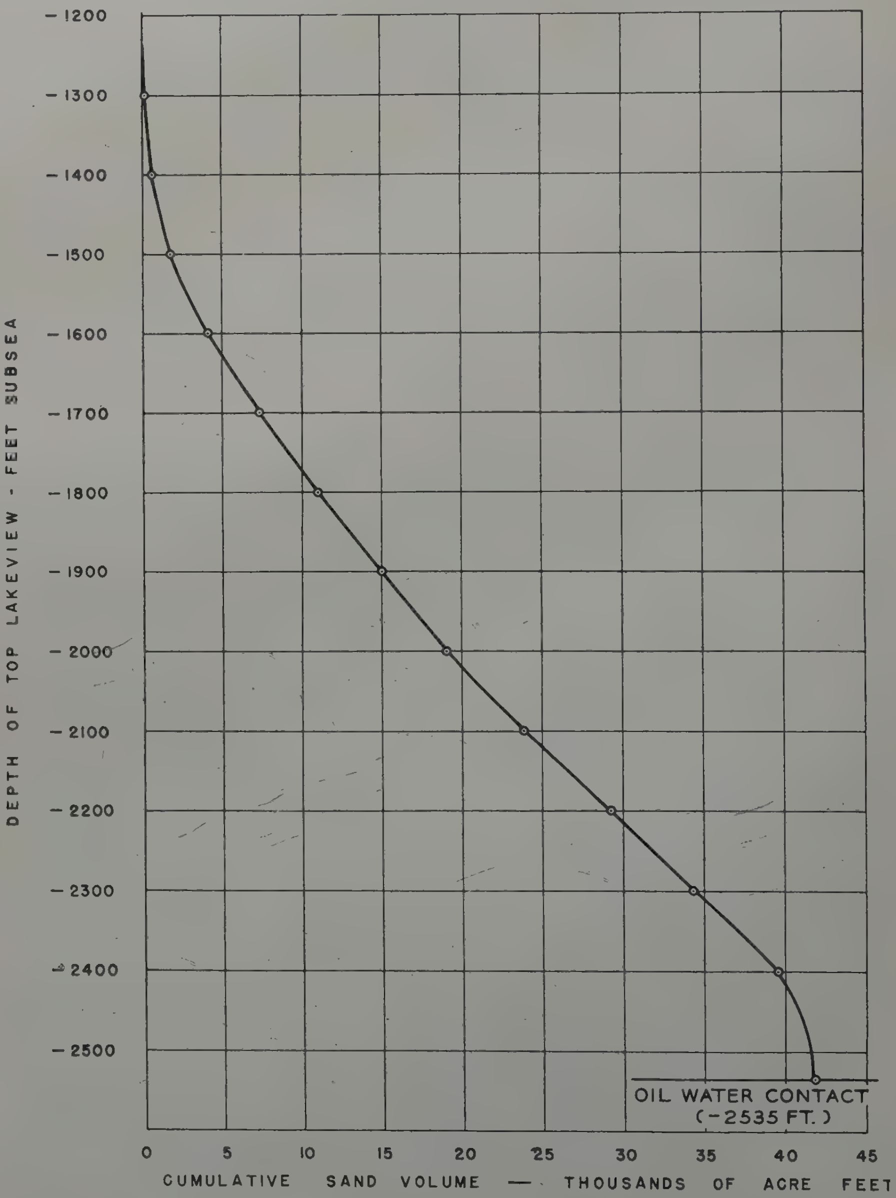

FIG. 9 — STRUCTURAL DISTRIBUTION OF SAND VOLUME

occurred in 1940 during a period of relatively high production which followed the completion of the majority of the wells. An inspection of fluid levels disclosed that the wells affected by water were surrounded by a pressure sink, which probably encouraged the movement of water into that region. During a period of reduced production in 1941, the water produced in this area declined noticeably. Concurrent with the increase in production during 1942, water again entered the area. Generally since about 1944, decreased gross production rates have resulted in gradually diminishing water cuts. Area 2 is characterized by initially clean wells which, after a period of approximately three months of intensive production, showed rapidly increasing water cuts. After 1937, following a decline in production rates, water receded from the area, only to reappear again during the period of heavy production which began in 1942. The water behavior thereafter has responded similarly to that in Area 1. Area 3 is a region which apparently has been invaded by water from other zones. A review of the mechanical conditions of wells which penetrated the Lakeview sand high on the structure suggests that any of several wells could have introduced foreign water into the Lakeview sand through unplugged sidetracked casing or from incompletely plugged sands. In addition, it appears that the low pressure Lakeview zone was readily susceptible to an invasion of foreign water. The belief that these structurally high wells were affected by a foreign water is further substantiated by the fact that wells highest on the structure produced water before the lower structure wells. Analyses of water produced by wells in Area 3 shows that water from the higher structure wells contained slightly smaller concentrations of salt than those further downstructure. Water produced from these downstructure wells in Area 3 was similar to Lakeview edgewater. It is conceivable, however, for a foreign water, in percolating through the Lakeview sand, to dissolve small quantities of salts so as to become similar to Lakeview water. The invasion in this area has not been serious since total water production seldom exceeded 200 bbl per day. There is no evidence that oil production was obstructed by this invasion. The ingression of alien water has been curbed to the point where it is now negligible.

Reservoir characteristics which are highly favorable to gravity drainage, make this pool particularly susceptible to effective gravity drive. The absence of active water drive and the depletion of gas by the "Lakeview Gusher" made gravity drive the dominant reservoir agent.

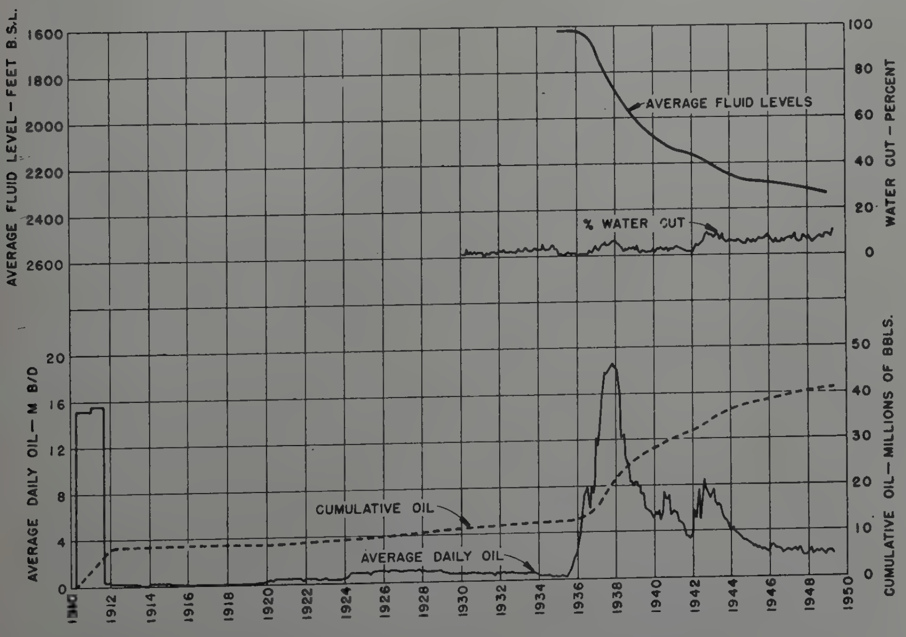

FIG. 10 — PRODUCTION HISTORY — LAKEVIEW POOL

The production decline characteristics of individual wells are dependent upon their structural location. Wells high on the structure exhibit rapid declines in production rate until they go dry. Wells lower on the structure produce for a substantial period of time at a relatively constant rate before their production declines rapidly due to the recession of the fluid level downstructure past the wells.

A comparison between the daily average production rate and fluid level decline represented by Fig. 10 shows that the decline in fluid level is intimately dependent upon the withdrawal rate. This relationship between withdrawals and fluid level is more strikingly illustrated on Fig. 13, which shows the fluid level versus the cumulative oil production. The straight line relationship between the fluid level and the cumulative oil production from January, 1942, to January, 1949, indicates that during that period the oil recovery has been essentially constant at about 53,000 bbl for each foot drop in fluid level. Such a relationship provides a simple means of estimating reserves, provided the lowest depth of drainage can be accurately determined. This method does not allow for thinning of the sands as the oil-water contact is approached.

The "Lakeview Gusher" was probably accompanied by an unstable localized reduction in pressure, which resulted in a release of the bulk of the original solution gas in the region affected. Following cessation of the "Gusher's" uncontrolled flow, a period of establishing equilibrium took place. During this period a low pressure free gas cap of small areal extent was apparently created. This was evidenced by later drilling. The establishment of equilibrium resulted from a movement of oil into the drained region and an equalization of pressures throughout the reservoir. The movement of fluid into the depleted area is substantiated by rising fluid levels and increased production in Wells No. 215, section 33, and No. 6, section 26, from 1921 through 1927. These data indicate the period to establish equilibrium was in excess of 16 years.

By relating the average fluid level at any particular time to the structural distribution of the sand volume, the number of acre feet drained at that time may be approximated. It is recognized that drainage is not complete above the fluid level and that the recovery is a function of time, but it is assumed that additional economic recovery from that region will be negligible. An analysis of Fig. 14, which associates the drained cumulative reservoir volume with cumulative production of oil, shows the ratio to approximate that of a straight line. This relationship indicates that such functions as formation volume factor, edgewater encroachment, water production, gas production, porosity, and interstitial water remain approximately constant over the period beginning with the rediscovery of the pool in 1935 through the present date. Of particular interest is a straight line extension of this curve

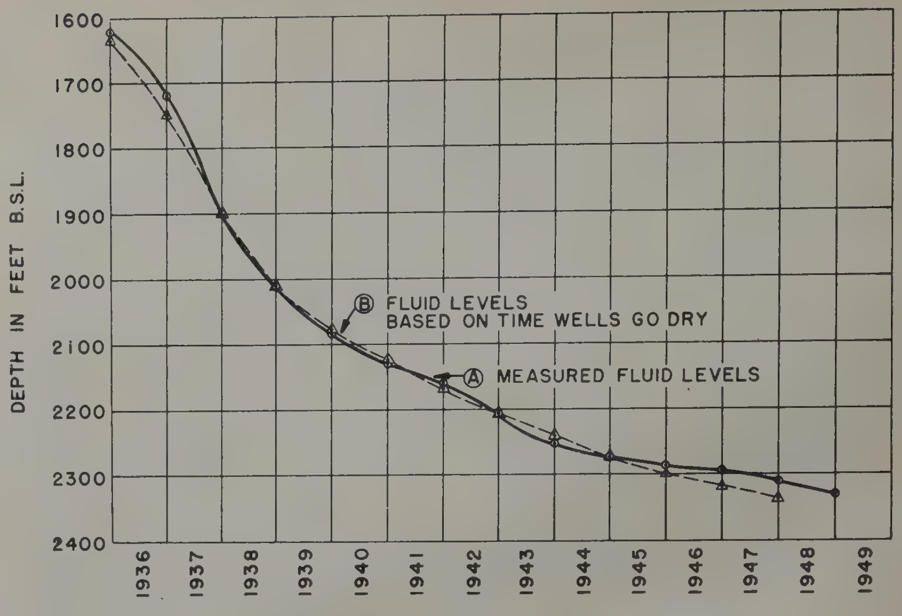

FIG. 11 — COMPARISON OF MEASURED FLUID LEVEL WITH TIME-DEPTH DEPLETION FLUID LEVEL

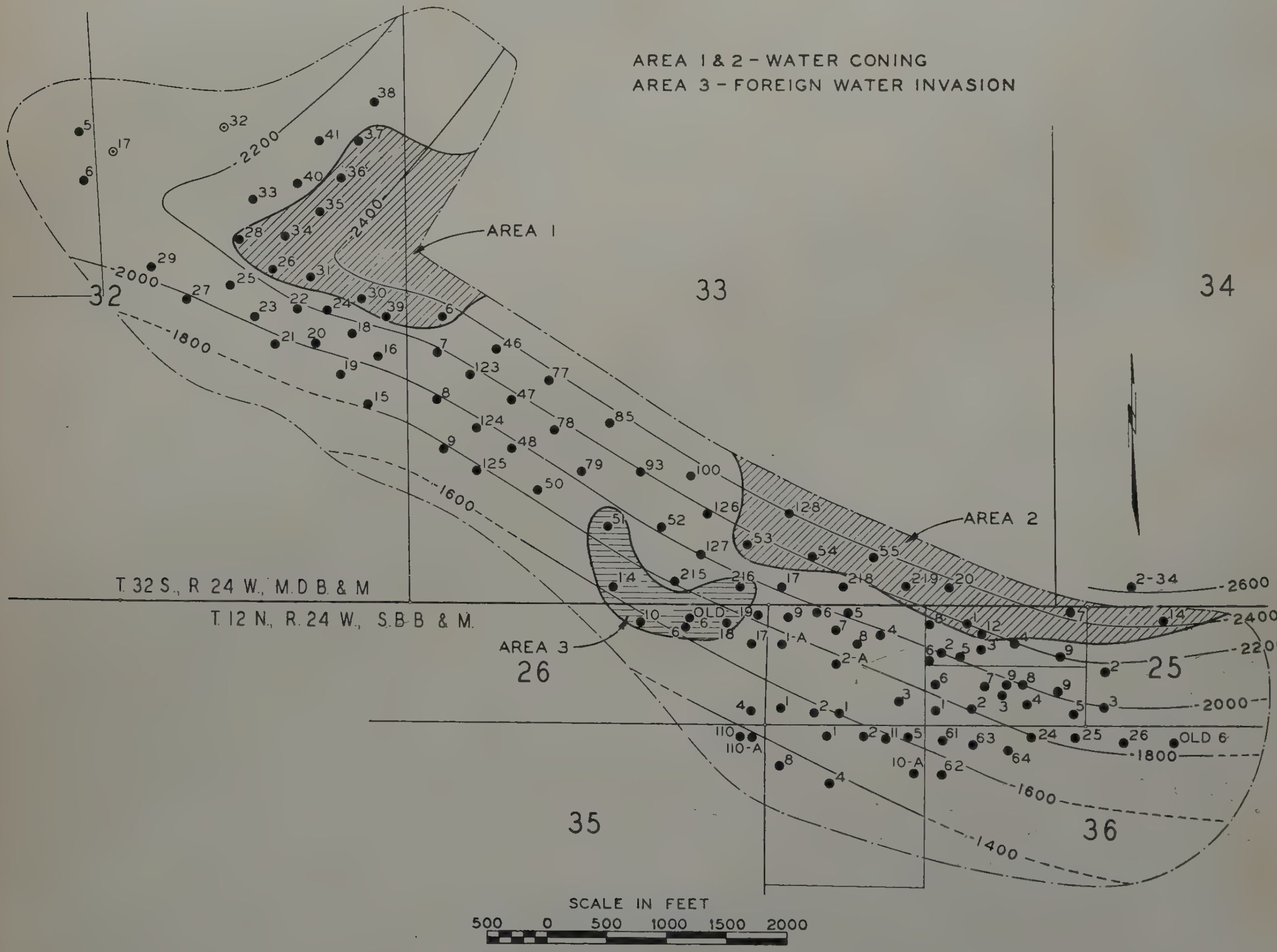
AREA 1 & 2 - WATER CONING
AREA 3 - FOREIGN WATER INVASION
AREA 1
AREA 2
AREA 3
32
33
34
26
25
35
36
T 32 S., R 24 W., M.D.B. & M
T 12 N., R 24 W., S.B.B. & M.
2200
2400
2000
1800
1600
2600
1400
SCALE IN FEET
500 0 500 1000 1500 2000

FIG. 12 — AREAS OF WATER CONING AND FOREIGN WATER INVASION

to represent a point of zero drainage. The first impression is that approximately 9,000,000 bbl of oil were produced without accompanying reservoir space being vacated. In the absence of edgewater encroachment, this apparent discrepancy must be related to the difference in physical properties of the fluid as it existed before and after the period of uncontrolled flow. Lewis[9] states that when original pressures are reduced, gas will come out of solution and expand. Some oil will be driven from the pores by the free gas and partial saturation conditions will be developed corresponding to the insular regions in a capillary system induced by gravity drainage. In the insular region, small globules of gas, separate and distinct from one another, are interspersed in the oil. In this stage the sand has no gas permeability, the gas is entrained in the oil and probably will move in the oil stream. In effect, single phase flow would still exist in the sand and the freed gas would merely reduce density and impart greater elasticity to the remaining liquid. The foregoing statements appear to be particularly applicable to the Lakeview Pool. It is believed that after the period of uncontrolled flow and during the period in which equilibrium was being re-established an accumulation of free gas in the insular region did occur and as a result of the imparted pseudo elasticity of the liquid the reservoir was essentially refilled with a fluid differing radically from the original fluid. The apparent production discrepancy of 9,000,000 bbl of oil as shown in Fig. 14 can be attributed to the refilling of the reservoir due to the accumulation of insular free gas.

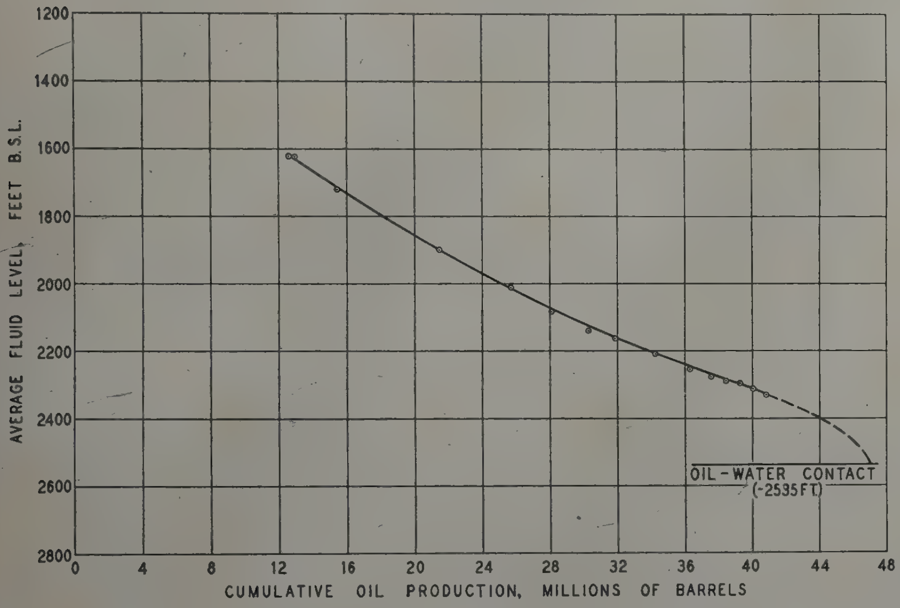

FIG. 13 — CUMULATIVE OIL PRODUCTION VERSUS FLUID LEVEL DECLINE

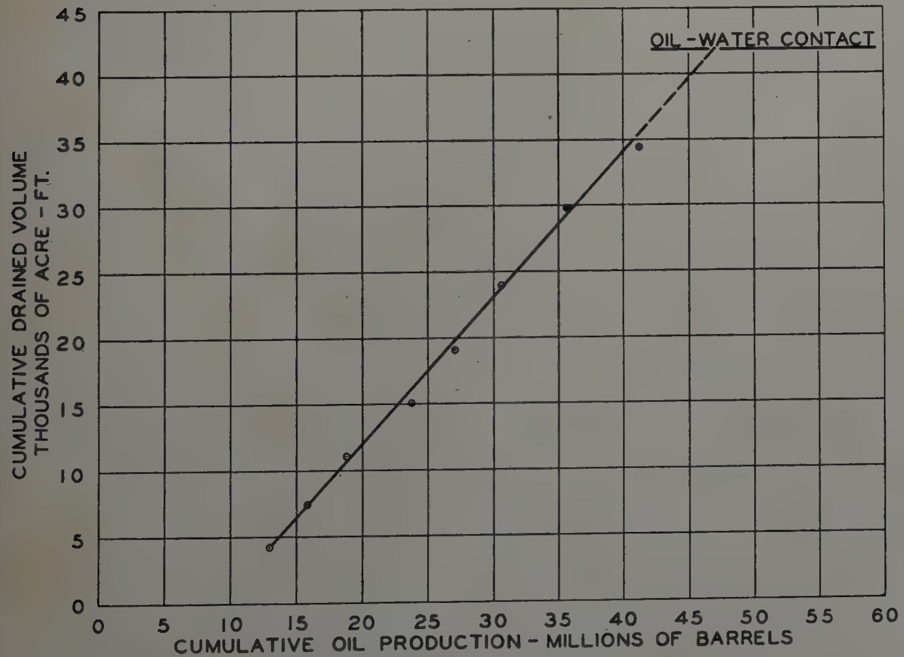

FIG. 14 — RESERVOIR DRAINAGE — PODUCTION RELATIONSHIP

An extrapolation of the curve of Fig. 14 to the oil-water contact gives an indication of the ultimate recovery attainable. It is not inferred that this recovery will be reached since neither the feasibility nor economies of draining the pool to the oil-water contact have been investigated.

Table II gives a resumé of estimated oil originally in place, recoveries as of May 1, 1949, and estimated ultimate recoveries assuming that the pool is drained down to the oil-water contact.

Table II — Oil Recovery

Tank oil originally in place, barrels	74,240,276
Barrels per acre foot originally in place	1,776
Tank oil produced to May 1, 1949, barrels	41,082,498
Barrels per acre-ft produced to May 1, 1949	983
Per cent recovery as of May 1, 1949	55.3
Estimated ultimate oil recovery, barrels	47,000,000
Estimated ultimate recovery in barrels per acre ft	1,124
Per cent ultimate recovery	63.3

CONCLUSIONS

The performance of the Lakeview Pool demonstrates the effectiveness of gravity drainage as a reservoir mechanism. In the absence of active edgewater and/or appreciable gas drive, gravity is the principal reservoir control. The pronounced dip and the favorable sand and fluid characteristics make gravity drive particularly effective. The recovery to date has been about 55.3 per cent of the tank oil originally in place, and it is estimated that an ultimate recovery of 63.3 per cent is attainable.

The greater portion of the pool's water production has been due to coning the inactive edgewater into low structure wells located along competitive property lines.

ACKNOWLEDGMENTS

Grateful acknowledgment is hereby made to the management of the Standard Oil Co. of California for permission to publish this paper, and to Miss L. R. Kirwan and N. R. Powley II for their assistance in assembling the data.

REFERENCES

1. Personal Communication, F. F. Hill, formerly Director of Production, Union Oil Company of Calif., 1949.
2. Department of Natural Resources, Division of Oil and Gas, History of Well Lakeview No. 1, Lakeview Oil Company.
3. T. P. Sanders: "Lakeview District Illustrates Value of Detailed Reserve Study." *Oil and Gas Journal* (June 23, 1938), Vol. 37, No. 6, 56.
4. E. V. Watts: "Some Aspects of High Pressures in the D-7 Zone of the Ventura Avenue Field." *Trans.* AIME (1948), 174, 191.
5. M. B. Standing: "A Pressure-Volume-Temperature Correlation for Mixtures of California Oils and Gases." *Drilling and Production Practice* (1947), 275.
6. Carlton Beal: "The Viscosity of Air, Water, Natural Gas, Crude Oil and Its Associated Gases at Oil Field Temperatures and Pressures." *Trans.* AIME (1946), 165, 94.
7. E. P. Burtchaell: "Reservoir Performance of a High Relief Pool." AIME *Jnl. of Petr. Tech.* (July, 1949), Vol. 1, No. 7, 171.
8. M. G. Arthur: "Fingering and Coning of Water and Gas in Homogeneous Oil Sand." *Trans.* AIME (1944), 155, 182.
9. J. O. Lewis: "Gravity Drainage in Oil Fields." *Trans.* AIME (1944), 155, 131.
10. Elkins, French and Glenn: "Lance Creek Sundance Reservoir Performance — A Unitized Pressure-Maintenance Project." Technical Publication No. 2401, *Petr. Tech.* (July, 1948).

DISCUSSION

By C. F. Gates, General Petroleum Corp., Los Angeles, Calif.

Sims and Frailing are to be commended for analyzing and summarizing the history of a pool which amply demonstrates how important gravity drainage can be as a recovery mechanism under favorable conditions. This pool is unique in having first a period of production in which the depletion mechanism dominated the recovery and then another distinct period in which recovery was almost exclusively by gravity drainage. Fluid level data shortly after the beginning of the second period of development, January, 1936, indicated an average pressure of about 185 psi or 14 per cent of the estimated initial pressure of 1300 psi. In order to visualize these relative values, one needs to examine Fig. 13 keeping in mind that the initial pressure was the equivalent of a fluid level about 1200 ft above sea level. Recovery to January, 1936, was 12.5 million bbl, or 17 per cent of the original oil in place. Assuming several wells and more uniform withdrawals, recovery by the depletion mechanism alone would probably have been about 20 per cent compared with 63 per cent estimated total for both depletion and gravity drainage.

It is of some interest to speculate about what the recovery might have been if no blowout had occurred and all produced gas had been returned to the top of the structure permitting gravity drainage to take place at higher pressure. Under present conditions about 37 per cent of the initial oil in place will remain in the reservoir. If the remaining oil saturation were the same at high pressure as at low pressure, then additional oil would be recovered because of the difference in formation volume factor of the residual oil. As an upper limit only 10 per cent of the residual oil would be recovered by this means. The total recovery would then be more than 63.3 per cent, but less than 67 per cent of the original oil in place.

DISCUSSION

By Vaughn S. Moyer

The Lakeview pool, in its latter production history, at least, is as fine an example of gravity drainage performance as can be found in California. Fortunately for the reservoir engineer, the drive appears to be uncomplicated by water or internal energy forces, permitting some more or less unencumbered calculations to be made for gravity drainage. Since a great many California pools react unpredictably — insofar as theoretical behavior is concerned—such calculations should enhance the knowledge of gravity drainage considerably. It is true, of course, that an isolated case such as this cannot of itself become the gauge whereby all gravity behavior is judged, but nevertheless it can serve as a guide to the trend to be expected.

Perhaps the authors have made such calculations. If so, a few words from them on the subject would be well worthwhile. It would be interesting to know if the observed gravity drainage deviates materially from the calculable values, and if so, in which direction—lesser or greater?

Author's Reply to Vaughn S. Moyer:

The successful application of theoretical gravity drainage equations to the Lakeview Pool is unfortunately hindered by the meager data available concerning sand and fluid characteristics. However, using the range of data that may be applicable, Darcy's equation for maximum downdip flow of oil[10] gives oil rates for 1938 in the order of 14,000 to 18,000 B/D. When this is compared to peak production rates of about 18,000 B/D in 1938, it appears that good agreement is indicated. Similar calculations for 1949 indicate maximum downdip oil movement in the range of 7,000 to 9,000 B/D. When compared with the present oil production rate of about 2,000 B/D, this may indicate that sufficient wells are not available to produce the pool to the maximum rate. Other factors that could contribute to this reduced rate include incomplete sand penetration and reduced effective oil permeability. ★ ★ ★

SOME PRELIMINARY INVESTIGATIONS OF QUANTITATIVE INTERPRETATIONS OF RADIOACTIVITY LOGS

ROBERT E. BUSH, LANE-WELLS CO., HOUSTON, TEXAS, AND **E. S. MARDOCK,** MEMBER AIME,

WELL SURVEYS, INC., TULSA, OKLAHOMA

ABSTRACT

The objective of this paper is to present practical methods of applying radioactivity logs to problems of interest both to those engaged in evaluating fundamental reservoir data as well as to those engaged in subsurface structural work. The basic theories underlying the operation of radioactivity logging methods are briefly discussed along with some of the problems arising in the interpretation of the log. Relative methods of quantitative interpretation are described, with a discussion of relative reference lines and specific examples are given showing the application of these relative quantitative interpretation methods. To show the variation of the methods described, specimen wells penetrating formations widely divergent in point of geologic age were selected to demonstrate the application. A relative reference line is determined for the Neutron Curve and by comparison to known petrophysical data such as porosities from diamond cores, a direct quantitative relationship is developed. The application of this relative calibration curve to logs of unknown wells will permit a reasonably accurate determination of porosity in limestone and dolomite formations. Specific examples are given showing the application of these relative methods of interpretation to logs of the Smackover limestone in Louisiana, the Edwards limestone and dolomites of South Texas, and Permian dolomites of West Texas.

INTRODUCTION

Radioactivity logs have been used extensively by the petroleum industry for a number of years and recognition of their value has grown steadily, not only as tools to aid in the solution of specific stratigraphic problems, but also as potential sources of the basic data necessary for the estimation of net pay and reserves. The value of radioactivity logs for stratigraphic work has been pointed out in the literature,[1,2,4,5,6] and now has long been recognized by the industry, but the quantitative application of the logs has advanced but little beyond the stage of a strong conviction that radioactivity logging curves will some day provide the information on such important quantities as the porosity and the liquid saturation of the formations.

During the past few years the staffs of the Lane-Wells Company and Well Surveys, Incorporated, have devoted a great deal of time, thought, and experimentation to the relationships existing between radioactivity curves and the lithologic conditions encountered, and this paper is, in a manner of speaking, intended as a progress report of this work and includes suggestions which the authors have found useful in the interpretation of radioactivity logs.

The section on theory is not intended as a complete exposition of the physical processes involved, but rather as a brief introduction to the reader of these processes so that he may acquire a better understanding of the behavior of the radioactivity curves under the varied conditions encountered in normal well logging.

Three relative methods for using neutron logs for the quantitative estimation of porosity in limestone or dolomite are presented. These methods are based on the comparison of logs and porosity data from wells in Louisiana, South Texas, West Texas, and New Mexico.

These areas were selected because not only were there more core data available from these areas but also the majority of these data were from limestone or dolomitic zones. The correlation between core data and logs is simpler for limestones and dolomites than it is for sandstones due to the fact that sandstones are more complex than limestones and differ more widely among themselves as to composition of cementing materials, siltiness, etc. When data applicable to the various types of sandstones are available, the authors hope to present a discussion similar to this paper covering sandstones or possibly a more general discussion covering all types of reservoir rocks.

The relative methods for estimating porosity which are presented in this paper fall short of the absolute method sought. However, these methods possess the advantage that they can be applied to almost any neutron log as long as the range of application is held within the limits imposed by the local lithologic conditions which prevailed during calibration, i.e., these methods are for short range application only.

THE THEORETICAL BASIS FOR RADIOACTIVITY LOGGING

The two radioactivity logging curves commercially available today are the

---

[1] References are given at end of paper.

Manuscript received at the office of the Petroleum Branch October 4, 1949. Paper presented at the Petroleum Branch meeting in San Antonio, October 5-7, 1949, and at the Petroleum Branch meeting in Los Angeles, October 20-21, 1949.

Gamma Ray Curve and the Neutron Curve. Each of these curves consists essentially of relative measurements of primary and/or secondary gamma ray intensities recorded as functions of depth.

The Gamma Ray Curve is obtained by lowering into the well a detector of gamma rays (Fig. 1-B) which is connected to surface recording equipment and the intensity of the gamma rays emitted naturally by the rock strata are recorded beside the proper depth marker, while the chamber is being raised to the surface.

The neutron survey is obtained with a short ionization chamber, to which there is attached a capsule containing a radium-beryllium mixture which serves as the source of neutrons, (Fig. 1-A). The ionization chamber of this instrument is affected by the gamma radiation resulting from the bombardment of the formation by neutrons and by the primary gamma radiation from the sources which is scattered by the formation whereby some of it is directed toward the ionization chamber. The natural radiation from the formations also affects the chamber, but the intensity of this radiation is very small compared to that of the gamma radiation from the other causes enumerated above.

Response of Curves to Various Conditions

Fig. 2 is a chart showing the response of the radioactivity logging curves for different lithologic conditions, and Fig. 3 shows the effect of hole size and casing.[4,5,6] These charts will not be discussed at this time but they will be discussed later in the text in connection with the description of the physical processes involved.

The Natural Gamma Ray Curve

The response of the natural gamma ray curve is clearly explained on the relatively simple basis that some rocks radiate more gamma rays than others, and Russell[3] has shown that there is a strong correlation between a rock classification and the intensity of the gamma radiation emitted by the members of the class (Fig. 4).

The Neutron Curve

The mechanism of response of the Neutron Curve is more complex than that of the Gamma Ray Curve, however, and in order to understand its behavior it will be necessary to discuss some of the basic factors affecting its operation.

Components of the Neutron Curve

The total gamma radiation reaching the ionization chamber of the neutron logging instrument while it is making a log has three main sources of origin, as follows:

I (total gamma radiation = $I_1+I_2+I_3$

Where:

I_1 is the intensity of the gamma rays induced by the action of neutrons upon the formation.

I_2 is the intensity of the scattered radiation, i.e., the gamma radiation which was originally emitted by the source capsule and which has been scattered by the formation.

I_3 is the intensity of the gamma radiation emitted by the formation rocks themselves.

The Neutron Induced Gamma Radiation Component (I_1)

The intensity of the gamma rays reaching a cavity in the rock from a point source distance r away would be[7]

$$I_1 = \frac{SQCe^{-\mu_1 r}}{r^2}$$

Where:

S is the source strength, a constant, characteristic for example, of the alpha

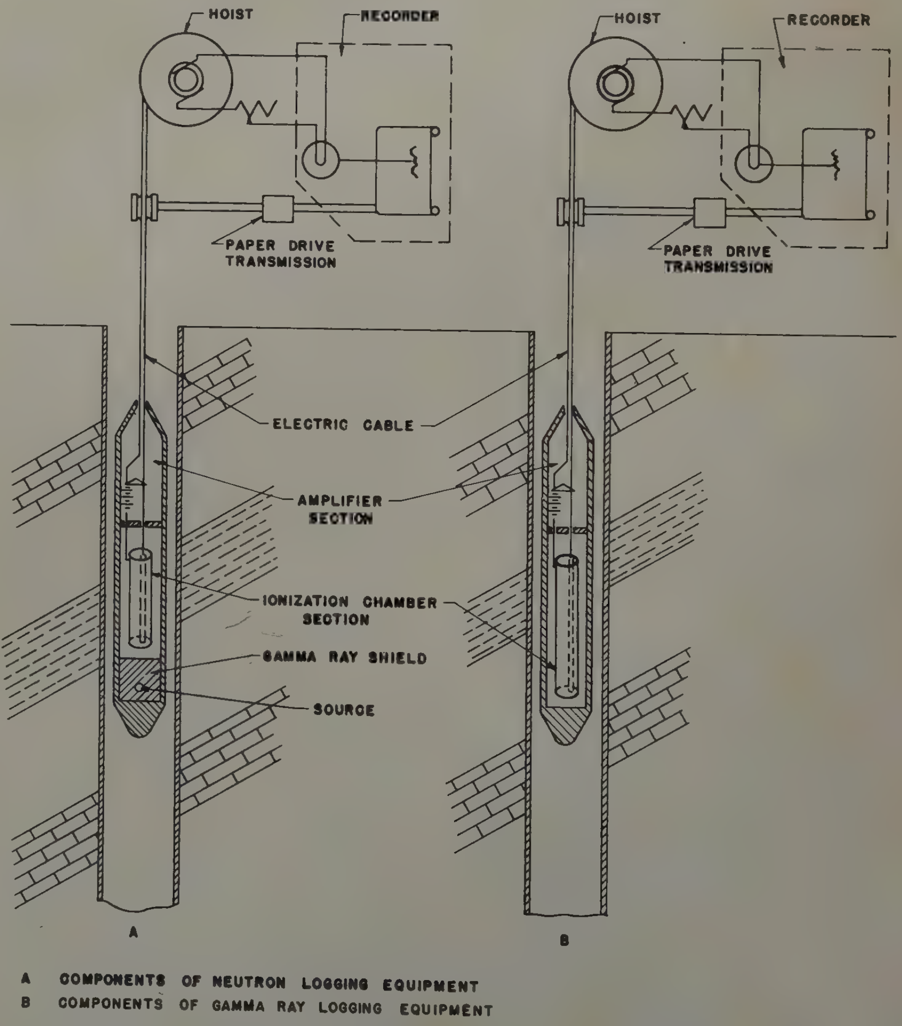

FIG. 1 — RADIOACTIVITY LOGGING EQUIPMENT

rayer used with the beryllium in the source capsule.

Q is a factor due to the neutron spectrum of the source flux. Q is a quantity which increases as the energy of the most populous group of neutrons in the source flux becomes larger. Q is constant for a given source.

C is a quantity which corresponds to the average effectiveness with which the elements present in the rock convert the neutron flux into a gamma ray flux. It varies with the chemical composition of the rocks, and it is larger for dry rocks than for wet ones (because, for example, gamma rays resulting from neutron capture are more energetic for most of the earth elements than they are for hydrogen).

μ_1 is the value to which the full absorption coefficient for the neutron flux converges as more rock is penetrated μ_1 is critically influenced by the hydrogen content of the formation; μ_1 increases with the concentration of hydrogen.

r is the distance through the rock from the source to the cavity.

The above reasoning also applies to a geometry which includes a well bore filled with oil or water whose diameter is small compared to the spacing between the source and ionization chamber. For closer spacing a more exact, and therefore more complex, treatment will be required and this is outside the scope of this paper.

For a given source, S and Q are constants and therefore do not affect the character of the well log except that if these constants are too small, the log will contain very high statistical fluctuations. All of the neutron sources used in logging comply very closely with standards which maintain the S and Q factors so that there are only very small deviations from one source to another.

The variable C affects the character of the log in that its main influence is exerted when the chemical composition of the rock changes. Sandstone and limestone, for example, have different C values.

The variable μ_1 is a determinative quantity affecting the I_1 component of the Neutron Curve; and therefore since this is the most important component, it can be said that with only a few exceptions μ_1 is determinative for the Neutron Curve.

The effects due to the influence of hydrogen on C and μ_1 cooperate to decrease the intensity of radiation for increasing hydrogen concentration; and it is for this reason that the neutron curve is a commercial means of studying the hydrogen content in the formations. This also explains the low response of the Neutron Curve opposite liquid filled porous zones, as shown in Fig. 2.

Fig. 5 shows how I_1 varies with porosity in limestone in an exponential manner.

On the other hand the increase in activity observed with anhydrite (Fig. 2) is mainly due to its larger C factor, although μ_1 is small due to the absence of water.

The log responds to shale in the same manner as to a porous zone (Fig. 2) because the C and μ_1 factors for shales are similar to those in porous zones, due to the high concentration of water, the presence of which is rendered less obvious by the fact that it is held in a loose state of chemical combination.

The Scattered Gamma Ray Component (I_2)

If the same geometry as above is considered but with a gamma ray source substituted for the neutron source, the intensity of the gamma radiation acting on the absorbing material in the rock cavity would be:

$$I = \frac{Pe^{-\mu_2 r}}{r^2}$$

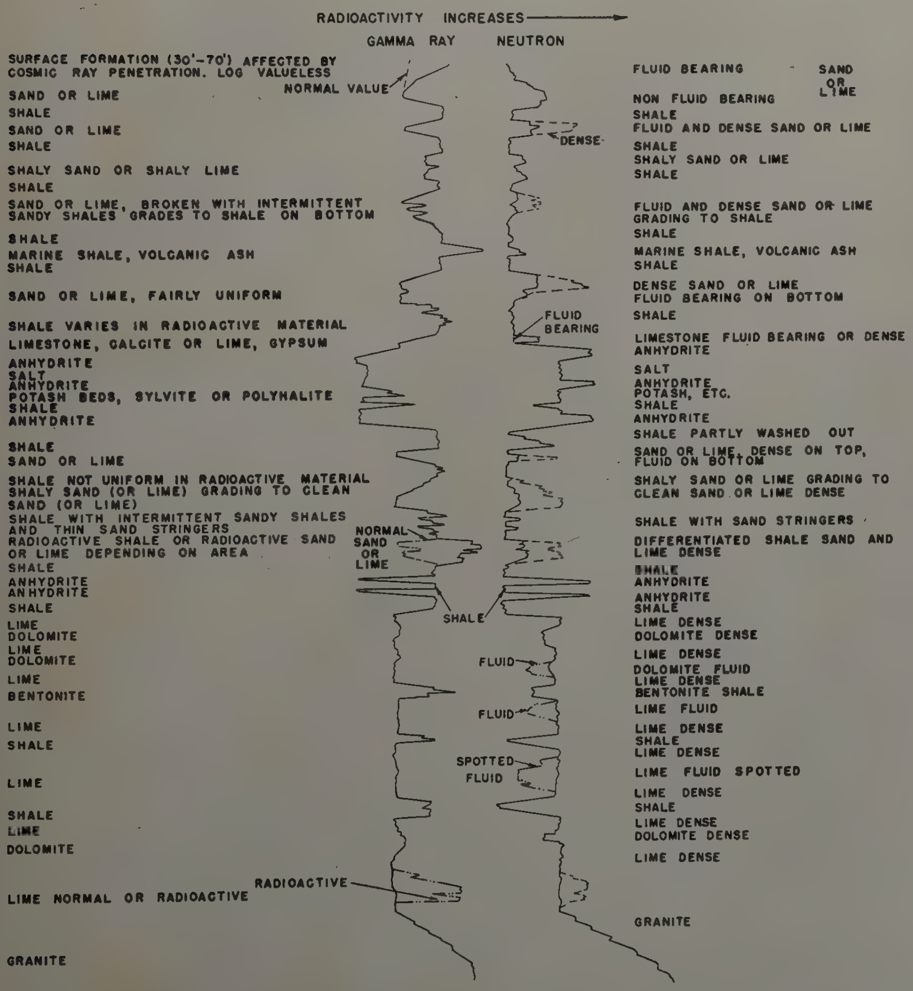
RADIOACTIVITY INCREASES
GAMMA RAY
NEUTRON
SURFACE FORMATION (30'-70') AFFECTED BY COSMIC RAY PENETRATION. LOG VALUELESS
NORMAL VALUE
SAND OR LIME
SHALE
SAND OR LIME
SHALE
SHALY SAND OR SHALY LIME
SHALE
SAND OR LIME, BROKEN WITH INTERMITTENT SANDY SHALES GRADES TO SHALE ON BOTTOM
SHALE
MARINE SHALE, VOLCANIC ASH
SHALE
SAND OR LIME, FAIRLY UNIFORM
SHALE VARIES IN RADIOACTIVE MATERIAL
LIMESTONE, CALCITE OR LIME, GYPSUM
ANHYDRITE
SALT
ANHYDRITE
POTASH BEDS, SYLVITE OR POLYHALITE
SHALE
ANHYDRITE
SHALE
SAND OR LIME
SHALE NOT UNIFORM IN RADIOACTIVE MATERIAL
SHALY SAND (OR LIME) GRADING TO CLEAN SAND (OR LIME)
SHALE WITH INTERMITTENT SANDY SHALES AND THIN SAND STRINGERS
RADIOACTIVE SHALE OR RADIOACTIVE SAND OR LIME DEPENDING ON AREA
SHALE
ANHYDRITE
ANHYDRITE
SHALE
LIME
DOLOMITE
LIME
DOLOMITE
LIME
BENTONITE
LIME
SHALE
LIME
SHALE
LIME
DOLOMITE
LIME NORMAL OR RADIOACTIVE
GRANITE
DENSE
FLUID BEARING
NORMAL SAND OR LIME
SHALE
FLUID
FLUID
SPOTTED FLUID
RADIOACTIVE
FLUID BEARING
NON FLUID BEARING
SAND OR LIME
SHALE
FLUID AND DENSE SAND OR LIME
SHALE
SHALY SAND OR LIME
SHALE
FLUID AND DENSE SAND OR LIME GRADING TO SHALE
SHALE
MARINE SHALE, VOLCANIC ASH
SHALE
DENSE SAND OR LIME FLUID BEARING ON BOTTOM
SHALE
LIMESTONE FLUID BEARING OR DENSE
ANHYDRITE
SALT
ANHYDRITE
POTASH, ETC.
SHALE
ANHYDRITE
SHALE PARTLY WASHED OUT
SAND OR LIME, DENSE ON TOP, FLUID ON BOTTOM
SHALY SAND OR LIME GRADING TO CLEAN SAND OR LIME DENSE
SHALE WITH SAND STRINGERS
DIFFERENTIATED SHALE SAND AND LIME DENSE
SHALE
ANHYDRITE
ANHYDRITE
SHALE
LIME DENSE
DOLOMITE DENSE
LIME DENSE
DOLOMITE FLUID
LIME DENSE
BENTONITE SHALE
LIME FLUID
LIME DENSE
SHALE
LIME DENSE
LIME FLUID SPOTTED
LIME DENSE
SHALE
LIME DENSE
DOLOMITE DENSE
LIME DENSE
GRANITE

FIG. 2 — GRAPHIC INTERPRETATION OF RADIOACTIVITY LOGS

Where:

P is a source constant which determines the source strength.

μ_2 is the average coefficient of absorption of the rock formation for the gamma rays emitted from the source. Since μ_2 is a function of density, it might be expected that the I_2 component would vary inversely with density. The I_2 component actually does behave in this manner but this density effect is greatly overshadowed by the effect of borehole diameter.

Fig. 6 shows that the I_2 component is directly proportional to the borehole diameter, although there is also an influence due to other factors, mainly the rock density.

This preponderance of the borehole diameter effect can be best understood by recalling that all of these scattered gamma rays have undergone losses of energy through the scattering process, so that only the photons which were scattered quite close to the well face are able to penetrate the rock and reach the ionization chamber. Hence, the relatively small effect of density. On the other hand, as the well face moves away from the instrument as it does when an enlarged section of bore-hole is traversed, a larger solid angle of the radiation from the source is subtended by the well face which becomes more thoroughly illuminated by the gamma rays some of which are backwards scattered. The ionization chamber can then "see" more of the scattered radiation. The I_2 component is therefore influenced principally by bore hole diameter changes and is responsible for the shift in the curve opposite borehole diameter changes (Fig. 3-A). I_2 is also affected strongly by casings and it is largely responsible for the shifts observed opposite casing seats in Fig. 3, (B, C, D and E).

The I_1 component is not as strongly effected by the steel casing; however, the cement behind the casing has an attentuating effect on the neutrons, and contributes to the casing shift observed in Fig. 3.

The Natural Gamma Ray Component (I_3)

While the Neutron Curve always has this component consisting of the gamma

GAMMA RAY CURVE (G/R) MAY SHIFT WITH CHANGE IN CASING STRINGS

NEUTRON CURVE (N) ALWAYS SHIFTS WITH CHANGE IN CASING STRINGS

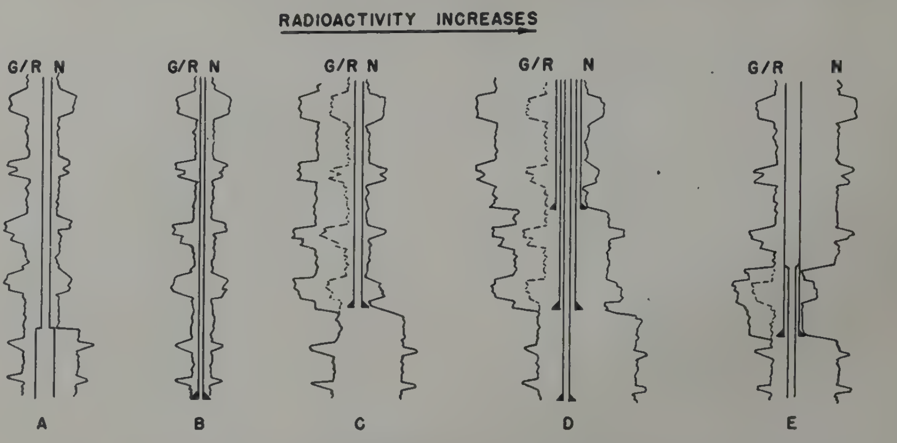

A OPEN HOLE WITH CAVITY. NEUTRON SHIFTS TO LEFT WITH DECREASE IN HOLE SIZE.

B ONE STRING OF CASING. CONTINUOUS UNIFORMITY.

C OPEN HOLE AND CASING. NEUTRON CURVE SHIFTS TO LEFT AT CASING SEAT.

D MULTIPLE CASING. NEUTRON CURVE SHIFTS TO LEFT AT EACH CASING SEAT.

E CASING AND LINER. NEUTRON CURVE SHIFTS TO LEFT AT CASING SEAT AND TO RIGHT AT LINER.

GAMMA RAY CURVE MAY ACT IN SAME MANNER AS NEUTRON CURVE BUT TO A LESSER DEGREE EXCEPT IN "A" WHERE THE GAMMA RAY CURVE REMAINS UNAFFECTED BY THE CHANGE IN HOLE SIZE.

FIG. 3 — EFFECT OF PHYSICAL BOREHOLE CONDITIONS ON GAMMA RAY AND NEUTRON CURVES

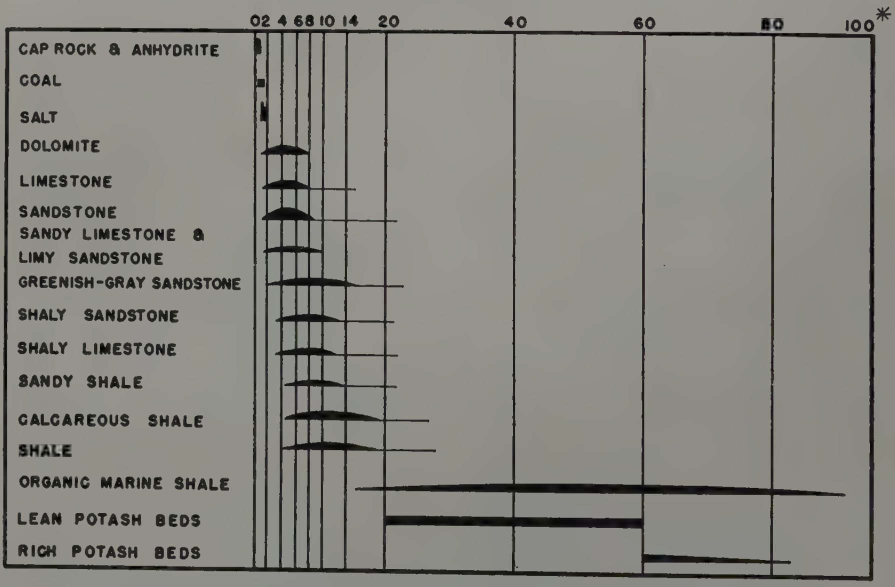

FROM W. L. RUSSELL, BUL. OF A.A.P.G., VOL. 25, NO. 9, SEPT. 1941, P1775.

* $\times 10^{-12}$ GRAMS RADIUM EQUIVALENT PER GRAM OF ROCK.

FIG. 4 — GAMMA RAY RESPONSE TO SEDIMENTARY ROCKS

radiation emitted by the rock through natural disintegration processes, it will usually be too small to merit consideration in most reservoir rocks.

However, important exceptions to this rule have been noted. Certain bentonitic sands of South Texas, partilly silted sands generally, radioactive limestone, and others elsewhere, exhibit sufficient natural gamma ray activity so that the Neutron Curve is seriously affected.

It is important to note that the Neutron Curve may be corrected for this natural activity by means of the Gamma Ray Curve. This is done by taking into account the relative sensitivities of the two ionization chambers for gamma rays. For any given sensitivity scale the gamma ray instrument will be found to be sixteen times more sensitive than the neutron instrument. For example, opposite a bentonitic sand the Gamma Ray Curve indicated a high intensity of natural gamma radiation by making an 8-inch swing to the right of the normal value for sands. The sensitivity scales were 6 and 10 inches respectively for the gamma ray and neutron curves. In order to calculate the correction to be applied to the Neutron Curve we have: $\frac{8}{16} \text{x} \frac{10}{6} = .833''$ = the correction to subtract from the Neutron Curve deflection in order to correct it for the natural gamma radiation.

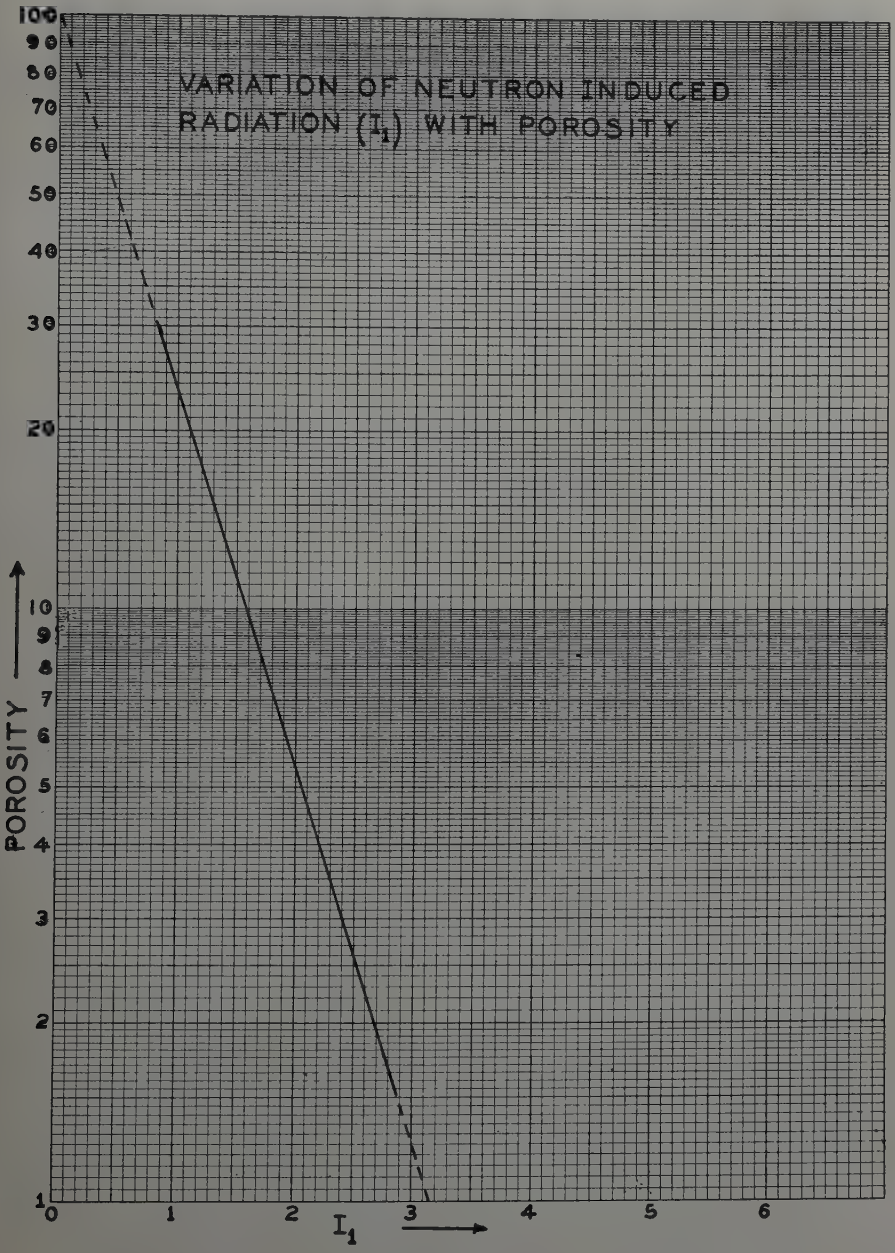

FIG. 5 — EFFECT OF POROSITY ON THE NEUTRON INDUCED RADIATION (I_1)

Relative Importance of the Three Components

The predominating component of the Neutron Curve is I_1. For most cases, where the bore hole diameter is small and does not change appreciably, the I_2 component is very small and exhibits no large variations. The I_3 component is usually small enough to be neglected when the log is used in stratigraphic correlation work; but where a quantitative application is to be attempted, it is sometime found necessary to perform the operation previously outlined and correct the neutron curve for the influence of natural gamma radiation.

Sampling of Radioactivity Logging

In order to understand the quantitative application of radioactivity curves the sampling process involved must be considered. Sampling as the term is used in geological investigations means the description of the manner in which a specific property of the earth is weighted throughout the portion of the earth being studied.

Sampling of the Gamma Ray Curve

Fearon[3] has shown that for gamma ray logging within a cylindrical bore hole, the weighing factor falls off radially as a function of the absorption coefficient of the rays emitted by the radioelement present.

The weight factor may be computed, for a stationary measure and for any particle in the vicinity of the detector by a calculation of the probability of radiation originating from any given particle arriving at the sensitive region of the detector. This probability is made up of three factors.

1. The solid angle subtended by the detector, with the particle as the vertex.
2. The average absorption factor which prevails for the radiation lying in the given solid angle.

3. The efficiency of the detector for radiation coming in from the direction of the particle.

The weighing factor falls off continuously with distance away from the detector, nowhere falling abruptly to zero. At considerable distances, however, the weighing factor is so close to zero that the neglect of all matter beyond the rather thick shell will cause a negligible influence on the measurement.

Fearon[8] has calculated the relative physical size of samples in gamma ray logging and coring and compared them in the table below. The two sets of samples have equal lengths.

Table (8)

Radioelement Predominately Responsible for Radiation	Wt. of Log Sample	Wt. of 3" Core Sample
Radium and series	370 lbs.	25 lbs.
Thorium and series	560 lbs.	25 lbs.
Potassium 40	160 lbs.	25 lbs.

Sampling of the Neutron Curve

The sampling of the Neutron Curve cannot be quantitatively treated as was the Gamma Ray Curve, because of the lack of information on the range of neutrons in the various rock substances. However, the available data on neutron ranges as well as that on the absorption of gamma rays of the hardness of those comprising the I_1 component tends to confirm the belief that the Neutron Curve sample is at least as large as that of the Gamma Ray Curve.

In neutron logging as in gamma ray logging the sampling process differs from that of coring and the weighing factor also falls off with distance from the instrument.

The manner in which the weighting factor varies in space differs markedly in the two cases making it a matter of particular interest to consider the shape of the sample observed.

Fearon[7] has also calculated the shape of the sample in neutron logging by first making the following definitions:

A. The weighting factor in neutron well logging is the rate of change in detecting secondary radiation (I_1) intensity with respect to molar density of representative substance at the point for which the weighting factor is determined.

B. The relative weighting factor is the ratio of the weighting factor at any given place to the value it would have at its minimum between source and detector, on a line joining them, if the space between source and detector were filled with material of the same nature as the surrounding rock.

C. The sample is the quantity of matter contained in a surface on which the relative weighting factor is 1/e.

The mathematical development of such surfaces is quite complicated and therefore only the shape of some simple examples will be considered.

Where both the neutron flux and the induced gamma ray flux have large penetrating power and neither is absorbed appreciably upon passing through the rock a distance equal to the space between the source and the detector, the log sample inside a surface of relative weighting factor, is the solid of revolution of which a section through the axis of rotation has the form:

$$r^2 = 4a^2\cos\theta - 2a^2 \qquad (7)$$

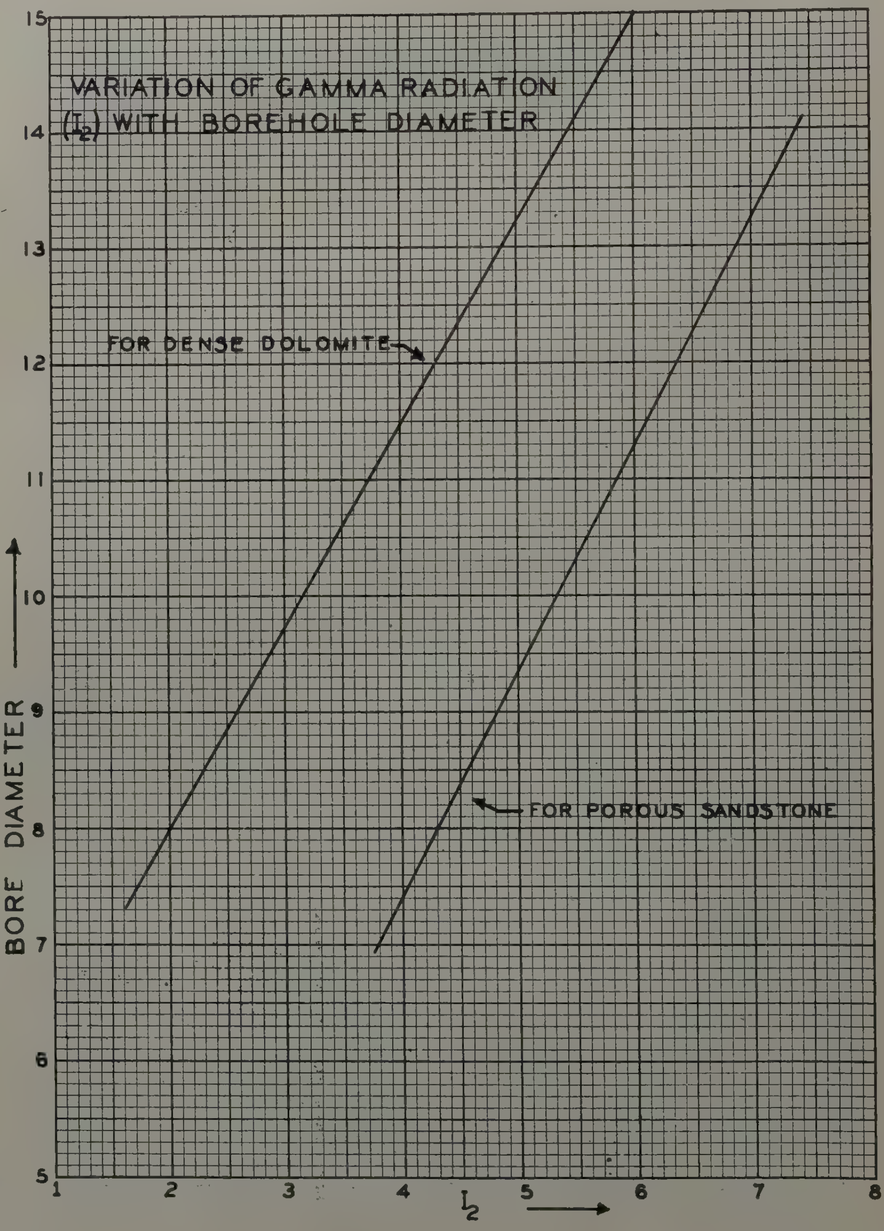

FIG. 6 — EFFECT OF BOREHOLE DIAMETER ON THE SCATTERED GAMMA RADIATION (I_2)

This equation is illustrated by the inner curve of Fig. 7a. The case where the emitted radiation is more penetrating than that detected is shown by the inner curve of Fig. 7b. The outer curves represent the pattern for a fractional weighting factor. The outer curve in Fig. 7b represents the zone sample by the existing commercial equipment.

In any case, however, when it is recalled to mind that μ_1 is the determining quantity, it will be apparent that the "core" sampled by the neutron log would be a reasonable approximation to a cylinder the radius of which would vary with μ_1, and therefore the radius would vary with the activity indicated by the neutron curve, i.e., the greater the activity encountered the greater the radius of the core sampled.

The log sample differs therefore, in several ways from samples secured within the borehole. In the first place the core obviously samples the zone within the radius of the borehole while the log samples the zone outside the borehole. This difference should be kept in mind when comparing core data with the neutron log for those formations where the hetergeneity of the porosity distribution is pronounced such as is the case with most of the limestones and dolomites, e.g., the Ellenburger in particular. In the second place, the log sample is much larger than the core sample. The core sample therefore cannot be expected to agree exactly with the log sample, for the types of formations enumerated and it is highly probable that the porosities calculated from the log may be more valuable than those obtained from cores for estimating net pay and reserves.

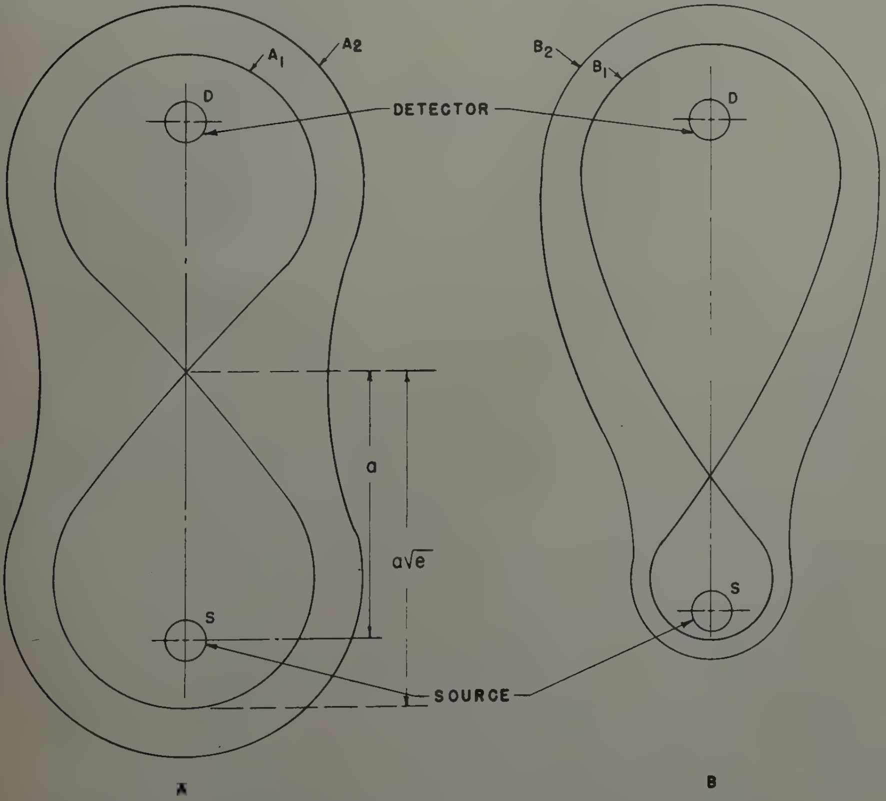

A_1 AND B_1 REPRESENT SURFACES CORRESPONDING TO WEIGHTING FACTOR OF ONE.
A_2 AND B_2 ARE SURFACES CORRESPONDING TO FRACTIONAL WEIGHTING FACTORS.
IN FIGURE A IT IS ASSUMED THAT THE EMITTED AND DETECTED RADIATIONS HAVE A VERY SMALL ABSORBTION IN PASSING A DISTANCE SD THROUGH THE ENVIRONMENTAL SUBSTANCE.
IN FIGURE B THE DETECTED RADIATION IS APPRECIABLY ABSORBED.

FIG. 7 — THEORETICAL SHAPE OF THE NEUTRON CURVE SAMPLE

METHODS OF QUANTITATIVE INTERPRETATION

Limited to Liquid Filled Porosities

The methods of interpretation presented in this paper apply only to liquid filled porosities. Unfortunately, the influences of saturation on the Neutron Curve are too complex to be discussed in this paper. The authors hope to be able to treat this subject in another paper, shortly.

General Discussion

The foregoing discussion of the basic theories has shown that there is a physical basis for the assumption that the Neutron Curve might be calibrated in terms of porosity. When this can be done, a powerful tool will be available for determining the porosity of reservoir rocks which will be simpler to apply to evaluation and other reservoir problems than similar data obtained from cores because of the better sampling of the neutron logging process.

Before this can be done a fairly complete background of information on the behavior of the variables C and μ_1 must be compiled. With this information together with the hole sizes, the casing record, and knowledge of the chemical nature of the lithology, it should be possible to determine the porosity of the zone sampled by an absolute method.

However, the information on the variables C and μ_1 is not available and therefore we must rely on relative methods which really offer almost all the advantages of the absolute method except those of flexibility and a wide range of applicability.

If the well completion procedures are the same (all wells were drilled to same bore diameter and have the same casing program) and the rock matrix is the same, the variables C and μ_1 will reflect only porosity changes and the component I_2 will be almost constant; hence the Neutron Curve will reflect mainly porosity changes. Therefore, if such a well is cored and logged, the relationship between the porosity of the cores and the log deflections can be determined, and this relationship can then be applied quantitatively to neutron logs of the other wells in the field in order to determine the porosities of their portion of the pay without determining the factors C and μ_1.

Relative Methods of Quantitative Interpretation

To determine the relationship between the deflections of a particular Neutron Curve and porosity it is necessary that sufficient core data be available in order that a wide range of porosity values will be at hand, and when these porosity values are compared with the Neutron Curve it must be kept in mind that there may be slight discrepancies in depth between the core log and the radioactivity log and the comparison must be made therefore with the core porosity log properly correlated as to depth with the radioactivity log. This is the first and one of the most important steps in making the interpretation.

The second important step is to establish the proper reference line for the Neutron Curve because it has no absolute zero.

Reference Lines

There are three possible choices for reference lines discussed in this paper. First there is the combination of a shale line and a dense limestone or anhydrite line; second, there is the shale line alone; and third, there is the dense limestone or anhydrite line alone.

These three possibilities give the interpretation method a wider field of application than would be possible with just one reference line, since a single standard reference line would not be applicable to all lithologies or to all types of completions.

Combination of Shale and Dense Limestone or Anhydrite Reference Lines

Where the formations are consistent and it is possible to log a thick shale and a limestone containing a dense zone or an anhydrite streak through the same number of casing strings or in open hole the difference between the Neutron Curve deflection of shale and that of the dense zone is considered to be the total neutron deflection and the deflections of the log are then converted to percentages of this total deflec-

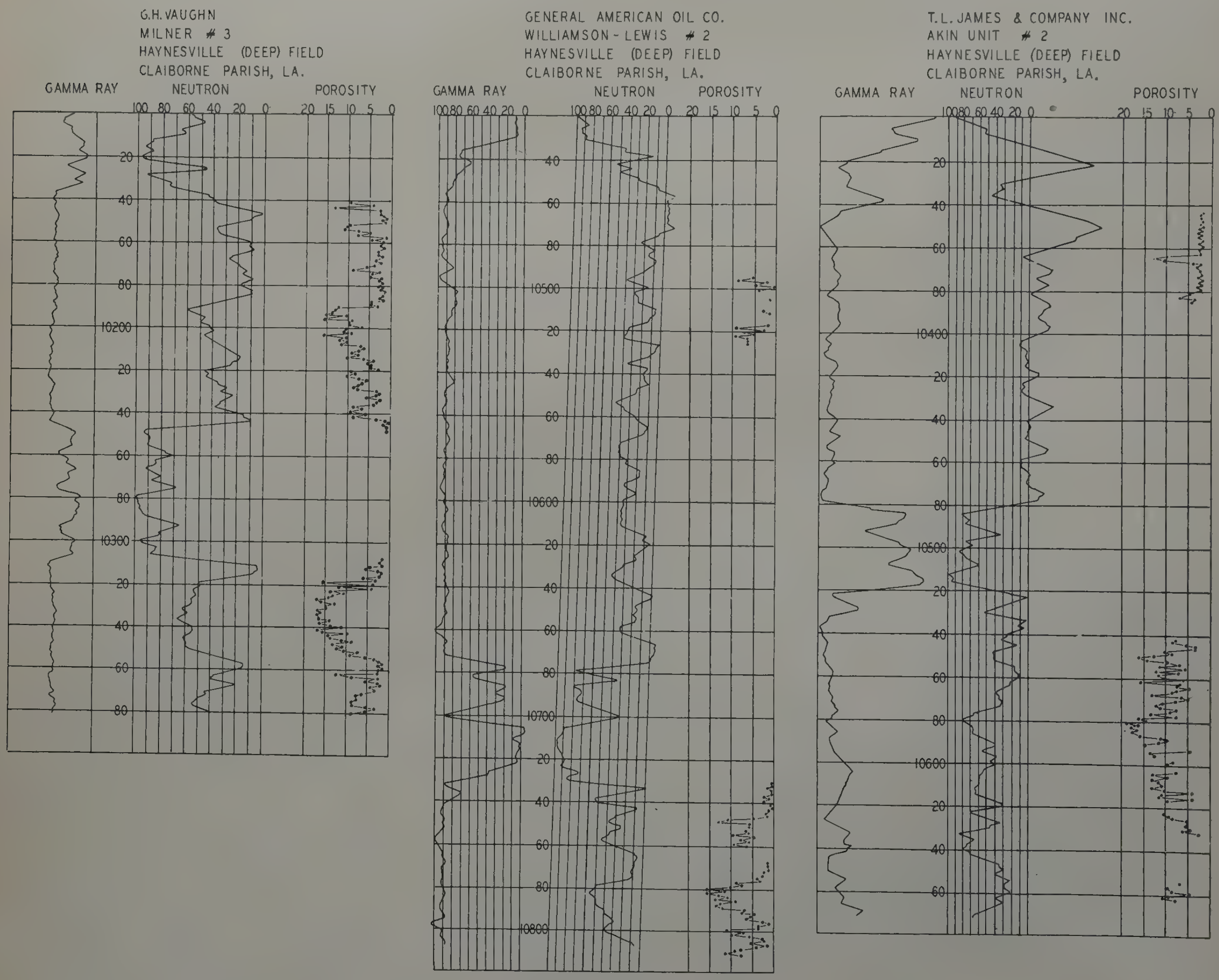

FIG. 8 — SMACKOVER LIMESTONE LOGS AND POROSITIES

tion. These percentages are then plotted against the porosities. Shale is assigned a value of 100 and the dense material a value of zero and the intervening distance is divided into 10 equal parts in order to provide a scale. This method will be referred to hereafter as the per cent of neutron deflection method or the percentage method.

This method has an important advantage over the others in that it is possible to compare curves run on different sensitivities without correcting for the sensitivity differences.

However the application of this method of choosing reference lines must be limited to those fields which exhibit consistent uniform shale lines and consistent dense zones. The hole diameter should be uniform and the shale there-

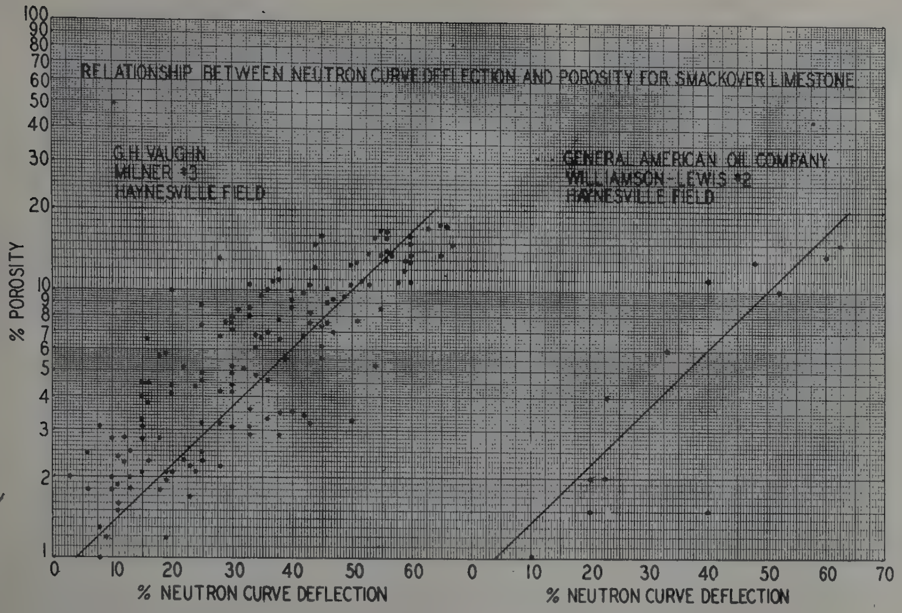

FIG. 9 — RELATIONSHIP BETWEEN NEUTRON CURVE DEFLECTIONS AND POROSITY FOR SMACKOVER LIMESTONE

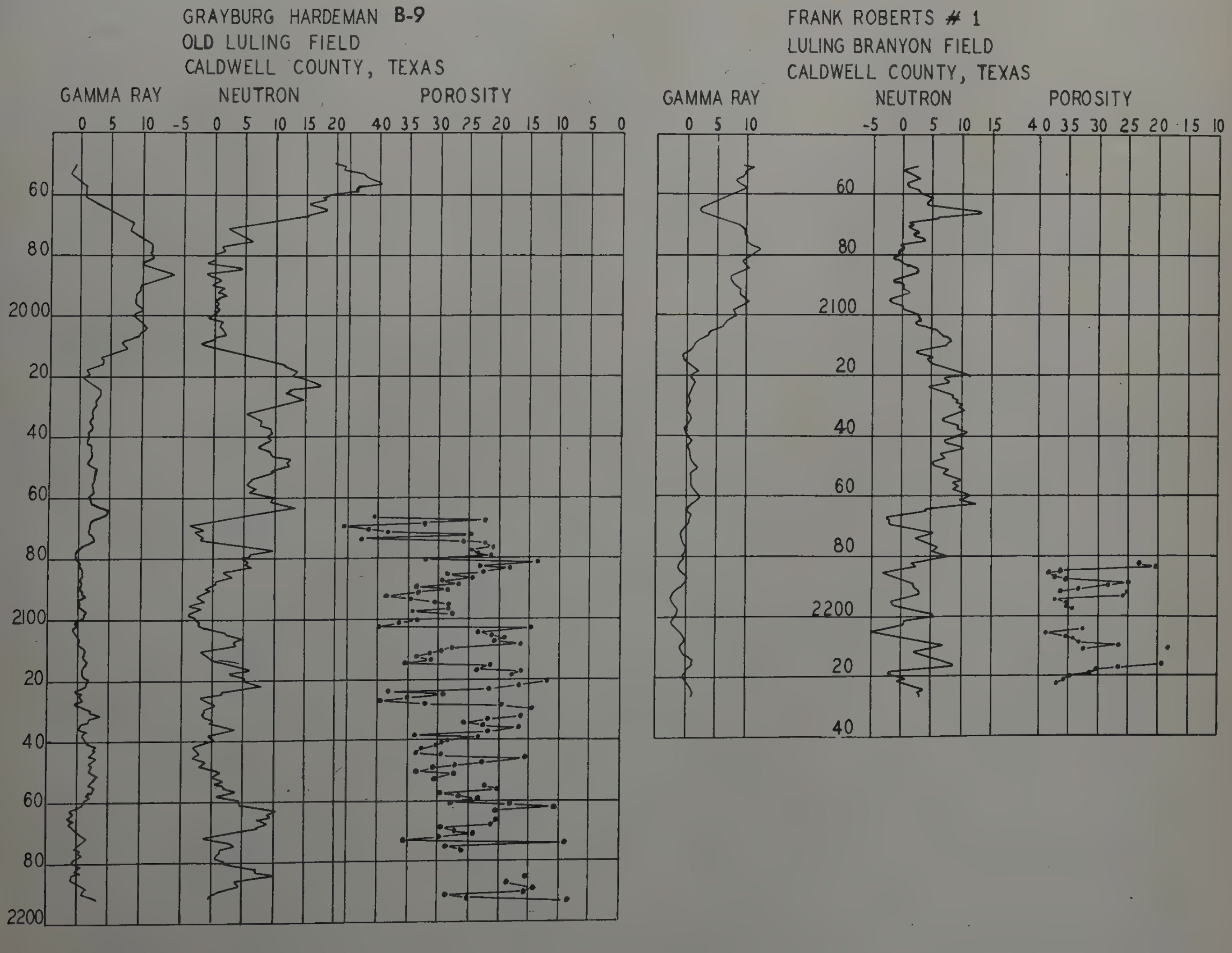

FIG. 10 — LULING — EDWARDS LOGS AND POROSITIES

fore should be stable in the drilling fluid and no sloughing should occur as this would result in enlarged bore diameters where the I_2 component of the log might be large enough to introduce error into the calibration curve.

The success of the method depends on the maintenance of the I_2 component at a very low level. If there is doubt as to the constancy of the bore diameter through the reference zones and the zone to be analyzed a caliper survey should be run. Usually if the zones to be studied all lie close to the bottom of the well, the diameter will be true to bit size and uniform and the value of the I_2 component therefore will be small and will vary only slightly from well to well.

Either dense limestone or anhydrite can be used for the other reference line. If an anhydrite zone is used it should extend throughout the field for an anhydrite reference line should not be used interchangeably with a dense limestone reference because the factor C apparently differs for anhydrite and limestone and the variation in the reference line will cause distortion of the calibration curve.

Fig. 8 shows an example of this method applied to three radioactivity logs of wells penetrating the oolitic Smackover limestone. The average shale line chosen is constant in all three wells, and is uniform throughout the field. It is obvious that the data derived from this group of logs is applicable only in this particular field, and only where the same casing program is followed. The per cent of Neutron Curve deflection is plotted as the abscissa and the per cent porosity as the ordinate on semilog graph paper and the points scattered along a straight line as shown in Fig. 9. Although the points do not all conform closely, they will fall in such a fashion that a straight line drawn through them will represent an average of the neutron derived porosity. This curve may then be applied to any other well in the field which has been completed in a similar manner, with a degree of accuracy which is limited by the quality of the sampling process, and the statistical and instrumental errors involved. (Unfortunately time and space do not permit a discussion of these latter factors in this paper).

Shale as the Reference Line

If a dense zone is not present under the same hole and casing conditions as the zone to be investigated but a shale is present under these conditions, the shale may be used as the reference line and the Neutron Curve deflections are then measured from this line.

Washing out of the shale may introduce the same errors in this method due to the greater I_2 component associated with larger hole diameters as it did in the case of the percentage method and it is therefore essential that the shale be stable and the borehole diameter true to bit size.

The Neutron Curve deflections, measured from the shale line are plotted against the porosities of the known well. The neutron derived porosities for the unknown wells may then be determined by directly comparing the Neutron Curve deflections from the unknown wells with the calibration curve, if the log sensitivities are the same.

If the log of the unknown well was run on a different sensitivity from that

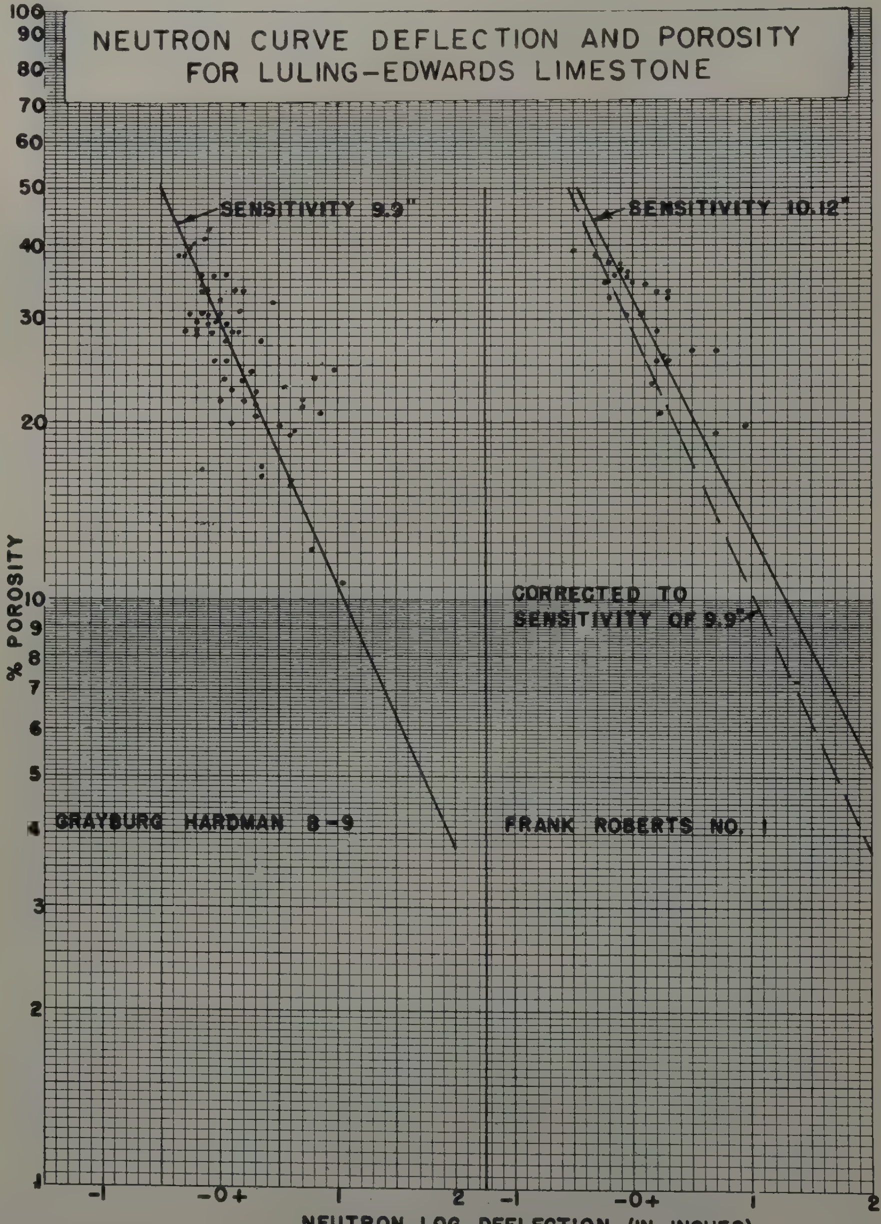

FIG. 11 — RELATIONSHIP BETWEEN NEUTRON CURVE DEFLECTIONS AND POROSITY FOR LULING — EDWARDS LIMESTONE

of the known well, the deflection of the unknown well must be corrected to correspond to the sensitivity of the log of the known well. The corrected curve deflection may then be compared with the calibration chart and the neutron derived porosity determined.

The correction for the change in sensitivities may be done as follows:

$$D_2 = \frac{S_2 D_1}{S_1}$$

Where:

D_2 is the corrected Neutron Curve deflection for the unknown well

D_1 is the deflection from the curve of the unknown well

S_1 = sensitivity of the curve of the unknown well

S_2 = sensitivity of the curve of the known well.

This correction has been made in this manner because it is believed that the reader will find it more convenient to convert the deflections of the unknown curve to the scale of the known curve and then compare these converted deflections to the calibration curve. However, it is easily possible to convert the calibration curve to the sensitivity of the unknown Neutron Curve. This may be done by allowing D_1 to represent some point on the cold calibration curve. D_2 will therefore represent the same point on the new curve.

This method of using a base line is illustrated by Fig. 10 showing two logs of Edwards limestone correlated with porosity data obtained from diamond cores. Fig. 11 shows the calibration curve resulting from plotting the neutron deflections measured from the shale line against the per cent porosities determined from core analysis.

Dense Zones as References

In the method first described, dense limestone was used as a reference line in that the difference on the Neutron Curve deflection in a shale zone and in a dense zone was used. It is quite frequently the case that casing programs require casing off shale and setting the casing shoe in the upper portion of the productive limestone or dolomite. In these cases a comparison with the cased off shale is not practical, and a dense zone within the limestone may be selected to be used as the reference line for the log. In this method the Neutron Curve deflection is measured from this reference and these deflections are plotted against the porosities of the base or known well. The neutron derived porosity for an unknown well in the field may then be determined by directly comparing the Neutron Curve deflection from the log of the unknown well with the calibration chart obtained on the known well, provided the log sensitivities are the same.

If the log of the unknown well was run on a different sensitivity from that of the known well, the deflections of the unknown well must be corrected to correspond to the sensitivity of the known well as has been described in the case of the shale line.

Fig. 15 illustrates the application of a dense zone as a reference line for the Neutron Curve.

Selection of the Most Applicable Method

Each of the described methods of using reference lines can provide a means of determining neutron derived porosities for a given zone by the application of the calibration curve determined for a base or known well to the neutron logs of the unknown wells. Due to the variations from area to area in the casing programs, borehole conditions, and lithology, the applicable method is that most commensurate with those conditions.

SPECIFIC APPLICATIONS

Smackover Limestone

To illustrate the technique used in the application of quantitative interpretation methods, widely differing

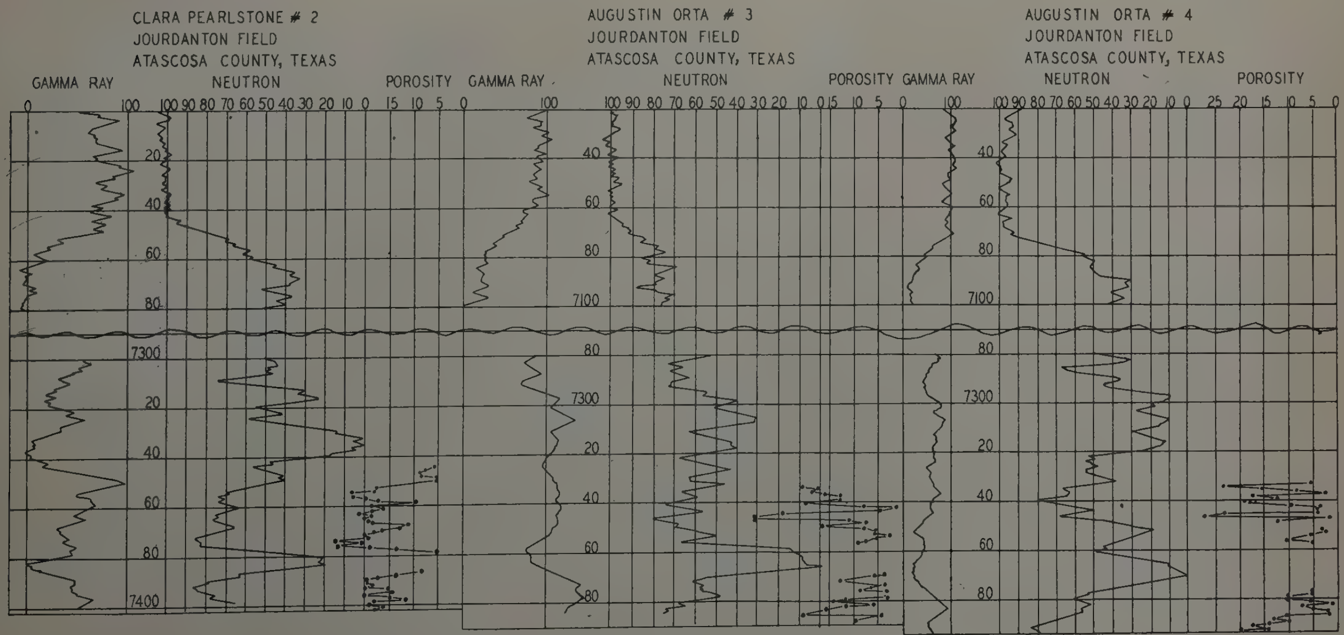

FIG. 12 — JOURDANTON — EDWARDS LOGS AND POROSITIES

fields, both geologically, lithologically, and geographically have been selected as examples. Fig. 8 shows three logs of wells located in the Haynesville (Deep) Field, Claiborne Parish, La., which have penetrated the Smackover limestone. The logs are aligned so that the correlation of the shales and limestone beds can be observed in order to illustrate the similarity of character of all three logs. The per cent neutron deflection method of porosity interpretation was chosen for this field because:

1. The hole was entirely cased.
2. Shales are present and are both consistent and correlative.
3. Dense limestone is scattered throughout the A and B Smackover zones.

Shale lines were determined by averaging the peaks of shale at the left of the log, the slope of which is found by extending the line several hundred feet up the log. A value of one hundred per cent is assigned this line, since it represents the lowest value on the log, and shows the greatest influence of hydrogen on the I_1 component. The greatest deflection within the Smackover was chosen as the dense limstone or zero point. The distance from zero to one hundred per cent was divided into parts of ten, with proportional dividers, and lines therefrom were extended over the zone of interest parallel to the shale line.

Due to excessive bottom hole temperatures the log of the General American Oil Company's Williamson-Lewis No. 2 has drifted to the right. This drift is corrected by drawing the zero line and the proportional division lines parallel to the slope of the shale line.

The curve is now prepared for correlation with the available core data. In this instance these data are already plotted and correlated on the same depth scale as the Neutron Curve. Correlations will vary slightly where coring is not continuous, and depth corrections must be checked for each individual core. A convenient method of recording data is to correct all depths to the Neutron Curve depth scale and to record the per cent neutron curve deflection directly from the log, opposite the corresponding porosity value. These data may be plotted on coordinate paper, and a curve drawn through the average of the points, but difficulty will be encountered in extending the curve past the limits of the available data, therefore semilog graph paper was selected for this purpose and reliance was placed on the behavior of the I_1 component as shown in Fig. 5.

Fig. 9 is the graph of the data obtained from the Milner No. 3 and the Williamson Lewis No. 2. It will be noted that a large dispersion of points occurs on either side of the average curve. However, dispersion is to be expected from the comparison of the neutron log deflections to the porosities due to the differences in sampling and the heterogeneity of the porosity distribution. The core analysis sample is obtained from a small plug representing only a small portion of one foot of core sample while the neutron sample would be very much larger. A smoother curve may be obtained by averaging three core samples, but no real improvement would be gained because the averaging is accomplished by using the same core samples as before.

When established for a field this curve may be applied to the log of an unknown well, and the neutron derived porosity determined.

Luling — Edwards Limestone

Two fields producing from the dolomitic Edwards Limestone of Southwest Texas have been selected as illustrations. This formation differs from the relatively homogeneous oolitic Smackover limestone in that the heterogeneity of the distribution of porosity in this dolomitic limestone is much more pronounced. Horizontal correlation in this type of material is poorer, and it will characteristically extend over only a few inches of sample. For this reason the two methods of sampling used in coring and well logging will cause wide dispersion of data.

Fig. 10 shows two logs of the Edwards limestone which were cored with a diamond core bit. Throughout the entire zone, high porosity is present, and no reliable dense material is available for use as a log reference line. The Grayson shale shown at the top of the log is quite extensive and constant throughout the area, and serves as an excellent marker. For this reason it was chosen as the relative log reference line.

The log reference line was established by drawing a line through the

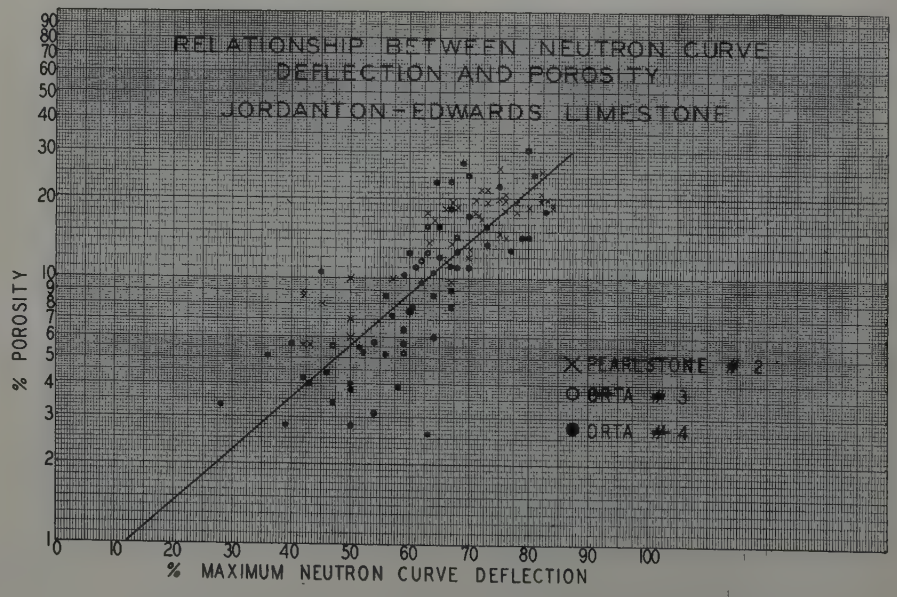

FIG. 13 — RELATIONSHIP BETWEEN NEUTRON CURVE DEFLECTIONS AND POROSITY FOR JOURDANTON — EDWARDS LIMESTONE

average of the shale peaks at the left of the log. A scale in inches is used to determine the changes in deflection from the reference line. In this example the porosities of the dolomite are high and the neutron deflection extends to the left of the reference line. To measure these intensity changes a negative scale in inches is established. The neutron curve is then correlated with a plot of the porosity, and the neutron log deflections from zero determined for the corresponding porosity. These data are plotted on semilog graph paper with the neutron log deflections as the abscissa and per cent porosity the ordinate, and an average line drawn through the points. The neutron derived porosity calibration curve is now established for this log. Fig. 11 shows the neutron derived porosity calibrations for the Grayburg Hardeman B-9 and the Frank Roberts No. 1.

To illustrate the procedure involved in correcting the Neutron Curve deflection for a given sensitivity to a different sensitivity, a deflection of the Frank Roberts No. 1, is two inches, and the curve was run on a sensitivity of 10.12 inches. This deflection may be corrected to apply to the log of the Hardeman B-9 which was run on a sensitivity of 9.9 inches, as follows:

$$D_2 = \frac{S_2 \times D_1}{S_1}$$

$$D_2 = \frac{9.9 \times 2}{10.12}$$

$$D_2 = 1.96 \text{ in.}$$

The corrected log deflection now may be applied to the calibration curve of Hardeman B-9. Since the Frank Roberts No. 1 was cored it is possible to check the accuracy of the neutron derived porosities with the porosities determined from cores.

Fig. 11, however, shows the derived porosity curve for the Hardeman B-9 corrected to the sensitivity of the Frank Roberts No. 1. This was done by taking points off the Hardeman B-9 calibration curve and substituting them in the above equation for D_1. Values of D_2 were then plotted against the porosity to obtain the new calibration curve.

Jourdanton — Edwards Limestone

Another example of Edwards limestone quantitative interpretation is shown in Fig. 12. In this example three logs are shown with corresponding core data. The neutron percentage method of quantitative interpretation was chosen for the Jourdanton Field because of the presence of the Grayson shale and an extensive anhydrite bed located within the productive Edwards. The procedure involved in this interpretation is identical with the method used for Fig. 8, with the exception of the reference line utilized. In the Jourdan-

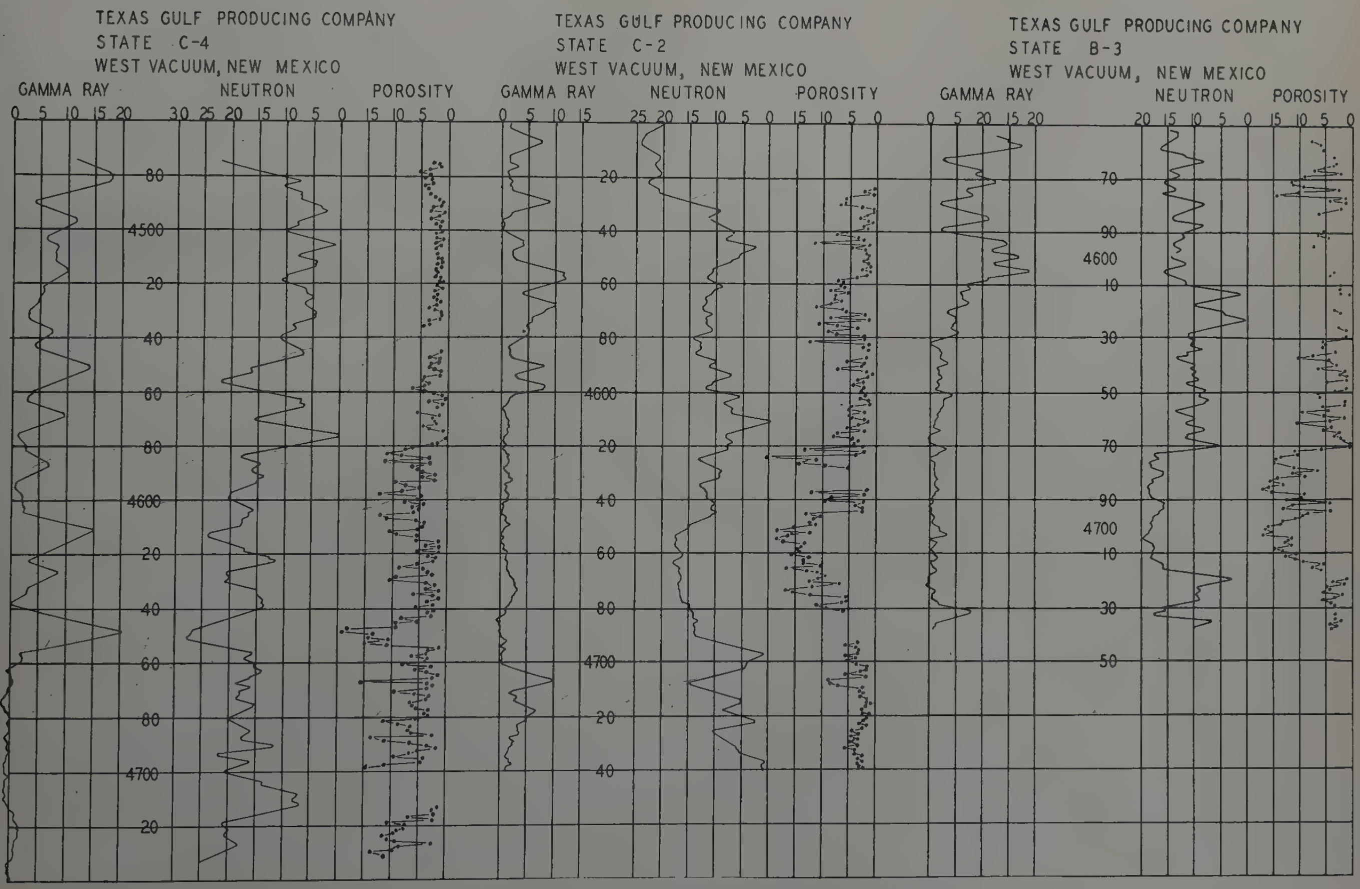

FIG. 14 — WEST VACUUM DOLOMITE LOGS AND POROSITIES

ton Field the anhydrite bed was chosen as the log reference instead of the dense limestone. Fig. 13 shows the combined plot of the per cent neutron curve deflection versus per cent porosity. No further correction is required for application of this neutron derived porosity calibration curve to logs of uncored wells in this field provided the same markers are available in each well.

Permian Dolomites

Permian dolomites of West Texas are highly hetergeneous and are quite often contaminated by silty material. The heterogeneity of these formations cause a wide dispersion of porosity values over extremely short intervals and samples taken from the borehole as cores, are highly dissimilar to the sampling of the Neutron Curve outside the borehole. For this reason neutron porosity curves determined from logs of this area exhibit a greater dispersion of points. A further complication is introduced by the presence of silty material which introduces deflections in the Neutron Curve similar to those due to porosity by the effect on the I_i component of the chemically combined hydrogen, characteristic of silty material. In zones of this type the normal procedure must be varied slightly to determine the effect of the silty material on the neutron porosity curve. The procedure followed in Fig. 16 accounts for and corrects for the effect of the silty material. Three logs shown are of wells located in the West Vacuum field, New Mexico, which have penetrated the San Andreas formation, a silty dolomite. The State C-2 was chosen as the base well for determining the neutron porosity curve. The highest deflection represents dolomite of very low porosity and is used as the log reference. A scale in inches was established by tracing the log on rectangular coordinate paper to show the intensity changes from zero. The neutron derived porosity calibration curve was determined by utilizing only porosity data obtained from a zone shown by the low intensity of the Gamma Ray log to be silt free. The points for this curve is shown by Fig. 15 and it represents the neutron derived porosity calibration curve for this particular log which was run on a sensitivity of 2.34 in. The data for wells C-4 and B-3 were also determined in the same fashion and their neutron derived porosity calibration curves plotted. To illustrate the application of the base neutron derived porosity calibration curve to uncored wells the State C-2 neutron porosity curve has been corrected to the logs of differing sensitivity of the State C-4 and B-3 and is shown by the broken line on each respective graph.

Correction for Silty Material

Correction for the effect of silty material is determined first by drawing an average of the lowest intensity values on the Gamma Ray Curve and establishing a scale in inches to determine the changes in its deflection. The Radioactivity log of the State C-4 was chosen for this determination because of the presence of much silty dolomite which had been cored. By referring the Neutron Curve deflections to the derived porosity calibration curve an apparent derived porosity is found and by subtracting from it the porosity of the core analysis the derived porosity subtractive component is found. The Gamma Ray Curve deflections are then plotted

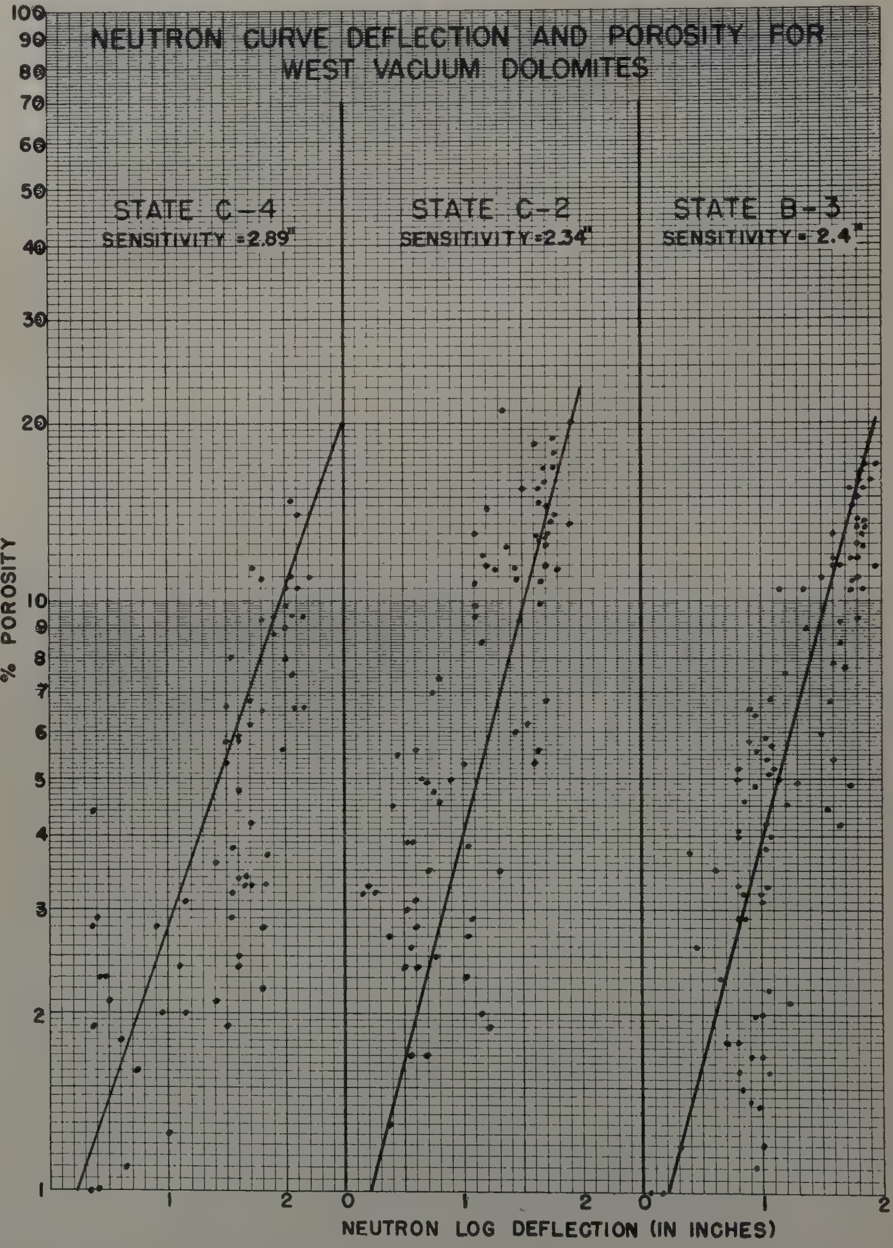

FIG. 15 — RELATIONSHIP BETWEEN NEUTRON CURVE DEFLECTIONS AND POROSITY FOR WEST VACUUM DOLOMITES

as the abscissae and the subtractive components are plotted as the ordinates on semilog graph paper and an average line is drawn through these points to provide a silt correction curve. The silt correction curve for the State C-4 is shown in Fig. 16, and has been corrected proportionally to the sensities of the Gamma Ray Curves of the State C-2 and State B-3. This procedure is the same as that shown by the formula previously shown for the correction of Neutron Curve deflections to a curve of different sensitivity. The complete determination of the neutron derived porosity may be expressed in the following formula:

$$P_n = P_{an} - P_s$$

Where:

P_n is the corrected neutron derived porosity,

P_{an} is the apparent neutron derived porosity read from the neutron deflection calibration curve.

P_s is the porosity difference caused by the decrease in intensity of the Neutron Curve due to the presence of hydrogen in silty material. This value is obtained from the silt correction curve, by referring to it the deflection of the Gamma Ray Curve. It is apparent that the dispersion of points on the silt correction curve should be extremely high due to the chemical heterogeneity of the dolomite plus the heterogeneity of the distribution of silty material plus the heterogeneity of the distribution of porosity.

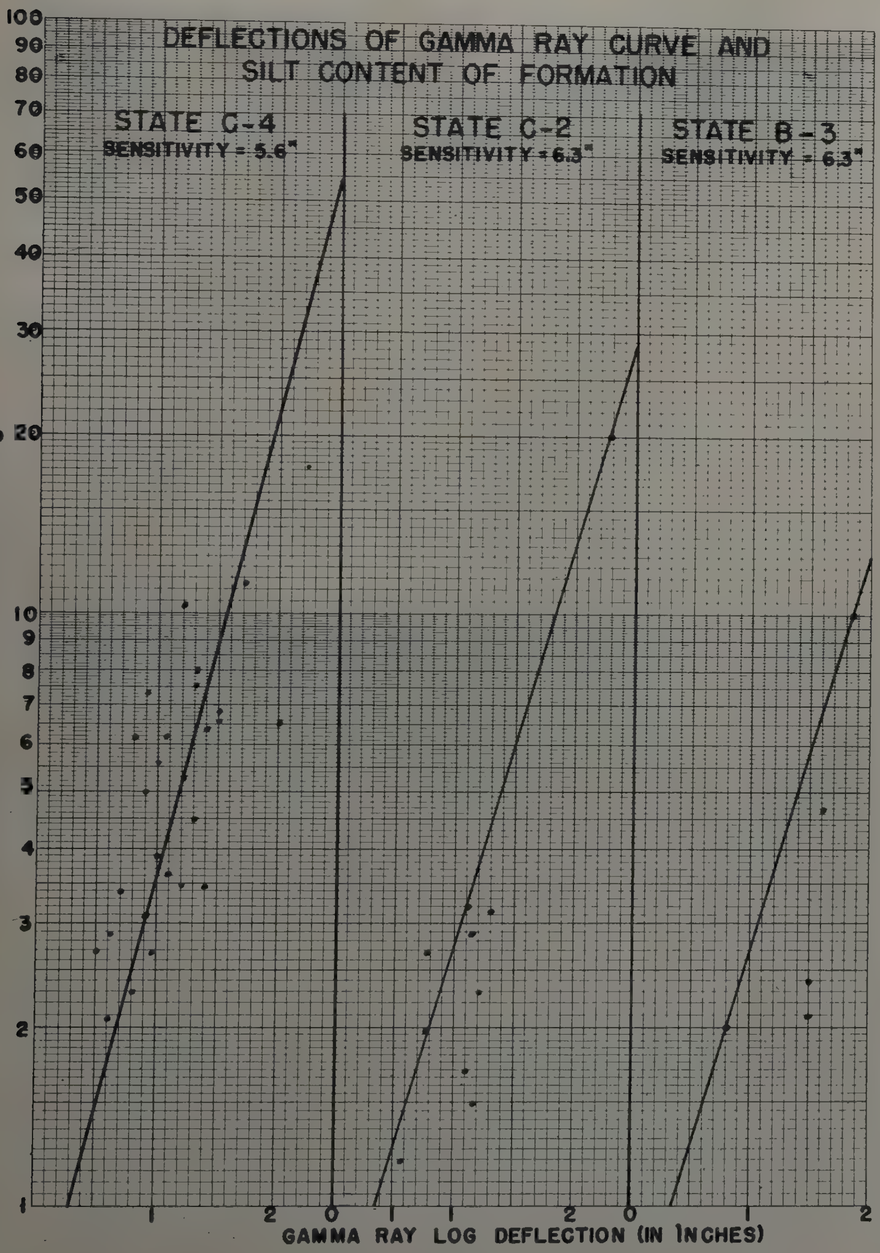

FIG. 16 — RELATIONSHIP BETWEEN GAMMA RAY CURVE DEFLECTIONS AND SILT CONTENT

SUMMARY AND CONCLUSIONS

The theoretical basis of radioactivity logging has been briefly discussed and the physical processes determining the logs have been described. The neutron log depends mainly on two variables, C a "chemical" factor which varies with the chemical composition of the sample on the surrounding rock and μ_1 the absorption coefficient for the neutron flux in the surrounding rock. μ_1 is largely a function of the hydrogen content of the rock and therefore is most strongly affected by fluid in the porosity.

The sampling of radioactivity curves is known to penetrate radially much deeper into the formation than other methods of sampling such as cores, reverse cuttings, and sidewall samples resulting in a much larger sample than those methods. The radioactivity curve sampling should therefore be superior for those formations exhibiting an extremely heterogeneous porosity distribution.

Relative methods of quantitative interpretation of radioactivity logs have been described which offer a means by which a neutron derived porosity can be determined for wells that have not been cored, by establishing a derived porosity curve from a selected base well, the data being applicable within limits of certain lithological and casing conditions. Versatility is obtained by utilizing the log reference points most applicable to the area. Homogeneous formations like the oolitic limestones show less dispersion of points plotted from these data, while heterogeneous formations such as Edwards limestone and dolomite and Permian dolomites show much greater dispersion.

While the methods presented in this paper offer the advantages of universal application to radioactivity logs, it is recognized that an absolute reference would offer greater accuracy to quantitative interpretation, and would increase the applicability of quantitative methods to data throughout the oil producing territories and remove the limitations imposed by changes in lithology and casing programs on relative quantitative interpretation methods. This development, however, still remains for the future.

ACKNOWLEDGMENT

The authors wish to thank the Lane-Wells Co. and Well Surveys, Inc., for permission to publish this paper.

They also wish to express their appreciation to the General American Oil Co., the T. L. James & Co., Inc., the Magnolia Petroleum Co., G. H. Vaughn, and the Texas-Gulf Producing Co. for their cooperation in supplying the logs and well data for this study.

The authors wish to acknowledge the assistance in this study and the criticism of this paper by C. I. Alexander of the Magnolia Petroleum Co.

The authors wish to acknowledge the assistance of the members of the staffs of the Lane-Wells Co. and Well Surveys, Inc., who have aided in the preparation of the manuscript. In this regard the helpful suggestions and criticisms of Chas. E. Duller, Robert E. Fearon, Gilbert Swift, John L. P. Campbell, and Robert M. Rutledge, Jr., were especially noteworthy.

REFERENCES

1. Wm. G. Green and R. E. Fearon, *Geophysics*, Vol. 5, July, 1940, p. 272.
2. Bruno Pontecorvo, *Oil and Gas Journal*, Sept. 11, 1941, p. 32.
3. William L. Russell, *Bull. A.A.P.G.*, Vol. 25, No. 9, Sept., 1941.
4. Warren Jackson and John L. P. Campbell, *Pet. Tech.*, No. 1923, Sept. 1945.
5. John L. P. Campbell and A. B. Winter, *Oil Weekly*, Jan. 6, 1946.
6. V. J. Mercier, *Oil Weekly*, Oct. 14 and 21, 1946.
7. Robert E. Fearon, *Nucleonics*, Vol. 4, No. 6, June, 1949, pp. 30-92.
8. Robert E. Fearon, *Nucleonics*, Vol. 4, No. 4, April, 1949, pp. 67-75.

★ ★ ★

ABILITY OF DRILLING MUD TO LIFT BIT CUTTINGS

H. N. HALL, HOWARD THOMPSON AND **FRANK NUSS,** MEMBER AIME,
STANOLIND OIL AND GAS COMPANY, TULSA, OKLAHOMA

ABSTRACT

Removal of bit cuttings is an important function of drilling muds. In an effort to obtain better understanding of the factors influencing the removal of cuttings, an extensive series of laboratory tests were made in which slip velocities of various sizes and shapes of particles were measured in muds of different physical properties. Empirical equations were then derived from these experimental data. These equations show that slip velocity is dependent on cutting size and shape, mud flow constants, and flow state of the mud. Applicability of these equations for field use is demonstrated by comparing computed slip velocities with slip velocities obtained from field tests.

INTRODUCTION

Drilling muds have many functions, but perhaps the most important is the removal of bit cuttings from the well. In a 10,000-ft well, the weight of rock which is drilled and must be carried to the surface is over 150 tons. In addition to this, the mud must remove any sloughings from the well bore. Failure of the mud to promptly remove either bit cuttings or sloughs from the well bore causes re-drilling and excessive wear on bit teeth, slows down drilling rate thereby increasing well costs, and greatly increases possibilities for stuck drill pipe when circulation is stopped for any length of time.

Drilling muds lift bit cuttings to the surface by means of the upward velocity of the drilling mud in the annulus. Because a density difference exists between the rock being drilled and the drilling mud, there is a difference between mud velocity and the rate of bit cutting travel, called the net rise velocity. To evaluate the ability of any type of drilling mud in respect to lifting cuttings, some method must be known for predicting the rate of fall of cuttings through mud traveling upwards in the annulus.

Equations for the rate of fall of particles through a true fluid have been satisfactorily determined by several authors.[1-6] Since drilling muds are not true fluids, but obey the laws of Bingham,[7] it should not be expected that equations for rate of fall of cuttings in a true fluid would be applicable to plastic fluids such as drilling muds. Several authors have attempted to compute cutting slip velocities in muds using a viscosity value obtained with a Stormer viscosimeter; however, unsatisfactory results were obtained. Pigott[8] took cognizance of the phenomenon of variation of viscosity with velocity in laminar flow, and calculated laminar slip velocities using a variable viscosity with Stokes law, and turbulent slip velocities using Rittingers law.

Drilling muds obey the laws of plastic flow which involve factors not affect-

---

[1] References are given at end of paper.

Manuscript received at the office of the Petroleum Branch October 28, 1949. Paper presented at the Petroleum Branch meeting at Columbus, September 25-28, 1949, and at the San Antonio meeting of the Petroleum Branch, October 5-7, 1949.

ing the flow of true fluids. Measurement of these plastic flow properties has been made possible by means of a rotational viscosimeter,[9] and it has been found possible to predict the flow performance of muds under actual drilling conditions.[10] Drawing an anology between flow of muds in circular pipes and fall of particles through drilling muds it was thought that cutting slip velocities should be affected by these plastic flow properties, and the proper approach to the problem of predicting bit cutting slip velocities in muds would be to investigate the relationships between plastic flow properties and slip velocities.

THEORY

The main problem to be considered in deriving expressions for rate of fall of particles through a fluid is that of the frictional resistance between a solid and a fluid in relative motion. If this frictional resistance can be expressed in terms of physical constants of the fluid and particle characteristics, then the problem of predicting slip velocities can be solved. The flow of fluids is a specialized case of the general case of frictional resistance between a solid and a fluid in relative motion, and the parameters which describe this should be applicable to cutting slip velocity relationships. Therefore, some mention must be made concerning the factors influencing flow of fluids in pipes.

When a true fluid is in laminar flow in a closed channel of any cross section, the parameters involved in predicting resistance to flow are the dimensions of the system, fluid velocity, density and viscosity. Whether a true fluid is in laminar or turbulent flow the viscosity is constant. Drilling muds are plastic fluids and do not behave as true fluids do in laminar flow. For a mud, viscosity is not constant in the laminar region and decreases with increasing velocity up to the critical velocity. Above the critical velocity, mud changes to turbulent flow and apparent viscosity is constant. Due to the phenomenon of changing viscosity in the laminar region, the mud properties must be described by some parameter other than viscosity in order to obtain an expression for resistance to flow for muds. Bingham[7] was the first to derive an equation for resistance to flow of plastic fluids in the laminar region. In place of viscosity, Bingham introduced the terms yield value (t_y) and rigidity (n) and the resulting equation is:

$$\triangle P = \frac{16\ L\ t_y}{3D_p} + \frac{32n\ V_m L}{gD_p^2} \quad . \quad (1)$$

As pointed out before, muds behave like true fluids when in turbulent flow and therefore Fanning's equation should hold for the turbulent flow of mud in circular pipes. Beck[9] has shown that Fanning's equation is applicable to drilling muds if Reynold's number is calculated using $\frac{n}{3.2}$ for the apparent viscosity.

Since flow of fluid through a pipe is but a specialized case of the general law of the resistance between a solid and a fluid in relative motion, it would seem probable that when particles are falling in laminar slip in a drilling mud, the mud will behave like a plastic material and for particles in turbulent slip, mud will behave like a true fluid with an apparent viscosity of $\frac{n}{3.2}$.

Presently used equations for slip in true fluid should therefore be modified to take this into account.

It has been shown both theoretically and experimentally that the resisting force acting on a particle moving in a true fluid depends on the size of the particle, some function of the area, velocity of the particle relative to the fluid, and the density and viscosity of the fluid. By rearrangement of the Fanning equation, a group known as the

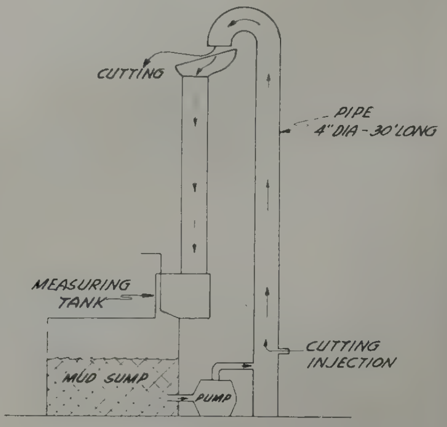

FIG. 1 — ARRANGEMENT OF EQUIPMENT.

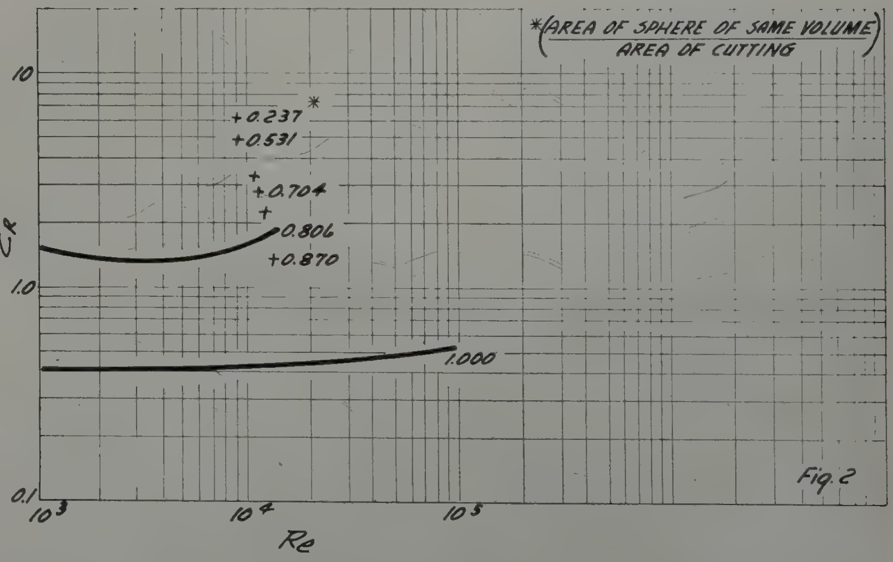

FIG. 2 — C_R VS. R_e FROM WADELL.

coefficient of friction, C_R, is obtained and this has been found to be a function of the Reynolds number. This gives the general relation for frictional resistance and the following equations are an expression of this relationship for laminar and turbulent slip.

For true fluids in viscous flow ($Re < .05$), resistance is proportional to viscosity, area, and relative velocity and Stokes law relates particle slip velocity to particle and fluid properties. Stokes law is:

$$V_s = \frac{2gD^2\,(\rho_s - \rho_m)}{36} \quad \text{for spherical particles} \qquad (2)$$

In the turbulent region ($Re > 2000$) resistance is largely due to transfer of momentum to larger masses of fluid, and is proportional to area, square of the relative velocity of the particle, and density of the fluid. In the turbulent region, Rittingers equation shows how particle slip varies with physical properties of the fluid and the particle. Rittingers equation is:

$$V = 9\sqrt{\frac{D\,(\rho_s - \rho_m)}{\rho_m}} \quad \text{for spherical particles} \qquad (3)$$

In the transition region, resistance is due to both viscous and turbulent forces, and neither Stokes nor Rittinger's equation applies. Even though neither one of these equations can be used, there is the relationship between C_R and Re, and with knowledge of this relationship slip velocities can be calculated.

Table I

Drilling Mud Characteristics
Laboratory Tests

Mud No.	Type	ty	n	ρ	V_c
1	Bentonite	0.	.00572	64.0	0.27
2	Bentonite	0.	.00893	64.5	0.83
3	Bentonite	.0007	.0131	65.0	1.30
4	Bentonite	.0189	.0276	65.4	3.4
5	Bentonite	.0420	.0409	66.0	5.2
6	Bentonite	.070	.0470	66.7	6.1
7	Bentonite	.0084	.0272	65.6	2.9
8	Bentonite	.0035	.0138	65.1	1.6
9	Bentonite	0.	.00893	63.8	0.8
10	Lubrigel	0.	.00277	62.4	0.27
11	Lubrigel	.0028	.00582	64.3	1.5
12	Lubrigel	.0378	.00631	65.7	2.8
13	Lubrigel	.0756	.00630	66.6	3.8
14	Lubrigel	.0854	.00630	67.0	3.9
15	Lubrigel	.1827	.00631	68.4	5.4
16	Bentonite	0.	.00108	62.9	0.3
17	Bentonite	0.	.00485	64.0	1.4
18	Bentonite and Baroid	0.	.0104	74.0	2.7
19	Bentonite and Baroid	.007	.0136	74.7	3.8
20	Bentonite and Baroid	.056	.0202	75.5	6.4
21	Lubrigel and Baroid	.434	.0262	77.7	11.4
22	Lubrigel and Baroid	.309	.0249	76.4	10.5
23	Aquagel	.217	.0182	65.8	9.1
24	Aquagel	.122	.0150	65.7	7.0
25	Aquagel	.056	.00875	65.5	4.6
26	Aquagel	.029	.00955	65.6	4.0
27	Aquagel	.163	.00448	68.5	5.7
28	Aquagel	.178	.00465	68.6	5.9
29	Aquagel	.130	.00410	68.1	5.3
30	Blanca Clay	.240	.00444	68.8	6.7
31	Blanca Clay	.045	.0175	66.8	6.1
32	Blanca Clay	.023	.0139	66.7	4.8
33	Blanca Clay	.015	.0098	66.6	3.5

Table II

Cutting Dimensions
Laboratory Tests

No.	ρ	Cuttings Description	Inches			Area Sq. in.	Volume Cu. in.	R_n
			1	2	3			
1	156	Glass Square	.657	.669	.210	1.436	.0954	.284
2	156	Glass Rectangle	.634	1.27	.210	2.410	.1775	.348
3	156	Glass Square	1.26	1.26	.210	4.23	.357	.440
4	156	Glass Sphere	.600D			1.13	.113	.300
5	152	Glass Sphere	.1857D			.1105	.00345	.09375
6	169	Al. Square	.250	.250	.125	.250	.00781	.1235
7	169	Al. Square	.250	.250	.0625	.1875	.003905	.0976
8	173	Al. Disk	.1875D		.0625	.0920	.001722	.0737
9	173	Al. Disk	.1875D		.125	.1288	.003444	.0927
10	156	Glass Sphere	.592			1.10	.1085	.296
11	156	Glass Rectangle	.458	.419	.215	.762	.0412	.214
12	156	Glass Rectangle	.570	.524	.130	.881	.0388	.210

APPARATUS AND PROCEDURE FOR LABORATORY TESTS

Determination of cutting slip velocities under conditions as nearly like those encountered in oil wells required the use of a tall pipe column through which the mud traveled upwards, a method of injecting cuttings into the mud stream near the lower end of the column, and a screen for removing cuttings at the top. Two systems with this type of arrangement were used. One was a large scale system having a column of 4 in. ID pipe with 33 ft of pipe from injection point to screen and the other had a column of 1.25 in. ID pipe, being 9 ft from injector to screen. Mud was returned to the reservoir by means of another pipe column which had a swinging spout so arranged that the discharge could be directed into a calibrated tank for measuring volume rates of flow. A 500 GPM centrifugal pump driven by a gasoline engine was used with the large scale apparatus and flow rates were varied by means of a hand throttle and automobile gear transmission. A 150 GPM centrifugal pump driven by an electric motor was used with the smaller apparatus and flow rates were varied with a by-pass valve, which returned some of the pump output to the reservoir. A sketch of the apparatus is shown in Fig. 1.

Each mud was constructed to the approximate desired flow properties, mixing being accomplished with a jet mixer. Circulation of the mud was continued long enough to make sure flow properties would remain constant during the test. Mud was then pumped through the pipe column and the rate was measured. Single cuttings of one type were injected and time of travel from injector to screen recorded. Groups of cuttings were then injected and their rate of travel was timed, after which the mud flow rate was rechecked. This procedure was followed throughout all tests. Mud flow properties were checked during the tests and velocity rates were selected at randon so that no hysteresis errors would be introduced. All cuttings were artificially constructed to the approximate shape of actual cuttings. Spherical particles were also used to check the application of the equations for laminar and turbulent slip. Flow properties were determined with the rotational viscometer.[9]

RESULTS OF LABORATORY TESTS

A fact well known among those who have experimented with colloids is the difficulty encountered in reproducing test results. For this reason a large number of tests were made and the average in each series was used. In turbulent flow ranges where mud acts as a true fluid the data were accurate to within ±10 per cent. In laminar flow, however, results varied from a mean value by an average of ±15 per cent.

Flow properties and critical velocities of muds used are given in Table I. These muds cover a greater range of flow properties than is normally found in actual drilling practice. Dimensions of cuttings are given in Table II.

Mud rate and cutting slip velocities for each test were separated into two parts; turbulent flow of drilling muds, Table III and for laminar flow, Table IV. Each of the slip velocities in these tables is an average of several tests. For cuttings falling in turbulent slip,

the relationship of the coefficient of friction, C_R, to Reynolds number is shown in Fig. 3. It should be noted that there are two distinct curves, one for spheres, and the other for flat or irregular particles.

In laminar slip, apparent viscosity is found to be a function of rigidity. This function was constant for a particular mud and the correlation of the function and yield value, t_y, is shown in Fig. 5. This relationship enables a modified form of Stokes law to be used in predicting laminar slip velocities.

From the laboratory data, empirical equations were derived in which cutting

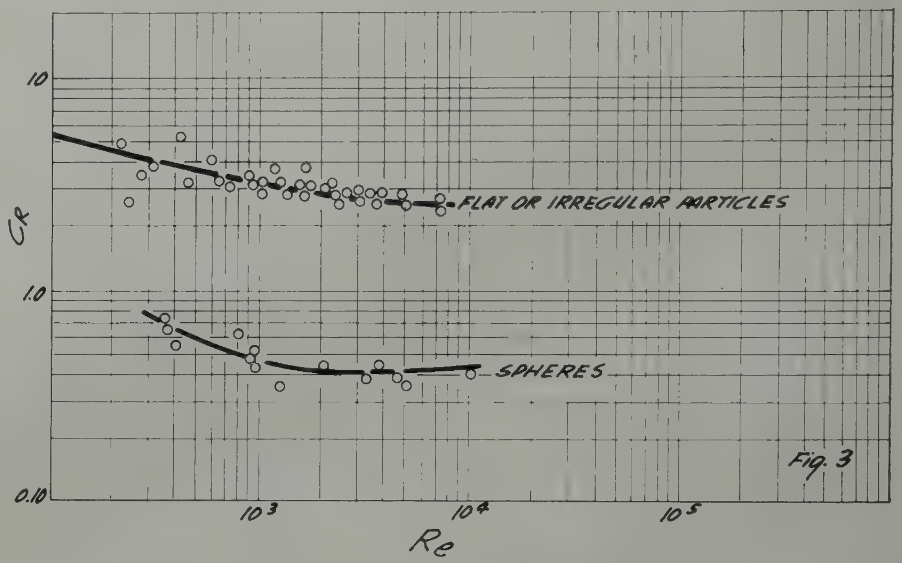

FIG. 3 — C_R VS. R_e LABORATORY DATA.

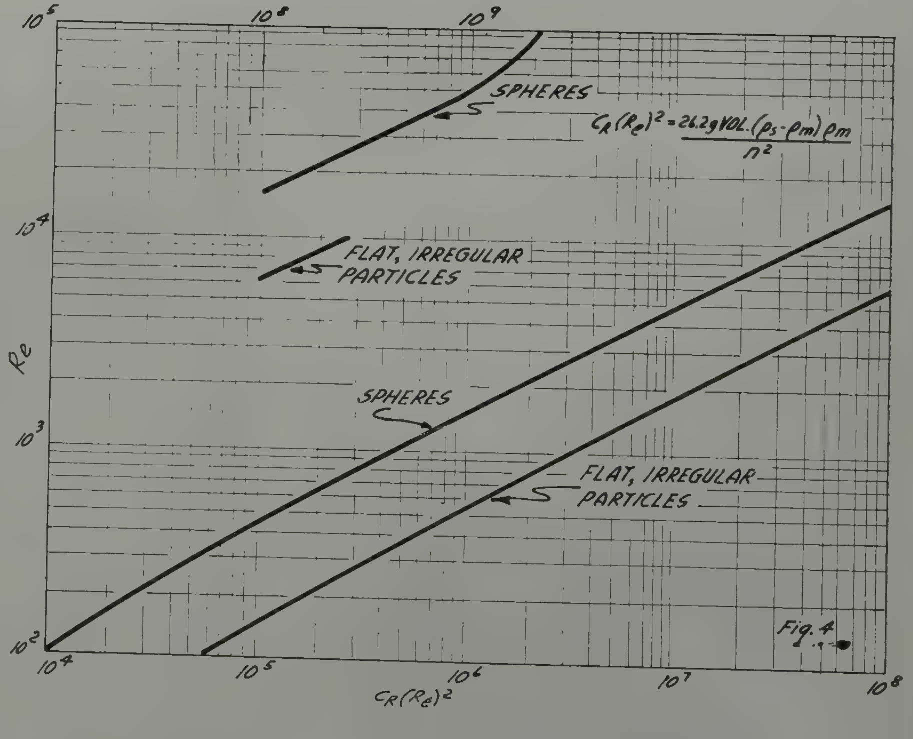

FIG. 4 — $C_R(R_e)^2$ VS. R_e FOR DRILLING MUDS LABORATORY DATA.

slip velocity is expressed as a function of cutting characteristics and mud flow properties.

DISCUSSION OF RESULTS

Turbulent Slip

Much data has been accumulated by various authors concerning slip velocities of spherical particles in true fluids. Relations between C_R and Reynolds number for spheres in true fluids have been accurately determined. Wadell[1] has shown that slip velocities of various flat particles require different C_R vs Re values, these relationships being dependent on relative flatness of the particles (see Fig. 2). Relative flatness termed sphericity, is defined as the ratio of the surface area of a sphere of the same volume as a particle to the surface area of that particle. Since the majority of bit cuttings are flat it was necessary to determine slip velocities in mud for both flat and spherical particles.

Table III

Turbulent Slip Data

Laboratory Tests

Mud #	Mud Velocity ft/sec	Cutting #1 V_s ft/sec	Cutting #2 V_s ft/sec	Cutting #3 V_s ft/sec	Cutting #4 V_s ft/sec
1	3.91	.97	1.14	1.25	2.74
	2.93	.99	1.15	1.25	
2	4.35	.98	1.05	1.21	2.81
	2.34	.95	1.08	1.24	
3	4.50	.96	1.03	1.09	2.70
	3.17	.93	1.06	1.15	2.66
	1.50	.89	1.00		
4	4.12	.84	1.02	1.14	2.60
7	3.76	.84	1.04	1.06	2.41
8	4.00	.94	1.03	1.08	2.58
	2.70	.80	1.00	1.23	
9	3.90	.96	1.05	1.10	2.76
	3.13	1.00	1.09	1.19	
10	4.30	1.06	1.15	1.41	2.79
	3.18	1.05	1.20	1.33	
	1.70	1.09			
11	4.24	1.00	1.12	1.26	2.88
	3.03	.99	1.17	1.20	
	2.35	1.02	1.08	1.17	
12	4.43	.96	1.06	1.20	2.80
	3.22	.98	1.06	1.25	
13	4.55	.96	1.05	1.21	2.71

Mud #	Cutting Mud Velocity ft/sec	Cutting #5 V_s ft/sec	Cutting #6 V_s ft/sec	Cutting #7 V_s ft/sec	Cutting #8 V_s ft/sec	Cutting #9 V_s ft/sec
16	3.75	1.00	1.00	.54	.47	.64
	3.04	1.31	1.01	.52	1.01	.65
	2.54	1.10	.51	.56	.60	1.04
17	3.79	1.62	.58	.97	.57	.57
	3.16	1.40	.89	.71	.20	.49
	2.67	1.21	.73	.60	.39	.55
	2.37	1.21	.51	.54	.60	.50
18	3.65	.98	.91	.43	.32	.54
	3.22	1.10	.48	.21	.31	.49
	2.91	1.01	.57	.32	.39	.35
19	4.11	.89	.65	.52	.78	.48

The coefficient of friction, C_R, is defined as:

$$C_R = \frac{2R}{A \rho_m V_s^2} \quad . \quad . \quad . \quad (4)$$

When the velocity has reached equilibrium; the retarding force on the particle is:

$$R = \frac{\pi D_e^3}{6} (\rho_s - \rho_m) g \quad . \quad . \quad (5)$$

$$A = \frac{\pi D_e^2}{4} \quad . \quad . \quad . \quad . \quad . \quad . \quad . \quad (6)$$

Therefore:

$$C_R = \frac{4 g D_e (\rho_s - \rho_m)}{3 \rho_m V_s^2} \quad . \quad (7)$$

The Reynolds number can be computed from the following relationship:

$$Re = \frac{3.2 D_e V_s \rho_m}{n} \quad . \quad . \quad (8)$$

Values of C_R and Re were computed from equations (7) and (8) respectively and C_R was plotted against Re as shown in Fig. 3. As can be seen from Fig. 3, there is a good correlation between C_R and Re. As it should be, there are two definite curves; one curve for spheres and one for flat particles. It was impossible to draw separate lines for varying sphericities from the data on flat and irregular particles. Such a situation as described by Wadell[1] probably exists, but due to the lack of reproducibility of results in colloidal systems and the amount of error introduced by the method of measuring slip velocities, the one line must suffice from data obtained.

From this relation between C_R and Re for drilling muds it should be possible to calculate turbulent slip velocity. This is possible, but since there are two unknowns, solution must be made by a tedious trial and error method. Multiplying C_R by $(Re)^2$ gives the following expression which contains only measurable properties:

$$C_R (Re)^2 = \frac{13.7 g D_e^3 (\rho_s - \rho_m) \rho_m}{n^2} \quad (9)$$

Fig. 4 shows a correlation of $C_R (Re)^2$ with Re. With this graph it is possible to compute values of Reynolds number for any situation, and the corresponding slip velocity is obtained from:

$$V_s = \frac{n\ Re}{3.2\ D_e\ \rho_m} \quad . \quad . \quad . \quad (10)$$

The equivalent diameter D_e used in the above equation is the diameter of a sphere whose volume is equal to that of the particle. For a non-spherical particle:

$$D_e = \sqrt[3]{\frac{6\ \text{Volume}}{\pi}} \quad . \quad . \quad (11)$$

The following general equations can be used for non-spherical particles:

$$C_R\ (Re)^2 = \frac{26.2g\ \text{Volume}\ (\rho_s - \rho_m)\ \rho_m}{n^2} \quad . \quad . \quad . \quad . \quad . \quad . \quad (12)$$

$$V_s = \frac{n\ Re}{3.97\ \rho_m\ \sqrt[3]{\text{Vol}}} \quad . \quad . \quad . \quad (13)$$

In computing slip velocities care should be taken to use the proper line on the plot of $C_R\ (Re)^2$ against Re.

Laminar Slip

Since muds behave like plastic materials when in the laminar flow region, a certain amount of force must be applied to overcome the yield strength of the mud, any force less than this does not cause shear of the mud. Muds will therefore support cuttings completely until the initial shear is overcome by some means. Stokes law for the resistance to slip for particles is:

Spherical Particles $R = 3\pi\ \mu\ D\ V_s$ . . . . . . (14)

Thin Disk Shaped Particles

$$R = \frac{16}{3}\ \mu\ D\ V_s \quad . \quad . \quad . \quad . \quad . \quad (15)$$

The force causing slip in a true fluid is:

$$F = \text{Volume}\ (\rho_s - \rho_m)\ g \quad . \quad (16)$$

In a plastic fluid such as mud, however, this force is reduced due to the yield strength and the resulting force causing slip is:

$$F = \text{Volume}\ (\rho_s - \rho_m)\ g - (\text{Surface Area})\ t_y g \quad . \quad . \quad (17)$$

When the particle undergoing slip reaches an equilibrium velocity, the two forces acting upon it, equation (14) or (15) and (17), are equal. Since apparent viscosity of a mud changes with rate of flow it was assumed that apparent viscosity would be a function of rigidity. This function was designated as (x) (n), and with this definition slip velocity equations in laminar flow are:

Spherical Particles:

$$V_s = \frac{gD^2\ (\rho_s - \rho_m) - 6g\ Dt_y}{18\ (x)\ (n)} \quad . \quad (18)$$

Flat Disks:

$$V_s = \frac{3\ \pi\ tDg\ (\rho_s - \rho_m) - 6\ \pi\ gt_y\ (D+2t)}{64\ (x)\ (n)} \quad . \quad . \quad . \quad . \quad . \quad . \quad (19)$$

Actual slip velocities in the laminar region of mud flow were compared with slip velocities calculated by the above equations, omitting the factor x. Although actual and calculated slip velocities differed widely, it was found that for any particular mud the actual and computed slip velocities differed by a constant factor. This factor itself varied with the yield value, t_y, of the mud and therefore a correlation between yield value and the factor x was established and is shown in Fig. 5. With this relationship, the equations for slip velocities of spherical and non-spherical particles in laminar flow were complete.

It should be pointed out that certain phenomena observed in cutting slip have no counterpart in pipe flow. In pipe flow systems, the flow region is selected as the one which requires the larger pressure drop. In bit cutting slip, this would be analogous to a bit cutting falling in whichever type of slip results in the least slip velocity. This is not a universal statement however. If the mud is in laminar flow, the cutting will fall in the type of slip giving lower slip velocities; but in the turbulently flowing mud the cutting can fall only in turbulent slip. Thus, in some cases the bit cutting may fall in turbulent slip even though laminar slip would be numerically less.

FIELD TESTS

Having obtained empirical equations for bit cuttings slip velocities based on laboratory tests, the next problem was to see how these equations would hold up when used in the field under actual operating conditions.

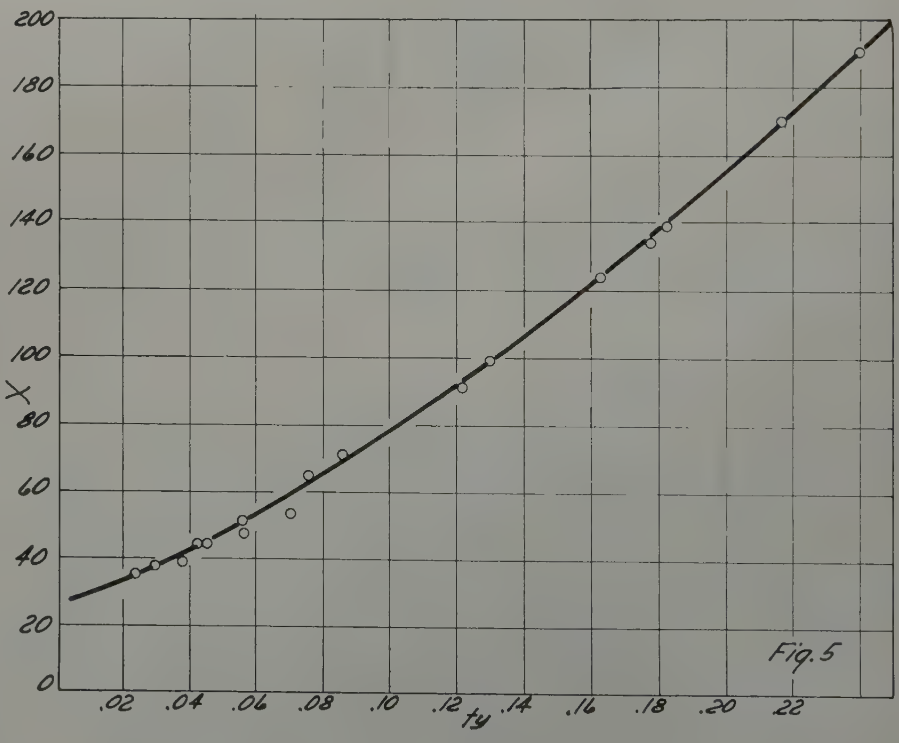

FIG. 5 — X VS. ty LABORATORY DATA.

PROCEDURE

It was decided that without causing excessive operating costs, the most accurate results on cutting slip velocities could be obtained by injecting artificial cuttings into the circulating system at the base of the standpipe and measuring the time of travel to the shale shaker or some other point where they could be caught as they came out of the hole.

Artificial cuttings used in the field tests were circular disks made from a thermosetting plastic and barytes. A combination of these two materials gave the desired hardness and proper density, which in all cases was close to 162 pounds per cu ft or a specific gravity of 2.6. These cuttings were developed as a result of laboratory experimentation. Circular disk shaped particles were used because they resemble fairly closely in shape the average type of cuttings delivered, and for the basis of these checks a definite size and weight particle had to be used in order to eliminate any errors due to inexact dimensions. From ten to twenty cuttings were introduced on each run through a special by-pass arrangement on the standpipe. Times of travel to the outlet point were taken, and corrections were made for time consumed in traveling down the flow line ditch in those cases where cuttings were timed at the shale shaker. Pump rates were adjusted for a series of runs by use of the hydraulic couplings with engines running at a governed speed. Frequent checks on pump rate were made to be sure it did not vary during a particular series of tests. Pump efficiencies were checked at the same time. Flow properties of each mud were measured frequently and an average used since variations were found to be minor. Due to the time and expense involved in changing mud flow properties over a wide range, only two muds were used in each series of tests. One check was run using water instead of mud as the drilling fluid.

Two series of tests were run. Equipment used varied slightly in the two tests, but in both cases the circulating system consisted of approximately 1000 ft of $4\frac{1}{2}$ in. drill pipe in $9\frac{5}{8}$ in. casing.

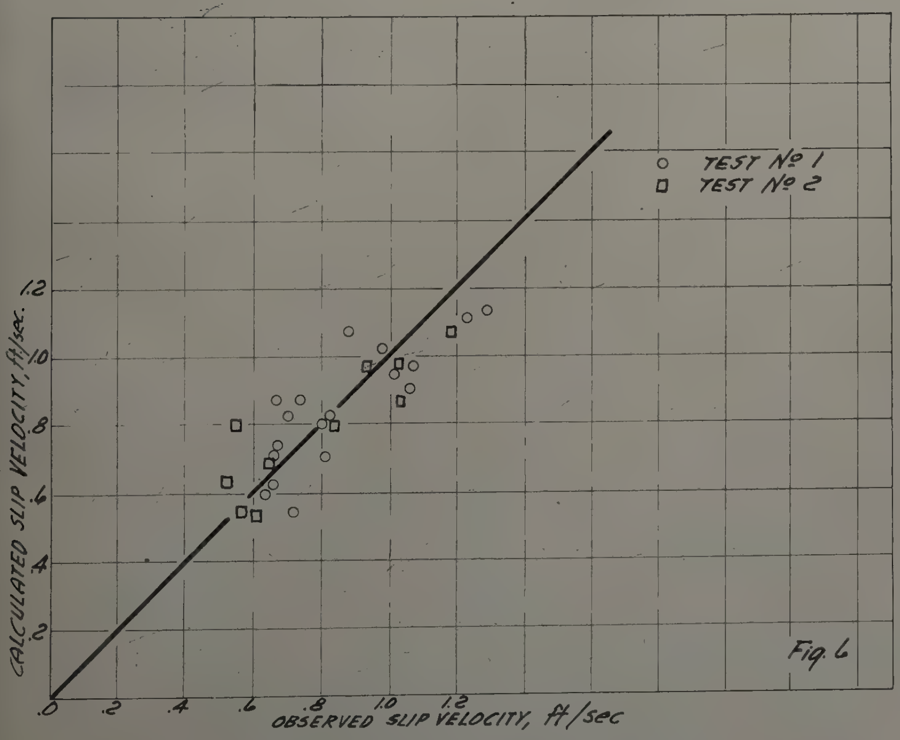

FIG. 6 — CALCULATED AND OBSERVED SLIP VELOCITIES FIELD DATA.

In the first series, cuttings were caught at the shale shaker, a Baker retainer being used as a bridging plug in the casing to insure return of cuttings from the bottom. A full opening Reed bit (jet nozzles removed) was run in on the $4\frac{1}{2}$ in. drill pipe and circulation established with the bit just barely clearing the retainer. Returns were through 12 in. blowout preventers, a 7 in. flow line angling at about 30° to the outside of the mast superstructure and on down a 13-in. pipe flow ditch to the shale shaker. Because of the extra restrictions and enlargements, it was found that cuttings were being slowed down and possibly settling out in these enlargements at the lower pump rates. Also, some were thought to be lost in the recesses of the retainer.

The second series of tests was made with a more convenient way of catching cuttings as they came out of the annulus, and resulted in a larger percentage of return of those injected. The blowout preventers were set aside and a side outlet of 7-in. casing made directly into the cementing joint of casing. This 7-in. pipe was only 5 ft long and discharged the mud into a board flume that was covered with $\frac{1}{4}$-in. mesh hardware cloth. Mud was discharged from this flume into a dug suction pit. A sub which directed flow back up the annulus was installed on the open ended drill pipe. With this type of arrangement, the erratic return of cuttings noted in the first test was entirely eliminated and nearly all the cuttings introduced were recovered.

Results of the field tests as compared with computed slip velocity values are shown in Tables V and VI. Three of the four muds shown in these tables were in turbulent flow in all parts of the annulus and at all circulating rates. The fourth was in laminar flow in most cases and sometimes exhibited turbulent flow around tool joints and drill pipe protectors. There was, therefore, sufficient data and duplication of results to evaluate the applicability of turbulent slip velocity equations. Laminar slip occurred in only one mud and this was run during the first series of tests. Some errors were introduced in the first test by the flow ditch and these were in turn further magnified by the high viscosity mud used to bring about laminar flow. Because of these factors it is thought that there were insufficient data to compare observed laminar slip velocities with calculated values.

For the muds which were in turbulent flow, turbulent slip therefore occuring, the data were more accurate and a larger number of tests were made than in the case of laminar slip. Because of these facts it is possible to get a better comparison between calculated and observed slip velocities. From Table V it can be seen that the difference between measured and calculated slip velocities ranges from –0.25 to +0.27 ft per sec. and from –0.24 to +0.18 ft per sec. in Table VI. Numerical differences between observed and computed slip velocities are of the order of ±0.15 ft per sec. The deviation of calculated slip velocities from the observed slip velocities is shown for each test as per cent of the observed value in Table V and VI. The per cent deviation is expressed as the ratio of the difference between computed and observed slip velocities to the measured slip velocity, being positive when calculated slip velocities are higher than observed values. Observed values of slip velocity used in computing per cent deviation are an average of values at the different circulating rates. The per cent deviation ranges from +45.5 per cent to –17.8 per cent with an average of these ranging from +15 to –10 per cent. Fig. 6 shows a correlation between calculated and observed turbulent slip velocities.

DISCUSSION OF FIELD TEST RESULTS

There are a number of the laminar cutting slip velocity measurements shown in Table V that are expressed as positive velocities. In these, the cutting velocity was measured to be higher than the average mud velocity. Such a thing can be understood when it is realized that in the laminar flow region there is a parabolic velocity distribution in the annular space with a central unsheared plug moving at the maximum velocity. A cutting which was trapped in this plug would probably have no tendency to be removed from its position so would naturally have a velocity greater than the average mud velocity. The phenom-

Table IV
Laminar Slip Data
Laboratory Tests

Mud #	Yield Velocity ty	Mud Vm	C_1 Vs	C_2 Vs	C_3 Vs	C_4 Vs
5	.0420	3.85	.20	.34	.37	.22
		3.03	.23	.30	.39	.20
	.0409	2.95	.19	.27	.41	.25
6	.070	4.39	.13	.22	.31	.22
	.0470	3.89	.20	.18	.22	.14
		2.43	.10	.23	.29	.09
12	.0378	1.85	1.55			
13	.0756	3.35	.84	1.01	1.40	1.01
		3.10	.94	1.20	2.00	.81
14	.0854	4.65	.98	.98	1.20	1.02
		3.20	.99	1.49		
		1.95	.43			
15	.1827	4.40	.37	.47	.52	.37
		3.55	.28	.41	.68	.31
		2.75	.23	.38	.79	.29
		1.33	.28	.37	.49	.15

Mud #	Yield Velocity ty	Mud Velocity Vm	C_{10} Vs	C_{11} Vs	C_{12} Vs
23	.217	.85	.08	.04	
		.675	.08	.03	
		.675	.09	.04	
		1.30	.10	.05	.03
		1.85	.09	.05	.03
		2.21	.09		.03
		1.78	.08	.05	.03
		1.10	.08	.045	.02
		1.12	.09	.04	.02
24	.122	2.90	.28	.12	.12
		2.31	.29	.13	.07
		1.60	.19	.17	.15
		2.90	.20	.20	
		2.53	.24	.30	
		1.76	.26	.09	.09
25	.056	.99		.61	.38
		1.50	.90	.67	.40
		1.31	.80	.60	.40
		1.20	.77	.55	.54
26	.029	1.71	1.21	.70	.63
		1.43	1.12	.79	.57
		1.25	.90	.80	.51
		1.09	.81	.71	.48
		.90			.49
27	.163	1.71	.59	.30	.19
		1.96	.51	.30	.19
		2.12	.59	.29	.19
		1.50	.55	.25	.21
		1.0	.50	.19	.20
		.63			.20
28	.178	1.25	.43	.25	.14
		1.78	.45	.27	.18
		1.44	.41	.26	.17
		1.01	.41	.27	.11
		.67		.20	.16
		.54			.16
29	.130	2.66	.90	.47	.32
		2.10	.69	.55	.27
		1.69	.65	.51	.32
		1.30	.80	.50	.28
		.97		.40	.30
30	.240	2.34	.35	.11	.06
		1.96	.33	.12	.06
		1.37	.32	.14	.05
		1.20	.31	.11	.055
		1.00	.30	.14	.06
		.91	.30	.13	.06
		.725	.23	.12	.07
31	.045	1.62	.50	.33	.25
		1.82	.35	.38	.20
		2.01	.40	.25	.25
		1.43	.43	.36	.25
		1.00	.43	.37	.26
		2.75	.46	.34	.21
		2.20	.47	.37	.21
		1.70	.41	.37	.27
32	.023	1.98	.74	.59	.34
		1.76	.80	.54	.37
		1.51	.71	.55	.38
		1.33	.71	.56	.40
		1.08		.50	.43
		.82			.42

enon of a parabolic velocity gradient could be a possible explanation of slip velocities which appear to be greater than their calculated value. Mud in the laminar flow region flows in a series of concentric shearing layers of mud and there is no turbulence present which would tend to move cuttings from one part of the stream to another. Because of this fact, a cutting could start out in a portion of the annulus having a velocity less than the average mud velocity and continue in it all the way up the annulus. Another possible explanation is that some of the cuttings might have been momentarily trapped in some part of the system. This would tend to give measured slip velocities greater than calculated values.

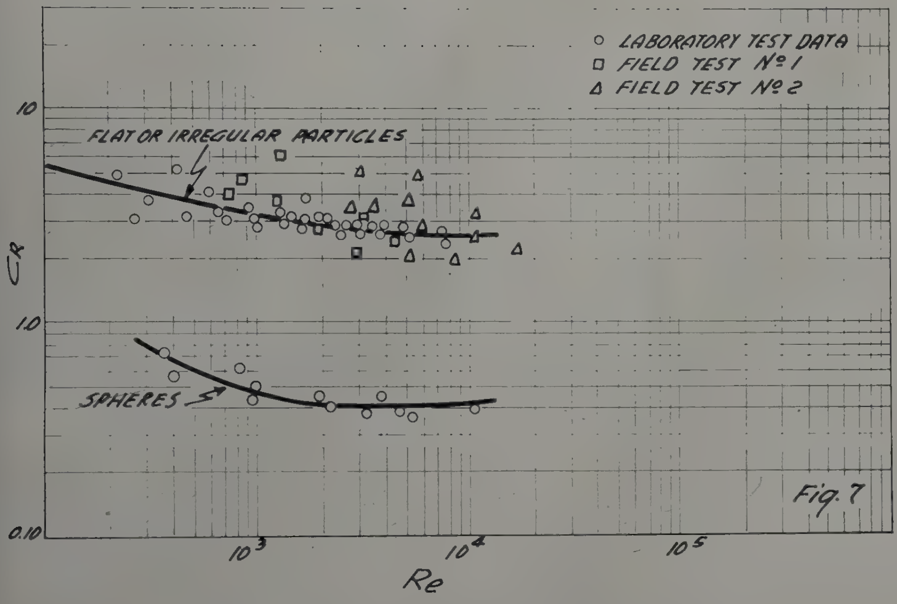

FIG. 7 — C_R VS. R_e, LABORATORY AND FIELD DATA.

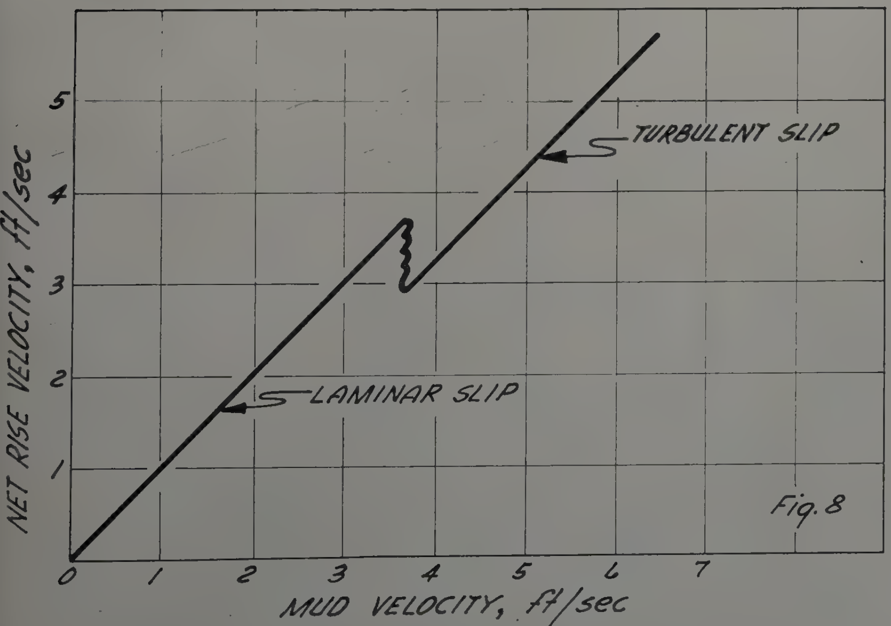

FIG. 8 — RELATION OF NET RISE VELOCITY AND MUD VELOCITY.

Since data from the laboratory tests did not reveal any such difficulty with laminar slip measurements, it is thought that the shorter travel distance did not allow the plug flow or velocity gradient phenomena to be so pronounced as they were in field tests. The laboratory apparatus had a uniform flow channel while tool joints and in the field tests drill pipe protectors set up restrictions which caused eddies and turbulence which could possibly have caused some error to be introduced.

Turbulent slip velocities measured from field data were used to compute C_R and the Reynolds number for the average slip velocity for each test. These values were then plotted on the original laboratory correlation of C_R and Reynolds number. The new correlation is shown in Fig. 7. Although the points are more scattered than laboratory values, they show the same trend and the wide variation is probably due to the difference between laboratory and field methods of determining slip velocities.

As the results were being tabulated, it seemed that mud velocity had some effect on measured slip velocities. This was evident in both types of cutting slip. The more complex circulating system used in the field tests allowed introduction of a number of errors, and prediction of the action of the cutting was almost impossible due to the changes of velocity and eddies and turbulent zones caused by restrictions such as tool joints and rubber drill pipe protectors. It is thought that the higher slip velocities noted with lower circulating rates was an indication of the above factors rather than the true slip velocity being affected by circulating rate.

It has been previously pointed out that the average per cent deviation for turbulent slip velocity figures was from +15 per cent to −10 per cent. The amount of deviation is not distressing when it is remembered that actual numerical differences between observed and computed values were on the order of ±0.15 ft per sec. Roughness of the system and methods of measurement could account for this magnitude of deviation. On the whole the correlation between observed and computed turbulent slip velocities are very satisfactory for engineering use, and qualitative results fall in line with what was predicted.

GENERAL DISCUSSION

With the knowledge that there is a means for determining the flow properties of drilling muds, and that these flow properties can be used to predict laminar and turbulent cutting slip velocities, much greater consideration can be given to intelligent design of muds to achieve best results in drilling. The ultimate aim of the mud program is to supply, as economically as possible, a mud which will: (1) have the proper weight characteristics, (2) be able to withstand chemical contamination from a formation being drilled, (3) be pumpable at all times and not cause excessive horsepower requirements, and (4) be able to effectively remove the bit cuttings, thereby lessening the possibilities of such serious problems as stuck drill pipe, excessive re-drilling, etc.

In the design of a mud system, assuming that all the requirements have been fulfilled with the exception of the last two mentioned above, three main items must be considered. These factors are: (1) with the given mud what will be the minimum mud velocity required to lift bit cuttings, (2) above this minimum velocity what would be the most advantageous pump rate, and (3) could the mud be further treated so that even with the added mud costs, an economic advantage could be realized due to lower horsepower requirements needed for cleaning the hole.

To illustrate a problem such as stated above, the following example is given:

Computation of Optimum Pump Rate

A well being drilled with mud of these characteristics:

Yield value (t_y)—0.110 lb per sq ft
Rigidity (n)—0.006 lb per sec ft
Density (ρ_m)—95 lb per cu ft
Critical Velocity—3.7 ft per sec

The pump is limited to a mud velocity of 4.0 ft per sec in the annulus.

To find the most desirable pump rate for removal of flat cuttings, turbulent and laminar slip velocities are computed.

Cutting Size—¼ in.x¼ in.x1/16 in.
Cutting Weight—170 lb per cu ft

Laminar Slip

$$V_s = \frac{3\pi t D(\rho_s - \rho_m)g - 6\pi g(D+2t)t_y}{64\ (x)\ (n)}$$

From Fig. 5, x = 84 when $t_y = 0.11$.

Substitution in the above equation gives $V_s = 0.0118$ ft per sec

Net rise velocity at 3.65 ft per sec = 3.64 ft per sec

Turbulent Slip

$$C_R\ (Re)^2 = \frac{835\ \text{Vol}\ (\rho_s - \rho_m)}{n^2} = 3.3\text{x}10^5$$

From Fig. 4, Re = 380

$$V_s = \frac{n\ Re}{6.4\ D_e\rho_m} = 0.77 \text{ ft per sec}$$

At a mud velocity of 4.0 ft per sec the net rise velocity of the cutting will be 3.23 ft per sec

Fig. 8 is based on the above data and shows the relation between net rise velocity and annular mud velocity in both laminar and turbulent flow.

From the example it can be seen that the laminar cutting velocity in this particular case is very small, and cuttings of this size would be lifted at almost any pump rate used. To properly insure the removal of cuttings and to remove them as quickly as possible, the next problem to be confronted is that of obtaining the maximum net rise velocity at practical pump rates. It can be seen that any mud in turbulent flow at a velocity less than 4.40 ft per sec will result in a smaller net rise velocity than was obtained with mud in laminar flow at 3.65 ft per sec. In the example given, a pump rate greater than 4.0 ft per sec was not possible, therefore, maximum cutting lift was obtained at the highest velocity at which the mud would remain in laminar flow.

Table V

Summary of Cutting Slip Velocities — Test No. 1

Cutting Size			Mud #1 Wt=10.9 #/gal n=0.00506 #/sec ft ty=0.0498 #/sq ft V_c=2.74 ft sec				%*	Mud #2 Wt=10.75 #/gal n=0.0213 #/sec ft ty=0.167 lbs/sq ft V_c=5.5 ft/sec					%*	Water		
			Calculated Turbulent Cutting Slip Velocity (ft/sec)	Observed Cutting Slip Velocity—(ft/sec)				Calculated Laminar Cutting Slip Velocity (ft/sec)	Observed Cutting Slip Velocity—(ft/sec)					Observed Cutting Slip Velocity—(ft/sec)		
Diam. (Inches)	Thickness (Inches)	Volume (Cu. In.)		Mud Vel. 4.75–4.77 ft/sec	Mud Vel. 3.78–3.96 ft/sec	Mud Vel. 2.84–2.96 ft/sec			Mud Vel. 4.68–4.70 ft/sec	Mud Vel. 4.04–4.15 ft/sec	Mud Vel. 3.24–3.34 ft/sec	Mud Vel. 1.72 ft/sec		Mud Vel. 4.91 ft/sec	Mud Vel. 3.47–4.40 ft/sec	Mud Vel. 2.04–2.06 ft/sec
1	½	0.392	1.07	.99	1.20	1.34	— 9.35	0.40	0.15	0.625			+12.6	1.55		
1	9/32	0.220	0.97	.93			+ 4.3	0.20			0.83		—76.0		1.16	
27/32	7/16	0.245	0.98	1.02			— 3.92									
27/32	7/32	0.122						0.12			0.62		—80.6		1.07	
23/32	11/32	0.139	0.87		1.02	1.04	—15.5	0.17	+0.04	0.24	0.20		+30.7	1.36		
23/32	6/32	0.076	0.80		.55		+45.5								0.91	
19/32	5/16	0.0865	0.80		.83		— 3.62	0.12	+0.385	+0.135			Out	1.33		
19/32	5/32	0.0433	0.70		.65		+ 7.70								0.870	
5/8	3/32	0.0288						0.017			+0.025		Out			
½	¼	0.0491												1.09		
½	⅛	0.0245	0.63	.56		.49	+17.3								0.88	.90
½	1/16	0.0123	0.54	.39	.81		—10.0	0	+0.72		+0.13		Out			
⅜	⅛	0.0138	0.55		.71	.42	— 1.79	0.015			+0.31	0.29	Out	.75	.81	.82

%*Deviation of Computed Average Value From Observed Value

To illustrate the balance between varying the cutting lift ability with increased horsepower or adding chemicals to change mud properties the above example is again cited, assuming that the annular mud velocity is not limited to 4.0 ft per sec. If the net rise velocity of cuttings had to be 4.5 ft per sec, the mud in its present state would have to be pumped at a velocity of 4.5 + 0.77 or 5.27 ft per sec. Chemical treatment of the mud could raise the critical velocity to 4.8 ft per sec. With the modified mud, laminar slip velocity would be about the same as shown in the example and at a mud velocity of 4.6 ft per sec the net rise velocity requirements would be satisfied. A knowledge of the relative costs of chemicals necessary for the above treatment and of the horsepower costs of pumping at the increased rate would allow an evaluation of this type problem.

Aside from the design of muds, the information presented in this paper could be useful in the event of trouble resulting from improper removal of cuttings. With empirical equations for calculating bit cutting slip velocities it is possible to determine how the mud should be treated to decrease slip velocity thereby increasing the net rise velocity. As an example take a case where the mud can only be in laminar flow and laminar slip prevails. An increase in either rigidity or yield value would result in an increased lifting ability. Perhaps the best way to solve a case such as this would be to add a bentonitic clay, which increases both yield value and rigidity, and treat with a viscosity reducer such as caustic-quebracho when the mud became too thick to pump efficiently. The caustic quebracho would tend to decrease the yield value greatly and change the high rigidity only slightly. For cuttings in turbulent slip an increase of rigidity in the mud will decrease slip velocity and therefore increase the ability of the mud to lift cuttings.

Annular dimensions used in the field tests were much more regular than are usually found in normal drilling operations, yet it was found that the cutting return was erratic. Given an irregular shaped open hole, centrifugal forces due to drill string rotation, turbulence or eddies caused by drill pipe whip and variation in mud velocity caused by the several different outside diameters of drill string, it is doubtful in normal operations that anywhere near the accuracy of the field tests presented could be obtained in predicting cutting slip velocity. It is felt, however, that if the lowest mud velocity in the annulus is greater than the calculated slip velocity of a certain size cutting, that cutting and any others smaller than it will be lifted out. Time of lifting, however, will probably be longer than calculations will show. All the factors such as restrictions, enlargements, etc., would not alter the true slip which can be predicted by the empirical equations, but would change the path of the cutting or momentarily deposit cuttings in quiescent pockets of mud.

CONCLUSIONS

1. Slip velocity values computed by the turbulent slip equations show deviations within ±15 per cent of slip velocity values measured under actual field conditions.
2. Laminar slip equations appear to be correct; however, the limited data obtained from field observations do not warrant any definite conclusions.
3. Turbulence due to restrictions, drill pipe vibration and rotations, etc., may tend to alter the path of cuttings moving upward in the annular space, causing errors in the prediction of cutting travel time. The ability of a mud to effectively lift cuttings is not affected by these factors, however, and if the annular mud velocity is greater than the calculated slip velocity, cuttings of a desired size will all be lifted and none allowed to settle back down the hole.
4. Results of field trials show that these slip velocity equations will be a useful tool in the overall design of mud systems. Use of these equations will enable determination of the most efficient pump speed for maximum cutting carrying capacity, and make it possible

Table VI

Summary of Cutting Slip Velocities — Test No. 2

Diameter (Inches)	Thickness (Inches)	Volume (Cu In)	Mud #1 Wt.=10.3 lbs/gal n=0.00128 lbs/sec ft ty=0.00154 lbs/sq ft V_c=0.508 ft/sec				% Deviation of Computed Average Value From Observed Value	Mud #2 Wt.=10.2 lbs/gal n=0.00141 lbs/sec ft ty=0.00767 lbs/sq ft V_c=1.055 ft/sec			% Deviation of Computed Average Value From Observed Value
			Calculated Turbulent Cutting Slip Vel. (ft/sec)	Observed Cutting Slip Velocity—(ft/sec)				Calculated Turbulent Cutting Slip Vel. (ft/sec)	Observed Cutting Silp Velocity—(ft/sec)		
				Mud Vel. 4.94—5.04	Mud Vel. 3.73	Mud Vel. 2.75			Mud Vel. 5.04	Mud Vel. 3.54	
1	1/2	0.392	1.11	1.11	1.35		− 9.75	1.13	1.29		−12.40
1	9/32	0.220	1.02	0.91	1.06		+ 3.56	1.02	0.98		+ 4.08
23/32	3/8	0.152	0.96	0.92	1.12		− 6.80	0.97	1.07		− 9.35
23/32	3/16	0.076	0.87	0.63	0.70		+30.8	0.88	0.74	0.75	+18.10
19/32	5/16	0.0865	0.88	0.85	1.12	1.26	−17.8	0.90	1.06	1.05	−14.7
19/32	5/32	0.0433	0.81	0.61	0.70	0.79	+15.70	0.82	0.70		+17.1
5/8	3/32	0.0288	0.73	0.77	0.96		−15.60	0.74	0.67		+10.45
1/2	1/4	0.0491	0.82	0.76	0.87		+ 0.62	0.81	0.817		− 0.86
1/2	1/8	0.0245	0.72	0.47	0.62		+32.2	0.71	0.62	0.69	+ 8.40
1/2	1/16	0.0122	0.63	0.59	0.60		+ 5.9	0.62	0.61	0.70	− 5.35
3/8	1/8	0.0138	0.64	0.46	0.65	0.72	+ 4.92				

to see how changing the mud flow properties by chemical treatment can aid in the removal of bit cuttings from the well.

ACKNOWLEDGMENT

The authors wish to express their appreciation to the Management of the Stanolind Oil and Gas Co. for permission to prepare and publish this paper, although it is recognized that the granting of such permission does not necessarily imply that Stanolind has incorporated or will incorporate these findings into its operating practice.

NOMENCLATURE

A = cross sectional area of cutting (perpendicular to direction of slip), sq ft
C_R = coefficient of resistance (particle slip), dimensionless
D = particle diameter, ft
D_e = equivalent particle diameter ($2 R_n$), ft
D_p = pipe diameter, ft
f = Fanning friction factor, dimensionless
F = force causing slip, lb ft/sec/sec
g = acceleration of gravity, ft/sec/sec
L = pipe length, ft
n = rigidity, lb/sec/ft
ΔP = pressure drop, lb/sq ft
ρ_m = mud density, lbs/cu ft
ρ_s = bit cutting density, lbs/cu ft
R = retarding force, lb ft/sec/sec
R_n = nominal radius, equal to radius of sphere of volume equal to that of the particle, ft
Re = Reynolds number, dimensionless
t = particle thickness, ft
t_y = yield value, lbs/sq ft
μ = viscosity, lbs/ft/sec
Vol. = particle volume, cu ft
V_c = critical velocity, ft/sec
V_m = mud velocity, ft/sec
V_s = particle slip velocity, ft/sec
x = empirical slip velocity factor for laminar slip, dimensionless.

REFERENCES

1. Wadell, H., "The Coefficient of Resistance as a Function of Reynolds Number for Solids of Various Shapes," *Journal of the Franklin Institute*, 217, (1934), 459-490.
2. Schmiedel, J., "Experimentelle Untersuchungen uber die Fallbewegung von Kugeln, Und Schieben in rechenden Flussigkeiten," *Physikalische Zeitschrift* Bd XXIX p. 605 (1928).
3. Pernolet, V., "A l'étude des préparations mechaniques des mineraux, ou expériences propres a établir la théorie des differént systemes usités ou possibles," *Annales des Mines*, 4 MD Series XX, (1851) p. 390.
4. Schulz, P., "Neue Bestiminungen de Konstanten de Tallgesetze in der nassen Aufoereitung mit Hilfe der Kinematograph and Betrachtungen uber das Gleichfalligkeitsgesetz," Doktor Ingenieurs Dishertation.
5. Sacks, V. K., "Technischen Hochschule ye Dresden in Verbindung mit der k. Sachs," Bergakademic yu Treiberg, (1914).
6. Richards, R. H., "Velocity of Galena and Quartz Falling in Water," *Trans.* AIME, 38, (1907), p. 219.
7. Bingham, E. C., *Fluidity and Plasticity*, McGraw-Hill, (1922).
8. Pigott, R. J. S., *Mud Flow in Drilling*, API Drilling and Production Practice, (1941), 91-103.
9. Beck, R. W., Nuss, W. F., and Dunn, T. H., "The Flow Properties of Drilling Muds," API *Drilling and Production Practice*, (1941), 9-22.
10. Thompson, H. M., Taliaferro, S. L. Basenburg, C. O., Nuss, W. F., "Application of Plastic Flow Studies to Mud Circulating Systems on Drilling Wells", Stanolind West Texas Drilling Research Report No. 2, October 15, 1947.

★ ★ ★

Discussion

By C. L. Prokop, Production Research Division, Humble Oil and Ref. Co., Houston, Texas

The authors have presented an interesting paper which should be a definite contribution toward a more thorough understanding of the factors which determine the carrying capacity of a drilling fluid.

The paper discusses the velocity distribution which exists across a mud stream flowing in laminar flow. In a low gel strength mud moving in laminar flow the velocity of the mud near the wall of the hole is very low. As one goes from the well out into the hydraulic center of the annulus the upward mud velocity will increase until it reaches a maximum of about 1½ times the average. After passing the center it again decreases to a very low value as one approaches the drill pipe. It is in this region of laminar flow that the calculated settling velocities showed their greatest deviation from those observed in the field tests. As Hall points out this should be expected because of the velocity distribution and the irregular flow channels that the mud may follow. These discrepancies may merit some attention as similar experiments have shown that a mud possessing a low gel strength and moving in turbulent flow often will be more effective in keeping a hole entirely clear than will the same mud made somewhat more viscous and flowing in laminar flow. It is true that particle slip velocities will be lower in the more viscous mud but the evidence is that a large number of cuttings may lodge in the hole. These particles which became stuck in the more or less stagnant portions of the mud stream near the hole wall will have little or no tendency to be thrown back into the moving stream. For this reason erratic cutting velocities in laminar flow may be the rule rather than the exception. In contrast a turbulent mud stream has a more constant velocity throughout its cross-section and probably washes the wall fairly clean of debris.

Whether or not these differences between laminar and turbulent flow would be sufficient to cause a dangerously large number of cuttings to collect in the hole would probably depend upon drilling conditions, but acknowledgment should be made of their presence.

★ ★ ★

THE PRESENCE OF CONDUCTIVE SOLIDS IN RESERVOIR ROCKS AS A FACTOR IN ELECTRIC LOG INTERPRETATION

H. W. PATNODE AND **M. R. J. WYLLIE,** GULF RESEARCH AND DEVELOPMENT COMPANY,
PITTSBURGH, PENNSYLVANIA

INTRODUCTION

In the quantitative interpretation of electric log data it is essential to know the formation factor, defined as the ratio of the resistivity of the formation 100 per cent saturated with brine to the resistivity of the brine.[1] This concept implies that the formation factor for any given rock is constant irrespective of the resistivity of the brine or solution with which it is saturated. It is apparent that this can be true only when the rock matrix is wholly non-conductive. As reservoir rocks may contain clay or shale having an appreciable conductance one may expect these constituents to influence the determination of true formation factor.

The formation factor may be theoretically derived from log data by dividing the resistivity of the mud filtrate invaded formation by the resistivity of the mud filtrate. Such a method of calculation has implicit in it the assumption that the fluids in the invaded formation are wholly replaced by mud filtrate, that the solid matrix is non-conducting, and that the formation factor of the invaded zone is identical with the formation factor of the uninvaded zone. Since the validity of the first two basic assumptions regarding the insulating character of porous matrices and the displacement of the interstitial fluids in porous media do not appear to be fully established, the formation factors of a number of cores and clay slurries have been measured under conditions suitable for verifying the assumptions and the extent of any errors inherent in them.

CORE STUDIES

Apparatus and Procedure

Resistivity measurements were made on short cylindrical permeable cores which had been previously mounted in lucite.[2] The cores were clamped by means of insulated bolts between brass plates about 5 cm square and 1 cm in thickness. The plates were provided with a ring seal to prevent leakage between them and the core mount, and had a centrally located orifice so that fluids could be flowed through the mounted core. The brass mounting plates were used as electrodes and any current flow between them necessarily passed only through the constituents of the intervening core.

Fluid saturation of the core, and fluid flow through the core, were effected by a centrifugal pump connected to the outflow end of the core, thus providing a differential pressure across the core of approximately one atmosphere.

The procedure used was first to evacuate each core by means of the pump and then to saturate the core with an aqueous sodium chloride solution of known resistivity. The resistance of the core was measured and flow of the solution through the core continued for sufficient time to establish a constant resistance reading. After equilibrium had been reached with one solution, another sodium chloride solution of a different resistivity was flowed through the core and the flow continued until a constant resistance reading was again obtained. This procedure was continued until resistance measurements of the core had been made with a series of solutions within a salinity range from 1.0N NaCl to distilled water.

The data obtained enabled the apparent formation factor of given porous rocks when saturated with fluids of different resistivity to be computed and also provided information regarding the ability of an invading fluid to displace interstitial water from a core.

Results

Berea Sandstone — The first core examined was a specimen of Berea sandstone.* This core had been cut essentially parallel to the bedding for permeability studies. The core was clamped in the core holder and saturated with 1.0N NaCl solution and the resistance determined. It was subsequently flushed and the resistance measured when saturated in turn with 0.1N, 0.025N, 0.01N, .005N sodium chloride solutions and finally with distilled water. In flushing the core with each

---

[1] References are given at end of paper.

Manuscript received at the office of the Petroleum Branch October 4, 1949. Paper presented at the Petroleum Branch meeting in San Antonio, October 5-7, 1949.

* All cores used were about 5 cm. in length and 2.75 cm in diameter.

solution, a large number of pore volumes was passed in each case and the saturated core allowed to rest for periods of 12 to 24 hours to insure mixing by diffusion of the saturating solution with any remaining unflushed solution of a different salinity. It was found that this precaution was unnecessary as, in accord with previous findings,[3] essentially all of the saturating fluid is flushed by the first few pore volumes of invading fluid.

It became evident from the resistance measurements that the calculated formation factor of the core was not independent of the resistivity of the saturating solutions, the calculated formation factor decreasing as the resistivity of the saturating solution was increased. It was apparent that current was being conducted through the core in part by some medium other than the saturating solution. Such conduction could be attributed to certain solid constituents in the rock and presumably to wet clay components in the form either of disseminated particles or shale streaks. Inspection of the data indicated that the total conductance of the core in each case appeared to be equal to the sum of the conductance of the solids and the conductance of the saturating solution. Calculations showed that the relationship was being followed and established that the conductivity of the solid materials was essentially constant, irrespective of the conductivity of the saturating solution.

The data and calculations for the Berea core are given in Table I. The true formation factor, F, may be defined as the formation factor that the core would have if none of the solid materials were conductive. The true formation factor thus expresses the texture of all the solid constituents of the rock. The apparent formation factor, Fa, is the measured resistivity of the core, ρ_{wa}, divided by the resistivity of the fluid with which it is saturated, ρ_c. The apparent formation factor becomes smaller as the resistivity of the saturating fluid is increased since the effect of the parallel resistance resulting from conducting solids then becomes relatively greater. Thus, a good value for true formation factor can be obtained by saturating cores with solutions of very low resistivity when making a measurement of formation factor. The values given for the resistivity of the core, ρ_{wa}, the resistivity due to the conductive solids as distributed in the core, ρ_f, and the resistivity of the fluid as distributed in the core, ρ_w, are computed from the relationship:

$$\frac{1}{\rho_{wa}} = \frac{1}{\rho_f} + \frac{1}{\rho_w} = \frac{1}{\rho_f} + \frac{1}{F\rho_c} \quad . \; . \; . \; . \quad (1)$$

The relatively good agreement between the measured and computed values of ρ_{wa} when ρ_f is a constant demonstrates the essential validity of this relationship.

Stevens Sandstone — In order to investigate further the effect of conductive solids in reservoir rocks, a core of Stevens sandstone from the Paloma field, California was obtained. This core was selected because of its known high clay content, it being thought that the specimen would have a relatively high solid conductivity as a result of the clay constituents.

The core was extracted to remove residual oil, and then mounted and saturated with solutions of different resistivity in a manner identical to that employed with the Berea sandstone. Data relating to the core of Stevens sandstone are given in Table I. The relatively close agreement between the measured and computed values of ρ_{wa} is apparent. The computed resistivity is based on a resistivity for the conductive solids, ρ_f, of 35.7 ohm-meters, and a true formation factor of 30.6.

Because of the high clay content, the actual permeability of the Stevens core to water was very low. Consequently, it was not practicable to flush this core with large volumes of solution as was done with the Berea core, only about three pore volumes being flowed before each measurement was made. Somewhat closer agreement between the calculated and measured resistivities might have been obtained had greater volumes of solution been flowed to insure more complete replacement of the interstitial solution by the invading solutions.

Nichols Buff Sandstone — The effective conductivity of the solid materials in a core of relatively clean Nichols Buff sandstone was determined. The core was saturated in turn with 1.0N sodium chloride solution and distilled water. The data for this core are given in Table I. The resistivity, ρ_f, of the conductive solid constituents is high, being 2230 ohm-meters, and the calculated formation factor is 18.4.

Alundum — In order to establish whether or not any of the conductivity attributed to solid conductive material in cores was actually due, in part, to ineffective flushing of fluid in the core by the invading fluids, the conductivity of an alundum core when saturated with different solutions was determined. It was found that the formation factor

Table I

Measured and Calculated Data for Rock Cores With and Without Conductive Solids

Core	F	Fa	ρ_c	$\rho_w = F\rho_c$	ρ_f	ρ_{wa} Measured	ρ_{wa} Computed
Berea SS	23.3	22.7	0.119	2.8	250	2.70	2.75
	23.3	20.8	0.97	22.6	250	20.2	21.0
	23.3	16.6	3.45	80.5	250	57.3	61.0
	23.3	13.0	8.21	191	250	107	108
	23.3	9.5	16.7	389	250	158	158
	23.3	0.08	3215	74919	250	246	249
Stevens SS	30.6	27.7	0.119	3.64	35.7	3.30	3.30
	30.6	13.5	0.97	29.6	35.7	13.1	16.0
	30.6	6.5	3.45	105.5	35.7	22.5	26.0
	30.6	1.9	16.7	511	35.7	32.0	32.3
	30.6	0.013	3215	98379	35.7	43.8	35.7
Nichol's Buff SS	18.4	18.4	0.126	2.32	2230	2.32	2.32
	18.4	0.7	2970	54650	2230	2140	2140
Alundum	12.4	12.4	0.119	1.47	∞	1.47	1.47
	12.4	12.4	8.21	10.2	∞	10.2	10.2

All resistivities in ohm-meters

of the core was constant when saturated with either 1.0N NaCl or .01N NaCl solutions, and that the first few pore volumes of the invading fluid appeared to replace all of the solution with which the core was saturated. The conductivity of the solids constituting the alundum core was thus zero, and the formation factor calculated at 12.4. The data for the alundum core are given in Table I.

Discussion

The results obtained demonstrate that reservoir rocks which contain wet clay or other conductive solids may have appreciable conductivity as a result of the presence of these materials, in addition to the conductivity of the pore water. In the cores examined the total measured conductivity is equal to the sum of the conductivity of the water in the pores and the conductivity of the solid material. It was found that the conductivity of the solid material in each core was essentially constant irrespective of the conductivity of the fluid which occupied the pores.

The number of pore volumes of solution necessary to displace effectively the original interstitial fluid in the cores appears to justify the assumption for a water sand that in the invaded zone surrounding the borehole the original connate water has been substantially 100 per cent replaced by mud filtrate. In the case of invasion of an oil sand an irreducible amount of oil must, of course, remain undisplaced.

SLURRY STUDIES

Although the relationship $1/\rho_{wa} = 1/\rho_f + 1/\rho_w$ was found to hold for the four cores examined, further study of the relationship with core material was not practicable because the only parameter that could be varied in any given core was the resistivity of the saturating solution. As mud slurries are analogous to porous rock and the type and quantity of the components may be varied at will, a series of mud slurries were prepared, and their properties measured. From these data further information regarding the above relationship was obtained.

Apparatus and Procedure

A large number of aqueous slurries were made using waters of different resistivity and various proportions and volumes of commercial grade fuller's earth* and powdered silica. As silica is non-conductive and fuller's earth has an appreciable conductance when wet, the effective conductivity of the solid constituents could be varied as well as the conductivity of the fluid.

Fuller's earth was used as the conductive solid principally because it is not readily dispersed and the flocculated clay settles out of suspension rather rapidly, thus expediting the experiment. Any other conductive clay material having this property would have been equally satisfactory.

The procedure for investigating the slurries was as follows. Known volumes of solids and fluid were placed in a glass tube 30 mm in diameter and 50 cm in length, the tube being closed at one end. After addition of the materials (whose volume never exceeded about one-half the capacity of the tube), the open end of the tube was closed by a rubber stopper through which was inserted a dipping-type resistivity cell having platinized platinum electrodes. The slurry was agitated thoroughly, and the tube then clamped vertically to allow the solids to settle. The slurry was then reduced to the desired volume by pipetting off part of the supernatant fluid. The resistance of this fluid (or filtrate), and the resistance of the slurry in the tube was then determined with the resistivity cell using a Kohlrausch bridge and telephone. The resistances were corrected to resistivities by multiplying by the cell factor. All resistance measurements were made at room temperature, i.e., about 26°C. The data given in Tables II, III and IV are measured resistivities and the relatively small corrections necessary to relate them to a constant temperature have not been made.

Results

In Table II are given the measured and calculated data for three slurries which are identical except that the resistivity of the solution in each slurry was different. The solid constituent in each case was fuller's earth. As in the cores already discussed, the resistivity of the fluid was the only parameter that was varied, and the calculated resistivity of the solid phase is essentially constant. While the true formation factor is

Table II

Data for Different Slurries Having a Constant Volume of Conductive Solids

Percent solids by volume, (1—P).100	5.72	5.72	5.72
Water resistivity, (ρ_c)	16.32	81.3	199.0
Apparent formation factor, (F_a)	1.096	0.57	0.308
Formation factor, $(F = P^{-1.6})$*	1.099	1.099	1.099
Measured resistivity of slurry, (ρ_{wa})	14.9	46.4	61.4
Resistivity of solid phase, (ρ_f)	85.5	96.7	85.5
True resistivity of slurry, $(\rho_w = F\rho_c)$	18.0	89.5	219

All resistivities in ohm-meters

---

* A value of 1.6 for slurries of this type was reported previously by H. W. Patnode.[4]

Table III

Data for Slurries Having Different Volumes of Conductive Solids and Constant Fluid Resistivity

Percent solids by volume (1—P).100	1.786	2.221	2.843	4.350	5.72	7.28
Water resistivity (ρ_c)	199.0	199.0	199.0	199.0	199.0	199.0
Apparent formation factor (ρ_{wa}/ρ_c)	0.714	0.584	0.476	0.389	0.308	0.257
Formation factor $(F = P^{-1.6})$	1.029	1.037	1.047	1.073	1.099	1.129
Measured resistivity of slurry (ρ_{wa})	142.0	116.0	94.7	77.5	61.4	51.1
Resistivity of solid phase (ρ_f)	461	264	177	121.5	85.5	66.0
True resistivity of slurry $(\rho_w = F\rho_c)$	204.6	206.2	208.2	214.0	218.8	224.5

All resistivities in ohm-meters

---

* Raw attapulgite clay.

constant, the apparent formation factor decreases as the water resistivity increases.

The data given in Table III are for a series of slurries made with fuller's earth in which the solution resistivity was kept constant and the per cent solid material, and consequently the formation factor, was varied. The data show the effective decrease in the resistivity of the slurry and consequent decrease in apparent formation factor as the percentage of conductive solids in the slurry is increased. Data from this table, plotted in Fig. 1, show an apparent linear relationship between per cent solids by volume and the conductivity of the solid phase for a series of slurries having a constant solution resistivity. A linear relationship indicates that the conductivity of a unit volume of the clay is constant irrespective of the total volume of clay in the slurry.

Table IV gives the data for a representative series of slurries containing both conductive and nonconductive solids, the percentage of conductive solids by volume varying from 22.8 to 100 per cent. In this series, measurements were first made on a slurry containing only fuller's earth followed by measurements of the slurry modified by adding increments of powdered silica. The value for resistivity of the conductive solids, ρ_s, given in the table is that calculated by application to these data of the relationship:

$$\frac{1}{\rho_{wa}} = \frac{N^x}{\rho_s}\left(1 - \frac{1}{F}\right) + \frac{1}{F\rho_c} \quad . \quad (2)$$

where, ρ_{wa} = resistivity of slurry,
ρ_s = resistivity of conductive solids,
N = fraction of solids, by volume, that are conductive,
x = an arbitrary exponent,
F = true formation factor,
ρ_c = resistivity of solution.

The validity of the relationship is shown by the relative constancy of the calculated value of ρ_s given in Table IV. Besides the data given, this relationship was further confirmed by calculations on eleven additional slurries. The value of the exponent, x, was found to be approximately equal to one, doubtless because of the rather uniform distribution of the conductive and nonconductive solids.

It should be recognized that the calculated resistivity of the fuller's earth, ρ_s, is only a relative value and is not a value for the resistivity of the clay when dry. The conductivity of the clay when in an aqueous system results in part from dissociation of the clay minerals. This dissociation is a function of the number and types of exchangeable ions on the clay, the extent of dispersion of the clay, the particle size, and other factors. The calculated value of conductivity is thus only a true value for the particular conditions under which the resistivity measurements are made.

EFFECT OF CONDUCTIVE SOLIDS ON LOG INTERPRETATION

True Formation Factor

It is clear that if reservoir rocks contain conductive solids the formation factor calculated from the ratio of the resistivity of the invaded zone, ρ_i, to resistivity of the mud filtrate, ρ_{mf}, (or the more common relation for a water sand, ρ_w/ρ_c where ρ_w = true resistivity of the sand and ρ_c = resistivity of the connate water), is an apparent formation factor which may differ considerably from the true formation factor.

It is an essential for reliable log interpretation that the true formation factor be obtained. For 100 per cent water-bearing sands an expression for the true formation factor may be derived from log data as follows:

Since ρ_f has been shown to be constant, we have,

$$\frac{1}{\rho_{ia}} = \frac{1}{\rho_f} + \frac{1}{\rho_i} = \frac{1}{\rho_f} + \frac{1}{F\rho_{mf}}$$

$$\frac{1}{\rho_{wa}} = \frac{1}{\rho_f} + \frac{1}{\rho_w} = \frac{1}{\rho_f} + \frac{1}{F\rho_c}$$

By difference,

$$F = \frac{(\rho_{mf} - \rho_c)\,\rho_{wa}\,\rho_{ia}}{(\rho_{ia} - \rho_{wa})\,\rho_c\,\rho_{mf}}$$

Where, ρ_{mf} = mud filtrate resistivity,
ρ_c = formation water resistivity,
ρ_w = true resistivity of the water-bearing formation (with solid conduction eliminated),
ρ_{wa} = true resistivity of the water-bearing formation from log data,
ρ_{ia} = true resistivity of invaded zone from log data,
ρ_i = true resistivity of the invaded zone (with solid conduction eliminated,
F = true formation factor.

The true formation factor of oil or gas-bearing reservoirs containing conductive solids cannot be calculated in this manner since the presence of hydrocarbons precludes a value for ρ_{wa} being obtained directly from the log. The true formation factor of such reservoirs must be extrapolated from adjacent water sands or from the reservoir rock below the oil-water contact if such a contact exists. Such an extrapolation must first be justified in the light of geologic conditions.

Resistivity Index

The resistivity index of a formation will also be modified by the presence of conductive solids. For example, the resistivity of the Stevens sandstone considered above theoretically could not exceed 37.5 ohm-meters, even in the event of all the available pore space be-

Table IV

Data for Slurries Containing Different Percentages of Both Conductive and Nonconductive Solids

Percent solids by volume (1—P).100..	4.350	5.41	7.74	10.90	13.85	16.65
Percent solids that are conductive, N.	100	79.7	54.2	37.1	28.2	22.8
Water resistivity (ρ_c)...............	57.5	53.4	51.6	46.9	44.1	42.5
Apparent formation factor, Fa.......	0.813	0.845	0.847	0.924	0.998	1.06
Formation factor ($F=P^{-1.6}$).........	1.073	1.093	1.138	1.203	1.269	1.339
Measured resistivity of slurry (ρ_{wa})...	46.7	45.9	43.8	43.3	42.8	45.0
Resistivity of solid phase (ρf)........	217	215	211	202	187	215
True resistivity of slurry ($\rho_w=F\rho c$)...	59.6	58.5	58.6	55.3	55.8	56.8
Resistivity of conductive solids (ρ_s)...	14.7	14.7	13.7	11.7	11.0	12.4

All resistivities in ohm-meters

ing occupied by oil. Thus the maximum apparent resistivity index of this formation will also be relatively small.

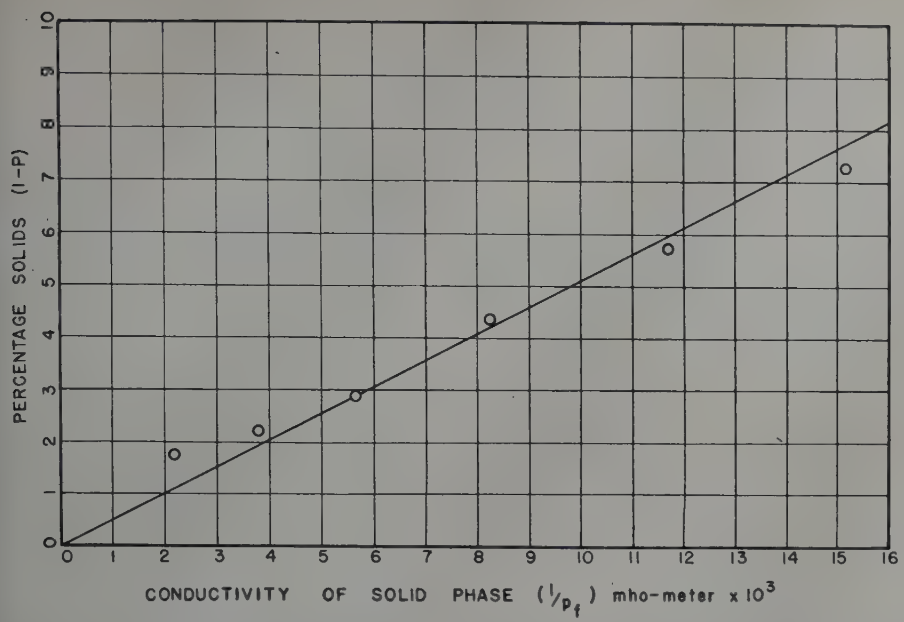

FIG. 1 — RELATIONSHIP BETWEEN VOLUME OF CONDUCTING SOLIDS AND APPARENT SOLID CONDUCTIVITY IN AQUEOUS SLURRIES OF CONSTANT SOLUTION RESISTIVITY.

The water saturation-resistivity index relationship for the Stevens sandstone core examined is shown in Fig. 2, when $\rho_c = 0.3$ ohm-meters, $\rho_f = 37.5$ ohm-meters and $F = 30.6$. The curves are drawn on the assumption that the resistivity index $= 1/S^n_w$ where $n = 2$, the value customarily assumed in log interpretation. The upper curve is the one obtained if there are no conductive solids or if the influence of conductive solids is eliminated by computation. The lower curve is based on the formation resistivities at various saturations which would obtain if the effect of conductive solids were ignored, and is calculated from the data given above. It may be noted that one effect of conductive solids is to give a resistivity index-saturation curve which could be interpreted in terms of variable and spuriously low values of the index n.

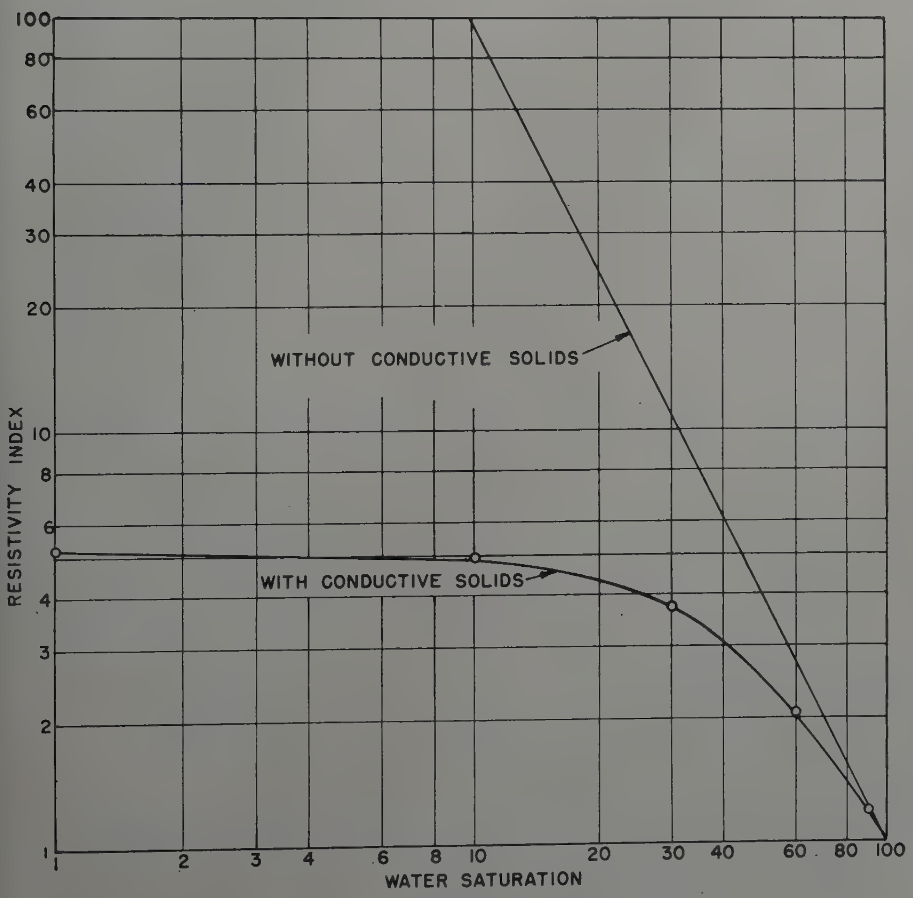

FIG. 2 — EFFECT OF CONDUCTIVE SOLIDS ON THE RESISTIVITY INDEX-SATURATION RELATIONSHIP IN STEVENS SANDSTONE CORE, ASSUMING $\rho_t/F\rho_c$ = SATURATION^{-2}.

CACULATION OF AMOUNT OF CONDUCTIVE SOLIDS IN FORMATIONS

In consideration of the relationship found for reservoir rocks discussed above, there appears to be no theoretical objection to extending the relationship established for slurries to include reservoir rocks. If this is true, a figure expressing the approximate percentage of shale or clay in reservoir rocks can be calculated in those cases where the electric log data permit the derivation of the true formation factor, F, the resistivity of the conductive material as distributed in the core, ρ_f, and the resistivity of the shale or clay in the formation, ρ_s. The latter resistivity may be assumed, to a first approximation, as the resistivity of the shales in the section adjacent to the sand investigated.

For example, using the value of $\rho_f = 37.5$ ohm-meters for the Stevens sandstone obtained above and taking the average value of 2 ohm-meters from electric logs as the resistivity of adjacent shale, the calculated per cent of solids in the core that are conductive is found to be 5.6 per cent by volume if Equation (2) is used. It is assumed that the distribution of conductive and nonconductive solids is such that $x \approx 1$. The extent of the variation of x for rocks and the practical applicability of Equation (2), has not yet been established.

SUMMARY

Several cores of reservoir rocks and a large number of slurries were studied and it was found that when conductive solids, such as wet clays, are present in the cores the calculated or apparent formation factor is less than the true formation factor. The true formation factor is defined as the formation factor that the rock would have if none of the solids in it were conductive. The apparent formation factor is thus not constant but decreases as the resistivity of the saturating fluid is increased.

It was established that the over-all conductivity of a core is the sum of the quotient of the true formation factor and the conductivity of the interstitial fluid and the apparent conductivity of any conducting solid material as distributed in the core. The conductivity of conducting solid materials appears to be essentially independent of the conductivity (salinity) of the interstitial fluid in the core.

Attention is called to the errors which may be made in the determination of formation factor and resistivity index from electric log data if the effects of conductive solids are not considered.

A method of determining the approximate quantity of conductive solids present in reservoir rocks when basic data can be obtained from the electric log is proposed and an example given.

ACKNOWLEDGMENTS

The writers thanks go to Paul D. Foote, executive vice-president, Gulf Research and Development Co., for permission to publish this paper and Ben B. Cox, director, Geology Division, for his help and encouragement in carrying out this work.

REFERENCES

1. G. E. Archie: "The Electrical Resistivity Log as an Aid in Determining Some Reservoir Characteristics." AIME Tech. Pub. 1422, *J. of Petr. Tech.* (January 1942), 5, (1), 8 pp. Also *Trans.* AIME (1942), 146, 54-62.
2. J. H. Henderson and S. T. Yuster: "Studies in Relative Permeability." *World Oil* (1948), 127, (12), 139.
3. R. G. Russell, F. Morgan and M. Muskat: "Some Experiments on the Mobility of Interstitial Waters." AIME Tech. Pub. 2054 (July 1946).
4. H. W. Patnode: "Relationship of Drilling Mud Resistivity to Mud Filtrate Resistivity." AIME Tech Pub. 2512, *J. of Petr. Tech.* (January 1949), 1, (1), 3 pp.

★ ★ ★

T.P. 2795

SQUEEZE CEMENTING OPERATIONS

GEORGE C. HOWARD, MEMBER AIME, AND **C. R. FAST,** STANOLIND OIL AND GAS CO., TULSA, OKLAHOMA

ABSTRACT

Laboratory and field testing of various squeeze cementing techniques and materials revealed that many improvements could be made in squeeze cementing operations. The use of a slow-pumping squeeze cementing procedure permitted the control of the quantity of cement displaced into a formation and aided in obtaining a high final squeeze pressure. Field testing indicated the desirability of obtaining high final squeeze pressures, the need for improved formation breakdown fluids, and the necessity of controlling the pressure differential during testing after a squeeze job.

INTRODUCTION

During the past few years, squeeze cementing operations have been investigated, both from the theoretical as well as the practical point of view, in an effort to arrive at some solution to the many and varied problems that arise with this type of operation. A review of well files indicated that in many instances, wells were being squeeze cemented four and five times before a satisfactory pressure buildup was obtained. There seemed to be considerable variation in opinion as to the proper method of squeeze cementing, as well as disagreement as to the proper breakdown agent, the quantity of cement that should be used, type retainer and length of WOC* time that was necessary. Consequently, it was deemed advisable to approach this problem theoretically, field testing each idea developed in hopes of eventually arriving at a squeeze cementing procedure that would give reasonable assurance of a successful job after one squeeze cementing operation. This investigation was, therefore, divided into two broad headings: (1) Preliminary studies, which include both theoretical and laboratory studies, and (2) Field investigations to determine the proper squeeze cementing methods.

PRELIMINARY STUDIES

Overburden Pressure Studies

Squeeze cementing problems are so intimately related to the earth's overburden pressure that solutions to them are very difficult, if not impossible, without an understanding of the nature and magnitude of the overburden pressures encountered at the depths of producing wells. It was thus felt that the first approach to research on squeeze cementing should be made through a study of these pressures.

Since there has been rather loose usage of a number of the terms related to overburden pressure by different writers, the terms to be subsequently used are defined here.

Theoretical overburden pressure is the calculated pressure at any given depth exerted by the theoretical weight of overlying formations as calculated from the average rock density.

Fluid displacement pressure is that pressure at which fluid can be injected into a formation after it has been broken down. It may be more or less than the theoretical overburden pressure.

Formation breakdown pressure is that pressure at which a formation parts or breaks and is usually thought of as fluid displacement pressure plus rock strength.

Breakdown agent is that fluid with which the formation is fractured.

The first step in the study of the earth's overburden pressures involved a review of pertinent technical literature. The general opinion expressed was that the overburden pressure gradient of the earth's formations is roughly 1.0 psi per foot of depth, and that application of sufficient pressure to stratified formations will cause them to part at or parallel to the bedding planes.

The second step in the study of overburden pressures involved a study of available well data in an effort to obtain some definite information as to the actual values experienced in the field for the above mentioned terms. Data from 115 cement squeeze jobs in the Gulf Coast area and 46 cement squeeze jobs and acid jobs in the West Texas-New Mexico area were closely analyzed.

The analysis of these data showed that the average formation breakdown

---

Manuscript received at the office of the Petroleum Branch September 29, 1949. Paper presented at the Petroleum Branch meeting in San Antonio, October 5-7, 1949.

* Waiting on cement.

pressure prior to squeeze cementing was less than 1.0 psi/ft of depth. The fluid displacement pressures, however, varied so greatly with depth due to structural stresses in the earth and elasticity of the earth's formations, that they could not be defined in general terms. For example, they were found to vary from 0.75 to 1.11 psi/ft at 2,000 ft, and from 0.57 to 0.85 psi/ft at 8,000 ft. Neither formation breakdown nor fluid displacement pressures varied linearly with depth. In general, it was found that the effective overburden pressure at a given depth, as determined from field data, was less than the theoretical pressure or the pressure calculated from the rock densities. This discrepancy can probably be best attributed to two factors. During the injection of fluid into a fracture in a formation, the entire overburden probably is not actually lifted by the injected fluid. The forces exerted in injecting the fluid probably tend to deform the rock in the vicinity of the fracture by a combination of bending and compressing, such that the actual overburden weight resisting deformation is measured from the formation fracture to some neutral plane well above it. The second factor tending to reduce the fluid injection pressure, as compared to the theoretical overburden pressure, is the structural position of the formations above the fracture. In some cases it is believed that the structure of the formations above the fractured section of the well bore may tend to support by beam or arch some of the weight of the overburden.

Some of the more pertinent data obtained from the review of available well files are plotted on Fig. 1, which presents the average formation breakdown pressures and average fluid injection pressures for the Gulf Coast and West Texas-New Mexico areas. Fig. 2 presents a comparison between the theoretical overburden pressures (rock density method) and the fluid displacement pressures obtained from field data. Shown also is a comparison of the corresponding overburden pressure gradients. The reasonably close agreement between the theoretical overburden pressure and the average field data at the shallow depths probably explains why many observers have concluded that 1 psi/ft of depth is applicable to deep well squeeze cementing operations.

It is interesting to note that, while the 161 wells used in the initial survey represent only a small portion of the total number of wells that have been squeeze cemented, the data obtained from these wells have been proved by subsequent field testing to be reasonably accurate, thus affording a means of estimating the breakdown and injection pressures that will be encountered during squeeze cementing operations.

While the information obtained in this theoretical investigation of pressures encountered in squeeze cementing operations did not offer any definite proof of what actually takes place down a hole, it did show that the pressures encountered on squeeze cementing jobs are sufficient to fracture and subsequently displace the fluid being squeezed out into the formation. This preliminary investigation indicated a definite need for extensive laboratory and field testing to establish whether or not cement is forced out into formations during the squeeze cementing operations. The answer to this question would permit steps to be taken to control the penetration of the cement slurry into the formation, which should increase the effectiveness of squeeze cementing operations. It was in an effort to obtain an answer to this last question that the next series of investigations was made.

Laboratory Shallow Well Experiments

During the past several years an extensive research program on squeeze cementing has been conducted with the objective of improving squeeze cementing operations. The initial portion of this program involved test work in wells at very shallow depths. A relatively hard sandstone was found a few feet below the surface in the test wells, making extensive testing of various cementing operations possible. These wells were drilled, squeezed using various techniques, and later excavated to observe the results.

Among the questions to be answered before improved squeeze cementing procedures could be recommended were:

1. Where does cement go during a squeeze job?
2. Where does cement go during successive squeeze jobs?
3. Should mud or water be used to break down formations prior to squeeze cementing?
4. Can cement be spotted at any desired elevation in the formation?
5. Will the cement that is forced out horizontally completely surround the well bore?

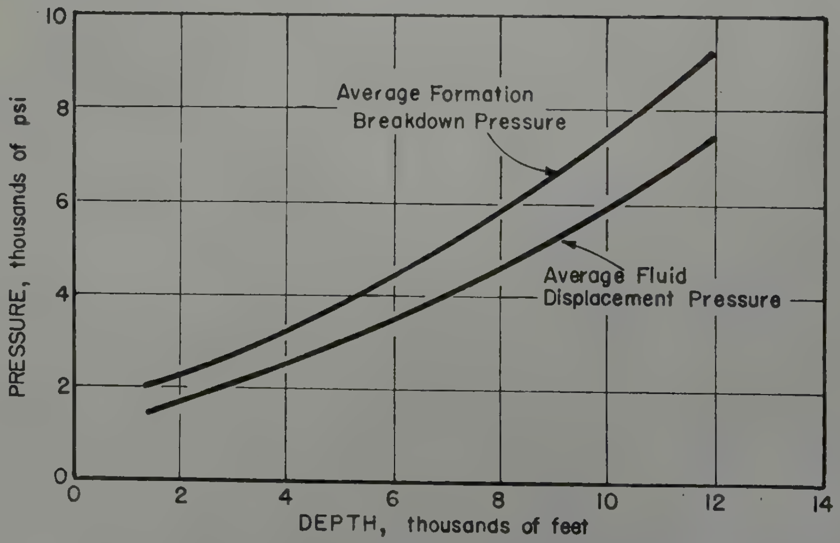

FIG. 1 — AVERAGE FIELD BREAKDOWN AND DISPLACEMENT PRESSURES.

6. Can perforations in casing be readily plugged by squeezing cement?
7. How can the quantity of cement placed out in the formation be controlled?

The ability to answer these questions by laboratory shallow well tests depended entirely upon the assumption that the results so obtained would at least reflect the behavior of cement slurries on squeze jobs at depths encountered in the field. How these shallow well tests compare with the actual behavior of cement in field practice is difficult to determine. The first impression is that, owing to the great difference in pressure at 10 ft and 10,000 ft, the behavior of cement slurries squeezed out at different levels should be entirely different. However, a comparison of the results of shallow well tests with the results obtained in coring two deep wells, discussed later in this paper, suggests that certain parts of the shallow well experiments reflect fairly accurately the actual behavior of cement slurries during field squeeze cementing operations.

The first point investigated in the shallow well tests was the question of where cement goes during a squeeze job. There are three main schools of thought on this question. One group holds that cement slurry squeezed against formations tends to compress soft sands and shales around the well bore thereby enlarging it. The pressure buildup at the end of the job is believed to be a result of maximum compaction of the formations. The second group believes that cement slurry squeezed in a well tends to follow a vertical path behind the primary cement job displacing any mud and mud filter cake present, with the pressure buildup being a result of both filling the space behind the pipe and dehydrating the cement against the formation. The third group holds that formations are fractured before injection of the cement and that the pressure buildup at the end of the job is a result of dehydration of the slurry in the fracture and about the well bore. In actual field practice probably all three schools of thought are partially valid with no one theory being entirely correct. However, shallow well experiments, that will be described later, gave evidence of only limited vertical movement of the cement slurry behind the pipe with a predominance of the cement being forced into the previously fractured formation in sheets or pancakes about the well bore.

Several shallow wells were squeeze cemented in an attempt to clarify this point. The first well was drilled to a depth of 9½ ft with 3-in. casing set at 7 ft in solid sandstone. The formation was broken down with water at a maximum pressure of 850 psi and 15 sacks of standard portland cement slurry were squeezed into the formation. A maximum squeeze pressure of 1500 psi was obtained. Before and after the squeeze cementing operations, ground elevations were taken at four stations spaced at 90° five ft from the test well. The following tabulation shows the results of this test:

Table I
Effect on Ground Elevations of Squeezed Cement

Location	Rise in Ground Elevation
Northwest of well	.430 inches
Northeast of Well	.586 "
Southwest of Well	.943 "
Southeast of Well	.860 "
Average Rise in Ground Elevation	.740 "

These data strongly indicate that the cement slurry was squeezed out in a horizontal sheet or "pancake" parallel to the bedding planes and actually lifted the overburden. This proved to be the case when this well was excavated to observe the results. A cement pancake 1½ in. to 2 in. thick, with a lateral spread of 360° around the well bore, was found just below the casing seat. This cement spread laterally from the well bore more than five ft (extent of the excavation) in all directions. Fig. 3 shows a sample of the cement pancake in a piece of the hard sandstone removed four ft from the well bore.

A total of 15 shallow wells were squeeze cemented during this series of laboratory tests, and in each case the cement spread horizontally from the well in relatively thin sheets approximately parallel to the bedding planes. If a zone of weakness such as a clay streak or bedding plane was encountered, the cement followed this zone of weakness. In some instances vertical fractures, which were generally believed to be caused by weathering, were encountered a few feet from the well bore and the cement followed these fractures. In only a few instances was any cement forced vertically between the casing cement and the formation. In these test wells only a small portion of the

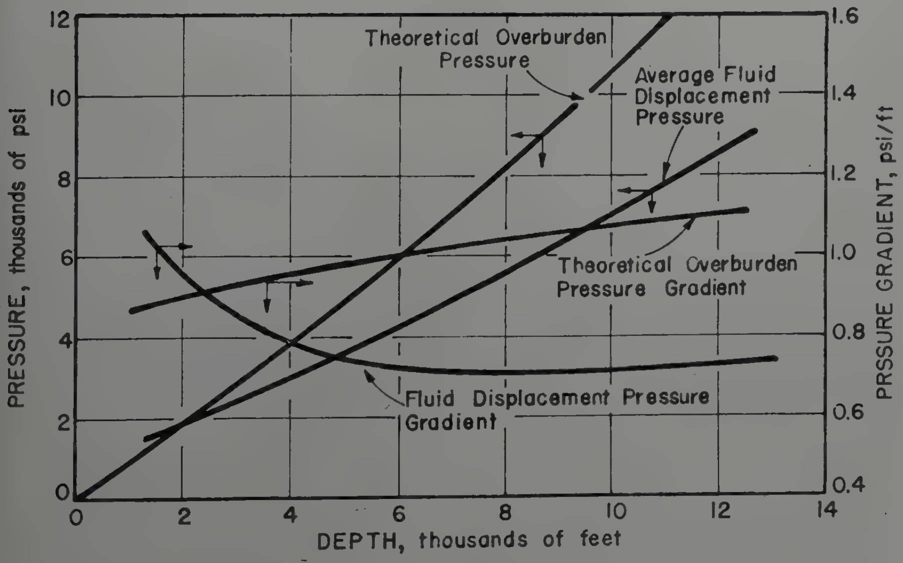

FIG. 2 — COMPARISON OF THEORETICAL OVERBURDEN AND FLUID DISPLACEMENT PRESSURES.

total cement slurry was lost in this direction, with the major portion of the cement slurry being displaced horizontally into the formation. This lack of vertical movement of cement slurry is probably accountable to the fact that good primary cement jobs were obtained in all test wells. In no case was the formation noticeably compacted or squeezed back, nor was the cement slurry forced into the interstices of the sandstone.

After determining in these shallow well tests that the majority of the squeezed cement slurry traveled in a horizontal direction from the well bore, the question arose as to where the cement goes when a well is squeezed and resqueezed at the same level. To investigate this problem a well was drilled to a total depth of 7 ft, 3-in. pipe set and cemented, and the well deepened approximately one foot. This well was squeeze cemented three times with different colored cement for purposes of identification. Red slurry was used on the first job, after breaking down with water, and nearly a cubic foot of slurry was displaced at a pressure of 50 psi before the pressure built up to approximately 500 psi. The following day the hole was cleaned out, the formation again broken down, and approximately 1½ cu ft of yellow colored cement slurry was squeezed out at 20 psi before the pressure increased to 500 psi. The third squeeze job was performed approximately four hours later after drilling out the cement plug and breaking down the formation a third time with water. Black cement slurry was squeezed into the well at 30 psi, and after 1½ cu ft of slurry had been placed, the pressure again increased to 500 psi. Subsequent excavation of this well showed that the cement slurry exhibited a general tendency to follow the squeezed cement of previous jobs. Figs. 4 and 5 are photographs taken after excavation of the well. The cement pancake observed in Fig. 4 is composed of a layer of red and yellow cement. The only evidence of black cement, the third squeeze job, is a thin layer at the extreme left of this photograph and about 3 in. above the main layer of cement. After taking this picture, further excavation revealed more streaks of black cement, the majority of which were between the other two layers, as is shown in Fig. 5. Other shallow wells subsequently squeeze cemented two or more times in the same interval exhibited a general tendency for the cement slurry to follow the same zone of weakness as did the cement of the first job. While these shallow well tests may not exactly represent what happens on a typical field squeeze cementing job, it is believed that these results do indicate the general behavior of a cement slurry on a deep well squeeze cementing job.

The question of whether water or mud should be used to break down a formation preceding a squeeze job has been asked many times. In view of the importance of this question, a number of shallow wells were utilized to evaluate this point.

When considering only the effects of the breakdown agent on the cement squeezed out into a formation, the advantages of water over mud were apparent early in the testing program. For example, shallow well tests showed that when formations were broken down with water prior to squeezing

Table II

Representative Data from Field Squeeze Cementing Tests

Well	Depth Ft	Breakdown Agent	Formation Breakdown Pressure, psi		Fluid Displacement Pressure, psi		Type Pumping Used	Final Squeeze Bottom Hole Pressure, psi	Number Sacks Used	Remarks
			Field	Calculated	Field	Calculated				
Experimental Squeeze Test Well No. 1	9530	Mud	9850	7800	8350	6800	Hesitation	8900	89	Core indicated vertical pancake.
2	2635	Mud	2600	2600	1800	2200	Hesitation	2705	137	Packer loosened. Core showed horizontal pancake.
3	6020	Mud	4900	4900	4400	4300	Hesitation	9428	87	3500′ tubing left full of cement.
4	6030	Mud	5050	4900	4400	4300	Slow Pumping	8025	112	Old tubing split at maximum squeeze pressure.
5	6030	Mud	4925	4900	4200	4300	Slow Pumping	8050	127	Job successful. No data on DST.
6	6000	Mud	4730	4900	4350	4300	Slow Pumping	8060	129	No test.
7	6015	Water	4500	4900	4100	4300	Slow Pumping	7750	112	50% water on DST. 2500 psi differential pressure on DST.
8	6015	Water	5000	4900	3750	4300	Slow Pumping	8164	115	50% water on DST. 2500 psi differential pressure on DST.
9	6018	Water	5300	4900	4800	4300	Slow Pumping	8444	117	Job successful. No DST.
10	6079	Water	4740	4900	4000	4300	Slow Pumping	8659	117	Job successful. 5000′ water cushion on DST.
11	6096	HCl + HF	4240	4900	3240	4300	Slow Pumping	7400	80	Plug not drilled and no test made.
12	6023	HCl + HF	5000	4900	4600	4300	Slow Pumping	10500	40	Dry DST. 4800′ water cushion on DST.
13	6061	HCl + HF	4645	4900	4445	4300	Fast Pumping	9000	50	Successful squeeze. 4500′ water cushion on DST.
14	6048	HCl + HF	4714	4900	3700	4300	Slow Pumping	8630	80	Plug not drilled.
15	6078	HCl + HF	4835	4900	3834	4300	Slow Pumping	7335	75	Successful squeeze. No data on DST.
16	6067	HCl + HF	4230	4900	3530	4300	Fast Pumping		150	Perforations cleared.
							Slow Pumping	7030	135	Dry on DST. 4500′ water cushion.
17	6080	HCl + HF	4230	4900		4300	Slow Pumping	7600	120	Now producing PLO.
18	6078	HCl + HF	4830	4900	3030	4300	Slow Pumping	7630	95	Now producing PLO.
19	6074	HCl + HF	4480	4900	3430	4300	Slow Pumping	8130	45	Now producing PLO. 4500′ water cushion on DST.
20	6079	HCl + HF	4230	4900	3330	4300	Fast Pumping		150	Cleared perforations 1st stage.
							Fast Pumping		150	Cleared perforations 2nd stage.
							Slow Pumping	7830	130	High final squeeze pressure obtained. Dry DST. 2500 psi differential on DST.

PLO—Pipe line oil
DST—Drill stem test
HCl—Hydrochloric acid
HF —Hydrofluoric acid

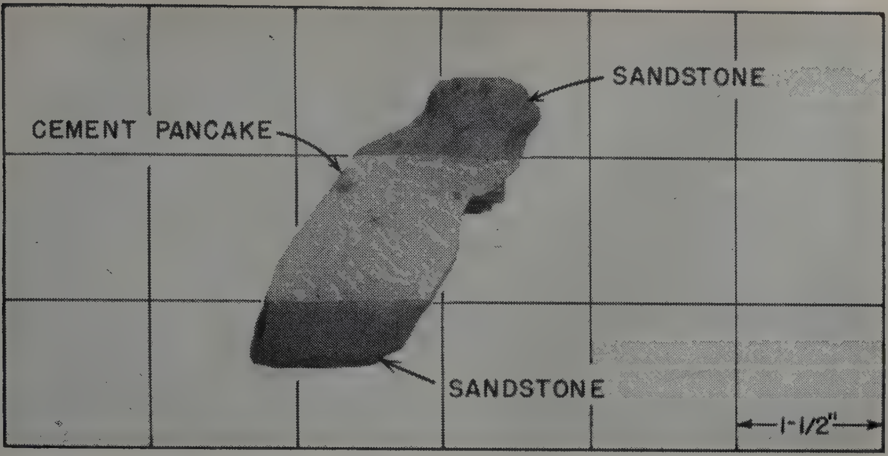

FIG. 3 — SAMPLE OF CEMENT PANCAKE FROM SHALLOW WELL.

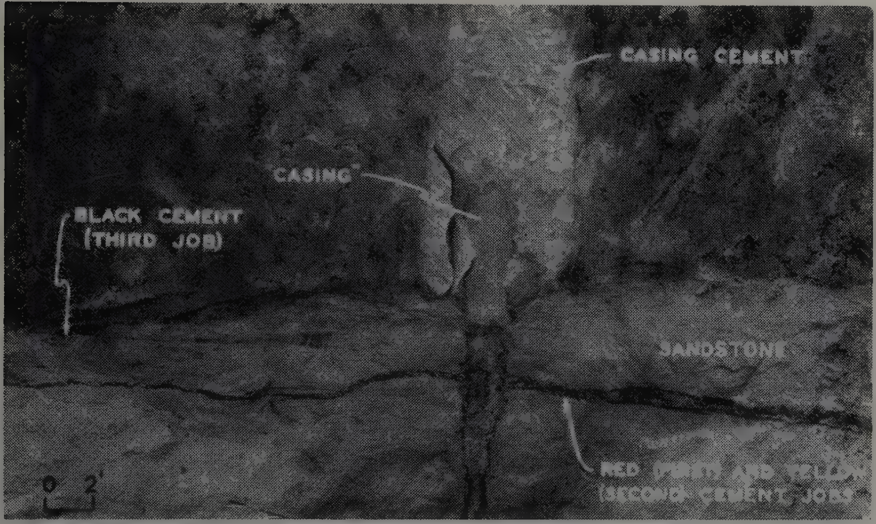

FIG. 4 — EXCAVATED SHALLOW WELL SHOWING LOCATION OF SQUEEZED CEMENT.

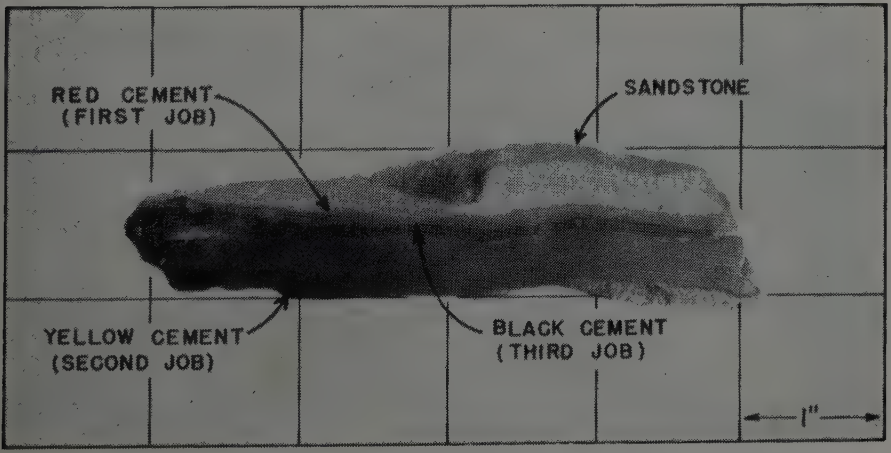

FIG. 5 — RELATIVE LOCATION OF CEMENT PANCAKES ON THREE SUCCESSIVE SQUEEZE JOBS.

cement, the cement bonded firmly and set hard against the formation. Figs. 3, 4 and 5, discussed previously, illustrate this point. Squeeze jobs in 5 shallow wells, where the cement was squeezed through perforations, indicated that water as a breakdown agent is more satisfactory than mud in obtaining perforation shutoffs. Water was used as a breakdown agent in 4 wells involving multiple squeeze cementing operations on 43 perforations. Only one of these perforations was not sealed by the cement slurry. Mud was used as a breakdown agent in 3 wells involving multiple squeeze cementing operations on 21 perforations. Of these 21, four were found to be open when exacavations were made to observe the results. A summation of these shallow well tests showed that approximately 98 per cent of the perforations broken down with water and squeezed with cement were sealed, as compared to an approximate 80 per cent shutoff attained on those squeeze jobs where the formation was broken down with mud.

In considering the possible application of these data to field usage, it should be remembered that the use of water as a breakdown agent presents the possible hazard of a partial drowning of the producing formation. Another objection to the use of water to break down formations is that it may not fracture highly permeable zones.

Mud, on the other hand, will break down highly permeable formations, and in field usage is believed to be less likely to damage oil sands, especially if the mud has low-water-loss characteristics. The injection of mud ahead of cement on squeeze jobs is likely to fracture the formation a greater lateral distance than would water. However, the mud film left on the face of the formation and on the primary cement sheath will tend to prevent a tight bond between the squeezed cement, cement sheath, and the formation. Experimental squeeze jobs in shallow wells at the laboratory, where the effects of breaking down formations with mud were demonstrated, showed that cement will not bond to a cement sheath or sand face covered with mud. Examples of the effects of mud on bonding characteristics are shown in Figs. 6 and 7.

This preliminary shallow well test work suggests that formations should be broken down with water in preference to mud before squeeze cementing in those cases where the formation characteristics are such as to permit its use; that is, where there is no danger of water blocking the pay and where the permeability is sufficiently low to permit fracturing with water. A low-water-loss mud would be preferable to water for use as a breakdown agent preceding squeeze jobs in formations susceptible to water blocking or in formations of high permeability.

Since neither mud nor water appears to be a satisfactory breakdown agent prior to squeezing cement in all formations, each material having certain advantages and disadvantages, the question is raised as to what would be an improved breakdown agent. Theoretically it appears from a study of the above mentioned shallow well tests that a low-water-loss cement would be a good material for this use since it would not possess the disadvantages of either water or mud.

The objective of some squeeze jobs is to displace the cement slurry into the formation at a given elevation to prevent the vertical migration of undesirable fluids. In order to determine the probability of success of this type of operation, a number of shallow well squeeze jobs were conducted.

Two methods were utilized to accomplish this purpose. In one method a special tool was used to V-notch the formation before it was broken down, to determine if the breakdown and subsequent cement pancake would be formed in the notch. Two squeeze jobs were conducted in a well under these conditions. In a second method, consisting of high density shooting, the casing was perforated at the desired level with 12 shots, approximately 30° apart, in a 2-in. band. Following this, the formation was broken down and the well squeeze cemented. Excavation of these two wells revealed that both of these attempts failed in their purpose. The cement pancake was opposite neither the notches nor the perforations because formation weaknesses found in both wells allowed the fracture to be formed more easily at other than the desired elevation.

These two wells demonstrated that in order to spot a cement pancake at a desired elevation, the formation must be relatively homogeneous. Due to the fact that such formations are seldom encountered in the field, the breakdown agent and the cement slurry will be squeezed out into the isolated section of the formation at the weakest point, whether it be a notch in the formation, a bullet hole, or a weakness caused by a bedding plane or a soft streak in the formation.

Subsequent shallow well squeeze jobs through perforations in pipe, where the formation was relatively homogeneous, indicated that the cement slurry entry point into the formation could be controlled by the elevation of the perforations. This was demonstrated in a well that was perforated with four shots spaced 90° apart at the same elevation in homogeneous sandstone. The formation was broken down with mud at 550 psi and four sacks of standard portland cement were squeezed into the formation with a final squeeze pressure of 2500 psi. Subsequent excavations revealed a horizontal cement pancake with a 360° lateral spread opposite the perforations.

Sometimes it might be desired that cement be squeezed so that it will penetrate the formation parallel to the bedding planes in all directions. This is to be desired in cases where the primary purpose of the job is to minimize the tendency for gas or water coning. In view of this problem, work was performed to determine whether or not cement that is forced out horizontally will completely surround the well bore when it is squeezed through perforations and in open hole.

Open hole squeeze jobs were performed on nine shallow wells with as many as three successive jobs in one well. In every case a 360° lateral spread of cement was obtained and the cement pancakes appeared to be of better quality and greater thickness than those formed by squeezing through perforations.

In order to determine the lateral spread of cement squeezed through perforations, three shallow wells were utilized. Cement was squeezed out 19 perforations, both singly and in sets, with a resulting average lateral spread of cement of approximately 140° per perforation. A minimum lateral spread per perforation of 45° and a maximum of 270° were noted.

It appears from the shallow well tests that a large number of perforations (possibly 10 or 20 shots) at the point of squeeze will tend to aid in obtaining a uniform squeeze pressure on the outside of the pipe. Then if formation conditions permit, the chances of creating a cement pancake parallel to the bedding planes and completely surrounding the well bore will be improved.

It has been demonstrated in field practice that perforations are sometimes difficult to plug by squeezing a cement slurry. This has been evidenced by the fact that many times, several squeeze jobs are required to seal completely one set of perforations. During these shallow well tests, squeeze jobs were conducted on nine sets of perfora-

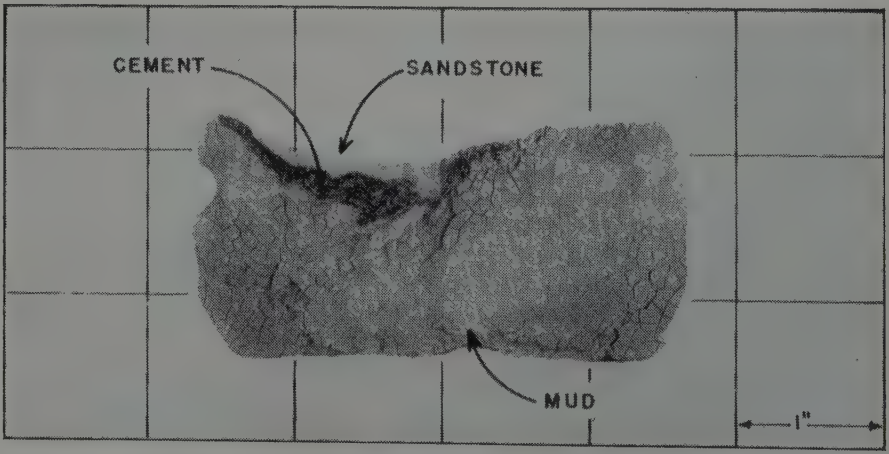

FIG. 6 — EFFECT OF A MUD BREAKDOWN AGENT ON SQUEEZED CEMENT.

tions in four wells; five perforations were found to be open after squeezing. On the other hand, a shallow well that was perforated and squeezed five successive times, one perforation at a time, had no unplugged perforations. An analysis of these test results would seem to indicate that, other factors permitting, a well probably should be perforated with as few shots as practicable at the time of testing; then, if it is found that the perforations must be plugged, they could be squeezed off with minimum effort.

Control of the quantity of cement placed out in the formation during a squeeze job is believed to be very important. Field experience has shown that on some wells large quantities of cement may be readily displaced out into the formation before a high final pressure is attained. On other wells it is difficult to displace any appreciable quantity of slurry out into the formation before the cement dehydrates and the pressure increases. It was found in shallow well tests that the quantity of cement squeezed out into the formation could be controlled to a certain extent by a variation in the squeeze cementing procedure. After the formation was broken down, it was possible to inject large quantities of cement slurry into the fracture at a relatively low pressure. In order to limit the quantity of cement placed during these jobs, slow pumping or hesitation pumping was employed. These procedures consisted of placing a predetermined quantity of cement in the normal manner, then either slowing or shutting down the pumps for short periods to initiate a pressure buildup. In this manner it was possible in many instances to attain high final pressures and limit the quantity of cement slurry displaced even in some of the soft streaks encountered in these shallow wells.

Large quantities of cement were displaced into the formation by the use of low-water-loss cement. This is a special cement that has an API fluid loss of less than 100 cc in 30 minutes.* Therefore, almost unlimited quantities of this cement can be placed without a pressure buildup because it will resist dehydration. Tests performed in a shallow well permitted the placement of 40 sacks of this cement, with five shutdowns ranging from 5 to 30 minutes without a pressure buildup in three hours of pumping. Yet when 10 sacks of standard portland cement were squeezed in a second well under similar conditions, the slurry dehydrated in 30 minutes with a pressure buildup of 2000 psi.

A number of shallow well tests were conducted using a phenol formaldehyde type plastic, with and without inert fillers, as a cementing medium. Generally speaking, the results of these tests were inconclusive due to difficulties experienced with the setting characteristics of the plastic at the low temperatures found at shallow depths. Excavation of these wells revealed that the plastics tested performed the same as cement slurries in the seeking of zones of weakness and in the formation of pancakes. A plastic pancake is illustrated in Fig. 8.

Before recommending extensive field testing of the improved procedure suggested by the shallow well squeeze jobs, it was deemed advisable to check, under controlled deep well conditions in the field, the applicability of the slow pumping or hesitation pumping squeeze cementing procedure to field squeeze cementing operations, and then by subsequent coring determine the direction of travel of the squeezed cement from the well bore.

Two such tests were performed in the Gulf Coast area in wells 9530 and 2635 ft deep. These tests, performed in a $3\frac{7}{8}$ in. diameter rat hole drilled below $9\frac{5}{8}$ in. casing in the first well and $10\frac{3}{4}$ in. casing on the second, definitely indicated not only that the slow pumping procedure as used in the laboratory was workable, but also furnished additional data for confirmation of the previously established overburden pressure theories. Coring the rat holes after the squeeze jobs showed that on one well the cement was squeezed out the bottom of the rat hole in a vertical fracture, while on the second the cement was squeezed out in a horizontal pancake. These tests illustrated that either type fracture may be formed, depending upon the formation against which the cement is squeezed. The vertical pancake from the well 9530 ft deep is illustrated in Fig. 9, which shows a portion of the core removed from this well. Fig. 10 shows a portion of the core taken from the second well 2635 ft deep, illustrating the horizontal pancake.

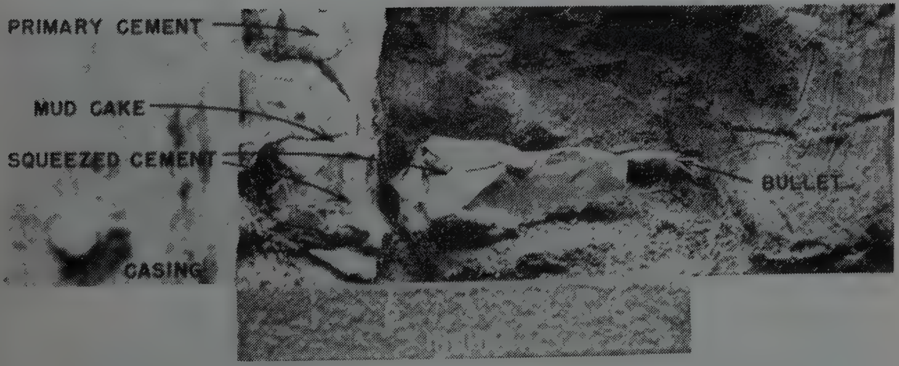

FIG. 7 — EFFECT OF MUD BREAKDOWN AGENT ON BOND BETWEEN PRIMARY AND SECONDARY CEMENT JOBS.

FIELD INVESTIGATION TO DETERMINE PROPER SQUEEZE CEMENTING METHODS

Reviewing the results obtained from the preliminary studies, it became apparent that the ability of a squeeze cement job to seal perforations is dependent upon the bond obtained between the squeezed cement and the primary cement sheath (see Fig. 7), rather than on the quantity of cement that can be displaced out into the formation. If the squeezed cement does not bond to the primary cement job, such as to prevent the entry of well fluids into the casing at this point, then all cement squeezed beyond this point serves very little purpose. The initial investigation also indicated that the quantity of cement required to obtain a high final squeeze pressure could be controlled by utilizing special squeeze cementing techniques.

---

* API Code 20 "Recommended Practices on Standard Field Procedure for Testing Drilling Fluids".

It is realized that a definite evaluation of a squeeze cementing procedure should be based on the ability of the squeeze job to accomplish the desired results. However, on many of the squeeze jobs conducted during this series of field tests, well conditions prevented a uniform testing program following each job, making a definite evaluation of the various squeeze cementing procedures difficult. As past field experience has indicated that a large majority of the successful squeeze jobs was characterized by a high final squeeze pressure, it appeared that this factor might be used as a criterion for judging various squeeze cementing procedures. By accepting this line of reasoning, it was then possible to rate a given procedure on the number of sacks of cement with which a high final squeeze pressure was obtained. For example, at the present time only 100 to 125 sacks of cement are required for a squeeze job, as compared to the estimated 250 or more sacks previously used.

Using these premises as the basis for forming an improved squeeze cementing procedure, a technique was recommended to the field for trial in several wells. The basic assumption was that the slow displacement of a cement slurry, once a breakdown had been obtained, would aid in the dehydration of the slurry, and thus help in compacting the squeezed cement into the perforations to be plugged. This procedure would allow control over the quantity of cement to be displaced before the final squeeze pressure is obtained.

To further verify the aforementioned slow pumping technique, field tests were set up to investigate each of the following variables:

1. Workability of the slow pumping or hesitation pumping squeeze cementing procedure.
2. Desirability of a high final squeeze pressure.
3. Type of retainer best suited for squeeze cementing operations.
4. Investigation of formation breakdown agents.
5. Required waiting on cement time.
6. Importance of the differential pressure imposed on perforations during testing.

Approximately 160 squeeze cement jobs have been conducted in the field to evaluate the aforementioned variables. Representative data from these jobs are included in Table II.

Slow Pumping Procedure

The slow pumping squeeze cementing procedure used on these field tests consisted principally of the following steps:

1. The retainer was lowered into the well until it was below the zone or perforations to be squeezed.
2. The proper breakdown fluid was circulated to bottom and up into the annulus so that it completely covered the zone to be squeezed.
3. The retainer was raised and set in the pipe a sufficient distance above the perforations to eliminate the hazard of dehydrating cement around the retainer.
4. Approximately 150 sacks of cement were mixed and displaced down the tubing, immediately following the breakdown agent.
5. The formation was broken down and 50 sacks of cement were pumped out into the formation at a high pump rate (2 to 3 bbl/min).
6. The next 50 sacks were displaced into the formation at a lower pump rate (approximately 1 bbl/min).
7. If a pressure buildup had not occurred by the time the third 50 sacks were started into the formation, the pumps were slowed down to a rate of ¼ to ½ bbl/min or lower as long as the cement was kept moving. This very slow pumping almost always resulted in a pressure buildup. Hesitation squeezing, or alternate pumping and shutting down periods, was also found effective, but this practice is somewhat hazardous in that the cement might gel or set while not in motion, and thus resist further movement up or down the tubing or drill pipe.
8. When the pressure buildup occurred, as much surface pressure was applied as the well equipment permitted. The pressure was held for approximately one minute before reversing out the excess slurry.

Prior to these tests, the field practice in many areas was to break down the formation with mud and then displace the cement slurry into the formation at as fast a rate as practicable until a pressure buildup occurred and no more cement could be displaced. Frequently, as many as 250 sacks of ce-

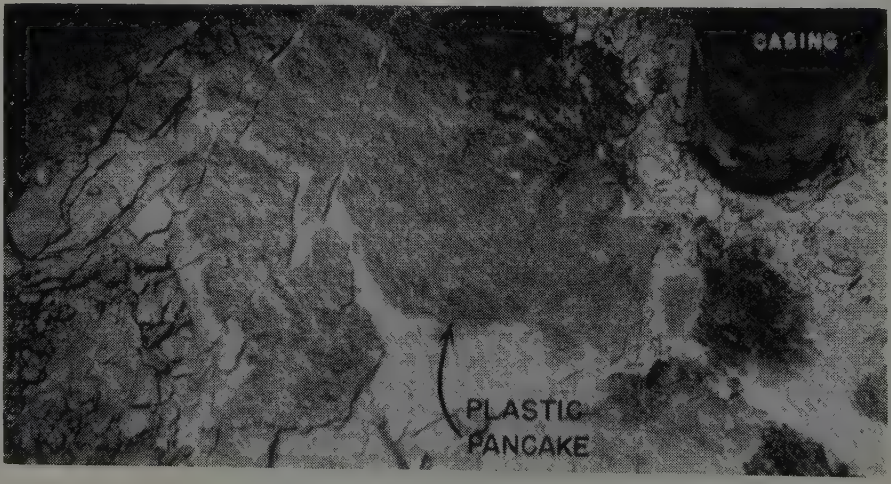

FIG. 8 — SQUEEZED PLASTIC PANCAKE.

ment and several stage jobs* would be required to attain the desired high final squeeze pressure.

An analysis of the fast pumping squeeze procedure used by the field, and the laboratory experiments previously described, suggested that part of the cement slurry on a field squeeze job was being displaced out into the formation away from the well bore. The pressure buildup was obtained only when sufficient water had been squeezed out of the cement slurry to leave a solid plug which resisted further movement and thus caused a buildup in pressure. The slow pumping procedure aided this rate of water loss by decreasing the displacement rate and allowing more time for the cement slurry to dehydrate. High final squeeze pressures were thus obtained with much smaller volumes of cement than had previously been possible.

Well conditions on eighteen squeeze cementing jobs, all conducted at depths of approximately 6000 ft, permitted an evaluation of the desirability of obtaining a high final pressure. Nine of the eighteen tests resulted in successful jobs, and the other nine failed to shut off all perforations. The bottom hole squeeze pressures of the successful jobs averaged 10,100 psi, or 7600 psi differential, while those of the unsuccessful jobs averaged only 7900 psi, or 5400 psi differential. Of course many other factors entered into the determination of success or failure of these jobs, but the over-all difference in final squeeze pressures is believed to be significant.

At the present time field practice in some areas has indicated that a final bottom hole squeeze cementing pressure equal to well depth x 1.0 + 2000 psi is generally giving satisfactory results. However, limited field experience has indicated that bottom hole pressures as high as well depth x 0.6 + 5000 psi may be required in shallow wells for satisfactory jobs. (See Fig. 11).

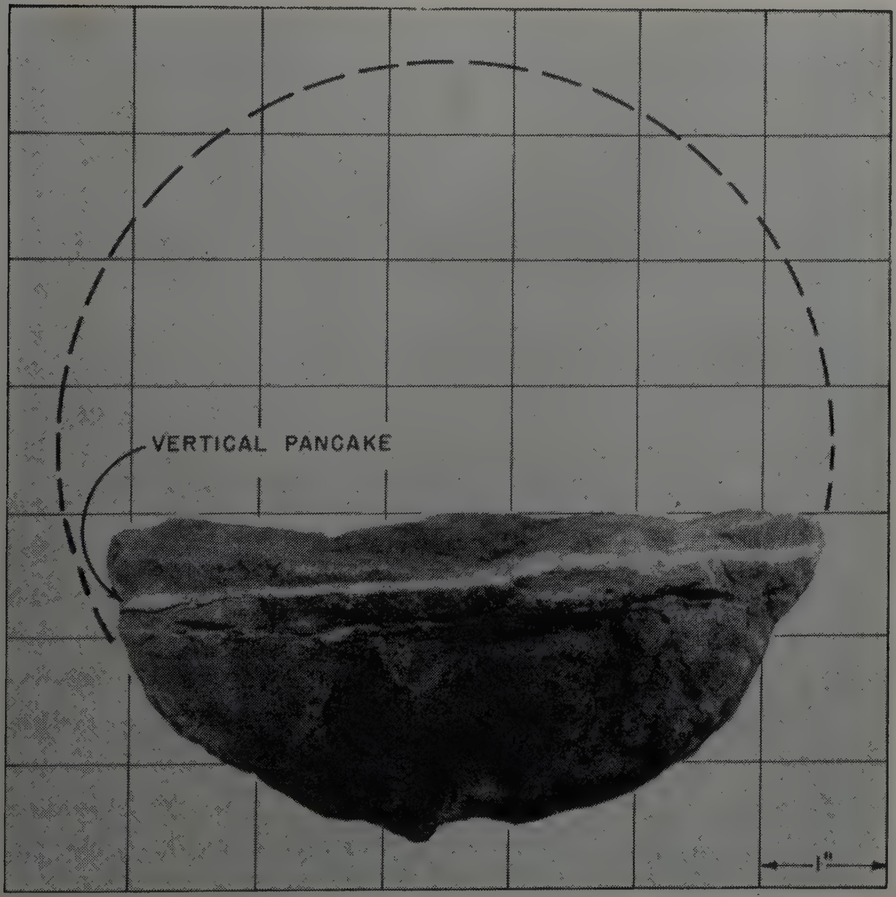

FIG. 9 — CORE FROM 9,530 FT WELL SHOWING VERTICAL CEMENT PANCAKE.

During these field tests a study was made to determine if drillable or retrievable cement retainers affected squeeze jobs differently, or if one type of retainer would be preferable to the other. At the beginning of these observations it was the thought that the drillable type retainer might be superior to a retrievable retainer in that it provided a means for retention of the full final squeeze pressure on the slurry during the entire curing period of the cement. The use of a retrievable type retainer, however, required that all of the surface pressure be bled off before starting the retainer out of the well. An investigation of 109 squeeze jobs, where a retrievable retainer was used, revealed that only 12 of these jobs were failures. Considering the many other factors that could have contributed to the 12 failures, it is difficult to visualize how any other type retainer could provide improved service. It can, based on these data and past field experience, be assumed that both retrievable and drillable type retainers are satisfactory for squeeze jobs.

The field investigation of formation breakdown agents involved three materials — mud, water, and a mixture of hydrochloric and hydrofluoric acids (HCl + HF). In order to establish a criterion for the three agents, the number of sacks of cement required to obtain a high final squeeze pressure was compared with each breakdown agent used. Table III below shows the data obtained on these evaluations.

Table III

Effect of Breakdown Agent on Quantity of Cement Required

Agent	No. Jobs Used	Avg. Sacks Cement Required to Obtain a High Final Squeeze Pressure
Mud	6	125
Water	6	126
HCl + HF	42	98

This table indicates that mud and water require about the same quantity of cement before a satisfactory pressure can be obtained, but that the mixture of hydrochloric and hydrofluoric acids appears to be the best breakdown agent tested based on the amount of cement required to obtain a high final squeeze pressure. In view of the encouraging results obtained with this material, and in an effort to improve on these results, additional tests have been planned with other chemical washes for use as improved breakdown agents.

---

* Stage job is defined as one part of a squeeze cementing job on which no pressure buildup is obtained with a predetermined quantity of cement. The perforations are subsequently cleared of cement in preparation for the next stage. This process is repeated until the desired high final squeeze pressure is obtained.

As no definite criterion had been established for the determination of waiting on cement time following squeeze cementing operations, 24 hours, which is accepted by many operators for casing cementing operations, was generally employed on this series of tests. This time was sufficient for every job where it was used and could be evaluated. Since a WOC time of less than 24 hours was successfully employed on some of these jobs as well as on other jobs, and since the temperatures and pressures are more severe than those encountered during casing cementing operations, it appears that a reduced WOC time may be used with reasonable safety.

By reducing the pressure in the casing, the pressure differential effected across a section of squeezed off perforations was found in some instances to be greatly in excess of the pressure that would be imposed across the perforated interval during the remaining life of the well. For example, some wells having producing differentials of 200 to 300 psi were being tested with differential pressures as high as 2500 psi. This high differential pressure was apparently a contributing factor in the resulting squeeze job failures. Believing that these conditions were unnecessarily severe, subsequent perforation testing was performed by imposing only as much differential pressure on the perforated interval being tested as would be imposed during the rest of the producing life of the well. Of the 160 squeeze cementing jobs reviewed in this investigation, it was possible to obtain complete data on the pressures used in testing the squeezed perforated intervals on only eight jobs. Of these eight, five were tested by imposing pressures comparable to those imposed on the well during its producing life. In each of the five wells tested the low differential pressure tests showed the squeeze job to be successful. (See Table II, Wells No. 10, 12, 13, 16, and 19.) The remaining three jobs were tested using a high differential pressure. Two of the three jobs tested showed an unsuccessful squeeze job, with the remaining well testing satisfactorily. (See Table II, Wells Nos. 7, 8, and 20.)

To date, insufficient data are available to permit accurate evaluation of the cements to be used for squeeze work. Fig. 12 illustrates the difference between the four bottom hole squeeze cementing temperatures obtained to date and the casing cementing temperatures that have been previously established by extensive field tests.* From the limited data on hand at this time it is believed that bottom hole temperature and pressure conditions are much more severe for squeeze cementing than they are for casing cementing.

Complete evaluations of all cements for squeeze work are planned for the future. Until these data are available, it is believed that care should be exercised in selecting cements for squeeze cementing operations, since cements tend to set more rapidly under high temperatures and pressures.

CONCLUSIONS

The results obtained from both laboratory and field investigations may be summarized as follows:

Laboratory Shallow Well Tests indicated that

1. Formations break down in any existing zone of weakness and a cement slurry subsequently squeezed into the well enters that zone in the form of a sheet or "pancake".
2. A cement slurry squeezed through a perforated section is most likely

---

* API Code 32 (Tentative).

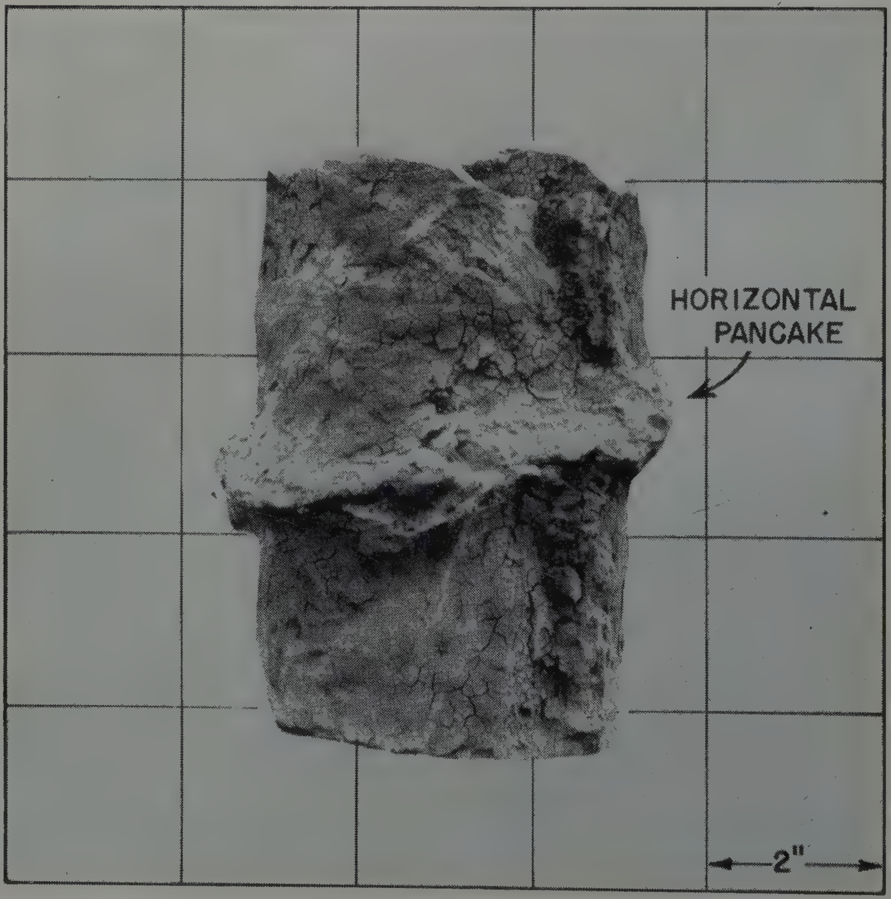

FIG. 10 — CORE FROM 2,635 FT. WELL ILLUSTRATING HORIZONTAL PANCAKE.

to enter only those perforations adjacent to or communicating with the zone of weakness.

3. Perforations opposite formations broken down with water are more easily sealed with cement than are those opposite formations broken down with mud.
4. The average lateral spread of a cement slurry squeezed from an open hole is approximately 360°; the spread of cement squeezed through perforations is erratic in that it varies from 45° to 270° per perforation, averaging 140°.

Field Tests indicated that

1. The slow pumping squeeze cementing procedure results in improved squeeze cementing operations utilizing less cement to obtain a high final squeeze pressure.
2. High final squeeze pressures appear to aid materially in accomplishing successful squeeze cement jobs, although a high final pressure does not necessarily insure plugging of all perforations.
3. Comparable results are obtained with either drillable or retrievable cement retainers.
4. The mixture of hydrochloric and hydrofluoric acids appears to be a more satisfactory breakdown agent than either mud or water.
5. A waiting on cement time of 24 hours appears to be ample, with some field data indicating that a shorter time may be sufficient.
6. The reduction of pressure in the casing during testing may be detrimental to the success of the squeeze job, if the resulting differential pressure across the perforated interval is greater than that expected during well production.

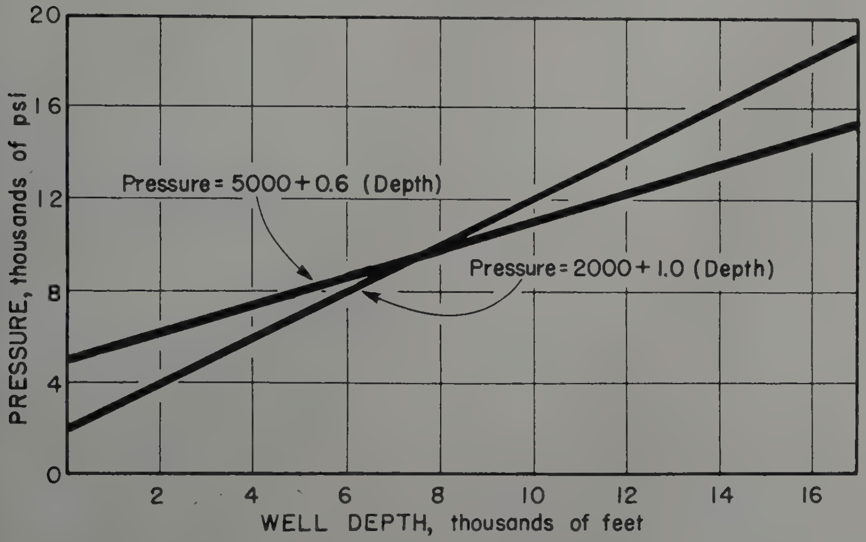

FIG. 11 — FINAL BOTTOM HOLE SQUEEZE PRESSURE.

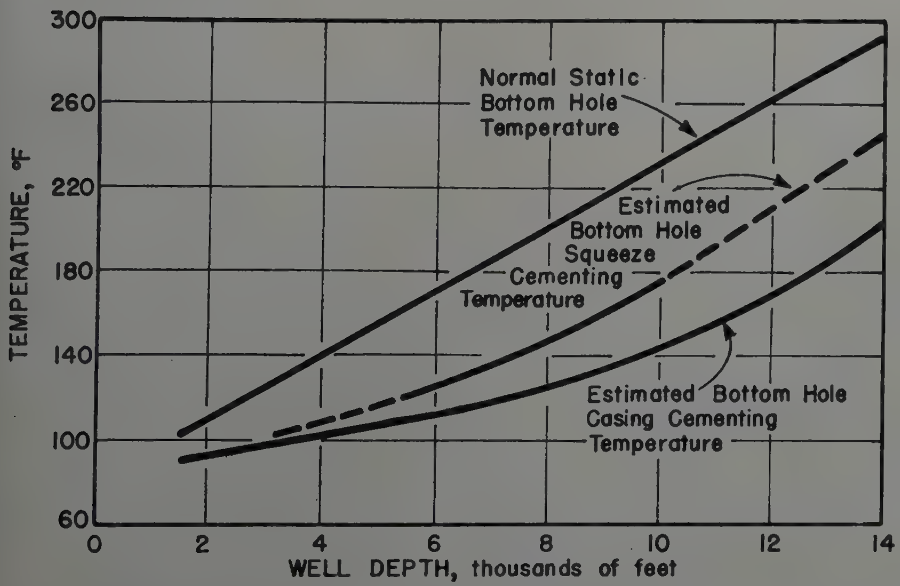

FIG. 12—COMPARISON OF BOTTOM HOLE CASING AND SQUEEZE CEMENTING TEMPERATURES.

FUTURE DEVELOPMENTS

Although much work has been done in the past on the improvement of squeeze cementing techniques and materials, there still remains a great deal of research and development work to be accomplished. There are some phases of this type of operation where the available knowledge is inadequate and others that need improvement. For example, the failure of many squeeze jobs to shut off completely all perforations, even though high final squeeze pressures are obtained, shows the need for improved squeeze cementing materials and procedures which will allow successive plugging of each perforation and still afford a means of obtaining a high final squeeze pressure. Considerable thought has also been given to the possibility of squeezing out into a formation an impermeable lens or pancake of cement at selected elevations in a well bore to control the migration of undesirable fluids into the producing well. The lack of definite measurements of bottom hole squeeze cementing temperatures represents another limitation of our present squeeze cementing knowhow. The solution to these and other equally important problems will undoubtedly permit further improvements in squeeze cementing operations.

ACKNOWLEDGMENT

The authors wish to express their appreciation to the management of the Stanolind Oil and Gas Co. for permission to prepare and publish this paper, although it is recognized that the granting of such permission does not necessarily imply that Stanolind has incorporated or will incorporate these findings into its operating practice. They also wish to express their appreciation to R. Floyd Farris and R. C. Clark, Jr., for their excellent assistance in accumulating these data; to J. B. Clark for helpful suggestions and criticisms; and to the Stanolind Oil and Gas Co.'s Division and Field personnel for arranging and conducting the field tests.

BIBLIOGRAPHY

L. F. Athy, "Density, Porosity, and Compaction of Sedimentary Rocks", *American Association of Petroleum Geologists Bulletin*, January, 1930.

G. E. Cannon and R. C. Craze, "Excessive Pressures and Pressure Variations with Depth of Petroleum Reservoirs in the Gulf Coast Region of Texas and Louisiana", *Petr Tech*, 1938.

Paul D. Torrey, "Progress in Squeeze Cementing Application and Technique", *Oil Weekly*, July 29, 1940.

John J. Grebe, "Tools and Aims of Research", *Chemical and Engineering News*, December 10, 1943.

C. A. Pitts, "Oil Well Cementing—Part 2", *Petroleum Engineer*, March, 1944.

Glenn M. Stearns, "Theory of Squeeze Cementing", *Engineering Fundamentals (Oil and Gas Journal*, August 12, 1944).

C. E. Reistle, Jr., "U. S. Patent No. 2,368,424", issued January 30, 1945.

S. T. Yuster and J. C. Calhoun, Jr., "Pressure Parting of Formations in Water Flood Operations—Part I", *Oil Weekly*, March 12, 1945.

S. T. Yuster and J. C. Calhoun, Jr., "Pressure Parting of Formations in Water Flood Operations—Part II", *Oil Weekly*, March 19, 1945.

F. B. Plummer, "Methods of Preventing Capillary Rise and Capillary Spreading of Water in Oil Wells", *Engineering Fundamentals (Oil and Gas Journal*, March 24, 1945).

P. A. Dickey and Kurt H. Andresen, "Behavior of Water Input Wells—Part 4", *Oil Weekly*, December 10, 1945.

A. J. Teplitz and W. E. Hassebroek, "An Investigation of Oil-Well Cementing", *Drilling and Production Practice*, 76, (1946).

★ ★ ★

RELATIVE PERMEABILITY TO GAS

W. J. LEAS, MEMBER AIME, **L. H. JENKS,** AND **CHARLES D. RUSSELL,** THE CARTER OIL CO., TULSA, OKLAHOMA

ABSTRACT

A detailed description is given of an experimental method for determining relative permeability of porous media to gas. Results are presented for natural and synthetic cores. The experimental data for two and three phase systems are compared. The reproducibility of the equilibrium gas saturation is demonstrated and the effects due to a variation in rate of gas flow are discussed. An attempt is made to correlate total permeability and rock textural factors with relative permeability to gas. Capillary pressure curves obtained simultaneously with the relative permeability curves are shown to be equivalent to those obtained in conventional displacement cells.

INTRODUCTION

The advances in petroleum reservoir technology during the past decade have made increasingly apparent the desirability of a simple, rapid, reliable method for obtaining relative permeability data on small cores. Such data are needed in order to study fluid mechanics in porous media and for the more refined reservoir behavior prediction calculations now under development.

The early experimental work in this field was done by Wyckoff and Botset[1] who measured relative permeabilities for gas-liquid mixtures flowing through

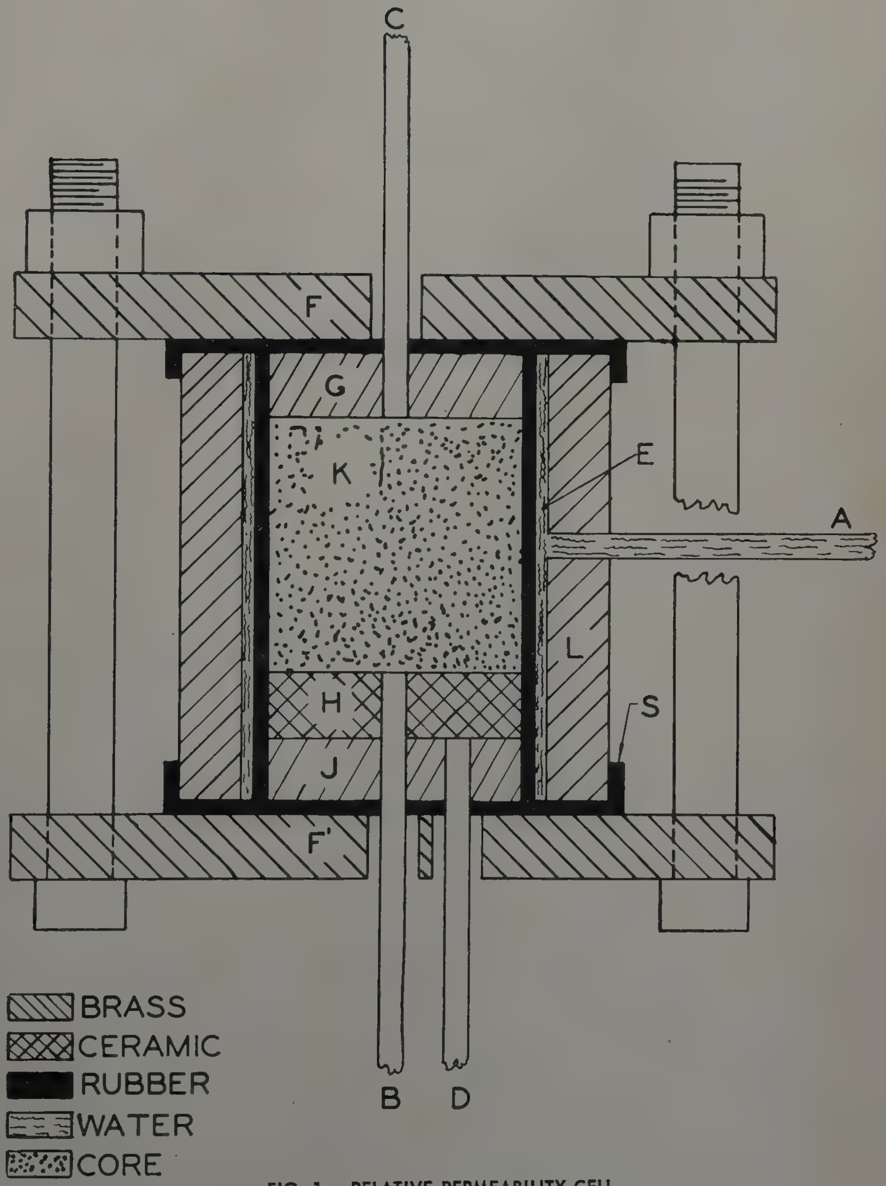

FIG. 1 — RELATIVE PERMEABILITY CELL.

---

[1] References given at end of paper.

Manuscript received at the office of the Petroleum Branch October 1, 1949. Paper presented at the Petroleum Branch meeting in San Antonio, October 5-7, 1949.

unconsolidated sands, and by Hassler, Rice, and Leeman[2] who measured the effective permeabilities to gas on small Bradford cores saturated with varying amounts of stationary liquid. Extensive studies have been made by Leverett[3] and Leverett and Lewis[4] on the behavior of fluids in packed columns of unconsolidated sand in which the two phases, oil and water, and the three phases, oil, water, and gas, were flowing in the sand simultaneously. Botset[5] extended his techniques to consolidated Nichols Buff sandstone and more recently Morse, Terwilliger, and Yuster,[6] and Henderson and Yuster[7] have developed relative permeability apparatus for small core samples. Hassler[8] has patented a method and apparatus for relative permeability determination which makes use of semipermeable barriers to maintain a pressure difference between fluid phases.

The experiments of the above investigators may in general be divided into two types depending upon whether or not a difference in pressure is mechanically maintained between the gas and liquid phases. In the experiments reported by Botset, Leverett, and Yuster et al the gas and liquid are allowed to flow through the core at the same pressure gradient and hence are classified as being those in which no difference in pressure is maintained between phases.

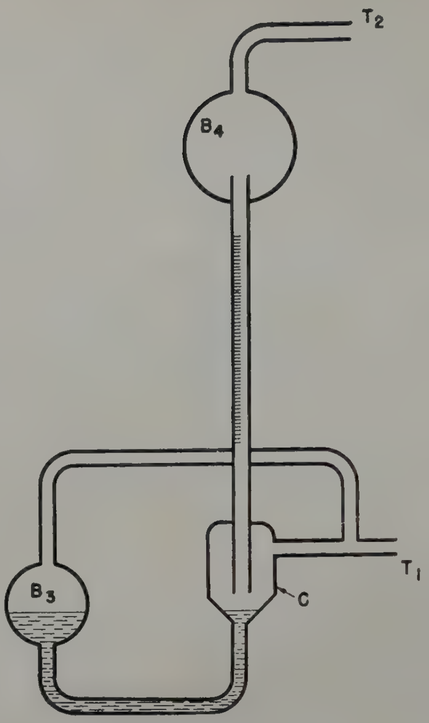

FIG. 2 — CROSS-SECTIONAL VIEW OF FLOWMETER.

In such experiments K_g and K_l are affected by the rate of flow.* At low rates, the end effect is quite pronounced and its effect is propagated back into the core to an appreciable extent. This and other rate effects limit this type experiment to a range of flow rates which may not correspond to reservoir rates.

To the authors' knowledge only limited data are available which have been obtained with the Hassler[8] method or modifications thereof.[13] In principle the elements necessary for establishing and maintaining a difference in pressure between the flowing phases are present in this technique. The geometry of the porous rings at the ends of the core, however, leaves much to be desired insofar as uniformity of saturation within the core is concerned. Moreover the auxiliary equipment appears to be unduly complex and not easily adaptable for inexpensive routine use.

The work presented in this paper has been directed toward overcoming the objections of the Hassler method. A cell has been designed which permits the maintenance of a pressure difference between the two phases, gas and oil; the oil phase is held immobile at each particular saturation while the gas is allowed to flow. The pressure gradient in the flowing gas phase is accurately known. The oil in the core is under reduced pressure and the gas at very

---

* For brevity, relative permeability to gas will hereinafter be referred to as K_g, relative permeability to liquid as K_l, and the equilibrium gas saturation as K_{eq}.

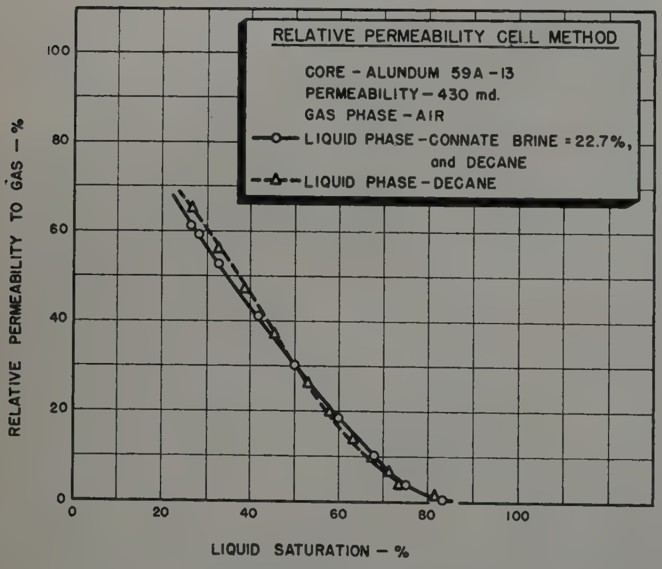

FIG. 3 — RELATIVE PERMEABILITY CELL METHOD.

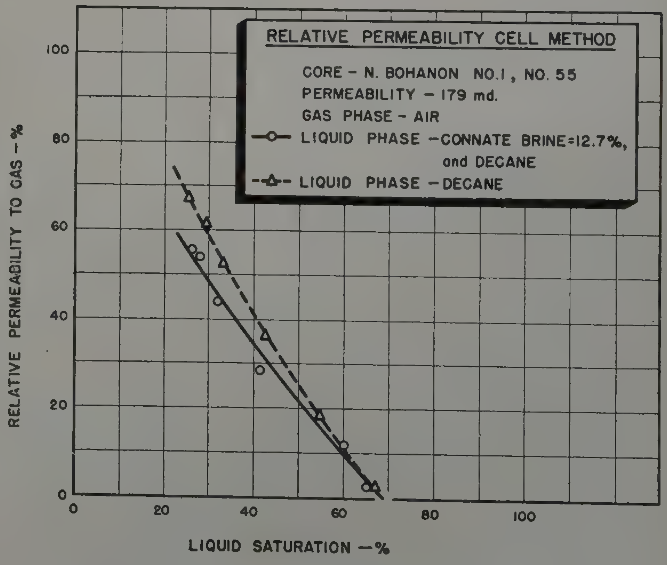

FIG. 4 — RELATIVE PERMEABILITY CELL METHOD.

nearly atmospheric. This cell has also been adapted to three phases, i.e., maintaining interstitial water at a fixed saturation in the core and measuring the permeability to gas at various oil saturations.

APPARATUS AND METHOD

The relative permeability cell shown in Fig. 1 is designed to maintain a pressure difference between fluid phases in the core sample. This cell, together with a gas pump, a manometer, and a flowmeter, makes it possible to measure the effective permeability of a core to gas at each discrete partial oil saturation. The oil saturating the core is held immobile during the measurement of effective permeability to gas.

In the operation of the cell, the core K, completely saturated with oil, is placed in capillary contact with the ceramic disc H which is also completely saturated with oil. The cell is then assembled as shown in Fig. 1 and bolted tightly together. The parts F, F′, G, J, L, C, B, D, and A are all made of polished brass or of chromium plated brass. The gas outlet tube C is soldered to disc G and the gas inlet tube B and tube D are soldered to disc J. The ceramic disc H is cemented to tube B and the brass disc J. Between plates G and J and the brass end plates F and F′ respectively, are sufficient rubber washers, so that when the end plates are drawn together by bolts, a seal will be provided between L and S at the ends of L and the disc-core assembly G-K-H-J will be compressed sufficiently to establish capillary continuity for the oil between H and K. To facilitate the insertion of the core and discs, a vacuum is applied to A to collapse the rubber sleeve S against L. After the cell has been bolted together, the annular space E between L and S and a few inches of tube A are filled with water. Gas pressure is then applied to force the rubber sleeve against the sides of the core and discs to make a peripheral seal. The ends of brass plate G and the ceramic disc H in contact with the core are grooved to permit a homogeneous distribution of gas as it flows in and out of the core. After the assembly is completed, tube D is filled with oil and is connected to one arm of a flexible U tube mercury manometer so that there is continuity of the saturating oil phase from the top of the mercury through D and H and into the core.

By lowering the mercury in the free arm of the U tube, a reduced pressure is imposed on the oil phase and the oil saturation of the core is reduced. When capillary equilibrium has been reached, gas is allowed to flow in B and out C and hence the effective permeability of the core to gas can be measured. Then the mercury in the free arm is again lowered. This cycle is repeated until the minimum attainable liquid saturation is reached, at which time the core is removed and weighed to determine its liquid saturation. From the calibration of the closed arm of the U tube and the position of the mercury interface in that tube, the saturations of oil at which the permeability is measured can be calculated. The effective permeability of the core to gas at each oil saturation divided by the permeability of the core to gas at zero oil saturation yields the relative permeability to gas at each oil saturation. These data are plotted versus the liquid saturation to give the conventional relative permeability curve.

The difference in level between the

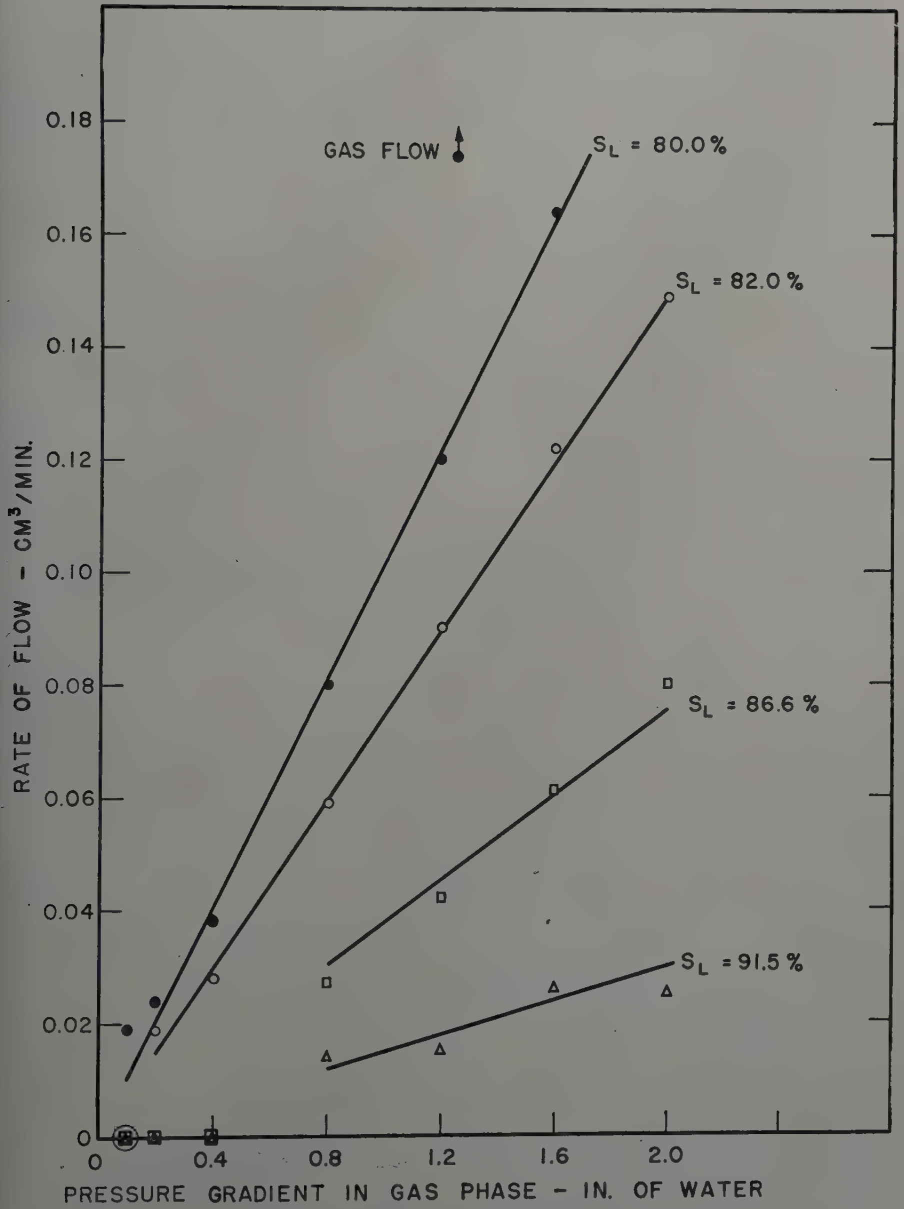

FIG. 5 — RATE OF GAS FLOW AS A FUNCTION OF PRESSURE GRADIENT AND LIQUID SATURATION, ALUNDUM CORE 5S-01.

mercury in the two arms of the U tube plus a correction for the liquid above the mercury in the closed arm yields data from which the capillary pressure curve can be obtained.

The maximum reduced pressure permissible on the liquid phase has been found to be about 5 psi. At reduced pressures greater than this value, the continuity of the liquid phase in tube D is interrupted by the formation of gas bubbles which preclude the accurate determination of both the liquid saturation and the capillary pressure. In those cases where capillary pressures in excess of 5 psi are necessary to obtain the requisite liquid saturation slight modifications can be made in the equipment to permit a constant pressure to be applied to the gas phase. This augments the reduced pressure on the liquid phase and the combination of the two suffice to desaturate the core.

After sufficient data have been obtained for the relative permeability to gas curve, the cell is disconnected from the gas flow lines, the tube B is capped, and tube C is connected to a pressure source capable of desaturating the core to its minimum liquid saturation. In this type of experiment either brine, oil, or both can be used as the saturating liquid. If only one liquid is used the initial saturation can be accomplished by the well known evacuation method. If both are used simultaneously and the brine preferentially wets the core, the brine is established in the core by first saturating a dry core with brine and displacing the brine with oil in a restored state displacement cell.[9] This modification requires that disc H in the relative permeability cell be treated with silicones to render it preferentially oil wetted so that the brine will remain in the core and only oil will be drawn out.

The flowmeter used in this research is of rather novel design and is shown in Fig. 2. Air flows in at T_1, up through the burette tube and out at T_2. A film across the burette is formed by lifting B_3 so that the liquid will rise in C and cover the lower end of the burette. B_3 is then lowered and the film travels up the burette. The time required for the displacement of a given volume is measured with a stopwatch and the volume rate of flow in cc/min is obtained. The film expands at the end of the burette in bulb B_4 and eventually breaks.

In all gas permeability measurements the phenomenon of gas slippage adjacent to the solid surfaces must not be overlooked. This slippage, frequently called the Klinkenberg effect[10], results in a higher permeability to gas than to liquid under conditions of single phase fluid saturation. The amount of slippage is a function of the ratio of the mean free path of the gas molecules to the radius of the channel through which gas is flowing. Any variations in experimental conditions which change either the mean free path of the gas molecules (such as pressure, temperature, etc.) or which change the average radius of the passages open for the flow of gas will affect the observed permeability to gas. An air permeability at atmospheric temperature and pressure may be greater than a liquid permeability on the same core by a factor of 2. Because of the possibility of changes in the average pore radius of passages available for gas flow as the partial liquid saturation of a porous medium decreases, the Klinkenberg effect should be taken into consideration in the ultimate evaluation of relative permeability to gas

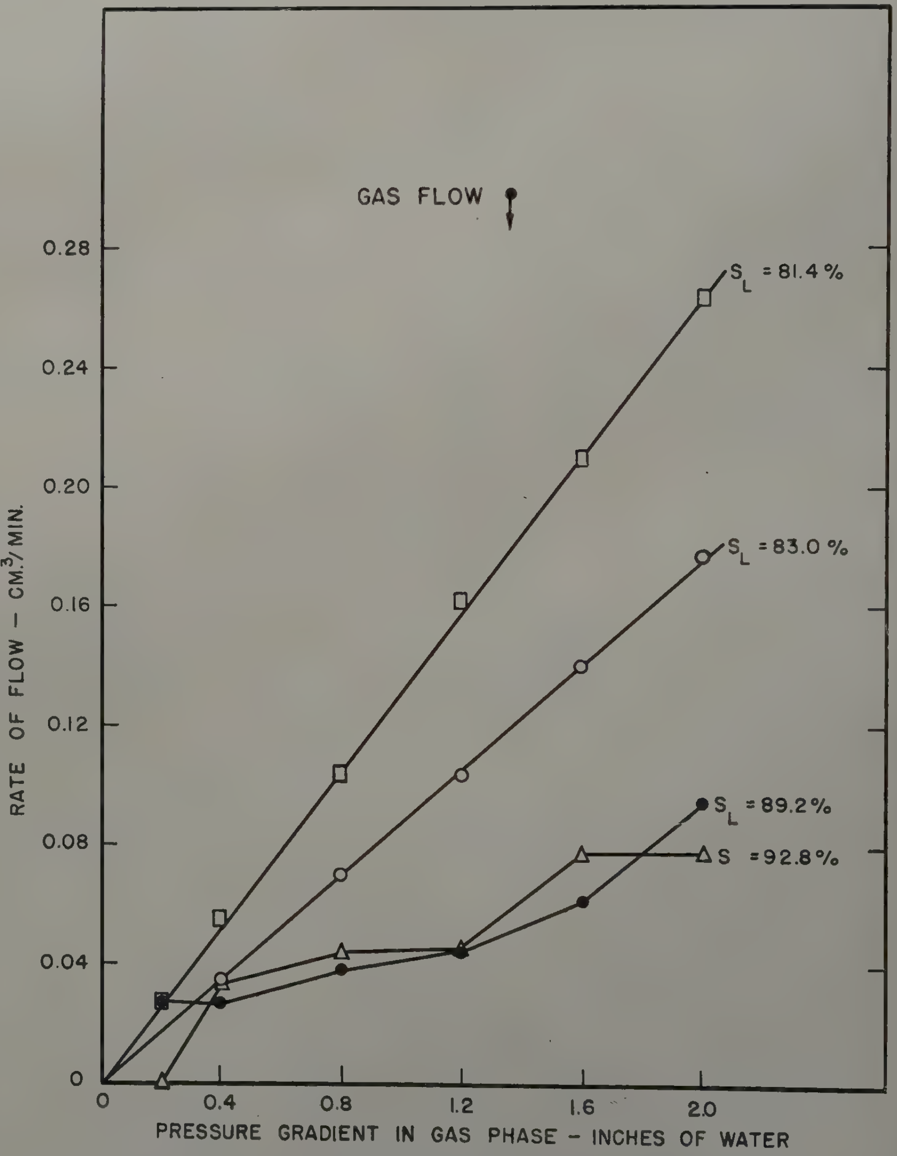

FIG. 6 — RATE OF GAS FLOW AS A FUNCTION OF PRESSURE GRADIENT AND LIQUID SATURATION, ALUNDUM CORE 5S-01.

data. According to Rose[11] this effect appears to be small.

RESULTS AND DISCUSSION

Quite early in the experimental program it became apparent that natural cores failed to meet the requirements as to uniformity, permeability range, similarity in textural properties, and durability which would be required of cores subjected to repeated handling of the sort which might be encountered in the development and testing of apparatus. Much of the work, therefore, has been done using 12 alundum cylinders 1-in. x 1-in. and varying in permeability from 30 to 3300 md. N-decane was used as the saturating liquid phase.

From time to time as the progress of the program warranted, runs were made on natural cores. Since considerably more data have been obtained than are shown in this paper, an attempt has been made to show data which are representative of the whole for illustrative purposes. A comparison between a decane-air system and a connate water-decane-air system using an alundum core is shown in Fig. 3 and a similar comparison using a natural core is shown in Fig. 4.

For both synthetic core material and natural reservoir rock, it is observed that there is good agreement between the results of two phase (gas-oil system) and those of three phase (gas-oil-connate water) systems. The agreement is slightly better in the region of the equilibrium gas saturation, i.e., at that saturation of liquid at which gas first flows. These figures show that the relative permeability to gas is determined by the total liquid saturation and is independent of the presence of water as a co-saturant.

Because of its importance in reservoir engineering calculations and reservoir exploitation, the equilibrium gas saturation is of particular interest. Hassler, Brunner, and Deahl[12] have indicated that the equilibrium gas saturation can occur over a range of several per cent depending mainly upon the extent of any "trap hysteresis" effect. They say, however, that one definite *highest* value of equilibrium gas saturation can be determined by experimental means. This value results from a continual desaturation process until the pressure that is just sufficient to start the flow of gas through the porous medium reaches zero. In other words no liquid has to be displaced or moved aside in order for gas flow to be accomplished. That value of equilibrium gas saturation is probably more significant than any other in regard to the production of oil from a dissolved gas-drive reservoir, and is therefore the value sought in most engineering uses. Some of the early work with the relative permeability cell method had indicated that Darcy's law might not be applicable in the region of the equilibrium gas saturation. Other investigators, using different methods, have exhibited data which indicate that the relative permeability of a core to gas is a function of the rate of flow.[6,7] In order to clarify this, two tests were made using an alundum core having a dry air permeability of 177 md. In the first test the core was set up in the relative permeability to gas cell so that the gas flowed through the core from bottom to top. At discrete liquid saturations a pressure difference was applied in successively increasing steps and the resulting gas flow rate was measured. The data are presented in Fig. 5.

At the higher liquid saturations, no gas flow is obtained for the lower pressure differences. However, once a pressure gradient giving flow has been reached, the rate of flow is more or less

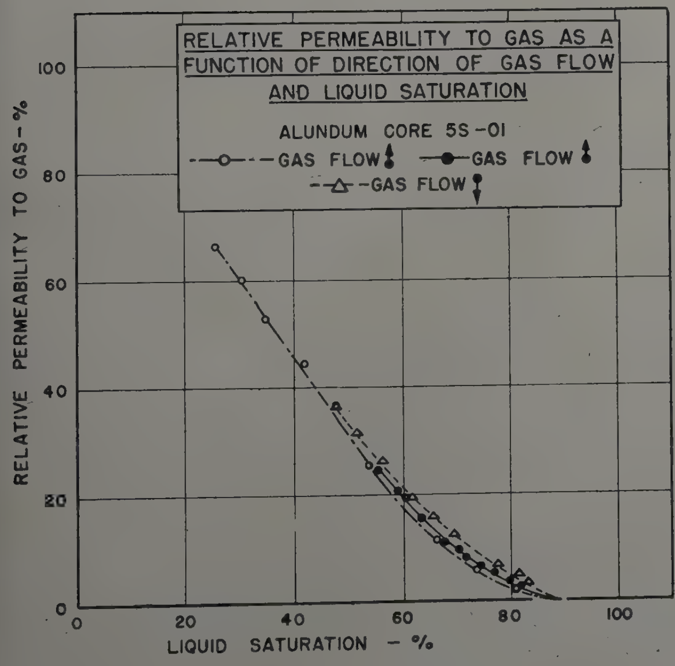

FIG. 7 — RELATIVE PERMEABILITY TO GAS AS A FUNCTION OF DIRECTION OF GAS FLOW AND LIQUID SATURATION.

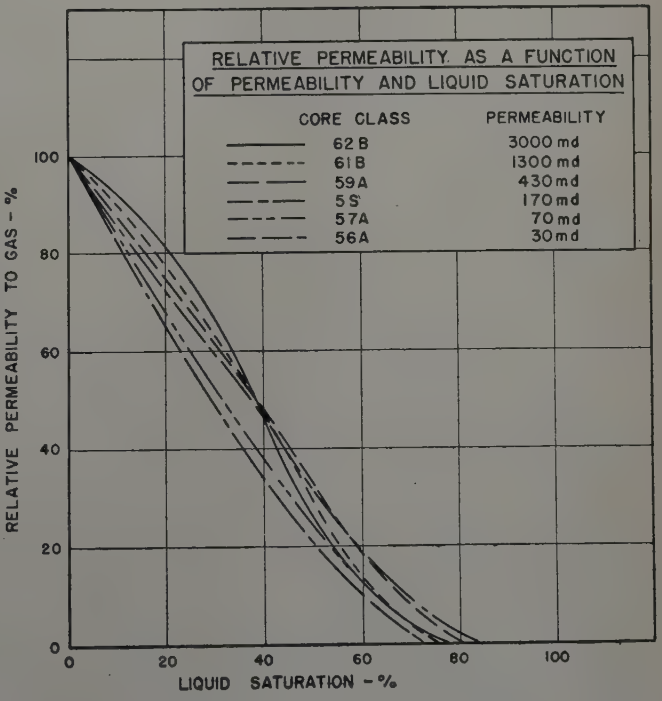

FIG. 8 — RELATIVE PERMEABILITY AS A FUNCTION OF PERMEABILITY AND LIQUID SATURATION.

linear with the pressure gradient. The line segments indicate the range over which flow was obtained. In going from 86.6 per cent to 82 per cent liquid saturation there is a decided improvement in the quality of the data and at the latter saturation gas flow was obtained at the lowest pressure gradient applied. This test therefore indicates that the maximum value of the equilibrium gas saturation lies between 82.0 per cent and 86.6 per cent.

In the second test, the core was set up in the same cell and the gas flow through the core was reversed so that it flowed through the core from top to bottom. The data for this test are shown in Fig. 6. Here, although there is gas flow for all applied pressure gradients at the higher liquid saturations, the data are quite irregular and Darcy's law does not appear to be valid. As in the first test, though, in passing from 89.2 per cent to 83.0 per cent saturation, there is again the distinct improvement in the data and at the latter saturation Darcy's law is valid. Here the maximum value of the equilibrium gas saturation is fixed between the limits of 83.0 per cent and 89.2 per cent.

When the first and second tests on this core are considered together the equilibrium gas saturation is bracketed between the values of 83.0 and 86.6 per cent. The relative permeability to gas curves from these two tests are shown in Fig. 7. The curves extrapolate to an equilibrium gas saturation of 88.0 per cent. The fact that this extrapolated value is slightly higher than the previously indicated maximum perhaps is explained by the fact that in the test cell approximately 50 per cent of one end of the core is in contact with the porous plate so that at liquid saturations very near the equilibrium gas saturation some passages, although filled with gas, are not available for its flow because they terminate at the porous plate. As the liquid saturation decreases the interconnection between passages increases and all become available for flow.

A review of the data of Figs. 3, 4, 5 and 7 shows that although there are deviations among sets at the lower liquid saturations, they converge in the region of the equilibrium gas saturation so that its determination is rather precise. The pressure gradients in the gas phase in these tests have been varied from 0.2 in. to 2.0 in. water. This is considerably less than has been used by other investigators[1,3,4,5,6,7] some of whom report a variation in relative permeability with rate of flow.[6,7] The data of Figs. 5 and 6 do not support this conclusion and the numerous other data obtained show that over this tenfold change in pressure gradient the relative permeability to gas is independent of rate of flow. The use of pressure gradients greatly in excess of those found in the reservoir can easily lead to experimental difficulties, such as displacement effects, which obscure the results. It appears that under the conditions of these experiments and in the reservoir the relative permeability to gas is independent of the rate of flow.

Some work was done to determine whether variations in the specific permeabilities of different cores would be reflected in the appearance of the relative permeability to gas curves of those cores.

For each of the six pairs of alundum cores an average relative permeability to gas curve was obtained in the following manner: Using the curves resulting from the two and three-phase experiments where decane was the displaced liquid phase, a mean liquid saturation value for a given relative permeability value was calculated and plotted against that relative permeability. Enough points were chosen for each pair of cores so that a complete curve resulted. The curves, six in number, were then plotted as in Fig. 8.

It appears that, at least for these alundum cores, there may be a correlation between permeability and relative permeability. At lower liquid saturations there is, without variation, a shifting to the right of the mean relative permeability curve for each step in increasing permeability. At liquid saturations above 40 per cent the trend is somewhat reversed, the shift being to the left with increasing permeabili-

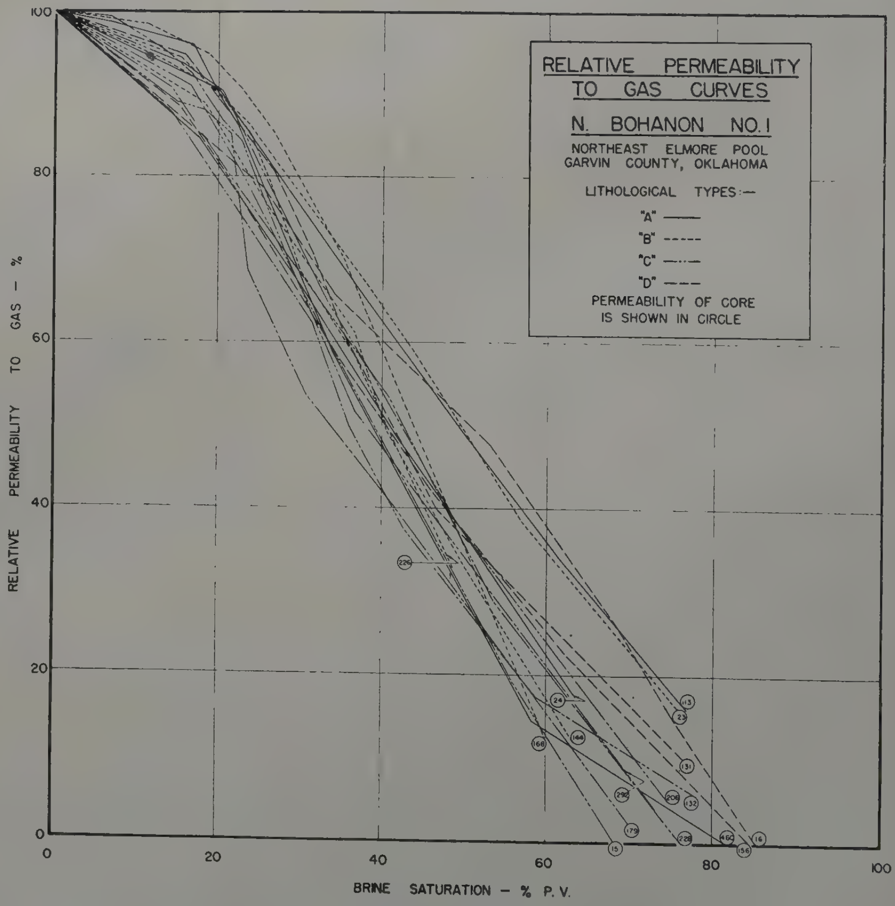

FIG. 9 — RELATIVE PERMEABILITY TO GAS CURVES.

ties. The disposition of the curves in this region, however, does not lend itself to such a generalization as at the lower liquid saturations, since exceptions occur here.

This apparent correlation should not be emphasized since it might be due mainly to the nature of the alundum cores. These particular cores all consist of the same two grain sizes, in varying percentages, and are entirely homogeneous. That the correlation does not exist for natural specimens can be seen from Fig. 9. Here the relative permeability curves are shown for 16 cores recovered from the N. Bohanon No. 1 well, Garvin County, Oklahoma. The figures in the circles are the dry air permeabilities. There is no apparent correlation between permeability and relative permeability. If a correlation exists it is masked by petrofabric variables.

As a matter of fact, the only variables encountered in the course of the laboratory experiments which have an appreciable effect on the relative permeability have been grain size distribution, rock surface characteristics, etc. This is brought out in Fig. 9 where cores of practically the same permeability have widely divergent relative permeability to gas curves. Additional data to illustrate this are shown in Fig. 10 where relative permeability to gas curves are presented for an alundum core, an N. Bohanon No. 1 core and a Nichols Buff sandstone core. Here it is seen that the equilibrium gas saturation for the Bohanon core is 69 per cent, whereas for the other two it is 88 per cent. The curves for the Nichols Buff core and the alundum core are practically identical above a saturation of 60 per cent. Below that saturation they diverge and the curve for the alundum core crosses the Bohanon curve at about 25 per cent saturation.

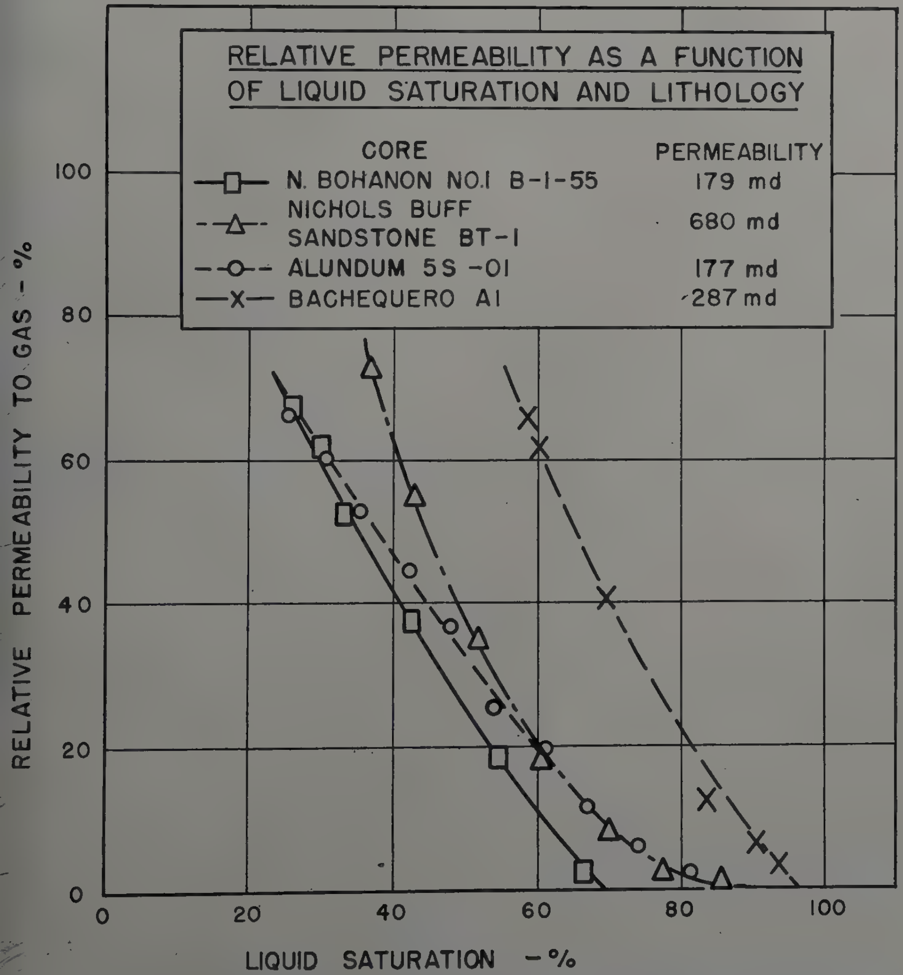

FIG. 10 — RELATIVE PERMEABILITY AS A FUNCTION OF LIQUID SATURATION AND LITHOLOGY.

In the section describing the relative permeability cell it was mentioned that a capillary pressure curve was obtained simultaneously with the relative permeability to gas curve. Since the equipment and procedure are different from those employed with the displacement cell a comparison of the capillary pressure curves obtained by the two methods is in order and is shown for two representative cores in Fig. 11. Also shown is the curve obtained with one of the cores when connate water was present in the core. It will be observed that the agreement between the curves is sufficient to justify the statement that the two methods give the same results.

CONCLUSIONS

From the foregoing discussion, the following conclusions may be drawn:

1. The data obtained by the method described above have a high degree of internal consistency and are reproducible from one test to another.
2. Rate of gas flow has no effect on relative permeability to gas as obtained by this stationary liquid method.
3. No definite correlation has been found between permeability and relative permeability to gas for the systems studied.
4. No definite correlation has been found between petrofabric factors and relative permeability to gas for the systems studied.
5. The capillary pressure curves obtained in the relative permeability cell agree with those obtained in a conventional displacement cell.

NOTE REGARDING USE OF DATA

In view of the fact that variations of relative permeability appear to exist within a single reservoir (see Fig. 9) it becomes necessary to deal with weighted average relative permeability values in the consideration of reservoir engineering problems. For the case of parallel non-connecting strata open to the same well, this averaging process would be as follows:

$$(K_g)\,\text{ave.} = \frac{\sum_{1}^{n} k_n\,(K_g)_n\,x_n}{\sum_{1}^{n} k_n\,x_n}$$

in which k_n is the specific permeability of a uniform stratum x_n thick.

Other more complex systems would require more elaborate means of averaging but would follow the same general principle indicated above.

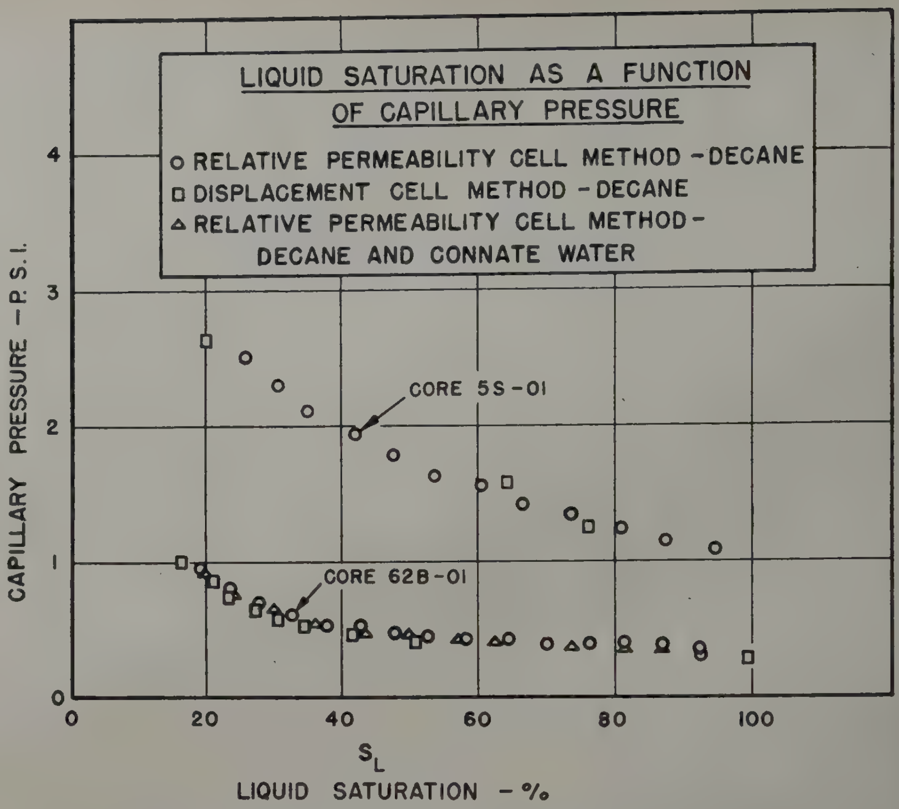

FIG. 11 — LIQUID SATURATION AS A FUNCTION OF CAPILLARY PRESSURE.

ACKNOWLEDGMENT

The authors wish to thank The Carter Oil Co. for permission to publish this paper. They are deeply indebted to W. A. Bruce for many helpful suggestions and contributions to this research program.

REFERENCES

1. Wyckoff and Botset, "The Flow of Gas-Liquid Mixtures Through Unconsolidated Sands", *Physics*, 7, 325 (1936).
2. Hassler, Rice and Leeman, "Recovery of Oil from Sandstones", AIME *Pet. Dev. and Tech.*, 1936.
3. Leverett, "Flow of Oil-Water Mixtures Through Unconsolidated Sand", AIME TP 1003.
4. Leverett and Lewis, "Flow of Gas-Oil-Water Mixtures Through Unconsolidated Sand", AIME TP 1206.
5. Botset, "Flow of Gas-Liquid Mixture Through Consolidated Sand", AIME TP 1111.
6. Morse, Terwilliger and Yuster, "Relative Permeability Measurements on Small Core Samples", Mineral Industries Experiment Station, Technical Paper 124, The Pennsylvania State College.
7. Henderson and Yuster, "Relative Permeability Studies", 11th Annual Secondary Recovery Conference, Penn. State, October 31-November 1, 1947.
8. Hassler, Patent No. 2,345,935, "Method and Apparatus for Permeability Measurements".
9. Rose and Bruce, "Evaluation of Capillary Character in Petroleum Reservoir Rock", AIME *Pet. Dev.* and *Tech.*, 1949.
10. Klinkenberg, L. J., "The Permeability of Porous Media to Liquids and Gases", API *Drilling and Production Practice*, 1941.
11. Rose, W. D., "Permeability and Gas-Slippage Phenomena", API Proceedings of the Twenty-Eighth Annual Meeting, Section IV, 1948.
12. Hassler, G. L., Brunner, E., and Deahl, T. J., "The Role of Capillarity in Oil Production", AIME *Transactions*, 1944.
13. Brownscombe, Slobod and Caudle, "Relative Permeability of Cores Desaturated by Capillary Pressure Method". API Meeting, May, 1949, Los Angeles, Calif.

★ ★ ★

T.P. 2777

DETERMINING FRICTION FACTORS FOR MEASURING PRODUCTIVITY OF GAS WELLS

R. V. SMITH, U. S. BUREAU OF MINES, BARTLESVILLE, OKLAHOMA

ABSTRACT

The theoretical background for calculating friction factors for flow in gas wells by two methods is presented. The first method, requiring pressures, temperatures and specific volumes of the flowing fluids at various depths in the well bore, shows how the mechanical-energy-balance equation for vertical flow may be graphically integrated over the actual path of the expansion of the fluid in the well. Thus, assumptions regarding the effective temperature and effective compressibility of the fluid in the well are avoided. The second method presents an equation derived on a basis of the assumptions that both the temperature and the compressibility are fixed at constant effective values throughout the flowing column of gas. The second method provides a convenient and practical means of calculating friction factors for gas wells and lends itself readily to the problem of calculating subsurface pressures in a flowing gas well. The application of both methods to actual test data taken on a flowing gas well is illustrated in the paper.

INTRODUCTION

As friction factors for the producing strings of flowing gas wells cannot be measured directly and must be calculated from flow-test data, study of the methods of arriving at friction factors is a necessary adjunct to understanding the characteristics of flow in gas wells. There are two methods of calculating friction factors for gas wells; they differ from one another mainly in the treatment of the path of expansion of the fluid in the well. In the flowing well, the energy consumed in lifting the fluid from the bottom to the top of the well, overcoming the friction between the moving fluid and the pipe walls, and increasing the velocity of the fluid as it flows up the producing string is supplied by expansion of the flowing fluid. The available energy is determined by the expansion of the fluid that follows a path determined by conditions of temperature, compressibility and phase changes of the fluid during the expansion. A means of evaluating the available energy in a flowing gas well and determining the proportion of the available energy used in lifting the gas, overcoming friction, and increasing the velocity of flow is developed in this report. Knowing how much energy is consumed in overcoming friction makes it possible to calculate friction factors for given flow rates in given sizes of pipes in wells.

Friction coefficients, as used in this report, are dimensionless proportionality multipliers used in the flow equations to satisfy the equality between the terms of the equation. The square root of the reciprocal of the friction coefficient is termed the friction factor.

It has been known for many years that friction factors may be computed directly from mathematical formulas based on certain assumptions regarding the temperature and compressibility of the moving fluid in a well. A general equation is presented in this report without assumptions for vertical flow of fluids and a conventional-type equation is derived on the basis of assumptions that fix the temperature and compressibility at constant values. Accurate pressures at the sand faces in wells are required in the method of determining the productivity of gas wells, as outlined by Rawlins and Schellhardt[1] in Bureau of Mines Monograph 7. Where measurements are not made with subsurface-pressure gauges or static gas columns are unavailable, flowing pressures customarily are calculated at the sand face in the well by the use of the well-known Weymouth formula[1]. Natural gas engineers have realized that errors introduced by the use of friction factors as given by the Weymouth formula are relatively unimportant in testing low-capacity gas wells; they also know that such factors are important considerations in testing large-capacity gas wells. Accordingly, present research on the productivity of gas wells at the Petroleum Experiment Station of the Bureau of Mines, Bartlesville, Okla., is being directed toward measurement of the pressure loss due to friction in flowing gas wells.

It is beyond the scope of this report to show how friction factors vary with rate of flow and in pipes of different diameters, as it is intended only to develop and illustrate the use of mathematical expressions for calculating friction factors from flow-test data. The equations presented apply only to turbulent flow in circular pipes.

ENERGY RELATIONS FOR FLOW OF FLUIDS[2]

The concept of conservation of energy is usually the basis of any study of fluid flow through vertical pipes as in gas wells, horizontal pipe lines, or orifices. In deriving equations, the following symbols are used:

---

[1] References given at end of the paper.

Manuscript received at the office of the Petroleum Branch September 20, 1949. Paper presented at the Petroleum Branch meetings in Columbus, Ohio, September 26-27, and in San Antonio, Texas, October 5-7, 1949.

[2] The explanation, in this report, of energy relations for fluid flow was taken from a discussion of flow of fluids by Cattell.[2]

A = cross-sectional area of the flow channel, sq ft
U = mean linear velocity of flow parallel to the axis of channel at a given cross section, ft per sec
g = acceleration of gravity, ft per sec per sec
E = total internal energy or intrinsic energy associated with one pound of fluid, ft-lb
p = pressure, lb per sq ft abs
P = pressure, lb per sq in. abs (psia)
v = specific volume of fluid, cu ft per lb
L = distance of a cross section above an assumed datum plane, ft
q = heat, in equivalent ft-lb, imparted to 1 lb of fluid from outside the fluid body
F = mechanical energy, ft-lb per lb of fluid, transformed into heat by frictional resistances.

Subscripts 1 and 2 applied to any of the symbols denote conditions at an upstream cross section A_1 and a downstream cross section A_2; respectively. In the example considered in this report, the upstream cross section A_1 is lower in elevation than the downstream cross section A_2.

Consider a fluid flowing upward from section A_1 to section A_2 through a circular vertical pipe in which A_1 equals A_2 in area. As the fluid under consideration is elastic, it fills the pipe completely, and no external forces except gravity act upon it between the two sections.

In considering a hypothetical well the following assumptions are made:

1. The fluid is homogeneous.
2. The flow is steady with respect to time; that is, in a unit of time the same weight of fluid flows through every cross section.
3. The fluid flows with mean linear velocity U_1 parallel to the axis of the pipe and at right angles to the plane of the cross section, A_1. The mean velocity may be defined as

$$U = \frac{Nv}{A}$$

where

N = weight rate of flow, lb per sec
v = specific volume of the fluid at the point under consideration, cu ft per lb
A = area of cross section under consideration, sq ft

As the flow is considered steady, 1 lb of the fluid passes through sections A_1 and A_2 in the same interval of time. When 1 lb of fluid passes the lower section A_1 it carries with it the following energy:

E_1, its internal energy, resulting from its temperature and the position of its molecules,

$\frac{U_1^2}{2g}$, its kinetic energy, attributable to its upward velocity,

p_1v_1, which represents the mechanical work performed in forcing the pound of fluid across section A_1,

L_1, which is the potential energy (referred to the assumed datum plane) of the pound of fluid resulting from the action of gravity upon it.

Applying terms used in hydraulics, $\frac{U_1^2}{2g}$, p_1v_1 and L_1 may be called, respectively, the velocity head, pressure head, and potential head of 1 lb of fluid at section A_1.

Under the conditions stipulated, the pound of fluid receives no mechanical energy from external sources while passing from A_1 to A_2, but it may receive heat q from sources outside the fluid. If the fluid loses heat, q has a negative value.

At Section A_2, 1 lb of fluid has the internal energy E_2, the velocity head $\frac{U_2^2}{2g}$, the pressure head p_2v_2 and the potential head L_2.

Balancing all forms of energy and expressing quantities of heat in units of equivalent work, it is apparent that:

> The internal energy, velocity head, pressure head, and potential head of 1 lb of fluid at section A_1, plus the heat per lb of fluid imparted from external sources to the fluid between sections A_1 and A_2, equals the internal energy, velocity head, perssure head, and potential head

of 1 lb of fluid at section A_2, or,

$$E_1 + \frac{U_1^2}{2g} + p_1v_1 + L_1 + q = E_2 + \frac{U_2^2}{2g} + p_2v_2 + L_2 \quad . \quad (1)$$

Between sections A_1 and A_2 each pound of fluid does the mechanical work $\int_{v_1}^{v_2} pdv$ upon the surrounding fluid; thus each pound of fluid must receive that amount of work from the rest of the fluid between the two sections. Such work can be done only by converting heat energy of the fluid into mechanical energy. As the work and heat must be equivalent, $\int_{v_1}^{v_2} pdv$ is the measure per pound of flowing fluid, not only of the work received but also of the heat (expressed in equivalent work units) that was transformed into that work. It may, therefore, be considered that each pound of fluid does the work $\int_{v_1}^{v_2} pdv$ upon itself at the expense of its own heat energy.

For each pound of fluid flowing from section A_1 to section A_2 the mechanical work F done against frictional resistance is converted into heat F (expressed in work units) absorbed by the fluid.

With these conceptions, and measuring heat in equivalent work units, a balance of heat (or nonmechanical) energy may be expressed as follows:

The internal energy of 1 lb of the fluid at section A_1, minus the heat energy per pound of fluid transformed into mechanical work by expansion of the fluid between the two sections, plus the heat per pound of fluid into which mechanical work is transformed in overcoming frictional resistance between the two sections, plus the heat per pound of fluid imparted from external sources to the fluid between the two sections, is equal to the internal energy of 1 lb of fluid at section A_2, or,

$$E_1 - \int_{v_1}^{v_2} pdv + F + q = E_2 \quad . \ . \ . \ . \quad (2)$$

Subtraction of equation (2) from equation (1) gives equation (3)[3]

---

[3] Equation (3) may be developed also by balancing mechanical energy. The velocity head, pressure head, and potential head of 1 pound of fluid at section A_1, plus the work per pound of fluid (derived from heat energy) done upon the fluid between the two sections, minus the mechanical energy per pound of fluid converted into heat by frictional resistances between the two sections, is equal to the velocity head, pressure head, and potential head of 1 pound of fluid at section A_2.

$$\frac{U_1^2}{2g} + p_1v_1 + L_1 + \int_{v_1}^{v_2} p\,dv - F = \frac{U_2^2}{2g} + p_2v_2 + L_2 \ . \ (3)$$

Equation (3) may be written in the form:

$$p_1v_1 + \int_{v_1}^{v_2} p\,dv - p_2v_2 = (L_2 - L_1) + \frac{U_2^2 - U_1^2}{2g} + F \ . \ (4)$$

Equation (4) may be considered a general one for the flow of fluids in pipes.

EQUATIONS FOR FLOW OF FLUIDS IN VERTICAL PIPES

Method I (graphic integration)

The application of equation (4) to the evaluation of friction factors for gas wells requires further treatment of term F or the mechanical energy per pound of fluid transformed into heat by frictional resistance. The work done in overcoming frictional resistance through distance dL equals frictional resistance times the distance through which the resistance is overcome. For turbulent flow the frictional resistance is proportional to the surface in contact with the fluid, to the density of the fluid, and approximately proportional to the square of the velocity. If the resistance is proportional to the square of the velocity it is also proportional to the first power of the kinetic energy $\frac{U^2}{2g}$ of 1 lb of fluid. Expressed by symbols, the frictional resistance is proportional to:

$$(dL) \quad (Per) \quad \left(\frac{U^2}{2g}\right) \quad (S)$$

where

dL = length of pipe, ft
Per = perimeter of pipe, ft
U = velocity, ft per sec
S = density, lb per cu ft

or

$$\text{frictional resistance} = (f)\ (dL)\ (Per)\ \left(\frac{U^2}{2g}\right)(S) \ . \ (5)$$

The term f then becomes a proportionality factor to satisfy the equality; it is commonly called the coefficient of friction.

Multiplying the frictional resistance as expressed in equation (5) by the length of pipe dL to obtain the work in overcoming the resistance and dividing by the pounds of fluid contained in the length of pipe dL, the work expended per pound of fluid in overcoming frictional resistance becomes:

$$dF = \frac{(f)\ (dL)\ (Per)\left(\frac{U^2}{2g}\right)(S)\ (dL)}{(A)\ (dL)\ (S)} \ . \ . \ (6)$$

where

A = cross-sectional area, sq ft.

For a circular pipe the perimeter divided by the area equals $\frac{4}{D}$ where D is the internal diameter in ft. Equation (6) becomes:

$$dF = \frac{4f\ U^2\ dL}{2gD} \ . \ . \ . \ . \ . \ . \ . \ . \ . \ . \ . \ (7)$$

or for a finite length of pipe

$$F = \frac{4f}{2gD}\int_{L_1}^{L_2} U^2\ dL \ . \ . \ . \ . \ . \ . \ . \ . \ . \ . \ . \ (8)$$

substiuting the value of the term F given in equation (8) into equation (4)

$$p_1v_1 + \int_{v_1}^{v_2} p\,dv - p_2v_2 = (L_2 - L_1) + \frac{U_2^2 - U_1^2}{2g} + \frac{4f}{2gD}\int_{L_1}^{L_2} U^2\ dL \ . \ . \ . \ . \ . \ . \ . \ . \ (9)$$

The expression at the left of the equality sign (as may be shown analytically or graphically), equals

$$-\int_{p_1}^{p_2} v\,dp$$

or

$$\int_{p_2}^{p_1} v\,dp.$$

If the pressures are expressed in psi instead of lb per sq ft, the expression equals

$$144\int_{P_2}^{P_1} v\,dP.$$

As equation (9) contains a velocity term U which is not commonly used in the gas industry, velocity in ft per sec may be converted to cu ft per 24 hours and specific volume expressed in cu ft per lb by:

$$U = \frac{Nv}{A}$$

where

U = velocity, ft per sec
N = rate of flow of fluid, lb per sec
v = specific volume, cu ft per lb
A = cross-sectional area of pipe, sq ft.

When the volume rate of flow is measured in cu ft of gas per 24 hours, the term N becomes:

$$N = \frac{QG}{86{,}400 \times 13.364}$$

where

Q = volume rate of flow, cu ft per 24 hours (absolute pressure base = 14.4 psi and temperature base = 60°F)
G = specific gravity of fluid, air = 1.0
86,400 = number of seconds in 24 hours
13.364 = volume of one pound of dry air at an absolute pressure of 14.4 psi and at a temperature of 60°F, cu ft.

Then the velocity term U becomes:

$$U = \frac{QGv}{1{,}154{,}600\ A} \quad \text{or}$$

$$U^2 = \frac{Q^2G^2v^2}{1.3331 \times 10^{12}\ A^2} \ .$$

By making the indicated substitutions and changing the subscripts 1 and 2 so that they indicate conditions at a depth s and at the wellhead (L = 0) respectively, taking the value of g, the acceleration of gravity, to be 32.17 ft per sec per sec, and changing elevations to depths, equation (9) becomes:

$$144\int_{P_w}^{P_s} v\,dP = L_s + \frac{Q^2G^2(v_w^2 - v_s^2)}{85.772 \times 10^{12}\ A^2} + \frac{fQ^2G^2}{21.443 \times 10^{12}\ DA^2}\int_0^L v^2 dL \ . \ . \ . \ . \ . \ . \ . \ . \ . \ . \ . \ . \ . \ . \ (10)$$

Changing A which is in units of sq ft into terms of inside pipe diameter, in in., and D, in ft, to in., equation (10) becomes:

$$144 \int_{P_w}^{P_s} vdP = L_s + \frac{Q^2G^2(v_w^2 - v_s^2)}{2.5515 \times 10^9\ d^4} + \frac{fQ^2G^2}{53.157 \times 10^6\ d^5} \int_0^L v^2dL \quad . \ . \ . \ . \ . \ . \ . \ . \ . \ . \ . \ . \ . \ . \quad (11)$$

where

P = pressure, psia

v = specific volume, cu ft per lb

L_s = energy required to lift 1 lb of the fluid from depth L in the well, ft-lb (as 1 lb of fluid is under consideration L_s is numerically equal to L)

L = depth of flowing column of fluid, ft

Q = volume rate of flow, cu ft per 24 hours (absolute pressure base = 14.4 psi and temperature base = 60°F)

G = specific gravity of fluid, air = 1.0

d = internal pipe diameter, in.

f = friction coefficient, dimensionless

The subscripts s and w refer to conditions at depth L and at the wellhead respectively.

As equation (11) does not contain assumptions which define the path of the expansion of the fluid, it may be considered general for the flow of fluids in wells.

Method II (mathematical integration)

Starting with equation (9)

$$p_1v_1 + \int_{v_1}^{v_2} pdv - p_2v_2 = (L_2 - L_1) + \frac{U_2^2 - U_1^2}{2g} + \frac{4f}{2gD} \int_{L_1}^{L_2} U^2dL \quad . \ . \ . \ . \ . \ . \quad (9)$$

and making the following assumptions:

1. The flow of fluid in a gas well can be considered to be isothermal at an "effective" temperature.
2. The deviation of the fluid from the ideal gas laws throughout the flow string of the well can be considered constant and can be expressed as an "effective" compressibility factor.

Then the following relationship exists:

$$p_1v_1 = p_2v_2 = ZTb$$

where

Z = effective compressibility factor, dimensionless

T = effective absolute temperature, °F + 459.6

b = gas constant in appropriate units for 1 lb of gas.

In accordance with the assumptions, equation (9) becomes:

$$\int_{v_1}^{v_2} pdv = (L_2 - L_1) + \frac{U_2^2 - U_1^2}{2g} + \frac{4f}{2gD} \int_{L_1}^{L^2} U^2dL \quad . \quad (12)$$

or in differential form[4] it is:

$$pdv = dL + \frac{UdU}{g} + \frac{4f}{2gD} U^2dL \quad . \ . \ . \ . \ . \ . \quad (13)$$

As shown in a previous section of this report, velocity equals rate of flow (weight basis) times specific volume divided by the cross-sectional area.

$$U = \frac{Nv}{A}, \text{ and } dU = \frac{Ndv}{A}.$$

Also, pressure may be expressed in terms of specific volume by the relationship:

$$pv = ZTb,\ p = \frac{ZTb}{v}$$

Substituting $\frac{Nv}{A}$, $\frac{Ndv}{A}$, and $\frac{ZTb}{v}$ for U, dU, and p, respectively, in equation (13),

$$ZTb \frac{dv}{v} = dL + \frac{N^2}{gA^2} vdv + \frac{4fN^2}{2gDA^2} v^2dL \quad . \ . \ . \quad (14)$$

Rearranging and collecting terms,

$$dL = ZTb \frac{dv}{v\left(\frac{4fN^2}{2gDA^2} v^2 + 1\right)} - \frac{N^2}{gA^2} \frac{vdv}{\left(\frac{4fN^2}{2gDA^2} v^2 + 1\right)} \quad (15)$$

Integrating between the limits, L = 0 and $v = v_1$ at the lower, or upstream, end of the length of flow string under consideration and L = L and $v = v_2$ at the wellhead, the result is,

$$L \Big]_0^L = ZTb \left[\frac{1}{2} \log \frac{v^2}{\frac{4fN^2}{2gDA^2} v^2 + 1} \right]_{v_1}^{v_2} - \frac{N^2}{gA^2} \left[\frac{1}{2\left(\frac{4fN^2}{2gDA^2}\right)} \log \left(v^2 + \frac{1}{\left(\frac{4fN^2}{2gDA^2}\right)} \right) \right]_{v_1}^{v_2} \quad . \ . \ . \ . \ . \ . \ . \ . \ . \ . \quad (16)$$

or

$$e^{\frac{2L}{ZTb}} = \left(\frac{v_2^2}{v_1^2}\right) \left[\frac{\left(\frac{4fN^2}{2gDA^2}\right) v_2^2 + 1}{\left(\frac{4fN^2}{2gDA^2}\right) v_2^2 + 1} \right]^{\left(1 + \frac{D}{2fZTb}\right)} \quad . \ . \ . \ . \ . \ . \ . \quad (17)$$

substituting pressure for specific volume according to the following relationships:

$$p_1v_1 = p_2v_2 = ZbT$$

$$v_1^2 = \frac{Z^2b^2T^2}{p_1^2},\ v_2^2 = \frac{Z^2b^2T^2}{P_2^2}$$

equation (17) becomes:

$$e^{\frac{2L}{ZTb}} = \left(\frac{p_1^2}{p_2^2}\right) \left[\frac{p_2^2\left(\frac{2fN^2Z^2T^2b^2}{gDA^2} + p_1^2\right)}{p_1^2\left(\frac{2fN^2Z^2T^2b^2}{gDA^2} + p_2^2\right)} \right]^{\left(1 + \frac{D}{2fZTb}\right)} \quad . \ . \ . \ . \ . \ . \ . \quad (18)$$

where

e = natural logarithm base = 2.71828+

L = length of pipe, ft

Z = effective compressibility factor, dimensionless

---

[4] Using the transformation of the terms to the left of the equality sign in equation (9), which is explained in the previous section of the text, an alternate differential form is obtained.

$$vdp + dL + \frac{UdU}{g} + \frac{4f}{2gD} U^2dL = 0 \quad . \ . \ . \quad (13a)$$

The solution of equation (13a) yields equation (18). Identical solutions for equations (13) and (13a) are made possible by the given assumptions regarding temperature and compressibility.

T = effective absolute temperature, °F + 459.6

b = gas constant = $\frac{1545.4}{M}$, cu ft, lb per sq ft, per degree F abs per lb, M = molecular weight

p_1 = pressure at lower, or upstream, end of section under consideration, lb per sq ft abs

p_2 = pressure at wellhead, lb per sq ft abs

f = friction coefficient, dimensionless

N = rate of flow of gas, lb per sec

g = acceleration due to gravity, ft per sec per sec

D = inside pipe diameter, ft

A = cross-sectional area of pipe, sq ft.

Further simplification of equation (18)[5] may be accomplished by considering the exponent $\left(1+\frac{D}{2fZTb}\right)$ and by substituting the values of the symbols shown later under Method I of this report. The inside diameter of the flow string was 5.012 in. and the average value of the friction coefficient was 0.003664 (see Table II) for the three depths considered. The effective compressibility factor may be assumed to be 0.964 and the effective temperature to be 540.9°F abs. The value of b, the gas constant for 1 lb of gas, may be computed from its specific gravity (0.708) by:

$$b = \frac{53.327}{G}$$

where 53.327 is the gas constant for 1 lb of dry air, and G is the specific gravity of the gas referred to air.

The value of the exponent $\left(1+\frac{D}{2fZTb}\right)$ becomes

$$1 + \frac{\frac{5.012}{12}}{2 \text{ x } .003664 \text{ x } .964 \text{ x } 540.9 \text{ x } \frac{53.327}{.708}} = 1.00145$$

The exponent 1.00145 means that the quantity in brackets, equation (18), is to be multiplied by its 690th root. Although the exact implications of the fractional part of the exponent are difficult to describe for all gas-well conditions, it is believed that the fractional portion of the exponent can be neglected for rates of flow used in testing gas wells. Also, the fractional portion of the exponent is derived from the kinetic energy term of equation (14) and usually is neglected in horizontal pipe line formulas.

Assuming that the exponent is unity, equation (18) becomes:

$$p_1^2 - e^{\frac{2L}{ZTb}} p_2^2 = \left(\frac{2fN^2Z^2T^2b^2}{gDA^2}\right)\left(e^{\frac{2L}{ZTb}}-1\right) \quad . \quad (19)$$

Rearranging and dividing by p_1^2

$$\frac{NZTb}{p_1} = Nv_1 = A\left[\frac{(Dg)}{(2fp_1^2)}\frac{\left(p_1^2-e^{\frac{2L}{ZTb}}p_2^2\right)}{\left(e^{\frac{2L}{ZTb}}-1\right)}\right]^{1/2} \qquad (20)$$

where Nv_1 = volume rate of flow at a pressure of p_1 and a temperature of T, cu ft per sec.

Equation (20) may be simplified further for use in the natural-gas industry by converting the variables to terms that are easily measured. It is customary to express the quantity that will flow in a well through a flow string of given dimensions, under various pressure conditions, in terms of cu ft per 24 hours at specific pressure and temperature bases. To convert volume Nv_1 in equation (20) from cu ft per second at temperature T and pressure p_1 to cu ft per 24 hours Q at a base temperature of T_o and base pressure of P_o it is necessary to multiply by

$$24 \text{ x } 3600 \frac{P_1T_o}{P_oZT}$$

Also, it is customary to express pressure in units of lb per sq in. abs (psia), pipe diameter in in., and area in sq ft in terms of diameter in in. Conversions in these units are obtained by substituting in equation (20) the following:

p = 144 P, where p is in lb per sq ft and P in psia,

$D = \frac{d}{12}$, where D is in ft and d in in., and

$A = \frac{\pi d^2}{4 \times 144}$

Also, gas constant b was shown to equal $\frac{53.327}{G}$. Substituting this quantity for b in the exponent of e, the exponent becomes $0.037504\frac{GL}{TZ}$

It is convenient to use the symbol s for the exponent of e in equation (20).

Equation (20) now becomes:

$$Q=24\text{x}3600\frac{P_1T_o}{P_oZT}\text{x}\frac{\pi d^2}{4\text{x}144}\text{x}\left[\frac{(32.17)\ (d)}{(2)\ (P_1^2)\ (12)\ (f)}\frac{(P_s^2-e^sP_w^2)}{(\ e^s-1\ )}\right]^{1/2} \quad \ldots\ldots \quad (21)$$

or

$$Q = 545.58\frac{T_o}{P_o}\left(\frac{1}{ZT}\right)\sqrt{\frac{1}{f}}\ \sqrt{d^5\left(\frac{P_s^2-e^sP_w^2}{e^s-1}\right)} \quad \ldots\ldots \quad (22)$$

If T_o = 60 + 459.6 = 519.6 °F abs and P_o = 14.4 psia equation (22) becomes

$$Q = 19{,}686\left(\frac{1}{ZT}\right)\sqrt{\frac{1}{f}}\ \sqrt{d^5\left(\frac{P_s^2-e^sP_w^2}{e^s-1}\right)} \quad \ldots\ldots \quad (23)$$

where

Q = volume rate of flow, cu ft per 24 hours (absolute pressure base = 14.4 psi and temperature base = 60°F)

Z = effective compressibility of gas, dimensionless (see text for explanation)

T = effective temperature, °F abs (see text for explanation)

f = friction coefficient, dimensionless

$\sqrt{\frac{1}{f}}$ = friction factor, dimensionless

d = inside diameter of pipe, in.

---

[5] This simplification of equation (18) was suggested by M. H. Cullender of the Phillips Petroleum Co., Bartlesville, Okla.

P_s = subsurface pressure at depth L in the well, psia
P_w = wellhead pressure, psia
e = natural logarithm base = 2.71828+
s = exponent of e in equations (22) and (23) = $0.037504 \dfrac{GL}{TZ}$
G = specific gravity of gas, air = 1.0
L = length of pipe, ft.

If the quantity to the right of the equality sign in equation (23) is multiplied by and at the same time divided by the square root of s, the terms may be rearranged into the following equation:

$$Q = 101{,}650 \sqrt{\frac{d^5}{GZT}} \sqrt{\frac{1}{f}} \sqrt{\left(\frac{P_s^2 - e^s P_w^2}{L}\right)\left(\frac{s}{e^s - 1}\right)} \quad \ldots\ldots\ldots (24)$$

Equations (23) and (24) are identical. However, equation (24) approaches the appearance of the equations for flow in horizontal pipe lines. Equation (24) contains terms, to correct for the weight of the flowing column of gas, that are identical with those derived by Ferguson.[3]

The accuracy of equation (23) depends entirely upon the validity of the three assumptions that were made in the development. Assuming that the temperature and compressibility of the gas in the well are constant at "effective" values defines the path of the expansion in the well. Actually the temperature and compressibility of the flowing gas vary with depth in the well. If the actual path of the expansion (adiabatic, polytropic or isothermal) were known for all conditions, the development of equation (23) could be modified so that the assumptions concerning temperature and compressibility would be eliminated. The third assumption, that the kinetic energy change is negligible, is justifiable for rates of flow used in testing gas wells. However, the exact implications of this assumption may be found by solving equation (18) for a specific well problem.

Equations (23) and (24) are more covenient than equation (11) for calculating subsurface pressures in a flowing gas well but the value of the friction factor must be known before this may be accomplished.

If the rate of flow Q is zero as in a static column of gas, equation (23) and (24) reduce to the familiar equation

$$P_s^2 = e^s P_w^2 \quad \ldots\ldots\ldots\ldots\ldots (25)$$

for computing pressures resulting from the weight of a static column of gas. Thus, the equations for flowing columns of gas meet the necessary conditions that they must describe static columns of gas when there is no flow.

APPLICATION OF EQUATIONS TO A SPECIFIC WELL PROBLEM

Method I (graphic integration)

Equation (11) is particularly useful in evaluating the friction coefficient f for gas wells. Pressures and temperatures must be measured in the flowing column of gas at several depths in the well and the flow rate must be measured by suitable means to permit the application of equation (11). As the foregoing equations show, the flow mechanism in a gas well is essentially a weight-lifting process with frictional effects. Therefore, the specific-gravity term G must convert the volume of gas into the weight of the total fluid lifted in the flow. Consequently, the specific gravity term must contain all the hydrocarbon liquid and water produced during the flow. For gas wells producing hydrocarbon liquid and water, the hydrocarbon liquid: gas and the water: gas ratios must be measured so that a combined specific gravity may be computed for the flow equation.

The specific volume of the fluid at various points in the flow string may be determined in the laboratory by pressure-volume-temperature studies of the fluid or it may be calculated from published sources of information on the compressibility of natural gases. The calculation of specific volumes from compressibility factors may introduce errors unless the factors are known to apply to the fluid.

Evaluation by mathematical means of the terms containing the integral signs in equation (11) involves assumption which define the path of the integral. It is thought that the study of the actual process of expansion in a gas well is not advanced to the point where the exact type of flow, with regard to heat transfer between the fluid and its surroundings, can be defined for all conditions. In a previous section of this report an equation was developed which is based on the assumption that flow in gas wells is isothermal.

Provided pressures, temperatures and specific volumes are at hand for a given flow rate in a gas well, equation (11) may be solved for the friction coefficient by graphic integration of $\oint_{P_w}^{P_s} v\,dP$ and $\oint_0^L v^2 dL$. Line integral signs are used because the values of specific volume required for the integration are a function of the temperature as well as of the pressure and the relation between temperature and pressure is not specified by the terms of the integral. Solutions for similar equations applied to flow in oil wells have been given by Cattell[2] and Eilerts, Smith and Cook[4]. The graphic integration may be done with a planimeter or other suitable means.

The data necessary for evaluating the friction coefficient for a given flow rate in a gas well by means of equation (11) are illustrated in Table I.

Table I

Data Required for Graphic Integration (Method I) to Evaluate Friction Coefficients and Friction Factors For a Flowing Gas Well in the Panhandle Field, Texas

Flow Rate, M cu ft per 24 Hours	Depth to Pressure Datum Point, ft	Temperature at Pressure Datum Point, °F	Pressure at the Indicated Depth, psia	Compressibility Factor at Datum Point	Specific Volume, cu ft per lb	Specific Volume Squared, v^2
5,904	0	74.9	244.6	0.966	1.1031	1.2168
5,904	50	75.2	245.0	.965	1.1018	1.2140
5,904	1,000	80.7	253.9	.964	1.0729	1.1511
5,904	2,000	85.7	263.4	.963	1.0427	1.0872
5,904	2,250	87.0	265.8	.963	1.0359	1.0731
5,904	2,500	87.6	267.5	.963	1.0305	1.0619

d, inside diameter of flow string, in.=5.012
G, specific gravity of gas (air=1.0)=0.708

The flow rate was measured with an orifice meter and computed to a pressure base of 14.4 psia and 60°F in accordance with Gas Measurement Committee Report No. 2 issued by the American Gas Association. Pressures at the various depths in the flowing column of gas were measured with an Amerada-type subsurface-pressure gage, and a recording-subsurface-temperature gage was run simultaneously with the pressure gage. The pressure-gage chart was interpreted according to the methods proposed by Smith and Dewees.[5] Wellhead pressures were constant throughout the test and were determined with a calibrated piston gage while the subsurface-pressure gage was at each indicated depth in the well. Compressibility factors at each pressure and corresponding temperature in the well were computed from the measured specific gravity of the gas using unpublished data in the files of the Bureau of Mines. Specific volumes and the squares of the specific volumes were computed from the compressibility factors.

The specific-volume data for a flow rate of 5904 Mcf per 24 hours (14.4 psia, 60°F) of Table I were plotted against pressure as is illustrated in Fig. 1. At a depth of 2500 ft, the specific volume was 1.0305 cu ft per lb, while at the wellhead the specific volume was 1.1031 cu ft per lb. At the same time, the temperature of the gas stream decreased from 87.6°F at a depth of 2500 ft to 74.9°F at the wellhead. The area on Fig. 1 bounded by the pressure ordinates between the wellhead pressure of 244.6 psia and the pressure of 267.5 psia at a depth of 2500 ft, the dashed lines to the curve and the curve itself, when multiplied by 144 is the energy in foot-pounds expended by 1 lb of gas in moving from a depth of 2500 ft to the wellhead or

$$\text{Energy, ft-lb per lb of gas} = 144 \int_{244.6}^{267.5} vdP$$

The area between the indicated pressure limits may be measured with a planimeter or by any other method of approximation suitable for a finite area. For example, the area within the limits outlined above as determined with a planimeter is equivalent to 3515.8 ft-lb of energy which is used in the flowing progress to overcome frictional effects, to increase the kinetic energy of the gas as represented by a velocity change, and to lift the lb of gas from a depth of 2500 ft to the wellhead.

Equation (11) requires the evaluation of another quantity:

$$\int_0^L v^2dL.$$

By plotting specific volume squared against depth as illustrated in Fig. 2, the quantity may be found by measuring the area between the curve and the depth ordinate within the proper depth limits. The actual measurement of the area is similar to that described in the preceding paragraph. The area on Fig. 2 bounded by the wellhead depth ($L = 0$) and a depth of 2500 ft was found by measurement with a planimeter to be 2839.3 units whose dimensions are volume squared times length divided by weight. Multiplication of these units by the proper quantities as indicated in equation (11) converts them to work in ft-lb.

The evaluation of the remaining terms of equation (11), the work required to lift 1 lb of gas to the wellhead and the work converted to kinetic energy requires the substitution of the proper quantities into the equation. The work necessary to lift 1 lb of gas through a vertical distance L is L ft-lb. The value of the kinetic energy term of equation (11) is found by substituting the values for the rate of flow, wellhead specific volume and specific volume at the given depth, and the inside diameter of the pipe.

The complete solution of equation (11) for the friction coefficient covering three successive depths for a flowing gas well (data presented in Table I) is given in Table II. The energy terms apply to 1 lb of gas flowing in the well. Item 1 shows the available energy for the flow process from the indicated depths to the wellhead. The energy required to lift the lb of gas to the surface and the energy used to increase the velocity of the gas are given opposite items 2 and 3, respectively. The excess of the available energy over that required to lift the gas and increase its velocity is transformed into heat by frictional effects (item 4). The remainder of the table illustrates the method of computing friction coefficients and friction factors from data on the amount of energy expended to overcome friction.

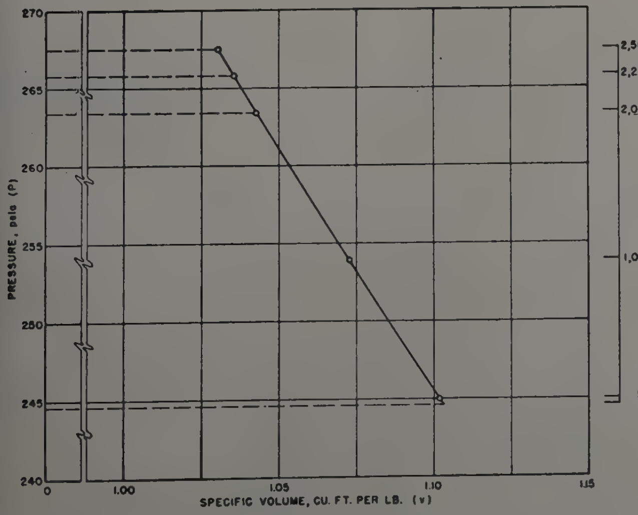

FIG. 1—GRAPHICAL EVALUATION OF ENERGY REQUIRED FOR MOVING ONE LB OF FLUID TO THE WELLHEAD FOR A FLOWING GAS WELL, $\int_{P_w}^{P_s} vdP$.

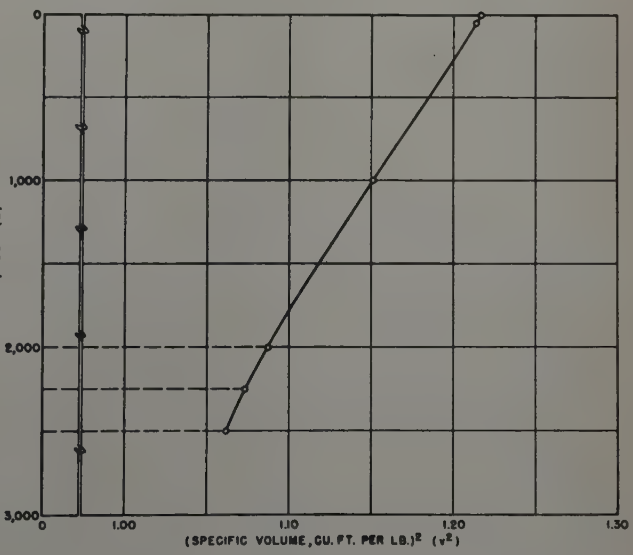

FIG. 2—GRAPHICAL EVALUATION OF THE INTEGRAL $\int_0^L v^2dL$ FOR A FLOWING GAS WELL.

Table II

Evaluation by Graphic Integration (Method I) of Frictional Effects, Friction Coefficients and Friction Factors for a Flowing Gas Well in the Panhandle Field, Texas

Depth considered, ft	2000	2250	2500
(1) Available energy, $144 \int_{P_w}^{P_s} v dP$, ft-lb	2903.8	3,262.9	3515.8
(2) Energy to lift gas, L_s, ft-lb	2000.0	2250.0	2500.0
(3) Energy converted to kinetic energy $= \frac{Q^2G^2(v_w^2 - v_s^2)}{2.5515 \times 10^9 d^4}$ ft-lb	1.4	1.6	1.7
(4) Frictional effects $= \frac{f\ Q^2G^2}{53.157 \times 10^6 d^5} \int_0^L v^2 dL$, ft-lb $= (1) - (2) - (3)$	902.4	1011.3	1014.1
(5) $\frac{Q^2G^2}{53.157 \times 10^6 d^5}$	103.92	103.92	103.92
(6) $\int_0^L v^2 dL$	2302.4	2572.5	2839.3
(7) Friction coefficient, $f = (4)/(5) \times (6)$, dimensionless	0.003772	0.003783	0.003437
(8) Friction factor, $\sqrt{\frac{1}{f}}$, dimensionless	16.28	16.26	17.06

Note: Well was flowing at the rate of 5904 Mcf per 24 hours (14.4 psia, 60°F) through a 5.012 in. inside diameter flow string.

The percentage distribution of the available energy among friction, lifting, and velocity increase is shown in Table III. For this particular well producing gas through a 5.012-in.-inside-diameter flow string at a rate of 5904 Mcf per 24 hours approximately 30 per cent of the available energy was consumed in overcoming friction; the remaining 70 per cent was used to lift the gas to the wellhead, and 0.05 per cent of the energy was used to increase the velocity of the gas. In comparison with frictional effects and lifting requirements the loss due to velocity increase was negligible.

The difference between frictional effects as reflected by energy, friction coefficient or friction factor as shown in Table II for the same flow rate in the same well but from different depths probably can be attributed to errors in the measurement of pressure.

Method II (mathematical integration)

Equation (23), (or equation (24)), which was obtained by mathematical integration of the energy-balance relationships is in convenient form for computing friction factors for flowing gas wells if the flow rate and the pressure at a given depth in the well is known.

Table III

Distribution of Available Energy for a Flowing Gas Well in the Panhandle Field, Texas

Distribution of Energy	Per Cent for Flow from Indicated Depths, ft		
	2,000	2,250	2,500
Lifting	68.87	68.96	71.11
Kinetic	.05	.05	.05
Frictional effects	31.08	30.99	28.84
Total or available energy	100.00	100.00	100.00

Employing the same data presented previously to illustrate the use of Method I, with estimated effective temperatures and compressibilities, friction factors may be computed by means of equation (23). The required data are illustrated in Table IV, which contains part of the data presented previously in Table I. In addition, Table IV shows effective temperatures and compressibilities estimated for the flowing column of gas to the indicated depths.

Exact methods of estimating the effective temperature and compressibility to describe adequately the behavior of a column of gas are not known. If the temperatures measured at different depths in the flowing well (Table I) are plotted as a function of depth on regular coordinates, a curve is obtained which changes from a straight line near the surface to a curved line at the lower depths. The values of effective temperatures presented in Table IV were obtained by determining the area within the limits of zero depth and the depth under consideration between the depth-temperature curve and a given reference temperature; the measured area was then divided by the specific depth under consideration to obtain an effective temperature.

Table IV

Friction Factors and Data Required for Their Computation by Mathematical Integration (Method II) for a Flowing Gas Well in the Panhandle Field, Texas

Flow Rate, M cu ft per 24 Hours	Depth to Pressure Datum Point, ft	Pressure at Indicated Depth, psia	Effective Temperature to Depth, °F	Effective Compressibility to Depth, Dimensionless	Friction Factor, $\sqrt{\frac{1}{f}}$ Dimensionless
5,904	0	244.6			
5,904	50	245.0			
5,904	1,000	253.9			
5,904	2,000	263.4	80.7	0.964	16.27
5,904	2,250	265.8	81.3	.964	16.25
5,904	2,500	267.5	82.0	.964	17.05

d, inside diameter of flow string, in.=5.012
G, specific gravity of gas (air=1.0)=0.708

Other methods of arriving at an effective temperature have been devised but the superiority of any one method is not known.

The effective compressibilities given in Table IV are those computed for the gas under pressure and temperature conditions at the midpoint of the flowing column of gas.

Substitution of the data shown in the first five columns of Table IV, with the values of the inside pipe diameter and the specific gravity of the gas, into equation (23) permits calculating the friction factor shown in the last column of Table

IV. For example, after substituting the values given for the depth of 2500 ft in Table IV into equation (23), the friction factor may be computed by completion of the indicated arithmetical operations in the following expressions:

$$\mathrm{s} = \text{exponent of e} = 0.037504\ \frac{.708 \times 2500}{.964 \times 541.6}$$

$$\mathrm{s} = 0.12714$$

$$\mathrm{e}^{\mathrm{s}} = \mathrm{e}^{.12714} = 1.1356$$

$$5{,}904{,}000 = 19{,}686\ \left(\frac{1}{.964 \times 541.6}\right)\sqrt{\frac{1}{\mathrm{f}}}$$

$$\sqrt{5.012^5\left(\frac{267.5^2 - 1.1356 \times 244.6^2}{1.1356 - 1}\right)}$$

or $$\sqrt{\frac{1}{\mathrm{f}}} = 17.05$$

Values of the number e raised to powers may be taken from mathematical tables, computed with logarithms or calculated by means of the infinite series:

$$\mathrm{e}^{\mathrm{s}} = 1 + \mathrm{s} + \frac{\mathrm{s}^2}{2} + \frac{\mathrm{s}^3}{6} + \frac{\mathrm{s}^4}{24} + \ldots\ .$$

Previously, friction factors for the same depths and basic data were computed by Method I, involving graphic integration, and were presented in Table II. Friction factors computed by Methods I and II and shown for comparison in Table V indicate that by either method virtually identical results are obtained. Data shown in Table V indicate for the given example that the estimation of effective temperatures and compressibilities by Method II gives accurate results.

The friction factors, presented in Table V, agree closely for depths of 2000 and 2250 ft but have a much higher value for a depth of 2500 ft; the difference probably is the result of error in pressure measurement at a depth of 2500 ft. Present-day knowledge of friction factors for gas wells is too limited to permit conclusions as to the accuracy of data shown in Table V, which are presented only to show the close agreement of friction factors calculated by two different methods.

Table V

Friction Factors Computed by Method I (Graphic Integration) for a Flowing Gas Well in the Panhandle Field, Texas

Flow Rate, M cu ft per 24 Hours	Depth Considered, ft	Friction Factors	
		Method I	Method II
5,904	2,000	16.28	16.27
5,904	2,250	16.26	16.25
5,904	2,500	17.06	17.05

SUMMARY

Two methods of calculating friction factors from data taken on flowing gas wells are presented in this report. Method I, which requires flowing pressures and temperatures at several points in the flowing gas stream, provides a solution for the energy-balance equation by graphic integration over the actual path of the expansion of the fluid in the well. In Method II, the energy-balance equation is integrated mathematically, the assumption having been made that the flow in a gas well is isothermal and at a constant compressibility, even though the temperature and compressibility of the fluid vary through wide limits.

The graphic integration of the energy-balance equation (Method I) provides a means of determining the energy available for lifting the fluid from the well and overcoming friction as the integration follows the expansion of the fluid along the path determined by temperature, compressibility and phase changes. Thus, condensation of liquids and wide variations in temperature and compressibility are taken into account without the necessity of making assumptions that may or may not apply. Method I, therefore, is particularly applicable in calculating friction factors for deep high-pressure and high-temperature gas wells.

The accuracy of Method I depends upon the efficiency of the graphic integration. The curves, illustrated by Fig. 1 and 2, should be plotted on suitable coordinates so that the areas are large enough to permit accurate measurement with a planimeter. If a planimeter is not available, one of several methods of estimating areas may be used.

The mathematically integrated equation (Method II) assumes a definite path for the expansion of the fluid in the well with both the temperature and the compressibility fixed at constant values. Its accuracy depends upon the degree to which the effective temperature and compressibility approximate conditions in the well. Method II provides a convenient and practical method for calculating friction factors from data on flowing gas wells and lends itself readily to the calculation of subsurface pressures in a flowing gas well which cannot be accomplished by Method I.

ACKNOWLEDGMENTS

The Bureau's study of the productivity of gas wells is being carried on in cooperation with the American Gas Association. The assistance given by E. L. Rawlins, chairman, Gas-Well Deliveries Subcommittee of the Natural Gas Department, American Gas Association, is gratefully acknowledged.

The investigations are under the general supervision of R. A. Cattell, chief, Petroleum and Natural Gas Branch, Bureau of Mines, Washington, D. C., and H. C. Fowler, supervising engineer, and C. J. Wilhelm, engineer in charge of production research, Petroleum Experiment Station, Bartlesville, Okla.

Acknowledgment is due the management of Phillips Petroleum Co. for granting the writer permission to publish certain data contained in the report. C. B. Carpenter, R. H. Espach, J. W. Ferguson, R. V. Higgins and H. C. Miller, of the Bureau of Mines, offered helpful suggestions in the preparation of the report. The comments of C. W. Binckley, of Phillips Petroleum Co., who reviewed the manuscript, are appreciated. S. E. Daniel prepared the illustrations. F. G. Archer assisted in the field testing.

REFERENCES

1. Rawlins, E. L., and Schellhardt, M. A., Back-Pressure Data and Their Application to Production Practices, Bureau of Mines Monograph 7, 1936, 210 pp.

2. Cattell, R. A., General Equations for Flow of Fluids, appended to: Lindsly, B. E., A Bureau of Mines Study of a "Bottom-Hole" Sample from the Crescent Pool, *Petroleum Engineer*, vol. 7, part 3, April 1936, pp. 38-42.
3. Ferguson, J. William, "Calculation of Back-Pressure Tests on Natural Gas Wells," *Oil and Gas Jour.*, vol. 37, Jan. 19, 1939, pp. 47-53.
4. Eilerts, K., Smith, R. V., and Cook, A. B., Properties of a Petroleum-Reservoir Liquid and Its Residua with Applications of the Data to Production Problems, Bureau of Mines Report of Investigations 3474, 1939, 32 pp.
5. Smith, R. V., and Dewees, E. J., "Sources of Error in Subsurface-Pressure Gage Calibration and Usage," *Oil and Gas Jour.*, vol. 47, Dec. 9, 1948, pp. 85-98.

DISCUSSION

By C. W. Binckley, Phillips Petroleum Co., Bartlesville, Okla.:

The vertical flow equation developed by Smith in his paper and described as equation (24) is the equation generally used to compute bottom-hole flowing pressures in gas and condensate wells. In the use of the equation, it is necessary to first obtain friction factors, an effective temperature factor of the gas stream and an effective compressibility factor. The accuracy of the computed bottom-hole working pressures is primarily dependent upon the accuracy of the friction factors and the validity of the methods used to determine the effective temperature and effective compressibility factors.

Several engineers have recently attempted to develop a general vertical flow equation for gas in which the temperature and compressibility are included as functions of depth and pressure. Such an equation could be used to compute bottom-hole flowing pressures by application of suitable friction factors. An equation of this nature has not been published and I do not believe one has been developed in a usable form.

Smith gives us a different approach to the problem. He describes a graphic integration method for determining friction factors by use of well test data. He then proceeds to show that by use of the general vertical flow equation, assuming an effective compressibility and temperature found at the midpoint of the flowing gas column, that a very close check is obtained for friction factors determined by the equation and by the graphic integration method. The check on friction factors was obtained by using data taken on a well with a relatively low pressure and low temperature flowing gas column.

The application of the procedures described in the paper to the determination of effective compressibility for high temperature and pressure gas columns of wells is not discussed by the author. This is an important point in improving the results of computed bottom-hole flowing pressures. For example, the graphic integration method can be used to establish friction factors. The friction factors can be used in connection with the general vertical flow equation and temperature gradient data to establish the effective compressibility. If the nature of the effective compressibility can be ascertained, we will have a better approach to the computation of reliable bottom-hole flowing pressures. In fact computed pressures should be as reliable as those measured with the bottom-hole pressure gage.

Furthermore, by proper correlation of experimentally determined friction factors with Reynolds numbers or other indexes and by use of a method for determining effective compressibility, it is probable that accurate bottom-hole flowing pressures can be established for all wells in a field by obtaining basic test data on a few representative wells. ★ ★ ★

T.P. 2708

PERFORMANCE CHARACTERISTICS OF A VOLUMETRIC CONDENSATE RESERVOIR

F. H. ALLEN AND **R. P. ROE,** MEMBERS AIME, STANOLIND OIL AND GAS COMPANY, TULSA, OKLAHOMA

ABSTRACT

The performance history of a volumetric gas condensate reservoir is presented. Curves depict the pressure-production relation and illustrate the phase behavior of the reservoir fluid. This performance is compared to calculated performance.

This Bacon Lime Reservoir was discovered in 1941 and has been produced to field separators and gas sales. Reservoir performance has been observed by periodic bottom hole pressure surveys and companion sample analysis of well effluents, in addition to gas and condensate production data.

The pressure-production history demonstrates that the reservoir has produced under volumetric control. The "retrograde" behavior of the reservoir fluid is illustrated by decreasing butanes-plus content of the well effluent, followed by revaporization as the reservoir pressure approaches abandonment. Calculated performance predictions are compared to actual performance and some discussion offered on apparent discrepancies.

INTRODUCTION

Since the late 1930's, many gas condensate reservoirs have been developed, the retrograde theory of phase behavior has been generally accepted, and a number of cycling programs have been initiated. Numerous technical papers have since appeared in the literature dealing with the theory and application of cycling the gas condensate reservoirs. Some cycling operations have now advanced to a stage where it is possible to determine performance characteristics to a fair degree of accuracy.

Field performance data for gas condensate reservoirs operated by pressure depletion have not been so extensively reported in the literature, although their probable behavior has been discussed in explanation of the retrograde theory. It is the purpose of this paper to compare calculated theoretical reservoir performance with field observations and well stream analyses which have been obtained throughout the practical producing life of a small volumetric gas condensate reservoir.

The reservoir under study is the Bacon Lime Zone of a field located in East Texas. The Bacon Lime occurs in the Lower Glen Rose Formation of Cretaceous Age. This Bacon Lime Reservoir is encountered at an average depth of 7600 ft (7200 ft subsea elevation) and comprises approximately 3100 acres located on a structural high with 80 ft of productive closure. The producing formation consists of approximately 50 ft of dense crystalline fossiliferous dolomite of generally low permeability with typical wide variation in both permeability and porosity, the more permeable stringers measuring 30 to 40 millidarcys. The average porosity is estimated to be 10 per cent with a connate water saturation of approximately 30 per cent of the pore space. The reservoir temperature was found to be 220°F and the original pressure was 3691 psia at –7200 ft elevation.

The reservoir was discovered in November, 1941, and is now essentially depleted. Throughout most of its productive life, from the standpoint of cumulative withdrawals, the reservoir has been produced by five wells. During its latter stages of depletion, 16 wells were completed in the Bacon Lime.

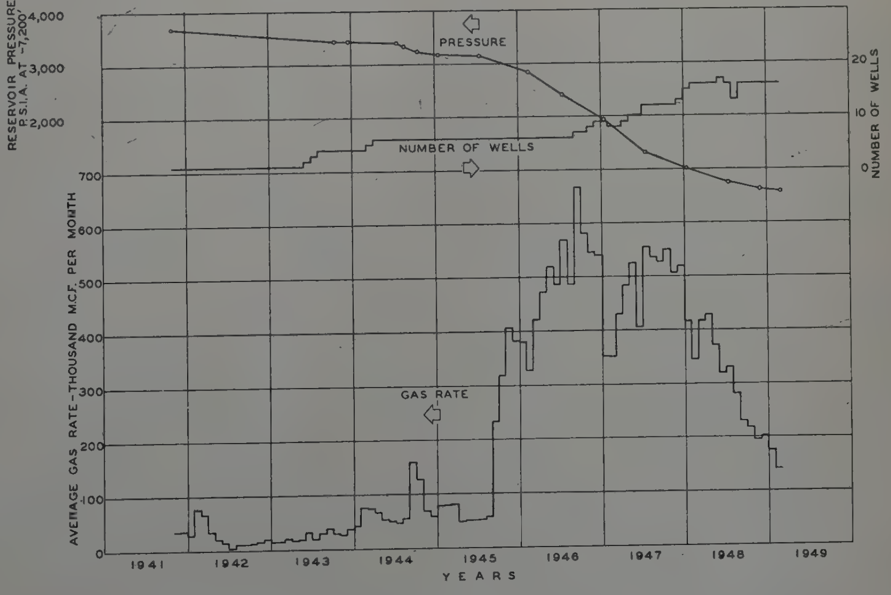

FIG. 1 — BACON LIME CONDENSATE RESERVOIR, RESERVOIR PERFORMANCE.

---

[1] References are given at end of paper.

Manuscript received at the office of the Petroleum Branch October 3, 1949. Paper presented at the Petroleum Branch meeting in San Antonio, October 5-7, 1949.

Remarkably poor communication has been observed between the wells producing from this zone. Early in the life of the reservoir, it was concluded that it would not be feasible to attempt cycling or pressure maintenance in this small reservoir. The reservoir has, therefore, been produced by pressure depletion with three-stage separation. The first separator has been operated at approximately 500 psig throughout most of the producing life of the reservoir and the second or intermediate stage at 40 psig. The estimated ultimate recovery by this means is in excess of 21,000,000 Mcf of gas and 850,000 bbl of condensate. The production history of the reservoir is shown in Fig. 1.

The initial composition of the reservoir fluid, based upon analyses of companion samples which were obtained from the discovery well soon after its completion, was determined to be as follows:

Table I

Initial Composition of Reservoir Fluid

	Mol Fraction
Methane	0.7690
Ethane	0.0770
Propane	0.0335
Butanes	0.0350
Pentanes	0.0210
Hexanes	0.0150
Heptanes - plus	0.0360
Carbon Dioxide	0.0135
	1.0000

Heptanes - plus:
Mol Wt 130
Sp Gr 0.7615

CALCULATED THEORETICAL PERFORMANCE

Employing this initial composition and the vaporization equilibrium constants of Roland, Smith and Kaveler[1] corrected to a convergence pressure of 4200 psia at 220°F, the theoretical performance of the reservoir was calculated under the two separate assumptions of flash and differential vaporization. These are comparable to two methods under which laboratory cell experiments are normally conducted in investigations to determine the changes which will occur in the composition of the production from a volumetric condensate reservoir during its depletion. The vaporization equilibrium constants which were used in these calculations

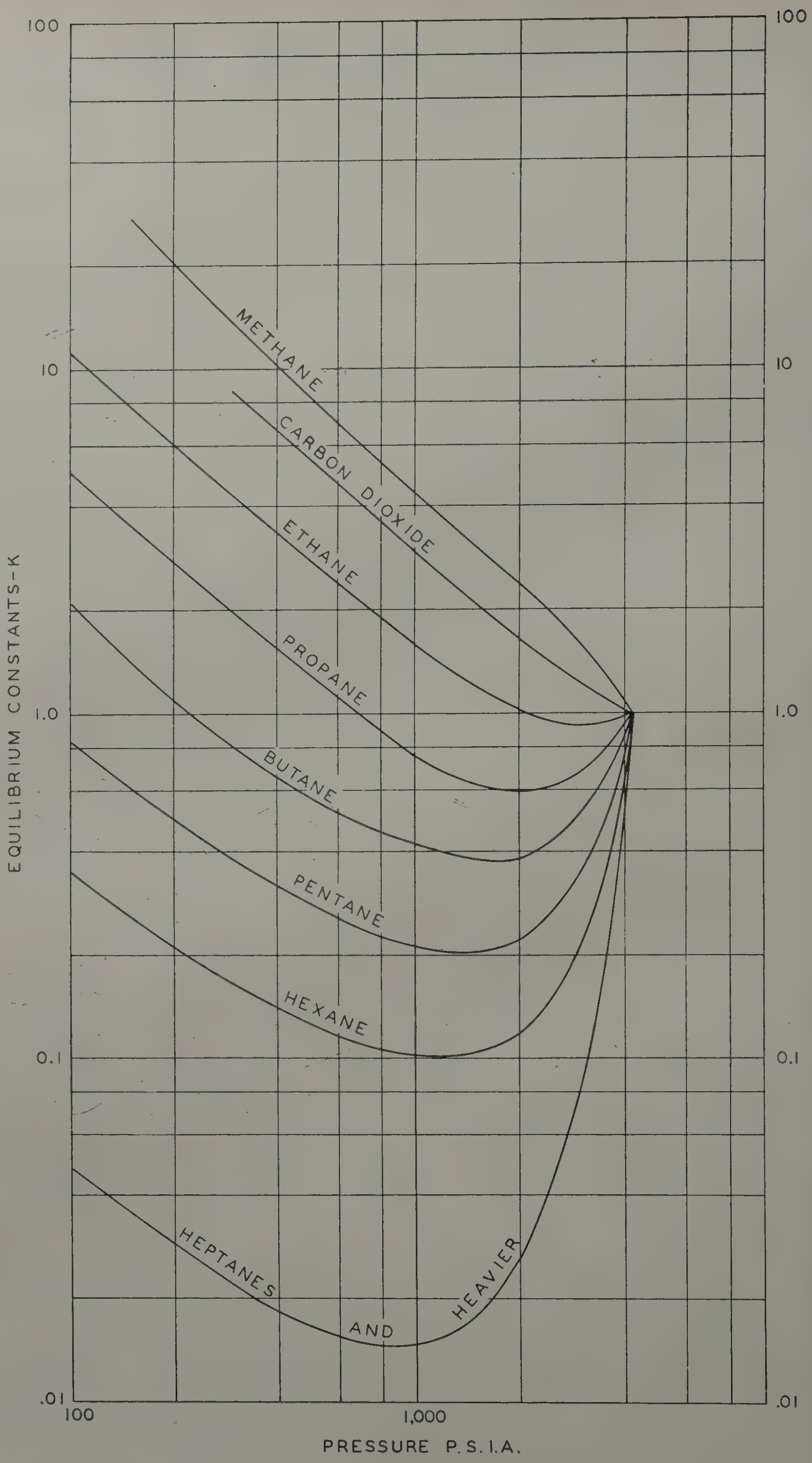

FIG. 2 — BACON LIME CONDENSATE RESERVOIR, VAPORIZATION EQUILIBRIUM CONSTANTS, RESERVOIR TEMPERATURE 220°F.

are shown plotted against pressure in Fig. 2. The constant for the Heptane-plus fraction was estimated, taking into account its reported molecular weight and specific gravity. The two types of estimated performance calculations are illustrated graphically in Fig. 3. The flash vaporization calculations were accomplished by assuming a constant composition of the whole system and computing the composition and volumes of each phase which resulted at successive reductions in pressure. The differential vaporization calculations were made by flashing the original composition to the first pressure from which the compositions and volumes of the two phases were computed. The volume of the vapor phase which it was necessary to produce in order to maintain a constant volume was then calculated and the number of mols of each component in the vapor represented by this volume was subtracted from the system. This resulted in a new over-all composition which was then flashed to the second or next lower pressure. This series of calculations representing differential vaporization assumed that only the vapor phase was produced from the reservoir with no flow, or production of the liquid phase. The resulting variations in composition of the vapor phase which was assumed to represent the composition of the well stream during the decline in reservoir pressure under both these methods of calculated theoretical performance are shown in Fig. 4. The two methods of calculation indicate the same well stream composition until the reservoir pressure drops to approximately 1500 psia after which differential vaporization produces greater revaporization of the ethane through hexanes components than is obtained from the flash vaporization process. Both vaporization processes indicate significant revaporization of the heavier components at reservoir pressures below 1200 psia. The pressure at which revaporization commences for each component varies progressively from approximately 3000 psia for ethane to about 1400 psia for the heptanes-plus fraction.

Gas deviation factors determined from reduced temperature and pressure correlations shown in Fig. 5 indicate essentially no difference in compressibility of the vapor phases obtained from the differential and flash vaporization proc-

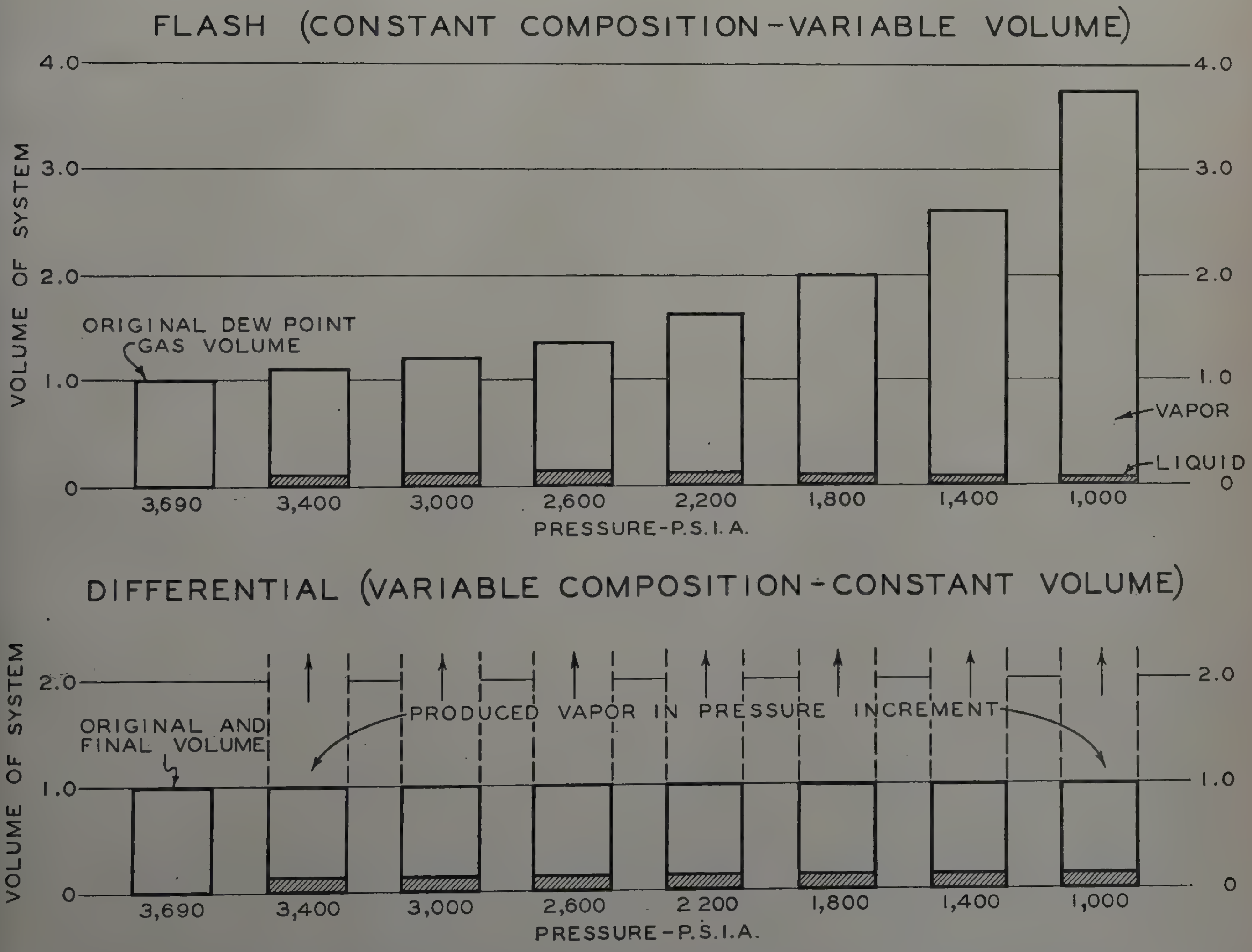

FIG. 3 — BACON LIME CONDENSATE RESERVOIR, METHODS OF CALCULATING THEORETICAL RESERVOIR PERFORMANCE.

esses. The calculated compressibility of the vapor phases, with and without retrograde condensation, differ markedly. The pressure reduction versus cumulative gas production relationship was practically identical for the two vaporization processes. The specific volumes calculated for the two phases as illustrated by Fig. 6, give some idea of the similarity of properties of the two phases at high pressures. Again, the difference in the two computations is demonstrated by different values of vapor specific volumes at the lower pressures. Definite variation in the volumes of liquid condensed by the two vaporization processes was computed as shown in Fig. 7. The reservoir fluid was indicated to be at its dew point initially.

A qualitative indication of the phase envelope based on the estimated original critical point and the upper dew point of the initial reservoir hydro-carbon system, and the liquid volume saturations at reservoir temperature as indicated from the flash vaporization process is shown in Fig. 8. It is of interest to note the changes which occur in the critical point and the upper dew point of the remaining reservoir hydrocarbon fluids at reservoir temperature as the pressure depletion progresses under differential vaporization.

OBSERVED RESERVOIR PERFORMANCE

The calculated performance of reservoir pressure decline with cumulative gas withdrawals, with and without correction for gas compressibility factors, is plotted in Fig. 9. Points represent average reservoir pressures obtained from field pressure surveys. Gas withdrawals have been converted to a wet gas basis and most pressures were obtained by bomb after a minimum of 48-hour shut-ins. Good agreement was obtained on most surveys in view of the apparent lack of communication between individual wells. A "best line" through the points indicates the actual pressure production trend to be leveling out slightly and is interpreted as being production from extremely tight portions of the reservoir rock. The same figure shows the recovery rate of stock tank liquid condensate and indicates no substantial increase in liquid recovery rate due to revaporization at the lower reservoir pressures.

Companion samples of the well stream from two wells and reservoir pressure measurements from several wells were obtained at intervals of six months throughout the productive life of the reservoir. The pressure measurement and sampling interval was reduced to three months during the latter stages of the reservoir depletion. The compositions of the well stream which were obtained from this series of sample analyses are indicated in Fig. 10. It will be noted that in the main, the observed changes in composition of the well stream during the depletion of the reservoir conformed reasonably well with the theoretical compositions reported in Fig. 4. The observed variation in molecular weight and specific gravity of the heptanes-plus fraction of the

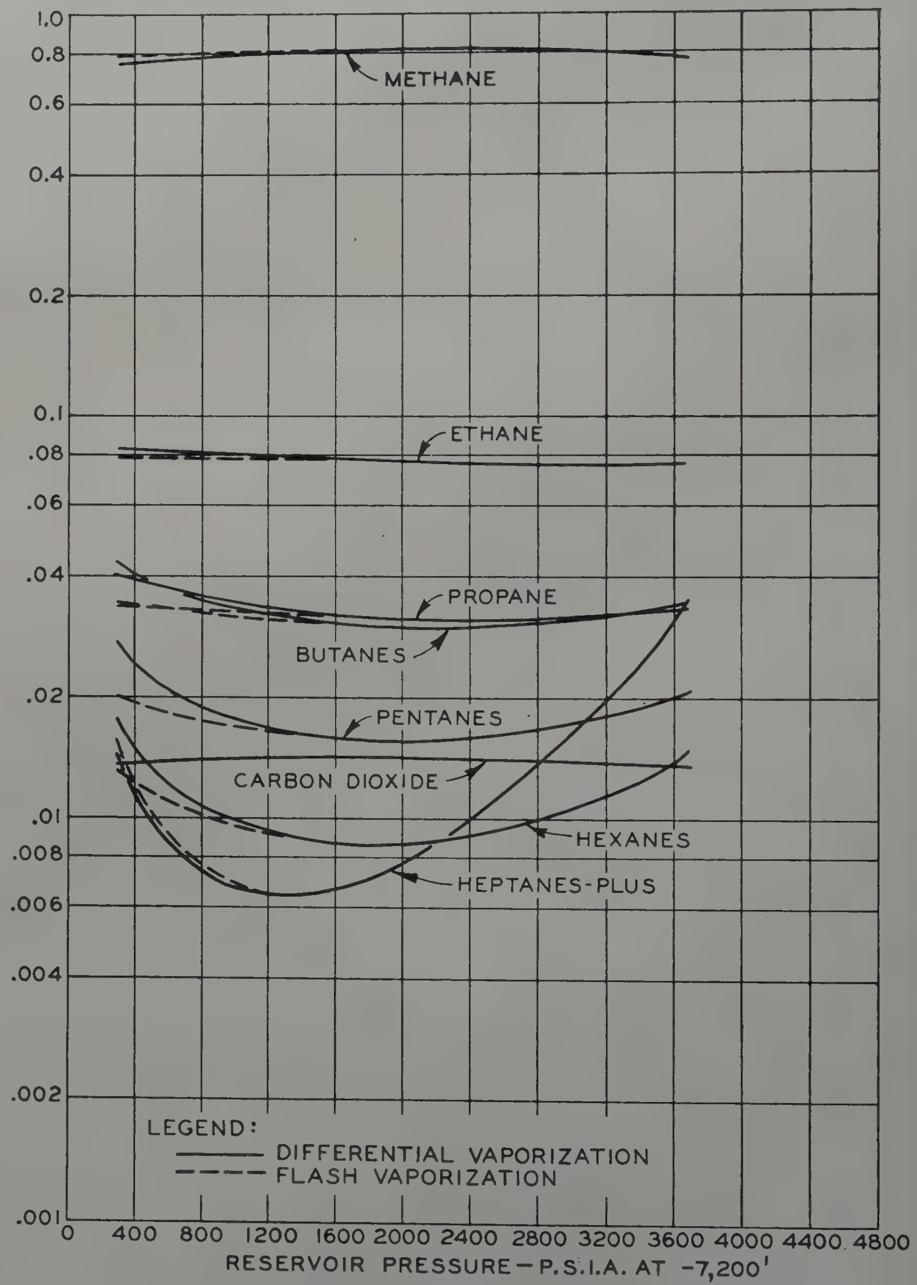

FIG. 4 — BACON LIME CONDENSATE RESERVOIR, CALCULATED THEORETICAL COMPOSITION OF WELL STREAM DURING PRESSURE DEPLETION.

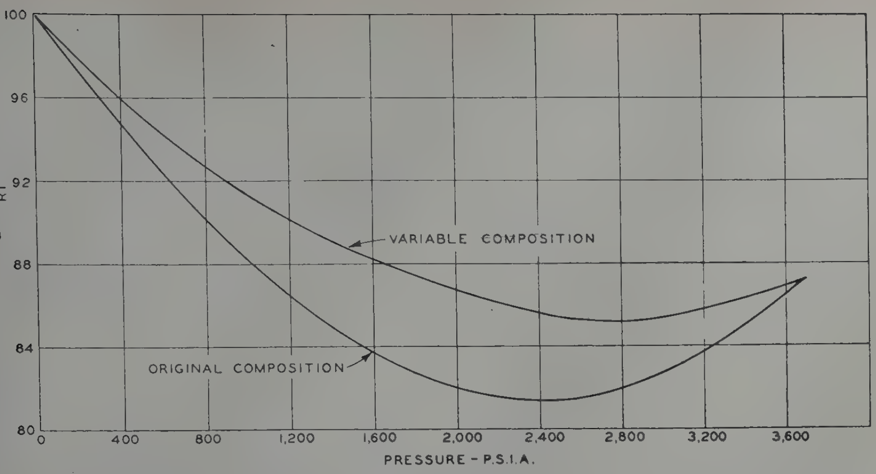

FIG. 5 — BACON LIME CONDENSATE RESERVOIR VAPOR PHASE COMPRESSIBILITY FACTORS.

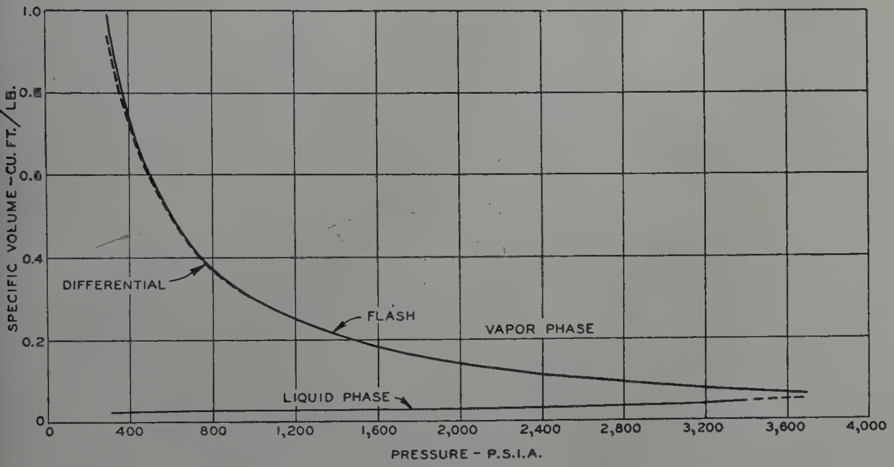

FIG. 6 — PHASE SPECIFIC VOLUMES 220°F, FLASH AND DIFFERENTIAL CALCULATIONS.

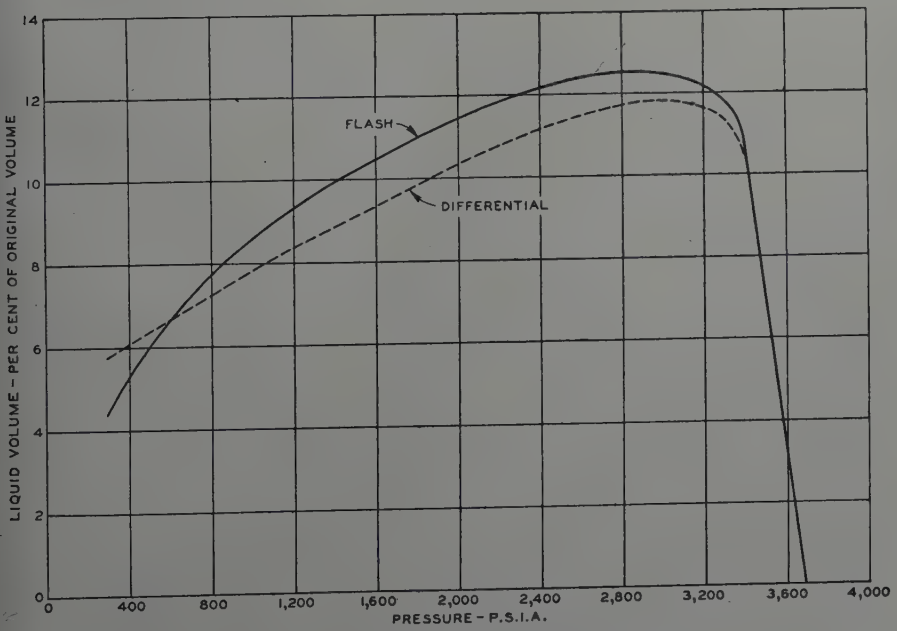

FIG. 7 — VOLUMES OF LIQUID CONDENSED, 220°F.

well stream which occurred during the productive life of the reservoir are indicated in Fig. 11. This variable nature of the heptanes-plus fraction was not considered in making the theoretical calculations.

Of principal interest in an economic analysis of condensate reservoir performance is the concentration of the butanes-plus fraction which occurs in the produced well streams throughout the depletion of the reservoir. The observed history of the butanes-plus concentration in the produced well streams as indicated from the series of companion samples is plotted in Fig. 12. These data illustrate definite revaporization of these fractions from the condensed liquid in the reservoir. This increase was not reflected in stock tank liquid recovery, however, as illustrated in Fig. 9. Superimposed on these data is the butanes-plus concentration which was calculated under the two assumptions of differential and flash vaporization. It was found that the early life of the reservoir is characterized by substantially higher concentration of butanes-plus in the well stream analyses than was predicted under the calculated theoretical performance. Theoretical calculations show that 54 per cent of the original butanes-plus material should be produced down to a reservoir pressure of 600 psia. Allowing for normal separator recovery factors, the cumulative stock tank recovery would be 1.54 GPM compared to initial recovery of 3.50 GPM. Actually, the cumulative stock tank recovery to 600 psia has been 1.70 GPM as compared to an initial average recovery of 3.60 GPM.

COMPARISON OF ESTIMATED AND ACTUAL RESERVOIR PERFORMANCE

Several possible interpretations have been proposed for the variation between the observed and the theoretical estimated reservoir performances which are most evident in Fig. 12. One of these lies in the possibility that the initial companion samples were not entirely representative of the original reservoir fluid due to the pressure draw-down which was required for production during the sampling operations. This might have resulted in condensation around the well bore to produce a well effluent, which was unduly rich in the lighter hydrocarbons. A second possible explanation is derived from the fact that small amounts of nitrogen, never in excess of one mol per cent, have been picked up in several of the sets of companion samples during the life of the reservoir. Nitrogen was not included in the original analysis of the reservoir fluids nor taken into account in the calculations. It is conceivable that the nitrogen exerted a depressing effect on the methane volatility which was not taken into account in the calculations. This effect may be discounted somewhat by the probably opposite effect nitrogen would have on the convergence pressure and thus on the equilibrium constants for the other components. An adjustment in the constant for the heptanes-plus fraction to account for its changing properties would tend to give a smaller calculated GPM content in the well stream.

A more likely interpretation, however, of the discrepancy between the observed and the estimated theoretical performance seems to be that liquid condensate was flowing into the well bore throughout most of the life of the reservoir which resulted in increasing the observed GPM of the well stream. Following this hypothesis, an approximate Kg/Ko relationship was estimated by assuming that the difference between the observed and calculated GPM values shown in Fig. 12 was produced from the reservoir formation as a liquid. The liquid hydrocarbon saturations obtained from the differential vaporization calculations were considered to be uniform throughout the reservoir rather than concentrated in the vicinity of the well bore. A connate water saturation of 30 per cent of the reservoir pore space and a constant gas-liquid viscosity ratio of 1:20 were employed in determining these approximate Kg/Ko relationships. The results of these calculations are shown in Fig. 13 along with several laboratory gas-oil relative permeabilities which have been reported in the literature. The estimated Kg/Ko relationship for the Bacon Lime Reservoir falls well within the range of the previously reported experimental data and closely approximates the limestone relative permeability relationships reported by Bulnes and Fitting[2] except for the steeper slope of the approximated Bacon Lime Kg/Ko curve. It must be recognized, however, that neither of the calculated reservoir performances assumed the possibility of the production of liquid condensate from the reservoir. Liquid condensate production would result in a progressive reduction in the reservoir liquid hydrocarbon saturation which should, in turn, decrease the slope of the approximate Kg/Ko curve shown on Fig. 13. This effect would, of course, be limited by the equilibrium saturation for liquid flow.

This part of the relative permeability relationship representing liquid saturations just in excess of the equilibrium value for liquid flow has not been emphasized in laboratory measurements of relative permeability relationships to

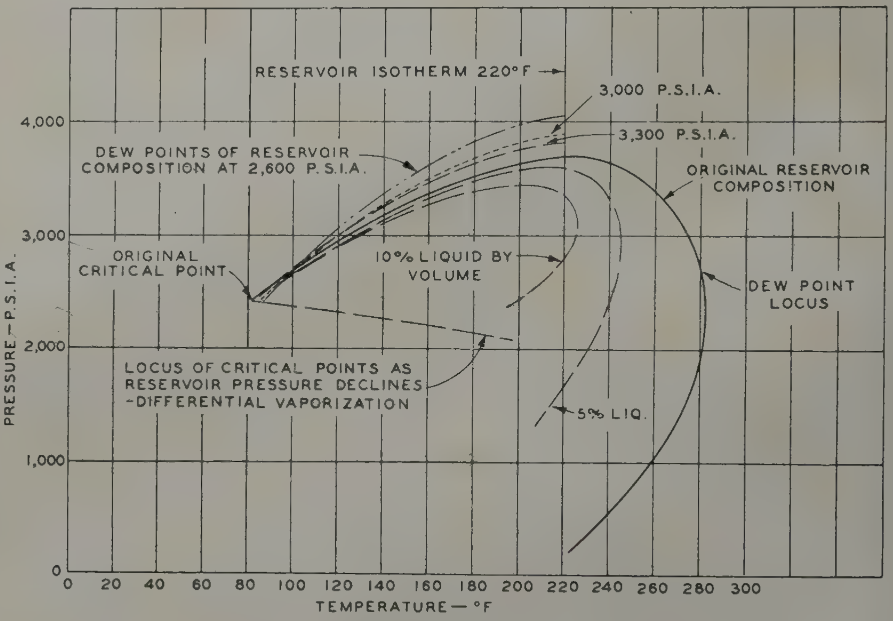

FIG. 8 — OUTLINE OF PHASE DIAGRAM CONSTANT AND VARIABLE COMPOSITION.

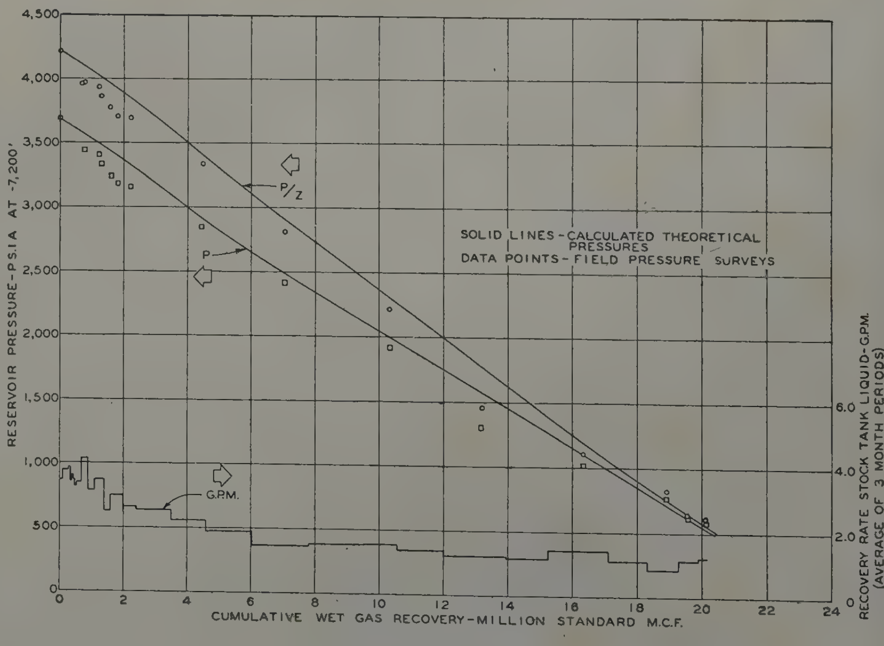

FIG. 9 — BACON LIME CONDENSATE RESERVOIR, RESERVOIR PERFORMANCE.

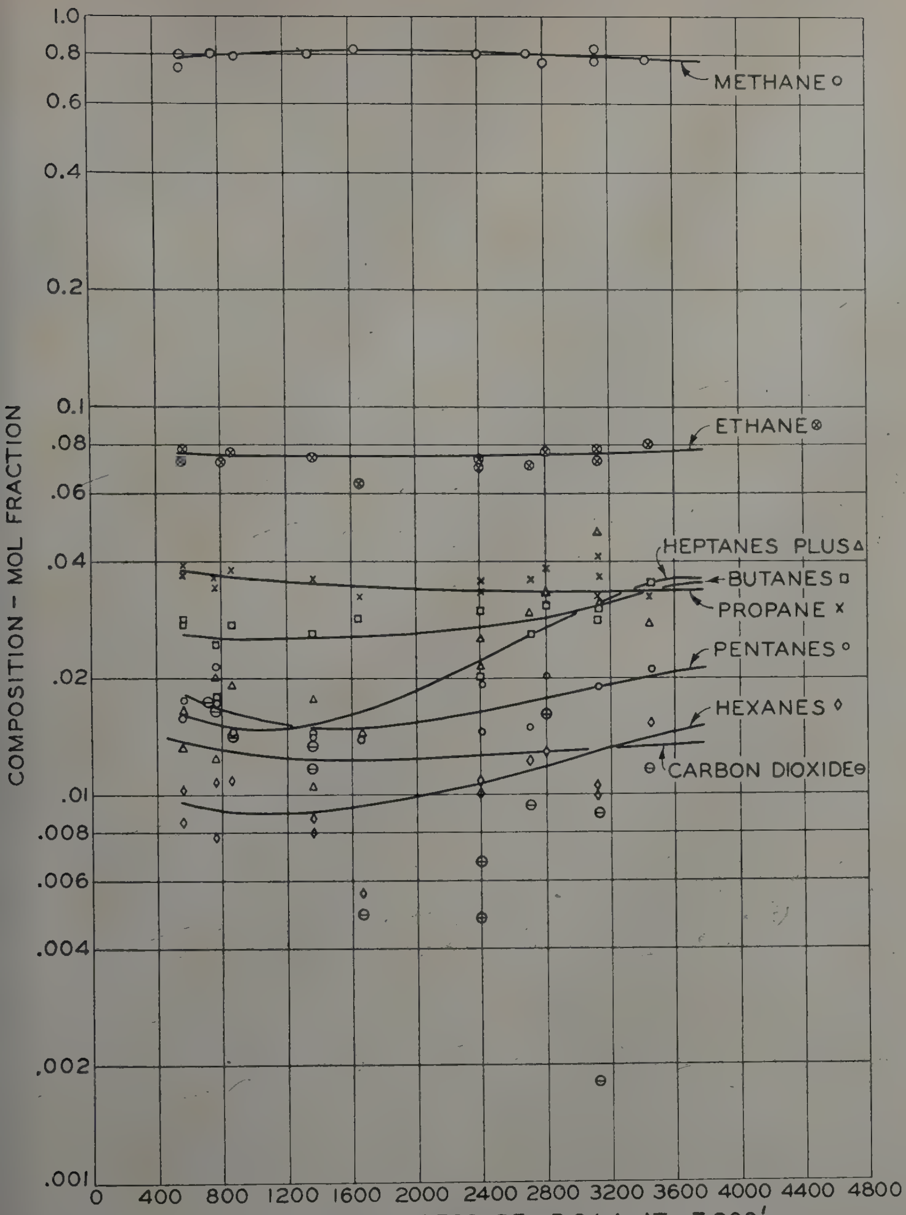

FIG. 10 — BACON LIME CONDENSATE RESERVOIR OBSERVED COMPOSITION OF WELL STREAM WITH PRESSURE DEPLETION.

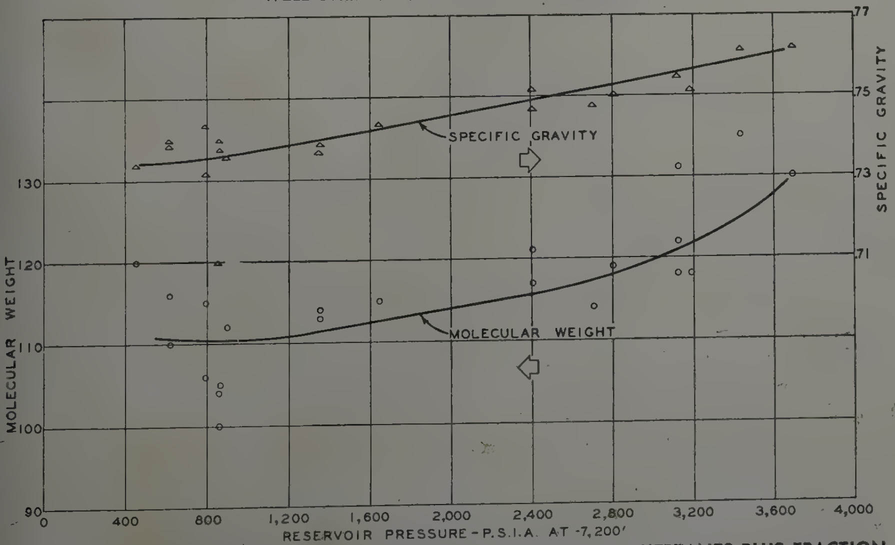

FIG. 11 — BACON LIME CONDENSATE RESERVOIR PROPERTIES OF HEPTANES PLUS FRACTION FROM OBSERVED WELL STREAM ANALYSES.

the same extent as the other end of the curve which includes the total liquid saturations in the vicinity of the equilibrium saturation for gas flow. Neither has it been possible to derive gas-oil relative permeability relationships in the region of the equilibrium point for liquid flow from actual field data. The availability of such gas-oil relative permeability data would make it possible to reverse the train of calculation from which the Kg/Ko relationship reported in Fig. 13 was derived and thus obtain an estimate by means of theoretical calculations of the flow rates of both gas and condensate from the formation and resulting enrichment of the well stream compositions. Reservoir performance predictions computed in this manner would closely reproduce the observed changes in composition of the production which occurred during the pressure depletion of the Bacon Lime Reservoir.

SIGNIFICANCE OF OBSERVED PERFORMANCE INDICATING CONDENSATE REVAPORIZATION

Although the data from actual companion samples of the produced well stream reported in Fig. 12 indicate definite revaporization of the heavier hydrocarbon components, no conclusive evidence of increased recovery of these fractions is indicated by the condensate recovery curve shown in Fig. 9. This lack of increased recovery due to revaporization during the final stages of depletion is apparently due to the low level of separator efficiency at these conditions. In the particular reservoir under study, the temperature of the high pressure separator gas increased steadily, with seasonal fluctuation, as reservoir pressure declined and is presently 40°F higher than those originally observed. This increase in separator temperature with decreasing reservoir pressure is interpreted as the result of decreasing effectiveness of Joule-Thomson cooling as the well production is flashed in the high pressure separator. At optimum separation pressures the liquid condensate recovery from stage separation is a direct function of the separation temperatures. It is, therefore, concluded that revaporization was taking place in the formation during the latter stages of depletion of this Bacon

Lime Condensate Reservoir, but the efficiency of the conventional three-stage separation system had declined to a level which prevented any significant additional recovery of liquid hydrocarbons from the revaporization process.

SUMMARY AND CONCLUSIONS

Predicted theoretical performance for a small volumetric condensate reservoir has been calculated on the two assumptions of flash and differential vaporization. The results of these calculations have been compared with observed performance determined from companion samples obtained throughout the producing life of the reservoir. It is concluded that the principal discrepancy between the computed and observed performance was due to the flow of liquid condensate from the formation which enriched the GPM of the well streams throughout most of the productive life of the reservoir. Revaporization of condensed liquids is indicated by the data representing the latter stages of reservoir depletion. It is evident, however, that the low level to which separator efficiency had declined by the time revaporization of the heavier hydrocarbons became appreciable prevented taking definite advantage of this increased GPM of the well streams.

ACKNOWLEDGMENT

The authors wish to acknowledge permission granted by the Stanolind Oil and Gas Co. to publish this paper. We also wish to acknowledge cooperation of field personnel in collecting samples and compiling the production data.

REFERENCES

1. Roland, Smith and Kaveler, "Equilibrium Constants for a Natural Gas-Distillate Mixture", *Oil and Gas Journal*, 39, No. 46, 128 (March 27, 1941).
2. Bulnes, Fitting, "An Introductory Discussion of the Reservoir Performance of Limestone Formations", AIME TP 1791 *Petr. Tech.*, January, 1945.
3. Brown, Katz, Oberfell and Alden, "Natural Gasoline and the Volatile Hydrocarbons", Section I, 1948, Midwest Printing Co., Tulsa. ★ ★ ★

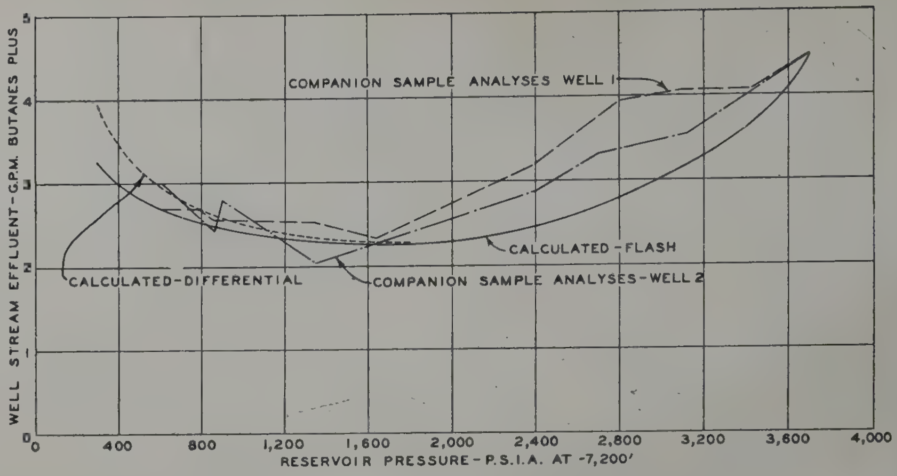

FIG. 12 — BACON LIME RESERVOIR WELL STREAM COMPOSITION.

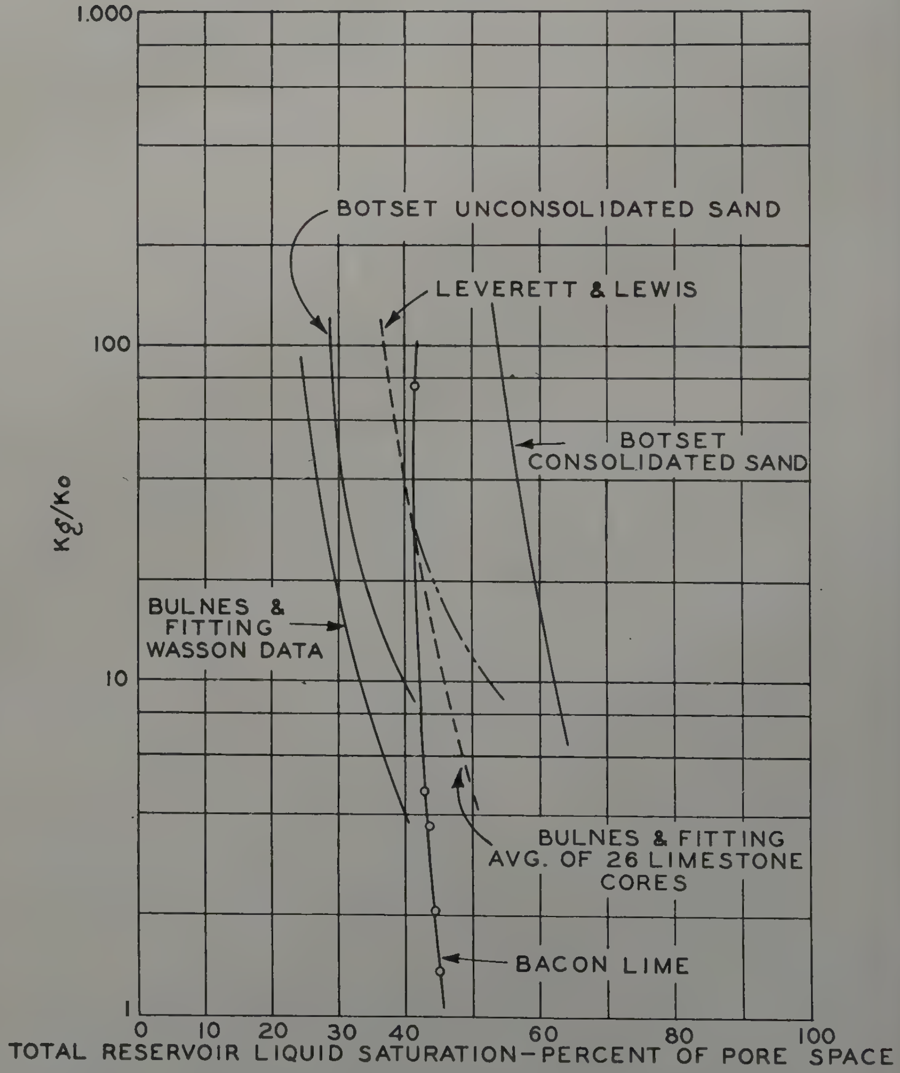

FIG. 13 — BACON LIME CONDENSATE RESERVOIR GAS OIL RELATIVE PERMEABILITY RATIOS.

T.P. 2849

THE ESTIMATION OF PERMEABILITY AND RESERVOIR PRESSURE FROM BOTTOM HOLE PRESSURE BUILD-UP CHARACTERISTICS

C. C. MILLER, MEMBER AIME, **A. B. DYES** AND **C. A. HUTCHINSON, JR.,** JUNIOR
MEMBER AIME, THE ATLANTIC REFINING CO., DALLAS

ABSTRACT

This paper presents a simple and practical method for the estimation of effective permeability and reservoir pressures from the rise in bottom hole pressure when a well is shut in. The equations on which the method is based consider a stabilized well producing from a uniform formation when flow is shut off at the sand face followed by the unsteady state flow of a compressible liquid from regions far from a well to points closer in during the build-up period. An approximation for extending the method for two-phase flow in the reservoir is also presented.

In order to compare the effects of extremes in the conditions existing at the external boundary of the reservoir, two general equations defining the build-up characteristics of the reservoir are shown: first, for a reservoir with constant pressure maintained at the radius of drainage, and second, for a reservoir with no influx over the radius of drainage. These equations define the build-up characteristics for the shut-in well as functions of time, the permeability and porosity of the drainage area, the viscosity and compressibility of the fluid flowing, the production rate prior to shut-in, and the radius of drainage of the well.

When a well is shut in at the surface, rather than at the sand face, flow will continue into the well bore after shut-in due to the compressibility of the fluids in the bore. The effect upon the build-up characteristics of this flow into the well after shut-in has been studied by means of the electrical analyzer. From the basic relationships and consideration of the limitations due to continued flow after shut-in, methods have been developed for the estimation of the effective permeability of an area from the plot of the build-up characteristics of the well producing that area. Likewise, equations are presented for the estimation of the reservoir pressure from an early portion of the build-up curve.

By means of the electrical analyzer, studies have been made concerning the variations in the build-up characteristics resulting from damaged or improved permeability in the immediate vicinity of the well bore. These studies show that the permeability estimated from the build-up curves represents the average effective permeability of the majority of the drainage area and that the permeability in the immediate vicinity of the well does not affect this estimate. Since the major portion of the drawdown is in the immediate vicinity of the well, variations in the permeability of this area greatly affect the productivity of the well as expressed by the productivity index. From pressure build-up and productivity index tests the ratio of the permeability of some arbitrarily specified area immediately surrounding the well and the effective permeability in the majority of the drainage area can be computed. This ratio is a measure of any damage to the well incurred in drilling or reworking and likewise any benefits as a result of remedial measures.

In build-up tests and many other tests that are made on a producing well it is at least desirable, if not absolutely necessary, that the well be stabilized prior to testing. A method is presented here for relating the time required to stabilize a well and the reservoir and fluid properties. An equation is also presented for approximation of the length of shut-in time required to obtain sufficient build-up data for the estimation of permeability and reservoir pressure.

---

[1] Reference given at end of paper.

Manuscript received at the office of the Petroleum Branch October 1, 1949. Paper presented at the Petroleum Branch meeting in San Antonio, Texas, October 5-7, 1949.

INTRODUCTION

The estimation of the effective permeability and of the reservoir pressure around a well has long been a problem for the petroleum engineer. Permeabilities were first estimated from direct analysis of the cores taken from the well and later supplemented by productivity index data. These methods, however, do not permit determination of the actual permeability of the formation in that the conditions in and around the well bore at the time of coring or testing cause considerable deviation from the actual values. It has been pointed out by many authors[1,2,3,4] that the rate of build-up in a shut-in well is affected by the permeability of the producing formation. It may be reasoned, therefore, that the build-up pressure tests should be valuable for a direct estimation of the effective permeability based on actual performance of a well. This is especially true since the build-up characteristics of a well are dependent upon the permeability in the majority of the area of drainage and not upon the permeability in the immediate vicinity of the well.

In order to secure valuable information from material balance studies of a reservoir, reliable reservoir pressure data are essential. These data are frequently obtained by shutting in the wells and allowing the pressure to build up and approach reservoir pressure. It is a familiar practice to shut in a well and after a fixed period of time record a bottom hole pressure measurement which is taken to represent the actual reservoir pressure. This, of course, is an erroneous assumption, for only in fields of very high permeability will the equilibrium reservoir pressure be recorded, and it is therefore inadequate to measure the reservoir pressure in this manner, especially in those tight formations where the rate of build-up is comparatively slow. Thus, several methods have been devised for the estimation of the reservoir pressure. These methods are dependent upon the build-up characteristics of the well. Among the contributions to the estimation of reservoir pressure from field data are the methods presented by Muskat[1] involving a semilogarithmic plot of the build-up characteristics and by Arps and Smith[2] employing a rectilinear plot of the rate of build-up. Included in these methods are the assumptions of an incompressible fluid which flows from the reservoir into an open flow string increasing the back pressure on the formation. A more fundamental approach to the problem has been presented by Muskat in which he considers a compressible fluid in a radial flow system with the pressure at the external boundary maintained constant.[5] The present paper gives further consideration to this method and includes a consideration of the effect of varying degree of migration over the radius of drainage as well as a consideration of the effect on the build-up curves of varying the permeability in the immediate vicinity of the well.

It is the object of this paper to present a simple method for the estimation of the effective permeability and reservoir pressure from the rise in bottom hole pressure when a producing well is shut in. A second objective is to show that build-up and productivity tests furnish complementary information for evaluating the degree of damage or improvement to the permeability in the area of the reservoir immediately surrounding the well bore. An illustrative example follows the discussion to assist in application of the method.

BUILD-UP EQUATIONS

The equations defining the build-up characteristics for a well shut in at the sand face and producing from a uniform formation containing a homogeneous compressible liquid with a steady state distribution prior to shut-in are*[5]

$$\Delta\bar{p} = \ln \bar{r}_e - 2\sum_{n=1}^{\infty} \frac{{}^{-x_n^2\bar{t}}}{(x_n)^2\, J_1^2\,(x_n)} \quad \ldots\ldots \quad (1)$$

for a radial drainage area with constant pressure maintained at the external boundary and

$$\Delta\bar{p} = \ln \bar{r}_e - \frac{3}{4} + \frac{\pi^2}{2}\sum_{n=1}^{\infty} \frac{J_1^2(x_n)\,U^2(x_n)}{J_1(\bar{r}_e x_n) - J_1(x_n)}\, e^{-\bar{r}_e x_n^2 \bar{t}} \quad (2)$$

for a radial drainage area with zero influx over the external boundary. In this later case a steady condition exists, referred to here also as a steady state, in which pressure gradients throughout the reservoir remain constant while the pressure throughout the reservoir is uniformly declining.

The dimensionless variables $\Delta\bar{p}$ and $\bar{t}$ are defined by the equations

$$\Delta\bar{p} = \frac{0.001127\ 2\pi kh\,(p - p_f)}{Q\mu F} \quad \ldots\ldots \quad (3)$$

and

$$\bar{t} = \frac{0.0002637\ kt}{fc\mu r_e^2} \quad \ldots\ldots\ldots\ldots \quad (4)$$

---

* See Appendix for derivations.

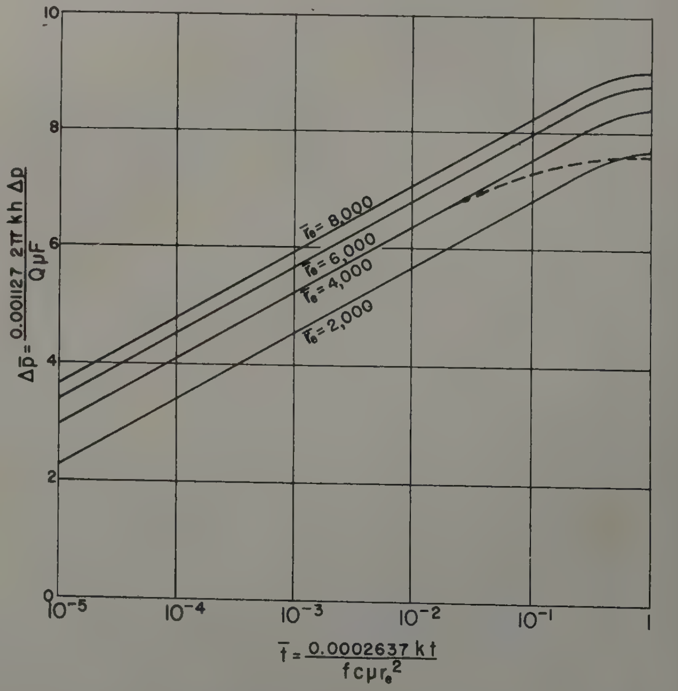

FIG. 1 — CALCULATED RISE IN BOTTOM HOLE PRESSURE IN A SHUT-IN WELL. STEADY STATE PRESSURE DISTRIBUTION OBTAINED PRIOR TO SHUT-IN BY CONSTANT PRODUCTION RATE. SOLID LINES FOR RESERVOIR WITH CONSTANT PRESSURE MAINTAINED AT THE RADIUS OF DRAINAGE. DASHED LINE FOR CLOSED RESERVOIR WITH NO INFLUX OVER RADIUS OF DRAINAGE AND $\bar{r}_e = 4{,}000$.

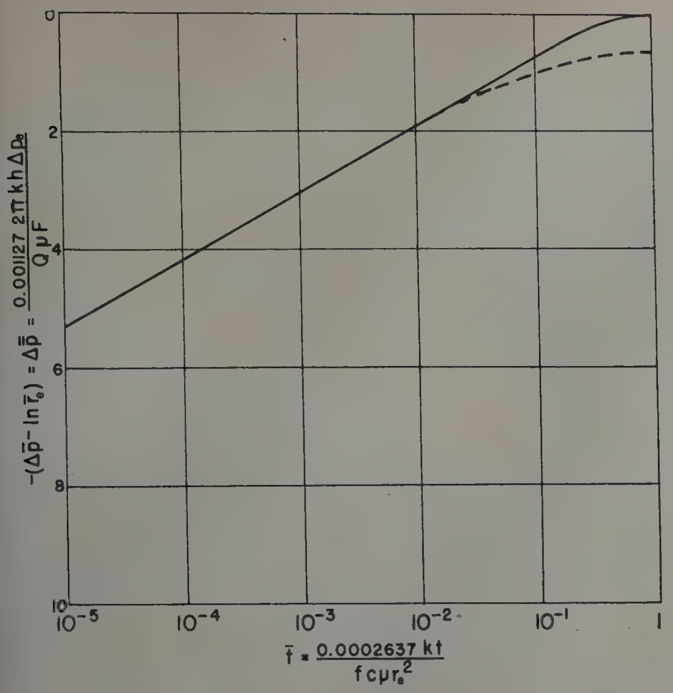

FIG. 2 — CALCULATED RISE IN BOTTOM HOLE PRESSURE IN A SHUT-IN WELL. STEADY STATE PRESSURE DISTRIBUTION OBTAINED PRIOR TO SHUT-IN BY CONSTANT PRODUCTION RATE. SOLID LINE FOR DRAINAGE AREA WITH CONSTANT PRESSURE MAINTAINED AT THE RADIUS OF DRAINAGE. DASHED LINE FOR CLOSED AREA WITH NO INFLUX OVER THE RADIUS OF DRAINAGE.

where

k = effective oil permeability, md
h = effective pay thickness, ft
Q = production rate prior to shut-in, STB/Day
μ = oil viscosity, cp
F = formation volume factor, $\frac{\text{Res bbl}}{\text{STB}}$
f = total porosity, fraction
c = mean liquid compressibility, psi^{-1}
r_e = radius of drainage, ft
pf = bottom hole flowing pressure at time of shut-in, psi
p = bottom hole pressure during build-up, psi, and
t = time, hours.

A numerical evaluation of equation (1) is presented in Table I. Values of $\bar{r}_e$ of 2000, 4000, 6000, and 8000 are used which correspond to 18, 72, 162, and 288-acre well spacings respectively for $r_w = 1/4$. The evaluation of equation (2) for $\bar{r}_e = 4000$, corresponding to a 72-acre well spacing and $r_w = 1/4$ is presented in Table II. The numerical values presented in Tables I and II are also presented in graphical form plotted as $\Delta\bar{p}$ vs. $\log \bar{t}$ in Fig. 1 and $\Delta\bar{p} - \ln \bar{r}_e$ vs. $\log \bar{t}$ in Fig. 2.

It may be seen in Fig. 2 that the early part of the build-up is independent of the conditions existing at the radius of drainage since the curves for the build-up in an area with constant pressure maintained at the external boundary and for the build-up with no influx over the external boundary coincide in this early section.

PERMEABILITY FROM THE BUILD-UP CURVE

Examination of Fig. 1 shows that the build-up characteristics plotted with dimensionless variables, $\Delta\bar{p}$ and $\log \bar{t}$, appears to be a straight line in the sections of $\bar{t} = 10^{-5}$ to approximately $\bar{t} = 10^{-1}$. This apparently straight section of the curve is not actually a straight line as might be determined by proper differentiation of either equations (1) or (2). However, this section of the curve is sufficiently straight for practical purposes. The straight line sections of the build-up curves in Fig. 1 are parallel as is indicated by the fact that the curves become coincident upon translation by the quantity $\ln \bar{r}_e$ as shown in Fig. 2. Though only one actual numerical evaluation of equation (2) has been calculated, additional curves also covering the range of $\bar{r}_e = 2000\text{-}8000$ were obtained on the electrical analyzer[6] which resulted in coincident curves when translated by the quantity $\ln \bar{r}_e$. The slope of these lines may be taken as 1.147. This slope is important in that it relates the permeability and the slope of the straight line section of the build-up curve (when pressure is plotted vs. log time instead of vs. time) according to the relation

$$\frac{\Delta(\Delta\bar{p})}{\Delta(\log \bar{t})} = \frac{\frac{kh}{141.2Q\mu F}\,\Delta(\Delta p)}{\Delta(\log\ t)} = 1.147 \quad . \quad (5)$$

Rearranging this equation the permeability, k, may be shown as a function of the slope, m, of the straight line section of the pressure-log time build-up curve as

$$k = \frac{162.5\ Q\mu F}{mh} \quad . \ . \ . \ . \ . \ . \ . \ . \ . \ . \quad (6)$$

The semilogarithmic plot of a field build-up test will generally show the straight line section as indicated for use in equation (6) for permeability estimation. However, an earlier

Table I

Build-Up Characteristics for a Shut-In Well in a Drainage Area Having Constant Pressure Maintained at the External Boundary in a Radial Flow System

Well Produced at Constant Rate Prior to Shut-In to Attain Steady State

$\bar{t}$	$\Delta\bar{p}$ $\bar{r}_e = 2000$	$\bar{r}_e = 4000$	$\bar{r}_e = 6000$	$\bar{r}_e = 8000$
10^{-5}	2.261	2.954	3.360	3.647
10^{-4}	3.401	4.094	4.500	4.787
2×10^{-4}	3.7743	4.4674	4.8729	5.1606
5×10^{-4}	4.2045	4.89865	5.30411	5.59180
10^{-3}	4.55070	5.24485	5.65031	5.93800
2×10^{-3}	4.89250	5.58665	5.99211	6.27980
5×10^{-3}	5.35590	6.04905	6.45451	6.74220
10^{-2}	5.70280	6.38595	6.80141	7.08910
2×10^{-2}	6.04944	6.74259	7.14805	7.43574
5×10^{-2}	6.50744	7.20069	7.60615	7.89384
10^{-1}	6.85404	7.54817	7.95263	8.24032
2×10^{-1}	7.19597	7.88912	8.29458	8.58227
5×10^{-1}	7.52970	8.22285	8.62830	8.91600
1	7.59695	8.29010	8.69556	8.98325

Table II

Build-Up Characteristics for a Shut-In Well in a Drainage Area with No Fluid Migration Over the External Boundary in a Radial Flow System

Well Produced at Constant Rate Prior to Shut-In to Attain Steady State

$\bar{t}$	$\overline{\Delta p}$ $\bar{r}_e = 4000$
6.25×10^{-4}	5.02
1.25×10^{-3}	5.354
3.125×10^{-3}	5.808277
6.25×10^{-3}	6.148454
1.25×10^{-2}	6.482556
3.125×10^{-2}	6.903227
6.25×10^{-2}	7.187298
1.25×10^{-1}	7.409087
3.125×10^{-1}	7.535509
6.25×10^{-1}	7.543964

apparent straight line section which is not accounted for by the build-up equations may be evident in this plot. The earlier straight line section will have a greater slope than that to be used in the permeability equation. In an attempt to discern the cause of this variation from the calculated build-up curve, possible deviations from the conditions specified in the derivations of the equations for the build-up relations were examined, and it was found that the most obvious deviation was the fact that the build-up relations were derived for a well shut in at the sand face. In actual field build-up testing the well is closed in at the surface and there is flow into the well after shut-in due to the compressibility of the fluids in the well bore. This flow into the well after shut-in will be at a rate equal to the production rate prior to shut-in at the start of the test and will drop to zero as the pressure is finally built up. Several methods were tried in an attempt to find an analytical solution for the build-up relations considering this declining rate of flow into the well after shut-in. However, because of the complexity of analytically describing changes occurring in the well bore a complete study of the effects was not made. The electrical analyzer[6] was used to illustrate these possible effects and their magnitudes on the build-up curves. Studies with the electrical analyzer were conducted such that the well was drawn down for a constant production rate to produce a steady state prior to shut-in. A constant pressure was maintained at the external boundary. Upon attainment of the steady state distribution, the well was shut in and the build-up measured as a function of time. It was found that for a well shut in at the botton the electrical analyzer produced a curve matching the calculated curve as obtained from equation (1). In the section of the build-up plot from $\bar{t} = 10^{-3}$ to 10^{-1} the analyzer curve and calculated build-up curve coincided precisely. However, in the section $\bar{t} = 10^{-4}$ to $\bar{t} = 10^{-3}$ slightly lower values were observed in the analyzer curve. This may be attributed to insufficient subdivision of the close in portion of the reservoir in the analyzer. The deviation, however, was insufficient to invalidate the use of the analyzer for these experiments. This problem might be attacked by the LaPlace Transformation methods of Hurst and Van Everdingen.[12] However, the authors have not investigated this possibility since the electrical analyzer was available.

In order to obtain the build-up characteristics of the well in the case where there is flow into the well bore after shut-in, it was necessary to simulate the well bore in the electrical analyzer. This was accomplished by means of the addition of capacitors at the well end of the reservoir. These capacitors were contained in an expansion unit such that the capacitance could be varied as the pressure at the bottom of the well varied. Of course, as oil flowed into the well after shut-in the average compressibility of the bore fluid decreased, necessitating a decrease in the electrical capacitance of the well bore unit of the analyzer. The capacitance of the bore was computed from the pressure-volume curve of the reservoir fluid. Two situations were considered for this type of test. The first case considered flow into the well bore after shut-in with the well containing only gas prior to shut-in. Although such a situation of only gas in the bore prior to shut-in will never actually exist in an oil well, this condition was studied as the large gas compressibility would cause a maximum deviation from the curve for a well shut in at the sand face. A 10,000-ft well drilled on a 72-acre spacing (1000-ft radius) was chosen for this study. The second case considered a 10,000-ft well bore filled with gas and oil prior to shut-in. Approximately 45 per cent of the bore volume was occuped by undissolved gas prior to shut-in for this test. The two curves that were produced from these tests of flow into the well bore after shut-in under the conditions just cited are shown plotted with dimensionless variable $\overline{\Delta p}$ and $\bar{t}$ in Fig. 3.

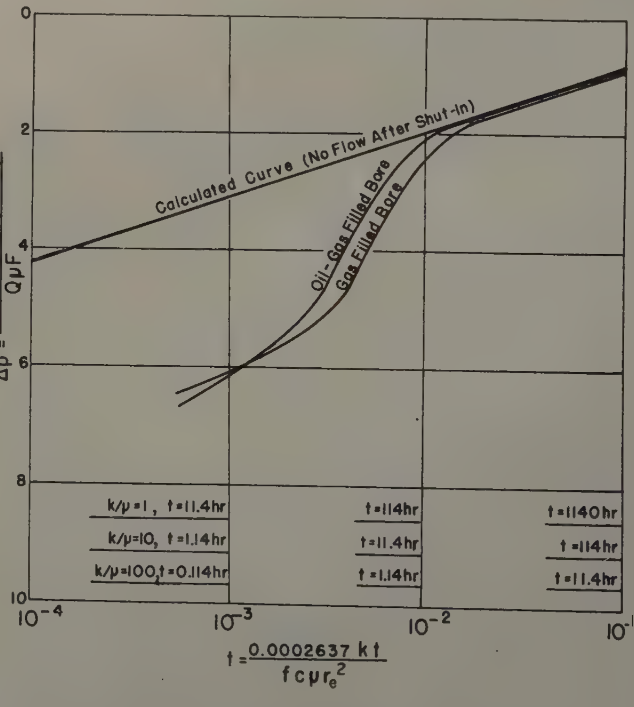

FIG. 3 — THE EFFECT OF FLOW INTO THE WELL AFTER SHUT-IN ON THE BUILD-UP CURVE.
OIL AND GAS FILLED WELL BORE 10,000-FT WELL.
GAS FILLED WELL BORE 10,000-FT WELL.
CALCULATED CURVE FROM EQUATION (3). TIMES GIVEN FOR K/μ VALUES ABOVE FOR SYSTEM $f = 0.2$, $c = 1.5 \times 10^{-5}$ psi^{-1}, AND $\bar{r}_e = 4{,}000$.

The calculated curve for the range of build-up considered is also included in Fig. 3 to provide a means for comparison. It will be noted that the flow into the well after shut-in causes a delaying action in the build-up as might be expected. However, after a comparatively short period of time a rapid build-up occurs and the curve becomes parallel if not practically coincident with the calculated curve assuming no flow into the well after shut-in. It will also be noted that an earlier straight line section which deviates from the calculated curve is present in these electrical analyzer build-up curves as had been expected. This is in direct correspondence with the earlier straight line section that is obtained in actual field build-up test curves.

The development for the equations for the build-up relations has considered that a uniform permeability exists in the reservoir. This situation, however, is not true and its effect has been considered by means of further electrical analyzer comparisons. It may justifiably be assumed that in the immediate vicinity of the well bore there may be a damaged or improved permeability area caused by the drilling procedures or treatment. The electrical analyzer was used to determine the effect on the build-up characteristics of such a damaged or improved area in the immediate vicinity of the well. This was accomplished by changing the resistance around the well in the analyzer, which change would depict a change in permeability immediately around the well. The radius of drainage of the well studied on the analyzer was 1000 ft. For the illustration of this effect the permeability to a radius of 23 ft from the well was changed to represent a twofold and a fivefold increase and a decrease to 1/2 and 1/5. A constant drawdown was maintained for these tests, so necessarily the production rates for these runs varied where there was a change in permeability. Pressure build-up curves obtained in these tests are shown plotted with dimensionless variables in Fig. 4. The dimensionless variable proportional to pressure, $\Delta\bar{\bar{p}}$, is defined by the equation

$$\Delta\bar{\bar{p}} = \frac{0.001127\ 2\pi kh}{FQ\mu}\ (p_e - p) \quad . \quad . \quad . \quad . \quad (7)$$

where k is the permeability of the majority of the reservoir and not that of the damaged or improved area in the immediate vicinity of the well and p_e is the pressure at the radius of drainage at shut-in. These curves show that the effects of this damage or improvement are very rapidly eliminated in the build-up and that the curves soon coincide with the calculated curve. It may be noted at this point in the case where either increase or decrease in the permeability is exhibited in the immediate vicinity of the well the drawndown will be greatly different from the drawdown that would be exhibited in the same reservoir with a constant permeability throughout the drainage area. Thus, the permeability that is calculated from the slope of the straight line section of the build-up curve represents the actual effective permeability in the majority of the drainage area of the reservoir and is not affected by high or low permeability sections in the immediate vicinity of the well. This fact suggests a method for evaluating the conditions in the immediate vicinity of the well. This type evaluation will be discussed later.

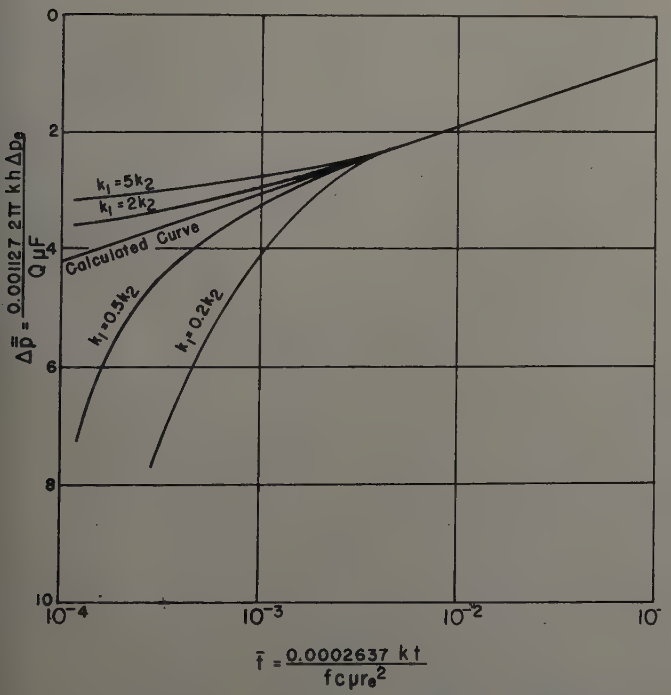

FIG. 4 — THE EFFECT OF A DECREASED OR INCREASED PERMEABILITY IN THE AREA IN THE VICINITY OF THE WELL ON THE BUILD-UP CURVE. WELL SHUT IN AT THE SAND FACE. $\bar{r}_e = 4{,}000$. EXTENT OF k_1 to $\bar{r} = 92$

The analysis of the effects on the build-up curve caused by existing conditions different from those assumed for the derivations of the equations should be continued to include the conditions where both local variation in permeability and flow into the well bore after shut-in exists. This problem was also treated by means of the electrical analyzer considering a 10,000-ft well filled with gas and oil prior to shut-in and including local permeability variations used in the previous tests. The results of these tests are shown plotted with dimensionless variables in Fig. 5. It may be seen in these curves, as in the curves for the tests considering damage or improvement and flow into the well bore after shut-in separately, that the curve approaches a condition where it is parallel to the calculated curve for a well shut in at the sand face and with uniform permeability throughout the drainage area. This would indicate that the section of the straight line that is parallel to the calculated curve may be used for permeability determination without error. However, much of the straight line section of the curve has been masked by the effects of flow into the well bore after shut-in, and it is necessary to make an opportune choice of the section of the curve that is to be employed in the permeability equation, since only a small portion of the total curve may be parallel to the calculated straight line section.

In order to develop a method to determine that the proper portion of actual field build-up test curve has been used in permeability determination, it is necessary to consider the calculated curve. The upper limit of the straight line section (Fig. 1) is approximately $\bar{t} = 2 \times 10^{-1}$ for a reservoir with constant pressure maintained at the radius of drainage and $\bar{t} = 3 \times 10^{-2}$ for a closed reservoir. A possible check of the upper limit of the straight line section of the actual field build-up test curve is suggested by this fact and may be accomplished by checking the upper limit of the actual field build-up plot for conformity with this upper limit of the straight line section of the calculated curve. In the calculation of $\bar{t}$ from equation (4) it is necessary to assume a value of r_e. If the well were stabilized prior to shut-in as required by equations (1) and (2) such that the pressure wave would have reached its maximum radius, the radius of drainage may be approximated from well spacing. If the final break in the field curve is included in the observed data (not an apparent break due to well bore effects), the calculated $\bar{t}$ for the last point of the straight line section should be of the order of 10^{-1}. Due to the long times required this final break is rarely obtained, in which case the last observed point usually gives a $\bar{t}$ falling in the range of 10^{-2} to 10^{-1}. If a straight line section is selected that is too early in the build-up curve and with too great a slope due to flow into the well after shut-in, the time as well as the permeability determined will be too low, giving a value well below the cited range.

NON-STABILIZED CONDITIONS

In actual practice there may be an additional deviation from the conditions assumed in the derivations for the build-up characteristic equations. This deviation arises from the fact that a considerable period of time is required for stabilization of the well to essentially steady state conditions prior to shut-in. However, the necessary steady state is sufficiently approximated in many cases to make the equations applicable. In the case of a well definitely unstabilized at the time of shut-in the analysis breaks down. The authors have found in such instances where the equations are not applicable that the electrical analyzer provides very satisfactory answers concerning the build-up characteristics and this method should be employed in such instances.

RESERVOIR PRESSURE FROM THE BUILD-UP CURVE

As pointed out before, many authors have examined the build-up characteristics to obtain methods for reservoir pressure estimation. However, the methods developed require that a considerable portion of the build-up curve be known before they are applicable. Also, flow into the well after shut-in and/or an increase or decrease in the permeability around the well cause erratic build-up curves and resulting erroneous estimation of reservoir pressure by the semilog plot of Muskat or the Cartesian rate plot of Arps and Smith.

The straight line section of the build-up curve corresponding to the straight line of the calculated curve in Fig. 1 may be used for reservoir pressure estimation in conjunction with the build-up equations. A measure of the reservoir or final build-up pressure around the well may be found in terms of the dimensionless $\Delta\bar{p}$ calculated for t increasing without limit. The final build-up, $\Delta\bar{p}_s$, for a reservoir with constant pressure maintained at the radius of drainage is given by the equation

$$\Delta\bar{p}_s = \ln \bar{r}_e \quad . \; . \; . \; . \; . \; . \; . \; . \; . \; . \; . \quad (8)$$

For the reservoir with no influx across the external boundary the equation for $\Delta\bar{p}_s$ is

$$\Delta\bar{p}_s = \ln \bar{r}_e - \frac{3}{4} \quad . \; . \; . \; . \; . \; . \; . \; . \quad (9)$$

Considering the method of derivation of these equations, in effect this is a method of material balance for the determination of reservoir pressure. The resolution of these two equations for the determination of reservoir pressure requires that the flowing pressure prior to shut-in be known. However, that flowing pressure measured by the pressure bomb is not in direct correspondence with the flowing pressure as required by the equations. This condition exists because of the possible difference in permeability in the immediate vicinity of the well and the permeability in the rest of the drainage area. Let us consider that it is therefore necessary to determine a hypothetical flowing pressure for use in the determination of the reservoir pressure. This flowing pressure is the pressure that would exist at the bottom of the well for the production rate at the time of shut-in if the permeability around the well were the same as that determined from the build-up curve. The determination of the hypothetical flowing pressure that is to be used may be accomplished in the following manner: An r_e corresponding to the well spacing is assumed. Employing this r_e the straight line section of the field build-up curve may be matched with the straight line section of the calculated curve, from which may be determined the hypothetical flowing pressure according to the equation

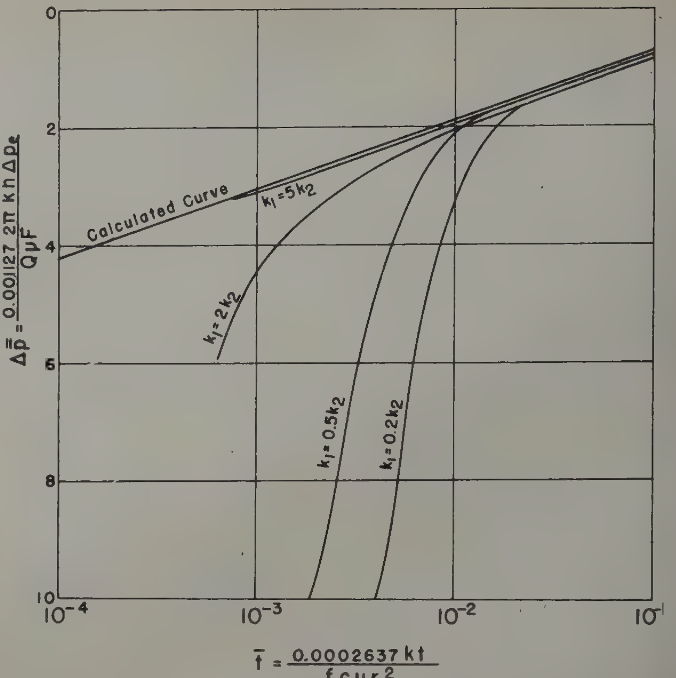

FIG. 5 — THE EFFECT OF FLOW INTO THE WELL BORE AFTER SHUT-IN AND A DECREASED OR INCREASED PERMEABILITY AROUND THE WELL ON THE BUILD-UP CURVE. $\bar{r}_e = 4{,}000$. k_1 EXTENDS TO $\bar{r} = 92$. OIL AND GAS FILLED BORE, 10,000-FT.

$$p_f = p - \Delta p = p - \frac{\Delta\bar{p}\ FQ\mu}{0.001127\ 2\pi kh} \quad . \; . \quad (10)$$

where the pressure p is taken from the field plot and $\Delta\bar{p}$ is the dimensionless pressure variable taken from the calculated curve at a $\bar{t}$ corresponding to the time that the pressure p was observed. Having determined the hypothetical flowing pressure the reservoir pressure may then be calculated by means of the equation

$$p_e = p_f + \Delta p_s = p + (\Delta\bar{p}_s - \Delta\bar{p}) \frac{FQ\mu}{0.001127\ 2\pi kh} \quad . \quad (11)$$

where $\overline{\Delta p}_s$ is calculated by equation (8) or (9), whichever is considered applicable. For wells with the drainage radius of approximately 250 ft to 1000 ft there is approximately a 10 per cent difference in the value of $\overline{\Delta p}_s$ as calculated from equations (8) and (9). It is necessary, therefore, to make an opportune choice of the equation to be employed for the determination of the reservoir pressure, and in such instances where neither is applicable some intermediate value may be chosen.

The chief point for error in this calculation is the assumption of the value of r_e which is usually done from well spacing. A 5 per cent error in the estimation of r_e leads to approximately a 1 per cent error in the theoretical drawdown, which in a high permeability formation means an error in the order of a few pounds. In a high pressure formation producing under open flow conditions where the drawndown is large this error may be in the order of 20 pounds.

BUILD-UP CURVES — TWO-PHASE FLOW

The relationships that have been presented to this point have considered the flow of a homogeneous compressible fluid through a porous medium. It would be of course advantageous to extend this method to include drainage areas in which both oil and gas were flowing. Considering that in the reservoir away from the well the pressure is fairly constant, the pressure functions μ_L, μ_g, F, ρ, and S may be assumed constant. Likewise, the saturation is fairly constant and the dependent variables k_{rg} and k_{rL} may also be assumed constant. These assumptions of essentially constant conditions have been reported to hold except for a very short transition period as the reservoir pressure falls below the saturation pressure of the oriignal reservoir fluid.[11] Applying these assumptions, Darcy's Law, and material balance considerations the build-up equations are shown to take the same form as for the single-phase flow case with a change in form of the dimensionless variables.* The resulting equation for effective oil permeability is the same as equation (6) where oil production rate and oil viscosity at approximately reservoir pressure are employed. The dimensionless variables $\overline{\Delta p}$ and $\bar{t}$ are defined by the equations

$$\overline{\Delta p} = \frac{0.001127\ 2\pi kh}{Q_L \mu_L F_L}\ \Delta p \qquad (12)$$

and

$$\bar{t} = \frac{0.0002637\ k}{f c_T \mu_L r_e^2}\left(\frac{\delta_L + \delta_g R}{F \delta_T}\right) t \qquad (13)$$

Equation (13) is used as equation (4) for checking the upper limit of the straight line section of the field build-up curve for conformity with a calculated curve. The same range of $\bar{t}$ applies. The total compressibility, C_T, is established at an estimated reservoir pressure as is the total density, δ_T. If the calculated pressure differs significantly from that estimated an adjustment may be necessary in these factors. In the authors' experience the quantity in parentheses has always been very nearly unity.

Table III

k/μ	t_s (days) 20 Acre Spacing	40 Acre Spacing	80 Acre Spacing	160 Acre Spacing
1	42	82	166	333
10	4.2	8.2	16.6	33.3
100	0.4	0.8	1.7	3.3

Time Required to Attain Steady State by Constant Production Rate (From equation (14). $C_L = 100\%$, $F = 0.2$, and $c = 1.5 \times 10^{-5}\ \text{psi}^{-1}$).

TIME TO APPROACH STEADY STATE

The preceding equations have all been derived for a system with a steady state density or presure distribution prior to shut-in of the well. This distribution is obtained by flowing the well at a constant production rate for a sufficient period of time prior to shut-in. A graphical method[7] for the transient solution of the diffusivity equation provides a means for the determination of this time. In a finite time of course steady state will not actually be attained, but it will be approximated sufficiently for all practical purposes. Employing this method, the time required to approach steady state conditions for either assumed boundary condition is a function of the radius of drainage, permeability, and porosity of the formation, and compressibility and viscosity of the fluid. It is independent of the rate of production and the net thickness of the pay. For one-phase flow this relationship is[7]

$$t_s = \frac{f c \mu r_e^2}{k} \qquad (14)$$

where t_s is the time in days required to approximate a steady state. A similar equation for two-phase flow may be obtained by replacing $fc\mu/k$ by the factors of K′, the modified diffusivity, obtaining

$$t_s = 50\ \frac{f c_T \mu_L r_e^2}{k\left(\dfrac{\delta_L + \delta_g R}{F \delta_T}\right)} \qquad (15)$$

where the values are obtained in the same manner as for equation (13). It will be noted that it is necessary to know the permeability in employing these equations. However, it is necessary to stabilize a well prior to a test before the permeability is known. In such instances the approximate time required to obtain a steady state distribution will be indicated by this equation if the range of permeability values that are expected is used in the equation. The initial pressure was assumed to be constant throughout the area for this derivation, and thus the time required for the steady state approximation represents the maximum period to be expected. Table III shows the range of time values that might be expected in single-phase flow. In such instances where the well has been produced for some time and it is desired to stabilize at a new production rate this time for the attainment of steady state at the new production rate will be less.

SHUT-IN TIME REQUIRED FOR PERMEABILITY DETERMINATION

Because it is undesirable to shut in a well over a long period of time, it is necessary in planning a pressure survey to estimate in advance the length of shut-in time required to obtain a sufficient section of the build-up curve for the determination of permeability. An expression for this time required may be derived directly from an examination of the calculated build-up relations as plotted in Fig. 2. This will give a relationship for the time required to obtain a sufficient section of the build-up curve for permeability determination as a function of the porosity, compressibility, viscosity, radius of drainage and permeability that are being considered. Approximate knowledge of these factors will enable the engineer to more accurately estimate the length of time that is required to shut in the well. The upper limit of the straight line section of the build-up curve plotted as pressure versus logarithmic time is in the region of $\bar{t} = 5 \times 10^{-2}$. This will be true in all cases. Employing this value in equation (4) and solving for t we have for one-phase flow

---

* For derivations see Appendix.

$$t_{si} = \frac{190\ fc\mu r_e^2}{k} \quad . \ . \ . \ . \ . \ . \ . \ (16)$$

where t_{si} is the time required in shut-in hours. This may be converted for two-phase flow in the same manner as equation (15). Table IV shows the range of time intervals that might be expected for single-phase flow. As in the case for the determination of the time required to approach steady state, it is necessary to know the value of the permeability prior to obtaining that value. It is necessary, therefore, to employ approximations of this permeability value with the answer of course resulting in an approximation of the time required to obtain a sufficient portion of the build-up curve for permeability determination. This equation though eliminates considerable uncertainty in the mind of the engineer requesting shut-in time of the well.

PERMEABILITY AROUND THE WELL

The permeability as determined by equation (6) from the slope of the build-up curve represents the effective permeability of the drainage area away from the well, as was indicated by the tests showing the changed permeability in the immediate vicinity of the well. The permeability as estimated from the productivity index using the steady state radial flow equation represents the average effective permeability of the entire drainage area. If these two permeabilities are different, there may exist a section in the immediate vicinity of the well with a permeability different from that of the majority of the area drained and their ratio is a measure of the degree of difference. This may be visualized more readily if an arbitrary radius of extent of the low or high permeability area around the well is taken. An equation relating these values is

$$\frac{k_2}{k_1} = \frac{\frac{k_2}{k} \log \bar{r}_e - \log \frac{\bar{r}_e}{\bar{r}_1}}{\log \bar{r}_1} \quad . \ . \ . \ . \ . \ (17)$$

where r is the radial extent of the permeability in the immediate vicinity of the well, k_1 the permeability in the immediate vicinity of the well, k_2 the permeability way from the well estimated from the build-up curve, and k the average permeability estimated from productivity index. In shot wells $\frac{k_2}{k}$ may appear to be small enough to give a negative k_1. This, of course, can not exist and has been caused by arbitrarily assigning too small a value to r_1.

If the permeability determined from the slope of the build-up curve is greater than the permeability that would be determined from the productivity index, there is an indication of a damaged or low permeability area in the immediate vicinity of the well. Likewise, if the productivity index permeability is greater than that permeability as determined from the slope of the build-up curve, there will be an area of higher permeability around the well. This will enable the reservoir engineer to determine the presence of a damaged or improved permeability region at the sand face. The obvious place for application of this analysis is in the determination of the effects of drilling fluid on the permeability near the sand face. This indicates whether treatment should be recommended to improve the productivity of the well. The method may also be used for quantitative evaluation of treatment designed to improve the permeability in the immediate vicinity of the well.

Table IV

k/μ	t_{si} hours 20 Acre Spacing	40 Acre Spacing	80 Acre Spacing	160 Acre Spacing
1	167	315		
10	16.7	32	63	126
100	2	3.2	6.3	12.6

Shut-In Time Required to Obtain Sufficient Data for Permeability Determination From (16). $C_L = 100\%$, $F = 0.2$, and $c = 1.5 \times 10^{-5}\ \text{psi}^{-1}$.

EXAMPLE ILLUSTRATING METHOD OF CALCULATION

In order to illustrate the method of procedure the following calculation is made for a typical well producing a tight formation. The build-up curve on this well, Well A, is shown plotted in Fig. 6. The following is a tabulation of the fluid and formation properties and flow information:

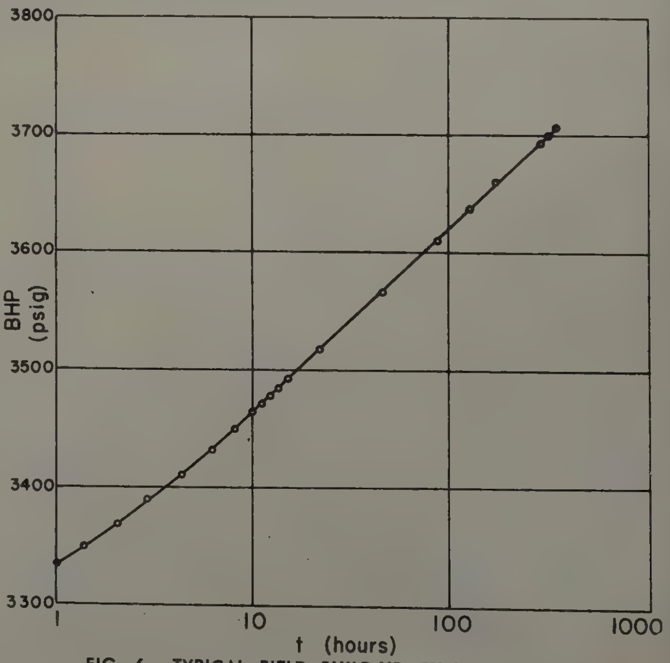

FIG. 6—TYPICAL FIELD BUILD-UP CURVE, WELL A.

$PI = 0.183$ BOPD/psi
$Q = 115$ BOPD
$h = 120$ ft
$r_e = 1300$ ft
$f = 0.15$
$F = 1.69$
$c = 1.52 \times 10^{-5}$ psi^{-1}
$\mu = 0.33$ cup

There were wells producing from the same formation in the immediate vicinity of Well A, and thus this case approaches a closed drainage area with zero influx over the external boundary. An unsaturated oil is flowing in the formation.

The slope of the straight line section of the build-up curve, Fig. 6, is determined as

$$m = \frac{p_2 - p_1}{\log \frac{t_2}{t_1}} = \frac{3705 - 3495}{\log \frac{335}{17}} = 162$$

where p_2 and t_2 are the upper end of the straight line section and p_1 and t_1 the lower end.

To estimate the effective permeability this slope value is used in equation (6) and the permeability calculated as

$$k_2 = \frac{162.5\ Q\mu F}{hm} = \frac{(162.5)(115)(0.33)(1.69)}{(120)(162)} = 0.537$$

At this point it is necessary to check that the slope of the proper section is used. This is done by calculation of the $\bar{t}$ for the upper end of the straight line section from equation (4)*

$$\bar{t} = \frac{0.0002637\ kt}{fc\mu r_e^2} = \frac{(0.0002637)(0.537)(335)}{(0.15)(1.52 \times 10^{-5})(0.33)(1300)^2} = 0.0374.$$

Since this value falls in the range of $\bar{t} = 10^{-2}$ to $\bar{t} = 10^{-1}$ the proper straight line section was used and the permeability estimation is valid.

For the estimation of reservoir pressure the value of $\Delta\bar{p}$ corresponding to the $\bar{t}$ just calculated and $\bar{r}_e = \frac{1300}{1/4} = 5200$ is obtained from Fig. 1 or Fig. 2.

$\bar{t} = 0.0374$ $t = 335$
$\Delta\bar{p} = 7.30$ $p = 3705$

The hypothetical flowing pressure is calculated from equation (10)* and $\Delta\bar{p} = 7.30$ as

$$p_f = p - \frac{\Delta\bar{p}\ Q\mu F}{0.001127\ 2\pi kh} = 3705 - \frac{(7.30)(115)(0.33)(1.69)}{(0.001127)(2\pi)(0.537)(120)}$$
$$= 2678 \text{ psig.}$$

The theoretical drawdown in terms of the dimensionless $\Delta\bar{p}$ is calculated from equation (9) since this case approaches a closed drainage area. Equation (8) would be used for constant pressure maintained at the radius of drainage. This $\Delta\bar{p}_s$ is calculated as

$$\Delta\bar{p} = \ln \bar{r}_e - \frac{3}{4} = \ln(5200) - \frac{3}{4} = 7.80$$

This dimensionless variable proportional to pressure may be converted to pressure, psi, and added to the flowing pressure to obtain reservoir pressure, or the reservoir pressure may be calculated directly from equation (11) as

$$p_e = p + (\Delta\bar{p}_s - \Delta\bar{p})\frac{Q\mu F}{0.001127\ 2\pi kh}$$
$$= 3705 + (7.80 - 7.30)\frac{(115)(0.33)(1.69)}{(0.001127)(2\pi)(0.537)(120)}$$
$$= 3775 \text{ psig.}$$

The over-all mean effective permeability of the drainage area may be calculated from the well-known radial flow equation as

$$k = \frac{PI\ \mu F \log \bar{r}_e}{0.00307\ h} = \frac{(0.183)(0.33)(1.69)(3.716)}{(0.00307)(120)} = 1.03 \text{ md.}$$

Since this is a higher permeability than that estimated from the build-up curve, it indicates that a high permeability exists in the immediate vicinity of the well. By use of equation (17) it may be estimated that to an arbitrary radius of 25 ft that $k_1 \cong 9k_2$.

FIELD BUILD-UP ANALYSES

The authors have subjected approximately 80 build-up curves to the analysis described in this paper. From these 80 curves, seven sets of data have been chosen to illustrate a number of possible conditions existing in build-up testing. These curves are shown plotted with the dimensionless variables in Figs. 7, 8, and 9. The curves plotted in Fig. 7 are from wells which are producing a highly unsaturated formation and in which the well bore was mostly filled with oil prior to shut-in, and thus there was very little flow into the well bore after shut-in since the average compressibility of the well bore fluid was low. The curves shown in Fig. 8 are for wells also producing an unsaturated formation but with a drawdown to approximately saturation pressure such that considerable gas was in the well bore prior to shut-in, allowing an appreciable flow into the well bore after shut-in. The curve plotted in Fig. 9 is for a well producing a two-phase formation, and thus the average compressibility of the well bore fluid was high permitting appreciable flow after shut-in.

Considering first the build-up curves that are shown plotted in Fig. 7, it may be seen that these curves generally follow the type shown in Fig. 4 from the analyzer build-up studies which might be expected since there was little or no flow into the well bore after shut-in. Well A indicates a high permeability region in the immediate vicinity of the well, and thus the early section of the curve falls above the calculated values (not shown but essentially coincident with curve C). The value of $k_1 = 5k_2$ has been estimated for a radius of extent of k_1 to 25 ft. Well B indicates an extremely high permeability in the immediate vicinity of the well, and the calculations estimate an approach to infinite permeability around the well to a radius of 25 ft. Unlike Well A, Well B had been acidized in an attempt to improve the permeability in the immediate vicinity of the well. However, this should not be construed to constitute a value of acidization correlation since it is entirely possible that Well B was drilled into a very high permeability lens. To attempt to evaluate the improvement obtained from acidization it is necessary to have tests before and after treatment. The build-up test of Well C indicates a well with very little difference in the permeability around the well and that away from the well, and thus the build-up curve is practically coincident with the calculated curve for a well producing a uniform formation. The build-up curve for a damaged well is shown by the build-up of Well D. It is known in this formation that most wells show a damaged condition. This may explain the finding that the permeability in the immediate vicinity of the well to a radius of 25 ft is one-fourth of the permeability in the majority of the drainage area away from the well. The point X marked on these curves corresponds to the point in Fig. 4 where the curves coincide with the calculated curve for the build-up of a well producing a uniform permeability zone. It will be noted that this is approximately the point of convergance of the curves shown in Fig. 7. However, it should not be expected that the curves of Fig. 7 correspond exactly to the curves shown in Fig. 4 in that there is some flow into the well after shut-in, which tends to result in lower values on the curves as may be seen by comparison of Fig. 4 and Fig. 5.

---

* For the two-phase flow of oil and gas in the drainage area equation (13) would be used in place of equation (4) and equations (10) and (11) altered for two-phase flow.

The curves shown in Fig. 8 are for build-up curves of a formation producing near the bubble point, and there is thus more flow into the well bore after shut-in than those curves just discussed. Well E represents a well producing from a relatively uniform permeability zone, while Well F represents a well producing a zone in which there is a low permeability region in the immediate vicinity of the well. Neither of these wells has been acidized. For the case of no flow into the well bore the point X again shows the point at which the effects of variation in permeability near the well are negligible. The point Y indicates the upper limit for the convergence of the analyzer curves where there is flow into the well bore after shut-in and increased or decreased permeability zones in the immediate vicinity of the well. It will be noted that in Fig. 8 the convergence of these curves with the theoretical curve occurs between the points X and Y as might be expected. The trends indicated in Fig. 8 are the same as those shown in Fig. 5. However, exact correlation should not be expected since the amount of flow after shut-in was different. The point Y does not indicate the maximum possible limit for convergence of the curves since a greater decreased in permeability around the well could exist and since gas accumulated in the immediate vicinity of the well would result in a material in that region with a compressibility higher than has been assumed. This additional compressibility may have an effect similar to flow into the well bore resulting in an even greater deviation from the calculated curve. However, for the 80 wells studied this value was not exceeded.

Fig. 9 shows the build-up curve of Well C producing an area containing both oil and gas. It will be noted in this curve that convergence with the calculated curve occurs near the point Y indicating appreciable flow after shut-in as would be expected for this type well. The points X and Y have the same significance as in the preceding figures. Comparison of the permeability from the build-up curve and the permeability from the productivity index tests in which the reduction to effective permeability near the well due to gas accumulation has been included indicates that production is from a practically uniform permeability area.

In Figs. 7, 8, and 9 the build-up data had been chosen to represent a number of various cases similar to those studied by means of the electrical analyzer, the results of which are plotted in Figs. 3, 4, and 5. It will be noted that an earlier straight line section than the one to be used for permeability determination is frequently present in these field build-up curves and that these sections correspond to those indicated from the analyzer work.

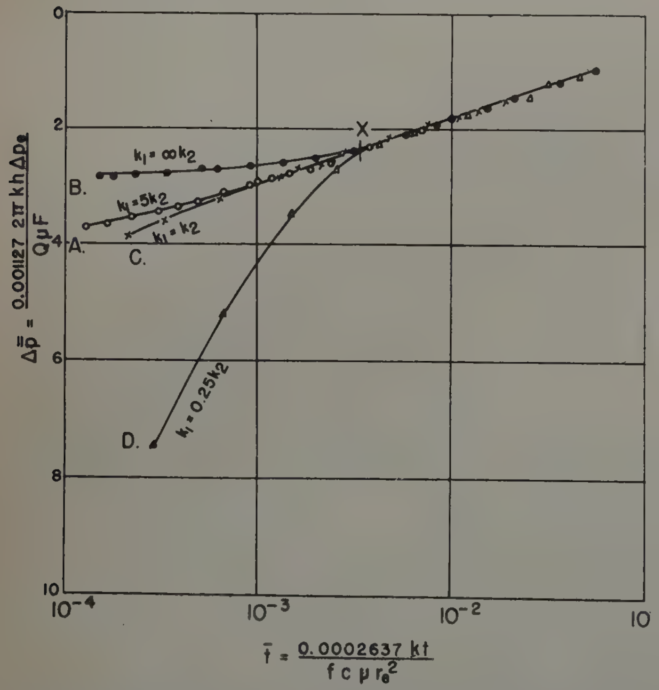

FIG. 7 — FIELD BUILD-UP CURVES; WELLS PRODUCING HIGHLY UNSATURATED FORMATIONS WITH FLOW INTO WELL BORE NEGLIGIBLE.

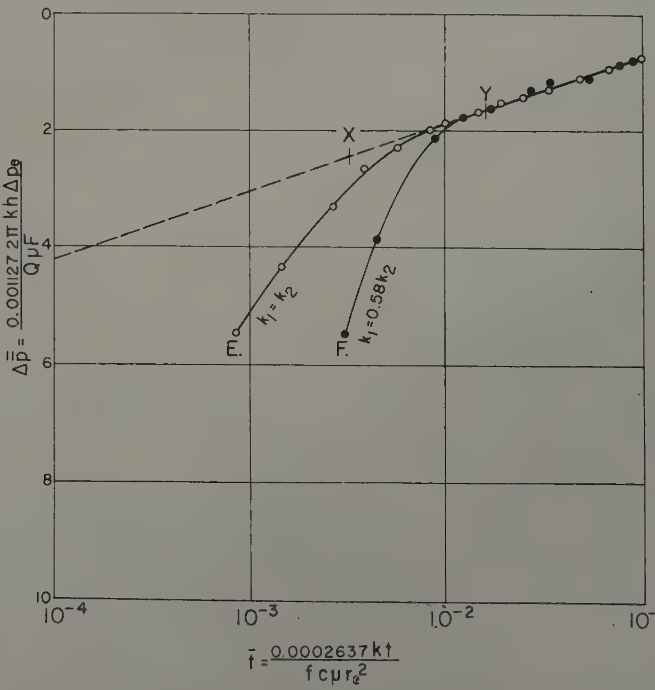

FIG. 8 — FIELD BUILD-UP CURVES; WELLS PRODUCING UNSATURATED FORMATIONS WITH FLOW INTO WELL BORE APPRECIABLE.

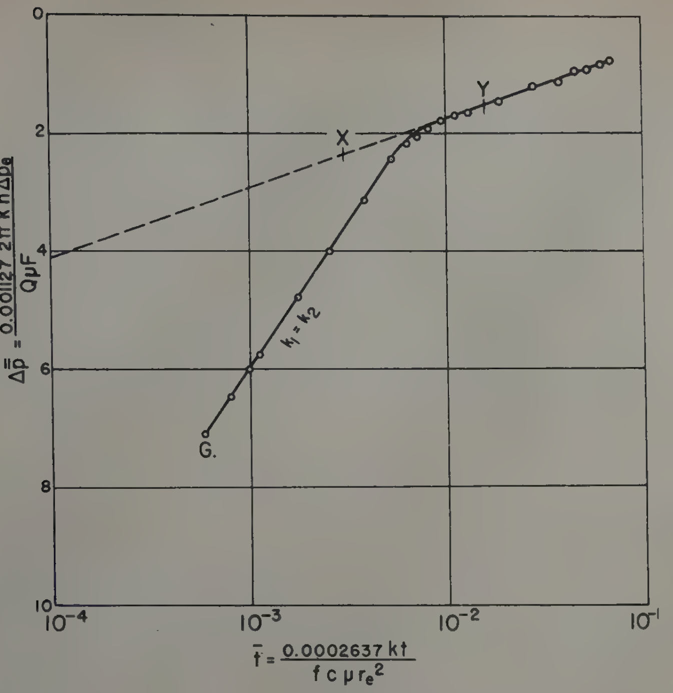

FIG. 9 — FIELD BUILD-UP CURVE; WELL PRODUCING FORMATION WITH OIL AND GAS FLOWING.

SUMMARY

The relationships developed in this paper enable the reservoir engineer to estimate the effective permeability and reservoir pressure from the early portion of the build-up curve provided the well is stabilized prior to shut-in. Relations are also presented to assist planning the pressure survey for estimating the length of time of constant production to stabilize the well and the shut-in time required to obtain sufficient data for analysis.

The method for analysis of build-up curves was derived for the flow of a homogeneous compressible liquid. However, the method may be extended to include an approximation for the condition of oil and gas flow in the reservoir where the gas is distributed throughout the reservoir rather than contained in a cap.

The early part of the build-up curve is independent of the amount of migration over the external boundary, and this portion of the curve is used for permeability estimation. It is not necessary therefore to know the magnitude of this migration for permeability estimation.

The build-up characteristics for the two cases of maximum and zero migration over the external boundary were considered. The difference in final build-up pressure for the two cases may be significant. It is therefore necessary to assume a value for the magnitude of migration in the estimation of reservoir pressure by this method. From the 80 wells studied, some of which were produced at relatively high allowables from zones of permeability in the order of one millidarcy, the error possible from the mid-value was found to be as large as 50 psi. High production rates and low permeabilities both lead to increases in the uncertainty arising from estimation of the degree of migration. This error would be practically constant in succeeding determinations, and the reservoir pressure decline would be considerably more accurate.

The equations developed for build-up characteristics consider a well producing from a uniform formation and shut in at the sand face. The existence of a high or low permeability zone in the immediate vicinity of the well and the flow into the well bore after shut-in to compress the fluids contained therein cause a deviation from the equations. Studies with the electrical analyzer show that such deviation is appreciable only in the very early portion of the build-up curve, becoming negligible after a short period of time, and these very early data should not be considered in interpreting build-up curves by this method.

The methods developed here are for a well stabilized prior to shut-in. The electrical analyzer may be used to extend this approach to instances in which the well is not stabilized prior to shut-in. However, analyzer runs take considerably longer to make than the method described here.

The permeability estimated from the build-up curve represents the permeability in the majority of the drainage area away from the well. The permeability estimated from the productivity index using Darcy's Law represents the permeability throughout the drainage area. Thus, the existence of a high or low permeability zone in the immediate vicinity of the well may be estimated by comparison of the permeabilities determined in these two ways. This offers a method to evaluate the possibility of having damaged the well in drilling or benefits occurring from treatment.

ACKNOWLEDGMENT

The authors wish to express their appreciation to Francis Collins, W. W. Schriever and V. J. Sikora for their suggestions and assistance in connection with this problem.

NOMENCLATURE

c = mean liquid compressibility, psi^{-1}
C = saturation, fraction
f = reservoir porosity, fraction
F = formation volume factor, $\frac{\text{Res bbl}}{\text{STB}}$
h = reservoir thickness, ft
k = effective permeability, millidarcys
K = diffusivity, $\frac{k}{fc\mu}$
m = slope of build-up curve = $\Delta p/\log t_2/t_1$
p = pressure, psia
Q = volume rate of flow, STB/Day
r = radial distance measured from center of well, ft
$\bar{r} = r/r_w$
R = gas-oil ratio, $\frac{\text{SCF}}{\text{Bbl}}$
S = solubility, $\frac{\text{SCF}}{\text{Res Bbl}}$
t = time, hours
v = velocity
μ = viscosity, centipoise
δ = density, lb/ft^3
ρ = gas conversion factor, $\frac{\text{SCF}}{\text{bbl}}$
ψ = mass rate of flow

Functions

$\ln$ = logarithm to the base e
$\log$ = logarithm to the base 10
$U(a_n r) = Y_1(a_n r_e) J_o(a_n r) - J_1(a_n r_e) Y_o(a_n r)$
$U'(a_n r) = a_n Y_1(a_n r_e) J_1(a_n r) + a_n J_1(a_n r_e) Y_1(a_n r)$
$U'(a_n f_w) = 0$
$f(\lambda)$ = time function of flux
$g(r)$ = initial density distribution function
J = Bessel function of first kind
Y = Bessel function of second kind
$x_n = a_n r_w$
$\bar{\Delta p} = \frac{0.001127\ 2\pi kh}{Q\mu F} \Delta p_f$
$\bar{t} = \frac{0.0002637\ kt}{fc\mu r_e^2}$
$\bar{\bar{\Delta p}} = \frac{0.001127\ 2\pi kh}{Q\mu F} \Delta p_e$
$\Delta p_f = p - p_f$
$\Delta p_e = p_e - p$
$K' = \frac{k(\delta_L + \delta_g R)}{fc_T \mu_L (F\delta_T)}$

Subscripts

e = conditions at radius of drainage
w = conditions at well
f = conditions with well flowing
g = gas phase
L = oil phase
o = initial conditions
r = relative
T = condition of the total system
s = static conditions
1 = in area near well
2 = in area away from well

REFERENCES

1. M. Muskat, "Use of Data on the Build-Up of Bottom Hole Pressures," *Trans.* AIME, 1937, p. 44.
2. J. J. Arps and A. E. Smith, "Practical Use of Bottom Hole Pressure Build-Up Curves," Reprint Paper No. 851-23-I, Tulsa, Oklahoma, Meeting API, March, 1949.
3. E. N. Kemler, "Applying Bottom Hole Pressure Data to Production Problems," Part 4, *The Oil Weekly*, September 21, 1942, p. 30.
4. N. Johnston and J. E. Sherborne, "Permeability as Related to Productivity Index," *API Drilling and Production Practice*, 1943, pp. 66-81.
5. M. Muskat, *The Flow of Homogeneous Fluids Through Porous Media*, McGraw-Hill Book Co., Inc., New York. 1937, p. 641.
6. W. A. Bruce, "An Electrical Device for Analyzing Oil-Reservoir Behavior," *Trans.* AIME, 1943, p. 388.
7. E. R. Brownscombe and L. R. Kern, "Graphical Solution of Single-Phase Flow Problems," Paper in Preparation.
8. M. Muskat, op. cit., p. 656.
9. E. R. Brownscombe and Francis Collins, "Steady States in Single Phase Reservoirs," Paper, San Francisco, California, Meeting of AIME.
10. M. Muskat and N. W. Meres, "The Flow of Heterogeneous Fluids Through Porous Media," *Physics* 7, 1936, p. 349.
11. Charles C. Miller, E. R. Brownscombe and W. F. Kieschnick, Jr., "A Calculation of the Effect of Production Rate Upon Ultimate Recovery by Solution Gas Drive," *Trans.* AIME, 186, 235, (1949).
12. A. F. Van Everdingen and W. Hurst, "The Application of the Laplace Transformation to Flow Problems in Reservoirs," *Trans.* AIME, 186, 305, (1949).

APPENDIX

Theoretical Build-up Relations

The fundamental differential equation defining the flow of a compressible homogeneous fluid through a porous medium in a radial flow system with no vertical flow is the familiar diffusivity equation

$$\frac{\partial^2 \delta}{\partial r^2} + \frac{1}{r}\frac{\partial \delta}{\partial r} = \frac{1}{K}\frac{\partial \delta}{\partial t} \quad \ldots\ldots \quad (1)$$

Before the integration of this equation for application to the problem at hand certain stipulations concerning the conditions of the reservoir and its fluid must be specified as boundary conditions. Muskat[5] has applied the equation to obtain the build-up relations for the following conditions:

1. An undersaturated fluid is flowing in the reservoir.
2. There is a steady state distribution in the reservoir prior to shut-in.
3. The well is shut in at the bottom. This excludes the possibility of flow into the well bore after shut-in due to the compressibility of the fluids.
4. A constant density and thus pressure is maintained at the external boundary, radius of drainage, during the build-up period.

This final specification of constant pressure at the external boundary at steady state indicates a reservoir under the condition of maximum migration of fluid across the external boundary for the given pressure difference between the external boundary and the well. This migration of course will be equal to the production rate at the time of shut-in and will drop to zero as the pressure is built up. By a direct integration of Darcy's Law the initial steady state density distribution for these conditions may be obtained in the form

$$\delta = \frac{\delta_e - \delta_w}{\log \bar{r}_e} \log \bar{r} + \delta_w \quad \ldots\ldots \quad (2)$$

Applying these boundary conditions to the diffusivity equation an integration results in an equation for the build-up characteristics which expressed in dimensionless variables takes the form as presented by Muskat

$$\frac{p_e - p}{p_e - p_f} \cong \frac{\delta_e - \delta}{\delta_e - \delta_f} = \frac{2}{\ln \bar{r}_e} \sum_{n=1}^{\infty} \frac{e^{-x_n^2 \bar{t}}}{(x_n)^2 J_1^2(x_n)} \quad . \quad (3)$$

where $J_0(x_n) = 0$. The dimensionless variable $\bar{t}$ is defined by the equation

$$\bar{t} = \frac{0.0002637\ kt}{fc\mu r_e^2} \quad . \quad . \quad . \quad . \quad . \quad . \quad . \quad . \quad . \quad . \quad (4)$$

where time is in hours, permeability in millidarcys, porosity as a fraction, compressibility in psi^{-1}, viscosity in centipoises, and radius in ft. Pressures may be substituted for density as was done in equation (3) because of the relation evolved from the equation of state where

$$\delta = \delta_0 e^{c(p_0 - p)} = \delta_0 [1 + c(p_0 - p)] \quad . \quad (5)$$

The conditions that exist at the radius of drainage may vary from a case of constant pressure at the external boundary to a condition of no influx as in a closed drainage area. It was therefore desirable to obtain equations defining the build-up characteristics for both cases as conditions of extremes at the external boundary or radius of drainage of the well.

The stipulations concerning the reservoir and its fluid that are specified in connection with obtaining the build-up characteristics for a well in a closed drainage area with no influx over the external boundary are the same as those just presented, with the exception of condition (4), which must be changed to consider the influx at the external boundary to be zero. This then represents a radial system in which the flux is specified over both boundaries. A system of this nature is governed by the equations[8] as derived from the diffusivity equation

$$\delta = \frac{2K}{r_e^2 - r_w^2} \int_0^t [f_e(\lambda) - f_w(\lambda)]\, d\lambda + \frac{2}{r_e^2 - r_w^2} \int_{r_w}^{r_e} rg(r)\, dr$$

$$+ \pi \sum_{n=1}^{\infty} \frac{a_n^2 J_1(a_n r_w) U(a_n r) e^{-Ka_n^2 t}}{J_1^2(a_n r_w) - J_1^2(a_n r_e)} \Bigg[\frac{\pi}{2} J_1(a_n r_w)$$

$$\int_{r_w}^{r_e} rg(r) U(a_n r)\, dr$$

$$+ K \frac{J_1(a_n r_e)}{a_n r_w} \int_0^t f_w(\lambda) e^{Ka_n^2 \lambda}\, d\lambda - K \frac{J_1(a_n r_w)}{a_n r_e}$$

where a_n is determined by the equation

$$\int_0^t f_e(\lambda) e^{Ka_n^2 \lambda}\, d\lambda \Bigg] \qquad (6)$$

$$U'(a_n r_w) = 0 \quad . \quad . \quad . \quad . \quad . \quad . \quad . \quad . \quad . \quad . \quad (7)$$

For the special case of a shut-in well in a closed reservoir that is considered here the flow function is zero at both boundaries.

$$f_w(\lambda) = f_e(\lambda) = 0 \quad . \quad . \quad . \quad . \quad . \quad . \quad . \quad . \quad . \quad (8)$$

The initial density distribution for this case is obtained in the same manner as before. This distribution, however, represents an equilibrium condition which is reached in the drainage area when the gradient is constant with time at all points.[9] Applying Darcy's Law as before the initial density distribution may be expressed in the form

$$g(r) = \delta_w + \frac{\psi c\mu}{4\pi kh(r_e^2 - r_w^2)} [2r_e^2 \ln \bar{r} + r_w^2 - r^2] \quad . \quad (9)$$

Making use of this expression in equation (6) the general expression for density as a function of position and time is

$$\delta = \delta_w + \frac{\psi c\mu}{2\pi kh} \Bigg[r_e^2 \frac{(r_e^2 \ln r_e - r_w^2 \ln r_w)}{(r_e^2 - r_w^2)^2} - \frac{1}{2} - \frac{r_e^2 + r_w^2}{4(r_e^2 - r_w^2)}$$

$$- \frac{r_e^2 \ln r_w}{r_e^2 - r_w^2} + \frac{\pi^2}{2} \sum_{n=1}^{\infty} \frac{J_1^2(a_n r_w) U(a_n r_w) U(a_n r)}{J_1^2(a_n r_e) - J_1^2(a_n r_w)} e^{-Ka_n^2 t} \Bigg]$$

$$. \quad . \quad . \quad . \quad . \quad . \quad . \quad . \quad . \quad . \quad (10)$$

In this particular application of this equation the interest is in the pressure, and thus the density, at the bottom of the well, requiring that $r = r_w$ be substituted in the Bessel function $U(a_n r)$.

The resulting density equation can then be converted to an equation for the bottom hole pressure using equation (5). Furthermore, the volume rate of flow is expressed by $FQ = \psi/\delta$ and in the terms involving r_e and r_w the r_w terms may be neglected without error since $r_e >>> r_w$. The pressure build-up expressed in dimensionless variables is

$$\Delta\bar{p} = \ln \bar{r}_e - \frac{3}{4} + \frac{\pi^2}{2} \sum_{n=1}^{\infty} \frac{J_1^2(x_n) U^2(x_n)}{J_1^2(\bar{r}_e x_n) - J_1^2(x_n)} e^{-\bar{r}_e^2 x_n^2 \bar{t}} \qquad (11)$$

The equation determining x_n is

$$J_1(\bar{r}_e x_n) Y_1(x_n) - J_1(x_n) Y_1(\bar{r}_e x_n) = 0 \quad . \quad . \quad (12)$$

The dimensionless variable proportional to pressure, $\Delta\bar{p}$, is defined by the equation

$$\Delta\bar{p} = \frac{0.001127\ 2\pi kh}{Q\mu F} \Delta p \quad . \quad . \quad . \quad . \quad . \quad (13)$$

where permeability is in millidarcys, height in ft, production in stock tank barrels per day, viscosity in centipoises, and pressure in psi. From equations (11) and (12) the pressure at the bottom of a shut-in well in a closed reservoir may be calculated as a function of time.

Equations (3) and (11) define the build-up characteristics for the two extremes in the magnitude of influx over the external boundary. For purposes of comparison of the numerical solutions of these equations it is necessary to convert $\frac{p_e - p}{p_e - p_f}$ to $\Delta\bar{p}$ or vice versa. Conversion of the former to $\Delta\bar{p}$ is accomplished by means of the well-known radial flow equation

$$Q = \frac{0.001127\ 2\pi kh \Delta p_f}{F\mu \ln \bar{r}_e} \quad . \quad . \quad . \quad . \quad . \quad (14)$$

Using this relation the conversion equation takes the form

$$\Delta\bar{p} = \left[1 - \frac{p_e - p}{p_e - p_f} \right] \ln \bar{r}_e \quad . \quad . \quad . \quad . \quad (15)$$

and equation (3) may be expressed as

$$\Delta\bar{p} = \ln \bar{r}_e - 2 \sum_{n=1}^{\infty} \frac{e^{-x_n^2 \bar{t}}}{(x_n)^2 J_1^2(x_n)} \quad . \quad (16)$$

A plot of $\Delta\bar{p}$ vs log $\bar{t}$ for equations (11) and (16) shows an apparent straight line section in the $\bar{t}$ range of 10^{-3} to 5×10^{-2}. This section, however, is not actually a straight line as might be determined by proper differentiation of equation (11) or (16). For practical purposes, though, this is a straight line and will be used as such. The straight line sections calculated from equation (16) are parallel since translation by the quantity $\ln \bar{r}_e$ results in coincident curves. Only one numerical evaluation of equation (11) was made, and this curve when translated by $\ln \bar{r}_e$ will coincide with those from equation (16). Electrical analyzer curves of equation (11) for various values of $\bar{r}_e$ show this same property of coincidence when translated by $\ln \bar{r}_e$. The slope of the build-up curve in the straight line section is important in that it is proportional to the permeability according to the relation

$$\frac{\triangle(\triangle\bar{p})}{\triangle(\log\bar{t})} = \frac{\dfrac{kh}{141.2\ Q\mu F}\triangle(\triangle p)}{\triangle(\log t)} \qquad (17)$$

Substituting the slope of the calculated curve (1.147) for $\dfrac{\triangle(\triangle\bar{p})}{\triangle(\log\bar{t})}$ in this equation results in an equation for the effective permeability as a function of the slope, m, of the straight line section of the build-up curve. This equation is

$$k = \frac{162.5\ Q\mu F}{hm} \qquad (18)$$

Build-up Curves — Two-Phase Flow

The relationships that have been developed to this point have considered the flow of a homogeneous compressible liquid through a porous medium. It would be, of course, advantageous to extend this method to include drainage areas in which both oil and gas were flowing. By making the approximations that are noted, this was done in the following manner.

By a material balance of the residual oil the mass transfer is expressed by the equation as modified from the approach of Muskat and Meres[10]

$$\nabla \cdot \frac{\delta_L k k_{rL}}{\mu_L F}\nabla p = -f\frac{\partial}{\partial t}\left(\frac{\delta_L C_L}{F}\right) \qquad (19)$$

The general equation for gas flow is

$$\nabla . \frac{\delta_g k k_{rL}}{\mu_L F} S\bar{\nabla} p + \nabla\frac{\delta_g k k_{rg}}{\mu_g}\rho\nabla p = -f\frac{\partial}{\partial t}\left(\delta_g C_g \rho + \frac{\delta_g C_L}{F} S\right) \qquad (20)$$

In the reservoir away from the well the pressure is fairly constant, and the pressure functions, μ_L, μ_g, F, ρ, and S are assumed to be considered constant. Likewise, the saturation is fairly constant and the dependent variables k_{rg} and k_{rL} will be assumed constant also. Applying these assumptions to the above equations the expression for gas flow becomes

$$k\left(\frac{k_{rL}\delta_g S}{\mu_L F} + \frac{k_{rg}\delta_g \rho}{\mu_g}\right)\nabla^2 p = -f\frac{\partial}{\partial t}\left(\delta_g C_g \rho + \frac{\delta_g C_L}{F} S\right) \qquad (21)$$

Applying the same to liquid flow

$$k\left(\frac{\delta L^{k}{}_{rL}}{\mu_L F}\right)\nabla^2 p = -f\frac{\partial}{\partial t}\left(\frac{\delta_L C_L}{F}\right) \qquad (22)$$

Adding these last two equations a general equation for the simultaneous flow of oil and gas through a porous medium is obtained. This is

$$k\frac{k_{rL}}{\mu_L F}\left(\delta_L + \delta_g S + \frac{\delta_g k_{rg}\mu_L F\rho}{k_{rL}\mu_g}\right)\bar{\nabla}^2 p$$
$$= -f\frac{\partial}{\partial t}\left(\frac{\delta_L C_L}{F} + \delta_g C_g \rho + \frac{\delta_g C_L}{F} S\right) \qquad (23)$$

The right side of this equation is a function of the total density, δ_T, of the system and may be converted to pressure by the introduction of a total compressibility term, c_T (see equation 5). Upon collection of constants the equation takes the form

$$\bar{\nabla}^2 p = \frac{1}{K'}\frac{\partial p}{\partial t} \qquad (24)$$

where

$$K' = \frac{k\dfrac{k_{rL}}{\mu_L F}\left[\delta_L + \delta_g R\right]}{f c_T \delta_T} \qquad (25)$$

since $$R = \frac{k_{rg}\mu_L F\rho}{k_{rL}\mu_g} + S \qquad (26)$$

Equation (24) is of the same form as the diffusivity equation for single-phase flow, and its solutions for the rise in bottom hole pressure when the well is shut in may be obtained by analogy.

The initial steady state presure distributions to be considered may be derived with the same conditions applying as were considered for single-phase flow with slight modifications

$$\int_{p_w}^{p}\frac{kh}{\mu F}dp = \frac{893\ Q}{2\pi}\ln\frac{r}{r_w} \qquad (27)$$

for constant pressure maintained at the external boundary and

$$\int_{p_w}^{p}\frac{kh}{\mu F}dp = \frac{893\ Q_L}{2\pi}\left(\ln\frac{r}{r_w} - \frac{r^2}{2r_e^2}\right) \qquad (28)$$

for a closed drainage area. Since it appears that during much of the history of the field when two phases are flowing, the saturation throughout the entire reservoir is relatively constant at any time the permeability may be considered constant. Although the pressure varies considerably, particularly near the well, the μF product will nevertheless remain fairly constant since μ increases and F decreases with pressure decline. With these assumptions the initial density distributions may be shown to take the same form as before, equations (11) and (16).

From these considerations the dimensionless variable proportional to pressure, $\triangle\bar{p}$, is defined as before,

$$\triangle\bar{p} = \frac{0.001127\ 2\pi kh}{Q_L\mu_L F_L}\triangle p \qquad (29)$$

The dimensionless variable proportional to time, $\bar{t}$, now requires a substitution of K′ for the diffusivity, K, in equation (4) giving

$$\bar{t} = \frac{0.0002637\ k}{f c_T \mu_L r_e^2}\left(\frac{\delta_L + \delta_g R}{F\delta_T}\right)t \qquad (30)$$

This change, however, does not require any changes in the equation for effective oil permeability which is

$$k = \frac{162.5\ Q_L\mu_L F_L}{hm} \qquad (31)$$

The pressure variables in these equations should be evaluated at or near the average reservoir presure, and with these modifications a well producing two phases may be handled in the same manner as a well producing only oil.

★ ★ ★

SOME THEORETICAL CONSIDERATIONS RELATED TO THE QUANTITATIVE EVALUATION OF THE PHYSICAL CHARACTERISTICS OF RESERVOIR ROCK FROM ELECTRICAL LOG DATA

M. R. J. WYLLIE AND **WALTER D. ROSE,** JUNIOR MEMBER AIME, GULF RESEARCH AND DEVELOPMENT CO.,
PITTSBURGH, PENNSYLVANIA

INTRODUCTION

The use of electrical well logs for the quantitative determination of such reservoir parameters as connate water saturation, formation permeability and connate water salinity has recently been attracting the attention of a number of workers[1,2,3,4,5].

While the theory of the determination of connate water salinity from the self potential S.P. log has received rather detailed treatment, relatively little attention has been paid to the theoretical aspects involved in the quantitative interpretation of resistivity data. It is clear that if electrical well logs can be used for the quantitative evaluation of physical characteristics of reservoir rock, they will provide a valuable tool to supplement cheaply information obtained by more laborious core analysis. In certain cases it is conceivable that the coring program could be considerably curtailed if the electric log could be relied upon to give reasonably accurate quantitative information.

It is our object in this paper to examine the theoretical basis of quantitative log interpretation as expressed in such well-established logging concepts as formation factor and cementation factor. It is also our object to investigate the physical aspects of the relationship which is presumed to exist between resistivity index and brine saturation in reservoir rock. In particular, we will endeavor to draw attention to the fact that it is possible to express these logging concepts in terms of capillary pressure-saturation relationships, permeability and tortuosity, parameters which we will consider in this paper to be fundamentally indicative of rock texture. The probability of being able to obtain from log recordings alone the data theoretically essential to permit quantitative log interpretation will be examined, and consideration will also be given to the problem of formulating simple semi-empirical relationships for use in the field.

THEORETICAL CONSIDERATIONS

The concept of formation resistivity factor, or as it is now commonly called, formation factor, appears to have been introduced by G. E. Archie[6,14]. Formation resistivity factor as defined by Archie is the resistivity of a rock 100 per cent brine-saturated divided by the resistivity of the brine. This relationship had previously been used by physical chemists and the concept is, for example, implicit in an early treatment by Fricke[7] of the conductivity of aqueous slurries. Archie was able to establish the fact that although the relationship between formation factor and porosity did not change too greatly for different rock textures, the relationship between formation factor and permeability was markedly dependent on rock texture. The relationship found by Archie between formation factor and porosity was expanded by H. Guyod[8]. Archie had suggested that the formation factor, F, could be expressed in terms of the porosity, ϕ, as follows:

$$F = \phi^{-m} \quad . \quad . \quad . \quad . \quad (1)$$

where, ϕ = effective porosity fraction of the sand,
and, m = an exponent greater than about 1.3.

Guyod introduced the term cementation factor for the exponent, m, since it may be qualitatively shown that formation factor for any given porosity tends to increase as the sand becomes more cemented. It would appear that the concept of m as an exponent representing the cementation in a sand is strictly only of qualitative value, since the quantitative estimation of m by means other than the determination of F and ϕ has not been possible. Guyod suggests that m can be estimated from a visual examination of a sample of rock, but this method appears to be both arbitrary and unreliable. It can be said, however, that in intergranular reservoirs of practical interest, the range of m is from about 1.4 to 3.0. A possible explanation for the fact that m is found to lie between these limits will be offered below.

The determination of formation factor is an essential preliminary to the

---

[1] References given at end of paper.

Manuscript received at the office of the Petroleum Branch October 6, 1949.

employment of the electric log for either the qualitative or quantitative interpretation of reservoir rocks for oil saturation. By Archie's original definition, F is a ratio and is independent of the resistivity of the brine used to saturate the formation. As shown elsewhere[9] this definition of F has implicit in it the assumption that the solid matrix of the formation is an insulator. If the solid matrix is a conductor, F will not be independent of the resistivity of the saturating fluid. However, in ideal cases a correction may be made for the presence of conductive solids in the rock matrix and if this correction is made, it is theoretically possible to determine F from log data.[9]

The calculation of the resistivity of the connate water in the formation may be made if the electrochemical S.P. applicable to the formation and the mud activity are both known.[5] The resistivity that the formation would have, if it were 100 per cent saturated with connate water, is then the product of the formation factor and connate water resistivity. A qualitative indication of the presence of oil or gas in the formation may be obtained by comparing this resistivity with the true resistivity of the formation obtained from resistivity departure curves.[10]

It may be said that, qualitatively, the effect of oil or gas in the formation will be to increase the resistivity of the formation. It has been widely assumed that the amount of oil or gas in the formation (if the formation has integranular porosity) may be calculated quantitatively from the relationship.

Resistivity Index $= S_w^{-n} = I$ . . (2)

where I, the resistivity index, is the ratio of the resistivity of the formation in situ to the resistivity which it would have at the same temperature if 100 per cent saturated with connate water, and S_w is the fraction of the pore volume saturated with connate water. The exponent, n, is normally given the value of 2.

This relationship, which is fundamental to the quantitative interpretation of electrical well logs, does not appear to us to have the requisite theoretical and experimental justification to warrant the universal applicability which is generally attributed to it. The relationship, in fact, appears to rest on the experimental findings of Wyckoff and Botset,[11] as supported by the work of Jakosky and Hopper,[12] Martin, Murray and Gillingham,[13] Leverett[28] and others. Some confirmation was also provided by Morse, Terwilliger and Yuster.[15] The data obtained by all these workers apply in most cases to unconsolidated sands, although a few data are applicable to moderately cemented sandstones. It is, however, important to note that the saturation processes used by these workers may not have always resulted in the same type of fluid distributions as that obtaining in reservoir rocks. The exponent found by these workers is actually an average of 1.96, although 2 is customarily assumed for log interpretation. The probability of this exponent being a universal constant for all reservoir rocks, irrespective of their texture, will be considered below, together with a consideration of the dependency of this exponent on fluid saturation distribution.

It will suffice to say here that available experimental evidence is not always correlatable to Equation 2, if the exponent n is assumed to be constant. It may be pointed out that the data of Morse, Terwilliger and Yuster, if substituted in Equation 2, will show an exponent which is not constant but varies from 8.5 at 90 per cent saturation to 2.8 at lower saturations. These results are for certain Bradford cores when using oil displacement of the brine and the variable exponents were attributed by these workers to the oil wettability of the sand. Henderson and Yuster[16] and Henderson and Mendrum[17] show a similar variation of the exponent n in a given sand depending upon the kind of non-wetting phase, the applied pressure inducing two-phase flow and other factors which affect the configuration of the non-wetting phase. Similarly, Guyod[18] has published a number of data showing the relationship found by Russian workers between resistivity index and saturation for cores of varying porosity when different types of non-wetting phase were employed. These data show that the water saturation index exponent is not independent of saturation and in addition varies from 1.7 to 4.3 at high water saturations, depending upon the type of porous medium and the nature of the non-wetting phase. The results, however, tend in most cases to an exponent of about 2.5 at water saturations less than 20 per cent. No details are available regarding the experimental technique employed by the Russian workers. Variable values of the exponent apparently less than 2 are explicable if formations contain conducting solids[9] but values of the exponent as high as 4.3 imply either a gross experimental error or a marked influence of formation texture or type of distribution of the conducting phase on the results obtained.

The effect of the formation texture on the validity of the resistivity index-saturation relationship does not appear to have been considered in detail either experimentally or theoretically. However, in recent years much information concerning methods of describing rock texture in terms of such parameters as tortuosity and specific internal surface area have been formulated by Carman[19] and others. These concepts recently have been linked to the study of capillary pressure phenomena in porous media.[20] It would appear that these rock textural relationships may be used also to give a more fundamental definition to formation factor and from this definition a theoretical treatment may be given to the concept of cementation factor and the exponent in the resistivity index-saturation relationship.

In order to accomplish this end, which involves the interrelation of electrical parameters with those relating to fluid movement, we make the fundamental assumption that the tortuosity pertaining to the flow of electrical current through conducting fluids in porous media is closely related to the tortuosity which appears in equations describing the mass transfer of fluids in the same media.

Tortuosity, it will be recalled, refers to the effective flow streamline length which determines the macroscopically observed variation in conductivity (whether it be electrical or fluid) as a function of the miscroscopic orientation characteristics of the individual pores comprising the interspaces. Therefore, the equivalence of hydraulic and electrical tortuosities seems to depend to some extent on the degree of uniformity of the pore structure.

In the treatment given below we will, for simplicity, assume that these two tortuosities are numerically identical and we will show that there is evidence in a number of cases to support this view. We would not, however, deny the contention that there may be an empirical constant connecting the two tortuosities; such evidence as we have obtained points, however, to such a constant, if it exists, being close to unity.

We would not infer that the mechanism of flow of electrical current through a porous medium containing a conducting fluid is identical with the flow mechanism of the fluid itself through that medium. Differences between the two mechanisms are immediately apparent and certain of these differences are discussed below. In particular we would not expect any similarity between the two processes unless the path available for hydraulic movement was the same as that available for electrolytic conduction. This limitation excludes any consideration of such porous media as shales, where the solid matrix is itself conducting. Similarly, in a porous medium composed of both conducting and non-conducting solids the similarity between fluid flow and electrolytic conduction can only be presumed to exist throughout the liquid phase. That is, any conductivity resulting from the presence of the conducting solids in the matrix must first be accounted for by independent processes.

Development of Formation Factor Concepts

The foregoing considerations imply that the formation factor concept is of fundamental importance to the development of applications based on electrical log data. From this, it follows that a definition of formation factor in terms of textural parameters of greater significance than the arbitrary cementation factor, m, of Equation 1 would be of considerable importance in the wider interpretation of electrical log data. Such a definition may be derived if the tortuosity applicable to fluid flow in porous media is assumed to be the same as that which affects the resistivity of porous media to electrolytic conduction.

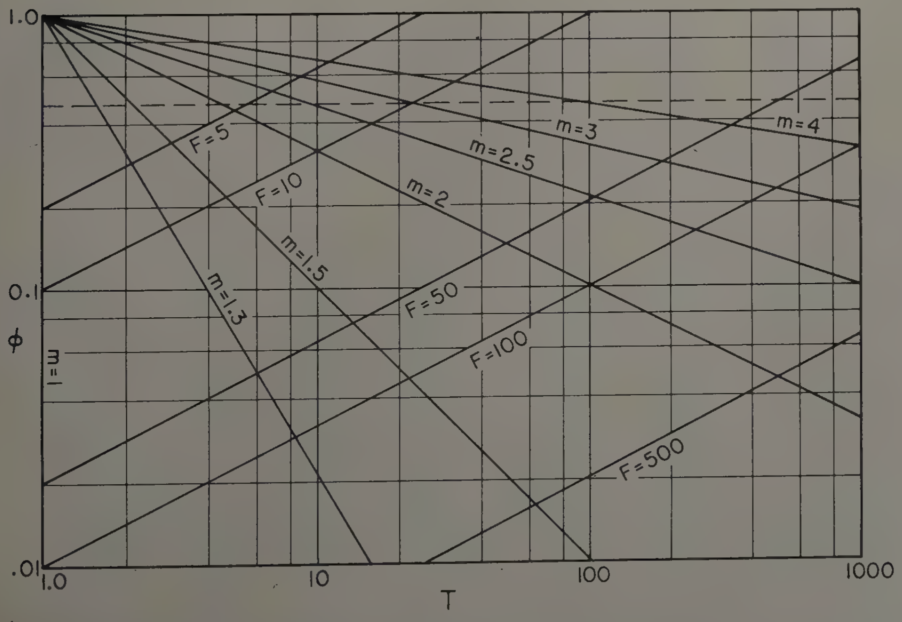

FIG. 1 — POROSITY AS A FUNCTION OF TORTUOSITY FOR CONSTANT VALUES OF FORMATION FACTOR AND CEMENTATION FACTOR

In considering the electrical resistance of a fluid saturated porous medium possessing a random* distribution of pores, we may express the resistance in terms of the electrical resistance of a single fluid-filled channel having a rather complex shape but of constant cross sectional area, ϕA_c, where ϕ is the fractional porosity and A_c is the total area of cross section. The length of this conducting channel may be taken as L_a, where L_a is greater than the actual length, L, of the porous medium. If ρ_c is the resistivity of the saturating fluid and ρ_w the resistivity of the saturated medium,

$$\rho_w \cdot \frac{L}{A_c} = \rho_c \cdot \frac{L_a}{\phi A_c}$$

Whence, $\rho_w = \rho_c \dfrac{L_a/L}{\phi}$

But, by definition,

$$F = \rho_w/\rho_c \qquad = (L_a/L)/\phi \quad = T^{1/2}/\phi \quad . \; . \; . \; . \; (3)$$

Where, $T = (L_a/L)^2$ = Tortuosity. It may be pointed out that Thornton's[21] recent treatment of relative permeability data has implicit in it concepts which lead also to Equation 3. In an extension of Thornton's treatment we derived[20] an expression for the hydraulic formation factor, F_f, in the form:

$$F_f = NT/\phi^2 \quad . \; . \; . \; (4)$$

Where N = number of pores in any cross-sectional area, A_c.

Comparison of Equations 3 and 4 gives:

$$F_f/N = F^2$$

and this calls attention to a fundamental difference between viscous resistivity to fluid flow and electrical resistivity. The former effect depends principally on the pore radius raised to the fourth power (r^4) and the latter to the radius squared (r^2). Hence, we observed that F_f from Equation 4 is the square of F from Equation 3 but includes an arbitrary parameter reflecting porous body geometry.

It is necessary now to examine Equation 3 in detail, especially with regard to its implications, since this definition of formation factor will serve as the basis for much of the other development to be given in this paper.

---

* Note that the fundamental definition of a porous medium possessing random pore distribution is that any plane through the medium will always expose a constant fractional void area proportional to the porosity.

Fig. 1 is a plot of fractional porosity versus tortuosity where a graphical solution can be made of Equation 3 for the formation factor. The dashed horizontal line refers to the porosity of the cubic packing of spheres, which is the maximum theoretical regular packing porosity which can obtain and which is somewhat above the maximum porosity which will obtain in practical instances. Minimum porosities for granular materials will generally exceed 0.05, and tortuosities will range from about 2.5 to perhaps 250; meaning the formation factors will generally fall in the range of 2.5 to perhaps 500. Fig. 1 also shows isocementation factor lines which are based on the following formulation for the cementation factor, m:

$$m = (\ln\phi/T^{1/2})/(\ln\phi) \quad . \ . \ (5)$$

arrived at by combining Equations 1 and 3. Although m can vary in the mathematical sense between 1 and infinity, it is clear from Fig. 1 that the variation to be encountered in practice lies well within the limits of 1.3 and 3.0 as originally observed by Archie, Guyod and others.† In the theoretical sense, however, values of m and limits in values of m are of little consequence since Equation 3 appears to be the fundamental definition of formation factor and Equation 1 is nothing more than a trivial definition which has been accepted in the past because of the coincidental fact that m appears to have a rather constant value in certain reservoirs. The theoretical implication of finding a reservoir where m is a true constant is that tortuosity will be equal to porosity raised to some constant exponent, $(2-2m)$. Previous investigations,[20] however, have shown that tortuosity may be expressed:

$$T = (\phi/Kt_s)(\delta/P_d)^2 \quad \text{(contact angle assumed 0)} \quad . \ . \ . \ . \ . \ . \ (6)$$

where δ and P_d are the interfacial tension and the displacement pressure, respectively, and t_s is the pore shape factor referred to by Carman.[19] This would give as another definition for m:

$$m = (\ln\phi^{1/2}K^{1/2}t_s^{1/2}P_d/\delta)/(\ln\phi)$$

implying that a log log plot of ϕ versus $(\delta/P_d)/(Kt_s)^{1/2}$ would be linear with slope equal to $(1-2m)/2$ and with zero intercept if m were constant. However, for texturally similar porous media, i.e., with identical tortuosities, it is seen from Equation 6 that this plot will have a slope of (–2) and intercept equal to T, and that for texturally dissimilar porous media the slope of $(1-2m)/2$ and zero intercept is not at all theoretically indicated as a unique requirement.

Equation 6 is of further interest in developing the relationship between formation factor and permeability. Combination with Equation 4 gives:

$$\ln F = -\tfrac{1}{2}\ln K + \ln(\delta/\phi^{1/2}t_s^{1/2}P_d)$$

which is a reasonable description of some of Archie's data[14] where a log log plot of F and K gave a slope of –½. The implication is that the term, $\delta/\phi^{1/2}t_s^{1/2}P_d$, was constant for the reservoirs giving such data plots. Such constancy, however, is not to be anticipated as unique since the above referred to intercept term can also be expressed as $(TK)^{1/2}/\phi$, showing its implicit dependence on K; and indeed Archie's data more generally show a slope of about –¼ on the log log plot of F versus K.

To conclude this discussion of formation factor as described by Equation 3, it is of interest to examine further the utility of the expression which has been developed. For instance, the claim that Equation 3 is a more theoretically sound description of F than is Equation 1 will have little or no appeal to those concerned with practical applications unless it can be shown that the term T in Equation 3 is more readily obtainable than the cementation factor,

Table I

Tortuosity of Regular Sphere Packings

Packing	F (Pirson)	ϕ	T	$T=(3-\phi/2)^2$
Cubic	2.64	.476	1.57	1.60
Rhombic	3.38 - 4.40	.395	1.33 - 1.73	1.70
Hexagonal	5.81	.259	2.26	1.88

Table II

Core	K md	ϕ	P_d psi	δ dynes/cm	F Measured	F Computed
Alundum	693	0.258	0.75	43.0	13.7	15.6
Alundum	667	0.254	1.05	43.0	11.3	11.0
Alundum	688	0.265	0.994	43.0	11.9	11.2
Alundum	657	0.262	1.05	43.0	13.0	11.0
Pyrex	2300	0.344	0.653	43.0	7.2	8.1
Nicholls Buff	232	0.200	1.73	43.0	12.5	12.8
Nicholls Buff	205	0.198	2.10	43.0	12.4	12.3
Berea	907	0.225	0.874	43.0	11.7	12.0
Berea	695	0.226	0.880	43.0	12.7	14.5
Alundum	64	0.236	4.24	54.2	11.5	10.1
Alundum	1305	0.294	1.23	54.2	8.0	6.9
Pyrex	322	0.298	2.13	54.2	7.7	8.0
Pyrex	353	0.303	2.82	54.2	5.7	5.8
Pyrex	342	0.304	2.13	54.2	7.1	7.5
Pyrex	149	0.268	2.55	54.2	8.4	10.3
Pyrex	129	0.366	3.86	54.2	4.04	6.25
Pyrex	105	0.325	5.21	54.2	6.4	5.5
Pyrex	8.2	0.374	18.0	54.2	4.4	4.2
Pyrex	3900	0.286	0.820	54.2	6.2	5.6
Alundum	60.8	0.232	4.71	54.2	10.9	9.5

---

† For example, varying the porosity ten-fold from 5 to 50 per cent and varying the tortuosity 100-fold from a value of 10 to 1000 changes the cementation factor, m, by about four-fold (i.e., from 1.36 to 6.01) if maximum porosity is associated with maximum tortuosity. On the other hand, the cementation factor will vary less than one-fold (i.e., from 2.15 to 2.67) if the more reasonable assumption is made that maximum porosity should be associated with minimum tortuosity. For these hypothetical systems the formation factor, F, will vary some 100-fold from 6.3 to about 630. (cf. Fig. 1 for other comparisons of this sort).

m, appearing in Equation 1 or that Equation 3 may be used to extend the value of formation factor measurements. Even though it has been shown by reference to Equations 3 and 4 that fluid flow and electrical conduction are not strictly analogous, we nonetheless believe our assumption that the tortuous path which provides added resistance to fluid conduction is the same as that which affects electrical conductivity in porous media is both useful and accurate. More direct proof of the essential similarity between the two tortuosities, fluid and electrical, are now given. Thus, using values of formation factor in Equation 3 quoted by Pirson[23] as applicable to systems of regular packed spheres, we can arrive at the values of tortuosity shown in Table I, since porosities are known for these packings. A number of values have been quoted as the proper tortuosity values to associate with systems of regular packed spheres, as 2.47 by Hitchcock,[24] 1.69 by Dalla Valle,[25] and 2 by Carman.[19] Moreover, implicit in the work of Fricke[7] is the definition of tortuosity as $(3-\phi/2)^2$. It is seen that the computed values in Table I at least fall within the range of possible values quoted by previous workers.

Further evidence bearing on the validity of the concepts implicit in the derivation of Equation 3 has been obtained as a consequence of the experiments summarized in Table II. It has been shown above in logarithmic form that combination of Equations 3 and 6 gives an expression for formation factor as:

$$F = \frac{\delta}{P_d}\left(\frac{1}{Kt_s\phi}\right)^{1/2} \quad . \quad . \quad . \quad (7)$$

In order to check this formulation values of P_d, δ, ϕ and K were measured by conventional means on a series of core samples consisting of both synthetic and natural oil field cores. A value of $t_s = 2.25$ was assumed, and the computed values of F are given in Table II. The formation factors were then measured and corrected where necessary for the effects of conductive solids. Fig. 2 illustrates the comparison obtained between the measured and computed values of F, and the calculated correlation coefficient of 0.986 is quite indicative of the general validity of the concepts relating formation factor to tortuosity and porosity.

The conclusion which we reach from the considerations and data given is that the similarity between the two tortuosities, hydraulic and electric, in porous media is extraordinarily close and that to a first approximation at least they may be considered to be identical. The consequence is that formation factor may be expressed in terms of a tortuosity-porosity function, thus providing the link which enables the formation factor concept to be interrelated with the important equations related to fluid movement in porous media. It is thus possible to formulate an expression (Equation 7) for formation factor in terms of porosity, permeability, interfacial tension, shape factor‡ and displacement pressure, and this expression we will show below to have certain application possibilities for the determination of permeability from electrical log data.

The expression for formation factor in terms of a tortuosity-porosity function is not of direct practical utility since tortuosity is not sufficiently readily obtainable to permit porosity to be deduced rapidly from formation factor data. Further reference to this point is made in a later section.

The new formulation of formation factor serves, however, to show that the cementation factor concept has little theoretical rationale and the use of specific values of the exponent m as characteristic of certain definite degrees of cementation is to be deprecated unless used with great caution.

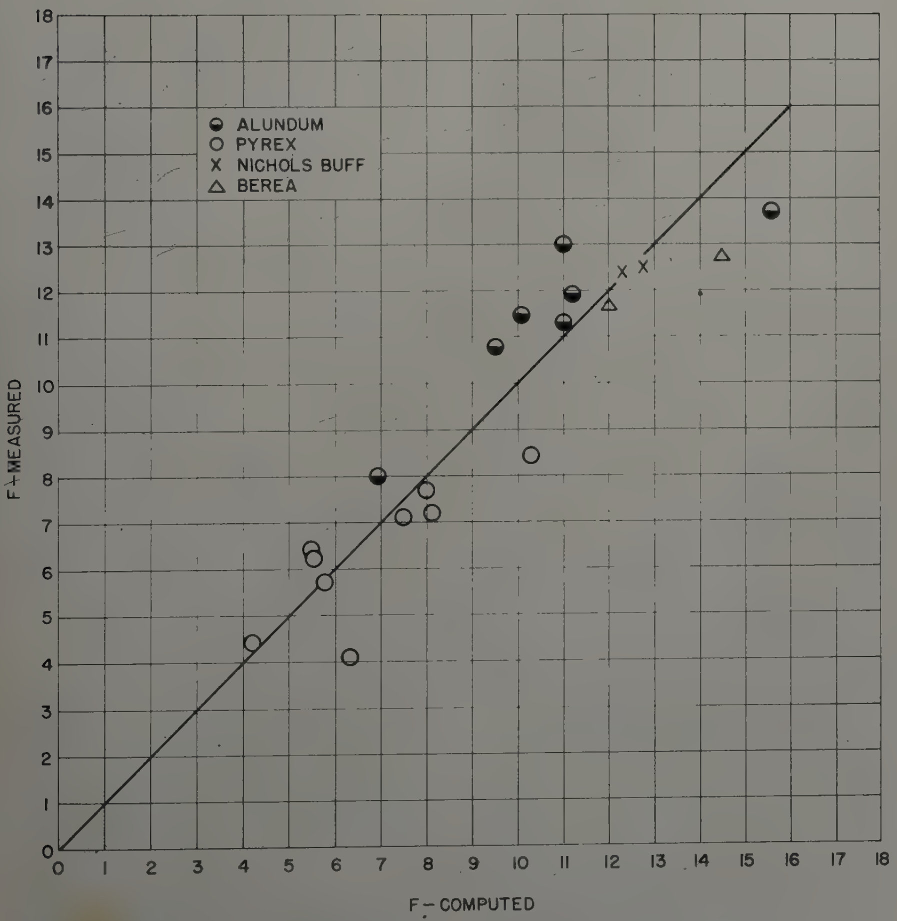

FIG. 2 — MEASURED AND COMPUTED VALUES OF FORMATION FACTOR

---

‡ The pore shape factor, t_s, appearing in Equation 7 has been shown by Carman[19] to vary within the narrow limits of 2.0 to 2.5, so that it may be assumed constant for computation purposes involving Equation 7.

In the case of unconsolidated porous media of relatively high porosity, the apparent constancy of m at a value of about 1.3 is probably a coincidental consequence of the compensating small changes in tortuosity which occur when the porosity of such systems is subjected to small changes.

The expression for formation factor in terms of an hydraulic tortuosity is also of considerable utility in the examination of the resistivity index concept, and we now consider this problem.

Development of Resistivity Index Concepts

By analogy to Equation 4 the effective formation factor characterizing the partially saturated porous system; that is, the ratio of the resistivity of the reservoir (or core sample) at brine saturation, S_w, to the brine resistivity, can be expressed as:

$$F_e = T_e^{1/2}/\phi S_w \quad . \ . \ . \quad (8)$$

where T_e is the tortuosity of the equivalent pores which may be regarded as making up the brine-filled portion of the system. Combination of Equations 3 and 8 gives:

$$\begin{aligned} I &= \text{Resistivity Index} = F_e/F \\ &= (T_e/T)^{1/2}/S_w \quad . \ . \ . \quad (9) \end{aligned}$$

as compared to the empirical relation which is given as Equation 2 above. The term, T_e/T, has been expressed previously[20] as:

$$T_e/T = S_w P_d^2/K_{rw} P_c^2 \quad . \quad (9A)$$

where K_{rw} is the wetting liquid relative permeability and P_c is the capillary pressure, both obtaining at saturation S_w. As before we assume that the hydraulic and electrical values of T_e are the same. This gives:

$$I = P_d/P_c(K_{rw}S_w)^{1/2} \quad . \ . \quad (10)$$

Unfortunately, there are only meager data available in the literature§ which can be employed to check the validity of equations 9 and 10, this being due principally to the fact that relative permeabilities are very difficult to measure, and when they are measured the necessary resistivity and capillary pressure data are not usually also obtained.

The first example to be considered is that of the single capillary tube saturated with various proportions of wetting (electrically conducting) and non-wetting fluids, where either the non-wetting fluid will be considered as dispersed in the wetting phase as droplets of radius less than the capillary tube radius, or the wetting liquid will be regarded as flowing as an annular cylinder around the centrally located flowing non-wetting fluid. In a recent paper[22] it was shown the right-hand term of Equation 10 reduces to $1/S_w$ for such a system, which is exactly what would be calculated for the resistivity index by Equation 9 under the conditions of saturation stated above (i.e., $T_e \approx T$ for all values of saturation). Only one other example will be cited as direct confirmation of Equation 10. If the capillary pressure data of Leverett[30] and the relative permeability data of Wyckoff and Botset,[11] obtained on comparable unconsolidated sands, are substituted in Equation 10, the resistivity index exponent, n, is computed for all values of saturation to lie between the limits of 1.75 and 1.90 as compared with the experimentally determined value of 1.96. On the other hand, indirect evidence bearing on the validity of Equation 10 may be derived from the relative permeability data of Morse et al.,[15] even though no capillary pressure data are available for the computation. In one case values of the ratio, P_d/P_c, can be computed as 0.89 at $S_w = 0.7$, 0.84 at $S_w = 0.5$, and 0.55 at $S_w = 0.3$ (cf. Morse et al data on their synthetic core); whereas, in another case values of the ratio are computed as being greater than unity (cf. the data on the oil-wetted Bradford core). The former values are certainly reasonable and perhaps of the right order; the latter values are certainly unreasonable and perhaps explicable in terms of experimental error or in terms of an inherent limitation in the application of the equations developed in this paper to oil-wetted media. In any event, Morse et al regarded their data on the Bradford core as anomalous, at least as compared to their other results.

It will be noted that the above examples, which tend to establish the validity of Equation 10, are of interest and importance since they are suggestive that Equation 10 will be found useful as an expression for wetting liquid relative permeability. Thus, it is seen that an experiment which includes the measurement of capillary pressure and resistivity index, both as a function of saturation, suffices for the computation of K_{rw} according to:

$$K_{rw} = (P_d/P_c)^2/I^2 S_w \quad . \quad (11)$$

Although Equation 11 depends on assuming a variation of T/T_e with saturation to be that described by Equation 9, it should not be interpreted that previously developed expressions for wetting liquid relative permeability[22] based on assuming a constant value for T/T_e will be too greatly in error. It appears probable, in some instances at least, that T/T_e will be nearly constant as an approximation over a considerable saturation range, as evidenced by the tendency of the resistivity index exponent, n, to approach low values as the saturation is decreased (cf. the Russian data cited by Guyod[18]).**

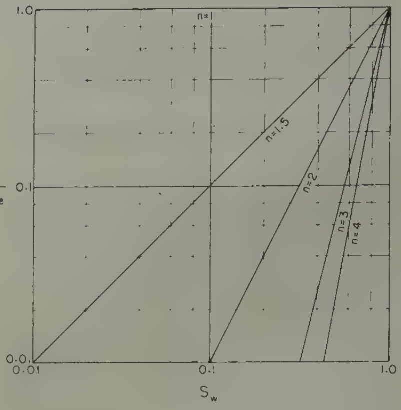

FIG. 3 — TORTUOSITY RATIO AS A FUNCTION OF SATURATION FOR CONSTANT VALUES OF THE RESISTIVITY INDEX EXPONENT

At this point it will be instructive to examine the implications of Equation 2 as brought forth on combination of

---

§ Attention is called to Thornton's recent work[21] where equivalent forms of Equations 8, 9, 10 and 11 are independently developed, and where some evidence is given bearing on the validity of these equations.

** Subsequent to the preparation of this paper and subsequent to the later appearance of Thornton's note in the literature,[21] we reinvestigated the utility of Equation 11 and we reported [29] certain inherent limitations related to its application, such as the difficulty of obtaining correct values for the ratio, P_d/P_c, associated with conditions of fluid distribution characterizing multi-phase fluid flow processes. In our note we arrived at an alternative equation for relative permeability as: $K_{rw} = I^{-2}$ . . . (11A) which is developed through interrelation of the consequences of Equation 4 with Equation 11. We also commented on the possibility of encountering experimental data which are fitted by neither Equations 11 nor 11A.

Equation 2 with Equations 9 and 10. Thus, we have:

$$n = (\ln S_w^2 T/T_e)/(\ln S_w^2) \quad . \quad (12)$$

as shown graphically by Fig. 3. As in the case of the cementation factor, m, (cf. Equation 5), we find the theoretical limits of the resistivity index exponent, n, to be between unity (as in a system of capillary tubes where T/T_e is unity for all values of saturation) and infinity. On the other hand, Fig. 3 is suggestive that the limits to be encountered in practice are perhaps 1.5 to 2.5 at saturations below 30 per cent, since from Equation 9 values of T/T_e less than about 0.01 are not to be expected. At high saturations, exponents as high as 4 appear to be possible. In connection with these practical limits, an interesting analysis can be made on the basis of Equation 12. By taking the relationships between the parameters, relative permeability, capillary pressure and saturation, as developed previously,[22] it is possible to solve Equation 12 for the exponent n. Fig. 4 shows the results of such approximation, and it is seen how n is indicated to vary with rock texture*** (as measured in terms of S_{wi}) and with saturation. With regard to the latter, it is our expectation that in practical instances n will be found to vary with saturation, although we do not imply that the variation as shown in Fig. 4 and arrived at by approximation processes is necessarily the type of variation which will be encountered. In fact, the majority of data available in the literature showing a variation in n with S_w in general indicate that n approaches a limiting constant value of about 2.5 or less with decreasing saturation (cf. Fig. 50 in the paper by Guyod[18]) and this is not the effect indicated by Fig. 4. Theoretically, however, at pendular saturation $I \rightarrow \infty$ and hence n must tend to infinity if S_w^{-n} is to equal I. In any event, Fig. 4 is of interest, in showing that the values of n encountered in practice are order of magnitude similar to those indicated from theory.

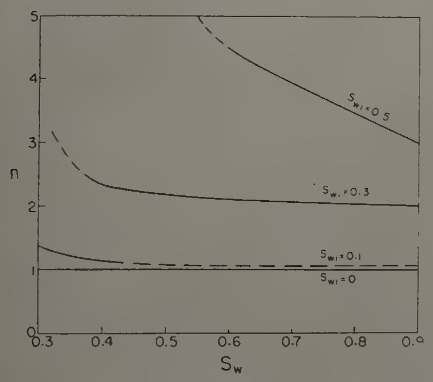

FIG. 4 — VARIATION OF RESISTIVITY INDEX EXPONENT WITH SATURATION

It is implicit in this discussion that the resistivity index exponent, n, as defined by Equations 2 and 12 is based less on theory than on the expedient desire to provide a simple empirical formulation of experimentally observed relations and in this connection our comments given previously with respect to the validity of constant values of m apply equally to values of n. It may be pointed out that if a continuous function is desired, it seems possible that the resistivity index, I, should be related by the exponent, n, to the term $(S_w - S_{wi})$, rather than to saturation alone as in Equation 2, where S_{wi} is the "irreducible" saturation reflecting on pendular configuration of the wetting phase. That is, our assumption regarding the equality of the hydraulic and electrical tortuosities breaks down at saturations in the vicinity of S_{wi} because the electrical resistivity becomes a surface effect in the event the brine wets the porous matrix, or it approaches infinity at pendular saturation when the angle of interfacial contact is greater than zero and the matrix is a con-conductor. At pendular saturation all fluid conduction has, however, ceased. In this connection it will be noted that available data relating I to S_w are often consistent with the surface conductivity concept given above. For example, Morse et al[15] show a relative electrical conductivity of about 10 per cent ($n = 1.96$) at saturations which are evidently pendular for their synthetic sandstone, and equivalent results can be found in most other published data. In addition, it will be clear from Equation 12 that the exponent, n, is dependent principally on the type of saturation distribution obtaining at given values of S_w, for the ratio, T/T_e, is a measure of fluid distribution. Therefore, the requirement is implicit that in laboratory experiments fluid distributions must be obtained which are analogous to those obtaining in the natural petroleum reservoir, if data for valid electrical log interpretation are desired. Moreover, Equation 12 is quite suggestive that values of n will vary for different types of porous media, and will vary for given types of porous media when saturation is varied, even though the same type of fluid distribution is maintained, and certainly when the fluid distribution type itself is varied. Admittedly, there is only meager evidence in the published literature substantiating these possibilities, and the common occurrence of values of $n \approx 2$ is difficult to interpret except as a fortuitous and otherwise non-unique result.

DEVELOPMENT OF PRACTICAL APPLICATIONS

In addition to application for the location of shale and sand intervals, it has been suggested that electric logs yield data which may be used to determine quantitatively three important reservoir parameters, viz., connate water saturation, porosity and permeability. In the light of the foregoing theoretical discussion, it is instructive to examine the inherent probability of being able to compute these three parameters. In so doing, we must bear in mind the fact that since electric logging is now an almost universal adjunct to standard drilling practice, any quantitative or even semi-quantitative data that can be derived from electric logs is in the nature of an operational bonus. Thus, we should recognize the fact that a purely academic approach to the problem of quantitative log interpretation is economically unjustified. If it can be shown that rigid and universal methods of log interpretations are not theoretically probable, we are still entitled to use the available theory to suggest such semi-empirical approximations as appear to be justified under certain specific conditions obtaining in certain limited geographical areas.

*** The recent experimental data of Dunlap, Bilhartz, Shuler and Bailey[33] and Williams[34] appear very strongly to confirm this theoretical prediction.

The Estimation of Connate Water Saturation from Log Data

The use of electric logs for the qualitative location of oil or gas saturation in reservoir rock depends fundamentally on the derivation of three parameters. These parameters are the true formation resistivity, the resistivity of the connate water at the formation temperature and the true formation factor. It is believed that the first two parameters can now be obtained with a high degree of accuracy in many instances. The estimation of formation factor is less readily made. It is not only difficult to determine formation factor with accuracy from present log data, but the apparent value, when deduced from the log, may be increased by residual oil saturation and decreased by conducting solids.[9] If an oil-water contact exists, it is theoretically possible to correct the apparent formation factor for the effects of conductive solids.[9] If such a condition does not obtain, the best method (in the absence of cores) still appears that of assuming the formation factor to be identical with the formation factor of a water sand adjacent to the one of interest. New techniques for estimating formation factor in situ are thus of prime importance to log interpretation. However, from a strictly qualitative approach, it is clearly desirable to overestimate the numerical value of formation factor, since the qualitative identification of hydrocarbon saturation in a formation is based on the relationship:

$$F\rho_c \ll \rho_t$$

Where,

F = true formation factor,
ρ_c = connate water resistivity,
ρ_t = true formation resistivity (corrected for conducting solids).

From the standpoint of quantitative log interpretation, the above difficulties are reinforced by the additional difficulty of finding the appropriate value for the exponent, n, in the resistivity index-saturation relationship,

$$I = S_w^{-n} \quad . \; . \; . \; . \; . \quad (2)$$

Fig. 5 shows a plot of water saturations, S_w, against values of the exponent, n, for various constant values of the resistivity index, I. Each curve of the family plotted may be shown to have a slope given by the relationship $(\partial S_w/\partial n)_I = -S_w \ln S_w/n$, and all curves may be calculated from the appropriate value of $(\partial^2 S_w/\partial n^2)_I = 0$ to have a point of inflection at a saturation of 0.136 (13.6 per cent).

It is clear from Fig. 5 that if the exact value of n for a particular formation is unknown to the log interpreter, the maximum error in a water saturation computed by arbitrarily assuming a value for n will result for true water saturations of about 14 per cent. Fig. 5 shows, however, that although maximum errors in interpretations are to be anticipated at saturations in the region of 14 per cent, the errors at any other saturations in the saturation range applicable to producing formations are also extremely serious. For example, if the probable range of n values in commercial oil-bearing reservoirs is assumed to be from 1 to 4, a resistivity index of 10 may be seen from Fig. 5 to indicate saturations anywhere from 10 per cent to 56.5 per cent, i.e., that reservoir may be computed to be either a potential producer of pipe line oil or a potential water sand, unless a more specific value of n for the reservoir is either definitely known or can be reliably as-

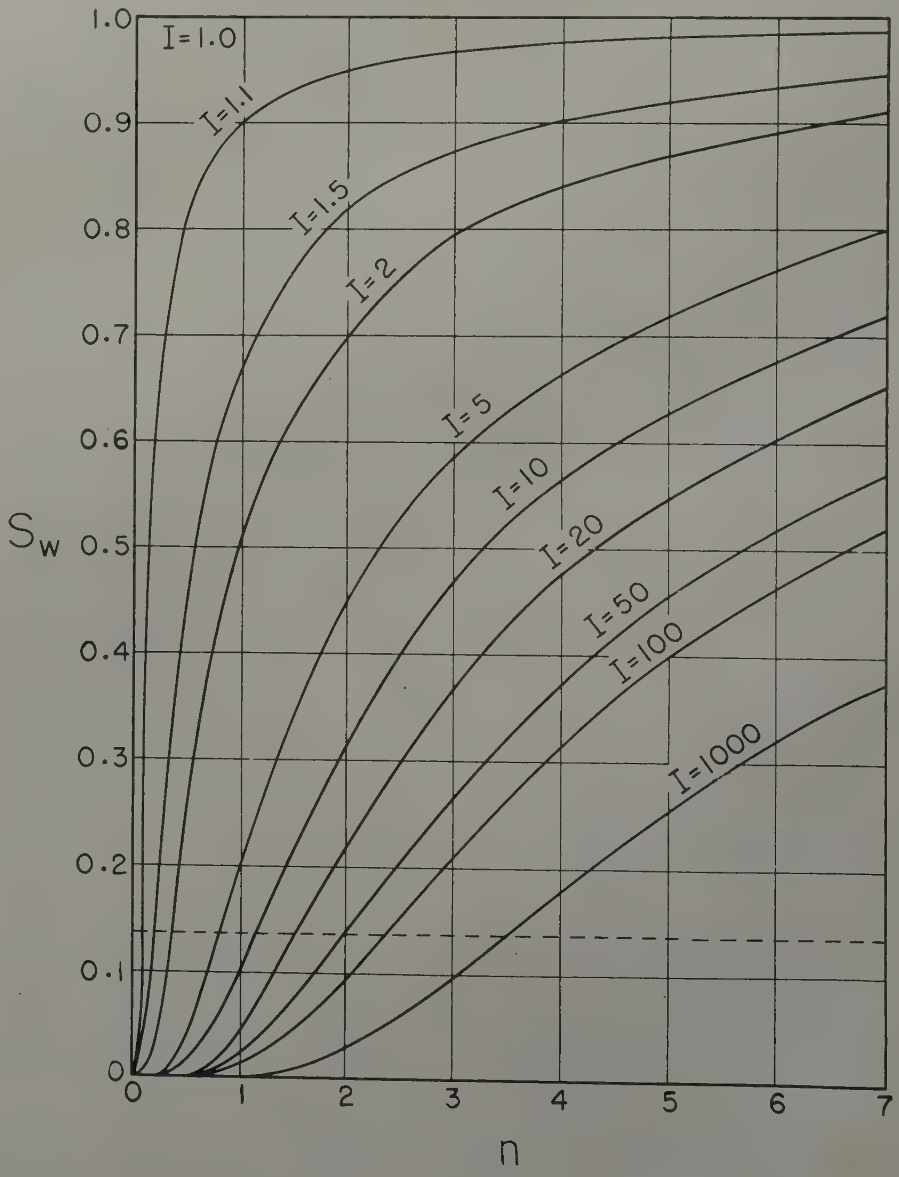

FIG. 5 — GRAPHICAL SOLUTION OF $I = S_w^{-n}$

sumed. However, Fig. 5 may be used to divide computed resistivity indices into three broad categories if the range of practical n values for all saturations is assumed to be from 1 to 4.

In the first category are resistivity indices less than 2. Such indices indicate water saturations in excess of 52 per cent and may almost invariably be assumed to be indicative of water sands.

In the second category are resistivity indices in the range 2-20. If possessed of such an index a formation may be either a pay sand or water producing since saturations may vary from 5 per cent to 84 per cent. Thus, in the absence of any information concerning the appropriate value of the exponent n to use, resistivity indices in this range give no reliable guide to production possibilities.

In the third category are resistivity indices which exceed 20. In this range the formations certainly contain less than 47 per cent water even for values of n as high as 4, and the probability of the formations containing oil or gas in commercial quantities is, in consequence, very high.

It appears probable from the theoretical treatment given above that the exponent n varies with the texture of the reservoir rock, the extent of wetting liquid saturation and other factors normally unknown to the log interpreter. While this conclusion requires further experimental elucidation, we do not consider that it is at present theoretically justifiable to regard the relation $I = S_w^{-n}$ as anything but a mathematical convenience. In practice, however, it would appear from the available experimental evidence that for reservoirs with low irreducible water saturations (in about the range 8-20 per cent) and probable variation of n may well lie within narrower limits than the range 1 to 4 previously discussed. For reservoirs with irreducible saturations from about 8-20 per cent, present experimental evidence indicates that n may only vary from about 1.7 to 2.5 in a large number of practical cases. If this is so, fairly reliable quantitative saturations may be calculated on the basis of the exponent $n \approx 2$, notwithstanding the fact shown above that in this saturation range errors in S_w arising from errors in n are at a maximum. Table III gives the saturations applicable to a number of resistivity indices for values of the exponent n of 1.7, 2.0 and 2.5.

Table III

n =	1.7	2.0	2.5
I	S_w	S_w	S_w
20	17.2	22.4	30.2
40	11.3	15.9	25.2
60	9.0	13.0	19.5
100	6.7	10.0	15.9

It will be seen that although the values of S_w in Table III differ considerably, an exponent of 2.0 would, nevertheless, give saturations of considerable utility to the reservoir engineer. If, in addition, it is recollected that no reservoir is texturally homogeneous or uniformly saturated, it is not unreasonable to believe that the intrinsic tendency of the log to yield average data for a large volume of reservoir rock may give rise to a computed saturation in excellent quantitative agreement with the mean of the irreducible water saturations obtained by core analysis techniques on a number of sample cores from the formation logged.

In the light both of available experimental data and theoretical considerations we would, however, strongly deprecate the attachment of undue importance to calculated numerical values of saturation in excess of about 30 per cent unless the textural constants of the reservior had previously been established.

The Estimation of Porosity From Log Data

From the theoretical section above it may be deduced that the porosity, ϕ, in Archie's relationship between porosity and formation factor and exponent, m, can be expressed as:

$$\phi = \frac{T^{1/2}}{F} = T^{\frac{1}{2(1-m)}} = F^{-\frac{1}{m}} \qquad \ldots\ldots (13)$$

Assuming that formation factor is obtainable from purely log data, porosity can only be computed if a reasonably accurate value of m can also be derived from log data. Equation 13 emphasizes that this is possible only in the event that tortuosity is obtainable from log data. Since no method of deriving tortuosity from log data alone is apparent, we conclude that the quantitative determination of porosity from the electric log is not at present possible. The nature of the problem, as exemplified by Equation 13, suggests that the only feasible practical methods for determining porosity, which will not involve a full coring program, will depend upon the combination of log data with such core analysis data as can be obtained on cuttings or side wall samples.

Qualitatively, Fig. 1 reinforces graphically the prevailing view that low formation factors will always be associated with rather high porosities. Tortuosity cannot be less than unity, hence a formation factor of 10 will mean a porosity of at least 10 per cent. Similarly, a formation factor of 5 implies a porosity greater than 20 per cent.[+]

The Estimation of Permeability From Log Data

Tixier has recently published[3] a method of determining permeability from log data which he shows to be of practical utility in the Mid-continent area. An examination of Tixier's treatment indicates that a number of assumptions are inherent in his approach and that these assumptions appear unnecessarily to limit any wide application of his method. Fundamentally, Tixier assumes that the exponent in the resistivity index-saturation relationship is 2.0, and that at any saturation, S_w, capillary pressure, P_c, is related to permeability, K, in the manner,

$$P_c = \frac{\text{Constant}}{K^{1/2}}$$

On the basis of these two assumptions he derives an expression for formation permeability in terms of the densities of brine and hydrocarbons in a porous formation and the slope of the resistiv-

---

[+] The fact that for a constant formation factor, Fig. 1 shows tortuosity to increase with increase in porosity can be rationalized by recollecting that constancy of formation factor with increasing porosity is inherently improbable in any real porous medium.

ity curve above the oil-water contact. Tixier's method is physically limited in scope by the relative paucity of logs showing valid oil-water contacts and the necessity for estimating the hydrocarbon density as it exists in the reservoir. More fundamentally however, the equation connecting capillary pressure and permeability at any saturation appears to us to represent a simplification which is in most cases quite unreal. The assumption regarding the value of n, with the reservations we have outlined above, we consider to be more justified.

Leverett has developed in two of his theoretical papers[30,31] a relationship for porous solids which may conveniently be expressed in the following form:

$$P_c = \left(\frac{\phi}{K}\right)^{1/2} j(S_w)\ \delta \operatorname{Cos} \theta \quad . \quad (14)$$

where P_c, ϕ and K have the same significance as before, δ is the interfacial tension, θ the contact angle, solid to liquid, of the wetting phase, and $j(S_w)$ is Leverett's capillary pressure function. From this equation the relationship between capillary pressure and permeability employed by Tixier follows, if ϕ, $j(S_w)$, δ and Cos θ are identical, or mutually compensating in their effects, in all the formations he studied. The universal constancy of δ Cos θ in water-wet oil field reservoirs is only acceptable as a first approximation, since it would seem that surface-active components of some crudes might markedly affect the interfacial surface tension. Wide variations in porosity are clearly to be expected, although in an area such as the Rocky Mountains a relatively constant porosity may have obtained. Independent values for the capillary pressure function at various saturations are unobtainable at present, although the value of $\lim_{S_w \to 1} j(S_w)$ has been shown by Rose and Bruce[20] to be equal to $(1/t)^{1/2}$, where t is the Kozeny rock textural constant. At any saturation, however, $j(S_w)$ is a function of the rock textural character of the formation and, hence, it may have wide variations not only from reservoir to reservoir but within any particular formation. Thus, the constant employed by Tixier, as Tixier noted, is certainly liable to vary very widely in different reservoirs and even in a particular area its constancy does not seem to be probable except in very ideal circumstances. It would appear from Tixier's results that the formations to which he applied his method were singularly texturally homogeneous and, thus, perhaps uniquely amenable to his treatment.

Since Leverett's equation indicates the factors which will affect Tixier's empirical "constant", it is reasonable to examine the possibilities of being able to express these factors in terms of measurable log data and thus to derive an expression of somewhat wider applicability.

Rose and Bruce[20] have shown that when S_w is unity,

$$P_d = \left(\frac{1}{K}\right)^{1/2} \delta \left(\frac{\phi}{t}\right)^{1/2}$$

(Contact angle assumed to be 0)

But it has been shown in the theoretical section that, $F = t^{1/2}/t_s^{1/2}\phi$.

Hence,

$$P_d = \delta/(K t_s \phi)^{1/2}\ F \quad . \quad (7)$$

The displacement pressure, P_d, does not seem to be obtainable from the electric log, but P_c may be derived in principle by using the same technique as that employed by Tixier. The gen-

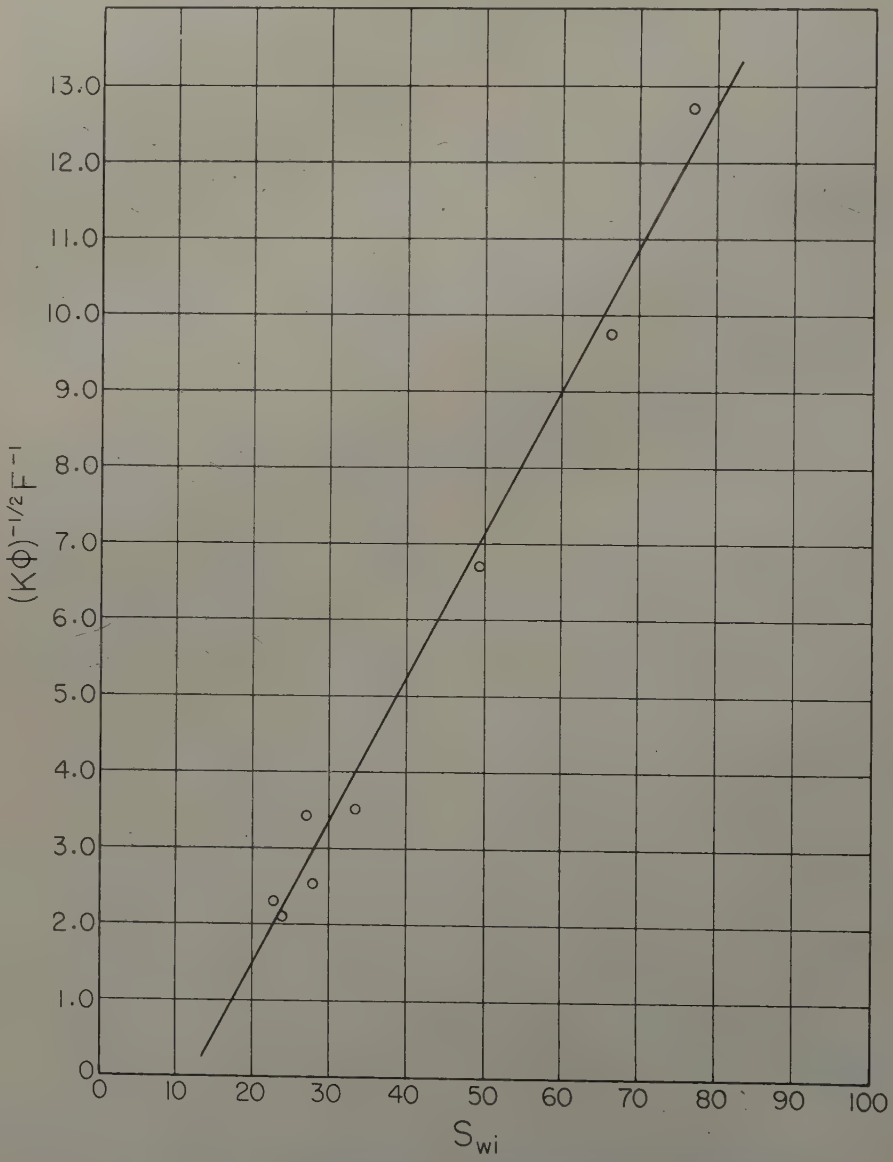

FIG. 6 — RELATIONSHIP BETWEEN IRREDUCIBLE SATURATION AND THE ROCK TEXTURAL FUNCTION $(K\ \phi)^{-1/2}F^{-1}$

eral relationship between P_c and P_d for all porous media undoubtedly is complex, but to a first approximation the relationship derived by Rose and Wyllie[29] may be used. This relationship states that $P_d = P_c S_w^{1/2}$. It then follows that,

$$P_c = \left(\frac{1}{K}\right)^{1/2} \frac{\delta}{F t_s^{1/2} \phi^{1/2} S_w^{1/2}}$$

or that,

$$K = \frac{\delta^2}{P_c^2 F^2 t_s \phi S_w} \quad . \quad . \quad . \quad (15)$$

In Equation 15 δ may be assumed constant, to a first approximation, and since t_s varies from about 2.0 to 2.5, it also is essentially a constant. The porosity, ϕ, is not calculable from log data directly, but by assuming a reasonable value for m in the expression $F = \phi^{-m}$, ϕ may be expressed in terms of F with an accuracy compatible with the other practically essential approximations. Thus, in terms of parameters which are obtainable from appropriate logs,

$$K = \text{Constant}\left[\frac{1}{P_c^2 F^{\left(2 - \frac{1}{m}\right)} S_w}\right]$$

where the constant is $\dfrac{21.2\,\delta^2}{t_s}$. (16)

for K in millidarcies, P_c in psi and δ in dynes/cm. In this expression, in the absence of other knowledge, a value of $m = 1.5$ is convenient. The constant, since it is dependent only on δ, θ and t_s may well have rather wide applicability unless variations in δ are in fact very large.++ The value of K deduced from this equation cannot, however, be expected to have more than an order of magnitude significance.

Our prime objection to the use of Tixier's method or the generalization of it outlined above, lies in the practical consideration that insufficient logs showing suitable oil-water contacts are obtained. Another inherent objection is the knowledge of the hydrocarbon density in situ which is required and which makes the method not immediately applicable when working in unknown territory. We have thus examined the possibility of devising a method of computing permeability under conditions where no oil-water contact exists and where no knowledge of the reservoir hydrocarbons has been obtained. With these severe limitations the problem becomes that of finding a relationship between permeability, formation factor and connate water saturation, since only the two latter quantities appear in principle to be calculable from log data. We make, in addition, the further assumption that the minimum water saturation computed in a reservoir is equal to the irreducible connate water saturation, S_{wi}. In this we follow the basic assumption of all capillary pressure core analysis.

The sole justification for attempting to connect permeability to irreducible water saturation and to formation factor lies in the probability that all three parameters are functions of rock texture. It is well-known that in rocks of similar texture, i.e., from the same reservoir, there is frequently a definite relationship between irreducible saturation and permeability. However, the permeability for the same irreducible saturation may differ by several orders of magnitude if the rock texture changes. In order to obtain a general expression which will give permeability

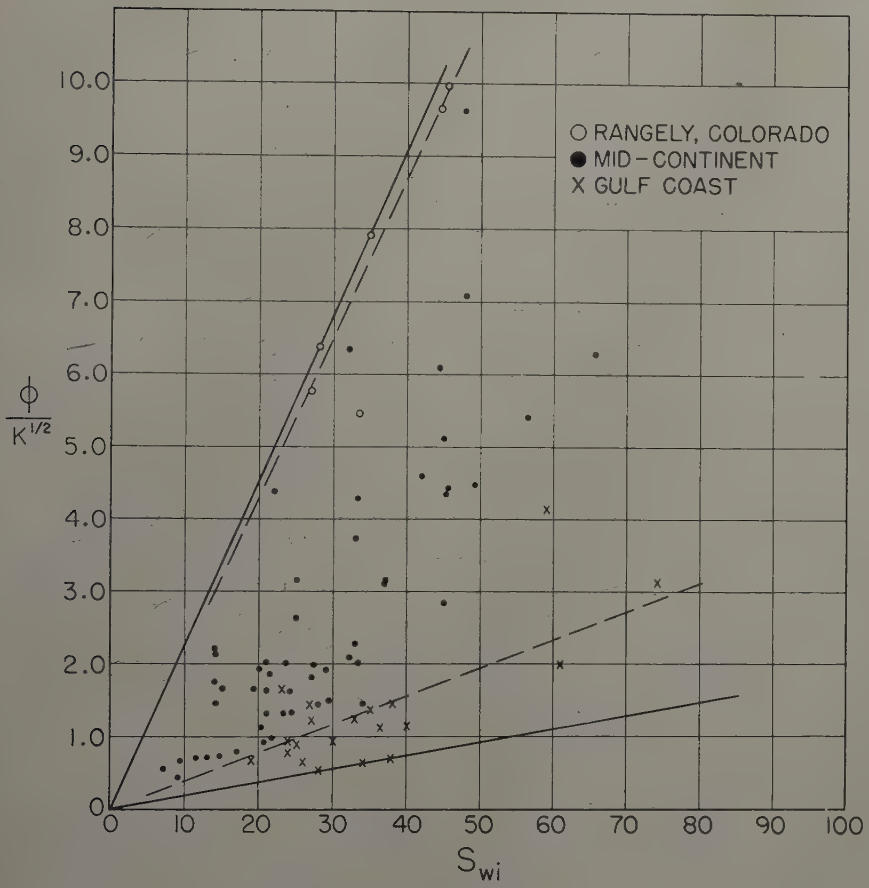

FIG. 7 — EMPIRICAL RELATIONSHIP BETWEEN IRREDUCIBLE SATURATION AND THE ROCK TEXTURAL FUNCTION $\phi/K^{1/2}$

++ From the logs published in Tixier's paper[3] the following approximate data may be derived. Formation factors are computed from the true resistivities of the water sands and the stated connate water salinities using temperatures appropriate to the depths shown.

Log	F	S_w	P_c psi	K(lab) md	Computed δ dynes/cm
Layton, Oklahoma	10	0.33	6.7	27	30.2
Cisco, North Texas	16	0.315	4.7	200-700	76.5-143
Tensleep, Wyoming	7	0.35	1	450	14.9
Rangely, Colorado	50	0.37	18.5	2.72	79.5

The values for interfacial tension are computed by solving for δ in Equation 16, m assumed 1.5 and n as 2 in every case. It will be seen that the values for δ so obtained are extremely variable and rather high. Errors in the assumed m are insufficient to reduce significantly the high computed values of δ, particularly as the high values of δ are associated with high formation factors. The fact that S_w appears to be independent of K points also to errors in n since the computed values of δ are directly proportion to $S_w^{1/2}$.

(or at least its order of magnitude) in terms of S_{wi} and F, it follows that F must appear in the desired expression in such a manner as to compensate these rock textural variations.

With these considerations in mind we have approached the problem in the following manner. Rose and Bruce[20] have discussed the application of the Kozeny equation for the estimation of interstitial surface areas and have found a reasonably linear relationship when surface area is plotted against irreducible connate water determined by the capillary pressure method.[+++] Now the Kozeny equation giving interstitial surface area, A, per unit of pore volume is:

$$A = \left(\frac{\phi}{K}\right)^{1/2}\left(\frac{1}{t}\right)^{1/2}$$

$$= \frac{1}{K^{1/2}\phi^{1/2}Ft_s^{1/2}}, \quad \text{substituting for} \quad t = F^2t_s\phi^2$$

If the assumption is made that $m=1.5$, $\phi^{1/2}$ may be expressed as $(1/F)^{0.33}$ whence,

$$A = \frac{1}{1.5K^{1/2}F^{0.67}}, \text{ since } t_s \approx 2.25$$

If S_{wi} is a straight line function of A, then we have,

$$S_{wi} = C\left[\frac{1}{K^{1/2}F^{0.67}}\right] + C^1 \quad . \quad (17)$$

where, C is a constant which must have the dimensions of a length, and C^1 is a dimensionless constant.

In a clean sand, S_{wi} is zero when the interstitial surface area is zero. Thus, for clean sands, i.e., with no interstitial water held in clays, the straight line must pass through the origin and $C^1 = 0$. Fig. 6 shows some data we have for a producing zone in a Californian field. In this figure S_{wi} has been plotted against $(1/K^{1/2}\phi^{1/2}F)$, no assumption being made regarding the value for m. The formation factors of the sands, all of which contained clay, were obtained with a fluid sufficiently saline to give good values of F.[9] It will be seen that the points fall on a moderately good straight line and that the value for the constant C^1 is about 12 per cent water.

The present dearth of data suitable for testing Equation 17 results from the scarcity of formation factor values, not from lack of determinations of permeability, porosity and irreducible saturations. However, as an approximation Equation 17 can be written in the form,

$$S_{wi} = C \cdot \frac{\phi}{K^{1/2}} + C^1 \quad . \quad . \quad (18)$$

if, $F = \phi^{-1.5}$ is assumed to hold in all cases. This form of the equation is likely to be considerably less accurate than that involving F, since the effect of the assumption concerning the value of m assumes greater importance.[‡‡] However, there are sufficient available data for Equation 18 to be used to test the approximate general validity of Equation 17, i.e., whether the constant which relates irreducible saturation to interstitial surface area is markedly dependent upon rock texture, or whether some mean value could be assumed for all types of formation. In the latter event it would be simple to set up curves giving a mean or minimum value for permeability in terms of the formation factor and irreducible saturation of any reservoir. It should be noted that Fig. 6 indicates that dirty formations are unlikely to fit this picture, since they may have an irreducible water saturation corresponding to an interstitial surface area of zero.

Fig. 7 shows a plot of S_{wi} against the function per cent porosity/(permeability in millidarcies)$^{1/2}$ for 80 determinations. The data for the Mid-continent are mean values of S_{wi}, porosity and permeability made on intergranular-type cores (including oolitic) from reservoirs in Kentucky, Illinois, Oklahoma and Texas. A few points refer to similar data on cores from California fields. It will be seen that while the scatter of points is considerable, the data for Rangely, Colorado, (given by Rose and Bruce[20]) tend to fall on a straight line passing through the origin. These points also define the minimum value of permeability for a given porosity. Conversely, Thornton and Marshall's data[32] which refer to a Louisiana Gulf Coast reservoir of Miocene Age, tend to fall about another line passing through the origin and correspond to maximum permeabilities at any given porosity. The Mid-continent and California data fall between these two extremes.

Fig. 7 in itself does not lend support to the hope that a reasonably accurate general constant can be found to express the relationship between S_{wi} and $\phi/K^{1/2}$. Fig. 7 shows, in fact, that for any given saturation and porosity the maximum possible permeability may be 150 times as great as the minimum possible permeability. It must be remembered, however, that Fig. 7 is greatly dependent upon the assumed value for the exponent m and, as shown above, the scatter is also likely to be considerably influenced by interstitial clay in the formations considered.

The data for the Mid-continent and California show a ratio of 22 between maximum and minimum values of permeability for any given porosity, and there is a probability of about 0.9 that under the same conditions the ratio between maximum and minimum permeabilities will not exceed 12. In general, it seems possible that plots similar to Fig. 7 but involving formation factor, may have some merit for the determination of the order of magnitude of permeabilities over quite wide ranges of formation texture. It also seems theoretically possible that when more data are available the constant C in Equation 17 may be expressible in terms of other formation texture parameters, in which case a unique curve relating all formations would be obtained. It may be mentioned that a constant C of the form $\phi^3/(1-\phi)^2$ serves markedly to reduce the scatter between the Rangely, Colorado data points and those of Thornton and Marshall, but does not consistently improve the Mid-Continent and California data. The term $\phi^3/(1-\phi)^2$ is the porosity function which appears in the Kozeny equation when the specific surface area is expressed in units of grain volume. Carman[31] shows that $\phi^3/(1-\phi)^2$ is that measure of rock texture which relates permeability to average grain diameter.

[+++] It is as well to note that this relationship is clearly not applicable to the elementary case of packed homogeneous spheres, since here A is a function of both sphere radius and porosity, whereas S_{wi} is independent of sphere radius. However, in consolidated porous media some relationship between A and S_{wi} is more plausible.

[‡‡] It may be noted that Equation 18 implies that $\phi = 1/t$, an equality not often encountered in practical cases and indicative of the errors involved in assuming a constant $m=1.5$.

SUMMARY AND CONCLUSIONS

In this paper we have had as our principal object the investigation of the inherent probabilities of deriving reliable information regarding the physical characteristics of reservoir rock from electrical log data. We have indicated that since electric logs are now an almost universal aid to well completion any information of a quantitative character which can be derived from electric logs is in the nature of a gift. It may also be pointed out that the value of this gift would be considerably enhanced if it led also to a curtailing or elimination of present coring and core analysis techniques.

Our analysis of the problem has enabled us to give physical interpretation to the significance of such logging parameters as cementation factor, formation factor and resistivity index exponent, and we have shown that these logging parameters are related to the rock textural parameters appearing in the Kozeny equation and expressions of capillary pressure phenomena. Our conclusions, from a strictly theoretical standpoint, do not, however, suggest that accurate estimates of reservoir rock parameters may presently be made from electrical log data alone, although possibilities exist that the judicious combination of log data and selected core analysis data may often give expressions for certain of these parameters which have fairly wide applicability.

Specifically we have derived, on the assumption that the tortuosity, T, applicable to fluid flow of the wetting phase in a porous medium is the same as the tortuosity affecting electrical conductivity through the fluid in the same medium, an expression for formation factor, F, of the form, $F = T^{1/2}/\phi$, where ϕ is the porosity of the medium. From this expression, we have shown that the common relationship $F = \phi^{-m}$ is of no fundamental significance and have indicated why the practical limits of m are likely to be from 1.3 to 3.0. We have also shown that the existence of reservoirs where a constant value of m will obtain, irrespective of porosity, is not to be anticipated. Experimental evidence for the formation factor relationship derived is also presented.

Applying the same assumption regarding the equality of the hydraulic and electrical tortuosities of the wetting phase in partially saturated porous media, e.g., brine-oil systems, we have derived an expression for the resistivity index, I, in terms of saturation and the ratio of the wetting liquid tortuosities at 100 per cent saturation and the saturation, S_w, considered. Thus, $I = (T_e/T)^{1/2} S_w$.

We show that the use of this expression leads to the conclusion that the resistivity index exponent n in the relationship $I = S_w^{-n}$ is dependent on the texture of the porous medium and the wetting liquid saturation. Thus, it appears that n is neither universally constant at a value of about 2 in all porous media, nor is it necessarily constant throughout the whole saturation range in any particular porous medium. However, both available experimental data and theoretical considerations appear to indicate that at low wetting phase saturations n may lie between 1.7 and 2.5 in a large number of practical instances, and thus a value of n = 2 has considerable practical utility.

We show that the accurate determination of porosity from log data alone is not possible, although limits to the porosity may be given. Thus, a formation factor of 5 implies a porosity in excess of 20 per cent, while one of 10 implies a porosity of at least 10 per cent.

We have expanded an empirical relationship proposed by Tixier and show that the order of magnitude of a formation permeability, K, may be obtained from the relationship:

$$K \doteq \text{Constant} \left(\frac{1}{P_c^2 F^{\left(2-\frac{1}{m}\right)} S_w} \right)$$

where the constant is equal to $\dfrac{21.2\,\delta^2}{t_s}$ for K in millidarcies, capillary pressure, P_c, in psi and interfacial tension, δ, in dynes/cm. The value for t_s lies between 2.0 and 2.5 and may be taken as 2.25.

In order to obtain an estimate of permeability when P_c is unobtainable (i.e., in the absence of an oil-water contact in the reservoir) we suggest a correlation between irreducible saturation, S_{wi}, permeability and formation factor of the form:

$$S_{wi} = C \left[\frac{1}{K^{1/2} F^{0.67}} \right] + C^1,$$

where C and C^1 are constants.

Evidence from a number of oil reservoirs in the United States is given to substantiate this type of correlation.

ACKNOWLEDGMENTS

We wish to acknowledge the help of Paul Fulton in obtaining certain of the experimental data incorporated in this paper, and our thanks are due to Paul D. Foote, executive vice-president, Gulf Research and Development Co., for permission to publish this paper.

NOMENCLATURE

A	Specific surface area of pores per unit of pore volume.
A_c	Area of face of core.
C	Textural constant with the dimensions of a length connecting irreducible water saturation to permeability and formation factor.
C^1	Dimensionless constant.
F	True formation factor of porous solid.
F_e	Effective true formation factor of a porous system partially saturated with a non-conducting non-wetting phase.
F_f	Hydraulic formation factor.
I	Resistivity index.
$j(S_w)$	Capillary pressure function.
K	Specific permeability.
K_{rw}	Relative permeability to wetting phase.
L	Actual length of core.
L_a	Mean effective length of pores in core.
m	Cementation factor exponent.
n	Saturation or resistivity index exponent.
N	Number of pores in any cross section A_c.
P_c	Capillary pressure.
P_d	Displacement pressure.
R	Radius of hypothetical cylindrical core of area A_c.
r	Pore radius.

S_w	Fractional wetting phase saturation.
S_{wi}	Fractional "irreducible" wetting phase saturation.
t	Kozeny rock textural constant.
t_s	Pore shape factor.
T	Tortuosity = $(L_a/L)^2$.
T_e	Effective tortuosity at any saturation of the wetting phase.
δ	Interfacial tension.
ϕ	Fractional porosity.
μ	Fluid viscosity.
ρ_c	Interstitial water resistivity.
ρ_t	True core or formation resistivity.
ρ_w	True resistivity of a core or formation 100 per cent saturated with a conducting wetting phase.
θ	Contact angle, solid to liquid, of the wetting phase.

REFERENCES

1. "Electric Log Analysis in the Rocky Mountains." M. P. Tixier. *Oil and Gas Jour.*, 48, No. 7, 143, (1949).
2. "Electric Logging." E. F. Stratton and R. D. Ford. Quarterly of the Colorado School of Mines, 302, (1949).
3. "Evaluation of Permeability from Electric Log Resistivity Gradients." M. P. Tixier. *Oil and Gas Jour.*, 48, No. 6, 113, (1949).
4. "A Quantitative Analysis of the Electrochemical Component of the S.P. Curve." M. R. J. Wyllie. *Trans.* AIME, 186, 17, (1949).
5. "A Statistical Study of the Accuracy of Some Connate Water Resistivity Determinations from Electric Log Data." M. R. J. Wyllie. Bull. AAPG 33, 1892, (1949).
6. "Electrical Resistivity as an Aid in Core Analysis Interpretation." G. E. Archie. *Trans.* AIME, 146, 54, (1942).
7. "A Mathematical Treatment of the Electric Conductivity and Capacity of Disperse Systems. I. The Electric Conductivity of a Suspension of Homogeneous Spheroids." H. Fricke. Physical Review, 24, 575. (1924).
8. "Fundamental Data for the Interpretation of Electric Logs." H. Guyod. *Oil Weekly*, 115, 38, October 30 (1944).
9. "The Presence of Conductive Solids in Reservoir Rocks as a Factor in Electric Log Interpretation." H. W. Patnode and M. R. J. Wyllie. AIME T.P. 2797, *Jour. Pet. Tech.*, 2, (2), 47, (1950).
10. "True Resistivity Determinations from the Electric Log — Its Application to Log Analysis." H. G. Doll, L. C. Legrande and E. F. Stratton. Presented to Pacific Coast District, Division of Production, API, Los Angeles, Spring (1947).
11. "The Flow of Gas-Liquid Mixtures through Unconsolidated Sands." R. D. Wyckoff and H. G. Botset. *Physics*, 7, (9), 325, (1936).
12. "The Effect of Moisture on the Direct Current Resistivities of Oil Sands and Rocks." J. J. Jakosky and R. H. Hopper. *Geophysics*, 2, (1), (1937).
13. "Determination of the Potential Productivity of Oil-Bearing Formations by Resistivity Measurements." M. Martin, G. H. Murray and W. J. Gillingham. *Geophysics*, 3, (3), (1938).
14. "Electrical Resistivity an Aid in Core Analysis Interpretation." G. E. Archie. Bull. AAPG. 31. 350. (1947).
15. "Relative Permeability Measurements on Small Core Samples." R. A. Morse, P. L. Terwilliger and S. T. Yuster. *Oil and Gas Jour.*, 46, (16), 109, (1947).
16. "Studies in Relative Permeability." J. H. Henderson and S. T. Yuster. *World Oil*, 127, (12), 139, (1948).
17. "Progress Report on Multiphase Flow Studies." J. H. Henderson and A. H. Mendrum. *Prod. Monthly*, 13, (5), 12, (1949).
18. "Electrical Logging Developments in the U.S.S.R." Part 6, H. Guyod. *World Oil*, 128, (4), 110, (1948).
19. "Fluid Flow Through Granular Beds." P. C. Carman. Trans. Inst. Chem. Engs., 15, 150, (1937).
20. "Evaluation of Capillary Character in Petroleum Reservoir Rock." Walter Rose and W. A. Bruce. *Trans.* AIME, 186, 127, (1949).
21. "A Note on the Valuation of Relative Permeability." Owen Thornton. *Trans.* AIME, 186, 328, (1949).
22. "Theoretical Generalizations Leading to the Evaluation of Relative Permeability." Walter Rose. *Trans.* AIME, 186, 111, (1949).
23. "Factors Which Affect True Formation Resistivity." S. J. Pirson. *Oil and Gas Jour.*, 46, 76, November 1 (1947).
24. "The Size of Pores in Collodion Membranes." P. I. Hitchcock. *J. Gen. Physiol.*, 9, 755, (1926).
25. *Micromeritics.* Pitman Publishing Company, New York, 2nd Edition (1948). J. M. Dalla Valle, P. 131.
26. Discussion on "Capillary Pressures—Their Measurement Using Mercury and the Calculation of Permeability Therefrom" by W. R. Purcell. Walter Rose. *Trans.* AIME, 186, 46, (1949).
27. "Capillary Pressures—Their Measurement Using Mercury and the Calculation of Permeability Therefrom." W. R. Purcell. *Trans.* AIME, 186, 39, (1949).
28. "Flow of Oil-Water Mixtures Through Unconsolidated Sands." M. C. Leverett. *Trans.* AIME. 132. 149, (1939).
29. "A Note on the Theoretical Description of Wetting Liquid Relative Permeability Data." Walter Rose and M. R. J. Wyllie. *Trans.* AIME, 186, 329, (1949).
30. "Capillary Behavior in Porous Solids." M. C. Leverett. *Trans.* AIME, 142, 152, (1941).
31. "Dimensional-Model Studies of Oil Field Behavior." M. C. Leverett, W. B. Lewis and M. E. True. *Trans.* AIME, 146, 175, (1942).
32. "Interstitial Water by the Capillary Pressure Method." O. F. Thornton and D. L. Marshall. AIME Pet. Tech. T.P. 2126, January (1947).
33. "The Relation Between Electrical Resistivity and Brine Saturation in Reservoir Rocks." H. F. Dunlap, H. L. Bilhartz, C. R. Bailey and E. Shuler. *Trans.* AIME, 186, 259, (1949).
34. "Estimation of Interstitial Water from the Electric Log." M. Williams. Abst.: *J. Pet. Tech.*, September (1949).

★ ★ ★

T.P. 2809

THE COEXISTENCE OF LIQUID AND VAPOR PHASES AT PRESSURES ABOVE 10,000 PSI

MICHAEL J. RZASA, STANOLIND OIL AND GAS CO., TULSA, OKLAHOMA, AND **DONALD L. KATZ,**
MEMBERS AIME, UNIVERSITY OF MICHIGAN, ANN ARBOR

ABSTRACT

With greater effort being devoted to the discovery of new oil and gas reserves and a consequent increase in bottom hole pressures due to greater drilling depths, the phase relationships of hydrocarbon fluids at pressures above 10,000 lb psi are becoming increasingly important.

The present paper discusses the results of research with a windowed cell on a methane-Kensol 16 system to pressures of 25,000 lb psi and temperatures to 260°F. Kensol 16 is a commercial high narrow-boiling-range oil. It is shown that for the temperature range of 60°F to 260°F, this particular system exists in two phases to pressures of approximately 14,000 lb psi, and data are presented giving the relative amounts of liquid and vapor phases coexisting under these conditions. Partial phase diagrams are shown for six different mixtures of methane and Kensol 16, three of which include the critical region.

In contrast to mixtures composed of substances of fairly close volatility, critical opalescence was noted for as much as ±200°F of the critical temperature.

The critical locus of the methane-Kensol 16 system was estimated and the conventional pressure-composition and temperature-composition diagrams were prepared. From these, the equilibrium vaporization factors for methane and Kensol 16 were estimated for temperatures from 60°F to 700°F and to pressures above 12,000 lb psi.

The relations of this study to petroleum production problems and other phase equilibria research are discussed.

INTRODUCTION

A knowledge of the physical behavior of naturally-occurring hydrocarbon mixtures is fundamental to a thorough treatment of nearly all operations involved in the recovery, refining, and transportation of petroleum. The operations may involve the applications of phase relationships, and the relative

---

[1] References given at end of paper.

Manuscript received at the office of the Petroleum Branch October 1, 1949. Paper presented at the Petroleum Branch meeting in San Antonio, Texas, October 5-7, 1949.

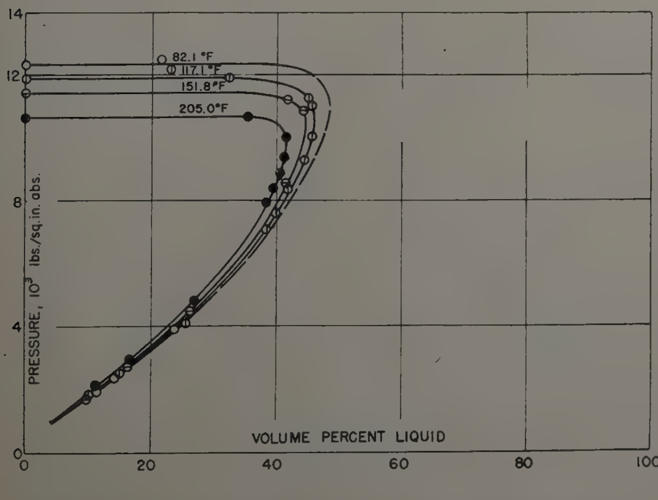

FIG. 1 — VOLUME PER CENT LIQUID 52.00 WT. PER CENT METHANE

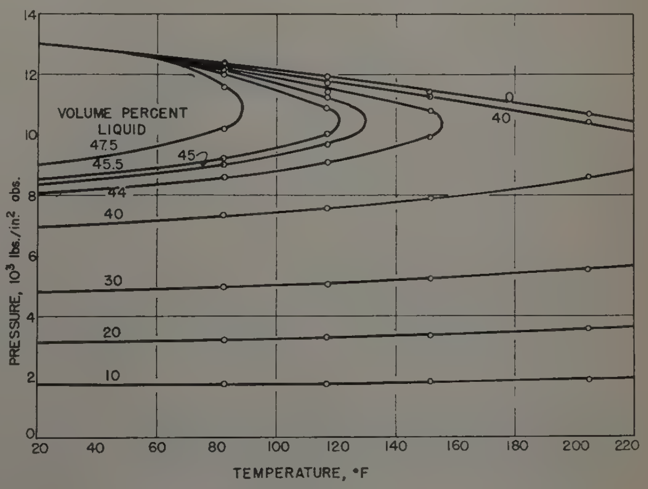

FIG. 2 — PHASE DIAGRAM 52.00 WT. PER CENT METHANE

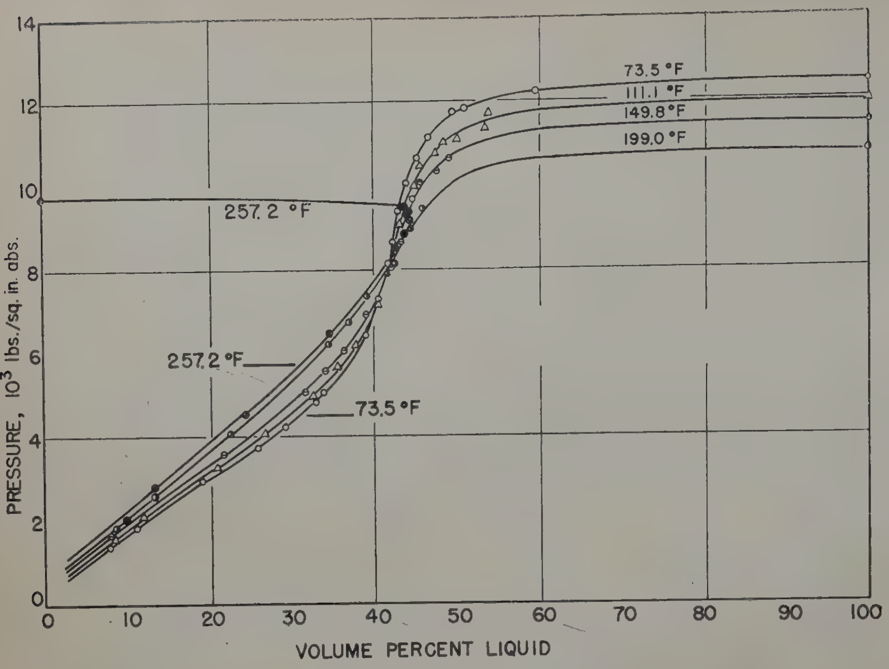

FIG. 3 — VOLUME PER CENT LIQUID 49.8 WT. PER CENT METHANE

amounts and compositions of phases coexisting at various pressures and temperatures.

The phase relationships of pure hydrocarbons are well understood. Binary systems containing methane have been studied from 60°F to 460°F and pressures to 10,000 lb psi.[1,3,5,9,11,15-17,19,24-32] No two-phase pressures in binary systems above about 5,300 lb psi have been studied. Several ternary[6,7,33] and complex systems[12,14,21,22,37,39] have been investigated. Two-phase pressures for a natural gas-crude oil system up to 10,000 lb psi have been studied by Roland.[21] Indications that two phases may exist at pressures to 25,000 lb psi were anticipated by Katz and Singleterry.[13] However, no cases have been reported where two phases were actually found to exist at pressures above 10,000 lb psi.

There have been recent indications that oil and gas pools having formation pressures approaching 10,000 lb psi are being discovered and exploited. It is entirely conceivable that reservoir pressures above 10,000 lb psi may become common in the near future, and it was with the idea of investigating phase relationships of hydrocarbon systems above this pressure that the present research was undertaken.

EQUIPMENT AND MATERIALS

The results presented in this paper were obtained with a high pressure cell containing ten windows which could be used for visual observations of phase phenomena occurring to pressures of 25,000 lb psi and temperatures to 300°F.[23]

The methane used in the present investigation had been furnished by the Phillips Petroleum Co. to Bicher for his study of the methane-propane viscosities.[2] The methane was guaranteed to have a minimum purity of 99.0 mol. per cent and was further purified by passing it through a train of tubes containing ascarite, activated charcoal, and granular calcium chloride.

Kensol 16 is a commercial narrow-boiling-range oil, two gallons of which were supplied gratis by the Kendall Refining Co. It had an initial boiling point of 567°F, midpoint of 574°F, and an endpoint of 589°F, and an experimentally determined molecular weight of 246.9.

EXPERIMENTAL RESULTS AND DISCUSSION

Nineteen different compositions of methane-Kensol 16 mixtures were in-

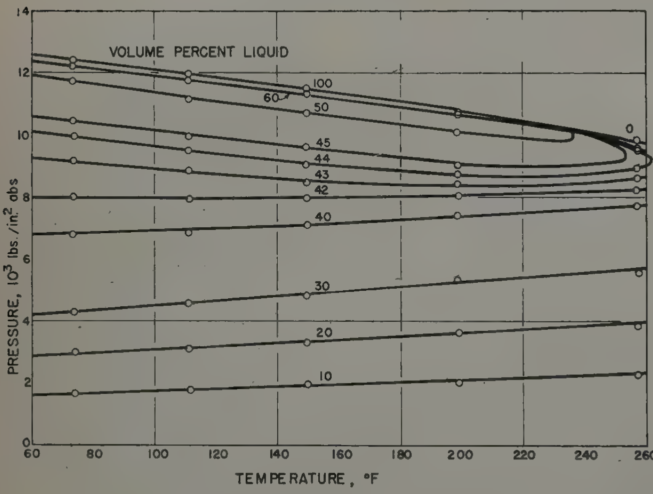

FIG. 4 — PHASE DIAGRAM 49.80 WT. PER CENT METHANE

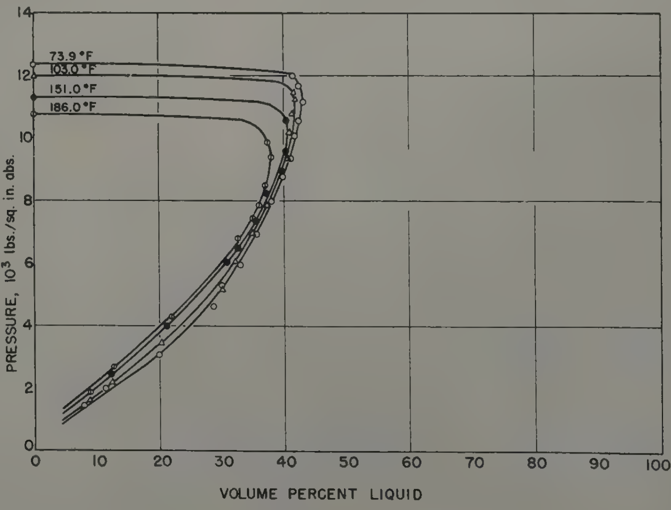

FIG. 5 — VOLUME PER CENT LIQUID 55.45 WT. PER CENT METHANE

vestigated during a series of 52 runs. The data obtained included densities of the entire system, saturation pressures, volume per cent liquid at various pressures and temperatures, and all accessory information on critical opalescence and that necessary for computing the compressibility factors.

Critical Opalescence

Critical opalescence was observed in all mixtures whose compositions varied between 45 and 55 weight per cent methane. Three mixtures, composed of 15.78, 72.70, and 75.78 weight per cent methane respectively, did not exhibit critical opalescence. Kurata and Katz[14] found that this color phenomenon occurred within a temperature range of ±50°F of the critical temperature for mixtures of volatile hydrocarbons such as natural gas and natural gasoline. In the present research, the color phenom-

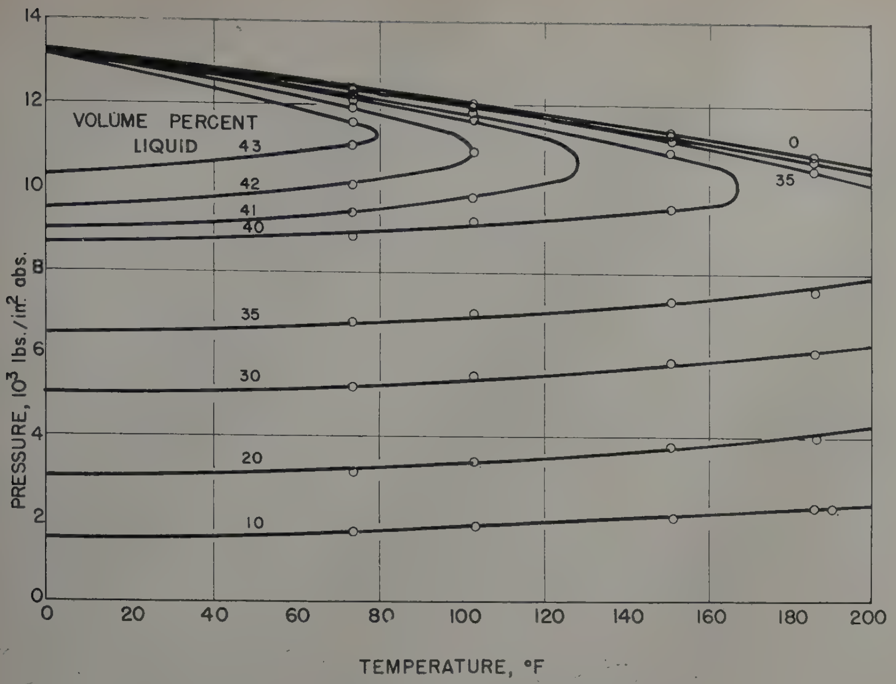

FIG. 6 — PHASE DIAGRAM 55.45 WT. PER CENT METHANE

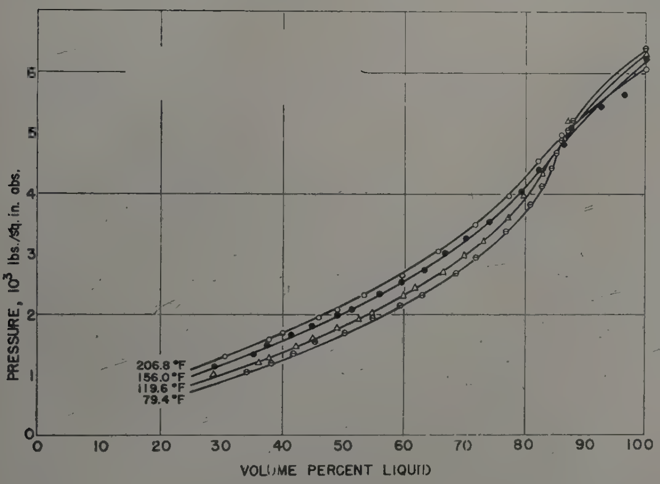

FIG. 7 — VOLUME PER CENT LIQUID 15.78 WT. PER CENT METHANE

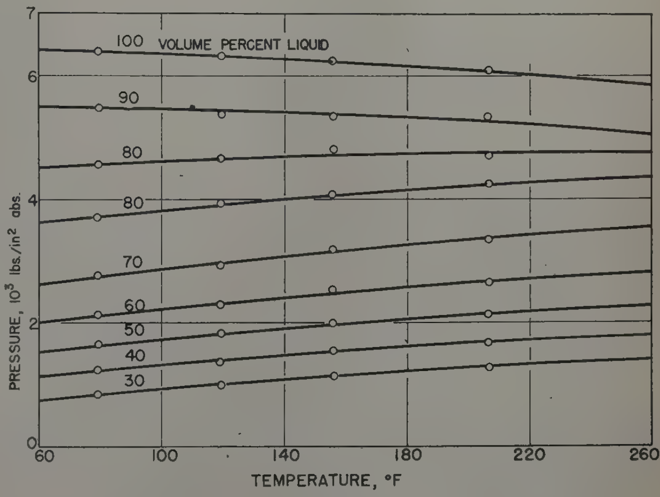

FIG. 8 — PHASE DIAGRAM 15.78 WT. PER CENT METHANE

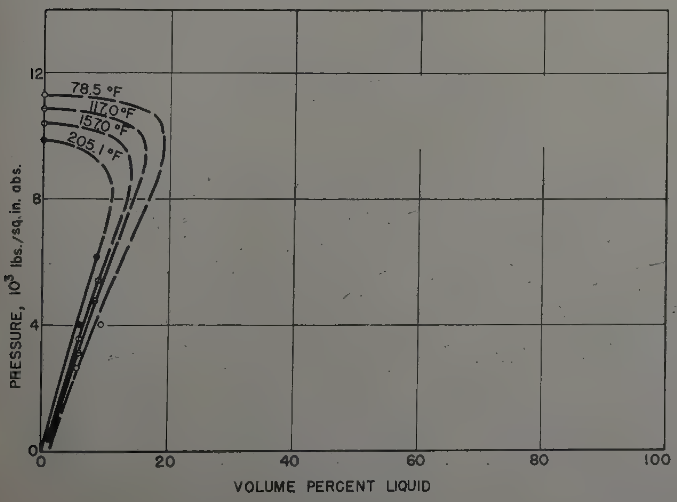

FIG. 9 — VOLUME PER CENT LIQUID 75.74 WT. PER CENT METHANE

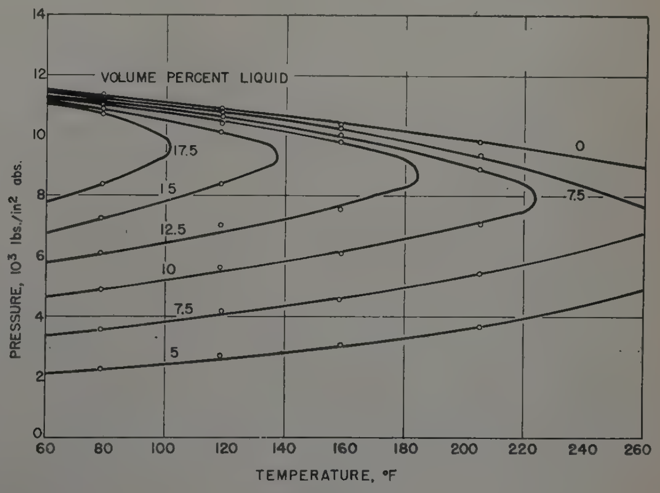

FIG. 10 — PHASE DIAGRAM 75.74 WT. PER CENT METHANE

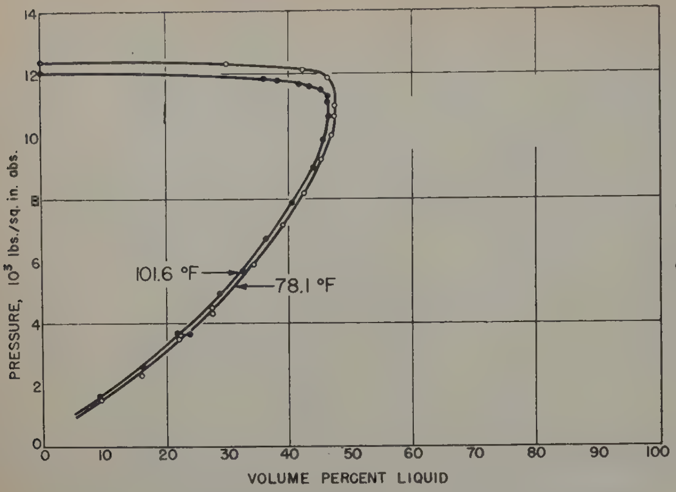

FIG. 11 — VOLUME PER CENT LIQUID 52.10 WT. PER CENT METHANE

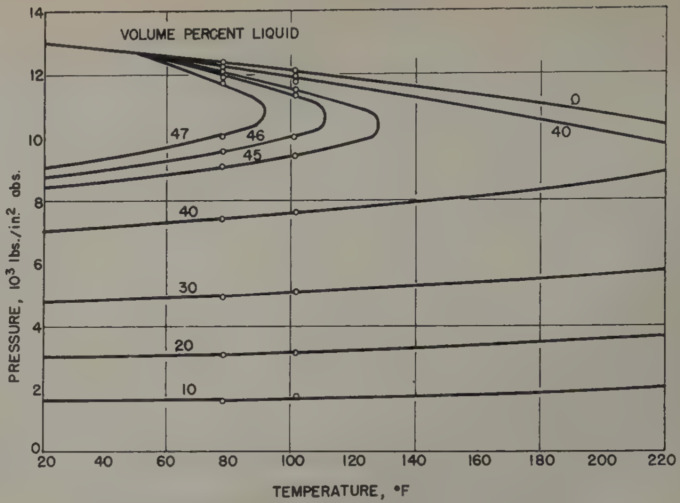

FIG. 12 — PHASE DIAGRAM 52.10 PER CENT METHANE

ena were definitely discernible over the entire range of temperatures investigated. This would indicate that the critical opalescence occurs over a wider temperature spread when the volatility spread between components comprising the system is increased.

As in the case of Kurata and Katz,[14] the mixtures appeared cherry-red to brown-red by transmitted light and blue-green by reflected light. Critical opalescence is believed to be caused by the association of molecules into tiny droplets of the liquid phase or bubbles of the vapor phase, which is about to appear.[14,20,38,41]

Phase Diagrams

Perhaps the most reliable method of determining experimentally the critical temperature and pressure of a hydrocarbon mixture is to plot a phase diagram of the constant-composition mixture from experimental liquid volume per cent data. These data are first plotted as volume per cent liquid versus pressure for the isotherms investigated, as shown in Fig. 1, 3, 5, 7, 9, and 11. Such graphs are then cross-plotted to give the conventional pressure-temperature diagram showing lines of constant volume per cent of liquid. These lines are extrapolated to a common point on the boundary curve, and this common point is the critical point of the mixture in question.

Fig. 1, 3, 5, 7, 9, 11 show the experimental liquid volume per cent data for six mixtures of methane and Kensol 16, while Fig. 2, 4, 6, 8, 10, 12 show these data cross-plotted to give the phase diagrams or the pressure-temperature projections.

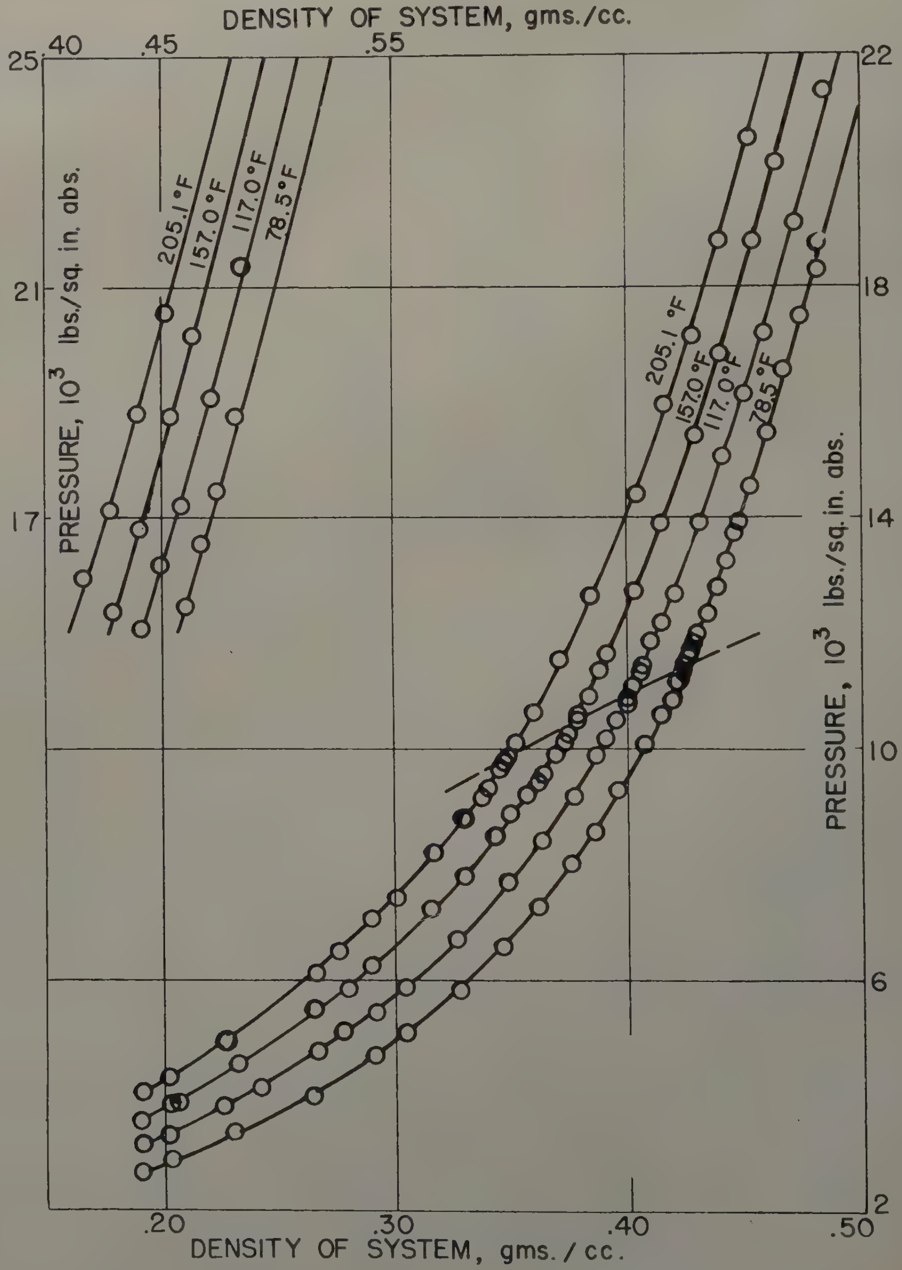

FIG. 13 — P-ρ CURVES 75.74 WT. PER CENT METHANE

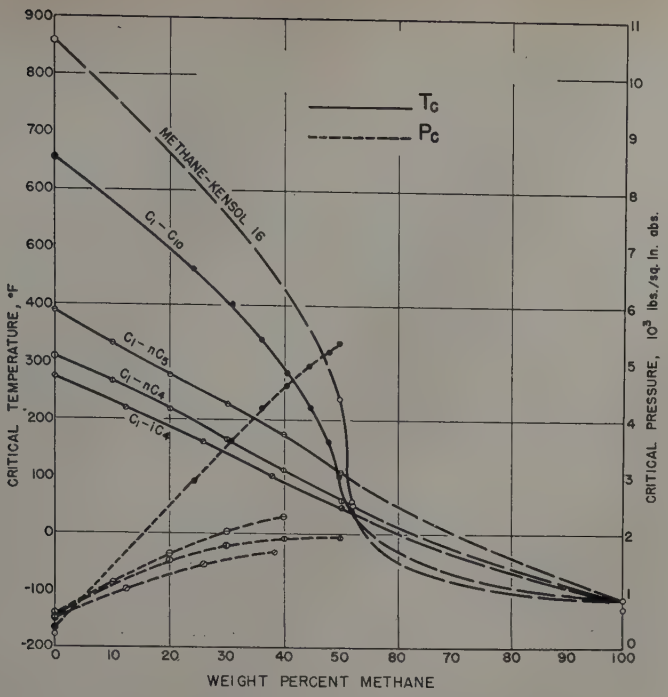

FIG. 14 — T_c AND P_c OF BINARY SYSTEMS

Experimental determinations of bubble points are quite frequently obtained from the break in the pressure-volume curves of the particular mixture studied. The present investigation stresses the difficulty in many instances of using this method in obtaining bubble or dew points. Fig. 13 shows experimental pressure-density isotherms for the mixture containing 75.74 weight per cent methane, the critical temperature of which was estimated to be –97°F. This mixture did not exhibit critical opalescence, so that it can be safely assumed that the actual critical temperature is fairly well removed from the experimental temperatures. Nevertheless, it can be seen from Fig. 13 that without visual means it would be very difficult, if not impossible, to determine the saturation pressure graphically. A pressure decrement of only a few pounds might result in complete "skipping over" of the break in the curve. This points out the fact that the visual method is perhaps the most reliable method of determining bubble points and upper dew points, even at temperatures well removed from the true critical temperature of the mixture.

Critical Properties

Only one mixture was investigated wherein the critical temperature was actually bracketed by the experimental isotherms. Limitations of the windows prevented the attainment of more isotherms and closer bracketing of the true critical temperature. The above-mentioned mixture contained 49.80 weight per cent, or 93.85 mol. per cent methane. By extrapolating the quality lines to a common point on the boundary curve, the critical temperature of this mixture was estimated as 235± 5°F, the critical pressure as 10,200± 100 lb psi absolute, and the critical density, as read from a pressure-density plot, was estimated as 0.458 grams per cubic centimeter.

Two other mixtures, one containing 52.00 weight per cent methane and the other 52.10 weight per cent methane, had their critical points close enough to the experimental isotherms to permit fair estimations of their critical points. The mixture of 52.00 weight per cent methane has a critical tempera-

Table I
Equilibrium Vaporization Factors as Computed From Fig. 15, 16 and 17

Pressure, psia	Temperature, °F	Equilibrium Factors Methane	Equilibrium Factors Kensol 16
2000	700	1.255	0.561
	600	1.628	.2195
	500	1.942	.0945
	400	2.160	.0398
	300	2.240	.0119
	200	2.255	.000585
	100	2.258	
	0	2.035	
4000	600	1.116	0.605
	500	1.350	.1918
	400	1.478	.0725
	300	1.543	.0200
	200	1.600	.00175
	100	1.620	
	0	1.595	
7000	400	1.100	0.364
	300	1.216	.073
	200	1.280	.0113
	100	1.302	.00252
	0	1.285	.00326
11,000	150	1.076	0.3065
	100	1.120	.1544
	0	1.152	.0848
12,000	100	1.035	0.597
	50	1.079	.3075
	0	1.089	.259

ture and pressure of 55±2°F, and 12,670±100 lb psi absolute, respectively. The mixture of 52.10 weight per cent methane has an estimated critical temperature, pressure, and density of 51±2°F, 12,700±100 lb psi absolute, and 0.545 grams per cubic centimeter, respectively.

The compositions investigated for critical properties were limited to a narrow range of weight per cent methane. It was discovered early in the research that the mixtures whose critical temperatures were between 60°F and 260°F or within the temperature range of this investigation, would probably have a composition of 50±1 weight per cent methane. This necessitated careful preparation of mixtures in order to bracket the critical temperatures.

Fig. 14 shows the critical temperatures and critical pressures of several binary mixtures containing methane plotted versus weight per cent methane. All the curves of critical temperature versus weight per cent methane exhibit inflection points at approximately 50 weight per cent methane, with the inflection becoming more marked as the molecular weight of the heavier hydrocarbon increases. The methane-decane system studied by Sage and Lacey[19] shows this inflection quite markedly. For a small change in composition in the vicinity of 50 weight per cent methane, the critical temperature of the methane-decane system exhibits a wide variation, from 217°F at 45 weight per cent methane to 80°F at 50 weight per cent methane. The same characteristics to a much greater degree were observed with the methane-Kensol 16 system, where the critical temperature varied from 235°F at 49.8 weight per cent methane to 51°F at 52.1 weight per cent methane. The estimated critical temperature locus for the methane-Kensol 16 system has been plotted in Fig. 14 for comparison.

The critical temperature and pressure for methane are -116°F and 673 lb psi absolute, respectively. From the specific gravity and molecular weight of the Kensol 16, its critical temperature and pressure were estimated as 859°F and 216 lb psi, respectively, by the method of Smith and Watson.[35] These values served as anchor points in plotting the critical locus of the methane-Kensol 16 system, as shown in Fig. 15.

Not all the points shown in Fig. 15 are experimental and many of them were obtained from the pressure-composition diagram of Fig. 16, which shows the experimental bubble and dew points plotted between the temperature range of 70°F to 260°F. Thus the shapes of the phase diagrams of Fig. 15 below 70°F and above 260° are estimated and open to question, but within the above temperature range, the curves are believed to be accurate to ±1.5 per cent.

Fig. 17 shows the conventional temperature-composition diagram for the methane-Kensol 16 system. Fig. 15, 16, 17 should be, and are consistent with each other and constitute the conventional pressure-temperature, pressure-composition, and temperature-composition plots.

As mentioned previously and seen from Fig. 14, the methane-Kensol 16 mixtures whose critical temperatures were between 70°F and 260°F were quite sensitive to composition changes. Fig. 18 shows the critical loci of binary

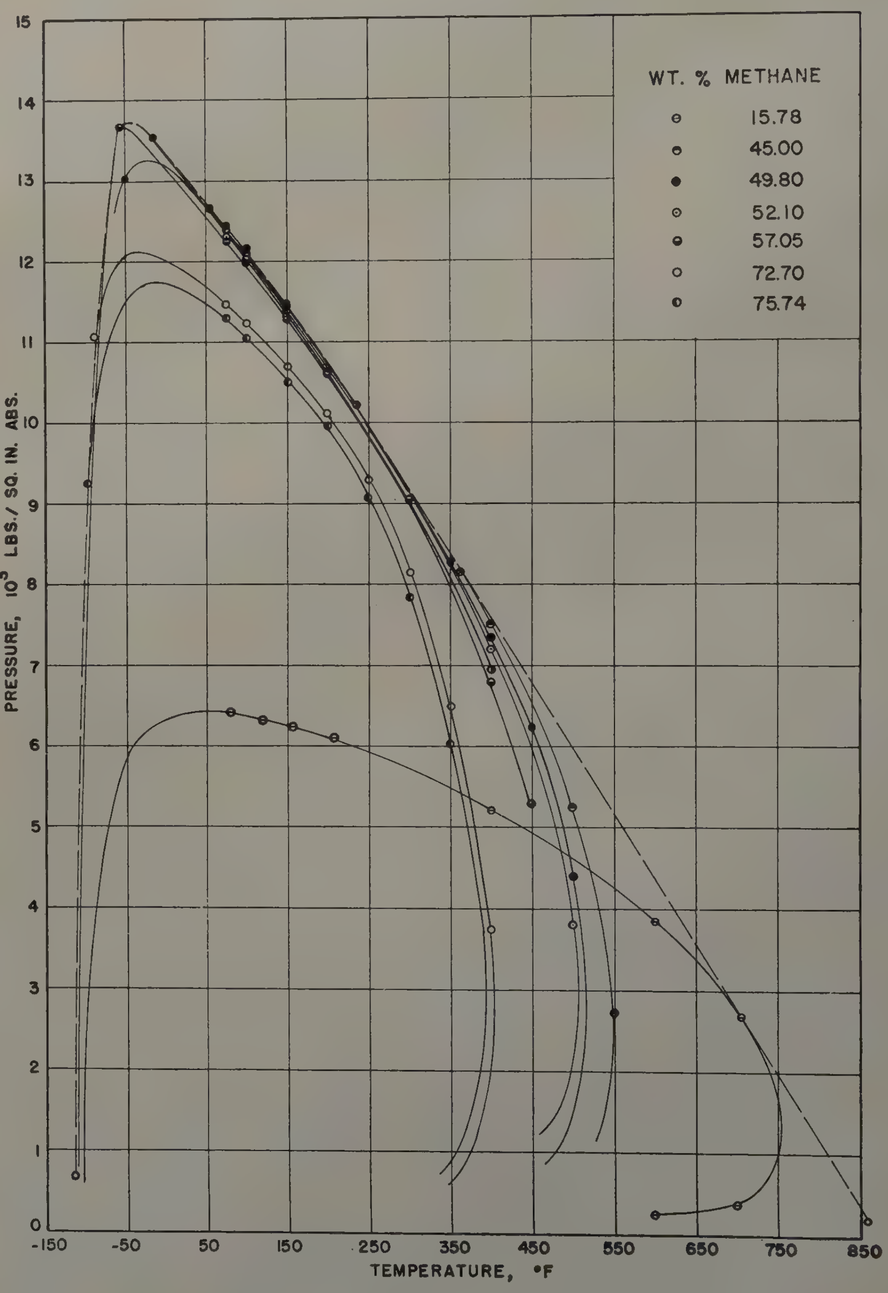

FIG. 15 — CRITICAL LOCUS OF METHANE-KENSOL 16 SYSTEM

hydrocarbon systems containing methane. Systems through the methane-hexane system exhibit fairly symmetrical critical loci curves. The methane-decane system shows a decided shifting of the maximum pressure toward methane. The methane-Kensol 16 exhibits similar reactions with the maximum critical locus pressure occurring at very high concentrations of methane, of the order of 56 weight per cent, or 95.14 mol per cent methane. Results on binary systems of carbon dioxide with propane, n-butane and n-pentane as investigated by Poettmann and Katz,[18] also indicate that the maximum pressure point on the critical loci curves shifts more and more toward the compound of higher volatility as the spread between the volatilities increases. For instance, the maximum pressure point of the carbon dioxide-butane system occurs at a composition of about 71 mol per cent carbon dioxide, and that of the carbon dioxide-pentane system at about 79.4 mol per cent carbon dioxide. Similar trends were observed in the carbon monoxide-propane system investigated by Widdoes and Katz[40] with the maximum pressure point occurring at about 90 mol per cent carbon monoxide.

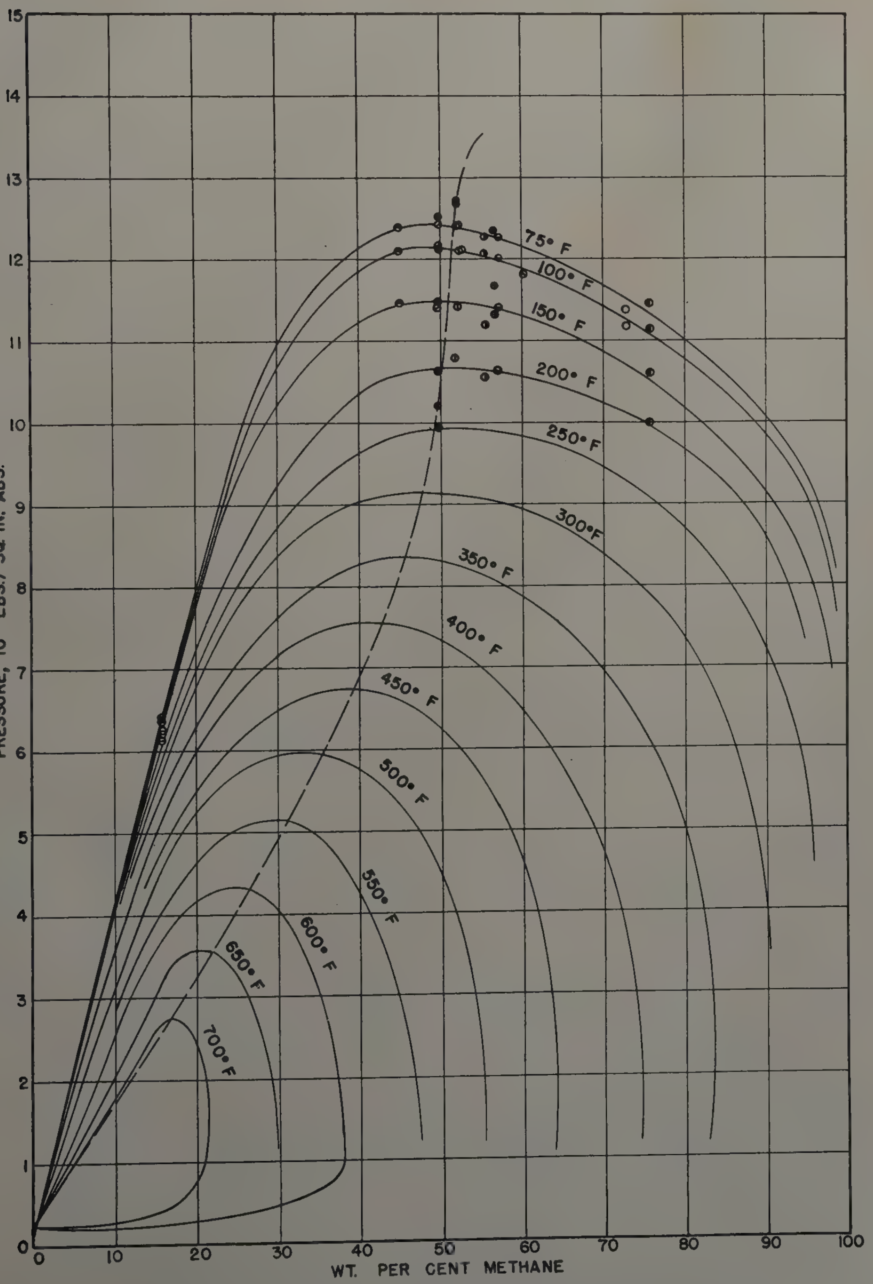

FIG. 16 — PRESSURE-COMPOSITION DIAGRAM OF METHANE-KENSOL 16 SYSTEM

The above discussion leads to a general conclusion: namely, that the greater the spread in the volatility of compounds comprising a binary system, the greater will be the deviation of the critical locus from symmetry, and the more will the critical locus curve be shifted toward the compound of highest volatility; the point of maximum pressure will occur at high percentages of the more volatile compound.

The assumption has almost always been made that the critical temperature of binary mixtures composed of pure substances or complex mixtures composed of various proportions of separator gas and liquid, would lie between the critical temperatures of the pure substances or of the separator gas and coexistent liquid. Recent work by Eilerts, et al.,[8] showed that it was possible to have the critical temperature of a complete system below the critical temperature of the more volatile component or fraction of that system. If the critical locus of the methane-Kensol 16 system is drawn between the critical temperatures of methane and Kensol 16, the critical locus curve will have a very sharp peak at about –50°F and it would appear more reasonable to expect that the critical locus curve extends below the critical temperature of methane. However, Fig. 15, 16, 17 were drawn so that the critical temperatures of methane and Kensol 16 bracketed the critical temperatures of mixtures.

Vapor-Liquid Equilibria

One of the most convenient tools in estimating the physical reactions of hydrocarbon systems to varying conditions of pressure and temperature is the equilibrium vaporization factor or "constant" as it is frequently called. It is used in the computations of bubble and dew points, the relative amounts of liquid and vapor phases and the compositions of the coexistent phases, under varying pressures and temperatures. The equilibrium vaporization factor was first proposed by Souders, Selheimer and Brown[36] and is defined as

$$K = y/x$$

where

K = equilibrium vaporization factor at equilibrium pressure and temperature,
y = mol fraction of component in vapor phase,
x = mol fraction of component in liquid phase.

Fig. 15, 16, 17 provide the means for computing the equilibrium vaporization factors for methane and Kensol 16. Table I gives the computed values of these factors. The equilibrium factors for methane are plotted in Fig. 19 as a function of temperature with lines of constant pressure, with a similar plot for Kensol 16 in Fig. 20.

A more convenient and clear method of presenting equilibrium factors is to plot the conventional log K versus log P charts with lines of constant temperatures, as has been done in Fig. 21 which shows isotherms of 0°F, 100°F, 400°F, and 600°F.

It is seen from Fig. 21 that the equilibrium vaporization factors converge to unity at different pressures for the different temperatures.

The pressures at which the factors converge to unity are called convergence pressures. It has been recognized that the convergence pressure is the critical pressure of the particular binary system which has its critical temperature at the temperature in question. For a binary system, therefore, the critical locus is the locus of the convergence pressures.

The equilibrium vaporization factor for a component in a binary system is fixed by specifying the temperature, pressure, and the particular binary system. It is also fixed by specifying the temperature, pressure, and convergence pressure at that temperature, in place of specifying the particular binary system.

Fig. 21 also shows how the factors for methane at 0°F cross the factors at 100°F and 400°F at successively lower pressures. This fact can also be seen from Fig. 19 which shows how the factors for methane rise at first with increase in temperature and then decrease to unity as the critical pressure, or convergence pressure, is reached.

In order to show the effect of convergence pressure on the equivalent vaporization factors for methane, Hanson, Rzasa and Brown[10] have presented a correlation based on binary paraffin systems, which was applied to the methane factors in the methane-Kensol 16 system. At all equilibrium pressures below about 4,000 lb psi absolute, the factors for methane are lower in the methane-Kensol 16 system than in the methane-decane system. Two possible explanations of this phenomenon may be advanced. First, the correlation presented by Hanson, Rzasa and Brown[10] applied to paraffin systems entirely, while in the present case the Kensol 16 is composed of only 64-66 per cent paraffins. Secondly, the peculiar shapes of the phase diagrams and critical locus of the methane-Kensol 16 system, with an extremely rapid shifting of the critical temperature with small changes in composition, may account for this decrease in the equilibrium factor. The same thing would be true if the factors for methane were correlated as a function of the molecular weight of the heavier constituent. The molecular weights of n-decane and Kensol 16

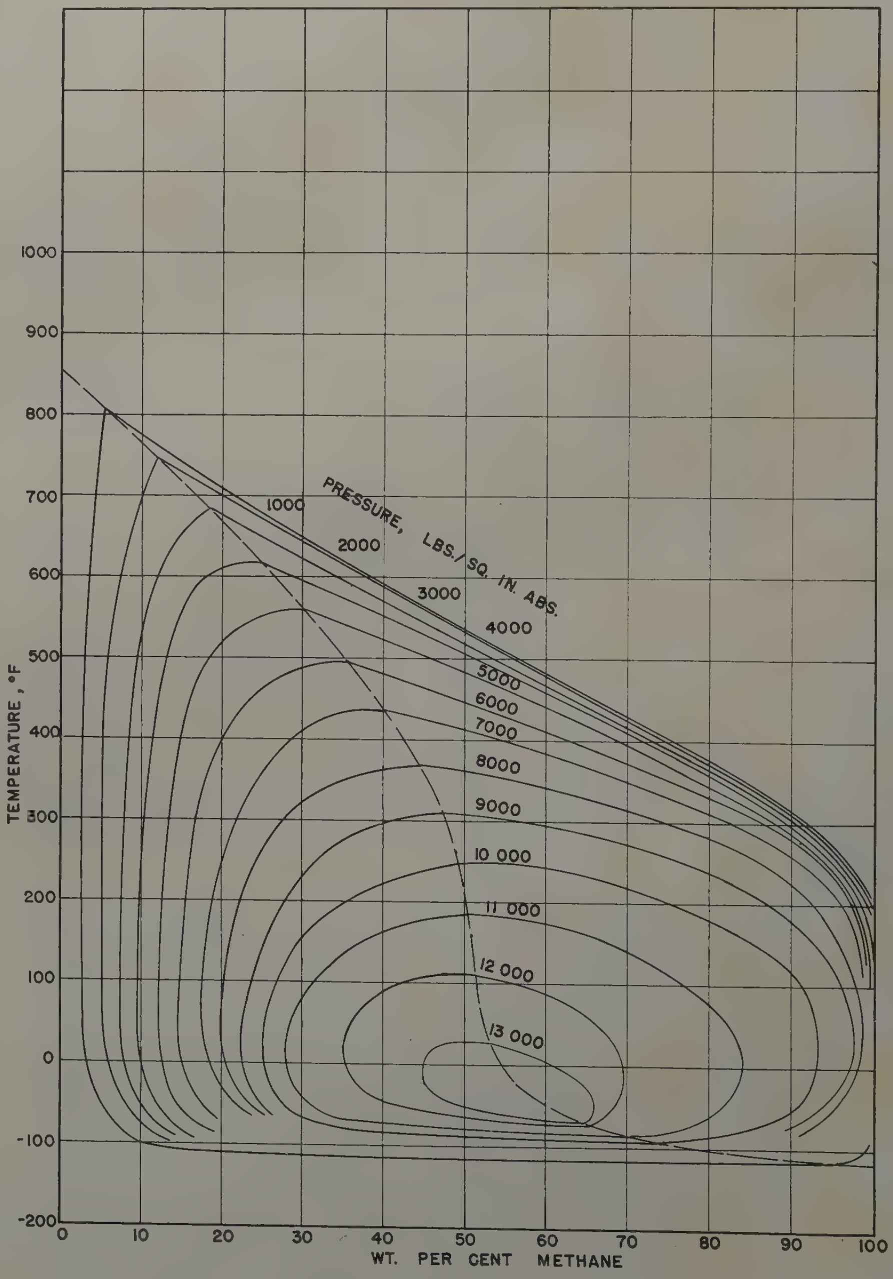

FIG. 17 — TEMPERATURE-COMPOSITION DIAGRAM OF METHANE-KENSOL 16 SYSTEM

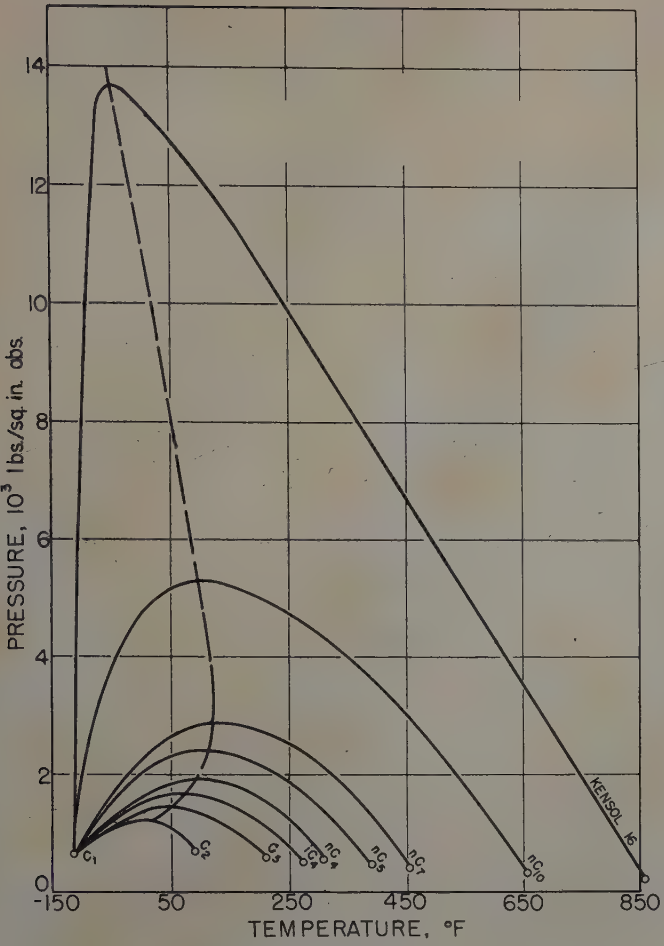

FIG. 18 — CRITICAL LOCI OF BINARY SYSTEMS CONTAINING METHANE

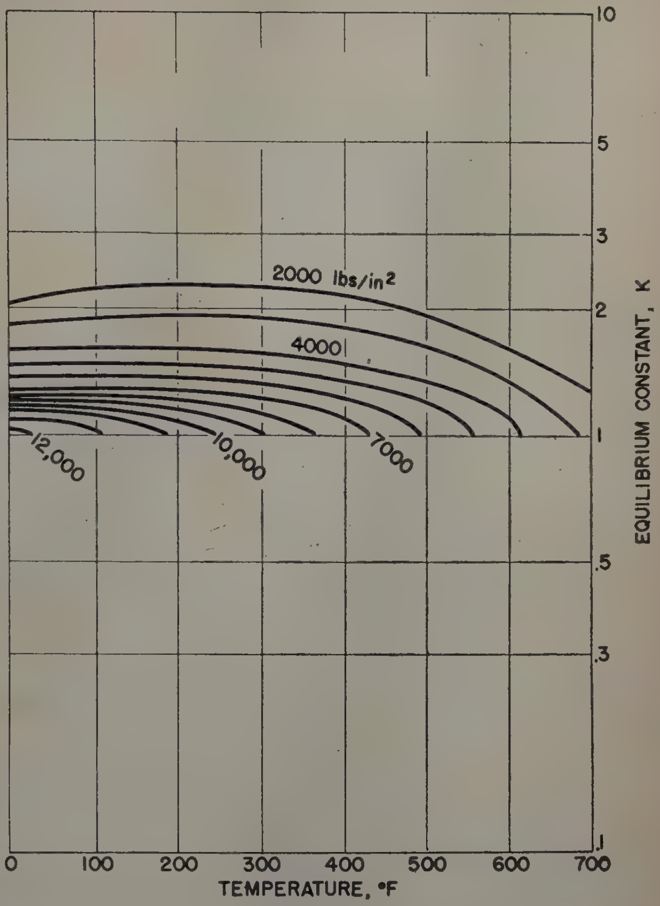

FIG. 19 — EQUILIBRIUM CONSTANTS FOR METHANE

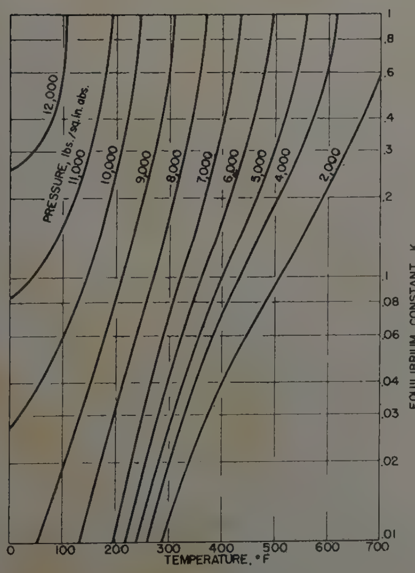

FIG. 20 — EQUILIBRIUM CONSTANTS FOR KENSOL 16

are 142.3 and 246.9, respectively, but the methane factors in the methane-Kensol 16 system are lower than they are in the methane-decane system. These observations are consistent with the results presented by Sage and Lacey.[34]

RELATIONS OF PRESENT WORK TO PETROLEUM PROBLEMS

Perhaps the most significant contribution of the present research to our knowledge of the physical reactions and phase behavior of petroleum fluids is the fact that two phases can coexist at pressures of 13,000 lb psi and above. As our search for oil continues, drilling depths will increase. Qualitatively, with increased depths we can expect to find oil pools with fluids containing more methane than that found in shallow wells. In that event, the control and production of these reservoirs may be complicated by the possible presence of two phases and operating techniques will be forced to take cognizance of that possibility. Heretofore it has been the general concensus that great well depths, of the order of 12,000 to 15,000 ft, would result in such high bottom hole pressures that the reservoir fluid would be expected to exist in the single phase. That this assumption may be invalid can be readily ascertained from the critical locus of the methane-Kensol 16 system.

Increase in drilling depths with consequent increase in bottom hole pressures will necessitate the study of phase relationships in the high pressure range, i.e., above 10,000 lb psi, and the present results are a step in that direction.

CONCLUSIONS

The following have been accomplished:

1. Phase diagrams for six mixtures of methane and Kensol 16 were ex-

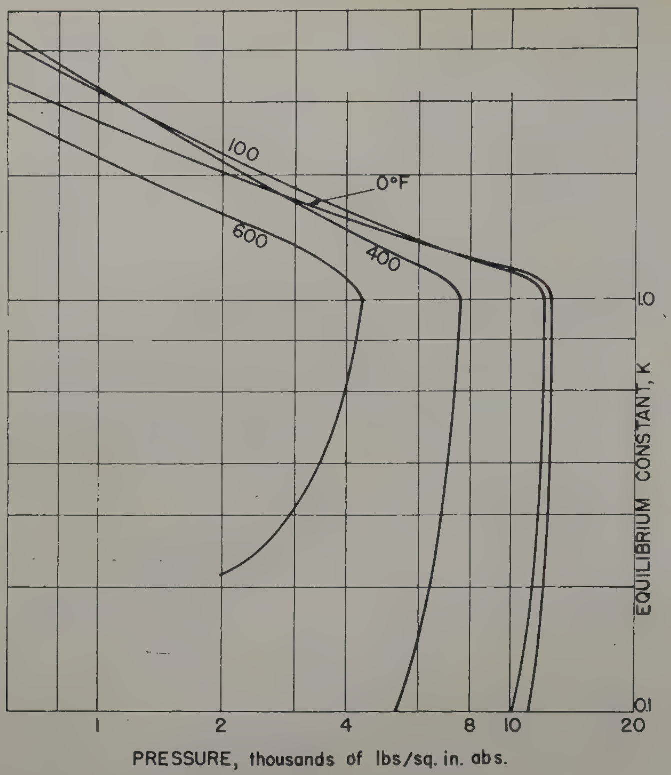

FIG. 21 — EQUILIBRIUM CONSTANTS

perimentally determined to pressures above 13,000 lb psi.

2. The coexistence of liquid and vapor phases above 10,000 lb psi was demonstrated.

3. The critical points of three methane-Kensol 16 mixtures were determined as follows:

Composition	T_c, °F	P_c, psia	ρ_c, gm/cc
49.80 wt. % methane	235	10,200	0.458
52.00 wt. % methane	55	12,670	
52.10 wt. % methane	51	12,700	0.545

4. A critical locus of the methane-Kensol 16 system was prepared from the experimental data.

5. The equilibrium vaporization factors for methane and Kensol 16 were estimated from the experimental data and extrapolated to 700°F.

6. The conclusion was reached that, for binary systems the influence of wide differences in volatility is such that the maximum pressure on the critical locus is shifted toward the compound of highest volatility, with the shift becoming more pronounced as the volatility spread increases.

7. For mixtures of wide-spread volatility it is very difficult, if not impossible, to determine the saturation pressures by the conventional pressure-volume curves, even at conditions well removed from the critical point. Visual means appear to be the most reliable method of determining these transition points.

REFERENCES

1. Amick, Ph.D. Thesis, Yale University (1939).
2. Bicher and Katz, *Ind. Eng. Chem.* 35, 754 (1943).
3. Boomer and Johnson, *Can. J. Research* 16, 328 (1938).
4. Boomer, Johnson, and Piercey, *Can. J. Research* 16, 319 (1938).
5. Boomer, Johnson, and Piercey, *Can. J. Research* 16, 396 (1938).
6. Carter, Sage, and Lacey, *Trans.* AIME 142, 170 (1941).
7. Dourson, Sage, and Lacey, *Trans.* AIME 151, 206 (1943).
8. Eilerts, Barr, Mullen, and Hanna, *Petr. Engr.* 19, 154 (1948).
9. Guter, Newitt, and Ruhemann, *Proc. Roy. Soc.* 176, 140 (1940).
10. Hanson, Rzasa, and Brown, *Ind. Eng. Chem.* 37, 1216 (1945).
11. Johnson, Ph.D. Thesis, Univ. of Alberta (1936).
12. Katz and Hachmuth, *Ind. Eng. Chem.* 29, 1072 (1937).
13. Katz and Singleterry, *Trans.* AIME 132, 103 (1939).
14. Kurata and Katz, *Trans.* AIChE 38, 599 (1942).
15. Lavender, Sage, and Lacey, *Oil and Gas J.* 39, No. 9 (July 11, 1940).
16. Middleton, Ph.D. Thesis, Univ. of Michigan (1935).
17. Nederbragt, *Ind. Eng. Chem.* 30, 587 (1938).
18. Poettmann and Katz, *Ind. Eng. Chem.* 37, 847 (1945).
19. Reamer, Olds, Sage, and Lacey, *Ind. Eng. Chem.* 34, 1526 (1942).
20. Roess, *J. Inst. Petroleum* 22, 665 (1936).
21. Roland, *Ind. Eng. Chem.* 37, 930 (1945).
22. Roland, Smith, and Kaveler, *Oil and Gas J.* 39, No. 46, 128 (March 27, 1941).
23. Rzasa, "Phase Equilibria of Methane-Kensol 16 System to Pressures of 25,000 lb psi and Temperatures of 60°F to 260°F", Ph.D. Thesis, Univ. of Michigan (1947).
24. Ruhemann, *Proc. Roy. Soc.* 171, 121 (1939).
25. Sage, Schaafsma, and Lacey, *Ind. Eng. Chem.* 26, 714 (1934).
26. Sage, Hicks, and Lacey, *Ind. Eng. Chem.* 32, 1085 (1940).
27. Sage, Budenholzer, and Lacey, *Ind. Eng. Chem.* 32, 1262 (1940).
28. Sage, Reamer, Olds, and Lacey, *Ind. Eng. Chem.* 34, 1108 (1942).
29. Sage, Webster, and Lacey, *Ind. Eng.* 29, 658 (1937).
30. Sage, Lavender, and Lacey, *Ind. Eng. Chem.* 32, 743 (1940).
31. Sage and Lacey, *Ind. Eng. Chem.* 30, 1296 (1938).
32. Sage, Bachus, and Lacey, *Ind. Eng. Chem.* 27, 686 (1935).
33. Sage, Billman, and Lacey, *Trans.* AIME 174, 13 (1948).
34. Sage and Lacey, API *Drill. and Prod. Pract.* 641 (1939).
35. Smith and Watson, *Ind. Eng. Chem.* 29, 1408 (1937).
36. Souders, Sellheimer, and Brown, *Ind. Eng. Chem.* 24, 517 (1932).
37. Standing and Katz, *Trans. AIME* 155, 232 (1944).
38. Travers and Usher, *Proc. Roy. Soc.* 78, 247 (1906).
39. Webber, *Trans.* AIME 142, 192 (1941).
40. Widdoes and Katz, *Ind. Eng. Chem.* 40, 1742 (1948).
41. Zernike, *Arch. neer.* IIIA, 4, 74 (1918).

* * *

SELECTIVE SP LOGGING

H. G. DOLL, MEMBER AIME, SCHLUMBERGER WELL SURVEYING CORP., RIDGEFIELD, CONNECTICUT

ABSTRACT

An earlier paper on the general subject of the SP log has analyzed the limitations of that log, in particular when dealing with thin permeable beds enclosed in thick highly resistive ones. Under such conditions, the SP log does not give a good definition of the permeable beds.

Selective SP logging is a new method which gives an accurate determination of the permeable beds, even in highly resistive formations, except when the salinity of the mud is extremely high. It also permits a close approximation of the static SP to be obtained.

The method consists generally in controlling the potential of auxiliary electrodes located in the drill holes in the vicinity of the measuring electrode. In this manner, the flow of SP current along the drill hole is modified to counterbalance the effect of highly resistive strata.

Several procedures and arrangements used to record selective SP curves and static SP curves are explained.

Field examples illustrating these methods are given and discussed.

INTRODUCTION

In an earlier paper,[1] the shape of the SP curves and the amplitude of the SP peaks were analyzed, considering how the circulation of the SP current is influenced by the subsurface media as a function of their geometrical configuration and their resistivities. It was shown, in particular, that the permeable beds situated between highly resistive formations are sometimes indistinctly indicated by the deflections of the SP log.

It is the purpose of this paper to discuss a new method now being developed, namely selective SP logging, whose principal feature is to enable a more accurate determination of the depths of the permeable beds present in highly resistive formations, such as occur in limestone fields.

It will be shown also how an additional curve called the static SP log can be derived from the selective SP log, or recorded directly, to facilitate the interpretation.

Another purpose of the static SP log is to provide an approach toward the determination of the value of the static SP, where this value is not readily given by the SP log. This application, although less important at the present time than that mentioned above, nevertheless is of interest, inasmuch as, according to laboratory and field experiments conducted by several investigators, the determination of oil saturation of reservoirs from the data of the electric log implies the knowledge of the resistivity of the connate water,[2,3] to which the static SP seems to be related.[4,5,6,7]

PRINCIPLE OF SELECTIVE SP LOGGING

The method of selective SP logging of the formations traversed by a bore hole consists in recording two curves under the following conditions:

The measuring device comprises one measuring electrode M and two additional electrodes G-G′, connected to each other, located above and below

---

[1] References given at end of the paper.

Manuscript received at the office of the Petroleum Branch October 24, 1949. Paper presented at the Petroleum Branch meeting in Columbus, September 25-28, 1949, and at the San Antonio meeting of the Petroleum Branch, October 5-7, 1949.

electrode M and preferably symmetrical with respect to M (Fig. 1). The distance between G-G′ is taken equal to a few feet. As the device is moved along the bore hole, the average of the potentials at electrodes G and G′ is maintained at a constant value, and the difference between the potential at M and the average of the potentials at G and G′ is continuously recorded. With this device, two curves are recorded corresponding respectively to two different values of the potential at G-G′,* suitably chosen, as will be discussed below.

When recording each of the curves, the potential at G-G′ is controlled by means of two other electrodes A-A′, also connected to each other and situated outside of and respectively very close to G-G′. A current whose intensity is adjusted, for example, by means of a potentiometric circuit (1), is fed to A-A′ from the surface through one of the conductors of the cable. The intensity of this current is controlled so as to keep the potential at G-G′ at a selected constant value. This current is called the monitoring current.

The electrodes G-G′ are connected to a reference electrode (3) at the surface by a second conductor, through a meter (2) which is used for controlling the potential at G-G′. Electrode M is also connected through a third conductor to the surface where a meter (4) permits the recording of the difference of potential between M and G-G′. The internal resistances of the meters (2) and (4) are great enough so that the measuring circuits do not interfere with each other, nor with the distribution of the potentials prevailing around the electrode system. These resistances are represented on the drawing by separate conventional symbols.

Remark—The potential at an electrode designates the potential prevailing in the mud around that electrode. In fact, however, the meters are connected to the metal of the electrodes so that the potentials which are recorded or controlled by the meters are the potentials in the mud plus the contact potentials between the mud and the metal. It is, therefore, desirable that the contact potentials of the electrodes M, G and G′ with respect to mud be equal and stable so that these contact potentials cancel out when the difference of the potentials between M and G-G′ is recorded. It is also desirable that the surface electrode (3) be stable, since the potential at G-G′, which must be kept constant, is referred to this electrode.

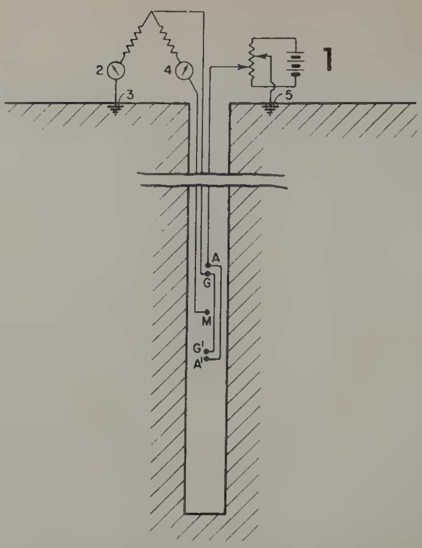

FIG. 1 — THEORETICAL CIRCUIT FOR THE SELECTIVE SP LOGGING.

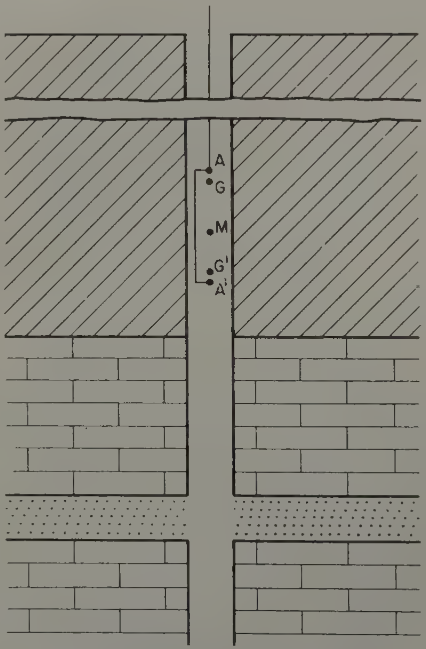

FIG. 2 — ELECTRODE SYSTEM OPPOSITE A THICK SHALE BED.

Analysis of the Procedure

A thick homogeneous, conductive, and impervious bed, such as a shale of low resistivity, is supposed to overlie a thick, highly resistive formation such as compact limestone, including permeable and impervious conductive beds. It is further supposed that the static SP's are the same respectively for all the shales and for all the permeable beds.‡

Two cases will be examined, according to whether the potential at G-G′ is brought to a value equal to the static SP of the shales V_c, or to the static SP of the permeable beds V_p. These two cases correspond respectively to the two curves which constitute the selective SP log.

Selective SP Curve No. 1 — The Potential at G-G′ Is Kept Equal to the Static SP of Shales

The device is placed in front of the thick shale bed at appreciable distance from its boundaries (Fig. 2) and no current is sent through A-A′. As the bed is thick and homogeneous the potential at G-G′ is equal to the static SP of shales: this potential is noted on the meter (2). On the other hand, the potential being constant in the mud in front of the shale bed, the difference of potential between M and G-G′, that is the selective SP, is equal to zero.

The device is then lowered while the potential of G-G′ is maintained constantly equal to the static SP of shales by means of the monitoring current.

The following circumstances are observed, depending on the formations successively traversed by the electrode system:

(a) When the device enters the highly resistive compact formation (Fig. 3), the potential at G-G′ tends to become negative with respect to the static SP of shale, as an effect of the flow of the original SP current prevailing in the mud column. A monitoring current of appropriate intensity and sign has, therefore, to be fed to A-A′ so as to keep that potential at G-G′ equal to the static SP of shale.

---

* In order to simplify the wording, the average of the potentials at electrodes G and G′ will be designated for short as "the potential at G-G′" throughout this paper.

‡ The static SP of a bed is the value of the potential which would be observed in the mud in front of this bed, in the ideal case where the SP current is prevented from flowing. Further explanations in this respect are given in reference 1.

With the monitoring current in operation, the current flows as shown schematically on the figure. No current can flow in the bore hole between G and the shale, since the potentials at G and in front of the shale are equal. Above electrode A, therefore, the current flows entirely in the conductor of the cable connecting electrode (5) to electrode A. From A to A′, the current flows in the low resistance conductor which connects them to each other. From A′ downward to the permeable bed, the current flows in the mud column. The current penetrates into the permeable bed to a great distance until sufficiently large cross sections are offered by the surrounding formations. From there on it flows toward the surface of the ground and reaches the surface of electrode (5).

The intensity of the monitoring current is such that the potential at G-G′ is maintained constant. The ohmic drop of potential due to the circulation of the current along the bore hole from G′ to the level of the permeable bed and along the permeable bed to surface electrode (5), minus the emf's occurring between G′ and electrode (5), is therefore constant. As the device goes down through the highly resistive formation, the total emf remains practically constant, whereas the path of the current along the bore hole becomes shorter and the total resistance offered to the current decreases. The intensity of the monitoring current, consequently, increases progressively.

The potentials at M and G-G′ remain equal, however, whatever the intensity of the current, since there is no possible exchange of current between the mud and the surrounding formations, which are supposed practically infinitely resistive, and the signal recorded remains equal to zero.

(b) When the device reaches the level of a thin permeable bed, and when electrode G′, for example, crosses the bed as shown in Fig. 4, a part of the current flows from A into the bore hole towards the bed, and another part goes directly down to A′, and from A′ into the bed. The potential at M is thus smaller than at G-G′ because of the ohmic drop of potential in the bore hole, and a negative signal is recorded.

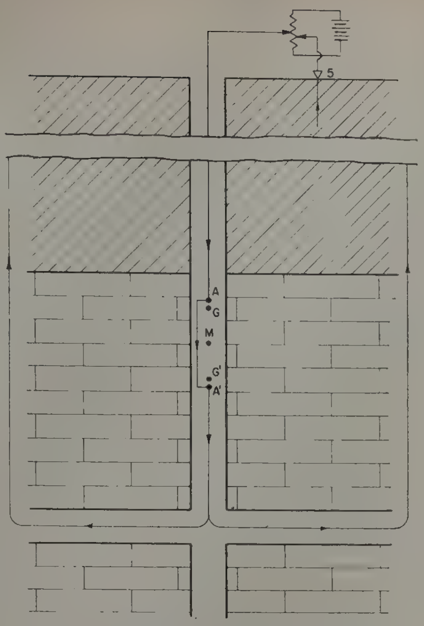

FIG. 3 — ELECTRODE SYSTEM OPPOSITE HIGHLY RESISTIVE FORMATION.

The boundaries of the recorded peak are situated at a distance from the boundaries of the layer equal to $\frac{GG'}{2}$: the width of the deflection is therefore equal to the thickness of the bed plus G-G′, i.e., plus approximately the over-all length of the device. Moreover, it can be demonstrated that in the case of a thin bed, enclosed in highly resistive formations, the peak has a triangular shape, the apex of the triangle being located in the center plane of the bed.

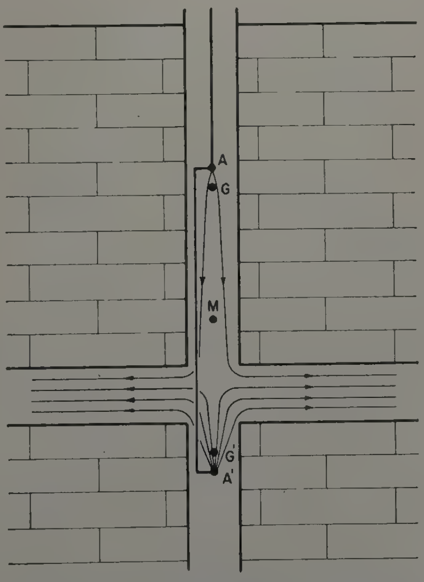

FIG. 4 — ELECTRODE SYSTEM OPPOSITE A THIN PERMEABLE BED COMPRISED BETWEEN HIGHLY RESISTIVE FORMATIONS.

(c) When the device is opposite a thick permeable bed, a plateau is obtained and the width of the deflection is still equal to the bed thickness plus the over-all spacing.

(d) When the device is opposite a thin shale bed encased between highly resistive formations, the potential in the mud, around G-G′, is made equal to the static SP of shales. By definition, this static SP is the potential which would be observed in the mud at the level of the shale bed, if the SP current were prevented from flowing. If any current flowed along the shale bed and the hole close to the bed, the potential at G-G′ could not be, therefore, equal to the static SP of the shales. The fact that the potential of G-G′ is equal to the static SP of shale implies, therefore, that no current flows in the thin shale bed.

Consequently, there is no ohmic potential drop in the mud, between G-G′ and M, and the potential at M is equal to the potential at G-G′, so that the selective SP meter reads zero potential.

Selective SP Curve No. 2 — The Potential at G-G′ Is Equal to the Static SP of Permeable Beds

The reasoning is quite similar to that of the preceding case, and symmetrical results are obtained.

The selective SP log gives zero readings in front of highly resistive formations and permeable beds. Deflections toward the positive sides are observed opposite shale beds. The width of each anomaly is also equal to the bed thickness plus G-G′, and the shape of the peaks, in front of thin shale beds, is triangular.

Conclusion—This analysis shows that the method of the selective SP logging can give the exact location of the conductive streaks interbedded with highly resistive formations, and can distinguish between shales and permeable streaks.

In the usual case where the SP in front of permeable beds is negative with respect to the SP in front of shales, the following pattern is observed, where U designates the potential maintained at electrodes G-G′:

1. If the potential U is kept equal to the static SP of the shales, the curve recorded stays on the zero line in front of the shales and the highly resistive compact formations, and shows sharp peaks toward the negative side in front of the permeable beds.

2. If the potential U is kept equal to the static SP of the permeable beds, the curve recorded stays on the zero line in front of the permeable beds and the highly resistive formations, and shows sharp peaks toward the positive side in front of the shale beds.

This is illustrated in Fig. 5 which shows a schematic cross section, comprising shale beds C_1 and C_5, hard formations H_2, H_4, H_6 and permeable beds P_3 and P_7. The conventional SP log and the selective SP curves recorded for U equal to static SP of shale (V_c) and for U equal to static SP of permeable beds (V_p) are also represented on the chart.

The pattern would be reversed, of course, in the rather exceptional case when the SP in front of permeable beds is positive with respect to the SP in front of shale, which occurs ordinarily when the salinity of the mud is higher than that of the connate water.

Quantitative Data

1. The magnitude of the peak obtained opposite a thin conductive bed, encased between hard formations, can be approximately computed through a simple reasoning.

Referring to Fig. 6-A, the device is shown centered with respect to a thin permeable bed, encased between highly resistive formations.

With the hole diameter and the thickness of the bed being supposed small with respect to A-A′, the resistances in the current path may be considered equivalent to linear resistances as shown in Fig. 6-B.

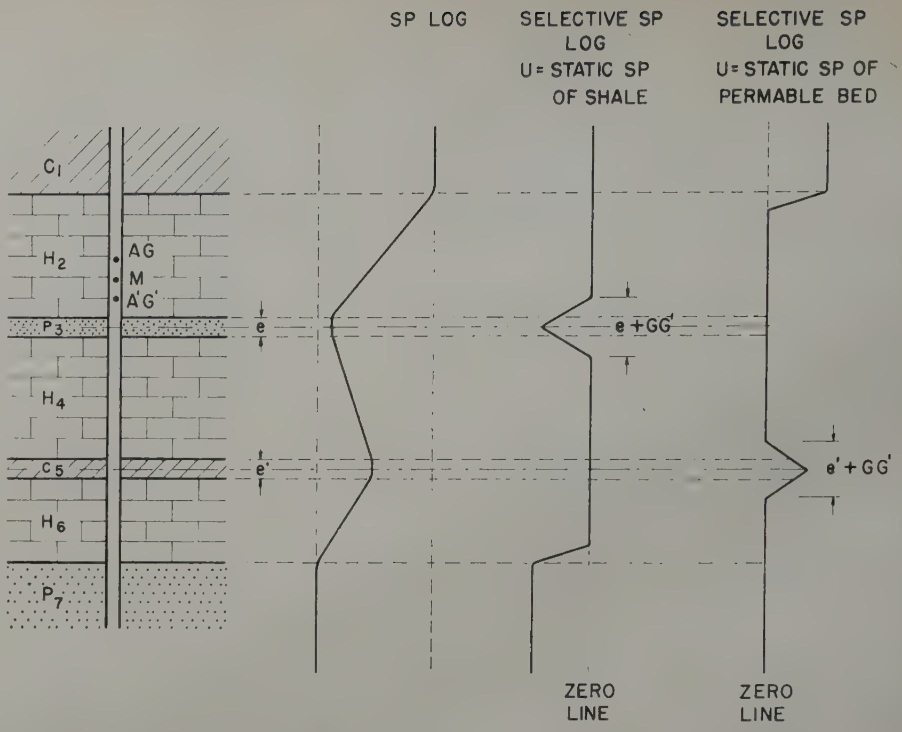
SP LOG
SELECTIVE SP LOG U= STATIC SP OF SHALE
SELECTIVE SP LOG U= STATIC SP OF PERMABLE BED
C1
H2
AG
M
A'G'
P3
e
H4
C5
e'
H6
P7
e +GG'
e'+GG'
ZERO LINE
ZERO LINE

FIG. 5 — SCHEMATIC REPRESENTATION OF SP AND SELECTIVE SP CURVES OPPOSITE CONDUCTIVE BEDS AND HIGHLY RESISTIVE FORMATIONS.

It is further assumed that the potential at G-G′ is kept equal to the static SP of shale.

Let V′ be the potential prevailing at some point N located at a great distance from the bore hole.

Further, let V_c and V_p be the static SP of shales and of permeable beds respectively.

R_o be the resistance between G and M, or G′ and M, along the bore hole.

R_1 be the resistance from the wall of the hole to N through the permeable bed and its surrounding formations.

Σ the sum of the electromotive forces occurring between the mud in front of the bed and N, and represented on Fig. 6-B by the conventional symbol of a battery.

i the intensity of the current circulating in the permeable bed.

The difference of the potentials between the mud around G-G′ and N is equal to the ohmic drop of potential due to the circulation of the current in the mud and in the bed, minus the total of the emf occurring along its path, which can be expressed through the equation:

$$V_c - V' = i\left(\frac{R_o}{2} + R_1\right) - \Sigma \quad . \quad (1)$$

If the current were prevented from flowing, the potential of the mud in front of the permeable bed would, by definition, be equal to the static SP of the permeable bed (V_p) and relation (1) would reduce to:

$$V_p - V' = -\Sigma \quad . \quad . \quad . \quad . \quad . \quad . \quad . \quad (2)$$

Combining (1) and (2),

$$V_p - V_c = -i\left(\frac{R_o}{2} + R_1\right)$$

The difference of potentials between M and G-G′ is equal and of opposite sign to the ohmic drop of the current in the same interval, namely:

$$-i\frac{R_o}{2}$$

The deflection ΔV of the selective SP curve is, therefore, given by the following expression:

$$\Delta V_1 = -i\frac{R_o}{2} = (V_p - V_c)\frac{R_o}{2R_1 + R_o} \quad . \quad . \quad . \quad . \quad . \quad . \quad . \quad . \quad (3)$$

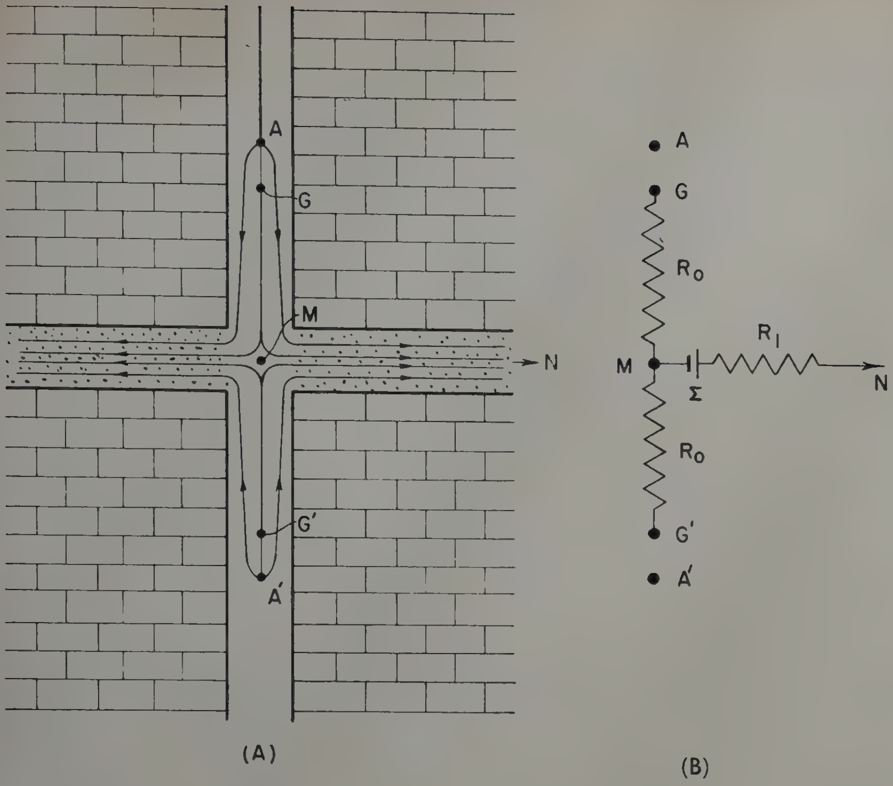

(A) (B)

FIG. 6 — SCHEMATIC DISTRIBUTION OF THE CURRENT AT THE LEVEL OF A THIN PERMEABLE BED AND EQUIVALENT LINEAR RESISTANCE NETWORK.

Quite a similar reasoning would show that if the potential at G-G′ is taken equal to the static SP of permeable beds, the selective SP in front of thin shale beds, situated within highly resistive strata, is given by:

$$\triangle V_2 = (V_c - V_p)\,\frac{R_o}{2R_1 + R_o} \quad . \quad (4)$$

The following conclusions can be deduced:

(a) The deflections of the selective SP log are proportional to the magnitude of the static SP of permeable beds with respect to that of shales, or vice versa.

(b) R_o is proportional to the spacing, and to the mud resistivity, and is inversely proportional to the sectional area of the hole.

Consequently, it might seem advisable to take G-G′ as great as possible so as to obtain the best possible contrast. But the spacing cannot, however, be exaggerated, lest the width of the peak be too large, and permeable beds at short distances from one another be not clearly separated. A spacing between G and G′ of sixty to eighty inches has been found satisfactory for field practice.

In the case where the salinity of the mud is very high, R_o is very small and the peaks of selective SP become also very small.

(c) R_1 has been calculated with good enough approximation. Using the following notations:

e is the thickness of the bed

d is the diameter of the hole

R_t is the resistivity of the bed

R_s is the resistivity of the adjacent formation

the value of R_1 is given by the formula:

$$R_1 = \propto \frac{R_t}{d}$$

the coefficient $\propto$ of which is given in the table below as a function of e, d. R_t and R_s.

	Rs/Rt					
e/d	0.5	1	2	3	4	5
10	0.70	0.41	0.25	0.18	0.14	0.11
20	0.92	0.52	0.30	0.21	0.17	0.13
50	1.20	0.65	0.37	0.26	0.20	0.16
100	1.4	0.77	0.42	0.29	0.23	0.18
200	1.63	0.87	0.47	0.33	0.25	0.20
500	1.97	1.02	0.55	0.38	0.29	0.23
1000	2.13	1.13	0.60	0.42	0.32	0.25

Computed example — Fig. 7 shows a schematic sequence of thick shales C_1, C_7, thick and resistive strata H_2, H_4, H_6 and thin permeable beds P_3 and P_5. The selective SP curve has been computed for the case of the potential at G-G′ being equal to the static SP of shales. The conventional SP curve has been also approximately computed and is traced on the chart for comparison.

CASE WHEN ALL THE PERMEABLE BEDS AND ALL THE SHALES DO NOT HAVE RESPECTIVELY THE SAME STATIC SP's

It often occurs that the static SP's of the permeable beds encountered in a bore hole are not the same. For example, the salinities of the interstitial waters may be different, so that the total SP emf's and, consequently, the static SP's, are different. Also, some permeable beds may contain an appreciable amount of shaly material, and show a pseudo-static SP, which is less than the static SP of permeable beds having the same connate water but a negligible content of shale.[1]

It also happens, although much less frequently, that different shale beds show different values of static SP.

In practice, two potentials U_1 and U_2, which are kept constant at electrodes G-G′ for the recording of the two curves, are preferably selected so that U_1 is equal to the most positive of the static SP's of shales, and U_2 to the most negative of the static SP's of permeable beds.

Let V_c and V_p now be respectively the most positive and the most negative static SP's in the section under investigation, and V_{cp} an intermediate value of the static SP, related, for instance, to shaly permeable beds. The deflections of the selective SP curves in front of these last beds will be respectively proportional to $(V_{cp} - V_c)$

and to $(V_{cp} - V_p)$ according to whether U is chosen equal to V_c or to V_p. The peak recorded is towards the negative side of the log in the first case, and towards the positive side in the second case.

Under these conditions, if it is supposed that all the conductive beds have approximately the same thickness and the same resistivity, the selective SP log will have the following features, on the average:

(1) Selective SP Curve No. 1—With U_1 being equal to V_c, that is, to the most positive of the static SP's, all permeable beds will give negative peaks, the greatest peaks being observed in front of the beds where the static SP is the most negative. Permeable beds with formation water of lower salinity, or with shale content, i.e., with a less negative static SP, will give smaller deflections. In general, all the shale beds will correspond to zero reading, because the static SP's of shales are practically equal. Quite exceptionally, however, some shale beds, whose static SP is less than V_c can give a negative deflection.

(2) Selective SP Curve No. 2—With U_2 being equal to V_p, that is, to the most negative of the static SP's, all shales will give positive peaks. The permeable beds, whose static SP is equal to V_p will correspond to zero reading, and the permeable beds, with a static SP less negative than V_p, will show positive peaks, but of lesser magnitude than shales.

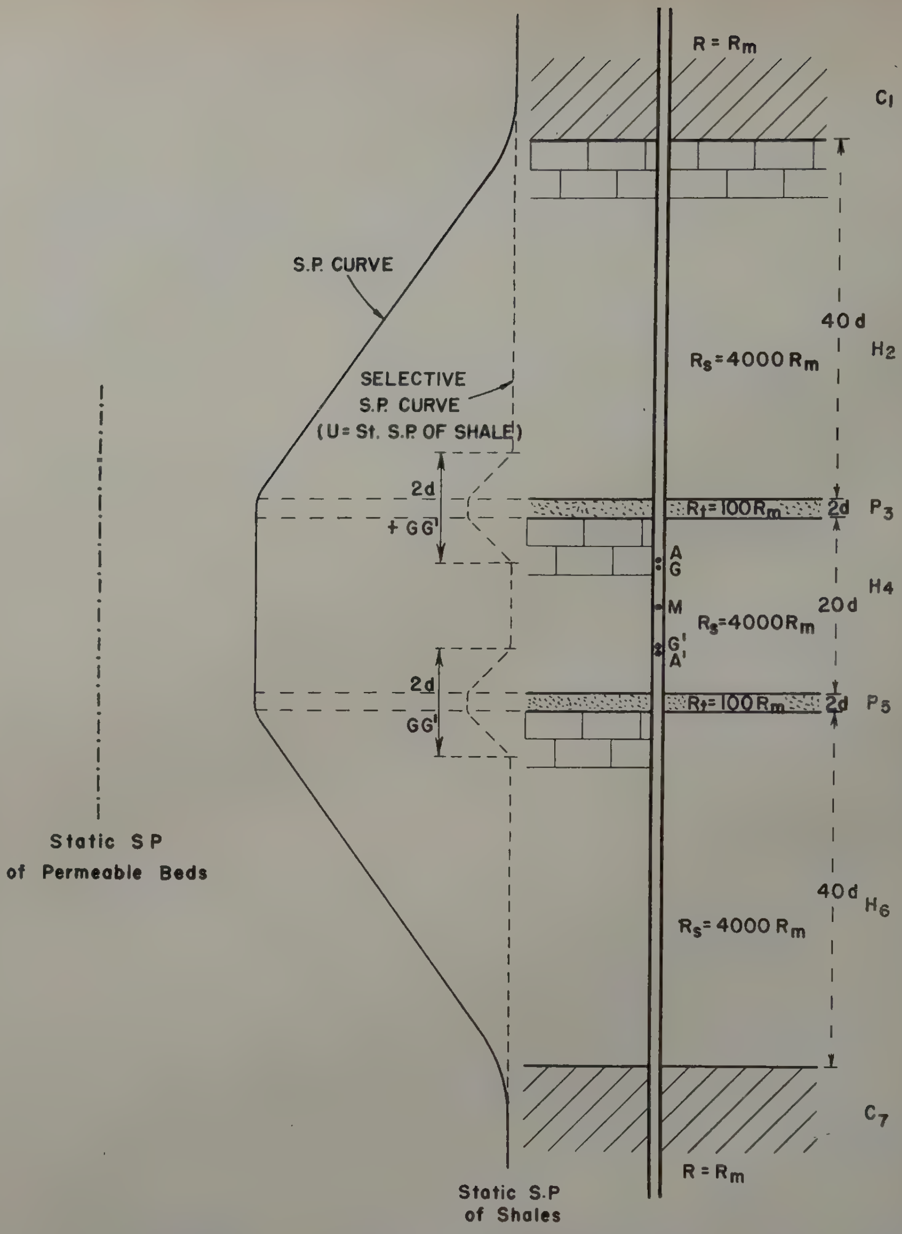

FIG. 7 — COMPUTED SP CURVE AND SELECTIVE SP CURVE OPPOSITE CONDUCTIVE BEDS AND HIGHLY RESISTIVE FORMATIONS.

REMARK REGARDING THE ADJUSTMENT OF THE POTENTIALS U_1 AND U_2

It is not always possible to find among the formations to be investigated thick enough shale beds or permeable beds such that the static SP of each can be accurately determined from the conventional SP log. It is, nevertheless, possible to determine the desired values for the potentials U_1 and U_2 by locating the device successively in front of a thin shale and of a thin permeable bed, provided, however, that each of these beds be comprised between highly resistive formations. The monitoring current is then adjusted in each case so as to bring the reading of the potential difference between M and G-G′ equal to zero. The potential at G-G′ is thus brought to a value equal to the static SP in front of the selected bed and can thereafter be maintained by monitoring at the value thus determined.

Such an adjustment, however, is not always easy to carry out because thin shale beds or thin permeable beds do not always appear clearly on the conventional logs. It results that, in practice, the values chosen for U_1 and U_2 are sometimes not exactly as they should be.

If it is supposed, for example, that U_1 is taken greater than V_c, and U_2 lower than V_p, both shales and permeable beds will give negative peaks on the first curve, and positive peaks on the second one. The distinction between shales and permeable beds by direct reading of the selective SP curves becomes difficult in this case.

Fortunately, it is always possible to deduce accurate conclusions from the selective SP logs, even if U_1 and U_2 were not suitably adjusted, by means of a simple computation method by which a static SP log can be derived from the selective SP curves, as explained hereafter.

COMPUTATION OF THE STATIC SP LOG FROM THE CURVES OF SELECTIVE SP

The above formulae (3) and (4) can be easily generalized. It can be shown that the magnitude of the deflection of a selective SP curve in front of a thin conductive bed enclosed in highly resistive formations is given by:

$$\triangle V = (V - U)\frac{R_o}{2R_1 + R_o} \quad . \quad . \quad (5)$$

where V is the static SP of the bed and U the potential maintained at G-G′, both being related to the same reference potential. It appears from this equation that, as already stated, when $\triangle V$ is equal to zero, in front of a conductive bed, the potential at G-G′ is equal to the static SP of the bed.

Supposing now that U_1 and U_2 are the two potentials at G-G′ during the recording of two selective SP curves No. 1 and No. 2, and that $\triangle V_1$ and $\triangle V_2$ are the corresponding values of the selective SP, it follows:

$$\triangle V_1 = (V - U_1)\frac{R_o}{2R_1 + R_o}$$

$$\triangle V_2 = (V - U_2)\frac{R_o}{2R_1 + R_o}$$

hence

$$V = U_1 - (U_2 - U_1)\frac{\triangle V_1}{\triangle V_2 - \triangle V_1} \quad . \quad (6)$$

If U_1, for example, is arbitrarily taken as reference potential, the equation simplifies as follows:

$$V = U_2\frac{\triangle V_1}{\triangle V_1 - \triangle V_2} \quad . \quad . \quad . \quad . \quad (7)$$

This equation shows that the value of the static SP can be deduced, at each depth, by a very simple proportionality rule, using the two curves of the selective SP log.

It is worthwhile to stress that the values computed for V are independent of the respective values of U_1 and U_2. In other words, the static SP can be computed even when the values U_1 and and U_2 have been so poorly chosen that the selective SP log is difficult to read directly.

The values of V, plotted in terms of depth, enable one to trace a curve which is the "static SP log." This curve can also be directly recorded, by means of a proper arrangement of the circuit. The explanation of this process is given in a later section.

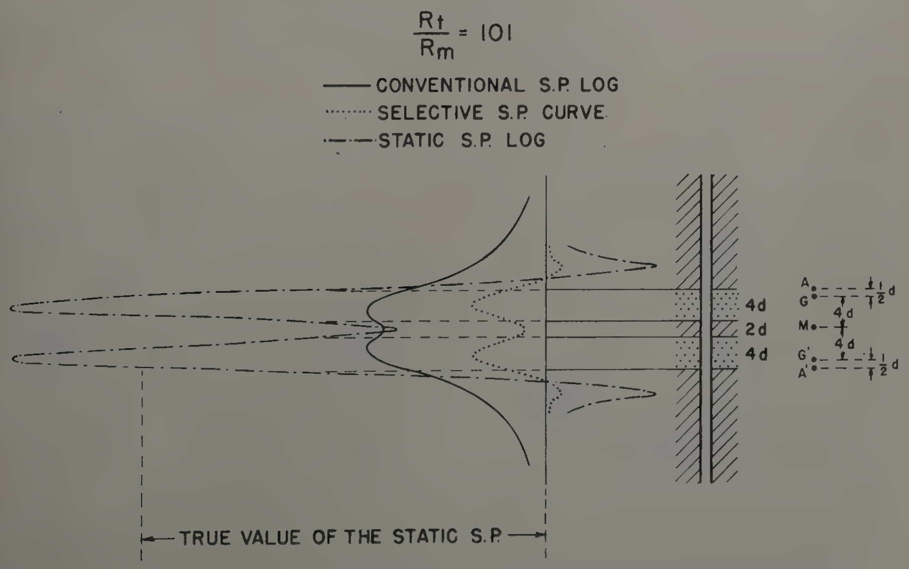

FIG. 8 — COMPUTED SP CURVE, SELECTIVE SP CURVE AND STATIC SP CURVE OPPOSITE A SEQUENCE OF CONDUCTIVE IMPERVIOUS AND PERMEABLE BEDS.

ESSENTIAL FEATURES OF THE STATIC SP CURVE

(a) In the general case, where the connate water of the permeable beds is more saline than the mud, the static SP log shows deflections towards the negative side in front of permeable formations, and deflections towards the positive side in front of shales. The indications are reversed in the exceptional case when the mud is more saline than the formation waters. An accurate record of the conductive beds inside highly resistive formations is obtained, and the distinction between permeable beds and shales is improved, even when the interpretation of the selective SP log is not easy at first glance.

(b) When the conductive beds under investigation are encased within compact formations, the amplitude of the deflections of the static SP log gives the true value of the static SP of these formations.

This second result, however, is not always completely obtained in practice. As shown above, the amplitude of the deflections of the selective SP is inversely proportional to the average resistivity of the formations surrounding the electrode system. When this resistivity is high, which often occurs, the deflections of the selective SP curves are very small and the smaller the deflections, the greater the graphical relative error in their determination. The value of the static SP deduced from the proportionality rule may, therefore, not be absolutely accurate in that case. The error is still greater if a certain drift occurred in the zero line as a consequence of the instability of the electrodes.

DIRECT RECORDING OF THE STATIC SP LOG

If the electrode system is placed in front of a thin conductive bed, included within highly resistive formations and if no current is sent through A-A′, a certain difference of potential occurs between M and G-G′. The potential at M, for example, is negative with respect to the potential at G-G′.

If a current is sent through A-A′, such that the potentials at M and G-G′ are made more negative, the potential at M is less modified than the potential at G-G′. The potential difference between M and G-G′ decreases, and the current can be adjusted until this difference becomes equal to zero. At this moment, both M and G-G′ are brought to the same negative potential which is equal to the static SP of the bed. The same process would take place, of course, if the original potential at M, before sending any current, were positive with respect to the potential at G-G′.

If the device is located opposite a thick conductive bed, the potentials at M and G-G′ are, evidently, both equal to the static SP of the bed, without any current being sent through A-A′.

The procedure for the recording of the static SP, therefore, consists in adjusting the monitoring current so that the potential difference between M and G-G′ be kept equal to zero when the electrode device is moved along the hole, and in recording the common potential at M and G-G′ versus depth.

This procedure is theoretically strictly equivalent to that which consists in deriving the static SP log from the selective SP curves by means of the proportionality rule, as already explained. In practice, however, and inasmuch as the techniques of application are different for each of these procedures, the errors in the values obtained for the static SP are not always the same, and some discrepancies may be observed between the recorded and computed static SP logs.

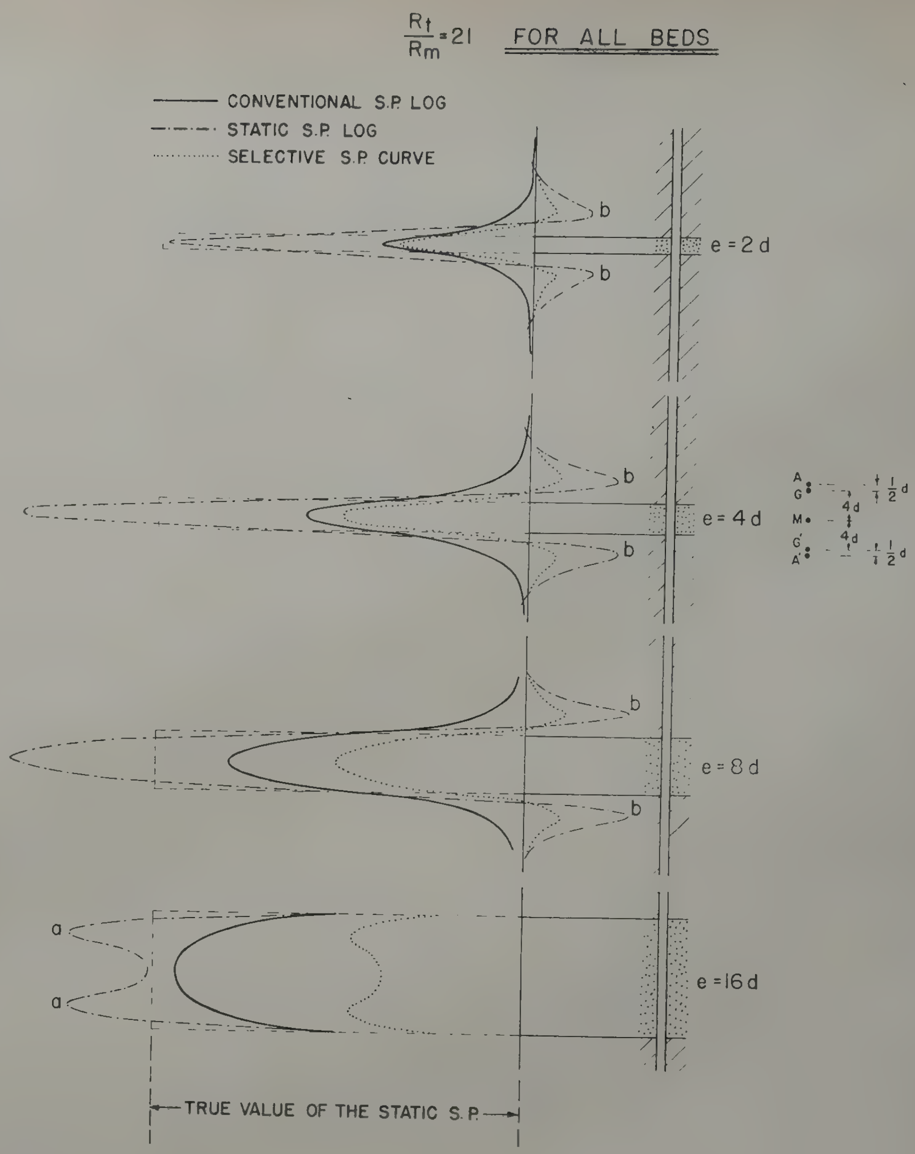

FIG. 9 — COMPUTED SP, SELECTIVE SP AND STATIC SP CURVES OPPOSITE A PERMEABLE BED COMPRISED BETWEEN CONDUCTIVE FORMATIONS.

CASE OF PERMEABLE BEDS SITUATED BETWEEN CONDUCTIVE FORMATIONS

The application of the new method has been described so far only for the case of conductive streaks interbedded in highly resistive formations. In the case of moderately resistive formations, such as sequences of shales and sands and, more generally, in the case of permeable beds bounded by conductive formations, the characteristics of the selective SP log and of the static SP log are somewhat different. The essential features of the logs in this case are reviewed below:

1. The selective SP and the static SP logs, on the average, show sharper breaks at the level of the boundaries of the beds than the conventional SP log. In Fig. 8 are shown, as an example, the conventional SP curve, the selective SP curve for U equal to the static SP of shales, and the static SP curve, computed for the case of two camparatively thin permeable beds, located within conductive impervious formations.

As shown on the figure, the thickness of each permeable bed is equal to 4 times the hole diameter, that is about 3′ - 4′, and the over-all spacing is equal to 9 times the hole diameter, that is about 7′ - 9′. The resistivity of the permeable bed has been taken equal to that of the surrounding formations, because this condition is one of the few for which mathematical computations are possible.

2. The ability of the new methods to locate thin beds depends on the electrode spacing. If the individual bed

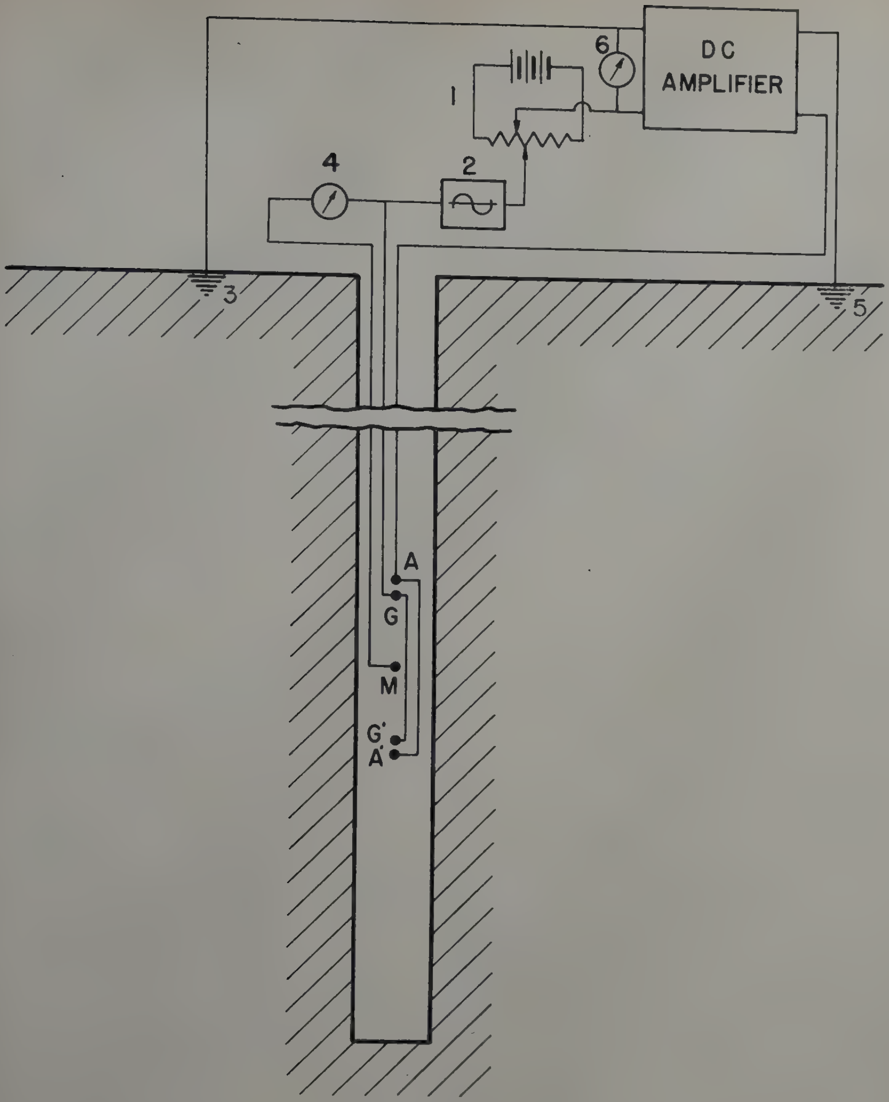

FIG. 10—SCHEMATIC RERESENTATION OF THE ACTUAL CIRCUIT USED FOR RECORDING THE SELECTIVE SP.

thickness in a sequence of permeable and impervious layers is such that too many of them are included within the over-all spacing, it is difficult to differentiate these layers. If the beds are very thin, only one average deflection is obtained and, therefore, the shortest possible spacings seem desirable.

Too short a spacing, however, may give too small deflections of the selective SP curves in front of the different layers, because the influence of the mud is too great. As for the static SP log, it would be theoretically possible to decrease the spacing so that the thinnest individual layers could be differentiated, but the disturbing effect due to zero instability of the equipment is substantially increased for short spacings. In practice, therefore, the electrode spacing should not be reduced under certain limits, lest inadmissible errors be introduced into the measurements. An average spacing, consequently, is applied, which is between 60 and 80 inches.

3. The magnitude of the deflections of the static SP log is a function of the spacing, of the geometrical configuration and of the resistivities of the media surrounding the electrodes.

4. For very thick permeable beds, the magnitude of the deflections of the static SP log from the shale line, gives the static SP with respect to that of shales, as is also the case with the regular SP log. A difference between the magnitude of the deflections and the true value of the static SP begins to appear for comparatively small values of the bed thickness. But, as a rule, this difference is always less than the difference observed from the regular SP log, all other conditions being the same.

This result is illustrated by Fig. 9, which shows the conventional SP curve, the selective SP curve for a monitoring potential U equal to the static SP of shales, and permeable beds of different thicknesses (e) ranging from 2 hole diameters (2d) to 16 hole diameters (16d). The beds are supposed included between impervious formations of same resistivity, equal to 21 times that of the mud.

In the present example, if the shale line is taken as the reference line, it appears that the deflection of the static SP log is almost equal to the true value of the static SP of the permeable beds for e equal to 2d, whereas the conventional SP curve gives a much smaller deflection. For e equal to 4d and to 8d, the deflection of the static SP log becomes greater than the true static SP, whereas the conventional SP deflection is smaller. For e equal to 16d, the shape of the static SP curve is more complicated. Instead of one single peak, the curve shows a central depression bounded by two symmetrical peaks (a) respectively below and above the upper and the lower boundary. The magnitude of the deflection at the level of the depression is approximately equal to the static SP.

A similar shape would be obtained for thicker layers; the curve would show a plateau corresponding to the true static SP, and two accessory peaks would occur at both boundaries of the bed.

It should also be mentioned that sharp depressions (b) are observed slightly above and below the boundaries of the beds, whatever the thickness of the bed.

These accessory peaks and depressions, such as (a) and (b), appear on the log when the electrode device crosses the boundaries between two different beds, and, for that reason, are designated under the general term of boundary effects.

APPLICATION OF THE STATIC SP LOG

Besides its application for the location of the boundaries of permeable beds inside highly resistive formations, the static SP log can be used for a closer determination of the true value of the static SP, wherever the convention Sp log fails to give it with close enough approximation, as, in particular, in the case of thin beds. This last feature is interesting, because the static SP of permeable beds is one of the elements used for the tentative evaluation of the saturation of reservoirs, as already mentioned in the introduction of the present paper.

It should be recalled that the static SP is a sum of emf's which are a function of different characteristics of the strata, such as salinity of the connate water, for example, but which are by no means connected directly with the value of the permeability, measured in millidarcys.[1]

FIELD TECHNIQUE

1. In field practice, instead of recording successively two selective SP curves with two different values U_1 and U_2 of the potential at G-G′, the same result is obtained more conveniently in only one run. To this effect, the potential at G-G′ is made periodically variable between two limits respectively equal to U_1 and U_2, and one single curve is recorded with only one galvanometer. The vibrated curve thus recorded is bounded by two envelopes, which are respectively identical to the curves which would be obtained if the potential at G-G′ were kept constant and equal to U_1 or to U_2.

2. The potential at G-G′ for selective SP logging, or the difference of potentials between M and G-G′ for static SP logging, are controlled automatically by means of a special DC amplifier.

3. For recording the selective SP (Fig. 10), one terminal of the input circuit of the amplifier is connected to electrodes G-G′, and the other terminal to the surface electrode (3). The input circuit further contains a potentiometer (1) and a generator of low frequency alternating emf (2). The output terminals are connected respectively to A-A′ and to the surface electrode (5). The meter (4) is used to record the selective SP and the meter (6) to control the accuracy of the monitoring.

4. For recording the static SP, the same amplifier is used, but the circuit is different (Fig. 11). The input terminals are connected respectively to the electrodes M and G-G′ and the output terminals to A-A′ and to the surface electrode (5). According to the design of the DC amplifier, when a difference of potential appears in the input circuit, a current is sent through the output circuit, and this current tends to bring this difference of potential between G-G′ and M back to zero. The potential difference between M and G-G′ is, therefore, automatically main-

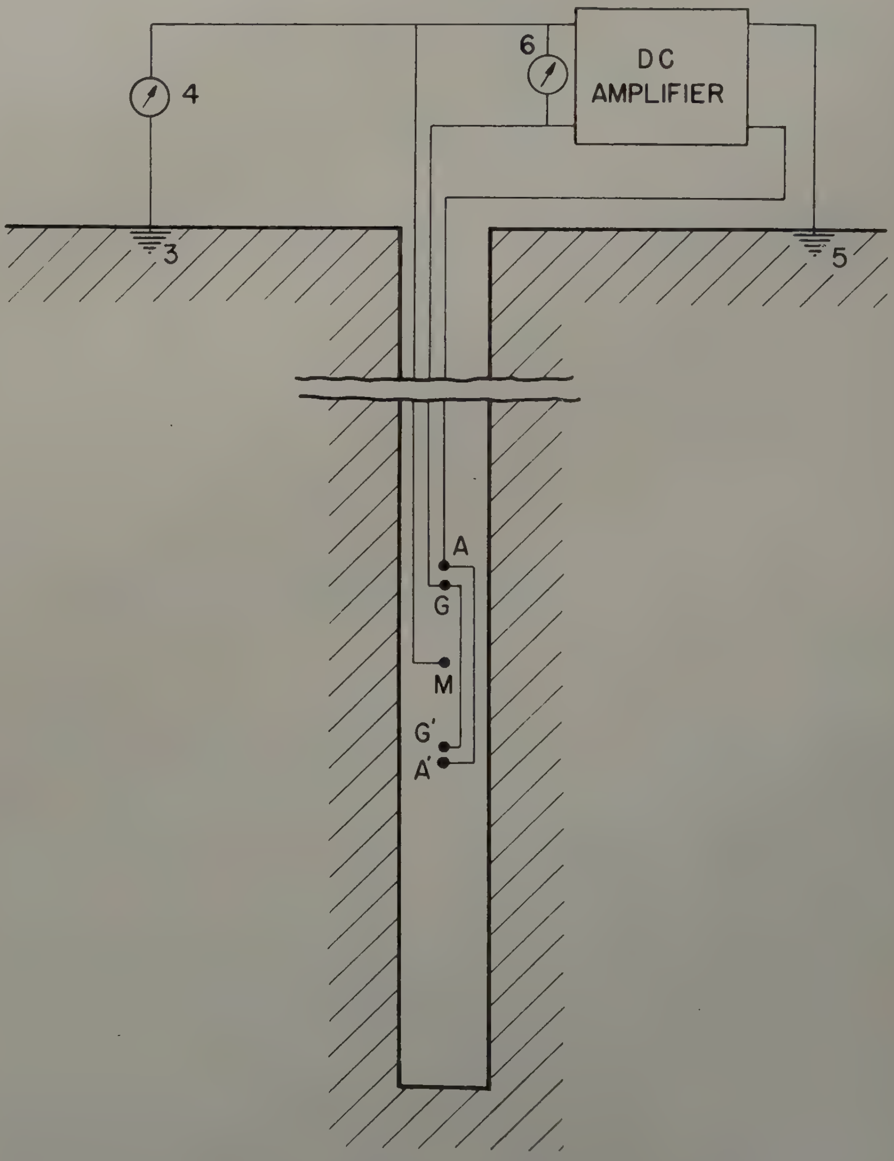

FIG. 11 — SCHEMATIC REPRESENTATION OF THE ACTUAL CIRCUIT USED FOR RECORDING THE STATIC SP.

tained equal to zero, or very near to it, and the resulting potential at M and G-G′ is recorded by means of meter (4). The curve thus recorded is the static SP log.

FIELD EXAMPLES

Fig. 12 is an example of a selective SP log recorded under rather favorable conditions, opposite limestone formations. The regular resistivity and SP logs are reproduced on the same chart.

Several depressions corresponding to conductive beds are noticeable on the resistivity log, and particularly on the curve recorded with the so-called "limestone device." Some of these depressions correspond to curvatures in the SP log, but the determination of the exact location of the boundaries of the beds, and the differentiation between permeable and impervious beds, are not always easy from the regular curves.

The selective SP log comprises two curves; the left-hand curve (selective SP Curve No. 1) corresponds to a potential at G-G′ practically equal to the static SP of shale, and the right-hand curve (selective SP Curve No. 2) to a potential at G-G′ which is not much different from the static SP of permeable beds.

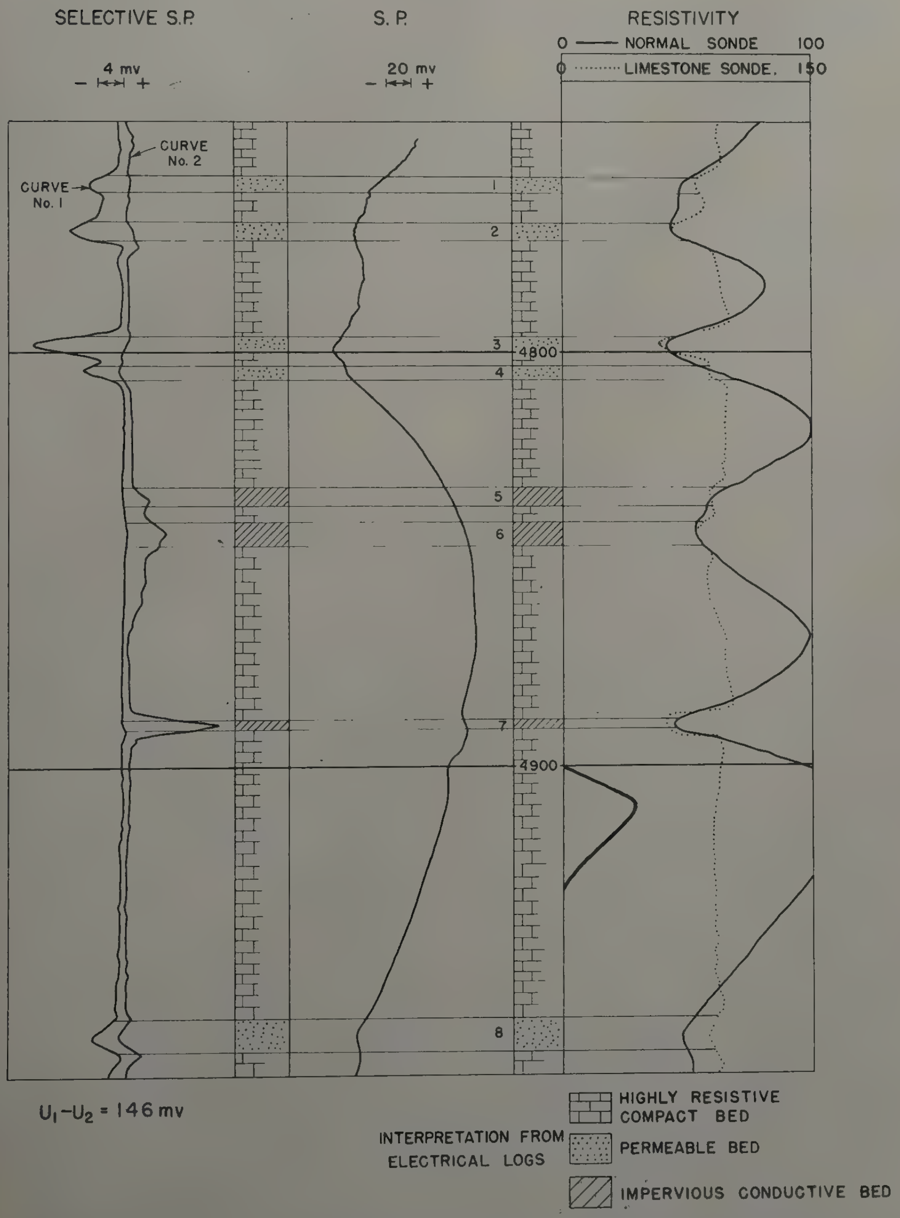

FIG. 12 — SELECTIVE SP, SP AND RESISTIVITY LOGS OPPOSITE LIMESTONE FORMATIONS.

It appears that at many levels both curves are very close to the zero line, which is characteristic of extremely resistive formations. The greatest part of the section, therefore is made of compact beds. Several sharp peaks appear, however, on either curve: the peaks towards the negative side are noticed only on Curve No. 1, whereas Curve No. 2 shows practically no deflections at the same levels. This feature is definitely indicative of permeable beds according to the schematic diagram shown in Fig. 5. Such peaks are numbered 1, 2, 3, 4, 8 on the drawing.

The peaks towards the positive side, conversely, exist only on Curve 2, and correspond to practically no deflection on Curve No. 1. This indicates conductive impervious beds, numbered 5, 6, 7 on the drawing.

All the deflections, either negative or positive, are sharp enough for the boundaries of the different beds to be determined with reasonable accuracy, the influence of the spacing being, of course, taken into account.

For the survey which is the matter of the present example the potentials U_1 and U_2 at G-G′, used respectively for curves No. 1 and No. 2, could be adjusted very close to V_c and V_p, which makes the interpretation unequivocal. The interpretation is furthermore remarkably easy, in this particular instance, because the conductive beds are few and clearly separated from one another by thick and definitely hard formations.

It was thought superfluous to compute the static SP log, which would not add anything to the data already recognizable on the chart, as far as the location of the conductive beds is concerned. The value of the static SP in front of each conductive bed can, however, readily be obtained in this case. At the level of permeable beds 1,

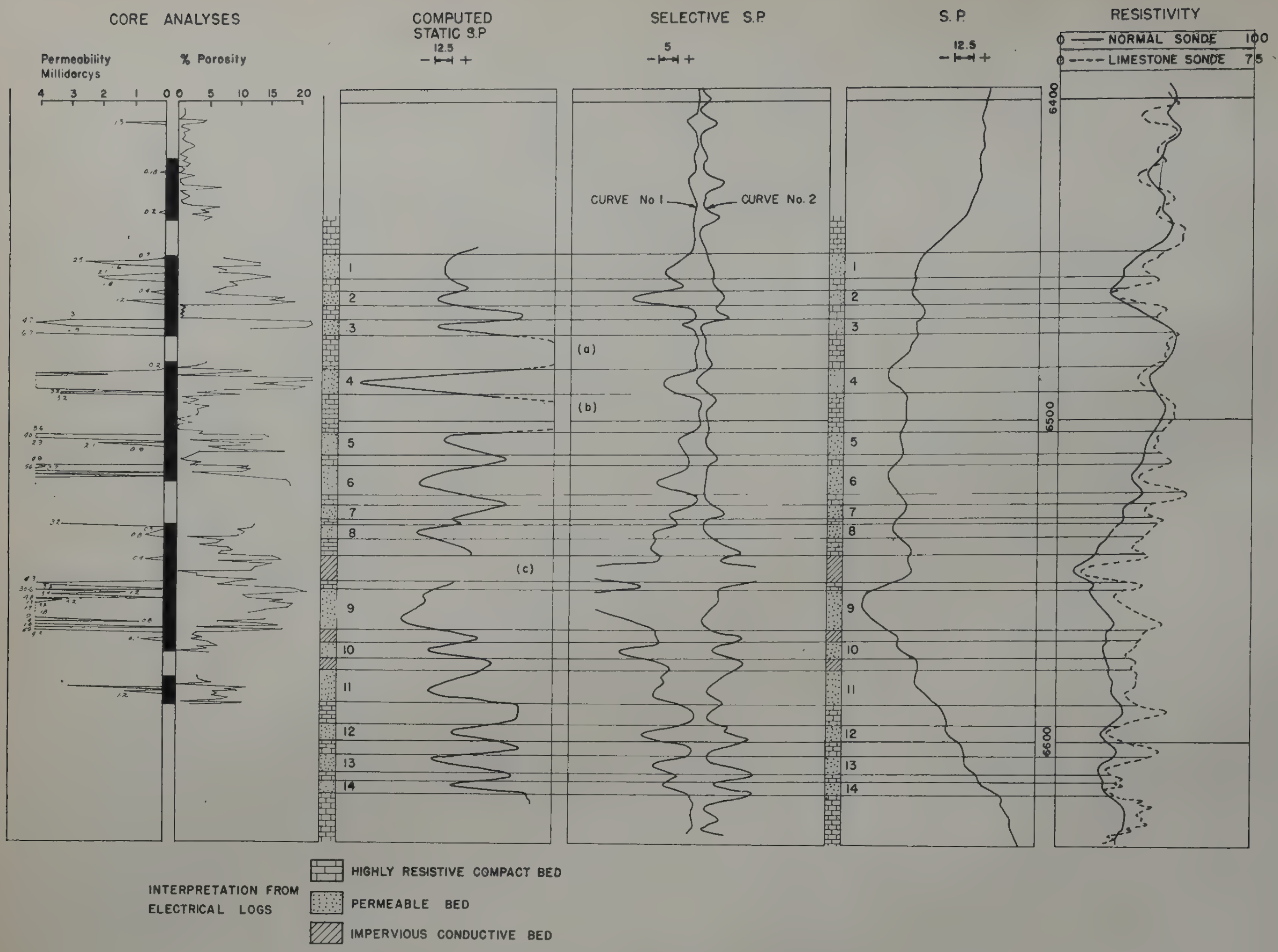

FIG. 13 — AN EXAMPLE OF AN IMPERFECT CHOICE OF THE POTENTIALS U_1 AND U_2.

2, 3, 4, Curve No. 2 gives practically no deflection, which means that the static SP of these beds is equal to the potential U_2 prevailing at G-G′ when Curve No. 2 was recorded. In the same way, the static SP of shale beds 5, 6, 7 is equal to the potential U_1 prevailing at G-G′ when the Curve No. 1 was recorded. The static SP of the permeable beds with respect to shales is, therefore, equal to $(U_1 - U_2)$, which itself can be read from the calibration of the monitoring equipment, namely, 146 mv, in the present instance.

Fig. 13 on the contrary, is an example of an imperfect choice of the potentials U_1 and U_2. This example is provided, however, because data of core analyses, regarding porosity and permeability, were available in the bore hole under survey, and could be compared with the results of the interpretation of the electrical logs.

Inasmuch as U_1 and U_2 were not adjusted correctly in this case, both selective SP curves No. 1 and No. 2 give deflections at the level of permeable beds and shale beds, so that the interpretation is not readily possible as in the preceding example.

The question is clarified by means of the static SP curve, which has been deduced from the selective SP curves by computation. Inasmuch as the value of the static SP cannot be accurately computed when the deflection of the selective SP log is very small, that is in front of compact highly resistive formations, the curve has been traced in dots along the corresponding intervals such as (a) and (b). Also, the selective SP curves go off scale at the level (c), and the corresponding value of the static SP cannot be determined: the computed curve is interrupted accordingly.

Generally, all the permeable streaks are marked by clear negative deflections on the static SP log. The interpretation is confirmed by the results of core analysis. Although the permeability record is not complete, the data plotted on the chart are nevertheless numerous enough to illustrate the conformity between the electrical interpretation and the laboratory results on cores, at the depths where both are available for comparison.

Fig. 14 is an example which shows a sequence of resistive permeable beds interbedded in conductive impervious formations.

The static SP curve has been both directly recorded and derived from the selective SP curves by computation. It may be observed in the chart that the two static SP curves coincide closely, except for the interval A-B. In this interval, the resistivity of the surrounding formation is very high, and the deflection of the selective SP curves is consequently very small, so that not only the possible shifts in the zero line, but also the graphical errors may result in important differences in the value computed for the static SP. The section of the computed curve between A and B cannot, therefore, be considered as reliable and has been reproduced in dots.

The boundaries of the different beds are marked by sharp breaks of the static SP log, whereas the corresponding deflections of the conventional SP log are very smooth. In this particular instance, the values of U_1 and U_2 for the recording of the selective SP curves were taken equal respectively to the static SP of shale bed (4) and of the permeable stratum (7). The difference $U_2 - U_1$ was equal to about 110 mv. The difference between the deflection of the static SP log opposite beds (1) and (2) gives, of course, the same value. But it is worth mentioning that permeable beds of moderate thicknesses, such as (3) and (7), show deflections on the static SP log which, although less than 110 mv, are nevertheless larger than the corresponding peaks on the regular SP log.

Attention is called also to sharp peaks, such as a_1, a_2, a_3, a_4 . . . , very close to the boundaries of the permeable beds, which are very likely "boundary effects," as described in the theoretical diagram of Fig. 9.

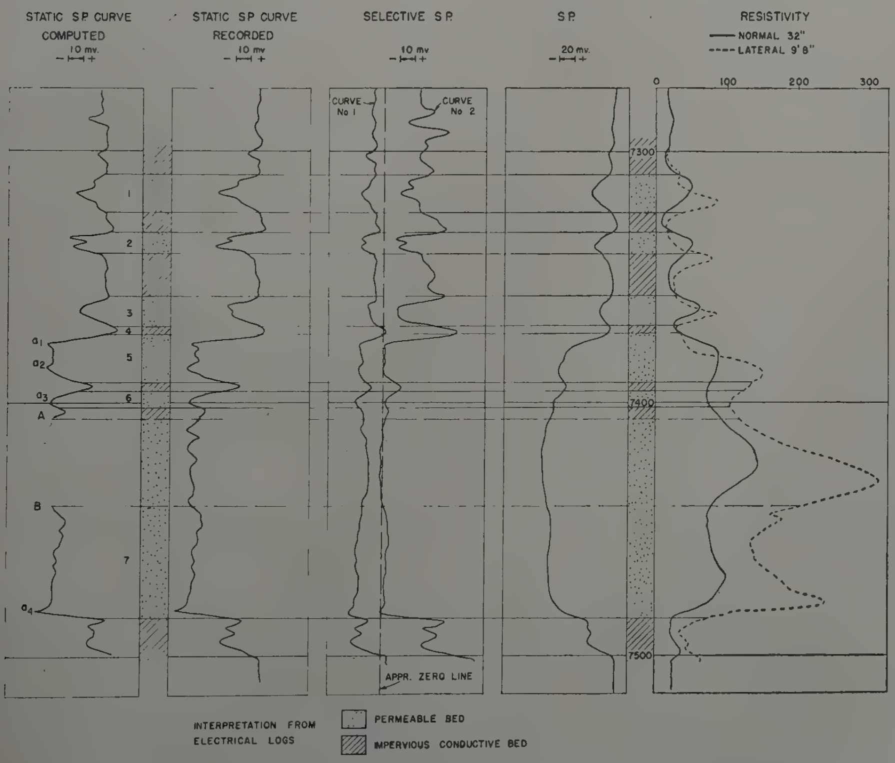

FIG. 14 — A SEQUENCE OF RESISTIVE BEDS INTERBEDDED IN CONDUCTIVE IMPERVIOUS FORMATIONS.

CONCLUSION

Until recently, the conventional methods of electrical logging have provided less information for the investigation of limestone fields than for the sequences of formations such as sands and shales.

The new methods of selective SP logging, and of static SP logging, which are now under development, promise a substantial improvement in the detection of the permeable strata located inside highly resistive formations, which are commonly found in limestone fields.

The new methods discussed in the present paper, under favorable conditions, can also determine the static SP of permeable formations, and should, therefore, prove useful wherever a quantitative value of the static SP is desired.

Several studies are under way to improve the equipment, but, even in the present stage of development, field results show that the new methods, although somewhat difficult in technique, should provide reliable interpretative data.

ACKNOWLEDGMENT

The author wishes to acknowledge the very important work done by M. Martin in the preparation of the paper. He would like to mention specially the outstanding contribution of J. Bricaud, who had the responsibility of developing the equipment and of working out all the details of the field technique. In addition credit should be given to W. C. Welz who designed the DC amplifier. The author wishes to show his appreciation to J. Bodin and R. Sauvage, who conducted the field experiments and discussed the results, and to J. K. Hallenburg for his assistance in these experiments. Acknowledgments are also due to the oil companies for their courtesy in making examples available.

REFERENCES

1. H. G. Doll: "The SP Log: Theoretical Analysis and Principles of Interpretation." *Trans.* AIME, Petroleum Branch, Vol. 179, page 146.
2. M. Martin, G. H. Murray and W. J. Gillingham: "Determination of the Potential Productivity of Oil-Bearing Formations by Resistivity Measurements." *Geophysics*, Vol. 3, July, 1938, page 258 ff.
3. G. E. Archie: "The Electrical Resistivity Log as an Aid in Determining Some Reservoir Characteristics." *Trans.* AIME, Vol. 146 (Petroleum Division), 1942 and 1943, page 54 ff.
4. C. and M. Schlumberger and E. G. Leonardon: "A New Contribution to Subsurface Studies by Means of Electrical Measurements in Drill Holes." *Trans.* AIME, Vol. 110 (Geophysical Prospecting), 1934, page 273 ff.
5. M. R. J. Wyllie: "A Quantitative Analysis of the Electrochemical Component of the SP Curve." *Jnl. Petr. Tech.*, Vol. 1, No. 1, January, 1949, p. 17 ff.
6. M. R. J. Wyllie: "A Statistical Study of the Accuracy of Some Connate Water Resistivity Determinations Made from SP Log Data." AAPG Meeting, St. Louis, March, 1949.
7. H. W. Patnode: "Relationship of Drilling Mud Resistivity to Mud Filtrate Resistivity." *Jnl. Petr. Tech.*, Vol. 1, No. 1, January, 1949, p. 14 ff.
8. M. P. Tixier: "Electric Log Analysis in the Rocky Mountains." *Oil and Gas Jnl.*, Vol. 48, No. 7, June 23, 1949, p. 143 ff.

★ ★ ★

T.P. 2853

AN ELECTRONIC ANALOG COMPUTER FOR SOLVING THE FLASH VAPORIZATION EQUILIBRIUM EQUATION

F. W. BUBB, WASHINGTON UNIVERSITY, ST. LOUIS, MISSOURI, **R. G. NISLE** and **P. G. CARPENTER,** MEMBER AIME,
PHILLIPS PETROLEUM CO., BARTLESVILLE, OKLAHOMA

SUMMARY

It is the purpose of this paper to describe an electrical computer which has been constructed to solve the equations for vapor-liquid equilibrium in multi-component systems. The instrument consists of seven component-computing units each with proper indicating means and power supplies. Each unit is a resistance network with a voltage matching servomechanism, and each provides an output voltage proportional to the mol-fractions for vapor and liquid phases. These voltages are summed and matched with a reference voltage to provide the solutions. Any reasonable number of such units may be put together to make a computer. The theory and operation of the computer is discussed. A number of applications and examples of computer results are given. The computer yields the over-all vapor or liquid fraction to a probable error of 0.002. An interpolation method is described which reduces the probable error to 0.0002.

INTRODUCTION

The process known as Flash Vaporization may be described as follows: A mixture of known composition of relatively volatile components is allowed to come to thermodynamic equilibrium at some given temperature and pressure by any path whatsoever. In general, a vapor and a liquid phase will be present at equilbrium. The problem is to determine the fractions of the mixture in the vapor and liquid phases, and to determine the mol fractions of the various components in each phase. The relations that exist between these various quantities at equilibrium are well known and will be given later. These equations are difficult to solve, yielding only to trial-and-error methods.

The virtues of the analog computer are its speed and the automatic character of its calculations. The device is operated by turning a crank which varies the value of v, the total vapor fraction. This actuates a number of servomechanisms which perform automatically all computations.

This computer facilitates the solution of such problems as (to mention a few): Analysis of separator operation, studies of changes in composition of reservoir fluids with pressure decline, and analysis of natural gasoline plant operation. Examples of some of these problems are given in detail later.

STATEMENT OF THE PROBLEM

The essential equations are

$$x_m = \frac{z_m}{1+(K_m-1)v} \quad . \; . \quad (1)$$

$$y_m = \frac{K_m z_m}{1+(K_m-1)v} \quad . \; . \quad (2)$$

$$\sum_{m=1}^{n} x_m = \sum_{m=1}^{n} \frac{z_m}{1+(K_m-1)v} = 1 \quad . \; . \; . \; . \; . \; . \; . \quad (3)$$

$$\sum_{m=1}^{n} y_m = \sum_{m=1}^{n} \frac{K_m z_m}{1+(K_m-1)v} = 1 \quad . \; . \; . \; . \; . \; . \; . \quad (4)$$

where

y_m = V_m/V = Mol fraction of m-th component in vapor phase.
x_m = L_m/L = Mol fraction of m-th component in liquid phase.
z_m = F_m/F = Mol fraction of m-th component in mixture.
K_m = y_m/x_m = Equilibrium constant for m-th component at the given temperature and pressure.
v = V/F = Mol fraction of vapor in the mixture.
F = Total mols of a mixture of n components.
V = Total mols of vapor in the mixture.
L = Total mols of liquid in the mixture.
F_m = Total mols of m-th component.
L_m = Mols of m-th component in liquid phase.
V_m = Mols of m-th component in vapor phase.

Assuming the total mols of the mixture F and its composition (all the F_m) to be known — either from a quantitative analysis or from the amounts put together to make the mixture — the $z_m = F_m/F$ may be regarded as known quantities. From the given temperature and pressure of the mixture the K_m are known (principally from experimental data). The primary problem is then: having given all the z_m and K_m to calculate v and all the fractions x_m and y_m. Having calculated these ratios, it is a simple matter to calculate V, L, V_m, L_m from their defining equations.

SOLUTION OF THE PROBLEM

Basic Computer Unit

The computer consists of n units, each of which provides voltages xE_o and yE_o proportional to x and y as in

---

Manuscript received at the office of the Petroleum Branch September 20, 1949. Paper presented at the Petroleum Branch meeting in San Antonio, October 5-7, 1949.

Equations (1-4). Fig. 1 shows the basic computing unit with the connections made for the case where $K<1$. Fig. 2 shows the same basic computing unit with connections made for the case where $K>1$. Certain modifications of this basic circuit are made for special values of K and v which render the basic circuit of Fig. 1 and 2 insensitive. Description of these modifications will be omitted. Provision is made for adding the voltages $x_m E_o$, or $y_m E_o$, for varying each voltage and hence their sum, and by means of a ganged variation of v for balancing the sum $\Sigma x_m E_o$ or $\Sigma y_m E_o$ to equal the line voltage E_o. When balance is attained by finding the correct value of v, cancellation of E_o yields Equation (3) or (4). The corresponding value of v which can be read from a dial is then the solution of (3) or (4).

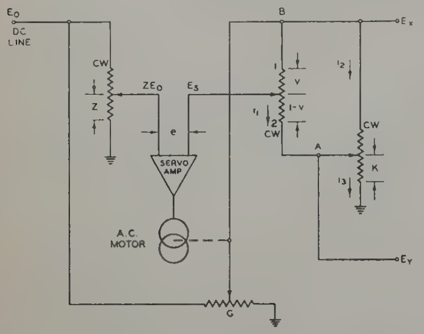

FIG. 1 — BASIC COMPUTER UNIT CIRCUIT FOR K<1 AND MODERATE VALUES OF "v".

Computing Unit —
Case Where K<1

The basic unit for providing the voltage $E_x = xE_o$ (and $E_y = yE_o$) for the case where $K<1$, is shown in Fig. 1. Four potentiometers marked x, v, G, K are connected as shown. The given fractions z and K are set by means of dials (calibrated to 0.1 per cent and which can be estimated by eye to 0.01 per cent). The potentiometer v is set by hand (and ganged with the v potentiometer of all other units so that the same value of the fraction v is simultaneously set on all units). The contact on the G potentiometer is set automatically by means of a servomotor. This motor is driven by an AC amplifier. The amplifier is actuated by the difference in voltages zE_o, from the contact on the z potentiometer, and E_s, from the contact on the v potentiometer. If $E_s<zE_o$, the motor moves the G contact to a position of higher voltage and raises the potential E_s. If $E_s>zE_o$, the motor moves the G contact to pick off a lower potential and reduces the E_s potential. In either case, the motor quickly positions the G contact so that

$$E_s = zE_o \quad . \; . \; . \quad (5)$$

an equation which we are now justified in using with the circuit equations below.

The following circuit equations, where R is the (large) resistance of the v potentiometer and r is the (small) resistance of the K potentiometer, are obvious:

$$Ri_1 = B - A \quad . \; . \; . \quad (6)$$

$$(1-K)ri_2 = B - A \quad . \; . \; . \quad (7)$$

$$Kri_3 = A \quad . \; . \; . \; . \quad (8)$$

$$i_1 + i_2 = i_3 \quad . \; . \; . \; . \quad (9)$$

$$E_s = vA + (1-v)B \quad . \; . \; . \; . \; . \quad (10)$$

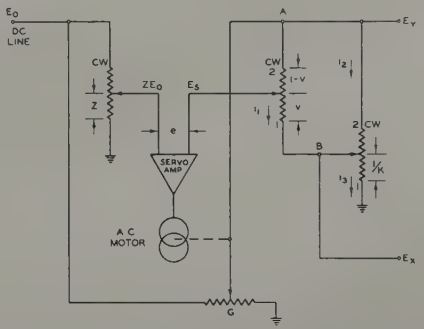

FIG. 2 — BASIC COMPUTER UNIT CIRCUIT FOR K>1 AND MODERATE VALUES OF "v".

Eliminating i_1, i_2, i_3, and E_s from the Equations (5-10), and solving for B and A, we have

$$B = \frac{zE_o[1 + K(1-K)\rho]}{[1 + (K-1)v] + K(1-K)\rho} \quad . \; . \; . \; . \; . \; . \quad (11)$$

$$A = \frac{zE_o[K + K(1-K)\rho]}{[1 + (K-1)v] + K(1-K)\rho} \quad . \; . \; . \; . \; . \; . \quad (12)$$

where

$$\rho = r/R \quad . \; . \; . \; . \; . \; . \; . \quad (13)$$

This ratio of the resistance, r, of the potentiometer, K, to the resistance, R, of the potentiometer, v, will be taken so small that the parts of (11) and (12) containing ρ can be reglected. Hence, to a sufficient approximation $B = E_x$ and $A = E_y$, where

$$E_x = \frac{zE_o}{1 + (K-1)v} \quad . \; . \quad (14)$$

$$E_y = \frac{KzE_o}{1 + (K-1)v} \quad . \; . \; . \quad (15)$$

Computing Unit —
Where K>1

The basic unit for a $K>1$ is the same unit as for $K<1$, but the setting of potentiometer, K is as shown in Fig. 2, and the connections to the potentiometer, v are reversed. The servomechanism sets potentiometer, G, as before so that Equation (5) is satisfied. The circuit equations differ slightly from Equations (6-10), but follow the pattern above and result in the same Equations (14) and (15).

Computer Assembly

The basic computing unit will be represented, for convenience, by the block shown in Fig. 3. The units are assembled as shown schematically in Fig. 4. Each output potential E_x, or E_y, is placed on one end of a high resistance R′. The other ends of these resistances are connected to a common lead whose potential is E, and which is connected to one terminal of a galvanometer M. The current, i_m, of the m-th unit through R′ is given by $x_m E_o - E = R' i_m$. The currents, i_m, will add; hence, summing the last equation from 1 to n, we have

$$E_o \sum_{m=1}^{n} x_m - nE = R' \sum_{m=1}^{n} i_m \quad . \; . \; . \; . \; . \quad (16)$$

A potential E_o/n is placed on the other terminal of the galvanometer. The ganged contacts on the v potentiometers are adjusted by hand until the galvanometer M reads zero. When this condition is attained $\sum_{m=1}^{n} i_m = 0$ and the last equation reduces to $E_o \sum_{m=1}^{n} x_m = nE$. But $nE = E_o$, and cancelling these equal factors, we have $\sum_{m=1}^{n} x_m = 1$ and

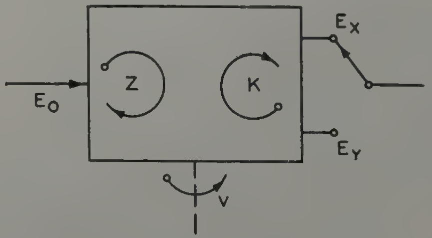

FIG. 3 — BASIC COMPUTING UNIT.

the v, so obtained, is the required solution of Equation (3).*

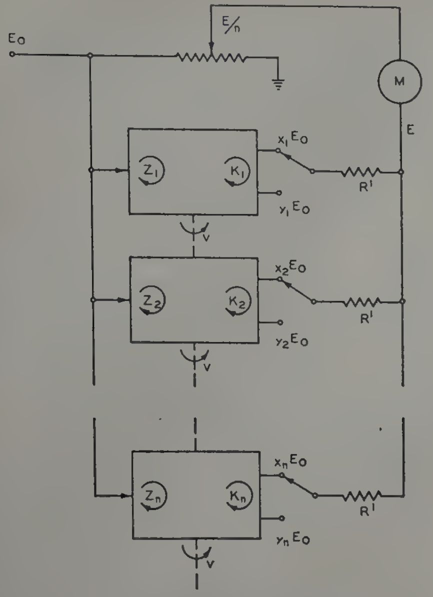

FIG. 4 — SCHEMATIC ASSEMBLY OF COMPUTER.

If the adding resistances R′ be switched to the other output terminals yE_o of the computing units, and if v be adjusted so that M reads zero, then v is the solution of the equation $\sum_{m=1}^{n} y_m = 1$, namely, the solution of the equivalent Equation (4). The two values of v should agree.

For conciseness, the complete wiring diagrams of this computer are omitted. For the same reason, we omit details concerning the sensitive units, the servomechanism details, the manual of operation, and design data.

The computer is packaged for convenience of operation and maintenance. The general arrangement is shown by the photographs (Figs. 5-7).

APPLICATIONS AND EXAMPLES

A few applications of this computer should be of interest.

Determination of Optimum Separator Operating Conditions

Just what is considered optimum may vary considerably. For instance, it may be desirable to obtain a maximum of stock tank liquid from a given crude; or, it may be desirable to maintain the gas composition uniform when a gas line is being fed from several separators. Since the crude composition, the temperature and pressure of the stock tank, and separator temperature are beyond control there remains only the separator pressure which may be varied to yield the desired product out of the separator. A series of flash calculations may, therefore, be made at different pressures intermediate between reservoir pressure and stock tank pressure. A second calculation gives the stock tank liquid and vapor compositions. That operating pressure is then selected which satisfies the requirements of the problem in question.

Evaluation of Reserves

Evaluation of reserves involves a study of changes in composition of the reservoir fluids during the life of a field. If the flash vaporization process is adopted as a simplifying assumption for small pressure increments, then this computer can be used as an aid in making such a study. Two general cases arise in this connection: (1) gas-condensate reservoirs, and (2) oil fields with gas-saturated crude. In either case, if the initial compositions of the phases present are known, and a reliable set of K constants is available, then the effect of pressure decline on composion may be calculated and an evaluation of recoverable fluids made. That is, the amount of condensation of heavy components with pressure decline can be calculated in the first case, or the loss of solution gas with pressure decline can be calculated in the second case.

Natural Gasoline Plant Calculations

At every stage where the pressure and/or temperature of the product is changed in natural gasoline plant operation, and natural gas processing, the flash vaporization process is involved, at least as a simplifying assumption, if not in fact. In cases where complete

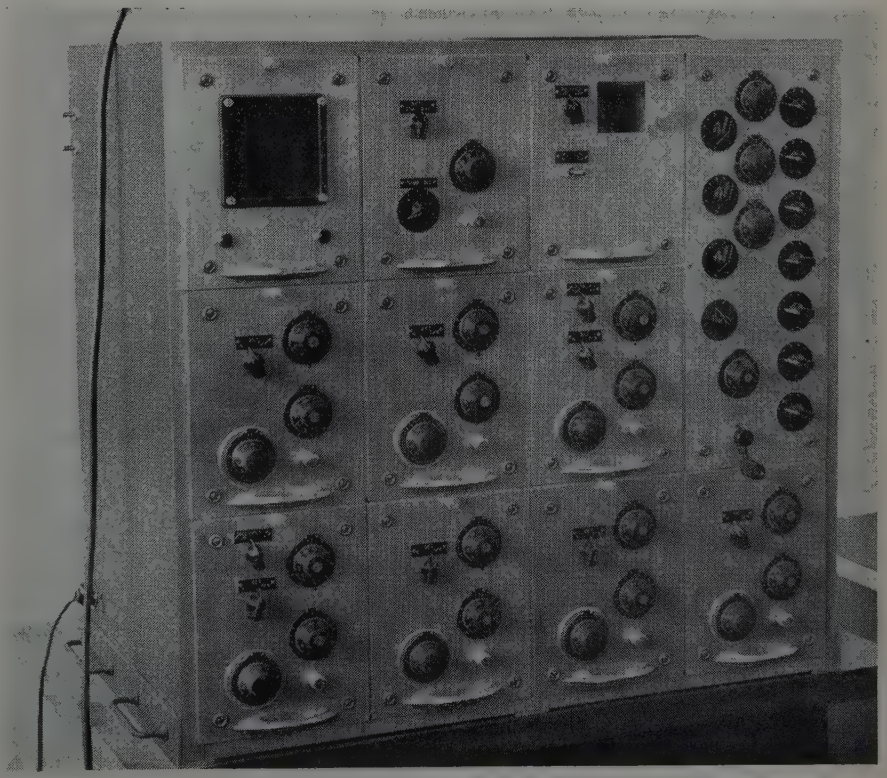

FIG. 5 — VAPOR LIQUID EQUILIBRIUM COMPUTER FRONT VIEW.

---

* The current, i_m, drawn from the X_mE_o terminal of Fig. 1 is drawn from the G potentiometer and does not disturb in any way the rest of the circuit. If the current, i_m, is drawn from the Y_mE_o terminal, this current must pass through a portion of the K-potentiometer and consequently i_2 in Fig. 1 will be disturbed. This effect is negligible, however, since the adding resistance R′ is very large (500,000 ohms) compared with the 500 ohm K-potentiometer. This disturbing effect is further reduced by the fact that the voltage at the opposite end of R′ is limited to E_o/n. This reduces the voltage drop across R′ and hence the current through it.

Similar considerations lead to the conclusion that this disturbing effect is also negligible when the connections shown in Fig. 2 are used.

equilibrium between liquid and vapor does not exist, conditions do differ from the ideal, but the fundamental calculations must be made before the deviations can be determined. The computer may be used to make these fundamental calculations.

Estimation of K Values

In the case of each of these applications only the straight forward operation of the computer is involved. However, other interesting variations are possible. One in particular was employed in this laboratory during the course of some PVT work. A quantity of reservoir fluid was equilibrated in a PVA cell. A portion of the vapor phase was bled off and analyzed. This process was repeated at constant temperature in a series of equal pressure steps. It was desirable to know the distribution of the components in the vapor and liquid states at each of the pressure points involved. The known quantities were initial composition of sample, weight per cent of total sample of vapor bled off, and composition of the vapor bled off. This process is a differential vaporization process, but if the pressure increments are small, flash vaporization calculations may be made as a first approximation. Such calculations will yield the desired information provided a reliable set of K-constants is available. In this particular case, the values of the K-constants for the heaviest components were in doubt, although the values for the lighter components were fairly well established. Before the desired information could be derived from the data, it was necessary, therefore, first to establish the values of the K-constants for the heaviest component. This is readily accomplished through the use of this computer.

The initial composition of the sample was set up on the Z-dials. The K-values at the temperature and pressure in question were set up on the K-dials using an approximate value for the seventh component (C_7). The computer was balanced to determine v and the vapor fraction of C_7 noted and compared with the experimental value obtained from the analysis of that portion of the vapor phase bled off. Since only an approximate value of K_7 was used, the computed C_7 vapor fraction differed from the experimental value. By resetting the K_7 dial and readjusting the v-dial for balance, a K_7 was found which would cause the computed C_7 vapor fraction to equal the experimental value. This process was repeated at each new pressure making allowance for the weight fraction of the sample bled off as a vapor. In this way a satisfactory set of K_7 values was obtained and the vapor-liquid distribution of each component at each pressure was obtained. The same results could have been obtained by cut-and-try methods, but probably would not have been attempted because of the time required to make such tedious calculations.

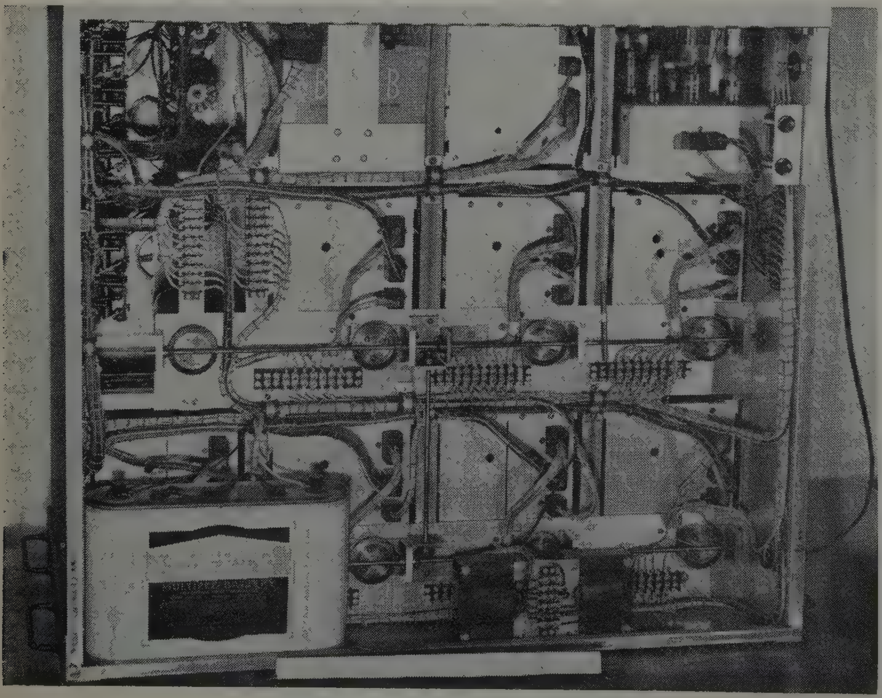
FIG. 6 — COMPUTER WITH BACK PANEL REMOVED.

Examples

As an example of the more usual type of problem solved with this computer, the results of a typical run are shown in Table I, together with a comparison between results obtained by the trial-and-error method and those obtained with the computer. The time required to make a complete calculation, including determining v and reading all liquid x_m and vapor y_m fractions is about ten minutes.

Error Studies

An evaluation of the accuracy of this computer has been made using data of the same type as that shown in Tables I and II. The results are shown in Fig. 8 and Table III. Fig. 8 is a frequency distribution curve of differences between computer and trial-and-error values of liquid and vapor fractions. Table III lists certain factors characterizing the frequency distribution of errors for this computer.

It will be noted that the standard deviation from the mean is $\sigma = .0015$. Accordingly, 68.3 per cent of the errors may be expected to fall in the range $+.0002 \pm .0015$. This range is indicated on the frequency curve in Fig. 8.

A similar comparison of the computer values of v with those obtained by the trial-and-error method for 20 examples indicates that the probable error is ± 0.0020.

Percentage errors have not been used in these studies, since the magnitude of the errors appears to be more or less uniform throughout the scale ranges. This would result in large percentage errors at small scale readings and small percentage errors at large scale readings. It was felt, therefore, that percentage errors would not give a true measure of the accuracy to be expected of this computer.

Second Approximation

The value of v as computed by this instrument may be considered a first approximation. The figures, just given, on the accuracy will then be a measure of the closeness of this approximation. If greater accuracy is desired, the computer may also be used to give a second approximation. This is accomplished by means of an interpolation formula and two additional readings on the instrument. This formula is

$$\epsilon_o = F \frac{v_2 - v_1}{|G_1| + |G_2|} \beta$$

in which

v_1 is a v-dial setting less than that required for balance $(v_1 < v_o)$

v_2 is a v-dial setting greater than that required for balance $(v_2 > v_o)$

G_1 is the galvanometer deflection in scale divisions corresponding to v_1.

G_2 is the galvanometer deflection in scale divisions corresponding to v_2

F is a proportionality constant found to be 336.5

$$\beta = 1 - \sum_{m=1}^{n} \frac{z_m}{1 + (K_m - 1) v_o}$$

ϵ_o is the correction to be applied to v_o to give the second approximation, $\bar{v}$, to the correct value of v, thus

$$\bar{v} = v_o + \epsilon_o$$

In the example given in Table I the quantities in the interpolation formula were found to be

$$v_1 = .480 \qquad G_1 = +2 \qquad v_o = .4837$$
$$v_2 = .490 \qquad G_2 = -3 \qquad F = 336.5$$
$$\beta = .001755$$

$$\epsilon_o = 336.5 \frac{.01 \times .001755}{5}$$
$$= \frac{336.5 \times 1.755 \times 10^{-5}}{5}$$
$$= 12 \times 10^{-4} = +.0012$$
$$\bar{v} = .4837 + .0012 = .4849$$

This value compares favorably with the trial-and-error value of .4850.

Eight similar examples were calculated as outlined above and gave results with an average probable error of 0.0002.

The additional time required to make the second approximation is largely that required to calculate β, which is a straight-forward operation, and the time required depends on one's skill with a desk calculator. The time required to make the two pairs of readings of V_1, G_1 and V_2, G_2 is negligible.

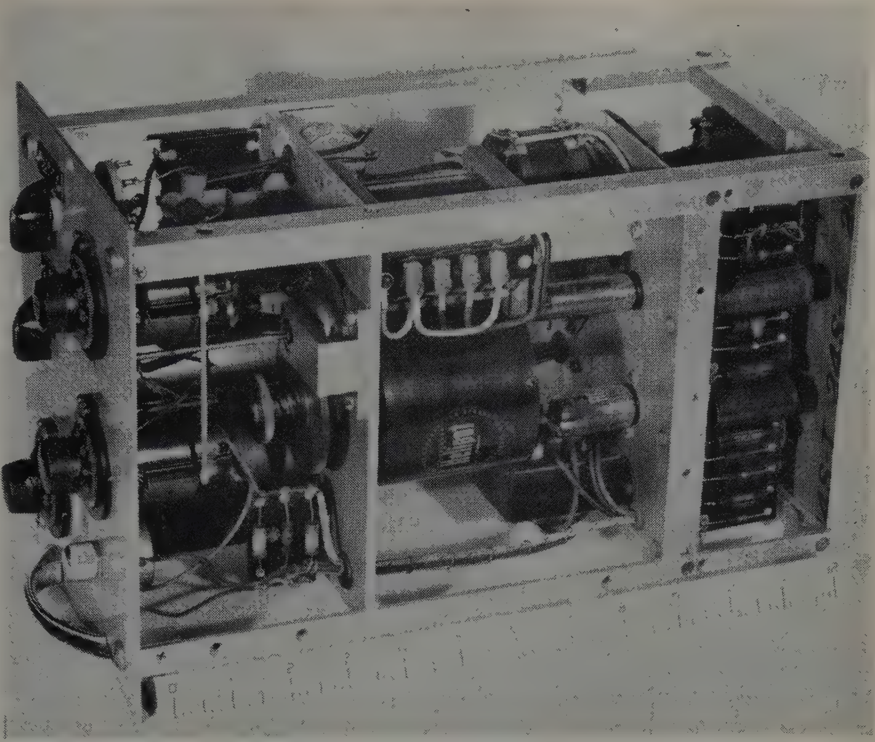

FIG. 7 — SINGLE COMPUTING UNIT.

Table I

Sample Problem with Comparison of Results

Component Number	z_m	K_m	Computer Values x_m	Computer Values y_m	Trial-and-Error Values x_m	Trial-and-Error Values y_m	Differences Δx_m	Differences Δy_m
C_1	.2085	173.0	.0040	.4285	.0025	.4277	+.0015	+.0008
C_2	.1185	21.0	.0123	.2328	.0111	.2327	+.0012	+.0001
C_3	.1069	5.35	.0350	.1834	.0344	.1840	+.0006	−.0006
C_4	.0776	1.67	.0585	.0970	.0586	.0979	−.0001	−.0009
C_5	.0590	0.46	.0800	.0372	.0799	.0368	+.0001	+.0004
C_6	.0485	0.162	.0805	.0142	.0817	.0132	−.0012	+.0010
C_7	.3810	0.0105	.7300	.0090	.7318	.0077	−.0018	+.0013
Totals	1.0000		1.0003	1.0031	1.0000	1.0000		

v (Computer value) = 0.4837 v (Trial-and-error value) = 0.4850

Table II shows another example. In this case one of the K's is large (247) and the v is small (0.0060), a case which calls for the use of one of the sensitive units not described in this paper.

Table II

Sample Problem Using One of the Sensitive Units

Component Number	z_m	K_m	Computer Values x_m	Computer Values y_m	Trial-and-Error Values x_m	Trial-and-Error Values y_m	Differences Δx_m	Differences Δy_m
C_1	.0025	247	.0013	.2474	.0010	.2470	+.0003	+.0004
C_2	.0111	30	.0096	.2840	.0095	.2809	+.0001	+.0031
C_3	.0344	7.6	.0332	.2460	.0331	.2500	+.0001	−.0040
C_4	.0586	2.4	.0575	.1372	.0581	.1394	−.0006	−.0022
C_5	.0799	.66	.0797	.0525	.0800	.0528	−.0003	−.0003
C_6	.0817	.23	.0815	.0196	.0821	.0189	−.0006	+.0007
C_7	.7318	.01	.7355	.0122	.7362	.0110	−.0007	+.0012
Totals	1.0000		.9983	.9997	1.0000	1.0000		

v (Computer value) = .0054 v (Trial-and-error value) = .0060

Table III

Factors Characterizing the Frequency Distribution Curve of Errors

Arithmetic Mean Error ($\overline{X}$)	$= +.0002$
Quadratic Mean Error (RMS)	$= \pm .0015$
Median Value	$= +.0004$
Mode	$= +.0005$
Standard Deviation (σ) from the Mean ($\overline{X}$)	$= \pm .0015$ (Approximately the RMS)

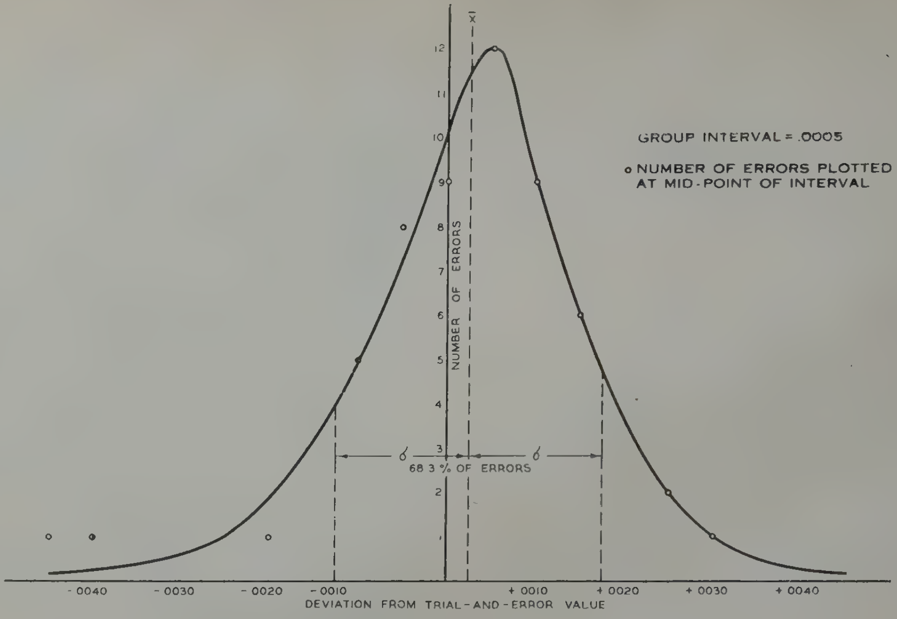

FIG. 8 — FREQUENCY DISTRIBUTION CURVE OF ERRORS IN X_m AND Y_m.

Use of the Sensitive Units

Special values of K and V which render the basic circuit insensitive are:

(a) $K \rightarrow 0$ and $V \rightarrow 1$

(b) K very large ($1/K \rightarrow 0$) and $V \rightarrow 0$

Condition (a) exists when one or more components are relatively involatile but are present only in small quantities. In such a case the denominators in Equations (14) and (15) approach zero and the units become insensitive. This occurs for values of $K < .01$ and of $V > .99$.

Condition (b) exists when one or more components are very volatile but are present in only small quantities. This is the case for the second example given. Because of the difference in connections shown in Figs. 1 and 2 the relative positions of the K and V potentiometers are the same as for condition (a) and the sensitive unit must be used. This occurs for values of $K > 100$ and of $V < .01$.

CONCLUSION

An electronic analog computer has been described which provides a solution to the vapor-liquid equilibrium problem. The computed value of v has a probable error of 0.0020 in the first approximation and 0.0002 in the second approximation. The operation is simple and rapid. In thus speeding up the solution, the way is opened for the application of the method to problems which would not otherwise be undertaken because of the amount of time required to obtain a solution. ★ ★ ★

T.P. 2846

THE FORCE EXERTED BY SURFACE WAVES ON PILES

J. R. MORISON, M. P. O'BRIEN, J. W. JOHNSON AND **S. A. SCHAAF,** UNIVERSITY OF CALIFORNIA, BERKELEY, CALIFORNIA

THE FORCE EXERTED BY SURFACE WAVES ON PILES

The force exerted by unbroken surface waves on a cylindrical object, such as a pile, which extends from the bottom upward above the wave crest, is made up of two components, namely:

1. A drag force proportional to the square of the velocity which may be represented by a drag coefficient having substantially the same value as for steady flow, and
2. A virtual mass force proportional to the horizontal component of the accelerative force exerted on the mass of water displaced by the pile.

These relationships follow directly from wave theory and have been confirmed by measurements in the Fluid Mechanics Laboratory of the University of California, Berkeley.

The maximum force exerted by breakers or incipient breakers is impulsive in nature, reaching a value much greater than that produced by unbroken waves but enduring for only a short time interval. This impulsive force represents the ultimate development of the accelerative force and is produced by the steep wave front and large horizontal acceleration at the front of a breaker. This impulsive force greatly exceeds the drag force computed from the particle velocities of the breaker.

The reader is cautioned that these preliminary results are applicable only to single piles without bracing and are likely to be modified somewhat where multiple piles are driven, one within the influence of the other or where multiple piles are connected by submerged bracing. This paper is essentially a preliminary report submitted at this time because of the current importance of wave forces in the design of offshore structures. An extended series of additional experiments is planned for the near future.

Theoretical Relationships

For the sake of simplicity of treatment, the theory will be developed from the equations for waves of small amplitude. The horizontal displacement of a water particle is described by the equation

$$X = \frac{H}{2}\,\frac{\cosh \frac{2\pi}{L}(d+z)}{\sinh \frac{2\pi D}{L}}\,\sin \frac{2\pi t}{T} \quad . \; . \; . \; . \; . \quad (1)$$

The horizontal component of the orbital velocity is obtained by differentiation with respect to time as

$$u = \frac{\pi H}{T}\,\frac{\cosh \frac{2\pi}{L}(d+z)}{\sinh \frac{2\pi d}{L}}\,\cos \frac{2\pi t}{T} \quad . \; . \; . \; . \quad (2)$$

The acceleration of the water particles at any position is obtained by again differentiating with respect to time as

$$\frac{\partial u}{\partial t} = \frac{-2\pi^2 H}{T^2}\,\frac{\cosh \frac{2\pi}{L}(d+z)}{\sinh \frac{2\pi d}{L}}\,\sin \frac{2\pi t}{T} \quad . \; . \quad (3)$$

where

H = wave height — ft

L = wave length — ft

d = still water depth — ft

z = depth below the still water measured negatively downward — ft.

T = wave period — sec

t = time — sec

The force exerted on a differential section, dz, in length is

$$dF = \left[C_M \left(\rho \frac{\pi D^2}{4}\right)\frac{\partial u}{\partial t} \pm C_D \frac{\rho D}{2}\,u^2\right] dz \quad . \; . \; . \quad (4)$$

where

D = pile diameter — ft

ρ = water mass density — slugs/ft^3

C_M = coefficient of mass

C_D = coefficient of drag

Substituting for $\partial u/\partial t$ and u^2 from Eqs. (3) and (2), the force per unit length at any position z is

$$\frac{dF}{dz} = \frac{\pi^2 \rho D H^2}{2T^2}\left[-f_M \sin\theta \pm f_D \cos^2\theta\right] \quad . \; . \; . \quad (5)$$

$$\frac{f_M}{C_M} = \pi A \frac{D}{H}\;;\; \frac{f_D}{C_D} = A^2\;;\; \theta = \frac{2\pi t}{T}$$

$$A = \frac{\cosh \frac{2\pi}{L}(d+z)}{\sinh \frac{2\pi d}{L}}\cdot \begin{cases} +\cos^2\theta \text{ for } 0 < \theta < \pi/2 \\ \qquad \frac{3\pi}{2} < \theta < 2\pi \\ -\cos^2\theta \text{ for } \frac{\pi}{2} < \theta < \frac{3\pi}{2} \end{cases}$$

The sin θ term (inertia) is negative for $0 < \theta < \pi$ and positive for $\pi < \theta < 2\pi$. Values of A and A^2 appear in Fig. 1

Manuscript received at the office of the Petroleum Branch October 23, 1949.

as functions of z/d and d/L. Values of f_M/C_M appear in Fig. 2 as a function of D/H. Values of d/L corresponding to values of d and L_o have been tabulated.*

The preceding equations permit several important conclusions as to the distribution and variation of the force exerted, namely,

1. The drag force decreases with distance below the surface more rapidly than does the inertia force.
2. The maximum force at any position (z/d) develops before the crest passes and the angle (or time) of advance increases with the ratio f_M/f_D.
3. The maximum forces applied at different values of z/d do not occur simultaneously and the angle of advance of the maximum forces, measured forward from the crest, increases from the surface to the bottom.
4. The relative importance of the inertia force increases with the ratio of pile diameter to wave height. The limiting effect occurs when the diameter is so great as compared with the wave length that the structure begins to act as a section of a wall; the maximum force then occurs when the run-up of water on the structure reaches its maximum elevation.

The angle θ corresponding to the maximum force may be obtained analytically from Eq. (5) by differentiating with respect to θ and equating to zero, as

$$+ f_M \cos\theta \pm 2f_D \sin\theta \cos\theta = 0$$

$$\sin\theta = \frac{f_M}{2f_D}$$

$$\cos^2\theta = 1 - \frac{f_M^2}{4f_D^2} = \frac{4f_D^2 - f_M}{4f_D^2}$$

Since the angle θ is in the fourth quadrant, i.e., the force leads the wave, we have

$$\left(\frac{dF}{dz}\right)_{max} = \frac{\pi^2 \rho D H^2}{2T^2}\left\{+\frac{f_M^2}{2f_D} + f_D\left(\frac{4f_D^2 - f_M^2}{4f_D^2}\right)\right\}$$

$$= \frac{\pi^2 \rho D H^2}{2T^2}\left\{f_D + \frac{f_M^2}{4f_D}\right\}$$

which is the maximum force at a particular depth z.

The moment exerted by the wave force about the bottom of the pile is

$$dM = (d + z)\ d\,F$$

$$M = \int_{-d}^{o} (d + z)\ d\,F$$

$$= \frac{\rho D H^2 L^2}{T^2}\left(-\frac{D}{H}\frac{\pi}{4} C_M K_1 \sin\theta \pm C_D K_2 \cos^2\theta\right) \qquad (6)$$

$$K_1 = \frac{1 + \frac{2\pi d}{L}\sinh\frac{2\pi d}{L} - \cosh\frac{2\pi d}{L}}{2\sinh\frac{2\pi d}{L}}$$

$$K_2 = \frac{1 + \frac{1}{2}\left(\frac{4\pi d}{L}\right)^2 + \frac{4\pi d}{L}\sinh\frac{4\pi d}{L} - \cosh\frac{4\pi d}{L}}{64\sinh^2\frac{2\pi d}{L}}$$

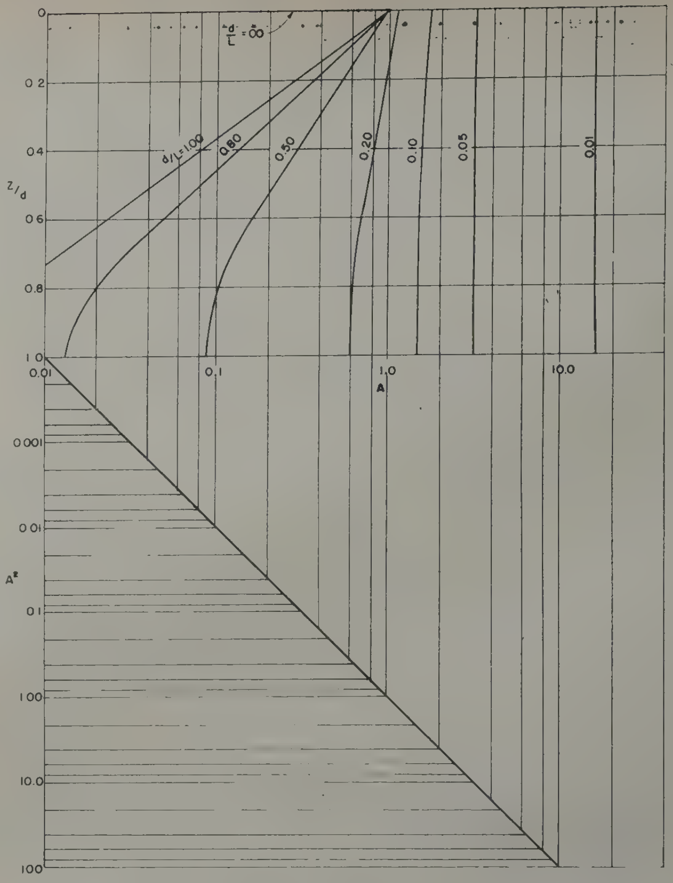

FIG. 1 — $\frac{Z}{d}$ VERSUS A AND A² FOR VARIOUS $\frac{d}{L}$

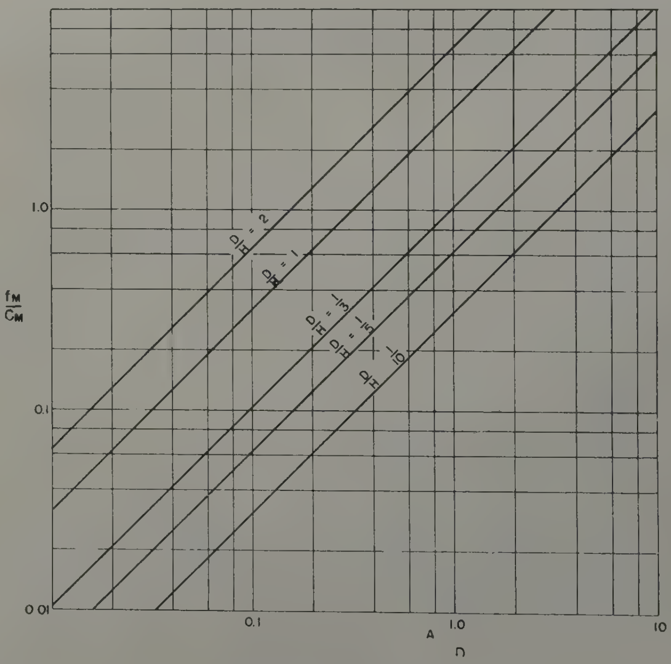

FIG. 2 — $\frac{f_m}{C_m}$ VERSUS A FOR VARIOUS $\frac{D}{H}$

---

* Wiegel, R. L. — Oscillatory Waves, The Bulletin of the Beach Erosion Board. Special Issue No. 1, Washington, D. C., July 1, 1948.

$$\sin\theta_{max} = \frac{-\pi D K_1 C_M}{8 H K_2 C_D}$$

Values of K_1 and K_2 appear in Fig. 3.

The development of these force and moment relationships was based on the sinusoidal wave theory for waves of small amplitude.

Theory and experiment show that the surface profile of a wave of finite amplitude departs from a sinusoidal form and is, in fact, very nearly trochoidal. The orbit velocities are also unsymmetrical, the forward velocity at the crest exceeding the backward velocity in the trough by approximately 10 per cent in a deep-water wave having a steepness ratio (H/L) of 0.02 and approximately 25 per cent for a steepness ratio of 0.10. Analysis of the data in this report has been based upon a sinusoidal variation in velocity and, in effect, the asymmetrical velocity variation is represented in the empirical coefficient. An extended series of experiments on piles, caissons, structural members, and flat surfaces under different exposures to wave action is planned. Measurement of orbital velocities in waves of varying H/L and d/L are in progress. When these experimental programs are completed, the data will be analyzed on the basis of the asymmetrical variation of velocity with time in waves of finite amplitude. The current importance of wave force in the design of offshore structures makes it desirable that the results to date be made available now. The force coefficients C_D and C_M reported here are regarded as sufficiently accurate for design purposes, provided that they are re-inserted in the equations from which they have been derived, namely, eqs. (4) and (6).

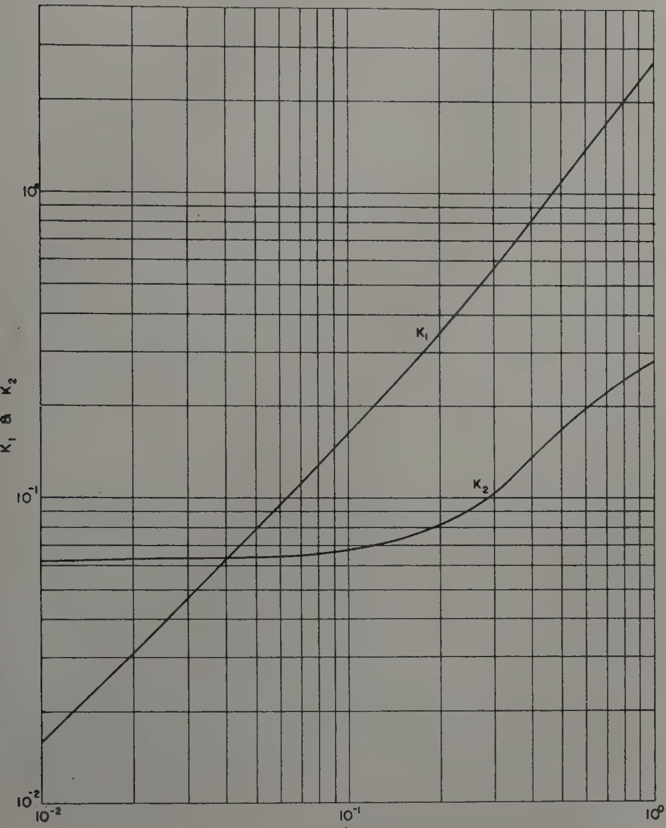

FIG. 3 — K_1 AND K_2 VERSUS d/L

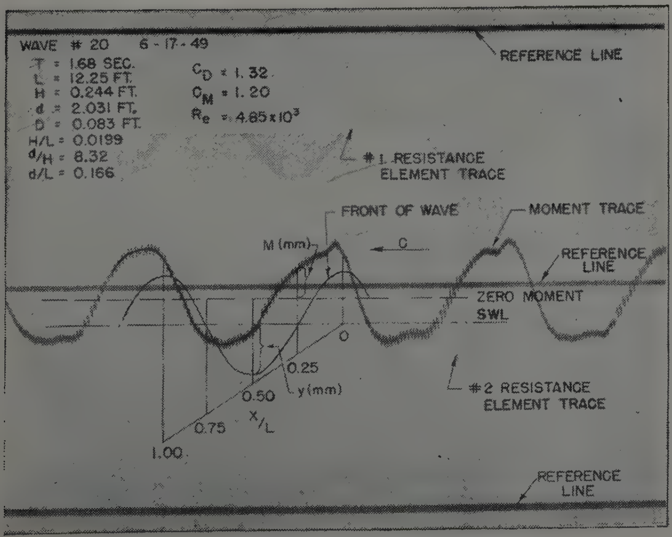

FIG. 4 — SAMPLE OSCILLOGRAPH RECORD

Laboratory Investigations

The laboratory measurements were planned on the basis of Eq. (6). The model pile was hinged at the bottom and the necessary restraining force was measured at a known moment arm above the hinge (Fig. 9). The wave profile at the pile and the wave force were recorded simultaneously on the same oscillograph record. The wave velocity just ahead of the pile was obtained by means of a second wave profile on the same record. Time was measured by a 60-cycle frequency traced by the oscillograph. Thus, all the data for analysis appeared on the same record, with the exception of the still-water depth which was measured directly. Details of the experimental equipment are available in reports of the Fluid Mechanics Laboratory and will not be presented here. Fig. 4 is a sample of the records obtained for each wave condition.

Analysis of the data took advantage of the fact that the two components of the total force are out of phase. Writing a dimensionless moment coefficient as

$$\overline{M} = \frac{M T^2}{\rho D H^2 L^2} = -\frac{\pi}{4} C_M \frac{D}{H} K_1 \sin\theta \pm C_D K_2 \cos^2\theta \ . \quad (7)$$

the equation may be solved for C_M and C_D by measuring the force when $\cos\theta$ or $\sin\theta$ are zero, respectively. When the crest passes the pile, $\theta = 0$ and $\sin\theta = 0$, and the value of $\overline{M}$ at this instant may be solved for C_D. When the instantaneous water-surface elevation is *at the still water* level, the velocity is zero and the corresponding value of $\overline{M}$ may be solved for C_M. It is to be noted that the actual wave profile, which is very nearly trochoidal, has been used and that the instant of zero velocity has been assumed to occur when the water surface crosses the still water level. The acceleration at the same instant has been taken as the theoretical value from Eq. (3). The important requirement is that the determination of C_M be made from the measured moment at the instant of zero velocity.

After determining the values of C_M and C_D at the instants of zero velocity and zero acceleration, these values were then employed to compute the remainder of the moment curve measured for each run. The agreement between the measured and computed moment curve was good over the entire wave length and this result confirms the analysis. Fig. 5 shows the wave profile as measured and the measured and computed moments.

The experimental values of C_M and C_D showed some scattering but no trend as a function of d/L, H/L or Reynolds number. The average values obtained for runs with the pile on a horizontal bottom and without impulsive forces, were

$$C_M = 1.508 \pm 0.197$$
$$C_D = 1.626 \pm 0.414$$

The Reynolds number, corresponding to the maximum surface orbital velocity, ranged from 0.22×10^4 to 1.11×10^4. The Reynolds number decreased from these maximum values both downward along the pile and with time. The drag coefficient of a cylinder varies not only with Reynolds number but also with the turbulence of the incident stream. Values of C_D for cylinders in a steady stream of air or water within this range of Reynolds numbers vary from 0.65 to 1.20.

The virtual mass coefficient of a cylinder accelerated perpendicular to its axis has been measured in a number of ways. The principle involved in the idea of a virtual mass is that the flow field around a cylinder contains kinetic energy in amount proportional to the square of the velocity of the cylinder and an increase in the velocity of the cylinder requires that work be done through the application of a force to increase this kinetic energy. Thus the cylinder appears to have a mass greater than its true mass. Measurements of the virtual mass of cylinders gives values between 0.5 and 1.0 to which must be added unity, representing the mass of water displaced by the pile, for comparison with the results of these experiments.

Surface profiles followed closely the trochoidal form corresponding to the ratio of the horizontal to vertical axis of the wave orbits which in turn depends upon the ratio d/L. In analyzing the data, the velocity and acceleration were assumed to follow Eqs. (2) and (3).

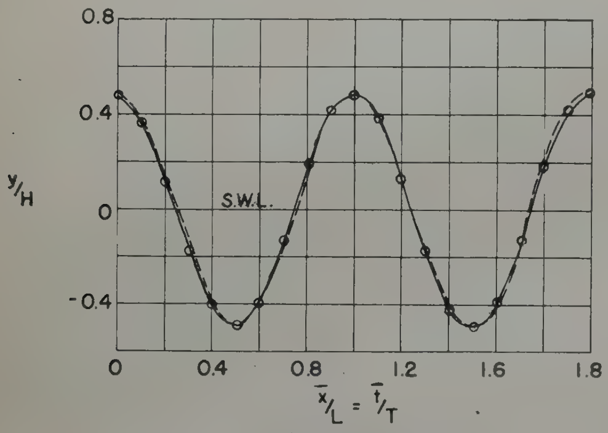

a. WAVE PROFILE

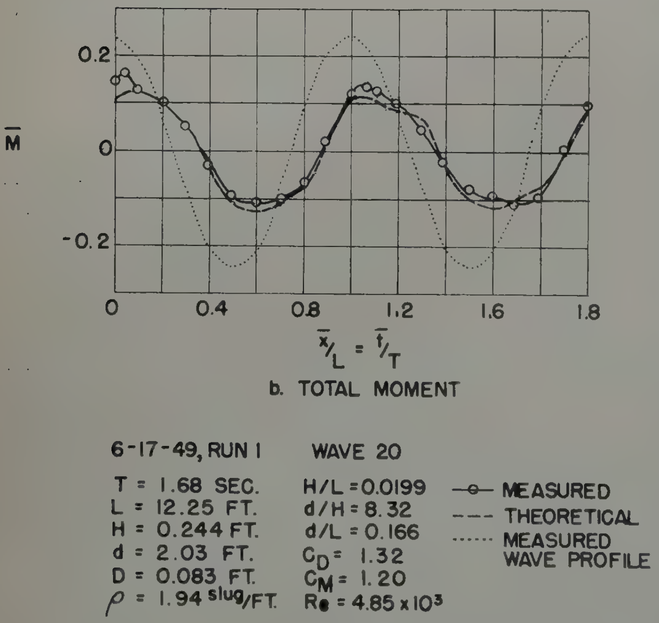

b. TOTAL MOMENT

FIG. 5 — COMPARISON OF THEORETICAL AND MEASURED TOTAL MOMENT AND WAVE PROFILE

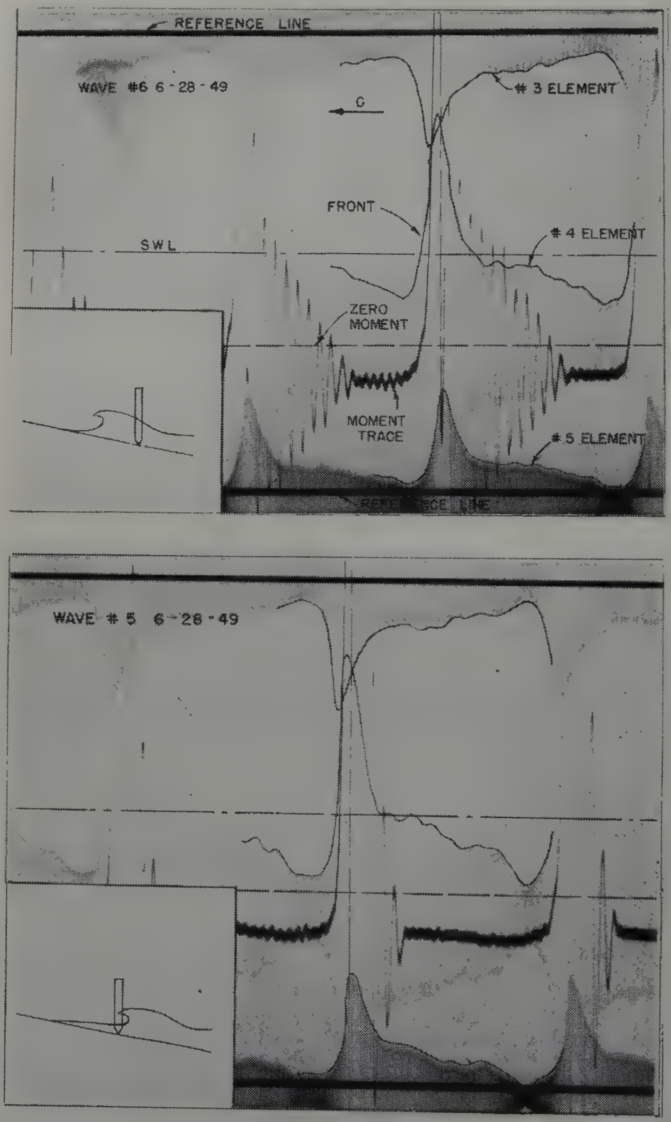

FIG. 6 — RECORD OF WAVE IMPACT

A — BREAKER SLIGHTLY AFTER PILE; WAVE PEAKED UP AS IT HITS PILE

B — WAVE BREAKING ON PILING

The variation in the moment arm between trough and crest was not considered in the integration to obtain M and has been neglected in the analysis. The effect is generally small for unbroken waves. Refinement of the analysis to consider this variation seems justified only in the case of breaking waves, where the percentage variation in moment arm would be large. The additional experiments contemplated will include measurement of the moment at three positions along the pile and the analysis of these data will include the effect of variation in the lever arm.

Fig. 6 show the record obtained for selected runs in which impact forces occurred. The trace of the force measurement shows that the instrument oscillated after impact and the values are not regarded as quantitatively reliable but it is evident that the maximum force produced by a breaker or incipient breaker greatly exceeds the force corresponding to the orbital velocity, which under breaking conditions, is the wave velocity. The impact force is of short duration and its impulse may not be great. In future work, the force measuring system will be revised in order to follow these impulsive forces and relate them to the wave velocity and height of breaker.

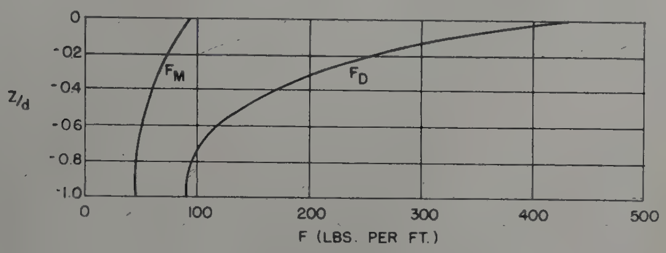

a. MAXIMUM FORCE DISTRIBUTION

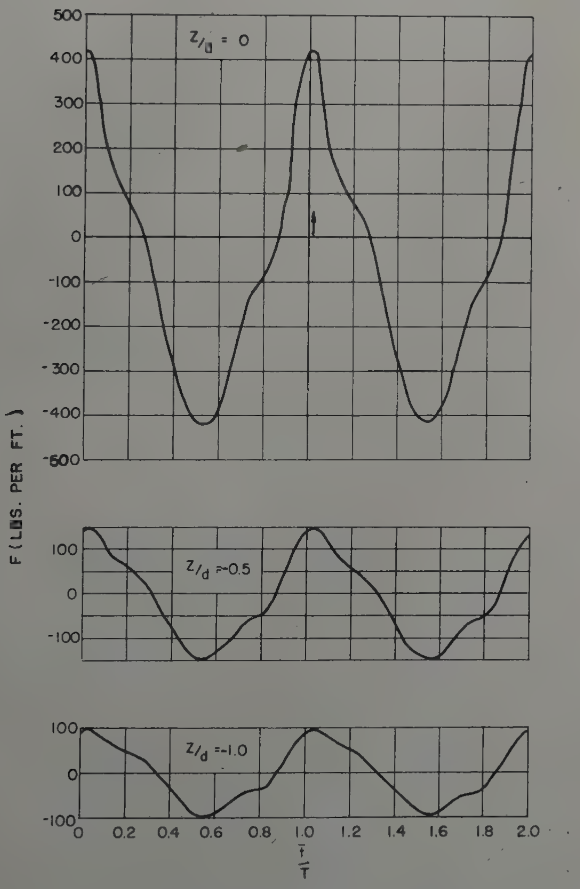

b. TOTAL FORCE VERSUS WAVE POSITION

FIG. 7 — EXAMPLE 1. FORCE RELATIONSHIPS

A — MAXIMUM FORCE DISTRIBUTION

B — TOTAL FORCE VERSUS WAVE POSITION

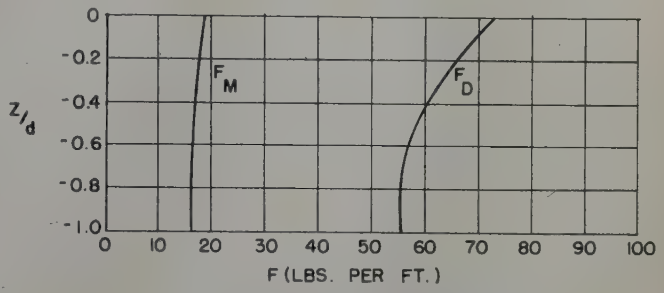

a. MAXIMUM FORCE DISTRIBUTION

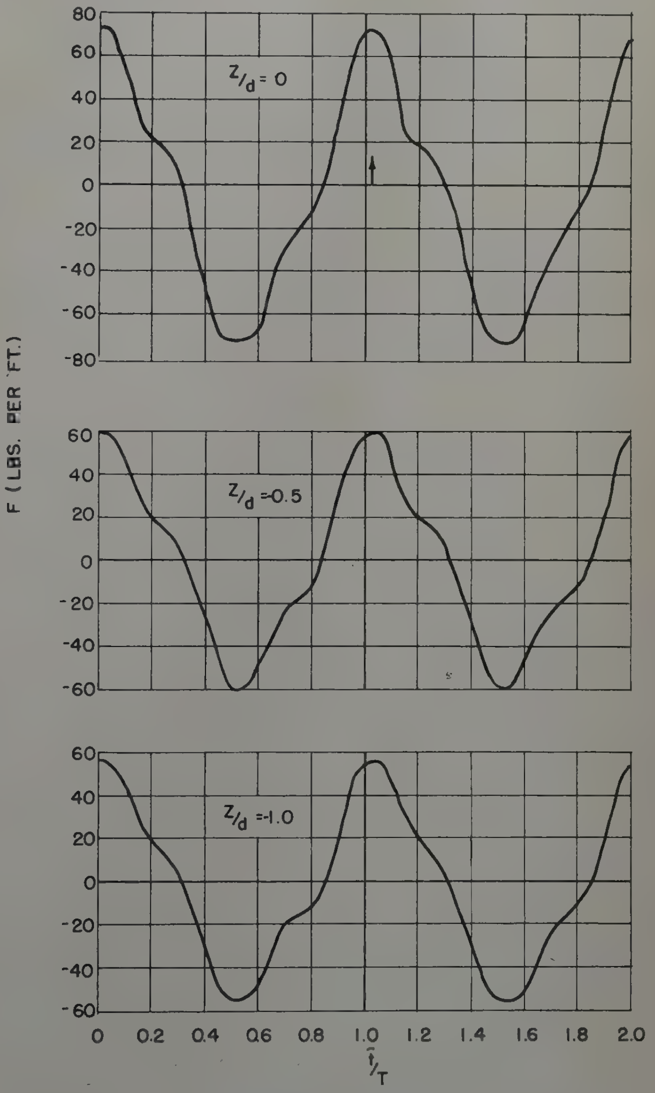

b. TOTAL FORCE VERSUS WAVE POSITION.

FIG. 8 — EXAMPLE 2. FORCE RELATIONSHIP

A — MAXIMUM FORCE DISTRIBUTION

B — TOTAL FORCE VERSUS WAVE POSITION

Ranges of Variables

The range of wave characteristics, water depths, and other variables used in the experiment were as follows:

$\frac{D}{H} = 0.212$ to 0.758

$\frac{D}{L} = 0.0090$ to 0.0419

$\frac{D}{d} = 0.0411$ to 0.0833

$\frac{d}{H} = 4.81$ to 18.15

$\frac{d}{L} = 0.102$ to 0.529

$\frac{H}{L} = 0.0090$ to 0.1135

$Re = 0.22 \times 10^4$ to 1.11×10^4

The experiments were performed in a constant depth channel. The above ratios were obtained from the records of 17 waves and one pile diameter. The range of variables will be extended in the contemplated program by testing model piles having three different diameters in the ratio 1:2:4.

Examples of Wave Forces

As an aid in applying these results to piles, the following simple examples have been developed:

Example 1.

A pile 2 ft in diameter is driven in 50 ft of water at a point at which the maximum wave is forecast as $H = 20$ ft, $T = 7$ sec. From Fig. 2, $f_M/C_M = 0.35$ at surface. Using $C_M = 1.705$ and $C_D = 2.040$, chosen on the high side of the average values for safety, the force per unit of length is expressed as

$$\frac{dF}{dz} = \frac{(3.14)^2 \cdot 2 \cdot 2 \cdot 400}{2 \times 49} \left(-f_M \sin\theta \pm f_D \cos^2\theta\right)$$

Fig. 7(a) shows the variation of the maximum velocity force and the maximum inertia force as a function of distance below the surface. These two forces are out of phase and their maxima do not occur simultaneously. Fig. 7(b) shows the variation in total force with time at the surface, mid-depth, and bottom. The arrow indicates the phase position of the maximum total moment given by Eq. (6), that is,

$$M = \frac{\rho D H^2 L^2}{T^2}\left(\frac{-D\pi}{H\,4} C_M K_1 \operatorname{Sin}\theta \pm C_D K_2 \operatorname{Cos}^2\theta\right)$$

where

$\rho = 2.0$ slugs/ft^3 (salt water)

$D = 2.0$ ft

$H = 20.0$ ft

$T = 7.0$ sec or $L_o = 5.12(7)^2 = 251$ ft

$d = 50.0$ ft

$d/L_o = 0.1995$

$L = 225$ft* (*See footnote page 150)

$C_M = 1.705$ Model study values; further experiments

$C_D = 2.040$ are required to completely evaluate the range to these terms.

$$K_1 = \frac{1 + \frac{2\pi d}{L}\sinh\frac{2\pi d}{L} - \cosh\frac{2\pi d}{L}\,*}{2\operatorname{Sinh}\frac{2\pi d}{L}} = 0.403$$

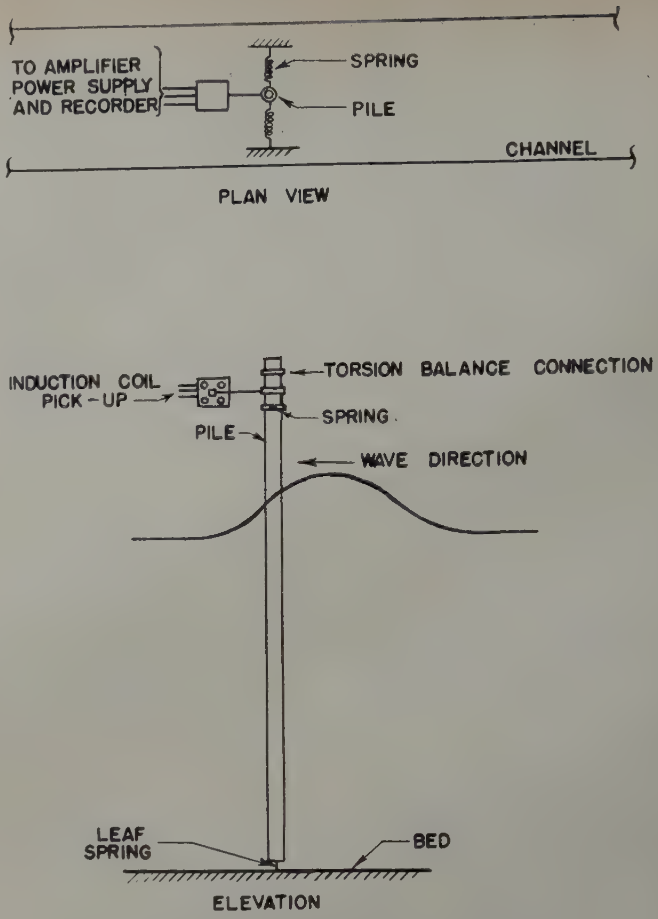

FIG. 9 — SCHEMATIC OF EXPERIMENTAL EQUIPMENT

$$K_2 = \frac{1 + \frac{1}{2}\left(\frac{4\pi d}{L}\right)^2 + \frac{4\pi d}{L}\sinh\frac{4\pi d}{L} - \cosh\frac{4\pi d}{L}}{64\left(\sinh\frac{2\pi d}{L}\right)^2} = 0.0852$$

$$\operatorname{Sin}\theta \text{ becomes } \operatorname{Sin}\theta_{max} = -\frac{\pi D K_1 C_M}{8 H K_2 C_D} = 0.1558$$

$$\operatorname{Cos}\theta_{max} = 0.9878$$

These values in equation (6) yield

$M_{max} = 293{,}000$ ft-lbs

$\theta_{max} = 8°57'$ (lead angle)

Example 2.

A pile 2 ft in diameter is driven in 50 ft of water where the maximum forecast wave is $H = 10$ ft, $T = 15$ sec.

$f_M/C_M = 1.67$ at surface

$$\frac{dF}{dz} = \frac{(3.14)^2 \cdot 2 \cdot 2 \cdot 100}{2 \cdot 225} \left(-f_m \operatorname{Sin}\theta \pm f_D \operatorname{Cos}^2\theta\right)$$

See Fig. 8(a) and 8(b)

$M_{max} = 77{,}600$ ft-lbs

$\theta_{max} = 8°5'$

ACKNOWLEDGMENT

The work described has been conducted under a contract with the Bureau of Ships and the Office of Naval Research. Kenneth Kaplan has participated in the analysis of the results. The authors are grateful to the late Harry Epstein of the Bureau of Yards and Docks for his critical review of this theory.

★ ★ ★

T.P. 2880

THE MICROLOG - A NEW ELECTRICAL LOGGING METHOD FOR DETAILED DETERMINATION OF PERMEABLE BEDS*

H. G. DOLL, MEMBER AIME, SCHLUMBERGER WELL SURVEYING CORP., RIDGEFIELD, CONNECTICUT

ABSTRACT

A new electrical logging method is described which measures the resistivity of small volumes of material near and behind the wall of the bore holes. The very small electrode systems used are supported in the face of the flexible insulator pad of appropriate dimension maintained in contact with the wall. The measurements are recorded simultaneously with two different electrode spacings.

This method provides a very detailed record of the formations and particularly of the permeable beds traversed by the bore holes.

The application of MicroLog to the location of permeable zones within compact formations, such as limestone, and to the determination of the amount of sand existing in sequences of thin shale and sand streaks is discussed.

The possibility of quantitative determination, providing a step toward the evaluation of formation porosity and mud cake thickness, is also examined.

Field examples illustrate the essential features of the method.

INTRODUCTION

In conventional electrical logging, the spontaneous potential (SP) log is used to delineate the permeable beds, and the resistivity logs are used primarily to provide indications concerning the fluid content of the beds.

When the formations are much more resistive than the mud, as happens, for example, in limestone fields, the SP currents are short-circuited by the more conductive mud column, with the result that the SP log is quite rounded. In that case, the SP log generally gives the approximate location of the permeable formations but it cannot be used for an accurate determination of the boundaries of each permeable bed.[1]

Solutions for the problem of obtaining a better determination of the permeable beds in limestone fields were developed from two angles. One approach consisted in improvements to the logging of the SP, as given by Selective SP logging and Static SP logging. These new methods, which have been described in an earlier paper,[2] give good results when the mud is not too salty, but they are still in a somewhat experimental stage, mostly because the development efforts have lately been concentrated on another approach to the problem, i.e., the MicroLog.

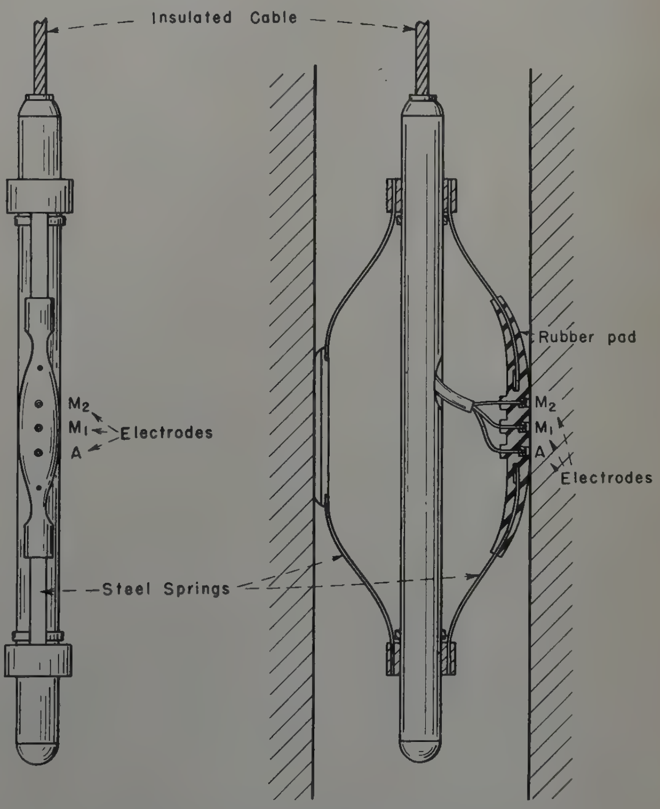

FIG. 1 — MICROLOGGING APPARATUS SHOWING DISTRIBUTION OF ELECTRODES

---

[1] References are given at end of the paper.

Manuscript received at the office of the Petroleum Branch February 6, 1950. Paper presented at the Annual Meeting of the AIME February 13-15, 1950 in New York, N. Y.

*MicroLog and MicroLogging: Trade Marks, Schlumberger Well Surveying Corp., Houston, Tex.

The MicroLog, which is the subject of the present paper, has been developed primarily as a means for the accurate determination of the permeable beds, where the SP log alone does not give a satisfactory answer. For that reason, this new development has found its first field of application in limestone areas, where the usefulness of MicroLogging is most obvious. The MicroLog is, however, also of importance in sand and shale formations, if only for a more precise determination of the boundaries between successive beds, and for a better evaluation of the sand count.

It is emphasized that the present paper is not intended to give an exhaustive and definitive description of the subject. In fact, the application of the new method has had a partly experimental character up to the present time, and several features of the corresponding technique are still being improved. It is possible that some of the improvements now under way will modify, to a certain extent, the response of the MicroLogs, and the procedure of interpretation. These differences, however, should not bring about any fundamental changes in the principle of this method, and should rather make its application easier and more reliable.

PRINCIPLE OF MICROLOGGING

A MicroLog is a resistivity log recorded with electrodes spaced at short distances from each other in an insulating pad which is pressed against the wall of the drill hole. Under those conditions, the system measures the average resistivity of the small volume of material—hereinafter referred to as a "microvolume" — which is located under the pad, and which is, therefore, electrically shielded against the short-circuiting action of the mud. Two different electrode systems, with different depths of investigation, are generally used in combination to provide two logs that are recorded simultaneously. For both electrode systems, the spacings are very small — usually one inch or two inches. In the discussion, the systems which have the smallest and the largest depth of investigation are respectively referred to as the "short spacing" and the "long spacing."

When the pad is applied to a permeable bed, the mud cake represents a substantial proportion of the microvolume. Inasmuch as the mud cake has a resistivity R_{mc} which can be estimated to be in general at most twice the resistivity R_m of the mud, the resistivities recorded through MicroLogging — hereinafter referred to as micro-resistivities — are never very high opposite permeable beds, and are appreciably related to the resistivity of the mud. The other part of the microvolume is constituted by a fraction of the solid structure of the permeable bed whose pores are almost completely filled by the mud filtrate. The resistivity of that part of the microvolume is, therefore, directly related to the resistivity of the mud.

It can easily be deduced from these considerations that the microresistivities measured opposite a permeable bed cannot generally be higher than a certain number of times the resistivity of the mud, unless the mud cake is very thin, and unless, simultaneously, the formation factor F is very high. A corresponding limit R_{lim} can be set at about 20 or 30 times the resistivity of the mud for the average case. This is why one of the rules of the interpretation for the MicroLog is to classify as most probably impervious all formations for which the microresistivities are higher than a certain limit R_{lim} directly related to the resistivity of the mud.

Because of a smaller depth of investigation, the short spacing is more influenced by the mud cake, and, therefore, generally gives a smaller apparent resistivity than the long spacing. This difference between the microresistivities recorded

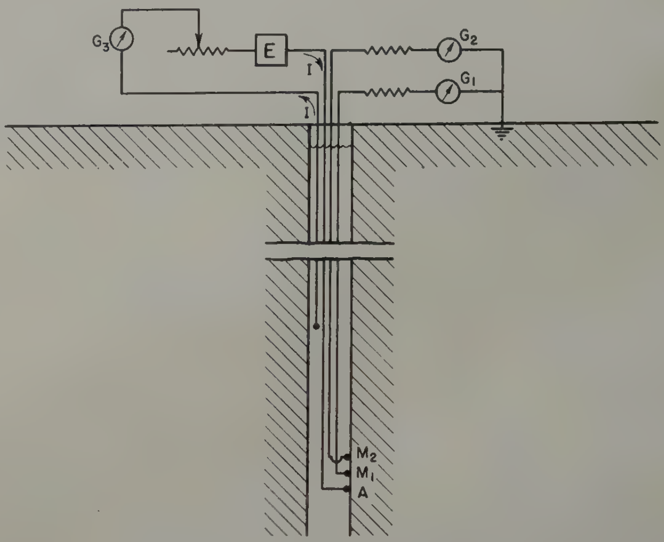

FIG. 2 — MEASURING THE RESISTIVITY OF THE SMALL VOLUME OF GROUND SURROUNDING THE ELECTRODES

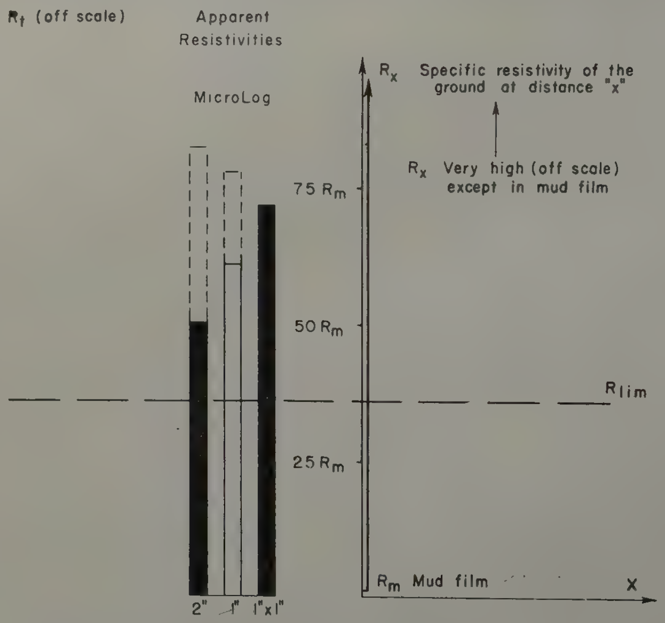

FIG. 3 — IMPERVIOUS FORMATION OF HIGH RESISTIVITY WITH A MUD FILM OF 1/64-IN. THICKNESS.

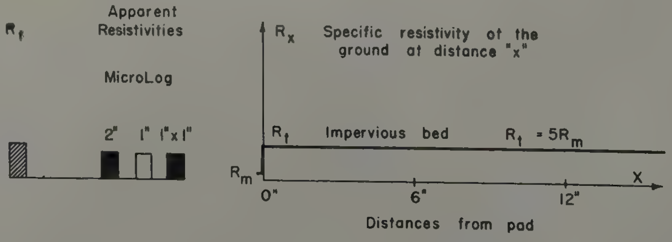

FIG. 4 — IMPERVIOUS BED OF LOW RESISTIVITY — SHALE (CATEGORY I_3)

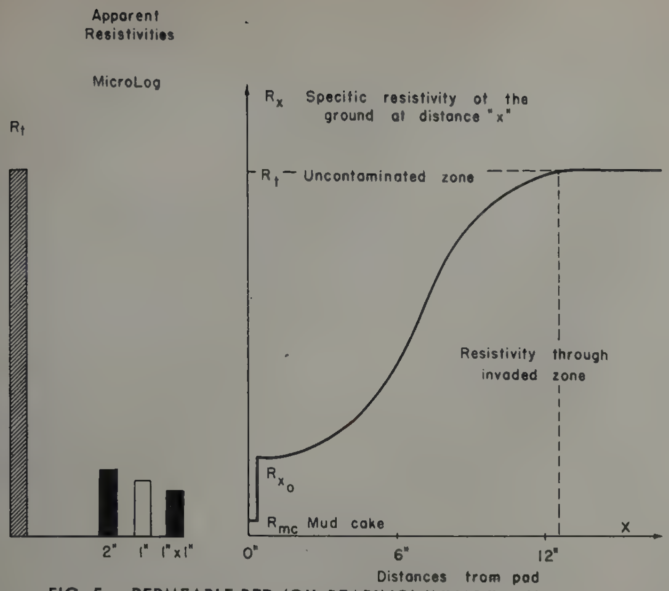

FIG. 5 — PERMEABLE BED (OIL BEARING) INVADED BY THE MUD FILTRATE
$R_t > R_{x_o}$
(CATEGORY P_2)

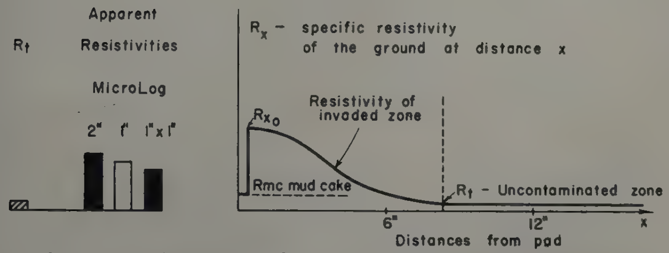

FIG. 6a — PERMEABLE BED (SALT WATER BEARING) WITH MODERATE INVASION BY MUD FILTRATE
$R_t < R_{x_o}$
(CATEGORY P_2)

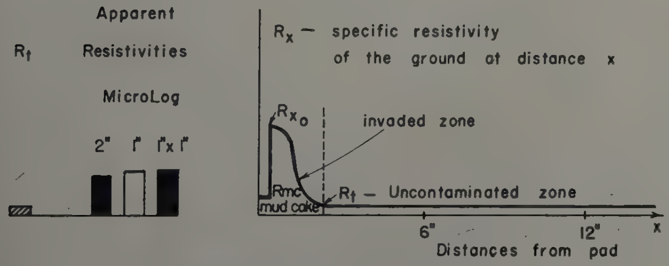

FIG. 6b — PERMEABLE BED (SALT WATER BEARING) WITH LITTLE INVASION BY MUD FILTRATE
$R_t < R_{x_o}$
(CATEGORY P_1)

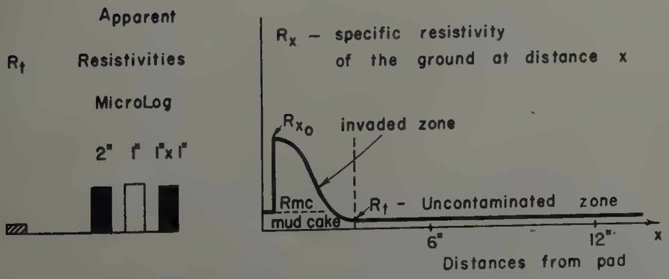

FIG. 6c — PERMEABLE BED (SALT WATER BEARING) WITH VERY LITTLE INVASION BY MUD FILTRATE
$R_t < R_{x_o}$
(CATEGORY P_1)

using two different depths of investigation is called "separation,"† and is said to be positive when the longer spacing gives the larger resistivity. When there is a large percentage of "positive separation," the formation can almost certainly be interpreted as permeable.

When the pad is applied to an impervious bed of low resistivity, both spacings measure substantially the same resistivity, which is that of the formation, and there is no appreciable separation between the microresistivity curves. If the resistivity of the impervious bed is very high, the microresistivities can differ appreciably from the formation resistivity, but they are both higher than the limit R_{lim} above which beds should be classified as impervious. For intermediate values of the resistivity, and because of the limited dimensions of the pad, a separation between the microresistivity curves is sometimes observed on impervious beds, but, in that case, the separation is negative, i.e., the longer spacing gives the smaller value of the apparent resistivity, so that there can be no confusion in the interpretation.

These different features of the interpretation will be discussed with more details in a later section.

DESCRIPTION OF THE EQUIPMENT

The MicroLogging apparatus consists essentially of a rubber pad, which is pressed against the wall of the drill hole, and in the face of which are inserted a certain number of electrodes. Several distributions of electrodes have been experimented with. One of the distributions is represented in Fig. 1A and 1B. The electrodes are nearly flush with the rubber surface, or slightly recessed, and each of them is connected by an insulated wire to one of the conductors of the cable used to lower the apparatus into the hole.

The rubber pad is molded on one of the branches of a spring guide whose design is such that the pressure applied to the pad is approximately independent of the diameter of the hole, provided that this diameter remains between certain limits which, for one of the guides presently in use, are respectively 4½-in. and 16-in. The rubber pad fits the wall of the drill hole over a substantial area surrounding the electrodes because of its shape and the pressure exerted upon it. The pad also shields the electrodes from the mud column, while the electrodes themselves are in direct contact either with the formation, or with the mud cake between the pad and the formation.

The resistivity of the small volume of ground surrounding the electrodes can be measured, for example, by sending a current of known intensity I through electrode A (Fig. 2), and by measuring, with galvanometer G_1, the potential difference created by that current between electrode M_1 and the reference electrode N.

Similarly, a slightly larger volume of ground can be taken into account by measuring, with galvanometer G_2, the potential produced at electrode M_2 by the same current. Because the spacing A M_2 is twice as long as the spacing A M_1, the corresponding investigation is also twice as deep. This is an important feature of the system; it is possible not only to measure the average resistivity of the ground under the pad, but also to determine whether or not the resistivity varies with depth from the pad. This determination is of significance, for a resistivity variation with depth from the pad usually occurs when there is a mud cake.

---

† The word "separation" has been introduced instead of the word "departure", previously used in the preprint of this paper, in order to prevent any confusion with the quite different acceptation of the word departure in the expression "resistivity departure curves."[4]

Electrode combinations other than A M_1 and A M_2 can, of course, be used. When a current is sent through electrode A, it is also possible to measure the potential difference between electrodes M_1 and M_2. The three-electrode system A M_1 M_2 is more influenced by the mud cake than the two-electrode system A M_1, so that a combination of the device A M_1 M_2 and the device A M_2 would generally give a larger separation opposite permeable beds than a combination of the two devices A M_1 and A M_2.

To simplify the wording, the two electrode and three electrode systems are called "micro-normal" and "micro-inverse" devices, respectively.‡

On most of the pads presently in use, the three electrodes are placed on a vertical line, in the middle of the pad, with a spacing of 1-in. between the successive electrodes. Three electrode combinations are thus obtained, which are listed herebelow for reference:

Measuring Device	*References*
A M_1 micro-normal	1-in. micro-normal (or 1-in.)
A M_2 micro-normal	2-in. micro-normal (or 2-in.)
A M_1 M_2 micro-inverse	1-in. x 1-in. micro-inverse (or 1-in. x 1-in.)

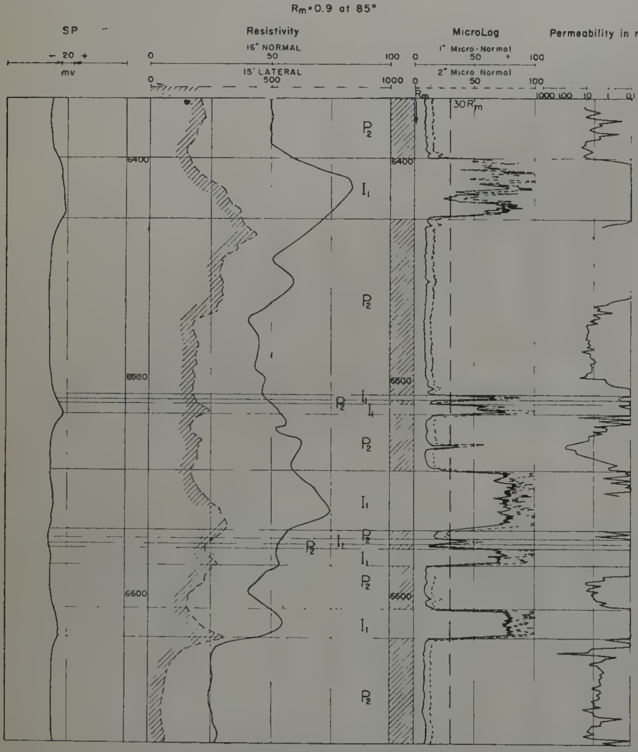

FIG. 7 — EXAMPLE OF MICROLOG

The combination of the 1-in. x 1-in. micro-inverse and the 2-in. micro-normal is preferred at the present time.

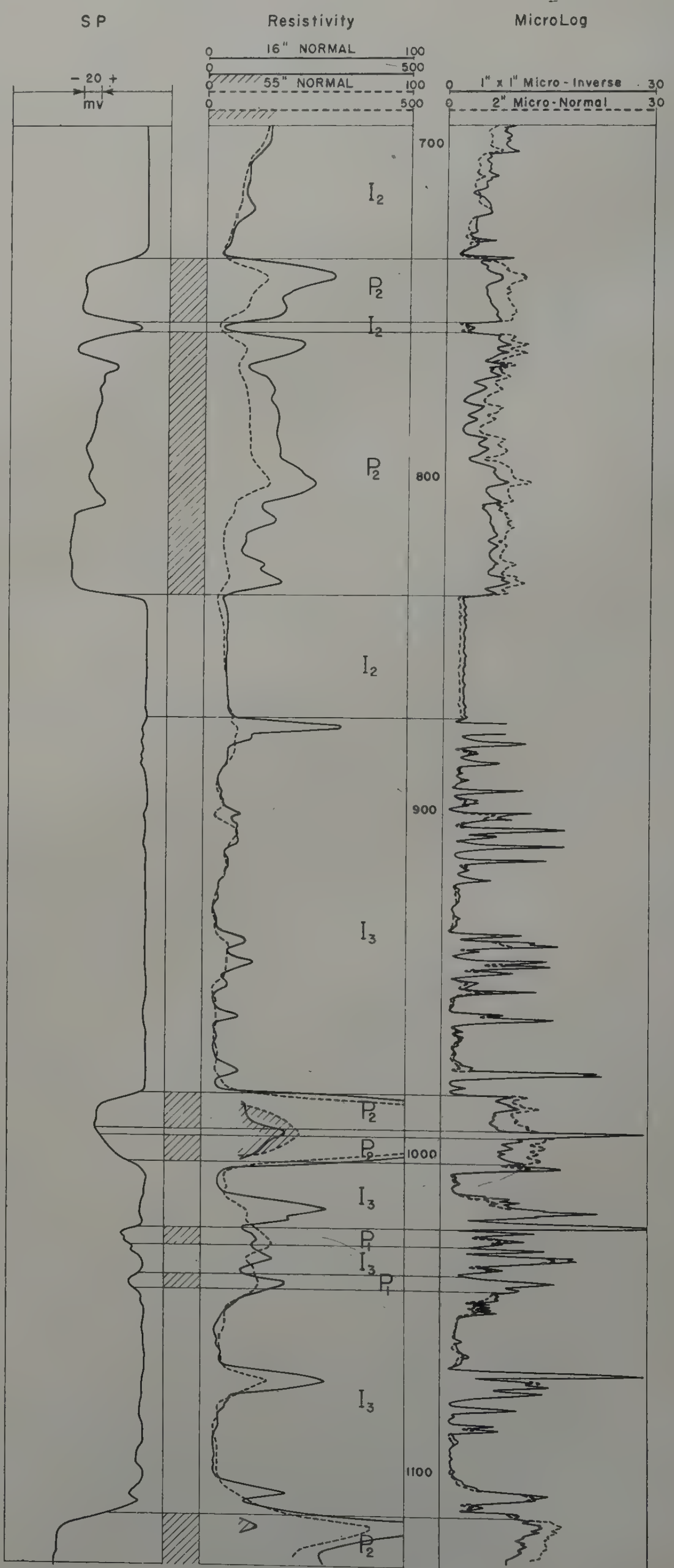

FIG. 8 — EXAMPLE OF MICROLOG

---

‡ The expression "micro-lateral" has been sometimes used instead of "micro-inverse." It should be pointed out, however, that MicroLogging devices, because they have much smaller depth of investigation and because the electrodes are shielded from the mud column, are different from the normal and lateral devices used in conventional logging.[4]

The electric circuit used for the recording of the microresistivity curves is somewhat similar to that used for conventional logging. Changes have been introduced, however, to compensate for the high resistance to ground of the small electrodes.

INTERPRETATION OF MICROLOGS

A discussion of the interpretation of the MicroLogs will be aided by placing the different cases usually encountered in practice into categories, which will be illustrated by schematic drawings (Figs. 3, 4, 5 and 6). Each category will be given a reference letter, namely, I_1, I_2, I_3 (Impervious beds), P_1, P_2 (Permeable beds). These letters will be placed on the field examples exhibited (Figs. 7 through 12) at the levels of each section of bore hole which can be considered as belonging to the corresponding category.

Highly Resistive Impervious Formations (Category I_1)

In impervious formations of high resistivity — i.e., whose resistivity is, for example, more than 50 times that of the mud — all the microresistivities are high. Because the wall of the drilled hole is generally somewhat rugose, the rubber pad cannot fit perfectly against it, and a sort of mud film may remain between the two. For that reason, and also because of the limited dimension of the rubber pad, the apparent resistivity recorded on the MicroLogs can be substantially lower than the true resistivity for that type of formation. When the formation resistivity is very high, the rugosity of the wall, which causes a mud film to remain under the pad, almost entirely controls the microresistivities. Too much importance should, therefore, not be attributed to the absolute values determined for the microresistivities, nor to the amount and type of separation between the two curves.

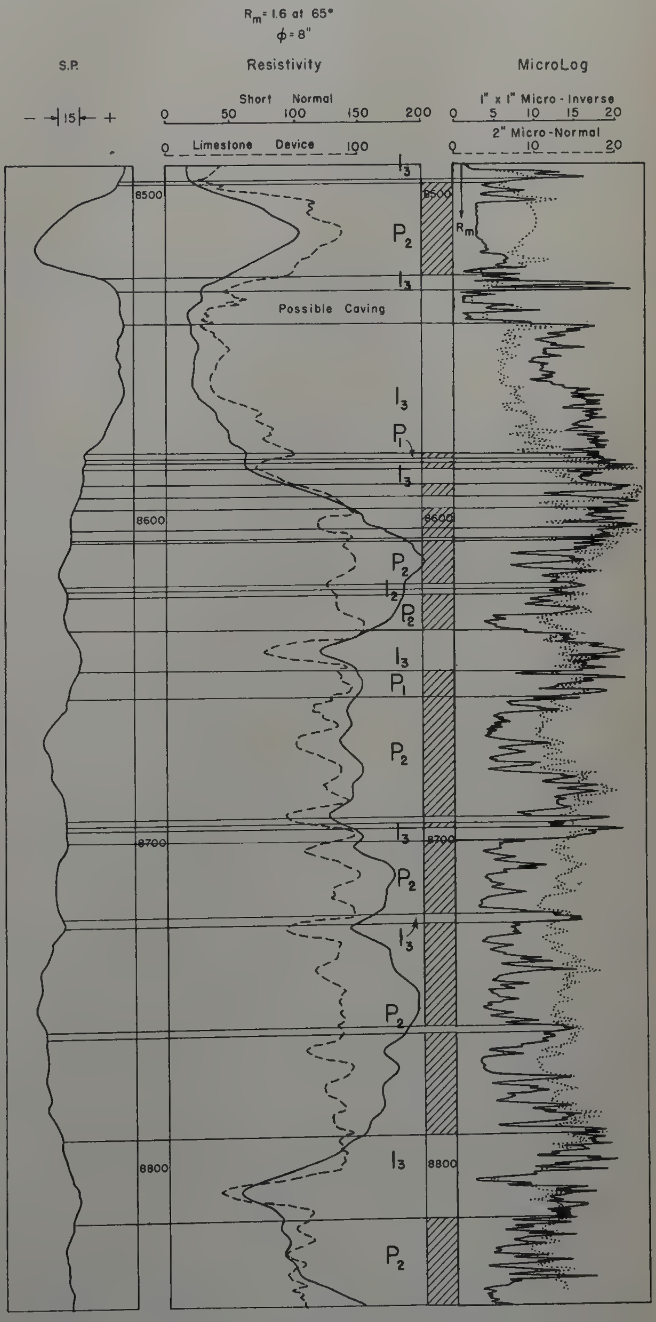

FIG. 10 — EXAMPLE OF MICROLOG IN VUGULAR LIMESTONE (ELLENBURGER)

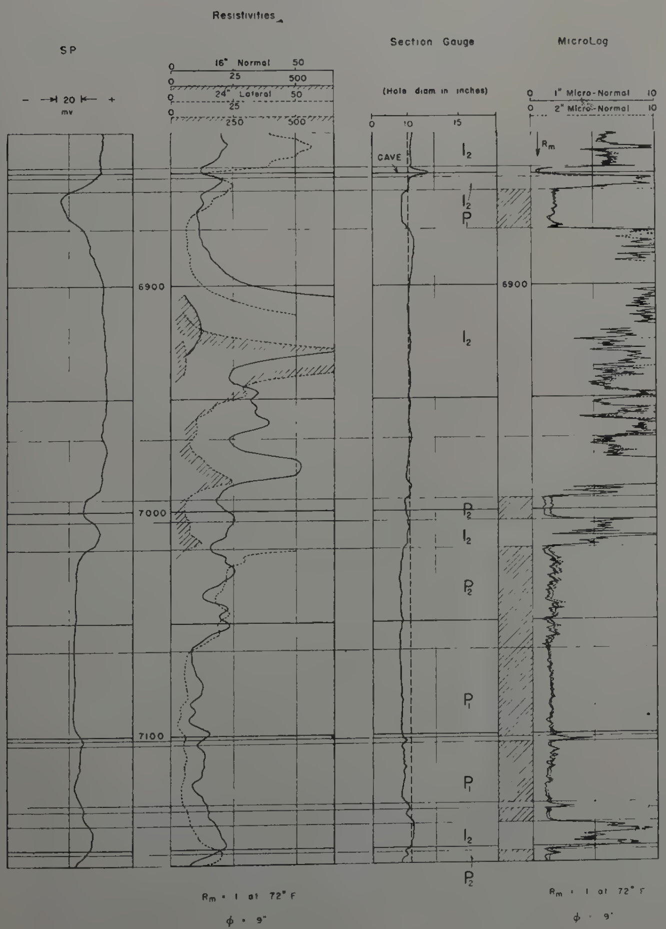

FIG. 9 — EXAMPLE OF MICROLOG

The diagnostic is based on this category on the fact that all microresistivities are superior to a certain limit R_{lim} which, as said before, can be taken equal to about 20 or 30 times the resistivity of the mud in the average cases. Such high microresistivities on both MicroLogs could not normally be recorded for a permeable formation. Both the invaded zone of the permeable formation and the mud cake would contribute to lower the apparent resistivity on the MicroLogs, and keep at least one of them, the 1-in. x 1-in. lateral or the 1-in. normal, under the limit R_{lim}.

The case of a compact bed of high resistivity is illustrated on Fig. 3, where it is supposed that the formation is more than 200 times as resistive as the mud, and that there is, between the pad and the formation, a uniform mud film 1/64-in. thick. The order of magnitude of the different microresistivities is about the same, but there can be a slight separation, either positive or negative, depending on the shape of the pad, the rugosity of the wall, the ratio formation resistivity to mud resistivity, etc.

Impervious Beds of Low Resistivity (Categories I_2 and I_3)

Fig. 4 represents the case of an impervious bed whose resistivity has been assumed to be five times the resistivity R_m of the mud. The resistivity diagram on the right of the figure illustrates the fact that the resistivity is uniform and does not vary with the distance from the pad, as would occur for a permeable bed. This diagram also shows the resistivity scale in relation to the resistivity R_m of the mud.

The rectangles at the left of Fig. 4 represent, at the same scale, the respective values of the different microresistivities that would be obtained in that case and the formation resistivity R_t. The apparent resistivities measured on the different micro-resistivity logs are slightly lower than the true resistivity R_t of the formation, because of the limited dimensions of the pad.

When the resistivity of the impervious bed is not much different from that of the mud, there is practically no separation between the microresistivity curves (Category I_3). When, on the contrary, the resistivity of the impervious bed is appreciably higher than that of the mud, there is generally, at least with the pads presently used, a substantial negative separation which is characteristic of an impervious bed (Category I_2).

Permeable Beds (Categories P_1 and P_2)

At the level of a permeable formation, the rubber pad slides over the mud cake against which it is applied, and the mud cake itself is separated from the uncontaminated part of the formation by the invaded zone, wherein the original fluid has progressively been replaced by mud filtrate.

Two cases must here be considered, depending on whether the invaded zone is less or more resistive than the uncontaminated zone.

The first case, which is the simplest as far as interpretation of the MicroLogs is concerned, is represented on Fig. 5, which is similar to Fig. 4 already discussed, except that now the resistivity varies in the formation with the distance from the pad. Here again, the abscissae on the diagram represent the depths from the pad, while the ordinates show the resistivity of the ground at the corresponding depths.

The resistivity R_{mc} of the mud cake has been assumed to be twice the resistivity R_m of the mud. The resistivity R_{xo} imme-

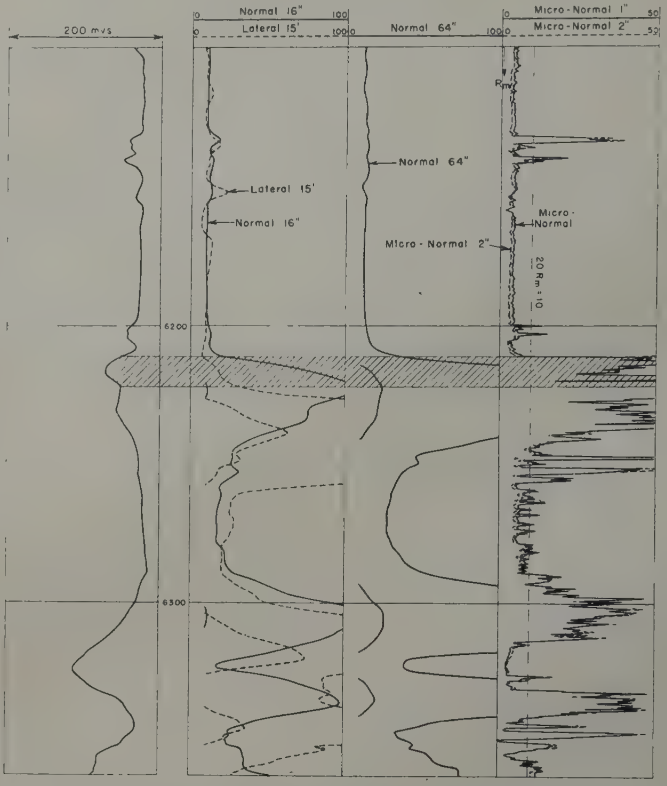

FIG. 11 — BED TESTED IN SPITE OF MICROLOG NEGATIVE INDICATION. NO FLUID RECOVERED AFTER CASING SET AND PERFORATED

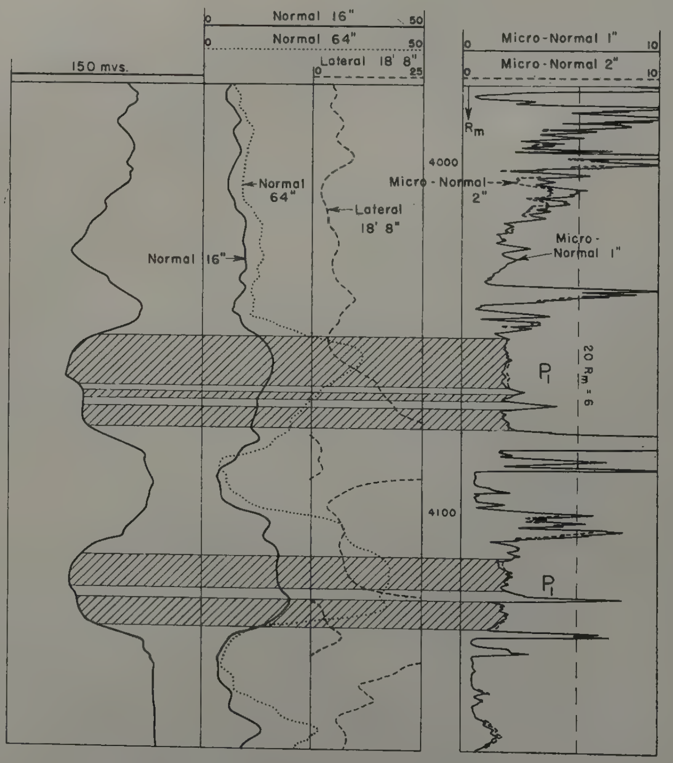

FIG. 12 — BEDS CONSIDERED AS TIGHT FROM CORE EXAMINATION AND SUBSEQUENTLY PUT TO PRODUCTION ON MICROLOG INDICATIONS

diately behind the mud cake, where the permeable bed should be practically saturated by mud filtrate, has been taken equal to 10 times R_m; this would correspond to a value of 10 for the formation factor, if the saturation by mud filtrate is complete,[3] and if the pores are reasonably free of conductive solids.[5]

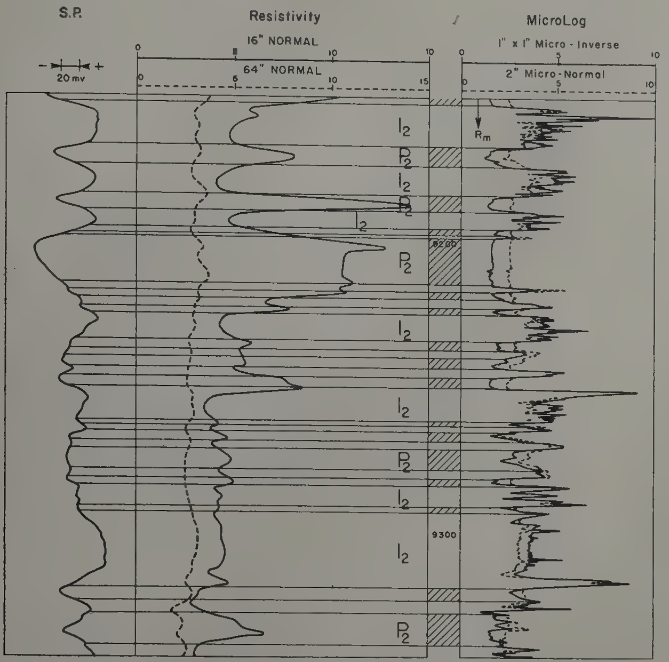

FIG. 13 — APPLICATION OF MICROLOG FOR A MORE ACCURATE DETERMINATION OF SAND COUNT IN SHALY SAND

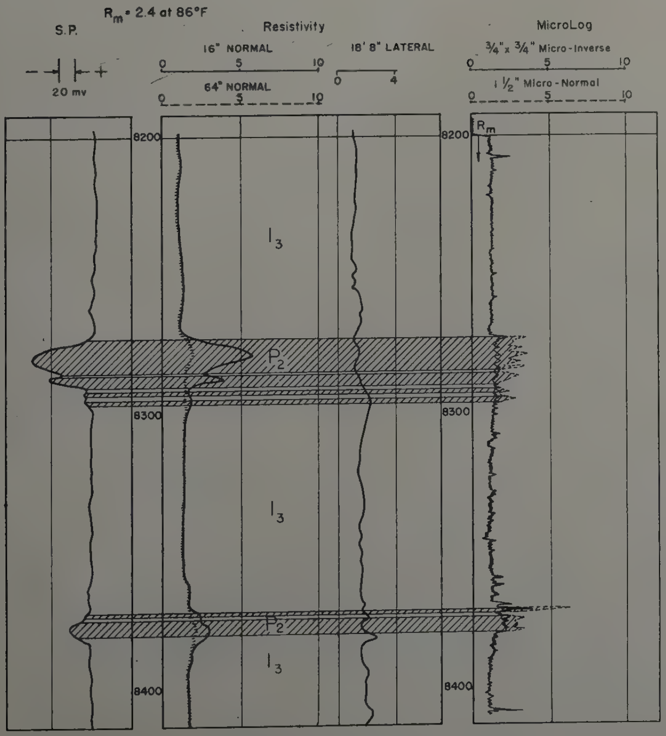

FIG. 14 — EXAMPLE OF MICROLOG IN SHALY SAND

On the left of Fig. 5 are represented, at the same scale, the approximate values of the microresistivities that would be obtained in that particular case from the MicroLog. As can be seen, the separation is positive and quite substantial. This result is general when R_t is larger than R_{xo}. A large positive separation between microcurves is characteristic of a permeable bed, provided, however, that the resistivity measured by the 1-in. x 1-in. lateral, or by the 1-in. normal, be lower than approximately 30 times that of the mud (Category P_2).

The interpretation is less definitive for beds, such as salt-water bearing beds, where the resistivity of the invaded zone is larger than that of the uncontaminated zone. This is particularly true when the mud is of the low water-loss type, with the consequence that the mud cake is thin and the formation is invaded by the mud filtrate to only a short distance from the wall.

When the mud cake has an appreciable thickness, and when, simultaneously, the depth of invasion is large enough, the micro-resistivities measured with the different electrode combinations show good positive separations (Category P_2). This case is represented on Fig. 6a. For a smaller penetration of the mud filtrate into the permeable bed, the separation would disappear (Category P_1), as represented on Fig. 6b. For still less invasion, the separation might even be slightly negative, as represented on Fig. 6c, but this negative separation never exceeds 20 per cent (Category P_1).

On the left-hand side of Figs. 6a, 6b and 6c are represented the approximate resistivities that would be measured on the MicroLog in the different cases, and for the different electrode combinations with the assumption that R_{xo} is about 5 times as high as the resistivity of the mud cake, which again corresponds to a formation factor of about 10. With them are also represented the formation resistivities. When the separation between the microresistivities is small, nil, or slightly reversed (within 20 per cent), the interpretation can be aided by the fact that these miroresistivities are larger than the formation resistivity, contrary to what would normally happen for an impervious bed of low resistivity, as discussed in connection with Fig. 4 above. It is simpler, however, to refer to the SP log to resolve the ambiguity in this case.

In all the cases represented in Figs. 3, 4, 5 and 6, the microresistivity corresponding to the 1-in. x 1-in. lateral could be computed with reasonable accuracy. The microresistivities corresponding to the 1-in. and 2-in. normals are only approximate, because the effect of the limited size of the pad cannot be accounted for accurately with these devices.

It is interesting to notice that the microresistivity for the 1-in. x 1-in. lateral is the same for the different cases represented on Figs. 4, 5 and 6, which cases differ only by the value of the true resistivity R_t and the depth of invasion by the mud filtrate. This illustrates the fact that the microresistivities, when measured with an electrode combination having a very small depth of investigation, are essentially responsive to the resistivity R_{xo} of the invaded zone and to the thickness and resistivity of the mud cake.

SUMMARIZED RULES OF INTERPRETATION

From the above discussion, it is possible to derive a certain number of simple rules of interpretation for the microresistivity logs of formations, whereby two electrode combinations of different depths of investigation have been run simultaneously. These rules which will apply in the great majority of cases, are schematically represented on Chart I.

Case I — The two microresistivities are higher than R_{lim}, that is, higher than about 20 or 30 times the mud resistivity. The formation then under study is a compact one, and should be interpreted as impervious, regardless of the separation (Category I_1).

Case II — The microresistivity determined by the shorter spacing, generally 1-in. x 1-in. lateral, is smaller than the limit R_{lim}. In that case, the sign and magnitude of separation should be examined, and, in case of doubt, the ambiguity resolved by reference to the SP log. This gives the following interpretation categories:

(a) Large negative separation (more than 20 per cent) — the formation is impervious (Category I_2).

(b) The separation is not definite enough (less than 20 per cent) — the MicroLog alone cannot determine, in general, whether the formation is permeable or not in this case, except that, when the resistivities of all formations are known to be much higher than that of the mud, the fact that the microresistivities are comparatively low gives a good probability that this is due to mud infiltration in a permeable bed. The ambiguity, if any, can be resolved by noting the trend of the SP curve. If that trend is positive, i.e., if the convexity is toward the positive side, or if the SP is on the positive limit (shale line), then the bed must be interpreted as impervious and the MicroLog gives its exact boundaries (Category I_3). If, on the contrary, the trend of the SP log is negative, the bed is permeable, and again the MicroLog gives the accurate boundaries (Category P_1).

(c) Large positive separation (more than 20 per cent) — the formation must be permeable (Category P_2).

Remarks

1. It is indeed wise to check the trend of the SP log in any case; unless this log is completely flat, it should always be possible to determine the trend of the SP.

When the mud is saturated with salt, the SP curve is usually flat. For limestone formations, however, there should be little doubt about the interpretation of the MicroLog in that case, because the permeable beds, which are invaded by the saturated mud filtrate, should be the only ones to give microresistivities lower than the limit R_{lim}, which itself is lower than the true resistivity of all impervious beds. The interpretation can then be based on the observation of the lows in the MicroLog, while a good positive separation, if it exists, brings a useful confirmation.

2. The interpretation is also facilitated by the consideration of the conventional resistivity log, insofar as this log makes it possible to evaluate the true formation resistivity R_t.

When the value of the microresistivity R_{micro} is less than R_{lim}, it can reasonably be assumed that a bed cannot be impervious unless R_t is comprised between values respectively equal to about R_{micro} and 2 R_{micro}. When R_t is between the two values, the SP log will generally give a definite anomaly that will make the interpretation safe. When R_t is not between the above limits, there is a strong probability that the bed is permeable.

3. In the particular case of a highly resistive permeable bed, with a comparatively conductive invaded zone, and interbedded with shales and highly resistive compact formations, the SP log may show no appreciable deflection with respect to the shale line. But, in that case, a good correct separation should be obtained from the MicroLog.

Exceptions to the Rules

There are a few cases which do not fall within the simple set of rules discussed in the previous section. Fortunately, these cases are rare, and the ambiguity can generally be resolved if the remarks made in the previous section are taken into account.

A first exception, which is obvious, corresponds to cavings whose diameters are larger than the maximum expansion of the spring system. If, in such a case, the pad remains a few inches from the wall, the two microresistivities will be equal to the resistivity R_m of the mud, irrespective of what the formation is. If, on the contrary, the pad happens to be near to the wall, the 1-in. x 1-in. micro-inverse will measure approximately the resistivity of the mud, whereas the 2-in. micronormal will already be substantially affected by the formation resistivity. Inasmuch as the formation resistivity is usually higher than that of the mud, even for a conductive shale, there will be a positive separation between the MicroLogs which could be falsely interpreted as indicating a permeable bed. These two cases can generally be detected by observing the abnormally low value given by the short spacing (1-in. x 1-in.) micro-inverse for which the microresistivity is frequently close to R_m in that case, and they would not fail to be recognized if a section gauge log were run, as is highly recommended when large cavings might exist. In those cases, the MicroLog indications should be disregarded, and the interpretation based on the conventional log, and, in particular, on the SP log, as far as the determination of the permeable beds is concerned.

Chart 1

$R_{1''\times 1''} > R_{lim}$	▨	▨	Impervious	Category I_1
$R_{1''\times 1''} < R_{lim}$	$R_{2''} < R_{1''\times 1''}$ large negative separation	▨	Impervious	" I_2
	$R_{2''} \simeq R_{1''\times 1''}$ separation nil or small	S P trend positive	Impervious	" I_3
		S P trend negative	Permeable	" P_1
	$R_{2''} > R_{1''\times 1''}$ large positive separation	▨	Permeable	" P_2

R_{lim} = equal to about
10 – 15 R_m for fresh mud
20 – 30 R_m for average mud
40 – 50 R_m for very salty mud

S P trend positive if convexity S P log toward positive, or if S P log on positive limit
S P trend negative if convexity S P log toward negative, or if S P log on negative limit

The interpretation rules could also be at fault if the mud cake, instead of being built on the wall, and within the hole, were built within the pores of the permeable bed. This case has not been encountered yet, but it seems that it could occur in coarse grain sands. If that did happen, the part of the permeable bed where the pores are filled with the mud deposit would be a little more resistive than the invaded zone behind, with the result that the 1-in. x 1-in. micro-inverse would measure an apparent resistivity slightly higher than that measured by the 2-in. normal. This would result in a negative departure, and the bed might, therefore, on the basis of the MicroLog, be falsely classified as impervious. Here again, the SP log would generally settle the question.

Other exceptions, which have not yet been observed, may exist and will reveal themselves when more examples are acquired. For that reason, it will always be useful to confront the indications given by the MicroLog with those obtained from the SP log, and also from the conventional resistivity logs, supplemented by the section gauge log when large cavings are to be expected.

FIELD EXAMPLES

Fig. 7 shows an example of a MicroLog recorded in a sequence of shales and limestone. In this instance, most of the compact beds give rise to microresistivities which are definitely higher than 30 R_m, so that the discrimination between permeable and impermeable formations is particularly easy. The permeability record, provided by core analysis, was available in this hole and is reproduced in the figure, as a check on the indications of the electrical logs.

In Figs. 8 and 9, sequences of sands, sandstones, limestones and shales are exhibited. At the upper part of Fig. 9, a sharp depression in the MicroLog brings the microresistivity down to approximately the resistivity R_m of the mud, a fact which is almost a certain indication of caving. This interpretation is confirmed by the section gauge log.

Fig. 10 shows the behavior of the MicroLog in the case of a thick limestone formation (Ellenburger), composed of compact zones and of fissured zones with vugular porosity.

Fig. 11 shows a limestone bed (cross-hatched zone), which corresponds to a deflection of the SP log, and which, however, appears as being impervious on the MicroLog. (Resistivity recorded on the MicroLog higher than 20 R_m—Category I_1.)

Despite the interpretation given by the MicroLog, the section was tested by gun perforation according to the deflection of the SP curve, and also to other indications (oil shows in cuttings . . .). No fluid was recovered. This is one among the numerous examples of formations which give rise to SP anomalies, although the permeability is too low for a commercial production to take place. In such cases of very low permeability (some fractions of a millidarcy), there is practically no penetration of mud filtrate, and therefore no mud cake built up. The MicroLog shows the formation as being tight, and therefore supplements, in a very useful way, the information given by the SP log.

Fig. 12 shows an example of sandstones (cross-hatched sections) which, contrarywise, had been first considered as tight, from core examination, and despite the negative deflection of the SP curve. The MicroLog shows low resistivities opposite these sections with a slight positive separation, which is a definite indication of permeability (Category P_1). It was accordingly decided to test the formations and production of gas was obtained.

Figs. 13 and 14 illustrate the features of the MicroLog in sequences of non-consolidated sands and shales, such as those commonly encountered in the Gulf Coast or in analogous geological provinces. In these regions, the conventional SP and resistivity logs differentiate very well the different sections where sands or shales are respectively predominant, but they are not capable of delineating each separate sand or shale streak, if these are thin. A very detailed record of the individual permeable and impervious beds is obtained from the MicroLog, as shown on the figures. This result is of interest for an accurate determination of the proportion of shale and sand in shaly sands, or, in colloquial terms, for the evaluation of the "sand count."

POSSIBILITIES OF QUANTITATIVE INTERPRETATION

To date, the MicroLog has been used primarily for a qualitative determination of the permeable beds and an accurate determination of their boundaries. It must be kept in mind, however, that the microresistivities measured for permeable beds are largely dependent on the resistivity and thickness of the mud cake, and on the resistivity R_{xo} of the formation immediately behind the mud cake. It is possible that the developments presently under way could bring the MicroLogging equipment to a point where R_{xo} and the thickness of the mud cake could be determined quantitatively from 2 micoresistivity curves. Pads which give a better fit on the wall of the hole, circular concentric electrodes and improved electric circuits are some of the steps being taken to raise the efficiency of the interpretation of the MicroLog, not only for its present qualitative use, but also in the hope that it might eventually lead to quantitative determinations.

When the first few inches of the permeable bed immediately behind the mud cake are practically saturated with mud filtrate, and when the mud cake is entirely built outside of the formation, and not partly within its pores, R_{xo} is equal to F R_{mf}, and, therefore, gives a direct measure of the formation factor F if the resistivity R_{mf} of the mud filtrate at the corresponding temperature is known. The possibility of determining the formation factor in situ and continuously would obviously be of great interest because of the close relation of that factor with the porosity[3], at least when the permeable material is reasonably free from conductive solids such as clay.[5]

It is more difficult to predict whether useful information could be derived from the thickness of the mud cake. Since laboratory experiments[6] have shown that, for a given mud, the thickness of the cake and the water loss are constants which do not depend on the nature of the permeable formation, and particularly on its permeability, it is logical to expect that all the mud cakes in a given hole will be found to have the same thickness. It is, however, possible that, even if the thickness of all mud cakes should be the same in a given well, a determination of that quantity would give valuable information about the behavior of the mud itself in the drill hole conditions. If further experience happens to show that the mud cake thickness varies from bed to bed, these variations could likely be related to some particular properties of the permeable formations, which might be of interest.

CONCLUSION

A new electrical logging method, called MicroLogging, has been discussed. This method makes use of electrodes applied to the wall of the drill hole under a non-conductive pad which shields them from the mud column. Two different microresistivity logs are recorded simultaneously, with two different electrode systems, which both correspond to very small electrode spacings.

Permeable beds are, in general, clearly indicated on the MicroLogs by a positive separation between the two microresistivity curves. Even when the separation is not definite, the interpretation is easy, thanks to simple rules based on the magnitude of the microresistivities, and on the behavior of the SP log. In all cases, the boundaries of the permeable beds are determined with great accuracy.

The MicroLog is, therefore, an important addition to the conventional electrical log, and should contribute to a better and more accurate determination of the permeable beds, particularly in limestone territories. Because of its accuracy in the determination of boundaries, the MicroLog should also render important services in sand and shale formations, where it could appreciably increase the accuracy of the sand count.

Finally, it is hoped that the MicroLog, after appropriate improvements, will permit quantitative determination and provide an approach toward the evaluation of porosity.

ACKNOWLEDGMENT

The author is indebted to the many engineers of the Schlumberger Well Surveying Corp. who, at headquarters and in the field, cooperated in the development of the method described in this paper. Acknowledgments are also due to the oil companies for their courtesy in making examples available.

REFERENCES

1. H. G. Doll: The SP Log: Theoretical Analysis and Principles of Interpretation. *Petroleum Technology*, Vol. II, September, 1948, or *Transactions AIME*, Petroleum Branch, Vol. 179, page 146.
2. H. G. Doll: Selective SP Logging. *Journal of Petroleum Technology*, Vol. 2, No. 5, p. 129.
3. G. E. Archie: The Electrical Resistivity Log as an Aid in Determining Some Reservoir Characteristics. *Petroleum Technology*, Volume J, 1942.
4. H. G. Doll, J. C. Legrand, E. F. Stratton: True Resistivity Determination from the Electric Log — Its Application to Log Analysis. *Oil and Gas Journal*, Vol. 46, No. 20, September 20, 1947, page 297 ff.
5. H. W. Patnode and M. R. J. Wyllie: The Presence of Conductive Solids in Reservoir Rocks as a Factor in Electric Log Interpretation. *Journal of Petroleum Technology*, Vol. 2, No. 2, p. 47.
6. H. T. Byck: The Effect of Formation Permeability on the Plastering Behavior of Mud Fluids. API Drilling and Production Practice, 1940, page 40.

★ ★ ★

T.P. 2854

DYNAMOMETER CHARTS AND WELL WEIGHING

L. W. FAGG, JOHNSON-FAGG ENGINEERING CO., TULSA, OKLAHOMA

The purpose of this paper is to present in a convenient form data and examples necessary in making dynamometer card analyses; also to outline a procedure of well weighing.

Many articles and papers have been written delving into the mathematical considerations relative to the shape and characteristics of dynamometer cards. However, it is recognized that there are too many unknown factors involved in such calculations to assure a workable degree of accuracy. For this reason the accepted procedure is to take dynamometer cards on wells in question rather than try to calculate the load curve.

The polished rod dynamometer is now recognized as a necessary tool for measuring loads, torque, and horsepower. It is also used to determine pump action and trouble-shoot for any seemingly abnormal pumping condition.

The apparently infinite variety of dynamometer cards that can be obtained is one reason for the general lack of usage of the dynamometer as a control instrument rather than a means for making routine measurements of loads and horsepower. When it is considered that the dynamometer card is a record of the *resultant* of all forces acting on the polished rod at any particular instant during the pumping stroke, the problem is then one of breaking down this resultant into its various components. As a means of a quick review we shall consider the examples shown in Figs. 1 to 9, and Tables I and II and then proceed to the interpretation of variously shaped cards caused by some abnormal operating condition.

In Table II, when we were considering the factors involved in calculating the peak polished rod load, it can be seen that the factors involved greatly oversimplify the problem. Certain assumptions are made which may or may not be even close to the actual field conditions, such as the specific gravity of the fluid generally considered as one; that the crank has constant angular velocity; that the down-hole friction is zero; and that the fluid lift is from the pump. In the following examples we shall see what a variation in *fluid weight* and *friction* can do to the general shape and magnitude of the dynamometer card. (Figs. 10 to 22.)

MAKING THE WELL STUDY

It is obvious that it would be impractical to consider in detail all of these factors each time a well study is made, inasmuch as each well study job could conceivably be extended into a research project rather than serve the practical requirements of finding the answer to a specific problem. For this reason it is important that some objective be established previous to the time the well study is made.

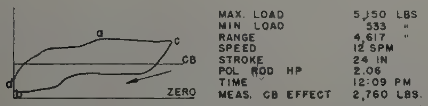

a = maximum load (height x scale constant)
b = minimum load. Range of load is difference between maximum and minimum load
speed — taken with stop watch
stroke — measured at polished rod
c = beginning of down stroke in direction of arrow. (End of up stroke)
d = beginning of up stroke. (End of down stroke).

Polished Rod Horsepower =

$$\frac{\dfrac{(\text{Area of card}) \times \text{Scale const.} \times \text{Stroke} \times \text{Length} \times \text{spm}}{(\text{Length of card})}}{33000 \times 12} = \frac{\dfrac{1.35}{2.53} \times 5300 \times 24 \times 12}{33000 \times 12} = 2.06$$

Approximate Peak Torque:
Upstroke = (2390) (12) (1) = 28,700 in. lb
Downstroke = (1860) (12) (.866) = 19,300 in. lb

Counterbalance should be increased to make up stroke and down stroke peak torque equal.

FIG. 1

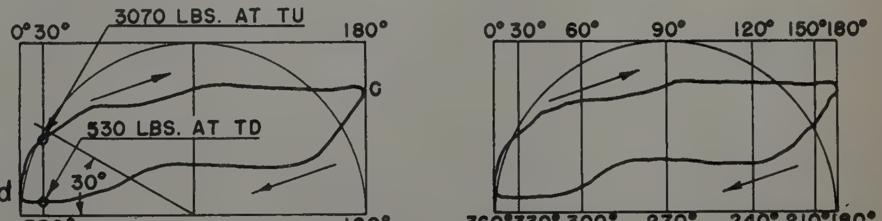

Load at TU = 3070 lb
Crank angle when polished rod is at position TU = θ
$\theta = 30°$
Maximum counterbalance effect at polished rod = 2760 lb

$$\text{Torque at TU} = (\text{Load at TU} - \text{Max. counterbalance effect-lbs}) \sin\theta \times \frac{\text{Length of Stroke}}{2}$$

$$= (3070 - 2760)\ .5 \times \frac{24}{2} = 1860 \text{ in. lb}$$

$$\text{Torque at TD} = (\text{Load at TD} - \text{Max. counterbalance effect-lbs}) \sin\theta \times \frac{\text{Length of Stroke}}{2}$$

$$= (530 - 2760) \sin 330° \times \frac{24}{2} = 13{,}400 \text{ in. lb}$$

Note: sin θ from c to d on UPSTROKE will be positive value.
sin θ from c to d on DOWNSTROKE will be negative value.
Torque at c and d is zero because θ is zero.

FIG. 2 — APPROXIMATE METHOD FOR CALCULATING TORQUE

Manuscript received at the office of the Petroleum Branch September 15, 1949. Paper presented at the Petroleum Branch meetings in Columbus, Ohio, September 26-27, and San Antonio, Texas, October 5-7, 1949.

In general the primary objectives are: (1) Information to be used as a basis for design of new installations; (2) Factual data to be used as a means for analyzing equipment failures; (3) Information necessary for proper control resulting in efficient pumping operation.

In order to satisfy the first consideration, design calculations as shown in Fig. 5 should be checked against dynamometer cards taken under comparable conditions. The pumping unit is usually designed to meet the capacity demand that will be expected, whether this be in the first or last stages. The bottom hole pump and sucker rod string, being more easily replaceable, are generally designed to meet the operating conditions anticipated for a reasonable time in the future.

If equipment failures are causing high operating expense, a bar chart such as shown in Fig. 4 will show failure frequency and serve as a guide when the well study is made. For instance, if most of the sucker rod breaks are in the top of the string, then a way should be found to reduce the peak load. If the failures are in the sucker

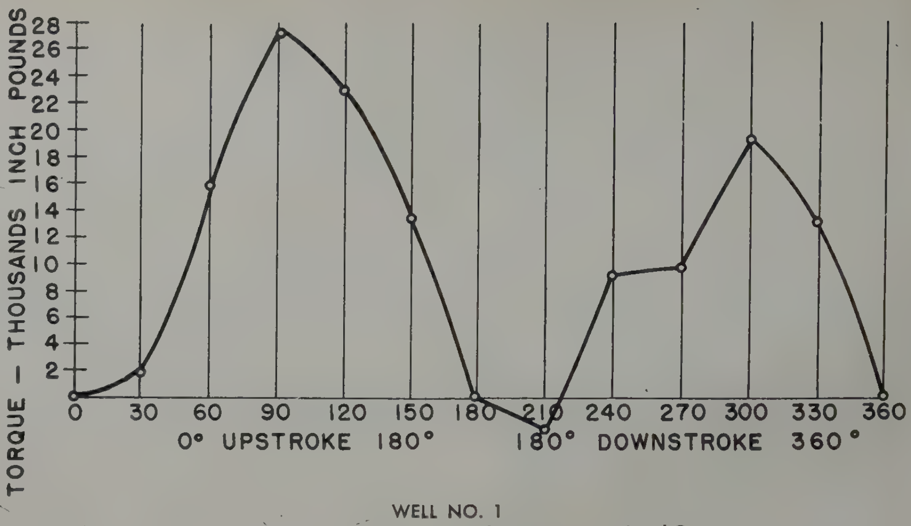

WELL NO. 1

Angle	Sine	Load	Counter Balance	Load Counter Balance	Torque
0°	0	1060	2760	— 1700	0
30°	.5	3070	2760	310	1860
60°	.866	4290	2760	1530	15900
90°	1.000	5040	2760	2280	27400
120°	.866	4980	2760	2220	23100
150°	.5	4980	2760	2220	13300
180°	0	4870	2760	2110	0
210°	— .5	3340	2760	580	— 3480
240°	— .866	1850	2760	— 910	9460
270°	— 1.000	1960	2760	— 800	9600
300°	— .866	955	2760	—1805	18750
330°	— .5	530	2760	—2230	13400
360°	0	1060	2760	— 1700	0

Torque may be figured at 15° intervals if more points are desired.

FIG. 3

ANALYSIS RECORD OF SUB-SURFACE EQUIPMENT FAILURES

COMPANY____________________
LOCATION____________________

REPORT NO.__________
LEASE__________
WELL NO.__________

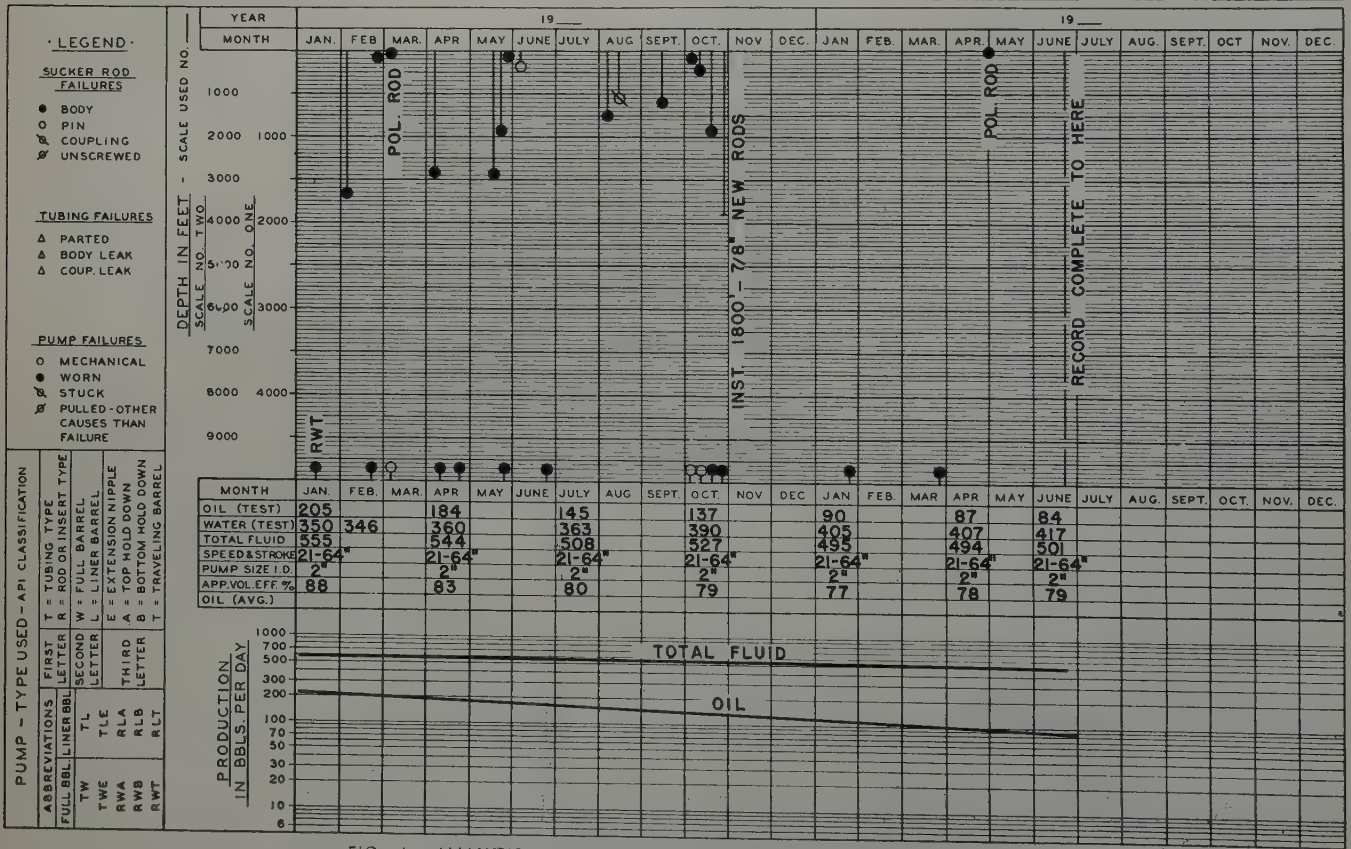

MONTH	JAN.	FEB.	MAR.	APR	MAY	JUNE	JULY	AUG	SEPT.	OCT.	NOV	DEC	JAN	FEB.	MAR	APR	MAY	JUNE	JULY	AUG.	SEPT.	OCT.	NOV.	DEC.
OIL (TEST)	205			184			145			137			90			87		84						
WATER (TEST)	350	346		360			363			390			405			407		417						
TOTAL FLUID	555			544			508			527			495			494		501						
SPEED & STROKE	21-64"			21-64"			21-64"			21-64"			21-64"			21-64"		21-64"						
PUMP SIZE I.D.	2"			2"			2"			2"			2"			2"		2"						
APP. VOL. EFF. %	88			83			80			79			77			78		79						
OIL (AVG.)																								

FIG. 4 — ANALYSIS RECORD OF SUB-SURFACE EQUIPMENT FAILURES

rod joint, then special attention should be given to joint makeup.

The dynamometer is now coming into wider use as a control instrument. After the proper equipment has been installed it is then important that it be adjusted to operate efficiently and under the most favorable load conditions.

The simplest way to do this is to take dynamometer cards at various speeds in order to determine the best load conditions that will give the desired production. The three variables that may be altered to satisfy this condition are the speed, stroke length, and pump size. Obviously, there is an optimum condition that will result in the least load and consequently the most trouble free operation.

In making a well study one of the most important considerations is to get a representative dynamometer card for the normal speed of operation. This is analogous to getting a representative sample of an oil-water mixture when metering a well's production.

When it is considered that a well operating at 20 strokes per minute makes approximately 28,800 strokes per day, it is easy to see that representative strokes are not always recorded. A procedure to lessen the possibility of an error of this kind is to take at least three dynamometer cards at intervals of fifteen minutes apart at the normal speed of operation. If these cards repeat or nearly repeat in shape it is reasonably safe to assume that representative cards have been taken. It is also advantageous to take dynamometer cards at various speeds throughout the considered pumping range so that the well may be operated under the most

Table I — Calculation of Apparent Volumetric Efficiency of Pump

Theoretical Production=Strokes per minute x Length of stroke x Pump constant.

$$\text{Apparent Volumetric Efficiency}=\frac{\text{Actual Production—As measured}}{\text{Theoretical Production}}$$

PUMP CONSTANTS

Size	¾″	15/16″	1″	1 1/16″	1¼″	1½″	1¾″	2″	2¼″	2½″	2¾″	3¾″	4″
Constant...	.065	.095	.117	.132	.182	.262	.357	.466	.590	.728	.881	1.64	1.86

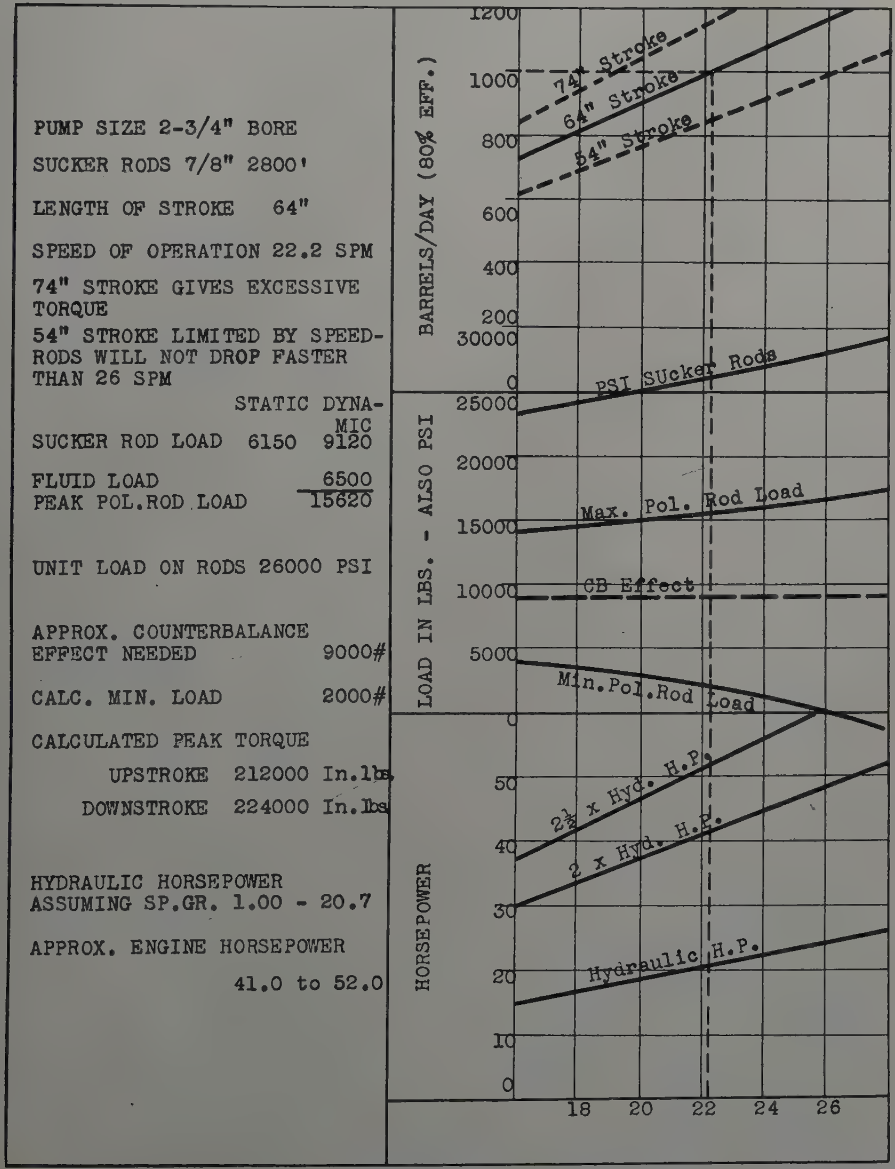
PUMP SIZE 2-3/4" BORE
SUCKER RODS 7/8" 2800'
LENGTH OF STROKE 64"
SPEED OF OPERATION 22.2 SPM
74" STROKE GIVES EXCESSIVE TORQUE
54" STROKE LIMITED BY SPEED-RODS WILL NOT DROP FASTER THAN 26 SPM

	STATIC	DYNAMIC
SUCKER ROD LOAD	6150	9120
FLUID LOAD		6500
PEAK POL. ROD LOAD		15620

UNIT LOAD ON RODS 26000 PSI
APPROX. COUNTERBALANCE EFFECT NEEDED 9000#
CALC. MIN. LOAD 2000#
CALCULATED PEAK TORQUE
UPSTROKE 212000 In.lbs
DOWNSTROKE 224000 In.lbs
HYDRAULIC HORSEPOWER ASSUMING SP.GR. 1.00 - 20.7
APPROX. ENGINE HORSEPOWER 41.0 to 52.0

FIG. 5 — DESIGN OF PUMPING INSTALLATION — 2800′ WELL. PRODUCTION 1000 BBL/DAY.

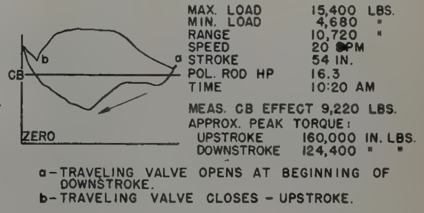

FIG. 6

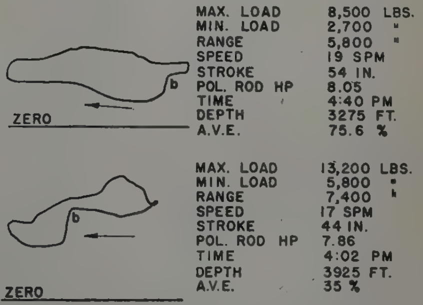

FIG. 7 — TYPICAL FLUID POUND; APPARENT VOLUMETRIC EFFICIENCY SHOWS VARIOUS STAGES OF PUMP OFF CONDITION.

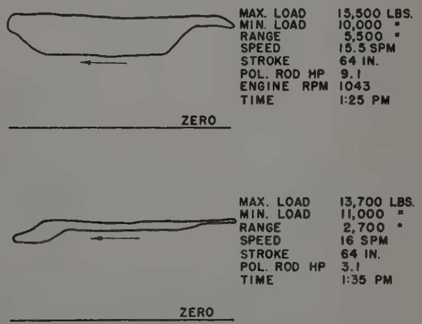

FIG. 8 — GAS POUND VARIOUS STAGES ON SAME WELL.

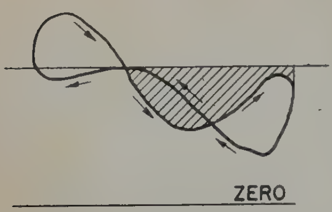

MAX. LOAD	14,000 LBS.
MIN. LOAD	4,000 "
RANGE	10,000 "
SPEED	22.5 SPM
STROKE	44 IN.
POL. ROD HP	3.5
TIME	1:47 PM

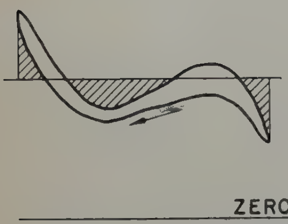

MAX. LOAD	15,500 LBS.
MIN. LOAD	5,500 "
RANGE	10,000 "
SPEED	20 SPM
STROKE	44 IN.
POL. ROD HP	3.1
TIME	3:15 PM

FIG. 9 — WELL IS AGITATING AND FLOWING. SHADED AREA SHOWS NEGATIVE TORQUE.

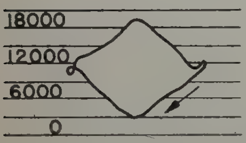

MAX. LOAD	19,800 LBS.
MIN. LOAD	2,000 "
RANGE	17,800 "
SPEED	22 SPM
STROKE	44 IN.
POL. ROD HP	18.8

30 RING PUMP PLUNGER

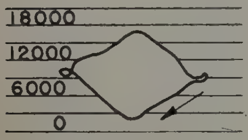

MAX. LOAD	17,000 LBS.
MIN. LOAD	2,000 "
RANGE	15,000 "
SPEED	23 SPM
STROKE	44 IN.
POL. ROD HP	18.5

15 RING PUMP PLUNGER

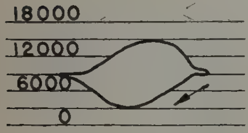

MAX. LOAD	14,800 LBS.
MIN. LOAD	3,000 "
RANGE	11,800 "
SPEED	23 SPM
STROKE	44 IN.
POL. ROD HP	15.4

7 RING PUMP PLUNGER

FIG. 11 — FRICTION IN PUMP.

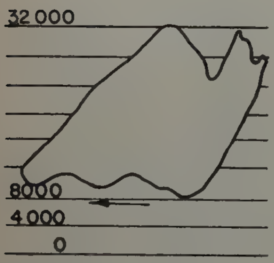

MAX. LOAD	32,000 LBS.
MIN. LOAD	8,000 "
RANGE	24,000 "
SPEED	5.8 SPM
STROKE	132 IN.
POL. ROD HP	25.4

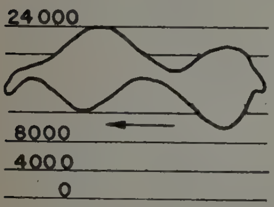

MAX. LOAD	24,000 LBS.
MIN. LOAD	10,000 "
RANGE	14,000 "
SPEED	8 SPM
STROKE	132 IN.
POL. ROD HP	16.8

SUCKER RODS: 2000 FT. — 1 IN.
4600 FT. — 7/8 IN.
PUMP 2 1/2 IN. X 1 3/4 IN. X 22 FT. RLB

FIG. 13 — SLACK IN TUBING.

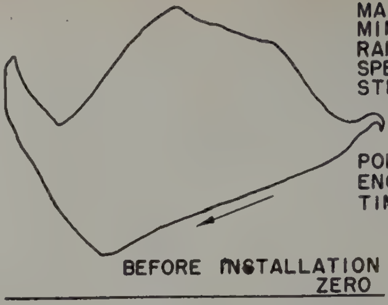

MAX. LOAD	21,000 LBS.
MIN. LOAD	3,700 "
RANGE	17,300 "
SPEED	19 SPM
STROKE	74 IN.
POL. ROD HP	30.7
ENGINE	786 RPM
TIME	8:30 AM

BEFORE INSTALLATION OF DUAL PUMP

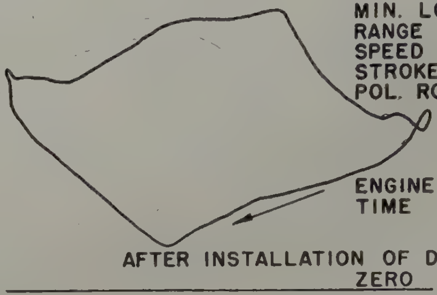

MAX. LOAD	20,700 LBS.
MIN. LOAD	4,000 "
RANGE	16,700 "
SPEED	19 SPM
STROKE	74 IN.
POL. ROD HP	30.5
ENGINE	780 RPM
TIME	3:15 PM

AFTER INSTALLATION OF DUAL PUMP

FIG. 10

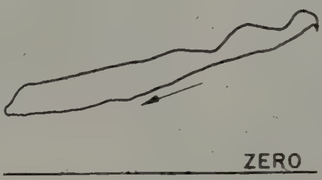

MAX LOAD	20,700 LBS.
MIN. LOAD	7,700 "
RANGE	12,930 "
SPEED	16 SPM
STROKE	64 IN.
POL. ROD HP	8.9
ENGINE RPM	810
TIME	12:30 PM

BEFORE

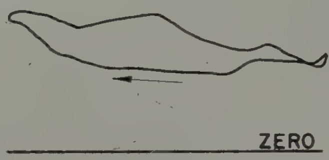

MAX. LOAD	17,700 LBS.
MIN. LOAD	9,800 "
RANGE	7,900 "
SPEED	16 SPM
STROKE	64 IN.
POL. ROD HP	9.4
TIME	9:45 AM

AFTER

FIG. 12 — BEFORE AND AFTER CLEANING PARAFFIN OUT OF TUBING.

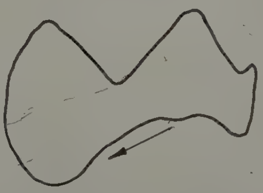

MAX. LOAD	19,000 LBS.
MIN. LOAD	7,000 "
RANGE	12,000 "
SPEED	22 SPM
STROKE	44 IN.
POL. ROD HP	19.1
TIME	2:30 PM
DATE	5-26-47

PUMPING THROUGH PACKER

ZERO

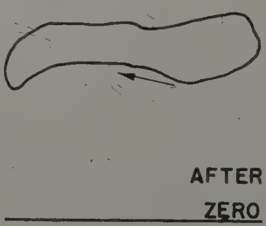

MAX. LOAD	14,700 LBS.
MIN. LOAD	9,800 "
RANGE	4,900 "
SPEED	23.5 SPM
STROKE	44 IN.
POL. ROD HP	9.9
TIME	2:45 PM
DATE	5-28-47

AFTER UNSEATING PACKER

FIG. 14

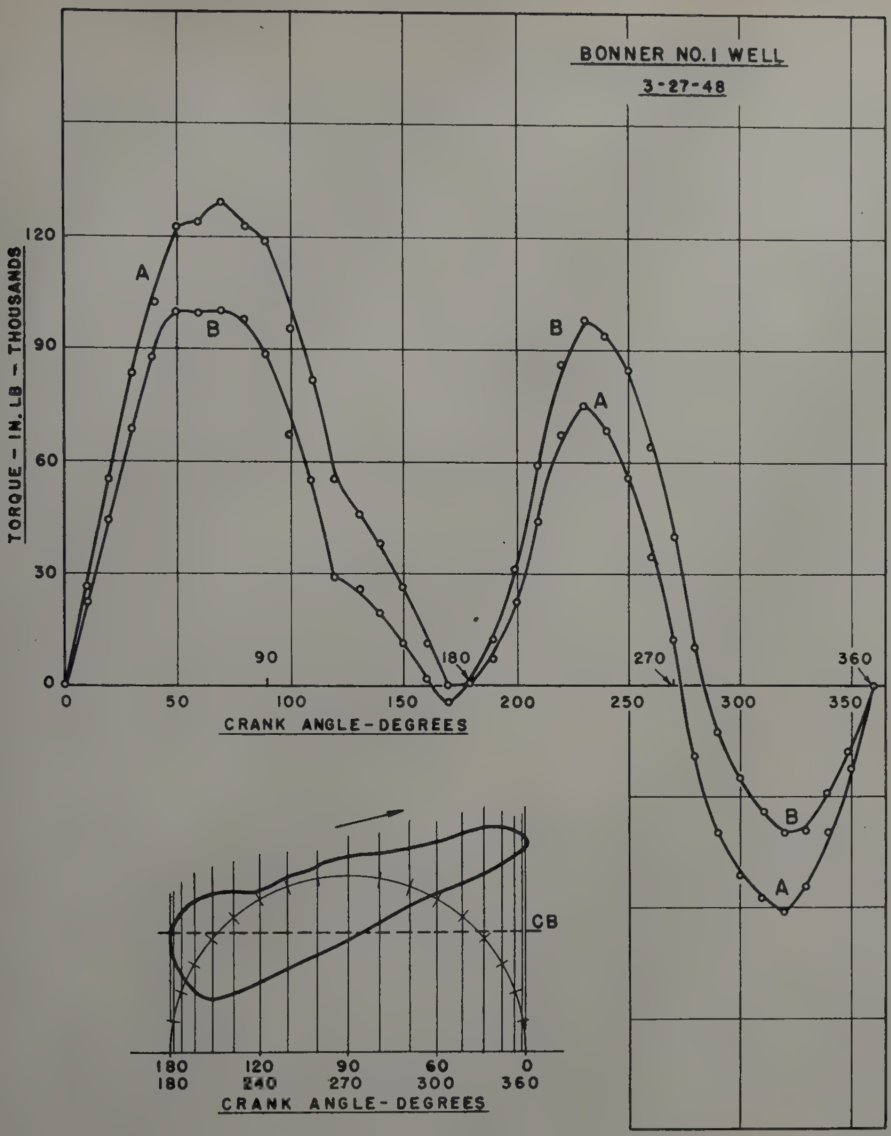

FIG. 15 — VISCOUS FLUID.

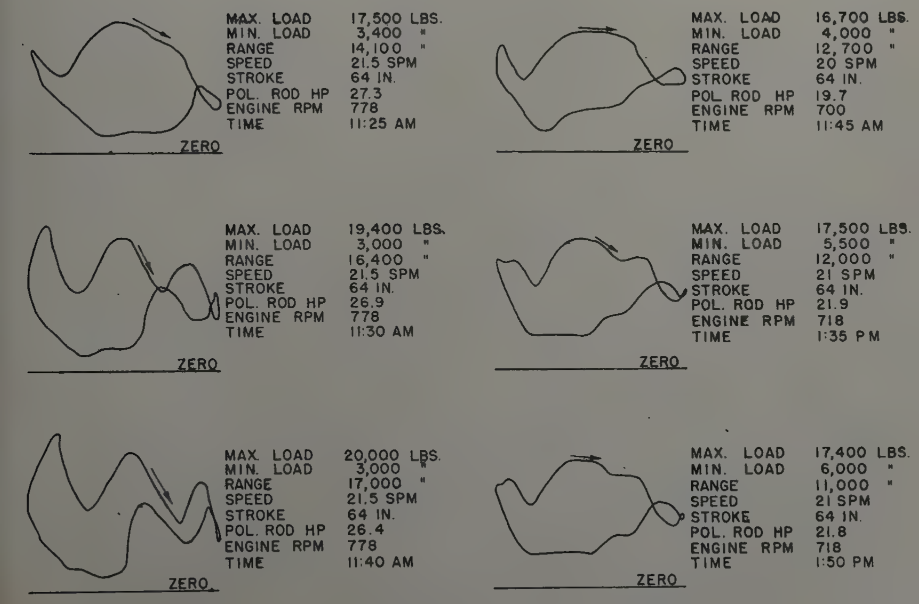

F.G. 16 — SAND PASSING PLUNGER CAUSING ABNORMAL CARD.

favorable load conditions. The author has frequently been asked to explain the pumping action of a well where only one dynamometer card was taken and which may or may not be anything like a second load curve would be. Inasmuch as all analytical work and subsequent recommendations are based on the character of the dynamometer card, the importance of having a card representative of normal operation cannot be overstressed.

CHECKING THE TRAVELING VALVE AND PLUNGER FOR LEAKS AND WEAR (FIG. 25)

After the desired number of dynamometer cards have been taken a new sheet of chart paper should be installed and the traveling valve checked as follows: The well should be stopped about the center of the upstroke with the stylii released so that the dynamometer is recording. The stroke component cord should be pulled at once. The recorded line represents the weight of the sucker rods plus the fluid weight on the plunger. The string should be pulled at about one second intervals and the rate of decrease of load noted. The time required for the load to reach the dead weight load of the rods will show how fast the fluid is leaking by the plunger or traveling valve. It is impossible by this method to differentiate between a leak in the traveling valve and fluid leakage past the plunger. The rate at which the load will equalize is dependent upon the plunger clearance and the depth to the pump, assuming the traveling valve is holding. Experience in making tests of this kind in conjunction with inspecting pumps that have been pulled will show when a pump is worn to the extent that it should be repaired or replaced.

CHECKING THE STANDING VALVE (FIG. 25)

The standing valve may be checked for leaks in a similar manner as that used in checking the traveling valve except the well is stopped near the end of the down stroke when the traveling valve is open and the standing valve is closed. The stylii are released on the chart paper and the stroke component cord pulled. This line will represent the dead weight of the rods in fluid. If the standing valve is not leaking this load line will remain in the same position. If the standing valve is leaking the load will increase showing that the standing valve is leaking and thus transferring a part of the fluid load on to the plunger and sucker rod string. A leaking standing valve then will show a build up in load on the polished rod under the above conditions.

CHECKING THE TUBING FOR LEAKS

The same procedure used for checking the standing valve should be followed, but in addition the bleeder valve should be opened to determine whether the fluid is falling in the tubing. If by means of the previous test it is shown that the standing valve is not leaking and yet the fluid level is dropping in the tubing, it is evident that the fluid must be leaking through the tubing. The rate at which the fluid drops in the tubing is generally not fast enough to register a noticeable load change on the dynamometer.

WEIGHING THE COUNTER-BALANCE EFFECT

While the instrument is still in place after taking a dynamometer card, it is

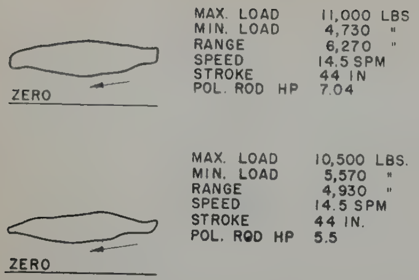

MAX. LOAD	11,000 LBS
MIN. LOAD	4,730 "
RANGE	6,270 "
SPEED	14.5 SPM
STROKE	44 IN
POL. ROD HP	7.04

MAX. LOAD	10,500 LBS.
MIN. LOAD	5,570 "
RANGE	4,930 "
SPEED	14.5 SPM
STROKE	44 IN.
POL. ROD HP	5.5

FIG. 17 — FRICTION IN STUFFING BOX

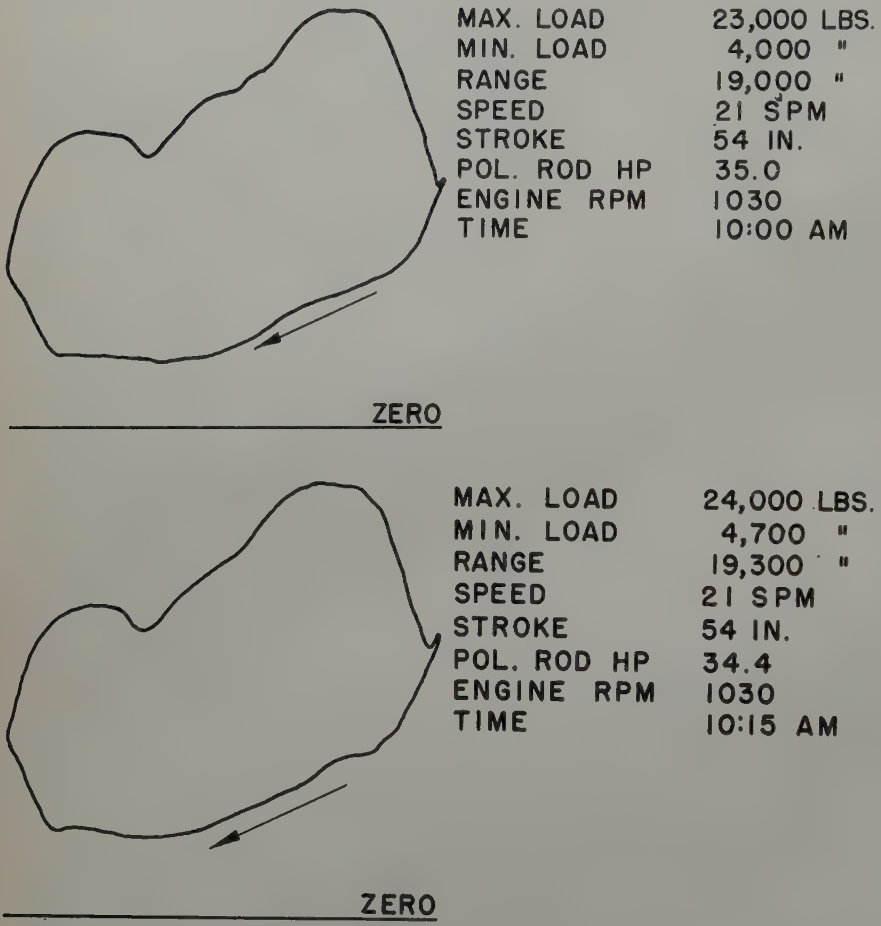

MAX. LOAD	23,000 LBS.
MIN. LOAD	4,000 "
RANGE	19,000 "
SPEED	21 SPM
STROKE	54 IN.
POL. ROD HP	35.0
ENGINE RPM	1030
TIME	10:00 AM

MAX. LOAD	24,000 LBS.
MIN. LOAD	4,700 "
RANGE	19,300 "
SPEED	21 SPM
STROKE	54 IN.
POL. ROD HP	34.4
ENGINE RPM	1030
TIME	10:15 AM

FIG. 18 — EXCESSIVE FRICTION CAUSED BY CROOKED HOLE T.D. 4600 FT SURROUNDING WELLS 4250 FT AVERAGE.

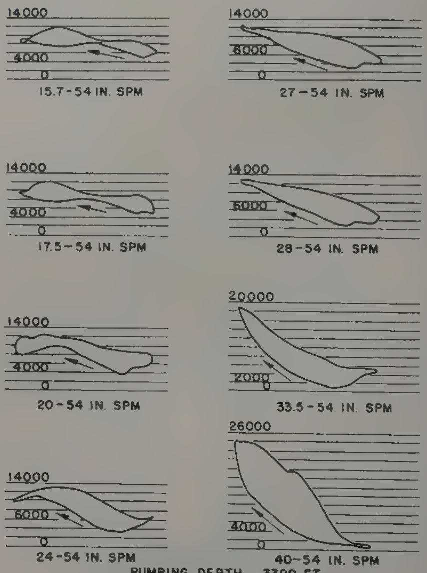

PUMPING DEPTH 3390 FT.
PUMP SIZE 2 3/4 IN. PLUNGER
SUCKER RODS 3375 FT. - 7/8 IN.

FIG. 20

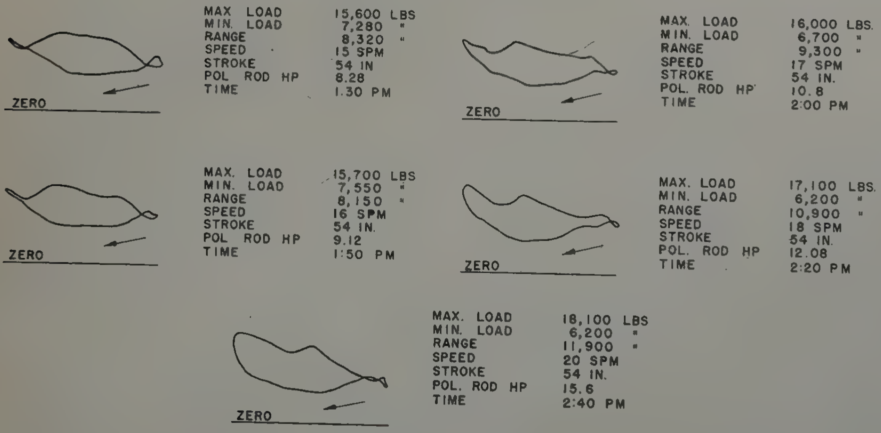

MAX LOAD	15,600 LBS
MIN. LOAD	7,280 "
RANGE	8,320 "
SPEED	15 SPM
STROKE	54 IN
POL ROD HP	8.28
TIME	1.30 PM

MAX. LOAD	16,000 LBS.
MIN. LOAD	6,700 "
RANGE	9,300 "
SPEED	17 SPM
STROKE	54 IN.
POL. ROD HP	10.8
TIME	2:00 PM

MAX. LOAD	15,700 LBS
MIN. LOAD	7,550 "
RANGE	8,150 "
SPEED	16 SPM
STROKE	54 IN.
POL ROD HP	9.12
TIME	1:50 PM

MAX. LOAD	17,100 LBS.
MIN. LOAD	6,200 "
RANGE	10,900 "
SPEED	18 SPM
STROKE	54 IN.
POL. ROD HP	12.08
TIME	2:20 PM

MAX. LOAD	18,100 LBS
MIN. LOAD	6,200 "
RANGE	11,900 "
SPEED	20 SPM
STROKE	54 IN.
POL. ROD HP	15.6
TIME	2:40 PM

FIG. 19 — SPEED CHANGE.

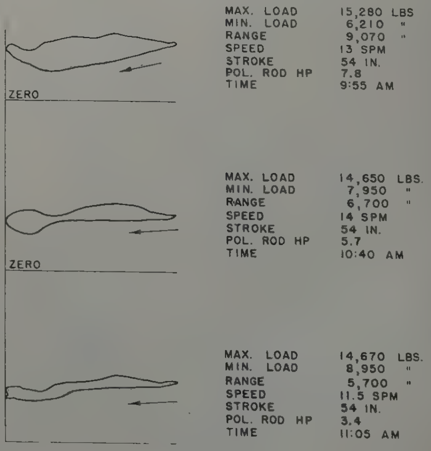

MAX. LOAD	15,280 LBS
MIN. LOAD	6,210 "
RANGE	9,070 "
SPEED	13 SPM
STROKE	54 IN.
POL. ROD HP	7.8
TIME	9:55 AM

MAX. LOAD	14,650 LBS.
MIN. LOAD	7,950 "
RANGE	6,700 "
SPEED	14 SPM
STROKE	54 IN.
POL. ROD HP	5.7
TIME	10:40 AM

MAX. LOAD	14,670 LBS.
MIN. LOAD	8,950 "
RANGE	5,700 "
SPEED	11.5 SPM
STROKE	54 IN.
POL. ROD HP	3.4
TIME	11:05 AM

FIG. 21 — FLUID IN TUBING AERATED.

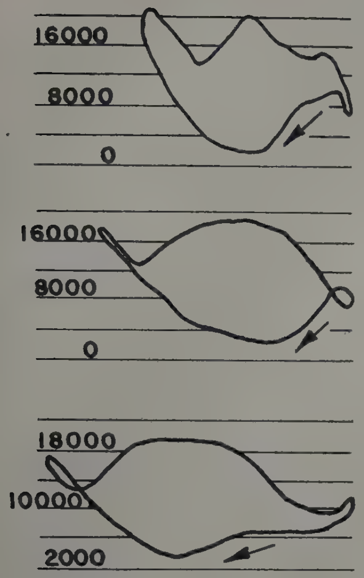

MAX. LOAD	20,500 LBS.
MIN. LOAD	2,000 "
RANGE	18,500 "
SPEED	28 SPM
STROKE	50 IN.
POL. ROD HP	34.4
PEAK TORQUE	231,000 IN. LB.
PROD	694 BBL. DAY
DISPL	117 FT PER MIN

MAX. LOAD	18,700 LBS.
MIN. LOAD	2,000 "
RANGE	16,700 "
SPEED	24.5 SPM
STROKE	62 IN.
POL. ROD HP	32.6
PEAK TORQUE	258,000 IN. LB
PROD	775 BBL DAY
DISPL	126.5 FT PER MIN

MAX. LOAD	19,000 LBS.
MIN. LOAD	3,000 "
RANGE	16,000 "
SPEED	21.5 SPM
STROKE	74 IN.
POL. ROD HP	29.8
PEAK TORQUE	296,000 IN. LB.
PROD	745 BBL. DAY
DISPL	132 FT PER MIN

FIG. 22 — LOAD AND TORQUE CHANGE DUE TO CHANGE OF STROKE LENGTH.

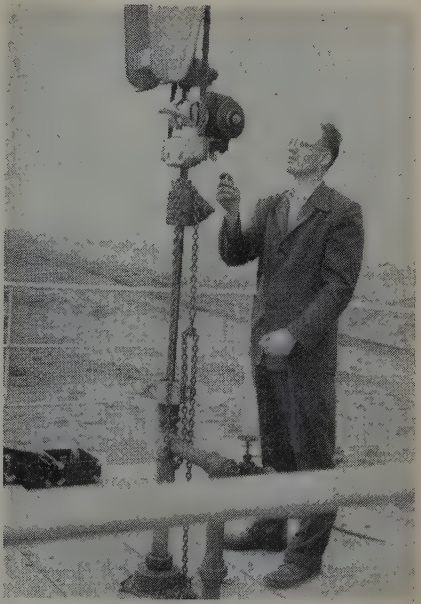

FIG. 23

a simple matter to weigh the actual counter-balance effect at the polished rod. The following procedure may be used.

(a) Stop the pumping unit at the position where the counterbalance effect is the greatest. That is, the point at which the crank is horizontal on the upstroke.

(b) Place a polished rod clamp a few inches above the stuffing box or above the polished rod liner if there happens to be one installed.

(c) Place a chain above the clamp just installed and wrap around the polished rod one turn, then run the chain under the casing head vent line or under the lead line and hook the chain together as closely as possible.

(d) Release the brake and check to see that the clutch is not dragging. Release stylii and pull the cord. This records the counterbalance effect as measured at the polished rod.

If the well is considerably underbalanced the rods will go down when the brake is released. In this case the clamp should be put directly over the stuffing box to prevent the rods from going down. No chain is necessary for this condition. For correct counterbalancing the measured counterbalance effect line should pass through the approximate center of the dynamometer card.

The maximum counterbalance effect must be known before instantaneous horsepower values can be calculated from the dynamometer card.

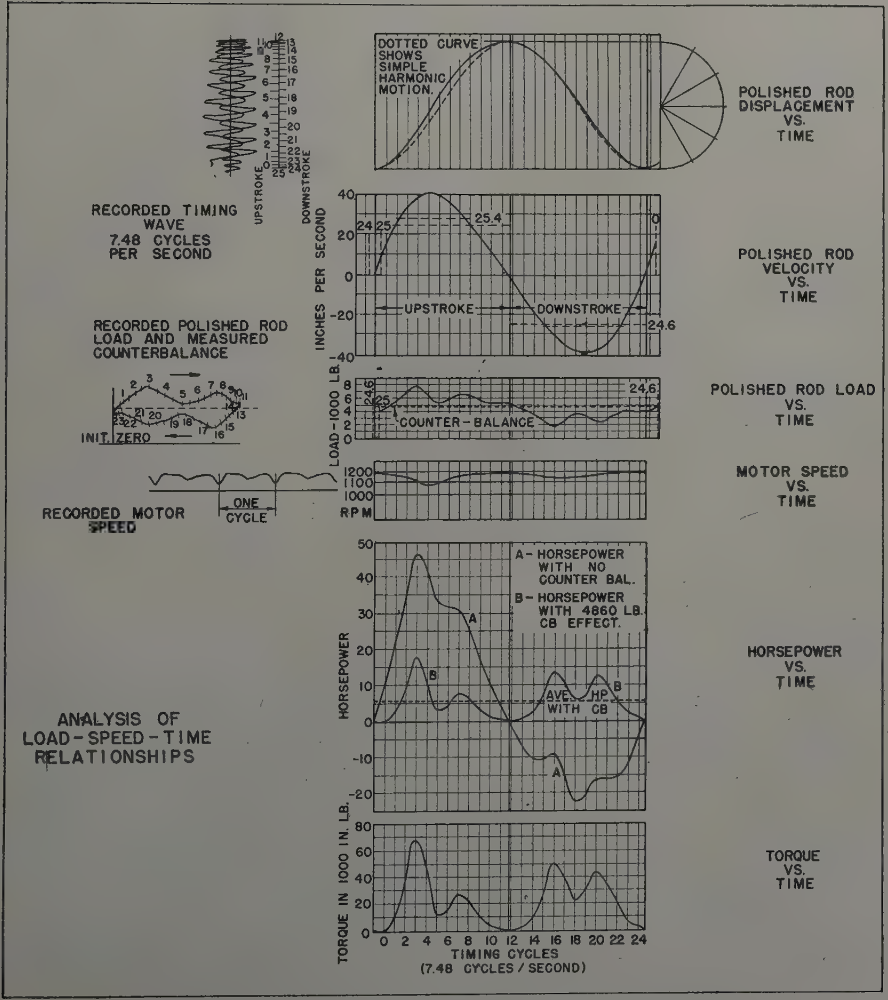

FIG. 24 — ANALYSIS OF LOAD SPEED-TIME RELATIONSHIPS

RECORDING THE TIMING WAVE

Release the stylii and press the end of the bar against the stop mechanism. Release it just before the bottom of the downstroke. The bar should then be allowed to vibrate through one complete stroke, at which time the stylus should be raised so there will not be an excessive number of lines recorded. The time constant for each cycle is given on the timing bar.

The timing wave is used to obtain instantaneous velocities which may be projected on the dynamometer card and used as a means for calculating instantaneous horsepower. (Fig. 24.)

RECORDS AND WELL DATA

In order to make proper analysis of the dynamometer cards and other information secured at the well it is necessary to have a detailed record of service of the principal components of the pumping system. These should include any major repairs to the engine or pumping unit; a record of sucker rod and polished rod failures showing date, depth, type of break (body, pin or coupling) and notations such as pitting due to corrosion or embrittlement due to hydrogen sulphide; a record of all pump changes with detailed information showing what caused the pump to fail.

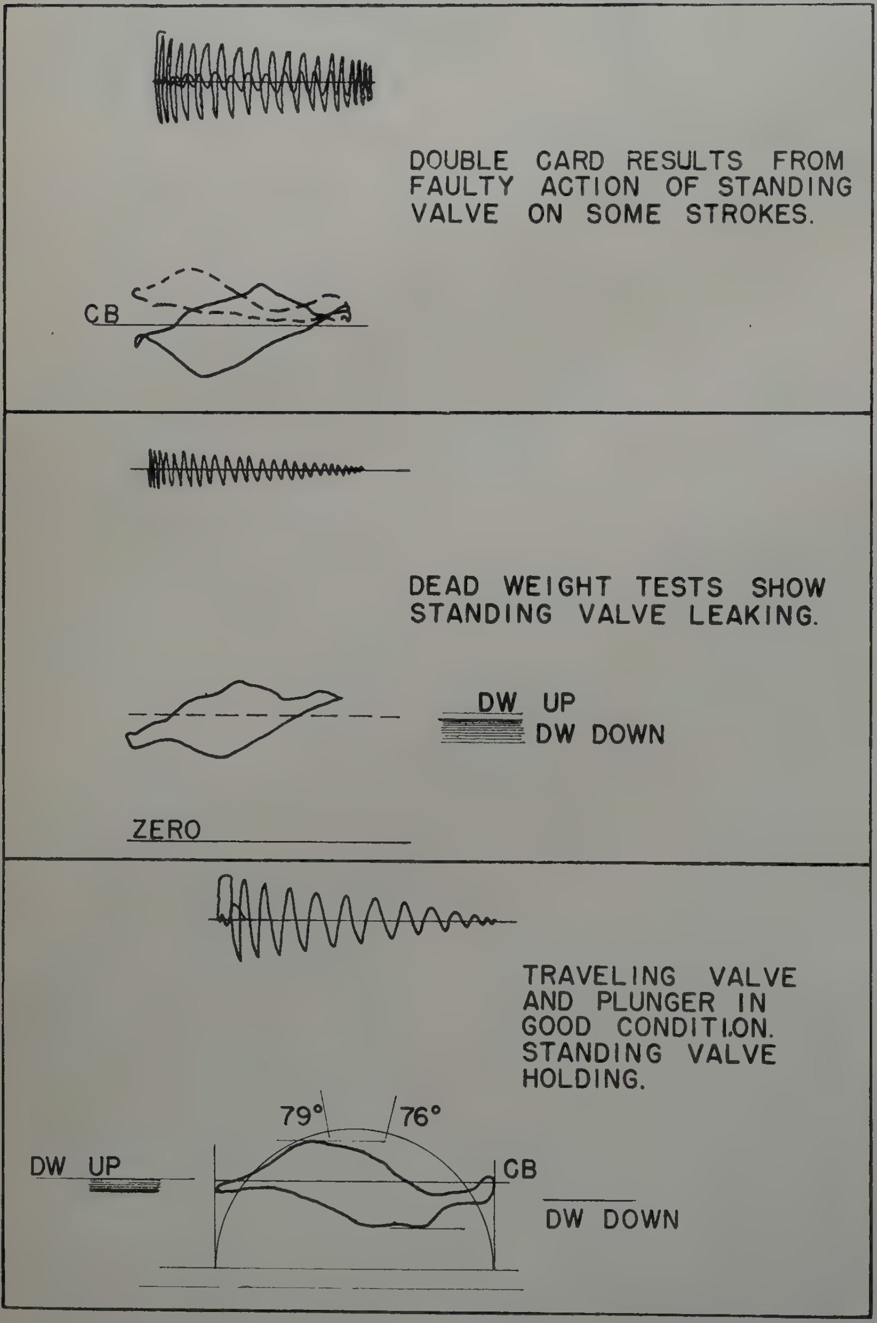

FIG. 25 — CHECKING THE TRAVELING VALVE, PLUNGER AND STANDING VALVE.

In one area where this type of record was kept it was shown that in twenty-six per cent of the pulling jobs due to pump failures there was nothing wrong with the pump. Cases of this kind are prevalent where a number of wells are pumping into a central tank battery and it is often difficult to know which well is failing when the lease production drops off. By having records and data as mentioned above and by making individual well studies, mechanical problems can be easily analyzed and very often their solution is obvious.

RECORDING TACHOMETER

Another useful instrument in making well studies is the recording tachometer. This not only gives the engine speed but also the engine speed variation during the pumping stroke. In certain cases it may be used for checking the well for proper counterbalance.

BALANCING CENTRAL POWER

Balancing of central power is covered by Figs. 27-30. The method used

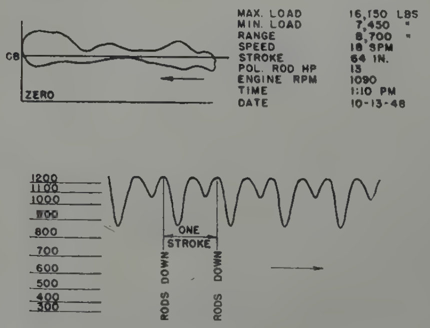

FIG. 26 — RECORDING TACHOMETER CHART.

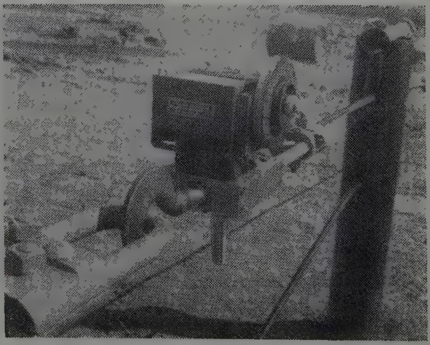

FIG. 27

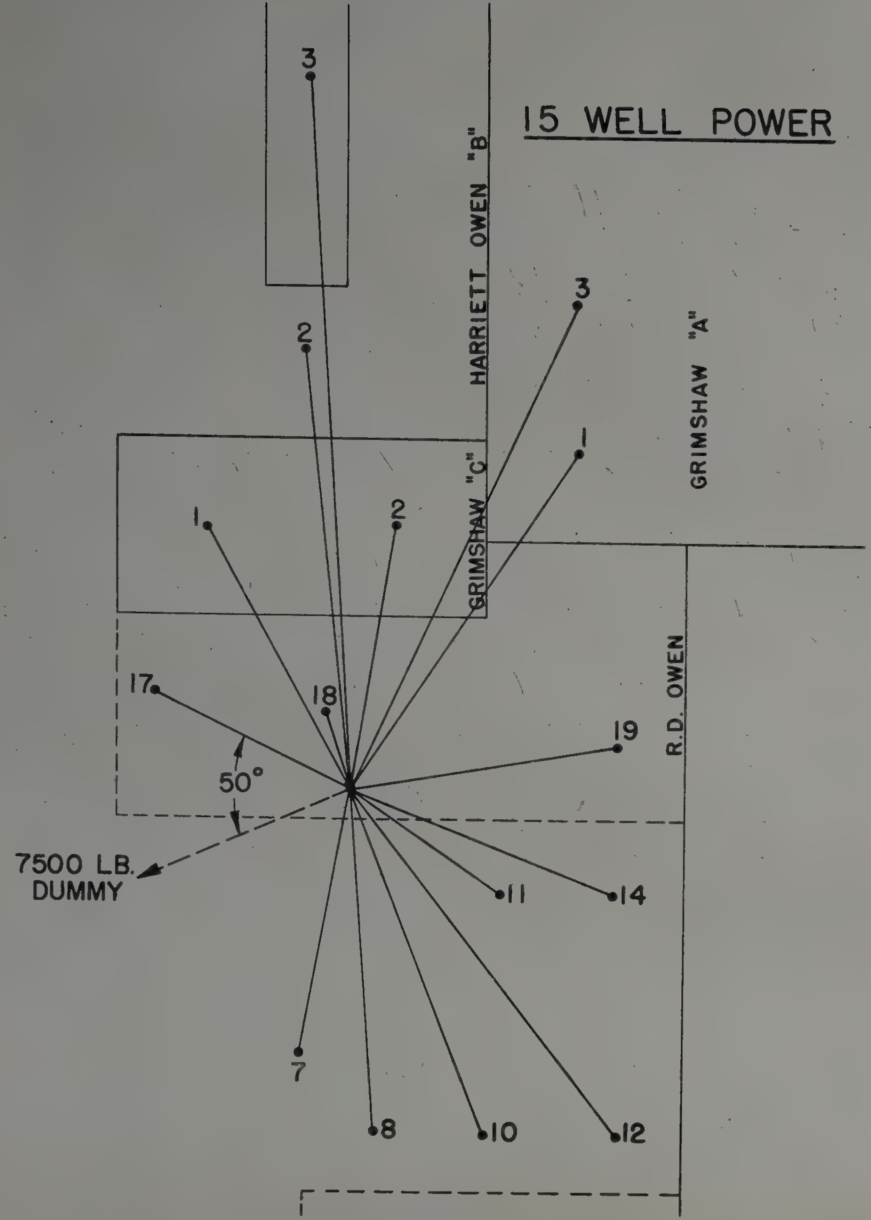
15 WELL POWER
HARRIETT OWEN "B"
GRIMSHAW "A"
GRIMSHAW "C"
R.D. OWEN
3
2
3
1
1
2
17
18
19
50°
7500 LB.
DUMMY
11
14
7
8
10
12

FIG. 28

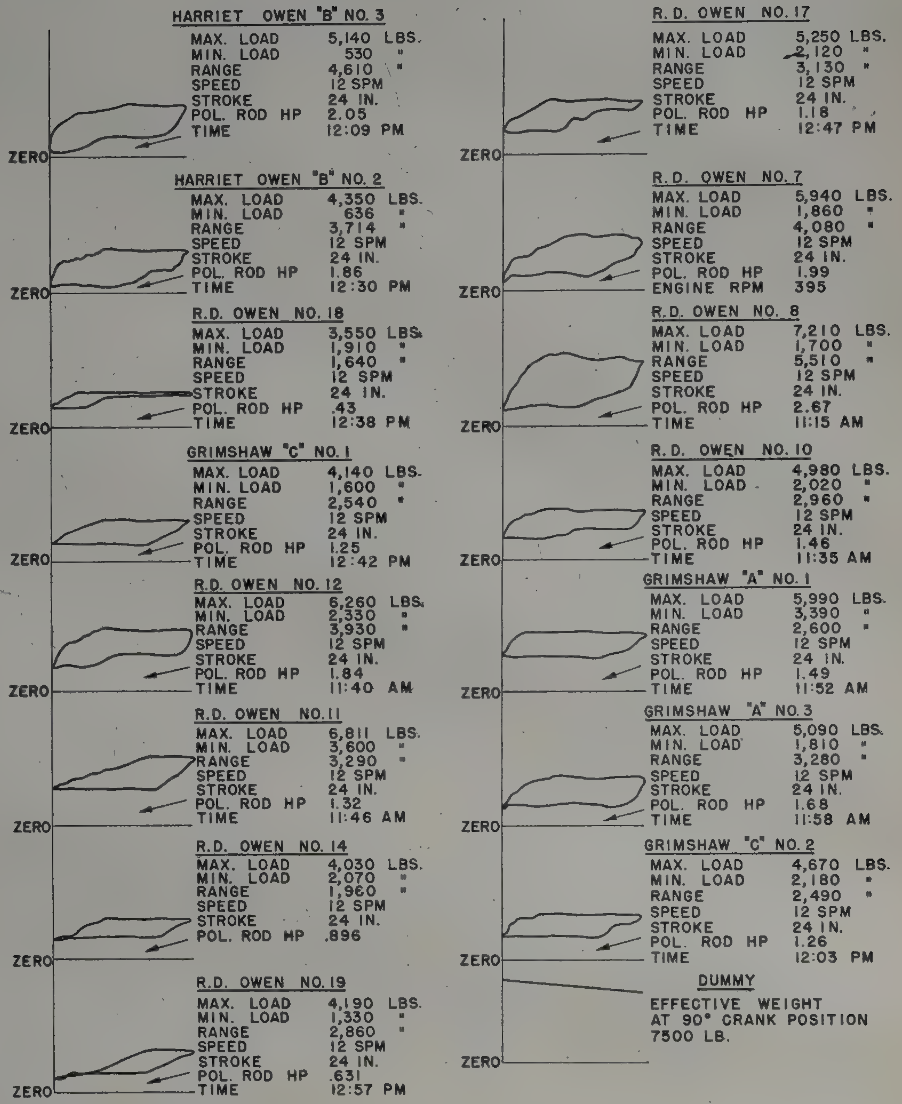
HARRIET OWEN "B" NO. 3
MAX. LOAD 5,140 LBS.
MIN. LOAD 530 "
RANGE 4,610 "
SPEED 12 SPM
STROKE 24 IN.
POL. ROD HP 2.05
TIME 12:09 PM
ZERO
HARRIET OWEN "B" NO. 2
MAX. LOAD 4,350 LBS.
MIN. LOAD 636 "
RANGE 3,714 "
SPEED 12 SPM
STROKE 24 IN.
POL. ROD HP 1.86
TIME 12:30 PM
ZERO
R.D. OWEN NO. 18
MAX. LOAD 3,550 LBS.
MIN. LOAD 1,910 "
RANGE 1,640 "
SPEED 12 SPM
STROKE 24 IN.
POL. ROD HP .43
TIME 12:38 PM
ZERO
GRIMSHAW "C" NO. 1
MAX. LOAD 4,140 LBS.
MIN. LOAD 1,600 "
RANGE 2,540 "
SPEED 12 SPM
STROKE 24 IN.
POL. ROD HP 1.25
TIME 12:42 PM
ZERO
R.D. OWEN NO. 12
MAX. LOAD 6,260 LBS.
MIN. LOAD 2,330 "
RANGE 3,930 "
SPEED 12 SPM
STROKE 24 IN.
POL. ROD HP 1.84
TIME 11:40 AM
ZERO
R.D. OWEN NO. 11
MAX. LOAD 6,811 LBS.
MIN. LOAD 3,600 "
RANGE 3,290 "
SPEED 12 SPM
STROKE 24 IN.
POL. ROD HP 1.32
TIME 11:46 AM
ZERO
R.D. OWEN NO. 14
MAX. LOAD 4,030 LBS.
MIN. LOAD 2,070 "
RANGE 1,960 "
SPEED 12 SPM
STROKE 24 IN.
POL. ROD HP .896
ZERO
R.D. OWEN NO. 19
MAX. LOAD 4,190 LBS.
MIN. LOAD 1,330 "
RANGE 2,860 "
SPEED 12 SPM
STROKE 24 IN.
POL. ROD HP .631
TIME 12:57 PM
ZERO
R.D. OWEN NO. 17
MAX. LOAD 5,250 LBS.
MIN. LOAD 2,120 "
RANGE 3,130 "
SPEED 12 SPM
STROKE 24 IN.
POL. ROD HP 1.18
TIME 12:47 PM
ZERO
R.D. OWEN NO. 7
MAX. LOAD 5,940 LBS.
MIN. LOAD 1,860 "
RANGE 4,080 "
SPEED 12 SPM
STROKE 24 IN.
POL. ROD HP 1.99
ENGINE RPM 395
ZERO
R.D. OWEN NO. 8
MAX. LOAD 7,210 LBS.
MIN. LOAD 1,700 "
RANGE 5,510 "
SPEED 12 SPM
STROKE 24 IN.
POL. ROD HP 2.67
TIME 11:15 AM
ZERO
R.D. OWEN NO. 10
MAX. LOAD 4,980 LBS.
MIN. LOAD 2,020 "
RANGE 2,960 "
SPEED 12 SPM
STROKE 24 IN.
POL. ROD HP 1.46
TIME 11:35 AM
ZERO
GRIMSHAW "A" NO. 1
MAX. LOAD 5,990 LBS.
MIN. LOAD 3,390 "
RANGE 2,600 "
SPEED 12 SPM
STROKE 24 IN.
POL. ROD HP 1.49
TIME 11:52 AM
ZERO
GRIMSHAW "A" NO. 3
MAX. LOAD 5,090 LBS.
MIN. LOAD 1,810 "
RANGE 3,280 "
SPEED 12 SPM
STROKE 24 IN.
POL. ROD HP 1.68
TIME 11:58 AM
ZERO
GRIMSHAW "C" NO. 2
MAX. LOAD 4,670 LBS.
MIN. LOAD 2,180 "
RANGE 2,490 "
SPEED 12 SPM
STROKE 24 IN.
POL. ROD HP 1.26
TIME 12:03 PM
ZERO
DUMMY
EFFECTIVE WEIGHT
AT 90° CRANK POSITION
7500 LB.
ZERO

FIG. 29

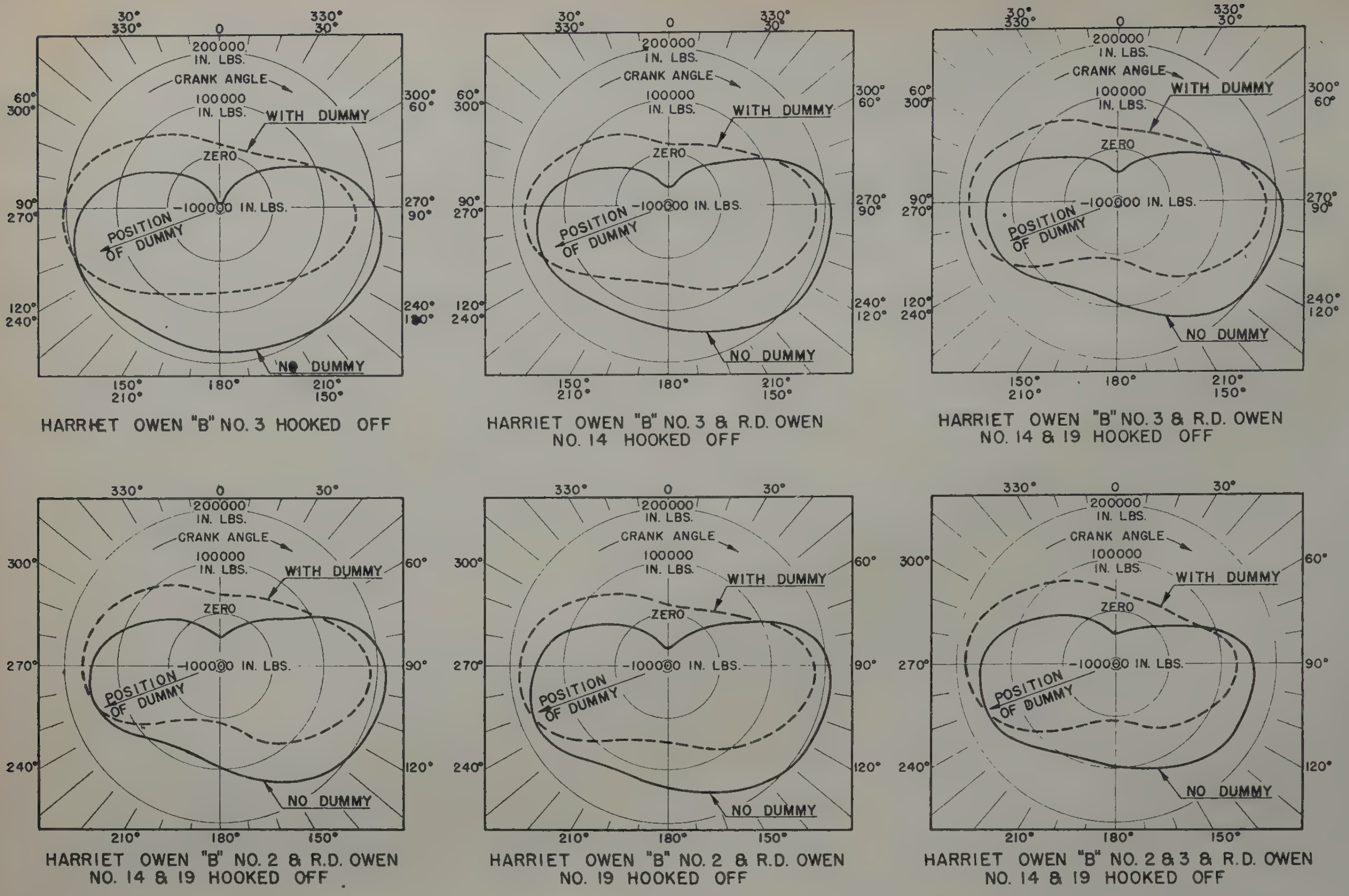

HARRIET OWEN "B" NO. 3 HOOKED OFF

HARRIET OWEN "B" NO. 3 & R.D. OWEN NO. 14 HOOKED OFF

HARRIET OWEN "B" NO. 3 & R.D. OWEN NO. 14 & 19 HOOKED OFF

HARRIET OWEN "B" NO. 2 & R.D. OWEN NO. 14 & 19 HOOKED OFF

HARRIET OWEN "B" NO. 2 & R.D. OWEN NO. 19 HOOKED OFF

HARRIET OWEN "B" NO. 2 & 3 & R.D. OWEN NO. 14 & 19 HOOKED OFF

FIG. 30

is that outlined by E. N. Kemler in *Drilling and Production Practice*, 1943, pages 100 to 103, inclusive. The charts and diagrams are self explanatory.

In conclusion, where procedures as outlined above have been used, substantially lower lifting costs invariably have been the result.

BIBLIOGRAPHY

1. Dr. E. M. Kemler, *Drilling and Production Practice*, 1943. Pp. 100-103.
2. D. O. Johnson, "Taking the Pulse of the Pumping Well," *The Oil Weekly*, March 25, 1940; presented before the API Mid-Continent District meeting at Wichita, Kansas, March 14-15, 1940.
3. Leo W. Fagg, "Lower Lifting Costs Through Proper Pumping Equipment Application," *World Oil*, November, 1947.
4. J. H. Field, "Comparison of Prime Movers for Pumping Wells," Petroleum Mechanical Engineering Conference, ASME, Houston, October, 1947.

★ ★ ★

Table II — Peak Load Calculation

Peak Polished Rod Load = Weight of Sucker Rods × Acceleration Factor + Fluid Load

AVERAGE WEIGHT OF RODS PER FOOT

	Diameter of Plunger											
Rod Comb.	⅝	¾	1	1¹⁄₁₆	1¼	1½	1¾	2	2¼	2½	2¾	3¾
⅝″	1.18	1.18	1.18	1.18	1.18	1.18	1.18	1.18				
¾-⅝″	1.30	1.31	1.32	1.32	1.34	1.36	1.39	1.42				
¾″	1.64	1.64	1.64	1.64	1.64	1.64	1.64	1.64	1.64	1.64	1.64	
⅞-¾″	1.76	1.77	1.78	1.78	1.79	1.81	1.83	1.86	1.88	1.91	1.92	
⅞″	2.20	2.20	2.20	2.20	2.20	2.20	2.20	2.20	2.20	2.20	2.20	2.20
1⅞-¾″	2.06	2.07	2.10	2.10	2.13	2 17	2.22	2.28	2.35	2.42		
1⅛″	2.34	2.34	2.35	2.35	2.36	2.38	2,39	2.41	2.43	2.44	2.48	2.62
1″	2.88	2.88	2.88	2.88	2.88	2.88	2.88	2.88	2.88	2.88	2.88	2.88
1⅛-1⅞-¾″	2.19	2.21	2.26	2.26	2.31	2.39	2.47	2.57	2.68			

ACCELERATION FACTOR $C = 1 + \frac{LN^2}{70500}$

		Length of Stroke in Inches									
		24	34	44	54	64	74	84	96	108	120
	8	1.023	1.031	1.040	1.049	1.058	1.068	1.076	1.088	1.099	1.110
	10	1.035	1.048	1.063	1.077	1.091	1.106	1.120	1.136	1.155	1.172
	12	1.051	1.070	1.091	1.111	1.131	1.152	1.172	1.198	1.222	1.247
	14	1.070	1.095	1.124	1.141	1.178	1.206	1.236	1.266	1.297	1.335
Strokes	16	1.091	1.125	1.162	1.197	1.232	1.281	1.307	1.348	1.390	1.437
	18	1.116	1.157	1.205	1.250	1.294	1.343	1.390	1.440	1.495	1.555
per	20	1.142	1.194	1.252	1.307	1.362	1.423	1.475	1.542	1.610	1.685
	22	1.180	1.235	1.305	1.372	1.440	1.512	1.605	1.655	1.740	
minute	24	1.205	1.280	1.362	1.440	1.520	1.610	1.690			
	26	1.242	1.330	1.427	1.515	1.610	1.705				
	28	1.278	1.386	1.495	1.595	1.710					
	30	1.320	1.437	1.562	1.685						
	32	1.365	1.495	1.642							

FLUID WEIGHT IN LB. PER FT. (SP. GR. = 1)

	Diameter of Plunger											
Rod Comb.	⅝	¾	1	1¹⁄₁₆	1¼	1½	1¾	2	2¼	2½	2¾	3¾
⅝″	.000	.0586	.208	.251	.399	.634	.910	1.037				
¾-⅝″	.000	.0416	.189	.233	.379	.610	.885	1.200				
¾″	.000	.000	.149	.193	.341	.575	.852	1.170	1.535	1.937	2.380	
⅞-¾″	.000	.000	.131	.175	.322	.554	.828	1.142	1.505	1.905	2.345	
⅞″	.000	.000	.080	.124	.272	.506	.784	1.105	1.465	1.870	2.310	4.540
1⅞-¾″	.000	.000	.093	.137	.281	.511	.782	1.093	1.448	1.850		
1⅞″	.000	.000	.063	.107	.253	.485	.761	1.080	1.437	1.840	2.275	4.480
1″	.000	.000	.000	.044	.192	.426	.704	1.022	1.385	1.790	2.240	4.460
1-⅛-1⅞-¾″	.000	.000	.073	.117	.259	.484	.751	1.058	1.410			

CORROSION MITIGATION WITHIN DEHYDRATING TANKS

ERNEST O. KARTINEN, MEMBER AIME, SIGNAL OIL AND GAS CO., LOS ANGELES

This report is the accumulation of eight years of experience on only one small phase in the business of oil production. It is not intended as a final report but rather as a progress report dealing with the internal corrosion of oil field dehydrating tanks.

The corrosion of dehydrating tanks continues to be a problem in the production of crude oil. The deterioration by corrosion of these tanks falls into three general classifications: (1) Atmospheric corrosion of exterior areas, (2) corrosion of the underside of deck and the rafters and top area of the upper row of staves in that part of the tank which is known as the vapor space, and (3) corrosion of the bottom and shell areas, and the steam coils which are normally immersed in water and thus exposed to the corrosive action of the water.

Atmospheric corrosion is primarily a paint problem, and has been omitted in this discussion.

The corrosion in the vapor space, in this company's experience, which has been of great concern only in one area, has also been omitted in this discussion.

The third, and most troublesome type of corrosion, and the one with which this report deals, is that which occurs in the water-exposed areas of dehydrating tanks, and, to a lesser degree, in some stock tanks.

The operating temperature of these waters varies from 80°F to 160°F and the salt counts run from a few thousand to as high as 25,000 parts per million. Corrosion in these tanks occurs in three forms: (1) pits, (2) ringworm type of attack along the vertical and horizontal bolt seams, and (3) as a general attack, spread over a wide area.

Steam Coils

In dehydrating tanks, our experience has been that the steam coils are the first to show signs of corrosion, and then the shell and bottom areas. This action is not uniform throughout this company's operations. Some installations have coil troubles with very little tank trouble, and some show just the opposite. But in the majority of cases the coils are the more seriously corroded areas. This may be partly due to the fact that we have tried by periodic application to keep a protective coating on the interior areas of the tanks, and some protection has been afforded by these coatings.

Through the years several types of hot and cold coatings have been tried with many various methods of cleaning the steel, ranging from use of cleaning solvents to hot and cold Oakite washes, as well as sandblasting. Although experience has shown that a longer life expectancy of a coating is possible after a very thorough steel cleaning job, it has still been necessary to recoat these tanks at least every two or three years.

Until a few years ago, vertical spiral steam coil bundles were installed when the tanks were originally erected. When these coils needed replacement, in some cases within 18 months, it was necessary to remove a couple of shell staves to accomplish this task. This required a down time period of several days and was often very inconvenient to the production operations of the leases.

This problem was considered on the basis that the coils were expendable, and thus, to eliminate any unnecessary down time when changing coils, the vertical spiral coils were discarded in favor of horizontal flat coils which could be taken in and out of the tanks by way of the cleanout openings, and put together with unions. This made a fairly easily replaceable and repairable coil. But it was still very much of a nuisance when repairs were necessary.

Efforts to increase the useful life of the dehydrating tanks led to the adoption of galvanized tanks at an increased initial cost. The zinc coating was depended upon for protection and no other protective coatings were applied.

In July, 1944, during the development of a new lease, a 3-ring 1,500 bbl, black iron water tank was converted into a dehydrating tank with steam coils to handle the new production. This tank was coated inside with a cold, brushed-on coating, for protection against corrosion. After approximately 18 months of service, holes developed in the tank and the steam coils. The tank was emptied and cleaned for repairs. The coils were so badly pitted that it was felt advisable to replace them.

Coating Becomes Loose

Inspection of the tank showed the protective coating to be still in place but loose, and numerous blisters were in evidence. A closer inspection showed that the interior of this tank was so badly pitted under the coating that any further attempt to use the tank was inadvisable. This tank was therefore discarded and a new galvanized tank ordered and set up at considerable expense and inconvenience.

In April, 1946, another dehydrating tank installation was made on an adjoining lease. This installation consisted of a 1,500 bbl, 3-ring galvanized tank with two sets of flat steam coils 12 in. and 24 in. up from the bottom. In September, 1947, seventeen months after installation, salt showed up in the boiler feed water. When the dehydrating tank was opened and cleaned, the steam coils were found to be badly pitted — several holes having penetrated through the wall of the pipe. New coils were installed.

Manuscript received at the office of the Petroleum Branch October 10, 1949. Paper presented at the Petroleum Branch meeting in Los Angeles, California, October 20-21, 1949.

The shell of the tank was also found to be very seriously corroded below the oil level. Large areas of the steel were very thoroughly pitted.

The most serious corrosion from a structural standpoint was the continuous corrosion along the vertical bolt seams and the chimes.

Numerous isolated pits were found in all the shell staves and the bottom. A pit depth gauge was used to measure some of the pits, and several were found to be .108 of an inch in depth. There were a great number of pits .050 of an inch or more in depth. The thickness of the metal in these staves is .1094 of an inch, which indicates that several pits had practically penetrated the steel. A further examination of these corroded areas disclosed a bright shining surface under the rust. The bottom of the tank was found to have only a few small pits. It was also observed at this time that the zinc coating had practically disappeared and had been replaced by a soft, light colored coating which brushed off and exposed black iron.

Cathodic Experiment

After this experience, it became apparent that some solution to the corrosion problem was necessary, and an investigation into the possibilities of protecting the water-immersed areas of dehydrating tanks by cathodic protection was undertaken.

The theory of cathodic protection is that if the iron wall of the tank and coil is made cathodic, that is, negative, with respect to some other point in the system which is anodic, or positive, a current will flow from the anodic to the cathodic surfaces. Rust cannot form at the point where current is entering the iron since iron cannot go into solution to start the corrosion process. In other words, cathodic protection is the use of an impressed current to prevent or to reduce the rate of corrosion of a metal in an electrolyte by making the metal the cathode for the impressed current.

In the application of cathodic protection, the metal to be protected is electrically connected to the negative terminal at a source of current such as a rectifier, generator, or battery. This type of installation is known as a forced drainage system.

Galvanic anode drainage is a form of forced drainage which uses an anode of an active metal such as zinc or magnesium. The drainage current depends on the galvanic potential between the metal to be protected and the anode.

The use of cathodic protection on the inside surfaces of dehydrating tanks presents many problems, such as:

(1) What current density is necessary for complete protection?

(2) What voltage is necessary to provide the required current for effective protection?

(3) How does the corrosiveness of the water affect current requirements?

(4) What effect has the presence of protective coatings upon current requirements?

(5) What anode spacing is necessary for complete coverage?

(6) Would the bolted seams in a tank provide sufficient contact between staves to prevent current from jumping from one stave to the other across the rubber gasket?

(7) Would there be any harmful effects to connecting pipe lines and structures which are not electrically insulated from these tanks?

From available literature, the following four conclusions were drawn:

TANK SIZE: 1500 BBL; 3-RING; STD. A.P.I.; GALVANIZED

ANODE NO. & SIZE: 6 - 16# ANODES - 4 CIRCUITS

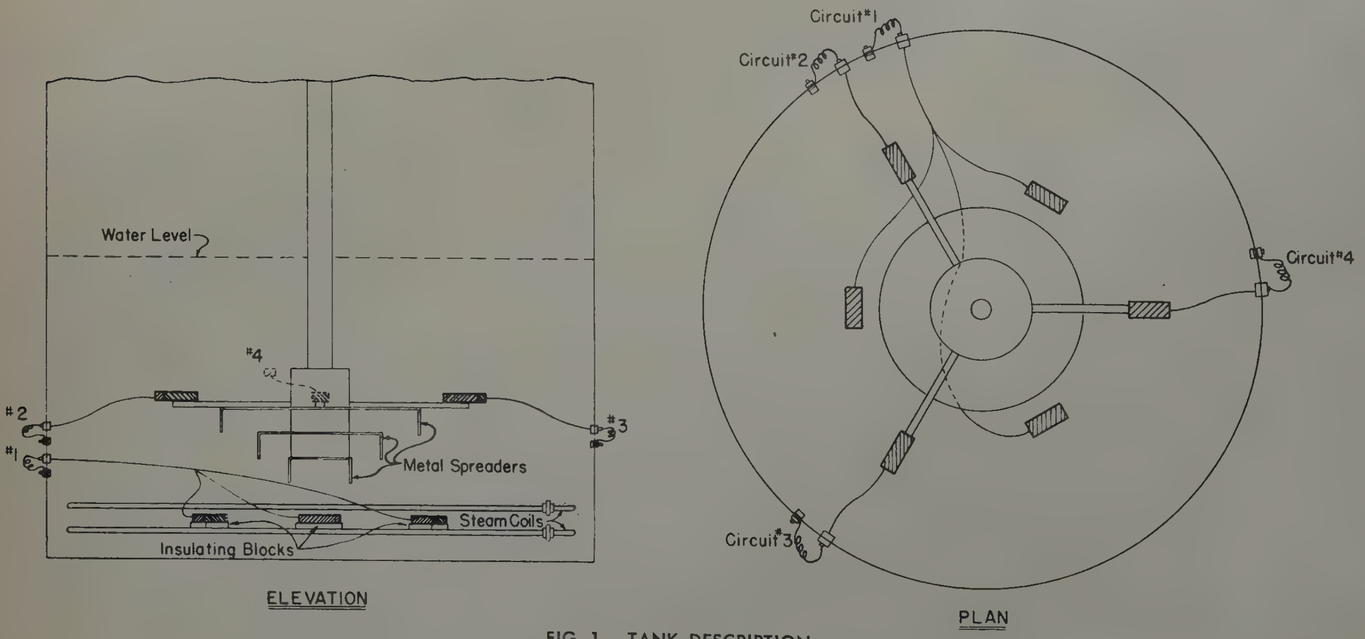

FIG. 1 — TANK DESCRIPTION

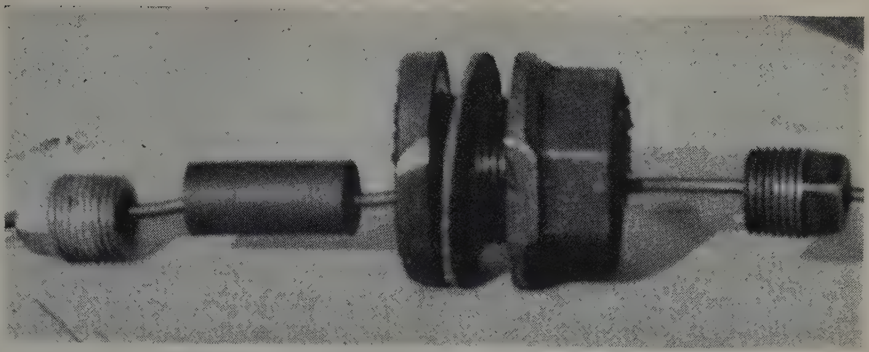

FIG. 2 — TANK FLANGE WITH RUBBER BUSHING AND PLUGS

(1) There are wide differences in the corrosiveness of water; so apparently no set of rules can be applied.

(2) The more corrosive brines require higher current densities for protection.

(3) In a tank, the anodes should be so located and their respective currents such that proper protection is obtained over the entire cathodic surface.

(4) In high resistivity water a greater number of anodes is needed in order to keep down the voltage required.

After some consideration, it was felt that at least partial protection of the dehydrating tank and the steam coils with a properly installed cathodic protection system was possible. There then arose the question of whether a forced drainage or a galvanic anode drainage system would be installed. Some experimenting with a 16-lb magnesium anode in oil field brine showed that it would develop approximately 2 amps. at .6 volts. Magnesium anodes were decided upon in this initial installation because of (1) their ease and simplicity of installation. The initial cost of magnesium anodes over a rectified installation was much less. (2) Magnesium has the greatest solution potential of all commercially available anodic metals. (3) It has a high content of stored energy — the electro chemical equivalent of 1-lb of magnesium being theoretically equivalent to 1,000 ampere hours. (4) It is now readily available because wartime production facilities are being used to fill peacetime markets.

In the dehydrating tank where the first anode installation was made there is approximately 262 sq ft of steam coil area, 158 sq ft of spreader area, 1,183 sq ft of shell and bottom area; or a total of 1,603 sq ft of steel which was subject to corrosion by exposure to the hot oil field brine. From literature on cathodic protection of installations in sea water, it was felt that 5 milliamps per sq ft would provide ample protection with a safe margin. Thus, it was determined that approximately 8 amps, if properly distributed, would be sufficient in this tank.

Four Circuits Used

We had on hand for experimental purposes six of the 16-lb magnesium anodes, and these were installed in this dehydrating tank in four circuits. One circuit had three 16-lb anodes in parallel, and the other three circuits were only single anodes. The three anodes of circuit 1 were placed on insulated pedestals between the two sets of coils, and circuits 2, 3, and 4, comprising one anode each, were set about 5 ft from the shell of the tank about 7 ft off the bottom (Fig. 1).

The lead wires were brought through the shell of the tank by means of a special bushing and then grounded to the shell on the outside of the tank. Fig. 2 shows the tank flange with rubber bushing and plugs to provide a watertight seal around the lead wire.

A Rhodes potentiometer was used to read the voltage, and shunts were used to calculate the amperage of the circuits. The readings of the four circuits a few days after installation were:

Circuit 1	5.7 Amps at .62 volts
Circuit 2	2.5 Amps at .62 volts
Circuit 3	2.6 Amps at .62 volts
Circuit 4	2.6 Amps at .62 volts
Total	13.4 Amps at .62 volts

This amperage provided a current density of approximately 8.04 milliamps per sq ft, and resistances were introduced into the four circuits to cut down the total amperage output to give a current density of approximately five milliamps per sq ft. Readings on all four circuits were taken at frequent intervals and the current output closely tabulated. Also, at this time, while waiting for new coils, this tank was painted inside with three coats of plastic coating.

It was proposed to run this test for six months before opening the tank for inspection. But in January, 1948, after four months' operation, large sections of coating were observed floating out into the waste water pit, and it was evident that the protective coating had disintegrated. The tank was opened and the coating was 100 per cent ineffective after 122 days. But, significantly, it was observed that the pits, which four months previously were shining and bright, now had a dull black luster. There were no traces of pitting on the new steam coils, and all the wrench and punch marks on the coils were sharp and dull in color. The entire exposed steel shell and steam coils had a dull black luster. With these observations, the anodes were removed and the loose coating washed off with a fire hose and new anodes installed. The tank was then closed and put into service.

Second Test

The second test period on this tank ran for 288 days. The tank was opened for inspection on October 28, 1948. As was previously observed, the tank steel had a dull color and the coils which had now been in the tank for 13 months showed no signs whatsoever of corrosion. The deep pits which had practically penetrated the steel after 17 months, have in this last 13 months shown no further corrosive action.

This dehydrating tank was opened again on June 7, 1949, for a routine washout and cleanup. At this time a detailed inspection of the tank was made and the anodes were approximately 75 per cent dissipated.

Pits were examined closely and found to have the same dull black color. The entire steel area of the coils and shell was coated with a thin, hard, black coating. This coating was very hard to remove by hand wire brushing. After a very careful inspection, no further trace of corrosion could be detected anywhere in the tank. This tank has been under cathodic protection for approximately 631 days without any further trace of corrosion.

It has been concluded from this experiment that (1) apparently 5 milliamps per sq ft provides sufficient current density for complete protection, (2) .6 volts potential between steel and magnesium provides sufficient voltage to provide the necessary current, (3) the anode spacing as was used provided ample coverage, (4) bolted seams provided sufficient contact between tank sheets and staves, (5) although the tank was not isolated from the rest of the system by insulating flanges, no harmful effects have been detected anywhere in the system.

It is felt from experience to date that this type of protection is economically feasible and offers better and more positive protection of the water immersed areas of dehydrating tanks while also protecting the steam coils than any protective coating which we have applied to date.

Summary sheet No. 1 (Fig. 3) shows some of the statistics and economics pertaining to this particular tank.

While some of the questions concerning the use of magnesium anodes for cathodic protection in this type of an installation were partially or wholly answered, there is much to be learned about such things as:

(1) Minimum current density necessary.
(2) Maximum anode spacing.
(3) Effect of electrolyte composition on anode behavior.
(4) Effect of pH on magnesium anode performance.
(5) Effect of current density on anode performance.
(6) Effect of anode current density on current efficiency.

We have at the present time 12 dehydrating tanks equipped with cathodic protection circuits. The tanks vary in size from 750 bbl to 2,000 bbl standard API bolted tanks. All of these tanks are several years old and show diversified degrees of corrosion. The protective coatings in these installations have been left intact for whatever protection they might afford. The installations are put in under varying conditions, with the magnesium anodes discharging at different rates and potentials. Efforts are being made to keep a close check on all these cathodic protection installations in an endeavor to compile data and experience which will provide answers to many of the unanswered questions as well as increase our knowledge concerning the practical application and limitations to which this simple principle, discovered by Sir Humphry Davy in 1823, can be applied in the battle against corrosion of this and other types of oil field equipment.

★ ★ ★

DESCRIPTION

Location	Lease Tank Farm	Job No.	Date of this Report	Instal. No.	Tank Bbls. Capacity	Tank No. Rings	Interior Treatment	Interior Condition	Area in Square Feet: Coils	Area in Square Feet: Spreader	Area in Square Feet: Shell & Bottom	Remarks
				1, 2, & 3	1,500	3			262	158	1,183	

ANODE SERVICE EFFICIENCY

Circuit No.	No. of Anodes	Total Anodes	Dates: Installed	Dates: Replaced	Days in Service	Hours in Service	Amps. (Avg.)	Total Amp. Hours Per Circuit	Total Amp. Hours for Tank	Milli Amps. Per Sq Ft Area
1	4	20	9 13 47	6-7-49	631	15,144	3.31	51,530	98,476	4.056
2	1						1.02	14,947		
3	1						.91	14,371		
	1						1.18	17,628		

ANODE SERVICE EFFICIENCY (Continued)

Circuit No.	Original Wt. (lb)	Final Wt. of Anodes	Anodes Weight Loss (lb.)	Amp. Hrs. Per Lb. Mg.	% Anode Efficiency
1	176	60.	116.	444	44.4
2	48	14.	34.	440	44.0
3	48	14.75	33.25	432	43.2
4	48	12.	36.	490	49.0

ANODE COST ANALYSIS

Cost of New Anodes	Cost of Magnesium Per Year	Total Anode
$77.00	$44.55	$81.00
21.00	12.15	
21.00	12.15	
21.00	12.15	

COST SUMMARY

New Coils Cost $400; Average Life of 2 Years; Per Coil	$ 200
New Tank Cost $2300; Average Life of 2 Years; Per Tank	$1150
Average Yearly Replacement Cost	$1350
Average Cost of Magnesium Anode Protection	$ 81
Average Yearly Savings	$1269

FIG. 3 — ANODE DATA SUMMARY SHEET

T.P. 2851

RELATIVE PRODUCTIVITY OF PERFORATED CASING-1

ROBERT A. HOWARD AND **MARSH S. WATSON, JR.,** JUNIOR MEMBER AIME,
UNIVERSITY OF OKLAHOMA, NORMAN, OKLAHOMA

ABSTRACT

An electrolytic model study has been made of the relative productivity of perforated casing. The results show that the relative productivity is roughly one-half to two-thirds of that predicted from point-sink calculations. This discrepancy can be satisfactorily explained on the basis of casing interference. The relative productivity was found to be insensitive to spatial arrangement of the perforations.

INTRODUCTION

The relative productivity of wells with perforated casing has been treated mathematically by Muskat.[1] In his treatment the perforations are represented by small spheres, thus enabling him to approximate the flow by that to point sinks. By neglecting interference between the flow into the various spheres representing the perforations, one may deduce the approximate formula

$$\frac{Q}{Q_o} = \frac{1}{1 + \dfrac{b}{2n} \, \dfrac{\dfrac{1}{r_p} - \dfrac{1}{r_w}}{\ln \dfrac{r_e}{r_w}}} \quad . \qquad (1)$$

Where Q is the flow rate into spherical sinks located in the median plane of the sand layer

Q_o is the open hole flow rate (uncased hole of radius r_w)

b is the thickness of sand layer under consideration (always one foot in this paper)

n is the number of spherical sinks in the sand layer

r_p is the radius of a spherical sink

r_w is the well radius

r_e is the drainage radius of the well.

Fig. 1 is a comparison of values calculated from equation (1) with Muskat's values. It will be observed that the approximate values are in error by less than 2½ per cent.

The disturbing effect of the casing on the flow lines is not explicitly taken into account by Muskat, but he reasons that interference between the flow patterns from the various point sinks will result in a negligible flow in the region within the well radius, and that no appreciable error will result from not explicitly excluding flow from this region. This line of reasoning is open to question, however, as the flow impedance, in the immediate vicinity of the well, of a hemispherical cavity in contact with an opening in the casing is twice that of a spherical sink in a continuous sand layer. There will be a difference, moveover, between the flow into a hemispherical cavity and that into a circular hole in the casing. This latter difference can best be appreciated by comparing the flow from a semi-infinite medium into a hemispherical cavity at the edge of the medium with the flow out of a circular opening of the same radius as the hemisphere and which is also on the edge of the medium. In this case[2] $\frac{Q_h}{Q_c} = \frac{\pi}{2}$, showing that the difference in flow rates into differently shaped cavities is quite appreciable.

It was the purpose of the investigation reported here to determine to what extent flow into circular perforations in casing departs from the values calculated by Muskat. For this purpose an electrolytic model was used.

Manuscript received at office of the Petroleum Branch October 12, 1949. Presented at AIME Annual Meeting, New York City, February 13-17, 1950.

[1] References are given at end of paper.

APPARATUS

The model tank was 36 in. in diameter, with a varnished plywood bottom, and vertical copper sides 1.75 in. high. A weak NaCl solution was used as the electrolyte. The casing was represented by a lucite cylinder, and the perforations by radial platinum wires cut off flush with the outer surface of the lucite cylinder. The platinum electrodes all lay in the median plane of the electrolyte. The fluid flow impedance was determined by measuring the resistance to 1000 cycle current with a General Radio type 650 A impedance bridge. A pure resistive balance was obtained by using an oscilloscope as a null detector. Each such resistance measurement was compared with that of a gold plated cylindrical copper electrode measured at the same temperature. The latter makes possible the comparison of perforation flow rates with open hole flow rates without making electrolyte conductivity measurements in a separate conductivity cell.

RESULTS

Since neither the open hole radius nor the drainage radius correspond to those used by Muskat, it was necessary to employ the two-dimensional radial flow equation to place our results on the same basis as his. To do this the following equation was employed,

$$\frac{Q}{Q_o} = \frac{1 + \dfrac{\ln \dfrac{r_e}{r_m} \cdot \dfrac{r_{oh}}{r_w}}{\ln \dfrac{r_m}{r_{oh}}}}{\dfrac{R}{R_{oh}} + \dfrac{\ln \dfrac{r_e}{r_m} \cdot \dfrac{r_{oh}}{r_w}}{\ln \dfrac{r_m}{r_{oh}}}} \quad . \quad (2)$$

Where Q is the flow rate into the perforations

Q_o is the flow rate into the open hole

r_e is the drainage radius (model rather than prototype)

r_m is the electrolytic tank radius (18 in.)

r_{oh} is the radius of the open hole electrode (0.249 in.)

r_w is the external radius of the casing (radius of lucite cylinder equals 0.384 in.)

R is the resistance measured with perforation electrodes

R_{oh} is the resistance measured with the open hole electrode.

The platinum wire employed to represent perforations was 0.032 in. in diameter, and the depth of the electrolyte was 0.768 in.

The results for the case where the prototype dimensions are:

casing radius	= 6 in.
perforation radius	= 0.25 in.
formation thickness	= 1 ft
drainage radius	= 660 ft

are shown in Fig. 2. It will be observed at once that the relative productivity is much less than that calculated by Muskat, which is consistent with the argument given above as to the probable effect of the casing. An equation of the same form as (1), namely,

$$\frac{Q}{Q_o} = \frac{1}{1 + \dfrac{c}{n}} \quad . \quad . \quad . \quad . \quad (3)$$

will fit the observed data to an accuracy of about 2 per cent if c is given the value 7.6. The flow lines in the vicinity of the perforation are of sufficiently complicated form that we have not been able to derive the value of c by simple physical considerations as was possible in the case of equation (1).

It is possible to derive an approximate equation for calculating the effect of increasing the casing radius and perforation radius by a factor k and the drainage radius by a factor h while leaving the perforation density constant. The equation which one obtains is:

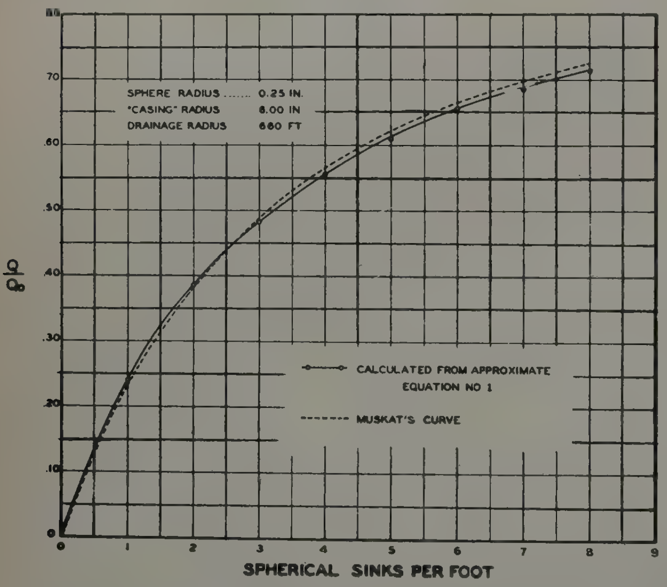

FIG. 1 — EFFECT OF NUMBER OF SPHERICAL SINKS PER FOOT OF CASING ON RELATIVE WELL PRODUCTIVITY.

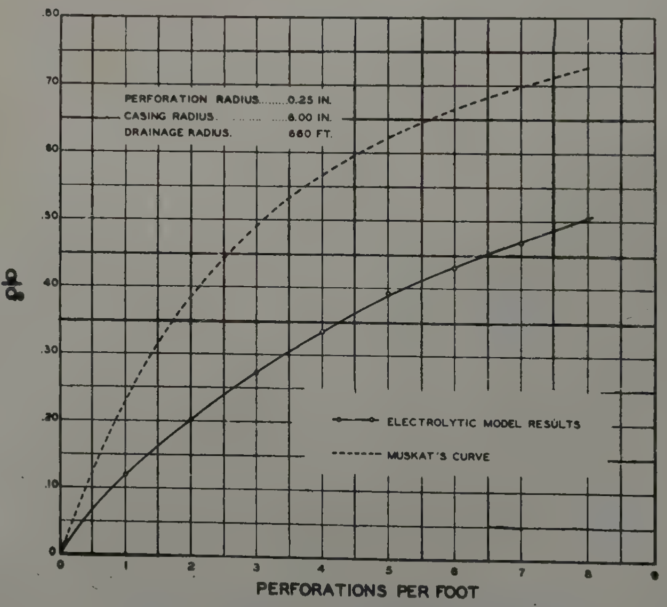

FIG. 2 — EFFECT OF NUMBER OF PERFORATIONS PER FOOT OF CASING ON RELATIVE WELL PRODUCTIVITY.

$$\left(\frac{Q}{Q_o}\right)' = \frac{1}{1 + \dfrac{\dfrac{1}{Q/Q_o} - 1}{k\left(1 - \dfrac{\ln k/h}{\ln r_e/r_w}\right)}} \qquad (4)$$

where

$(Q/Q_o)'$ is the desired relative productivity,

Q/Q_o is the relative productivity which is known for certain casing and perforation radii

r_e is the drainage radius for the known case

and r_w is the casing radius for the known case.

The electrolytic model results for the following prototype dimensions:

casing radius = 3 in.

perforation radius = 0.125 in.

formation thickness = 1 ft

drainage radius = 660 ft

are compared in Fig. 3 with the values computed from equation (4), using the electrolytic model results shown in Fig. 2, and also with the values given by Muskat for this case. It will be observed that the values calculated from equation (4) are in good agreement with those determined experimentally, but are much lower than the values given by Muskat.

LOCATION OF PERFORATIONS

No special study was made of the effect of spatial distribution of the electrodes, but, as will be seen from Fig. 4, the 2, 4, and 8 perforation patterns are symmetrical arrangements, while the remainder are asymmetric. It will be noted that a smooth curve drawn through the points corresponding to symmetrical arrangments will not deviate by more than the experimental error from those corresponding to asymmetrical arrangements.

FLOW TO SPHERICAL SINKS

As a check on our method, we had three brass spheres of 0.040 in. diameter turned on the ends of small brass rods. All of the rod but the sphere was coated with insulating material. The sphere itself was gold plated. Since flow of current to the sphere was cut off where the rod joined the sphere, the cross sectional area of this piece was subtracted from the total area of the sphere and the radius of the equivalent sphere having the resultant area calculated. The observed resistances were converted by means of equation (2), using new values of r_w (= 0.458 in.) and r_e (corresponding to an effective sphere diameter of 0.038 in.). The results are shown in Fig. 5. The agreement with Muskat's calculated values is good, showing that the calculations are correct but that the point sink representation is inadequate to portray flow in the region of the impermeable casing.

CONCLUSION

The limitations to the applicability of electrolytic model studies and potential theory calculations to actual field conditions are now so widely appreciated that they will not be discussed further. There is, however, one limitation to this particular investigation which is worth mentioning. Our model represents a perforation which consists of a circular hole through the casing which just exposes the undisturbed sand face in contact with the casing, or it may be interpreted as a circular hole through the casing and cement if the well radius is

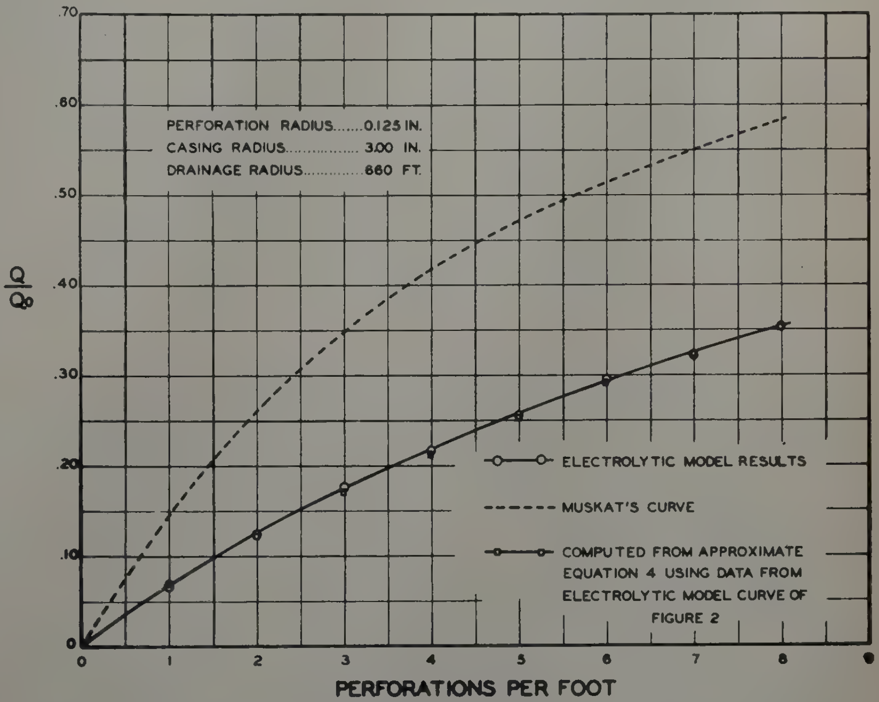

FIG. 3 — EFFECT OF NUMBER OF PERFORATIONS PER FOOT OF CASING ON RELATIVE WELL PRODUCTIVITY.

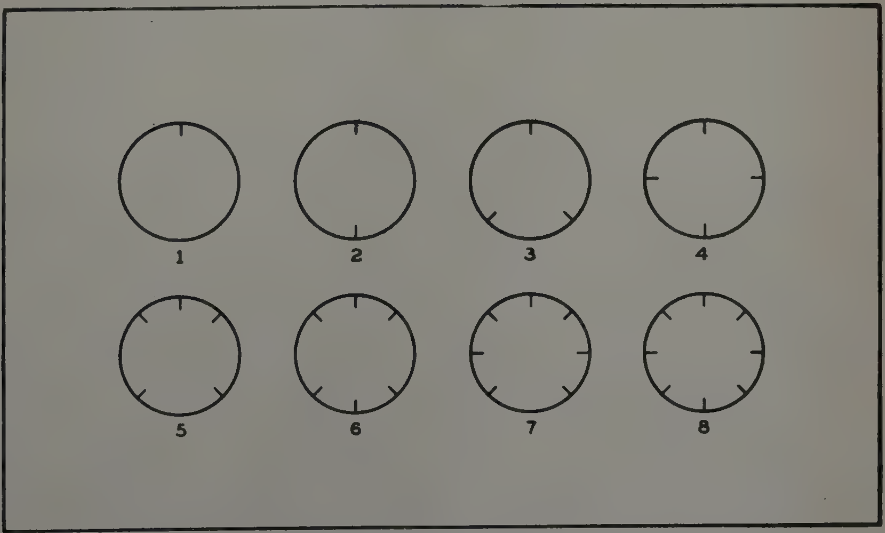

FIG. 4 — DIAGRAMMATIC PLAN OF THE NUMBER AND ARRANGEMENT OF PERFORATION ELECTRODES.

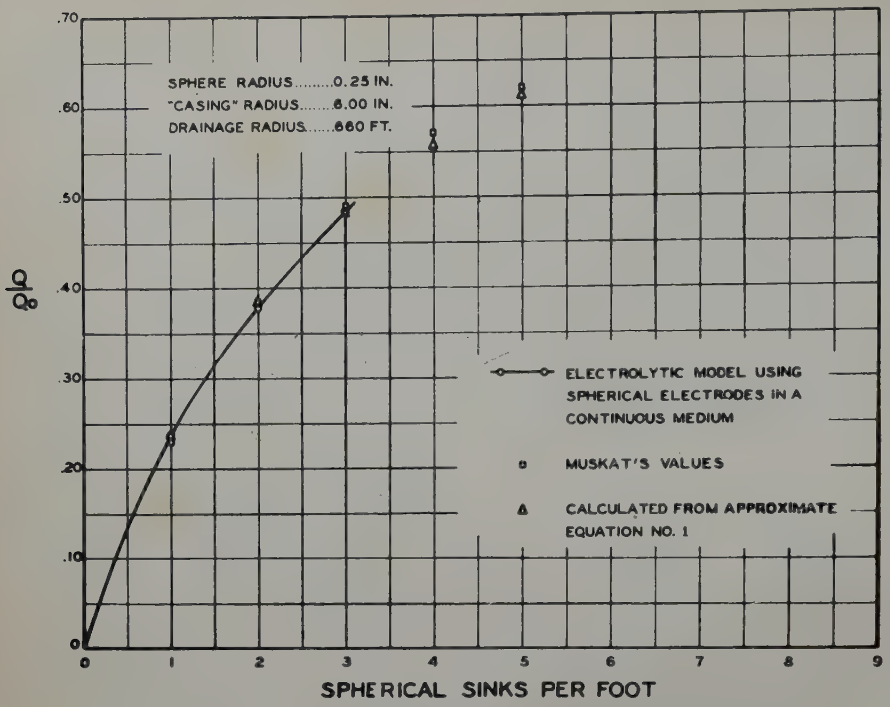

FIG. 5 — EFFECT OF NUMBER OF SPHERICAL SINKS PER FOOT OF CASING ON RELATIVE WELL PRODUCTIVITY.

interpreted as the radius of the cemented hole instead of the casing radius. In any case, the perforating bullet could hardly cut a hole through the casing and expose undisturbed formation. For this reason the authors are now investigating the effect of formation penetration on relative productivity.

ACKNOWLEDGMENT

We are indebted to the Shell Union Oil Co. for a fellowship granted to Marsh S. Watson which made possible his graduate work in the Department of Petroleum Engineering and for an equipment grant to cover, in part, the cost of the apparatus used.

REFERENCES

1. M. Muskat, Petr. Dev. & Tech., 151, 175 (1943).
2. J. H. Jeans, *Electricity & Magnetism*, Cambridge University Press (1933).

★ ★ ★

T.P. 2881

IMPROVEMENTS IN THE X-RAY SATURATION TECHNIQUE OF STUDYING FLUID FLOW

F. MORGAN, J. M. McDOWELL AND **E. C. DOTY,** GULF RESEARCH AND DEVELOPMENT CO.,
PITTSBURGH, PENNSYLVANIA

ABSTRACT

Improvements in the X-ray method of measuring liquid saturation and saturation distribution are presented. Two identical direct current amplifiers have been added to measure continuously the intensities of the X-ray tube output and the beam which has passed through the core under test. The ratio of these intensities is automatically recorded on a modified Brown Electronik Recorder. Arrangements have been made to drive the core automatically and in synchronism with the recorder chart so as to give a continuous curve showing the variation of liquid saturation along the length of the core. By determining the ratio of the two X-ray beam intensities simultaneously the measurements are made essentially independent of small fluctuation in voltage and current supplied to the tube. This improved technique has been used for investigating the fluid distribution along the length of cores and core assemblies when one fluid is displaced by another. Typical results of these studies are shown.

INTRODUCTION

In a previous publication[1] a method was described for measuring the oil saturation in cores which was based on the absorption of X-rays by the fluid content of the core. While that technique is capable of yielding accurate results, the original apparatus was not especially convenient for determining the fluid distribution along the length of a core. This was primarily due to the slow response of the amplifier and galvanometer and the necessity of making a point by point survey of the material under investigation. It was, therefore, not only possible for sections of the core having a variable or unusual saturation distribution to escape observation entirely, but changes in output of the X-ray generator between readings on the unknown and the monitor introduced errors in the measurements that could be avoided only by further stabilization of the source or by taking a large number of readings.

This paper describes a method and apparatus for recording continuously and automatically the intensity of the X-ray beam that is transmitted by a core. The variation of saturation with time at a given section of the core may thus be found, or by scanning the core by driving it in synchronism with the recorder the saturation distribution may readily be determined.

As indicated in the previous paper, the X-ray method possesses an advantage over the weighing technique in relative permeability experimentation in that the core need not be removed from the holder for the purpose of making a saturation measurement. Furthermore, the actual distribution of fluid and the effects upon that distribution of inflow and outflow heads may be investigated. And errors due to gas bubbles or loss of liquid that are frequently sources of error in volumetric methods of saturation determination are avoided.

PRINCIPLE OF THE METHOD

The energy in an X-ray beam that has passed through an absorbing material is expressed by the well known formula:

$$E = E_o \, e^{-\mu c d} \qquad (1)$$

where E_o is the energy in the incident beam, μ the mass absorption coefficient, c the density or concentration of absorbing material, and d is the length of path of the beam in the absorber. The coefficient μ varies with the wavelength of the radiation as well as with the absorbing material.

The output of an X-ray tube varies in an approximately linear manner with the tube current, but to the second or higher power of the anode voltage. Moreover, the quality or wavelength distribution of the radiation varies with the voltage.

---

[1] References given at end of the paper.

Manuscript received at the office of the Petroleum Branch October 4, 1949. Paper presented at the Petroleum Branch meeting in San Antonio, October 5-7, 1949.

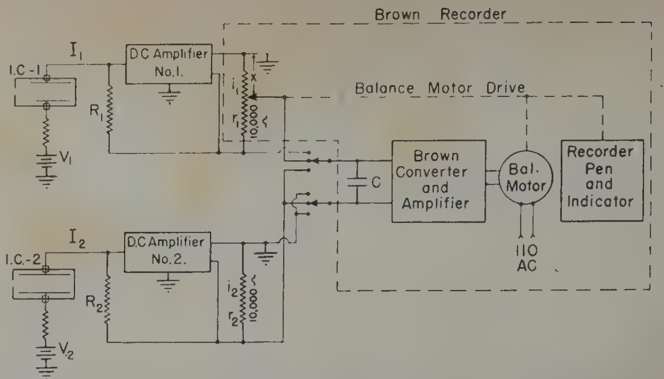

FIG. 1 — SCHEMATIC AND BLOCK DIAGRAM OF THE X-RAY MEASURING AND RECORDING SYSTEM.

Current regulators have been developed which satisfactorily control the tube current, but entirely suitable voltage regulators are not readily available. Consequently, in this application, as in the earlier apparatus, a second beam is taken off at a small angle to the main beam and used as a control.

For the greatest precision in the measurement of X-ray absorption at various saturations, homogeneous or monochromatic X-rays should be employed unless a standard can be used that always exactly matches the unknown in absorption qualities. If more than one wavelength is present, the longer waves will be strongly absorbed by the first sections of the absorber making the fraction of the energy removed per unit of path decrease with the thickness traversed. In core studies, however, the use of a homogeneous beam is generally not practical because of the great loss in intensity that is incurred in monochromating the X-rays. Moreover, tests have shown that for moderate concentrations of tracer materials in the core, the error introduced even in assuming a constant value of μ will be small. And further corrections may readily be made by calibrating the system with absorbers consisting of cells of varying thickness filled with the test fluid.

In Fig. 1, I_1 and I_2 represent the currents flowing in the monitor and test ionization chambers, respectively, due to the passage of X-rays through the gas inside the chambers. These currents are directly proportional to the X-ray beam intensity as long as the voltages applied to the ionization chambers are sufficient to render recombination of the ions negligible. Consequently the current flowing in resistance R_1 due to the ionization current in chamber 1 may be written:

$$I_1 = k_1E_1 = k_1E_oe^{-\mu_m c_m d_m} = C_1E_o \qquad (2)$$

where c_m and d_m, the density and thickness of the absorber in the monitor beam, are fixed quantities, and μ_m is essentially constant for the small variations normally encountered in the intensity of the incident beam. The current I_1 is therefore a measure of the X-ray tube output.

For the test core the ionization current may similarly be expressed as:

$$I_2 = k_2E_2 = k_2E_oe^{-(\mu_t c_t d_t + \mu_a c_a d_t)} \qquad (3)$$

where the subscript t designates the test core and a refers to the absorbing fluid containing the tracer material. Since μ_t, c_t and d_t are constant, or nearly so, for a given core section, they may be incorporated in the constant of proportionality. Also the effective density or concentration of the tracer material in the core is given by:

$$c_a = f\rho\gamma \qquad (4)$$

where f and ρ are the porosity and saturation of the core and γ is the true density of the fluid containing the tracer. Therefore:

$$I_2 = C_2E_oe^{-\mu_a f\rho\gamma d_t} \qquad (5)$$

In the inverse feed-back amplifier, of voltage gain g, indicated in Fig. 1, the entire output voltage, ir, is fed back in opposite polarity to the input voltage IR, so that:

$$g(IR - ir) = ir \qquad (6)$$

or:

$$ir = \frac{g}{g+1}IR \qquad (7)$$

When the gain is high, as in the present application, the output voltage is for practical purposes equal to the input voltage. The output is thus not only independent of the gain, but the swing of the grid voltage is reduced by the factor g and the linearity of the amplifier is consequently improved. Moreover, by the use of feed-back, the effective grid to cathode resistance of the first tube is increased and the time constant of the input circuit is reduced.

Therefore to a good approximation:

$$i_1r_1 = I_1R_1 = C_1E_oR_1 \qquad (8)$$

Similarily:

$$i_2r_2 = I_2R_2 = C_2E_oR_2e^{-\mu_a f\rho\gamma d_t} \qquad (9)$$

and:

$$\frac{i_2r_2}{i_1r_1} = \frac{C_3R_2}{R_1}e^{-\mu_a f\rho\gamma d_t} = C_4e^{-\mu_a f\rho\gamma d_t} \qquad (10)$$

since R_1 and R_2 normally remain fixed for a given experiment.

In practice the ionization currents are fed to two identical DC amplifiers which were patterned after the feedback amplifier of A. O. Nier, E. P. Ney, and M. G. Inghram.[2] As the internal gain of these amplifiers is about 500, the input and output voltages are very nearly equal. In the present application r_1 is a 10,000 ohm 10-turn helipot, the slider of which is geared to the balancing motor of a Brown Electronik Recorder. The test core amplifier has a fixed output resistance of 10,000 ohms. As indicated in Fig. 1, the input of the recorder amplifier is connected between the high side of the fixed resistor and the slider of the helipot. The recorder thus serves as a null indicating instrument. In response to a signal the amplifier tends to drive the balancing motor in such a direction that a balance will be restored. The arrangement is such that the helipot will be driven through its 10 turns while the recorder pen is moved across the full scale of the chart. The pen position thus indicates directly the fraction of the output of amplifier No. 1 which is equal to the output of amplifier No. 2. In operation the standard absorber in the monitor beam is first adjusted until the voltage drop across the helipot is equal to or a little greater than the drop across the output of amplifier No. 2, the saturation of the test core having its minimum value. For any saturation of the test core the balancing motor comes to rest indicating zero input when:

$$i_2r_2 = xi_1r_1 \qquad (11)$$

where x is the fraction of the total helipot resistance that lies between the movable contact and the grounded point.

Substituting Eq. (10) and letting x_o be the value of x when f or $\rho = 0$,

$$x = x_oe^{-\mu_a f\rho\gamma d_t} \qquad (12)$$

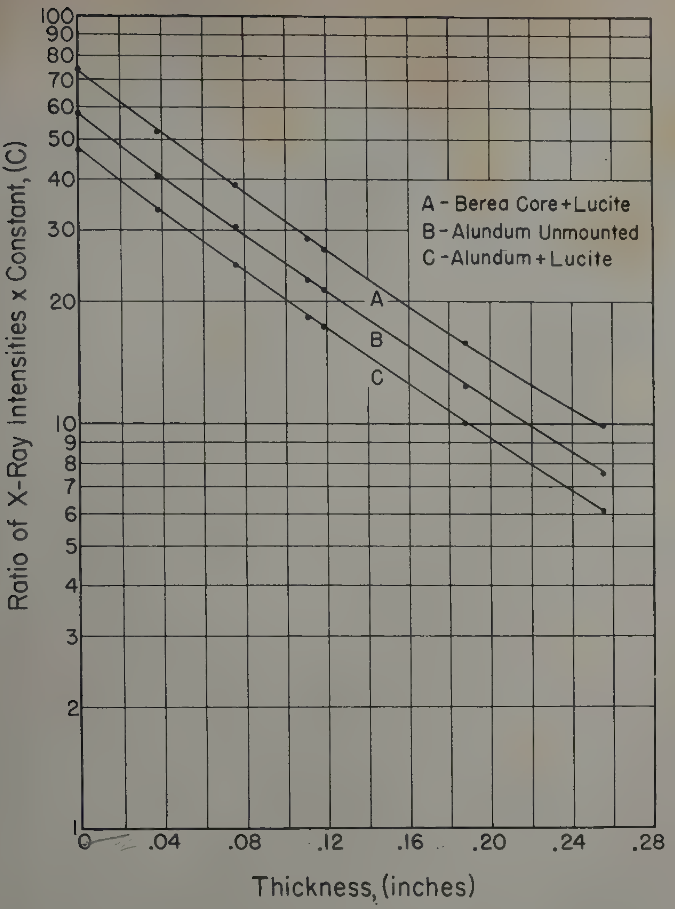

FIG. 2 — THE VARIATION OF INTENSITY OF A TRANSMITTED X-RAY BEAM WITH THICKNESS OF AN ABSORBER CONSISTING OF AN AQUEOUS SODIUM IODIDE SOLUTION (CALIBRATION CURVE). RECORDER READINGS ARE PLOTTED AS ORDINATES.

Again for a given core section and test fluid, μ_a, f, γ, and d_t may be treated as constants. Then:

$$x = x_o e^{-\mu' \rho} \qquad (13)$$

and a plot of the logarithm of the recorder reading against the core saturation should be a straight line, the position of which is readily determined from the recorder readings for both the dry and saturated core. In practice, such semi-log plots are generally slightly concave upward due to the variation of absorption of the tracer fluid with wavelength. However, if the concentration of tracer is low and a monitor absorber is selected which approximately matches the test core in its absorbing qualities, the deviation from linearity will be small.

Equation (12) may also be applied in determining the porosity of a core. Since the absorption of X-rays depends upon the number of absorbing molecules in the beam and not on their specific location, cells containing various thicknesses of the tracer fluid may be inserted in the path of the X-rays, along with the dry core, and the transmission determined. The thickness of tracer liquid that gives the same ratio of x/x_o as is found for the saturated and dry core will be equal to the product of the length of path of the X-ray beam in the core and the porosity of the core.

In Fig. 2 the recorder reading, which is proportional to the ratio of the intensity of the beam that has passed through the test liquid to the incident beam, is plotted as a function of cell thickness for three combinations of alundum and Berea cores in series with the cell. Lucite was used with the Berea sample to keep the deflection on the scale. The three lines are parallel within the error of reading the chart thereby verifying the theory. By using this liquid to saturate a core the porosity may be determined by the method described above. Also the thickness of tracer fluid corresponding to a fully saturated core can be read from the curve and the deviation from linearity on the semi-log saturation plot determined, or a true calibration curve of recorder reading vs. per cent saturation prepared.

In deriving the above equations, the assumption was made that the pore space in the core not occupied by the tracer fluid was filled with gas or a liquid with a very low absorption coefficient. This hypothesis, although convenient, is not necessary. If one liquid is a weak absorber in comparison with the other, it is easy to show that a semi-log plot of the recorder reading against saturation of the tracer containing liquid will be approximately a straight line when the deflections for zero and 100 per cent saturation are taken equal to those for 100 per cent saturation of the weak absorber and the tracer liquid respectively.

DESCRIPTION OF THE APPARATUS

The same X-ray tube and power supply have been used as described in the previous paper. However, a Westinghouse electronic tube current regulator and a Sorenson voltage regulator have been added to help stabilize the X-ray output. The latest arrangement of the apparatus is shown by the photograph of Fig. 3, while a schematic diagram of the X-ray tube and the beam paths is shown by Fig. 4. The test core, C_2, can be driven automatically by the motor so that the entire length of the core can be scanned in either direction with the X-ray beam. Since the beam at the core is approximately ⅛ in. wide in the direction of scan, the average value of the saturation will be obtained over this length of core. However, the exact position of any abrupt change in saturation may be accurately determined when the core is scanned in both directions.

The ionization chambers have parallel plate electrodes as shown in Fig. 4. The plates in both chambers are one inch wide, and the separation is also one inch, the length being

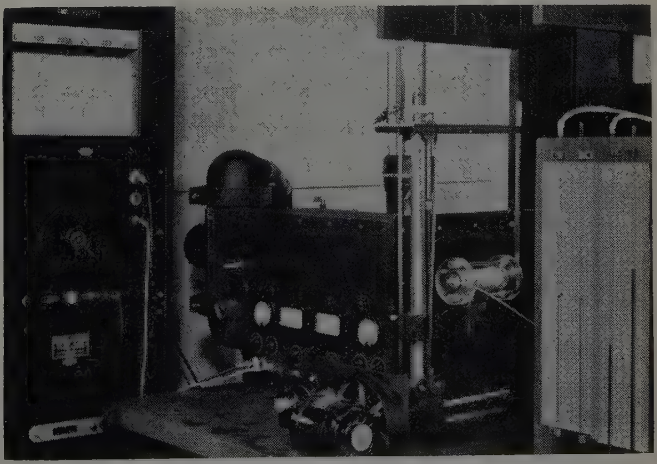

FIG. 3 — VIEW OF APPARATUS.

eight inches in IC-1 and 16 inches in IC-2. The plates, which are of aluminum, are mounted in brass tubes having lucite windows on the ends through which the X-rays enter. The chambers are filled with Freon gas to increase their efficiency and 45 volts is normally applied to the electrodes. Tests at higher voltage have shown no improvement in linearity and only a slight increase in ionization current. Freon gas has been used in spite of its comparatively low efficiency because of its stability, availability and freedom from harmful effects. The electrodes are insulated from the walls of the chamber by means of Teflon.

The first stage of each amplifier, consisting of a 959 acorn tube and grid resistor of 10^9 or 10^{10} ohms, is mounted in a shielded can next to the ionization chamber to reduce the grid capacitance, diminish the leakage paths and minimize possible interference from external sources. The other stages in each amplifier consist of two 1S5 tubes and a 6J5 output tube. The amplifiers are entirely battery operated and all components are completely shielded.

As indicated before, the Brown Recorder is used as a null indicating device which records the fraction of the output of amplifier No. 1 which is required to balance the output of amplifier No. 2. The signal is connected directly to the input of the recorder amplifier, the bridge circuit being disconnected entirely. The chart can be driven at the same speed as the test core or at some multiple speed, if desired, to give an expanded scale for the curve. Scanning speeds of ½ in., ¾ in., 1 in. and 1½ in. per minute have been provided.

The switch indicated in Fig. 1 is used for connecting the total output of each DC amplifier directly to the recorder in order to set the zero adjustments to give zero output voltage when there is no input signal. This is indicated when the recorder pen does not move in either direction. The amplifiers should be adjusted to zero output before each core scan or measurement since they are subject to slight drift even after the warm-up period. The zero position is also subject to change from excessive vibration. Extensive measures have been taken to reduce this drift and interference as much as possible, but conditions are not favorable for eliminating them entirely. However, with care in operation the results are quite satisfactory.

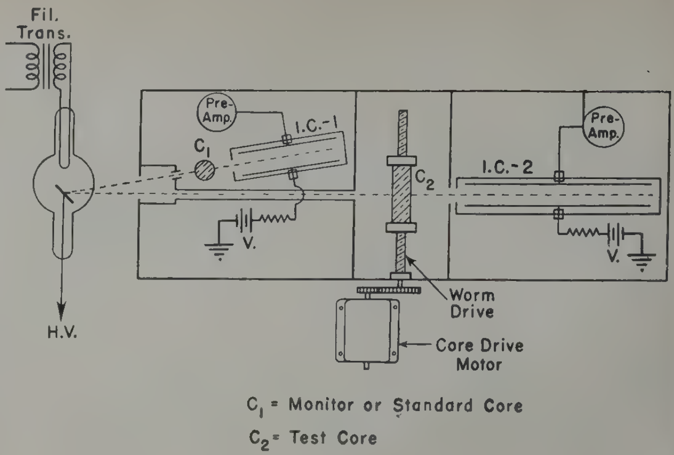

FIG. 4 — SCHEMATIC DIAGRAM OF X-RAY BEAM PATHS.

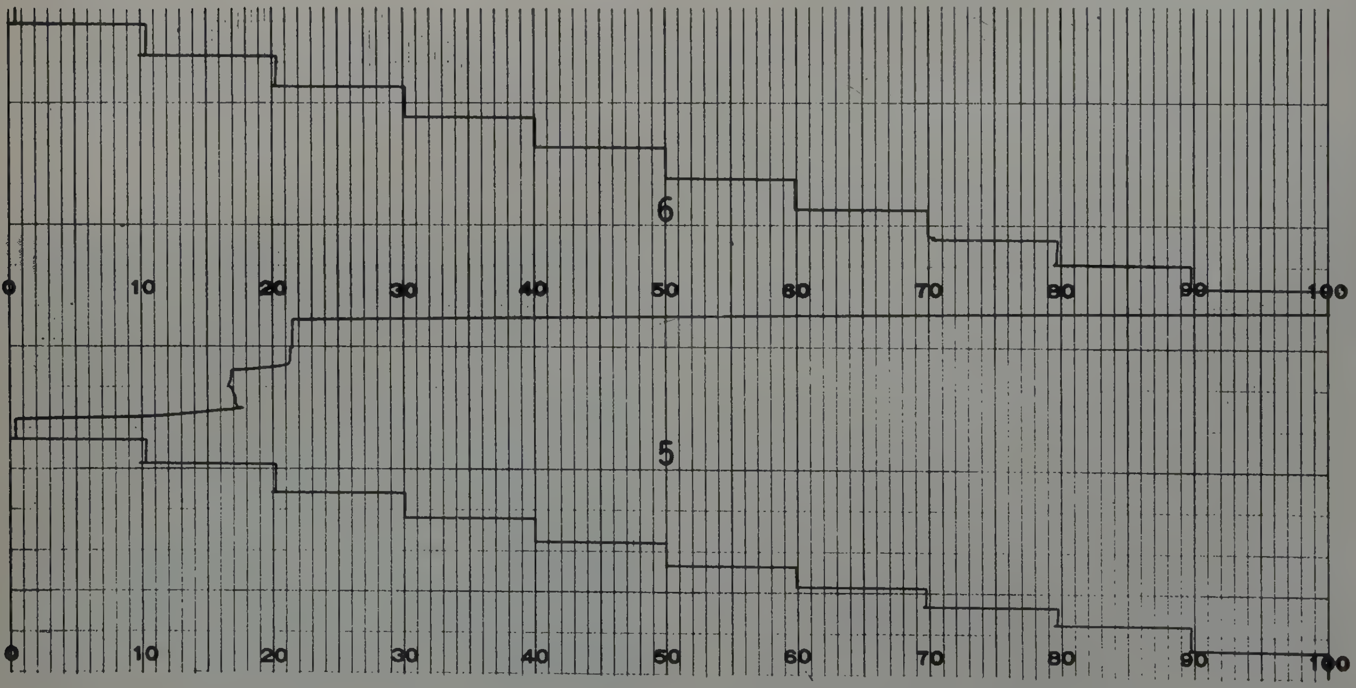

FIG. 5 — RESPONSE OF RATIO METER TO EQUAL INCREMENTS IN VOLTAGE RATIO.

TEST OF RATIO METER

To test the amplifiers and, at the same time, obtain information on the suitability of the apparatus for determining the ratio of currents or voltages, potentials were applied to the preamplifier tube grids by means of potentiometers. The potential divider in the grid circuit of amplifier 2 was so set that the voltage could readily be reduced to zero in ten equal increments and the grid of amplifier number 1 was biased until the recorder registered full scale. Fig. 5 shows the results of the test. As the voltage ratio was decreased from unity to zero by tenths, the recorder pen moved approximately one major division at a time. Deviations from the exact values are due in part to drift of the amplifier zero and in part to lack of linearity in the helipot resistance.

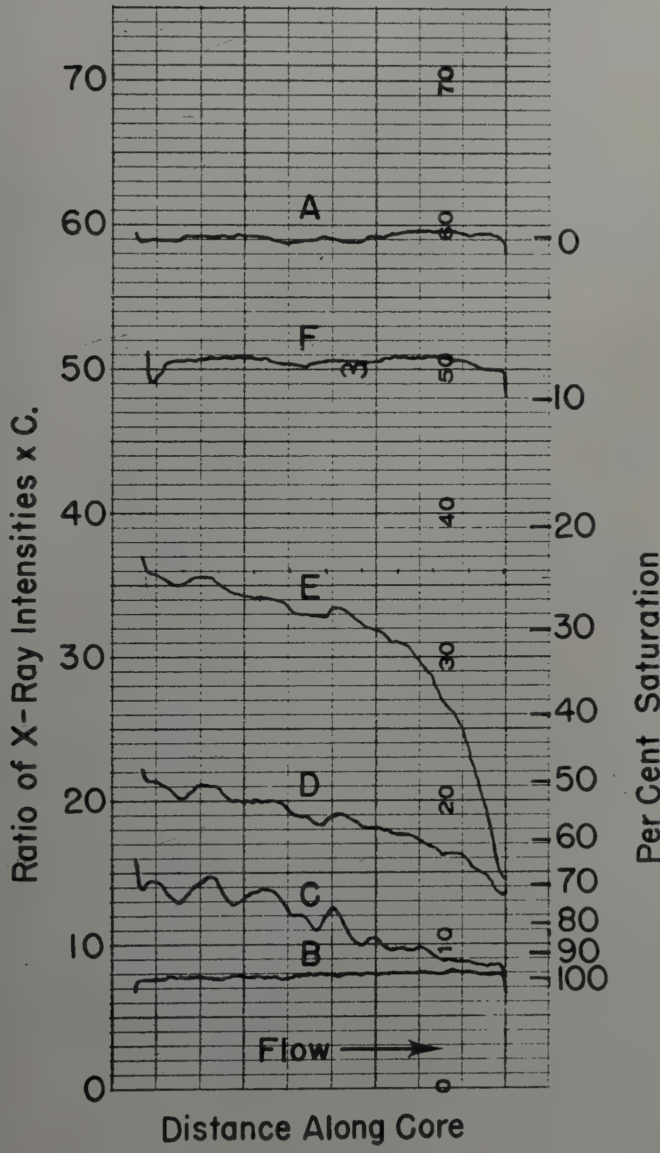

FIG. 6 — WATER DISTRIBUTION IN AN ALUNDUM CORE SUBJECTED TO A GAS DRIVE. TRACER, SODIUM IODIDE. A — DRY CORE, B — SATURATED CORE, C. D. E — SATURATION DISTRIBUTION AT VARIOUS STAGES OF THE DRIVE, F — INTENSITY THROUGH CORE AFTER FLOWING ONE PORE VOLUME OF DISTILLED WATER (THE SATURATION SCALE AT THE RIGHT IS NOT APPLICABLE TO CURVE F DUE TO THE ADDITION OF A THIRD COMPONENT, DISTILLED WATER).

CORE EXPERIMENTS

Saturation Distribution During Gas Drive

As a preliminary step in a series of experiments on multicore sections, the distribution of fluid in a core subjected to a gas drive was determined at various stages of desaturation. It is well known that water tends to accumulate at the outflow face of such a core, due to capillary forces or the "end effect," and this behavior has been observed experimentally.[1,3] The new apparatus is very convenient for demonstrating such effects and is also well adapted for the investigation of saturation variations inside a core. In this case it was considered desirable to scan an undivided core to obtain a picture of the liquid distribution before proceeding with the experiments which involved cutting the core into sections. As stated before, the width of the beam in the direction of scan was approximately ⅛ in. Its height was roughly ¼ in. These dimensions can undoubtedly be reduced, if necessary, to obtain better resolution.

An alundum core approximately four inches long and one inch in diameter was mounted in lucite, inserted in the X-ray unit core holder, and scanned in its dry state. It was then saturated, after evacuation, with an aqueous solution consisting of 200 grams of sodium iodide per liter. This concentration is high, but since no ill effects have been observed, with the exception of a mild corrosive action when metal fittings are used, there seemed to be no necessity for reducing the tracer concentration. The air permeability of the core at atmospheric pressure was 410 md. and the porosity, as computed from the amount of sodium iodide solution required for saturation, was 23.8 per cent. This compares favorably with the value 24.3 determined by the method of Equation (12). The dry scan, depicted as the trace *A* of Fig. 6, shows that there are no major cavities or unconformities along the central section of the core. The small differences in absorption observed in passing from one end of the sample to the other may easily be accounted for by small variations in the core diameter.

Trace *B* is for the saturated core. A slightly greater absorption at the inflow than at the outflow end indicates either that the core was not entirely saturated at the ouflow end or the porosity was somewhat lower there. The maximum difference in saturation — about three per cent — is of little significance in this experiment. Furthermore, since great accuracy in saturation determination was not required in this experiment, a scale of saturation based only on the logarithmic formula has been appended to the chart. Due to the previously mentioned change of absorption with wavelength the indicated saturations will be a little higher than the true values except near the ends of the scale. Curves *C*, *D*, and *E* follow the course of the saturation distribution during progressive desaturation by flow of nitrogen, which had been bubbled through water, starting with an inflow pressure of approximately 3 psi and then increasing the gas pressure by steps until the differential pressure across the core was about 12 psi. No attempt was made to run the experiment at each pressure until equilibrium had been attained. Shortly after the initiation of gas flow, for example in trace *C*, large variations were observed in saturation along the length of the core. Such changes are apparently due to gas pockets, trapped inside the core, which are not readily flushed out by the flow of liquid and gas. In traces *C* to *E* the piling up of water at the outflow face due to capillarity became more and more evident as the gas pressure was increased. Following this phase of the study the tracer material was washed out of the core preparatory to the first step of the multi-core experiment. Curve *F* shows that distilled water is quite effective in flushing the sodium iodide solution

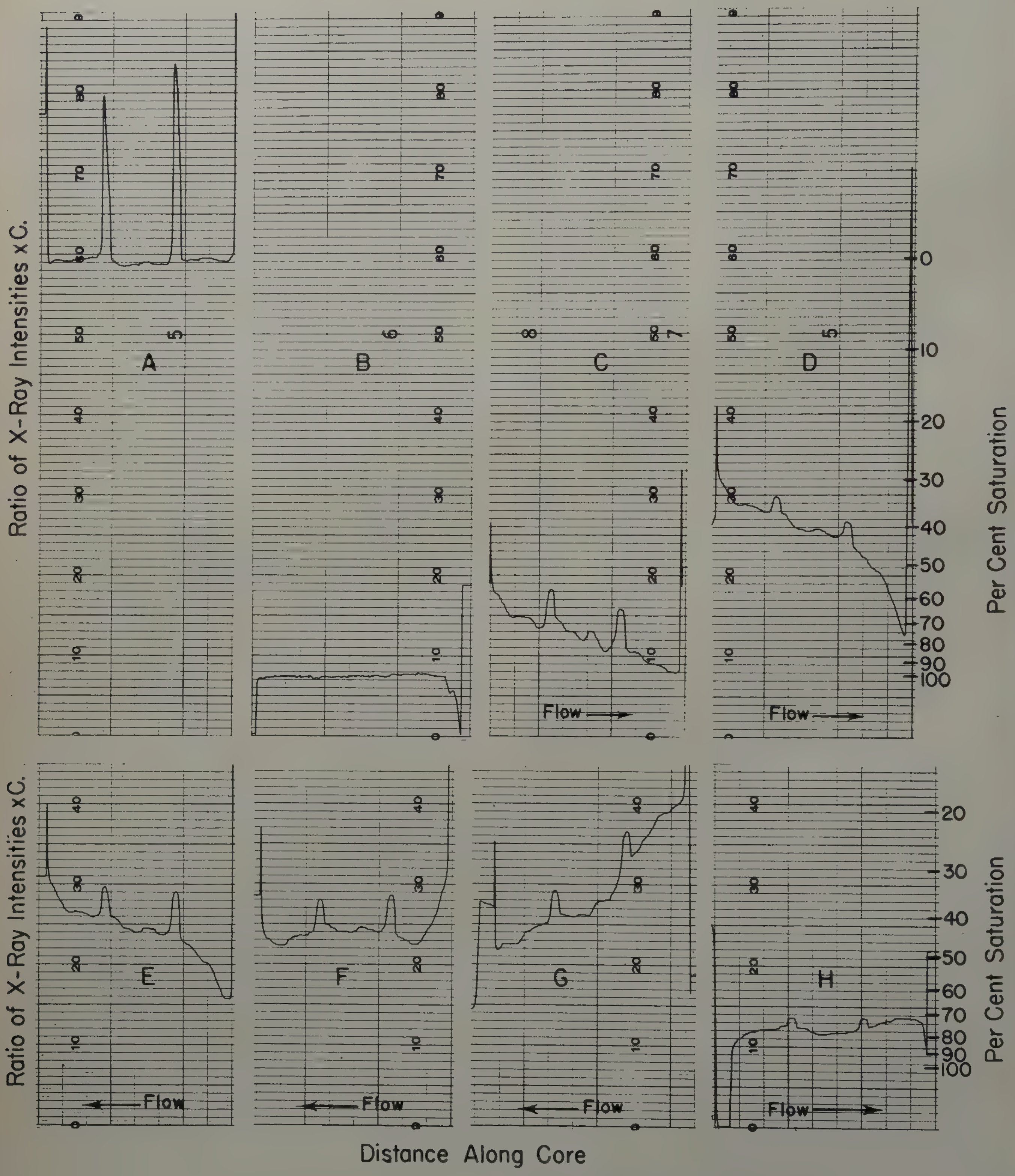

FIG. 7 — THE VARIATION OF TRANSMITTED BEAM ENERGY AND WATER SATURATION IN A THREE SECTION CORE. ALL CONTACTING SURFACES UNDERGROUND 0.0005". A — DRY CORE; B — SATURATED CORE; C, D, E, F, G — VARIOUS STAGES OF A GAS DRIVE; H — AFTER FLOWING SODIUM IODIDE SOLUTION. THE VERTICAL CHART LINES ARE NOT COORDINATED WITH THE CORE LOCATION.

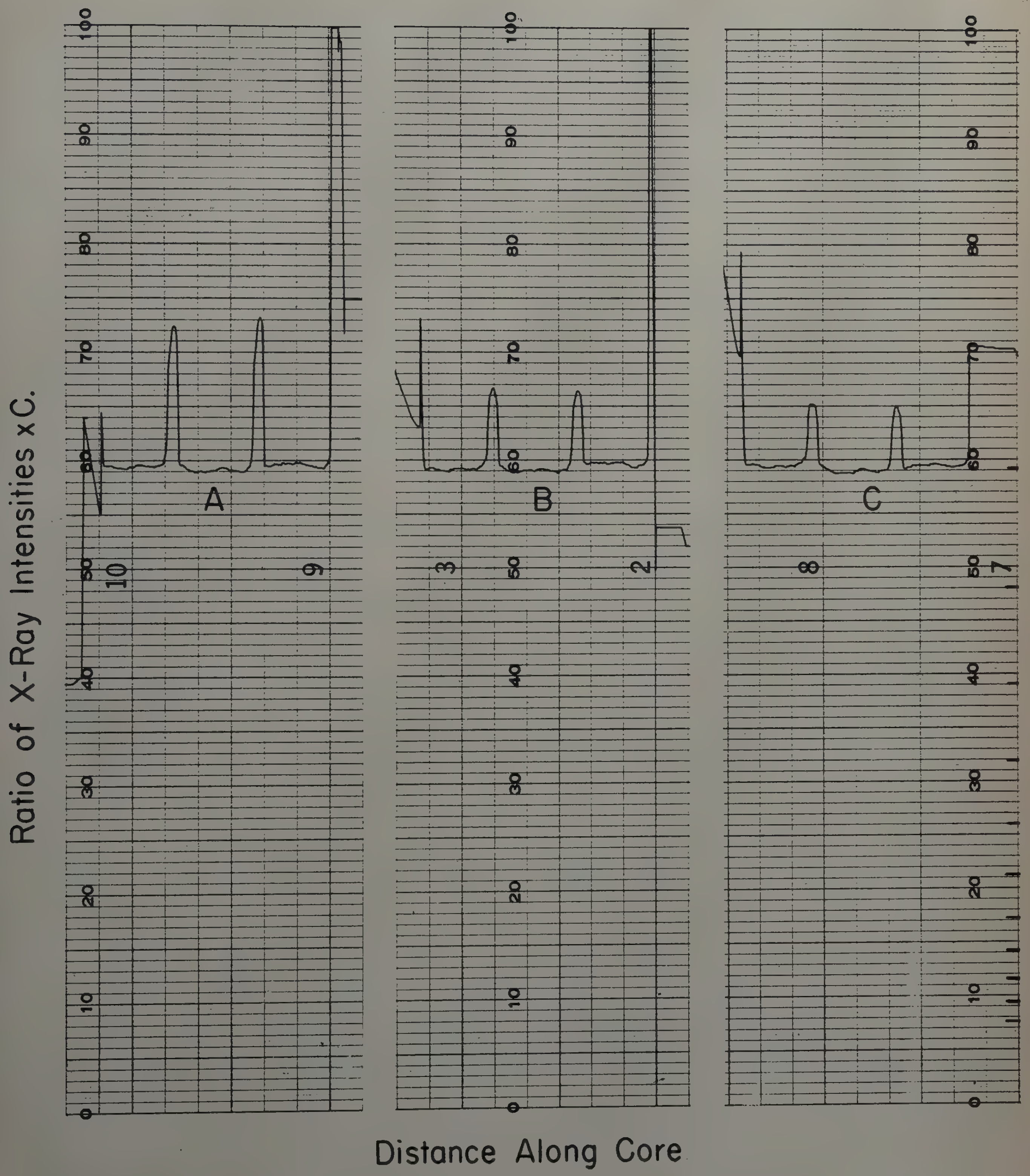

FIG. 8 — THE INTENSITY OF THE TRANSMITTED X-RAY BEAM THROUGH A DRY, THREE SECTION CORE, UNDER VARIOUS COMPRESSIVE FORCES INCREASING FROM A TO B TO C. TEST CORE FLUSH WITH ENCASING LUCITE.

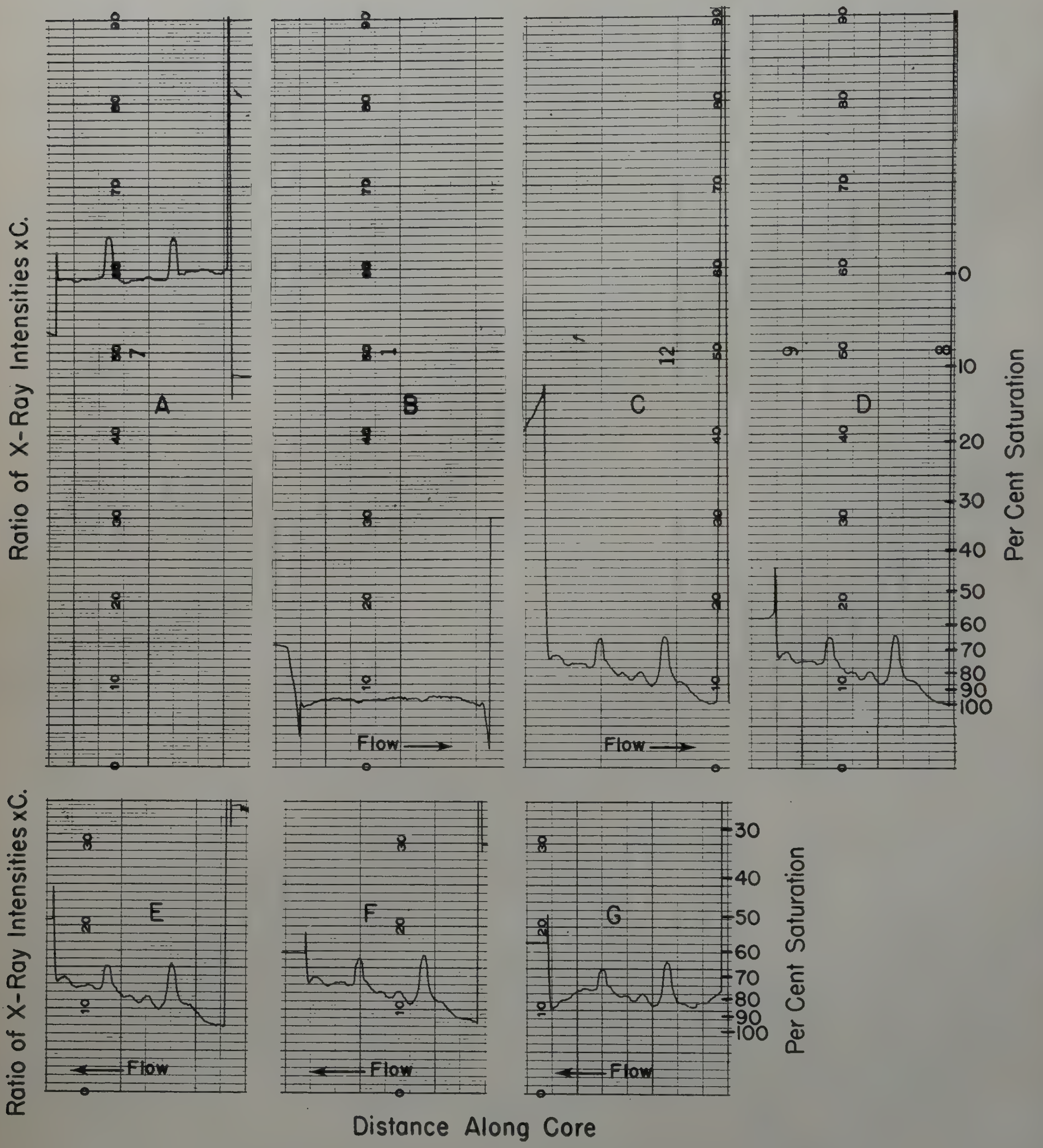

FIG. 9 — THE VARIATION OF TRANSMITTED BEAM INTENSITY AND WATER SATURATION IN A THREE SECTION CORE. ALL CONTACTING SURFACES CUT FLUSH WITH ENCASING LUCITE. A — DRY CORE; B — SATURATED CORE; C, D, E, F, G — VARIOUS STAGES OF SATURATION DURING A GAS DRIVE.

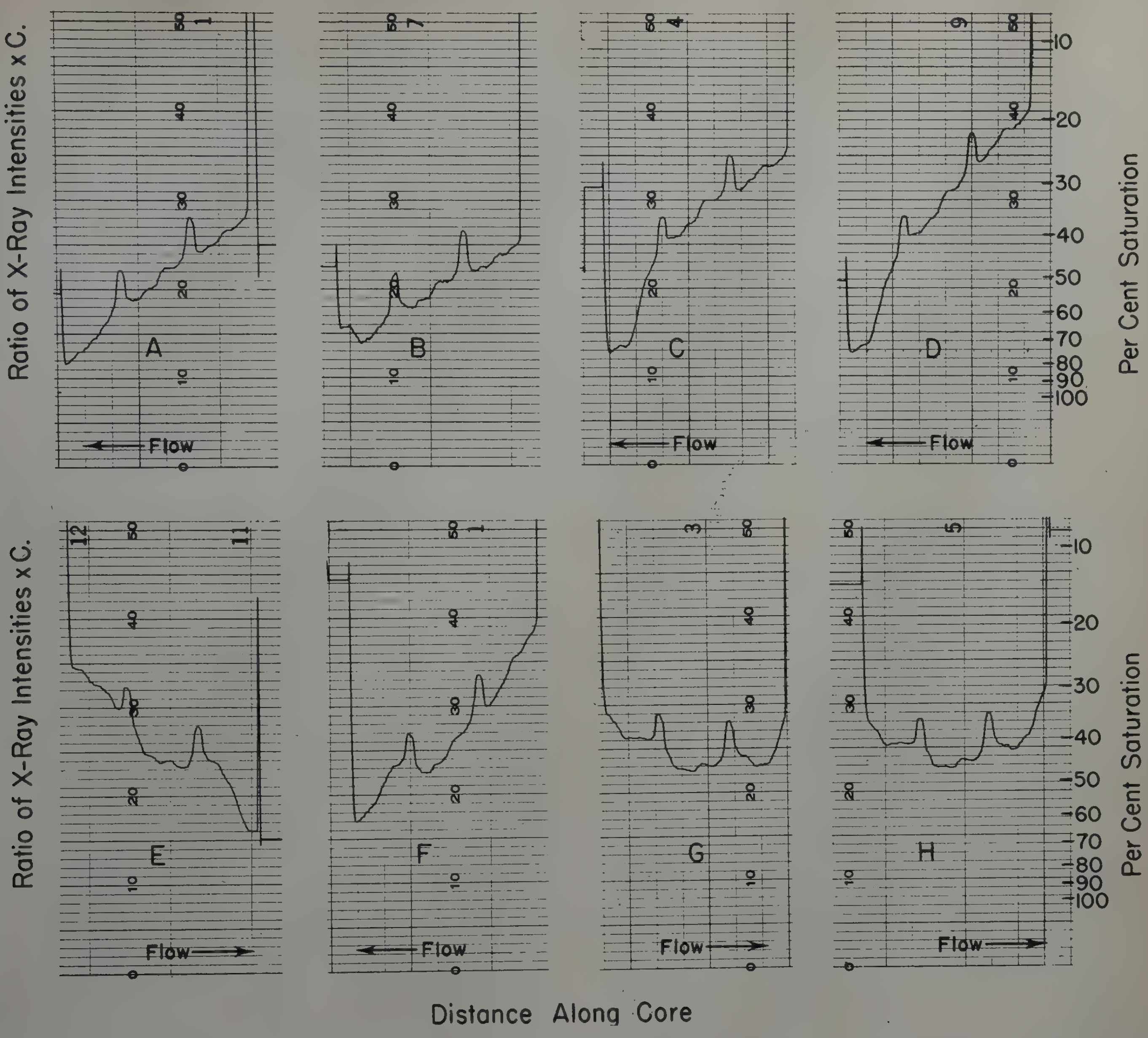

FIG. 10—THE VARIATION OF TRANSMITTED BEAM INTENSITY AND WATER SATURATION IN A THREE SECTION CORE AT VARIOUS STAGES DURING A GAS DRIVE. (CONTINUATION OF FIG. 9.)

out of the core. Only one pore volume of liquid had been collected at that stage, but the absorption already was reduced nearly to the value expected for a core containing water devoid of iodide tracer.

Effect on Fluid Distribution of Sectioning a Core

A method has recently been described[4] for measuring relative permeabilities of short cores in which core sections are pressed tightly against the test piece on both the inflow and outflow ends. All three sections are mounted in lucite and the cores themselves are undercut slightly at the contact faces in order that leak tight joints may be provided on compression of the lucite. Pressure taps are inserted at the junctions and the assumption is made that end effects will be avoided as the three pieces will for practical purposes behave as a single continuous core. A series of experiments was undertaken with the X-ray apparatus to test the hypothesis that no discontinuities would be found at the junctions of the cores.

After several hundred milliliters of water had been flowed through the core used in the previous experiments, it was cut into three sections corresponding to inflow and outflow heads and a test core. All four contacting faces were then undercut 0.0005 in. below the lucite sleeve. The three sections were next dried and inserted in a core holder in which considerable pressure could be applied parallel to the length of the specimen. With the exception of the joints the dry scan, shown as the trace *A* in Fig. 7, is in all respects nearly an exact duplicate of the dry scan of the core in its original condition. The marked increase in intensity at the joints definitely indicates a lack of uniformity in core structure at these points.

Evidently, under the conditions of this experiment, the three sections are not equivalent in all respects to a single core. Trace *B*, of the saturated core, also compares favorably with that for the undivided piece. The junctions may now be located, however, by small dips in the record which indicate that the bulk concentration of the tracer is greater in the cavities between the sections than in the cores themselves. When the third scan, *C*, was taken, after the start of a gas drive, peaks in the saturation curve were present where the dips had previously occurred. Due to the gaps between sections, the calibration curve for the core segments is not applicable at the junctions nor are the saturation scales at the right of the figure valid there. Rather, at the junctions, the X-ray energy reaching the detector will consist of two or more components arriving from parallel beam elements, one of which passes through the gap between the sections while the others traverse portions of the cores. Calibration curves, determined as before but based on the maximum and minimum deflections observed at the junctions, indicate that the dips will just disappear when the saturation in both the cores and gaps is approximately 80 per cent (60 per cent in Fig. 9). A more precise calibration, obtained by considering parallel elements, indicates, however, that both of these figures are too high and that all the peaks at the junctions for the partially saturated

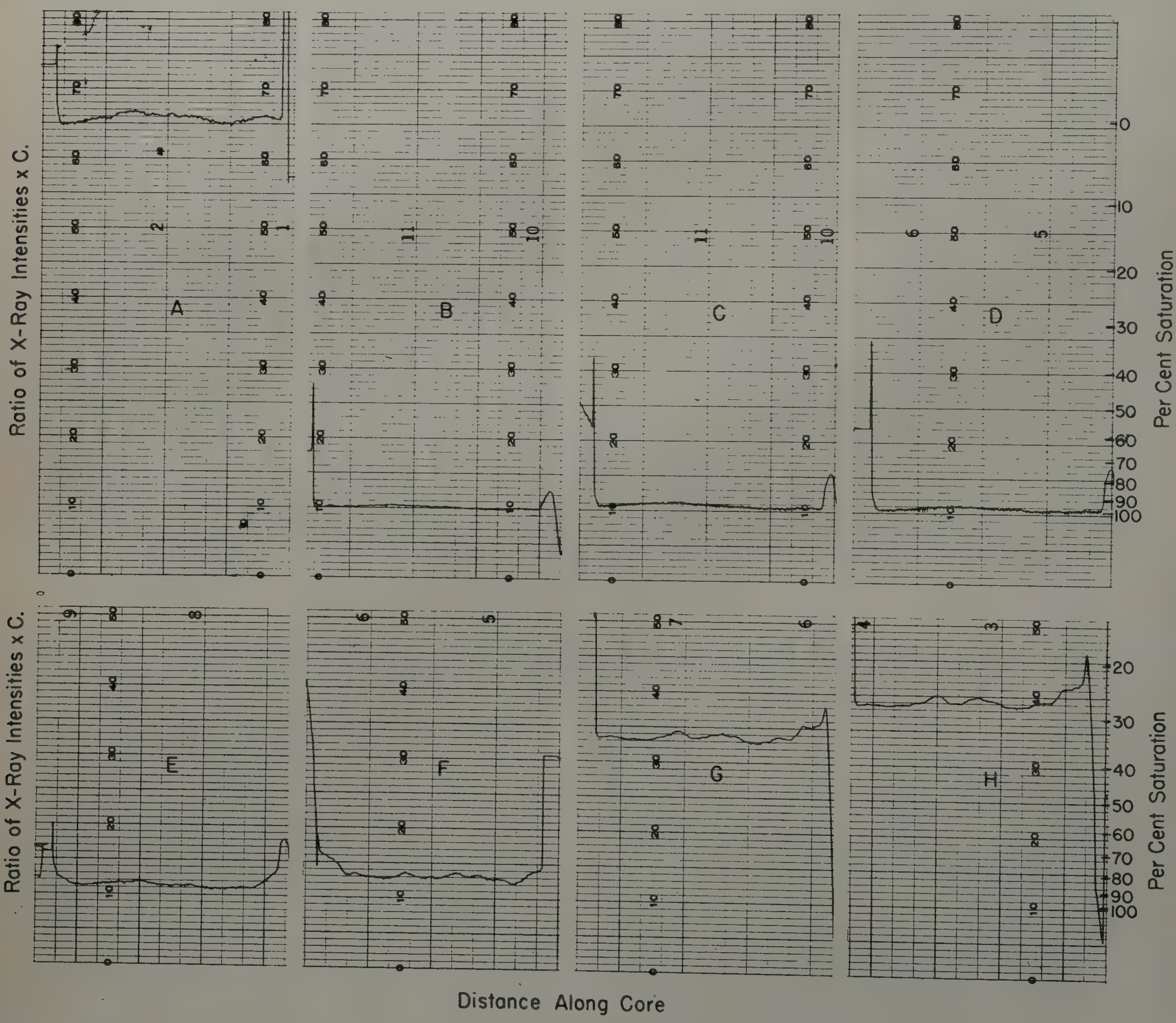

FIG. 11 — THE VARIATION OF TRANSMITTED BEAM INTENSITY AND WATER SATURATION WITH DISTANCE ALONG A CORE DURING DESATURATION BY THE CAPILLARY PRESSURE TECHNIQUE. BARRIER AT RIGHT, CORE UNMOUNTED. DISPLACING MEDIUM, GAS. A — DRY CORE; B — SATURATED CORE; C, D, E, F, G, H — SATURATION DISTRIBUTION AT VARIOUS STAGES AS GAS PRESSURE WAS INCREASED.

states must be ascribed to a local concentration of gas in excess of that in the neighboring segments. Exact determinations of these saturations are difficult, if not impossible, because of the limited response of the detectors and uncertainty in the effective width of the gaps.

Curve *D* shows the effect of continuing the gas flow at increased pressure and trace *E* was taken after gas had flowed slowly through the core in the reverse direction at a rate of about 2.5 milliliters per minute for 40 minutes. Not much redistribution of fluid took place under these conditions. However, when the pressure drop over the core was increased to about 5 psi the liquid distribution changed rapidly. Curve *F* shows the distribution after gas had been flowing at 1 ml/sec for three hours, while *G* corresponds to 2 ml/sec for the next hour. Once gas has collected at the junctions it is not readily displaced by flowing sodium iodide solution as indicated by curve H, which was made after a large quantity of sodium iodide solution had flowed through the core at 9 psi.

As the next step the ends of the test core were finished flush with the lucite after washing with water, and the dry core was examined as before. Fig. 8 shows the results of three scans with compressive forces applied to the core assembly increasing from left to right. Since it was evident that sufficient force could not be applied to close the gaps, the remaining contacting surfaces were immediately ground flush with the lucite preparatory to the final phase of the experiment.

The core sections were next inserted in the core holder and a compressive force applied that seemed on the verge of cracking the lucite. The top left trace of Fig. 9, corresponding to the dry core, still shows the discontinuity although it is not so pronounced as before. Curve *B* is for the liquid filled core. The drift of the amplifiers in this case was more than usual and the latter trace appears to be a little too high. After the flow of several pore volumes of sodium iodide solution failed to increase the saturation, the flow of nitrogen was started at a pressure slightly above the displacement pressure and trace *C* was obtained shortly thereafter. As before, the absorption of X-rays is least at the junctions of the core sections indicating the existence of a saturation discontinuity and the collection of more gas at the interface than corresponds to the gas-water ratio in other parts of the core. On the basis of these experiments it therefore appears that even by grinding the core faces flush with the encasing lucite the contact cannot be made sufficiently intimate to eliminate entirely all boundary effects. The remaining scans of Fig. 9, as well as those of Fig. 10, illustrate the saturation distribution which accompanies the flow of gas through the core at various pressure gradients. The trapping of excessive gas at the junction is evident in all of the examples. After taking curve *C*, the core was shut in for 24 hours with no appreciable change of fluid distribution, as indicated by trace *D*. Neither did the flow of gas for one hour in the reverse direction at a very slow rate, under a head of one cm. of Hg., nor a flow for one and a half hours at four times that gradient change the picture appreciably as shown by traces *E* and *F*. However, at 11.3 cm Hg. pressure the distribution, *G*, was altered considerably in one hour.

To obtain *A* of Fig. 10 the gas pressure was increased to 17.9 cm. of Hg. for 40 minutes and additional liquid was recovered. This time, *B*, the distribution changed when the core was shut in with pressure applied for 16 hours. Further liquid was produced and curve *C* obtained after flowing for 30 minutes at 22.9 cm. of Hg. pressure. In *D* gas had flowed for three hours at a pressure of 22.0 cm. of mercury, while in *E* the flow was reversed for 30 minutes at 22.5 cm. Hg. It was again reversed in *F* for 15 minutes at approximately the same pressure. On stopping the flow after it had continued for five minutes from left to right, *G* was obtained. The saturation distribution then remained practically unchanged for 30 minutes while flow was continued in the same direction, as shown by trace *H*, at 1.6 cm. Hg. pressure.

If the results obtained after sectioning the core can be considered to be representative of such samples, it appears that a discontinuity in capillary properties must be expected over at least a portion of the core face in passing from the body of a core into the space between the sections. How serious this effect will be in the measurement of relative permeabilities has not yet been determined. In many of the experiments there seems to be no noticeable piling up of liquid at the outflow end of the test core. However, if the observed saturation gradients persist when flowing mixtures, unequal pressure drops in the two phases will normally be encountered. Moreover, at the joints equilibrium will generally be attained only after long intervals of flowing and considerable variation with time will probably be observed.

In addition to the features already emphasized are the sharp saturation breaks that occur at the same location in the core in all the experiments. Particularly outstanding in this respect are the traces *C* of Figs. 6, 7 and 9. These variations were entirely unexpected as this core was found, on first scanning, to be more uniform than the average.

Fluid Distribution During Desaturation by Capillary Pressure Method

In experimentation of the capillary pressure type in which semipermeable barriers are employed, it is generally tacitly assumed that, at equilibrium, a discontinuity in saturation will exist at the interface between the core and the barrier. While it appears that this conclusion is justified from a theoretical point of view, no direct experimental tests of its validity seem to have been made. Furthermore, the saturation distribution during the transient stage before equilibrium is established has not been investigated. As the X-ray method of saturation is particularly suited to this type of study, experiments were started with the view of following the liquid distribution in a core during the desaturation process.

For this purpose an alundum core, 9.6 cm. in length and 2.58 cm. in diameter, having a permeability of 220 md. and porosity of 24 per cent was selected. The core was enclosed in a loose fitting lucite sleeve and mounted in a horizontal position so that it could be moved parallel to its length by means of the scanning motor. A spring pressed the core tightly against the barrier and Kleenex was used between the core and barrier to insure phase continuity. Sodium iodide was the saturating liquid and air the displacement medium. The results of the experiments are shown by the recorder charts reproduced in Fig. 11. The traces are of somewhat greater length than in the previous examples due to an increase in chart speed.

The first trace *A* shows the dry scan of the core. While this sample lacks the uniformity of the core used in the previous experiment, it nevertheless was the best of several that were available at the time. Scan *B* is for the saturated core. Here as in all the records in the figure, the barrier is located at the end of the core corresponding to the right end on the scan. Trace *C* was taken two days later after the displacing pressure had been gradually increased to 12 cm. of mercury and about 0.4 ml. of liquid had been collected. The shift of this trace from the original saturated scan is too small to be entirely reliable. Scan *D* was made about an hour after the pressure was increased from 12 to 14 cm. Trace *E* followed by about half an hour a further increase of pressure to 16.6 cm. of Hg., and *F* corresponds to the same conditions one day later. A scan taken just before the increase of pressure did not differ significantly from *E*. Traces *E* and *F* both indicate a lower saturation at the ends of the core than at the middle. The saturation was again recorded, G, after the pressure had been increased to 30.5 cm. of Hg. and maintained for 20 hours. The pressure was then increased to 39.8 cm. and four days later the core was scanned giving the trace *H*. In contrast to traces *E* and *F*, *G* and *H* show a low value of saturation only at the barrier end. The saturation, corresponding to trace *H*, was approximately 26.5 per cent when computed from the volume of liquid displaced, while the average value from the X-ray surve using the simple absorption formula is about 27.0 per cent.

The shutter was not opened in time to catch the barrier in scan *F*, while traces *G* and *H* show a sharp hump at the core-barrier contact which is followed by the anticipated rapid decrease in intensity due to the high saturation in the barrier itself. A decrease in saturation is apparent at or in the immediate vicinity of the barrier-core contact possibly indicating lack of complete areal contact between the core face and barrier.

DISCUSSION AND CONCLUSIONS

The adoption of a second ionization chamber, which led to the development of the ratio circuit, followed the observation that saturation determinations were variable from day to day and even from one time to another during the same day due to changes in the intensity of the X-ray beam. It is obvious that the apparatus would be considerably simplified if the X-ray source could be stabilized to the extent that sufficient accuracy would be obtained with a single ionization chamber. Moreover, if only approximate saturation values are required, or if minor variations in fluid distribution are not significant, it is quite possible that a recorder comparable to those recently developed or under development by several instrument manufacturers may be sufficiently sensitive and stable to measure the extremely small values of current that are available by this method.

Since an X-ray generator is a rather costly piece of equipment and the output is subject to fluctuations due to variations in the power supply, some preliminary experiments have been made using γ-ray sources. With the materials that have been commonly available, however, the sensitivity has not been as good as with the X-ray apparatus. On the other hand, for studies of saturation in thin core sections a beta ray recording gauge that is commercially available may be satisfactory.

As stated before, the experiments on the three section core indicate that sufficiently intimate contact between the faces to eliminate all boundary effects cannot be obtained. How serious this effect will be on the determination of relative permeabilities is difficult to ascertain and will require more experimentation and analysis. From some aspects the assembly seems to be approximately equivalent to three separate cores. At high pressure gradients the saturation along the length of the test core is far from uniform, as is to be expected, and the pressure gradients will generally not be equal in the two phases. Furthermore, the segregation of gas at the boundaries may be expected to lead to discontinuities in the pressures which may seriously affect the results.

The experiments do show that under certain conditions flow, in the non-wetting phase at least, may be maintained without seriously influencing the saturation distribution in a core. In relative permeability experimentation it therefore appears that the X-ray method may prove to be useful, not only for determining the saturation of a core, but also to indicate when conditions are appropriate for the measurement.

The above saturation distribution measurements on three section cores duplicate essentially some results obtained previously for air-water and oil-water mixtures with the point by point X-ray saturation technique. The measured permeability saturation curves were not reproducible, however, and the results were not considered to be reliable. Whether the inconsistency in results was due to failure to continue flow until equilibrium was attained, to an inherent variability in phase distribution and pressure gradients or to faulty experimental technique is problematical. In any case, work is being continued on this method as it seems to be better adapted than the capillary desaturation technique to the solution of some problems.

ACKNOWLEDGMENTS

The authors wish to thank Morris Muskat and W. L. Kehl for many valuable discussions during the progress of this work, and Paul D. Foote, executive vice-president of the Gulf Research and Development Co., for permission to publish the material.

REFERENCES

1. R. L. Boyer, F. Morgan, and M. Muskat, *Trans.* AIME, 170, 15 (1947).
2. A. O. Nier, E. P. Ney, and M. G. Inghram, *Rev. Sci. Inst.* 18, 294 (1947).
3. E. Brunner and E. S. Mardock, *Trans.* AIME 165, 33 (1946).
4. R. A. Morse, P. L. Terwilliger and S. T. Yuster, *Producers Monthly* 11, No. 10, 19 (1947).

★ ★ ★

T.P. 2893

PORE SIZE DISTRIBUTION OF PETROLEUM RESERVOIR ROCKS

N. T. BURDINE, L. S. GOURNAY, AND **P. P. REICHERTZ,** MEMBER AIME,

MAGNOLIA PETROLEUM CO., DALLAS

ABSTRACT

An investigation of equivalent pore entry radii in typical samples of petroleum reservoir rock and the pore volume associated with each value of pore entry radius has been made. Theoretical discussions together with experimental procedures for obtaining pore entry radii and the distribution of pore volume with pore entry radii are presented. Experimental results on a number of core samples, along with typical distribution curves, are shown. Data on the per cent of the pore volume filled by mercury at a pressure of 1500 psi are included. The results of re-runs of samples, made possible by regenerative apparatus, show the repeatability of the data and indicate the amount of physical change in the samples by mercury penetration. Theoretical equations for calculating permeability from pore size distribution data were derived and the results of such calculations are compared with measured gas permeability data. The effect of the shape, surface area, and weight of the sample on the pore size distribution of reservoir rocks was investigated experimentally. Mercury capillary pressure curves are compared with those obtained by the porous diaphragm method using gas to displace water.

INTRODUCTION

Standard core analysis techniques, in general, lead to quantities which are statistical averages of the varying properties of the samples under examination. Although such statistical information has real value in predicting the gross performance of porous bodies, it fails to provide fundamental information concerning the properties of the porous medium itself or any processes which may be occurring in it. For example, a gas permeability measurement on a core sample is an indirect way of determining an average pore radius for that particular sample. Since there are many combinations of pore radii that will give the same radius, and, hence, the same permeability, no information is obtained on the pore size distribution. Furthermore, similar values in permeability do not imply similarity in other properties of a porous medium. For instance, it is possible to have two core samples with identical permeability which would have different residual oil contents at the end of an air-oil drive, or even different amounts of interstitial water.

It has been recognized for some time by the petroleum industry that a determination of pore size distribution for porous reservoir rocks offered promise of increased understanding of fundamental flow processes in the porous matrix, and therefore of petroleum reservoir performance in general. There have recently been published several methods for determination of pore size distribution in porous materials. A report is given here of the modifications in equipment and technique required to adapt one of these methods to measurements on petroleum reservoir core samples. Although only a few correlations or applications of the method are available for presentation at this time, the technique is brought to the attention of the industry so that the opinions and experience of others with this or similar techniques may be exchanged. It seems possible that the method will have wide application in the future.

METHOD

There are three general methods which may be employed to measure the pore size distribution in naturally occurring rock formations. One method[1] is based on experimentally determined adsorption isotherms for calculating the surface area of the porous medium. Knowing the surface area and the pore volume, a rough estimate of the pore radius can be made. Since this method depends on the thickness and uniformity of the adsorbed layer, the validity of the results would be highly questionable.

A second method utilizes capillary pressure data obtained by static dis-

---

Manuscript received at office of the Petroleum Branch August 12, 1949. Presented at Branch Fall Meeting, San Antonio, Texas, October 5-7, 1949.

[1] References are given at end of paper.

placement of a wetting fluid from a sample in contact with a semi-permeable porous diaphragm. Although partially successful for the determination of interstitial water curves, the inherent errors and limited pressure that may be used eliminate this method for pore size distribution studies.

A third method, employed by Purcell[2] in an investigation of capillary pressures in reservoir rocks, and by Drake and Ritter[3] in the measurement of the pore size distribution of catalysts, uses a "non-wetting" fluid, mercury. The technique of Drake and Ritter, with modifications, has been applied to the study of pore entry radii and the distribution of pore volume with pore entry radii in reservoir rocks.

In the theory of Drake and Ritter[3] two equations were developed, for the penetration of a "non-wetting" liquid into a porous solid, namely,

$$pR_i = -2\,\sigma\cos\theta \quad . \quad . \quad . \quad (1)$$

and

$$D(R_i) = \frac{p}{R_i}\,\frac{d(V_o - V)}{dp} \quad . \quad . \quad (2)$$

A pressure-volume curve is plotted from experimental data. By graphical differentiation of this curve, values of the derivative in Equation (2) required to evaluate $D(R_i)$ are readily obtained. For a number of values of p, the pressuring curve is differentiated to obtain $d(V_o - V)/dp$, R_i is calculated from Equation (1), and $D(R_i)$ from Equation (2). Plotting $D(R_i)$ against R_i gives the distribution curve.

The value of $\overline{D(R_i)}$ may be determined directly from the pressure volume curve, where $\overline{D(R_i)}$ is the average value of the distribution function in the radii interval R_i to $R_i + \Delta R$. By definition[3]

$$\overline{D(R_i)} = \frac{v_i}{\Delta R} \quad . \quad . \quad . \quad (13)$$

The incremental volume, v_i (fractional), is read off the pressure-volume curve, divided by ΔR, and plotted against $R_i + \frac{1}{2}\Delta R$, giving the distribution curve. This type of graphical differentiation employs the chord instead of the tangent, with accuracy inversely proportional to the length of the increment.

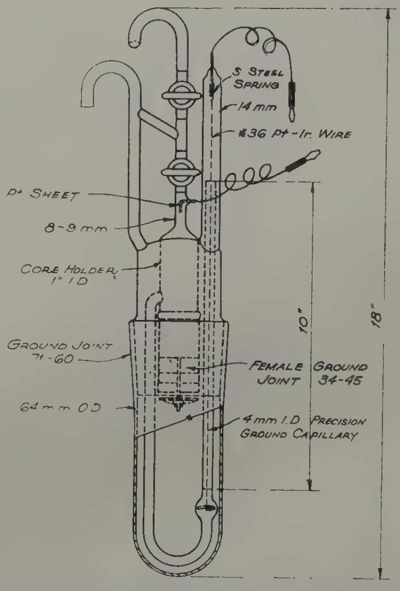

FIG. 1 — DILATOMETER, MOD. IV FOR PORE SIZE DISTRIBUTION MEASUREMENTS.

APPARATUS AND PROCEDURE

An apparatus suitable for determining the pore size distribution in porous media has the following essential components: (1) a system wherein the pressure can be varied from small absolute values (high vacuum) to 2000 psig or higher; (2) a closed system for evacuating the sample and immersing it in the "non-wetting" liquid at a few microns (Hg) pressure; (3) and, finally, a system for measuring the quantity of "non-wetting" liquid that penetrates

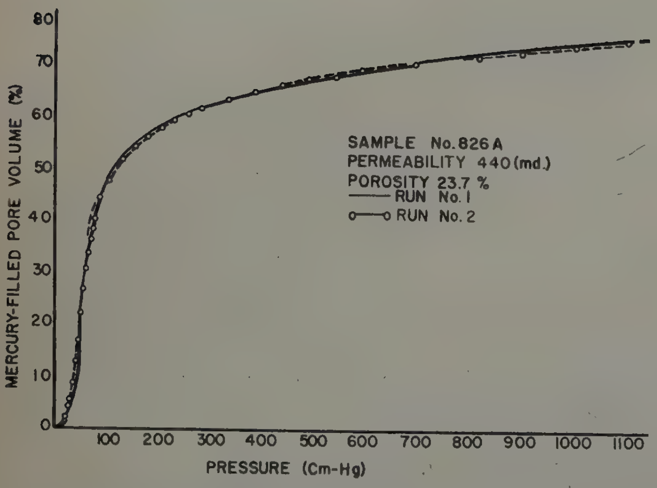

FIG. 2 — MERCURY IMBIBITION CURVES; MERCURY-FILLED PORE VOLUME VS. PRESSURE.

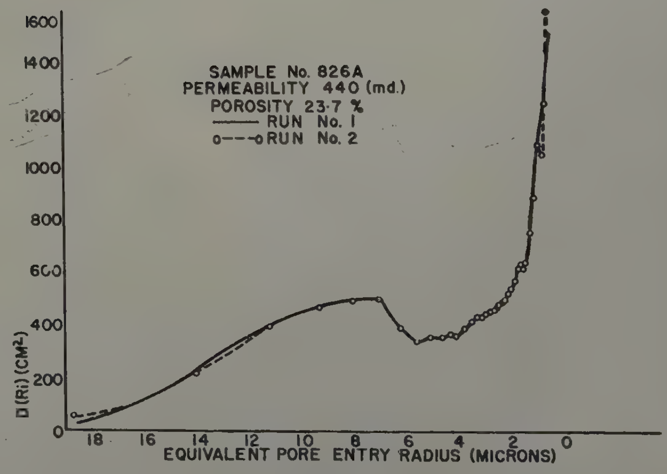

FIG. 3 — EQUIVALENT PORE ENTRY RADIUS VS. DISTRIBUTION FUNCTION.

the sample for a given pressure change. The component parts of the apparatus used in this investigation are described below.

The vacuum system consists of a single stage, high speed, mercury diffusion pump backed by a Welch Duo-Seal, Hy-vac pump. A McLeod gauge and mercury manometer are inserted for pressure (or vacuum) measurements and a tube filled with calcium sulphate ($CaSO_4$) for admitting dry air to the system is included.

The electrical system is used for measuring the quantity of "non-wetting" liquid (mercury) that penetrates the sample for a given pressure change. The essential components are: a type K, L&N potentiometer, a standard 100-ohm resistance, a Rubicon galvanometer, variable resistance boxes, and the platinum resistance wire installed in the capillary of the dilatometer. If the current in the circuit is adjusted to a constant value by means of the potential drop across the standard 100-ohm resistance, the resistance to be measured (the platinum wire) is then determined directly by its potential drop.

Table I

Dilatometer Calibration

Ohms/cc	Pressure (psi)	Volume Variation (cc)
2.2953	0–1500	±.0006

For readings above atmospheric pressure, a high pressure steel chamber or bomb of sufficient size to contain the dilatometer was constructed. The bomb was connected to a high pressure (2000 psi) nitrogen bottle with suitable pressure gauges, valves, and fittings, and wired electrically for resistance measurements.

The dilatometer used in these studies, Fig. 1, was made of pyrex glass. It consisted of a sample chamber connected to a capillary tube and surrounded by a jacket. This arrangement reduced the pressure differential between the inside

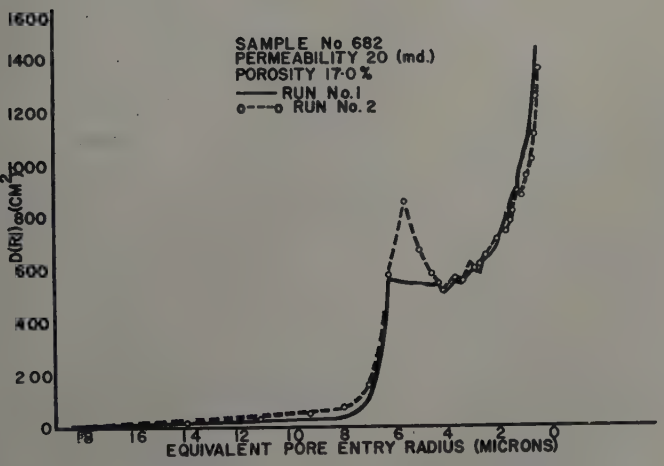

FIG. 4 — EQUIVALENT PORE ENTRY RADIUS VS. DISTRIBUTION FUNCTION.

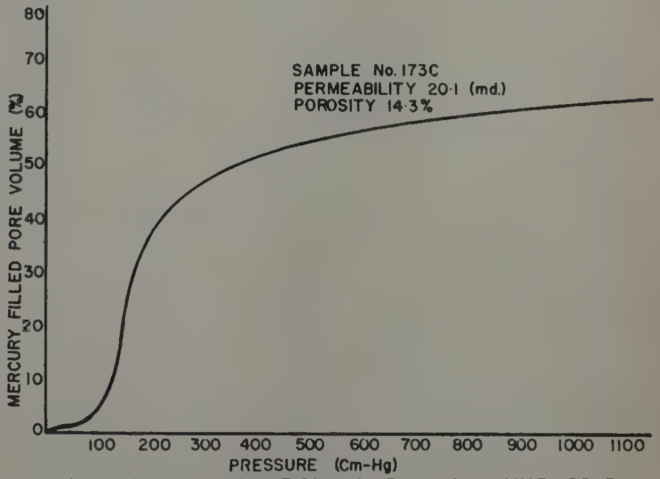

FIG. 5 — MERCURY IMBIBITION CURVE; MERCURY FILLED PORE VOLUME VS. PRESSURE.

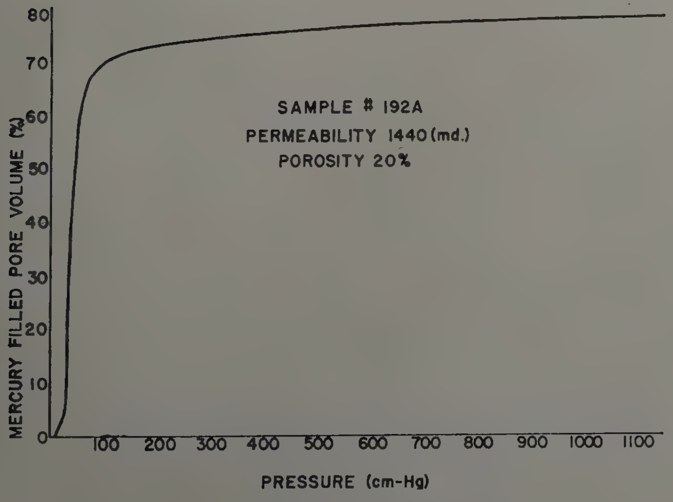

FIG. 6 — MERCURY IMBIBITION CURVE; MERCURY-FILLED PORE VOLUME VS. PRESSURE.

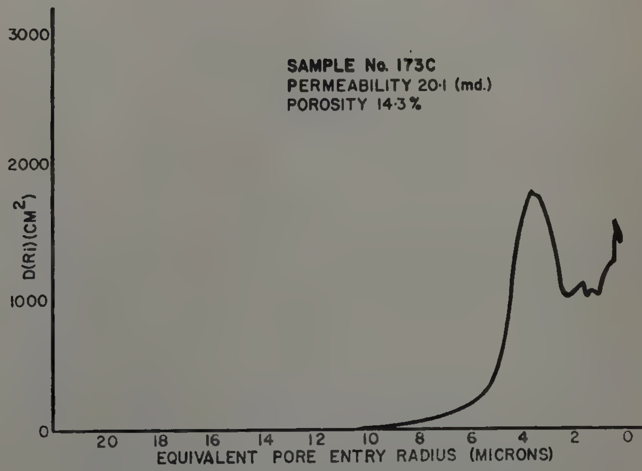

FIG. 7 — EQUIVALENT PORE ENTRY RADIUS VS. DISTRIBUTION FUNCTION.

and outside of the sample chamber to a minimum for all pressures. A No. 36 B&S gauge platinum-iridium wire with appropriate leads for electrical connections to the outside was mounted inside the capillary tube. The dilatometer calibration results are shown in Table I.

After preparations* the sample is placed in the dilatometer and the system is evacuated to a final pressure of 2 to 3 microns of mercury. The capillary tube and the sample chamber are now filled with mercury and the resistance of the capillary wire recorded. The pump is isolated from the dilatometer and dry air is admitted in increments to the system, thereby increasing the pressure on the mercury surrounding the sample. The volume of mercury entering the sample for a given pressure change and, hence, the pore volume associated with this particular increment in the value of pore entry radius, is determined by the increase in resistance of the capillary wire, as the mercury recedes in the capillary upon entering the porous sample. Due to temperature changes in the system by admission of air, or due to an apparent lag in the mercury penetrating the sample for a given pressure increase, or both, the initial resistance readings are too low. It is therefore necessary to wait until the system stabilizes for each pressure increase before the final resistance is measured and recorded. (The ambient temperature changes of the air-conditioned room are considreed to be negligible.) This procedure of alternately increasing the pressure and measuring the change in resistance is continued until atmospheric pressure is reached. The inside of the dilatometer surrounding the pressure chamber and the pressure bomb are partially filled with water to minimize temperature variations and to reduce the air space. The dilatometer is then transferred to the bomb and the readings are continued, as above, to 1500 psig or higher, using nitrogen for the pressurizing gas. After converting the resistance readings to volumes of mercury by a previously determined calibration curve, a pressure-volume curve may be plotted for the particular sample.

Physical Effects of Sample Regeneration

After several experimental tests were made to determine the pore size distribution in reservoir rock samples, it became apparent that much additional information could be obtained if reruns on the test samples were possible. Such information would show, (1) the physical changes in the sample due to the penetration of the mercury into the pore spaces, and, (2), the magnitude and effect of the experimental errors on the repeatability of the data. Also, incompleted runs that were halted during the experiment for various reasons could be started anew. The preparation of a sample for the re-run necessitated the removal of mercury imbibed during the previous run. This was accomplished by vacuum distillation.

The apparatus for sample regeneration consisted of a pyrex glass tube sample chamber surrounded by a heating coil and connected to a Hy-Vac pump through a CO_2 trap.

Samples containing mercury are placed in the sample chamber, evacuated and heated to 180°C. (356°F.) for several hours. When the weight of the sample has been reduced to the weight before imbibition of mercury, it is assumed that all of the mercury has been removed from the sample.

Table II

Measured (Gas) Permeabiilty Before and After Pore Size Experiments

Sample Number	Permeability (md)	
	Before Pore Size Run	After Pore Size Run
261A	0.47	0.50
12A	97.8	94.0
12B	100.8	95.2
174C	37.9	38.2

---

* Samples are extracted in a Soxhlet extractor using benzene for 24 to 48 hours and dried for at least 24 hours in an oven at 90°C.

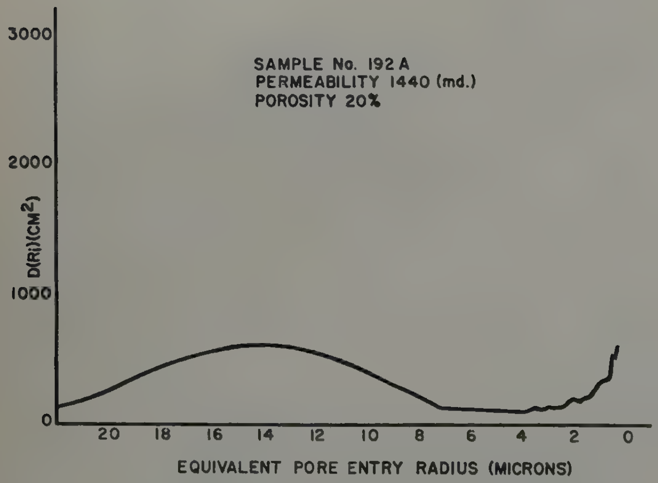

FIG. 8 — EQUIVALENT PORE ENTRY RADIUS VS. DISTRIBUTION FUNCTION.

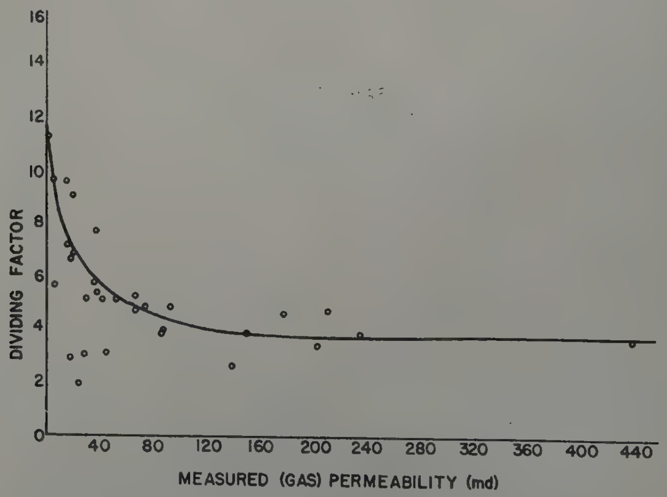

FIG. 9—DIVIDING FACTOR VS. MEASURED (GAS) PERMEABILITY CURVE.

The pressure-volume curves (Fig. 2) for the first and second runs on a reservoir rock sample show excellent repeatability of data and indicate low order of magnitude of experimental errors. Also, the distribution function curves (Fig. 3) for the same sample are very similar. An extreme case, that was observed on only one sample (Fig. 4) gave a broad peaked distribution curve for the first run and a considerably sharper peak for the second run. When the imbibed mercury was being removed from this sample by vacuum distillation a fine gray powder formed on the walls of the chamber and the outside of the sample. The chemical composition of the powder or the cementing material of the sample was not determined.

If the entrance openings to the pore spaces are enlarged by the penetration of the mercury, the gas permeability should be increased by successive pore size distribution runs. To test this, gas permeability measurements were made on a number of reservoir samples before the pore size data were taken and after the removal of the imbibed mercury. No appreciable increase in permeability, Table II, was observed for any of the samples.

Table III

Per Cent Pore Volume Filled During Mercury Imbibition to 1500 PSIA

Sample No.	Meas. (Gas) Permeability (md)	Pore Volume Filled (%) at 1500 psia	Sample No.	Meas. (Gas) Permeability (md)	Pore Volume Filled (%) at 1500 psia
171C	17	76	190A	93	80
164C	86	69	174B	36	71
171B	2.6	85	173C	20	78
261A	0.5	56	311B	52	68
174C	38	75	192A	1440	82
164B	41	78	169B	30	55
311A	67	53	171D	22	85
161B	7	72	295A	20	84
173D	16	77	261B	<0.01	60
163A	29	78	686	46	57
681	81	61	867	88	77
866	88	73	683	16	62
680	38	61	696	75	61
682	20	59	14564	112	80
826A	440	85	13302	5	68

Table IV

Dividing Factor - Permeability Data

FRL Sample No.	Per Cent Porosity	Meas. (Gas) Permeability (md)	Calculated* Permeability (md)	Dividing Factor
295A	13	19.6	131	6.7
13302	25	5.1	49.7	9.7
14564	20	112	709	6.3
13232	20	140	359	2.6
826A	24	440	1610	3.7
866	21	88.2	357	4.1
867	21	88.4	356	4.0
682	17	20	181	9.1
696	17	75	366	4.9
680	19	38	292	7.7
683	15	16	154	9.6
681	17	67	318	4.7
686	16	46	401	8.7
161B	18	6.7	38.3	5.7
163A	16	29	151	5.2
164B	15	40.8	213	5.2
164C	18	86.1	333	3.9
169B	17	29.6	90.4	3.1
171B	10	2.6	29.4	11.3
171C	12	17.1	50.9	3.0
171D	10	22	43.2	2.0
174B	17	35.5	205	-5.8
174C	17	37.9	203	5.4
173D	14	16	115	7.2
173C	14	20.1	139	6.9
190A	19	93.0	456	4.9
192A	20	1440	4390	3.1
311A	23	66.6	354	5.3
311B	18	51.9	269	5.2
261A	17	0.5	4.1	8.2
12618	17	237	937	4.0
13996B	20	493	1860	3.8
15809	20	150	590	3.9
6	20	213	1020	4.8
951	23	179	841	4.7
53	20	205	718	3.5
Shale Sample	Not Measurable	0	Negligible	—

*No dividing factor used.

It may be concluded from the above tests that the apparatus and procedure for acquiring pore size distribution data on a reservoir sample are satisfactory and that the physical characteristics of the sample are not, in general, altered in the process.

RESULTS

Pore size distribution data have been obtained on 100 samples taken from several reservoir formations. Typical pressure-volume curves are shown (Figs. 5 and 6) for samples that have widely different gas permeabilities. Also, the distribution function curves for the same samples (Figs. 7 and 8) illustrate the type of distribution and the size of the pore entry radii to be expected in the respective permeability ranges.

Pore Volume Filled by Mercury

The per cent of the pore volume filled by mercury at maximum pressure (1500 psig), Table III, varied with the permeability of the sample and ranged from 53 to 85.

According to Equation (1), the smallest pore filled at 1500 psig has an equivalent entry radius of 716Å (1Å = 10^{-8} cm). Hence, a large percentage of the pore space (over 45 per cent for one case above) has entry radii less than 716Å and is not filled with mercury at the maximum pressure used.

An apparatus has been assembled that will increase the pressure range to 10,000 psi. If Equation (1) is applicable[3,4], this will extend the lower radii region filled by mercury to 108Å and will include an estimated 95 per cent of the total pore volume of most reservoir samples.

Geological Correlation

A study of pore size distribution data obtained to date shows that distribution curves for samples from a particular geological formation sometimes have similar characteristics, whereas distribution curves from another formation may have very little in common. If geological formations are found to have characteristic distribution curves in general, the exceptions to this trend may perhaps be ascribed to relatively large amounts of clays and various chemical compounds occluded in the formation. When sufficient data are available, definite conclusions may be made in regard to this possible type of correlation.

Permeability Calculations and Results

Two equations were developed for calculating the permeability of a porous medium from pore entry size distribution data. (See Appendix for derivations). One equation contains the distribution function, and the other, the pressure-volume relationship. The equations are:

$$k = \frac{100\,\phi}{8C}\;\frac{\displaystyle\sum_{i=0}^{n} \frac{\overline{D(R_i)}\;\overline{R_i^4}}{x_i^2\,\overline{R}_i^2}}{\displaystyle\sum_{i=0}^{n} \overline{D(R_i)}} \quad . \quad (15)$$

and

$$k = \frac{100\,\phi}{8C} \sum_{i=0}^{n} \frac{v_i\;\overline{R_i^4}}{x_i^2\,\overline{R}_i^2} \quad . \quad (17)$$

In these equations all factors are known or determinable except the factor, x_i, which is proportional to the "effective" capillary length. If the "effective" capillary lengths of all the pores for all samples are the same, the factor, x_i^2, may be written as a "dividing factor", f, in the equations above. The value of f may be shown both theoretically and experimentally for close-packed spheres of uniform size to be $(\pi/2)^{2(2)}$. Since naturally occurring rock structures vary considerably from this ideal "sand" pack, the values of the factors, f, for various permeability ranges apparently can be determined only by experimental measurements. Data obtained by the authors have been plotted with the measured gas permeability versus the "dividing factor" (Fig. 9) that makes the calculated values the same as the measured values. A curve was drawn through the data points to show the general trend. Table IV shows the detailed data used.

An analysis of the data indicates that the factor, f, varies inversely with the permeability of the sample. Since the pores with the smaller radii might be expected to have the more random paths through a porous medium, the factor, f, would be greater for the smaller pores than for those of larger radii. Values of the "effective" capillary lengths were estimated from the accumulated data. These results, the general trend of the "dividing factor" curve, and the probability that the pores of larger radii approach more closely those of the "ideal" sand pack were instrumental in the formulation of the empirical formula

$$x_i = 5\,e^{-0.4R_i} + 1.83 \quad . \quad . \quad . \quad (18)$$

using the values of x_i determined by this equation permeabilities were calculated (Table V) and plotted against the measured gas permeabilities, Fig. 10, for the samples tested.

It is observed that the calculated permeabilities for five of the samples were low and probably outside the range of experimental error. These samples were taken from a field in which a considerable amount of fine interstitial material was present. Further study and accumulation of data are necessary to verify the empirical Equation (18).

Of special interest are those samples which gave abnormally low or high dividing factor values. A study was made of the distribution curves, Fig. 11, for three samples, the data for two of which deviated from the norm, despite the fact that the measured gas permeabilities of all three were about the same: 20 md. All three of these curves indicated different mean pore entry radii, enclosed different total areas and, therefore, different pore volumes for a chosen radii interval; but the one with the least mean pore entry radius had the largest pore volume, the one with the next larger mean pore entry radius had the second largest pore volume, and the one with the largest mean pore entry radius had the least pore volume. These facts, in conjunction with the variations in dividing factors, explain qualitatively how it is possible for the three samples to have the same permeability, although being widely different structurally.

It is seen from the foregoing that Equations (15) or (17) may be used to calculate the permeability of porous media from pore size distribution data.

Table V
Measured (Gas) Permeability vs. Calculated Permeabilities

FRL Sample No.	Per Cent Porosity	Measured (Gas) Permeability (md)	Calculated* Permeability (md)
13232	20	140	68
686	16	46	98.5
161B	18	6.7	2.9
163A	16	29	20
164B	15	40.8	35.8
164C	18	86.1	71.2
169B	17	29.6	11.6
171C	12	17.1	5.6
171D	10	22	4.4
173C	14	20.1	20.5
173D	14	16	15.8
174B	17	35.5	34.2
174C	17	37.9	35.9
190A	19	93.0	93.7
311A	23	66.6	71.3
311B	18	51.9	63.5
261A	17	0.5	0.2
12618	17	237	245
13996B	20	493	524
15809	20	150	140
6	20	213	264
951	23	179	209
53	20	205	166
682	17	20	23.8

*Used $x_i = f(R_i)$.

Table VI
Physical Measurements of Samples

Sample No.	Gas Permeability (Meas.) md	Run No.	Weight (gms)	No. of Pieces	Surface Area (cm²)	Total Pore Volume Filled (%)	Permeability (Calc.) md
14564	112	1	22.42	1	29.2	85	709
14564	112	2	16.10	Sample	Crushed	84	1240
13302	5.1	1	27.69	1	31.8	68	49.7
13302	5.1	2	26.09	2	40.3	66	56.5
13302	5.1	3	22.61	4	58.0	67	67.2
13302	5.1	4	18.73	16	69.2	64	80.7
174-B	35.5	1	27.28	1	29.8	71	205
		2	15.90	2	21.5	73	244
		3	16.03	4	51.2	79	306

The results of the investigation indicate a reasonably accurate and satisfactory method for permeability measurements. If the permeability is known and the pore size distribution data are available, the lithology factor, f, may be determined by similar equations.

Water Capillary Pressure Determinations

Equation (1), namely,

$$pR_i = -2\,\sigma \cos\theta$$

may be used to determine capillary pressure curves for "wetting" fluids as well as for "non-wetting" fluids in porous media. The difference lies in the values of the constants, σ and θ. The value of contact angle between the reservoir solid and water was assumed to be that determined between quartz and water. This value, as well as the value of surface tension for the mercury-air interface, was taken from the International Critical Tables. The values so obtained were $\sigma = 72.75$ dynes per cm and $\Theta = 0°$.

Using the mercury capillary pressure data (for about ten sandstone samples), water capillary pressure data were calculated by Equation (1), plotted, and compared with the results obtained by the porous diaphragm method. A typical curve is shown in Fig. 12. The porosities of these samples were estimated. Considering the assumptions made and experimental errors involved, the correlations of results are very good. The discrepancies that appear, especially at the extremes of pressures, are under investigation theoretically and experimentally as more data are accumulated.

External Surface Area, Weight, Shape Factor Effects of Samples

In the study of iregularly shaped samples, experimental measurements were made to determine the effect of external surface area, weight, and shape of the sample on the pore size distribution data. This necessitated pore size measurements on a sample and re-runs, on the same sample, with successive changes in one or more of the physical factors. For example, the first run was taken on a sample in one piece and the re-run data were taken with the sample crushed into many pieces. The pressure-volume curves showed increased volume values in the low pressure range for the second run and the calculated permeability was 75 per cent higher than that for the first run.

The procedure for making multiple samples by cutting the originals was altered to make possible plane area measurements, uniform shapes, and constant weights. Physical measurements, calculated permeabilities, and other data are shown in Table VI. A typical set of pressure-volume curves and distribution function curves are shown in Fig. (13) and (14), respectively.

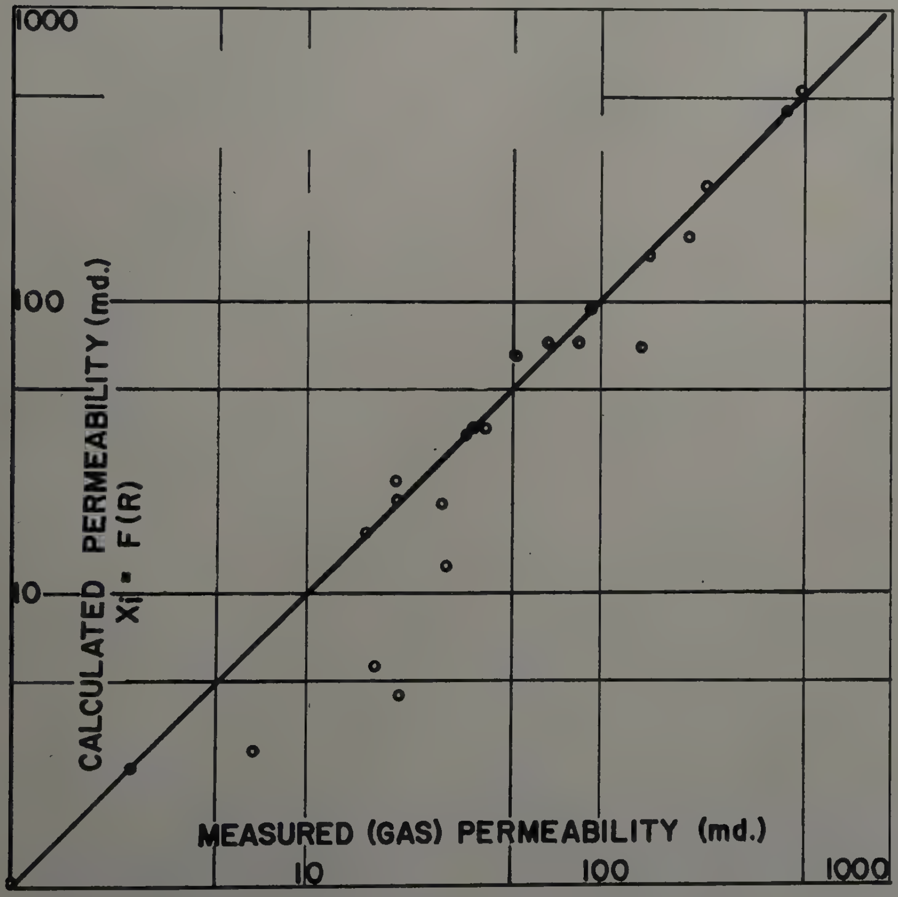

FIG. 10 — PERMEABILITY CALCULATED BY EFFECTIVE CAPILLARY LENGTH VS. MEASURED GAS PERMEABILITY.

General observation of these data reveal that the volume of mercury penetration in the low pressure range increases as the surface area per unit weight increases, but a quantitative relationship between the two has not been determined. Too, the increase in calculated permeabilities with increase in surface area is erratic and inconsistent and the per cent of pore volume filled by mercury at maximum pressure (1500 psi) varies from run to run for every sample. These variations may be explained partially by the change in effective pore volume when the sample is cut, due either to secluded pores being made available to mercury penetration or to the destruction of pores in the line of cut.

An apparatus was developed to measure the bulk volume of the sample in place in the dilatometer and thus make possible the ultimate determination of the porosity from total imbibed mercury at a pressure of 10,000 psi. This was accomplished by measuring the volume difference to fill the sample chamber with and without the sample. The accuracy of measurement on cylindrical aluminum plugs of known bulk volume was approximately ±0.1 per cent, whereas reservoir samples gave porosity values consistently higher by this method than by independent methods. The apparent increase in porosity was caused by void spaces formed between the sample and the walls of the sample chamber. The effect of such voids on the pressure-volume curves is as if the sample had pores with large radii. Too, the data taken on samples with various surface areas were undoubtedly affected by these and other voids between the sample pieces, to the extent that correlation between the increase in surface area and the increase in calculated permeability was impossible.

CONCLUSIONS

The invesigation of pore entry size distribution in naturally occurring reservoir rocks has involved the development of an apparatus for experimental measurements, the accumulation of pore entry size distribution data on samples taken from various formations, and the derivation of theoretical equations for applications and correlations of the data.

The apparatus is simple to operate, accurate, and reliable. For all practical purposes, the range of data is not limited by the equipment that may be built. For example, the pressure range is now being extended to 10,000 psig with no experimental difficulties anticipated. The operating procedure is straightforward and on a routine basis. The time required for a complete test, starting after preparation of the sample and ending with the calculation of the data and plotting of the curves, is from 3 to 4 hours.

The data obtained from the 100 samples on which this report is based, with the corresponding pressure - volume curves and distribution function curves, represent a cross-section of the type of information to be expected from pore entry size studies of reservoir rocks.

The investigation of the effect of weight, shape, and external surface area of the sample on the data has not been completed. Probably the external surface area effects observed thus far were caused mainly by the apparent pore volume between the sample pieces or between the sample pieces and the walls of the sample chamber. When the apparent pore volume has been eliminated, it is expected that the effect of the shape and external surface area on the measurements will be negligible.

Using the theoretical Equation (17) and the empirical Equation (18), permeabilities can be calculated from pore size distribution data within engineering accuracy, except for rare cases. These equations in conjunction with pore size distribution data are of prime importance in fundamental flow studies of porous media.

The data accumulated so far indicate that water capillary pressure curves may be determined from mercury capillary pressure data taken from small, irregularly shaped samples, with the pressure range greatly exceeding that possible by the porous diaphragm method.

Finally, work is continuing to accumulate more data, to refine the method, and to extend the range of application in the study of porous media.

SYMBOLS

The following definitions are applied to the symbols used in this report:

σ	Surface tension (dynes/cm)
θ	Contact angle (degrees)
R_i	Pore entry radius (cm or microns, $i = 1,2,3$ - - -
p	Pressure (cm-Hg, psi, dynes/cm^2)
$D(R_i)$	Distribution function (cm^2)
V	Volume (cc)
v_i	Incremental volume (fraction of total pore volume)

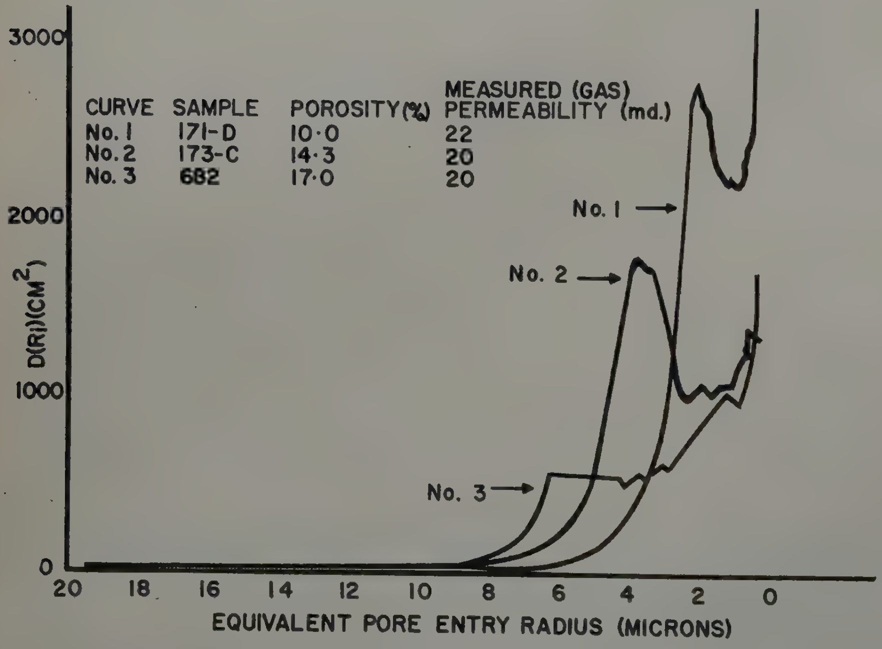

FIG. 11 — EQUIVALENT PORE ENTRY RADIUS VS. DISTRIBUTION FUNCTION.

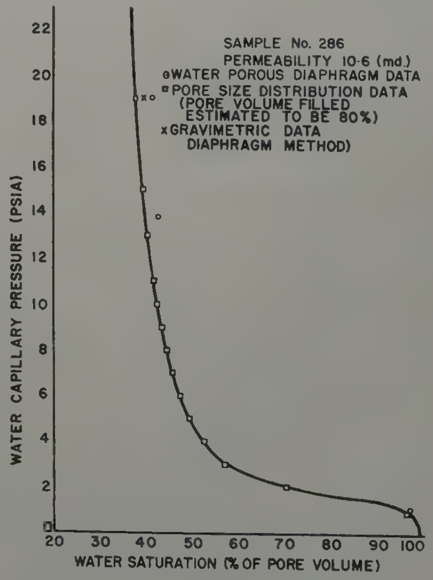

FIG. 12 — WATER CAPILLARY PRESSURE CURVE.

V_o	Total pore volume (cc)
$\overline{D(R_i)}$	Average distribution function (cm^2)
ΔR	Constant pore entry radii interval (cm)
Q	Rate of flow (cc/sec)
μ	Viscosity (poises, dyne-sec/cm^2)
L	Length of sample (cm)
n_i	Number of pores in the range ΔR
n	Number of terms included in sum
k	Permeability (darcys)
ϕ	Porosity (fractional)
C	Conversion constant (9.87×10^{-7} atmos/dynes/cm^2)
f	Dividing factor
L_i	"Effective" capillary length (cm)
x_i	Proportionality factor (ratio of L_i to L)
A	Area of cross-section of sample (cm^2)
k_g	Measured gas permeability (darcys)
v_p	pore volume (cc)
v_{Hg}	Total volume of pore space filled by mercury (cc)

REFERENCES

1. C. G. Shull: "The Determination of Pore Size Distribution from Gas Adsorption Data." *Jour. Amer. Chem. Soc.* 70, 1410, (1948).

2. W. R. Purcell: "Capillary Pressures—Their Measurement Using Mercury and the Calculation of Permeability Therefrom." *Petr. Tech.*, 1, 39, 1949. T.P. 2544.

3. L. C. Ritter and R. L. Drake: "Pore Size Distribution in Porous Materials." *Ind. Eng. Chem.*, An. Ed., 17, 782, (1945), and "Macropore-Size Distributions in Some Typical Porous Substances." Ibid 17, 787, (1945).

4. James H. Henderson: "The Effect of Surface Curvature on Surface Tension." Penn. State Doctoral Dissertation Series, M.S. degree 1947.

APPENDIX

The rate of flow of a fluid through a single capillary is according to Poiseuille's Equation

$$\frac{Q\mu}{\Delta p} = \frac{\pi R_i^4}{8L} \quad \ldots\ldots \quad (3)$$

The equivalent expression for the rate of flow of a fluid through an assemblage of parallel capillaries, each of the same length but having varying values of radius, is

$$\frac{Q\mu}{\Delta p} = \frac{\pi}{8L} \quad \underset{i}{\quad} n_i \, \overline{R_i^4} \rightarrow_{i+x} \quad \ldots\ldots \quad (4)$$

where

$$\overline{R_i^4} = \sum_{i}^{i+x} \frac{R_i^4 \rightarrow_{i+x}}{n}$$

and n_i is the number of pores in the range ΔR.

Now,

$$\phi = \frac{\pi}{A} \sum_{i} n_i \, \overline{R_i^2} \rightarrow_{i+x} \quad \ldots\ldots \quad (5)$$

where ϕ is the fractional porosity, A is the area of cross-section, and

$$\overline{R_i^2} = \sum_{i}^{i+x} \frac{R_i^2 \rightarrow_{i+x}}{n}$$

$$\therefore \frac{Q\mu}{\Delta p} = \frac{\pi}{8L} \sum_{i=o}^{n} \left[n_i \sum_{i}^{i+x} \frac{R_i^4}{n} \right] \quad \ldots \quad (6)$$

$$\phi = \frac{\pi}{A} \sum_{i=o}^{n} \left[n_i \sum_{i}^{i+x} \frac{R_i^2}{n} \right] \quad . \quad (7)$$

Instead of assuming that the capillaries have equal lengths consider each radii interval with an "effective" capillary length, L_i. Also, let

$$L_i = x_i L \quad \ldots\ldots \quad (8)$$

Then Equation (6) becomes

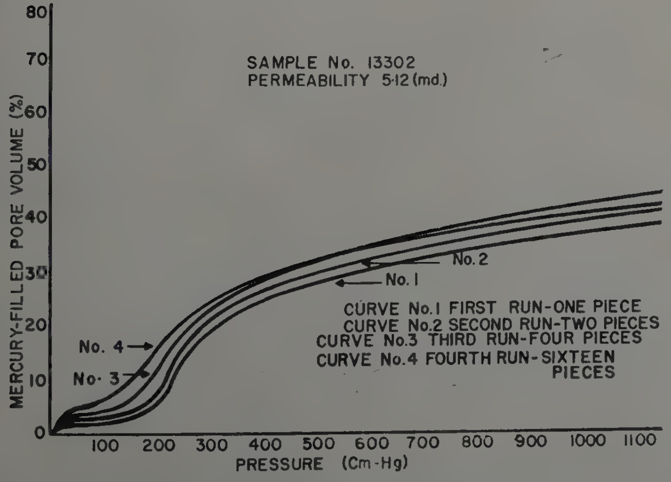

FIG. 13—MERCURY IMBIBITION CURVES; MERCURY-FILLED PORE VOLUME VS. PRESSURE.

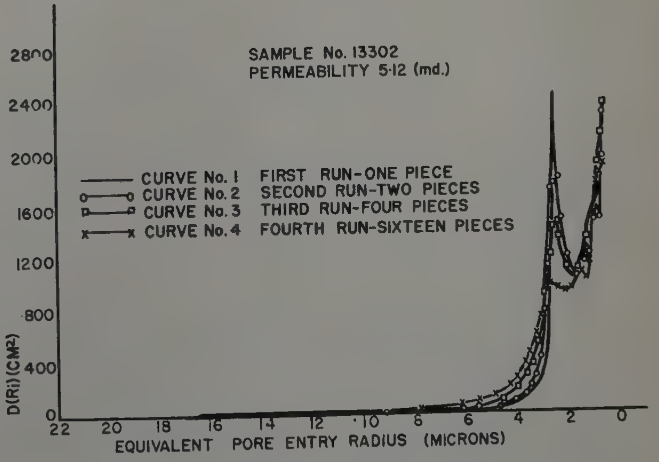

FIG. 14—EQUIVALENT PORE ENTRY RADIUS VS. DISTRIBUTION FUNCTION.

$$\frac{Q\mu}{\Delta p} = \frac{\pi}{8L}\sum_{i=o}^{n}\left[\frac{n_i}{x_i}\sum_{i}^{i+x}\frac{R_i^4}{n}\right] \quad . \quad (9)$$

Similarly,

$$\phi = \frac{\pi}{A}\sum_{i=o}^{n}\left[x_i n_i\sum_{i}^{i+x}\frac{R_i^2}{n}\right] \quad (10)$$

Also, the rate of flow through this same system is given by Darcy's Law:

$$\frac{Q\,\mu}{\Delta p} = \frac{CA}{100L}\cdot k \quad . \quad (11)$$

where k is the permeability in darcys. Combining Equations (9), (10), and (11) gives

$$k = \frac{100\,\phi}{8C}\;\frac{\sum_{i=o}^{n}\left[\frac{n_i}{x_i}\sum_{i}^{i+x}\frac{R_i^4}{n}\right]}{\sum_{i=o}^{n}\left[x_i n_i\sum_{i}^{i+x}\frac{R_i^2}{n}\right]} \quad . \quad . \quad (12)$$

By definition

$$v_i = \overline{D(R_i)}\cdot\Delta R = \pi x_i L\sum_{i}^{i+x}\frac{n_i R_i^2}{n} \quad . \quad . \quad . \quad . \quad (13)$$

where v_i is the fractional of total pore volume in the radii interval R_i to R_{i+x}.

$$\therefore\; n_i = \frac{\overline{D(R_i)}\;\Delta R}{\pi x_i L\sum_{i}^{i+x}\frac{R_i^2}{n}} \quad (14)$$

Substituting Equation (14) in (12),

$$k = \frac{100\,\phi}{8C}\;\frac{\sum_{i=o}^{n}\frac{\overline{D(R_i)}\;\overline{R_i^4}}{x_i^2\;\overline{R_i^2}}}{\sum_{i=o}^{n}\overline{D(R_i)}} \quad . \quad . \quad . \quad . \quad . \quad . \quad . \quad (15)$$

Also, from Equation (13)

$$n_i = \frac{v_i}{\pi x_i L\sum_{i}^{i+x}\frac{R_i^2}{n}} \quad . \quad (16)$$

Combining Equations (16) and (12)

$$k = \frac{100\,\phi}{8C}\sum_{i=o}^{n}\frac{v_i\,\overline{R_i^4}}{x_i^2\;\overline{R_i^2}} \quad (17)$$

★ ★ ★

THE SP LOG IN SHALY SANDS

H. G. DOLL, MEMBER AIME, SCHLUMBERGER WELL SURVEYING CORP., RIDGEFIELD, CONNECTICUT

ABSTRACT

As a continuation of the earlier paper on the general subject of the SP log, a more complete analysis of certain features of the SP log in shaly sands is given. The pseudo-static SP in front of shaly sands is compared, on a theoretical basis, to the static SP in front of clean sands, as a function of the respective amount of shale and sand in the formation, and of the relative resistivities of the shale, of the uncontaminated part of the sand, and of the invaded zone of the sand.

As a conclusion, the advantage of using reasonably conductive mud in this case is shown.

The discussion is illustrated by field examples.

INTRODUCTION

The discussion reported in the present paper is based on a theoretical analysis, and not on experiment. The field examples, joined to the text, are shown only as qualitative illustrations of the essential results of this analysis. Although the hypotheses made in the theoretical developments may perhaps be somewhat improved, it seems, nevertheless, that the results obtained account reasonably well for the actual phenomena, and give a fair approximation of their order of magnitude.

The paper contains a mathematical analysis of a tri-dimensional distribution of potentials and current lines, due to spontaneous electromotive forces arising at the contact of shales and free electrolytes, as a function of the geometry and of the respective resistivities of the different media involved. It is assumed, although this hypothesis is not proven, that the emf's remain the same even if the shale occurs in very thin layers or in dispersed particles.

It has already been pointed out[1,2,3] that, all other conditions being the same, the deflection of the SP log in front of a shaly sand is smaller than opposite a clean sand. When the thickness and the conductivity of a clean sand are large enough, the deflection of the SP log reaches a limiting value which is equal to the "static SP" of the clean sand. It is generally convenient to take the static SP of shale as the reference value or "base line." As a consequence, and for the sake of abbreviation, the expression, "static SP of a clean sand," is often used to designate the difference between the static SP of that sand and that of the shales, which difference is a measure of the total electromotive forces involved in the chain mud sand-shale.

A similar limiting value is also observed for the SP deflection opposite a thick shaly sand, but it is smaller, just as if the total electromotive force involved were smaller in that case. This limiting value has been called the "Pseudo-Static SP" of the shaly sand.

The static SP of a clean sand depends on the salinity of its connate water with respect to that of the mud, and, to a certain extent, on the differential pressure which controls the electro-filtration potentials, but it does not depend on the resistivity of the sand. On the contrary, the pseudo-static SP of a shaly sand depends not only on the salinity of its connate water and on the differential pressure, but also on the percentage of shale and on the resistivities of the shale, of the uncontaminated part of the sand, and of the zone invaded by the mud filtrate.

If the three resistivities above were equal, the pseudo-static SP would be proportional to the percentage of sand in the shaly sand, and its departure from the static SP of a clean sand having the same connate water would simply be proportional to the percentage of shale. In that case, the pseudo-static SP of a shaly sand containing 10 per cent of shale would be 10 per cent less than the static SP of a clean sand.

When, however, the sand is, on the average, substantially more resistive than the shale, the percentage of departure of the pseudo-static SP from the static SP of a clean sand is much larger than the percentage of shale. For that reason, the peaks of the SP log opposite shaly sands are systematically of smaller amplitude when the sands are oil-bearing than when they are water-bearing, all other conditions being the same. This feature is observed even when the sand beds are thick, and even when they do not contain a large percentage of shale.

All this has already been described in an earlier publication[3], but mostly in a qualitative way. The present paper will analyze in more detail the action of the local SP currents which are generated inside of the shaly sands, and which are responsible for the abnormally low value of the pseudo-static SP. The quantitative computations have been extended to the general case of thin interbedded layers of sand and shale, where the resistivities of the shale and sand streaks do not have the same value: they are summarized in charts giving values of the pseudo-static SP of a shaly sand as a function of the different parameters involved.

DEFINITIONS

The static SP of a clean sand has been defined as the potential that would exist in the mud opposite that sand, were the SP current prevented from flowing. Such an ideal condition is represented on Fig. 1-A.

By analogy, the pseudo-static SP of a shaly sand can be defined as the potential that would exist in the hole, if the circuit shaly sand — surrounding shales — mud column were interrupted by the insulating plugs placed at the boundaries

---

[1] References are given at end of the paper.

Manuscript received at the office of the Petroleum Branch October 18, 1949. Paper presented at the Petroleum Branch meeting October 20-21, 1949.

between the shaly sand and the surrounding shales, as represented in Fig. 1-B, in which it is assumed that the connate water in the invaded zone has been completely displaced by the mud filtrate, and that there are no electromotive forces between the mud column and the invaded zone in the sand layers. Under these conditions, the potential in the mud corresponds to the diagram represented in solid line, and the pseudo-static SP is, as defined, the average value of the potential opposite the shaly sand (i.e., disregarding the ripples, which, in fact, are negligible if the individual beds of sand and shale are thin enough).

It must be remarked that in Fig. 1-B, the insulating plugs interrupt only the circuit of the SP current which normally would flow into the shaly sand, from the shaly sand into the surrounding shales, and back from the surrounding shales through the mud column and the invaded zone. This SP current should be differentiated from local currents whose whole paths are small and remain inside of the shaly sand itself. The former will be referred to as the "external SP current" (dashed lines on Fig. 1-B), the latter as the "internal SP current" (solid lines on Fig. 1-B). Under normal conditions, i.e., in the absence of insulating plugs, the external SP current is free to flow and produces in the mud column, by ohmic effect, the potential differences which are recorded on the SP log (dashed diagram, Figs. 1-A and 1-B).

The internal SP currents represented on Fig. 1-B, and which flow from the invaded zone of each sand streak into its uncontaminated part, and back through the surrounding shale streaks, are generated in exactly the same way as the external SP currents, because of the existence of the electrolytic chain mud filtrate — connate water — shale. These internal currents produce potential differences by ohmic effect both in the shale streaks and in the sand streaks, and the respective values of these ohmic drops of potential, in the shale parts and in the sand parts of their circuit, determine the value of the pseudo-static SP, as explained later on.

QUANTITATIVE ANALYSIS OF THE PSEUDO-STATIC SP IN SHALY SANDS

The following assumptions will be made:

1. The shaly sands are thick and are constituted of alternating sequences of pure thin sands and pure thin shales.
2. In a given shaly sand, all the thin sand beds are identical and have the same thickness h, whereas all the thin shale beds are also identical and have the same thickness h', so that the average proportion of sand and shale is the same at all levels.
3. The individual thicknesses, h, of the sand beds, and, h', of the shale beds are both small in comparison with the diameter of the hole.
4. The depth of penetration of the mud filtrate into the individual sand beds is large in comparison with their thicknesses.
5. The effect of the electrofiltration potentials can be neglected* and there is no other electromotive force across the mud cake.

For reasons of convenience, the following cases will be considered in succession:

(a) Shaly sand with 50 per cent sand and 50 per cent shale, in which there is no diffusion between the mud filtrate and the connate water. This is an ideal case in which the thickness of the sand beds is supposed to be the same as that of the shale beds. Moreover, in the sands the zone which is invaded by the mud filtrate, and the uncontaminated zone, are both considered to be homogenous, and to make a sharp contact with each other.

(b) Shaly sand with 50 per cent sand and 50 per cent shale, with diffusion between mud filtrate and connate water, and with a continuous variation in the oil saturation throughout the invaded zone.

(c) Shaly sand in which the thickness of the sand beds is not the same as that of the shale beds, also with diffusion and a continuous variation of the oil saturation.

Shaly Sands with 50 Per Cent Shale, 50 Per Cent Sand and No Diffusion

This case is, of course, of a purely theoretical nature, but it is very useful to consider it as a first step in the analysis. Fig. 2 represents a very thick shaly sand of that category, and shows schematically the internal currents which flow in each sand bed from the invaded zone — supposed to be homogeneous — into the uncontaminated zone, and back

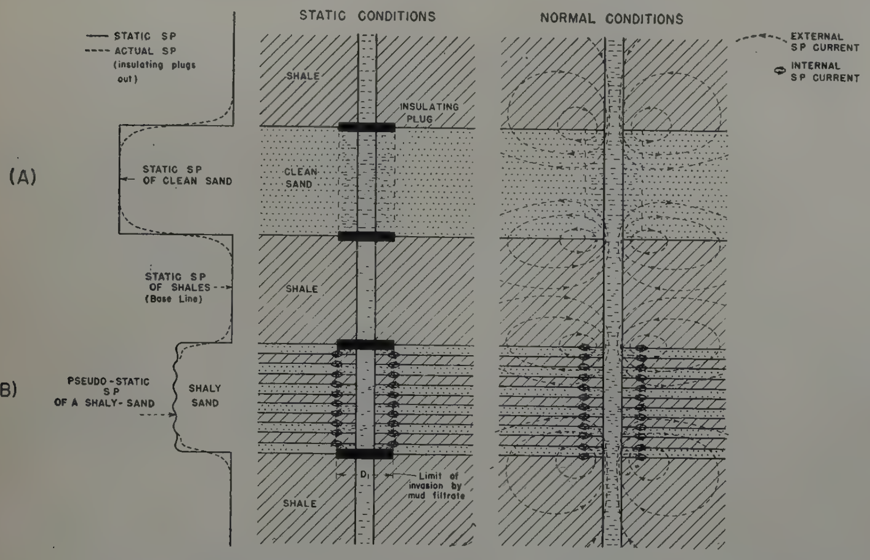

FIG. 1A — SCHEME OF STATIC AND NORMAL CONDITIONS, CLEAN SAND.
1B — SCHEME OF STATIC AND NORMAL CONDITIONS, SHALY SAND.

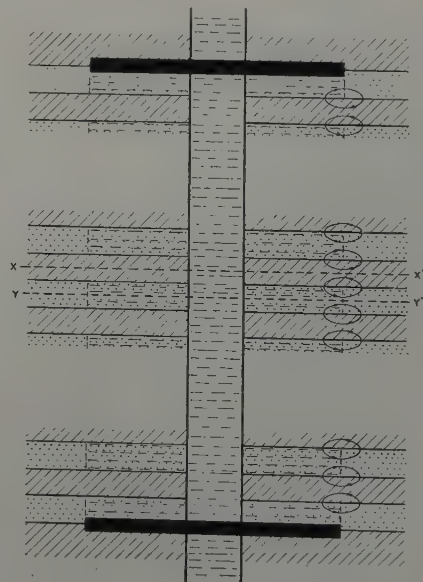

FIG. 2 — PSEUDO-STATIC CONDITION.

---

*This effect is analyzed in another paragraph at the end of the paper.

through the adjoining shale beds. By reason of symmetry, no line of current flow crosses the planes like XX' or YY' which divide any of the beds into equal parts. Nothing is changed, therefore, in the space between planes XX' and YY', from the point of view of the current and potential distribution, if all the surrounding formations are removed in order to isolate the two half beds. The case of the shaly sand represented in Fig. 2 can, therefore, be reduced to that of two adjoining beds, respectively of sand and shale, and both in contact with the mud, as represented in Fig. 3.

In Fig. 3-A it is assumed that an insulating plate is preventing the internal SP current from flowing. The potential is arbitrarily taken equal to zero at all points in the shale bed which are far enough from the mud column so that the SP current has no influence on their potential. In that case, the potentials in the different regions have the values indicated in rectangular frames in Fig. 3-A, namely:

Zero in the shale,
$V_o = +c$ in the mud opposite the shale,
$-b$ in the uncontaminated sand,
$-a -b = V_o - (a + b + c)$ in the mud opposite the sand, and in the invaded zone.

(This last expression has been placed in Fig. 3-A in a rectangle which covers both the mud and the invaded zone, because the potential is the same in these two regions, it being assumed that there is no electromotive force across the mud cake.)

In these expressions:

a is the boundary emf between mud filtrate and connate water,

b is the boundary emf between connate water and shale,

c is the boundary emf between shale and mud or mud filtrate.

When the insulating plate is removed, the internal SP current flows as schematically represented in Fig. 3-B, and produces potential drops by ohmic effect in the shale and in the sand. These potential drops have been designated by PD_{sh}, PD_i and PD_t respectively for the shale bed, the invaded zone, and the uncontaminated sand. The potential in the mud—that is the pseudo-static SP—can be computed by considering the ohmic drops and the boundary emf's encountered when following a path from the shale in the direction toward the hole, either along the shale bed or along the sand bed.

In the first case, the value obtained is expressed by:

$$-PD_{sh} + c$$

In the second case, the expression is:

$$-b + PD_t - a + PD_i$$

This second expression has also been placed in Fig. 3-B in a rectangle which covers both the mud and the invaded zone.

The two expressions above are identical with the assumptions made, because the total drop of potential along the path of the internal current i must be equal to the total electromotive force involved, or

$$PD_{sh} + PD_i + PD_t = a + b + c$$

so that:

$$-PD_{sh} + c = -b + PD_t - a + PD_i$$

Under the hypothesis made that the potential is zero at a great distance inside the shale, $+c$ represents the static SP of the shales, whereas $(-a -b)$ represents the static SP of clean sands, having the same connate water. The pseudo-static SP can, therefore, be written in either of two ways:

Pseudo-static SP = Static SP of shales $- PD_{sh}$

or

Pseudo-static SP = Static SP of clean sands $+ PD_i + PD_t$

A shaly sand can, therefore, be considered as a shale in which internal currents due to sand streaks create potential drops that make its pseudo-static SP more negative than that of a pure shale. It can also be considered as a sand in which internal currents due to the presence of shale streaks create potential drops that make its pseudo-static SP more positive than that of a clean sand. Both definitions are equivalent, and this illustrates once more the symmetrical character of the SP log with respect to sand and shales, and more generally, with respect to impervious and permeable beds.

It remains to evaluate quantitatively the values of PD_{sh}, or of PD_i and PD_t, as functions of the different resistivities of the three media.

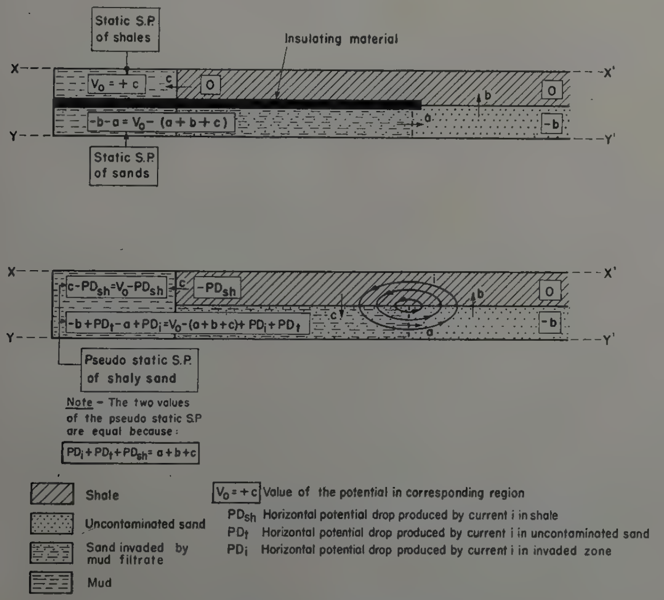
Static S.P. of shales
Insulating material
X
X'
Y
Y'
V₀ = + c
c
0
0
b
a
-b-a = V₀ - (a+b+c)
-b
Static S.P. of sands
c-PDsh=V₀-PDsh
-PDsh
0
i
b
c
-b+PDt-a+PDi=V₀-(a+b+c)+PDi+PDt
a
-b
Pseudo static S.P. of shaly sand
Note - The two values of the pseudo static S.P. are equal because:
PDi+PDt+PDsh= a+b+c
Shale
Uncontaminated sand
Sand invaded by mud filtrate
Mud
V₀ = + c Value of the potential in corresponding region
PDsh Horizontal potential drop produced by current i in shale
PDt Horizontal potential drop produced by current i in uncontaminated sand
PDi Horizontal potential drop produced by current i in invaded zone

FIG. 3A — THEORETICAL STATIC CONDITIONS.
3B — PSEUDO-STATIC CONDITIONS.

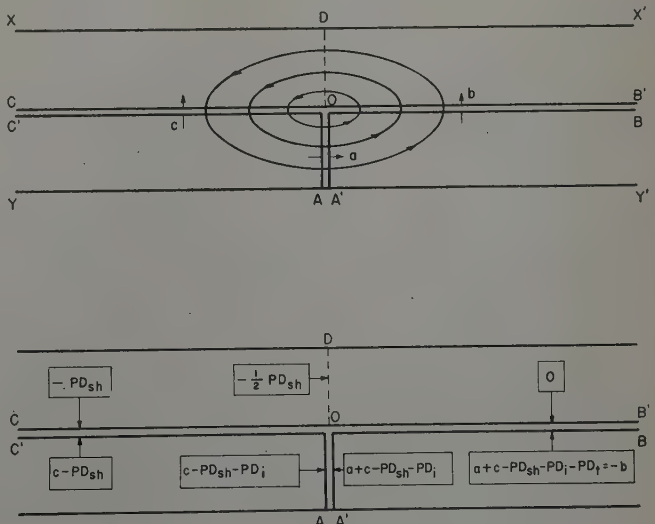

FIG. 4A — BOUNDRY EMF's AND LINES OF RESULTING CURRENT FLOW.

4B — POTENTIALS EXISTING IN THE SEPARATE ZONES.

Computation of PD_{sh}, PD_i and PD_t

When the depth of penetration of the mud filtrate in the sand streaks is large in comparison with their thickness, the internal SP current, which flows essentially in the vicinity of the boundary between the invaded zone and the uncontaminated zone, does not reach the mud column. On the other hand, that boundary can be likened to a plane, even though it actually is a cylinder, since its radius of curvature is large in comparison with the thickness of the individual layers of sand and shale. It is therefore sufficient to study the simplified case represented in Fig. 4-A and Fig. 4-B, where there are only three media separated by plane surfaces which are perpendicular to the plane of the figure, and to compute PD_{sh}, PD_i and PD_t for that case.

In Fig. 4-A, the boundaries between the different media have been represented by double lines to illustrate the fact that there is an electromotive force at each boundary and, therefore, a constant potential difference between the two sides of the same boundary.

In Fig. 4-B, the values of the potentials prevailing in the shale and in the sand, at great distances from the hole, near to the boundary of the invaded and uncontaminated zones, and close to the hole, have been placed in rectangular frames.

When the three resistivities R_{sh}, R_i and R_t are equal, the figure has two planes of symmetry *DOA* and *COB*. This same symmetry, therefore, applies to the lines of current flow which are represented in Fig. 4-A by solid lines with arrows. These lines of current flow across the boundaries, and also across the plane *DO*, perpendicularly. Either side of any boundary is, therefore, an equipotential surface, and there is a potential difference equal to the boundary emf between the two sides of that boundary.

By reason of symmetry, the resistance between the equipotential planes *OB'* and *OD* is equal to that between *OD* and *OC*, and to those respectively between *OC'* and *OA*, and between *OA'* and *OB*. If r is one of these resistances, i the intensity of the current, g a geometrical factor which is a function of the thickness of the individual layers, and R the common resistivity of the three media, one can write:

$$PD_{sh} = i \times 2r = i \times 2gR$$
$$PD_i = i \times r = i \times gR$$
$$PD_t = i \times r = i \times gR$$

If now the resistivities of the three homogeneous media are made different from each other, and respectively equal to R_{sh}, R_i and R_t, the lines of current are not changed, and the resistances in the different sectors respectively become gR_{sh}, gR_i and gR_t. The intensity of the current is changed, because of the change in the total resistance of the circuit. The shape of the equipotential surfaces, whether at the boundaries or elsewhere, remains unchanged, but the potential of each of these equipotential surfaces is changed. The new values of the potential drops in the three media are given by:

$$PD_{sh} = i \times 2gR_{sh}$$
$$PD_i = i \times gR_i$$
$$PD_t = i \times gR_t$$

and since the total potential drop must be equal to the total electromotive force along the circuit:

$$PD_{sh} + PD_i + PD_t = a + b + c = E$$

From the above relations, it is easy to deduce:

$$-PD_{sh} = -E \frac{2R_{sh}}{2R_{sh} + R_i + R_t} \quad . \; . \; . \; . \; . \; . \; . \; . \quad (1)$$

and

$$PD_i + PD_t = E \frac{R_i + R_t}{2R_{sh} + R_i + R_t} \quad . \; . \; . \; . \; . \; . \; . \quad (2)$$

which give respectively the pseudo-static SP with respect to the static SP of shales (base line), and the departure of the pseudo-static SP with respect to the static SP of a clean sand.

It is interesting to consider the ratio α of the pseudo-static SP of a shaly sand to the static SP of a clean sand with, of course, the same connate water. These two quantities are respectively equal to $-PD_{sh}$ (Eq. 1) and to $-E$, so that their ratio α is given by:

$$\alpha = \frac{\text{pseudo-static SP shaly sand}}{\text{static SP clean sand}} = \frac{1}{1 + \dfrac{R_i + R_t}{2R_{sh}}} \quad . \quad (3)$$

The coefficient α is called the "reduction factor."

Relation (3) applies only to the present case of a shaly sand with 50 per cent sand, 50 per cent shale and no diffusion in the invaded zone.

The exact distribution of the potentials and of the current lines, established through computations, is given in Fig. 5. This figure demonstrates that, at reasonable distances from the boundary between mud filtrate and uncontaminated sand, the potentials in the shale are on either side respectively equal to zero and $-PD_{sh}$.

Shaly Sand with 50 Per Cent Shale, 50 Per Cent Sand and with Diffusion in the Invaded Zone

This condition can be treated by assuming the diffusion occurs in steps, as represented in Fig. 6. If it is furthermore supposed that the diffusion takes place over a distance great in comparison with the individual thickness of each shale or sand bed, the invaded zone can be divided into a sequence of homogeneous sections with respective resistivities R_1, R_2, R_3, . . . , such that the length of each section, measured along the stratification, is much greater than its height, measured in the perpendicular direction. If $E_{1.2}$, $E_{2.3}$, $E_{3.4}$, . . . , are the total electromotive forces involved at each of the successive boun-

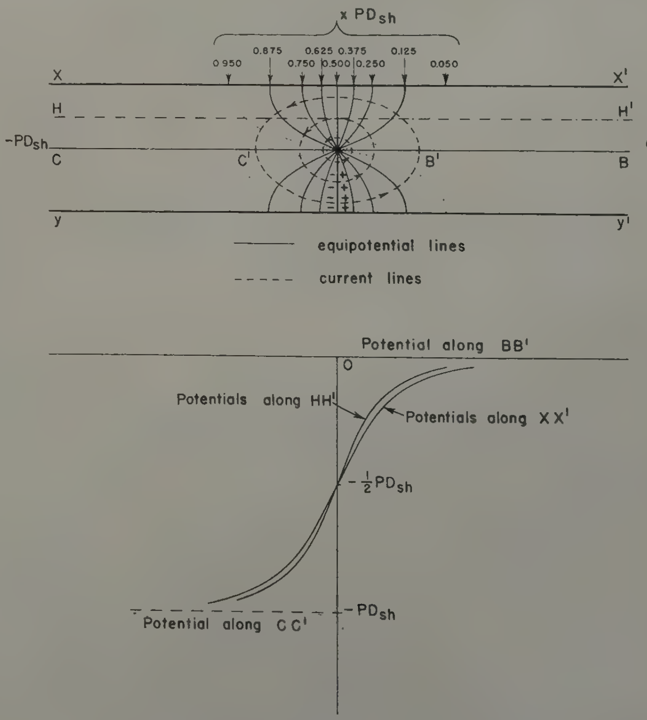

FIG. 5 — DISTRIBUTION OF EQUIPOTENTIALS AND CURRENT LINES (COMPUTED).

daries between these sections, the total potential drop along the shale is given by:

$$PD_{sh} = E_{1.2}\frac{1}{1+\frac{R_1+R_2}{2R_{sh}}} + E_{2.3}\frac{1}{1+\frac{R_2+R_3}{2R_{sh}}} + \ldots$$

It is convenient to replace this summation with an integral:

$$PD_{sh} = \int_l^L E(x)\frac{1}{1+\frac{R(x)}{R_{sh}}}dx \quad \ldots \ldots \quad (4)$$

in which:

$E(x)$ is the electromotive force per unit length along the shaly sand, prevalent at the radial distance x from the axis of the hole.

$R(x)$ is the resistivity of the invaded zone at the radial distance x.

l and L are the radial distances of the two limits of the invaded zone.

The value of $E(x)$ at any radial distance is proportional to the relative change of salinity per unit length at that radial distance. If $R_w(x)$ designates the resistivity of the water in the sand at the radial distance x, the value of $E(x)$ is given by:

$$E(x) = -K'\frac{\frac{dR_w(x)}{dx}}{R_w(x)} \quad \ldots\ldots\ldots\ldots \quad (5)$$

so that the general expression for PD_{sh} becomes:

$$PD_{sh} = -K'\int_l^L \frac{\frac{dR_w(x)}{dx}}{R_w(x)}\,\frac{1}{1+\frac{R(x)}{R_{sh}}}dx \quad \ldots\ldots \quad (6)$$

It is interesting to consider the case where the diffusion follows an exponential law, as would seem natural. In that case, one must have:

$$R_w(x) = R_{mf}\left(\frac{R_w}{R_{mf}}\right)^{\frac{x-l}{L-l}} \quad \ldots\ldots\ldots \quad (7)$$

where R_w and R_{mf} are the resistivities of the connate water and of the mud filtrate.

Relations (5) and (7) give:*

$$E(x) = -K'\frac{L_n\frac{R_w}{R_{mf}}}{L-l} = K\frac{\log\frac{R_{mf}}{R_w}}{L-l} \quad \ldots\ldots \quad (8)$$

The expression for PD_{sh} given by equation (6) then becomes:

$$PD_{sh} = \frac{K\log\frac{R_{mf}}{R_w}}{L-l}\int_l^L\frac{dx}{1+\frac{R(x)}{R_{sh}}} \quad \ldots\ldots \quad (9)$$

$(-PD_{sh})$ is the value of the pseudo-static SP, referred to the static SP of shales, and can be computed through equation (9) as a function of the different resistivities within the sand streaks. In particular, when the resistivity of the sand varies from a value R_i, at the beginning of the zone of diffusion radial distance l), to a value R_t at the end of that zone (radial distance L), and this according to an exponential law, $R(x)$ is given by the expression:

$$R(x) = R_i\left(\frac{R_t}{R_i}\right)^{\frac{x-l}{L-l}} \quad \ldots\ldots\ldots\ldots \quad (10)$$

and, after reduction, the expression for PD_{sh} becomes:

$$PD_{sh} = K\log_{10}\frac{R_{mf}}{R_w}\left(1-\frac{\log\frac{R_t+R_{sh}}{R_i+R_{sh}}}{\log\frac{R_t}{R_i}}\right) \quad \ldots \quad (11)$$

so that:

$$\alpha = \frac{\text{Pseudo-static SP of shaly sand}}{\text{Static SP of clean sand}} = 1-\frac{\log\frac{R_t+R_{sh}}{R_i+R_{sh}}}{\log\frac{R_t}{R_i}} \quad (12)$$

which, after transformation and with simplified notations, can be written:

$$\alpha = \frac{\log\frac{u+q}{1+q}}{\log u} \quad \ldots\ldots\ldots\ldots \quad (13)$$

where

$$u = \frac{R_t}{R_i} \qquad q = \frac{R_t}{R_{sh}}$$

This expression applies to a shaly sand with 50 per cent sand, 50 per cent shale, in which both the salinity and the resistivity in the invaded zone vary exponentially with the radial distance from the axis of the hole.

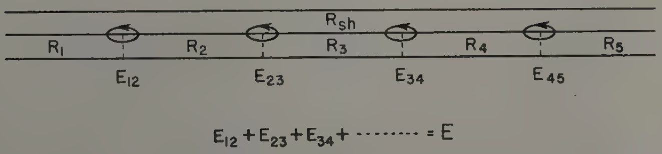

FIG. 6 — ILLUSTRATION OF CONCEPT OF DIFFUSION INCREMENTS.

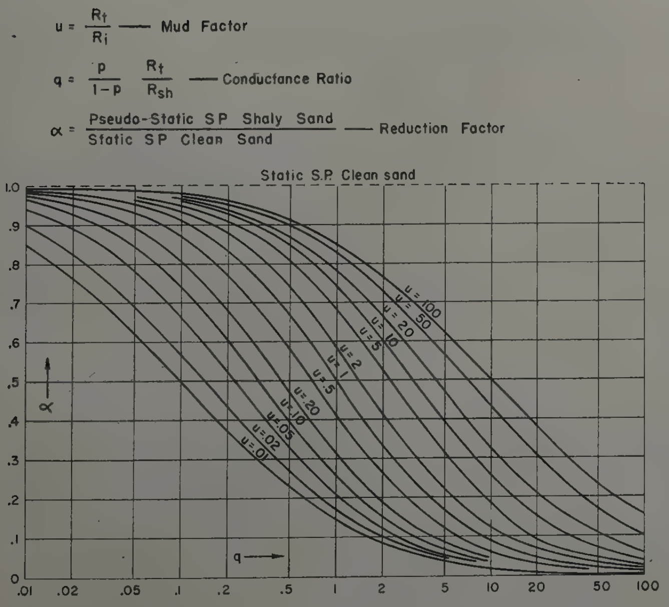

FIG. 7

---

*The present mathematical development implies that the electro-chemical SP is related to mud resistivity and connate water resistivity by an expression such as $SP = K\log_{10}\frac{R_{mf}}{R_w}$.

Shaly Sand in Which the Thickness of the Sand Beds is Not the Same as That of the Shale Beds

The formulae established in the previous section, for shaly sands having 50 per cent of shale and 50 per cent of sand, can be extended to the case where the proportion of sand and shale has any given value. Without going through the demonstration, and in order not to extend the discussion, it can simply be stated that the expressions 9, 11 and 12 above can be used to compute PD_{sh} and α in the general case, provided that R_{sh}, R_t, R_i be respectively replaced by $\frac{R_{sh}}{p}$, $\frac{R_t}{1-p}$ and $\frac{R_i}{1-p}$, p being the proportion of shale, and, consequently, $(1-p)$ the proportion of sand, in the shaly sand. With this change, expressions (9) and (13), for example, will read for the general case, after making obvious simplifications:

$$PD_{sh} = \frac{K \log \frac{R_{mf}}{R_w}}{L-l} \int_l^L \frac{dx}{1+\frac{p}{1-p}\frac{R(x)}{R_{sh}}} \quad . \; . \; . \quad (14)$$

and

$$\alpha = \frac{\text{Pseudo-static SP shaly sand}}{\text{Static SP clean sand}} = \frac{\log \frac{u+q}{1+q}}{\log u} \quad . \quad (15)$$

with

$$u = \frac{R_t}{R_i}$$

$$. \; . \; . \; . \; . \; . \; . \; . \quad (16)$$

$$q = \frac{p}{1-p}\frac{R_t}{R_{sh}}$$

p = proportion of shale in the shaly sand.

PRACTICAL APPLICATION — CHARTS

Expression (15) has been used to compute the chart of Fig. 7. This chart gives the pseudo-static SP of a shaly sand as compared to that of a clean sand having the same connate water. To use the chart, it is necessary to determine for each particular case the two quantities:

$$u = \frac{R_t}{R_i}$$

and

$$q = \frac{p}{1-p}\frac{R_t}{R_{sh}}$$

in which:

p is the proportion of shale,

R_t is the resistivity of the sand streaks in the uncontaminated zone,

R_i is the resistivity of the sand streaks in the invaded zone. immediately behind the mud cake,

R_{sh} is the resistivity of the shale streaks,

u represents the relative influence of R_i, which is a direct function of mud resistivity, which consequently, may be called the "mud factor,"

q represents the ratio of the respective contributions of the shale and sand streaks to the horizontal conductivity of the shaly sand in its uncontaminated zone. It may therefore be referred to as the "conductance ratio."

This chart applies to all cases where both the salinity and the resistivity in the sand streaks vary exponentially through the invaded zone. It can be demonstrated that the chart also applies to shaly sands that contain no oil, whatever the law of variation of salinity through the invaded zone, provided that the variation of salinity be continuous, i.e., without large changes occurring over radial distances which are small in comparison with the individual thickness of the individual layers of sand and shale.

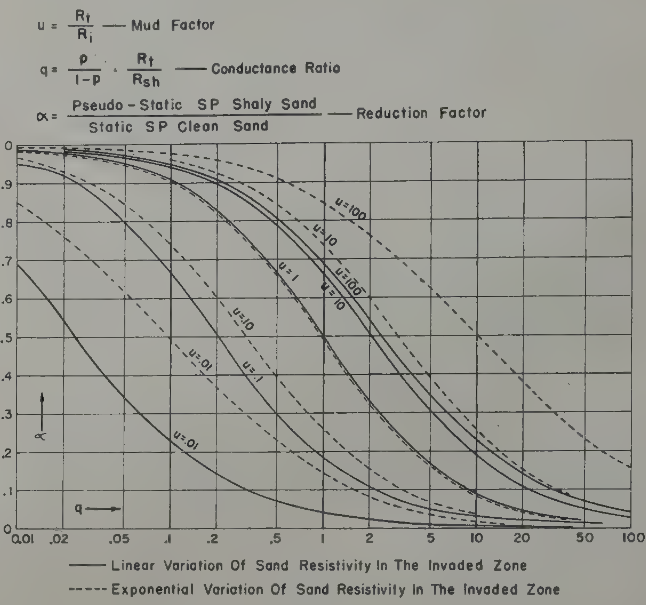

FIG. 8

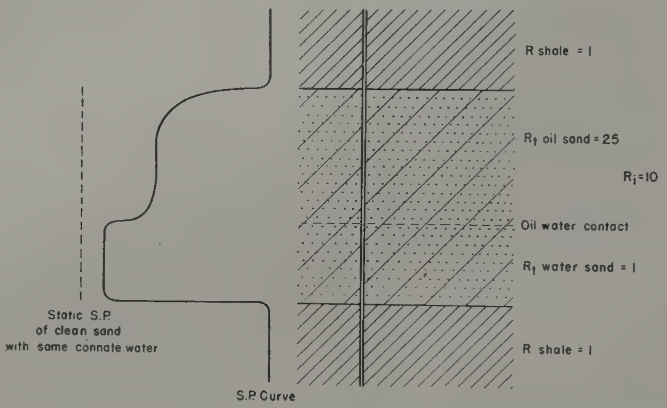

FIG. 9 — SHALY SAND WITH 4 PER CENT SHALE; OIL BEARING AT THE TOP AND WATER BEARING AT THE BOTTOM (COMPUTED CURVE).

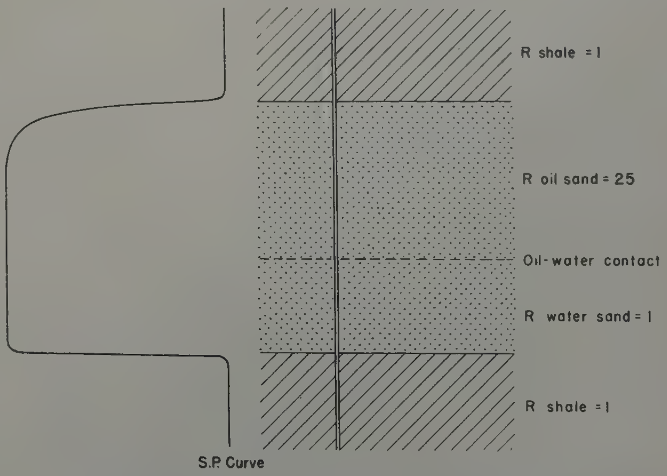

FIG. 10 — CLEAN SAND; OIL BEARING AT THE TOP AND WATER BEARING AT THE BOTTOM (COMPUTED CURVE).

In the case of an oil sand where the resistivity varies linearly instead of exponentially,* in the invaded zone, the value of α is smaller than that indicated on the chart. This is illustrated by Fig. 8, on which a few curves computed for the linear law are compared to the corresponding curves for the exponential law extracted from chart of Fig. 7.

Example: An oil-bearing shaly sand, with 20 per cent shale, is considered, where:

R_{sh} = 1 ohm-m — Resistivity of shale
R_t = 25 ohm-m — Resistivity of uncontaminated sand
R_w = .1 ohm-m — Resistivity of connate water
R_m = 2 ohm-m — Resistivity of mud
Formation factor = 10

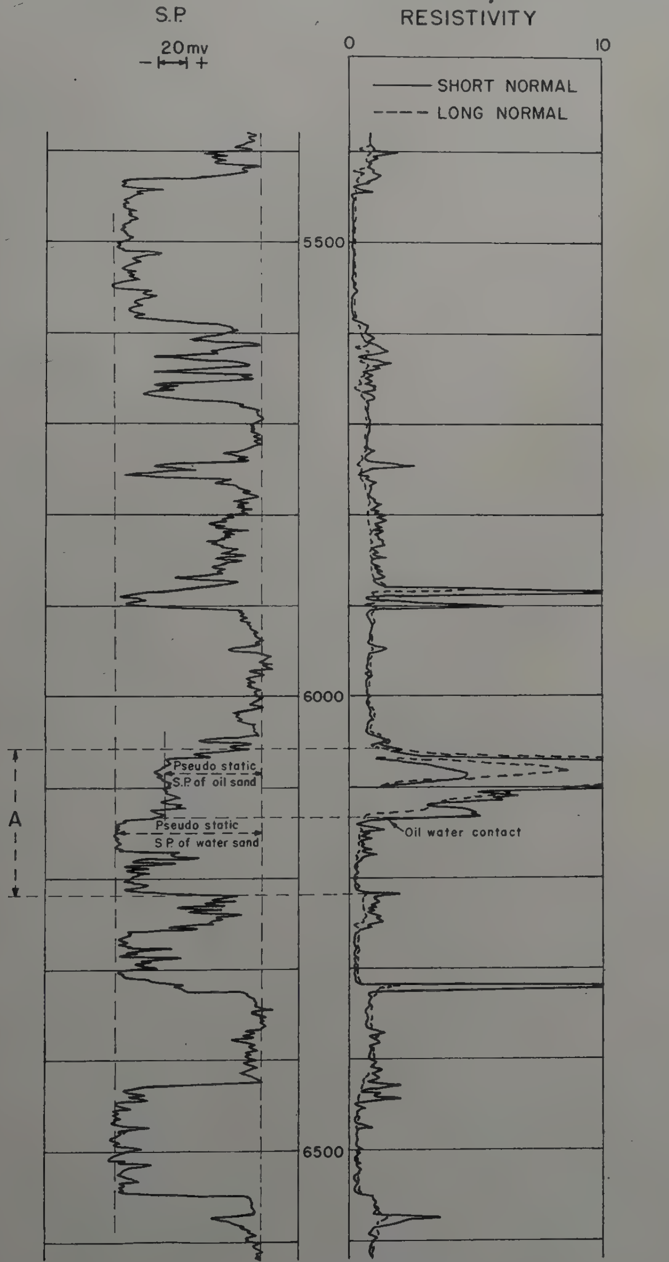

MUD RESISTIVITY
(Corrected for temperature) 0.9 ohm-meter

FIG. 11 — FIELD EXAMPLE OF SP LOG IN SHALY SAND.

Hence:
$u = 1.25$ — mud factor
$q = 6.2$ — conductance ratio
Chart of Fig. 7 gives:
$\alpha = .15$ — Reduction factor.

Pseudo-Static SP of Water Sands and Oil Sands

The pseudo-static SP of a shaly sand is of smaller magnitude if that sand is oil-bearing, than if it is water-bearing, because in the first case, R_t is much larger and affects the conductance ratio q accordingly. This is the reason why sands, which are seldom quite clean, frequently show less SP deflection opposite their oil-bearing section than opposite their water-bearing section. This is illustrated by Fig. 9 which represents a computed SP log for a thick, shaly sand, partly oil-bearing, partly water-bearing. It is interesting to compare this theoretical log with that of a clean sand, having otherwise exactly the same characteristics, namely the same connate water and the same saturation (Fig. 10).

It should be pointed out that the proportion of shale in a shaly sand is seldom constant throughout the whole bed. In particular, the percentage of shale generally decreases from the top and bottom boundaries towards the center of the bed. In the case of water-bearing sands, the pseudo-static SP is little different from the static SP of clean sands, and therefore is affected little by the variation of the shale content. On the contrary, the pseudo-static SP of oil-bearing sands is very sensitive to the proportion of shale. In practice, the shape of the SP curve, at the level of the boundaries of an oil-bearing bed, is therefore smoother for a shaly sand than for a clean sand, all other conditions being the same. Also, the SP curve generally does not involve a plateau opposite thick oil-bearing shaly sands, but more often shows fluctuations according to the variations of the pseudo-static SP, i.e., of the percentage of shale.

Field Examples

Fig. 11 is a practical example of SP log opposite a sequence of shales and shaly sands. For the sake of completeness, the resistivity curves, recorded with both the short and the long normal devices, have been reproduced on the figure. On this example, all the water-bearing sands of sufficient thickness show the same pseudo-static SP. Bed (A), is oil-bearing at the top, water-bearing at the bottom. The pseudo-static SP opposite the oil-bearing part is strikingly less than the pseudo-static SP of the water-bearing sands. Moreover, the shape of the average contour of the peak, opposite bed (A), is quite similar to that of the theoretical curve, Fig. 9.

Fig. 12 illustrates the case of a clean sand, and should be compared to Fig. 10.

Fig. 13 shows the logs obtained opposite the same shaly sand, in two different bore holes. In one hole, the sand is oil-bearing, and the pseudo-static SP is equal to 20 mv; in the other, the sand is water-bearing, and the pseudo-static SP is equal to 50 mv.

Computation of the Resistivity of the Connate Water from the Pseudo-Static SP of a Shaly Sand

It has been proposed[1,5,6] to compute the resistivity R_w — and, therefore, the salinity — of the connate water in a sand from the static SP by the formula:

$$E = K \log_{10} \frac{R_{mf}}{R_w} \qquad \qquad (17)$$

in which E is the absolute value of the static SP, corrected for the electrofiltration potential, if that quantity is not negligible, R_{mf} is the resistivity of the mud filtrate, and K is a coefficient theoretically equal to approximately 70 when E is expressed in millivolts (4). This relation can also be written:

---

*Of course, the law of variation of resistivity in the invaded zone is not exactly known, and has been here taken linear chiefly as a simple example.

$$\log R_w = \log R_{mf} - \frac{E}{K} \quad \ldots\ldots\ldots \quad (18)$$

In the case of a thick shaly sand, the pseudo-static SP, as determined from the log, is equal to αE, and instead of R_w, the formula gives a false value R_{wa}, such that:

$$\log R_{wa} = \log R_{mf} - \alpha\frac{E}{K} \quad \ldots\ldots\ldots \quad (19)$$

By combined relations (18) and (19), the following relation is obtained:

$$\log\frac{R_{wa}}{R_w} = (1-\alpha)\frac{E}{K} = (1-\alpha)\log\frac{R_{mf}}{R_w} \quad \ldots \quad (20)$$

which makes it possible to compute the relative error made in the computation of R_w if no correction is made to the pseudo-static SP taken from the SP log. The value of α in relation (20) can be taken from the chart of Fig. 7.

It is interesting to study how, for a given shaly sand, the relative error on R_w is influenced by the resistivity of the mud, as represented by that of the mud filtrate R_{mf}. Fig. 14 shows three computed curves corresponding to the same shaly sand, containing 5 per cent of shale. For each curve, all conditions are maintained constant, except the resistivity of the mud: the different curves correspond to different values of the oil saturation. In particular, it is assumed that for a given curve the distribution of the fluids in the sand beds is the same for all values of R_{mf}. It is interesting to see that the error is small provided that the resistivity of the mud is not too different from that of the connate water. However, when the resistivity of the mud is substantially larger than that of the connate water, and particularly when there is a large oil saturation, the error, as computed, becomes very large. Were it not for the fact that a sharp SP log is necessary for the detection of the permeable beds and for correlation purposes, there would be a definite advantage in using muds having a resistivity as near as possible to that of the connate water. It seems at least interesting to compromise by using muds that are resistive enough to give a decent SP log — for example, about five times as resistive as the average connate water — but not excessively resistive, lest the computation of connate water salinity from the SP become too erroneous.

Effect of the Use of Two Successive Muds of Different Salinities on the Pseudo-Static SP of a Shaly Sand

In the case of a clean sand, the static SP depends almost entirely on the ratio between the resistivity of the last mud used and the resistivity of the connate water. It can be demonstrated that this is also the case for a shaly sand if it is one hundred per cent water-bearing, because, in that case, the resistivity of the sand varies proportionally with the resistivity of its impregnating water.

In the case of an oil-bearing shaly sand that has been penetrated successfully by two different muds, the resistivity of the sand streaks varies through the invaded zone, not only because the salinity of the water varies continuously, but also because the oil saturation increases progressively toward the uncontaminated zone.

A computation using the relation given earlier in this paper shows that the pseudo-static SP in such an oil-bearing shaly sand depends not only on the resistivities of the last mud and of the connate water, but also on the resistivity of the water in the intermediate zone. This result is illustrated by the numerical application of Fig. 15, which represents the variations of the pseudo-static SP of a shaly sand as a function of the resistivity half-way between the limits of the invaded zone, all other conditions remaining the same. The figure shows also the pseudo-static SP that would have existed for that same shaly sand, if it had been entirely water-bearing, and if it had the same salinity of connate water: in this case, the pseudo-static SP is independent of the variations of salinity through the invaded zone, provided that they are continuous.

It is interesting to note that, according to the above theory, the use of a first mud, more conductive than the connate water, improves the pseudo-static SP of an oil-bearing shaly sand as finally measured with a fresh mud, and brings it nearer to the static SP of a clean sand.

Shaly Sand in Which the Clay Material is Disseminated in the Sand

The clay material is frequently disseminated in the sand, as a coating around the sand grains. In that case, the thin network of clay is everywhere side by side with the network

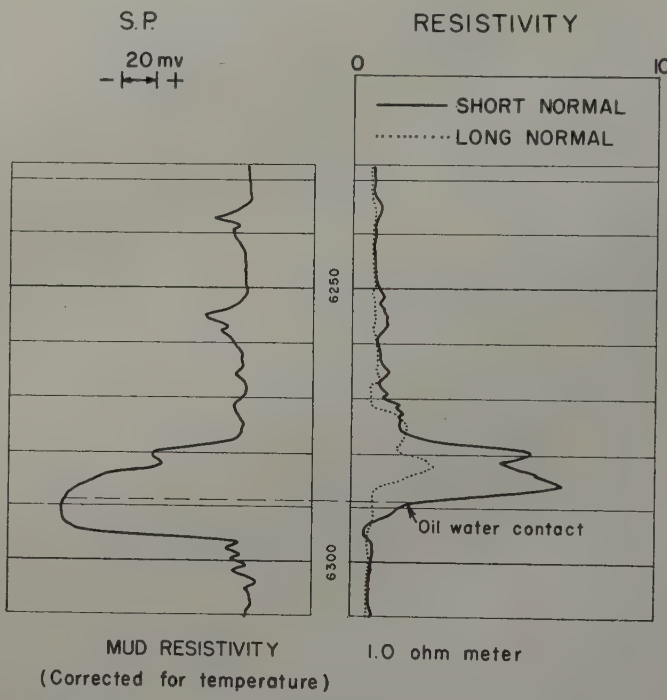

FIG. 12 — FIELD EXAMPLE OF SP LOG IN CLEAN SAND.

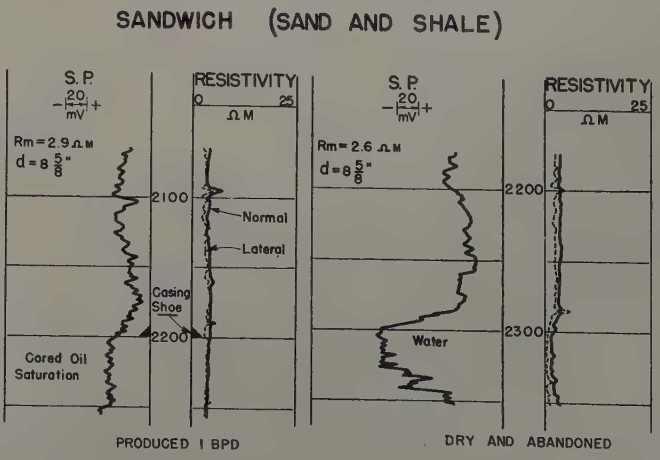

FIG. 13 — A PENNSYLVANIAN SAND IN HEWITT AREA, SOUTHERN OKLAHOMA.

of capillary water. This case is equivalent to that of alternate thin layers of sand and shale, except that the alternate layers have become of microscopic thickness. The conclusions arrived at for alternate thin layers remain valid, but should be considered only in a qualitative way.

The case where clay is present in the sand, in the form of clay grains isolated from each other, can also be considered. Such an occurrence may result from the transformation of feldspar grains that were originally deposited with the sand. In that type of shaly sand, the clay grains that are surrounded by a homogeneous electrolyte, as is the case in the uncontaminated zone, for example, are electrically in equilibrium, and therefore inert. On the contrary, the clay grains which are in the diffusion zone, where the salinity varies continuously with the radial distance from the hole, form with the heterogeneous electrolyte that surrounds them as many small cells, each of which produces only a very small amount of current. All these small currents flow from the clay grains into the electrolyte on the side where the salinity is minimum, flow around the clay grains, and back into them from the side where the salinity is maximum. Since the salinity gradient is always radial, with respect to the hole, and in the same direction, all the small potential drops produced in the ground by the small SP currents around the clay grains add their effect to build up a potential difference across the invaded zone.

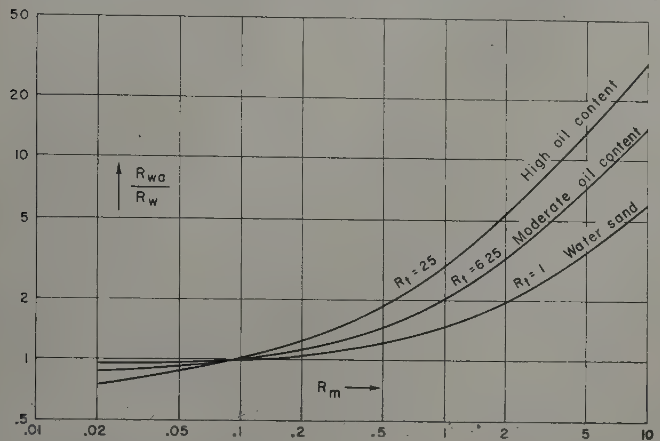

Numerical characteristics
for the computation:
5 % Shale
R_{sh} Shale = 1 ohm - meter
Formation factor of the sand : 10
R_w Connate Water = 0.1

FIG. 14 — RELATIVE VALUE $\frac{R_{wa}}{R_w}$ OF THE APPARENT CONNATE-WATER RESISTIVITY IF COMPUTED FROM THE DATA OF THE SP CURVE OPPOSITE A SHALY SAND, AS A FUNCTION OF THE MUD RESISTIVITIES.

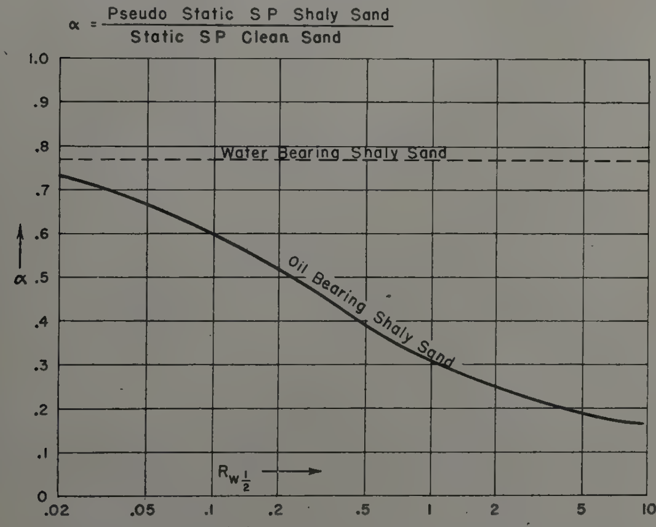

Numerical characteristics
for the computation:
Formation factor of sand : 10
R_{sh} Shale = 2 ohm - meter
R_t Oil Sand = 25
R_t Water Sand = 1
R_m Mud = 2
R_w Connate Water = 0.1
10 % Shale

$R_{w\frac{1}{2}}$: Resistivity of water midway from the limits of the invaded zone

FIG. 15 — PSEUDO-STATIC SP OF A SHALY SAND PENETRATED BY TWO SUCCESSIVE MUDS OF DIFFERENT RESISTIVITIES.

If both the resistivity of the shaly sand, and that of its impregnating water, vary throughout the invaded zone according to an exponential law with respect to the radial distance, the SP reduction coefficient for the case of disseminated clay grains, can be expressed approximately by:

$$\alpha = 1 - 3p\frac{\log\dfrac{2R_{sh}+R_t}{2R_{sh}+R_i}}{\log\dfrac{R_t}{R_i}} \qquad . \ . \ . \ . \ . \ . \ . \ . \ (21)$$

with as usual:

$$\alpha = \frac{\text{pseudo-static SP of shaly sand}}{\text{static SP of clean sand}}$$

This expression has been established by a mathematical reasoning which involves a certain measure of approximation. It should be considered only as rough approach to the value of α when the percentage p of clay by volume is small (less than 5 per cent), and it becomes otherwise quite erroneous.

In the general case where shales are present in the sand bed, both as continuous layers and as disseminated grains, an approximate value for α can be roughly determined from the charts of Fig. 7 and 8, by taking p equal to the total percentage of shale, either stratified or granular.

Effect of the Electrofiltration EMF's

The electrofiltration emf's are due to the differential pressure between the mud column and the sand beds: they are located across the mud cake, as represented in Fig. 16.

If the mud cake is very thin, and if the thicknesses of the individual beds of sand and shale are small in comparison with the radius of the hole, the contribution of the electrofiltration phenomenon to the pseudo-static SP can be established in a way very similar to that used for the case of the electrochemical emf's. In this case, the potential drop, PD_f, which measures the pseudo-static SP due to electrofiltration, occurs partly in the mud and partly in the shale beds, and it is given approximately by the formula:

$$PD_f = E_f\frac{1}{1+\dfrac{p}{1-p}\dfrac{R_m+R_i}{R_m+R_{sh}}} \qquad . \ . \ . \ . \ . \ . \ (22)$$

where:

E_f = electrofiltration emf,
p = proportion of interbedded shale,
R_m = resistivity of the mud,
R_i = resistivity of the invaded zone in the sand streaks immediately behind the mud cake,
R_{sh} = resistivity of the shale.

The expressions (4), (9) and (14), given in the earlier part of this paper, are valid only when the depth of invasion of mud filtrate is very great, at least in comparison with the individual thickness of each bed. In the case of moderate invasion, the pseudo-static SP would have a value intermediate between those derived from these equations and equation 22.

It is interesting to notice that, in the ideal case where no invasion is present, the pseudo-static SP involving both electrochemical and electrofiltration emf's, would be given by the same expression, where E_f would be replaced by the total electromotive force.

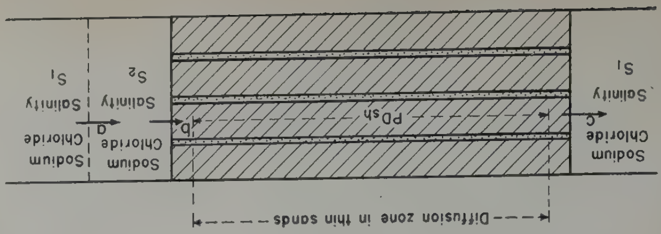
Sodium Chloride Salinity S_1
Sodium Chloride Salinity S_2
a
b
PD_{sh}
c
Sodium Chloride Salinity S_1
Diffusion zone in thin sands

FIG. 16 — EFFECT OF THE ELECTROFILTRATION EMF.

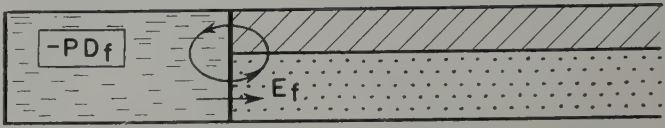

FIG. 17 — SODIUM CHLORIDE CHAIN CONTAINING SHALE BRIDGE WITH VERY THIN LONGITUDINAL SAND STREAKS.

Variation of the *K* Coefficient of Shale Samples When Measured with Solutions of High Salinities

The behavior of certain shales, which do not show the same *K* coefficient when placed between concentrated solutions of sodium chloride as when placed between dilute solutions, might be explained by considering these shales as being in fact shaly sands with a very large proportion of shale, and only a few very thin permeable streaks. This is illustrated schematically in Fig. 17 which represents such a type of shale placed in a sodium chloride chain.

Using the usual notations *a*, *b* and *c* for the emf's at the different boundaries, and designating by PD_{sh} the potential drop produced horizontally in the core by the internal SP current due to the salinity change along the thin permeable streaks, one obtains for the apparent total emf E_a measured between the two extreme solutions:

$$E_a = a - b - PD_{sh} + c = (a + b + c) - PD_{sh}$$

When the salinities S_1 and S_2 are low, the resistivity of the permeable streaks, as impregnated by either of the two solutions, or their mixture, is high. Since, in addition, the permeable streaks are much thinner than the adjoining shale streaks, the conditions are those of a shaly sand for which the conductance ratio:

$$q = \frac{p}{1-p}\frac{R_t}{R_{sh}}$$

is very high. In that case, and according to relation (15) or the chart of Fig. 7, PD_{sh} is very small, and, therefore, E_a is equal to E and satisfies the formula:

$$E = K \log \frac{S_1}{S_2}$$

When, however, the salinities S_1 and S_2 are high, the resistivity of the permeable streaks becomes low and the conductance ratio q falls down to a level where PD_{sh} is no longer negligible. The apparent emf E_a, as measured, should, therefore, be less than that indicated by the above relation.

There might be other reasons, for example of electro-chemical nature, for the abnormal value of the emf given by certain shales with concentrated solutions, and the above reasoning should be considered only as a suggestion toward a reasonable and simple explanation which needs to be checked by laboratory measurements.

CONCLUSION

The problem of shaly sands has been approached from a purely theoretical point of view in order to analyze the respective influence of the different parameters involved on the value of the pseudo-static SP of these shaly sands, as compared to the static SP of clean sands under similar conditions.

The conditions asumed may well have been oversimplified, but the theory, as it is, seems sufficient to explain most of the facts that have been observed in practice. This does not mean that other phenomena are not involved, and a careful check of data from electric logs and core analyses in favorable cases will determine to what extent the computed formulae can be considered better than a qualitative approximation. Two of the essential conclusions should remain, at least qualitatively. One is that the pseudo-static SP of a shaly sand is not only a function of the shale content but is also influenced, to a very large extent, by the relative resistivities of the sand and shale, so that the corresponding SP deflection decreases in a large measure when oil saturation increases. The other is that, if the salinity of the connate water is to be computed from the amplitude of the SP, it is essential not to use muds that are a great deal more resistive than the connate water.

The charts and formulae established by computations, which are shown in this paper, obviously could be used to determine certain parameters involved if the other parameters are known. It seems reasonable, therefore, to assume that the above analysis could lend itself to quantitative approximations of certain characteristics of shaly sands. Such an application seems, however, premature, at least until field experiments have determined the practical value of the theoretical deductions.

In any case, it is hoped that the discussion will prove useful as a help toward a better understanding of the SP phenomena in the case of shaly sand, and that it will encourage further studies of the problem.

ACKNOWLEDGMENT

The author wishes to acknowledge the efficient cooperation of M. Martin and A. Poupon in the preparation of the final draft and in the computation of the theoretical examples given in the paper. He also wishes to express his appreciation to the oil companies for their courtesy in making examples available.

REFERENCES

1. Park A. Dickey: "Natural Potentials in Sedimentary Rocks," *Transactions* AIME, Petroleum Branch, 1944, Vol. **155**, p. 37.
2. W. D. Mounce and W. M. Rust, Jr.: "Natural Potentials in Well Logging." *Transactions* AIME, 1944, Vol. **155**, p. 47.
3. H. G. Doll: "The SP Log: Theoretical Analysis and Principles of Interpretation." *Journal of Petroleum Technology*, Vol. 11, September, 1948, or *Transactions* AIME, Petroleum Branch, Vol. **179**, p. 146.
4. M. R. J. Wyllie: "A Quantitative Analysis of the Electrochemical Component of the SP Curve." *Journal of Petroleum Technology*, Vol. 1, No. 1, January, 1949, p. 17 ff.
5. M. R. J. Wyllie: "A Statistical Study of the Accuracy of Some Connate Water Resistivity Determinations Made from SP Log Data." AAPG Meeting, St. Louis, March, 1949.
6. M. P. Tixier: "Electric Log Analysis in the Rocky Mountains." *Oil and Gas Journal*, Vol. 48, No. 7, June 23, 1949, p. 143 ff.

★ ★ ★

LIQUID-LIQUID DISPLACEMENT IN POROUS MEDIA AS AFFECTED BY THE LIQUID-LIQUID VISCOSITY RATIO AND LIQUID-LIQUID MISCIBILITY

J. P. EVERETT, MEMBER AIME, OKLAHOMA A&M COLLEGE, STILLWATER, OKLAHOMA, **F. W. GOOCH, JR.,** U. S. NAVY, AND **JOHN C. CALHOUN, JR.,** MEMBER AIME, UNIVERSITY OF OKLAHOMA, NORMAN, OKLAHOMA

SUMMARY

The results of two sets of displacement experiments are reported. In the first set of experiments various solutions of sugar in water were displaced by other solutions of sugar in water. In the second set oils were displaced by water. Each set of experiments was performed on a linear system made of cemented silica sand grains.

These displacement tests were made to evaluate the behavior when the ratio of fluid viscosities between the displacing and displaced phases was varied. A further consequence of the test results is a comparison between displacement behavior when the displaced and displacing phases are miscible as with sugar solutions and when they are immiscible as with oil and water.

INTRODUCTION

Buckley and Leverett[1] have presented a theory for the displacement of oil by gas or water based upon the relative permeability concept. This theory presents the displacement of oil as occurring in two phases, an initial or primary phase preceding the breakthrough of the displacing phase and a subordinate or secondary phase during which both oil and the displacing phase flow simultaneously through the same porous section. These authors gave the results of calculations to show that the percentage of oil displaced during the primary phase by water drive would be dependent upon the ratio of the viscosity of the oil to that of the water. No experimental evidence was reported by these authors to substantiate their theory. Qualitatively, however, it has been found to be in agreement with many observed field results.

Laboratory investigators have been in general agreement in reporting for air or gas drive[2,3] a small primary phase of production and a large secondary phase. Reported investigations on water drive[3,4,5] have shown instances where both primary

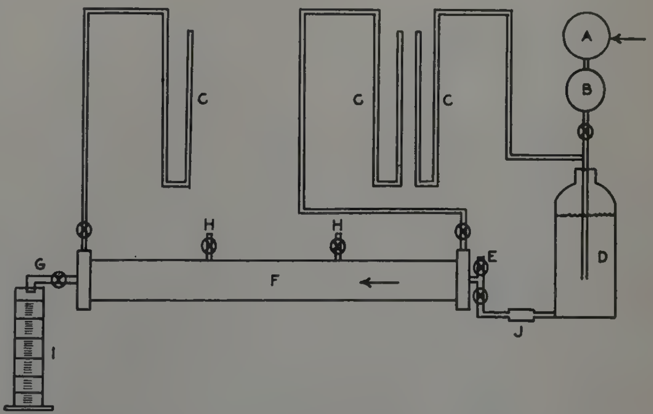

FIG. 1 — SCHEMATIC FLOW ARRANGEMENT FOR DISPLACEMENT OF SUGAR SOLUTIONS BY WATER. A, B — PRESSURE REGULATOR; C — MERCURY MANOMETERS; D — GLASS FLUID RESERVOIR; E — VALVE FOR CLEANING FLUID SYSTEM; F — POROUS SECTION OF SAND; G — OUTLET CONTROL VALVE; H — PRESSURE CONNECTIONS; I — GRADUATED CYLINDER; J — FILTER.

---

[1] References are given at the end of the paper.

Manuscript received at the office of the Petroleum Branch October 1, 1949. Paper presented at the Petroleum Branch meeting in San Antonio, October 5-7, 1949.

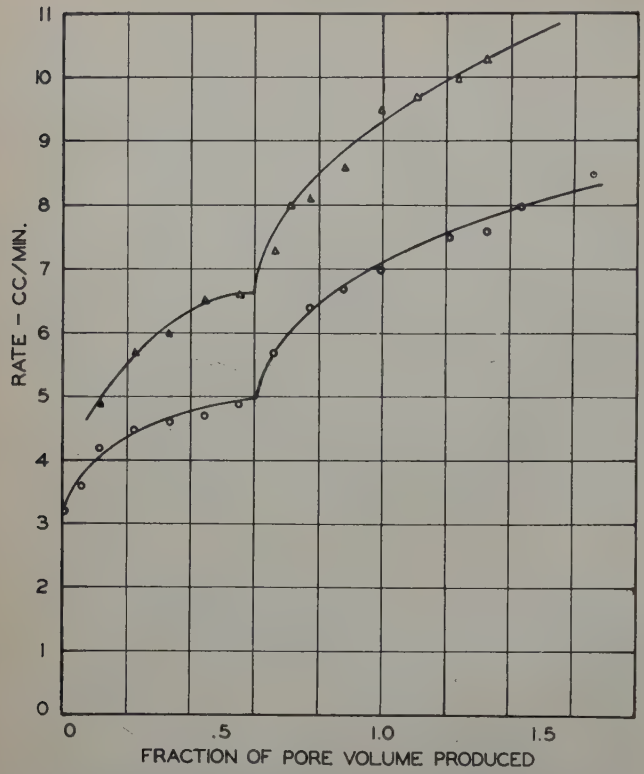

FIG. 2 — INCREASE OF PRODUCTION RATES DURING DISPLACEMENT. VISCOSITY RATIO (DISPLACED OVER DISPLACING FLUID) IS 4.25; PRESSURE IMPOSED IS 220 mmHg. △ HORIZONTAL RUN. ⊙ VERTICAL RUN DOWNWARD.

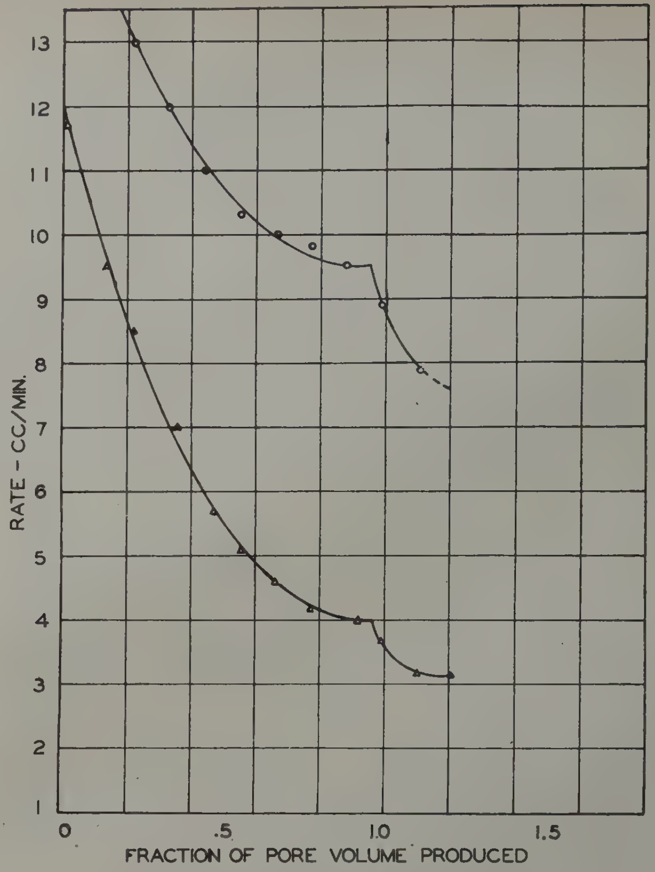

FIG. 3 — DECREASE OF PRODUCTION RATES DURING DISPLACEMENT. △ — VISCOSITY RATIO (DISPLACED OVER DISPLACING FLUID) IS 0.235; PRESSURE IMPOSED IS 220 mmHg. VERTICAL RUN UPWARD. O — VISCOSITY RATIO (DISPLACED OVER DISPLACING FLUID) IS 0.874; PRESSURE IMPOSED IS 220 mmHg. HORIZONTAL RUN.

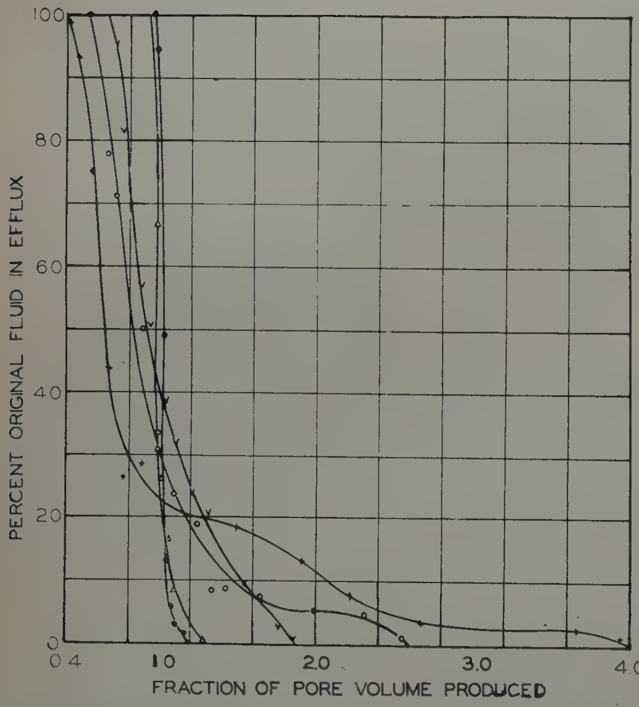

FIG. 4 — EFFLUX COMPOSITIONS VERSUS CUMULATIVE IN PORE VOLUMES (HORIZONTAL RUNS). VISCOSITY RATIO (DISPLACED OVER DISPLACING FLUID) X = 9.1; O = 4.25; V = 2.34; △ = 1.14; ⊙ = 0.437.

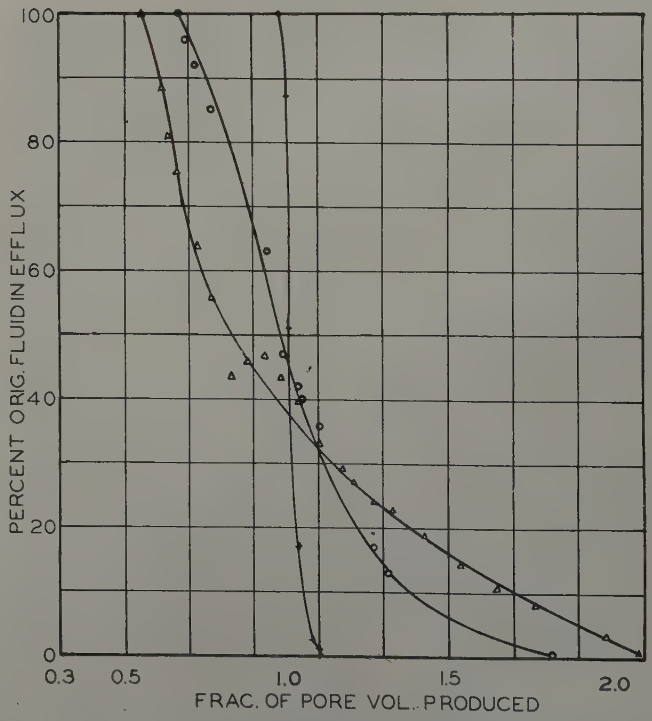

FIG. 5 — EFFLUX COMPOSITION VERSUS CUMULATIVE IN PORE VOLUMES (VERTICAL RUNS). VISCOSITY RATIO (DISPLACED OVER DISPLACING FLUID) △ = 4.25; 0 = 2.29; X = 0.235.

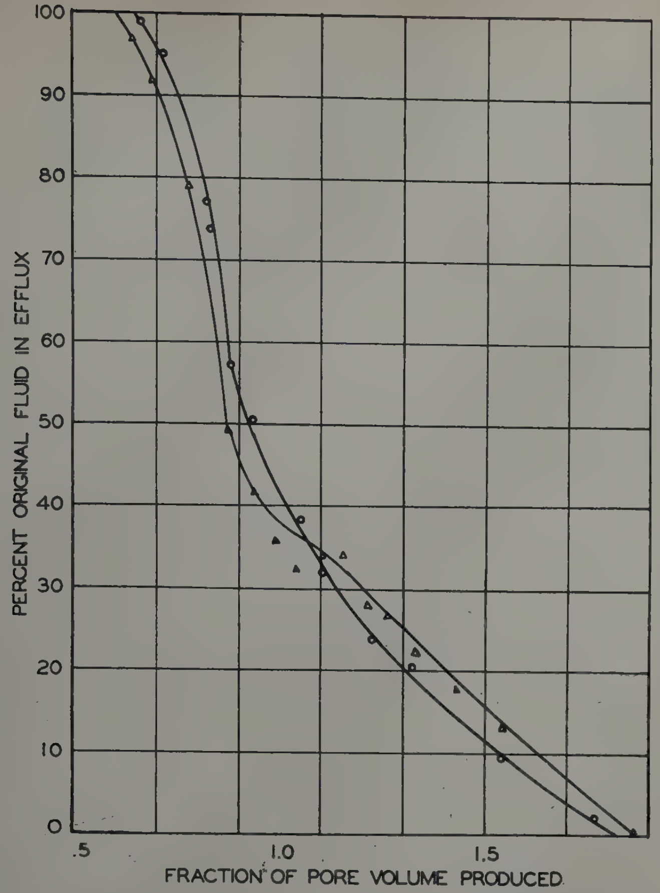

FIG. 6 — DISPLACEMENT AT TWO PRESSURE GRADIENTS (HORIZONTAL RUNS) VISCOSITY RATIO (DISPLACED OVER DISPLACING FLUID) IS 2.35. ○ = IMPOSED PRESSURE IS 220 mmHg. △ = IMPOSED PRESSURE IS 760 mmHg.

and subordinate phases were important, with the former in general being more significant.

Other investigators have presented data on other types of displacement. Data on the mobility of connate water was presented[6] with the conclusion that displacement efficiency would be high. One of the present authors in a former work[4] noted but did not report comprehensive data on the removal of connate water by a fresh water drive. These data also supported the belief that connate water would be displaced effectively from a porous material by invading water.

Huntington and others[7,8] have given data on the displacement of one gas by another and on the displacement of carbon tetrachloride by hexane from a column of unconsolidated sand. These experiments indicated the occurrence of displacement in primary and secondary phases, even for the displacement of one gas by another. Their data is presented in terms of mixing rather than in terms of displacement efficiency. The data reported for hexane-carbon tetrachloride displacement indicated a variation in displacement efficiency during the primary phase as the speed of displacement varied. For gas-gas displacement these investigators found a variation in efficiency with the pressure of the gas system.

The literature also contains reference to displacement in ideal capillary systems and in pipe lines,[9] which situations may not be directly applicable to petroleum production but they nevertheless provide a basis for analyzing results of displacement from porous media.

The present work was undertaken in an effort to supply data which it was hoped might be added to that cited to form support for a comprehensive displacement theory. In particular, it was felt that Buckley and Leverett's[1] analysis pointed to the viscosity ratio between displaced and displacing fluids as an important variable. A perusal of other cited references led to the thought that the displacement from a porous medium of one fluid by another miscible with it would be in many

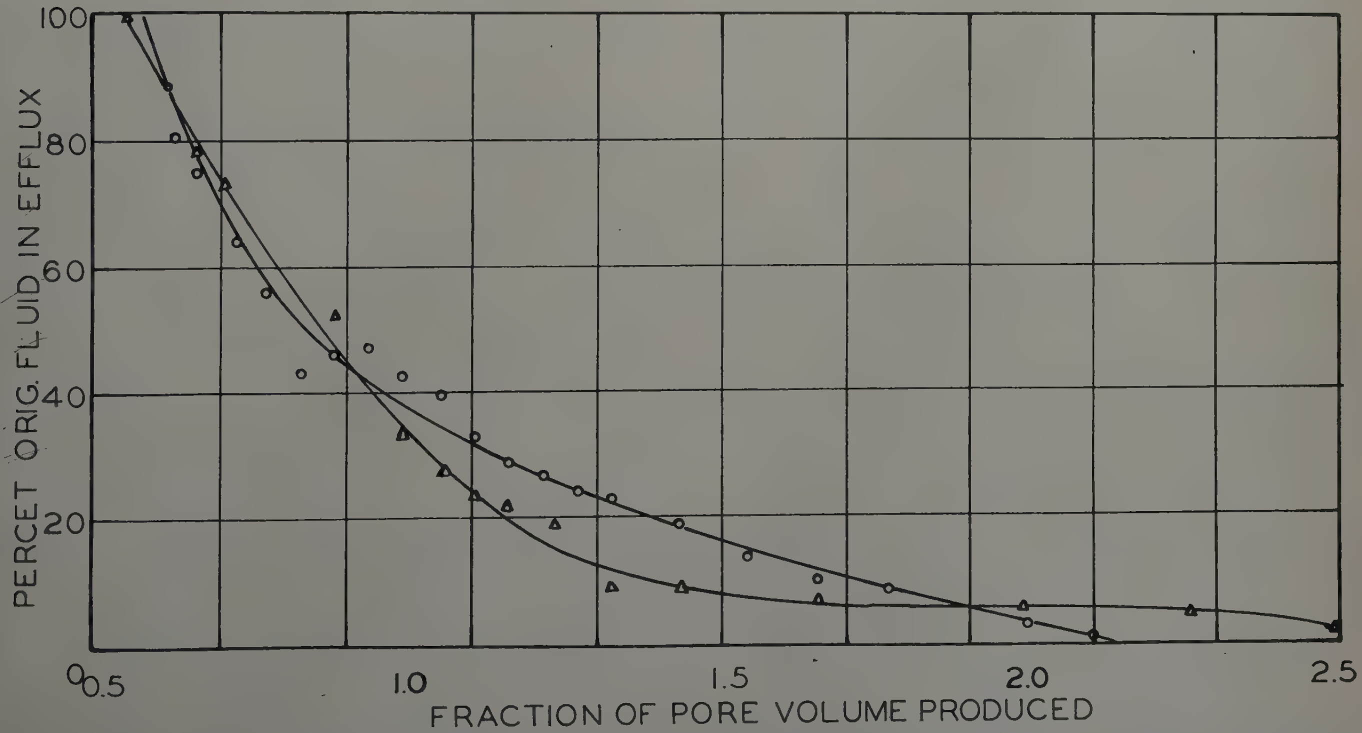

FIG. 7 — COMPARISON OF VERTICAL AND HORIZONTAL RUNS. VISCOSITY RATIO (DISPLACED OVER DISPLACING FLUID) IS 4.25; PRESSURE IMPOSED IS 220 mmHg. ○ = VERTICAL RUN. △ = HORIZONTAL RUN.

respects similar to the displacement of a fluid by one immiscible with it. It was anticipated that observation of such comparison might lead to a simpler basis for a theoretical approach to displacement calculations.

The experimental work reported in the following sections was carried out as two different problems on similar sand systems. Some of the details of experimental technique differ therefore. The problems were approached in similar fashions and are hence reported here together.

DISPLACEMENT OF A LIQUID BY ANOTHER WITH WHICH IT IS MISCIBLE

This portion of the work was performed on a sand column, 93.7 cm in length and 6.35 cm inside diameter. An unconsolidated sand, cleaned and fired, of 80-140 mesh was packed by vibration into a lucite tube filled with a colloidal suspension of silica. After the tube was filled with sand and liquid, the excess silica suspension was displaced by air. The sand filled tube was then dried by passage of hot air and evacuation. The resulting sand system was, therefore, lightly consolidated. The resulting system had a pore volume of 907 ccs and an average porosity of 30.7 per cent as found by water saturation. The permeabilities to air of the three sections shown in Fig. 1 were 3.81, 4.01, and 3.82 darcies.

Fig. 1 is a schematic drawing of the manner in which this porous sand section was set up for displacement tests. The liquids used were water and solutions of sucrose in water. By varying the amounts of sucrose in solution the viscosities were varied.

Displacement was measured in terms of the concentration of sucrose in the effluent. This was determined by measurement of refractive index. The effluent was collected in increments which varied from 50 to several hundred ccs. The porous system was cleared of its liquid after a given run and prepared for a new run by the continued flowing of the liquid which was to be the new saturant.

Runs were made with the sand system in both the vertical and horizontal positions. Vertical runs were made because it was noted that a slight gravitational settling was occurring on the horizontal runs. During vertical runs the displacing liquid was injected at the bottom when it was heavier than the displaced liquid and from the top when it was the lighter of the two. All runs were made with a constant pressure differential imposed across the two ends of the system. This resulted in a variation of displacement velocity during the course of a given displacement test.

The results of these displacement tests are shown in graphical form in Figs. 2 to 10. Table I gives a summary of information on these runs. In this table μ_o denotes the viscosity of the displaced phase and μ_w the viscosity of the displacing phase. On all runs except 1 and 6 sugar solutions were displaced by water. On runs 1 and 6 water was displaced by sugar solution.

DISPLACEMENT OF OILS BY WATER

The second group of experiments were performed on a column of sand similar to that described in the previous section. Unconsolidated sand between 65 and 270 mesh was the starting material. This was partially consolidated by packing it in a suspension of colloidal silica. Further consolidation was performed by saturating the column with an alcoholic solution of tetraethyl orthosilicate, displacing as much of this liquid as was possible by air and hydrolizing the remainder. Several repetitions of this cementing procedure were used. Finally, one end of the core system was cut off and discarded because the cementing material had built up excessively due to concentration of the cementing liquid by capillary forces.

Pressure taps were placed along the sand column and the air permeabilities of the various linear portions were measured as 2.77, 2.44, 2.54, and 2.99 darcies. The average porosity of the system was found to be 27.2 per cent with a total pore volume of 980 ccs. The overall column was 115.8 cm long and 6.35 cm inside diameter.

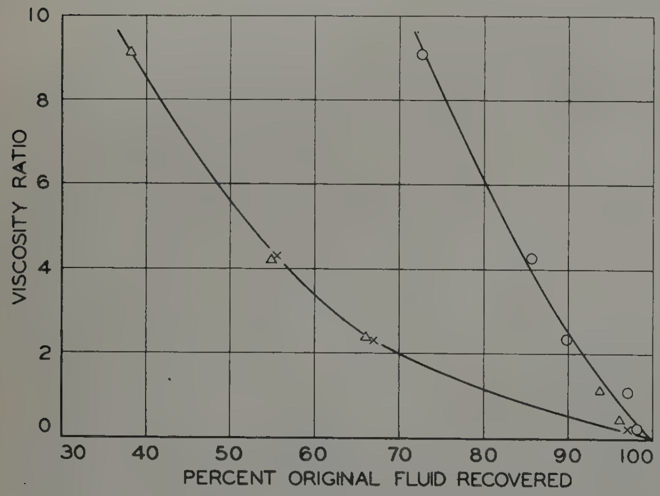

FIG. 8 — PER CENT OF ORIGINAL FLUID RECOVERED AS A FUNCTION OF VISCOSITY RATIO. △ — AT BREAKTHROUGH (HORIZONTAL RUNS). X — AT BREAKTHROUGH (VERTICAL RUNS). ⊙ — AT ONE PORE VOLUME CUMULATIVE.

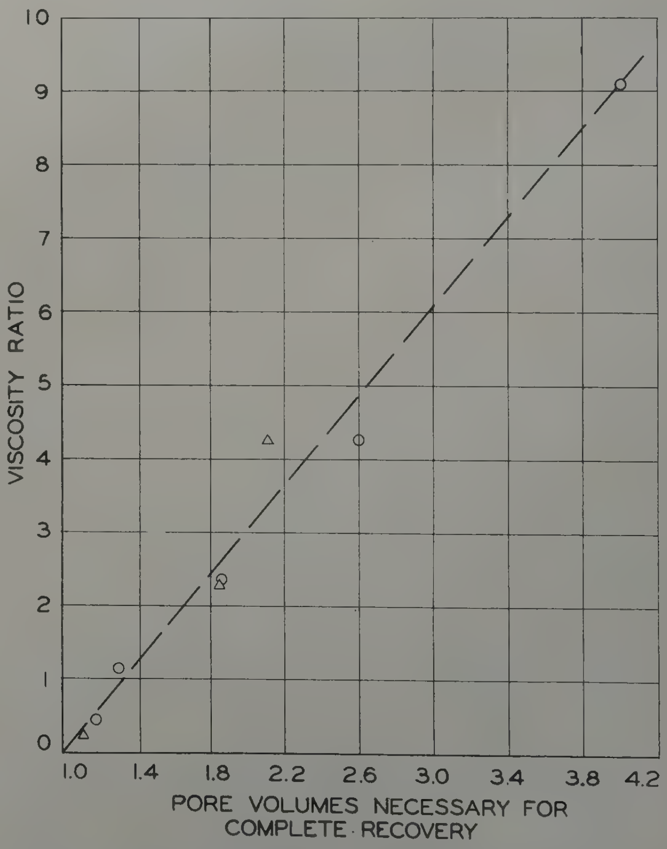

FIG. 9 — CUMULATIVE NECESSARY TO COMPLETE DISPLACEMENT (WATER-SUGAR SOLUTION DISPLACEMENTS). 0 — HORIZONTAL RUNS. △ — VERTICAL RUNS.

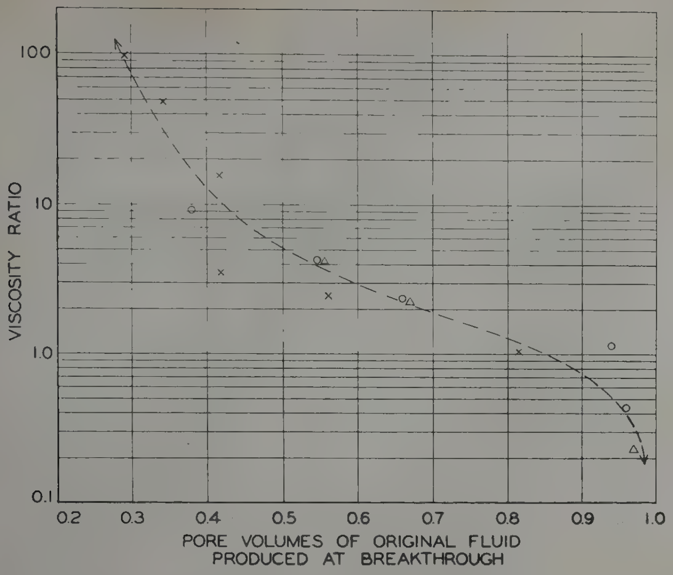

FIG. 10 — PORE VOLUMES PRODUCED AT BREAKTHROUGH OF DISPLACING LIQUID AS A FUNCTION OF VISCOSITY RATIO. 0 — WATER-SUGAR SOLUTION DISPLACEMENT (HORIZONTAL RUNS). △ — WATER SUGAR SOLUTION DISPLACEMENT (VERTICAL RUNS). X — WATER-OIL DISPLACEMENT.

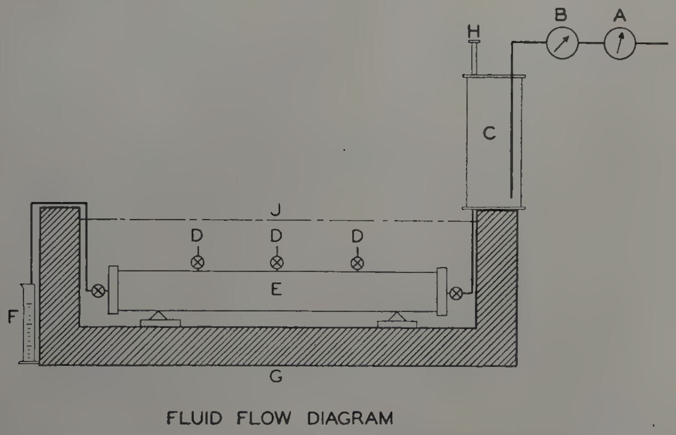

FIG. 11 — SCHEMATIC FLOW ARRANGEMENT FOR DISPLACEMENT OF OIL BY WATER. A, B — PRESSURE REGULATORS, C — METAL FLUID RESERVOIR, D — PRESSURE CONNECTIONS, E — POROUS SAND SECTION, F — GRADUATED CYLINDER, G — WATER BATH, J — WATER LEVEL IN BATH.

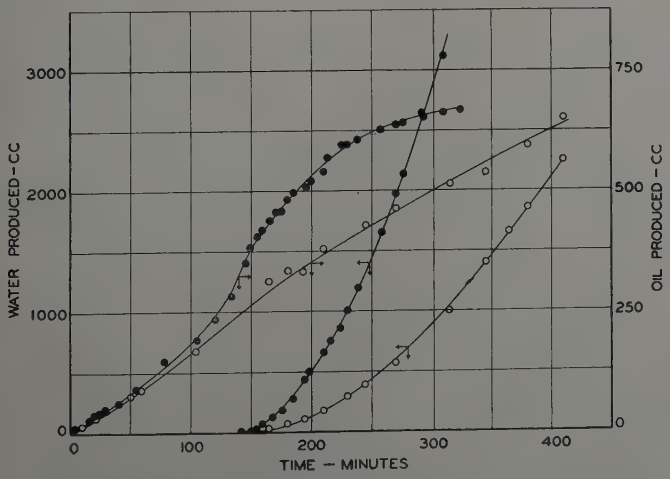

FIG. 12 — OIL AND WATER PRODUCTION AS A FUNCTION OF TIME. O — OIL-WATER VISCOSITY RATIO IS 98.6. ● — OIL-WATER VISCOSITY RATIO IS 48.53. PRESSURE IMPOSED IS 20 PSIG.

Fig. 11 gives a diagrammatic sketch of the flow set up. Runs were made with the core always in a horizontal position and with the assembly placed in a water bath so that the viscosities of the liquids could be controlled to desired values. A constant pressure differential was imposed for the duration of each run and rates were permitted to vary. Pressure was imposed by applying nitrogen to a reservoir chamber containing the displacing liquid as shown in Fig. 11.

The oils were standard grade lubricating oils, kerosene, deodorized naphthas, and blends of lubricating oils with naphthas. By varying the type oil and the temperature during displacement the desired ratios of oil viscosity to water viscosity were obtained. The displacing liquid was always water.

The results of the water-oil displacement experiments are shown in Figs. 12 to 20 and in Fig. 10. Table II gives a summary of conditions and numerical results on these displacements.

DISCUSSION OF EXPERIMENTAL RESULTS

An examination of the results of both sets of experiments will show that displacement always occurred in two phases — the primary phase prior to breakthrough of the displacing liquid and the secondary phase from breakthrough until cessation of production. Figs. 4, 5, 15, 16 and 17 show point of breakthrough and per cent of original fluid in the efflux as a function of the total pore volumes of fluid produced. The point of breakthrough always was followed by a sharp drop in the amount of displaced fluid in the efflux.

In both sets of experiments the relative importance of the primary and secondary phases varied with the fluid viscosities.

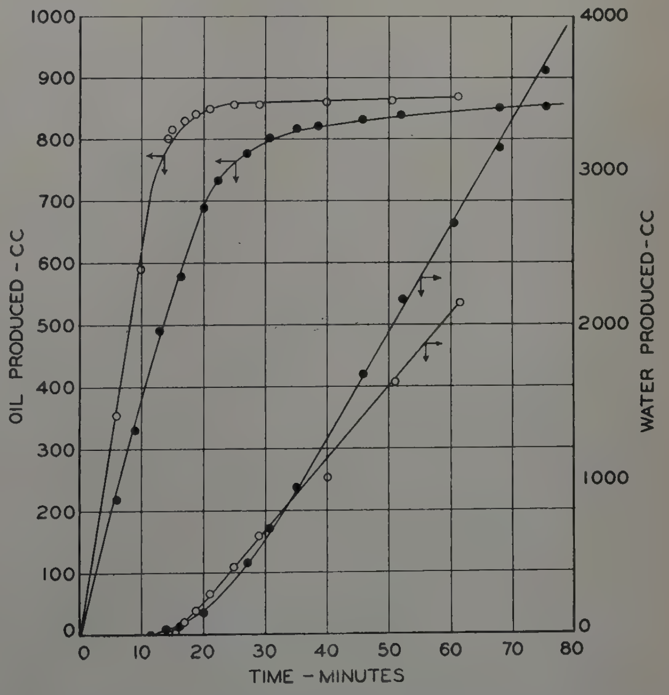

FIG. 13 — OIL AND WATER PRODUCTION AS A FUNCTION OF TIME. O — OIL-WATER VISCOSITY RATIO IS 1.04. ● — OIL WATER VISCOSITY RATIO IS 3.51. PRESSURE IMPOSED IS 20 PSIG.

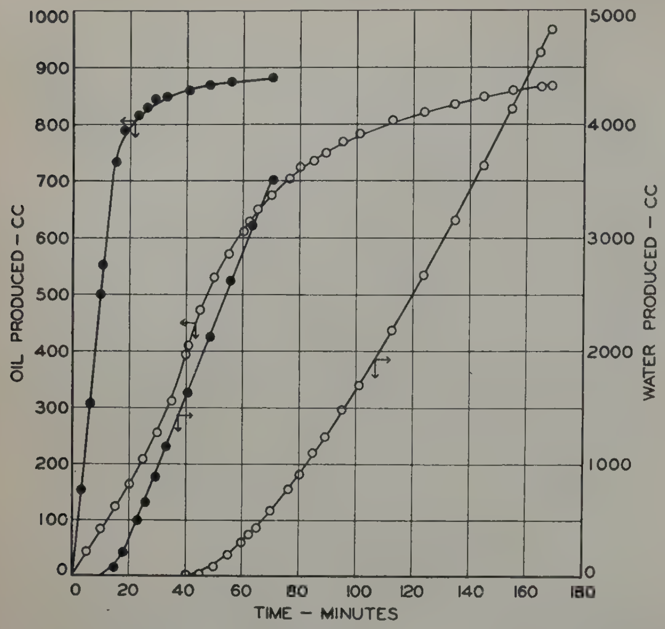

FIG. 14 — OIL AND WATER PRODUCTION AS A FUNCTION OF TIME. O — OIL-WATER VISCOSITY RATIO IS 15.49. ● — OIL-WATER VISCOSITY RATIO IS 2.41. PRESSURE IMPOSED IS 20 PSIG.

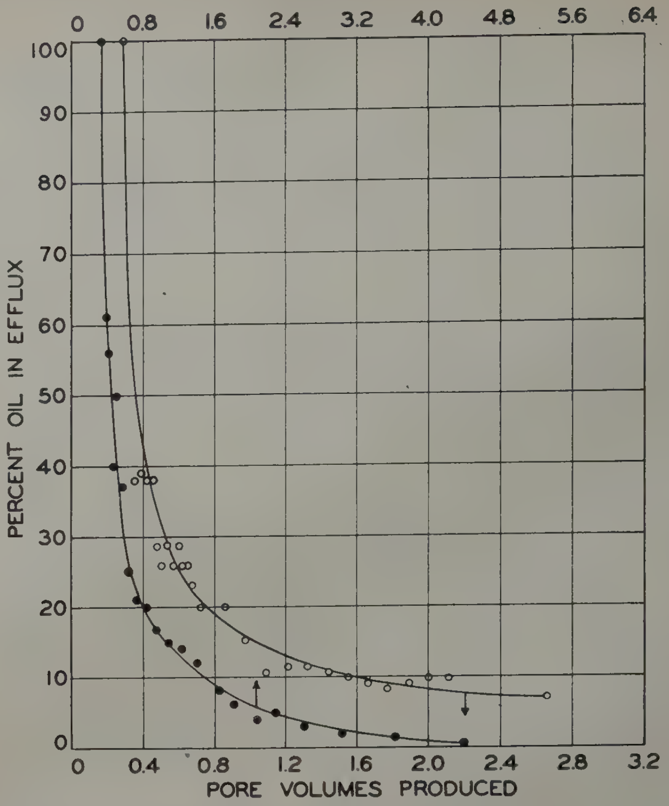

FIG. 15 — PER CENT OIL IN EFFLUX VERSUS TOTAL CUMULATIVE PRODUCTION. O — OIL-WATER VISCOSITY RATIO IS 98.6. ● — OIL-WATER VISCOSITY RATIO IS 48.53. PRESSURE IMPOSED IS 20 PSIG.

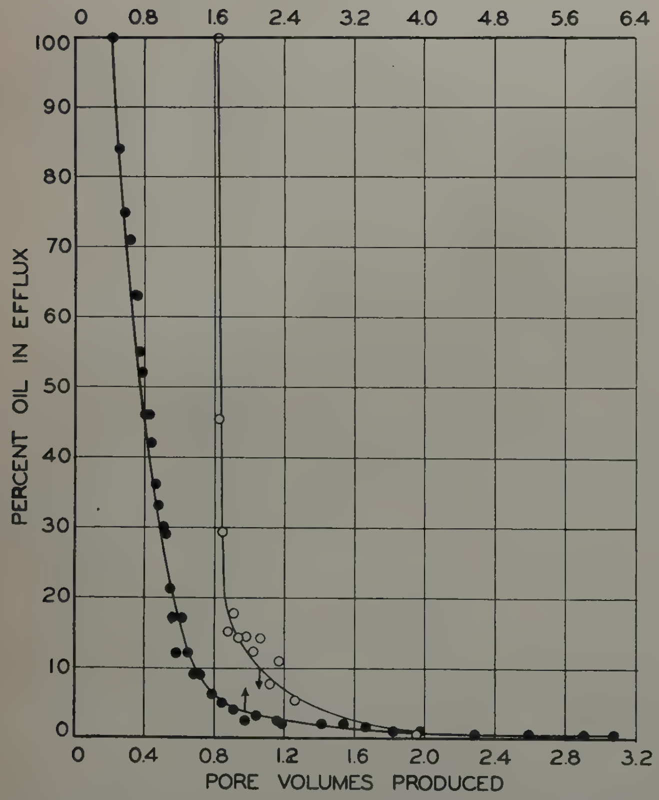

FIG. 16 — PER CENT OIL IN EFFLUX VERSUS TOTAL CUMULATIVE PRODUCTION. O — OIL-WATER VISCOSITY RATIO IS 1.04. ● — OIL-WATER VISCOSITY RATIO IS 3.51. PRESSURE IMPOSED IS 20 PSIG.

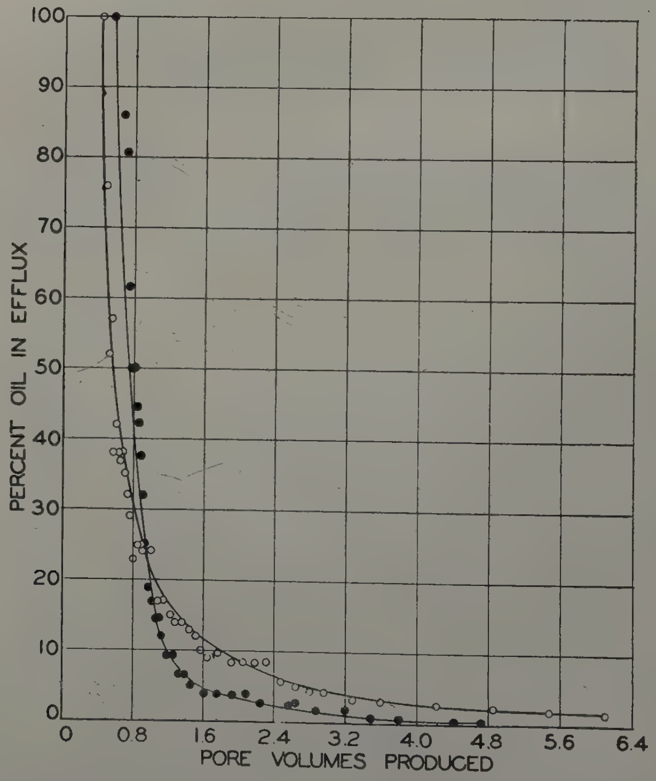

FIG. 17 — PER CENT OIL IN EFFLUX VERSUS TOTAL CUMULATIVE PRODUCTION. O — OIL-WATER VISCOSITY RATIO IS 15.49. ● — OIL-WATER VISCOSITY RATIO IS 2.41. PRESSURE IMPOSED IS 20 PSIG.

Following the lead of Buckley and Leverett[1] this variable has been expressed as the viscosity of the displaced liquid divided by the viscosity of the displacing liquid.

Fig. 8 indicates the effect of the viscosity ratio upon the recovery at breakthrough and at one pore volume cumulative for the water-sugar solution displacements. Fig. 9 is a plot of the cumulative throughput necessary to effect complete recovery on these same displacements.

The primary phase displacement was very close to 100 per cent for low viscosity ratios. The theoretical limit for this type displacement would be 100 per cent recovery in the primary phase at a viscosity ratio of zero. This is shown on both Figs. 8 and 9.

Fig. 18 gives the effect of viscosity ratio for the water-oil displacements. Here also the primary phase yields higher recoveries for lower viscosity ratios. The apparent upper limit for displacement during the primary phase is 91 per cent at a viscosity ratio of zero. Fig. 18 indicates that all water-oil displacements might ultimately have reached this recovery had they been carried to a sufficiently high water-oil ratio. All these runs were terminated before an ultimate point was reached. Table II gives total recovery at cessation of displacement.

In these experiments a pressure differential for carrying on the displacement was arbitrarily assigned. No particular attention was paid to rates of displacement except to note that the displacement speeded up or slowed down depending on whether the displacing liquid had the lower or higher viscosity. Figs. 2 and 3 show typical rate data recorded for the water-sugar solution displacements. It is to be noted in these figures that the rates for the horizontal and vertical runs differ because the imposed pressure differential on the vertical runs was not corrected for the gravitational head.

Fig. 6 gives the results on a pair of runs made at two pressure differentials. At the higher differential, which would also mean the higher rate of displacement, the percentage recovery during the primary phase was noted to be slightly less than at the lower pressure differential. Also at the higher pressure gradient a slightly higher cumulative recovery was found to be necessary to effect complete removal of the displaced liquid.

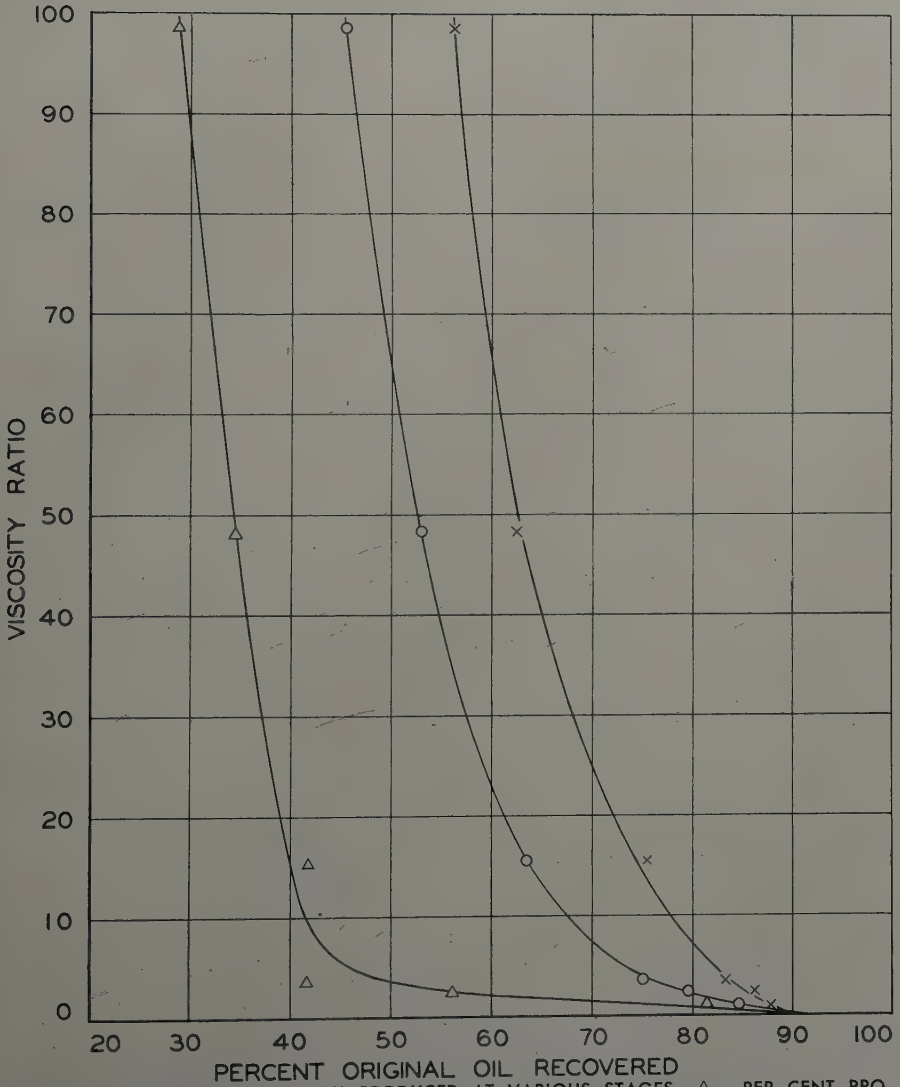

FIG. 18 — PER CENT ORIGINAL OIL PRODUCED AT VARIOUS STAGES. △ — PER CENT PRODUCED AT BREAKTHROUGH. 0 — PER CENT PRODUCED AT ONE PORE VOLUME TOTAL CUMULATIVE. X — PER CENT PRODUCED AT 1.95 PORE VOLUMES TOTAL CUMULATIVE.

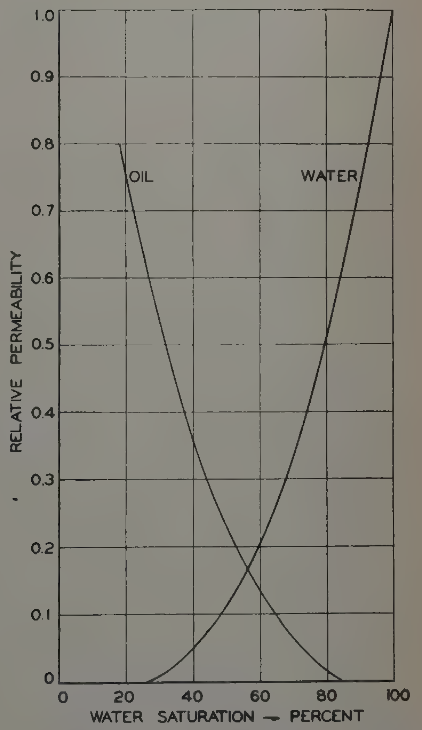

FIG. 19 — RELATIVE PERMEABILITY TO OIL AND WATER (AFTER LEVERETT, AIME, 1939).

These results are in agreement with those shown by Hendrix and Huntington[8] in their Fig. 3.

During the horizontal displacement test there was some visual evidence of a separation of displaced and displacing liquids due to difference in their densities. Therefore, vertical runs were made for comparison but only on the water-sugar solution displacements. The displacement histories on horizontal runs are shown in Fig. 4 and on vertical runs in Fig. 5. Fig. 7 compares one particular set of such runs for the same viscosity ratio. It was noted that the curves for horizontal runs show a hump after breakthrough but that the curves for vertical runs do not. Data from both horizontal and vertical runs are plotted in the correlations of Fig. 8, 9, and 10. From these plots it can be noted that the effects of gravity were probably not very important.

To further compare the results of the two types of displacement, the percentage recoveries at breakthrough for all runs were plotted in Fig. 10. All data can be represented by a single function from which individual observations do not deviate markedly. As pointed out previously, however, the water-sugar solution displacement can approach 100 per cent efficiency at zero viscosity ratio whereas the water-oil must approach a value of 91 per cent.

Further correlation was attempted between the observed data on water-oil displacement and calculated histories by the method of Buckley and Leverett.[1] The method will not be described here. Basic to the calculation are relative permeability curves. Such curves were not procured for the systems studied but inasmuch as they were very close to unconsolidated sands it was assumed that the relative permeability curves of Buckley and Leverett would apply. Fig. 19 shows the curves used for the calculations.

After several intermediate calculations the method gives a distribution of water saturation as a function of distance, U, along the linear system being flooded. Different distributions are calculated for different values of total cumulative liquid injected. Fig. 20 gives the results of such saturation distribution calculations for the case where the viscosity ratio was 1.04. From this figure and from the data necessary to calculate it, there was also obtained a calculation of per cent oil in the efflux as a function of cumulative throughput. These results are given in Fig. 21 along with experimental observations for the same viscosity ratio. The agreement in this case is quite good.

Fig. 22 gives an overall comparison between the calculated results for recovery during the primary phase as given by Buckley and Leverett and experimental results for the same quantity in the present work. The curves for the two sets of experimental data shown here are as taken from Figs. 8 and 18. Buckley and Leverett's calculations were not carried on for a system strictly analogous to the experimental ones described. They assumed a system containing connate water originally, a condition not used in the experiments being reported. However, their calculation of per cent water saturation at breakthrough should be comparable to per cent recovery at breakthrough from a system containing no connate water.

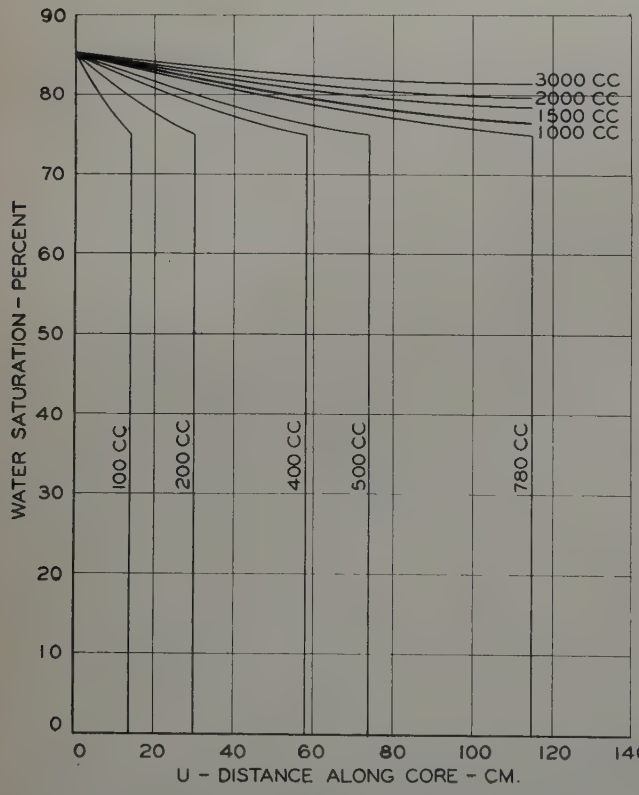

FIG. 20 — CALCULATED DISTRIBUTION OF WATER SATURATION AT VARIOUS VALUES OF TOTAL CUMULATIVE. BY METHOD OF BUCKLEY AND LEVERETT FOR OIL-WATER VISCOSITY RATIO EQUAL TO 1.04.

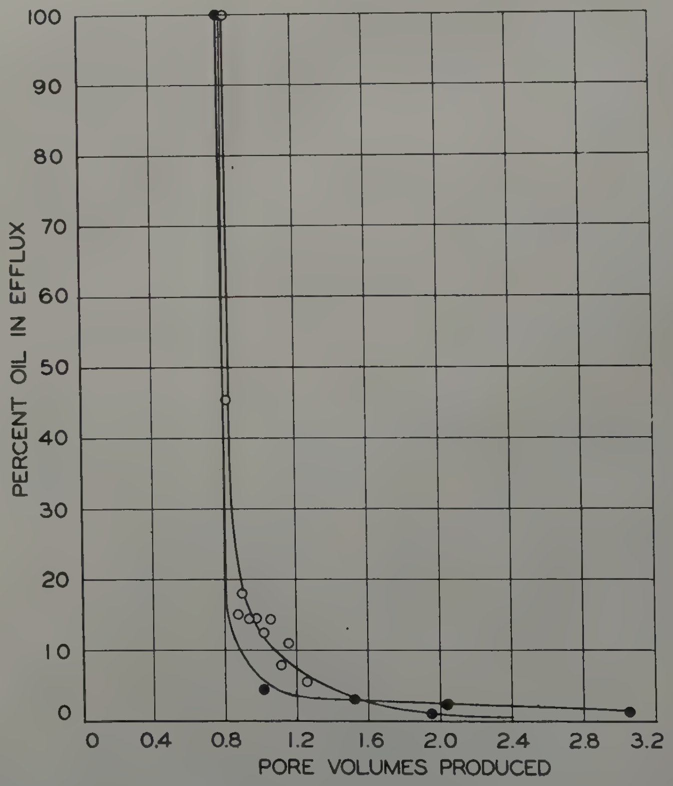

FIG. 21 — COMPARISON OF EXPERIMENTAL DATA WITH CALCULATED PERFORMANCE. 0 — EXPERIMENTAL DATA OIL-WATER VISCOSITY RATIO IS 1.04. ● — POINTS TAKEN FROM CALCULATED DATA OF FIG. 20.

It is significant to note that a water flood at the highest viscosity ratio of 98.6 produced only 29 per cent oil at breakthrough. This approaches the values ordinarily expected for gas displacement. It is suggested that the difference in mechanism between a water-drive and a gas-drive may be very slight if viscosity ratios are identical.

The comparison of the water-oil displacement results to a gas-oil displacement is further shown in Fig. 23, where water-oil ratios are plotted versus cumulative oil produced. For constant viscosity and pressure gradient conditions the water-oil ratio should be proportional to K_w/K_o. The cumulative oil produced can be plotted negatively as residual oil which would be proportional to an average oil saturation. Fig. 23 is comparable, therefore, to the familiar K_g/K_o versus oil saturation curve.

CONCLUSIONS

The general agreement between the behaviors of the two types of displacements observed in these experiments would lead to the thought that the main forces to be considered are viscous rather than interfacial. The interfacial forces undoubtedly control to a large degree the maximum possible displacement, i.e., the difference between 91 per cent and 100 per cent in the two instances reported. However, the manner of displacement where the interfacial forces were non-existent is comparable in a large degree to that where interfaces were present, which indicates that up to the final stages of displacement viscous forces were most important.

It is further suggested, therefore, that a theory of displacement of oil from porous media might be approached by a consideration of the displacement behavior between fluids which are mutually miscible. No complete analytical approach for this situation was found in the literature, even for simplified systems. The application of such data, aside from a contribution to a general theory of displacement, would be to the displacement of very mobile reservoir fluids by injected gases or to the recovery of oil by injected hydrocarbons.

These experiments point out the desirability of carrying on a water flood under conditions of as low a viscosity ratio as possible. Flooding at high pressures before solution gas is liberated, or flooding with waters containing high amounts of salts would both be advantageous from this standpoint. A further suggestion from these experiments would be that a high efficiency of displacement could be obtained by displacing reservoir liquids with other hydrocarbon liquids. Practically, however, this would not be feasible unless the displacing hydrocarbon could be readily recovered, a situation which could possibly be met by the use of a close cut, high vapor

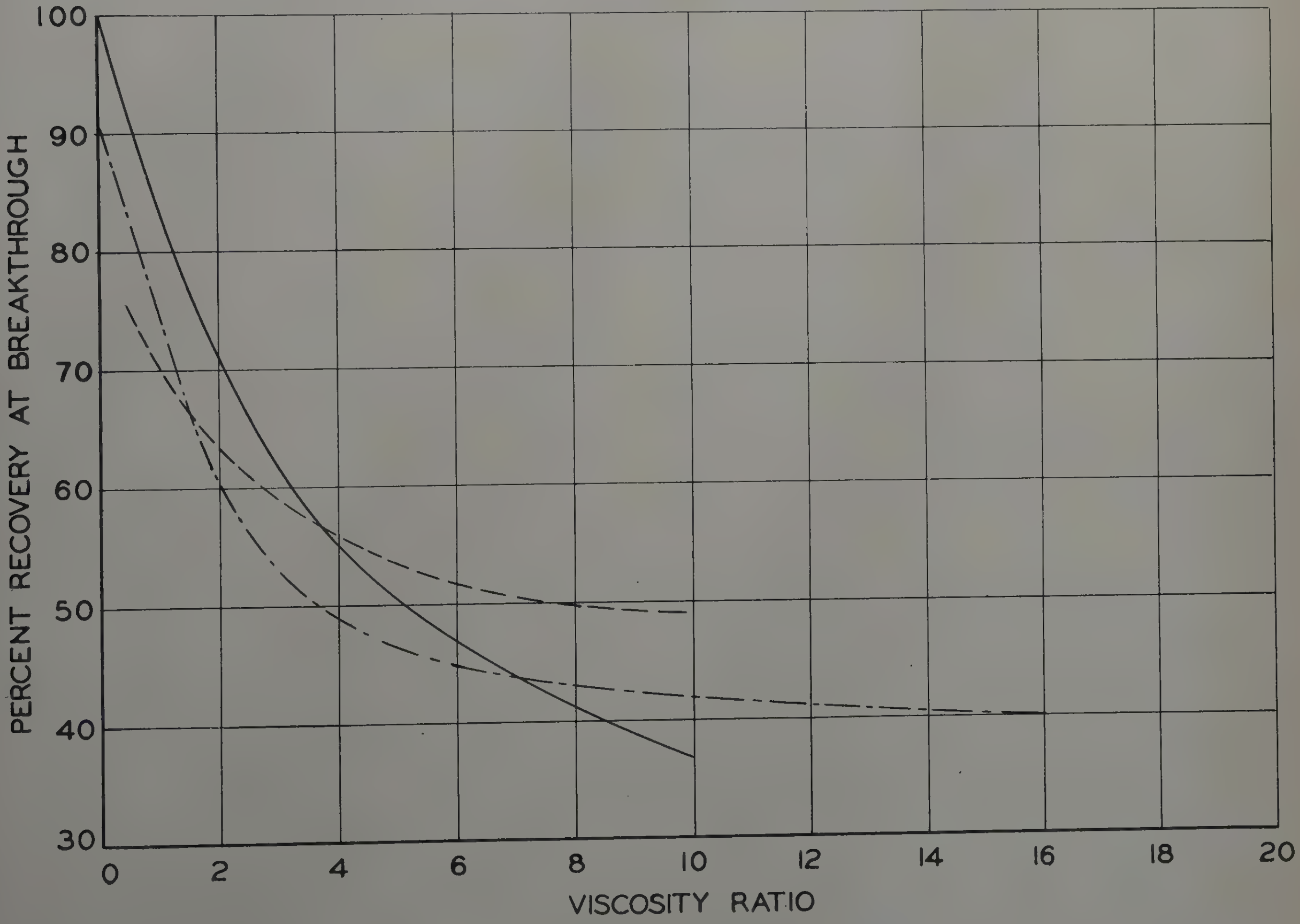

FIG. 22 — COMPARISON OF PER CENTS PRODUCED AT BREAKTHROUGH.
– – – – – – CALCULATIONS OF BUCKLEY AND LEVERETT.
———— WATER-SUGAR SOLUTION DISPLACEMENTS.
—·—·— WATER OIL DISPLACEMENT.

Table I

Summary of Results on Water-Water Solution Displacements

Run No.	Tube Position	μ_o	μ_w	$\frac{\mu o}{\mu w}$	Pressure Gradient	Pore Volumes Recovered at Breakthrough	% of Original Fluid Recovered at One Pore Volume Cumulative	Cumulative Pore Volumes Necessary for Complete Recovery
3	Horizontal	8.1	0.894	9.1	220 mm Hg	.38	72.7	4.0
4	Horizontal	3.8	0.894	4.25	220 mm Hg	.55	85.8	2.6
2	Horizontal	2.08	0.894	2.35	220 mm Hg	.66	89.7	1.86
5	Horizontal	2.05	0.874	2.35	760 mm Hg	.585		
11	Horizontal	1.0	0.876	1.14	220 mm Hg	.94	97.0	1.30
1	Horizontal	0.855	1.95	0.44	220 mm Hg	.96		1.18
7	Vertical	3.7	0.874	4.25	220 mm Hg	.55		2.1
9	Vertical	1.95	0.854	2.29	220 mm Hg	.67		1.85
6	Vertical	0.874	3.7	0.24	220 mm Hg	.97	98.0	1.11

Table II

Summary of Results on Water-Oil Displacements

Run No.	μ_o	μ_w	$\frac{\mu o}{\mu w}$	Pressure Gradient	Pore Volumes Recovered at Breakthrough	% of Original Fluid Recovered at One Pore Volume Cumulative	Total Pore Volumes Through at Termination	Cumulative Recovered at Termination
1	63.5	0.644	98.6	20 psig	29.0	45.5	2.70	62.0
3	33.0	0.68	48.53	20 psig	34.5	53.0	4.39	68.4
4	10.3	0.665	15.49	20 psig	41.8	63.3	6.09	89.0
5	2.21	0.63	3.51	20 psig	41.8	75.0	6.13	88.4
6	1.52	0.63	2.41	20 psig	56.1	79.6	4.72	89.7
2	0.835	0.80	1.04	20 psig	81.6	84.7	1.95	87.8

pressure fraction, which could be vaporized from the reservoir after displacement was complete.

It is apparent that the ratio of viscosities between displaced and displacing fluids is an important consideration in attempting to evaluate the success of displacement. Further examination of this concept might lead to control of maximum displacement efficiency by control of the viscosity of the displacing medium. The consideration of this concept might suffice also to compare gas and water displacements more fruitfully.

The experiments described here have been necessarily simplified. Experimentation on the displacement of oils by hydrocarbon liquids in the presence of connate water would be among desirable future experiments. Further simplification would also be desired in order to better understand the water-sugar solution displacement as a basis for theoretical calculations on water-oil or gas-oil displacements.

REFERENCES

1. Buckley and Leverett, "Mechanisms of Fluid Displacement in Sands," AIME *Trans.*, 1942, Vol. **146**, p. 107.
2. Yuster and Day, "Gas Requirements in Gas Drive Recovery," *Producers Monthly*, Vol. **10**, No. 12, pp. 21-28, Oct. 1946.
3. Holmgren, "Some Results of Gas and Water Drives on a Long Core," *Petr. Tech.*, July, 1948.
4. Calhoun, McCormick and Yuster, "The Effect of Pressure Gradients and Saturations on Recovery in Water Flooding," *The Petroleum Engineer*, 16 (4): 82-90, Jan. 1945.
5. Morse and Yuster, "Water Flood Tests on Long Cores," *Oil Weekly*, April 7, 1947.
6. Russell, Morgan and Muskat, "Some Experiments on the Mobility of Interstitial Waters," AIME *Trans.* 1947, Vol. **170**, p. 51.
7. Mertz and Huntington, "Gas Mixing in Porous Media," *Oil Weekly*, Sept. 8, 1941.
8. Hendrix and Huntington, "The Effect of Velocity on the Mixing of Liquids in Porous Media," *Petroleum Engineer*, Oct. 1941.
9. Fowler and Brown, "Contamination by Successive Flow in Pipe Lines," AIChE *Trans.*, Aug. 1943.

* * *

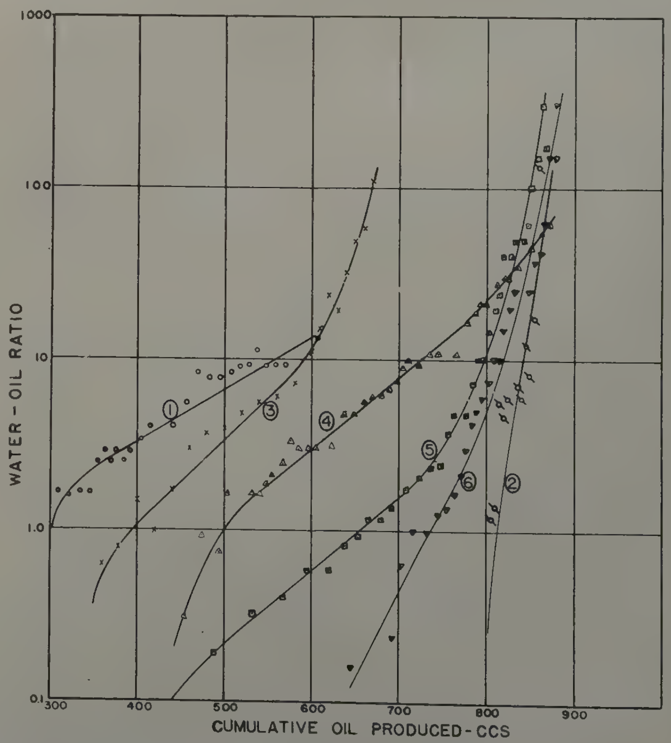

FIG. 23 — DISPLACEMENT HISTORY DURING SECONDARY PHASE TO SHOW SIMILARITY TO K_G/K_O CURVES. NUMBERS INDICATE RUN NUMBERS FROM TABLE II.

ANALYSIS OF FRACTURED LIMESTONE CORES

FRANK C. KELTON, MEMBER AIME, CORE LABORATORIES, INC., DALLAS, TEXAS

ABSTRACT

A method is outlined for the analysis of large cores, developed primarily for the purpose of obtaining reliable data on fractured or vugular limestones.

Porosity and fluid saturations are determined by a modified Dean-Stark extraction, after initially bringing the samples to 100 per cent liquid saturation by a vacuum-pressure method. Horizontal permeabilities on the whole samples are determined in two directions, parallel and perpendicular to the direction of principal fracturing.

Results are presented for various types of formations. A comparison is made between data obtained by this special method and the method of conventional analysis, and discussion is given of the relative advantages and limitations of each. In view of this comparison a modified method for the analysis of fractured and vugular formations is proposed, which method retains the advantages of the previously outlined techniques but gives promise of speeding up the analysis.

INTRODUCTION

For many years the greater part of the production in the Permian Basin was from formations of Permian and Pennsylvanian age. While production from these formations is still the predominant production, deeper prospecting has brought to light older formations with oil productive characteristics. Attempts to core these deeper horizons were at first usually characterized by poor recovery. The old rule of thumb, "good core recovery — poor well" was originated and remained in effect until recently. With the advent of diamond coring and the increased efficiency in drilling and coring operations, the old adage has lost its significance. Formations of Devonian, Silurian and Ordovician ages were successfully cored with varying degrees of recovery. The cores thus obtained were surprising and in some cases disappointing. Good recovery from these formations led to speculation as to the feasibility of analysis and the meaning of data obtained from conventional analysis. Commercial laboratories were engaged to analyze these cores, and their results indicated that data obtained by conventional methods would be of little value. From visual inspection it was apparent that in many cases the effective porosity for storage of hydrocarbons, and permeability, were contained largely in fractures and solution cavities rather than in the primary crystalline structure of the formation. In other cases the solution cavities augmented the effective porosity of the primary crystalline structure, or fractures enhanced the permeabiilty of the latter so that the formation might respond favorably to acidization and become commercially productive. Since the spacing of the cavities and fractures was often comparable to the core diameter, it was evident that the entire core should be analyzed instead of small fragments.

On the basis of these observations, commercial laboratories were requested to devise a system of analysis which would yield data of practical value. Procedures have accordingly been developed which seem to meet this requirement, and to date nearly 12,000 large core samples have been analyzed. It is the purpose of this paper to describe the methods used, to present typical results for several fractured formations and to compare the data obtained by this special analysis with that obtained by conventional analysis. Certain modifications and alternative procedures are finally suggested to speed up the analysis.

CORE ANALYSIS PROCEDURE

Fluid Saturations and Porosity

The core sample, in segments up to 15 in. in length, is marked, weighed and examined under ultra-violet light to determine the presence of oil saturation. If present, the approximate quantity of oil and its location on intercrystalline, fracture or vugular surfaces is noted. This information is carefully recorded. The degree of fracturing and/or vugular development is also noted. The sample is then placed in a pressure cell and the air evacuated with a high speed vacuum pump. This evacuation is continued only long enough to reduce the pressure to approximately the vapor pressure of water in order not to remove excessive amounts of water. Water is admitted to the cell and allowed to penetrate the sample under atmospheric pressure, filling the pore space initially occupied by air and replacing the small amount of water removed by evacuation. Pressure up to 200 psi is applied to force water into the smaller capillaries, and the sample is left sub-

---

[1]References at end of the paper.

Manuscript received at the office of the Petroleum Branch October 5, 1949. Paper presented at the meeting of the Petroleum Branch October 5-7, 1949, in San Antonio, Tex.

merged under presure for an hour or longer. It is then removed from the cell, surface water wiped off, and reweighed. The gain in weight is a measure of the residual gas content of the original sample. If large surface vugs are present an alternative procedure is used to prevent them from draining fluid, as will be discussed later.

The sample, now fully saturated with oil and water, is placed in an extraction pot, Fig. 1, and covered with toluene. The pot is placed in an insulated oil bath, Fig. 2, connected to a jacketed condenser tube, and allowed to heat up until the water of the sample and the toluene are vaporized. This process is similar to the familiar Dean-Stark extraction; as the water is condensed it drops into the receiving tube and collects at the bottom while the condensed toluene runs back into the pot. The water is drained from the receiving tube at intervals and measured.

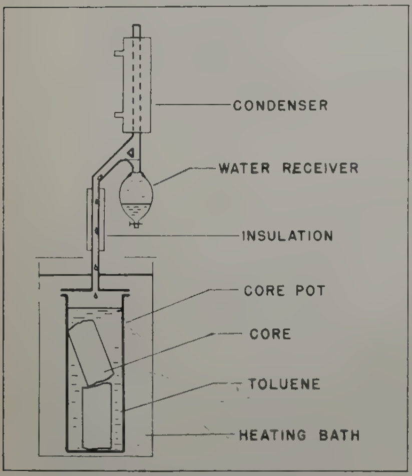

FIG. 1 — EXTRACTION APPARATUS SCHEMATIC.

The largest part of the water in the sample is removed after one day's extraction, but the remainder comes over very slowly. Typical rates of water removal are shown for various formations in Fig. 3. Since it is necessary to determine the water content to within a fraction of a cubic centimeter in order to be able to determine the oil content acurately, the process is continued until the amount of water removed daily has dropped to 0.1 to 0.3 cc. This may require from three days to three weeks or even longer; the average time is about one week. During this time the oil content of the core sample is being replaced by toluene. If the visual examination showed oil saturation only on fracture planes and/or vugular surfaces, the extraction is asumed to be complete when there is no sensible gain in water in the receiving tube. If, on the other hand, the examination indicated oil in intercrystalline pore spaces, the extraction of oil may not be complete, and in this case the sample is removed from the pot and placed in an oversize soxhlet extractor where extraction with toluene is continued.

After extraction is complete the sample is placed in a constant temperature oven and dried for a period of one to two days. After cooling to room temperature it is re-weighed. The loss of weight, less the amount of water measured during the extraction, is the weight of the oil contained in the sample. This weight is corrected for an assumed density of oil to give the volume of oil in the sample. The summation of oil and total water gives the pore space of the sample, since the original gas content has previously been replaced by water.

A representative number of samples are immersed in water until capillary penetration of water has for practical purposes ceased, and their bulk volumes determined by the bouyancy or apparent decrease in weight when re-immersed in water. For the purpose of this measurement of bulk volume it is necessary only that no appreciable further penetration of water occurs during the second immersion; this is easily realized even though the samples are far from being 100 per cent saturated. These bulk volumes together with the dry weights give apparent densities, and these divided by one minus the respective fractional porosity give true grain density. An average true grain density figure is thus obtained, which is used together with the extracted weights of the other samples to determine their grain volume, and pore volume is added to give bulk volume. Pore volume divided by this bulk volume gives the porosity.

Permeability

The extracted sample, or the largest segment if the sample consists of more than one piece, is placed in the cylindrical holder shown in Figs. 4 and 5. The sides of the core are covered with two rectangular rubber gaskets, with openings whose length extends to within 1 to 1½ in. of the shortest length of the core and whose width extends over about one fourth the circumference. Two sections of split pipe of suitable diameter and with hinged pieces along their sides to provide a

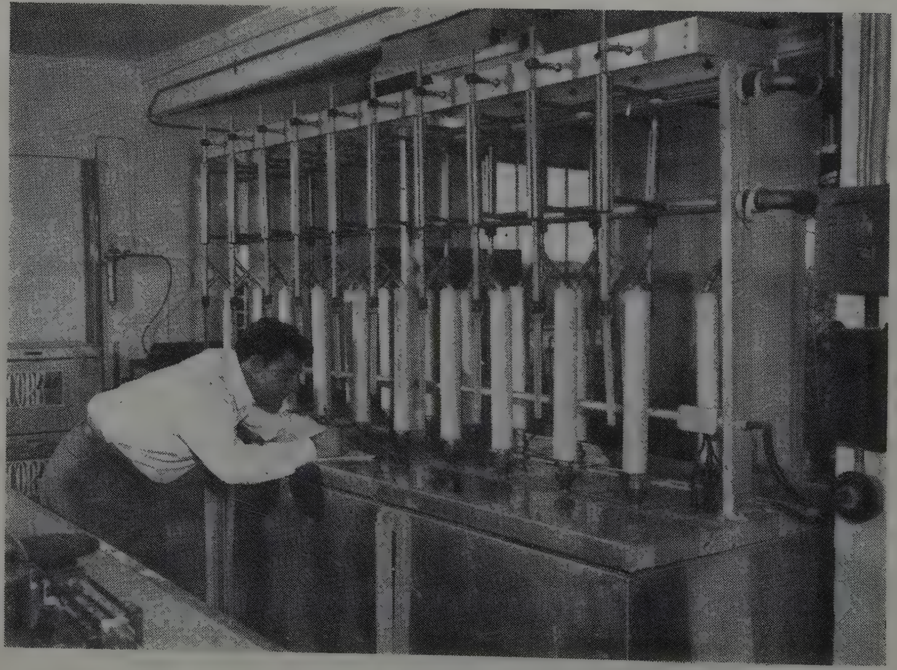

FIG. 2 — EXTRACTION APPARATUS.

good fit, are placed around the gaskets, and a number of stranded wire cables are wrapped around the pipe. By means of a crank and worm gear these cables are tightened simultaneously so that considerable pressure is applied to all sides of the gaskets. This seals the core except for the two rectangular openings in the gaskets, a thin line along the sides of the core between the gaskets, and the ends of the core.

Air pressure is applied to the opening on one side of the core, and the rate of air flow out of the other side is measured directly by means of a burette and soap film so that no back pressure is exerted on the downstream side. Permeability is calculated as though the flow were uniformly distributed across the rectangular cross section between the gasket openings and through the length between the straight edges of the gasket openings. Corrections are then applied to take into account the nonlinearity of flow and the loss through the ends of the core and through the slits between gaskets.

The orientation of the core in the holder is such that the flow is across the direction of principal fracturing. The permeability so obtained is designated as K_{max}. The core is then turned 90° in the holder and permeability again measured. This is called $K_{90°}$.

The correction applied to take care of the loss of air through the ends of the core is called the shape factor. Typical values of this factor, for a 3 in. core, are shown in Fig. 8. This shape factor is proportional to the fraction of entering air that gets to the gasket opening on the opposite side of the core. It may be noted that for the length of core usually available and the length of the seal between the gasket opening and the ends of the sample, the shape factor generally lies between 85 per cent and 95 per cent, i.e., a relatively small loss to the ends of the core. In addition to the above shape factor, a constant factor is applied to take care of the widening of the flow lines and loss of air at the sides between the gaskets, as may be visualized by reference to Fig. 4.

The above correction factors were derived by extensive experiments on a synthetic core of nearly uniform permeability. The flow through a series of

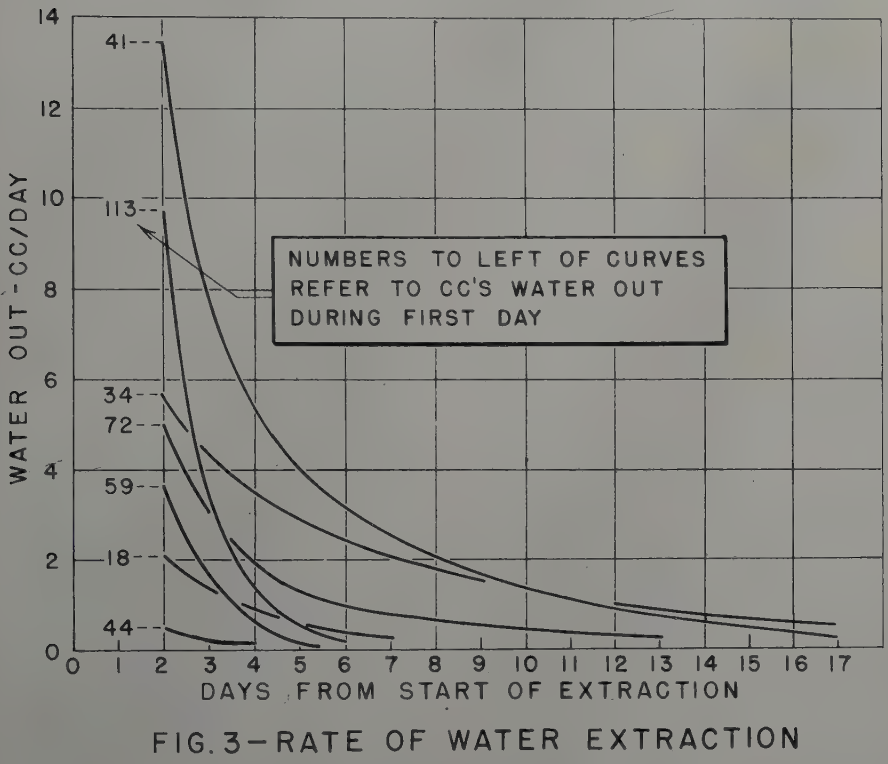

FIG. 3 — RATE OF WATER EXTRACTION.

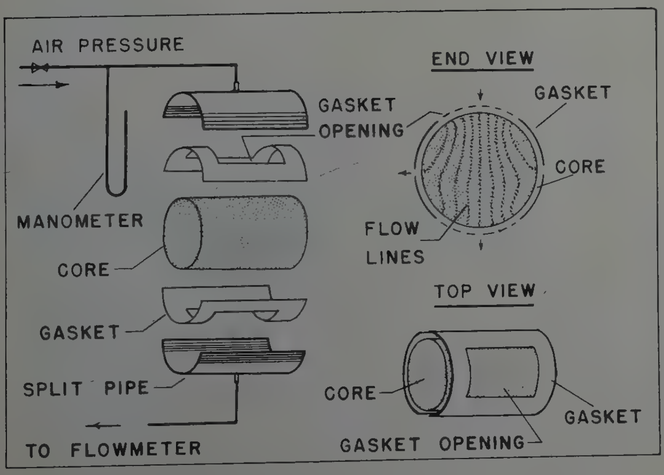

FIG. 4 — CLAMP TYPE PERMEAMETER SCHEMATIC.

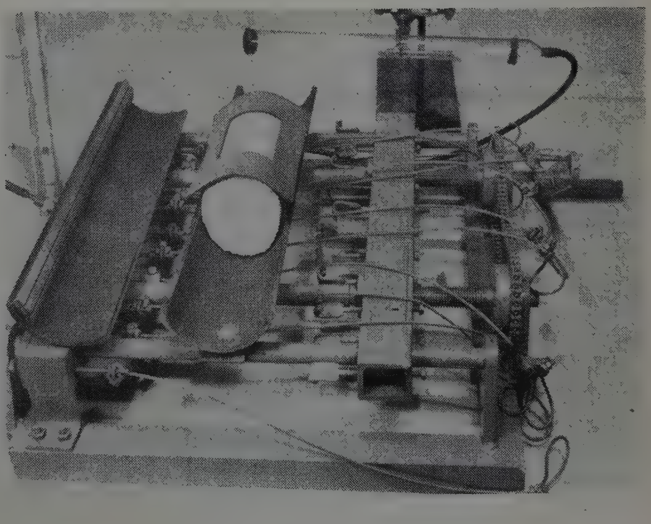

FIG. 5 — CLAMP TYPE PERMEAMETER.

gasket openings was measured using a long core, and the series of measurements repeated after cutting off 2 cm at a time from each end of the core. A direct measurement of the permeability of each such section of the core was then made. A subsequent check was obtained from electrolytic model experiments simulating the non-linear flow through the core.

DISCUSSION AND ALTERNATIVE PROCEDURES

Fluid Saturations and Porosity

It may be noted that two checks are available on the porosity as determined by the above outlined procedure. If the sample, after extraction, is allowed to cool under toluene and then weighed prior to drying, the weight of toluene divided by its specific gravity furnishes a check on the porosity. The agreement is generally found to be good. Another check is furnished, after extraction and drying, by resaturating the sample with water and determining the weight increase. The agreement here is also good. For example, a series of such measurements on seven samples of porous limestone gave a porosity value of 10.06 per cent by toluene and 10.13 per cent by resaturation. On eight low porosity samples of the same formation, the corresponding averages were 1.30 and 1.27 per cent respectively. On another formation, the corresponding values were 10.01 and 9.40 per cent; on still another, 4.94 and 5.16 per cent.

If there is a question as to whether the volatility of a particular oil might give rise to incorrect saturations if vacuum is applied, the above technique of resaturation after extraction may be used. It is also used where there are a large number of surface vugs. In this case the extraction is carried out directly on the original sample. The extracted and dried sample is then sprayed with a webbing plastic material which bridges the gaps across the surface vugs. Additional plastic is applied until a coating is built up which is thick enough to prevent loss of water from the vugs but still permeable enough to permit the entrance of water when vacuum and pressure is applied. Actual experience has indicated that this method of applying a plastic coating is required in only a small percentage of cases.

In a check on six cores of 5⅜ in. diameter, an average porosity of 7.63 per cent was obtained after extraction and resaturation with a 25 per cent brine (for purposes of electrical resistivity measurements), as compared to an average of 7.93 per cent from the original Dean-Stark extraction, and an average of 8.03 per cent from a gas expansion method. The last mentioned method will not be described in detail in this paper, but in brief consisted of using a large size Hassler holder to seal over the surface of a faced sample, followed by measurement of pressure change as air or helium was admitted to the evacuated sample. The accuracy of this porosity method is felt to be good, but it has the disadvantage of requiring extra steps in the procedure, i.e., sawing the core and subsequent drying, and also the attainment of pressure equilibrium is slow if the core matrix has extremely low permeability.

It may be mentioned that one example was encountered where the Dean-Stark extraction method failed to remove the water completely. If the procedure is applied blindly one would in this case come out with an incorrect high oil content and a low water content. In the example noted the apparent oil content was 0.6 per cent of bulk volume, the water content 0.8 per cent, the total porosity 1.5 per cent. The formation was a dense dolomitic shale, of permeability less than 0.001 md. It was evident, however, both from the appearance of the sample and the fact that the gas content was almost zero, that the formation was so tight that it would not give up all its water under the conditions of the extraction. This serves to emphasize that each analysis must be treated as an individual problem and solved accordingly.

Permeability

It has been suggested that the use of the above mentioned clamp type permeameter may give rise to considerable error due to the end effect when dealing with fractured core samples, i.e., there may be a channel connected to one end of the core which carries a disproportionately large amount of air. It is not denied that this may occur in some instances, but it is believed that the errors will be in both directions and will tend to balance out when a large number of samples are measured.

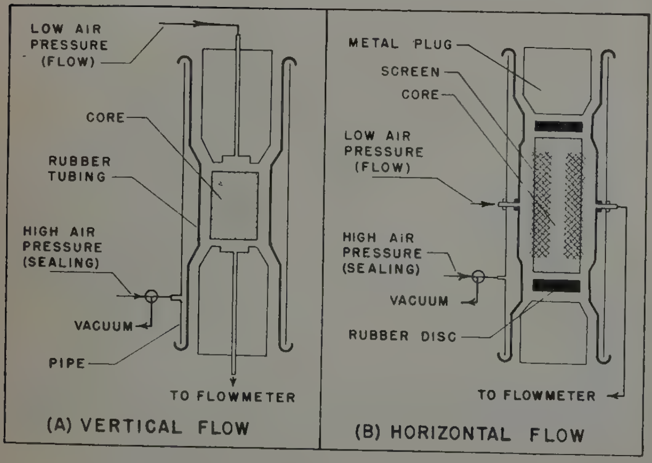

FIG. 6 — HASSLER TYPE PERMEAMETER SCHEMATIC.

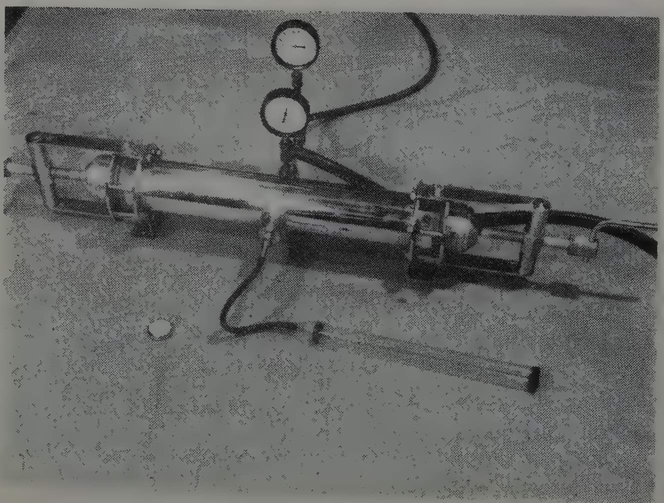

FIG. 7 — HASSLER TYPE PERMEAMETER.

The accuracy of any one measurement is not high, but the approximate magnitude of the "equivalent" permeability is at least indicated and the measured value does take into account the flow capacity of both the matrix and the fracture or vugular system. Measurements so far made on samples of intergranular porosity have shown reasonable agreement with permeabilities of drilled plugs from the samples.

A different type of permeameter has been devised, as shown in Figs. 6 and 7, not because it was felt that the open-end clamp type permeameter was not good, but to permit a different method of analysis which is described in the last part of this paper. Screens covering opposite sides of the core replace the rectangular gasket openings of the clamp type permeameter, and the remaining surface of the sample is sealed by rubber tubing and air pressure. This Hassler type permeameter may be used for both horizontal unidirectional permeabilities and vertical permeabilities on the same sample. It requires that the permeability sample be faced off on both ends with a diamond saw. The two sizes of this permeameter which have been built will accommodate core samples of diameter from 2¾ to 5⅜ in., and length from 2 to 20 in. Shape factor corrections have been determined by three-dimensional electrolytic model experiments simulating the controlling factors in the fluid flow, i.e., the ratios of screen length and width to core length and diameter. The accuracy of permeability determination with this apparatus is probably slightly better than that of the clamp type permeameter; however, the latter is believed to be adequate for the purposes to which it is applied, considering the erratic and capricious nature of the permeability of fractured systems.

Matrix Measurements

A technique which was used in certain instances consisted of making measurements of total porosity by extraction and resaturation, and measurements of porosity on a number of small pieces of the matrix, using the difference as an indication of the amount of secondary, or fracture and vug porosity. This method has been described by Atkinson and Johnston.[1] Further experimental data in this connection is presented below. It is felt that this method is useful but is limited to those cases where the matrix is quite dense and the secondary porosity well defined.

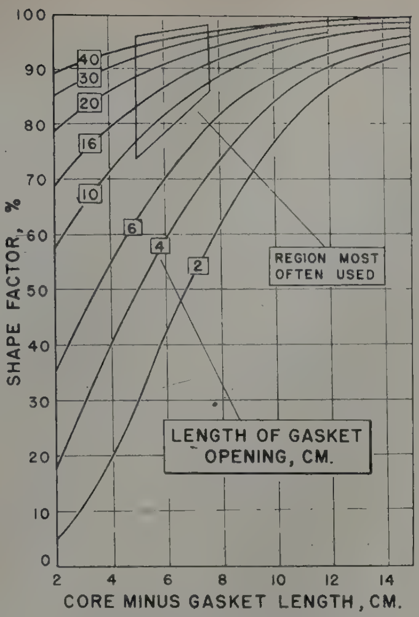

FIG. 8— SHAPE FACTOR

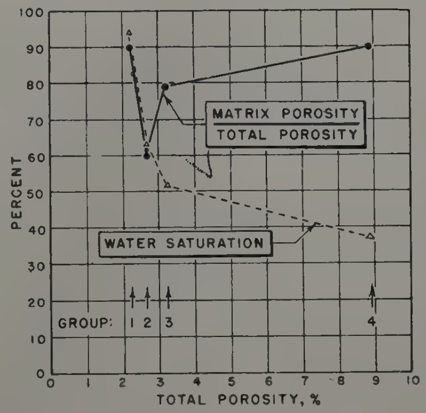

FIG. 9 — MATRIX POROSITY VS. WATER CONTENT.

ANALYSIS RESULTS FOR TYPICAL FORMATIONS

Matrix Measurements

After obtaining analysis results on large cores from a section of Ellenburger formation from the Fullerton field, additional measurements of matrix porosity and permeability were proposed in order to obtain a clear understanding of the relationships involved. Fortunately the available samples showed a rather wide variety of characteristics ranging from dense and finely fractured to spongy, vuggy formation. Accordingly, on the basis of the special analysis results only, four groups of samples were selected. Group 1 consisted of 14 samples with very low gas bulk (from 0 to 0.29 per cent) and low oil bulk (0 to 0.40 per cent). Group 2 contained 13 samples of intermediate gas bulk (0.41 to 1.52 per cent) and low oil bulk (0 to 0.16 per cent). Group 3 contained 15 samples of intermediate gas bulk (0.06 to 0.89 per cent) and intermediate oil bulk (0.17 to 2.10 per cent). Group 4 contained 7 samples of high gas bulk (1.43 to 5.63 per cent) and high oil bulk (1.05 to 2.40). In general, group 1 consisted of dense samples with limited fracture development, group 2 had somewhat larger fractures and some open vugs, group 3 showed more development of intergranular porosity, and group 4 samples were intergranular and/or highly vugular.

In Table I a summary is presented of average values of fluid contents, porosity and permeabilities by special analysis, and average values of porosity and permeability of matrix samples. The latter were small (¾ in. diameter) drilled plugs. Matrix porosity was determined by the vacuum-saturation method, but pressure was not used. Fig. 9 is a graphic comparison of the

Table I

Matrix vs. Whole Core Data, Ellenburger, Fullerton Field

Group		1	2	3	4
Gas,	% bulk	0.08	0.91	0.63	3.72
Oil,	% bulk	0.06	0.06	0.88	1.84
Water,	% bulk	2.07	1.65	1.66	3.27
	% pore	94	63	52	39
Matrix porosity,	% bulk	1.98	1.58	2.56	7.92
	% total pore	90	60	81	94
Total porosity,	% bulk	2.21	2.62	3.17	8.40
K_{max},	md	10	409	28	94
$K_{90°}$,	md	0.6	1.2	10	38
Matrix K,	md	0.3	0.2	0.3	3.7

averages of water saturation (as per cent of pore space) with the average ratio of matrix to total porosity, for the four groups.

Table 1 and Fig. 9 show agreement, considered good for the number of samples represented, between the water content for groups 1 and 2 and the matrix porosity. However, this agreement disappears for groups 3 and 4. This illustrates quantitatively what had been inferred, i.e., that matrix porosity measurements would be an approximation to the water content of the large cores, and hence useful in reserve estimates, only when the matrix is dense and representative pieces can be selected such that no small vugs or intergranular porosity is included.

The magnitudes and ratios of K_{max} and $K_{90°}$ in the different groups reflect the amount and distribution of secondary porosity between fractures and vugs.

Fig. 10 shows photographs of six core samples from the above groups together with the corresponding special core analysis data. Out of these, samples 50 and 96 are from group 1, sample 91 from group 2, samples 32 and 78 from group 3, and sample 29 from group 4.

Average Data for Several Formations

Table II presents a summary of special analysis data for three types of formation. Between 300 and 500 samples are included in each set of data. The group of samples listed as "low porosity fractured formation" consisted primarily of Ellenburger and Devonian. The "fractured limestone" group included relatively high porosity samples with considerable fracture and vug development. The "non-fractured dolomite" group was comprised of samples from three crystalline dolomite formations possessing negligible fracture development. It is of interest to note the average water saturations, 60.0, 45.8 and 41.8 per cent of pore space respectively. These decrease in the same order that the $K_{90°}$ values increase. It should be pointed out, if the average measured total water saturations seem high compared to the values usually associated with such formations, that these averages include values for the lowest porosity samples as well as the high porosity samples, and that no attempt was made to differentiate between "barren" and "productive" pay. The percentages of samples with K_{max} less than 0.1 millidarcys were 29 per cent, 5 per cent and 4 per cent for the three respective groups. The average oil saturations were, respectively, 16.6, 12.4 and 15.0 per cent of pore space. On the premise that the measured water content is equal to the connate water content, the calculated values of reservoir oil in place are, respectively, 73, 381 and 432 bbl per acre ft.

The maximum individual values of K_{max} in the three groups of samples of Table II are, respectively, 5,060, 27,400 and 970 millidarcys. These may be compared to the permeability values reported by Bulnes and Fitting[2] ranging up to 2,670,000 millidarcys and porosities up to 36.5 per cent, for ¾ in. test plugs cut from a cavernous limestone. The average values of K_{max} and $K_{90°}$ shown in Table II are quite respectable values, and their ratios reflect the degree of fracturing of the three groups of samples. It is probable that reducing sample size and length of flow in permeability measurements on fractured and vugular formations tends to cause a poorer permeability distribution as compared to larger samples. That is, in two series of permeability measurements on small samples and on large samples from the same formation, the measurements made on small samples would show more extremely high and more extremely low values than the measurements made on large samples.

The data on the fractured limestone of Table II are further split into groups according to porosity range, as shown in Table III. The two lowest porosity groups, 0 - 3, 3 - 6 per cent, are also divided into two subgroups according to whether K_{max} is less than or greater than 0.1 millidarcy. The regular trends in the oil, water and gas saturations as functions of porosity are pointed out. The water and oil saturations are plotted in Fig. 11 as "Field B," where they are compared with the corresponding water and oil saturations of a considerably lower porosity fractured Devonian formation, "Field A." It may be noted from Fig. 11 that the water saturation for the highest porosity group in Field B is practically the same as the water saturation for the next highest porosity group, in contrast to what one might expect from capillary considerations. This same effect has been noted in other cases; in some, the water saturation curve shows a decided minimum. This may be due to one of several physical causes. It may be a reflection of the connate water characteristics of the reservoir, caused by qualitative changes in the character of the pore space. Or it could be due to differences in relative permeability characteristics in the low and high porosity formation.

Table II

Summary of Average Data for Three Types of Formations

Formation:	Porosity	Water		Oil		K_{max}, md		$K_{90°}$, md	
	% Bulk	% Bulk	% Pore	% Bulk	% Pore	Aver.	Range	Aver.	Range
Low-porosity fractured formation	2.38	1.41	60	0.39	16	96	0-5060	7.8	0-756
Fractured limestone	9.05	4.14	46	1.12	12	106	0-27400	12	0-313
Non-fractured dolomite	8.72	3.65	42	1.31	15	42	0-970	19	0-857

Table III

Breakdown by Porosity Groups of Data on a Fractured Limestone

Porosity Range, %	0 - 3		3-6		6-10	10-15	>15
Permeability md	<0.1	>0.1	<0.1	>0.1	——	——	——
Number Samples	12	75	8	88	94	105	99
Porosity							
% Bulk	1.57	1.89	4.34	4.36	7.82	12.43	17.53
Oil							
% Pore	0.9	4.5	8.6	7.5	12.7	16.7	19.9
Water							
% Pore	85.1	73.9	59.7	55.0	42.4	30.5	29.7
Gas							
% Pore	14.0	21.6	31.7	37.5	44.9	52.8	50.4
K_{max}, md	0.04	11	0.05	133	335	28	28
Range	0.00- 0.10	0.13 228	0.00- 0.08	0.11- 9,680	0.08- 27,400	0.00- 334	3.01- 793
$K_{90°}$, md	0.03	3.33	0.02	11	10	16	18

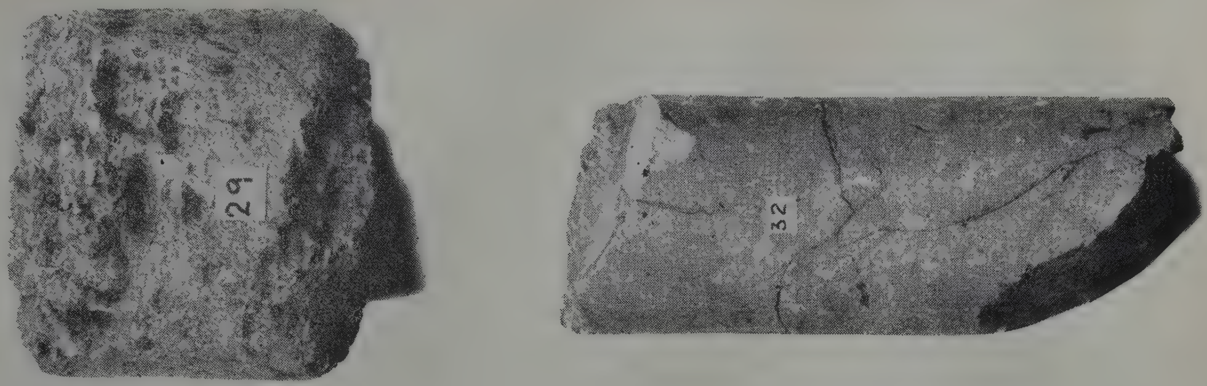

SAMPLE 29	
Porosity	8.66%
K_{max}	23 md
K_{90°	0.3 md
Gas	65%
Oil	21%
Water	14%

SAMPLE 32	
Porosity	1.60%
K_{max}	108 md
K_{90°	24 md
Gas	9%
Oil	36%
Water	55%

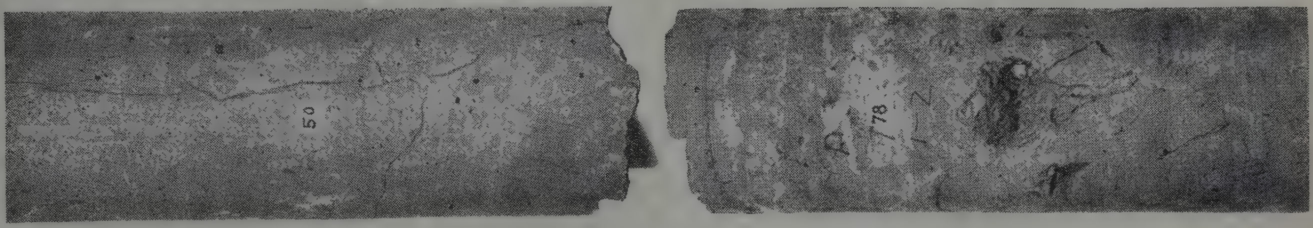

SAMPLE 50	
Porosity	2.02%
K_{max}	124 md
K_{90°	1.9 md
Gas	3%
Oil	0%
Water	97%

SAMPLE 78	
Porosity	4.17%
K_{max}	125 md
K_{90°	25 md
Gas	22%
Oil	11%
Water	67%

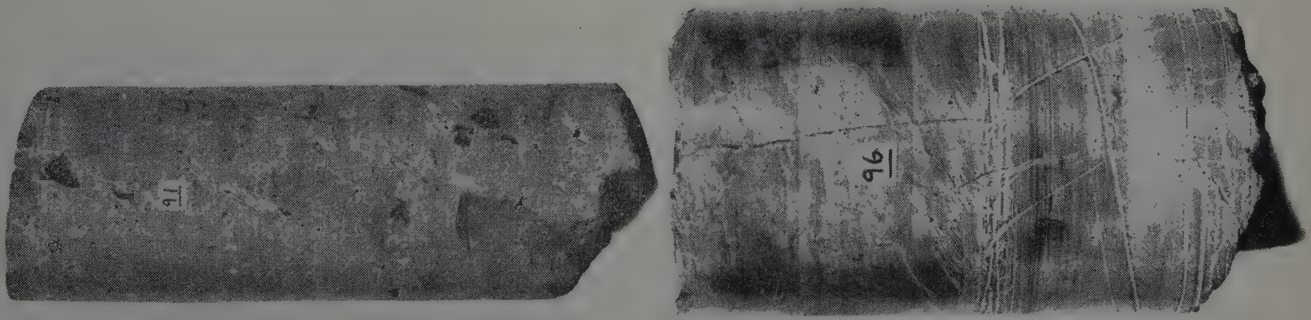

SAMPLE 91	
Porosity	2.87%
K_{max}	3.1 md
K_{90°	1.6 md
Gas	38%
Oil	3%
Water	59%

SAMPLE 96	
Porosity	2.00%
K_{max}	15 md
K_{90°	.006 md
Gas	17%
Oil	5%
Water	78%

FIG. 10 — DATA ON ELLENBURGER SAMPLES.

Flushing of pore space with water from the drilling mud may have occurred and subsequent expulsion of water by liberated gas as the core was raised to the surface may have resulted in a final water saturation higher than the original connate water saturation. However, another possible cause is a statistical phenomenon which is often overlooked, but is known definitely to be of appreciable effect. The water saturations are averaged in groups with porosity as the controlling parameter. Since there is not a one-to-one correspondence between individual values of porosity and saturation, the average saturation for the next to highest group includes some low values which correspond to the porosity group below it and some high values which correspond to the porosity group above it. The average saturation for the highest porosity group can draw upon some values corresponding to the porosity group below it, but none for a higher porosity group, therefore, the average saturation for this end group is higher than would be the case if there were a still higher porosity group present. Incidentally, it may be noted that if this statistical effect did not exist, the average values of K_{max} and $K_{90°}$ for the highest porosity group of Table III would be higher, and perhaps more consistent with the values from the adjacent group if the presumption is made that the permeabilities for the adjacent group are not greatly influenced by fracturing.

Fig. 12 shows the permeability averages by groups for the fractured limestone of Table III, as compared to the corresponding data for the non-fractured dolomite samples of Table II. The fractured limestone permeability averages exhibit a significant feature in that the greatest permeability ratios occur for the intermediate porosity groups 3-6 and 6-10 per cent, whereas for the inter-crystalline dolomite the trend is for both permeabilities to increase steadily with porosity, with a gradual decrease in the ratio between K_{max} and $K_{90°}$.

In concluding this section on typical core analysis data for fractured formations, it may be remarked that the interrelationships between the measured quantities appear very similar to those for sandstone or non-fractured reservoirs, but with certain differences in the magnitudes of the porosity and in the directional character of the permeability. If one considers the fractured reservoirs in terms of larger volumetric units, the differences in reservoir behavior between these and sandstone reservoirs become a matter of degree, not of kind. It would appear that the core analysis of fractured reservoirs, once considered an impossibility, is now well on the way to becoming a useful tool in reservoir engineering. Continued study based in part on this tool should in time contribute materially to our understanding and evaluation of such reservoirs.

COMPARISON OF SPECIAL VS. CONVENTIONAL CORE ANALYSIS

The comparison betwen special and conventional analysis which is discussed here is not concerned with obvious differences which arise from the failure of conventional analysis to properly take into account the effect of fractures or large vugs, but rather with the basic differences due to the respective methods applied to formation which should lend itself to analysis by either method.

A portion of each sample used for special analysis was set aside and run by conventional methods of analysis. A total of 296 samples were run by each method. These samples were from three different reservoirs of crystalline dolomite. The extent of fracturing was

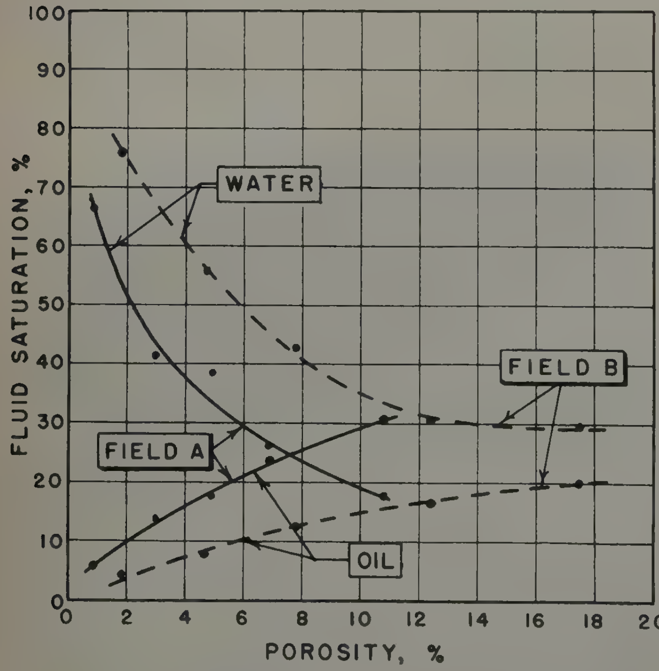

FIG. 11 — SATURATIONS VS. POROSITY FOR TWO FRACTURED FORMATIONS.

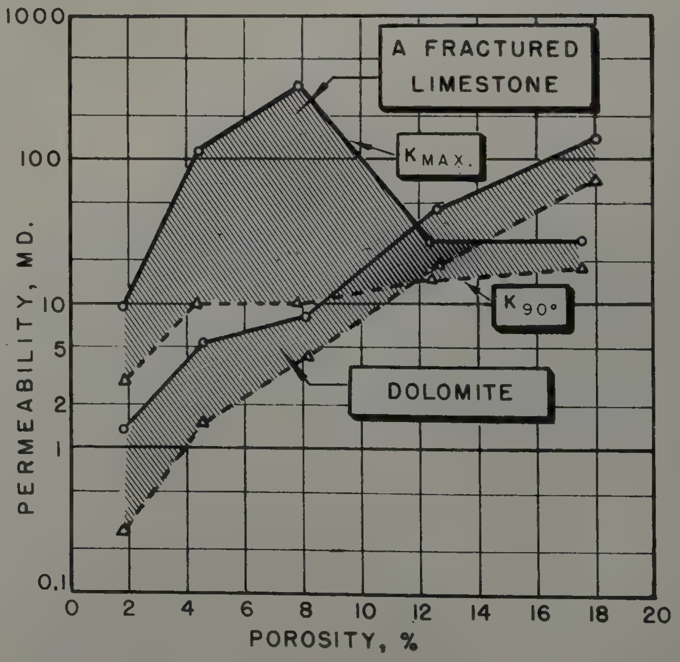

FIG. 12 — PERMEABILITY VS. POROSITY.

Table IV
Comparison of Special and Conventional Analysis

Dolomite	Special Analysis	Conventional Analysis
Porosity		
% Bulk	8.7	9.6
Oil		
% Bulk	1.3	1.2
Water		
% Bulk	3.7	2.2
Gas		
% Bulk	3.7	6.2
K_{max}		
md	42.1	26.9
$K_{90°}$		
md	18.9	26.9

so slight that it can be neglected insofar as its effect on porosity and fluid saturations is concerned, although possibly not in regard to permeability. The resultant average values for porosity, oil, water and gas bulk, and K_{max}, $K_{90°}$ and conventional permeability, are shown in Table IV.

In the conventional analysis, a 180 gram sample of formation was retorted to arrive at water and oil content. Corrections were applied which had proved applicable to sandstone and presumably to higher porosity lime and dolomite. The gas bulk was measured on a separate 20-40 gram sample by injecting mercury at 750 psi presure into the gas-filled pore space, with corrections for the compressibility of mercury and its closer conformation to the chamber walls as pressure is applied. Porosity was calculated as the sum of the oil, water and gas bulk. Permeability was measured on a drilled plug from ¾ to 1¼ in. in diameter.

Referring to Table IV, it is noted that porosity by special analysis is 9 per cent lower than porosity by conventional analysis. The oil contents by the two methods checked closely, 1.3 per cent of bulk volume by special as against 1.2 per cent by conventional analysis. The difference in porosity is seen to be due to the combined effect of a higher water bulk by special analysis and a higher gas bulk by conventional analysis.

To realize the reasons for these differences it is necessary to go back to the original data and to study critically the individual steps of the methods and calculations. In the special analysis there is evidence (e.g., weight of core saturated with toluene) that in some cases the measured gas content is slightly low. In the oil content determination there are sources of possible error which, however, tend to compensate each other except in extreme cases which can usually be anticipated. Incomplete extraction of oil by the toluene results in low measured oil content, whereas incomplete removal of water gives high measured oil content. In general, the measurement of water content of the sample is considered quite accurate.

In the conventional analysis the water content is appreciably lower than by special analysis, and there is reason to believe that more time should be allowed for distillation of water from the sample. By taking the final water reading in the retorting instead of an intermediate water reading, the water bulk for the data of Table IV would be increased from 2.2 to approximately 3.3. The water is read at an intermediate time in the case of sandstone samples in order to allow for combined water or water of crystallization, but apparently in the case of dolomitic formation the water is held in the fine capillaries in free rather than in combined form, and the reason the water is slow in coming over during the distillation is that the permeability of the matrix is so low.

The high measured gas bulk in conventional analysis seems to be the most important source of discrepancy. It should be realized that in the low porosity material involved we are stretching the limits of accuracy of this measurement. The reason for the high gas bulk probably lies largely in the fact that there is a surface effect and that the mercury conforms more closely to the grains when pressure is applied. This effect causes a greater percentage error when the total pore space is low. It is not believed that measurement of total porosity by the Washburn-Bunting method would appreciably increase the accuracy since in this method there is an error from absorption of air on the pore surfaces, and this error would be appreciable due to the number of fine capillaries and the large surface area. It is possible that a helium porosimeter would work satisfactorily. At any rate, investigation is being made as to ways to reduce the error in the gas bulk measurement of conventional analysis, and also to choose suitable retorting conditions to improve the accuracy of the water measurement.

In summary, it is believed that the special analysis methods give somewhat more accurate fluid saturation and porosity values than conventional analysis, even on non-fractured formation. The special analysis may possibly tend to give slightly conservative values for reservoir oil in place. Conventional analysis on low-porosity formation which does not have fractures or large vugs has in the past probably given values for reservoir oil in place which are too high, but there is reason to believe that improvements in accuracy can be made here.

Individual foot-by-foot interpretations should not be made from special analysis data since examination reveals very poor correlation between porosity, fluid saturations and permeability of individual samples when fracturing or solution cavities are present. However, statistical examination of the overall data on a given reservoir does reveal relationships which should be useful in reservoir studies and reserve estimates. The need for analysis of all of the productive horizon is even more apparent than in the case of sand reservoirs.

POSSIBLE MODIFICATIONS OF SPECIAL ANALYSIS METHODS

A major limitation of the special analysis technique heretofore described is its slowness. This is a consequence of the size of the samples and the time required for complete extraction. Due to this long extraction time, even a large and expensive laboratory installation is limited in the number of samples it can turn out per day. The slowness of extraction is not the entire reason, of course, since the process involves a large number of separate time-consuming steps on which detailed and careful records must be kept. In order to obtain core analysis data of more immediate use for completion purposes, it would be highly advantageous to have a faster method.

It has been observed that some operators have insisted that special analysis rather than conventional analysis be made in cases where the fracture or vugular development of the formation was minor. Since in the past the analysis of small amounts of core had proved inadequate for all cases, this was probably a natural reaction or swing to the other extreme. However, for a good many formations, statistical considerations show that conventional analysis will be adequate, and should be chosen where quickness of results are important.

One compromise which should prove applicable in many cases would be to run conventional analysis except for permeabilities which would be run on the large cores as needed. This would be particularly suited to cores which are in part fractured and whose porosity is of the intergranular type or shows only small to medium size vugs. The contribution of fractures to the total porosity will in general be quite small.

For those formations on which special analysis is specifically required, three alternative modifications are proposed in order to shorten the time required to complete the analysis. These are as follows:

1. On those reservoirs where the oil section is known or can be determined by examination under ultraviolet light, it is proposed to saturate the samples as before, and then combine, say, 100 ft of contiguous cores in one large-scale Dean-Stark extraction apparatus. In this way the total water content and the total oil content is determined for the combined group of samples which represents all of the core available and individual measurements of porosity and permeability are made on the separate samples. The composite oil and water content of each 100-ft section can be used to establish reserves, and should be as useful as individual values since for this purpose the individual values would have to be combined anyway.
2. It is proposed to take 6 to 9-in. specimens of core for extraction, face them off, and determine permeability using the Hassler type permeameter shown in Figs. 6 and 7. In this apparatus vertical as well as two horizontal permeabilities can be measured. Adjacent 9 to 12-in. specimens of core can be taken for determinations of porosity and fluid content. For this purpose the core will be crushed by a rock crusher to the size of walnuts or smaller. Preliminary tests indicate that the extraction will be complete in 1 to 2 days by this procedure. The total analysis time will of course not be shortened a comparable amount since we are actually adding additional steps of cutting, crushing, handling and calculating; however, the statistical average characteristics of the formation should be affected only to a very small extent by thus using ½ to ⅔ of the sample size that has been previously used in special analysis.
3. Other entirely different methods of analysis are possible, such as vacuum distillation, which shows possibilities of being made into a fast and acurate method.

It is believed that the above described procedures can be developed to be as accurate as the methods of special analysis originally used and described in this paper. It is hoped they will be used to speed the accumulation of reservoir data on the increasingly important class of fractured and vugular reservoirs.

ACKNOWLEDGMENT

Acknowledgment is made to the companies who have kindly given permission to use their data herein, and to H. W. Brennan, Jr., Lloyd N. Johnson and W. R. Bailey who have assisted in the preparation of this paper.

REFERENCES

1. Burton Atkinson and David Johnston: "Core Analysis of Fractured Dolomite in the Permian Basin," AIME *Petr. Tech.*, TP 2432, Sept. 1948.
2. A. C. Bulnes and R. U. Fitting, Jr.: "An Introductory Discussion of the Reservoir Performance of Limestone Formations," AIME *Petr. Tech.*, TP 1791, January, 1945.

★ ★ ★

T.P. 2848

VAPOR-LIQUID EQUILIBRIUM DATA ON THE SYSTEM NATURAL GAS-WATER-TRIETHYLENE GLYCOL AT VARIOUS TEMPERATURES AND PRESSURES

JOE A. PORTER,* BLACK, SIVALLS AND BRYSON, INC., KANSAS CITY, MO., AND **LAURANCE S. REID,**

UNIVERSITY OF OKLAHOMA, NORMAN, OKLA., MEMBER AIME

Gas dehydration plays an important part in the production of natural gas. Effective dehydration prevents formation of gas hydrates and the accumulation of water in transmission systems,[2,6,7] insuring uninterrupted gas deliveries at maximum efficiency under the most adverse weather conditions. At the present time, most gas companies require a maximum water vapor content of seven lb per million standard cu ft of gas, so that virtually all gas tendered for sale must be dehydrated to meet this specification.

For a number of years it has been common practice to produce gas and gather it at a common point for dehydration prior to discharge into the transmission system.[1,3,11,16,17] However, higher transmission line pressures, long gathering lines and relatively low ground temperatures have made it necessary to dehydrate gas at, or near, individual wells in order to gather gas from a number of newly developed fields without unusual difficulty. Where gas has been dehydrated at pressures ranging from 300 to 800 psi in the past, future trends indicate that these processes may be operated at pressures as high as 2,000 psi.

Economics of gas dehydration are of great importance, particularly where facilities must be provided to process relatively small quantities of gas, such as the production from an individual well. Although the adsorption of water vapor from gas on a granular sorbent material such as activated bauxite, activated alumina, or one of the alumina-silica gels is highly effective and produces virtually "bone dry" gas, the cost of a small unit of this type is substantially greater than that of an absorption process which, through proper selection of the absorbing liquid, will dehydrate the gas sufficiently to meet pipe line specifications. For this reason, a great deal of emphasis has been placed on the development of small, inexpensive dehydration units[8,24] and the search for more effective absorbent liquids has been intensified.

A wide variety of methods for dehydrating gas are known[2] and many of these have been used in industry. Earlier applications of the absorption process employed concentrated solutions of calcium and lithium chlorides as the absorbent. The severe corrosion problems inherent in handling these solutions and the relatively small dew point depressions obtained caused early abandonment in favor of, or conversion to, diethylene glycol when it was found that aqueous solutions of this organic liquid were more hygroscopic than the brines and were noncorrosive. Processes employing diethylene glycol-water solutions are widely used for gas dehydration at pressures ranging as high as 1,200 psi.[13,14,15] At nominal pressures a dew point depression of 45° to 50°F may be obtained and the data of Russell et al.[14] indicate that a minimum dew point is obtained from the effluent gas at a pressure of approximately 1,200 psi when the gas is in equilibrium contact with a 95 per cent by weight diethylene glycol solution. In a number of instances the dew point depression obtained with diethylene glycol-water solutions is not sufficient to produce a specification product without cooling the inlet gas. In a recent search for a better absorbent, triethylene glycol was used in a small commercial dehydration unit and subjected to rather exhaustive field tests.[8] The data obtained were encouraging and indicated that, at pressures ranging from 300 to 500 psi, triethylene glycol produced a substantially greater dew point depression than diethylene glycol. These results led to an investigation of the system natural gas-water-triethylene glycol in an effort to obtain vapor-liquid equilibrium data, to determine pressure limitations, and to develop other data pertinent to the design of gas dehydration processes.

A review of the literature has failed to reveal any data which permit reasonably accurate calculation of the vapor-liquid equilibrium conditions for a solution of water and triethylene glycol in contact with natural gas at high pressure. Since these constituents form a non-ideal system, the Poynting equation[18,21] or the usual combination of Raoult's and Dalton's laws[19,20,22] would not be valid. Correction of Raoult's and Dalton's laws by the use of activity coefficients[21] is not feasible for available data are insufficient for the prediction of the actual increase in the ratio of the activity of one component in the vapor phase to its activity in the liquid. Therefore, experi-

---

[1] References are given at end of paper.

Manuscript received at the office of the Petroleum Branch September 27, 1949: Paper presented at the Branch Fall Meeting in San Antonio, Texas, October 5-7, 1949.

*American Gas Association Supply Men's Research Fellow in Chemical Engineering at the University of Oklahoma. This paper is a condensation of a thesis submitted by J. A. Porter in partial fulfillment of the requirements for the M.Ch.E. degree, conferred by the University of Oklahoma in August, 1949.

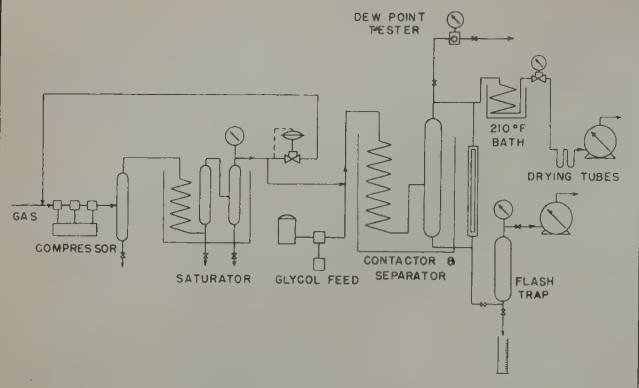

FLOW DIAGRAM OF APPARATUS

FIG. 1

mental equilibrium data were observed in the laboratory, using 95 per cent by weight triethylene glycol, 5 per cent water solution in contact with a relatively nitrogen-free natural gas at pressures ranging from 500 to 2,000 psig and at temperatures ranging from 60° to 100°F.

APPARATUS

The experimental apparatus used in this investigation is shown in Fig. 1 and is, essentially, a duplicate of the continuous flow system used by Russell[13] to investigate the system natural-gas-water diethylene glycol. In this system, the natural gas was compressed to the desired pressure by a three-stage Rix compressor and passed through a coil in a constant temperature bath to a saturator where the moisture content of the gas was adjusted to the desired level. Saturated gas from this vessel then passed through a gas scrubber where any entrained water was separated and removed from the gas. Saturation conditions were checked by dew point measurement of the gas at a point immediately downstream from this scrubber.[9]

A measured quantity of saturated gas was then passed to a second constant temperature bath containing the gas-liquid contactor and a separator. A measured quantity of 95 per cent triethylene glycol solution was pumped into the contactor coil by means of a gas-powered plunger pump so that the gas and glycol solution flowed concurrently in intimate equilibrium contact to the separator, where the two phases were separated and removed from the system.

The effluent gas stream was split, with one portion passing through a U. S. Bureau of Mines Dew Point Tester maintained at system pressure, thence to a pressure-reducing regulator prior to measurement at atmospheric pressure in a wet test meter. The second portion was passed to a second pressure-reducing regulator, thence to a train of drying tubes filled with anhydrous magnesium perchlorate where water and glycol vapors were adsorbed prior to measuring the gas in a second wet test meter. Gas from both meters was then vented to atmosphere.

The glycol solution was withdrawn from the separator at a constant rate in order to maintain a uniform level in that vessel. A portion of this solution was accumulated under pressure in a separate vessel, equipped with a high-pressure reflex liquid level gauge glass, where the solubility of gas in the glycol solution was determined at the end of each run.

Accessory apparatus included a special viscosimeter used to determine the glycol concentration of all solutions used in this investigation.[10]

EXPERIMENTAL MATERIALS AND TECHNIQUES

The natural gas used in this investigation was obtained from the mains of the Oklahoma Natural Gas Co. at Norman, Okla. A representative analysis of this gas is shown in Table I.

The triethylene glycol used was a technical grade obtained from the Carbide and Carbon Chemicals Division of Union Carbide and Carbon Corp. Physical constants and other data pertaining to this glycol are shown in Table II. The glycol was blended with distilled water to the desired concentration of 95 per cent by weight glycol and 5 per cent by weight water.

A specific operating procedure was used throughout the investigation which was developed from preliminary experiments. In pressuring the apparatus, the saturator was bypassed to prevent condensation of moisture in the system. When system pressure reached 200 psig, glycol injection was started. After the desired operating pressure was attained, the gas was turned through the saturator and the gas flow to the contactor was adjusted to a rate of six standard cu ft of gas per hour. The glycol injection rate was adjusted to 60 gal per Mcf of gas. These rates, and the established temperatures and pressures, were maintained constant throughout the run. After operating conditions were established, the system was operated for one hour before any samples were drawn for analysis or effluent gas dew points observed. At the end of this preliminary period, an inlet gas dew point was observed to start the run and the drying tube train was connected into the proper effluent gas stream. A total volume of approximately 20 standard cu ft of gas was passed through the drying tubes in order to minimize error. The weight of the glycol vapor in the effluent gas stream was obtained by difference, calculated from the pounds of water and glycol adsorbed from one cu ft of gas passing through the drying tubes, minus the pounds of water vapor per cu ft of gas as determined by dew point measurement in conjunction with the water vapor content correlation by McCarthy et al.[9] Prior to use, the adsorbent used in the drying tubes was saturated with hydrocarbons by passing dehydrated gas through the train, thus insuring that only glycol and water vapors would be adsorbed during the investigation.

Dew points of inlet and effluent gas were determined by means of a U. S. Bureau of Mines Dew Point Tester, using liquid propane as the refrigerant. Preliminary investigation of the effect of glycol vapors on the dew point of gases treated with triethylene glycol failed to reveal errors of the magnitude predicted by Reisenfeld and Frazier[12] so that the dew point method was accepted as adequate. It is interesting

Table I
Analysis of Natural Gas

Component	Gas Volume % or Mol %
Carbon Dioxide	0.70
Nitrogen	1.95
Methane	82.52
Ethane	8.20
Propane	3.67
Butanes	1.86
Pentanes	0.72
Hexanes	0.19
Heptanes and Heavier	0.19
	100.00

Specific Gravity (Re: Air = 1.000): 0.6932

Table II

Some Physical Constants and Properties of Triethylene Glycol[23]

Structural Formula	$HO\text{-}CH_2\text{-}CH_2\text{-}O\text{-}CH_2\text{-}CH_2\text{-}O\text{-}CH_2\text{-}CH_2\text{-}OH$
Molecular Weight	150.17
Specific Gravity at 20°/20°C	1.1254
Boiling Point at 760 mm Hg.	287.4°C
Decomposition Temperature[5]	206.5°C
Solubility in Water	Completely miscible in all proportions

to note that the dew points obtained were sharp and unmistakable; wholly unlike the results of similar determinations on gases treated with diethylene glycol solutions. This is probably due to the fact that triethylene glycol exhibits approximately 15 per cent of the vapor pressure of diethylene glycol at the temperatures employed.

The water concentration of the glycol solution was determined using an adaptation[10] of the method proposed by Fried, Bigg and Jennings.[4] This method is based on the fact that the viscosity of a glycol-water solution is directly related to the glycol concentration. The specially constructed apparatus was calibrated at a constant temperature of 30°C using solutions of known concentrations prepared from a sample of 100 per cent triethylene glycol supplied by the Carbide and Carbon Chemicals Division of Union Carbide and Carbon Corp.

All glycol solution used in this investigation was collected, analyzed and re-blended to 95 per cent glycol concentration by adding fresh glycol. Fresh solution requirements were small due to the fact that the glycol-gas circulation rate was so great that, even at 500 psig pressure and 100°F, the solution was diluted to but 94.0 per cent by weight glycol. At higher pressures and lower temperatures, the dilution was of the general order of magnitude of one to two-tenths of one per cent so that the equilibrium data obtained were, substantially, for 95 per cent glycol concentrations throughout the investigation.

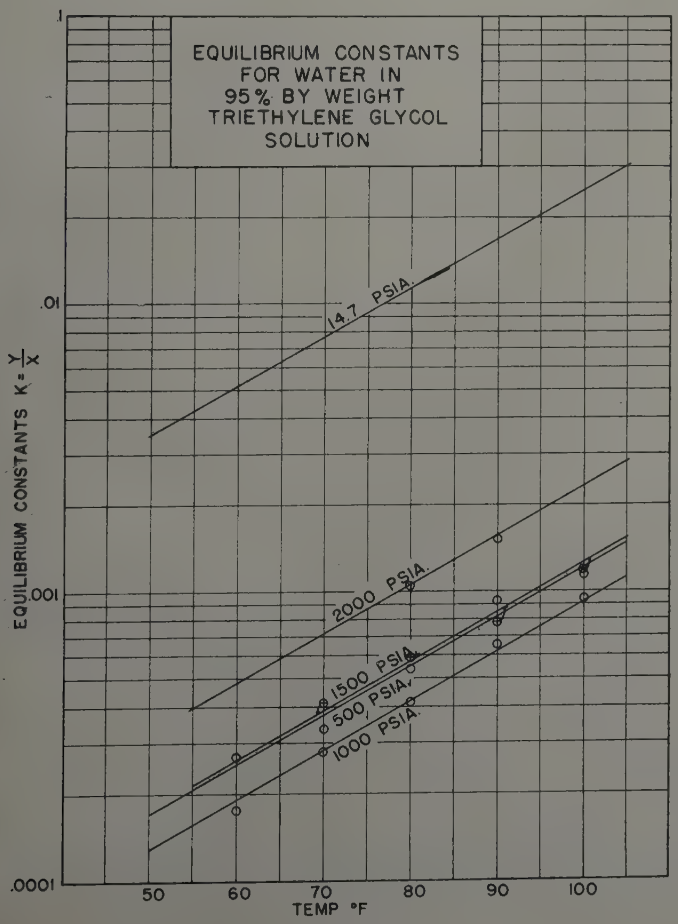

FIG. 2

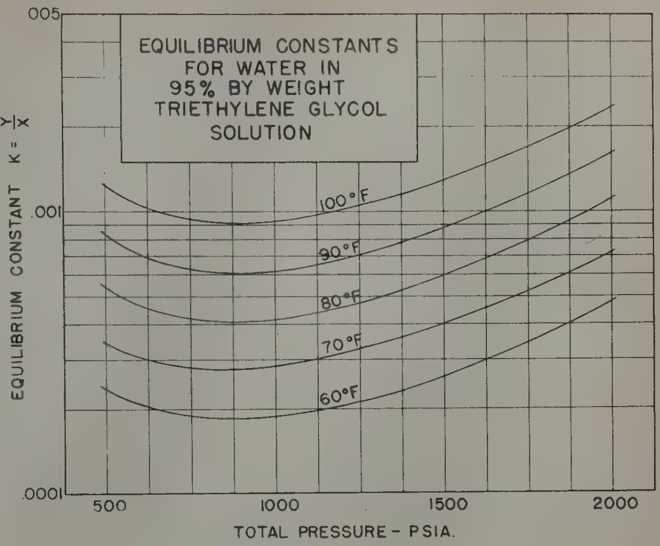

FIG. 3

Solubility of gas in glycol solution was determined by liberating the gas evolved from solution differentially and measuring it by means of a wet test meter. The gas was liberated at a very low rate so that the process was substantially isothermal. The volume of the residual glycol solution was measured in a standard 1,000 ml graduated cylinder.

Accuracy of the data obtained in this investigation is considered to be quite satisfactory. Dew point measurements were reproducible to 2°F. Determination of the glycol concentration of the various solutions was accurate to 0.1 per cent, and check determinations on gas solubility in glycol solutions varied from 3 to 5 per cent. The method employed for the determination of glycol concentration in the effluent gas proved unsatisfactory, particularly at pressures exceeding 1,000 psig and at the lower temperatures employed, due to the fact that it depended on a small weight differential between two relatively large weights. As this weight differential became progressively smaller the error became larger.

DISCUSSION OF RESULTS

The data obtained from this investigation are shown in graphical form for sake of brevity. Fig. 2 is a semi-logarithmic plot of the equilibrium constants for water, calculated from the observed data, versus temperature using pressure as the parameter. The curve for atmospheric pressure was calculated from published equilibrium data.[23] The best straight line has been drawn through the experimental data points for each higher pressure, parallel to the atmospheric isobar. From this plot the equilibrium constant for water may be obtained at intermediate temperatures. Fig. 3 is a cross-plot of Fig. 2, where the equilibrium constants for water are plotted versus system pressure with temperature the parameter. This plot indicates that, over the temperature range investigated, a mini-

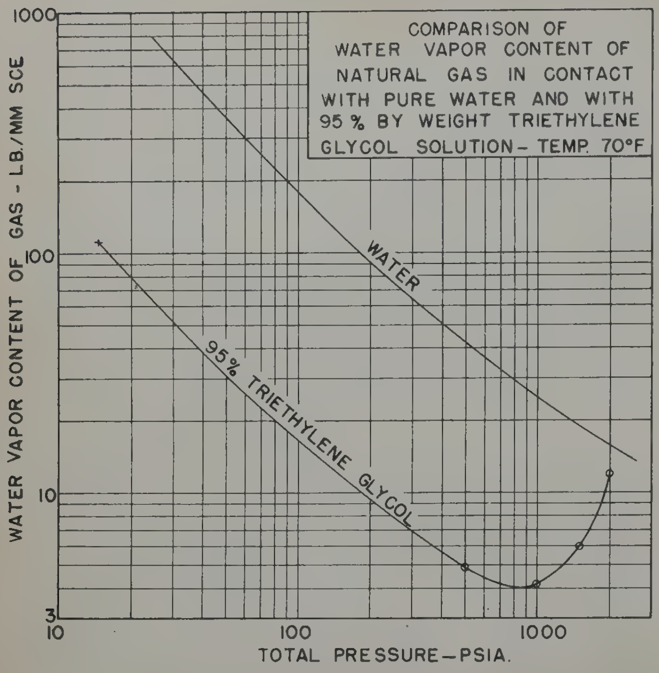

FIG. 4

mum value of K is found at a pressure of approximately 900 psia.

Figs. 4, 5 and 6 show graphical comparisons of the water vapor content of natural gas in equilibrium contact with (a) pure water, and (b) 95 per cent by weight triethylene glycol-water solution at temperatures of 70°, 80° and 90°F, respectively. It is of interest to note that the water vapor content of the gas in equilibrium contact with the glycol solution passes through a minimum in the pressure range 800 to 1,000 psia. An extrapolation of the glycol curve indicates a retrograde phenomenon at pressures exceeding 2,000 psia wherein water is stripped from the glycol solution by the gas. This indicated behavior has been verified by laboratory experiments conducted since this investigation was concluded. It is postulated that the pressure at which the two curves intersect would be increased by use of more highly concentrated glycol solutions.

If the gas entering the absorber is saturated with water vapor at the contact temperature, then the dewpoint depression is obtained by subtracting the dew point temperature of the effluent gas from the contact temperature. Dew point depressions for inlet saturation temperatures of 70°, 80° and 90°F may be determined from the data of Figs. 4, 5, and 6, respectively. However, dew point depression is plotted versus pressure for a constant inlet temperature of 80°F in Fig. 7. Inspection of the data of Figs. 4, 5, and 6 and similar data for temperatures of 60° and 100°F, not shown, indicates that there is virtually no difference in dew point depression resulting from varying the contact temperature from 60° to 100°F, indicating that the dew point of the effluent gas is a function of the inlet temperature and the system pressure. Fig. 7 shows that the maximum dew point depression is practically constant at pressures ranging from atmospheric to 500 psia where the differential temperature is approximately 60°F. At higher pressures, this differential temperature declines quite rapidly.

Data obtained showing the concentration of triethylene glycol in the effluent gas are presented in Table III. These data were found to be inconclusive at higher pressures and lower temperatures, because of the analytical method employed, but they are presented here to indicate the probable magnitude of the glycol vapor losses attending gas dehydration under comparable conditions. Further investigation of this phase of the problem is now under way, employing a modification of the analytical method used by Russell.[13]

The solubility of natural gas in 95 per cent by weight triethylene glycol-water solution at a temperature of 80°F and various pressures is shown in Fig. 8. These data are based on the volume of the residual solution measured after the gas was liberated. Solubility data observed at other temperatures employed in this investigation were in very close agreement

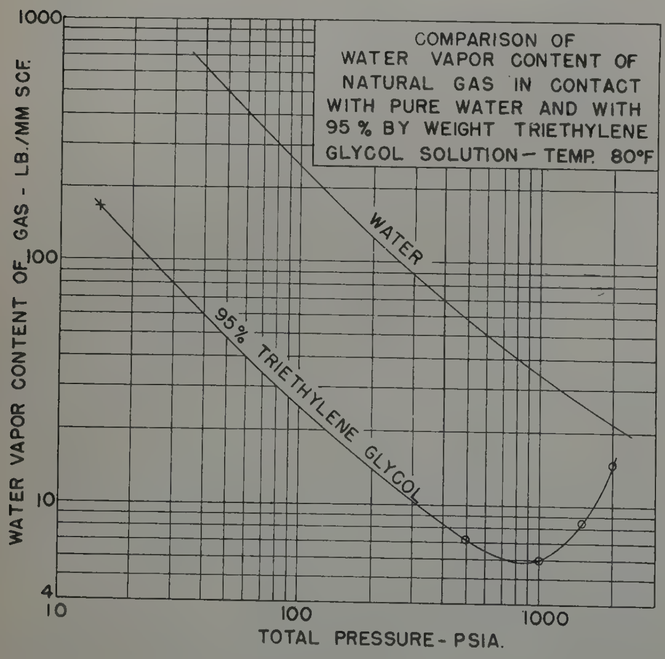

FIG. 5

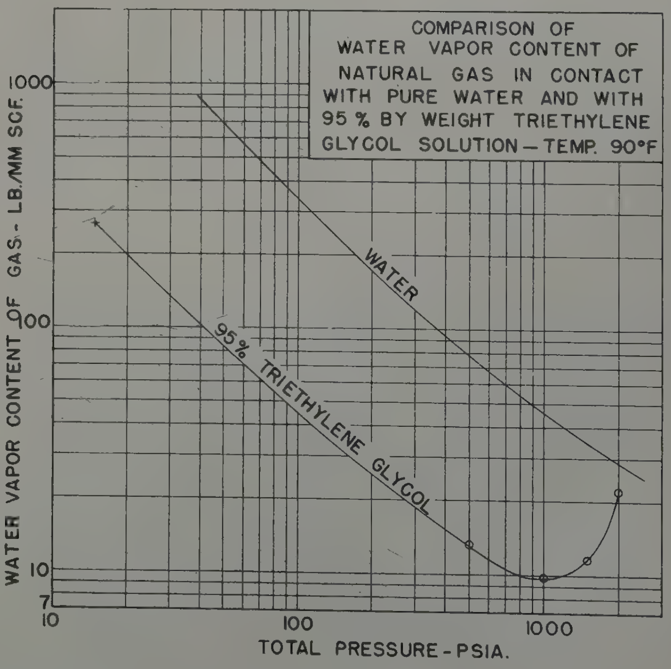

FIG. 6

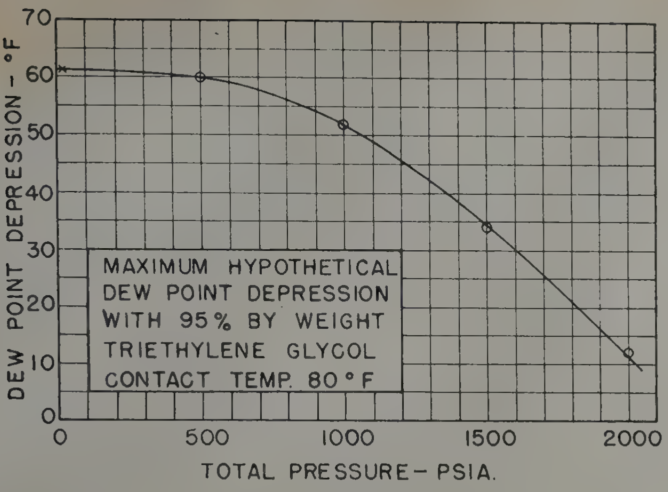

FIG. 7

with the data of Fig. 8 so that this curve properly represents the solubility of gas in 95 per cent triethylene glycol solution at temperatures ranging from 60° to 100°F.

A comparison of some of the physical properties of triethylene glycol and diethylene glycol[23] suggests that the former is probably better suited for natural gas dehydration service. In the atmospheric temperature range, the vapor pressure of triethylene glycol is approximately 15 per cent of the vapor pressure of diethylene glycol, indicating that vaporization losses from atmospheric storage would be lower if triethylene glycol were used. Although the boiling points of the pure substances vary appreciably, 549°F for triethylene glycol versus 473°F for diethylene glycol, the aqueous solutions exhibit virtually identical boiling points in the range 95-98 per cent by weight glycol. However, the extent to which these solutions may be concentrated by application of heat at atmospheric pressure is limited by decomposition temperatures.

Table III

Equilibrium Concentrations of Triethylene Glycol in the Vapor Phase at Various Pressures and Temperatures

Temperature °F	Lb of Glycol per MMSCF Gas
At 500 psia:	
60	2.71
70	0.52
80	0.21
90	0.35
100	1.75
At 1,000 psia:	
60	1.68
70	0.65
80	0.50
90	——
100	——

Diethylene glycol has a decomposition temperature of 328.1°F[5] so that the maximum concentration attainable without deterioration due to progressive decomposition is slightly less than 97 per cent. On the other hand, triethylene glycol has a decomposition temperature of 403.7°F[5] which permits concentration of the solution to approximately 99 per cent by weight. In view of the fact that dew point depression is a function of glycol concentration under equilibrium conditions,[23] it follows that triethylene glycol can be used with greater effectiveness at operating pressures ranging upward to 1,100 psig.

CONCLUSIONS

The results of this investigation may be summarized as follows:

1. Sufficient experimental vapor-liquid equilibrium data have been obtained on the system natural gas-water-triethylene

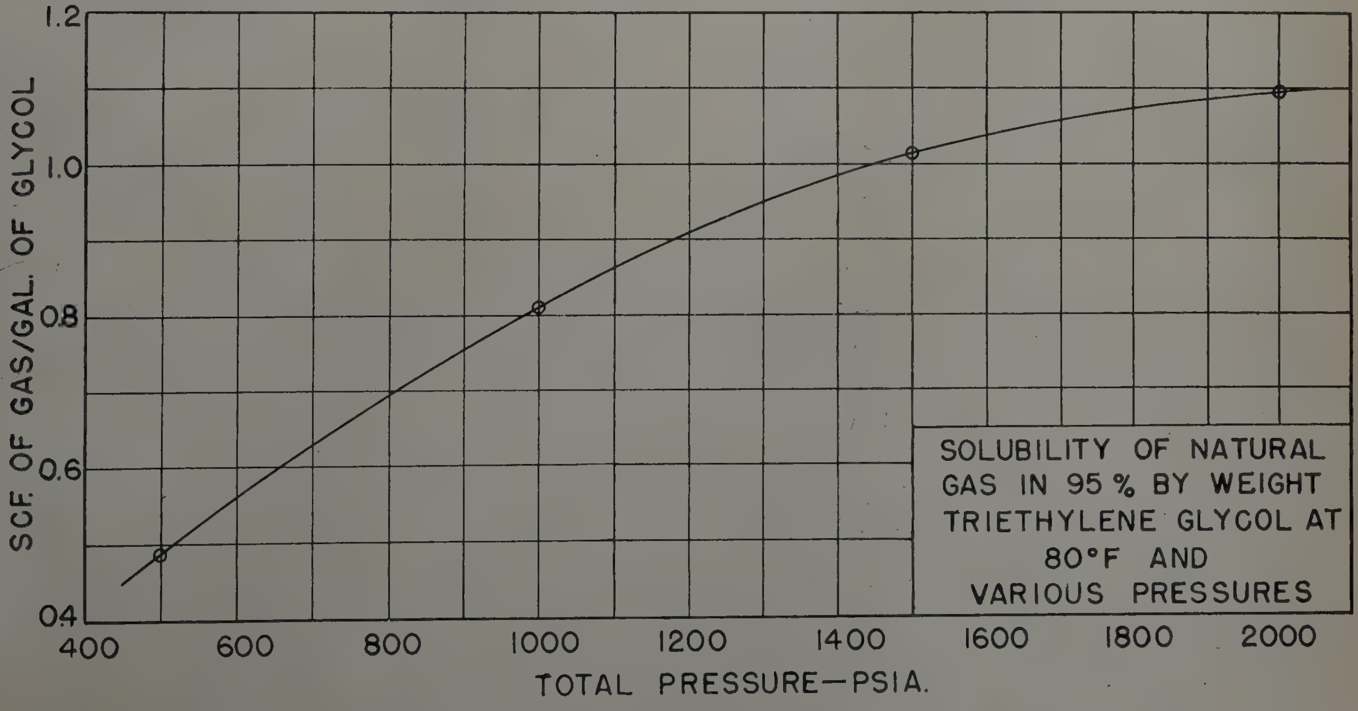

FIG. 8

glycol to permit design of gas dehydration facilities operating at temperatures ranging from 60° to 100°F and at pressures ranging from atmospheric to 2,000 psig.

2. Equilibrium dew point depression in a triethylene glycol dehydration system operating at a specific pressure is a function of the contact temperature alone, over the range of temperatures investigated.
3. The solubility of natural gas in a 95 per cent by weight triethylene glycol-water solution varies with pressure, but it is not a linear function of pressure. Variation in temperature has a negligible effect on gas solubility within the temperature range investigated.
4. The practical pressure limit for natural gas dehydration processes employing 95 per cent by weight triethylene glycol-water solutions is approximately 1,500 psig. The dew point depression diminishes rapidly at pressures greater than 1,000 psig.
5. At pressures as high as 1,100 psig, 95 per cent by weight triethylene glycol-water solution effects a greater dew point depression than a diethylene glycol-water solution of the same concentration.
6. Triethylene glycol has a lower vapor pressure and greater thermal stability than diethylene glycol.

ACKNOWLEDGMENTS

This research was supported by a research fellowship established in the School of Chemical Engineering at the University of Oklahoma by the American Gas Association Supply Men. The assistance provided by this grant is gratefully acknowledged.

Special thanks are due the Carbide and Carbon Chemicals Division of Union Carbide and Carbon Corp. for providing a sample of pure triethylene glycol and pertinent viscosity data, and to Black, Sivalls and Bryson, Inc., for donating the high-pressure glycol pump used in this investigation.

REFERENCES

1. T. S. Bacon, *Gas Age*, 89, 11, 17-20 (May 21, 1942).
2. W. M. Deaton and E. M. Frost, Jr., *Monograph 8*, U. S. Bureau of Mines, 1948.
3. W. F. Fulton, *Am. Gas Assn. Bull.*, "Symposium on Long Distance Transmission of Natural Gas," pp. 26-34, AGA Natural Gas Dept., 1944.
4. S. Fried, E. Bigg and E. H. Jennings, *Science*, **98**, 479-80 (1943).
5. A. F. Gallaugher and H. Hibbert, *J. Am. Chem. Soc.*, **59**, 2521-5 (1937).
6. E. G. Hammerschmidt, *Ind. Eng. Chem.*, **26**, 8, 851 (1934).
7. D. L. Katz, *Trans.* AIME, **160**, 140, T.P. 1748 (1945).
8. L. L. Laurence and L. S. Reid, *World Oil*, **129**, 2, 156-9 (June 1949).
9. E. L. McCarthy, W. L. Boyd and L. S. Reid, *Trans.* AIME, **189**, (1950).
10. J. A. Porter and L. S. Reid, *Petroleum Engineer*, **22**, 5, D-9 (May 1950).
11. J. L. Morris, *World Oil*, **128**, 8, 194-8 (Dec. 1948).
12. F. C. Reisenfeld and H. D. Frazier, *Oil and Gas Journal*, **48**, 12, 238, (July 28, 1949).
13. G. F. Russell, M.Ch.E. Thesis, University of Oklahoma, 1944.
14. G. F. Russell, L. S. Reid and R. L. Huntington, *Trans.* AIChE, **41**, 315 (1945).
15. N. K. Senatoroff, *Proc. Pacific Coast Gas Ass'n.*, **36**, (1945).
16. H. N. Wade, *Petroleum Engineer*, **14**, 6, 184-90 (March 1943).
17. H. N. Wade, *Petroleum Engineer*, **14**, 7, 100-4 (April 1943).
18. B. F. Dodge, *Chemical Engineering Thermodynamics*, McGraw-Hill Book Co., Inc., New York, (1944).
19. G. H. Getman and F. Daniels, *Outlines of Theoretical Chemistry*, John Wiley and Sons, Inc., New York, (1937).
20. S. Glasstone, *Textbook of Physical Chemistry*, D. Van Nostrand and Co., New York, (1940).
21. G. N. Lewis and M. Randall, *Thermodynamics and the Free Energy of Chemical Substances*, McGraw-Hill Book Co., Inc., New York, (1923).
22. F. N. McDougall, *Thermodynamics and Chemistry*, John Wiley and Sons, Inc., New York, (1939).
23. Tech. Bull. *Glycols*, Carbide and Carbon Chemicals Division, Union Carbide and Carbon Corp., New York, (1948).
24. L. H. Peahl, *Oil and Gas Journal*, 49, 10, 92-96 (July 13, 1950).

★ ★ ★

T.P. 2914

THE WATER VAPOR CONTENT OF ESSENTIALLY NITROGEN-FREE NATURAL GAS SATURATED AT VARIOUS CONDITIONS OF TEMPERATURE AND PRESSURE

EUGENE L. McCARTHY, BLACK, SIVALLS AND BRYSON, INC., KANSAS CITY, MO.; **WILLIAM L. BOYD,** CONTINENTAL OIL CO., PONCA CITY, OKLA.; AND **LAURANCE S. REID,** UNIVERSITY OF OKLAHOMA, MEMBER AIME

ABSTRACT

Proper control of the moisture content of natural gas is essential to reliable operation of gas transmission and distribution facilities serving northern markets. The moisture content of natural gas is usually determined by dew point measurement at the existing pressure. For any gas of constant moisture content, the dew point varies with the pressure.

A correlation of the data of several investigators is presented in graphical form by the authors. These data were correlated by the authors and F. M. Townsend, C. C. Tsao, M. D. Rogers, Jr., and J. A. Porter, graduate students in chemical engineering at the University of Oklahoma.

Of particular interest are the hitherto unpublished low temperature data observed by Wickliffe Skinner, Jr., which are included in this correlation.

PRESENTATION OF DATA

The problem of interpreting water dew points, or saturation temperatures, of natural gas in terms of specific moisture content has increased in importance during the past decade because of extensive developments in the transmission and petro-chemical phases of the natural gas industry. Virtually all gas transported to northern and eastern markets must be dehydrated to a low water vapor content to prevent hydrate formation in transmission and distribution lines and resultant interruptions in gas deliveries. Complete dehydration is required in certain phases of the petro-chemical industry involving low-temperature operations.

It is a well-known fact that the water vapor content of pure hydrocarbon vapors and their mixtures at superatmospheric pressures cannot be predicted with accuracy by assuming validity of the ideal gas laws.[12] Earlier interest in the general problem was concentrated on the water vapor content of pure hydrocarbons and hydrocarbon mixtures in the pressure and temperature ranges common to gas and oil producing reservoirs in order to obtain fundamental data for the improvement of production techniques and the furtherance of reservoir studies. Excellent data are published for pressures ranging from atmospheric to 10,000 psig and for temperatures ranging from 100° to 460°F[4,9,10,11] and are found to be in close agreement. However, experimental data at high pressures and temperatures below 100°F are comparatively limited in scope.

Experimental data in the lower temperature range have been reported by Laulhere and Briscoe,[8] Deaton, et al,[2,3] Hammerschmidt,[5,6] and Wade.[14] In general, the pressures employed in these investigations ranged from atmospheric to 1,000 psig while temperatures ranged from 32° to 120°F; i.e., the usual conditions encountered in gas transmission line operations. Additional data were reported by Russell, et al,[12] at pressures as high as 2,000 psig and covering a rather narrow atmospheric temperature range. In 1947, Hammerschmidt published a correlation of all available data,[7] in which the water vapor content of gases at saturation, under high pressure and low temperature, was predicted by extrapolation. In 1948, Wickliffe Skinner, Jr., presented data on the moisture content of a low nitrogen content gas at low temperature and at pressures ranging upward to 1,500 psia.[13] Comparison of Skinner's experimental data with the extrapolated data of Hammerschmidt revealed an appreciable variation in the lower temperature range, emphasizing the need for a new correlation which would rely on Skinner's data at lower temperatures.

Careful scrutiny of available data suggested that presence of an appreciable quantity of nitrogen in a gas mixture may affect its saturated moisture content so that data obtained from gases with more than three per cent nitrogen were not used in this correlation.

CORRELATION OF DATA

Data employed in this correlation are presented in Table I. The data of Dodson and Standing,[4] McKetta and Katz,[9] and Olds, Sage and Lacey[10] were compared and found to be in close agreement so that the data of Olds, et al, re-plotted in a more convenient form by the Humble Oil and Refining Co.,[1] were used for temperatures of 100°F and above. Skinner's data were used for temperatures below 40°F. Between these intermediate temperature limits, the data of Hammerschmidt,[7] Wade[14] and extrapolated data of Olds, et al,[1] were tabulated

---

[1] References given at end of paper.

Manuscript received at the office of the Petroleum Branch September 30, 1949. Paper presented at the Petroleum Branch meeting in San Antonio, Texas, October 5-7, 1949.

Table I

Sources of Data Used in Correlating the Water Vapor Content of Essentially Nitrogen-Free Natural Gas at Saturation

Investigator	Reference	Pressure Range psig	Temperature Range
Hammerschmidt	7	50-2,000	20° to 120°F
Olds, Sage and Lacey	10	300-10,000	100° to 460°F
Skinner	13	30-1,500	–60° to 40°F
Wade	14	25-1,000	–10° to 120°F

and averaged. These average values, together with the smoothest curve drawn to join the data plots of Skinner and Olds, et al, determined intermediate values between 40° and 100°F. Accuracy of this method was confirmed by comparison with a Duhring plot of the data of Skinner and of Olds, et al, at 700 psia which was prepared by F. M. Townsend.* The water vapor content of gas at atmospheric pressure was calculated from the vapor pressure data of Zimmerman and Lavine.[15]

CONCLUSIONS

Experimental data concerning the moisture content of essentially nitrogen-free natural gases have been correlated and plotted versus saturation, or dew point, temperature using pressure as the parameter. Pressures range from atmospheric to 6,000 psia, while temperatures range from –60° to 280°F. These data have been used successfully in the production of gas from high pressure wells, in the design of dehydration processes and in the operation of high pressure gathering and transmission lines.

REFERENCES

1. S. E. Buckley, personal communication to L. S. Reid.
2. W. M. Deaton, *Gas*, (1936), 12, 6, 20, 58-59.
3. W. M. Deaton and E. M. Frost, Jr., "Water Content of Compressed Gases," presented before Natural Gas Section, AGA, Dallas, Texas, May 5-8, 1941.
4. C. R. Dodson and M. B. Standing, *API Drilling and Production Practice*, (1944), 173.
5. E. G. Hammerschmidt, *Western Gas*, (1933) 9, 9-11, 29.
6. E. G. Hammerschmidt, *American Gas Association Monthly*, (1934), 18, 853-855.
7. E. G. Hammerschmidt, *Chem. Engr. Progress*, (1947), 43, 7, 361.
8. B. M. Laulhere and C. F. Briscoe, *Gas*, (1939), 15, 21-24.
9. J. J. McKetta, Jr. and D. L. Katz, *Trans.* AIME (1947) **170**.
10. R. H. Olds, B. H. Sage and W. N. Lacey, *Ind. Eng. Chem.*, (1942), 34, 1223.
11. H. H. Reamer, R. H. Olds, B. H. Sage and W. N. Lacey, *Ind. Eng. Chem.*, (1943), 35, 790.
12. G. F. Russell, R. B. Thompson, F. P. Vance, and R. L. Huntington, *Trans.* AIME, (1945), **160**.
13. Wickliffe Skinner, Jr., M.Ch.E. Thesis, University of Oklahoma (1948).
14. H. N. Wade, *Petr. Engineer*, (1943), 14, 7, 102.
15. O. T. Zimmerman and I. Lavine, *Psychometric Tables and Charts*, Ind. Res. Service, (1945), Dover, N. H.

★ ★ ★

---

*Graduate Student in Chemical Engineering, University of Oklahoma, Norman, Okla.

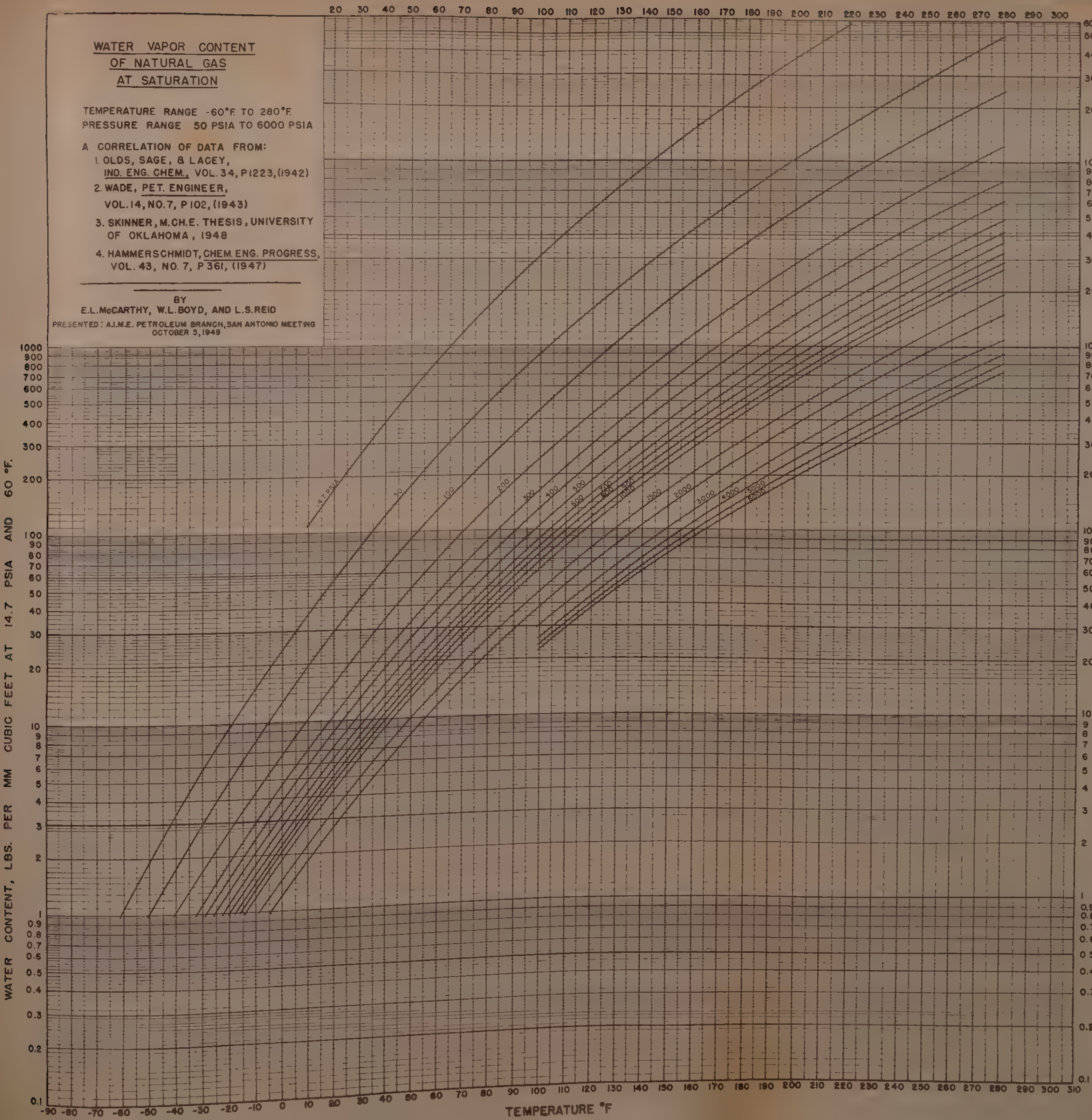

WATER VAPOR CONTENT OF NATURAL GAS AT SATURATION

TEMPERATURE RANGE -60°F. TO 280°F.
PRESSURE RANGE 50 PSIA TO 6000 PSIA

A CORRELATION OF DATA FROM:

1. OLDS, SAGE, & LACEY, IND. ENG. CHEM., VOL. 34, P1223, (1942)
2. WADE, PET. ENGINEER, VOL. 14, NO. 7, P102, (1943)
3. SKINNER, M.CH.E. THESIS, UNIVERSITY OF OKLAHOMA, 1948
4. HAMMERSCHMIDT, CHEM. ENG. PROGRESS, VOL. 43, NO. 7, P361, (1947)

BY
E.L.McCARTHY, W.L.BOYD, AND L.S.REID

PRESENTED: A.I.M.E. PETROLEUM BRANCH, SAN ANTONIO MEETING
OCTOBER 3, 1949

A STUDY OF RESERVOIR PERFORMANCE OF THE FIRST GRUBB POOL, SAN MIGUELITO FIELD, VENTURA COUNTY, CALIFORNIA

WAYNE E. GLENN, CONTINENTAL OIL CO., LOS ANGELES, CALIF., MEMBER AIME

ABSTRACT

The San Miguelito Field of Ventura County, California, lies along the coast approximately five miles northwest of the city of Ventura. The structure is one of several in the Ventura anticline, a series of anticlinal folds trending northwest-southeast through the San Miguelito Field. The Ventura Avenue Field lies to the southeast along the anticline, and Padre Canyon and Rincon Fields lie to the northwest; the series then extends beneath the Pacific Ocean. Production is obtained from the Lower Pico and Repetto formations of Pliocene age, and oil accumulation is controlled by faulting, lithology and structure. The first well in the First Grubb Pool was completed in November, 1931, and to date 48 producing wells have been drilled on the 276 productive acres. Approximately 685 ft of net pay are contained in the eight sand bodies grossing 1,220 ft of section. Production of oil to date has been 15,600,000 bbl. A gas injection project was instigated in April, 1940, but was discontinued in September, 1949.

This paper is confined to a discussion of the development and performance history of the First Grubb Pool of the San Miguelito Field.

LOCATION AND GEOLOGY

The San Miguelito Oil Field is located in Ventura County about five miles northwest of the city of Ventura along the coastal highway to Santa Barbara. It is located within sections 23, 24, 25, and 30 of Township 3 North, Range 24 West, San Bernardino Base and Meridian. Surface elevation in the field ranges from sea level to plus 1,200 ft, and the terrain is extremely rugged. The structure is well defined on the surface and on the wall of the Amphitheatre Canyon where appears a so-called "text book" anticlinal section.

The San Miguelito structure is an asymmetrical, elongated anticline about two miles long and three-fourths of a mile wide. The trend of the axis of the anticline is northwest-southeast. Fig. 9 illustrates the contours and major faults of this structure. Dips on the southwesterly flank average about 40 degrees, whereas the northeasterly flank ranges from 60 to 75 degrees. There are several faults striking generally east and west. These faults do not appear to affect materially the area of accumulation or performance behavior. It is believed that accumulation was affected by steeply dipping beds and extremely low permeability of the northeast flank of the structure.

As shown by the typical log, Fig. 1, the San Miguelito Field is divided into two stratigraphic producing intervals. The First Grubb Pool comprises the interval from the "G" to "L" markers; the Second Grubb Pool from the "L" to "M" markers. The First Grubb Pool, ranging in thickness from 1,105 to 1,680 ft, with an average of 1,220 ft, includes approximately 685 ft of oil-bearing sands. The First Grubb zone consists of eight sand intervals separated by shales.

The shale bodies separating the eight sand intervals within the First Grubb Pool are continuous throughout the major part of the structure and serve as an effective barrier. Many of the thin, irregular shale or siltstone streaks within these sand bodies are discontinuous and do not affect well performance appreciably.

The productive horizons in the First Grubb Pool are siltstones and sandstones of the Lower Pico and Repetto formations of Pliocene age.

It is apparent from inspection of the typical log that the "G" to "L" interval might have been separated into at least six producing zones and selectively produced. Unfortunately the electric log and some of our modern tools were not available or were in their infancy during the period 1931 through 1937. Not until 1937 when eight wells had been completed were there sufficient geological data to permit definition of the sand bodies. Then the problem of reservoir control in this multiple-sand field, where all sands are open to a common

---

[1]References given at end of paper.

Manuscript received at the office of the Petroleum Branch October 26, 1949. Paper presented at the Petroleum Branch meetings at San Antonio, October 5-7, 1949, and at Los Angeles, October 20-21, 1949.

Table I

Summary of Formation Characteristics

Sand Interval	Weighted Average		Average Strat. Thickness, Ft	Average Net Effective Pay, Ft	Acres Within Productive Limit
	Perm. md	Porosity Per Cent			
G - H	237	17.2	100	71.3	97
H - Ha	79	18.1	125	77.5	148
Ha - I	71	17.2	130	75.2	180.5
I - Ia	56.6	19.5	115	65.4	158.3
Ia - J	47.8	17.9	140	70	258
J - Ja	109	18.5	125	82.7	262
Ja - Jc	107	19.2	215	111.1	165.3
Jc - K	56	17	240	131.3	276
K - L	36.2	17.6			
Pool	86	18	1220	685	1545

well bore, was recognized. Because of the number of wells completed, cost considerations, and the complexity of the structure, however, the decision was made to produce all oil-bearing sands simultaneously. Fig. 2, typical sections, illustrates the complex geologic problem that accounts to a large extent for this type completion and for the slow development rate.

The First Grubb Pool of the San Miguelito Field was discovered with completion of Grubb Well No. 1 in November, 1931, at a depth of 6,750 ft for an initial potential of 616 B/D of 32-degree API gravity. In August, 1932, it was recompleted with an initial production of 2,449 B/D. As of September 1, 1949, 48 producible wells had been drilled to the first Grubb horizon.

FORMATION AND FLUID CHARACTERISTICS

The reservoir rocks are quite typical of California Pliocene sands. They are generally rather poorly sorted and contain a large amount of silty argillaceous material, ranging from firm well consolidated sands of low permeability to unconsolidated highly permeable sands, as shown by the typical log and as summarized in Table I.

Porosity and permeability determinations are somewhat limited as only some 800 samples from 20 wells were analyzed. The weighted average porosity is 18 per cent, and the average permeability is 86 millidarcies. The pool weighted average porosity and permeability were determined by arriving at an average value for each foot of sand, measured from the top of each sand marker. These average values were then applied to the corresponding sand interval of each well penetrating the First Grubb Pool.

The permeability variation is extremely high, but there does seem to be some correlation between wells. Based on the information available, it is estimated that 27 per cent of the average pore space is occupied by water.

In contrast to the typical California reservoir, the sand intervals increase in areal extent with depth; that is, the "G" to "H" interval contains a productive area of 97 acres while the "Jc" to "L" interval contains 276 acres. Permeability generally decreases with depth except for the "Ja" to "Jc" interval which is comprised of a "coarse pebble bed." The productive limits are in general defined by the Padre fault and permeability on the north, faulting and permeability on the east, water on the south, and permeability on the west flank. The productive limit along the southwest flank, as defined by water-oil contact, is very irregular as would be expected in a reservoir of this type. Faulting and permeability are the controlling factors. The Isopachous maps, Figs. 3 through 3c, indicate the relative sand volume and productive limits of each sand interval. The average gross sand thickness is 1,220 ft, whereas the net effective thickness averages about 685 ft. (The well numbers followed by "-2" indicate Second Grubb Pool wells.) The total bulk sand volume of the First Grubb Pool was calculated to be 136,600-acre ft. The essential formation characteristics are shown in Table I.

As there was but one rather poor analysis of a bottom hole fluid sample taken in 1940 at a static pressure of 2,700 psig, reservoir fluid characteristics were recalculated. The recalculation was based on reservoir performance, published papers, and early stage separation work. The original saturation pressure is estimated to be 3,000 psig

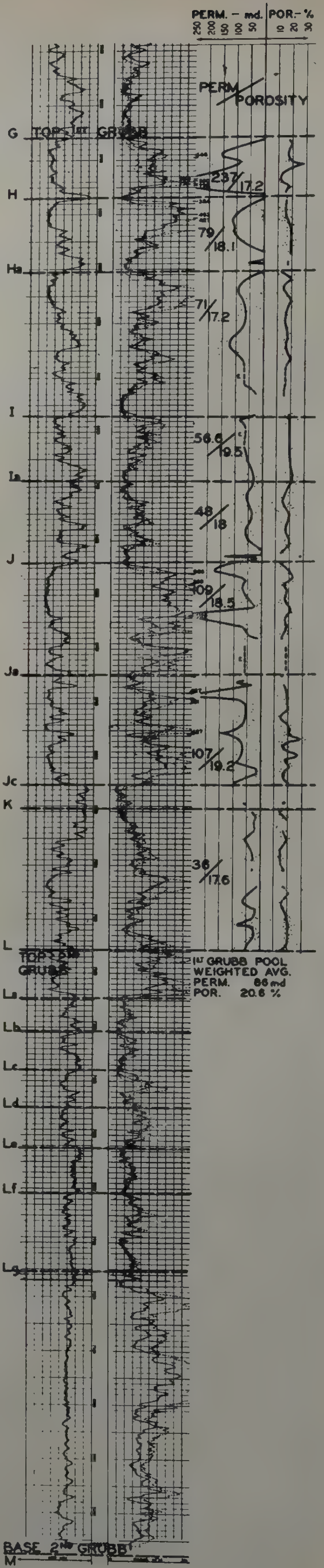

FIG. 1 — TYPICAL LOG.

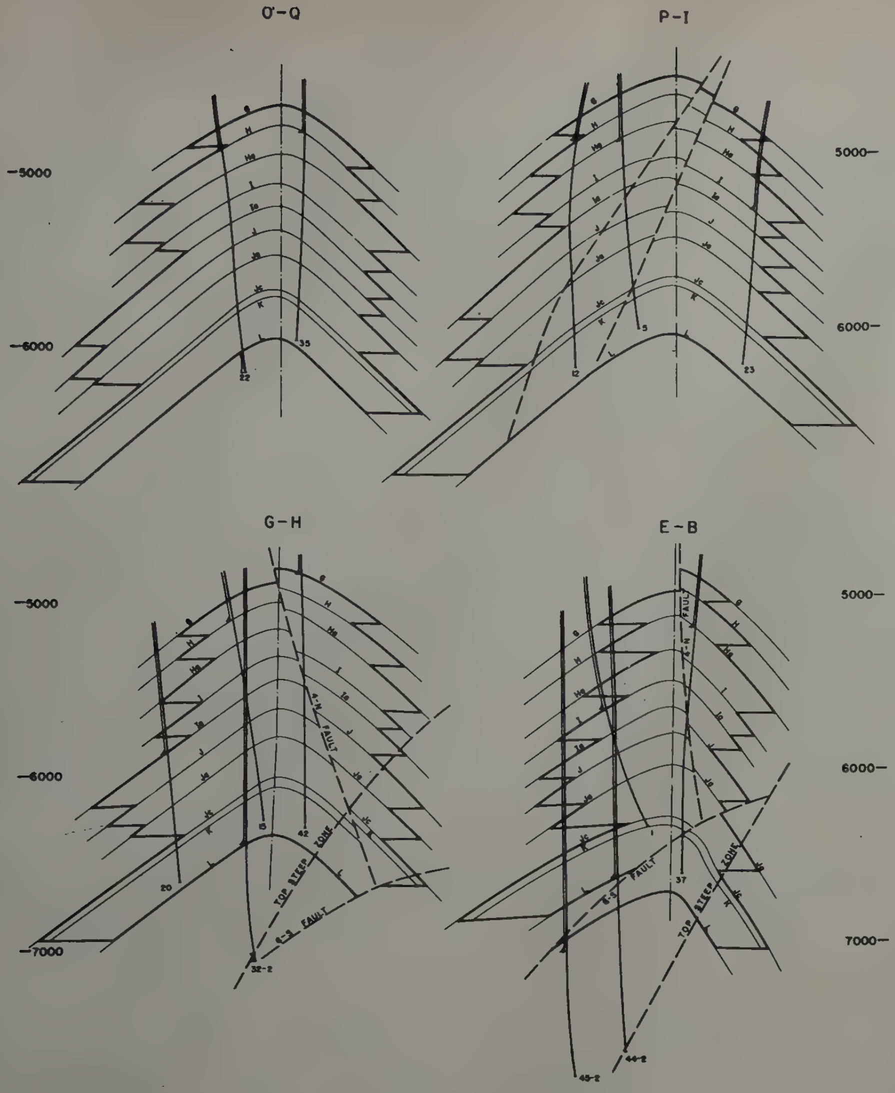

FIG. 2 — TYPICAL SECTIONS.

at the –5,500 ft field datum and 158°F. Subsurface sample data were extrapolated to these conditions, and a formation volume factor of 1.428 bbl per bbl was used to correct reservoir volumes to stock tank conditions.

The viscosity of the oil at subsurface temperatures of 158° and 3,000 psig was 0.92C$_p$. The produced oil gravity was 32 degrees API at 60°F. This gravity varies with trap pressure and temperature. The solution gas-oil ratio was calculated to be 890 cu ft per bbl. With the exception of three wells near the axis of the structure and considering trap pressure, the original produced gas-oil ratios verify this figure.

Average original pressures were calculated by zones using the water gradient through each oil saturated interval from top to bottom. This procedure was justified due to the fact that water existed at the productive limit of each zone. The temperature of each oil saturated interval was measured by means of a recording thermometer. The pressure and temperature gradients under estimated original conditions are shown in Fig. 4.

Original tank oil contained in each sand interval was determined by using fluid data shown in Table II. Using the pore volume, mean temperature and pressure (Fig. 4 and Table III), and the reservoir fluid characteristics as determined, the original tank oil in place was calculated for each of the eight sand intervals. In the remainder of the calculations, the reservoir was treated as a single producing unit, it being impossible to determine the performance of individual zones since all were open to a common well bore.

RESERVOIR PERFORMANCE

Production statistics of the pool are unusually complete and accurate. Individual well oil, gas, and water measurements have been recorded since inception. These data plus frequent reservoir pressure and P.I. surveys make individual well and reservoir performance studies more reliable than is often the case in a field of this age.

A record of reservoir performance is shown by Fig. 5. To illustrate the individual well performance, which is often more indicative of true reservoir performance than is the pool curve, Figs. 6 and 6a are included. These figures show the performance history of individual wells. Correlation of well and pool behavior, as to spread of high gas-oil ratios, water production, gas-oil segregation and gas channeling, with the cumulative oil production and gas injection map shown by Fig. 7, yields a panorama of the extent to which gas-oil segregation is achieved.

Pool performance history is characterized by effects of concentrated development, localized withdrawal at high rates, gas channeling, and gas-oil segregation. The magnitude of these effects is obscured in Fig. 5 by selective well production in later years. Recent well completions of down-structure wells and selective reservoir control have resulted in the lowering of pool gas-oil ratios as reflected by Figs. 5 and 8. A study of individual well behavior in conjunction with structural position, penetration, subsurface pressure characteristics, P.I., and gas-oil ratio histories discloses a typical low permeability, solution gas drive pool. Water encroachment in thin, high permeability sands in the "I" and "J" intervals and gravity drainage are now affecting well and reservoir performance.

While gas-oil ratios vary to some degree with oil rates in the high-structure wells where there exist zones of low liquid saturation, this is not believed to be the case in the early stages of development, nor is it true now in low-structure wells where liquid saturation is high.

The declining oil production rates, as shown by Fig. 5, reflect the reduction imposed by MER adjustments rather than the actual decline in producing capacity of the wells. This fact is borne out by the completion of 20 wells since the peak production year, several of which had potentials in excess of 1,200 B/D.

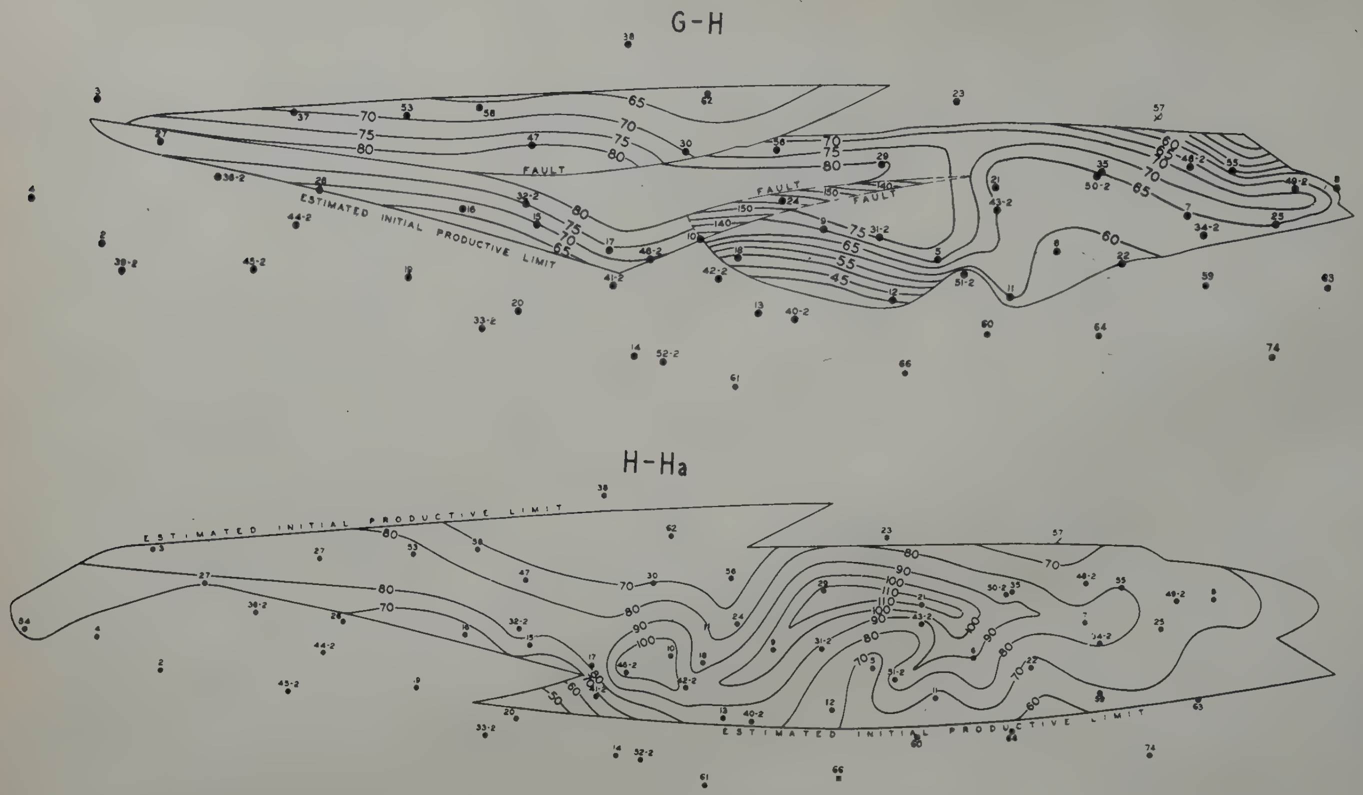
G-H
FAULT
FAULT
FAULT
ESTIMATED INITIAL PRODUCTIVE LIMIT
65
70
75
80
140
150
60
55
45
H-Ha
ESTIMATED INITIAL PRODUCTIVE LIMIT
ESTIMATED INITIAL PRODUCTIVE LIMIT
80
70
90
100
110
60
50

FIG. 3 — ISOPACH MAP — G-H AND H-Ha SECTIONS.

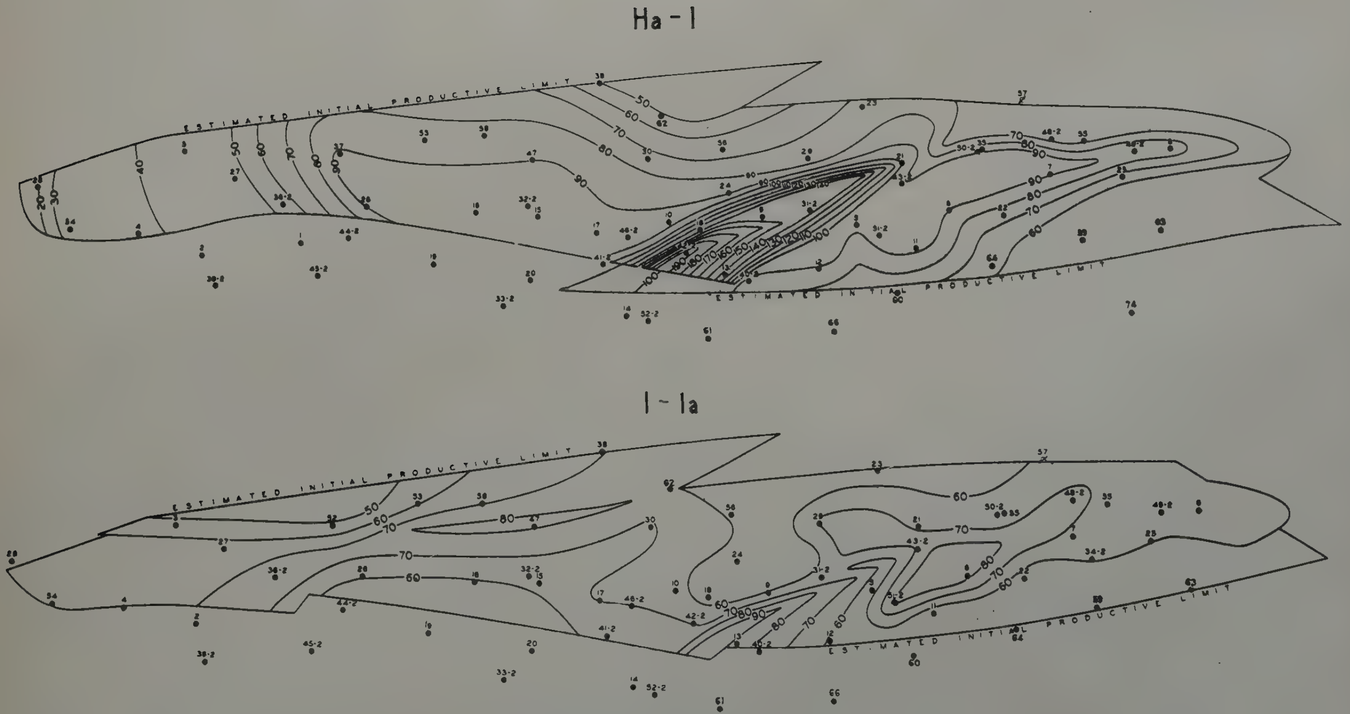
Ha - I
ESTIMATED INITIAL PRODUCTIVE LIMIT
ESTIMATED INITIAL PRODUCTIVE LIMIT
20
30
40
50
60
70
80
90
100
110
120
130
140
150
160
170
180
I - Ia
ESTIMATED INITIAL PRODUCTIVE LIMIT
ESTIMATED INITIAL PRODUCTIVE LIMIT
50
60
70
80
90

FIG. 3a — ISOPACH MAP — Ha-I AND I-Ia SECTIONS.

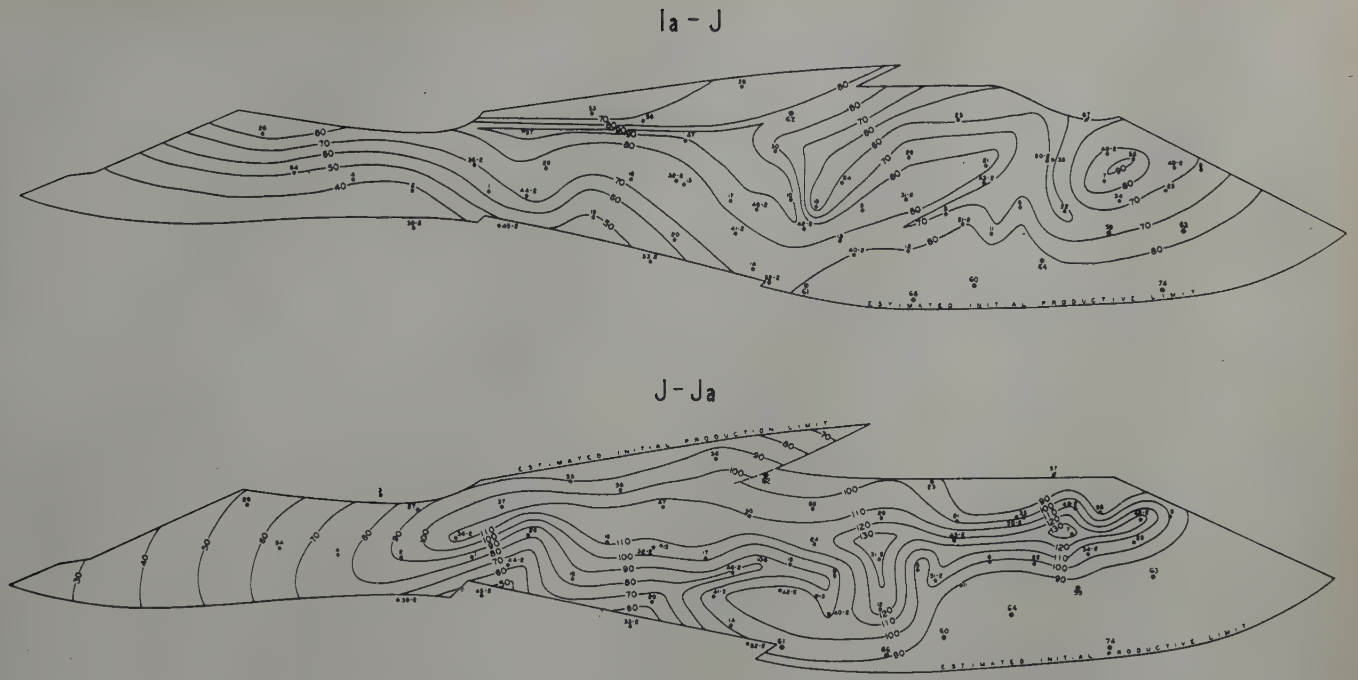
Ia - J
ESTIMATED INITIAL PRODUCTIVE LIMIT
J - Ja
ESTIMATED INITIAL PRODUCTION LIMIT
ESTIMATED INITIAL PRODUCTIVE LIMIT

FIG. 3b — ISOPACH MAP — Ia-J AND J-Ja SECTIONS.

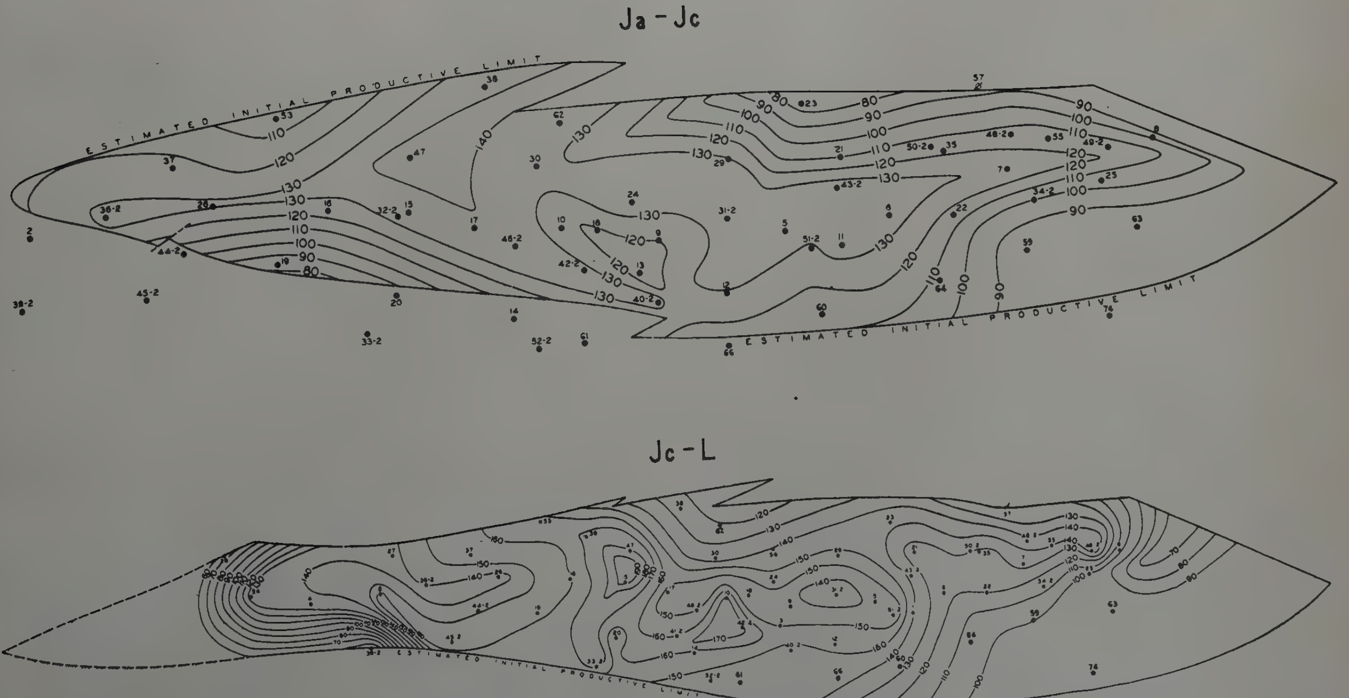
Ja - Jc
ESTIMATED INITIAL PRODUCTIVE LIMIT
ESTIMATED INITIAL PRODUCTIVE LIMIT
Jc - L
ESTIMATED INITIAL PRODUCTIVE LIMIT

FIG. 3c — ISOPACH MAP — Ja-Jc AND Jc-L SECTIONS.

Table II
P.V.T. Data

Sand Interval	Original Mean Sand Interval		Formation Volume of Saturated Oil B/B.S.T.O.	Saturation GOR
	Pressure	Temp.		
G - H	2770	149	1.406	830
H - Ha	2817	151	1.410	840
Ha - I	2875	154	1.416	852
I - Ia	2930	157	1.422	866
Ia - J	2985	159	1.427	875
J - Ja	3042	162	1.433	888
Ja - Jc	3105	165	1.438	898
Jc - K	3195	169	1.448	915
Pool Datum	3000	158	1.428	890

Throughout 1943, the pool production rate increased with development to reach a maximum daily oil rate of 5,500 bbl. During the period from early 1944 through 1947, only an average of 1.3 wells per year were completed in the First Grubb Pool. To permit control of withdrawal and to develop the productive sands that would not be adequately drained otherwise, the development rate was increased during the period 1947 through 1949 by completion of 15 wells. With the completion of four additional wells in 1950, development will be complete.

The high production rate of well No. 5 for approximately 18 months after completion created a low-pressure area, the effects of which have been erased by pressure depletion only in the past two years.

Gravity drainage has been effective in maintaining a high oil saturation in the down flank wells as evidenced by the gas-oil ratio performance of the individual wells. The effectiveness has been minimized by high up-dip differential pressures until very recently. It is practically impossible to calculate the amount of gravity drainage taking place in a field of this type where several sand intervals are open to the same well bore. A recent 46-day shutdown of the field gave strong indication of gravitational migration of the oil and gas, as noted from declines in gas-oil ratios of down-structure wells.

GAS-OIL RATIO

Initial produced gas-oil ratios (Fig. 9) were equivalent to the solution ratio in those early wells in which the "H" marker is located below –4,800 ft elevation. The variation in value as reported is due largely to gas remaining in solution at separation pressure.

The abrupt rise of the pool gas-oil ratio during 1936 and 1937 coincides with the completion of Grubb Well No. 5, which had an initial gas-oil ratio of 5,500 cu ft per bbl, six times the solution ratio of 890, and the completion of Well No. 7, which initially produced 9,561 cu ft of gas per bbl of oil. Gas-oil ratios of both of these wells declined with dissipation of a small gas cap in the thin gas sands located in the "Ia" and "J" interval near the axis of the structure so that by 1940 the ratios of these two wells compared with the pool ratio of 1,250 cu ft per bbl. It is significant that Grubb Well No. 1, while produced at rates equivalent to Well No. 5 had produced approximately 1,530,000 bbl of oil before the gas-oil ratio exceeded 1,300 cu ft per bbl. The comparative performance of the two wells is shown in Figs. 6 and 6a. Several original small stray gas sands occurred above the –4,800 ft contour; and although the free gas was rapidly dissipated, wells completed as late as 1941

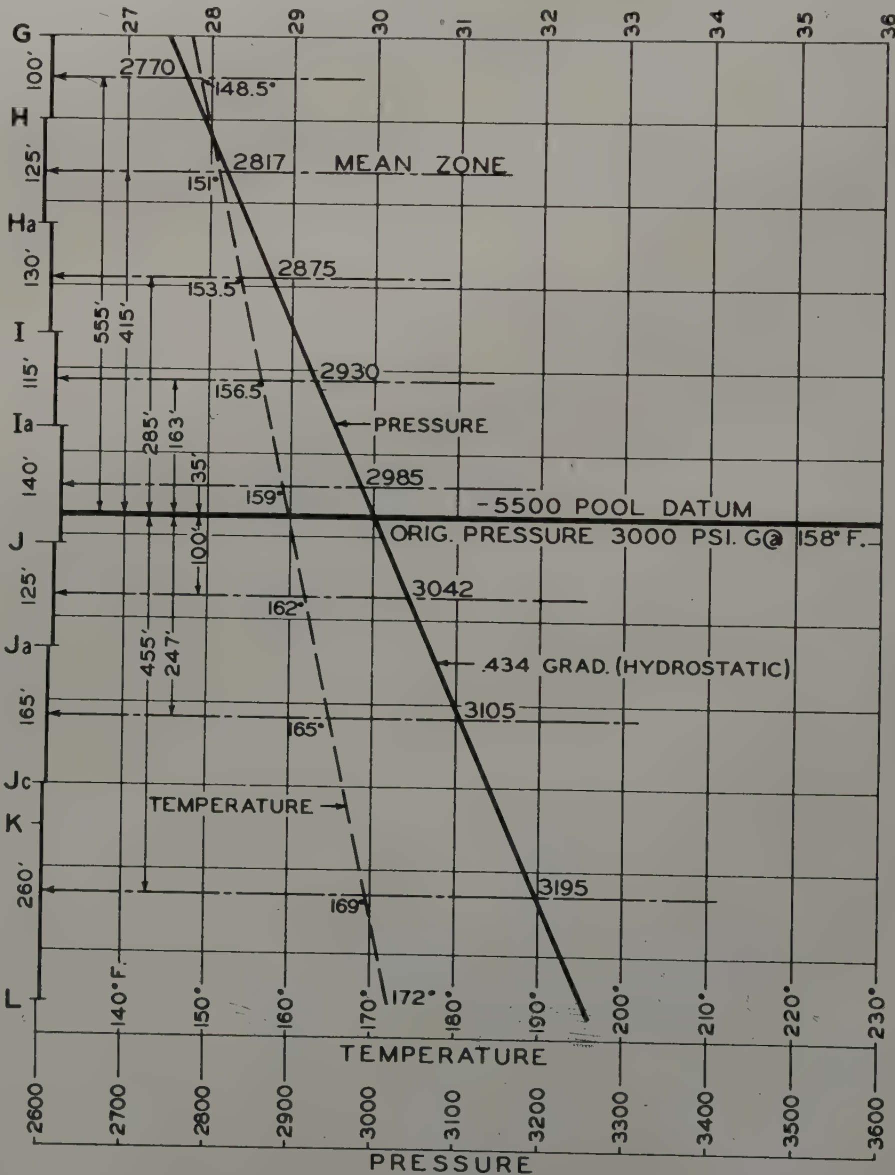

FIG. 4 — PRESSURE AND TEMPERATURE CHART.

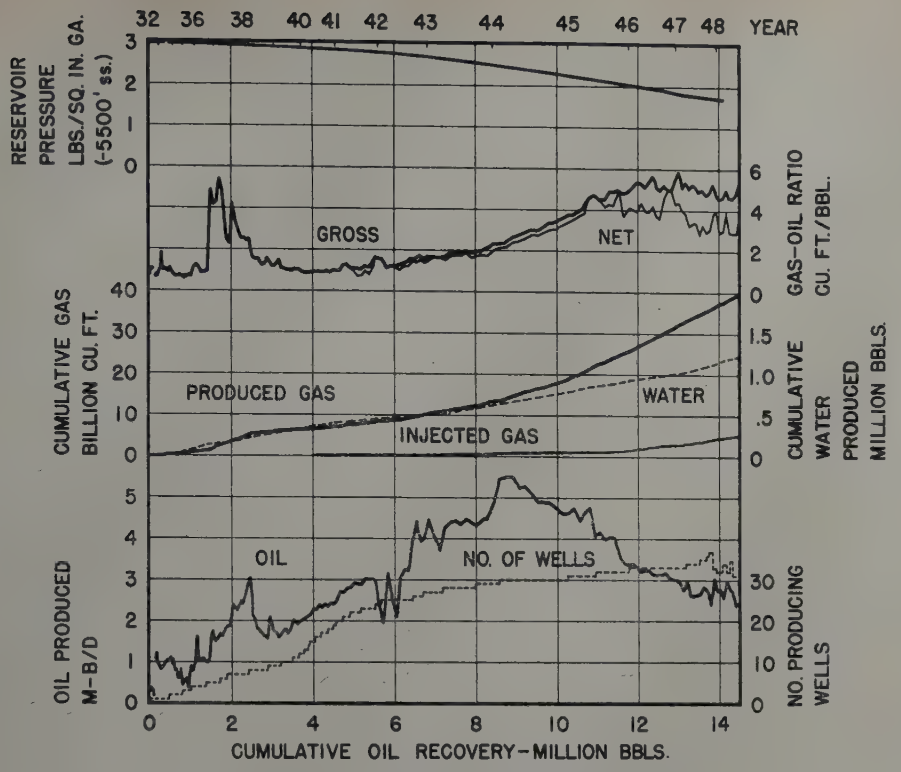

FIG. 5 — RESERVOIR PERFORMANCE.

produced free gas, as indicated by the initial ratio of Well No. 21. This well's initial ratio of 5,892 cu ft per bbl declined to near normal by 1943. Well No. 8 demonstrated similar characteristics although located across the 3N fault.

The high initial ratio of Well No. 27 reflects gas injection in the upper part of the "I" to "Ia" interval in Well No. 3. These wells are not separated by the 4N fault, as the fault intersects both wells above the "H" marker.

In general, the gas-oil ratio trend maps, Figs. 10, 10a, and 10b, illustrate effective gas-oil segregation, localized gas channeling, and the effects of high withdrawal rates.

The upward trend of the pool gas-oil ratio during the war years reflects the effect of heavy withdrawals from structurally high wells which caused local areas of low liquid saturation and low pressure. Gas injection initiated in 1940 adversely affected the gas-oil ratio due to channeling of the injected gas. The reversal of the pool gas-oil ratio trend in 1946 was due to the completion of low gas-oil ratio wells downstructure and shutting in high ratio wells.

Until excess gas is excluded in the "intermediate" and "high" ratio group wells, maximum withdrawal should be obtained from the current low ratio and newly completed wells. The exclusion might be accomplished by selectively plugging gas sands or changing injection intervals. When this work is successfully completed, all wells will be selectively produced.

Even though gas channeling, permeability distribution, and method of operation may affect recovery, it is well to remember that the cumulative ratio is an index to ultimate recovery, not considering gravity drainage. Ratio control in a reservoir of this type is difficult because of the fluid and reservoir characteristics, stage of depletion of some sands, and inter-communication between sand intervals within the First Grubb Pool.

GAS INJECTION

The First Grubb reservoir is primarily a solution-gas-drive and gravity drainage type; therefore, operating procedure is based on the performance of that type of reservoir. A small-scale gas-injection project was initiated in April, 1940, as a conservation measure and to determine the feasibility of augmenting the natural reservoir energy and sweeping the oil sands with injected gas, thereby increasing the ultimate recovery of oil. The relatively small volume of gas injected to date has not affected over-all reservoir mechanics other than to serve as a gas sweep through a very limited sand volume. Gas channeling has minimized the effectiveness of gas injection. The initial gas-injection well, Grubb Well No. 3, is located on the north flank of the structure in the western part of the field. The injection intervals were "H" to "Ha," "Ha" to "I," and "I" to "Ia," comprising about 180 ft of effective oil sand. During 1941 and 1942, the daily average of 0.450 MMcf of gas was injected at a well head pressure 3,200 psi. This volume was increased to 0.75 MMcf daily during 1943. By November, 1943, a total volume of 511 MMcf of gas had been injected. At this time gas injection in Well No. 3 was discontinued because of gas channeling evident in Grubb Well No. 27. This well was completed in September, 1942, offsetting the injection well, with an average gas-oil ratio of 2,285 cu ft of gas per bbl of oil. Considering the low effective permeability of the sands open to production in this well, the low initial productivity index, the abnormally high pressure, and a gas-oil ratio three times solution ratio which increased 600 cu ft per bbl within a month, it became evi-

Table III
Pressure and P. I.

Year	Field Datum -5,500 Weighted Areally Surface-Acres	Well Datum Weighted by Bulk Vol. in Drainage Area	Number of Wells in Survey	Prod. Index Range
Original	3,000	3,160		
July, 1938	2,954	2,934	8	1.40-2.25
June, 1939	2,914	2,890	10	.07- .76
December, 1940	2,877	2,808	19	.70-4.16
December, 1941	2,847	2,759	23	.15-3.19
December, 1942	2,742	2,626	27	.13-1.80
December, 1943	2,566	2,438	29	.04-1.54
November, 1944	2,323	2,156	30	.14-1.80
August, 1945	2,129	1,939	32	.09-1.14
September, 1946	1,956	1,783	33	.04-1.04
March, 1947	1,830	1,640	34	.08- .96
March, 1948	1,745	1,547	38	.08-1.04

dent gas injection into Well No. 3 was channeling through highly permeable streaks and adversely affecting Well No. 27.

After again placing Well No. 3 on production, a total of 25,565 Mcf gas was produced at an average ratio of 3,909 cu ft per bbl with a pressure drawdown of approximately 1,100 psig before a normal producing ratio was reached. This indicates the very small volume of gas that was stored in the reservoir in a period of three years.

Well No. 24 was converted to injection in November, 1943. The initial daily injection rate was approximately 1,600 Mcf. Upon addition of compressors in 1945, the daily rate was increased to 5,000 Mcf, which rate has been maintained. From 1943 until September, 1946, approximately 2,000,000 Mcf of gas was injected into Well No. 24 with the sand interval from "H" through "K plus 190" ft open. The high permeability, high gas-saturated sands from "Ia" to "Jb" were receiving the injected gas. The K_g/K_o relation in these thin sands resulted in by-passing the remaining liquid saturation. A review of gas-oil ratio and performance trends of individual wells led to an attempt in November, 1946, to inject gas selectively into the "K plus 190" ft sand interval. The blanks between each sand interval were squeezed prior to setting a packer in the blank liner opposite the "Jc" to "K" shale. After injecting 2,600,000 Mcf of gas in this interval, a review of well performance was made in order to determine future injection policy. The study revealed gas entry into two thin permeable streaks within the "K" to "L" interval. This gas migration is shown on the temperature and flow meter survey chart, Fig. 11. After a review of these data, the injection interval in Well No. 24 was changed from the "K" to "L" to the "Jb" to "Jc" interval. The "K" to "L" interval was plugged with a temporary bridge plug. To date this has proved an effective means of controlling gas channeling within zones. Well Nos. 5, 6, and 12 and other high-structure wells have shown a marked decrease in gas-oil ratio. Several flowing wells have required artificial lift equipment since changing this injection interval. Subsequent flow meter surveys and temperature surveys have clearly indicated a rapid decrease in gas channeling, and the character of these surveys has changed appreciably.

Gas injection has affected all high-structure wells above –4,850 ft, Well No. 13 at –5,025 ft, and Well Nos. 15 and 17 at an elevation of –5,080 ft.

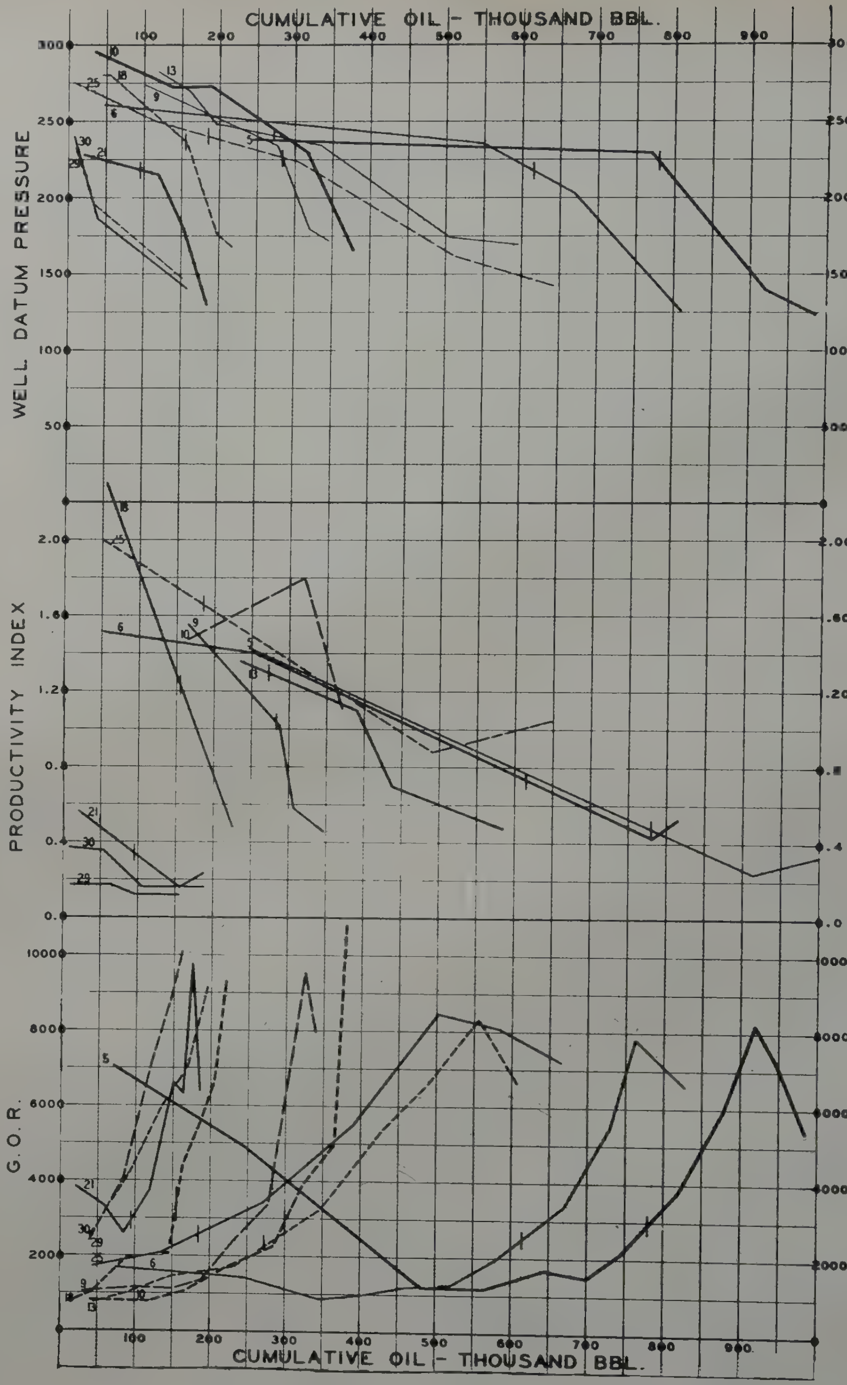

FIG. 6 — P.I., G.O.R., PRESSURE VS. RECOVERY — HIGH GAS-OIL RATIO WELLS.

Performance trends of significant wells, grouped as to gas-oil ratio, are shown by Figs. 6 and 6a. The gas-oil ratio curves of Well Nos. 9, 10, and 18 indicate channeling within one to three months after injection started in Well No. 24. The second change in Well Nos. 10 and 18 occurred in September, 1945, the month the injection rate was increased to 5,000 Mcf per day. Well No. 6 produced 56,000 bbl while Well No. 5 recovered only 41,000 bbl of oil before gas-oil ratio trends reflected gas injection. Productivity indices increase with a corresponding decrease in gas-oil ratio of the high ratio wells. This is not true in the low ratio group of wells. The low-structure wells are not adversely affected by gas injection; therefore the gas-oil ratios remained relatively low due to gravity segregation and to some extent gravity drainage.

To date about 7,000,000 Mcf of dry

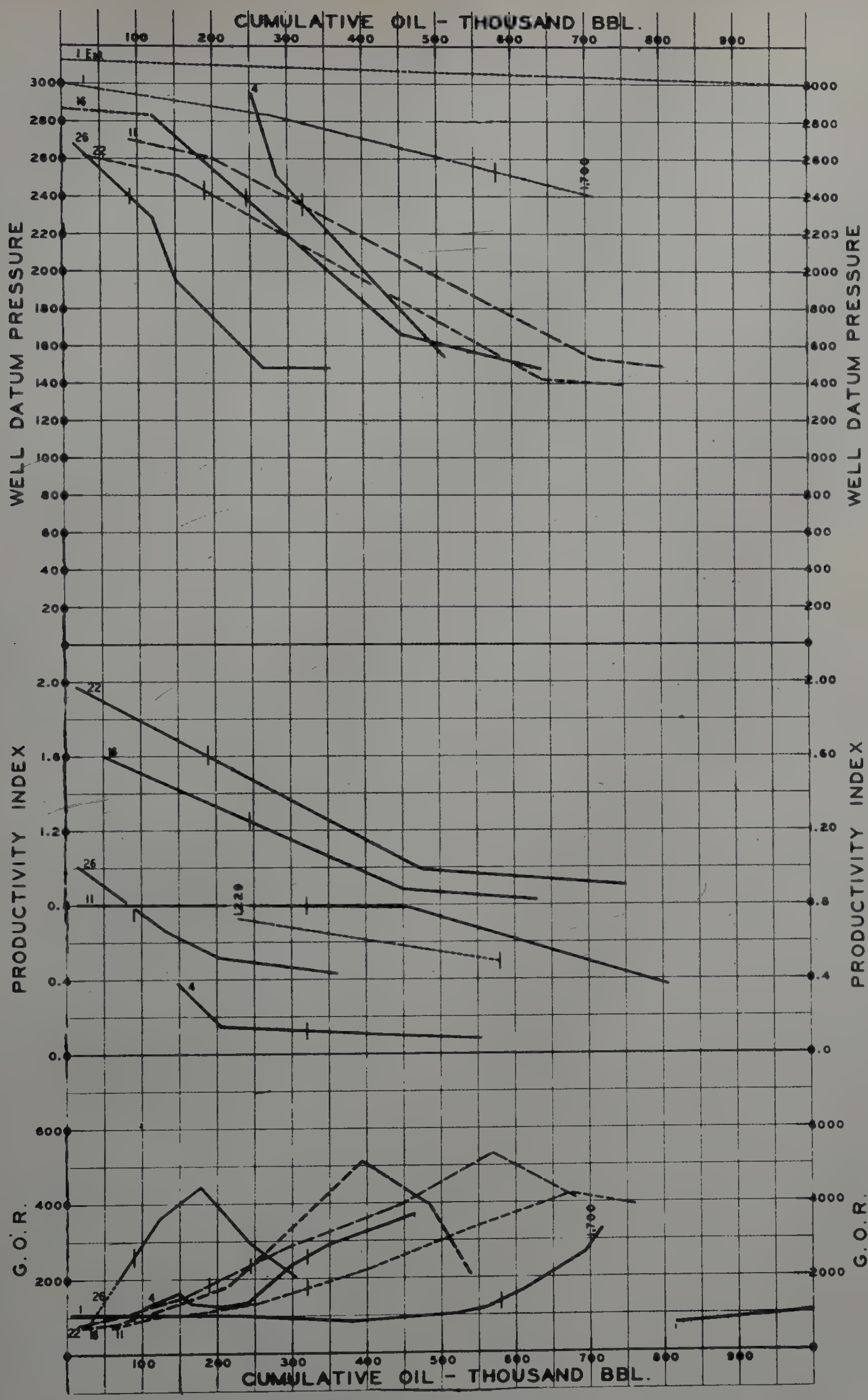

FIG. 6a — P.I., G.O.R., PRESSURE VS. RECOVERY — LOW GAS-OIL RATIO WELLS.

gas has been returned to the First Grubb Pool. This represents about 15 per cent of the wet gas produced. Gas injection in the First Grubb Pool was never intended solely as a pressure maintenance project. It was for the purpose of gas storage, to prolong the flowing life of wells, to determine the feasibility of gas sweep to increase oil recovery, and to some degree to retard pressure decline. This project was successful only in prolonging flowing life of wells and as a guide to future injection methods. Selective low-pressure gas injection is proposed, which is more favorable and more easily controlled in a reservoir of this type.

The total volume of gas injected into the First Grubb Pool is by no means sufficient to arrive at a conclusive answer as to what full-scale pressure maintenance might have done; however, it is hard to conceive how reservoir performance and ratio control could have been greatly different from that which has been experienced by injection in Well No. 24. It does not seem feasible that high-pressure gas injection into an interval of this thickness could be controlled. There are two definite schools of thought as to the type gas injection project that is most efficient and economical. Some factors favor injection of gas at high pressure, while other factors favor injection at low pressure. Unfortunately, there are no general rules to follow. Any program is thusly compromised to meet optimum economic considerations while still striving to obtain maximum oil recovery.

Factors favoring maintenance of high pressure are indirect effects on oil characteristics such as high formation volume factors, low viscosity, and low surface tension by keeping gas in solution in oil. Operating benefits at high reservoir pressures include extended flowing life of wells, providing gas storage for possible use or sale, and preventing premature water encroachment. Unfortunately, gas storage and prevention of water entry is not practicable in the First Grubb Pool due to the number of zones open to a common well bore, and permeability profile. For example, if the current high gas-oil ratio wells were shut in permanently, as would be necessary under high-pressure injection, approximately 82 per cent liquid saturation would remain in this area, not considering gravity drainage. Water entry is confined to possibly two relatively thin sand zones and will require shutting off as the pool is depleted regardless of pressure.

Factors favoring injection of gas at low pressure are lower compression ratios and costs, larger displacement volume in the reservoir per surface unit of gas handled, effective utilization of the natural existing energy and agent for oil displacement (gas dissolved in oil), and greater control of fluid movement in the reservoir by selective injection and producing well control.

Since it has been demonstrated that oil is recovered primarily due to actual displacement by gas, it is necessary that the introduction of gas into the reservoir be controlled to assure that it will flow through the maximum oil-filled pore space. Herein lies an important distinction between the displacing ability of gas dissolved in oil in a reservoir and gas injected through wells. Expansion of gas released from solution provides energy and a displacing agent in each pore in which oil exists;

while injected gas, from necessity in following the line of least resistance, is capable of displacing oil from only a part of the reservoir before the ratio of gas circulation to oil recovery becomes economically prohibitive.

The part of the First Grubb reservoir which can be effectively swept by high-pressure gas, a function of permeability profile, has been determined by injection in Nos. 3 and 24. In keeping with the above, maximum recovery and ultimate economic gain should result from the injection of low-pressure gas as a sweep of each sand interval which is separated from adjacent sands by major shales.

RESERVOIR PRESSURE

First pressure observations were made in 1936 and subsequently at six-month intervals. The estimated original pressure of 3,000 psig at –5,500 ft is based upon maximum recorded well pressures of 2,895 lb in Well No. 10 in 1939, and 2,900 lb original pressure in Well No. 14 in 1940. Other factors considered were hydrostatic head calculations, experience in similar pools of Ventura Avenue, and study of pressure recovery data.

Detailed pressure build-up time studies have been made throughout the life of the First Grubb Pool. The time required to obtain maximum build-up has varied from 12 hours in the early life of the field to more than 30 days in a recent survey. Some wells were still building up at the end of this period. A build-up curve should be obtained on every well in order to arrive at the relative "static pressure" in each well. The value of a correlation of pressure, average production rate for a period prior to the survey, and shut-in time in a low permeability reservoir of this type cannot be overemphasized.

From detailed study of the pressure history of this pool and its application to reservoir performance and material balance calculations, it was determined that two pressure values should be determined.

(1) For comparative well and reservoir performance studies to observe the effect of selective withdrawal, injection, or change in operating practices, the field datum (–5,500 ft) pressure is desirable. These values are shown on Figs. 12 through 12c and the weighted average value in Table III. The pool weighted average pressure is determined by planimetering areas between isobaric lines within the estimated productive limit of the pool.

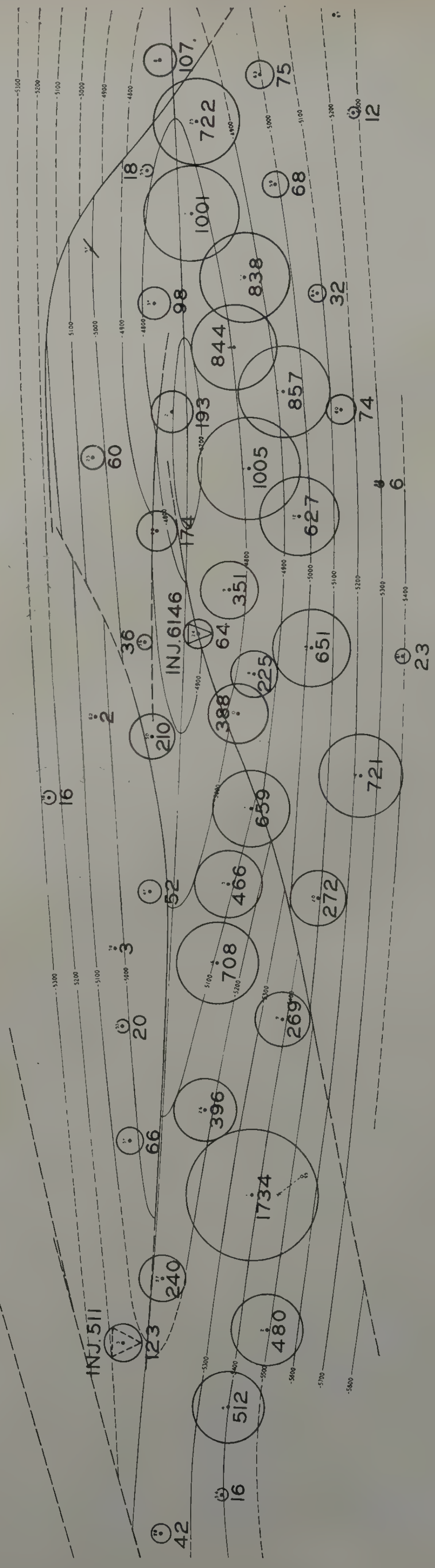

FIG. 7 — CUMULATIVE OIL RECOVERY AND GAS INJECTION — JULY 1, 1949.

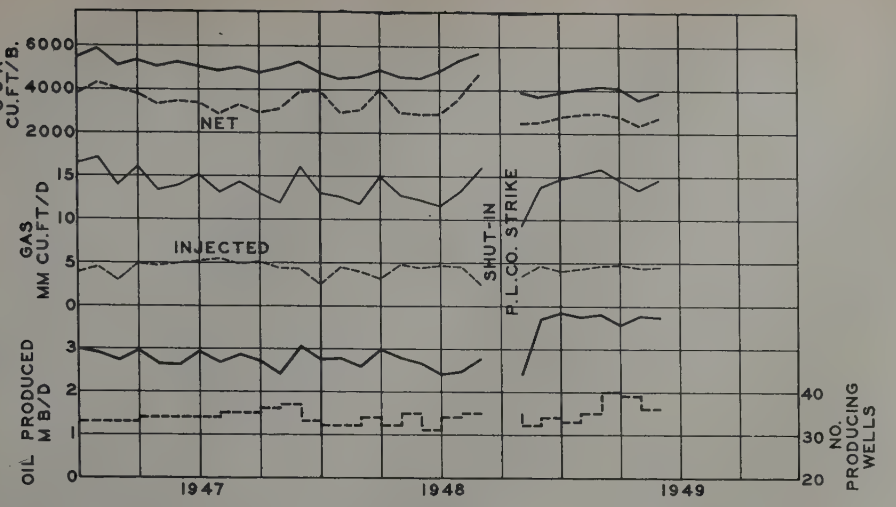

FIG. 8 — COMPARATIVE RESERVOIR PERFORMANCE.

(2) The true mean reservoir pressure is the fluid pressure at the mean depth in a whole interval, under conditions of static equilibrium. It is impractical or impossible to determine fluid distribution under static equilibrium conditions in the reservoir rock surrounding each well. Thus, a fluid gradient correction for the oil, water and gas (if gas cap exists) within the drainage area of the well bore is applied to the measured mean well datum pressure to determine the true mean pressure in the theoretical drainage area of each well. This corrected pressure is then multiplied by the net effective sand bulk volume within the wells' drainage area. The sum of these values (pressure x net acre-ft) is then divided by the total pool acre-ft to arrive at the volumetrically weighted mean reservoir pressure. This procedure was also followed in determining the pressure of the crestal, intermediate, and low structure wells (as grouped in Table IV) and in turn relative oil and gas saturation. The mean formation pressure so calculated is shown in Table III.

Reservoir pressure maps, Figs. 12 through 12e, reflect concentrated withdrawal along the southeasterly property line and subsequent pressure equalization as development progressed and withdrawals were taken more ratably. The low average permeability and permeability distribution of the north flank is evident by slow equalization and variation in pressure of offset wells. Although faults are a pressure barrier between individual sand intervals, from a reservoir standpoint faults do not alter or affect pressure performance in a pool where all zones are open to a common well bore.

Reservoir pressure decline to date is a direct function of net fluid withdrawal. Although masked by high gas-oil ratios and oil production rates since 1942, water influx has had a small effect on retarding rate of pressure decline. Since the volume and rate of water encroachment are relatively small as compared to total fluid withdrawal, it is doubtful that water will influence pool performance to any great extent until the pool nears depletion.

WELL INTERFERENCE

In spite of the heterogeneity of the producing sand, lamination of sand and shales, and faulting, there is communication between wells, as evidenced by channeling of injected gas between offset wells. The flowing characteristics of Well Nos. 9, 10, 13, and 18 are also affected by changes in production rates of nearby wells.

Gas-oil ratio and pressure maps clearly illustrate this condition. Interference between wells other than the above-mentioned is difficult to detect during the relatively short test periods involving comparatively small volumetric withdrawals.

Well No. 11 offers an excellent example of the detrimental effect of poor mud on productivity. After an initial clean-up period, the productivity index in August, 1939, was found to be 0.76 B/D per psi. This is an abnormally low value for a south flank well, as shown on Fig. 7a. The well reached its peak productivity of 1.2 B/D per psi after having produced 126,000 bbl. This characteristic is apparent in a number of the early water base mud completions.

WATER PRODUCTION

Water production during the early life of the field was of relatively minor importance. Subsequent to 1939, when several wells were drilled along the southern flank of the central and western part of structure, water encroachment through highly permeable parts of the "Ia" to "J" and "J" to "Ja" intervals was found to be sufficient to warrant expense of shut-off operations. The water front is moving along the 4S fault in a northeasterly direction. The front has reached as far into the field as Well No. 13 where the water cut increased twenty-fold since 1942. Further downstructure, in Well No. 19, the water cut has increased from 32 per cent in 1942 to 68 per cent in 1949. Total water production from the First Grubb Pool amounts to 1.3 million bbl. Five wells account for 70 per cent of the total pool water production of 370 B/D. Control of water entry has been difficult and expensive because of the long sections of slotted liner separated by 30 to 60 ft blanks set opposite shales. Water entry can be located and shut off but only at the expense of sealing off oil-productive sands of low permeability.

Table IV

Summary of Recovery Factors

	Cum. Prod. Bbl.	Acres	Ac. Ft.	B/Ac.	B/Ac. Ft.	B/Lb. Drop
GOR above 10,000	954,865	10.6	7.995	90.081	119	528
GOR 5,000 to 10,000	6,151,811	85.26	59.733	72,154	103	3,529
GOR below 5,000	7,324.234	159.94	83,253	45.794	88	5,093
Structural Elev. at top of "H" —						
above –4,800	1,603,234	38.18	21,460	41,990	75	851
–4,800 to –5,000	5,700,309	97.84	71,734	58,261	79	3,242
–5,000 to –5,500	7,041,647	112.49	54,928	62,598	128	4,596
North Flank	1,050,531	93.54	57,712	11,230	18	688
South Flank	13,445,045	169.37	98,516	90,617	136	8,022

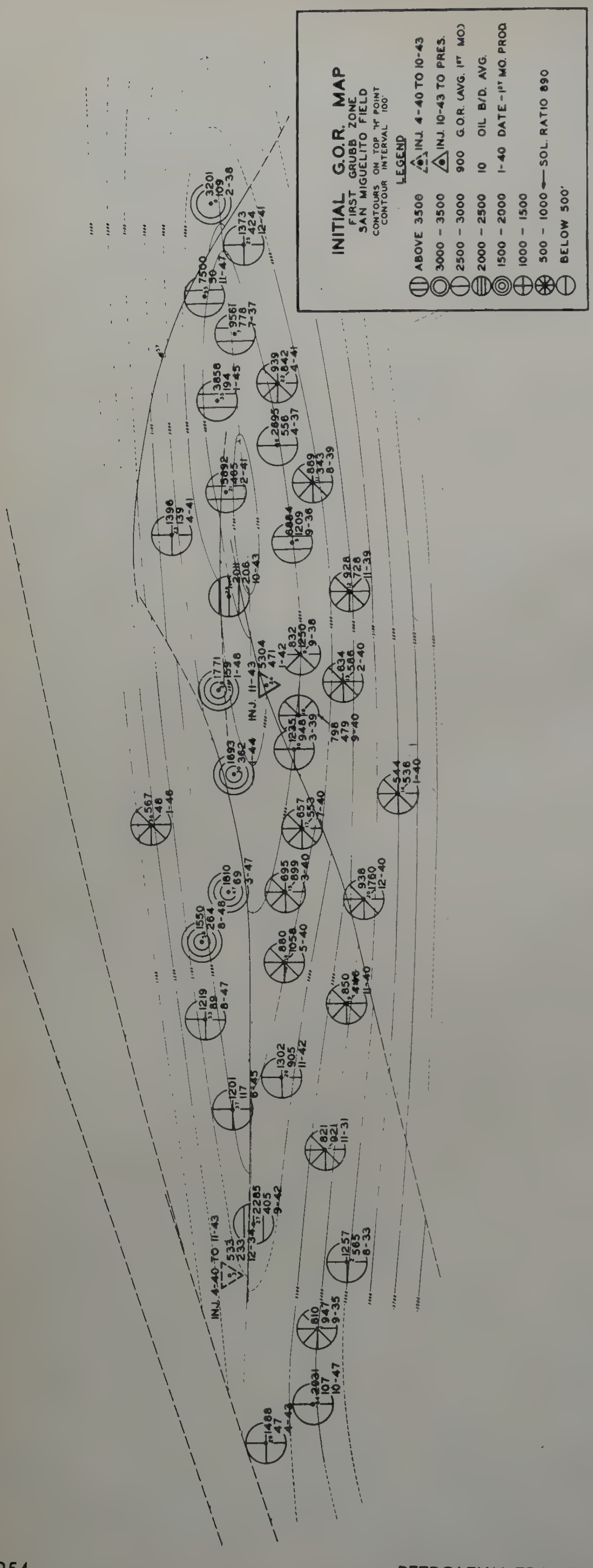

FIG. 9 — INITIAL GAS-OIL RATIO MAP.

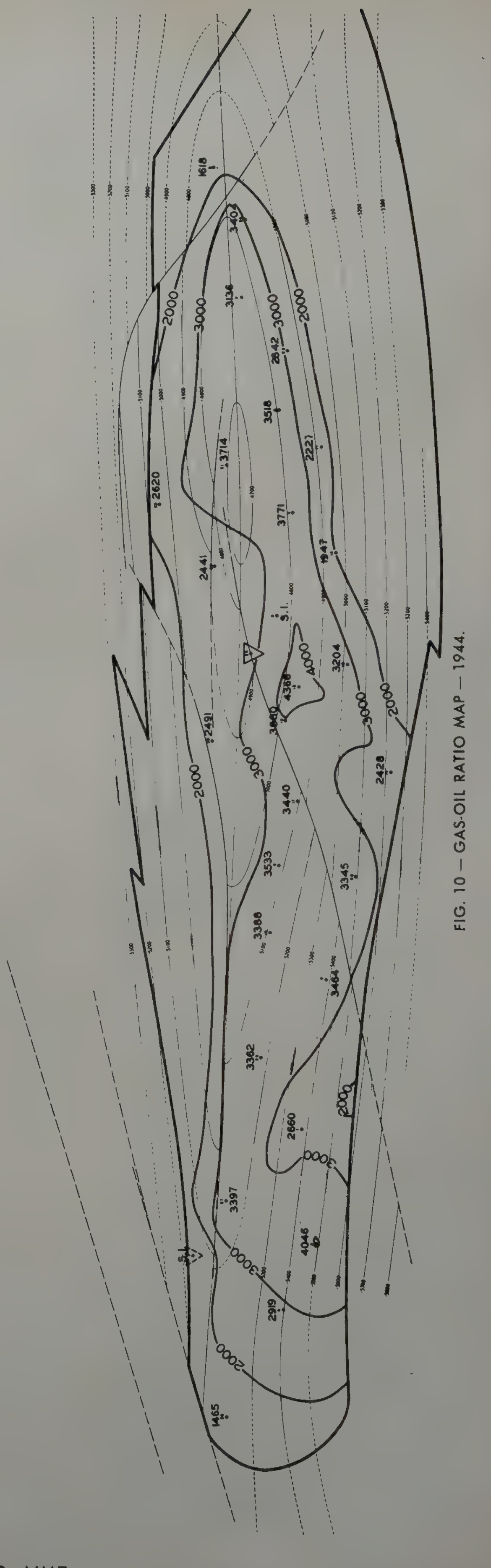

FIG. 10 — GAS-OIL RATIO MAP — 1944.

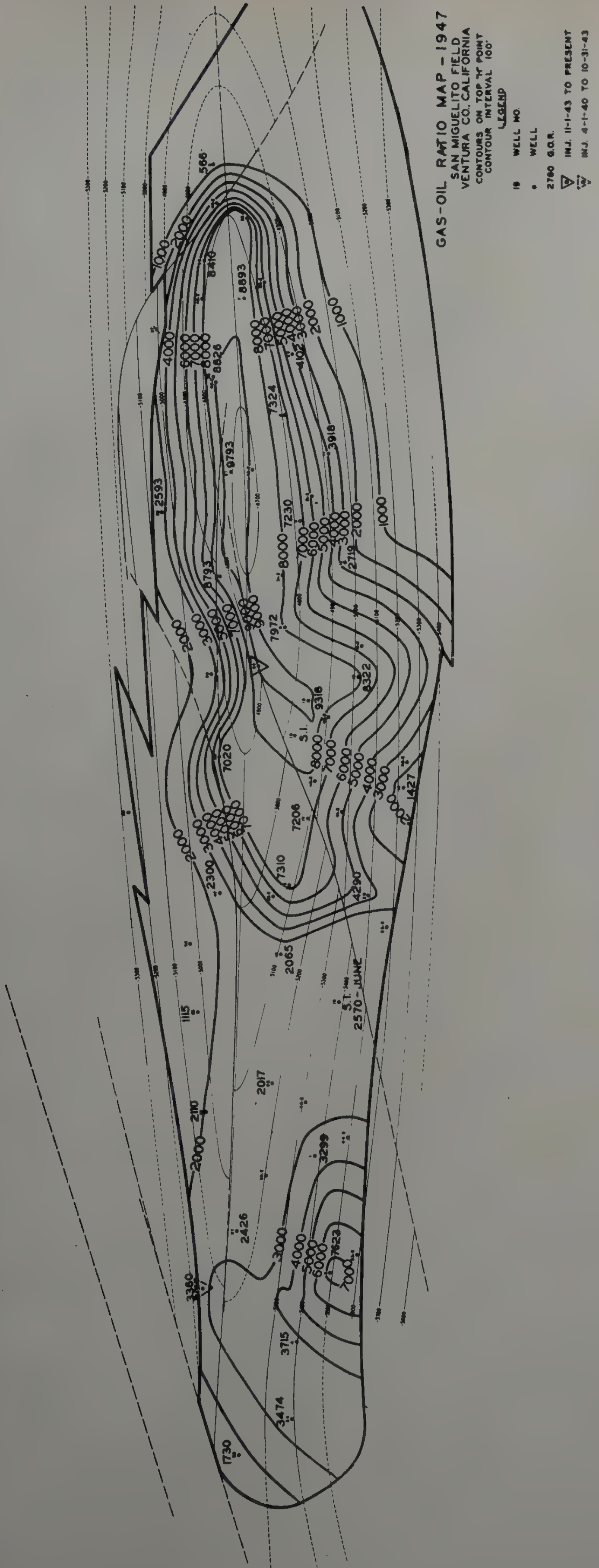

FIG. 10a — GAS-OIL RATIO MAP — 1947.

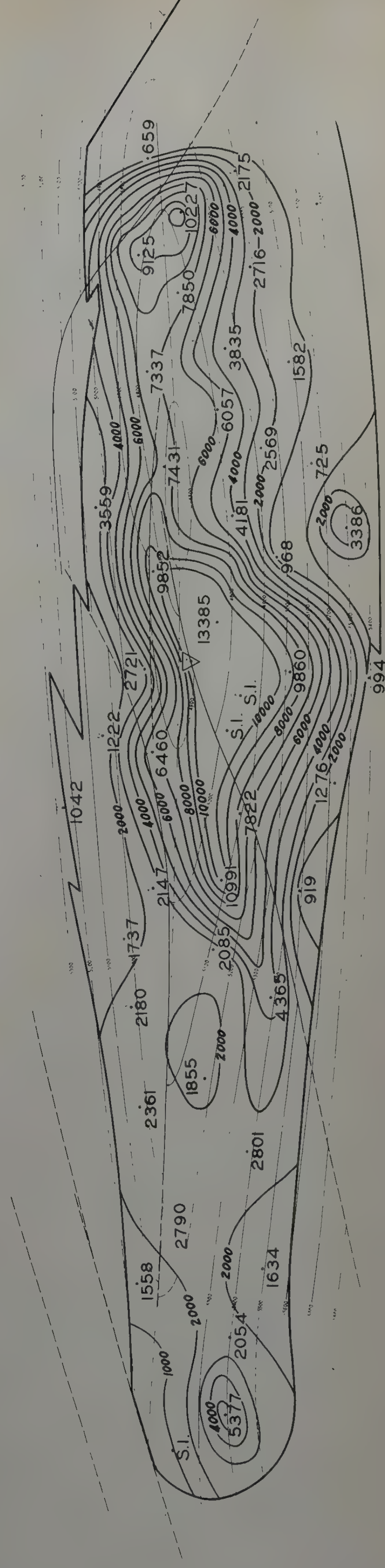

FIG. 10b — GAS-OIL RATIO MAP — MARCH, 1949.

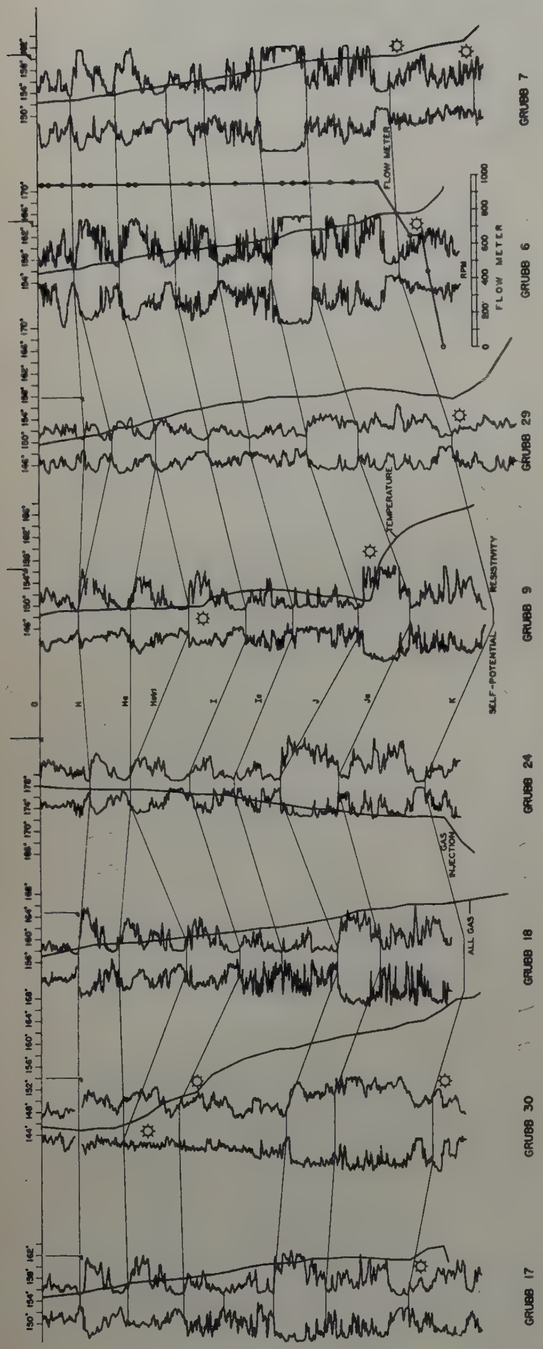

FIG. 11 — FLUID FLOW CHART.

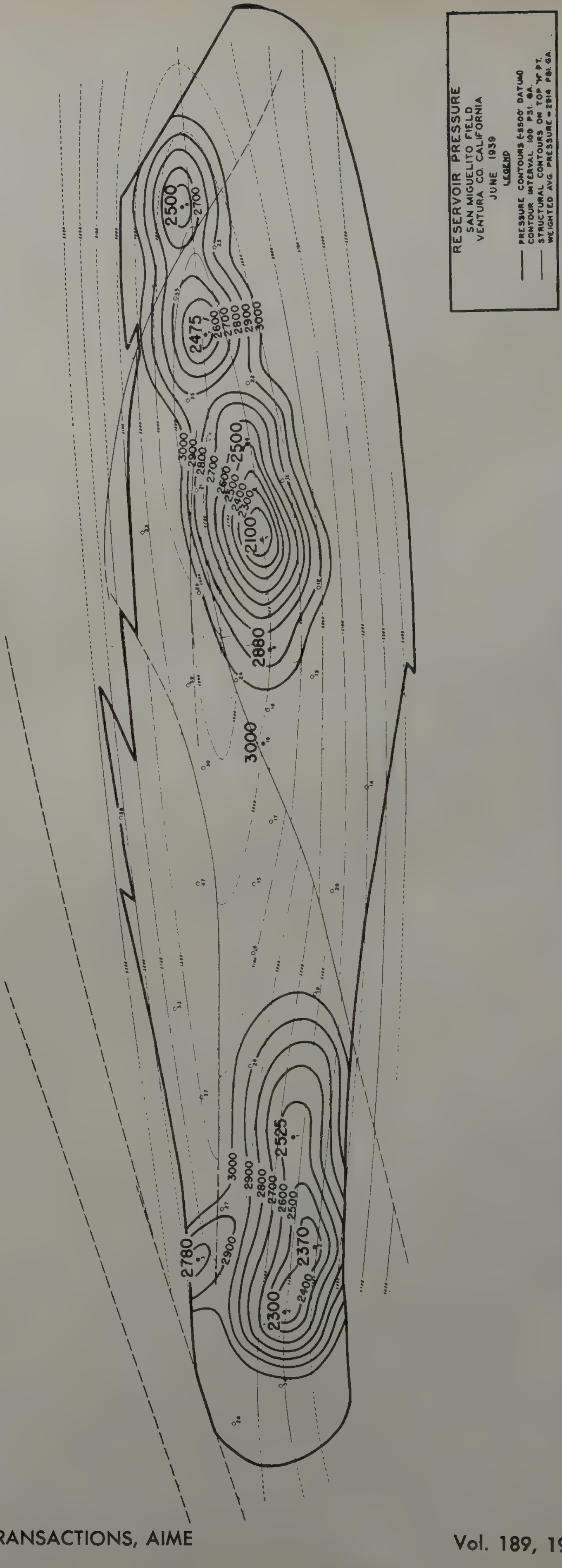

FIG. 12 — RESERVOIR PRESSURE MAP — JUNE, 1939.

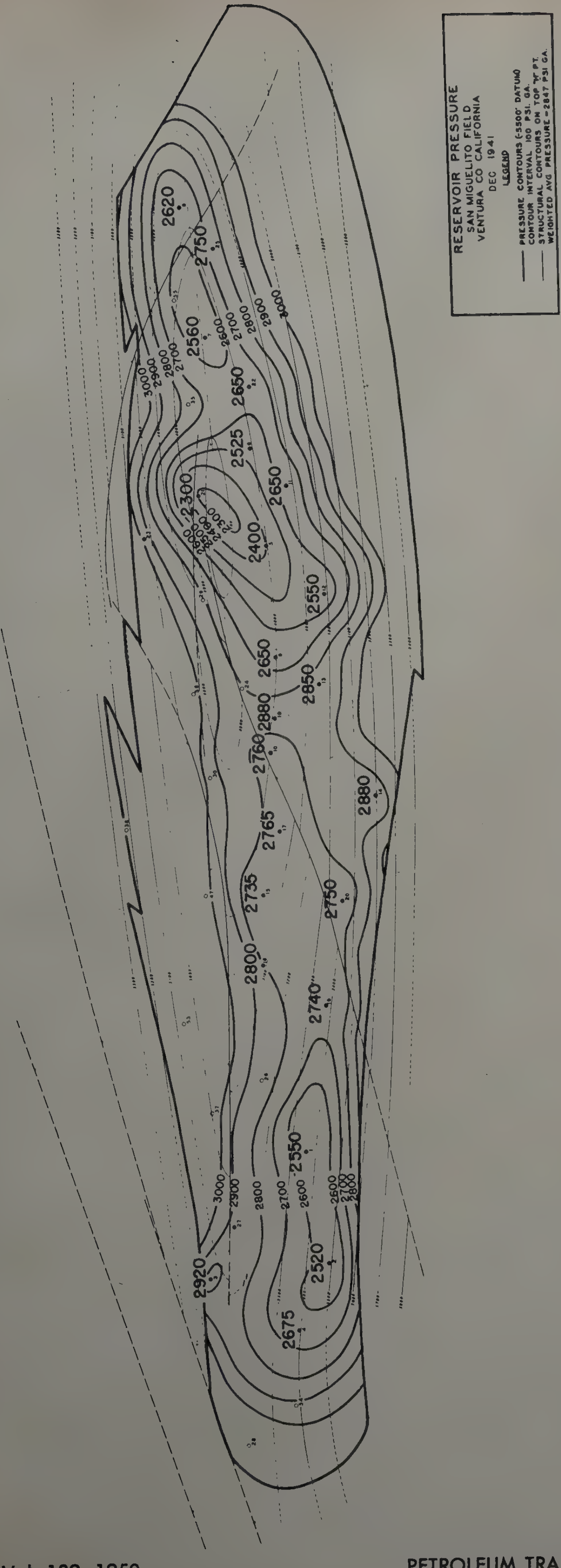

FIG. 12a — RESERVOIR PRESSURE MAP — DECEMBER, 1941.

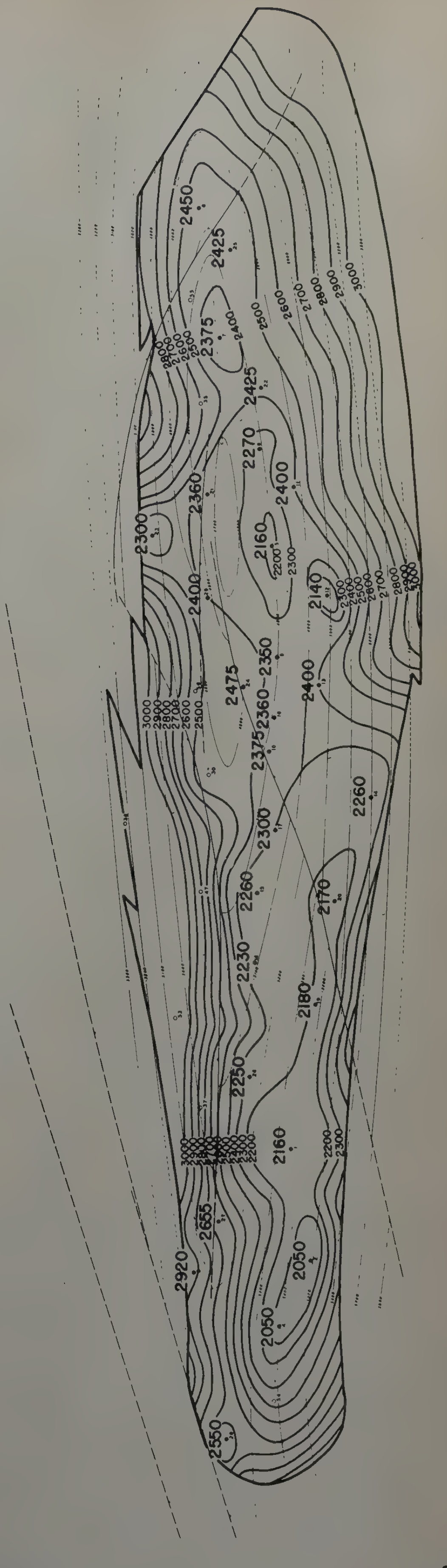

FIG. 12b — RESERVOIR PRESSURE MAP — DECEMBER, 1943.

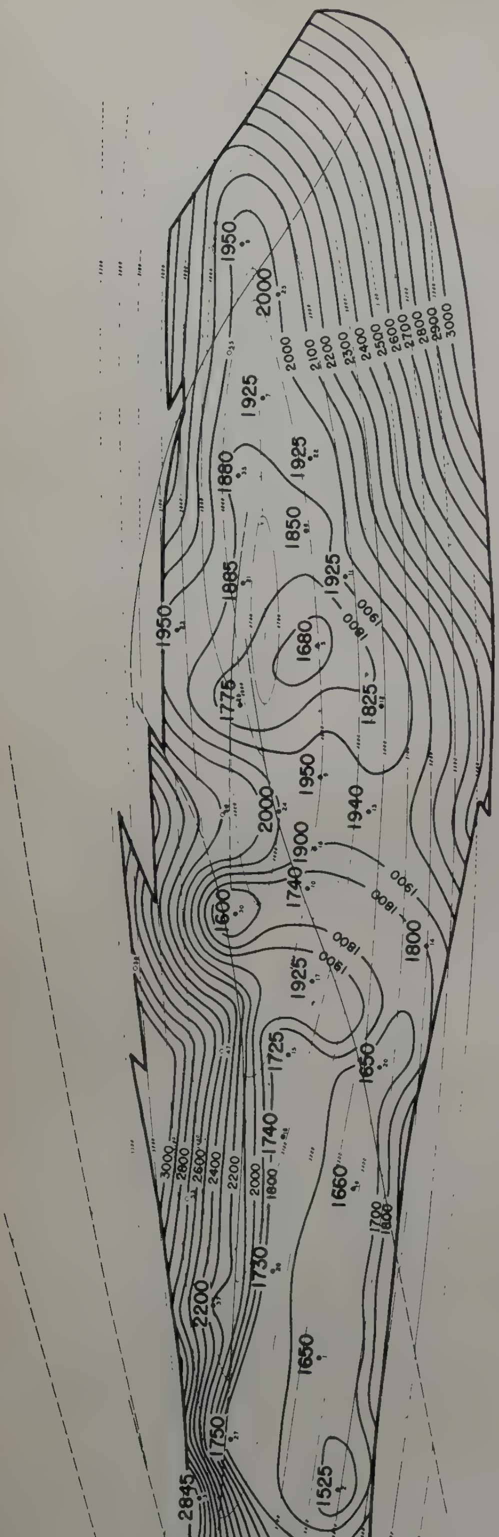

FIG. 12c — RESERVOIR PRESSURE MAP — SEPTEMBER, 1945.

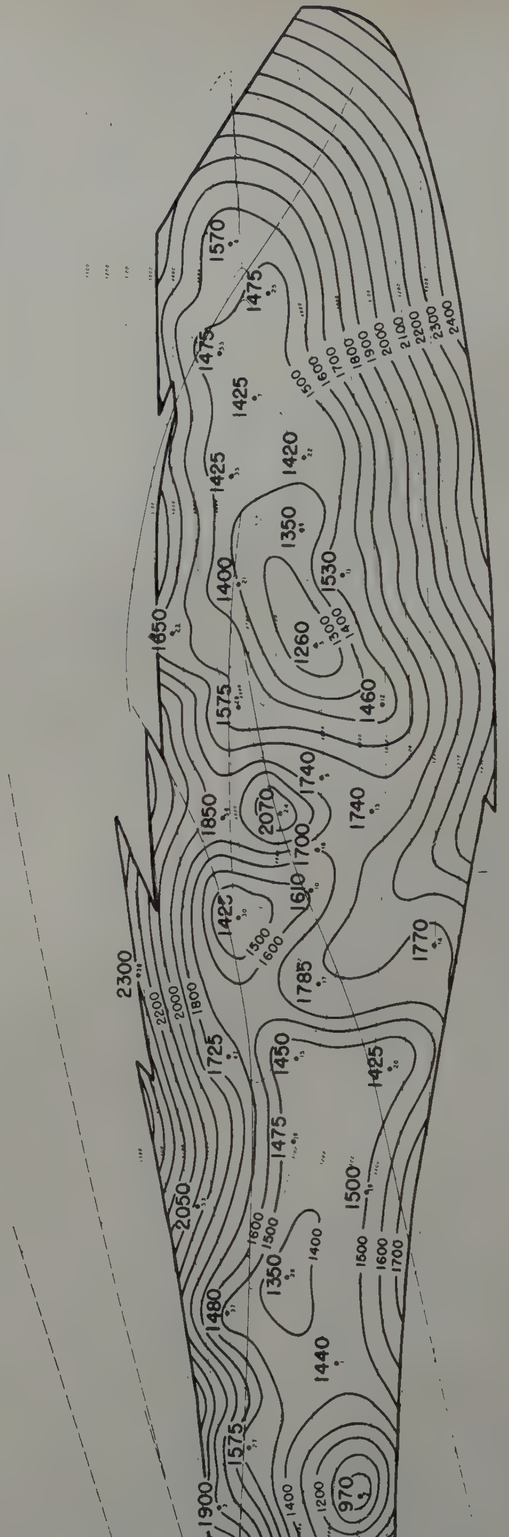

FIG. 12d — RESERVOIR PRESSURE MAP — MARCH, 1948.

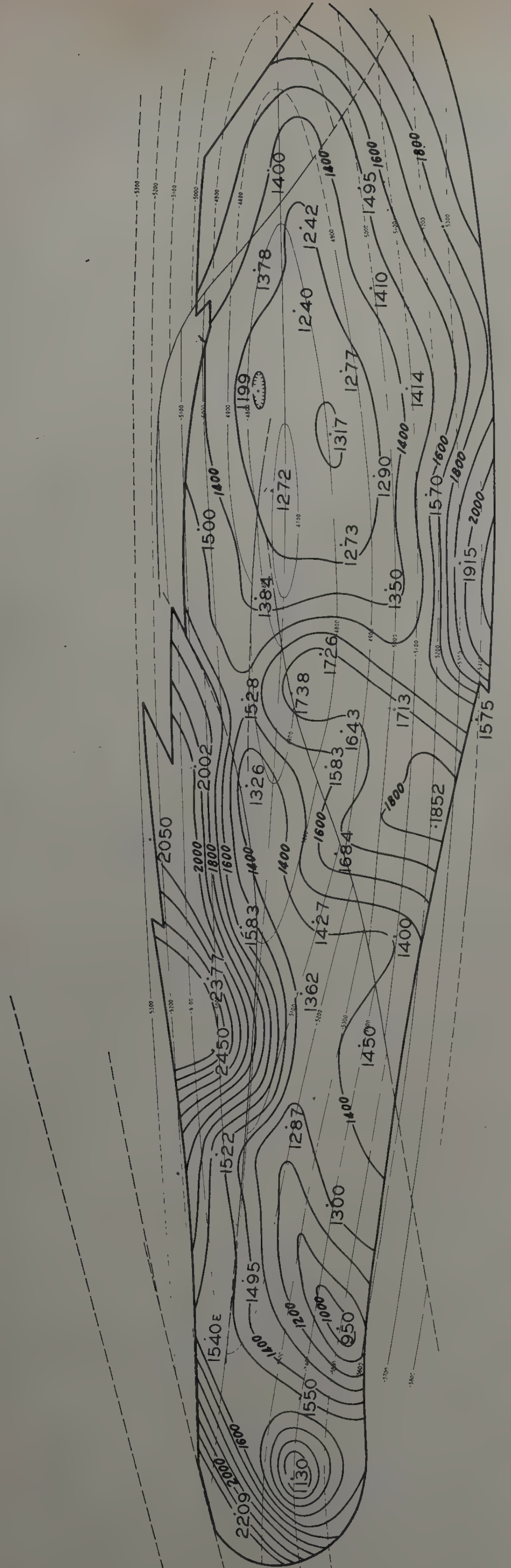

FIG. 12e — RESERVOIR PRESSURE MAP — MARCH, 1949.

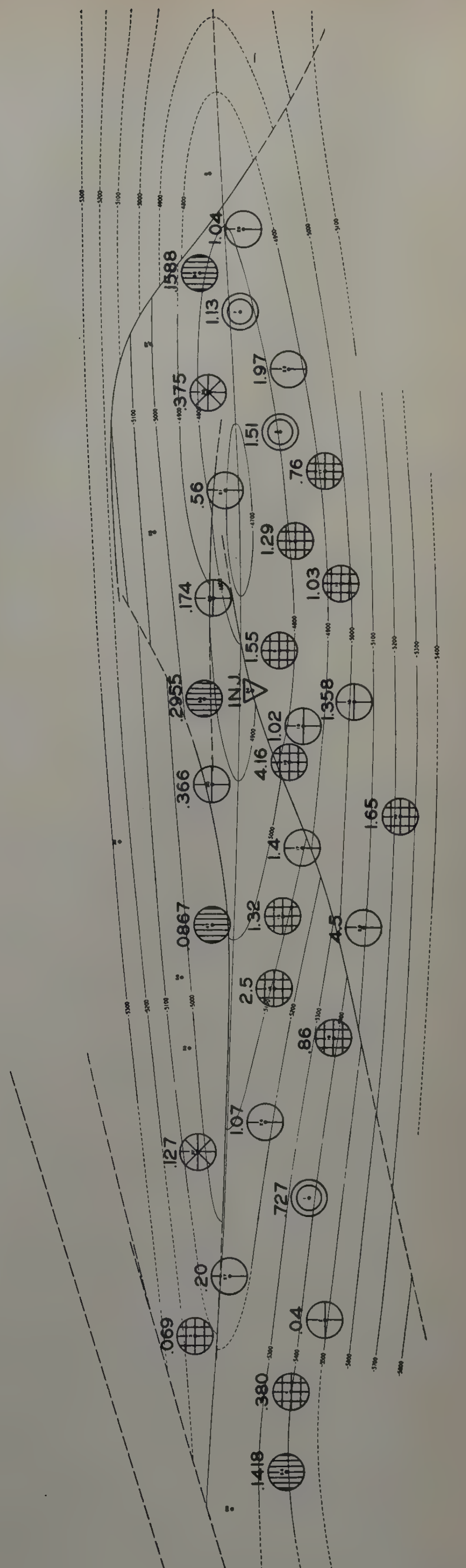

FIG. 13 — INITIAL PRODUCTIVITY INDEX MAP.

PRODUCTIVITY INDEX

A study of Fig. 13, Initial Productivity Index Map, reveals the uniform low permeability of the north flank and westerly area of the First Grubb Pool. Productivity indices of the recently completed south flank wells range from 1.7 to 2.1 B/D per lb per square in. pressure drop. The indicated potential of two of these wells was in excess of 1,000 B/D. This fact is significant in view of the stage of depletion of the reservoir, limited interval open and pressure decline to approximately 60 per cent of the estimated original well datum pressure.

The productivity index history of the high ratio wells, Fig. 6, reflects declining productivity indices with increasing gas-oil ratios. As the peak ratio is passed, the productivity index increases or its rate of decline is arrested. This characteristic may reflect relative saturation of oil and gas in a zone or zones not affected by gas channeling. As a rule, the rate of productivity index decline is directly proportional to permeability to oil and in turn structural position.

SPACING AND RECOVERIES

The spacing density of the First Grubb Pool was originally 10 acres per well. The density was based on such considerations as an average net sand thickness of 685 ft, relatively low permeability, topography, and other factors. As development proceeded, average density was increased to 6.5 acres per well. Present well density of the developed acreage ranges from 2.54 to approximately 8 acres per well.

Recoveries to date range from an average of 18 bbl per acre-ft on the north flank to an average of 136 bbl per acre-ft on the south flank. The recovery factors as shown by Table IV are grouped to illustrate stage of depletion, gravity drainage, and gas-oil segregation by gas-oil ratio brackets, structural elevation, and flank of the structure. The north flank low recovery reflects low permeability and productivity indexes of less than one-half of those on the south flank. The greater bbl per acre-ft recovery of the high gas-oil ratio group reflects stage of depletion and gas-oil segregation. This is further evidenced by the low recovery efficiency index of 52 bbl per lb drop for the area above 10,000 GOR as compared to 5,093 bbl from the low ratio group.

The recovery in terms of bbl per acre-ft and recovery index of bbl per lb drop of the low structure wells indicate effect of gravity segregation and drainage. This effect should become even more pronounced as the downstructure pressures are dissipated. Until recently, the low pressure area on the crest of the structure caused a pressure differential greater than gravity head, thus a tendency to flow oil up-dip. For this reason, gravity drainage in a part of the reservoir has been negligible.

As of August, 1948, the discovery well was pumping 27 B/D oil with a cut of 75 per cent after a cumulative recovery of 1,730,000 bbl. At that time it was whipstocked some 270 ft upstructure and recompleted in the "K to L" interval of the First Grubb zone, for an oil potential of 100 B/D. It is estimated that the ultimate recovery from this well will be nearly 2,000,000 bbl at the time of abandonment. Several wells have recovered nearly a million bbl. Pool cumulative recovery is 15,600,000 bbl.

CONCLUSIONS

The San Miguelito-First Grubb Pool has produced 15,500,000 bbl of oil, 45 billion cu ft of gas and one-third million bbl of water. Although there is evidence of a partial water drive in some sands within the First Grubb zone from the southern flank of the structure, the current rate of water encroachment is of such small magnitude that it does not affect the behavior of the solution-gas-drive reservoir. Material balance calculations have shown that water contiguous to this reservoir has been ineffective in maintaining pressure. The relatively small volume of gas injected in the crest of the structure has had no material effect on ultimate recovery. Gas injection has had an adverse effect on offset wells as a result of gas channeling. Past reservoir performance history under high pressure gas injection should not be construed as being indicative of the results to be obtained under future selectively controlled low-pressure gas injection.

Reservoir performance to date reflects gas channeling, effective gas-oil segregation, and effects of high withdrawal rates in a reservoir of relatively low permeability.

Faults, lamination of sands and shales, and heterogeneity of the producing sands affect the pressure and gas-oil ratio distribution within the First Grubb reservoirs; however, faults are not pressure barriers, with the possible exception of the one in the vicinity of Well No. 8.

The importance of determining true reservoir pressures in a steeply dipping high relief California type pool cannot be overemphasized. There is a 500-lb pressure differential between the top and bottom of the First Grubb zone. Volumetrically weighted mean well datum pressures have proved to be more accurate for reservoir mechanics calculations. Due to the time required for this method of pressure analysis, it is often desirable to determine a mean formation datum pressure, as is the custom, which is satisfactory for use in well comparisons and selective withdrawal control.

ACKNOWLEDGMENTS

The author wishes to express his appreciation to the management of the Continental Oil Co. for permission to publish the data used in this report. He desires to acknowledge the capable assistance of R. T. Hanson, J. H. Bolstad, John Van Riper, and Leroy Witt of the Pacific Coast Region. In addition, credit should be given M. H. Dubrow, Ponca City Production Department, John A. Murphy, and others of the Development and Research Department of Ponca City, Okla., for their valuable assistance and suggestions.

REFERENCE

M. B. Standing, "A Pressure-Volume-Temperature Correlation for Mixtures of California Oils and Gases." *API Drilling and Production Practice* (1947).

★ ★ ★

T.P. 2950

VOLUMETRIC BEHAVIOR OF OIL AND GAS FROM A LOUISIANA FIELD I

H. H. REAMER AND **B. H. SAGE,** CALIFORNIA INSTITUTE OF TECHNOLOGY, PASADENA, CALIF., MEMBER AIME

ABSTRACT

An experimental investigation was conducted upon five different paired samples of oil and gas from a field in Louisiana. The study, with each pair of samples, included the measurement of the formation volume and the volume of the liquid phase for three mixtures of the oil and gas. The gas-oil ratio varied from approximately 200 to over 40,000 cu ft per bbl and measurements were made at temperatures between 40° and 250°F. The gravity of the tank oil for the five samples under investigation varied between 38.0° and 55.8° API.

The composition of the oil and gas samples and their mixtures is submitted in tabular form. A number of diagrams depicting the effect of temperature and gas-oil ratio upon retrograde dew-point pressure are presented.

INTRODUCTION

During the past two decades a fairly large number of investigations were made of the volumetric behavior of naturally occurring hydrocarbon mixtures. The earlier work of Beecher and Parkhurst[1] and a more recent report on samples from Dominguez Field[2] are typical of research of this nature. Such studies have been used in estimating the volumetric behavior of fluids in producing fields other than those from which samples were taken. Progress has been made[3,4,5] in correlating the influence of pressure, temperature, and composition upon the specific and formation volume of hydrocarbon mixtures of relatively low gas-oil ratios, but attempts to extend this correlation to higher ratios have not been particularly successful. The influence of composition upon the volumetric behavior of such systems cannot be simply related to a single parameter such as gas-oil ratio. In order to aid in the extension of the correlation of the volumetric behavior of mixtures of oil and gas to higher ratios, a rather complete study was made of five different pairs of samples from a Louisiana field. The complexity of the influence of composition upon the volumetric and phase behavior of such systems in the regions of retrograde condensation was indicated by earlier work,[6,7,8,9,10] and it is doubtful if simple correlations can be established in these regions with the information currently available. The terminology employed in this paper is identical to that utilized earlier.[10]

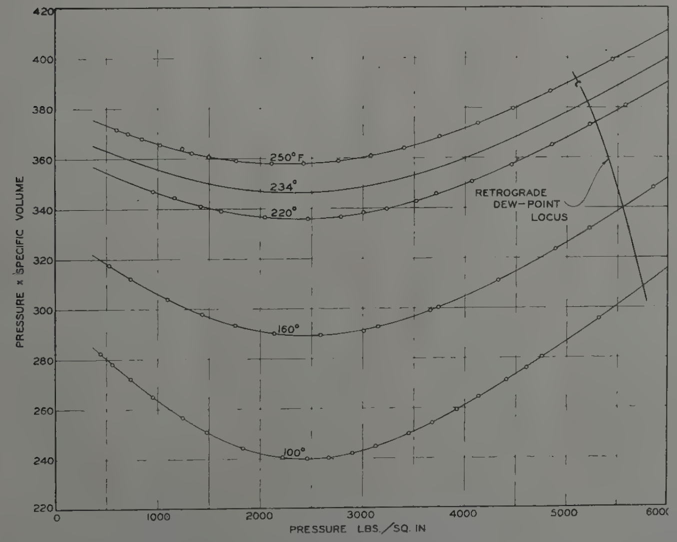

FIG. 1 — PRESSURE, SPECIFIC VOLUME PRODUCT FOR SYSTEM C CONTAINING 0.6912 WEIGHT FRACTION TRAP GAS.

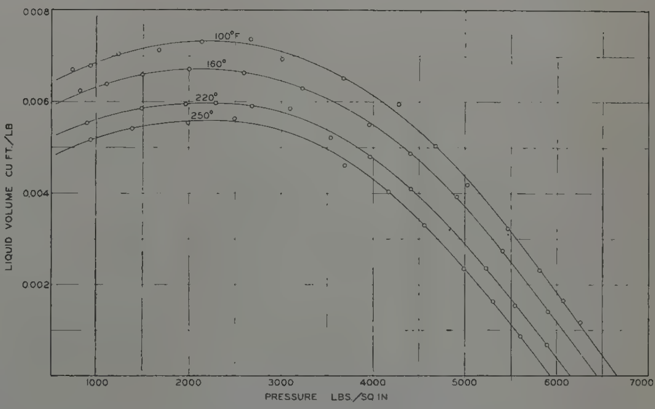

FIG. 2 — VOLUME OF LIQUID PHASE FOR SYSTEM C CONTAINING 0.6912 WEIGHT FRACTION TRAP GAS.

---

[1] References given at end of paper.

Manuscript received at the office of the Petroleum Branch February 21, 1950.

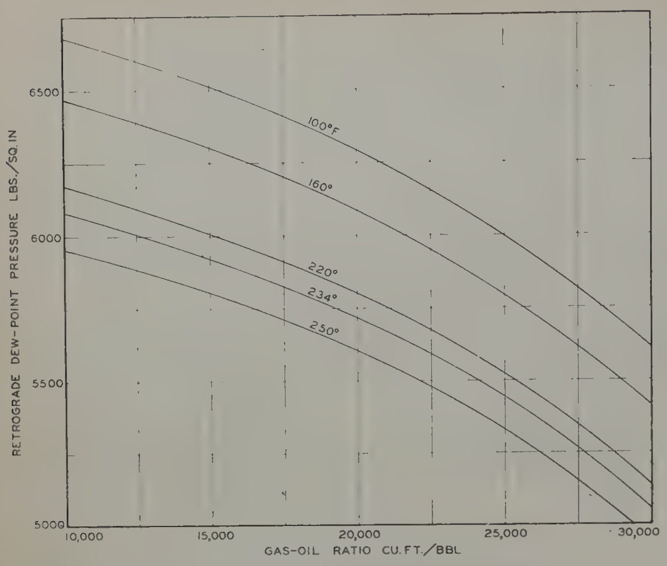

FIG. 3 — RETROGRADE DEW-POINT PRESSURES FOR SYSTEM C.

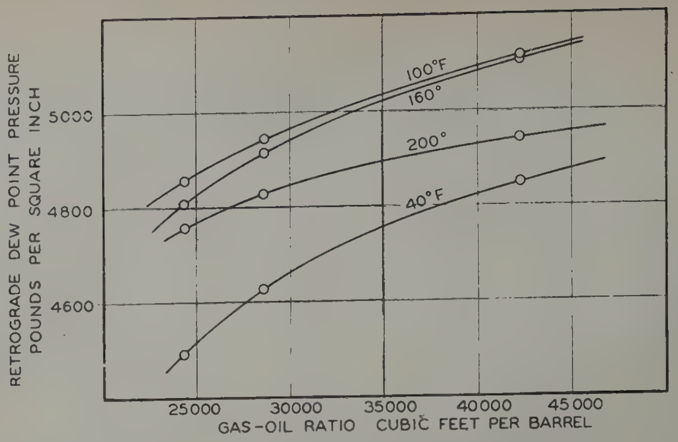

FIG. 6 — RETROGRADE DEW-POINT PRESSURE FOR SYSTEM A.

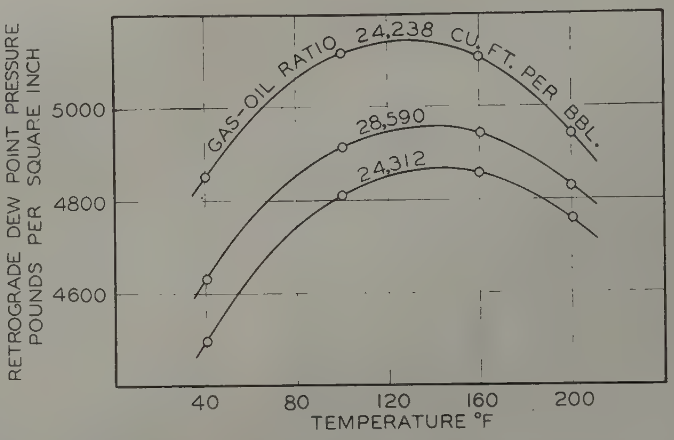

FIG. 7 — INFLUENCE OF TEMPERATURE UPON RETROGRADE DEW-POINT PRESSURE FOR SYSTEM A.

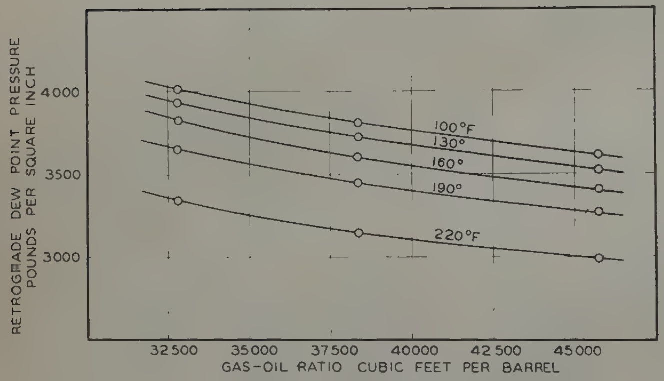

FIG. 4 — RETROGRADE DEW-POINT PRESSURES FOR SYSTEM *E*.

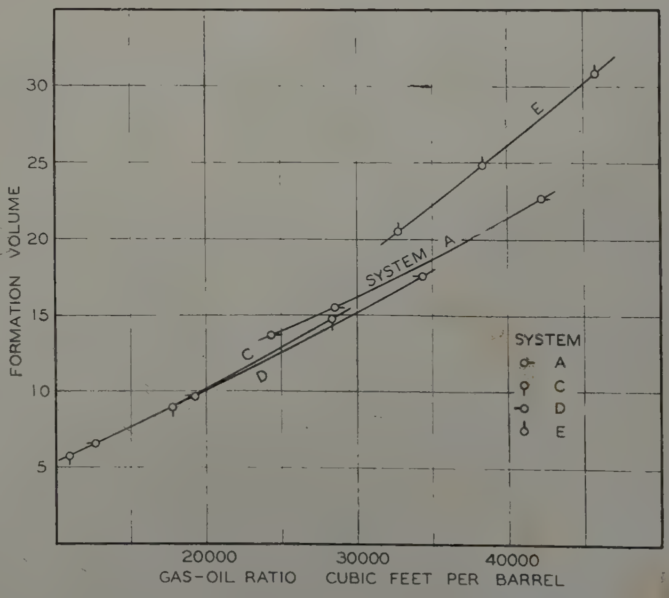

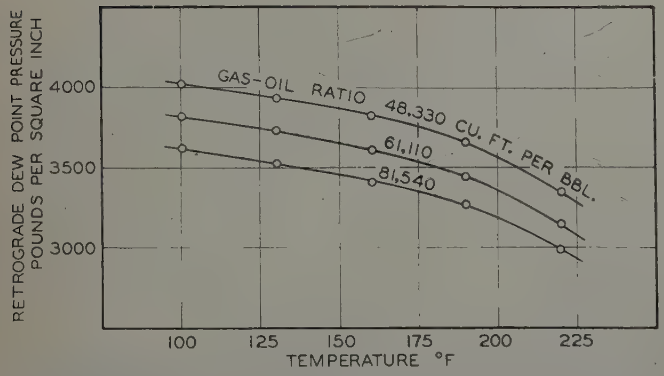

FIG. 5 — INFLUENCE OF TEMPERATURE UPON RETROGRADE DEW-POINT PRESSURE OF SYSTEM *E*.

FIG. 8 — FORMATION VOLUME AT RETROGRADE DEWPOINT FOR 100°F.

Table I

Composition of Trap Samples

Component	Gas Mole Fraction	Gas Weight Fraction	Liquid Mole Fraction	Liquid Weight Fraction
SYSTEM—A				
Methane	0.94204	0.8582	0.1110	0.0163
Ethane	0.02820	0.0482	0.0214	0.0059
Propane	0.01303	0.0326	0.0353	0.0142
Isobutane	0.00433	0.0143	0.0252	0.0133
n-Butane	0.00303	0.0100	0.0299	0.0158
Isopentane	0.00154	0.0063	0.0575	0.0379
n-Pentane	0.00090	0.0037	......	......
Hexanes	0.00129	0.0063	0.0875	0.0689
Heptanes	0.00070	0.0040	0.1274	0.1166
Carbon Dioxide	0.00400	0.0100	0.0042	0.0017
Octanes and heavier	0.00094[a]	0.0064	0.5006[f]	0.7094
SYSTEM—B				
Methane	0.9150	0.8096	0.0334	0.0027
Ethane	0.0379	0.0628	0.0113	0.0017
Propane	0.0197	0.0479	0.0188	0.0041
Isobutane	0.0050	0.0160	0.0118	0.0034
n-Butane	0.0046	0.0147	0.0141	0.0041
Isopentane	0.0018	0.0072	0.0115	0.0042
n-Pentane	0.0010	0.0040	0.0135	0.0048
Hexanes	0.0013	0.0062	0.0385	0.0166
Heptanes	0.0005	0.0028	0.0765	0.0383
Octanes and heavier	0.0002[b]	0.0014	0.7706[g]	0.9201
Carbon Dioxide	0.0080	0.0194	......	......
Air	0.0050	0.0080	......	......
SYSTEM—C				
Methane	0.9184	0.8134	0.1149	0.0159
Ethane	0.0378	0.0627	0.0347	0.0090
Propane	0.0148	0.0360	0.0349	0.0133
Isobutane	0.0038	0.0122	0.0191	0.0096
n-Butane	0.0071	0.0228	0.0247	0.0124
Isopentane	0.0028	0.0112	0.0266	0.0166
n-Pentane	0.0010	0.0040	0.0202	0.0126
Hexanes	0.0010	0.0048	0.0802	0.0597
Heptanes	0.0008	0.0044	0.1412	0.1222
Octanes and heavier	0.0005[c]	0.0035	0.5035[h]	0.7287
Carbon Dioxide	0.0070	0.0170	......	....
Air	0.0050	0.0080	......	......
SYSTEM—D				
Methane	0.9281	0.8366	0.1190	0.0165
Ethane	0.0382	0.0645	0.0349	0.0091
Propane	0.0144	0.0357	0.0343	0.0131
Isobutane	0.0034	0.0111	0.0160	0.0081
n-Butane	0.0032	0.0104	0.0267	0.0134
Isopentane	0.0016	0.0065	0.0261	0.0163
n-Pentane	0.0007	0.0028	0.0214	0.0133
Hexanes	0.0015	0.0073	0.0827	0.0616
Heptanes	0.0007	0.0039	0.1317	0.1142
Octanes and heavier	0.0002[d]	0.0014	0.5072[i]	0.7344
Carbon Dioxide	0.0080	0.0198	......	......
SYSTEM—E				
Methane	0.9628	0.9011	0.1333	0.0217
Ethane	0.0168	0.0295	0.0178	0.0054
Propane	0.0089	0.0229	0.0242	0.0108
Isobutane	0.0025	0.0085	0.0131	0.0077
n-Butane	0.0030	0.0102	0.022	0.0134
Isopentane	0.0013	0.0055	0.0231	0.0169
n-Pentane	0.0008	0.0034	0.0221	0.0162
Hexanes	0.0014	0.0070	0.0876	0.0765
Heptanes	0.0011	0.0064	0.1579	0.1604
Octanes and heavier	0.0004[e]	0.0029	0.4977[j]	0.6708
Carbon Dioxide	0.0010	0.0026	0.0005	0.0002

Average molecular weight of less volatile constituents:
a. 120.0 c. 125 e. 125
b. 125 d. 125
Average molecular weight as determined from freezing-point lowering of benzene:
f. 155.2 h. 167.6 j. 133
g. 238.9 i. 167.4

MATERIALS

The samples of oil and gas from each of several surface primary separators were obtained and forwarded to this laboratory in appropriate pressure vessels. Subsamples were withdrawn from each of the pressure vessels containing liquid phase samples by appropriate displacement procedures involving the use of ethylene glycol. These subsamples were dried by passage through chambers packed with granular calcium chloride. The samples of the trap gas were withdrawn from the primary gas containers after the vessels had been maintained at a temperature in excess of 250°F for several hours. This procedure was followed in order to avoid the possibility of the partial condensation of portions of the trap gas in the original container. The subsamples were forwarded to an industrial laboratory where the composition of the trap liquid and trap gas was determined by appropriate fractionation analysis.

The results of these analytical measurements are reported in terms of both mole and weight fractions. The latter variable is included because of uncertainties as to the molecular weight of the octanes and heavier fractions of the trap liquid and trap gas samples. In the case of the trap liquid samples, the molecular weight of the octanes and heavier hydrocarbons was obtained from the freezing point of benzene.

PROCEDURES

The equipment used in this study[11] and the techniques employed in the determination of the quantity of each of the phases have already been presented in the literature.[10,12,13] For this reason, it is not necessary to review in detail the laboratory approach to this investigation. In principle, it consisted of introducing appropriate quantities of the trap liquid into a closed vessel in which the sample was confined over mercury. The quantity of this hydrocarbon sample was established from volumetric measurements carried out upon a trap liquid sample of known weight. The weight of trap gas was established by direct gravimetric techniques making use of weighing bombs.[14] The total volume of the mixture of trap liquid and trap gas was determined as a function of pressure for a series of temperatures. In addition, the total volume of the liquid phase was established throughout the greater part of the heterogeneous region. This information was obtained by the direct measurement of the relative elevation of the mercury-hydrocarbon and the hydrocarbon liquid-gas interfaces. The details of this method have been described.[11] These measurements were carried out at temperatures between 40° and 320°F. In all cases at least three different temperatures were investigated and in some cases as many as five were studied.

Experimental data were obtained for a series of different gas-oil ratios for each set of samples of trap liquid and trap gas. An effort was made to use as nearly identical methods as possible in the studies of each set of samples. Some minor changes in procedure were required but it is not believed that these variations significantly influenced the results.

DESCRIPTION OF SAMPLES

Five sets of corresponding samples of trap liquid and trap gas were obtained from the field and are identified in this text by the letters *A* to *E* inclusive. The composition of the trap liquid and trap gas for each set is presented in Table I. The weight and mole fractions of the lighter hydrocarbons were tabulated with similar information for each of the fractions making up the octanes and heavier portion of the trap liquid samples. In the footnotes to Table I, attention is called to additions or variations in the tabular information for the several sets of trap samples.

The physical properties of the octanes and heavier portion of the five trap liquid samples are presented in Table II. These data are supplemented by more limited information concerning the characteristics of several portions of the overhead obtained from the fractionation of the octanes-and-heavier portions at reduced pressures. As an added characterization, the viscosity-gravity factor[15] was computed for each of the fractions as well as for the octanes-and-heavier parts of the trap liquid samples as a whole. It is believed that the information contained in Tables I and II permits a fairly complete evaluation of the quantities of the lighter hydrocarbons in each of the mixtures of trap sample investigated and gives at least a rough indication of the principal characteristics of the octanes-and-heavier hydrocarbons making up these samples. Since the data submitted for each of the corresponding sets of samples are similar, a direct comparison of the characteristics may be obtained.

The relative quantities of the lighter hydrocarbons in the liquid phase recovered from the stock tank for each of the trap samples are recorded in Table III. The compositions of the corresponding trap samples and tank oil have been

Table II

Properties of Octanes and Heavier — Portion of Trap Liquid Sample

	System-A	System-B	System-C	System-D	System-E
Specific Gravity °API 60°F, atmospheric pressure	47.5	35.4	43.8	43.2	49.8
Specific Volume 60°F, atmospheric pressure	0.020276	0.018917	0.01987	0.01980	0.020543
Average molecular weight	155.2	238.9	167.6	167.4	133
Kinematic viscosity: centistokes					
77°F	1.5541	......	......	.....	......
100°F	1.2779	......	......	.....	......
Viscosity gravity factor	0.8080	......	......	.....	......

SYSTEM—A

Cut No.	Specific Gravity 60°F/60°F	Kinematic Viscosity Centistokes		Viscosity Gravity Factor	Boiling Range °F	Weight* Fraction
		77°F	100°F			
1	0.7489	0.7395	0.6430	0.792	244–266	0.06740
2	0.7545	0.7912	0.6839	0.795	266–284	0.06790
3	0.7641	0.8890	0.7617	0.801	284–318	0.06876
4	0.7674	1.0487	0.8880	0.798	318–347	0.06906
5	0.7756	1.2627	1.0514	0.800	347–377	0.06980
6	0.7881	1.5762	1.3018	0.806	377–415	0.07092
Residue	0.8211	3.8393	2.8759	0.816	....	0.29558

SYSTEM—B

Cut No.	Specific Gravity 60°F/60°F	Kinematic Viscosity Centistokes		Viscosity Gravity Factor	Boiling Range °F	Weight* Fraction
		77°F	100°F			
1	0.7682	0.896	0.796	0.805	240–340	0.0833
2	0.7880	1.381	1.135	0.811	340–419	0.0855
3	0.8099	2.511	1.942	0.815	419–484	0.0879
Residue	0.8735	35.05	21.53	0.829	484 ...	0.6634

SYSTEM—C

Cut No.	Specific Gravity 60°F/60°F	Kinematic Viscosity Centistokes		Viscosity Gravity Factor	Boiling Range °F	Weight* Fraction
		77°F	100°F			
1	0.7684	0.729	0.636	0.8164	248–268	0.0694
2	0.7717	0.806	0.693	0.8160	268–302	0.0697
3	0.7798	0.977	0.831	0.8160	302–347	0.0704
4	0.7884	1.299	1.075	0.8148	347–392	0.0712
5	0.7992	1.777	1.433	0.8146	392–436	0.0722
6	0.8109	2.465	1.928	0.8166	436–472	0.0732
Residue	0.8377	7.454	5.119	0.8181	472 ...	0.3026

SYSTEM—D

Cut No.	Specific Gravity 60°F/60°F	Kinematic Viscosity Centistokes		Viscosity Gravity Factor	Boiling Range °F	Weight* Fraction
		77°F	100°F			
1	0.7750	0.725	0.641	0.8240	236–274	0.0702
2	0.7755	0.783	0.685	0.8210	274–298	0.0703
3	0.7811	0.913	0.787	0.8202	298–336	0.0708
4	0.7894	1.218	1.027	0.8173	336–379	0.0715
5	0.7988	1.663	1.361	0.8161	379–428	0.0724
6	0.8141	2.392	1.872	0.8216	428–473	0.0738
Residue	0.8422	7.339	5.106	0.8240	473 ...	0.3053

SYSTEM—E

Cut No.	Specific Gravity 60°F/60°F	Kinematic Viscosity Centistokes		Viscosity Gravity Factor	Boiling Range °F	Weight* Fraction
		77°F	100°F			
1	0.7494	0.779	0.683	0.7892	252–276	0.0641
2	0.7536	0.807	0.700	0.7940	276–285	0.0645
3	0.7606	0.871	0.759	0.7975	285–304	0.0651
4	0.7685	0.962	0.822	0.8032	304–321	0.0658
5	0.7758	1.097	0.923	0.8060	321–348	0.0664
6	0.7837	1.296	1.084	0.8100	348-376	0.0671
7	0.7930	1.610	1.315	0.8120	376–412	0.0678
8	0.8029	2.134	1.695	0.8120	412–446	0.0687
Residue	0.8264	4.268	3.141	0.8190	446 ...	0.1413

* Based upon the entire trap liquid sample.

Table III

Composition of Tank Oil

Component	Mole Fraction	Weight Fraction
SYSTEM—A		
Methane	......	......
Ethane	......	......
Propane	0.01461	0.00500
Isobutane	0.01986	0.00895
n-Butane	0.02585	0.01165
Pentanes	0.06235	0.03488
Hexanes	0.09830	0.06568
Heptanes	0.14919	0.11591
Octanes and heavier	0.62984	0.75793
SYSTEM—B[a]		
Methane	......	......
Ethane	......	......
Propane	0.0161	0.0034
Isobutane	0.0099	0.0027
n-Butane	0.0125	0.0034
Isopentane	0.0112	0.0038
n-Pentane	0.0133	0.0046
Hexanes	0.0347	0.0142
Heptanes	0.0812	0.0386
Octanes and heavier	0.8211	0.9293
SYSTEM—C[b]		
Methane	......	......
Ethane	......	......
Propane	0.0144	0.0046
Isobutane	0.0123	0.0051
n-Butane	0.0248	0.0103
Isopentane	0.0422	0.0218
n-Pentane	0.0127	0.0065
Hexanes	0.0826	0.0510
Heptanes	0.1499	0.1075
Octanes and heavier	0.6611	0.7932
SYSTEM—D[c]		
Methane	......	......
Ethane	......	......
Propane	0.0208	0.0067
Isobutane	0.0168	0.0071
n-Butane	0.0254	0.0108
Isopentane	0.0338	0.0178
n-Pentane	0.0259	0.0136
Hexanes	0.0823	0.0517
Heptanes	0.1596	0.1167
Octanes and heavier	0.6354	0.7756
SYSTEM—E[d]		
Methane	0.0092	0.0013
Ethane	0.0049	0.0013
Propane	0.0158	0.0061
Isobutane	0.0118	0.0060
n-Butane	0.0228	0.0117
Isopentane	0.0258	0.0164
n-Pentane	0.0250	0.0159
Hexanes	0.1026	0.0780
Heptanes	0.1877	0.1659
Octanes and heavier	0.5944	0.6974

Gravities of the tank oil at 60°F.
[a] 38.0° API
[b] 49.5° API
[c] 49.4° API
[d] 55.8° API

used to determine the relationship of the gas-oil ratio to the composition of the mixture. The methods whereby this was accomplished have already been described.[10,12,13]

EXPERIMENTAL RESULTS

The compressibility factors of trap gas sample *A* are shown in Table IV. The behavior of this multicomponent hydrocarbon mixture is similar to that reported in earlier investigations.[12] The information submitted forms additional confirmation of the possibility of predicting within reasonable limits the volumetric behavior of natural gas.[16,17]

The composition of the experimentally studied mixtures for each of the several sets of samples is recorded in Table V. The corresponding values of the gas-oil ratio as well as the weight and mole fraction of the principal components are included in this tabulation. The methods employed in arriving at the several derived quantities presented in Table V have already been described.[12] The results of the experimental investigation of the five sets of mixtures are available.[18] A sample of these data for System *A* at 40°F is shown in Table VI. In each table, the specific volume, the volume of the liquid phase per unit weight of mixture, and the formation volume are recorded for a series of even valued pressures for each of the temperatures studied.

The qualitative significance of the results is already available in the literature [10,12,13] and for this reason only a limited number of figures pertaining to the volumetric behavior are included in this text. In Fig. 1 for System *C* is presented the product of the pressure and the specific volume for a mixture containing 0.6912 weight fraction trap gas. As a matter of interest the locus of the retrograde dew-point state has been indicated. No significant discontinuity in the relationship of the first derivative of the product of the pressure and volume with respect to pressure is discernible at dew point. Fig. 2 portrays the variation in the volume of the liquid phase per unit weight of mixture as a function of pressure for the same system. The nearly linear decrease in the volume of the liquid phase with increase in pressure for states at pressures above 4,500 psi is characteristic of materials of this type.

In Fig. 3 the variation of the retrograde dew-point pressure with gas-oil ratio is shown for System *C*. Similar information is presented in Fig. 4 for System *E*. In both of these cases an isothermal increase in gas-oil ratio causes a decrease in the retrograde dew-point pressure. The influence of temperature upon the retrograde dew-point pressure for System *E* for several different gas-oil ratios is indicated in Fig. 5. An increase in temperature results in a decrease in the retrograde dew-point pressure for both Systems *C* and *E*. A somewhat different behavior is presented in Fig. 6 for System *A*. In this instance an increase in gas-oil ratio is associated with an increase in the retrograde dew-point pressure but this effect is less pronounced at the higher temperatures. Fig. 7 shows that the retrograde dew-point pressure for System *A* reaches a maximum at temperatures between 120° and 150°F for gas-oil ratios between 42,000 and 24,000. This indicates a somewhat more complex behavior than was encountered for the other mixtures.

The formation volume at retrograde dew-point is depicted as a function of gas-oil ratio in Fig. 8 for 100°F. In this instance there is a similarity in the behavior of the several systems investigated. In each case an increase in gas-oil ratio resulted in an increase in formation volumes at retrograde dew-point. Similar behavior was found at the higher temperatures.

No simple relationship of retrograde dew-point pressure to the properties of tank oil appears to exist for this system as was the case for another investigation[10] of a similar nature. With the exception of System *B* all of the formation volumes in the heterogeneous region can be related to the prevailing gas-oil ratio, temperature, and pressure by the following expression:

$$v = \frac{ArT}{P} \quad \ldots\ldots \quad (1)$$

The values of the coefficient *A* are presented as a function of temperature and pressure in Table VII. It is apparent that there is but little variation in this constant with change in pressure and temperature. Equation 1 should not be employed at gas-oil ratios below 5 Mcf per bbl since large discrepancies are encountered at the lower gas-oil ratios. The data for System *D* which were limited to gas-oil ratios below 1,500 cu ft per bbl were not employed in the establishment of the coefficients of Table VII. These coefficients apply only to systems of the same general type as have been studied here. However, their magnitude is similar to such coefficients found earlier.[10] The ability to obtain a simple correlation over a wide range of gas-oil ratios, temperatures, and pres-

Table IV

Compressibility Factors for Trap Gas Sample

Pressure PSI Absolute	40°F.	100°F.	160°F.	200°F.
0	1.0000	1.0000	1.0000	1.0000
200	0.9563	0.9693	0.9808	0.9853
400	0.9134	0.9417	0.9628	0.9716
600	0.8731	0.9165	0.9458	0.9590
800	0.8344	0.8935	0.9305	0.9480
1000	0.7970	0.8725	0.9236	0.9383
1250	0.7540	0.8495	0.9035	0.9282
1500	0.7210	0.8303	0.8924	0.9203
1750	0.6985	0.8158	0.8844	0.9143
2000	0.6864	0.8060	0.8788	0.9103
2250	0.6835	0.8009	0.8758	0.9085
2500	0.6882	0.8002	0.8750	0.9089
2750	0.6990	0.8039	0.8770	0.9112
3000	0.7145	0.8115	0.8815	0.9155
3250	0.7333	0.8228	0.8888	0.9218
3500	0.7548	0.8369	0.8980	0.9297
3750	0.7784	0.8531	0.9096	0.9390
4000	0.8032	0.8710	0.9227	0.9500
4250	0.8294	0.8905	0.9373	0.9620
4500	0.8565	0.9114	0.9533	0.9752
4750	0.8838	0.9334	0.9703	0.9395
5000	0.9118	0.9559	0.9880	1.025

Table VI

Sample

Volumetric Behavior of Experimentally Studied Mixtures

SYSTEM—A

Weight Fraction Trap Gas = 0.7972
Gas-Oil Ratio = 24,312

Pressure PSI Absolute	Specific Volume Cu Ft/Lb.	Liquid Volume Cu Ft/Lb.	Formation Volume
	40°F		
R.D.P.	(4494)[a] 0.04903	0	12.34
0	∞	....	∞
200	1.1908	....	299.7
400	0.7509	....	189.0
600	0.3563	0.00502	89.67
800	0.2552	0.00542	64.23
1000	0.1964	0.00571	49.42
1250	0.1509	0.00593	37.98
1500	0.1219	0.00597	30.67
1750	0.1020	0.00586	25.67
2000	0.08803	0.00562	22.15

Table VII

Values of Coefficient

Ax10^3

Pressure PSIA	40° F[a]	100°	160°	220°	250°[b]
600	4.45	4.75	4.90	5.03	5.08
1000	4.07	4.51	4.74	4.93	5.00
1500	3.75	4.29	4.59	4.84	4.93
2000	3.59	4.16	4.51	4.80	4.89
3000	3.70	4.21	4.52	4.81	4.93
4000	4.19	4.55	4.75	5.01	5.09
5000	....	4.99	5.11	5.30	5.36

[a] Based on data for System A only.
[b] Based on data for Systems C and D.

Table V

Compositions of Experimentally Studied Mixtures

SYSTEM—A

Component	Weight Fraction Trap Gas					
	0.7972		0.8222		0.8727	
	Mole Fraction	Weight Fraction	Mole Fraction	Weight Fraction	Mole Fraction	Weight Fraction
Methane	0.90940	0.68748	0.91410	0.70856	0.92323	0.75102
Ethane	0.02793	0.03958	0.02797	0.04063	0.02804	0.04277
Propane	0.01390	0.02889	0.01378	0.02935	0.01355	0.03028
Isobutane	0.00515	0.01410	0.00503	0.01412	0.00481	0.01417
n-Butane	0.00408	0.01119	0.00393	0.01104	0.00365	0.01075
Isopentane	0.00374	0.01272	0.00342	0.01194	0.00282	0.01033
n-Pentane	0.00086	0.00294	0.00087	0.00303	0.00061	0.00322
Hexanes	0.00468	0.01900	0.00418	0.01744	0.00327	0.01428
Heptanes	0.00568	0.02681	0.00496	0.02401	0.00361	0.01832
Octanes and heavier	0.02057	0.14898	0.01774	0.13136	0.01241	0.09592
Carbon Dioxide	0.00401	0.00831	0.00402	0.00852	0.00400	0.00894
Gas-Oil Ratio =	24,312		28,590		42,238	

SYSTEM—B

	Weight Fraction Trap Gas					
	0.05611		0.09859		0.13645	
Methane	0.3827	0.0480	0.5156	0.0822	0.5937	0.1128
Ethane	0.0218	0.0051	0.0259	0.0077	0.0282	0.0100
Propane	0.0191	0.0066	0.0193	0.0084	0.0194	0.0101
Isobutane	0.0091	0.0041	0.0081	0.0047	0.0075	0.0051
n-Butane	0.0103	0.0047	0.0089	0.0052	0.0081	0.0056
Isopentane	0.0077	0.0043	0.0062	0.0044	0.0053	0.0046
n-Pentane	0.0085	0.0048	0.0066	0.0048	0.0055	0.0047
Hexanes	0.0238	0.0160	0.0182	0.0156	0.0149	0.0152
Heptanes	0.0464	0.0363	0.0349	0.0348	0.0282	0.0334
Octanes and heavier	0.4654	0.8686	0.3492	0.8295	0.2809	0.7948
Carbon Dioxide	0.0032	0.0011	0.0044	0.0019	0.0051	0.0026
Air	0.0020	0.0004	0.0027	0.0008	0.0032	0.0011
Gas-Oil Ratio =	398.7		705.3		1003.9	

SYSTEM—C

	Weight Fraction Trap Gas					
	0.6912		0.8051		0.8928	
Methane	0.8659	0.5672	0.8891	0.6580	0.9035	0.7280
Ethane	0.0376	0.0462	0.0377	0.0523	0.0377	0.0570
Propane	0.0161	0.0290	0.0155	0.0316	0.0152	0.0336
Isobutane	0.0048	0.0114	0.0044	0.0117	0.0041	0.0119
n-Butane	0.0082	0.0196	0.0077	0.0208	0.0074	0.0217
Isopentane	0.0044	0.0128	0.0037	0.0122	0.0032	0.0117
n-Pentane	0.0022	0.0066	0.0017	0.0057	0.0014	0.0049
Hexanes	0.0062	0.0217	0.0039	0.0154	0.0025	0.0106
Heptanes	0.0100	0.0408	0.0059	0.0274	0.0034	0.0171
Octanes and heavier	0.0334	0.2274	0.0189	0.1448	0.0098	0.0812
Carbon Dioxide	0.0065	0.0118	0.0067	0.0137	0.0069	0.0152
Air	0.0047	0.0055	0.0048	0.0064	0.0049	0.0071
Gas-Oil Ratio =	13,398		24,589		49,412	

SYSTEM—D

	Weight Fraction Trap Gas					
	0.7073		0.7996		0.8972	
Methane	0.8796	0.5964	0.8980	0.6722	0.9141	0.7521
Ethane	0.0380	0.0483	0.0381	0.0534	0.0381	0.0588
Propane	0.0156	0.0291	0.0151	0.0312	0.0147	0.0334
Isobutane	0.0042	0.0102	0.0039	0.0105	0.0036	0.0108
n-Butane	0.0046	0.0113	0.0041	0.0111	0.0036	0.0108
Isopentane	0.0031	0.0094	0.0025	0.0085	0.0020	0.0075
n-Pentane	0.0019	0.0059	0.0015	0.0049	0.0011	0.0039
Hexanes	0.0064	0.0232	0.0045	0.0182	0.0029	0.0129
Heptanes	0.0085	0.0362	0.0056	0.0260	0.0030	0.0153
Octanes and heavier	0.0306	0.2160	0.0190	0.1482	0.0090	0.0768
Carbon Dioxide	0.0075	0.0140	0.0077	0.0158	0.0079	0.0177
Gas-Oil Ratio =	14,780		24,300		52,938	

SYSTEM--E

	Weight Fraction Trap Gas					
	0.9308		0.9097		0.8884	
Methane	0.9522	0.8403	0.9487	0.8218	0.9451	0.8030
Ethane	0.0168	0.0278	0.0168	0.0273	0.0168	0.0268
Propane	0.0091	0.0221	0.0092	0.0218	0.0092	0.0216
Isobutane	0.0026	0.0084	0.0027	0.0084	0.0027	0.0084
n-Butane	0.0033	0.0104	0.0033	0.0105	0.0034	0.0105
Isopentane	0.0016	0.0063	0.0017	0.0065	0.0018	0.0067
n-Pentane	0.0011	0.0043	0.0012	0.0045	0.0013	0.0048
Hexanes	0.0025	0.0118	0.0029	0.0133	0.0032	0.0148
Heptanes	0.0031	0.0171	0.0037	0.0203	0.0045	0.0236
Octanes and heavier	0.0067	0.0491	0.0088	0.0632	0.0110	0.0775
Carbon Dioxide	0.0010	0.0024	0.0010	0.0024	0.0010	0.0023
Gas-Oil Ratio =	81,540		61,110		48,330	

sures for the four systems investigated indicates a similarity in behavior. The average deviation of the values of the coefficient *A* for the several systems at a given pressure and temperature was 0.057. The maximum deviation encountered was 0.13 at 5,000 psi at 100°F for System *A*.

ACKNOWLEDGMENT

The cooperation and financial support of The Texaco Development Corp. made this study possible. The samples were obtained by The Texas Co. in whose laboratories the analyses of the trap samples were carried out. The assistance of W. W. Robinson in the coordination of the program was particularly helpful.

REFERENCES

1. Beecher and Parkhurst: *Petr. Dev. and Tech. in 1926*, AIME (1927) 51.
2. Sage and Lacey: Amer. Petr. Inst. *Drill. and Prod. Prac.*, 1935 (1936) 141.
3. Standing and Katz: *Trans.* AIME (1942) **146,** 159.
4. Sage and Lacey: Amer. Petr. Inst. *Drill. and Prod. Prac.*, 1941 (1942) 308.
5. Standing: *Oil and Gas Jnl.* (1947) **46,** (2) 95.
6. Kurata and Katz: *Trans.* Amer. Inst. Chem. Engrs. (1942) **38,** 995.
7. Carter, Sage and Lacey: *Trans.* AIME (1941) **142,** 170.
8. Standing and Katz: *Trans.* AIME (1942) **146,** 140.
9. Smith and Watson: *Ind. Eng. Chem.* (1937) **29,** 1408.
10. Sage and Olds: *Trans. AIME* (1947) **170,** 156.
11. Sage and Lacey: *Trans.* AIME (1948) **174,** 102.
12. Olds, Sage and Lacey: *Trans.* AIME (1945) **160,** 77.
13. Olds, Sage and Lacey: *Trans.* AIME (1949) **179,** 287.
14. Sage and Lacey: *Trans.* AIME (1940) **136,** 136.
15. Hill and Coats: *Ind. Eng. Chem.* (1928) **20,** 641.
16. Kay: *Ind. Eng. Chem.* (1936) **28,** 1014.
17. Sage and Lacey: *Refiner and Natl. Gasoline Mfr.* (1939) **18** (11) 88. *Oil and Gas Jnl.* (1939) **38** (27) 189. Amer. Petr. Inst. *Drill. and Prod. Prac.*, 1939 (1940) 641.
18. Reamer and Sage: American Documentation Institute, Document 2920, Washington, D. C. (1950).

★ ★ ★

T.P. 2938

CRITICAL ANALYSIS OF THE EFFECT OF WELL DENSITY ON RECOVERY EFFICIENCY

W. O. KELLER, KELLER AND PETERSON, MIDLAND, TEXAS, MEMBER AIME, AND **F. H. CALLAWAY,** STANOLIND OIL AND GAS CO., TULSA, OKLAHOMA, JUNIOR MEMBER AIME

ABSTRACT

The various theories as to the well spacing-recovery relationship are reviewed in considerable detail and these theories analyzed in terms of their consistency with modern reservoir engineering concepts. It is concluded that the well spacing problem must be analyzed in terms of recovery efficiency and that a positive answer to the relation between well density and recovery efficiency is not available from direct comparisons of the production histories of wells and fields.

The results of an engineering analysis designed to permit approximate calculation of recovery efficiencies as a function of well spacing in a depletion type reservoir from basic reservoir data is presented. Results of this type analysis indicate that the effect of well spacing on recovery efficiency in depletion type reservoirs can be expected to be very small. Limitations of this approach are pointed out, particularly with respect to its application in lenticular reservoirs.

Testing techniques are outlined which should indicate whether or not a reservoir is continuous between wells and whether or not satisfactory drainage is being obtained with present spacings. A mass of data of this type indicates continuity to exist in most fields.

INTRODUCTION

The purpose of this paper is to review critically the engineering aspects of the well spacing problem, both from the standpoint of certain concepts and from the standpoint of reservoir mechanics. The well spacing problem is primarily an economic problem in which the optimum well density for a particular field is that density which will yield the greatest oil recovery consistent with justifiable development costs. The well spacing answer in terms of economic conditions, however, is extremely sensitive to the variation in recovery efficiency with well density. The variation in recovery efficiency with well density is properly an engineering problem. Different opinions as to the correct answer to this engineering problem is the basis for most of the wide difference in opinion among various members of the industry as to optimum well spacing. This paper will be confined to the engineering problem of the relation between well density and ultimate oil recovery; economic considerations necessary for the evaluation of optimum well density for any particular field will not be discussed.

The paper can be logically divided into two parts. The first part deals with a critical examination of the background and logic of the Cutler Rule and of similar studies by other authors and of related well spacing concepts. It is indicated that the variations in recoveries with well density* observed by Cutler and others can be logically attributed to regional migration. Theoretical justification of the Cutler type relation wherein observed variations in recovery with well density in the same field is attributed to variations in recovery effiiency, in terms of energy relations, is refuted.

The second part consists of a review of concepts of reservoir mechanics with regard to the well density-recovery relation. It is indicated that little variation of recovery efficiency with well density can be expected in a depletion type reservoir, unless lenticular conditions prevent communication between wells. The significance of field test data with regard to the existence or non-existence of lenticular conditions is pointed out.

THE CUTLER RULE†

The first published article concerning the engineering aspects of the well spacing problem to receive wide attention was the work of W. W. Cutler[1] of the U. S. Bureau of Mines, published in 1924. In a study of decline curves from a large

---

[1] References given at end of paper.

Manuscript received at the office of the Petroleum Branch October 2, 1949. Paper presented at the Petroleum Branch Meeting in San Antonio, Texas, October 5-7, 1949.

*The expression "well density" as utilized herein refers to the number of acres attributed to each well in a uniform well pattern, and is expressed in acres per well. The term "well spacing" is utilized to denote the average distance between adjacent wells in a uniform well pattern.

†Although the Cutler rule is treated critically in this discussion, the authors intend no personal criticism of W. W. Cutler or of his work. The currently accepted concepts of reservoir mechanics were non-existent at the time of Cutler's work, as were even the most basic tools (such as the bottom hole pressure bomb) for observing reservoir behavior.

number of fields, Cutler observed a variation in physical recoveries of wells on tracts developed to different densities in the same field. He analyzed, with regard to the well spacing relation, the recoveries of tracts drilled to different well densities in the same field, including data from seven separate fields. These data consisted only of examples which apparently satisfied the following requirements:

1. The wells being compared had approximately the same initial productive capacity as exhibited by the first year's production and were completed at approximately the same time, in areas of approximately equal pay thickness.
2. The wells being compared exhibited interference with offset wells as indicated by changes in the slope of decline curves of old wells upon completion of nearby new wells.

From these comparative data was developed the following tentative rule: *The ultimate production for wells of equal size where there is interference . . . seem approximately to vary directly as the square roots of the areas drained by the wells.* The *areas drained by the wells* is considered to be the area of the tract in question divided by the number of wells on that tract; in short, the areas attributed to those wells. The rule can be restated to the effect that the average recovery per acre should be inversely proportional to the square roots of the area drained by (attributed to) each well. All the examples represented by Cutler's data apparently were depletion type gas drive reservoirs which were produced at unrestricted rates.

It is apparent that the variation in recoveries with well density observed by Cutler must be attributed to either or both of two factors:

1. Regional migration into the areas of closer spacing.
2. Higher recovery efficiency from beneath the areas of closer spacing.

If the variations in recovery can be attributed to variations in recovery efficiency, then it follows that Cutler's Rule can be applied on a field-wide basis with regard to total recovery from the field. If the variation in recovery is due to regional migration, the rule cannot be applied on a field-wide basis with regard to field-wide recoveries. Although the rule itself makes no provision with regard to the cause of the observed variation of recovery with well density, it is apparent from Cutler's justification of his rule, in terms of energy relations, that he attributed the variation in recovery entirely to a variation in recovery efficiency. It is in the light of this interpretation that the Cutler Rule has been advanced by advocates of close spacing as a guide to increasing oil recoveries. An examination of Cutler's justification of the rule on the basis of energy relations, wherein the variation in recovery with well spacing is attributed to variation in recovery efficiency with well spacing, indicates the justification to be invalid on two separate grounds:

1. Linear flow principles were utilized, whereas radial flow conditions actually apply.
2. Energy relations themselves are incorrectly applied.

A quantitative evaluation of the severity of regional migration between tracts drilled to different densities in the same field indicates that the behavior reflected by Cutler's Rule might easily be attributed entirely to regional migration.

Cutler's justification, on the basis of energy relations, of his opinion that the observed differences in recovery should be attributed to a variation in recovery efficiency is perhaps most clearly stated in his own words: "This (tentative) rule seems to rest on the fundamental mechanical law that the energy required to move a fluid (either liquid or gas) through a pipe or analogous conductor is proportional to the distance. Thus, to force water twice as far through a pipe line requires twice the force. According to this theory, doubling the spacing means doubling the distance the oil must be forced to the well, and inasmuch as the proportion of gas energy to oil is not increased, it would naturally be expected that the energy would be effective to only half the degree and, hence, result in only half the recovery, which accords with the facts." This justification, as indicated above, is unsound, due to the fact that flow through a reservoir was assumed to be analogous to flow through a pipe line (linear flow). It is also in error in the assumption that recovery efficiency is a direct function of energy consumption in the reservoir.

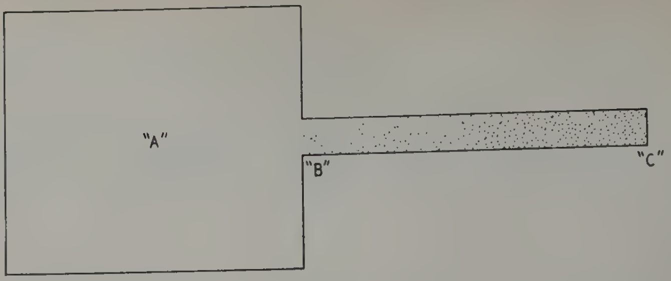

FIG. 1 — SIMPLIFIED FLOW SYSTEM FOR ILLUSTRATION OF ENERGY RELATIONS, CONSISTING OF CONSTANT VOLUME CHAMBER A, DISCHARGING THROUGH SAND PACKED COLUMN BC, TO OUTLET C.

The error of comparing flow through an oil reservoir to flow through pipe line has been pointed out repeatedly. The former is linear in geometry and is represented by parallel flow paths and by a constant cross sectional area available for flow, while the latter is near radial in geometry and is represented by converging flow paths and varying cross sectional area available for flow. Differences between the flow and energy consumption characteristics of linear and radial flow systems can be demonstrated quantitatively by the comparison of the integrated (steady state) form of the Darcy Equation for the two types of flow systems. This has been done by Miller and Higgins of the U. S. Bureau of Mines,[2] who show that, with ordinary well spacings and well bore diameters, doubling the spacing will result in a nine to 12 per cent increase in flow resistance and energy consumption. For a linear flow system, as used in Cutler's reasoning, the flow resistance and energy consumption would be doubled under the same circumstances. Thus, on the basis of the flow pattern alone, Cutler's theoretical justification of his rule should indicate the effect of well density on recovery efficiency to be approximately 10 per cent of what the rule provides and the data indicate.

Over and above the error of utilizing linear flow principles, Cutler's justification on the basis of energy relations relies upon the false assumption that recovery efficiency is inversely proportional to the energy utilized in overcoming flow resistance within the reservoir. His reasoning represents essentially a simple energy balance, in which the potential expansive energy initially present in the reservoir fluids is equated to the product of the number of barrels of oil to be recovered times the energy consumption of the flow system per barrel production.

$$E = NF \qquad (1)$$

where E = initial energy content of the reservoir

N = number of bbl of oil to be recovered

F = units of energy utilized per bbl to overcome flow resistance in the rock or $$N = \frac{E}{F} \qquad \text{(1-A)}$$

The energy balance so written is incomplete and its implications erroneous. It fails to distinguish between energy consumption within the system to overcome flow resistance and total energy removed from the system, i.e., energy voidage. Energy content of the produced fluids after they reach the well bore has been ignored completely and tacitly assumed to be zero under all circumstances. If we let $H =$ the energy content per bbl of produced fluid after it reaches the well bore, the correct equation may be written.

$$(E_1 - E_2) = N(F + H) \qquad (2)$$

where subscripts 1 and 2 refer to initial and abandonment conditions, respectively. It is obvious from this expression that the recovery efficiency from a reservoir cannot be evaluated in terms of the energy utilized to overcome flow resistance in the system and that Cutler's logic, as represented by Equation 1, is invalid.

The true significance of energy relations in a producing reservoir becomes readily apparent upon application of an energy balance between the fluids remaining in the reservoir and those produced. Such an analysis indicates that recoveries cannot be expected to be directly related either to energy content of the reservoir fluids or to the manner in which that energy is utilized. Consider a constant flow system of the type illustrated in Fig. 1, which will be assumed to contain a homogeneous (single phase) compressible fluid, such as a gas or an under-saturated crude oil. Fluid is being produced isothermally through a sand packed tube, *BC*, to an outlet, *C*, by virtue of expansion of fluid within the chamber, *A*. The volume of fluid contained in the flow channel, *BC*, may be considered to be negligible. The energy content of the system at any time in its depletion history may be written as follows:

$$E = g \int_{v}^{v_{14.7}} pdv = \frac{y}{v} \int_{v}^{v_{14.7}} pdv \qquad (3)$$

where $E =$ expansive energy content of fluids contained in the system, referred to atmospheric condition.

$g =$ volume, at atmospheric conditions, of fluids contained in the system

$p =$ pressure

$v =$ relative fluid volume, at reservoir conditions, referred to volume at atmospheric conditions

$y =$ volume of the system

For any particular fluid, the relative volume (v) is a function of pressure. The rate of change of energy content of the system with respect to pressure is expressed:

$$\frac{dE}{dp} = \frac{d}{dp}\left[\frac{y}{v}\int_{v}^{v_{14.7}} pdv\right] \qquad (4)$$

The expression $\frac{dE}{dp}$ represents, of course, the energy voidage from the system per unit pressure drop, and is expressed as a function of the volume of the system, the pressure therein, and the pressure-volume characteristic of the contained fluid. The quantity of fluid within the system can be described in terms of the volume of the system, the pressure therein, and the pressure-volume characteristic of the contained fluid.

$$g = \frac{y}{v} \qquad (5)$$

Differentiating with respect to pressure,

$$\frac{dg}{dp} = y \frac{d}{dp}\left(\frac{1}{v}\right) \qquad (6)$$

Combining Equations 4 and 6,

$$\frac{dE}{dg} = \frac{\frac{d}{dp}\left[\frac{1}{v}\int_{v}^{v_{14.7}} pdv\right]}{\frac{d}{dp}\left(\frac{1}{v}\right)} \qquad (7)$$

The expression $\frac{dE}{dg}$ represents the energy voidage from the system per unit of production from the system, as a function of the pressure existing in the system and the pressure volume characteristic of the contained fluid. Note that the energy voidage per unit production is entirely independent of the dimensions of the system, the number of outlets, the flow resistance of the withdrawal system, or the rate of production.

The energy voidage of the system per unit production must be accounted for in terms of the energy consumption of the flow system, (F), and the energy content of the produced fluids, (H), per unit production. For a system containing a given fluid,

$$(F + H) = \frac{dE}{dg} \phi\ (p) \qquad (8)$$

which indicates that the total energy voidage per unit of pro-

Table I

Effect of Regional Migration Upon Recovery for Various Spacing Patterns

Case	1	2	3	4	5	6
Recovery—Bbls/Acre for 10-Acre Development	9,723	——	8,581	6,685	5,320	——
Recovery—Bbls/Acre for 20-Acre Development	——	6,630	——	——	——	4,784
Recovery—Bbls/Acre for 40-Acre Development	3,193	3,578	2,769	2,545	2,534	3,060
Recovery—Bbls/Acre Average	3,919	3,917	3,932	3,926	3,927	3,922
Recovery Ratio—Close to Wide Development	3.045	1.853	3.098	2.626	2.099	1.563
Recovery Ratio—Required by Cutler's Rule	2	1.414	2	2	2	1.414

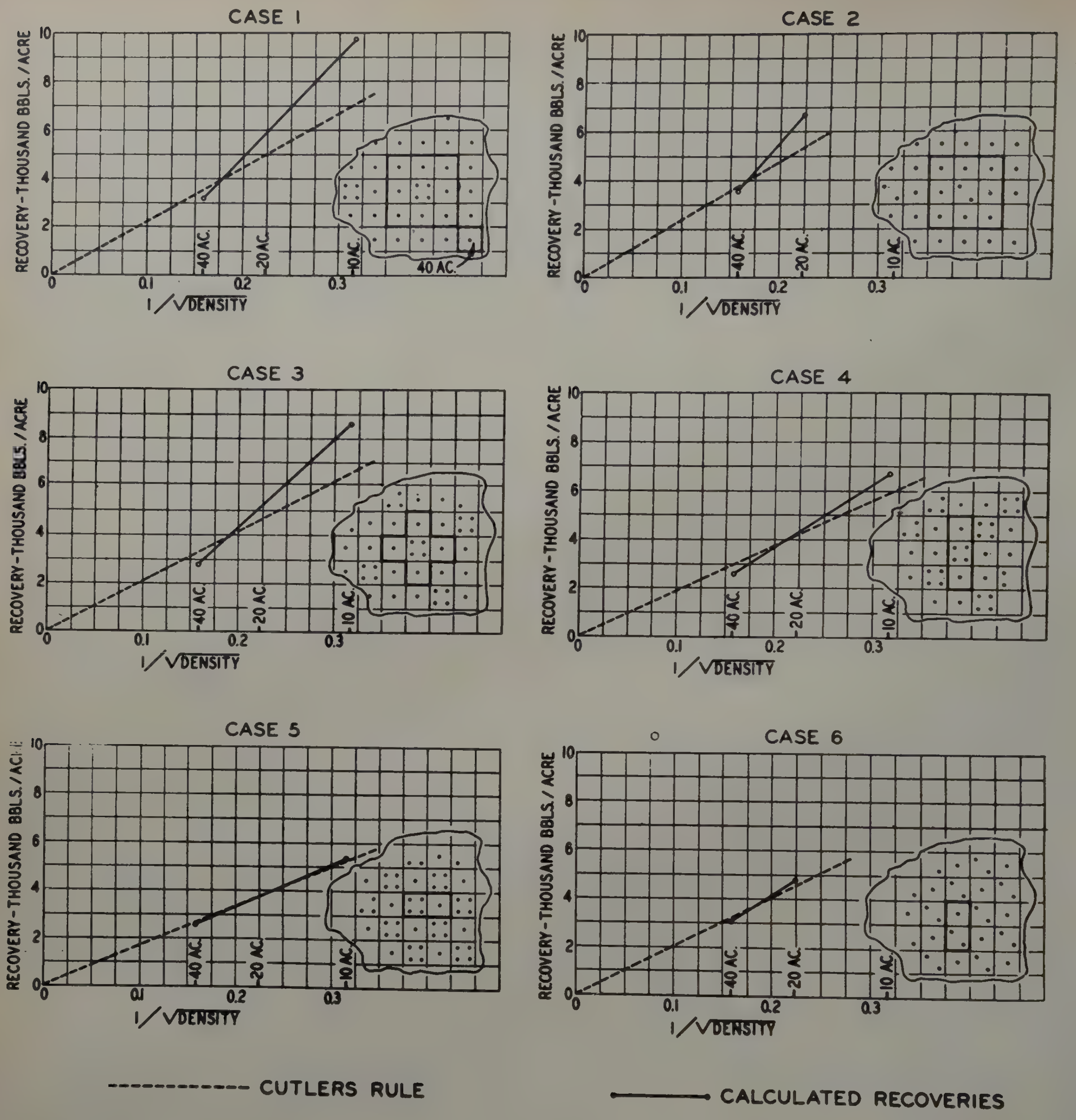

FIG. 2 — VARIATION IN RECOVERY WITH WELL DENSITY DUE TO REGIONAL MIGRATION FOR VARIOUS SYMMETRICAL SPACING PATTERNS.

duction is always equal to the sum of the quantities F and H but that the value of either is of no consequence to the total energy voidage per unit production, which is uniquely related to pressure and fluid characteristic. The energy voidage cannot be changed by altering the quantity of energy utilized to overcome flow resistance; such will only serve to alter by a like amount the quantity of energy to be produced with the fluids at the outlet of the system.

What, then, is the significance of energy relations in the flow system illustrated in Fig. 1? Actually, the energy to be voided from a system per unit production at any particular time, as expressed by Equation 7, will determine the maximum rate to which those fluids can be produced. The maximum flow rate from the system illustrated in Fig. 1 will exist when the outlet pressure is atmospheric and the energy content of the produced fluids, H, is equal to zero. The total energy voidage of the system $\frac{dE}{dg}$ will then be utilized to overcome fluid friction in the rock. The value of this energy voidage per unit production will, therefore, determine the maximum rate at which the system can be produced at any particular time in its depletion history. The energy voidage per unit production will, therefore, determine, in the same fashion as the permeability, viscosity, dimensions and geometry of the flow system, the maximum production rate at any time from the system. It will not, as such, determine the quantity of fluid to be recovered.

Although the relations expressed in Equations 3 through 8 have, for the purpose of simplification, been derived for the system diagramed in Fig. 1, they will apply to a continuous porous system with negligible error provided that average pressures be utilized.

Three generalizations with regard to energy relations of a flow system producing expansible fluids by virtue of their expansion alone are in order:

1. Potential expansive energy content of the system is determined uniquely by the volume of the system, the pressure, and the pressure-volume characteristic of the contained fluid.
2. Energy voidage per unit production is determined uniquely by the pressure and the pressure-volume characteristic of the fluid and cannot be altered by varying the dimensions of the system or the flow rate.
3. The energy voidage per unit production, together with the geometry of the flow system, its permeability and the viscosity of the fluid, will determine the maximum productive capacity of the system.

The discussion of energy relations presented above is confined to homogeneous fluid (single phase) depletion type systems. Cutler's Rule was developed and intended to apply to depletion type oil reservoirs, wherein two phases (oil and gas) ordinarily co-exist and are produced simultaneously. The fluid content of a depletion type oil reservoir can be arbitrarily broken into two components; that part of the fluid which will exist in the liquid phase at stock tank conditions and that part which will exist in the vapor phase at stock tank conditions. The potential expansive energy of that part of fluid which will exist in the liquid phase at stock tank conditions is very small compared to that of the portion which will exist in the vapor phase. The potential expansive energy of the portion which will exist in the liquid phase can for all practical purposes be ignored and the energy content of the system considered to exist solely in the form of free and solution gas.

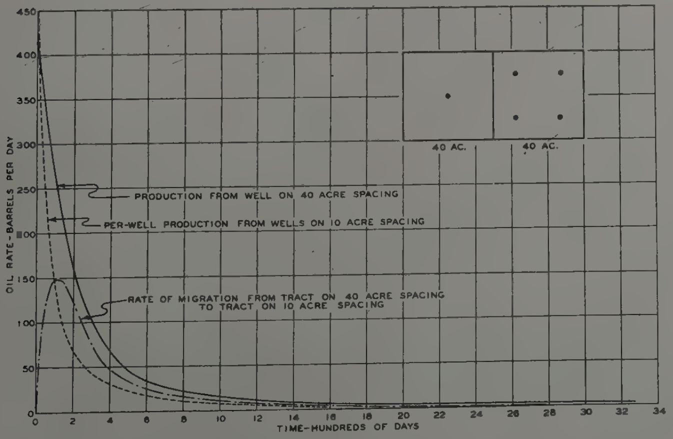

FIG. 3 — CALCULATED PRODUCING RATES AND MIGRATION RATES FOR THE SPACING PATTERN ILLUSTRATED IN CASE 5, FIG. 2.

Under these circumstances, the generalizations developed with regard to the energy relations for a homogeneous fluid system can be expected to hold between the reservoir and the well bore for a depletion type oil reservoir when applied specifically to that portion of the reservoir fluid which would exist in the vapor phase at atmospheric conditions. It follows that the energy relations at any particular time in a depletion type oil reservoir cannot be altered except by altering the producing gas-oil ratio or injecting extraneous fluids.

As pointed out previously, the logical explanation for the relation observed by Cutler and others between recovery and well density for wells in the same field is regional migration. The requirements which Cutler placed upon his data with regard to the utilization of wells of approximately the same size, completed at approximately the same time, in areas of uniform pay thickness and that interference existed between wells, is such that regional migration from the areas of wider spacing to areas of closer spacing is inevitable. The more densely developed areas will be subject to more rapid withdrawal rates per acre and per acre foot of pay and will be subject to a more rapid rate of pressure decline than the areas of wider spacing. This situation can only result in the development of pressure "sinks" around the areas of dense development and pressure "highs" around the less densely drilled areas, which in turn will result in migration from the high to low pressure areas or from the areas of wider spacing to areas of closer spacing. The influence of migration upon the per acre recoveries of tracts drilled to different densities in the same pool has been recognized by many writers, including Miller and Higgins[2] who state that at least part of the increased production credited to more densely drilled tracts must be attributed to regional migration.

Calculations intended to evaluate quantitatively the effect of migration under conditions of varying well densities have been prepared for a typical set of reservoir conditions. These calculations have been prepared for six geometrical configurations of tracts of different well densities representing portions of six symmetrical spacing patterns. Reservoir conditions underlying the tracts were assumed to be identical in order to duplicate the conditions which Cutler strove to find, and all wells were assumed to be opened to production at the same time and produced to capacity until a limiting economic rate of three bbl per well per day was reached. The performance of the six systems was derived by a step-wise solution combining simultaneously the depletion drive behavior, as outlined by Muskat,[3] and well production and regional migration rates in terms of Darcy's Law. Since regional migration operates in a system of complex geometry (i.e., not simple radial or linear geometry), a constant for insertion in the Darcy equation to reflect the flow pattern which the migrating oil would assume was evaluated for each of the six cases by means of the electric analyzer.

These calculations are based upon the assumption that the variation of recovery efficiency with well spacing will be negligible; therefore, the entire difference in recovery as reflected thereby must be attributed to regional migration. The results of these calculations are presented in Fig. 2 and in Table I. The points representing actually calculated values in the graphs on Fig. 2 are connected with straight lines solely for the purpose of comparison with the slope of the line representing Cutler's Rule for the various spacing patterns. Fig. 3 illustrates the rates of production and migration as a function of time for Case 5. Note that the variation in per acre recoveries with well density from migration alone is in each instance somewhat more severe than that predicted by Cutler's Rule. These data lead to the conclusion that the well density-recovery relation observed by Cutler and by others on intra-field recovery comparisons might very easily have resulted from migration alone, even if there were no variation in recovery efficiency with well density.

Consideration of the variables at work in the preceding calculations points to the conclusion that the effect of the magnitude of the permeability of the rock, together with other factors, such as viscosity, which determine the productivity index of the wells, will not affect appreciably the relative recoveries for a given geometrical arrangement of wells. This is to be expected because the same factors which govern the ability of the wells to produce oil also govern the ability of the oil to migrate. It is believed that any reasonable set of depletion type reservoir conditions, under the specified requirement of simultaneous well completion, unrestricted production, uniform permeability, porosity, and pay thickness, would yield relative recoveries for the geometrical patterns analyzed of the same order of magnitude as those shown in Fig. 2. Under otherwise similar conditions artificial restriction of producing rates would, if allowables were on a per-well basis, increase the severity of migration, the per-well recovery approaching equality (per acre recoveries inversely proportional to well density) if the allowables were very small. However, artificial restriction with allowables on an acreage basis would prevent migration completely during the prorated period; migration would be confined to the period of decline and total migration over the life of the system reduced.

The preceding considerations indicate strongly that the variations in recovery with well density for intra-field comparisons can be attributed primarily to regional migration and that Cutler's Rule cannot be applied in evaluating field-wide recoveries. The explanation of such variation in terms of energy relations which would attribute the different recoveries to variations in recovery efficiency with well density has been refuted. One fact is quite apparent; the relation between well density and recovery efficiency cannot be isolated by means of intra-field comparisons. Data obtained from intra-field comparisons are of no real significance with regard to the effect of well density upon recovery efficiency.

FIELD-WIDE COMPARISONS

Since the effect of regional migration makes evaluation of the relation between well density and recovery efficiency impossible by means of intra-field comparisons, it appears that the relation can be isolated from actual production data only by comparing in their entirety the recoveries from different fields developed to different well densities. Several investigators have attempted to evaluate the relation between density and recovery efficiency by this method. Two somewhat different techniques for evaluating the relation from field-wide data are possible, one consisting of the direct comparison of recoveries from two or more fields which are identical in all respects except well spacing; the other consisting of a statistical analysis of a large number of fields for the purpose of developing a "trend" between recovery efficiency and well density.

The first method, consisting of direct comparison of recoveries from fields of identical reservoir charateristics but different spacings, is subject to severe practical limitations due to the difficulty of finding two or more fields which are known to be identical in all respects other than well spacing, which might affect recovery efficiency, and in which basic reservoir data are of sufficient accuracy to permit close evaluation of the recovery efficiencies in each. An example of the uncertainties of this approach is available in the analyses by Clark, Tomlinson and Royds[4] and by Vietti, Mullane, Thornton and vanEverdingen[5] of data presented by Hill and Guthrie[6] on the Mexia-Powell Fault Line Fields of Texas. The two analyses resulted in exactly contrary conclusions as to the effect of well density upon recovery efficiency by use of the same data. An impartial observer must conclude that the data were of insufficient basic accuracy to permit a definite conclusion either way.

The second method for evaluating the well density-recovery efficiency relation by means of field-wide comparisons is the statistical analysis, represented in the literature by the work of Craze and Buckley.[7] This analysis reflected no significant variation of recovery efficiency with well spacing for a group of approximately 70 water drive fields. Although the basic data utilized by these authors may not have been of sufficient accuracy to detect a relatively small variation in recovery efficiency with well density, the fact that the effect of certain other reservoir factors, such as oil viscosity, did show up indicates that any pronounced variation in recovery efficiency with well density would have been reflected in the analysis. A variation in recovery efficiency with well density of the order

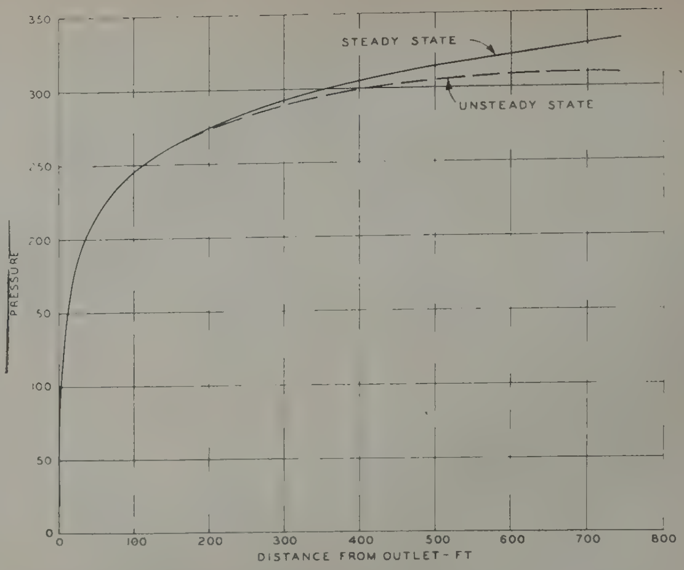

FIG. 4 — COMPARISON OF STEADY AND UNSTEADY STATE PRESSURE DISTRIBUTION IN RADIAL FLOW SYSTEM PRODUCING A SLIGHTLY COMPRESSIBLE FLUID AT EQUAL RATES.

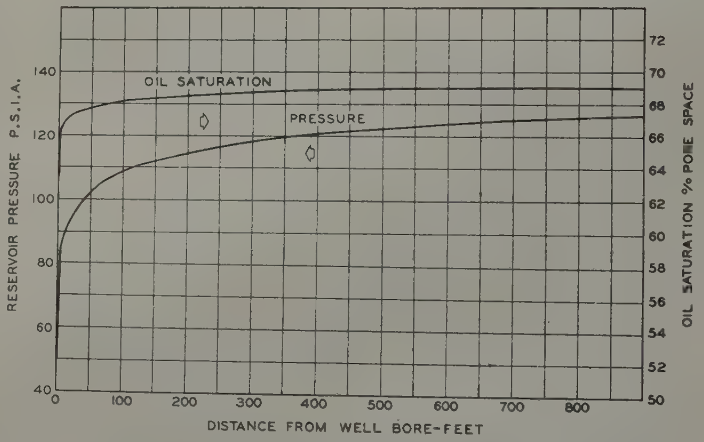

FIG. 5 — CALCULATED PRESSURE AND OIL SATURATION DISTRIBUTION. AT ABANDONMENT. $K = 15$MD.

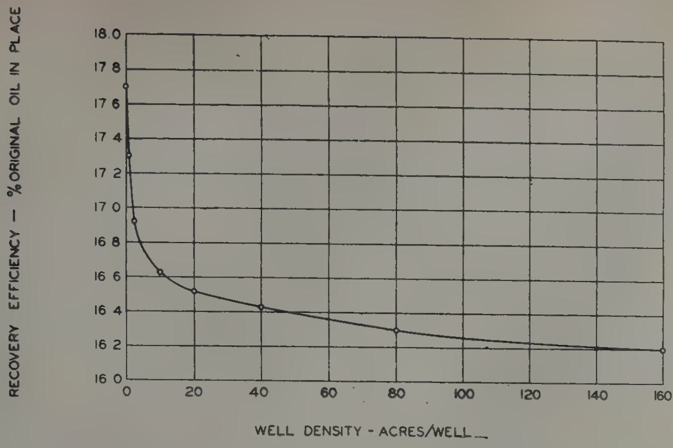

FIG. 6 — CALCULATED VARIATION IN RECOVERY EFFICIENCY WITH WELL DENSITY.

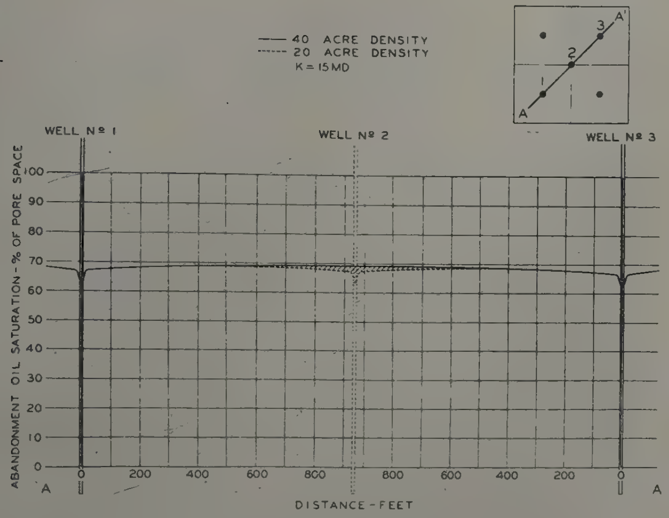

FIG. 7 — OIL SATURATION DISTRIBUTION AT ABANDONMENT CONDITIONS.

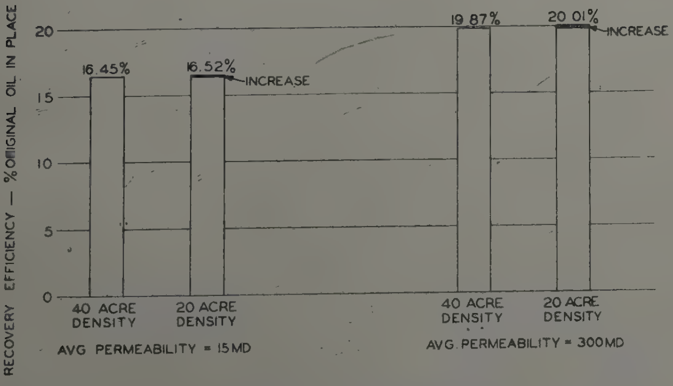

FIG. 8 — CALCULATED VARIATION IN RECOVERY EFFICIENCY WITH WELL DENSITY AND PERMEABILITY.

of magnitude of Cutler's Rule would most assuredly have appeared in Craze and Buckley's analysis.

WELL SPACING IN TERMS OF RESERVOIR MECHANICS

The relation between well density and recovery efficiency is inherently incapable of being isolated by means of intra-field comparison. Due to practical limitations, the relation has not as yet been quantitatively developed from field-wide comparisons. Any relation which does exist must have some logical basis in terms of reservoir mechanics and should be apparent in the mechanism of fluid displacement from porous rock. From a consideration of the currently accepted concepts of the mechanism of fluid displacement in porous rock and of the principles governing the behavior of oil reservoirs, it appears that no appreciable variation in recovery efficiency with well density is to be expected. The results of a quantitative analysis for a particular set of depletion type reservoir conditions indicate that the variation in recovery efficiency with well density will be extremely small. Consideration of the variables at work indicates that the same general situation may be anticipated for any reasonable set of depletion type reservoir conditions, provided that the reservoir is continuous between wells.

It is apparent that the relation between well density and recovery efficiency will be a function of the saturation distribution throughout the well drainage radius at the time the well must be abandoned. Conversely, the well spacing relation can be evaluated quantitatively in terms of the saturation distribution at abandonment with respect to distance from the well bore. Evaluation of saturation distribution in a depletion type oil reservoir requires that the entire production history of the system be reproduced. The rigorous reproduction of the entire history of a two-phase system of finite dimensions producing in the unsteady state involves the solution of a non-linear differential equation of such complexity that it has not been accomplished to date. It is possible, however, to reproduce approximately the production history of such a system and the abandonment saturation conditions in such a system by means of a judiciously chosen set of simplifying assumptions. Approximate solutions of this type have been advanced by at least three writers,[8,9,10] which although slightly different in the method of attack, arrive at approximately the same results. These analyses are all based upon the proposition that the unsteady state performance can be reproduced closely by means of a succession of steady states, utilizing the depletion drive theory advanced by Muskat[3] and others for vanishing pressure gradients and the Darcy equation. Actual calculations consist of the construction of a series of steady state solutions, both in regard to time as the reservoir as a whole undergoes depletion and in regard to distance from the well bore at any particular time.

Consideration of the geometry of a near-radial flow system, wherein the majority of the pressure drop occurs in the immediate vicinity of the well bore, and wherein the bulk of the producing formation lies near the outer boundaries of the system,* leads to the conclusion that the composition of the flowing stream will, in a depletion type oil reservoir and in the absence of transient conditions, be relatively constant from the well bore to the extreme radius of drainage, and will be closely consistent with the composition of the production from that part of the rock which lies near the outer limits of the drainage radius. This generalization is derived from the fact that the area from which most of the produced fluids originate is an area of small pressure gradients in which the depletion drive theory for vanishing pressure gradients can be expected to hold very closely (Fig. 4). The area near the well bore, where large pressure gradients exist, contribute very little to the well efflux and acts primarily to transmit fluids produced from outlying elements. Saturation conditions in areas near the well bore are determined, therefore, to a much greater extent by the producing gas-oil ratio of the outlying elements than by the depletion drive theory for vanishing pressure gradients.

---

*This situation is a reflection of the fact that the volume of a cylindrical solid is proportional to the square of its radius; thus only one-quarter of the volume of such a solid lies within the inner half of its radius.

Calculations intended to evaluate abandonment saturation distribution, based upon the approximation of constant total gas-oil ratio throughout the drainage radius as determined by pressure and saturation conditions in the outlying elements, have been prepared for two particular sets of reservoir conditions. The permeability of the rock was taken to be 15 millidarcys in one instance and 300 millidarcys in the other; all other reservoir factors were identical in both calculations. The economically limiting (abandonment) oil producing rate was assumed to be three bbl per well per day. The results of these calculations are presented in Figs. 5 through 9. Fig. 5 represents the calculated variation in pressure and oil saturation at an abandonment oil production rate of three bbl per well per day for the set of calculations using a permeability of 15 millidarcys. Abandonment oil saturation gradients are very small and the recovery efficiency practically the same at all distances from the well bore except for a small saturation sink in the immediate vicinity of the well bore. The effect of these saturation gradients in terms of recovery effiiency for the $K = 15$ md. calculation is illustrated in Fig. 6. Note that there is very little variation in recovery efficiency with well density except for very close spacing. Fig. 7 is included only for illustrative purposes, showing saturation and pressure distribution at abandonment in the area surrounding three wells. Under the conditions of saturation distribution outlined, it is apparent that the only effect with regard to recovery efficiency of drilling the center well will be to develop a small saturation sink in the immediate vicinity of that well. Fig. 8 represents the relative recovery efficiencies for permeability values of 15 millidarcys and 300 millidarcys, all other reservoir conditions being identical. It is interesting to note that the effect of permeability is to cause some variation in recovery efficiency. However, the drilling of additional wells will have no greater effect upon recovery efficiency in the low permeability situation than in the high permeability situation. In either instance, however, the effect of number of wells upon the rate of production from a given reservoir is appreciable, provided that the wells are produced at capacity or that allowables are on a per well basis. Fig. 9 represents the entire producing history of a representative 40-acre tract under the assumed reservoir condition ($K = 15$ md.) for a 20-acre development and for a 40-acre development.

The basic reasons for the flat saturation gradients and small effect of well density upon recovery efficiency in a continuous depletion type reservoir are:

1. The radial geometry of the drainage pattern.
2. The mechanism of oil displacement by gas.

Indeed, the authors are unable to conceive of a set of conditions under radial drainage and consistent with the mechanism of oil displacement by gas under which the steep saturation gradients necessary for an appreciable effect of well spacing on recovery efficiency could exist. If an appreciable effect does exist, the currently accepted concept of fluid displacement is in need of radical revision.

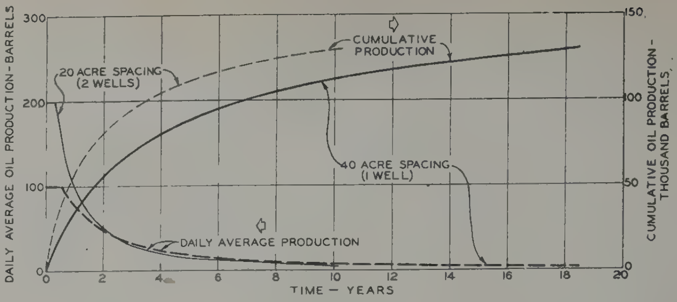

FIG. 9 — EFFECT OF WELL DENSITY UPON PRODUCTION RATES FOR A 40-ACRE TRACT. $K = 15MD$.

An analysis of the well spacing problem in terms of abandonment saturation conditions is obviously inapplicable when a lenticular condition exists throughout the producing reservoir; that is, when the pay zone is not continuous between the producing wells. In order to obtain maximum recovery from a reservoir composed of separate lentils, it is necessary that at least one well bore penetrate each and every separate lentil. The generalizations developed above with regard to depletion drive reservoirs are, therefore, strictly limited to those instances in which continuous communication between wells exists.

The depletion drive theory, together with the well spacing calculations derived therefrom, is based upon the assumption that gravitational segregation of fluids within the rock is negligible in the time interval required to produce the reservoir. Gravitational segregation is known to be appreciable in many depletion type fields, particularly those of high permeability, and the depletion drive theory together with the well spacing calculations of the type illustrated above cannot be expected to hold quantitatively. However, since the gravitational influence is not related to the distance which a particular segment of the rock lies from the well bore and since drainage must still occur through a radial system, it is not believed that the presence of the gravitational segregation will itself cause an appreciable variation in recovery efficiency with well density.

Table II
Completion Pressure Data — Field "B"

Well No.	Date of Test	*Completion Pressure PSIA	Pressure Decline Prior to Completion PSIA
1	4-29-46	2,021 (Field Orig.)	0
2	11-4-47	1,982	39
3	2-5-48	1,945	76
4	6-29-48	1,807	214
5	8-10-48	1,787	234
6	8-16-48	1,812	209
7	8-20-48	1,653	368
8	8-23-48	1,729	292
9	8-27-48	1,685	336
10	8-29-48	1,735	286
11	9-8-48	1,343	678
12	9-9-48	1,723	298
13	9-13-48	1,868	153
14	9-15-48	1,218	803
15	9-16-48	1,730	291
16	9-22-48	1,594	427
17	9-24-48	1,565	456
18	10-6-48	1,739	282
19	10-15-48	1,631	390

*Completion pressures are maximum build-up bottom-hole pressures taken immediately after initial potential tests.

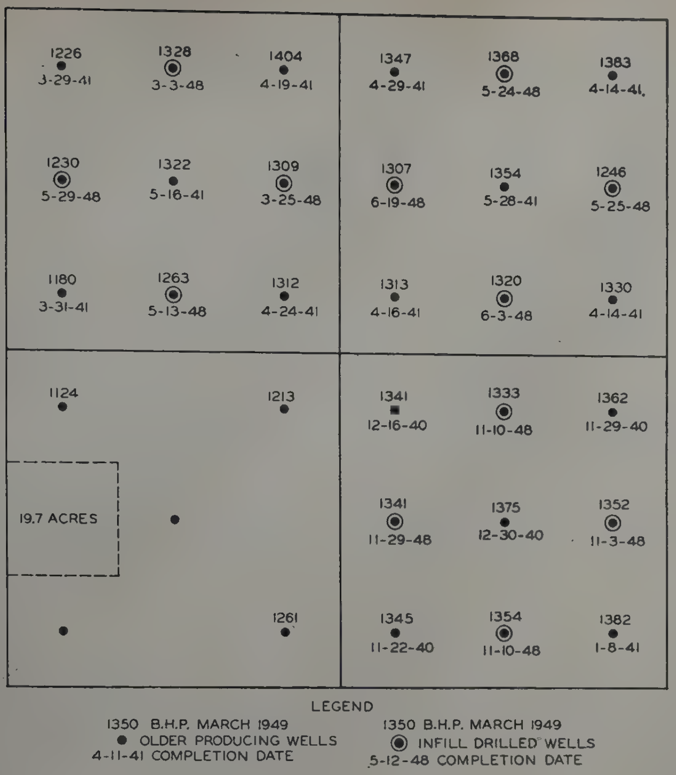

INITIAL RESERVOIR PRESSURE = 1771 P.S.I.A.
AVERAGE PRESSURE OF OLDER WELLS = 1332 P.S.I.A.
AVERAGE COMPLETION PRESSURE OF INFILL WELLS = 1313 P.S.I.A.
AVERAGE PRESSURE DECLINE IN INFILL AREAS DUE TO DRAINAGE TO OLDER WELLS = 458 P.S.I.A.

FIG. 10 — COMPARISON OF COMPLETION PRESSURES OF LATER-DRILLED INFILL WELLS AND OLDER WELLS — FIELD A.

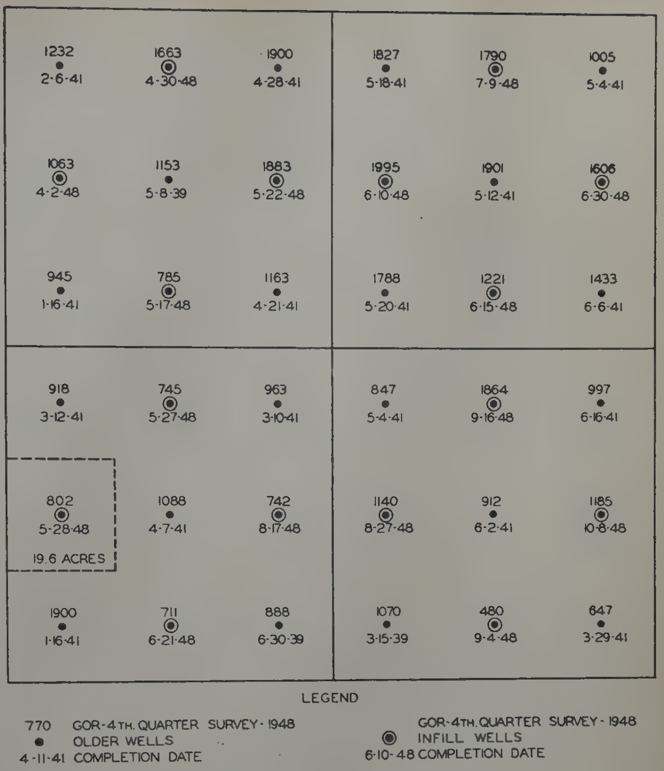

INITIAL SOLUTION GAS-OIL RATIO = 470 CU.FT/BBL.
AVERAGE COMPLETION GAS-OIL RATIO OF INFILL WELLS = 1228 CU.FT/BBL.
AVERAGE GAS-OIL RATIO OF OLDER WELLS = 1229 CU.FT/BBL.

FIG. 11 — COMPARISON OF COMPLETION GAS-OIL RATIOS OF INFILL WELLS WITH GAS-OIL RATIOS OF OLDER WELLS IN A DEPLETION TYPE RESERVOIR — FIELD A.

The application of depletion drive theory to actual reservoir rocks has been questioned by some, due to the fact that such rocks are not uniform with respect to permeability and porosity as must be assumed for quantitative calculations. It seems reasonable to expect, however, that if the recovery efficiency does not vary appreciably with distance from the well bore for any reasonable set of conditions of uniform permeability and porosity (as indicated to be the case), the variations in recovery efficiency in a heterogeneous system will not vary appreciably for any particular segment of rock with its distance from a well bore.

The well spacing problem in water drive reservoirs has not been the cause of as great concern as in depletion type reservoirs due to the superabundance of expansive energy and displacing fluid furnished by encroaching water. A water drive reservoir is ordinarily abandoned when the water-oil ratio reaches an economically limiting value. The recovery efficiency, therefore, depends upon the average oil saturation in the reservoir at which limiting water-oil ratios can be expected, and a variation in recovery efficiency with well spacing must be the result of reaching the limiting water-oil ratio at different average oil saturations with different well spacings. There is no reason to believe that the variation in recovery efficiency with well density on a uniform pattern will be appreciable; however, abandonment oil saturation conditions with respect to distance from the well bore in a water-drive reservoir cannot be sensibly generalized in terms of reservoir mechanics, due to the fact that abandonment saturations surrounding any particular well depend preponderantly upon the sand and well bore conditions peculiar to that well. It is readily apparent that the recovery efficiency in a water drive reservoir will depend considerably upon well location; strategic location of wells at or near the top of the reservoir or of separate sand stringers is essential for maximum recovery.

CONTINUITY

Since it is indicated that the effect of well density upon recovery efficiency for reasonable variations in well density is small in continuous reservoirs, and since it is obvious that infill wells will obtain additional oil in a lenticular reservoir, it appears that the well spacing problem in a particular field can be resolved into the problem of determining whether or not the reservoir is continuous. Fortunately, engineering and production data are capable of yielding a positive answer as to the presence or absence of continuity in most reservoirs.

There is no doubt as to the existence of continuity between wells in a field in which an effective water drive exists. The observation of the results of water influx in terms of pressure behavior is in itself a reflection of continuity and freedom of migration of fluids throughout the reservoir.

In depletion type fields, the presence or absence of continuity must be established from certain specialized testing techniques. Depletion drive theory indicates that the pressure existing in the inter-well area should be very closely equal to the maximum shut-in bottom-hole pressure of the currently producing wells. Furthermore, it is to be expected that the gas-oil ratio of an infill well completed between old producing wells will be of the same magnitude as those existing at the same time in the older offset wells and that the well productivity should be approximately equal. The drilling of an infill well into an area which has been produced by other wells for a considerable time provides, therefore, an excellent opportunity for observing the pressure and stage of depletion existing in the inter-well area and of determining whether or not the inter-well area is being adequately drained from the old producing wells.

If an infill well between older wells on any certain spacing pattern exhibits a pressure upon completion equal to the virgin reservoir pressure, that fact constitutes positive evidence that the inter-well area has suffered no drainage from the offset wells and that a lenticular condition exists in which the additional wells can be expected to recover appreciable additional oil. The exact quantity of additional oil to be recovered cannot be evaluated, because it depends upon the size and number of previously untapped lentils which the new well happens to penetrate.

If, on the other hand, an infill well immediately upon completion exhibits a bottom-hole pressure consistent with the current shut-in bottom-hole pressure of older offset wells and if the gas-oil ratio and other producing characteristics of the well are similar to those of the offset wells, it can reasonably be concluded that the inter-well area is at approximately the same stage of depletion as the areas surrounding the older wells. The inter-well area has been and is capable of being drained by the offset wells and an appreciable increase in ultimate recovery cannot be expected. The infill well will simply deplete reservoir space which would have otherwise been depleted by the older wells and recover oil which would otherwise have been recovered by the older wells on wider spacing. The productivity of the infill well should furthermore be of the same magnitude as that currently existing in the older wells and considerably below the initial potential of the early completions in the field. Productivity data, however, must be used with care due to normal variation in permeability and pay thickness within the reservoir, and due to the effect of transient conditions if the new well has not completely stabilized. Frequently, also, the condition of the hole is considerably better in a new well than in the old wells, resulting in productivities which at first glance may yield an erroneous impression. Several examples of actual field data, including initial completion pressures, gas-oil ratios, and well productivities of the type required to indicate whether or not continuity exists between wells are presented in Figs. 10 through 12 and in Table II.

Continuity in depletion gas drive reservoirs can also be determined by means of planned interference tests where pressure measurements are taken on a shut-in well surrounded by producing wells. Since the production from the shut-in well during the test period is zero, any pressure drop observed in the shut-in well can only be accounted for by movement of fluids away from that area due to the production of surrounding wells. The time required to conduct such interference tests is dependent upon the build-up period required for the shut-in well to reach maximum build-up pressure and the average rate of reservoir pressure decline in the area of the test. The time required to conduct such tests is usually lengthy, except where high rates of production are maintained or where the expansibility of the reservoir's fluids is small, as in an undersaturated reservoir. Care must be taken in such tests to allow sufficient time for the average reservoir pressure to decline a measurable amount; otherwise, the results may be subject to misinterpretation. Fig. 13 presents the results of a test in a

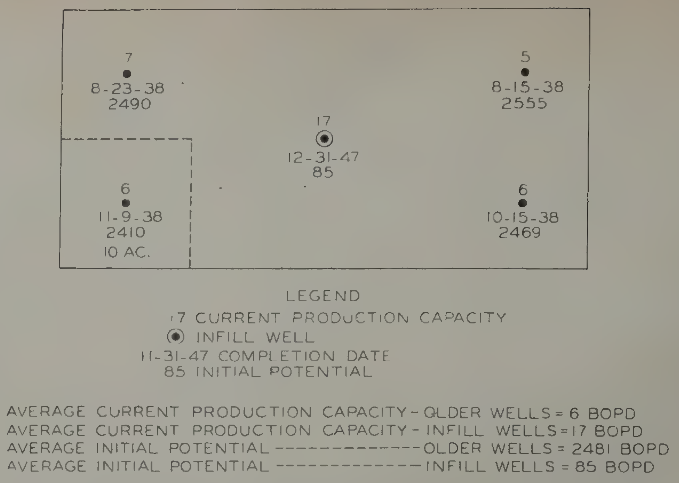
7
8-23-38
2490
5
8-15-38
2555
17
12-31-47
85
6
11-9-38
2410
10 AC.
6
10-15-38
2469
LEGEND
17 CURRENT PRODUCTION CAPACITY
⊙ INFILL WELL
11-31-47 COMPLETION DATE
85 INITIAL POTENTIAL
AVERAGE CURRENT PRODUCTION CAPACITY - OLDER WELLS = 6 BOPD
AVERAGE CURRENT PRODUCTION CAPACITY - INFILL WELLS = 17 BOPD
AVERAGE INITIAL POTENTIAL ------------- OLDER WELLS = 2481 BOPD
AVERAGE INITIAL POTENTIAL ------------- INFILL WELLS = 85 BOPD

FIG. 12 — COMPARISON OF PRODUCTIVITY OF INFILL WELL WITH OLDER WELLS IN A DEPLETION TYPE RESERVOIR — FIELD D.

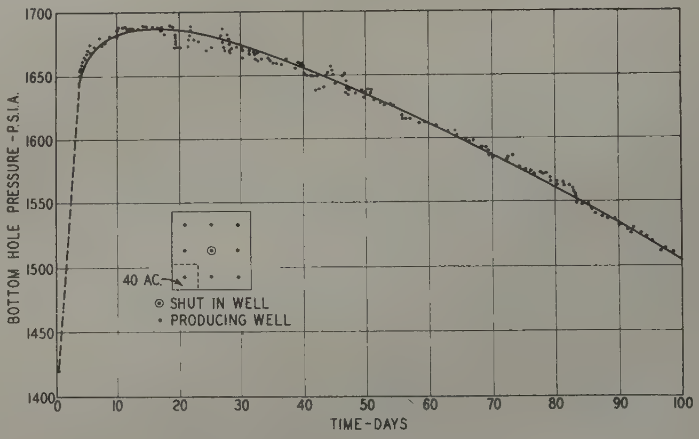

FIG. 13 — INTERFERENCE TEST — FIELD B.

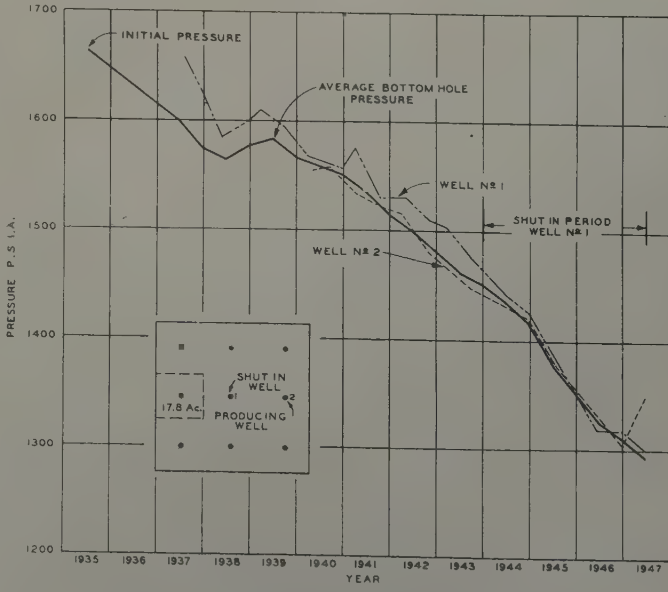

FIG. 14 — PRESSURE PERFORMANCE OF A SHUT-IN WELL IN A GAS DRIVE FIELD — FIELD C.

reservoir containing an under-saturated crude in which appreciable pressure drop occurred over a fairly short period of time. Fig. 14 reflects the behavior of a shut-in well over a longer period of time in a reservoir producing fluid below bubble point pressure.

Data of the type required to indicate whether or not continuity exists are available to the authors on a large number of fields. These data indicate continuity to exist in most reservoirs and that lenticular conditions are the exception. In most instances, therefore, the effect of well spacing upon recovery efficiency can be expected to be very small. A number of instances have come to the attention of the authors in which actual pressure, gas-oil ratio, and productivity data indicated communication to exist, but in which geological correlation of porous zones in the various wells was not possible. The presence or absence of continuity must be proven by means of behavior which is the direct result of continuity; in particular, pressure behavior. Speculation as to the presence or absence of continuity between wells on the basis of geological data alone is extremely risky.

CONCLUSIONS

The following conclusions appear to the authors to be in order:

1. Justification of an appreciable variation in recovery efficiency with well spacing in terms of energy relations is not valid.
2. Observed variations in actual recoveries with well density between different leases in the same field can be attributed largely to regional migration.
3. Comparison of field-wide recoveries, though representing a fundamentally sound approach, has not as yet furnished a positive answer to the well spacing question.
4. Consideration of the principles of reservoir mechanics indicates that the variation in recovery efficiency with well density will be very small for a continuous reservoir.
5. The well spacing problem in most fields can be resolved, in terms of whether or not continuity exists, by means of properly planned and executed testing programs.

ACKNOWLEDGMENT

Acknowledgment is made to the Stanolind Oil and Gas Co. for permission to present this material.

REFERENCES

1. W. W. Cutler, Jr., "Estimation of Underground Oil Reserves by Oil Well Production Curves," *U. S. B. M. Bulletin 288,* (1924), 89.
2. H. C. Miller and R. V. Higgins, "Review of Cutler's Rule of Well Spacing," *U. S. B. M., R. I. 3479,* (1939).
3. M. Muskat, "Production Histories of Oil Producing Gas Drive Reservoirs," *Journal of Applied Physics,* Vol. 16, No. 3, (March, 1945).
4. S. K. Clark, C. W. Tomlinson and J. S. Royds, "Well Spacing — Its Effect on Recoveries and Profits," *Bull. Am. Assoc. Petroleum Geol.,* 28, 2, (1944), 321-56.
5. W. V. Vietti, J. J. Mullane, O. F. Thornton and A. F. Van Everdingen, "The Relation Between Well Spacing and Recovery," *API Drlg. and Prod. Prac.,* (1945), 160-77.
6. H. B. Hill and R. K. Guthrie, "Analysis of Oil Production in the Near Depleted Mexia-Powell Fault Line Fields of Texas," *U. S. B. M., R. I.* 3479, (1939).
7. R. C. Craze and S. C. Buckley, "A Factual Analysis of the Effect of Well Spacing on Oil Recovery," *API Drlg. and Prod. Prac.,* (1945), 144-59.
8. W. H. Barlow and W. B. Berwald, "Optimum Oil-Well Spacing," *API Drlg. and Prod. Prac.,* (1945), 129-43.
9. R. G. Loper and J. C. Calhoun, Jr., "The Effect of Well Spacing and Drawdown on Recovery from Internal Gas Drive Reservoirs," Petroleum Branch, AIME, in Dallas, Tex., October, 1948.
10. C. C. Miller, E. R. Brownscombe and W. F. Kieschnick, "A Calculation of the Effect of Production Rate Upon Ultimate Recovery by Solution Gas Drive," AIME *Trans.,* Vol. 186, (1949), 235-50.

APPENDIX

Pressure and saturation distribution around a well bore in a depletion-drive system, from which recovery efficiency as a function of well spacing can be evaluated, was approximated as shown in Figs. 5 through 9. The methods of arriving at these approximate solutions were chosen upon the basis of the logic expressed in the text, in which it was concluded that the total composition of the flowing stream (liquid *and* vapor phases) at any particular time in the history of the system can be expected to:

1. Be approximately the same from the extreme radius of drainage to the well bore.
2. Be controlled by the composition at the extreme radius of drainage whereat the behavior of the system can be accurately predicted by the depletion-drive concept, due to the fact that vanishing pressure gradients exist at that point.

The relations developed may be derived as follows:

For a given element of reservoir rock,

$$(1) \quad GOR = F\,(K_g/K_o) + r_s$$

$$(2) \quad F = \frac{\mu_g}{\mu_o} \times \frac{14.7}{p} \times \frac{5.61}{Z} \times \frac{520}{T_R}$$

Also,

$$(3) \quad q_o = \frac{7.073\ Kt\ K_o/K}{\mu_o\beta} \quad \frac{r\,dp}{dr}$$

Rearranging (3),

$$(4) \quad q_o \int_{r_e}^{r_w} \frac{dr}{r} = \frac{7.073\ Kt\ K_o/K}{\mu_o\beta} \int_{p_e}^{p_w} dp$$

By the logic expressed above and in the text,

(5) Let $GOR = \phi\ (p_e)$ (from material balance)

Assuming uniform contribution of various elements to the total flow stream into the well bore (in the absence of transient conditions),

$$(6) \quad q_o = Q_o\left(1 - \frac{r^2}{r_e^2}\right) \quad \text{(Approximately)}$$

From (2),

$$(7) \quad F = \phi\ (p)$$

Also,

$$(8) \quad r_s = \phi\ (p)$$

Substituting (5), (7), and (8) in (1), it follows that, for a given value of p_e

(9) $K_g/K_o = \phi\ (p_e, p)$

From relative permeability relations, for a given s_w,

(10) $K_g/K_o = \phi\ (s_1)$

And

(11) $K_o/K = \phi\ (s_1)$

Therefore,

(12) $K_o/K = \phi\ (K_g/K_o)$

Combining (9) and (12)

(13) $K_o/K = \phi\ (p_e, p)$

Also,

(14) $\mu_o = \phi\ (p)$

(15) $\beta = \phi\ (p)$

Substituting in (4),

(16) $$Q_o \int_{r_e}^{r} \left(1 - \frac{r^2}{r_e^2}\right) \frac{dr}{r} = 7.073\ KT \int_{p_e}^{p} \frac{K_o/K}{\mu_o \beta}\ dp$$

This relation must be evaluated (integrated) graphically from r_e to r_w, and intermediate points to obtain p as a function of r. Since, at abandonment condition, Q_o is determined by economic factors and p_w by physical factors, value of these variables must be fixed in evaluating pressure and saturation distribution at abandonment conditions. The total gas-oil ratio, however, is chosen as a function of p_e. The solution of the relation therefore becomes a trial and error proposition, in which a value for p_e is arbitrarily chosen and p_w evaluated for the desired Q_o until a value of p_e has been found which will yield the desired value of p_w. Elimination of expression (6) and substitution of Q_o directly for q_o will result in only a slight modification of the calculated pressure distribution.

Once the pressure distribution has been determined, the oil saturation and oil in place at abandonment, as a function of r, can be evaluated.

Since s_o is a function of liquid saturation (for a given s_w), it follows from (16) that

(17) $s_o = \phi\ (K_o/K) = \phi\ (p_e, p) = \phi(r)$

(18) Oil in place/unit pore volume $= s_o/\beta$

(19) $$\text{Abandonment oil in place} = 2\pi t f \int_{r_w}^{r_e} \frac{s_o}{\beta}\ r dr$$

(20)

$$\text{Oil Recovery} = \pi t f \left[\frac{(1 - s_w)}{\beta_i} (r_e^2 - r_w^2) - 2 \int_{r_w}^{r_e} \frac{s_o}{\beta}\ r dr \right]$$

NOMENCLATURE

ϕ = Symbol denoting "function of"

GOR = Total gas-oil ratio (free and solution gas)

p = Pressure

p_e = Pressure at the extreme radius of drainage

p_w = Pressure at the well bore

r = Radius, distance from the center of the well bore

r_w = Well bore radius

K = Permeability

K_o = Effective permeability to oil

K_g = Effective permeability to water

t = Pay thickness

μ_o = Oil viscosity

μ_g = Gas viscosity

Z = Compressibility factor of free gas

β = Reservoir volume factor of oil phase at any pressure, p

β_i = Reservoir volume factor of oil phase at initial pressure

q_o = Instantaneous rate of flow at any radius, r

Q_o = Rate of flow into the well bore (at r_w)

s_o = Oil saturation

s_w = Connate water saturation

s_1 = Liquid saturation (oil plus water)

T_R = Reservoir temperatures

f = Fractional porosity

REVIEW OF CYCLING OPERATIONS IN THE LA GLORIA FIELD

W. H. JUSTICE, LA GLORIA CORP., CORPUS CHRISTI, TEX., MEMBER AIME

PURPOSE

Cycling operations have been successfully conducted in the La Gloria Zone for eight years. The cycling of this zone is now virtually completed. It is proposed that this report shall review the cycling operations of this reservoir so that the industry can more accurately evaluate the cycling process as a production method.

INTRODUCTION

The La Gloria project is one of the largest cycling operations in the State of Texas. The gas rights in the field are unitized in three operating units. By mutual agreement Magnolia Petroleum is the designated operator of the project for the 12 operators owning the gas rights. The La Gloria Corp. is the owner and operator of the cycling plant. The development and operation of the field are under the direction of an Operators Committee comprised of a representative of each operator. The Operators Committee is assisted by an Engineering and Geological Sub-Committee.

The La Gloria gas field is situated approximately three miles north of Falfurrias, Tex., and lies principally in the extreme south end of Jim Wells County, with its outer limits extending into the north end of Brookes County, Tex. It is a simple elliptically-shaped dome which has a closure of 350 ft. The field encompasses a surface area of 5,500 acres. The gas reserves are found in 20

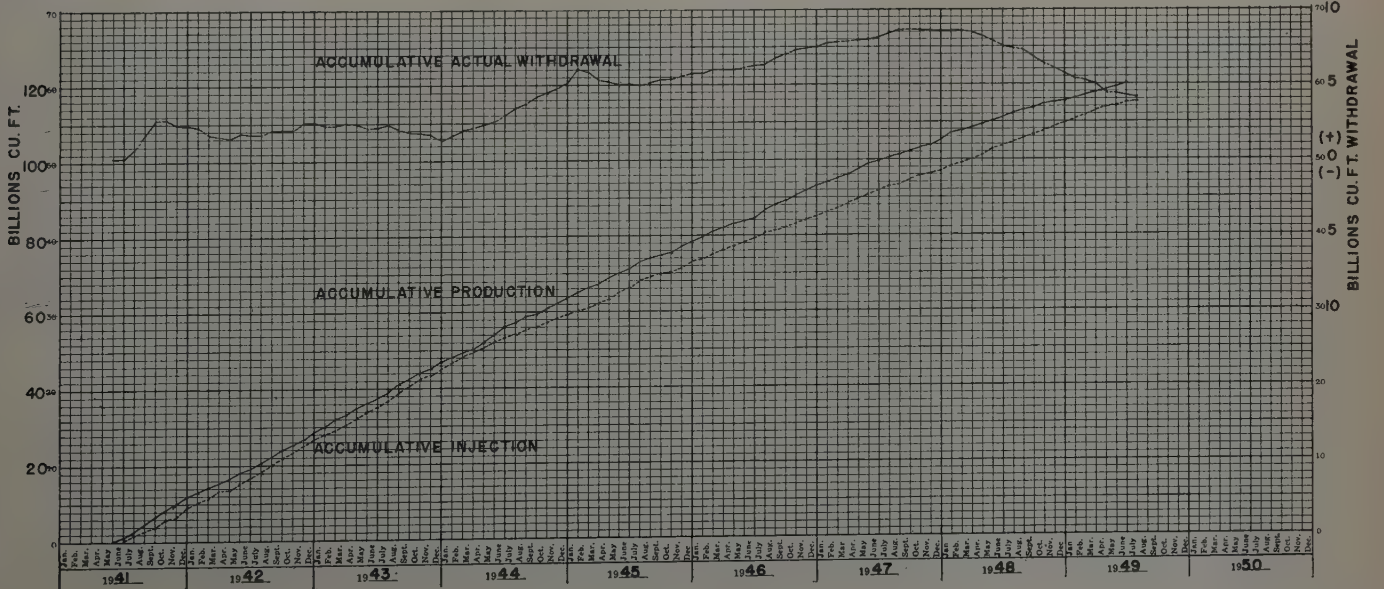

FIG. 1 — LA GLORIA ZONE, LA GLORIA FIELD

Manuscript received at the office of the Petroleum Branch October 4, 1949. Paper presented at the Fall Meeting of the Branch October 5-7, 1949, in San Antonio, Tex.

major sand zones lying in the lower Frio formation and Transition Zone of the Upper Vicksburg formation. Approximately 40 gas wells have been drilled in exploring and developing the gas reserves of the field.

DISCUSSION

The La Gloria sand occurs in the lower Frio formation at a depth of 6,515 ft at the crest of the structure. The average sand thickness for this zone is 32 ft. The reservoir initially had a gas column of 125 ft and did not have an oil column. The sand has an average porosity of 22.2 per cent and an average permeability of 521 MD. The productive area of this zone is 2,680 acres. The original bottom hole pressure was 3,470 psia and the formation temperature is 203°F. The average percentage connate water in the reservoir space has been estimated at 20 per cent. The original gas reserve for the La Gloria Zone is estimated at 139,284,000 cu ft at 14.65 psia and 60°F. The initial condensate reserve in place is estimated at 6,727,000 bbl of propane and heavier condensate, of which 4,011,000 bbl consist of pentanes and heavier hydrocarbons, 1,128,000 bbl of iso and normal butanes and 1,588,000 bbl of propane. The initial hydrocarbon content of the gas was 1.21 GPM or 28.8 bbl per MMcf of pentanes and heavier hydrocarbons, .34 GPM or 8.10 bbl per MMcf of iso and normal butanes and .48 GPM or 11.40 bbl per MMcf of propane. The reservoir data on the La Gloria Zone is summarized in Table XII.

Table I

Summary

La Gloria Zone Gas Production and Injection
La Gloria Field, Jim Wells County, Texas

	Gas Produced		Gas Injected	
Year	Yearly Total Volume-Mcf	Average Daily Volume-Mcf	Yearly Total Volume-Mcf	Average Daily Volume-Mcf
1941 (6.5 mos.)	11,126,467	54,800	8,693,048	42,800
1942	17,449,830	47,800	17,584,239	48,175
1943	18,230,414	49,950	19,070,512	52,250
1944	16,858,497	46,200	14,741,921	40,400
1945	14,838,079	40,650	12,989,308	35,600
1946	14,401,905	39,450	12,596,668	34,500
1947	13,009,921	35,650	12,006,362	32,900
1948	9,642,063	26,400	12,455,192	34,100
1949 (7 mos.)	4,549,873	21.360	7,474,602	35,091
Total production to date	120,107,050		117,611,852	
Estimated total production and completion of cycling program:	126,428,400		123.801,900	

Cycling operations were begun in the La Gloria Zone in May, 1941. For initial cycling operations in this zone there were available six producing and two injection wells. Another injection well was made available in 1942 along with another producing well. An average of 50 MMcf per day was produced from the reservoir during the first four years of operations. With the abandonment of producing wells because of dry gas encroachment the producing rate has been gradually decreased to the present rate of 21 MMcf per day.

During the cycling operations of the La Gloria reservoir a volume of gas equivalent to 97 per cent of the gas produced has been returned to the reservoir through three injection wells. The return of this high percentage of residue gas to the reservoir was made possible by using gas from uncyclable reservoirs for plant fuel. The low net volumetric withdrawal of gas from this reservoir has resulted in a very small average pressure drop in the reservoir. Since the average pressure of the reservoir was not appreciably reduced during cycling, the retrograde loss of condensate in the reservoir was largely prevented. This is evidenced by the fact that a well recently completed in the uncycled portion of the reservoir has a condensate content practically equivalent to the content of the gas produced from the original wells.

The condensate content testing of the produced gas is extremely important in the control of the cycling operations. These tests were conducted on samples obtained by the split-stream method and were conducted on each well every

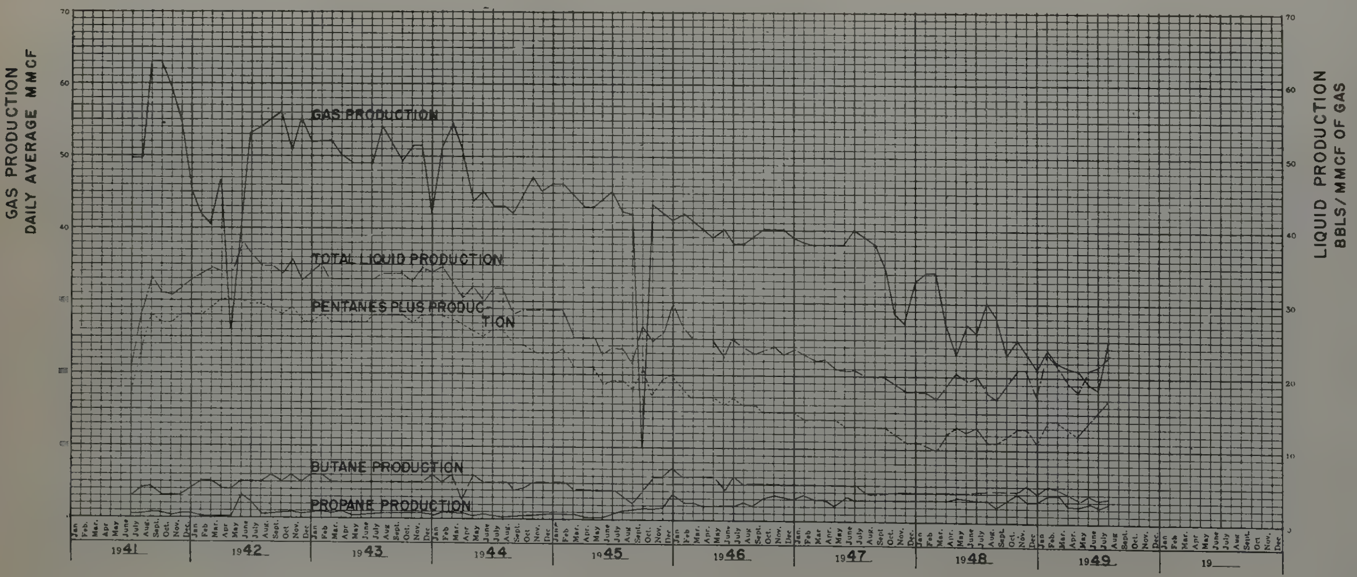

FIG. 2 — LA GLORIA ZONE PRODUCTION

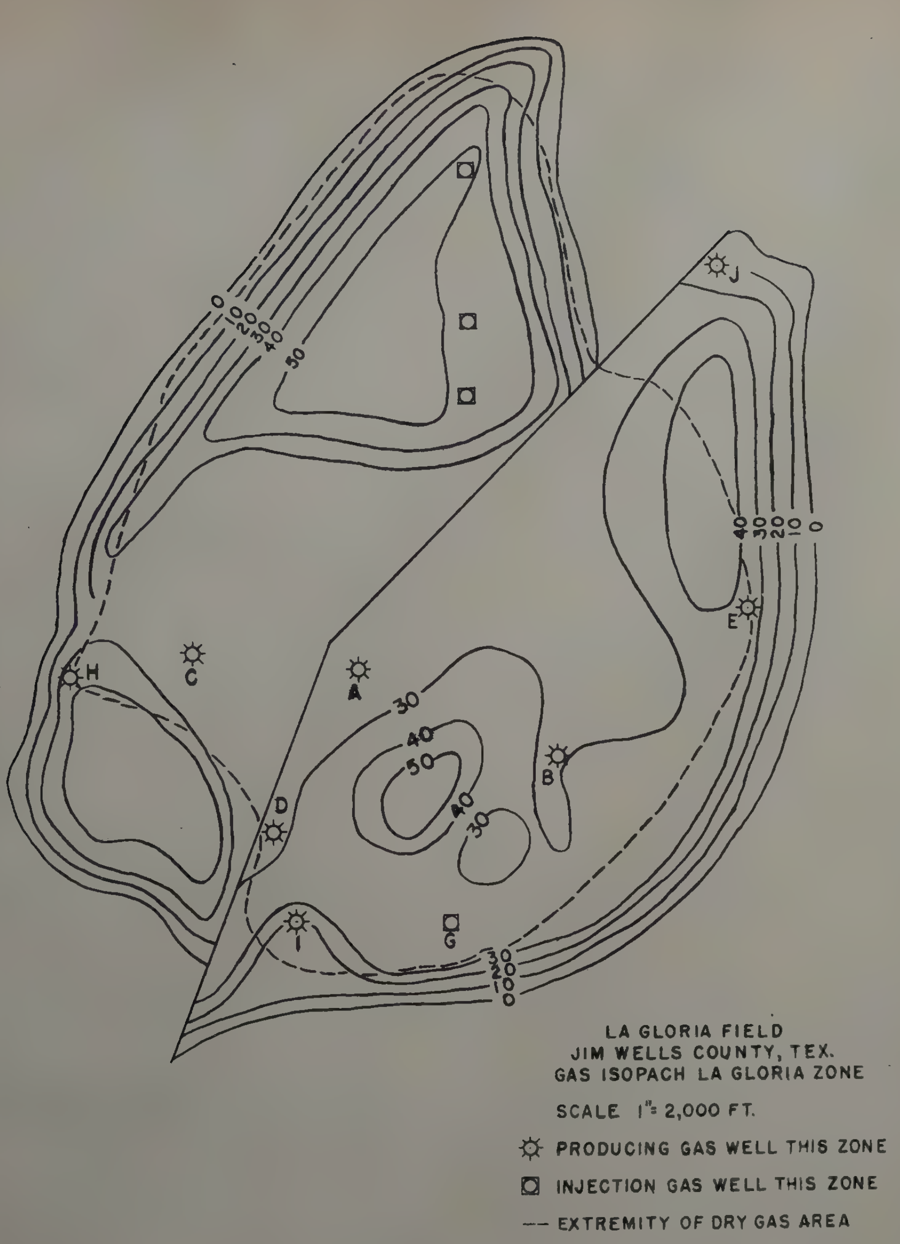
0
10
20
30
40
50
A
B
C
D
E
G
H
I
J
LA GLORIA FIELD
JIM WELLS COUNTY, TEX.
GAS ISOPACH LA GLORIA ZONE
SCALE 1" = 2,000 FT.
PRODUCING GAS WELL THIS ZONE
INJECTION GAS WELL THIS ZONE
-- EXTREMITY OF DRY GAS AREA

FIG. 3 — GAS ISOPACH, LA GLORIA ZONE

three months. The travel of the dry gas in the reservoir was followed by this testing program. It is indicated that the dry gas has displaced approximately 80 per cent of the wet gas in the invaded area. The gas was injected in wells located in the extreme north end of the reservoir and the gas was produced for a "ring" of wells located in the south half of the reservoir (Fig. 3). The use of this "end-to-end sweep" cycling pattern has resulted in the invasion by the dry gas of 85 per cent of the original reservoir volume.

It is estimated that the cycling program of the La Gloria reservoir is now 95 per cent completed. When the cycling and depletion of this reservoir are completed, it is estimated that the following recoveries will have been realized:

2,725,000 bbl or 68 per cent of original C5+ condensate in place recovered during cycling.

836,000 bbl or 20.8 per cent of original C5+ condensate in place recovered during depletion to 500-lb. abandonment pressure.

3,561,000 bbl or 88.8 per cent of original C5+ condensate in place recovered during cycling and depletion.

The condensate recovered during cycling was accomplished by handling a volume of gas equivalent to 91 per cent of the original gas in place or 126,428,400 cu ft of which 25 per cent or 31,602,000 cu ft was dry gas.

SUMMARY

Cycling of the La Gloria Zone resulted in the following:

(1) The recovery and sale of 68 per cent of the pentanes and heavier con-

Table II
Summary
La Gloria Zone Liquid Production
La Gloria Field, Jim Wells County, Texas

Year	Yearly Total Pentanes + Bbl	Average Bbl/M^2cf	Yearly Total Propanes + Bbl	Average Bbl/M^2cf	Yearly Total Butanes Bbl	Average Bbl/M^2cf	Yearly Total Liquid Bbl	Average Bbl/M^2cf
1941 (6.5 mos.)	291,768	26.2	1,195	0.1	40,247	3.6	333,210	29.9
1942	500,940	28.7	6,994	0.4	88,444	5.1	596,378	34.2
1943	502,454	27.6	9,169	0.5	93,186	5.1	604,809	33.2
1944	424,519	25.2	8,183	0.5	80,131	4.8	512,833	30.5
1945	291,347	19.6	13,961	0.9	64,788	4.4	370,096	24.9
1946	233,106	16.2	34,342	2.4	76,101	5.3	343,549	23.9
1947	168,407	12.9	38,352	2.9	56,629	4.6	263,388	20.4
1948	112,704	11.7	28,750	3.0	37,091	3.8	178,545	18.5
1949 (7 mos.)	64,205	14.1	13,624	3.0	17,686	3.9	95,515	21.0
Total production to date	2,589,450	21.6	154,570	1.3	554,303	4.6	3,298,323	27.5
Estimated total production and completion of cycling program:	2,725,260	21.6	162,700	1.3	583,470	4.6	3,471,430	27.5

Table III

Gas and Liquid Production — Well A, La Gloria Zone La Gloria Field, Jim Wells County, Texas

	Gas Production		Liquid Production			All Liquids	
Year	Yearly Total Volume-Mcf	Avg. Daily Volume MMcf	Pentanes + Bbl/M^{2}cf	Propane Bbl/M^{2}cf	Butane Bbl/M^{2}cf	Yearly Total Bbl	Bbl/M^{2}cf
1941 (6.5 mos.)	2,635,942	13.5	25.4	0.2	3.3	76,261	28.9
1942	2,848,117	7.8	24.6	0.6	4.6	84,967	29.8
1943 (1 mo.)	94,403	3.0	9.5	0.3	2.0	1,121	11.8
1944							
1945							
1946							
1947							
1948							
1949							
Total production to date	5,578,462					162,349	29.1

Table V

Gas and Liquid Production — Well C, La Gloria Zone La Gloria Field, Jim Wells County, Texas

	Gas Production		Liquid Production			All Liquids	
Year	Yearly Total Volume-Mcf	Avg. Daily Volume MMcf	Pentanes + Bbl/M^{2}cf	Propane Bbl/M^{2}cf	Butane Bbl/M^{2}cf	Yearly Total Bbl	Bbl/M^{2}cf
1941 (6.5 mos.)	1,535,986	7.8	28.1	.20	3.18	48,811	31.8
1942	2,788,085	7.6	28.9	.6	5.5	97,591	35.0
1943	2,822,440	7.7	28.9	.6	5.6	99,180	35.1
1944	2,832,173	7.7	22.9	.3	4.0	76,944	27.2
1945	2,705,814	7.4	13.6	2.0	4.6	49,903	18.4
1946	3,059,543	8.4	13.0	1.2	4.3	56,591	18.5
1947	3,160,615	8.6	10.7	2.4	3.9	53,826	17.0
1948	3,178,736	8.7	9.0	1.8	2.9	43,677	13.7
1949 (5 mos.)	949,459	6.3	5.5	1.7	1.0	7,774	8.2
Total production to date	23,032,851					534,297	23.2

Table VII

Gas and Liquid Production — Well E, La Gloria Zone La Gloria Field, Jim Wells County, Texas

	Gas Production		Liquid Production			All Liquids	
Year	Yearly Total Volume-Mcf	Avg. Daily Volume MMcf	Pentanes + Bbl/M^{2}cf	Propane Bbl/M^{2}cf	Butane Bbl/M^{2}cf	Yearly Total Bbl	Bbl/M^{2}cf
1941 (6.5 mos.)	1,694,046	8.7	28.5	0.7	3.4	55,226	32.6
1942	3,186,941	6.2	29.9	0.7	5.3	115,245	35.9
1943	3,640,227	7.1	29.9	0.5	5.2	129,524	35.6
1944	3,146,349	6.1	27.4	0.4	5.6	105,184	33.4
1945	3,475,926	6.8	20.3	1.5	6.4	98,009	28.2
1946	3,795,844	7.4	19.2	3.2	6.4	109,302	28.8
1947	2,831,731	5.5	16.2	3.6	5.2	70,757	25.0
1948	2,430,028	4.7	8.7	2.2	2.8	33,281	13.7
1949 (7 mos.)	1,293,418	6.1	8.8	2.2	2.6	17,584	13.6
Total production to date	25,494,510					731,112	28.7

Table IV

Gas and Liquid Production — Well B, La Gloria Zone La Gloria Field, Jim Wells County, Texas

	Gas Production		Liquid Production			All Liquids	
Year	Yearly Total Volume-Mcf	Avg. Daily Volume Mcf	Pentanes + Bbl/M^{2}cf	Propane Bbl/M^{2}cf	Butane Bbl/M^{2}cf	Yearly Total Bbl	Bbl/M^{2}cf
1941 (6.5 mos.)	1,307,703	6,700	26.0	0.5	3.0	38,575	29.5
1942	1,852,645	5,100	29.0	0.6	4.6	63,330	34.2
1943	1,594,141	4,400	23.0	0.4	4.1	43,975	27.5
1944	1,694,232	4,600	13.9	0.3	3.0	29,186	17.2
1945 (6 mos.)	544,934	3,000	11.3	0.1	2.0	7.319	13.4
1946							
1947							
1948							
1949							
Total production to date	6,993,655					182,385	26.1

Table VI

Gas and Liquid Production — Well D, La Gloria Zone La Gloria Field, Jim Wells County, Texas

	Gas Production		Liquid Production			All Liquids	
Year	Yearly Total Volume-Mcf	Avg. Daily Volume MMcf	Pentanes + Bbl/M^{2}cf	Propane Bbl/M^{2}cf	Butane Bbl/M^{2}cf	Yearly Total Bbl	Bbl/M^{2}cf
1941 (6.5 mos.)	2,133,647	10.9	28.0	0.2	3.1	66,780	31.3
1942	3,549,019	9.7	29.4	0.3	5.5	124,842	35.2
1943	3,994,764	10.9	26.0	0.2	4.9	124,346	31.1
1944	4,009,299	11.0	28.0	0.3	5.6	135,981	33.9
1945	3,636,429	10.0	20.0	1.5	4.9	92,335	25.4
1946	4,136,046	11.3	11.0	1.1	3.9	65,755	16.0
1947	4,160,911	11.4	6.7	1.5	2.3	43,879	10.5
1948	1,005,920	4.5	4.8	1.3	1.5	7,664	7.6
1949							
Total production to date	26,626,035					661,582	24.9

Table VIII

Gas and Liquid Production — Well G, La Gloria Zone La Gloria Field, Jim Wells County, Texas

	Gas Production		Liquid Production			All Liquids	
Year	Yearly Total Volume-Mcf	Avg. Daily Volume MMcf	Pentanes + Bbl/M^{2}cf	Propane Bbl/M^{2}cf	Butane Bbl/M^{2}cf	Yearly Total Bbl	Bbl/M^{2}cf
1941							
1942	2,623,145	7.2	28.8	0.2	5.0	89,018	34.0
1943	3,045,264	8.3	29.0	0.5	5.3	105,928	34.8
1944 (6 mos.)*	1,159,048	6.4	27.0	0.8	3.2	35,837	31.0
1945							
1946							
1947							
1948							
1949							
Total production to date	6,827,457					230.783	33.8

*This well converted to injection well.

Table IX

Gas and Liquid Production — Well H, La Gloria Zone
La Gloria Field, Jim Wells County, Texas

	Gas Production		Liquid Production			All Liquids	
Year	Yearly Total Volume-Mcf	Avg. Daily Volume MMcf	Pentanes + Bbl/MMcf	Propane Bbl/MMcf	Butane Bbl/MMcf	Yearly Total Bbl	Bbl/MMcf
1942	601,878	2.0	29.6	0.7	5.2	21,385	35.5
1941							
1943	1,561,178	4.3	29.0	0.7	5.2	53,915	34.5
1944	2,379,692	6.5	29.0	0.8	4.2	80,805	34.0
1945	2,723,058	7.5	29.0	1.0	6.0	98,108	36.0
1946	2,940,897	8.0	25.0	3.1	8.7	108,166	36.8
1947	2,856,664	7.8	21.6	4.7	6.9	94,926	33.2
1948	2,692,438	7.4	20.1	4.9	6.4	84,635	31.4
1949 (7 mos.)	1,683,937	8.0	17.5	3.4	5.2	43,737	26.0
Total production to date	17,439,742					585,677	33.6

Table X

Gas and Liquid Production — Well I, La Gloria Zone
La Gloria Field, Jim Wells County, Texas

	Gas Production		Liquid Production			All Liquids	
Year	Yearly Total Volume-Mcf	Avg. Daily Volume MMcf	Pentanes + Bbl/MMcf	Propane Bbl/MMcf	Butane Bbl/MMcf	Yearly Total Bbl	Bbl/MMcf
1941							
1942							
1943	1,477,997	4.0	29.9	1.1	6.4	55,269	37.4
1944	1,637,704	4.5	23.5	0.4	6.0	48,896	29.9
1945	1,751,918	4.8	11.3	0.5	2.2	24,422	14.0
1946 (5 mos.)	469,575	3.1	5.5	0.5	2.0	3,735	8.0
1947							
1948							
1949							
Total production to date	5,337,194					132,322	25.0

Table XI

Gas and Liquid Production — Well J, La Gloria Zone
La Gloria Field, Jim Wells County, Texas

	Gas Production		Liquid Production			All Liquids	
Year	Yearly Total Volume-Mcf	Avg. Daily Volume MMcf	Pentanes + Bbl/MMcf	Propane Bbl/MMcf	Butane Bbl/MMcf	Yearly Total Bbl	Bbl/MMcf
1941							
1942							
1943							
1944							
1945							
1946							
1947							
1948 (4 mos.)	334,941	3.0	28.2	7.6	9.6	15,224	45.4
1949 (7 mos.)	623,050	3.0	28.6	5.5	8.3	26,420	42.4
Total production to date	957,991					41,644	43.5

Table XII

La Gloria Field, Jim Wells County, Texas
La Gloria Zone
PHYSICAL FACTORS

Average Porosity	22.2%
Average Permeability	521 M.D.
Connate Water — Estimated	20.0%
Condensates — Pentanes+ G.P.M.	1.21
Condensates — Pentanes+ Bbl/MMcf	28.8
Depth to Edgewater	6,900 ft
Average Pressure	3,470 psia
Average Temperature	203°F

ORIGINAL GAS AND CONDENSATE RESERVES

All gas computed to 14.65 psia and 60°F

	Field
Productive acres of gas	2,680
Average net productive sand ft	32
Acre ft productive sand	87,600
Gas per acre ft Mcf	1,590
Gas reserves Mcf	139,284,000
Condensate reserves Pentanes and heavier Bbl	4,011,000

densate content of gas in this zone during the cycling period. This has provided a substantial income from this gas reserve during this eight-year cycling period.

(2) The cycling of this reservoir has reduced the retrograde loss that would have occurred if the reservoir had not been cycled. The amount of this loss varies with the pentanes plus content of the reservoir gas. The gas in the La Gloria reservoir had a moderate recoverable pentane plus condensate content of 28.8 bbl per MMcf so that the increased recovery of condensate due to cycling was not as large as it would have been for a gas containing a greater amount of condensate.

(3) Cycling has also increased the ultimate recovery of condensate from this reservoir since 68 per cent of the gas remaining in the reservoir at the abandonment pressure will be gas that has already been processed. We have estimated the abandonment pressure for this reservoir at 500 psia which will result in the abandonment of 13 per cent of the gas initially in place. The retrograde loss of the pentanes and heavier content of this gas during depletion is estimated at 25 per cent.

(4) At the time cycling was started in this reservoir, there was only available a small seasonal gas sale and the prevailing price for residue gas was extremely low. In this particular case, cycling has not resulted in the deferment of any income from the sale of residue gas since the available seasonal gas sale has been fulfilled from uncyclable reservoirs. A substantial gas sale at a much improved price will become available to this field during the first quarter of 1951 and this sale will be met initially with gas produced from this reservoir that has been cycled. Gas will become available from the other reservoir now being cycled and from uncyclable reservoirs in the field in time to fulfill the volume demand of this sale during the next 20 years.

CONCLUSION

The cycling of the La Gloria Zone has been highly successful in increasing the ultimate recovery of condensate from this reservoir and in providing a substantial income during the cycling period from what would have otherwise been a very low income property.

It is not to be concluded, however, that the cycling of other fields containing gas with the same condensate content would be as economically profitable. Because of the change in the availability of substantial gas markets at prices considerably higher than were formerly available, increased construction cost and other changes, each project should be critically examined to determine the most economical production method.

ACKNOWLEDGMENTS

The writer wishes to express his thanks to the management of the Magnolia Petroleum Co. and the other operators in the La Gloria Field for permission to publish this paper. The information contained in this paper has been accumulated through the years by F. H. Stone, W. H. Speaker, C. L. Wheless and J. P. Nielson et al., and they are to be credited for their assistance in preparing this data. The geological reports of J. O. Lewis and Bruce Scrafford are credited for the geological data.

★ ★ ★

PERFORMANCE OF LIMESTONE RESERVOIRS

R. C. CRAZE, HUMBLE OIL AND REFINING CO., HOUSTON, TEX., MEMBER AIME

ABSTRACT

During the past 20 years, research and development in the study of reservoir behavior have dealt principally with flow of oil through sandstones. Many reservoir studies of sand fields have proved valuable in promoting recovery efficiency.

This paper discusses fundamental principles governing oil and gas production from sandstone and limestone alike and presents the results of investigations relating to the application of analytical techniques used for sandstone reservoir studies to the study of limestone reservoir performance. The characteristics of limestone porous systems, porosity-permeability relationships, distribution and occurrence of oil, and characteristics of flow through such systems are discussed. Recognition is made of the similarities or differences which these factors exhibit in limestone and sandstone systems. Comparisons between operating data for typical limestone and sand reservoirs are presented. It is indicated that the distribution and movement of fluids in and through porous limestones follow the same fundamental principles underlying such processes in sandstones. This fundamental similarity may readily be discernible in the performance of many limestone reservoirs.

The volumetric balance and unsteady state radial flow equation, the fluid displacement equation, use of electrical analogue devices, and other analytical techniques to study the behavior of limestone fields appear fundamentally applicable, but do require thorough understanding of the properties of the formation, of the fluids, their behavior during flow, and adequate production operating data. Need for more complete coring and comprehensive examination of core properties is stressed. The results of "active oil" studies, and of flow and interference tests are presented. Well spacing, well completion, and efficient rates of production in limestone reservoirs are briefly discussed.

INTRODUCTION

Limestone and dolomite reservoirs constitute the largest source of supply of crude oil in the world, an estimated 60 per cent of present production coming from carbonate reservoirs. In many large geologic provinces such as Mexico, the Middle East, and more recently Canada, almost all the oil is found in this type of rock. In the United States, all of the major oil-producing areas except California and Pennsylvania contain oil-bearing carbonate formations. The discovery in recent years of large oil reserves in the Silurian, Devonian, and Ordovician formations in West Texas, in addition to the large reserves in the Permian, has accentuated the interest of operators, geologists, and engineers in limestone formations and in the many problems associated with understanding the performance of these reservoirs. The rapid increase in discovery of oil in limestone formations and the present-day position of prominence held by these fields in the production and reserve picture in all parts of the world emphasize the horizons opened to the reservoir technologist in the field of geological and production research.

Pertinent to an interpretation of the behavior of limestone reservoirs are the methods of analysis which may be utilized and a possession of full knowledge of the many factors which influence the analytical procedures. During the past 20 years a well-developed science of reservoir engineering has been built upon the research of many workers who studied the fundamental nature of oil reservoirs, characteristics of the porous media, properties and behavior of the contained fluids, and the mechanics of flow. Application of these studies to production practice has resulted in greater recoveries and more efficient field operation. The major portion of this evolutionary process has been founded upon studies of sand fields. The applicability of these more thoroughly developed techniques for studying sand fields to the study of the behavior of limestone fields becomes a factor of technical and practical significance.

In the light of the technological background available to the reservoir analyst, this paper discusses fundamental principles governing oil and gas production from sandstone and limestone alike and presents the results of investigations relating to the application of analytical techniques used for sandstone studies to the study of limestone reservoir performance.

LIMESTONE RESERVOIR CHARACTERISTICS

The characteristics of limestone and sandstone reservoirs are similar in many respects and they both may occur under similar structural conditions. Fundamentally, the distribution and movement of fluids in and through the porous limestone media follow the same basic principles which dictate such processes in sandstones. Herein lies a fundamental similarity, which may readily be discernible in the performance of many limestone reservoirs. In some limestone fields, as in many sand fields, widely varying formation properties and distribution may reveal themselves in deviations in the performance of the reservoir, in the behavior of wells, and in fluid flow through the rock, and make difficult the delineation of reservoir behavior. Only by reservoir studies, core analyses, and coordinated laboratory and field experimentation can the effects of the many influencing factors upon the nature of limestone production be determined.

FORMATION CHARACTERISTICS

The chief difference between limestone and sandstone, aside from their chemical compositions, is the difference in the geometry and origin of the porous systems in the two kinds of rock. In sandstone the porous system results entirely from the openings among individual sand grains which occur during deposition. The geometry of the openings between the sand

---

[1] References given at end of paper.

Manuscript received in the office of the Petroleum Branch May 16, 1950. Paper presented at a meeting of the Permian Basin Section of the Branch in Midland, Tex., Feb. 27, 1950.

grains is determined by the geometry of the grains. Although the pore channels are tortuous and highly irregular, nevertheless they are intercommunicating and, macroscopically, impart to the sand segment fairly regular properties of porosity and permeability.

In a limestone, the void system is characterized by a wide variation in the shapes and distribution of pore sizes. Some intercrystalline or intergranular limestones may have porous systems which geometrically are similar to the systems of some sandstones. The behavior of such limestone reservoirs may be quite similar to that of sandstone reservoirs. However, complicating processes of secondary solution, recrystallization, and fracturing markedly influence the geometry of limestone porous systems, imparting to the formations where such processes have occurred considerable variations in the pore shapes and a high degree of variation in pore size distribution. Such conditions make it more difficult to obtain representative sampling, to measure the rock properties, and to ascertain the influence of the porous system upon the reservoir behavior.

Recent research has been conducted to study the occurrence of oil in carbonate reservoirs. This project combined a petrographic study of dolomitic and calcitic limestone cores with laboratory examination of the same cores. More than 3,700 core samples obtained from various formations and ages in West Texas, Southwest Texas, and North Texas, from the Devonian zones at Leduc, Canada, and from the Quaternary surface limestones in the Bahama Islands were examined. Porosities and permeabilities were measured on the samples.

In this study, four basic porosity types were recognized: intercrystalline, intergranular, fissure, and vug. Core analyses and detailed lithologic examination of the samples indicated a relationship between the type of porosity and the porosity-permeability properties of the carbonates. Table I summarizes this relationship.

Table I

Porosity Type	Porosity, Per Cent	Permeability, *md.*
Intercrystalline		
Microgranular	High (20-35)	Low (1-10)
Fine- to Coarse-Grained	Moderate (10-20)	Moderate (10-100)
Intergranular	Very high (25-45)	Very high (300-5000+)
Fissure	Low (2-10)	Very high (unmeasured)
Vug (highly variable)	Low to very high	Moderate to very high

In Fig. 1 is shown the relationship between porosity and permeability for a series of samples from the Cretaceous Edwards lime of intercrystalline porosity type. It became evident during this study that textural variations of the formation within a porosity type influenced the porosity and permeability relations. These influences were also found to vary with the formation and with composition. This textural relationship is also illustrated in Fig. 1. As the texture ranges from microgranular to coarse-grained, the permeability increases for a given porosity. The texture-composition relation noted for the Edwards lime was also found in samples from the Ellenburger and Permian formations in West Texas. In the Ellenburger, for example, limestones are microgranular, and the dolomites range from fine- to coarse-grained.

In conjunction with the correlations made on the results of these core analyses, statistical methods were applied to attain more complete interpretation. Such methods have utility in establishing relationships between porosity and permeability probabilities and in characterizing the porosity type or combinations of types that make up the productive zones.

The existence of different types of porosity and the conditions of their formation affect the accumulation of oil and the behavior of reservoir and well. Correlation with production tests on wells shows the influence of porosity type on well potentials. In the fracture type such as the Keystone and Martin Ellenburger fields, potentials are medium to high and vary less than in other types. Reservoir pressures are quite uniform and a high degree of intercommunication is apparent. In the vug-type reservoir, well performance and reservoir pressures in some areas may vary widely from those in other portions of the reservoir. In the intercrystalline type reservoir, potentials generally are lower and their distribution more uniform than those of wells in vug-type formations. Pressure distribution may vary from one area to another. An understanding of the variations in well behavior with properties of the formation may aid considerably in interpreting reservoir performance, in applying auxiliary aids to increase production efficiency, and in well completion and control.

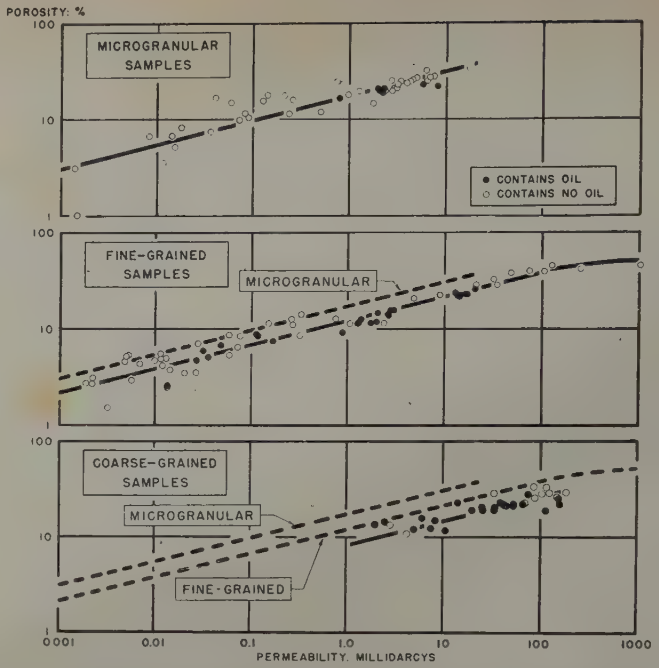

FIG. 1 — POROSITY-PERMEABILITY RELATIONS EDWARDS LIMESTONE SAMPLES.

DISTRIBUTION OF OIL OCCURRENCE

In connection with studies of the textural-porosity-permeability relations in limestone core samples, an analysis of the distribution of the presence or absence of oil with permeability and porosity was made for a group of cores from the Edwards limestone in the Jourdanton Field in Atascosa County. The presence of oil appeared dependent upon high porosities and permeabilities, and similarly, the absence of oil the result of low porosities and permeabilities. It was indicated that little oil was present in those cores having porosities less than 5 per cent and no oil present in those with less than 2 per cent porosity and 0.01 *md.* permeability.

An interesting study of fractured dolomite cores from the Martin Ellenburger Field has also been made. Large core samples were obtained from a well cored with oil-base drilling fluid and porosities were measured in the laboratory. Total porosity averaged 3.3 per cent of the bulk volume of the samples. Porosities of small samples of the intercrystalline matrix averaged 1.51 per cent, leaving 1.79 per cent porosity for the fracture and vug system. The ratios of the matrix porosity to the total porosity for individual cores averaged 0.474. The ratio of the matrix porosity to total porosity was the same as the fractional water saturation of 0.473 observed for the large samples. This indicated that water occupied practically all the matrix porosity and oil all the fracture porosity. This distribution was observed visually when the cores were obtained. The matrix was intercrystalline dolomite having a low permeability of around 0.1 *md.*

In another Ellenburger field, Yarbrough and Allen, a similar study indicated that the fractures and interconnected vugs contained the major portion of the recoverable oil.

FLUID MECHANICS

Relative Permeability

The rate of flow of a fluid in a reservoir rock is proportional to the effective permeability of the rock to that fluid. Where two fluids, oil and gas, are flowing simultaneously, the effective permeability to each depends upon the fraction of the pore space occupied by each fluid. These effective permeabilities are usually expressed as a relative permeability to the particular fluid flowing.

Relative permeability-saturation relations for gas and oil are useful in predicting gas-oil ratios, reservoir pressures, and recoveries to be expected under various operating conditions. Relative permeability curves, however, for the various reservoir rocks are quite different and it becomes necessary to determine these relations for the particular formation under study. Relative permeabilities may be determined experimentally in the laboratory on small core samples through use of several techniques. Other methods involve the determination of relative permeability-saturation relations from field and well production behavior.

Relative permeability curves obtained to date on sandstone and limestone cores indicate no marked characteristic variations which could be attributed specifically to the formation composition — whether limestone or sandstone. Rather, the variations which do occur in the displacement of the curves are functions of the textural differences and the pore size distributions for both sands and limestones. Very wide distribution of pore sizes and a large fraction of very fine pores give sharply decreasing oil permeabilities and rapidly rising gas permeabilities with decrease in oil saturation. This would result in rapid increase in gas-oil ratios with depletion and comparatively low oil recovery. A more uniform pore size distribution is reflected in more moderate changes in oil and gas permeabilities, giving rise to less rapid increase in gas-oil ratios and higher recovery.

The ultimate test of the reliability of laboratory measurement of relative permeabilities on small core samples will be the accuracy with which such measurements reflect actual field behavior. Correlation of a relative permeability-saturation relation determined from field and well performance with that averaged from laboratory measurements on cores should shed light on the applicability of such experimental measurements on cores to the interpretation of field behavior.

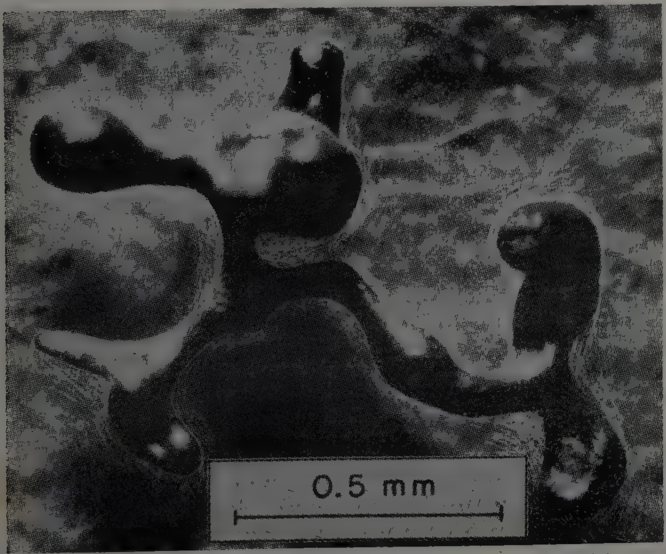

FIG. 2 — RESIDUAL OIL IN SAND (21 PER CENT SATURATION).

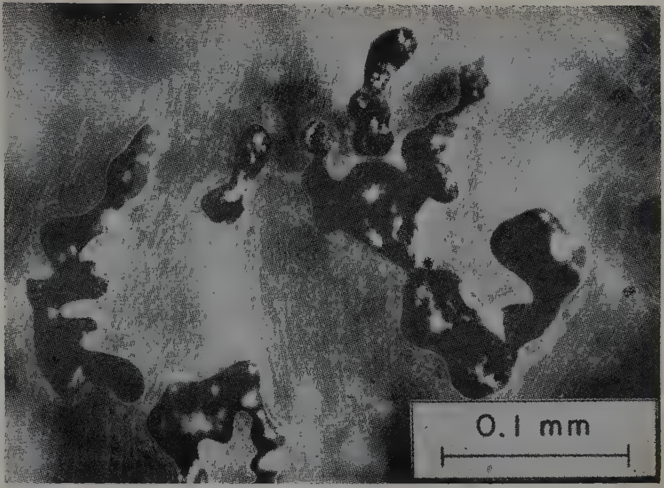

FIG. 3 — RESIDUAL OIL IN LIMESTONE (31 PER CENT OIL SATURATION).

Capillary Pressure

An important piece of information about the capillary properties of a rock is its characteristic curve of capillary pressure versus saturation. These curves reflect the capillary forces which govern the distribution of fluids in the porous system and influence the flow of fluids. The shapes of the capillary pressure-saturation curves do not appear to be a unique function of either sandstone or limestone, but reflect the pore size distribution in the rock.

Capillary pressure measurements have been found useful through the restored state technique in determining interstitial water in reservoir formations. Capillary pressure-saturation relations have been correlated with permeabilities and porosities of cored formations through use of the dimensionless quantity[1] $(P_c/\gamma)\ (K/\phi)^{0.5}$ where P_c is the capillary pressure, γ the interfacial tension, K the permeability, and ϕ the porosity. From results obtained on cores from the Edwards limestone at Jourdanton, there is some indication that this correlation is best for cores in the same lithologic classification and in the same formation. Use of the more rapid mercury-injection method to obtain capillary pressure curves, developed by W. R. Purcell[2] of Shell Oil Co., may increase the utility of this correlation in obtaining permeabilities of tight limestone cores and irregular fragments or cuttings.

The possibility exists that there may be a unique relationship between the permeability-saturation curves and the capillary pressure-saturation curves. The discovery of such a relationship could greatly reduce the amount of laboratory testing necessary for complete information on a core.

Correlation of relative permeability-saturation relations and capillary pressure-saturation relations for limestone cores with core analyses and lithologic examination should be helpful in obtaining a more complete knowledge of the occurrence and flow characteristics of oil in limestone reservoirs.

Residual Oil

To determine the shape of the residual oil at reservoir abandonment conditions, unconsolidated sand and limestone cores were saturated with water, the water displaced with molten Wood's metal, and the Wood's metal flushed with water. The sand and limestone were then removed. The remaining Wood's metal is believed to have the same configuration as the residual oil in depleted water-flushed reservoirs. A photomicrograph of residual oil in unconsolidated sand is shown in Fig. 2. The shape of the residual oil in a limestone is presented in Fig. 3. This limestone was a sample from the Edwards formation having only intercrystalline porosity. Comparison between the residual oil in unconsolidated sand and in this limestone shows no significant difference in shape. In both formations the residual oil existed in the pores not as discrete droplets or spheres, but as irregularly shaped blobs interconnected by tortuous links. The size of the residual oil shapes in this limestone sample was smaller than in the sand because of the lower permeability and much smaller average pore size of the limestone. The similarity observed in the shape of the residual oil in sand and in the intercrystalline limestone is not surprising in view of some similarity between the geometry of the porous system of the intercrystalline limestone and that of a sandstone. However, it is expected that significant differences in the shapes of residual oil would be observed between those in sands and those in limestones whose porous systems comprise fractures, vugs, or combinations of these with intercrystalline or intergranular pores.

LIMESTONE RESERVOIR PERFORMANCE

Oil fields have been classified by technologists according to the following categories: dissolved gas drive, gas cap drive, and water drive. These categories are convenient, descriptive, and practical. The type of drive fixes the operating characteristics and to a large extent determines the ultimate recovery. Limestone reservoirs, as well as sandstone fields, may be so classified, according to the type of drive predominant in the expulsion of oil from the reservoir.

Identification of Type of Drive

The determination of the reservoir pressure variations with production of oil is highly important in interpreting and controlling the behavior of oil fields. This is only natural, since the pressure is an index of the efficiency with which the natural forces available for the production of oil are utilized. A vast amount of subsurface pressure data and information on the withdrawals of oil, gas, and water have been accumulated by field engineers and operators on a great number of fields, both sand and limestone. Correlation of these pressure-production relations with geologic information, formation characteristics, fluid properties, and well behavior has permitted better interpretation of field behavior, particularly in sand reservoirs. Fairly well-defined characteristics may be assigned to the three types of drive and identification facilitated through inspection of the pressure-production relations.

For limestone as well as sandstone fields producing under dissolved gas drive, the rapid and continuous decline in pressure, the sharp rise in gas-oil ratio, and the production of very little water are typified by the operating data on the Fullerton Field, a limestone reservoir in the Clear Fork zone of Permian Age (Fig. 4).

The gas cap drive has as its chief characteristics segregation of free gas in the reservoir as a gas cap, moderate and continuous decline in pressure, increasing gas-oil ratios as the expanding gas front reaches the wells, and little water production. Typical of the gas cap drive field is the Goldsmith Field producing from the San Andres dolomite (Fig. 5).

The Henderson Field, producing from cavernous Yates-Seven Rivers limestone of Permian Age is an example of a limestone reservoir operating under an extremely active water drive (Fig. 6). The high degree of pressure maintenance, the production of gas at essentially the dissolved gas-oil ratio, and the rapidly increasing water production to very high percentages are characteristic of fields in this classification.

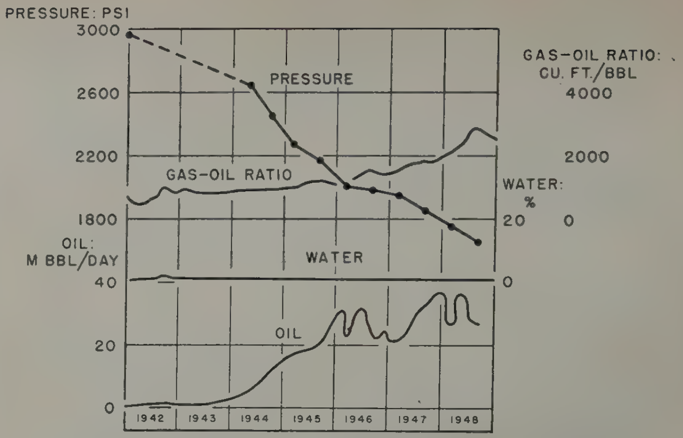

FIG. 4 — OPERATING DATA — FULLERTON DISSOLVED GAS DRIVE.

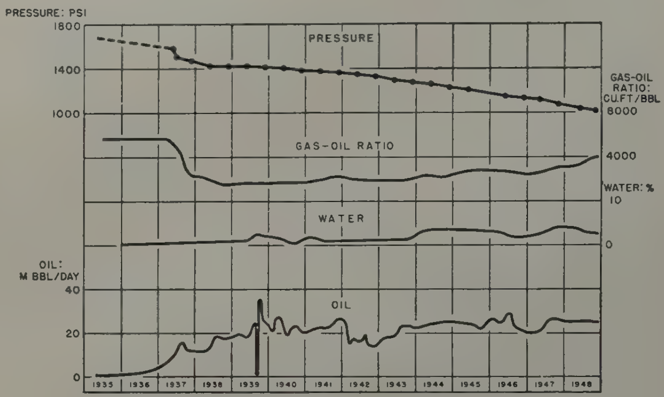

FIG. 5 — OPERATING DATA — GOLDSMITH GAS-CAP DRIVE.

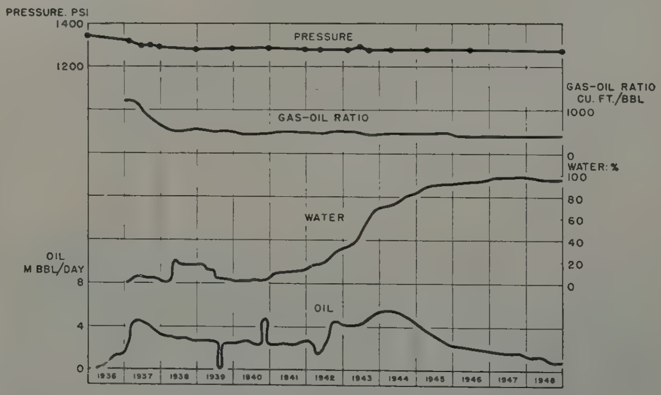

FIG. 6 — OPERATING DATA — HENDERSON WATER DRIVE.

COMPARISON BETWEEN OPERATING DATA FOR LIMESTONE AND SANDSTONE FIELDS

Having viewed the above fields as typical limestone fields operating respectively under the three types of drive, one might compare pressure-production trends in limestone reservoirs with those for sand fields to ascertain whether there are any similarities or marked dissimilarities in the operating data. In Fig. 7 is shown a comparison between the pressure-production data for the Henderson Field, mentioned before as a typical water drive limestone reservoir, and the Amelia Field, producing from the Frio sand in the Texas Gulf Coast. Both reservoirs have very active water drives, and the degree of pressure maintenance, and the gas-oil ratio and water production trends have been remarkably similar for the past 12 years. The only dissimilarity has occurred during the last four years when Henderson's oil production rate has suffered a severe decline, the result of near-depletion of its reserves.

Two other fields, both with large gas caps and inefficient water drives, show comparable performance. In Fig. 8 are presented operating data for the Eunice Field, a limestone reservoir in the Seven Rivers Permian formation, and for the Conroe (Upper Cockfield) reservoir, producing from the Cockfield sand of Eocene Age. Here too, the pressure variations are similar, as are the gas-oil ratio and water production trends.

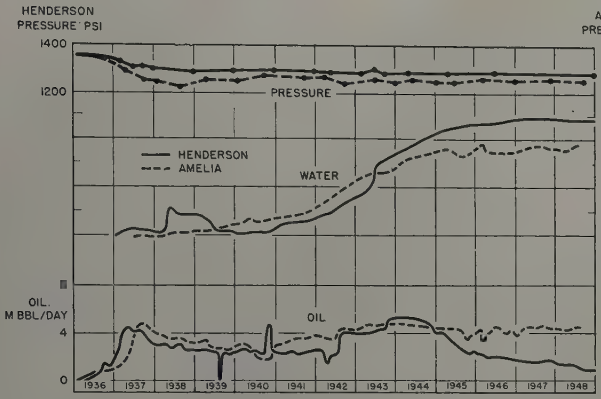

FIG. 7 — COMPARISON RESERVOIR PERFORMANCE HENDERSON AND AMELIA.

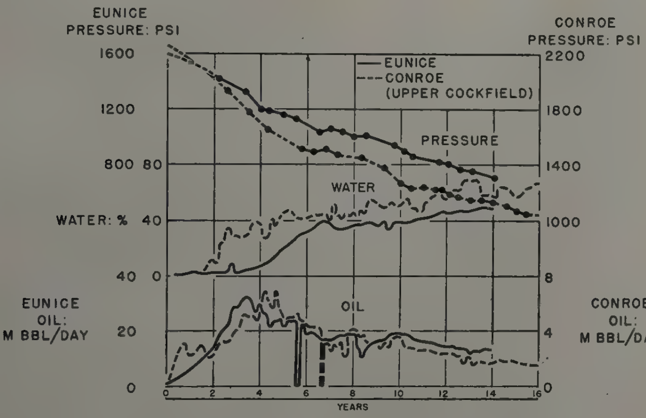

FIG. 8 — COMPARISON RESERVOIR PERFORMANCE EUNICE AND CONROE (UPPER COCKFIELD).

It is interesting to observe the similarity in the production behavior of two older and typical "decline" fields, Hendricks, producing from cavernous Seven Rivers Permian limestone, and the Yegua (Eocene Age) sand field production in the Humble Field. These fields, the production data for which are presented in Fig. 9, were drilled up rapidly many years ago and began producing as flush fields at peak open-flow rates. Their production rates soon began to decline, however, and during the ensuing years these two reservoirs have produced at relatively low oil rates accompanied by production of large quantities of water. It is significant to note that despite the differences in the porous media and in their relative sizes, the percentage rates of decline in the production of oil has been almost identical.

Comparative performances such as illustrated here lead one toward the conclusion that limestone reservoirs fundamentally behave like sandstone reservoirs.

ANALYSIS OF LIMESTONE RESERVOIR PERFORMANCE

Comprehensive analyses of sand and limestone reservoirs have proved useful in promoting better operating practices and recovering additional oil. Determination of the type of drive, estimation of recovery, prediction of pressure, feasibility of gas and water return, determination of maximum efficient rates, evaluation of recovery participation, well production control and well spacing are but a few of the problems which find their solution through application of the reservoir analysis.

Accumulation of more complete field production data, associated field and laboratory investigations, and deeper searching into the theory underlying fluid flow have been coordinated into methods of analysis which have been applied to studies of reservoir performance. The volumetric balance, the unsteady state radial flow equation, the fluid displacement equations, and the dissolved gas drive procedure have been utilized successfully, particularly in studies of sand fields. It is realized that these methods frequently must rely on simplifying assumptions and inadequate data. Lack of sufficient knowledge of the characteristics of the reservoir and of the properties and behavior of the contained fluids can render application of these methods difficult, whether the reservoir be sandstone or limestone.

WATER DRIVE FIELDS

In the study of water drive fields, the volumetric balance equation has been employed to compute the volume of water influx into a reservoir. This equation requires complete production data, correct average reservoir pressure variations, detailed subsurface oil and gas examination, and a thorough knowledge of the reservoir rock, the distribution of fluids, and the configuration, continuity, and volumes of those portions of the reservoir occupied by oil and gas. The unsteady state radial flow equation, another tool applied to water drive evaluation, further requires a knowledge of the properties and extent of the surrounding porous continuum. For the sand field, the properties of the formation, the oil and gas in place, and the continuity of the reservoir and its surrounding aquifer are often more readily determined because of the higher degree of uniformity of the sand porous system and the greater ease of representative sampling. Reservoir pressure trends are usually more precisely determined because of the usual rapid response of sand wells in attaining pressure equilibrium following shut-in during pressure surveys. The long, slow buildup observed in wells in many tight limestone fields has made

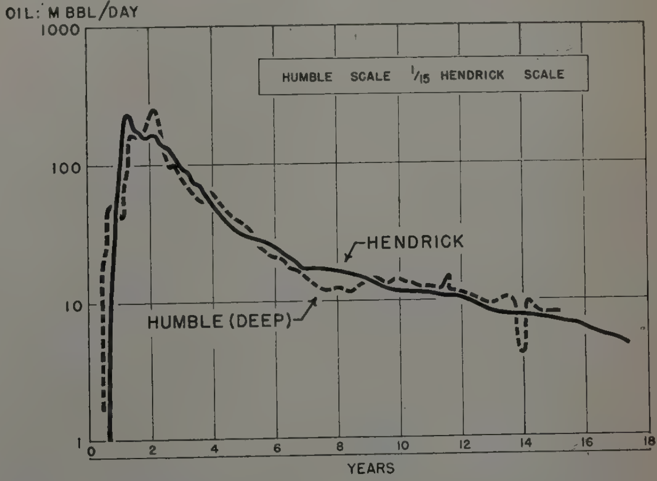

FIG. 9 — COMPARISON DECLINE CURVES HENDRICK AND HUMBLE (DEEP).

difficult an accurate determination of the average formation pressure variations. Build-up characteristics of individual wells reflect the well production rate prior to shut-in. Hence, the average pressure of a low-permeability reservoir may be modified by the field production rate prior to the time of the survey. Flow tests and build-up curves on key wells can assist in determining the correct reservoir pressure.

As an example of the utility of the volumetric balance and unsteady state equations in a reservoir study of a limestone field, a study of the Bateman Ranch (5,100-ft horizon) is cited. This field, situated in a local anticlinal closure, produces undersaturated oil from a cavernous zone in the Canyon lime (Pennsylvanian Age) showing little evidence of fracturing and having widely varying porosity and permeability. Rapidly declining pressures during the first four years of its history raised the question as to whether a water drive was effective, and the rate at which the field should be produced to assure full benefit of the available drive. Analysis of the reservoir performance indicated an effective water drive. It was then possible to evaluate the maximum efficient rate of production and to recommend operating procedures to promote recovery. Nearly identical values of the water influx calculated by the volumetric balance and those by the unsteady state equation gave evidence of successful correlation of the pressure-production relations, and assured reliability of predicted behavior.

Studies of water-drive limestone reservoirs have also been carried out successfully through the use of such devices as the Carter oil reservoir analyzer and potentiometric models. Application of these devices in the future may find even greater utility in handling problems the solution of which by mathematical means may become particularly complex.

GAS CAP DRIVE FIELDS

In the mechanism of gas cap drive, the gas cap invades the oil zone in a manner very similar to that by which water encroaches into and displaces oil from the sand. The effectiveness of the displacement of oil by gas depends on the ease with which the two fluids can move. This in turn is a function of the relative permeability-saturation relations for gas and oil in the specific formation under study, the properties of the oil and gas, and the formation characteristics and geometry. With data on these variables at hand, the calculation of oil recovery by gas cap drive under existing or projected conditions of operation may then be made through use of the fluid displacement equation. The derivation and use of this equation are explained in a paper by S. E .Buckley and M. C. Leverett.[3] Methods of analysis employing this equation are equally as applicable to limestone reservoirs as to sand fields.

DISSOLVED GAS DRIVE FIELDS

Evaluation of the pressure-production behavior of dissolved gas drive fields and the prediction of ultimate recovery may be accomplished for limestone reservoirs by the same analytical procedure developed for sand fields. The volumetric balance is helpful in delineating past performance, but is not adequate to predict pressures and oil recoveries because of its inability to predict gas-oil ratio variations. The stepwise depletion procedure employing the relative permeability-saturation relations for gas and oil is necessary to delineate the behavior and recovery of fields operating under this type of drive. Here again, relative permeability data, formation characteristics, and fluid properties are requisite. Where core data are insufficient to obtain representative relative permeability measurements, resort to well production data and pressure variations with depletion may assist in obtaining the necessary relative permeability curves.

ACTIVE OIL CALCULATIONS

A recent study employed the volumetric balance, rearranged into the "active oil" equation, to determine the apparent "active oil" variations with production for eleven limestone reservoirs. The purpose of this study was to investigate the possibility and extent of oil migration or "bleed-in" from zones of very low permeability into more permeable channels as pressure was reduced in the reservoir. It was stated by Bulnes and Fitting[4] that recoveries from a number of fields "tend to eliminate the possibility that only the permeable (i.e., greater than 1 md. permeability) zones are producing." Some have proposed that to recover the oil from low-permeability zones, fields should be produced at high rates, pulling the pressure down in the permeable strata and thereby creating a pressure differential in the tight pores sufficient to expel that oil into the larger pores and hence to the well.

It has been postulated that the slow rates of pressure build-up for wells producing from limestone reservoirs of relatively low permeability reflect both the slow movement of oil over considerable distances and the gradual migration from the dense part of the reservoir into zones of higher permeability. It was conceivable that there could be a lag in this latter migration which would result in higher rates at the greater pressure differentials resulting from depletion and that this would be reflected as an increase in the active oil calculated by a volumetric balance. To check this point, volumetric balances were made in five fields believed to have no significant water drive. Data for six limestone reservoirs with water drives were included for comparison.

The active oil study of the Goldsmith Field, producing from the San Andres dolomite, is summarized in Fig. 10 as an example of this investigation. Core analyses indicated an average porosity of 10 per cent, a permeability of 33 *md.*, and a connate water saturation of 15 per cent. Pressure-production relations have been shown previously in Fig. 5. The active oil, computed at each pressure survey, showed little variation with cumulative production of oil, and remained fairly constant at 525 MM bbl. On an increment basis, the variations were more pronounced because of the effects of pressure variations following changes in field production rate. However, these variations were consistent with the anticipated effects upon the apparent active oil, and the average trend remained the same as that on the cumulative basis.

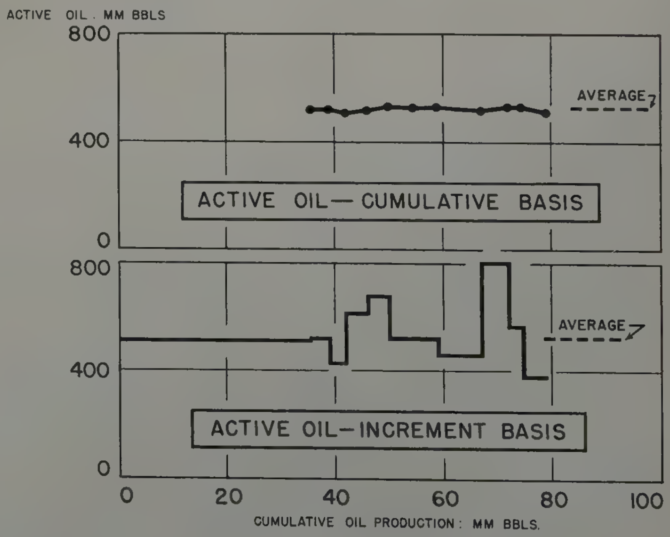

FIG. 10 — ACTIVE OIL CALCULATIONS GOLDSMITH.

The results of these active oil studies indicated:

1. There is no evidence that delayed oil entry from regions of low permeability is of significant importance.

2. The differences in behavior of limestone and sand reservoirs appear not to be fundamental.

3. Active oil volumes for fields without effective water drives may be used to check volumetric estimates, to serve as a basis for predictions, to smooth the pressure-production curve, and to estimate oil in place for fields without adequate core data.

4. Active oil calculations may be used to check the presence of a water drive.

5. Active oil studies for fields on which data are available will serve as a background for studying fields with incomplete data or where proper interpretation of available data is doubtful.

6. More complete core data are needed for checking active oil volumes. Core data provide the best approach to the estimate of ultimate production and are necessary for the proper analysis of reservoir behavior.

FLOW AND INTERFERENCE TESTS

As part of the study of limestone reservoirs, a series of flow and interference tests was conducted in the Martin Field in West Texas, a water drive reservoir producing undersaturated crude from the Ellenburger dolomite. These tests were made to obtain information which might aid in determining whether or not the unsteady state radial flow equation used so frequently in the interpretation of fluid flow behavior in sand media precisely predicts transient behavior in a limestone reservoir. It was hoped by using the pressure variations observed in the wells during the interference tests, the time at which those variations were measured, the distances of the offset shut-in wells to the producing well, the rate of oil production, and properties of the reservoir oil that the porosity and permeability of the formation could be calculated through use of the unsteady state equation. Furthermore, should the porosity be determined, the product of porosity, thickness, and the appropriate area would yield the volume of fluid in place in the total reservoir or any areal unit.

During the flow and interference tests in these wells, producing from the highly permeable, fractured dolomite at Martin, the resulting small pressure drops were measured accurately by means of a dead-weight tester attached to the tubingheads of the wells. Since the tubing remained full at all times with undersaturated oil, pressure drops as low as 0.1 psi were measurable. These tests showed definite interference between wells, pressure drops of 13 psi being observed after 24 hours in wells 1,867 ft from the producing well, and 3 psi in a well 3,733 ft away. The average rate of flow in the producing well was 1,831 B/D.

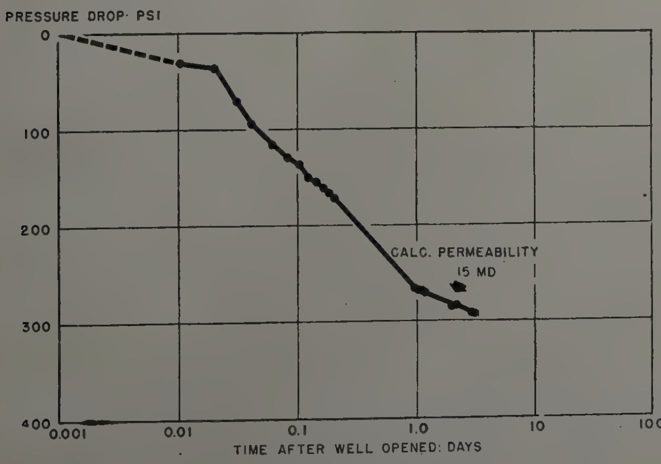

FIG. 11 — RESULTS OF FLOW TEST L. P. BENNETT 15 — WASSON.

Values calculated for the permeability-thickness product and for the porosity-thickness product were reasonably consistent for the offset wells. However, extrapolation of the flow test data for the producing well failed to check these quantities for the offset wells. The measured pressure drop in the producing well was more than ten times too high to be consistent with the pressure drops observed in the offset wells and with the corresponding formation properties. The results further indicated that a reasonable check of the porosity determined by the flow tests with that from core data could be obtained only if the entire Ellenburger formation thickness be used, and not just the thickness of the productive oil zone. Since this was so, it was felt that the determination of oil in place from these interference test data was not possible.

Further studies of pressure-production-time relations obtained during flow tests on a number of wells in West Texas fields have been made to determine the applicability of the unsteady state equation in depicting the flow characteristics of limestone wells. The results have indicated that the unsteady state radial flow equation represents the flow relations in limestone wells equally as well as in sandstone producers. Interpretation of flow test data through this equation has permitted computation of the formation permeability of wells producing from limestone. Particularly, for those wells with declining productivity factors, from the slope of the pressure drop versus logarithm of the time relation, the permeability of the formation has been computed and checked reasonably well with permeability values from core data. The chief requisite for an accurate permeability measurement from flow test data is a test of longer-than-usual duration. The sensitivity of the equation to changes in porosity, however, is not adequate to permit its use in calculating this important characteristic from flow test data with any accuracy. In Fig. 11 is shown the pressure-time relations for a flow test obtained on a well in the Wasson Field.

More research is needed to amplify the interpretation of well and reservoir behavior through the medium of flow and interference tests.

PRODUCTION PRACTICES

Well Spacing

The spacing of wells in limestone reservoirs has in recent years been relatively wide. Proof that much wider spacing of wells than has been employed in many fields in the past can adequately drain the porous formation throughout a continuous reservoir has been amply demonstrated in the comparatively high recoveries obtained to date in many of our sandstone and limestone reservoirs. The results of interference tests of short duration in highly permeable fractured limestones have given conclusive evidence of fluid movement throughout the reservoir. Even in limestones of low permeability, the pressure-production behavior of infill-drilled wells in many instances has indicated that the portion of the intercommunicating reservoir penetrated by the infill well had been drained by the wider-spaced wells to the same degree as the rest of the reservoir and hence that the closer-spaced wells would not increase the ultimate field recovery.

Such information as this has corroborated the fact that well spacing, solely through its influence of distance between wells, appears not to have any appreciable effect upon the ultimate recovery to be obtained from a reservoir. The properties of the formation, the continuity of the structure, the characteristics of the oil, and the degree to which the operator efficiently controls and utilizes the forces available for production of oil do have a profound effect upon the recovery of oil. The proper spacing of wells becomes a problem governed by their structural position in the reservoir and not by distance between wells as such.

Well Completion

Completion of wells in limestone or sandstone reservoirs must satisfy two conditions. First, a well should be completed so as to provide, along with other wells, the maximum ultimate recovery from the reservoir. Secondly, the well should be completed in such fashion as to permit workover for the exclusion of gas or water or change in the completion interval in a manner which is straight-forward and least expensive. These conditions lead to completion normally within a limited interval in the lower, rather than the upper, portion of the reservoir.

In a water drive reservoir, such completion permits control of water encroachment, allowing the lower portions of the reservoir to be flooded first, followed by flooding of successively higher sections as wells are progressively worked over. This is practical from the workover standpoint as wells are drilled originally to their maximum depth and selectively plugged back to shut off water. In fields without water drives, and with or without initial gas caps, this type of completion is also preferable. In such reservoirs, completion near the base of the productive zone is conducive to higher ultimate recovery in that maximum advantage is taken of the benefits of gravitational segregation and retention of gas in the reservoir. Initial completion near the top may later require expensive deepening to deplete lower portions, and exclusion of gas may become impossible.

It appears to be good completion practice in limestone formations to drill wells to the bottom of the productive section and complete within the minimum interval required to yield a satisfactory productivity factor. The distance above the water, if a water drive is present, should be sufficient only to prevent immediate production of water. This distance would depend upon the continuity and permeability of the producing zone.

If the permeability is so low that a satisfactory productivity factor cannot be obtained even by opening the entire productive section, it would be preferable to sacrifice productivity factor rather than open the entire section. In such event, completion within the lowest one-fourth of the productive interval should be reasonably satisfactory.

Maximum Efficient Rates

The maximum efficient rate of production for a reservoir is the maximum rate which can be maintained without creating appreciable waste. In limestone fields, as well as in sand fields, the maximum efficient rate is dependent primarily upon the type of drive available, and upon the individual characteristics of each field.

For water drive fields, the maximum efficient rate of production is that rate which will maintain reservoir pressure at or above 70-80 per cent of the initial pressure or of the saturation pressure of the oil, will permit uniform pressure distribution over the reservoir, will lead to uniform rate of water advance through the productive zone, and assure uniform flushing of the flooded portions. Efficient reservoir production demands efficient operation of the wells tapping the reservoirs. It is important, then, to avoid excessive localized pressure drop, to maintain high oil saturation, and to prevent or minimize fingering or coning of gas and water into the wells.

For gas cap drive fields, maximum recovery of oil is obtained only through efficient displacement of oil from the reservoir as the gas cap expands and invades the oil zone. Maximum efficient producing rates permit uniform encroachment and flushing of the oil zone, avoid waste of gas, and take advantage of the benefits of gravity forces where reservoir conditions are favorable.

For dissolved gas drive fields, the maximum efficient rate must be based on other factors. Some degrees of restriction in withdrawal rate will assist in maintaining uniform saturation, in eliminating localized areas of large pressure drop, high gas saturation and ultimate reduction in recovery, and may permit some degree of gravitational segregation to take place. For fields which have produced at high rates since their discovery, restriction of withdrawal rates to those for water drive fields may permit a water drive to become evident under more favorable producing conditions.

The most precise estimate of the efficient producing rate for a limestone reservoir may be obtained through a complete reservoir study and detailed analysis of field and well performance.

CONCLUSION

The differences between the performance of limestone reservoirs and sandstone reservoirs appear not to be fundamental. The distribution and movement of fluids in and through the porous limestone media follow the same basic principles which dictate such processes in sandstones. This fundamental similarity may readily be discernible in the performance of many limestone reservoirs.

The primary difference between limestone and sandstone reservoirs is the difference in the geometry and origin of the porous systems in the two kinds of rock. The pore spaces in the limestone are characterized by a wide variation in their shapes and in the distribution of pore sizes. These widely varying characteristics of limestone formations give a complexity to the porous system which may modify the reservoir and well behavior in such a fashion as to make difficult the application of analytical techniques to delineate the performance, to understand the recovery processes, and to predict the results of operating practices to increase recovery. The solutions to the questions which surround the interpretation of limestone reservoir performance appear to lie in obtaining a thorough knowledge of the characteristics of the limestone porous system, of the occurrence of oil in that media, and of the influences of the porous system upon the flow characteristics. Application of that understanding may then be made to the fundamental principles governing oil and gas production, which principles are basic and identical for both sandstone and limestone. This path of research seems most promising, rather than the necessity for development of a completely new and different explanation of fluid occurrence and behavior specific for limestone reservoirs.

Acquiring this knowledge means research in many phases of the broad problem. Coordinated effort of geologists, engineers, and production technologists should result in success — success measured in greater recovery of oil from our limestone reserves.

ACKNOWLEDGMENT

The author wishes to thank the Humble Oil and Refining Co. for permission to publish this paper. He also expresses his appreciation to S. E. Buckley for his helpful suggestions and to W. B. Everett, J. G. Richardson, W. L. Crothers, and Burton Atkinson for their contributions.

REFERENCES

1. M. C. Leverett: *Trans.* AIME, (1941), **142**, 151.
2. W. R. Purcell: *Trans.* AIME, (1949), **186**, 39.
3. S. E. Buckley and M. C. Leverett: *Trans.* AIME, (1942), **146**, 107.
4. A. C. Bulnes and R. U. Fitting, Jr.: *Trans.* AIME, (1945), **160**, 179.

★ ★ ★

ESTIMATION OF INTERSTITIAL WATER FROM THE ELECTRIC LOG

MILTON WILLIAMS, HUMBLE OIL AND REFINING CO., HOUSTON, TEXAS, MEMBER AIME

ABSTRACT

A comparison is made between the amount of interstitial water found by analysis in cores and that estimated from the resistivity curve of the electric log for the corresponding strata of producing reservoirs. It is shown that while the determined and the estimated water saturations are in good agreement in some cases, this agreement may be due to a fortuitous compensation of errors. Estimates of water saturations made from the electric log by use of existing relations should, therefore, be employed with caution. Also presented are data on the variation of salinity of interstitial waters in reservoir sands, and on the effect of variation of salinity and porosity on the validity of estimates of water content made from the electric log.

INTRODUCTION

Throughout the history of electric logging there have been recurrent cycles of optimism and pessimism as to the value of the electric log in the quantitative estimation of reservoir fluid content. The very early days of electric logging were an optimistic period, in which there was widespread faith in the ability of the resistivity curve to reflect fluid content, and in the ability of the potential curve to indicate textural characteristics. In time the accumulation of exceptions to this idealistic behavior brought about a general disillusionment, and caused the more pessimistic of those dealing with electric logs to believe that the sole importance of the log lay in stratigraphic correlation.

Within the last several years optimism as to the quantitative use of the electric log has been revived, primarily as the result of the stimulating work of G. E. Archie[1] on the estimation of interstitial water in sands from resistivity data. Even though the general trend of thought on the quantitative value of the electric log reflects optimism, it is inevitable that there are some widely divergent opinions of the validity of quantitative estimates based on the electric log.

A valid method of estimation of fluid content by means of the electric log and a general knowledge of the textural character of the reservoir rock would be of signal importance, not only in that it would save time and money in securing information on reservoirs now being drilled, but also because it would permit the evaluation of reserves in many fields drilled without adequate core data subsequent to the advent of electric logging.

Because of this importance, Humble's Production Research Division, in cooperation with various other company divisions, initiated several years ago a series of tests designed to evaluate the reliability of estimates of fluid content made from the electric log. The investigation was limited at the outset to sand reservoirs, since it was felt that the inclusion of limestone reservoirs would entail needless complications.

In devising these tests it was immediately apparent that the chief difficulty in evaluating the worth of any method of estimation lay in establishing the true value of fluid content. The results of direct analyses of cores cut with ordinary mud were not sufficient, because of the probability of contamination of the fluids by filtrate from the drilling mud; the results of restored state tests on cores were deemed unsuitable because these results can hardly be said to furnish a primary standard.

The method adopted was the direct analysis of cores cut with an oil-base drilling fluid. Such cores, when properly handled, are believed to afford the most precise determination of water content available at the present, and, in addition, lend themselves readily to the determination of various other properties which are pertinent to the estimation of fluid content from the electric log.

Since it was desired to compare the fluid contents estimated from the electric log run in ordinary mud with cores cut in the same hole, the use of oil-base fluid necessitated the changing over, after all cores were cut, to a conventional mud. This procedure presented several advantages, one of which was that the use of oil-base fluid permitted

---

[1] References are given at end of paper.

Manuscript received at office of the Petroleum Branch August 12, 1949. Presented at Branch Fall Meeting, San Antonio, Texas, October 5-7, 1949.

the drilling of the hole closely to gauge. Again, use of oil-base fluid allowed a comparison to be made between electric logs made in the same hole in oil-base and in natural mud.

EXPERIMENTAL PROCEDURE

Two wells in the Hawkins Field, a field in East Texas which produces from a thick Woodbine sand section, were chosen for the initial tests. One of the wells was located near the edge of the structure, and penetrated both the oil zone and a portion of the underlying water zone. The other well was located nearer to the center of the structure, and penetrated a gas cap and a portion of the oil zone. The thickness of pay in this particular field is quite large in comparison with that in most of the reservoirs encountered east of the Rockies. The electric logs made in this field are usually considered to be reliable and diagnostic.

After completion of the experimental work on these two wells, additional data pertinent to the evaluation of methods of estimation of fluid content were obtained in the Charlotte Field in Southwest Texas. In this case cores of the Navarro sand were obtained by use of oil-base fluid, and electric logs were run in the same fluid by use of scratcher electrodes. Since the primary purpose of the use of oil-base fluid in this field was to increase productivity, it was not practical to change to a natural mud after completion of coring. The results of tests in this field were therefore limited, but served to throw some light on the validity of connate water estimates made from the electric log.

In all cases, every attempt was made to minimize contamination of the cores by filtrate from the oil-base fluid. To obtain large enough samples to permit discarding of the outer part of the core, a conventional core barrel was used. It was found most important to bring each core to the surface immediately after it was cut, and to remove the core from the barrel as soon as possible. After removal from the barrel, the cores were first wiped dry, and then the outer portion was removed by use of either a wire brush or a knife. Unless this procedure was followed with all possible dispatch it was observed that, on standing at the surface, the cores imbibed the oil-base fluid.

Samples for analysis were selected after the cleaning process was completed and were subjected to the following determinations:

Resistivity of the Core

The resistivity of each sand core sample was determined immediately after the core had been removed from the barrel and cleaned.

In preparing the core samples for this determination, the ends of the sample were sawed off with a diamond saw, run with no lubricant. The sample, usually some 5 in. in length, was then placed in a holder which was fitted with current plates which could be brought to bear against the ends of the core, and with two sets of probes which could be driven into the core for the measurement of potential gradient along the length of the sample. Each set of probes consisted of three pointed brass rods spaced equally around the circumference of the core sample.

Alternating current (60 cycles per second) was passed through the current plates and through the core. This current was determined precisely by measurement with a vacuum tube voltmeter of the voltage drop across a calibrated resistor in series with the core sample. The potential gradient along the core between the two sets of probes was measured with the same vacuum tube voltmeter, which had an input impedance of 1 megohm. A switching arrangement made possible the measurement of potential gradient either between individual probes of the two sets or between the collective probes of the two sets. Comparisons of the potential drop between each of the three pairs of single probes and between the two sets of probes, with the probes in each set in parallel, showed close agreement. In most cases separate determinations of resistance were made over different portions of the core, and, in all cases, if it appeared possible that the core sample had not been freed of all portions contaminated by oil-base fluid, the sample was pared down until it included only the center of the core.

The resistivity of each core sample was computed from the resistance, as determined above, and from the dimensions of the sample.

Salinity of Interstitial Water

The salinity of interstitial water contained in each core sample was determined directly by inserting into a crushed sample of the core a small chloride-sensitive electrode, together with a reference half-cell. The chloride-sensitive electrode was prepared by fusing a thin coating of silver chloride on the point of a rod of pure silver. The potential developed between this electrode and the reference cell (a calomel half-cell) reflects the chloride content of the fluid with which the two are in contact. This method of determination, it will be noted, is a *direct* salinity measurement and does not depend on a knowledge either of water content or of the total amount of salt present in the sample. In spite of the fact that the interstitial water content of some of the core samples tested was quite low, there was still present enough continuous water phase to permit the determination of salinity by this method.

The salinity measurements were made in the field within an hour or so after removal of the core from the barrel. The crushed core sample used in this determination was then employed in the determination of fluid content. as described below.

Determination of Interstitial Water Content

The content of interstitial water in the core samples was determined by two independent methods, and as a further check, by a variation of one of these.

One method used was that of vaporization of the water from a weighed, crushed core sample, and absorption of the vaporized water in a weighed drying tube. This method has been described by Schilthuis[2].

An independent method consisted in the addition to a weighed, crushed sample of the core of a known volume of a chloride-free solution of an electrolyte, followed by the determination, by a procedure similar to that used in determining the salinity of the interstitial water, of the salinity of the mixture of interstitial water and added electrolyte. Since the salinity of the interstitial water itself, the salinity of the diluted interstitial water, and the volume of diluent were known, the original volume of interstitial water present in the sample could be computed from the relationship:

$$V_1 = \frac{C_2 V_2}{C_1 - C_2}$$

where

C_1 is the salinity of the interstitial water,

C_2 is the salinity of the mixture of interstitial water and diluent,

V_1 is the volume of interstitial water present in the sample, and

V_2 is the volume of diluent added.

The use of a solution of an electrolyte as a diluent in this method, rather than the use of pure water, was found to be necessary in order to coagulate the clay normally present in core samples. If this clay is not coagulated by the electrolyte, adsorption by the clay of a portion of the water added in the dilution will introduce some error into the determination. A suitable electrolyte was found to be calcium nitrate, used in the diluent solution in 2½ per cent concentration.

A variation of the foregoing method consisted in the determination of the original salinity by use of the chloride-sensitive electrode, followed by the determination of the mass of chloride present in a weighed portion of the core. The volume of interstitial water in the core sample is given by $V_1 = \frac{m}{C_1}$ where m is the mass of chloride present, and V_1 and C_1 are as before.

A comparison of the results of analysis of individual samples by each of the three foregoing methods showed an extremely close correspondence for all. The values of interstitial water content finally chosen were average ones from all three methods, although, because of the good concordance, the results of any one method could have been employed with equal confidence.

Determination of Oil Content

In the case of the two wells drilled in Hawkins, the oil content of each core sample was determined by difference according to the method described by Schilthuis[2]. The cores from the Charlotte Field were subjected to this same treatment, and also to a method of direct determination which was found to be quite rapid and reliable. The direct method consisted in adding to the crushed and weighed core sample a small volume of calcium nitrate solution and a small known volume of a liquid which was miscible with oil, immiscible with water, and of high refractive index. The organic compound alphabromnaphthalene was used for the latter liquid, and, in practice, was added to the same core sample used for water assay by the salinity method. The mixture of core, diluent solution, and organic liquid was shaken vigorously for a few seconds, and a droplet of the mixture of alphabromnapthalene and oil contained in the core was fished out. The refractive index of this droplet was determined by use of a compact portable refractometer, and the oil content of the droplet was determined by reference to a calibration chart which showed the refractive index as a function of the percentage of the particular crude present in the mixture. Since a known volume of the liquid of high refractive index was employed, the oil content of the core could then be computed.

This method was found to be quite rapid, and gave results in close agreement with those obtained by use of the more conventional method.

Porosity

Porosity of each of the core samples was determined both by the Washburn-Bunting method, and by a comparison of bulk and grain density. In the case of the Hawkins cores, porosity measurements were made on samples adjacent to those used for the determination of fluid contents. In the case of the Charlotte cores, the determination of porosity by a comparison of bulk and grain densities was made on the same core sample used for assay for fluid contents. This was done by determining the bulk density of the wet core (containing interstitial water and oil), crushing this sample, determining the fluid contents, and then correcting the wet bulk density to dry bulk density. The latter, together with the grain density, was used for the computation of the total porosity. The use of the identical sample for both porosity and fluid content determinations resulted in consistent fluid saturation values, and eliminated a common source of uncertainty in computing saturations.

In general, the total porosity was found to be somewhat higher than the apparent porosity as determined by the Washburn-Bunting method. Since it is thought that the latter is subject to greater error, the total porosity was used in the computation of fluid saturations.

Permeability

Permeability, both parallel and perpendicular to the bedding plane, was determined by conventional methods.

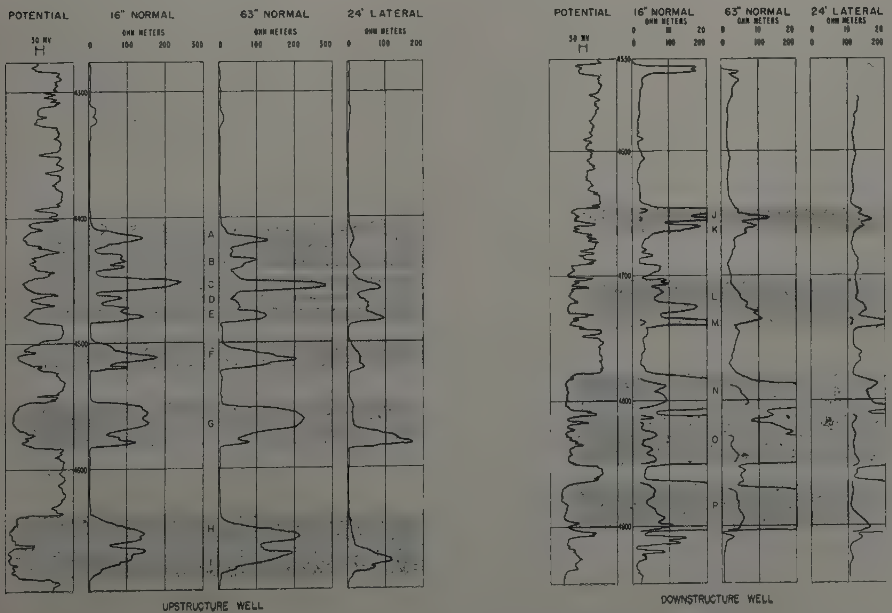

UPSTRUCTURE WELL

DOWNSTRUCTURE WELL

FIG. 1 — ELECTRIC LOGS — HAWKINS WELLS

Formation Factor

The ratio of the resistivity of a core sample completely saturated with a saline solution to the resistivity of the solution alone, defined by Sundberg[3] as the "formation resistivity factor" and by Archie[1] simply as the "formation factor," was determined for all samples which were competent enough to withstand the treatment involved. Small test cylinders were cut from the core samples by use of a diamond drill, and then were cleaned by flowing through them under pressure successive portions of toluene, acetone, and salt water. The salt water duplicated in composition the water produced from the respective fields. Following this treatment, the core samples were submerged in a vessel of salt water. The vessel was evacuated to remove all air from the samples, then a pressure slightly higher than atmospheric was applied. The core samples were removed, and resistance determinations were made immediately by means of a four-electrode system using alternating current. The resistivities of the cores were computed from the resistance values and the physical dimensions. The formation factors were then determined by dividing the resistivities of the cores by the resistivity of the water used to saturate them.

Table I

	Upstructure Well	Downstructure Well
Mud resistivity at surface, ohmmeters	3.3 (at 88°F)	4.8 (at 78°F)
Bottom-hole temperature, °F	158	168
Estimated mud resistivity at bottom-hole temperature, ohmmeters	1.8	2.4
Nominal hole size, in.	6¼	6¼

Mounce Potential

All core samples, including those which were shale or predominantly shale, were subjected to a determination of the Mounce potential. This potential, described by Mounce and Rust,[4] arises when a shale or clay containing saline water is brought into contact with water of a different salinity. The magnitude of the potential, when salinities of the interstitial and extraneous waters are held constant, appears to reflect the percentage of shale or clay present in the sample.

The determination was made by interposing the core sample between two hollowed-out rubber stoppers, one of which contained water equivalent in composition to water produced from the respective field, and the other of which contained fresh water. Nonpolarizable electrodes immersed in the two solutions were connected to a vacuum tube

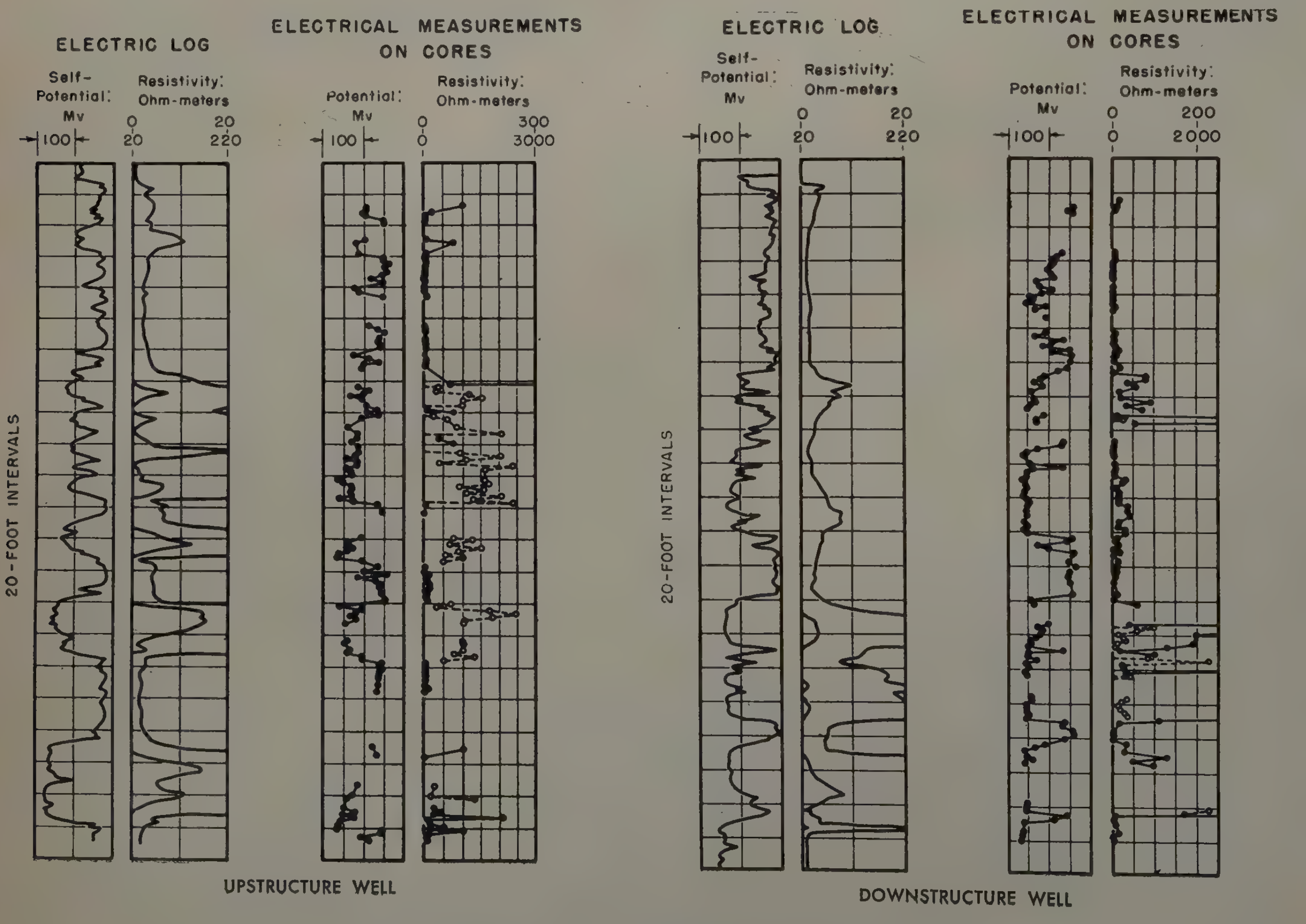

FIG. 2 — ELECTRIC LOGS VS. CORE LOGS, HAWKINS FIELD

voltmeter, which indicated the value of the Mounce potential.

In an attempt to correlate the results of measurements of the Mounce potential with clay content, measurements were made of the dye adsorptivity of the core samples, a method purported to be indicative of clay content. The latter method proved to be ineffective. Since the results of Mounce potential measurements were in agreement with visual observations of clay content, no use was made of the results obtained from the dye adsorption method.

ELECTRIC LOG DATA

Hawkins Wells

Electric logs were run in both wells in the Hawkins Field immediately after the oil-base fluid used in coring had been displaced with conventional water mud. In each case, the hole was then underreamed from a nominal diameter of 6¼ in. to a nominal diameter of 8 in., and additional logs were run. In each well the electric log made in the hole before underreaming was not significantly different from the log made in the reamed hole, nor was it materially different from logs made in nearby wells drilled entirely with ordinary water muds. This agreement indicates that the use of oil-base fluid in drilling had little or no effect on the log made after displacement of oil-base fluid with conventional mud.

Fig. 1 is a reproduction of conventional electric logs made in the two Hawkins wells before the holes were underreamed. Table I gives the information which would ordinarily be utilized in the quantitative interpretation of these logs.

The measurements of mud resistivity at the surface were made with no particular care either in selecting samples which would be representative or in attempting to secure a high degree of accuracy in the technique of the measurement.

Caliper logs made in both wells showed that the actual diameters of the holes were very close to the nominal size.

In addition to the logs shown in Fig. 1, electric logs were also made with a point electrode device and with other multielectrode configurations.

Charlotte Wells

Although several wells drilled to the Navarro sand of the Charlotte Field were cored with oil-base fluid, only one yielded a sufficient number of core samples to justify the making of a comparison between the results of determinations on cores and results derived from the electric log.

Two different electric logs were run in oil-base fluid in this one well. Although the resistivity curves of both logs showed essentially the same features, the numerical values of resistivity highs did not agree. A consideration of the different systems of instrumentation used in making the two logs dictated the choice of that log which gave the higher resistivity values as being the more nearly correct.

A three-electrode tool of the scratcher type was used in making this log. The two potential electrodes were separated by a distance of 24 in., and a single current electrode was located 66 in. above the midpoint of the two.

The oil-base fluid had a water content at the time of logging of roughly 10 per cent. Attempts to measure the resistivity of surface samples of the fluid gave various results, none of which were considered reliable, but all of which indicated very high values. It is estimated that the contact resistance between each scratcher and the strata being logged was several thousand ohms.

A comparison of the logs made in oil-base fluid in several wells in the Charlotte Field with logs made in conventional mud in offset wells indicated that both resistivity and potential curves of the oil-base logs were diagnostic of the character and fluid content of the reservoir rock, but that the oil-base resistivity curves gave generally higher resistivity values opposite the producing intervals than did the logs run in neighboring wells in ordinary muds.

CORRELATION OF RESULTS

The data obtained from the foregoing determinations were deemed sufficient not only to permit a comparison between analytical values of interstitial water and those estimated from the electric log, but also to evaluate the validity of certain relations upon which commonly-used methods of estimating interstitial water from the electric log are based. For example, the data permit an examination of:

1. The relation of the apparent resistivity of a stratum, read from the electric log, to the true resistivity of the cores from the stratum,

2. The relation of the resistivity of a core to its interstitial water content, and

3. The effects of variable physical quantities such as porosity, shale and clay content of the rock, and salinity of the interstitial water on the relation of resistivity to interstitial water content.

Comparison of Apparent Resistivity from Electric Log with Resistivity of Cores

In order to compare the apparent resistivity values read from the electric log with the resistivity measurements made on the cores immediately after removal from the core barrel, it was necessary to:

1. Adjust the latter values to correct them to bottom-hole temperature, and

2. Select values from the electric log which would correspond in depth to the depths of the core samples.

The temperature correction was made on the assumption that the resistivity of the interstitial water had the same temperature coefficient as that of a solution of pure sodium chloride.

In general, since core recovery was exceptionally good, there was no difficulty in assigning depths to the majority of core samples in order that resistivity values could be read from the electric logs at corresponding depths. There were a few exceptions, however, where the depths of incompletely recovered cores were in doubt by a matter of three or four feet. In such cases, a comparison of a plot against depth of the Mounce potential of the recovered portion of the core with the potential curve of the electric log proved a valuable aid. Correspondence between the two could usually be found readily, and was used to establish the true depth of the incomplete core.

Fig. 2 shows a comparison of the resistivities and Mounce potentials of the Hawkins cores with the potential and 63 inch-spaced resistivity curves of the electric logs made in these wells. The Mounce potential values measured on the cores agree very well in magnitude with the potential values of the electric log. Though the logs of resistivities measured on the core samples show striking similarities in character to the resistivity curves of the electric logs, it is obvious that the apparent resistivity values of the electric logs were generally much less than the resistivities measured on the cores.

The question immediately arises as to how closely the resistivity of the cores approximates the resistivity of the same material in situ. This resolves itself into the questions of:

1. How much aqueous fluid was lost from the cores prior to the measurement of resistivity at the surface, and

2. Whether or not the resistivity measurements at the surface were affected by contamination of the cores by the oil-base fluid.

It is certain that a small amount of water was lost from the core samples by evaporation during the time necessary to clean and select the samples. This amount, however, was minor, as shown by reasonably close agreement of the average value of salinity of the interstitial water in the core samples with the salinity of water produced from the Hawkins Field, and, more strikingly, by the fact that the water saturation found by analysis in samples recovered from the water zone encountered in the downstructure Hawkins well was in excess of 95 per cent.

Contamination of the cores by the oil-base fluid is thought not to have been serious. The core sample from the water bearing zone referred to, which was quite permeable, had absolutely no oil present, showing that in this case no flushing by the oil-base fluid had taken place. It is interesting to note that the water saturations in the upper part of the Woodbine section of Hawkins were in some cases as low as 2 or 3 per cent. Even this, however, cannot be ascribed to flushing by the oil-base fluid, since it is inconceivable that any flushing possible during the drilling operations could reduce the water saturation to such low values. It is likewise inconceivable that interstitial water could be lost from the cores to the mud by reaction with the quicklime postulated by some to be present in the oil-base fluid. Actually, the fluid used in Hawkins contained at least 1 per cent free water, as do all oil-base fluids in practice. It is not likely that any water-reactive substances capable of abstracting water from the cores could exist in such an environment.

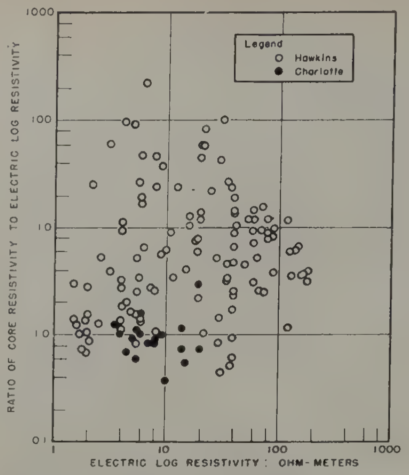

FIG. 3 — COMPARISON OF CORE RESISTIVITIES WITH POINT VALUES OF ELECTRIC LOG RESISTIVITY

Consideration of the foregoing factors indicated that the true resistivity of the strata in situ was not far different from the resistivity of the cores corrected to bottom-hole temperature.

To investigate the relationship between the apparent resistivity read from the electric log and the true resistivity as indicated by the measurements made on the cores, a comparison was made of the core resistivities and of point values of resistivity at corresponding depths read from various log curves. Fig. 3 is a plot of core resistivity data and of point values of resistivity read from the 63 in. spaced curves made in the Hawkins wells and from the oil-base run made in the Charlotte well. In this figure the ratio of core resistivity (corrected to bottom-hole temperature) to the apparent resistivity given by the electric log is plotted against the resistivity read from the electric log.

In this figure, if close correspondence of the core resistivity data with the electric log data had been obtained, the data points would lie along a horizontal line whose ordinate would have a value of one. It is seen from the figure, however, that the data for the two Hawkins wells indicate a wide disparity between the two resistivity values, except possibly at low values of resistivity, and indicate further that there is no relation between the magnitude of the deviation and the magnitude of the resistivity. It is apparent from Fig. 3, however, that the agreement of core resistivities and

Table II

Comparison of Resistivities Estimated from Electric Log with Average Core Resistivities — Hawkins Wells

Designation of Interval	Depth Interval	Thickness of Interval, feet	Maximum Apparent Resistivity from Electric Log ohmmeters		Computed "True" Resistivity from Electric Log ohmmeters	Average Core Resistivity over Interval ohmmeters (Corr. to Subsurface Temperature)	No. Core Samples from Interval	Ratio Core Resistivity to Computed "True" Resistivity from Electric Log
			16″ Curve	63″ Curve				
A	4403-25	22	140	130	150	350	9	2.3
B	4429-42	13	100	100	145	370	4	2.5
C	4447-60	13	250	285	360	1160	7	3.2
D	4462-69	7	90	50	135	700	4	5.2
E	4471-84	13	140	125	180	910	3	5.1
F	4497-4522	25	175	205	190	430	8	2.3
G	4547-82	35	155	210	180	530	9	2.9
H	4636-60	24	145	215	190	140	2	0.7
I	4662-87	25	150	195	190	27	9	0.14
J	4646-58	12	40	15	20	95	6	4.8
K	4660-67	7	20	10	25	75	4	3.0
L	4704-31	27	20	10	10	11	12	1.1
M	4734-43	9	30	10	20	210	3	10.5
N	4778-4808	30	90	85	70	220	9	3.1
O	4812-52	40	60	40	50	240	13	4.8
P	4865-4905	40	100	60	60	370	6	6.2

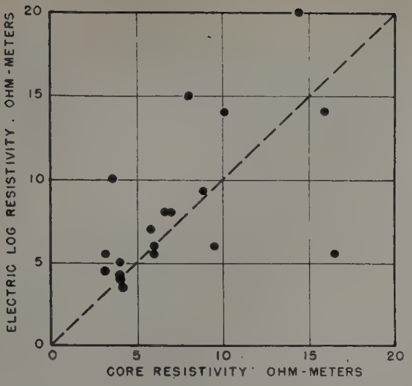

FIG. 4 — COMPARISON OF CORE RESISTIVITIES WITH RESISTIVITIES FROM ELECTRIC LOG MADE IN OIL-BASE MUD, CHARLOTTE

log resistivities was fairly good for the Charlotte oil-base run. This agreement may be examined more closely in Fig. 4, in which the electric log resistivities are compared directly with the core resistivities by plotting both on Cartesian coordinates.

It is realized that the point values of resistivity read from the electric log which were used in Fig. 3 included some values which were spuriously low because of the geometry of the electrode configuration used in making the log. These low values would normally be discounted in the estimation of interstitial water saturation by use of the resistivity curve. An attempt was consequently made to eliminate these values from those data from the Hawkins wells which were used for comparison. The procedure used in this attempt was identical with that currently employed by many of those engaged in the quantitative interpretation of electric logs. In this procedure the section logged in each of the Hawkins wells was first, by reference to the potential curve, divided into depth intervals which appeared to embrace only homogeneous sand. These intervals are indicated in Fig. 1. The maximum values of resistivity given by the 16-in. and 64-in. curves were then tabulated from each interval. So-called "true" resistivities were then computed from these maximum values by use of "departure curves."[5] The procedure used in the computation was in accordance with the directions for use accompanying the curves.

Table II lists the depth intervals chosen in the Hawkins wells, the maximum values of apparent resistivities given by the 16-in. and 63-in. curves in the various intervals, the "true" resistivities computed from the apparent resistivities, the average resistivity of cores from each interval, and the number of core samples upon which this average was based. Also shown is the ratio of the average core resistivity to the computed log resistivity for each interval.

An examination of Table II reveals that the log resistivity values, derived as described above, were, in general, materially lower than the average core resistivity values, even though the log resistivities were computed from the extreme peak value of apparent resistivity read from the log. The exceptions to this were Intervals *H*, *I*, and *L*.

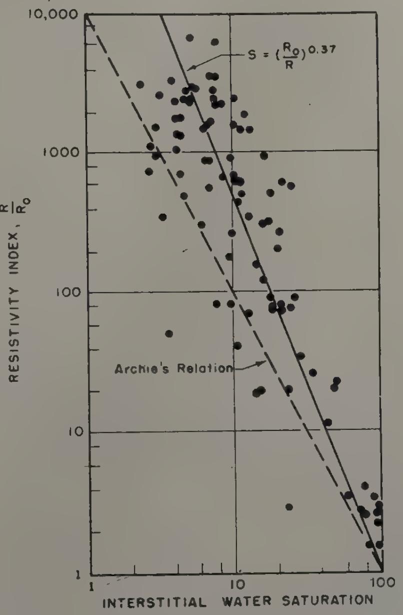

FIG. 5 — RESISTIVITY INDEX VS. INTERSTITIAL WATER SATURATION

In Interval *H* only two samples were available for measurement of core resistivity, and these two samples were from the bottom of the interval. In Interval *L*, where there was very good agreement between log and core values, it should be noted that both resistivities were relatively low.

In Interval *I*, where the computed log value was much higher than the average core resistivity, the 16-in. and 63-in. log curves showed a definite decline in resistivity from top to bottom of the section. Moreover, core analysis revealed a marked increase in water saturation from top to bottom of the interval. These facts cast doubt on the validity of the practice of utilizing the peak value of resistivity in estimating some mean resistivity of the interval. Perhaps of more importance, they also lead logically to the question of how, by the use of logs made with currently available equipment, one may distinguish between resistivity effects which are predominantly due to the geometry of equipment and strata, and those which are caused by real changes in rock texture or fluid content.

It is believed to be significant that the Hawkins log resistivities, either as read directly from the log or as corrected by the use of published departure curves, were generally lower than the core resistivities, whereas good agreement was obtained at Charlotte. It may be concluded from this that the effect of ordinary mud, in juxtaposition with resistant beds, in shunting a portion of the electric current used in making the resistivity log may be quite serious, and that the various methods proposed in the past for correcting for this effect and for the analogous effect of filtrate invasion are inadequate. Parenthetically, it may be observed that the use of wide electrode spacing, originally introduced to minimize the effects of the presence of mud and of filtrate invasion, usually offers no satisfactory solution to the problem because of the averaging effect

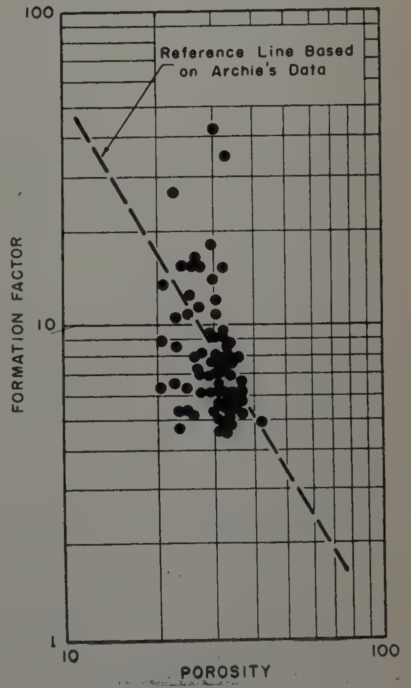

FIG. 6 — FORMATION FACTOR VS. POROSITY

of the wide spacing. The average resistivity obtained with wide spacing ordinarily encompasses low resistivity shale streaks as well as the higher resistivity sand members of interest. The assumption under which very wide spacing is presumed to be of advantage, that the productive interval is a very thick, entirely homogeneous bed, is a naivete in the light of the actual texture and bedding of most reservoir material.

Insofar as the resistivity of a productive sand enters into the quantitative estimation of fluid content, it really matters little whether the resistivity is actually the true resistivity or whether it is some other quantity—provided, if it be some other quantity, that it bear some recognizable relation to the true resistivity or to the fluid content.

The effect of fallaciously low electric log resistivities, when used in the estimation of interstitial water, is, in the absence of compensating errors, to make the computed water saturation too high.

Relation Between Water Content and Resistivity

To investigate the relationship between interstitial water content and resistivity, use was made of the results of analysis for interstitial water and the resistivity data obtained on the cores. Following the procedure used by Archie, the "resistivity index" was plotted against the interstitial water saturation expressed as a percentage of the total pore volume. The resistivity index is defined by Archie as the ratio of the core resistivity at a given saturation of interstitial water to the resistivity of the core completely saturated with interstitial water. Fig. 5 shows a plot of these data for samples from the two Hawkins wells. Since most of the cores from the Charlotte well were altered during the process of saturating with salt water, no data from these determinations were considered. Shown in Fig. 5 is a dotted line representing Archie's relation of saturation to resistivity index, which he found to be approximately

$$S = \sqrt{\frac{R_o}{R}}$$

where

S is the interstitial water saturation

R_o is the resistivity of the core completely saturated with interstitial water

R is the resistivity of the core at the interstitial water saturation considered.

In general, the data points in Fig. 5 lie above Archie's line. For these particular data a representation somewhat better than the square root relation is given by the empirical relationship

$$S = \left(\frac{R_o}{R}\right)^{0.37}$$

Even for this relationship there is considerable deviation of individual determinations.

Archie's square root relation apparently was based primarily on data obtained in the laboratory with reasonably clean sands. Since it is apparent from the data shown in Fig. 5 that the Hawkins samples did not conform very well to the square root relationship, it is reasonable to suppose that the sands found in other reservoirs may also yield a different relationship. Indeed, Archie pointed out this possibility.

It is interesting to note that the effect of the discrepancy between the square root relation and the relation indicated by Fig. 5 is such that the use of the square root relation in estimating interstitial water content would, in the absence of other disturbing factors, yield erroneously low values for the particular sand cored in this study.

Effect of Variation of Properties of Sand and of Interstitial Water

It is generally recognized that variations of porosity and of sand texture introduce some uncertainty into the values of interstitial water estimated from the electric log. To investigate the effects of these quantities, the formation factor, following Archie's procedure, was plotted against the porosity for all samples from the two Hawkins wells. This plot is shown in Fig. 6.

Archie has found that the formation factor, which enters into the relationship between resistivity and interstitial water saturation, is in turn related to the porosity and other textural properties of a sand by the relation

$$F = p^{-m}$$

where

F is the formation factor, i.e., the ratio between the resistivity of a sand completely saturated with brine to the resistivity of the brine alone,

P is the sand porosity, expressed as a fraction,

m is a "cementation factor," dependent upon the cementing material associated with the sand.

Archie has reported that the value of m varies from about 1.3 for clean, unconsolidated sands to more than 2 for well-cemented or silty sands.

In Fig. 6, should Archie's relation between formation factor and sand texture hold, and should the sand samples under consideration not vary too much in textural characteristics, the data points would be expected to lie along a straight line of slope −m. Although the data cannot very well be represented by a straight line of reasonable slope, the line joining the center of mass of the points with the lower right-hand corner of the graph has a slope of about −1.7, which is a reasonable value of Archie's cementation factor for the moderately clean Woodbine sand at Hawkins.

Individual values of m, as computed from the data on each core sample, ranged from slightly over one to almost three. In view of this large spread, an effort was made to determine whether or not a relation exists between the value of m for a particular sample and the content of clay as reflected by the Mounce potential. The results of this examination were inconclusive.

Table III

Comparison of Average Water Saturation Values Computed from Point Resistivities with Saturations Found by Core Analysis — Hawkins Wells

	Upstructure Well	Downstructure Well
Average Saturation from Core Analysis	8.5%	31.8%
Average Saturation Computed from 16″ Normal Curve	13.4	21.3
Average Saturation Computed from 63″ Normal Curve	15.6	33.8
Average Saturation Computed from 25′ Lateral Curve	18.0	41.3
Average Saturation Computed from Single Electrode Curve	16.6	26.9
Average Saturation Computed from 4Z18 Curve	14.7	26.0

It is evident from the scattering of the data shown in Fig. 6 that additional information on the geometry and textural characteristics of sands is urgently needed.

In spite of the apparent lack of correlation of porosity with other textural characteristics of Hawkins samples, it is felt that only minor errors are introduced by variation of sand texture alone into the estimation of interstitial water from the electric log.

The variation of salinity of the interstitial water in the samples both from Hawkins and from Charlotte was much greater than had been anticipated. In the case of the two wells in the Hawkins field, the variation of salinity was found to be erratic over short intervals, but with a definite trend of increasing salinity with increasing depth. This is shown by Fig. 7, in which the salinity is plotted against subsea depth for both of the Hawkins wells and for the Charlotte well. The salinity of water produced from wells low on structure in Hawkins is approximately equal to the average salinity of the interstitial water found in the structurally lower well, which penetrated the water producing zone. There was no apparent correlation of salinity with either sand texture or shale content of these samples.

Because of the short interval included in the productive section of the Charlotte well it was not possible to determine whether or not there was a trend of salinity with depth. Contrary to experience in the Hawkins field, however, there appeared to be a well-defined trend in the Charlotte samples of decreasing salinity with increasing shale content of the cores as reflected by the Mounce potential. This is illustrated in Fig. 8. The more silty samples, which yielded higher potentials, had substantially lower salinities than the cleaner ones. The water produced from an edge well in this field, which may be presumed to flow from a permeable sand member having a low Mounce potential, had a salinity of approximately 30,000 ppm. This salinity is close to that indicated by the curve in Fig. 8 for a sample of zero Mounce potential.

It is evident from Figs. 7 and 8 that variation of salinity may complicate the problem of estimating the interstitial water content of a reservoir sand from the electric log. Since, however, the effect of salinity of interstitial water on the resistivity is relatively small, such a variation probably introduces only minor errors into the estimation.

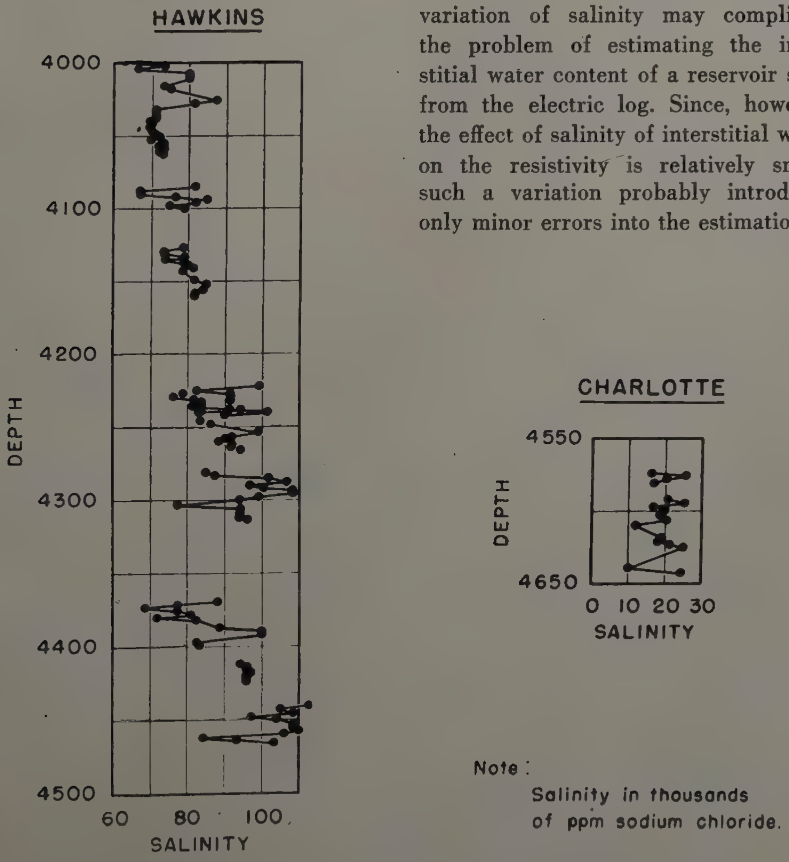

Note:
Salinity in thousands of ppm sodium chloride.

FIG. 7 — SALINITY OF INTERSTITIAL WATER VS. SUBSEA DEPTH

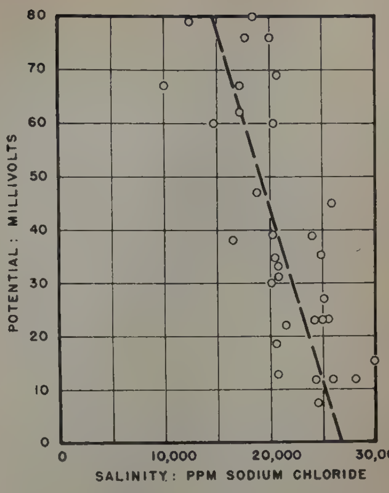

FIG. 8 — MOUNCE POTENTIAL VS. SALINITY OF INTERSTITIAL WATER, CHARLOTTE CORE SAMPLES

Comparison of Estimated Water Saturation with Saturation Determined by Analysis

In the preceding discussion, it has been pointed out that the apparent resistivities read from the electric log were generally too low. It has been shown that the relation found to obtain between true resistivity and water saturation deviated from the square root relation, and that the use of the true resistivity in the square root relation should yield computed values of interstitial water saturation which are lower than the actual values. It follows that the deviation from the square root relation was such that it tended to compensate for the error introduced by use of the resistivity values from the electric log. Although only a limited amount of data has been considered, it seems logical to suppose that the two major sources of error are present to some extent in practically all cases. If, therefore, the successful estimation of water content from the electric log depends on the compensation of errors which may not always be compensatory, it is not surprising that the method has reputedly yielded very good results in some cases, and results of questionable value in others.

To investigate this possible compensation of errors, the water saturations computed by the use of various electric log curves obtained with different electrode configurations in the Hawkins wells were compared with the saturations found by analysis. The resistivity index used in these computations was obtained from that portion of the electric log run in the water zone, and was checked by computation from the average formation factor for the reservoir. The use of a single average value of the resistivity index implies, of course, the use of average values of porosity, salinity of interstitial water, and textural factor.

Fig. 9 shows this comparison for the various electrode configurations employed in the downstructure well. In this figure both the interstitial water saturations found by core analysis and the saturations estimated from the point values of apparent resistivity read from the electric log at corresponding depths are plotted against depth. A comparison of the average values of the productive intervals in both the downstructure and the upstructure wells is shown in Table III.

It is interesting to note in Fig. 9 and in Table III that the average interstitial water saturations computed from all electrode configurations look entirely reasonable in spite of the fact that all of the various resistivity curves yielded values which were generally different from the true resistivities as revealed by measurements on cores. Parenthetically, though the average values of water saturation estimated from point resistivity values in the upstructure well were considerably in error percentagewise, at such low water saturations a fairly large percentage error is of little consequence either from the standpoint of computation of reserves or from the standpoint of prediction of fluid production.

Reference to Fig. 9 shows that perhaps the best concordance between estimated and analytical values for the downstructure well is seen in the case of saturations estimated from the impedance curve obtained with a single electrode. Heretofore, the use of the single electrode device has been questioned because of the difficulty of conversion of impedance values given by the device to earth-resistivity values. It has been assumed that the values given by multielectrode devices are more easily converted to true resistivity values. The Hawkins data indicate that difficulties attend the use of either device.

Table IV shows a comparison between the water saturation values estimated from the maximum resistivity values read from the electric log for each of the intervals considered previously, and the average water saturations found by core analysis for the corresponding intervals.

Again, in general, all of the estimated values of water saturation appear entirely reasonable. Better correspondence with analytical values was obtained by this procedure than was obtained by use of the point resistivity values.

It will be remembered that the only intervals in which the log resistivities were higher than the average core resistivities were intervals *H*, *I*, and *L*. In interval *L*, in which there was very good control from the standpoint of number of samples, there was very good agreement between log and core resistivities. It is interesting to note in Table IV that the interstitial water saturation estimated from the log resistivity for interval *L* is much lower than the saturation found by analysis. This circumstance corroborates the remarks made previously on the lack of conformance of the Hawkins core samples to the square root relationship between water saturation and resistivity.

It is apparent from Fig. 9 and from Tables II and III that the errors in resistivity and in the relation between true resistivity and water saturation were compensated fairly satisfactorily in the Hawkins wells. The estimation of the water saturation throughout this particular field by use of the electric log might, therefore, be undertaken with some confidence. This may not be true in other fields, however, particularly where conditions are such that erratic logs are obtained.

In illustration of the latter point, various cases have been observed[6] in which any attempt to estimate quantitatively the interstitial water content

Table IV

Comparison of Water Saturation Values Computed from Electric Log with Average Saturations Found by Core Analysis — Hawkins Wells

Designation of Interval	Water Saturations Computed from Electric Log			Water Saturation from Core Analysis	No. Core Samples from Interval
	$S=100\sqrt{\frac{0.6}{R_a}}$ R_a from 16″ Normal	$S=100\sqrt{\frac{0.6}{R_a}}$ R_a from 63″ Normal	$S=100\sqrt{\frac{0.6}{R}}$ R from Departure Curves		
A	6.6%	6.7%	6.4%	5.8%	10
B	7.7	7.7	6.5	6.0	6
C	4.9	4.6	4.0	5.1	7
D	8.2	10.9	6.6	6.3	4
E	6.6	6.8	5.8	8.0	2
F	5.9	5.4	5.6	5.7	8
G	6.2	5.2	5.7	6.4	11
H	6.5	5.3	5.6	4.9	9
I	6.4	5.5	5.6	18.7	9
J	12.2	20.0	17.2	20.0	6
K	17.2	24.5	15.6	21.4	4
L	17.2	24.5	24.5	39.8	12
M	14.0	24.5	17.2	19.7	3
N	8.2	8.3	9.2	13.1	9
O	9.9	12.2	10.9	14.2	13
P	7.7	9.9	9.9	10.7	9

S=Water Saturation

R_a=Maximum Apparent Resistivity from Electric Log

R=Computed "True" Resistivity

Table V

Comparison of Average Water Saturation Values Computed from Point Resistivities with Saturations Found by Core Analysis — Charlotte Well

Average Saturation from Core Analysis	68.0%
Average Saturation estimated from log, using relation, $$S = 100\sqrt{\frac{R_o}{R}}$$	53.2%
Average Saturation estimated from log, using relation, $$S = 100\left(\frac{R_o}{R}\right)^{0.37}$$	62.5%

of producing sands would have yielded ridiculously high values because of resistivities which were much too low. The electric logs may have been deficient because of faulty equipment, faulty operation, or because of circumstances beyond control. Regardless of the cause of spuriously low resistivities, had complete reliance been placed on the quantitative interpretation of the electric log some very good producing sands might have been condemned.

It will be remembered that there was very good agreement between the resistivities measured on the cores and point values read from the electric log run in oil-base fluid in the Charlotte well. It is instructive to compare the interstitial water saturations computed from these resistivities by use of the square root relationship between resistivity and saturation with that computed by use of the exponential relationship found to apply better to the Hawkins samples. Table IV shows comparisons of the water saturation estimated by use of both relationships with the water found by analysis.

When the square root relationship was used, the computed water saturations were too low, as might be expected from a consideration of the direction of the error introduced by this relationship. When, however, the exponential relationship found to apply for Hawkins was used, the agreement between computed and determined water saturations was fairly good. This may have been happenstance, or it may indicate a similarity in some undefined textural features of Hawkins Woodbine and Charlotte Navarro sands.

CONCLUSIONS

The following conclusions and generalizations may be drawn from this work:

1. The apparent resistivities of high-resistivity beds read from electric logs made in ordinary mud were generally much lower than the true resistivities of the strata as revealed by core resistivities. This is also undoubtedly true in many cases other than those studied.

2. Existing methods for deriving true resistivities from the apparent resistivities of logs made in ordinary mud were ineffectual. It is believed that this is likewise true in the general case in strata of high resistivity.

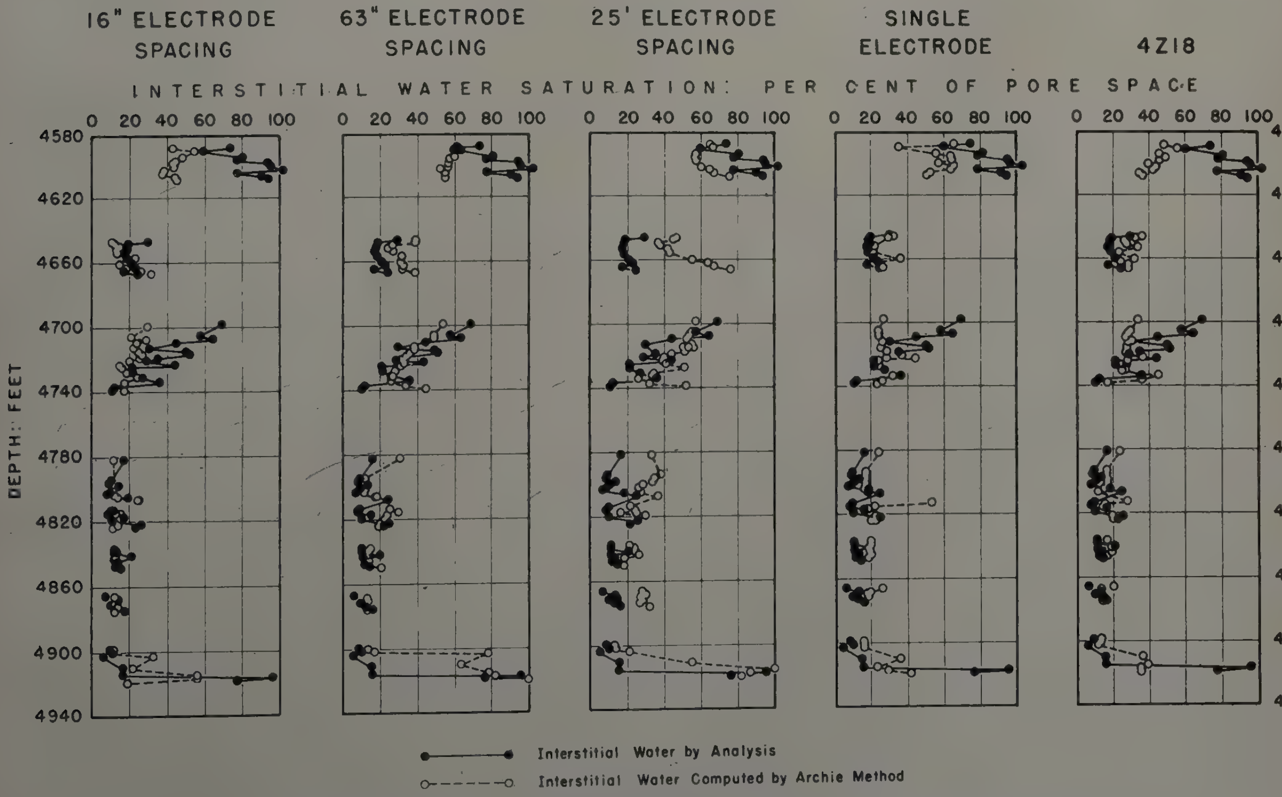

FIG. 9 — INTERSTITIAL WATER SATURATIONS FROM CORE ANALYSIS VS. SATURATIONS COMPUTED FROM POINT RESISTIVITY VALUES OF ELECTRIC LOGS, DOWNSTRUCTURE WELL, HAWKINS

3. The square root relation between the interstitial water saturation and the true resistivity which has been proposed failed to conform to the data obtained in this study.

4. Variations in salinity of interstitial water and in the texture of reservoir sands complicated the estimation of interstitial water from the electric log, but these factors alone probably contribute only minor errors to the average values of water saturation computed from the electric log.

5. The successful estimation of interstitial water saturations from the electric log appears to depend upon the compensation of errors introduced by use of erroneous resistivity values and by use of a questionable relation of water content to true resistivity.

These conclusions in themselves do not furnish a direct answer to the all-important question of how much reliance can be placed in the values of interstitial water content of sands estimated from the electric log. It is evident, however, that there definitely can be cases in which estimates made from the electric log are seriously in error. The existence of such cases, even in the absence of any knowledge as to the frequency of their occurrence, limits the utility of the method.

In considering the reliability of the method, it should be borne in mind that fallacious results may be caused not by the introduction of an error of infrequent occurrence, but by the aggravation of one of the several sources of error generally present, and, in particular, by the failure of errors in opposition to cancel.

These considerations preclude the use of the water saturation estimated from the electric log as what might be called a "primary standard." For this purpose there is at present no substitute for competent core data. If, however, sufficient information in a particular field or locality demonstrates the agreement of estimates made from the electric log with determination made on cores, the electric log method may be profitably used as a "secondary standard." In such case estimates of water saturation may be made with some assurance for parts of the field or locality where core data are not available. In this usage estimates made from the electric log may effect substantial savings in coring costs.

With regard to the possible improvement of estimates of interstitial water made by use of the electric log, the most critical weakness lies in the reliability of the resistivity curve. Possibly the development of new logging techniques and improvements of present practice may alleviate some of the difficulties experienced at present. Even if better electric logging devices or techniques become available, both logging companies and users of logs must still maintain constant vigilance to assure intelligent utilization and interpretation of the electric log.

ACKNOWLEDGMENTS

The work and results described herein could only be achieved by the cooperative effort of a large number of individuals within the Humble organization. Prominent among these were T. A. Huber and the groups within the Petroleum Engineering Dept. headed by Huber and by J. L. Battle. J. A. Newsome, Jr., formerly of Humble's Production Research Division and now with Parks Engineering Co., deserves particular mention for his contribution to this work.

REFERENCES

1. G. E. Archie, "The Electrical Resistivity Log as an Aid in Determining Some Reservoir Characteristics," *Trans.* AIME, **146** (1942), 54-61.
2. R. J. Schilthuis, "Connate Water in Oil and Gas Sands," *Trans.* AIME, **127** (1938), 199-212.
3. Karl Sundberg, "Effect of Impregnating Waters on Electrical Conductivity of Soils and Rocks," *Trans.* AIME, *Geophysical Prospecting* (1932), 367-391.
4. W. D. Mounce and W. M. Rust, Jr., "Natural Potentials in Well Logging," *Trans.* AIME, **155** (1944), 49-54.
5. Schlumberger Well Surveying Corp., "Resistivity Departure Curves," Schlumberger Document Number 3, (1949).
6. Joseph Zaba, "Limitations of Electrical Logging," *API Drilling and Production Practice,* (1940), 20-29.

DISCUSSION

By G. E. Archie, Shell Oil Co., Houston, Tex., Member AIME

There appears to be some question about the basic data used to reach the conclusions. This is shown in Fig. 3, which compares resistivity measurements made on cores with corresponding electrical log resistivities. It can be seen that no relation or trend exists. Certainly the electrical resistivity log is related to the resistivity of the formations, and if this cross check cannot be made, it appears to me that no conclusions using core resistivities can be made on this well, let alone applying the conclusions generally to the industry.

No doubt the author took all possible precautions in making measurements of the core. In spite of this, however, it is very difficult to make good electrical contact with the water network when the water content is low.

It is highly improbable that the resistivity curves recorded in the bore hole are in error by a factor of 10 to 100 because of the recording equipment. Several different curves were recorded in two different wells; also, these logs can be compared with adjoining wells.

The above indicates that the data in Fig. 5 are controversial and actually the equation, $S = (R_o/R)^{0.37}$, when applied to the electrical logs, would result in considerable error.

Fig. 6 is questionable, for it is hardly conceivable that the resistivity of a water-bearing sand could vary five-fold for the same porosity.

I would like to make the following comments on the author's conclusions:

Conclusion 1: This conclusion is based on resistivity measurements made on cores. Fig. 3 indicates conclusions based on these measurements are not valid.

Conclusion 2: There is no reason to discredit departure curves, as they are straightforward calculations using specific geometry. Application to specific well conditions can be made only after accounting for this geometry.

Conclusion 3: The author states that the square root relation failed to conform to the data. Actually, this rela-

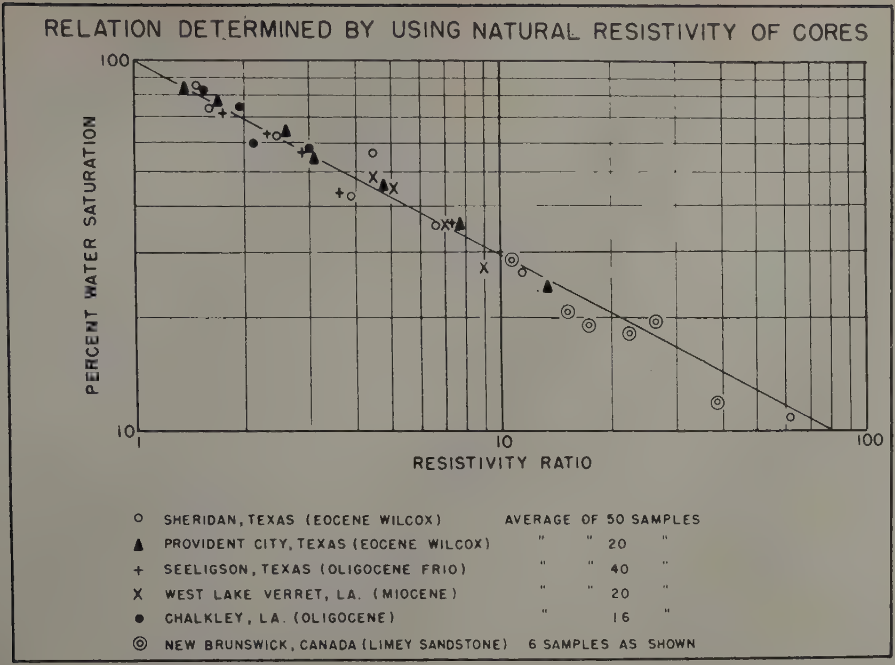

tion when applied to the resistivity log checked well with the actual water found in the cores, see Table III, and Fig. 1 for relatively uniform intervals where the maximum resistivity value is representative of the interval. The author's conclusions are based on what may be erroneous resistivity measurements of cores.

Conclusion 4: The basis for this conclusion is not well grounded, for the author's basic data do not correlate (Fig. 3).

It is unfortunate that the experiment was performed on a reservoir with such low connate water, making the resistivity measurements of cores difficult. However, the remainder of the data are useful (Table III), for it adds another oil-producing reservoir to the list that has been cored with oil base mud and the connate waters check reasonably well with the equation,

$$S = \sqrt{R_o/R}.$$

For completeness, I would like to present a chart from a paper I gave at the Houston Geological Society meeting of September 12, 1949. This chart presents the resistivity ratios versus water saturation of six different reservoirs. The resistivity measurements were made on the cores as they were extracted from the well and the water saturation determined in the laboratory. Note that the average trend is close to the square root relation predicted several years ago for sandstone formations "in situ;" saturation exponent n equals about 1.9 (where $n = 2$ for the square root relation when the formula is written

$$S = (R_o/R)^{1/n}.$$

It should be pointed out that no cores containing less than about 10 per cent water saturation are recorded. This point was mentioned previously;[1] it was stated that the approximate equation, $S = (R_o/R)^{1/n}$, applies for water saturations down to about 15 to 20 per cent. It appears now that this limit may be extended to about 10 per cent or even below in some cases, as Table III appears to indicate.

I do not agree with the author's further conclusion: "With regard to the possible improvement of estimates of interstitial water made by use of the electric log, the most critical weakness lies in the reliability of the resistivity curve." I am of the opinion that the experiments indicate that much can be done to improve the sampling preparation and laboratory measurement of the resistivity of cores.

REFERENCE

1. G. E. Archie: *AAPG* (May, 1950) 34.

★ ★ ★

AUTHOR'S REPLY TO G. E. ARCHIE

I gather from Archie's comments that his concern results primarily from failure of the log resistivities to agree with the core resistivities. I gather, furthermore, that he has more faith in the former than in the latter.

As I understand Archie's views, he believes that the core resistivities are questionable because

1. No relation or trend is discernible in Fig. 3.
2. It is very difficult to make good electrical contact with the water network (in the cores) when the water content is low.
3. It is highly improbable that the resistivity curves recorded in the bore hole are in error by a factor of 10 to 100.

The fact that there was no discernible quantitative relation between core resistivities and log resistivities need not mean, in itself, that the former are wrong and the latter right. I have preferred to examine the probable error in each, and to choose as the more correct that measurement least subject to error. It may be pertinent to review the probable errors involved both in the measurement of core resistivities and in the measurement of earth resistivities by means of the electric log.

In the measurement of the resistivity of a core there may always arise errors due to the human factor — the misreading of a meter, the misplacing of a decimal in the computation, etc. Such errors may also occur occasionally in the measurement of earth resistivity by the electric log, or of any other physical quantity. I do not believe that Archie had such errors in mind, and see no occasion to dwell upon this source of uncertainty.

Undoubtedly, the possibility of error in core measurements due to improper contact with the water network deserves consideration. Such an error might have its origin in either or both of two sources: first, microscopic inhomogeneity of the core material which might result in paths of different resistance being tapped at various positions of the potential probes used in the four-electrode configuration; and, second, high electrode resistance in the measuring circuit. Actually, the first of these possible sources of uncertainty was demonstrated to be of no consequence in the cores under test by the close agreement of multiple determinations made at different positions on the cores. The second possible source of error, that of high electrode resistance, is, I imagine, what Archie had in mind as a major source of error.

Although there may be some effect due to high electrode resistance, consideration of the basic principles of the resistance measurement shows that the effect is to make the measured resistance of the core, and consequently its resistivity, too *low*. Hence, the elimination of any error from this source would lead to a wider disparity between core and log resistivities than that shown in Fig. 3. Fortunately, actual rough measurements of the electrode resistances demonstrated them to be of reasonable magnitude and of little significance.

In spite of the fact that I can visualize no serious errors which might have attended the measurement of the core resistivities, it should not be thought that these measurements were of a high degree of accuracy. They were not intended to be, nor was there any necessity for them to be.

In examining the possible errors involved in log resistivities, one must differentiate between those incurred in the physical measurements actually made and those which arise when the results of these measurements are converted to *resistivity*. The physical quantities actually measured in electric logging by use of a multielectrode system are the current flowing between the current electrodes and the potential between the potential electrodes. Even though errors from instrumental or human sources may sometimes inadvertently occur, I do not question the ability of the electric log in the usual case to reflect the potential difference between the pickup electrodes for a given current input.

If the electrodes are points in an infinite homogeneous medium, the computation of the resistivity of the medium from the current input and from the potential difference is not a particularly difficult problem. Such an ideal case, however, is never met in practice. In reality, the electrodes are not points, there exists a low resistance path between them through the mud in the hole, and, of paramount importance, the earth material of interest is not of infinite extent and most decidedly is not homogeneous or isotropic.

One may refer to the many excellent and instructive papers written by Guyod to gain an idea of the complexities of the problem of deriving earth resistivities from the quantities actually measured by the logging equipment. When it is recalled that the cases dealt with by Guyod are usually extreme simplifications of reservoir stratigraphy, it is obvious that the values of "resistivity" read from the electric log are subject to question.

A comparison of the nature and magnitude of the probable errors attending the measurement of core resistivity with those incurred in the determination of resistivity by the electric log leads me to conclude that the core resistivities are the more reliable.

I am somewhat puzzled by Archie's allusion to departure curves as "straightforward calculations using specific geometry." If Archie refers to the application of published departure curves as being a straightforward procedure, I am not sure that I agree. If Archie refers, on the other hand, to the derivation of the curves being a matter of straightforward deduction from logical assumptions, I am quite sure that I must abstain from agreeing. To the best of my knowledge I have never seen a complete published exposition of the derivation. From the results obtained by their use at Hawkins, I must conclude that published departure curves are deficient in yielding the true resistivity of high resistance strata.

I do not believe that the determination of the true resistivity of reservoir material by electrical measurements made in the borehole presents insurmountable difficulties. I do believe that our methods used to date have shortcomings, and that a prerequisite to future progress is the recognition of these shortcomings in order that they may be rectified.

★ ★ ★

T.P. 2891

THE EFFECT ON WELL PRODUCTIVITY OF FORMATION PENETRATION BEYOND PERFORATED CASING

JAMES M. McDOWELL AND **MORRIS MUSKAT,** MEMBER AIME, GULF OIL CORP., PITTSBURGH, PA.

ABSTRACT

A report is given of electrical analog experiments on the effect of casing perforation completions on well productivity for ideal uniform reservoirs under steady state homogeneous fluid flow conditions. Graphical results are presented for the effect of perforations of different densities and various degrees of penetration into the formation surrounding the casing or cement sheath. The latter range from perforations which terminate flush with the casing to those which extend into the formation a distance equal to the casing diameter. For the special case where the perforations terminate immediately beyond the casing with semi-spherical protrusions the electrical analog results correct and supersede previously reported theoretical calculations. It is found that the penetration of the perforations into the surrounding productive section may so increase the resultant productivity as to approach or even exceed that for open hole completions.

INTRODUCTION

A theoretical analysis of the effect of casing perforation on well completion, without additional penetration of the formation, was reported several years ago.[1] In this treatment the perforations were represented by mathematical sinks and no explicit account was taken of the imperviousness to flow of the casing in which the perforations were made. This procedure was justified by consideration of the mutual interference between the sinks, which seemed to indicate that the analytical method automatically eliminated flow across the casing radius between the perforations. However, both further theoretical investigation and the electrical analog measurements described below showed that this assumption in the previously developed theory was not valid and that the calculated well capacities would considerably exceed the correct values.§

Even if this simplifying assumption were retained the generalization of the theory to situations where the perforations extend into the producing formation would be extremely difficult. On the other hand, the electrolytic model analog of this type of steady-state homogenous fluid system is, in principle, so simple that it has not been worthwhile to attempt to develop the exact analysis even for the more limited case of strict casing perforation. The whole problem has therefore been studied anew by electrical models to cover the range from holes in the casing which terminate flush with the casing surface to such as extend into the surrounding rock to a depth equal to the casing diameter.

It is to be expected that the productivity of a well completed with casing radius* r_w, perforated with holes of radius r_p, and extending to depths d into the surrounding rock, would depend primarily on the dimensionless geometrical parameters of the system, such as $\frac{r_e}{r_w}$, $\frac{r_w}{a}$, $\frac{r_p}{a}$, and $\frac{d}{r_w}$, where r_e is the external boundary radius and a is the mean vertical separation between the perforations. It will also depend, of course, on the number of perforation lines or total perforation density. While such parameters automatically control analytical treatments, it would require a very extensive series of model experiments to fully disclose their functional effect on the well productivity. For practical purposes, however, a rather limited range of the variables suffices to give the effects of interest. Accordingly, in the experimental study reported here the casing diameter has been kept fixed† at six in., the perforation diameter has been taken as either one-fourth in. or one-half in., their density has been varied from one to eight per ft, and their penetration into the formation has ranged from zero to six in., with a primary scaling factor of one to six.

EXPERIMENTAL METHOD AND RESEARCH

Although electrolytic model experiments have been made for years, there still seems to be some question as to what set of conditions will give the best results. For this reason a number of electrode materials and electrolytes were tried. Those chosen for the final experiments were copper electrodes and a weak copper sulphate solution as the electrolyte. This

---

[1] Reference given at end of paper.

Manuscript received in the office of the Petroleum Branch January 12, 1950.

§Similar results with respect to perforations which do not penetrate into the formation have been recently reported by R. A. Howard and M. S. Watson, Jr., *Jnl. Petr. Tech.* (1950), 2, 179-82.

*Assuming that the casing has been cemented with a uniform and impermeable cement sheath, the effective casing radius is to be interpreted as the external radius of the cement annulus. It is also assumed here that the casing is set through the complete producing section, that it is perforated throughout with a uniform density and that the formation has a constant and isotropic permeability.

†As noted later, however, a uniform scale change permits reinterpreting the primary measurements to correspond to a casing diameter of 12 in.

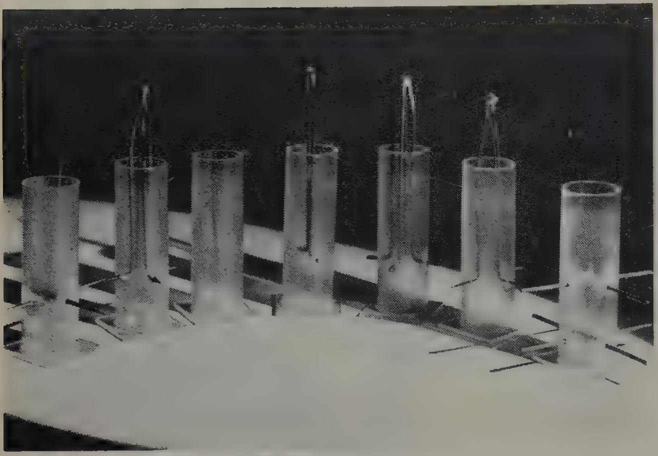

FIG. 1 — A PHOTOGRAPH OF SEVERAL MODEL WELL SYSTEMS FOR PERFORATED CASING COMPLETIONS.

combination gave electrical stability and satisfactory accuracy, as established by a number of experimental checks with theoretical calculations for simplified systems.

The model consisted of a cylindrical tank four feet in diameter with a plywood bottom coated with paraffin, and a stainless steel wall lined with thin copper foil about six in. high. This tank was filled with a weak $CuSO_4$ solution to a depth of two in. (one lb of $CuSO_4$ in 15.6 gal of distilled water). The open well was represented by a one in. dia. copper rod placed at the center of the tank. The well casings were represented by one in. OD polystyrene tubing closed at one end. The perforations were represented by copper wire electrodes extending through the tubing. The copper wire and foil were cleaned with nearly concentrated nitric acid just prior to making the measurements. A General Radio Bridge type 650-A was used in making the resistance measurements, with an external 1,000 cycle signal source.

The well models representing the well, where only the casing is perforated and no hole is made in the formation, had the ends of the wire electrodes smoothed off flush with the polystyrene tubing. Models were made with 1, 2, 4, and 8 electrodes representing a corresponding number of perforations per ft. A ratio of one to six related the model to the actual reservoir units, so that the two in. depth represents one ft. Various perforation patterns were used, but the results indicated that no detectable variation in productivity was apparent whether the perforations were all on one vertical line of the casing or evenly distributed around it. In each case, however, vertical symmetry was maintained so that the measurement would correspond to a horizontal layer of the reservoir one ft thick, representing a unit of symmetry in the composite system of arbitrary thickness. Perforations of one-half in. dia were represented by No. 12 A.W.G. copper wires (0.081 in. dia) and one-fourth in. dia. perforations were represented by No. 18 A.W.G. copper wire (0.040 in. dia).

To represent wells in which the perforating bullet or charge produced a hole in the formation extending beyond the casing and cement sheath models were made in which the wire electrodes protruded horizontally out from the tubing a corresponding distance. Models were made with semi-spherical protrusions only, and others with the wires extending one-fourth in., one-half in., and one in., which correspond to ratios of one-fourth, one-half and one with the casing diameter. A photograph of several of these model well systems is reproduced in Fig. 1.

It was assumed* that the flow would be essentially radial in the reservoir at a distance from the well corresponding to the radius of the tank. This distance was equivalent to 12 ft. It is necessary then to add to the resistance measured for each model the value of the calculated resistance for the area beyond the tank extending to the radius of drainage, which was chosen as 660 ft, as used in the previous theoretical calculations. The ratio of the productivities for any perforation pattern to that of the uncased well will be equal to the inverse ratio of their total resistance measured or calculated to the radius of drainage.

If R_m equals the measured resistance in the tank of radius r_o, R_t equals the total resistance to the radius of drainage r_e expressed in units of the model, and R_d equals the resistance between the radius of the tank and the radius of drainage, then:

$$R_t = R_m + R_d \quad \ldots\ldots\ldots\ldots \quad (1)$$

$$R_d = \frac{\rho \log r_e/r_o}{2\pi h} \quad \ldots\ldots\ldots\ldots \quad (2)$$

where ρ is the resistivity of the electrolyte and h is its thickness.

For the open or uncased well,

$$R_t = \frac{\rho \log r_e/r_w}{2\pi h} \quad \ldots\ldots\ldots\ldots \quad (3)$$

and:

$$R_m = \frac{\rho \log r_o/r_w}{2\pi h} \quad \ldots\ldots\ldots\ldots \quad (4)$$

Using the measured value of resistance of the tank, with the one in. dia copper electrode, of 41.5 ohms, the value of ρ as calculated from Equation (4) = 342.2 ohm-cm. From Equation (3) we find $R_t = 84.4$ ohms, and from Equation (2), $R_d = 42.95$ ohms. The ratio of the productivities of a cased well with a given pattern of perforations and the open well is therefore given by:

$$Q/Q_o = \frac{R_t \text{ (open well)}}{R_m + R_d} = \frac{84.4}{R_m + 42.95} \quad . \quad (5)$$

The ratios thus calculated are plotted in Fig. 2 for one-half in. dia perforations and six in. dia casing, and in Fig. 3 for one-fourth in. dia perforations and six in. dia casing. By

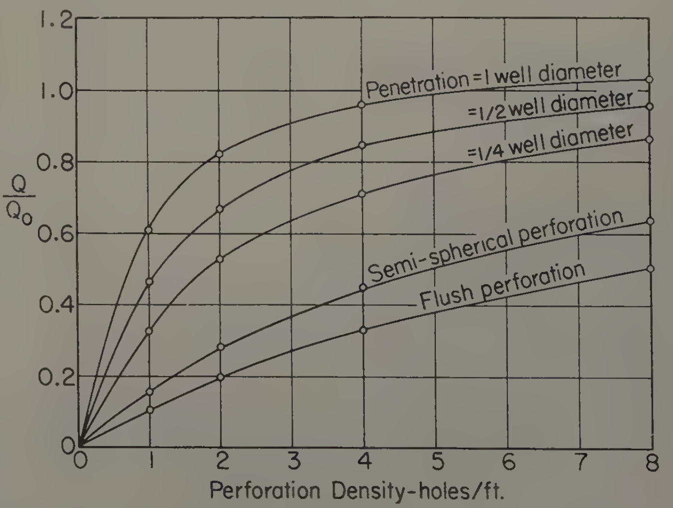

FIG. 2 — THE EFFECT OF THE PERFORATION DENSITY ON THE PRODUCTIVITY OF PERFORATED CASING COMPLETIONS, WITH VARIOUS PERFORATION PENETRATIONS INTO THE PRODUCING FORMATION. Q/Q_o = (PRODUCTIVE CAPACITY OF CASED AND PERFORATED WELL)/(PRODUCTIVE CAPACITY OF UNCASED WELL). CASING DIAMETER = SIX IN.; PERFORATION DIAMETER = ONE-HALF IN.

---

*While probes of the actual potential distributions in the models showed slight variations near the external boundaries, these were considered to be of negligible importance.

changing the ratio between the model and the reservoir distances to one-twelfth instead of one-sixth and recalculating R_t; R_d and the ratios Q/Q_o, the curves of Fig. 4 were obtained for one-half in. dia perforations and 12 in. dia casing.* Since this scale transformation must also be applied to the perforation density, the original data of Fig. 3 apply only to perforation densities as high as four per ft. The recalculated curves have therefore been extrapolated for the higher perforation densities, as indicated by the dash segments in Fig. 4.

Replotting the data of Figs. 2 and 3 for fixed perforation densities while varying the formation penetration the curves of Fig. 5 are obtained. Here the depth of the perforation has been expressed in units of the casing or cement sheath diameter to provide a dimensionless measure of this parameter. Along the ordinate axes are plotted the relative productivities for the perforations terminating flush with the casing or formation surface. For plotting purposes the data for the semi-spherical protrusions were arbitrarily assumed to have "penetrations" equal to the perforation diameter divided by the casing diameter.

To show the relative effect of the casing diameter on the well productivities, the basic data have been further replotted in Fig. 6. The solid curves are for a six in. dia casing (well bore) and are the same as the solid curves of Fig. 5. The dashed curves are for a 12 in. dia casing, but all other parameters are the same. It will be noted that, except for nearly zero penetration, the relative productivity for the same relative penetration increases with the casing diameter, but this is largely the result of the penetration into the formation being greater in actual depth. Where the perforations merely penetrate the casing and cement, the relative productivity Q/Q_o is slightly less for the larger diameters. The reason is that whereas the area of the perforation holes through which the fluid can enter the casing is the same in both cases, the area through which the fluid would enter the uncased well increases with increasing diameter. This results in a larger open hole productivity Q_o for the larger size well, but a smaller value for the ratio, Q/Q_o. For the same reason, the relative productivities for fixed absolute depths of penetrations will be somewhat smaller for the larger casing diameters.

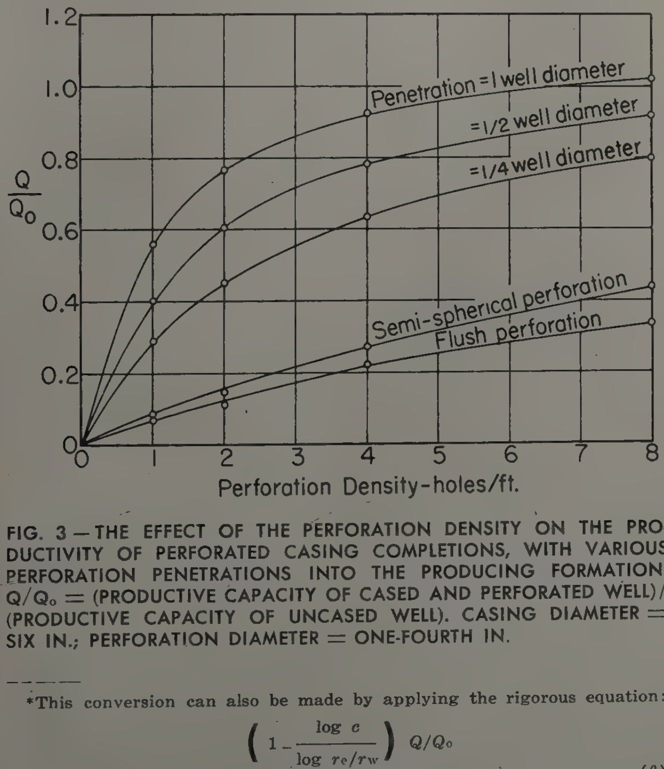

FIG. 3—THE EFFECT OF THE PERFORATION DENSITY ON THE PRODUCTIVITY OF PERFORATED CASING COMPLETIONS, WITH VARIOUS PERFORATION PENETRATIONS INTO THE PRODUCING FORMATION. Q/Q_o = (PRODUCTIVE CAPACITY OF CASED AND PERFORATED WELL)/(PRODUCTIVE CAPACITY OF UNCASED WELL). CASING DIAMETER = SIX IN.; PERFORATION DIAMETER = ONE-FOURTH IN.

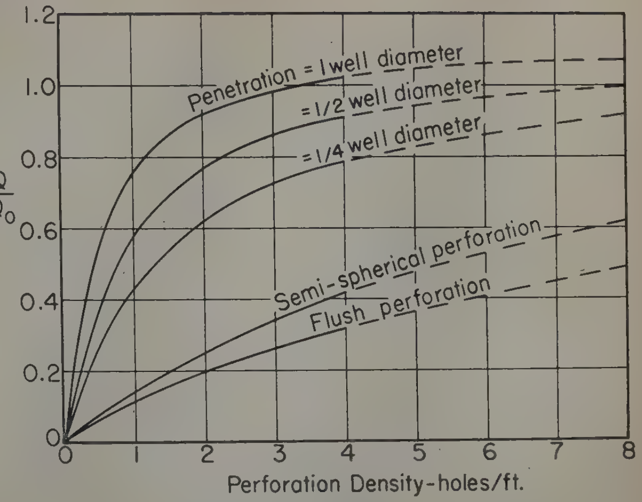

FIG. 4—THE EFFECT OF THE PERFORATION DENSITY ON THE PRODUCTIVITY OF PERFORATED CASING COMPLETIONS, WITH VARIOUS PERFORATION PENETRATIONS INTO THE PRODUCING FORMATION. Q/Q_o = (PRODUCTIVE CAPACITY OF CASED AND PERFORATED WELL)/(PRODUCTIVE CAPACITY OF UNCASED WELL). CASING DIAMETER = 12 IN.; PERFORATION DIAMETER = ONE-HALF IN. DASHED SEGMENTS ARE EXTRAPOLATIONS.

DISCUSSION

Perhaps the most significant implication of the results plotted in Fig. 2-4 is the marked increase in relative well productivity resulting from even limited degrees of extension of the perforation holes into the producing formation. An appreciable increase is indicated even for the simple extension of the flush perforations so as to have nothing more than semi-spherical protrusions.* Moreover, as the formation penetration is increased, the resultant productivity, for densities of four per ft or greater, approaches and may even exceed that for the open hole completion. However, as is to be expected, the added gains from increased penetration continually decline, so as to give an asymptotic character to the curves of relative productivity vs. penetration as indicated in Fig. 5. It will be noted also from Fig. 5 that whereas the well productivity is quite sensitive to the perforation radius at zero or low penetration depths, at high values of the latter the perforation radius, if uniform, becomes of little importance.

To check on the effect of the assumption that the holes penetrating the formation beyond the steel casing are strictly uniform, several additional experiments were performed using uniformly tapered perforation electrodes of one-half in. equivalent diameter at the casing. It was found that for a perforation density of one per ft, the tapering would reduce the relative productivity by 9.1 and 12.2 per cent for penetrations of 25 per cent and 100 per cent of the casing diameter respectively. The corresponding reductions for a perforation density of four per ft were 4.7 and 9.0 per cent respectively. For still

---

*This conversion can also be made by applying the rigorous equation:

$$(Q/Q_o)' = \frac{\left(1 - \frac{\log c}{\log r_e/r_w}\right) Q/Q_o}{1 - Q/Q_o\left(\frac{\log c}{\log r_e/r_w}\right)} \quad \ldots\ldots \quad (6)$$

where Q/Q_o is the relative productivity for a known case corresponding to a drainage radius r_e, well radius r_w, perforation radius r_p, perforation penetration d, and n perforations per ft; and $(Q/Q_o)'$ is the relative productivity for r_e, $c\,r_w$, $c\,r_p$, cd, and n/c, where c is the common scaling factor.

*The previously mentioned theoretical treatment, which referred to such perforations, gave relative productivities exceeding those indicated in Figs. 2-4 by 25-70 per cent, depending on the perforation density.

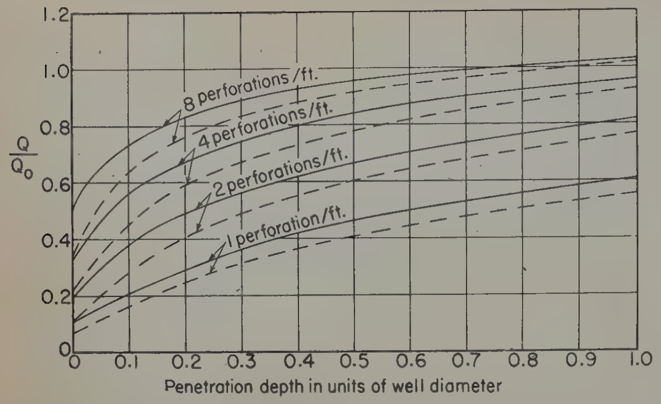

FIG. 5—THE EFFECT OF THE DEPTH OF PERFORATION PENETRATION INTO THE FORMATION SURROUNDING THE CASING ON THE WELL PRODUCTIVITY FOR VARIOUS PERFORATION DENSITIES. Q/Q_o = (PRODUCTIVE CAPACITY OF CASED AND PERFORATED WELL)/(PRODUCTIVE CAPACITY OF UNCASED WELL). CASING DIAMETER = SIX IN.; ——— PERFORATION DIAMETER = ONE-HALF IN.; — — — — PERFORATION DIAMETER = ONE-FOURTH IN.

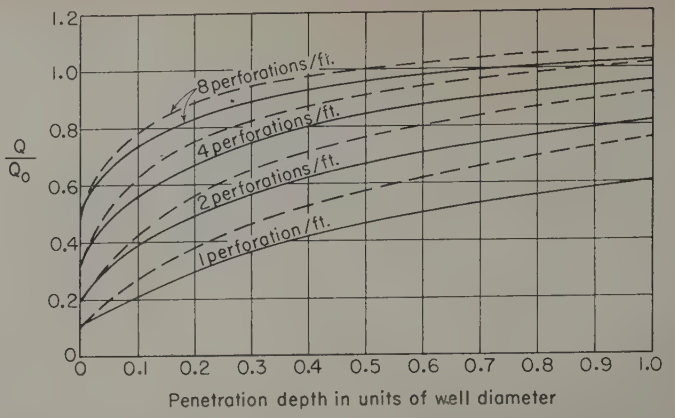

FIG. 6—THE EFFECT OF THE DEPTH OF PERFORATION PENETRATION INTO THE FORMATION SURROUNDING THE CASING ON THE WELL PRODUCTIVITY FOR VARIOUS PERFORATION DENSITIES. Q/Q_o = (PRODUCTIVE CAPACITY OF CASED AND PERFORATED WELL)/(PRODUCTIVE CAPACITY OF UNCASED WELL). ——— CASING DIAMETER = SIX IN.; . . . . . CASING DIAMETER = 12 IN.; PERFORATION DIAMETER = ONE-HALF IN. FOR ALL CURVES.

higher perforation densities the effects of the hole tapering would be even lower. While other variations in the geometry of the extended perforations could be visualized, these specific results indicate that for practical purposes the uniform perforation charts of Figs. 2-4 should suffice to give at least a semi-quantitative relative evaluation of the various perforation programs which might be considered for actual well completions.

The results presented here are essentially empirical, and do not reveal the full scope of the dependence of the well productivity on the basic dimensionless parameters of the producing systems. From a practical standpoint, however, the ranges of variables covered in the experiments span the conditions corresponding to actual well systems in which the perforations are uniformly distributed over the whole producing formation. With respect to the absolute magnitudes of the well productivities, it is to be noted that if the perforations just penetrate the casing or cement sheaths the need for relatively high perforation density is even greater than had been previously indicated by the theoretical calculations. However, if the perforations can be extended for appreciable distances into the producing formation productive capacities approaching those for uncased holes should be obtained even for moderate perforation densities. On the other hand, it is to be emphasized that the gains indicated by Figs. 2-5, either by increasing the perforation density or penetration, are to be expected only if the cementing of the casing has provided a perfect seal. If channels have been left in the cement sheath even a single perforation opening into such channels will give high well capacities which may not be appreciably increased by additional perforation.

ACKNOWLEDGMENT

The authors are indebted to R. D. Wyckoff for helpful suggestions in choosing the optimum conditions for operating the electrical analogs, and to P. D. Foote, executive vice-president of the Gulf Research and Development Co., for permission to publish this paper.

REFERENCE

1. Morris Muskat: *Trans.* AIME, (1943), 151, 175.

DISCUSSION

By Robert A. Howard, Department of Physics, University of Oklahoma, Norman, Okla.

It is indeed fortunate that this excellent paper appears at this time, as the data presented here complement those presented by Watson and myself. Our data cover the range of penetration from zero to slightly over one-third the casing diameter, while the data presented here have a gap between zero and a penetration of one-fourth casing diameter, but go on to a penetration of one casing diameter. The authors also give data on one-half in. holes in six-in. casing, a case which is not covered in our paper.

It is gratifying to find that there is good agreement between the experimentally determined points in the two papers. The relative productivities obtained for six-in. casing with one-fourth in. perforations, however, show that the approximate scaling equation which we found to be valid for flush perforations, gives results which are somewhat high for deeper penetration. If one uses the scaling procedure of McDowell and Muskat (which is an exact, rather than approximate, scaling procedure, but which alters the vertical distribution of perforations) to convert our data for one-half in. perforations in 12-in. casing to one-fourth in. perforations in six-in. casings, the results agree well with those shown in Fig. 5 except in the region between zero penetration and a penetration of one-fourth casing diameter. In general, our data indicates that the interpolated sections of the curves in Fig. 5 do not rise quite steeply enough, or in other words, that the initial bit of penetration is even slightly more important than indicated by this figure. This may indicate that the arbitrary assignment of penetration equal to the perforation diameter for hemispherical perforations is not satisfactory. The extrapolated portions of Fig. 4 are confirmed by our results out to a perforation depth of one-third casing diameter.

Relative productivities greater than one which were predicted in our paper, have actually been found here for the greater depths of penetration. It is interesting to note that the differences between the results obtained by McDowell and Muskat and by ourselves vary by little more than the experimental error involved in the measurements in spite of the fact that they used round rather than flat-ended penetration electrodes such as we used, their electrodes were about 2.5 per cent undersized, and their eight electrode distribution is in two layers rather than a single horizontal layer. ★ ★ ★

T.P. 2953

THE KOBE POROSIMETER AND THE OILWELL RESEARCH POROSIMETER

CARROL M. BEESON, MEMBER AIME, PETROLEUM ENGINEERING DEPARTMENT, UNIVERSITY OF SOUTHERN CALIFORNIA, LOS ANGELES, CALIF.

ABSTRACT

Reasons are given for using a Boyle's-law porosimeter in conducting core analysis for either routine or research purposes. Among other things, it is pointed out that such a porosimeter permits the measurement of all basic properties on the same sample, thereby eliminating the sources of error inherent in the use of adjacent samples. References are made to investigations of gas adsorption on various porous materials, to show that the use of helium in Boyle's-law porosimeters reduces to negligible proportions the error due to the adsorption or desorption of the operating gas.

Two Boyle's-law instruments are described, which permit accurate and rapid measurements of porosity. Schematic sketches and explanations are included, along with derivations of equations required in performing precise determinations.

Summaries of data obtained during calibration are tabulated and analyses of the data are presented as indications of the precision and accuracy of each device. Comparisons are also shown for measurements made with each of the instruments on the same test pieces and cores.

INTRODUCTION

An accurate porosimeter, operating on the principle of Boyle's law, is of considerable value in the analysis of cores for either routine or research purposes. This is due primarily to the fact that the measurement of porosity with such an instrument leaves the sample free of contamination by any liquid.

When used in conjunction with an extraction apparatus[1] for determining oil and water saturations, a Boyle's-law porosimeter permits the measurement of all basic properties on the same sample. This eliminates the sources of error inherent in the use of adjacent samples, or the necessity of determining porosity after all other properties have been obtained.

Large errors may result from combining measurements made on adjacent samples in order to obtain a single property. This type of error is definitely involved when oil and water are measured with one sample and the pore volume is measured with an adjacent one. Furthermore, the source of error would be present to some extent, even if the analyst could choose the samples so they were truly adjacent from a geological standpoint.

The use of adjacent samples in routine core analysis also necessarily decreases the probability of correlating core properties. For example, the chance of correlating the "irreducible" interstitial-water saturation with permeability, is bound to be greatly reduced by measuring these properties on "adjacent" samples.

For research purposes, amplification is scarcely required concerning the greater flexibility of a method for measuring porosity which leaves the core free of contamination by any liquid. Even under those circumstances which require that the core be saturated with a liquid, a previous measurement of porosity with a gas is useful in determining the degree of saturation that has been attained in the process.

Furthermore, for comparable accuracy, porosity usually may be determined more rapidly with a gas than with a liquid. This advantage of the Boyle's-law instrument is most outstanding when the determination time is compared with that required in obtaining porosity by evacuation of the core followed by saturation with a liquid of known density.

Several porosimeters which operate on the principle of Boyle's law have been described[2,3,4,5,6,7] in the literature. No comparison will be attempted between those instruments and the ones described herein.

Before helium gas became readily available, Boyle's-law porosimeters were subject to an appreciable error due to the adsorption of the operating gas on the surface of the core solids. There is considerable direct and indirect evidence in the literature to support the contention that the adsorption of helium on porous solids is negligible at room temperature.

In discussing the use of Boyle's-law porosimeters, Washburn and Bunting[2] stated that "for most ceramic bodies dry air is a satisfactory gas, but hydrogen will be required in some instances. Helium could, of course, be employed for all types of porous materials at room temperatures or above." Howard and Hulett[3] obtained evidence that the adsorption of helium was negligible at room temperatures, even on activated carbon; for the density measured with this gas was unaffected by changes in pressure or by changes in temperature from 25°C to 75°C. For oil-well cores, Taliaferro, Johnson, and Dewees[6] obtained lower porosities with helium than with air, but apparently did not study helium adsorption.

From the work of these investigators, it follows that the use of helium in Boyle's-law porosimeters reduces the error due to gas adsorption to negligible proportions. This makes it possible to construct instruments which permit the determination of porosity with (1) a high degree of accuracy, (2) with great rapidity, and (3) without contamination.

THE KOBE POROSIMETER

The fundamental design of the Kobe Porosimeter was developed by Kobe, Inc., which firm built about 12 of the instruments during 1936 and 1937. Since that time, seven or eight more have been constructed with their permission, making a total of about 20 that have been put into operation.

---

[1] References given at end of paper.

Manuscript received in the office of the Petroleum Branch, October 20, 1949.

In this porosimeter, the bulk volume is determined from the volume of mercury displaced by the sample, whereas the volume of sand grains and disconnected voids depends upon the volume of a gas displaced by the sample.

Although many modifications have been made in the design, method of calibration, and method of use, the manner of application of Boyle's law has remained the same. That is, in the relation $P_1V_1 = P_2V_2$, the initial pressure P_1 is fixed at that of the room, the initial volume V_1 is chosen, the final pressure P_2 is fixed at a definite higher value, and the final smaller volume V_2 is measured. However, volume differences instead of volumes are actually determined, as shown in the Appendix.

The Appendix contains a detailed description of the device, including the method of operation and accuracy of results. As indicated there, bulk volumes of steel balls of from 5 to 15 cc may be measured very rapidly, with errors which should not exceed 0.5 per cent. Sand-grain volumes in this range may be measured almost as rapidly, with errors which should not exceed 0.1 per cent. The above value for the accuracy of measuring bulk volume does not include the effect of any penetration of mercury into a core nor the effect of trapping air around a core, during a determination. With these limitations in mind and applying these figures to differences in porosity, a core with a bulk volume of 5.00 cc and a sand-grain volume of 4.00 cc should yield a value for porosity of 20.0 ± 0.5 per cent.

Various users of the Kobe Porosimeter have made modifications in the original design of the instrument. Several of these have been enumerated in the Appendix.

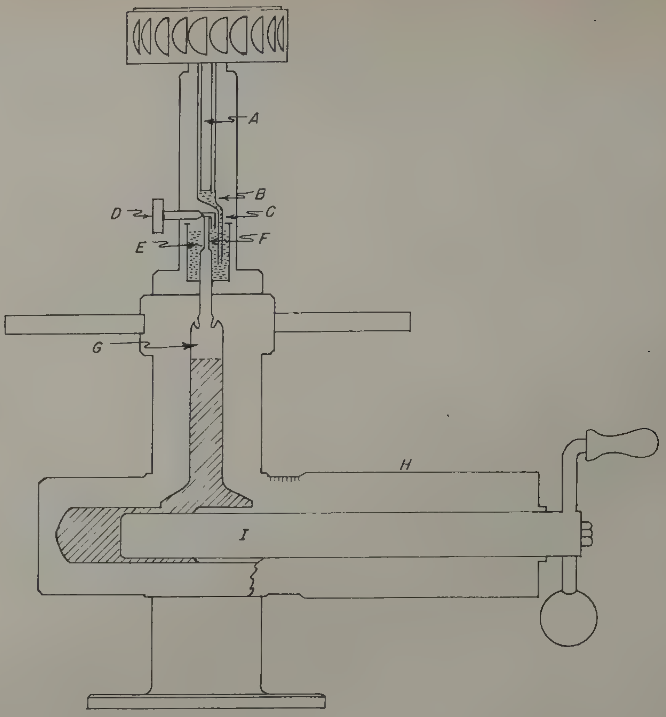

FIG. 1 — SCHEMATIC SKETCH OF KOBE POROSIMETER.

THE OILWELL RESEARCH POROSIMETER

Despite the many modifications that have been made in the design, method of calibration, and method of use of the Kobe Porosimeter, there were several reasons for developing a new instrument.

Chief among these was the amount of manual labor involved in making the necessary changes in the volume of the cell during a determination. For a large number of consecutive measurements the process becomes sufficiently tiring that one laboratory designed equipment for changing the volume mechanically. However, the device would have made the porosimeter considerably more complex, so the idea was abandoned without actual trial.

Another consideration involved the belief that a less expensive instrument might be developed, which would be quite useful for many production laboratories.

An analysis of the original Kobe Hydrogen Porosimeter described by Coberly and Stevens[5] indicated that modifications in this instrument, chiefly to increase accuracy, should yield an excellent porosimeter. During the time since construction of the Kobe Hydrogen Porosimeter, much more accurate gauges had been made available, and it was believed that the accuracy of the stock item might be increased still further. In addition, Coberly and Stevens had observed that decreasing the volumes of the chambers would increase accuracy.

The Oilwell Research Porosimeter was developed along these lines, using the principle of the original Kobe Hydrogen Porosimeter. That is, in the relation $P_1V_1 = P_2V_2$, the initial pressure P_1 is fixed at a definite value, the initial volume V_1 is fixed at that of the first chamber, the final lower pressure P_2 (or its equivalent) is measured on a bourdon-type gauge, and the final volume V_2 is the volume of the first chamber plus the volume of the second chamber diminished by the sand-grain volume. As explained in the Appendix, however, sand-grain volumes obtained with this instrument are not calculated with the use of Boyle's law.

The Appendix contains a detailed description of the instrument, including the method of operation and accuracy of results. As substantiated there by a statistical analysis of the calibration data, the design and method of operation permit very rapid measurements of sand-grain volumes from 4.0 cc to at least 13.5 cc, with errors which continually decrease in this range from ± 1.1 per cent to ± 0.2 per cent.

Transforming these limits to differences in porosity, a core with a sand-grain volume of 12.00 cc and a pore valume of 3.00 cc should yield a value for porosity of 20.0 ± 0.2 per cent, providing the sand-grain volume were measured in the instrument and the bulk volume were known exactly. Under the same conditions, a core with a sand-grain volume of 4.00 cc and a pore volume of 1.00 cc should yield a value for porosity of 20 ± 0.9 per cent. Single measurements should be within these limits 90 per cent of the time, and the limits could be still further reduced by using the average of several measurements.

ACKNOWLEDGMENTS

The men who have helped directly or indirectly in the preparation of this paper are too numerous to recount. However, the author wishes to express his gratitude to Kobe, Inc., for their generous cooperation, and to Oilwell Research, Inc., for release of the major portion of the data contained herein.

REFERENCES

1. C. G. Rall and D. B. Taliaferro: A Method for Determining Simultaneously the Oil and Water Saturations of Oil Sands, U. S. Bureau of Mines R. I. 4004, (Dec. 1946).
2. E. W. Washburn and E. N. Bunting: Determination of Porosity by the Method of Gas Expansion, *J. Amer. Ceramic Soc.*, (1922) 1, 112.

3. A. E. MacGee: Several Gas Expansion Porosimeters, *J. Amer. Ceramic Soc.*, (1926) **9**, 814.
4. G. H. Fancher, J. A. Lewis and K. B. Barnes: Some Physical Characteristics of Oil Sands, Penn. State College, Mineral Industries Experiment Station Bulletin 12, p. 65, (1933).
5. C. J. Coberly and A. B. Stevens: Development of Hydrogen Porosimeter, *Trans.* AIME, (1933) **103**, 261.
6. D. B. Taliaferro, T. W. Johnson and E. J. Dewees: A Method of Determining Porosity. A list of Porosities of Oil Sands, U. S. Bureau of Mines R. I. 3352, (Sept. 1937).
7. E. Kaye and M. L. Freeman: An Air Porosimeter, *API Drilling and Production Practice*, (1948) 187.
8. H. C. Howard and G. A. Hulett: A Study of the Density of Carbon, *J. Phys. Chem.*, (1924) **28**, 1082.

APPENDIX

THE KOBE POROSIMETER

Description and Operation

A schematic sketch of one of the instruments is shown in Fig. 1. The dead-weight gauge A slides into a closely machined cylinder and rests on the surface of a quantity of oil confined in the chamber B just above the valve D. The oil in the chamber is connected by the tube C to the oil reservoir E in a plastic walled chamber. Pressure exerted on the surface of the reservoir is transmitted by the oil, through the tube, to the dead-weight gauge. The lower portion of the instrument contains mercury, the quantity of which is adjusted so that the micrometer barrel H reads approximately zero when the mercury level G is raised to the mark F in the tube centered in the plastic walled chamber. Turning the micrometer actuates the piston I inside the horizontal cylinder which raises or lowers the mercury level (shown at G) and the displacement volume is measured on the micrometer to 0.001 cc. The tube centered in the plastic walled chamber opens through the valve D to dried air at atmospheric pressure, and is also connected to the air space above the reservoir.

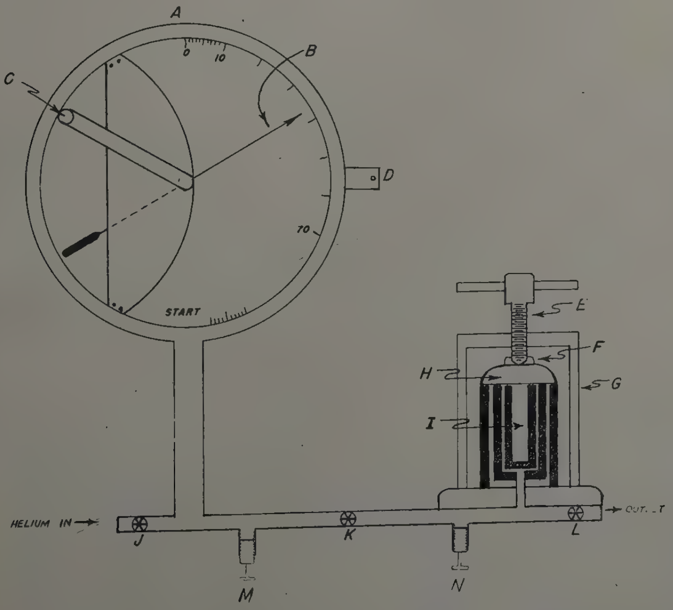

FIG. 2—SCHEMATIC SKETCH OF OILWELL RESEARCH POROSIMETER.

Table I—Determination of Constant from Operation of Kobe Porosimeter

R_1	R_1'	R_2	R_2'	K
85.000	20.027	50.000	11.095	1.343
70.000	16.210	50.000	11.095	1.341
50.000	11.095	40.000	8.546	1.342
50.000	11.095	20.000	3.438	1.342
30.000	5.989	20.000	3.438	1.343

For correct operation of the porosimeter, it is essential that the floating position of the gauge be accurately reproduced. This may be accomplished by projecting, on a screen, the image of a pointer mounted at the center of the gauge. The screen may be so situated that the movement of the gauge is magnified more than ten fold by the motion of the image. To insure free motion of the gauge at the floating position, it is rotated by a jet of air of constant direction and intensity.

Derivation of Equations for Determining Constant and Measuring Porosity

Considerable difficulty was experienced in obtaining reproducible values of the porosimeter constant by the method originally provided. Accordingly the author derived the relations given below and helped develop the following method of measuring porosity.

In determining the volume of sand grains (and disconnected voids) V_s, the gas is compressed from barometric pressure P_b to the floating pressure P_f by rotating the micrometer barrel from some chosen initial reading R to a reading R' at which the dead-weight gauge floats. The sample is then placed in the instrument and the process repeated by starting at the same initial reading and obtaining the final reading R_s'.

The total volume occupied by the gas when the micrometer reading is at R'' may be represented by the symbol B. The application of Boyle's law to the above operations then yields the following relations:

$$P_b(B + R - R') = P_f B$$
$$P_b(B + R - R' - V_s) = P_f(B + R_s' - R' - V_s).$$

Elimination of B and R from these two equations gives,

$$V_s = \frac{P_f}{P_f - P_b} \cdot (R_s' - R').$$

The bulk volume is equivalent to the difference between the micrometer readings made at barometric pressure when the mercury has been forced up to the reference line, with and without the sample. Denoting the bulk volume by $R_s^\circ - R^\circ$, the porosity becomes,

$$P = 1 - \frac{P_f}{P_f - P_b} \cdot \frac{R_s' - R')}{(R_s^\circ - R^\circ)}$$

This equation shows that, providing P_f is determined, the porosity may be computed from the barometric pressure and the micrometer readings.

Equating the forces which act in opposite directions on the floating dead-weight gauge yields the relation,

$$P_f A = P_b A + W \cos d,$$

where A represents the cross sectional area of the piston, W signifies the weight of the gauge and $\cos d$ corresponds to the cosine of the angle by which the piston deviates from the vertical. Since A, P_b, W and $\cos d$ can be determined with considerable accuracy, the expression permits the evaluation of P_f. For example, the measured values, $P_b = 14.64$ psi (75.67 cm of Hg at 32°F), $W = 4.794$ lbs, diameter of piston $= 0.377$ in., and the assumed value $\cos d = 1.000$, lead to $P_f = 57.64$ psi (3.924 atm., absolute) and $K = P_f/(P_f - P_b) = 1 - AP_b/W \cos d = 1.341$.

Table II — Data Obtained by Kobe Porosimeter with Test Pieces and Cores

Sample	$R_s°$	$R°$	$R_s° - R°$	R_s'	R'	$R_s' - R'$
7/8″ ball	13.841	8.060	5.781	23.723	19.430	4.293
15/16″ ball	15.166	8.063*	7.103	24.718	19.430*	5.288
1 1/8″ ball	20.349	8.065*	12.284	28.579	19.430*	9.149
1 1/8″ cylinder	20.131	8.068*	12.063	28.367	19.430*	8.937
3/4″ core	17.603	8.070	9.533	25.442	19.430	6.012
1″ core	19.866	8.073*	11.793	26.039	19.432*	6.607
1″ alundum	21.434	8.077*	13.357	25.934	19.434*	6.500
1 1/8″ alundum	23.048	8.080*	14.968	28.288	19.436*	8.852
7/8″ ball	13.855	8.080	5.775	23.740	19.435	4.305
15/16″ ball	15.187	8.080*	7.107	24.734	19.433*	5.301
1 1/8″ ball	20.358	8.080*	12.278	28.584	19.432*	9.152
1 1/8″ cylinder	20.133	8.080*	12.053	28.369	19.431*	8.938
3/4″ core	17.610	8.080	9.530	25.432	19.430	6.002
1″ core	19.884	8.083*	11.801	26.042	19.432*	6.610
1″ alundum	21.442	8.085*	13.357	25.929	19.435*	6.494
1 1/8″ alundum	23.046	8.088	14.958	28.280	19.437	8.843

*These values were interpolated from the measured ones.

Note: The constant was measured before and after the tests, by using values of R_1 and R_2 of 70.000 and 50.000. The values obtained for R_1' and R_2' were 19.418 and 14.383 before the tests, and 19.430 and 14.395 after the tests. Each of these sets of results yields a value of 1.3365 for the constant.

A second method of determining the porosimeter constant depends upon the operation of the instrument. With no sample present, the air is compressed from barometric pressure to the floating pressure by movement of the micrometer barrel from R_1 to R_1', and similarly, from a different initial reading R_2 to R_2'.

The constant was also computed from operations of the porosimeter at other values of the barometric pressure. At $P_b = 75.6$ cm of *Hg* at 32°F, the calculated values of *K* were 1.340, 1.340 and 1.339. At $P_b = 75.5$ cm of *Hg* at 32°F, the values were 1.338 and 1.338.

The last five values of the constant average 1.339 with an average barometric pressure of 75.56 cm of *Hg* at 32°F, while those of Table I average 1.342 with a barometric pressure of 75.9 cm of *Hg* at 32°F. These figures yield a grand average of $K = 1.340$ at $P_b = 75.7$ cm of *Hg* at 32°F. This agrees quite satisfactorily with the value of 1.341 calculated from the weight of the gauge and the diameter of the piston. Furthermore, the variation in the determined values of the constant, with barometric pressure, agrees with the expression derived above.

Accuracy of Kobe Porosimeter

To obtain an indication of the precision and accuracy of the Kobe Porosimeter, a pair of measurements was made on each of various test pieces and samples. Three steel ball bearings and one cylinder were included. Cylindrical cores were also used, two having been drilled from California oil sands and two from alundum. Helium was used as the operating gas.

The data have been recorded in Table II, with columns headed by the symbols defined in the section of Derivation of Equations for Determining Constant and Measuring Porosity. The figure given with each sample indicates the diameter of the sphere or cylinder.

Calculations made from the original data of Table II have been given in Tables III and IV. The bulk volume V_b is the volume of mercury displaced by the sample, whereas V_s is the volume of the solids and disconnected voids, as determined by Boyle's law. The differences, $\triangle V_b$, $\triangle V_s$, and $\triangle P$, between each pair of measurements of the bulk volume, the solid volume, and the calculated values of porosity serve to indicate the magnitude of variations in measurements made with the instrument.

The total volume occupied by the gas when the micrometer reading is at R_2' may be represented by the symbol *C*. The application of Boyle's law to the above operations then yields the following equations:

$$P_b(C + R_1 - R_2') = P_f(C + R_1' - R_2')$$

$$P_b(C + R_2 - R_2') = P_f C.$$

Elimination of *C* from these two relations gives,

$$P_f/P_b = (R_1 - R_2)/R_1' - R_2'), \text{ or}$$

$$K = P_f/(P_f - P_b) = \frac{R_1 - R_2}{(R_1 - R_2) - (R_1' - R_2')} .$$

Determination of Porosimeter Constant

Determinations of *K* at various initial settings of one porosimeter, for $P_b = 75.9$ cm of *Hg* at 32°F, have been recorded in Table I.

The volumes of the steel balls were known to ±0.003 cc, from measurements made with a micrometer to ±0.0001 in. Accordingly, Table IV indicates the errors involved in measuring such test pieces with the instrument. It appears from the table that bulk-volume measurements were 0.5 per cent too high, while solid-volume measurements were within 0.1 per cent of the known values.

The above statement for the degree of accuracy of measuring bulk volume does not include the effect of any penetration of mercury into a core nor the effect of trapping air around a core, during a determination. With these limitations in mind and transforming the above figures to differences in porosity, a core with a bulk volume of 5.00 cc and a sand-grain volume of 4.00 cc would yield a value for porosity of 20.0 ± 0.5 per cent.

Modifications in Design of Kobe Porosimeter

Various users of the Kobe Porosimeter have made modifications in the original design of the instrument. These have been mainly to facilitate operation, as is apparent from the examples that follow.

Some users have replaced the dead-weight gauge by a Bourdon gauge. This change also facilitates counterbalancing the removable cap, which is the part above *G* in Fig. 1. Another user has moved the dead-weight gauge to the side of the

Table III — Deviations in Measurements with Kobe Porosimeter

Sample	Bulk Volume V_b, cc		Solid Volume V_s, cc		Porosity P, %		Differences $\triangle V_b$, cc	$\triangle V_s$, cc	$\triangle P$, %
7/8″ ball	5.781	5.775	5.738	5.754	0.74	0.36	—0.006	+0.016	—0.38
15/16″ ball	7.103	7.107	7.067	7.085	0.51	0.31	+0.004	+0.018	—0.20
1 1/8″ ball	12.284	12.278	12.228	12.232	0.46	0.37	—0.006	+0.004	—0.09
1 1/8″ cylinder	12.063	12.053	11.944	11.946	0.99	0.89	—0.010	+0.002	—0.10
3/4″ core	9.533	9.530	8.035	8.022	15.71	15.82	—0.003	—0.013	+0.11
1″ core	11.793	11.801	8.830	8.834	25.13	25.14	+0.008	+0.004	+0.01
1″ alundum	13.357	13.357	8.687	8.679	34.96	35.02	±0.000	—0.008	+0.06
1 1/8″ alundum	14.968	14.958	11.831	11.819	20.96	20.99	—0.010	—0.012	+0.03

Table IV — Errors in Measurements of Ball Bearings with the Kobe Porosimeter

Dia. of Ball	Meas.* Vol., V_m,	Avg.‡ Bulk Vol., $\overline{V}_b$;	Avg.‡ Solid Vol., $\overline{V}_s$	$\overline{V}_b - V_m$		$\overline{V}_s - V_m$	
in.	cc	cc	cc	cc	%	cc	%
⅞	5.750	5.778	5.746	+0.028	+0.49	–0.004	–0.07
$\frac{15}{16}$	7.068	7.105	7.076	+0.037	+0.52	+0.008	+0.11
1⅛	12.224	12.281	12.230	+0.057	+0.47	+0.006	+0.05

*The measured volumes of the balls were computed from measurements made with a micrometer to ±0.0001 in.

‡The average bulk volume $\overline{V}_b$ and the average solid volume $\overline{V}_s$ were obtained by averaging the values given in Table III.

instrument, connection being made by a coil of tubing with small bore.

Portions of the threads on the cap and barrel have been removed, so the cap may be dropped in place and tightened with about a one-quarter turn. A zero adjuster has also been added by some, in the form of an adjustable reservoir of mercury attached to the main reservoir.

THE OILWELL RESEARCH POROSIMETER

Description and Operation

A schematic sketch of the Oilwell Research Porosimeter is shown in Fig. 2.

It consists of the 12-in. gauge *A* connected to the sample chamber *H* through the needle valve *K*. Similar valves *J* and *L* are also in the line to control the flow of a gas, such as helium, into the gauge and to exhaust the gas from the sample chamber. This is equivalent to two interconnected chambers, with the Bourdon tube of the gauge and the connecting lines being one, and the sample chamber and connecting lines being the other. Valves *M* and *N* have been added since the original calibration, to permit adjustment of the zero point by altering the amount of either valve stem included in the system.

In operation, helium is forced into the gauge chamber until the needle *B* on the dial attains the "start" position (100.00 psi), as seen through the illuminated eye piece *C* mounted on a swivel attached to the gauge. This reading of the gauge, as well as all others, is made while the attached buzzer *D* is in operation, to eliminate the effect of friction on the position of the needle. The gas is then expanded into the sample chamber and the position of the needle is noted. This reading, together with the calibration table, yields the volume of the sand grains and disconnected voids of the sample contained in the chamber.

The sample chamber may be opened or tightly sealed by means of the hinged yoke *G* and the hand screw *E*. These operations may be made very rapidly, as the thrust bearing *F* is so close to the top of the yoke that only three or four turns of the screw are required. In addition, the hinge of the yoke is automatically stopped at the proper position. Speed of operation is also increased by the presence of the removable sample holder *I*.

The seal at the cap of the sample chamber is obtained with an O-ring gasket, while metal-to-metal contact restricts any change in the volume of the sample chamber.

The gauge dial has 360 graduations equally spaced throughout a range which is equivalent to 48 to 82 psi, although the markings on the graduations bear no direct relation to pressure. The illuminated eye piece, with hairline, permits locating the position of the needle to the nearest half division, with no difficulty.

Calibration and Accuracy

The Oilwell Research Porosimeter was calibrated by means of chrome-alloy ball bearings that had been measured to 0.0001 in. with a micrometer. Combinations of the ball bearings were used so as to increase the total volume in increments of about 0.2 cc throughout the range from 1.072 to 10.970 cc. The range was similarly extended to 13.555 cc by using combinations of the ball bearings with two steel cylinders.

This method of calibration minimizes errors due to deviations of the gas from the perfect gas law, as well as errors due to uncertainties involved in assigning a definite value of pressure to each graduation on the dial and errors due to changes in the volume of the Bourdon tube. All that is required is to determine, with the desired accuracy, what sand volume is represented by each graduation on the dial, when the instrument is operated under the given conditions.

Readings made during calibration were corrected to a zero point of 8.40 by adding to the reading the difference between 8.40 and the measured or interpolated zero point. The zero point is the reading obtained when the helium gas is expanded into the empty chamber. This reading has been found to change gradually, during a series of measurements, from a value not less than 8.20 to a value not exceeding 8.95. Since obtaining the data given in the tables, the necessity of making the correction has been eliminated by installing zero adjusters in the system. It has also been found that the change in zero point may be decreased considerably, in a non-thermostated room, by removing the sample holder when the instrument is not in use.

The corrected readings were plotted against the ball volumes on a scale sufficiently large to produce a curve four feet in length. Curve readings were obtained by determining from this curve the reading which corresponded to the ball volume. The difference between the corrected reading and the curve reading gives an indication of the accuracy to be expected from the instrument. Unfortunately, space permits including only the following analysis of the calibration data.

The differences between the corrected reading and the curve reading conform very well to the normal curve of errors, and the standard deviation amounts to 0.073. Consequently, 90 per cent of all readings made with the instrument in a similar manner should lie within ± 0.12 units of the true reading. This statistical analysis of the 90 single readings made during calibration is well supported by the pairs of readings of the same volumes, taken on different days. Not a single one of the 17 pairs of readings taken in this manner differs by more than 0.10 units.

It was apparent from the data that the errors in readings are relatively independent of the volume of the test piece. Accordingly, the percentage error increases with decreasing

Table V — Data Obtained by Oilwell Research Porosimeter with Test Pieces and Cores

Sample	Reading*	Solid Vol., V_s, cc	Reading*	Solid Vol., V_s, cc
⅞″ ball	23.00	5.77	23.10	5.80
$\frac{15}{16}$″ ball	26.90	7.08	26.90	7.08
1⅛″ ball	44.50	12.22	44.50	12.22
1″ cylinder	43.50	11.97	43.60	12.00
¾″ core	30.10	8.12	30.10	8.12
1″ core	32.60	8.90	32.60	8.90
1″ alundum	31.80	8.65	31.80	8.65
1⅛″ alundum	43.00	11.84	43.00	11.84

*The zero point was maintained at 8.40 by using the zero-point adjuster after each pair of determinations, as well as just before and just after the series of measurements was made.

volume. Multiplying the deviation of ± 0.12 by the rate of change in volume with respect to reading yields at 12.210 cc and 4.002 cc, for example, the respective differences of ± 0.030 cc or ± 0.25 per cent and ± 0.044 cc or ± 1.1 per cent.

Transforming these limits to differences in porosity, a core with a sand-grain volume of 12.00 cc and a pore volume of 3.00 cc should yield a value for porosity of 20.0 ± 0.2 per cent, providing the sand-grain volume were measured in the instrument and the bulk volume were known exactly. Under the same conditions a core with a sand-grain volume of 4.00 cc and a pore volume of 1.00 cc should yield a value for porosity of 20.0 ± 0.9 per cent. Single measurements should be within these limits of error 90 per cent of the time and the limits could be still further reduced by using the average of several measurements.

A test was made of the accuracy of the device by measuring the solid volumes of the same test pieces and cores that were used in obtaining a measure of the accuracy of the Kobe Porosimeter. Three steel ball bearings and one steel cylinder were included. Cylindrical cores were also used, two of California oil sands and two of alundum. The data have been compiled in Table V.

Table VI lists the deviations in measurements made with the Oilwell Research Bulkvolumeter and Porosimeter, while Table VII shows the errors made in determining the volumes of the ball bearings by means of these devices. The deviations and errors are in keeping with the analysis made of the accuracy of the porosimeter. Space does not permit a discussion of the bulkvolumeter.

The measurements of the cores with the Oilwell Research Porosimeter and Bulkvolumeter have been compared in Table VIII with those obtained with the Kobe Porosimeter. As seen there, the differences are within the limits of the experimental errors that have been given for each of the instruments. ★ ★

Table VI — Deviations in Measurements with Oilwell Research Bulkvolumeter and Porosimeter

Sample	Bulk Volume V_b, cc		Solid Volume V_s, cc		Porosity P, %		Differences ΔV_b, cc	ΔV_s, cc	ΔP, %
⅞" ball	5.728	5.797	5.77	5.80	–0.73	–0.05	+0.069	+0.03	+0.68
$\frac{15}{16}$" ball	7.120	7.051	7.08	7.08	0.56	–0.41	–0.069	±0.00	–0.97
1⅛" ball	12.232	12.180	12.22	12.22	0.10	–0.41	–0.052	±0.00	–0.51
1⅛" cylinder	11.938	11.964	11.97	12.00	–0.27	–0.30	+0.026	+0.03	–0.03
¾" core	9.492	9.497	8.12	8.12	14.45	14.50	+0.005	±0.00	+0.05
1" core	11.807	11.807	8.90	8.90	24.62	24.62	±0.000	±0.00	±0.00
1" alundum	13 318	13.292	8.65	8.65	35.05	34.92	–0.026	±0.00	–0.13
1⅛" alundum	14.833	14.907	11.84	11.84	20.18	20.57	+0.074	±0.00	+0.39

Table VII — Errors in Measurements of Ball Bearings with Oilwell Research Bulkvolumeter and Porosimeter

Diameter of Ball, in.	Meas.* Vol., V_m, cc	Avg.‡ Bulk Vol., $\overline{V}_b$, cc	Avg.‡ Solid Vol., $\overline{V}_s$ cc	$\overline{V}_b - V_m$ cc	%	$\overline{V}_s - V_m$ %	cc
⅞	5.750	5.762	5.785	+0.012	+0.21	+0.035	+0.61
$\frac{15}{16}$	7.068	7.086	7.08	+0.018	+0.25	+0.012	+0.17
1⅛	12.224	12.206	12.22	–0.018	–0.15	–0.004	–0.03

*The measured volumes of the balls were computed from measurements made with a micrometer to ±0.0001 in.

‡The average bulk volume $\overline{V}_b$ and the average solid volume $\overline{V}_s$ were obtained by averaging the values given in Tables VI and V, respectively.

Table VIII — Comparison of Core Measurements Made by Kobe Porosimeter and by Oilwell Research Bulkvolumeter and Porosimeter

Sample	Avg. Bulk Vol., $\overline{V}_b$ Kobe, cc	O.R., cc	Avg. Solid Vol., $\overline{V}_s$ Kobe, cc	O.R., cc	Avg. Porosity $\overline{P}$ Kobe, %	O.R., %	$\Delta\overline{V}_b$, cc	$\Delta\overline{V}_s$, cc	$\Delta\overline{P}$, %
¾" core	9.532	9.495	8.03	8.12	15.77	14.48	–0.037	+0.09	–1.29
1" core	11.797	11.807	8.83	8.90	25.14	24.62	+0.010	+0.07	–0.52
1" alundum	13.357	13.305	8.68	8.65	34.99	34.98	–0.052	–0.03	–0.01
1⅛" alundum	14.972	14.870	11.83	11.84	20.98	20.37	–0.102	+0.01	–0.61

T.P. 2932

PHASE EQUILIBRIA IN HYDROCARBON-WATER SYSTEMS

II – The Solubility of Ethane in Water at Pressures to 10,000 psi

O. L. CULBERSON* AND **J. J. McKETTA, JR.,**** MEMBER AIME, DEPARTMENT OF CHEMICAL ENGINEERING,
THE UNIVERSITY OF TEXAS, AUSTIN, TEX.

ABSTRACT

A preliminary investigation was made to determine the time required to attain equilibrium within the equilibrium cell for this system.

Experimental and smoothed data are presented for the solubility of ethane in water for temperatures of 100°, 160°, 220°, 280° and 340°F at pressures to 10,000 psia.

The minimum solubility phenomenon disappears at 10,000 psia within this temperature range.

INTRODUCTION

As a continuation of the investigation of the behavior of hydrocarbon-water systems, the experimental data on the solubility of ethane in water have been extended to 10,000 psia. The experimental apparatus, technique, materials, and analytical methods are essentially the same as previously reported.[1]

TIME-CONCENTRATION STUDY

Prior to the initial determinations of solubility in the ethane-water system, it was desired to establish the time

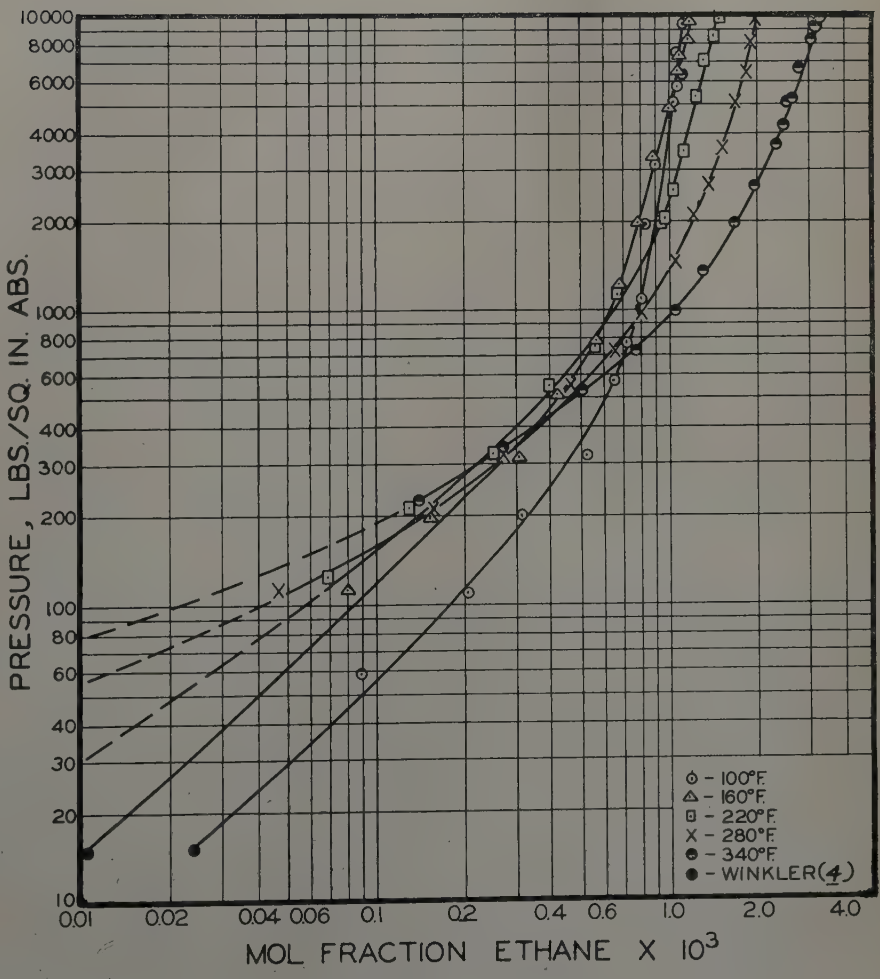

FIG. 1 — SOLUBILITY OF ETHANE IN WATER AT CONSTANT TEMPERATURE.

---

*Gulf Research & Development Co., Harmanville, Pa.

**Associate Professor of Chemical Engineering.

[1] References given at end of paper.

Manuscript received at the office of the Petroleum Branch, March 14, 1950. The first of this series of papers by the authors may be found on Page 1, Vol. 189, *Trans.* AIME, 1950.

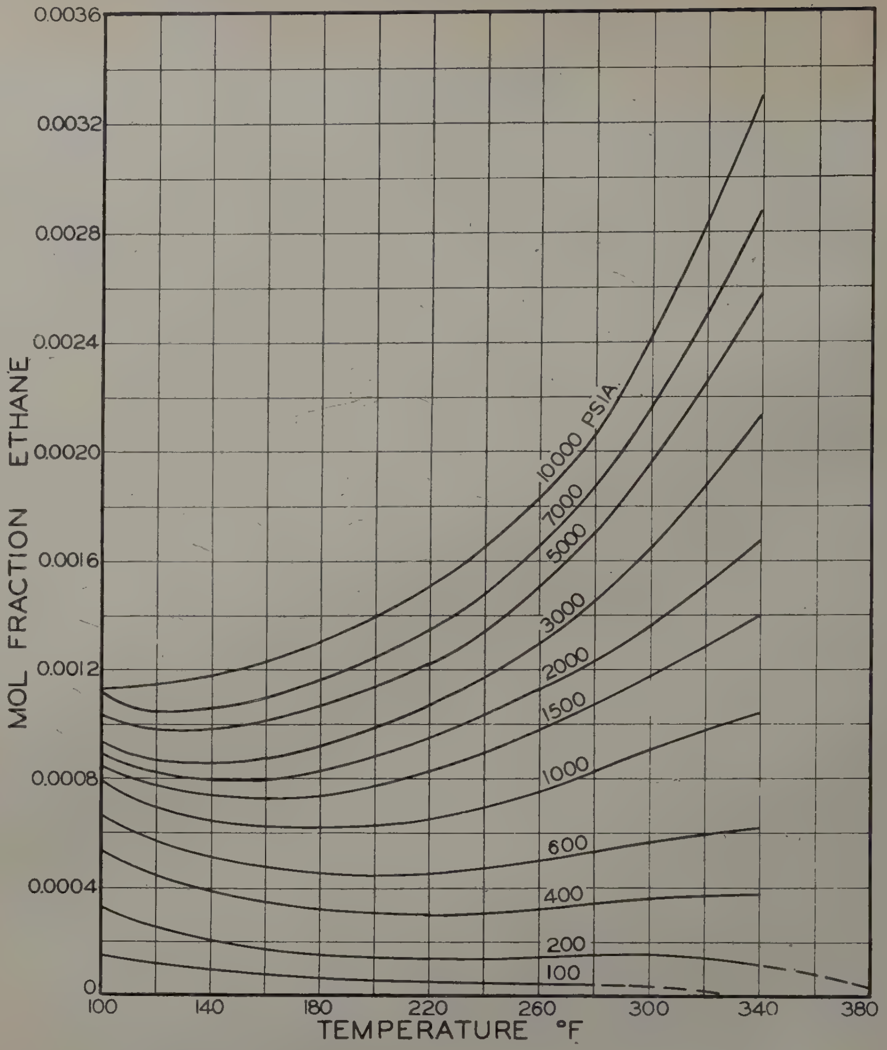

FIG. 2 — SOLUBILITY OF ETHANE IN WATER AT CONSTANT PRESSURE.

necessary to agitate the liquid and vapor at equilibrium temperature and pressure in order to have equilibrium between the phases. This was done by bringing the equilibrium cell to the equilibrium temperature, charging it with ethane to a pressure of 800 psia, and then charging with water to a pressure which was the same for each time-solubility determination. The temperature of the determinations was 100°F and the pressure, having been 6,330 psia for the first determination, was maintained at this same value on each subsequent determination. When the water was charged to the equilibrium cell, the cell temperature departed from 100°F and a period of time averaging about 40 minutes had to elapse before the cell came back to equilibrium temperature. During this time, the cell and its contents were not agitated. When the system had returned to equilibrium temperature, agitation was started and timing was begun. The results of the time-solubility determinations are given in Table I. Reading down a column in Table I, the figures represent respectively: the time of agitation for the particular run; the time at which water was charged to the cell, taken as zero; the time elapsing after charging the water and until the cell returned to equilibrium temperature where agitation was begun; the hours relative to zero time elapsing before agitation was stopped; and the solubility determined for the particular run. Since the ethane and water were in contact during the period when the temperature was returning to the equilibrium temperature, the time measured against the solubility values determined is not a true measure. Considerable diffusion undoubtedly occurred under the pressures involved; however, the technique used was necessary in view of the fact that for the shorter runs, the system may not have been at equilibrium temperature when the desired time had elapsed. From Table I it may be seen that equilibrium was attained within one hour after agitation was begun. Regardless of the indications toward a shorter agitation period, in subsequent determinations the system was agitated for three hours before a sample was taken.

Table I — Time-Concentration Determinations for Ethane in Water (100°F, 6330 psia)

Agitation Time, Hours	Elapsed Time, Hours				
	½	1	2	3	10
Water Charged	0.00	0.00	0.00	0.00	0.00
Agitation Begun	0.67	0.50	0.33	1.67	1.00
Agitation Stopped and Sample Taken	1.17	1.50	2.33	4.67	11.00
Solubility, *MF* C_2H_6*	0.001047	0.001122	0.001100	0.001107	0.001102

*Concentration in mole fraction ethane.

SOLUBILITY DATA

The solubility of ethane in water has been experimentally determined for temperatures of 100°, 160°, 220°, 280°, and 340°F at pressures extending to 10,000 psia. These data are shown in Table II and in Fig. 1 along with data previously reported.[1] The data for the entire range of pressures are cross-plotted in Fig. 2. From the curves in Figs. 1 and 2, the smoothed data are presented in Table III. It was necessary to adjust the smoothed values previously reported for the lower pressure range[1] in order to tie in the solubilities determined for the higher pressures.

The behavior of the ethane-water system in the vapor-liquid region as represented by Fig. 2 indicates a minimum solubility zone at pressures to about 9,000 psia. Although there is no maximum solubility indicated in Fig. 3 for pressures above 300 psia, it seems reasonable to expect a maximum in the isobaric curves at higher temperatures since the concentration of the solute is zero when the solvent is at its saturation temperature and pressure. For example, water has a vapor pressure of

2,000 psia at a temperature of 635.82°F.[3] Therefore, although the 2,000 psia isobar of Fig. 2 indicates an increasing solubility with increasing temperatures, at some temperature this isobar must reach a maximum in order to approach zero at 635.82°F. The maximum concentrations at pressures below 300 psia are shown in Fig. 2 and have been discussed earlier.[1] From Fig. 2 one can see that the temperature at which minimum solubility occurs on an isobar decreases as the pressure for the isobar increases. Although the limited temperature range of this work prevents the appearance of maximum solubilities at pressures above 300 psia, one might expect that the temperatures for the maximum solubility would increase as the pressure for the isobar increases.

The solubility of ethane in water is given on a volumetric basis in Fig. 3 and is compared to the data of Dodson and Standing[2] for the solubility of natural gas in water. In Fig. 3 the solubility is given in cu ft of the vapor (at 60°F and 14.7 psia) per bbl of water at the same conditions. The natural gas used by Dodson and Standing contained 88.51 per cent methane and only 6.02 per cent ethane. The difference in the solubilities of ethane and natural gas in water indicates that the solubility characteristics of methane and ethane are vastly different. As may be seen from Fig. 3, at 5,000 psia the solubility of methane in water may be approximately two times the solubility of ethane in water.

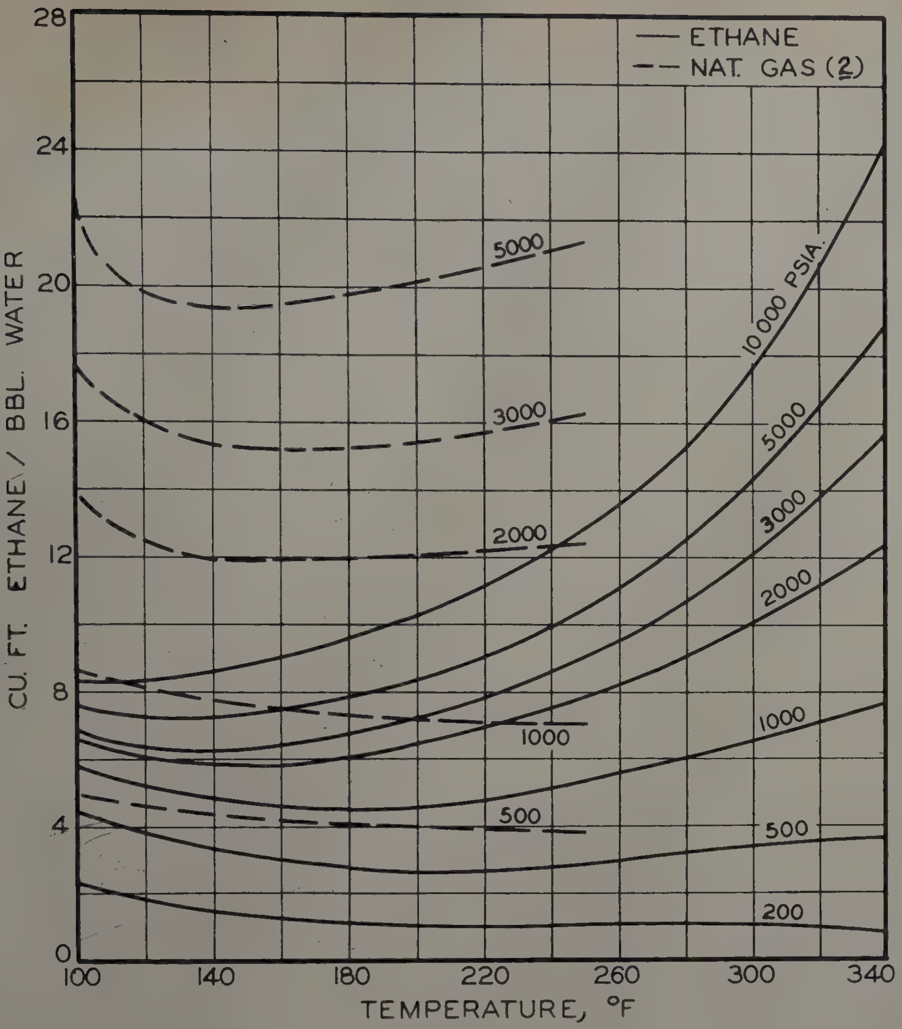

FIG. 3 — VOLUMETRIC SOLUBILITY OF ETHANE IN WATER REFERRED TO 60°F AND 14.7 PSIA.

Table II — Experimental Values for the Solubility of Ethane in Water

Pressure: Lb/Sq. In. Abs.

Solubility: Mol Fraction C_2H_6

100°F		160°F		220°F		280°F		340°F	
Pressure	MF C_2H_6	Pressure	MF C_2H_6	Pressure	MF C_2H_6	Pressure	MF C_2H_6	Pressure	MF C_2H_6
59	0.0000893	113	0.0000812	123	0.0000698	113	0.0000475	226	0.000140
110	0.0002040	196	0.0001540	212	0.0001300	210	0.0001580	334	0.000261
200	0.0003110	315	0.0003090	322	0.0002560	320	0.0002720	529	0.000503
340	0.000521	512	0.000417	548	0.000391	557	0.000464	737	0.000770
568	0.000647	785	0.000570	752	0.000560	736	0.000660	992	0.001039
767	0.000709	1215	0.000679	1120	0.000661	979	0.000803	1370	0.001311
1080	0.000801	1985	0.000788	1965	0.000944	1470	0.001065	1985	0.001671
1925	0.000821	3275	0.000895	2030	0.000964	2105	0.001208	2605	0.001970
3115	0.000890	4885	0.001011	2535	0.001042	2680	0.001384	3640	0.002325
5035	0.001018	6485	0.001078	3455	0.001132	3585	0.001530	4285	0.002480
5800	0.001066	7350	0.001100	5320	0.001249	5045	0.001703	5035	0.002515
6330	0.001105	8330	0.001178	7010	0.001329	6465	0.001867	5250	0.002635
7605	0.001060	9650	0.001166	8480	0.001434	8055	0.001901	6630	0.002790
9455	0.001130			9935	0.001514	9775	0.002005	8320	0.003060
								9335	0.003200
								9835	0.003300

ACKNOWLEDGMENT

The writers wish to express their appreciation to the Gulf Oil Corp. for extending the Gulf Oil Fellowship to O. L. Culberson for this investigation. The Phillips Petroleum Co. generously supplied the research grade ethane used in this work.

REFERENCES

1. Culberson, Horn and McKetta: *Trans.* AIME, (1950) **189,** 1.
2. Dodson and Standing: *API Drill. and Prod. Prac.,* (1944) 173.
3. Keenan and Keyes: *Thermodynamic Properties of Steam,* John Wiley and Sons, (1936) 39.
4. Winkler: *Z. Physik. Chem.,* (1899) **9,** 171.

★ ★ ★

Table III — Smoothed Values for the Solubility of Ethane in Water
Mole Fraction C_2H_6 x 10^3

Pressure, psia	100°F	160°F	220°F	280°F	340°F
200	0.328	0.173	0.144	0.151	0.110
400	0.534	0.348	0.299	0.341	0.370
600	0.667	0.478	0.449	0.528	0.620
800	0.749	0.569	0.559	0.697	0.841
1000	0.793	0.628	0.647	0.825	1.039
1250	0.822	0.683	0.742	0.962	1.236
1500	0.849	0.729	0.823	1.071	1.395
2000	0.888	0.788	0.955	1.229	1.677
2500	0.915	0.831	1.020	1.341	1.920
3000	0.933	0.873	1.073	1.440	2.127
3500	0.959	0.913	1.121	1.518	2.291
4000	0.982	0.951	1.163	1.582	2.413
4500	1.009	0.986	1.192	1.640	2.498
5000	1.032	1.014	1.222	1.698	2.571
6000	1.080	1.060	1.287	1.791	2.721
7000	1.112	1.098	1.350	1.867	2.867
8000	1.126	1.142	1.412	1.930	3.011
9000	1.129	1.187	1.464	1.998	3.154
10000	1.133	1.228	1.500	2.063	3.290
14.7	0.0240*	0.0105*			

*Winkler.

T.P. 2933

RELATIVE PRODUCTIVITY OF PERFORATED CASING - II

ROBERT A. HOWARD AND **MARSH S. WATSON, JR.,** JUNIOR MEMBER AIME, UNIVERSITY OF OKLAHOMA, NORMAN, OKLAHOMA

ABSTRACT

The effect of depth of formation penetration by casing perforations has been studied by means of an electrolytic model. It is found that the relative productivity of perforated casing is profoundly affected by the depth to which the formation is penetrated. The first in. of penetration is of especial importance. A scaling equation which was shown to agree with experimental results at zero penetration is used to calculate the relative productivity of a scaled down casing with scaled down perforations.

INTRODUCTION

In an earlier paper[1] the authors showed that the point sink representation of casing perforations is inadequate. It was pointed out at that time that while the electrolytic model results were a marked improvement over point-sink calculations, they still left a great deal to be desired in that the electrolytic model represented a case not realizable in practice, namely, a clean hole through the casing but undisturbed formation on the other side of the casing. Obviously, to be effective, the perforation must penetrate a finite distance into the producing formation. It was the purpose of the present investigation to find how the relative productivity of perforated casing varies with depth of penetration.

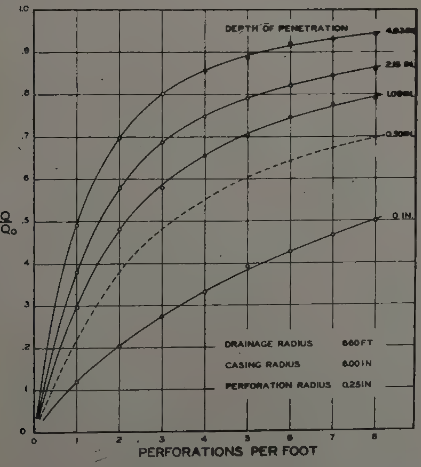

FIG. 1 — VARIATION IN RELATIVE PRODUCTIVITY WITH PERFORATION DENSITY FOR 12-IN. CASING WITH 0.5-IN. DIAMETER PERFORATIONS FOR VARIOUS PENETRATION DEPTHS.

The term "depth of penetration" as used in this paper refers to the distance which the perforation penetrates the producing formation. The amount of casing and cement penetrated is not taken into account, a fact which is discussed more fully later. The "casing radius," therefore, is to be interpreted as the radius of the boundary between cement and formation wall, in cases where the casing is not in contact with the formation wall.

APPARATUS

The electrolytic model experimental setup was identical with that described in the previous paper[1] except that the platinum electrodes were now allowed to project from the lucite cylinder by varying amounts. When fewer than eight electrodes were used, the unused ones were covered with a coat of insulating material to minimize disturbances to the current flow-lines. Comparison runs made with the unused electrodes uninsulated, however, showed that the values of Q/Q_o so obtained did not vary by more than the experimental error from the values obtained with the unused electrodes insulated.

RESULTS

The variation of relative productivity* with perforation density is shown for various penetration depths from 0 to 4.03 in. in Fig. 1. It will be seen that even one in. of penetration into the formation results in a huge increase in the relative productivity. Moreover, as the depth of penetration increases, it becomes less and less advantageous to use large perforation densities, 80 per cent of open hole productivity being obtained with only three 0.5-in. diameter holes per foot when the penetration is 4.03 in.

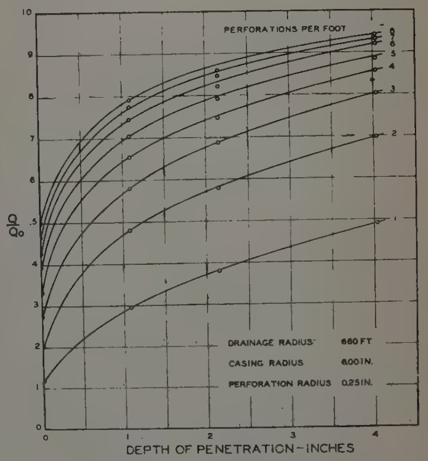

FIG. 2 — VARIATION IN RELATIVE PRODUCTIVITY WITH DEPTH OF PERFORATION PENETRATION FOR 12-IN. CASING WITH 0.5-IN. DIAMETER PERFORATIONS FOR VARIOUS PERFORATION DENSITIES.

---

[1] Reference given at end of paper.

Manuscript received in the office of the Petroleum Branch March 10, 1950.

*Relative productivity is defined here as the ratio of the production through the perforations to the production through an uncased hole of the same radius as the "casing radius." This ratio does not correspond exactly to actual field conditions, for the comparison between rates of flow in the cased and uncased hole assumes the same pressure differential between the outer boundary and the well bore in each case. Since fluid friction will cause a pressure drop along the casing or tubing which is proportional to the rate of flow, the pressure at the formation face will not be quite the same in the two cases.

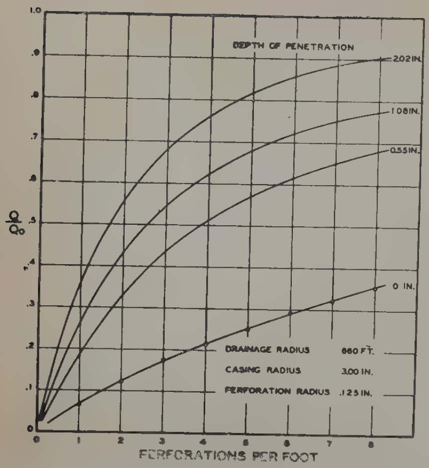

FIG. 3 — VARIATION IN RELATIVE PRODUCTIVITY WITH PERFORATION DENSITY FOR 6-IN. CASING WITH 0.25-IN. DIAMETER PERFORATIONS FOR VARIOUS PENETRATION DEPTHS.

Fig. 2 shows the variation of relative productivity with depth of perforation penetration for various perforation densities from 1 to 8 per ft. From these curves it is evident that the initial in. of penetration is, relatively, much more important than an additional in. of penetration.

The platinum electrodes used in this work had a conductivity about 2 x 10^8 times that of the electrolyte, so that they could be considered to be effectively perfect conductors, corresponding, therefore, to perforation holes offering no flow resistance. Under such circumstances one would expect, from theoretical considerations, that the productivity would increase without limit as the depth of penetration is increased. The flattening of the curves of Fig. 2 at the greatest depth of penetration is an indication that this expectation would be borne out by electrolytic model studies if the penetration depths were increased. Since the perforation hole does offer a small flow resistance, the productivity will, in actual practice, approach a limiting value as the depth of penetration is increased. It is altogether possible, however, that the productivity from perforated casing may exceed 100 per cent of open hole production even when the flow resistance of the perforation hole is taken into account. This will certainly be true in the case of formations of low permeability.

It has previously been shown that one may construct an approximate formula for computing the relative productivity of perforated casing when the dimensions of casing and perforation hole are each k times those for which the variation of relative productivity is known. The equation which was obtained was

$$\left(\frac{Q}{Q_o}\right)' = \frac{1}{1 + \dfrac{\dfrac{1}{Q/Q_o} - 1}{k\left(1 - \dfrac{\ln k}{\ln r_e/r_w}\right)}}$$

Where

$(Q/Q_o)'$ is the desired relative productivity,

Q/Q_o is the relative productivity which is known for certain casing and perforation radii

r_e is the drainage radius for the known case

and r_w is the casing radius for the known case. Fig. 3, which shows the variation in relative productivity with perforation density for various penetration depths for 6-in. casing with .25-in. diameter perforations, was obtained from calculations using the above formula and the experimental results shown in Fig. 1. Fig. 4, using the results of the calculations for Fig. 3, shows the variation in relative productivity of 6-in. casing with 0.25-in. diameter perforations with depth of penetration for various perforation densities.

CONCLUSIONS

Since the curves of Figs. 2 and 4 are very steep for small depths of penetration, it will be seen that, if the permeability of the formation very near the well bore is in any way markedly reduced during completion of the well, the effective depth of penetration will be reduced and the productivity appreciably lessened. Obviously any plugging of the shot holes which results in appreciable resistance to the flow of fluids through them will result in markedly decreased productivity. Finally, the reader is reminded that such electrolytic model studies as this represent the flow of a single, homogeneous, incompressible fluid through an isotropic permeable formation.

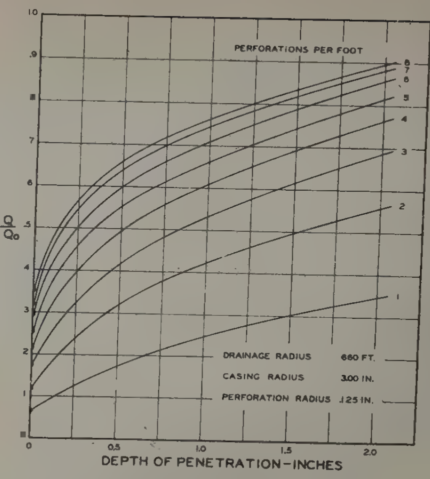

FIG. 4 — VARIATION IN RELATIVE PRODUCTIVITY WITH DEPTH OF PERFORATION PENETRATION FOR 6-IN. CASING WITH 0.25-IN. DIAMETER PERFORATIONS FOR VARIOUS PENETRATION DENSITIES.

ACKNOWLEDGMENT

We are indebted to the Shell Union Oil Company for a fellowship granted to Marsh S. Watson which made possible his graduate work in the Department of Petroleum Engineering and for an equipment grant to cover, in part, the cost of the apparatus used.

REFERENCES

1. R. A. Howard and M. S. Watson: *Trans.* AIME, (1950), 189, 179.

★ ★ ★

T.P. 2939

HIGH PRESSURE WATER INJECTION FOR MAINTAINING RESERVOIR PRESSURES, NEW HOPE FIELD, FRANKLIN COUNTY, TEXAS

ALBERT S. TRUBE, JR., TIDE WATER ASSOCIATED OIL CO., HOUSTON, TEX., AND **SAM N. DeWITT,** SEABOARD OIL CO. OF DELAWARE, DALLAS, TEX., MEMBERS AIME

ABSTRACT

This paper presents a discussion of the pressure maintenance operations which were begun in the New Hope Field, Franklin County, Texas, in 1944. The project has required the injection of extraneous waters at depths from 7,300 to 8,000 ft with intake well-head pressures up to 4,000 psi in three different reservoirs — the Bacon, Hill, and Pittsburg.

Records of oil and water production, water injection and the GOR have been kept for each reservoir and reservoir pressures were taken at regular intervals. These data indicate that the Bacon Reservoir had no apparent water encroachment up to the time of water injection. However, the Pittsburg and Hill reservoirs had some natural water influx but not sufficient to prevent pressures from declining below the bubble point. The Bacon and Hill reservoirs responded almost immediately to water injection, while the Pittsburg, which is the least permeable, has shown good pressure response only since August, 1948.

The principle objective of the project has been to increase ultimate recovery. Success of the project to date also has resulted in reduced lifting costs. Estimates based on the initial water break-through patterns indicate that the primary objective of substantial additional recovery will be accomplished, and there is a possibility that the original estimates of oil recovery with pressure maintenance will be exceeded.

INTRODUCTION

This pressure maintenance project was one of the earliest primary pressure maintenance programs to be attempted on a multiple zone field. There are three producing reservoirs into which water is being injected for the purpose of maintaining pressure and increasing the ultimate recovery from each. This paper is limited in scope to an account of the development of the project, the pressure production relationship prior to the injection of water and the effect of water injection on the producing reservoirs. Also discussed are the nature of the injection system and the indicated results on initial water break-through in the Bacon Reservoir.

FIELD CONDITIONS

The New Hope Field, which is located about 12 miles northeast of Winnsboro, Franklin County, Texas, is an elongated symmetrical anticline containing four known oil reservoirs. The reservoirs are of the Trinity group of the Comanchean or Lower Cretaceous period and are found in Table I.

The oil productive portion of each reservoir is not present in all of the producing wells because their areas and positions vary with respect to one another. Fig. 1 shows the relative position of the four reservoirs and illustrates how some wells could penetrate all four, while others are restricted to three, two, or perhaps one, depending on structural location. The first three reservoirs contain undersaturated oil. The deepest, the Elledge, has a primary gas cap. Although this reservoir covers a considerable area of the field, it has a very thin section and a low order of permeability. Elledge producing wells have generally been characterized by an early increase in GOR, making it necessary to recomplete them in other reservoirs. (At present, one well is completed in the Elledge, which is still producing.) Because of the difficulties encountered in producing oil from this reservoir, and the small quantity of oil actually present, future attempts at producing it will probably be on a salvage basis during the later life of the program. For this reason, the remainder of this report will be confined to a discussion of the Bacon, Hill and Pittsburg reservoirs.

---

[1] References given at end of paper.

Manuscript received in the office of the Petroleum Branch September 10, 1949.

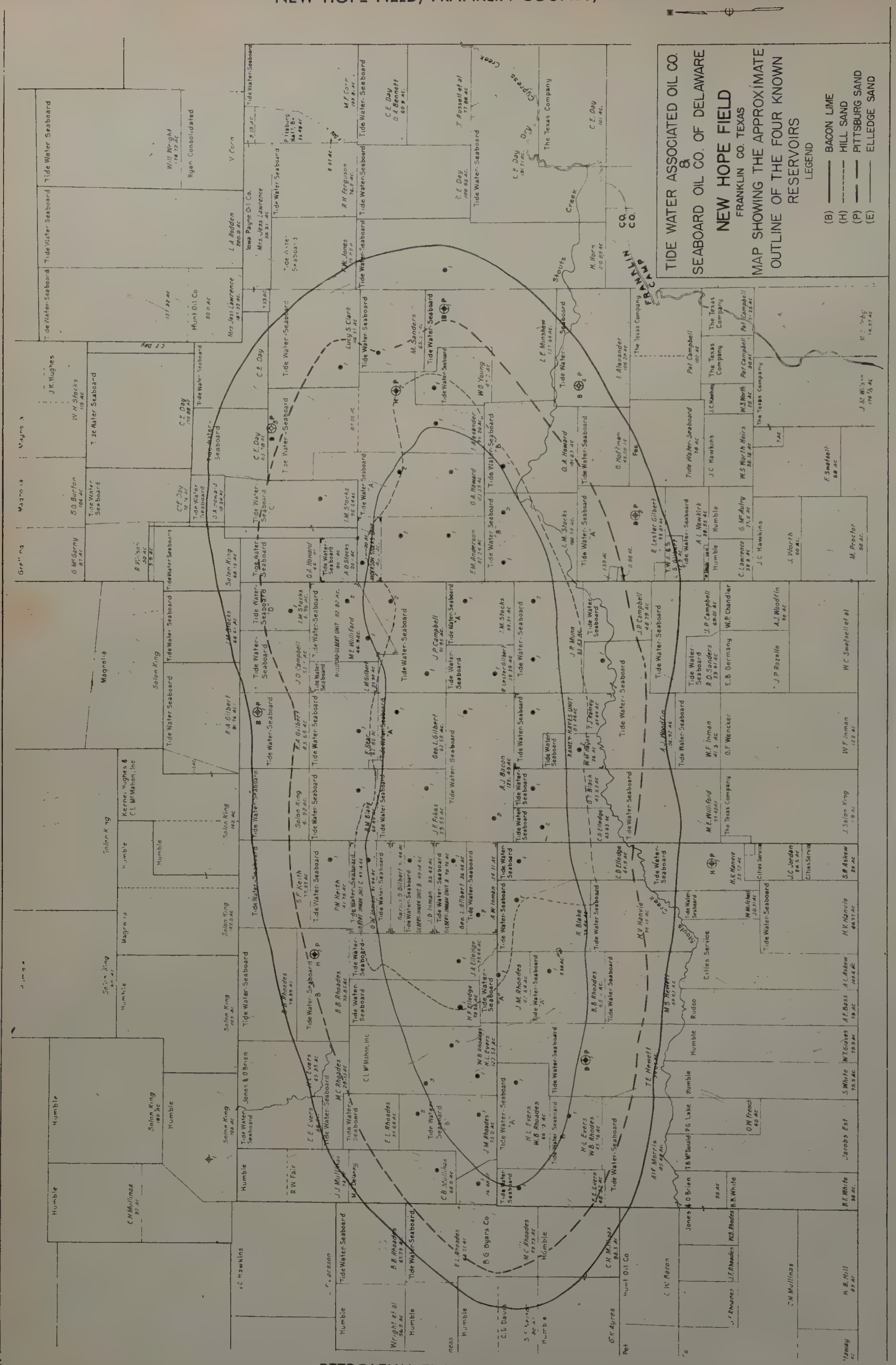

FIG. 1 —MAP SHOWING THE APPROXIMATE OUTLINE OF THE FOUR KNOWN RESERVOIRS, NEW HOPE FIELD.

Table I

Reservoir Name	Type Formation	Average Depth Ft	Estimated Productive Area—Acres
Bacon	Oolitic Limestone	7,300	4,609
Hill	Sandstone	7,400	1,284
Pittsburg	Sandstone	7,900	3,304
Elledge	Sandstone	8,200	2,890

The location of the reservoirs with respect to each other has been conducive to dual completions. Fifty-nine producing wells have been drilled in the field to date; not included in this figure are two non-commercial Bacon producing wells, and one dry hole, each of which was converted into a water injection well. Two wells which were drilled as injection wells are not included. Three of the 59 producing wells have been converted into water injection wells, making a total of 56 producing wells and nine dual water injection wells as of October, 1950. Most of these 56 have been dually completed at one time or another and at the present time there are still 11 dually completed producing oil wells, while eight of the nine injection wells are also used as dual water injection wells.

The data in Table II represent average values which have been obtained from an analysis of many samples of the producing formations, all of which were cored with water base drilling mud. Electric logs were made on all wells prior to setting casing, which in turn has furnished an additional means of checking the position and content of the various reservoirs. Representative bottom hole oil samples were obtained early in the life of each reservoir and these data have also provided a valuable basis for evaluating reservoir behavior. The estimated quantities of original oil in place in each of these reservoirs are based on the above factors, all of which have been well established on a statistical basis.

Using the oil in place value and the compressibility of the saturated oil (Items 8 X 15), the volume of stock tank oil production per pound drop was determined for each reservoir and is shown in Item 19. Item 19 represents the expected behavior of all of the stock tank oil in place between original and saturation pressure if no water drive is present. In this determination, errors are introduced by neglecting the change in formation volume factor and by assuming the compressibility factor to be constant over the entire pressure range. These errors are very small, however, in comparison with the substantial differences caused by water encroachment and will be considered negligible in comparing with actual reservoir performance.

PRODUCTION HISTORY

Pressure performance and production data have been recorded and are shown on a semi-annual basis in Tables III, IV, and V, and in graphical form on Figs. 3, 4, and 5. Available data on the Elledge Reservoir are incomplete and are not included in this report. As previously pointed out, the oil in the Bacon, Hill and Pittsburg reservoirs is considerably undersaturated in each case. Because of this, it was possible to determine the presence or lack of water influx in each reservoir, and to show definite need for water injection long before pressures approached the bubble point.

Bacon Lime Reservoir

Referring to Table III and Fig. 3, it can be seen that the rapid rate of pressure decline even with low average producing rates becomes evident at once. Reservoir pressure dropped 365 psi between May 1, 1943, and August 9, 1944, during which time the average producing rate was 436 B/D. During the following period, between August 9, 1944, and April 1, 1945, the reservoir lost 890 psi while averaging 1,229 B/D of oil. In each case, the reservoir

Table II — Characteristics of Reservoir and Contents

Item No.		Bacon Lime	Hill Sand	Pittsburg Sand	Elledge Sand
1.	Zone				
2.	Discovery Date	5-4-43	3-5-44	4-26-43	2-19-44
3.	Well Spacing	440′-900′	440′-900′	440′-900′	440′-900′
4.	Proration Unit, acres per well	40	40	40	40
5.	Interstitial Water, % (1)	25.41	30.58	28.73	35.42
6.	Porosity, % (1)	18.9	16.6	13.4	10.8
7.	Permeability, md (1)	379	390	61.1	17.3
8.	Original Reservoir Pressure, Po, psig	3,425	3,425	3,523	3,741
9.	Saturation Pressure, Ps, psig	907	1,110	1,682	3,741 (2)
10.	Formation Volume Factor at Ps	1.233	1.287	1.456	1.952 (2)
11.	Reservoir Temperature, Tr. F°	203	208	216	217
12.	Reservoir Oil Viscosity at Ps and Tr. cent	0.71	0.73	0.38	—
13.	Stock Tank Oil Gravity, °API	43	45	49	52
14.	Solution Gas/Oil Ratio, cu ft/bbl	256	286	577	1,475
15.	Avg. compressibility of saturated oil between Po and Ps at Tr, bbl per million bbl per psi change in pressure	12.00	13.26	15.30	—
16.	Est. avg. net pay thickness, ft	10.98	13.55	17.30	3.42
17.	Est. avg. initial productivity index, bbl/day/psid	1.2	2.4	0.67	—
18.	Est. volume of original stock tank oil in place. Millions of bbl	44.89	12.84	29.92	2.74
19.	Est. stock tank oil recovery between Po and Ps if no water drive present, bbl./psid. (3)	538	170	458	—

(1) Weighted average from core analysis data.
(2) Elledge reservoir contains a primary gas cap.
Original conditions estimated from available data.
(3) Barrels of stock tank oil per pound per square inch drop in pressure.

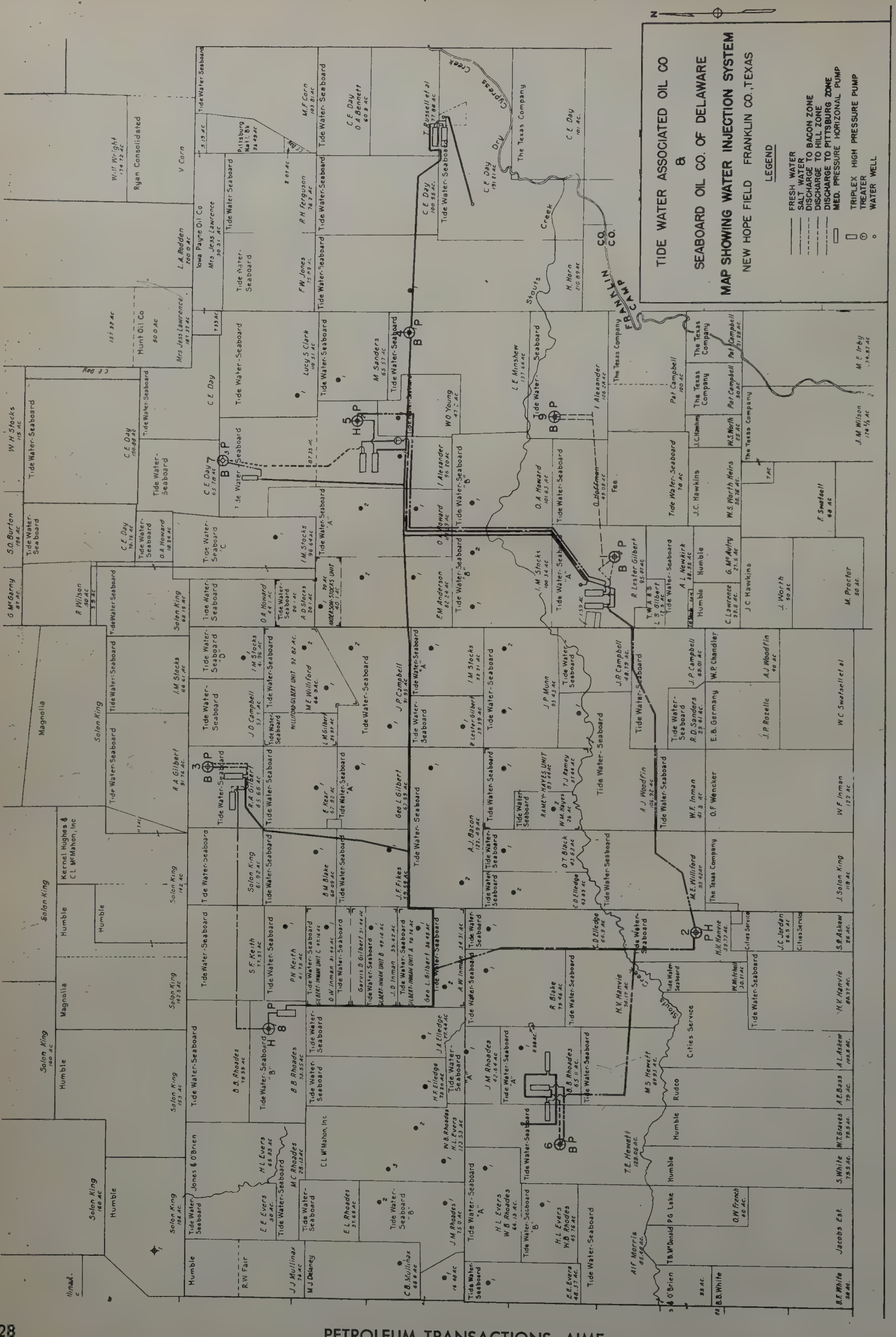
TIDE WATER ASSOCIATED OIL CO
&
SEABOARD OIL CO. OF DELAWARE
MAP SHOWING WATER INJECTION SYSTEM
NEW HOPE FIELD FRANKLIN CO., TEXAS
LEGEND
FRESH WATER
SALT WATER
DISCHARGE TO BACON ZONE
DISCHARGE TO HILL ZONE
DISCHARGE TO PITTSBURG ZONE
MED. PRESSURE HORIZONAL PUMP
TRIPLEX HIGH PRESSURE PUMP
TREATER
WATER WELL
Scale · Feet
1000 0 1000 2000 3000 4000 5000
FRANKLIN CAMP CO.
Dry Cypress Creek
Stouts Creek

FIG. 2 — MAP SHOWING WATER INJECTION SYSTEM, NEW HOPE FIELD.

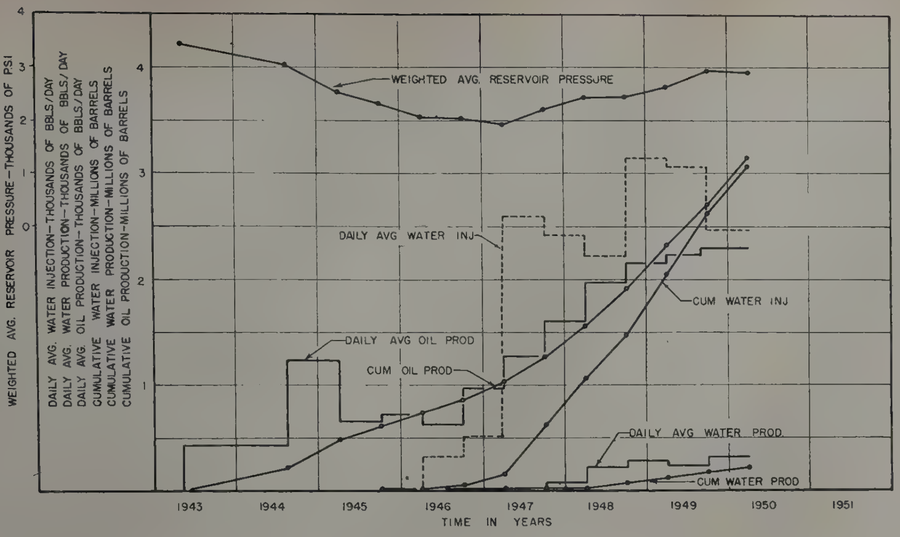

FIG. 3 — PRESSURE AND PRODUCTION STATISTICS FOR THE BACON LIME RESERVOIR.

was producing about 550 bbl of stock tank oil per lb drop. This rate of recovery is remarkably close to the value of 538 bbl psid referred to in Item 19, Table II. The fact that these, and subsequent surveys, showed little change in the rate of recovery was considered a definite sign of little or no natural water influx. This conclusion was necessary even though the average reservoir permeability indicated that at least a partial water drive should develop if such permeability continued out into the surrounding aquifer. It should be noted that the low production pressure drop relationship was consistent until the time water injection began, but that the response to water injection was immediate even though the pressure continued to decline for one year after injection began. During the period October 1, 1946, to April 1, 1947, the production/pressure relationship increased from 570 to 3,076 bbl/psid, or from 555 to 624 bbl/psid on a cumulative basis. Subsequently, as additional injection facilities were installed, the downward pressure trend was reversed and has been increased from the low point of 1,936 psig on April 1, 1947, to 2,913 psig as of April 1, 1950.

The behavior of the producing wells was consistent with the pressure history. As the pressure declined, more and more Bacon wells ceased flowing. As the most shallow reservoir, the Bacon had been used for annulus production in the dual completion program. The Hill producing wells have always flowed but the Pittsburg Reservoir, as will be shown later, was concurrently producing with a high rate of pressure decline. The net effect was that only the Hill wells were available for dual completion and this in turn resulted in greatly curtailed production from the Bacon and Pittsburg. In addition to this, it was obvious that an attempt to produce at high withdrawal rates would surely result in reservoir pressures declining below saturation pressure. The producing rates, therefore, declined to an average of 639 B/D for the Bacon prior to the time definite signs of improvement were shown. With the favorable response to water injection, and the subsequent return of reservoir pressures to higher values, more and more Bacon wells began to flow. All water free Bacon wells are flowing and average reservoir withdrawal rates are at an all-time high of 2,316 B/D.

Hill Sand Reservoir

Table II shows that the permeability of the Hill sand reservoir averages 390 md. This reservoir also has the most favorable distribution of permeability of all the zones. In referring to Table IV and Fig. 4, a contrast between Bacon and Hill reservoir performance is immediately evident. The expected rate

Table III — Pressure and Production Statistics for the Bacon Oolitic Lime Reservoir, New Hope Field

Date	Wtd. Avg. Reservoir Pressure psig	Pressure Change		Cum. Stock Tank Oil Prod. Bbl	Cumulative Wtr. Prod. Bbl	Cumulative Water Inj. Bbl	Time Interval Days	Interval Rate of Prod. or Injection, B/D			Oil Recovery Stock-Tank Bbl/psi Drop	
		Per Interval psi	Cumulative psi					Oil Prod.	Wtr. Prod.	Wtr. Inj.	Per Inter.	Cumulative
5-1-43	3,425			0			—	—			—	—
8-9-44	3,060	—365	—365	203,000			466	436			556	556
4-1-45	2,535	—525	—890	490,540			234	1,229			548	551
10-1-45	2,316	—219	—1,109	611,285			183	656			551	551
4-1-46	2,082	—234	—1,343	744,731	8,640		182	733	48		570	555
10-1-46	2,044	—38	—1,381	861,634	14,317	62,000	183	639	31	339	3,076	624
4-1-47	1,936	—108	—1,489	1,040,085	22,164	158,178	182	981	43	528	1,659	699
10-1-47	2,207	+271	—1,218	1,273,490	29,526	634,790	183	1,275	40	2,604		1,046
4-1-48	2,435	+228	—990	1,566,832	44,823	1,079,157	183	1,603	84	2,428		1,583
10-1-48	2,448	+10	—977	1,928,232	83,803	1,486,965	183	1,975	213	2,228		1,974
4-1-49	2,638	+190	—787	2,322,388	137,567	2,061,695	182	2,166	295	3,158		2,951
10-1-49	2,952	+314	—473	2,732,768	189,092	2,625,083	183	2,243	243	3,079		5,778
4-1-50	2,913	—39	—512	3,154,281	241,547	3,075,713	182	2,316	327	2,476		6,161

of recovery from laboratory data was 170 bbl/psid. (See Table II, Item 19.) The closest approach to this value was 248 bbl/psid which was observed during the first interval between March 5, 1944, and August 8, 1944. Thereafter the rate of recovery increased enormously, averaging 1,147 and 6,061 bbl/psid during the following two intervals. This was very good evidence of the presence of natural water influx. Conclusive evidence was obtained when the producing rate was decreased to 1,027 B/D between October 1, 1945, and April 1, 1946, resulting in a 42 psi increase in reservoir pressure for that period.

The pressure behavior indicates that the natural water influx can sustain only a total outlet of about 1,000 B/D of stock tank oil with no water production. Water injection, therefore, was considered necessary in order to achieve a higher producing rate, to increase ultimate recovery by maintaining reservoir pressure and to control water influx. Water injection was started and, on Table IV and Fig. 4, it should be noted that pressures are now fairly stable around 3,000 psi at an average withdrawal rate of about 1,500 B/D. The bbl/psid relationship becomes meaningless on an interval basis once pressure begins increasing but on a cumulative basis, a tendency for the figure to level off indicates stable conditions. On Table IV it is noted that the cumulative bbl/psid was at a fairly constant value between October 1, 1945, and October 1, 1947. This indicated fairly stable conditions at rates of about 1,000 B/D. Subsequent increase in injection rates resulted in better movement of water into the reservoir, as evidenced by an increase to 3,547 bbl/psid at a 1,510 B/D average withdrawal rate.

Evidence of water influx into the reservoir has also been apparent from the behavior of producing wells located low on the structure. Table IV indicates some water production between October 1, 1945, and October 1, 1946. These wells were subsequently recompleted as Bacon or Pittsburg oil producing wells, and no water was produced during the following year. Beginning with the October 1, 1947, period, however, other edge wells began producing small quantities of water, which has increased steadily and which will probably continue to increase as the reservoir is depleted. Reference to Fig. 2 shows that the Hill reservoir is the smallest of all in area and, because of this, it also contains the fewest number of producing wells — 16 at present. In order to combat the problem of water production from Hill wells, plans are now under way for the injection of water at rates sufficient to return the reservoir pressure at least to its original value. The attainment of this goal would permit the flowing of Hill production to a much higher water cut, resulting in a saving in lifting costs.

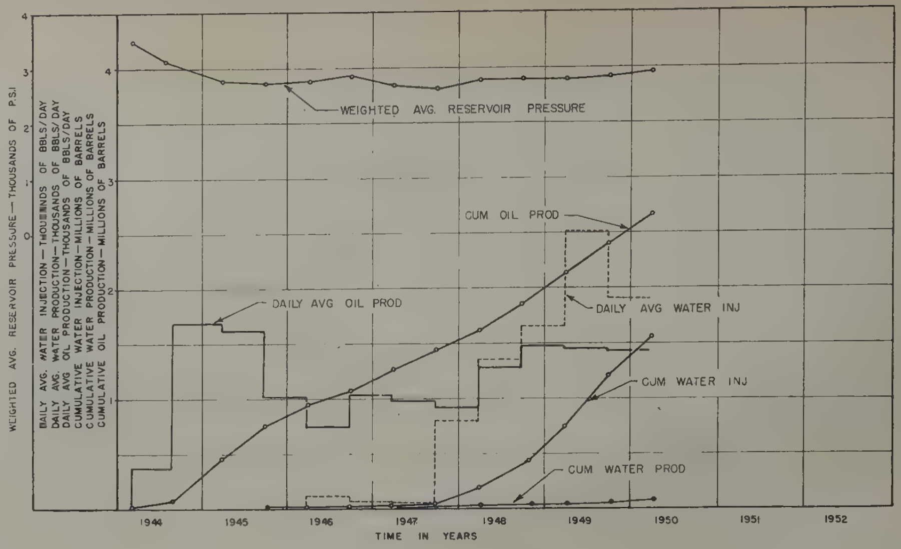

FIG. 4 — PRESSURE AND PRODUCTION STATISTICS FOR THE HILL SAND RESERVOIR.

Table IV — Pressure and Production Statistics for the Hill Sand Reservoir, New Hope Field, Franklin County, Texas

Date	Wtd. Avg. Reservoir Pressure psig	Pressure Change		Est. Volume Cumulative Stock Tank Oil Produced Bbl	Cumulative Water Produced Bbl	Cumulative Water Injected Bbl	Time Interval Days	Interval Rate of Prod. or Injection, B/D			Oil Recovery Stock-Tank Bbl/psi Drop	
		Per Interval psi	Cumulative psi					Oil Prod.	Wtr. Prod.	Wtr. Inj.	Per Inter.	Cumulative
3-5-44	3,425											
8-8-44	3,135	—290	—290	72,000			156	462			248	248
4-1-45	2,789	—346	—636	469,000			234	1,697			1,147	737
10-1-45	2,740	—49	—685	766,000			183	1,623			6,061	1,118
4-1-46	2,782	+42	—643	953,000	3,000		182	1,027	33			1,482
10-1-46	2,872	+90	—553	1,091,000	17,653	27,000	183	754	80	143		1,973
4-1-47	2,717	—155	—708	1,283,000	17,653	43,619	182	1,055	0	91		1,812
10-1-47	2,662	—55	—763	1,465,932	17,653	54,092	183	1,000	0	58		1,921
4-1-48	2,809	+147	—616	1,639,608	19,244	206,150	183	949	9	831		2,662
10-1-48	2,828	+19	—597	1,879,286	23,149	461,199	183	1,310	21	1,394		3,148
4-1-49	2,817	—11	—608	2,156,432	31,764	768,479	182	1,523	47	1,688		3,547
10-1-49	2,894	+77	—531	2,428,662	38,842	1,234,059	183	1,488	39	2,544		4,574
4-1-50	2,984	+90	—441	2,694,899	59,854	1,654,551	182	1,463	115	2,310		6,109

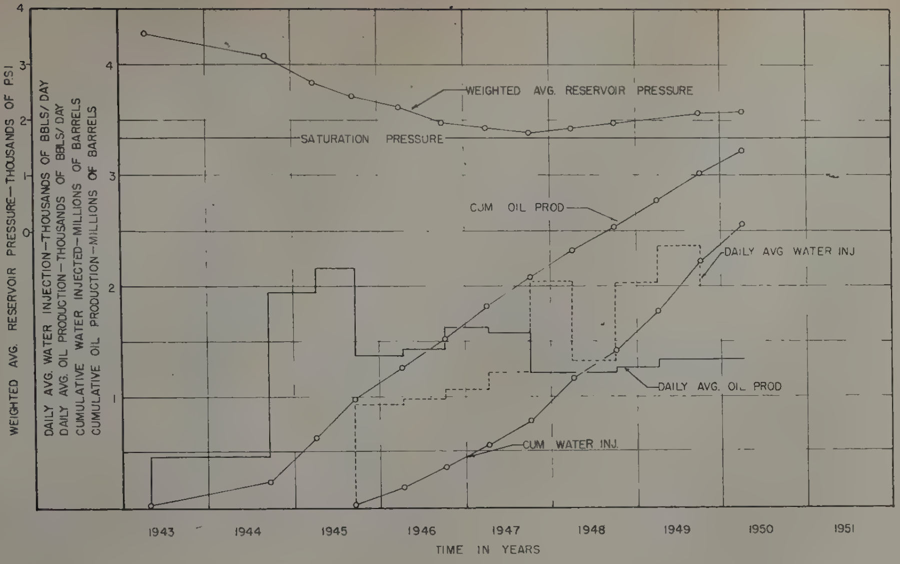

FIG. 5 — PRESSURE AND PRODUCTION STATISTICS FOR THE PITTSBURG SAND RESERVOIR.

Pittsburg Sand Reservoir

Table II shows that the permeability of the Pittsburg Reservoir averages 61.1 md, which is the lowest permeability of the three reservoirs under consideration. In addition to this, the Pittsburg sand has the least favorable permeability distribution of the three reservoirs. Table II, Item 19, also indicates that the production pressure behavior of the Pittsburg Reservoir should be on the order of 458 bbl/psid if no natural water influx is available. The first production pressure relationship, as shown on Table V, was observed for the period April 26, 1943, to September 12, 1944, to be 583 bbl/psid. This value is consistent in that with low initial water influx it was, and should have been the lowest value observed from field data. This relationship continued to increase with observation of successive intervals, indicating the presence of some natural water influx. However, the slow rate of increase (in comparison with the Hill Reservoir for instance) indicated that the natural water drive was not effective. Note that the production relationship for the Hill Reservoir, on an interval basis, increased almost 25 times over its initial observed value and that, at best, that rate could sustain only 1,000 B/D of oil production from that reservoir. By contrast, the production pressure relationship for the Pittsburg Reservoir over an equivalent period barely doubled in value. These indications, together with the high rate of pressure decline and the high order of saturation pressure, made it imperative that the first water injection equipment obtainable be placed in operation for the Pittsburg Reservoir. The first water injection experiments were conducted on Pittsburg Reservoir wells and, until April 1, 1949, more water had been injected into this reservoir than into either the Hill or the Bacon. Table V shows that, although the Pittsburg response has been poor, a reversal in downward pressure trend was finally achieved just short of saturation pressure by the combined influence of decreased average oil producing rates and increasing average water injection rates. It should be noted that pressures have been increasing since October 1, 1947, resulting in a steady increase in the cumulative pressure/production relationship.

OIL RECOVERY

Reservoir performance history shows that the Bacon and Pittsburg reservoirs would have been controlled by solution drive, and that the Hill Reservoir had a partial water drive. Estimates of recovery by natural means were made using the method outlined by Babson[1] for the Bacon and Pittsburg. For the Hill, however, additional estimates based on availability of reservoir water,

Table V — Pressure and Production Statistics for the Pittsburg Sand Reservoir, New Hope Field

Date	Wtd. Avg. Reservoir Pressure psig	Pressure Change		Est. Volume Cumulative Stock Tank Oil Produced Bbl	Cumulative Water Injected Bbl	Time Interval Days	Interval Rate or Prod. or Inj. B/D		Oil Reccvery-Stock Tank Bbl/psi Drop	
		Interval, psi	Cumulative, psi				Stock Tank Oil Prod.	Water Injection	Per Interval	Cumulative
4-26-43	3,523			0						
9-12-44	3,126	—397	—397	231,400		504	459		583	583
4-1-45	2,671	—455	—852	619,400		200	1,940		853	727
9-12-45	2,409	—262	—1,114	975,899		165	2,161		1,361	876
4-1-46	2,220	—189	—1,303	1,251,798	188,000	200	1,379	940	1,460	961
10-1-46	1,958	—262	—1,565	1,514,450	367,000	183	1,435	978	1,002	968
4-1-47	1,858	—100	—1,665	1,809,371	562,396	182	1,620	1,073	2,949	1,087
10-1-47	1,790	—68	—1,733	2,096,596	784,898	183	1,570	1,216	4,224	1,210
4-1-48	1,840	+50	—1,683	2,318,222	1,159,671	183	1,211	2,048		1,377
10-1-48	1,971	+131	—1,552	2,540,735	1,401,052	183	1,216	1,319		1,637
4-1-49	2,012	+41	—1,511	2,770,235	1,771,041	182	1,261	2,033		1,833
10-1-49	2,126	+114	—1,397	3,013,257	2,203,385	183	1,328	2,363		2,157
4-1-50	2,131	+5	—1,392	3,255,257	2,567,285	182	1,330	2,000		2,339

flood pot experiments, and permeability distribution were made. As a result of this work it was found that normal recovery from the Bacon Reservoir would have been 170 bbl per acre ft, from the Hill 260 bbl per acre ft, and from the Pittsburg 155 bbl per acre ft. The increase in recovery, due to water injection, was originally estimated to be at least 45 per cent on the basis of permeability distribution.

Indications to date are that the three reservoirs have been responding to water injection with no evidence of channeling. Because of the favorable reaction it is now believed that the ultimate recovery from the three reservoirs will be increased at least 70 per cent over that recoverable by natural means.

HISTORY OF FLOOD PATTERN DEVELOPMENT

Bacon Reservoir

In the Bacon Reservoir a breakthrough pattern became evident early in 1948, after injection well No. 4, which, at that time, had taken 410,000 bbl of injected water. This volume of water in turn represented reservoir oil which had been displaced out of the partially flooded area. The three producing wells immediately adjacent to injection well No. 4 were affected: the first on December 23, 1947, with an initial water cut of 15 per cent, the second on January 8, 1948, with initial water cut of 5 per cent, and the third on March 1, 1948, with an initial water cut of 34 per cent. The fact that these wells began making water within three months of one another indicated that the invaded region was expending uniformly. This in turn was an indication of the absence of channeling. Subsequent history shows that by October 1, 1948, the water production from these wells had increased to 72, 40, and 80 per cent respectively. About that time injection well No. 7 (see Fig. 2) was completed and water input into injection well No. 4 was reduced to that quantity produced only by the three adjacent oil wells. As of August 1, 1949, the water production from these same three wells was 67, 44, and 4 per cent respectively, injection well No. 4 having taken 634,764 bbl of water.

On September 1, 1950, the status of these wells was as follows: NI0, 60 and 4 per cent respectively. The first well, a west offset, has been shut down and its allowable transferred to other wells in the field, as provided by Railroad Commission field rules. The third well, a northwest offset, lies between injection wells 4 and 7. The behavior of this well proves the effectiveness of injection well No. 7.

In May, 1949, one of the producers offsetting injection well No. 3 began making 3 per cent water and by September, 1949, water had broken into the three nearest wells. At that time injection well No. 3 had taken 634,000 bbl of water into the Bacon. In June, 1950, one additional offset well began making water, bringing the total water producers in this group to four. Beginning in April, 1950, however, the rate into injection well No. 3 was reduced to the equivalent water production from its offsets, and in September, 1950, water injection into this well was discontinued. Prior to curtailing water injection into No. 3 the offset water producing wells tended to make increasing amounts of water. After curtailing water injection into No. 3, the water production from the offset wells either stopped rising or began to decrease. One well lying between injection wells 3 and 7 started flowing pipe line oil again. This is further evidence of the effectiveness of injection well No. 7.

Injection well No. 7 was drilled for the purpose of flooding oil out of the north and northeast portions of the Bacon and Pittsburg reservoirs. This well was completed and water injection into the Bacon started in September, 1948. Initial water break-through into the two nearest offset producing wells took place almost simultaneously in March, 1950, and by this time injection well No. 7 had taken 526,000 bbl of water. By September 1, 1950, this well had taken 698,000 bbl of water. The west offset producer had been shut down and the southeast offset was making 65 per cent water.

Injection well No. 1 had taken 815,000 bbl of water as of September 1, 1950, but as yet there has been no water break-through into its immediate offsets.

Injection well No. 6 had taken 244,000 bbl of water by March, 1950, at which time one Bacon producer on the west edge of the field began to make water. As of September 1, 1950, well No. 6 had taken 322,000 bbl of water and the break-through well was producing 20 per cent water.

Injection well No. 9 was drilled for

Table VI — Summary Showing Average Performance of New Hope Field Water Injection Wells in the Order in Which They Were Converted

No. on Map I	Injection Well Zones	Date of Initial Injection	Water Injection Capacity (1) B/D	Well Head Injection Pressure (1) psig	Average Injection Rate 9-1-50, B/D
1.	Lester Gilbert "A"-2				
	Bacon	Apr., 1946	700	3,900	200
	Pittsburg	Oct., 1945	350	3,800	300
2.	H. V. Hanvie #1				
	Hill	June, 1946	1,450	1,400	—
	Pittsburg	Oct., 1945	490	4,000	220
3.	R. A. Gilbert #1				
	Bacon	Apr., 1947	750	1,900	—
	Pittsburg	Feb., 1948	370	4,000	250
4.	L. E. Minshew #1				
	Bacon	May, 1947	1,190	1,800	450
	Pittsburg	Mar., 1947	260	4,000	—
5.	I. Alexander #2				
	Hill	Nov., 1947	1,360	750	1,170
	Pittsburg	Aug., 1947	550	750	350
6.	T. E. Hewett #1				
	Bacon	July, 1948	475	1,850	450
	Pittsburg	Sept., 1948	810	3,750	500
7.	I. Alexander #3				
	Bacon	Oct., 1948	1,550	1,500	1,400
	Pittsburg	Sept., 1948	330	3,000	300
8.	B. B. Rhoades B-1				
	Hill	Sept., 1950	1,800	1,800	1,700
	Pittsburg	Sept., 1950	250	3,200	250
9.	New Hope Unit 11				
	Bacon	Sept., 1950	1,500	2,000	1,100
	Pittsburg	Sept., 1950	800	3,000	700

the purpose of flooding oil out of the south and southeast portions of the Bacon and Pittburg reservoirs. This well was completed and water injection started in September, 1950. Although this well has not had time to take a large volume of water, it is anticipated that it will function equally as well as injection well No. 7.

One characteristic observed is that the principal direction of a water front is toward the center of the reservoir, rather than around the periphery. The reason for this behavior may lie in the fact that the average capacity (md-ft) approaches zero near the reservoir limits and that most of the oil withdrawal is from the central area which has a high relative capacity. The location and behavior of the water producing wells is particularly encouraging. The experience accumulated to date gives evidence that as yet there has been no channeling of injected water.

Hill Sand

In the Hill there is evidence of water encroachment along the south and east flanks of the reservoir. Evidence concerning the present position of the water front on the north flank of the reservoir is still inconclusive because most of the Hill producing wells in that area are completed high in the sand. Injection well No. 8 was converted from a Bacon producer to a Hill-Pittsburg water injection well in September, 1950. Water injection into this area has not been sufficient to warrant further discussion at this time.

Pittsburg Sand

In the Pittsburg sand one water break-through has been observed, this being in the offset producer nearest injection well No. 6, which occurred in June, 1950. At that time the injection well had taken 323,000 bbl of water. As of September 1, 1950, well No. 6 had taken 356,000 bbl of water and the break-through well was producing 67 per cent water.

DEVELOPMENT OF THE WATER INJECTION PROGRAM

Because the initial calculations had indicated that the Pittsburg would be the most difficult reservoir to handle, it was decided that injection should be started there first. Accordingly, a dry hole (see Injection Well No. 1 on Fig. 2) located on the south flank of the reservoir was converted into an injection well. During the following experimental period, it developed that, instead of taking 7,000 B/D of water at 1,300 psi injection pressure as calculated from permeability data, the well required from 3,500 to 4,000 psi injection pressure to take only 400 B/D. The experience with this well indicated that the permeability of the Pittsburg Reservoir had decreased materially below the oil-water contact. This also accounted for the poor water drive as evidenced by pressure behavior. Injection of unaerated water into the shallow, low permeability sands in the Bradford Field in Pennsylvania under pressures in the 1,000 to 2,000 psi range had been proved practical, but there were no previous experience data available on water injection into deep horizons under the pressure conditions outlined above.[2]

The experimental period had to be continued. During this time, additional studies of the physical and chemical nature of the reservoir formations, together with the chemical properties of the available salt and fresh unaerated water, were made. No means were found by which injection pressures could be lowered without also decreasing the rate of water injection. Established practices in which the formations were shot with nitroglycerine and acidized, together with chemical and bacterial control of the injected waters, also failed to disclose any means of combating the problem. In short, the results of the experimental period disclosed that the only means of injecting water into the Pittsburg Reservoir was by the continued injection of unaerated water into the first well at low rates and under the high pressures.

A second attempt was made by converting another dry hole into a Pittsburg injection well in the hope that a better injection well could be obtained. (See Injection Well No. 2, Fig. 2.) Water injection was started into this well on October 23, 1945. By that time, the first injection well had taken about 13,000 bbl into the Pittsburg while the Pittsburg Reservoir itself had produced about 1,000,000 bbl of oil with no water. The second Pittsburg injection well proved to be no better than the first as it would also take only about 500 B/D of unaerated water at 4,000 psi well-head injection pressure. Subsequent history shows that these two wells averaged about 940 B/D, while reservoir withdrawal rate was held to about 1,400 stock tank B/D. Although the 940 B/D rate was considered sufficient to cause some reflection in pressure decline, it was noted that no definite reaction was apparent which could be credited to water injection alone. Well No. 1 was subsequently converted to a Bacon-Pittsburg injection well. The Bacon section in Well No. 2, however, had neither porosity nor permeability and, for this reason, it was completed dually as a Hill-Pittsburg injection well. Subsequent development of the injection well program took place as shown on Table VI. The location of these wells, with respect to the various reservoirs, is shown on Fig. 1. All of the injection wells, with two exceptions, were converted from dry holes, non-commercial producers, or producing wells located within the reservoir limits.

Injection wells Nos. 7 and 9 were drilled intentionally as Bacon-Pittsburg water injection wells.

WATER SUPPLY AND FIELD SYSTEM

Extraneous water for the injection system has been supplied from three fresh water wells in the shallow Wilcox sands and one salt water well which is completed in the Woodbine sand. This water is delivered under pressure as needed to surface storage tanks by means of deep well centrifugal pumps. Particular caution has been exercised in keeping air away from this water once it reaches the surface. The system is completely closed and at no point is the line pressure allowed to go below five psig. Vessels are equipped so as to maintain a gas seal.

No difficulties are encountered in the injection of air-free extraneous water other than the unusually high injection pressures. No plugging action has been experienced to date because of extraneous water injection. Considerable difficulty has been experienced, however, in the attempt to inject produced water along with extraneous water into the Bacon Lime. A preliminary investigation disclosed the formation of precipitates with various mixtures of extraneous and produced water. A complete account of the problem is beyond the scope of this report. It should be stated, however, that to date the injection of the comingled water along with various treating agents has been unsuccessful. Two injection wells (Nos. 4 and 7) were almost completely plugged as a result of these experiments, necessitating clean-out and acidizing operations to get them back in condition. The problem has since been overcome by injecting only produced-water into the Bacon section of injection well No. 4. This well is now taking all of the produced-water under vacuum. Although the injection of comingled water has presented a challenge, it is believed that additional research and experiments will eventually provide a complete solution of the problem.

The water is injected into the high pressure wells by means of vertical type, positive displacement, triplex pumps. These pumps can operate at pressures up to 5,000 psi. Water for the lower pressure wells is injected by means of horizontal, positive displacement reciprocating pumps similar to those used in the East Texas Field and other areas. These pumps can operate up to about 2,000 psi.

Experience has shown that it has not been practical to inject the salt water at very high pressures. Much difficulty was encountered in the attempt to inject salt water into the Pittsburg Reservoir under pressures in the 4,000 psi range. Most of the down-time was caused by plunger scoring and packing failures resulting from this attempt. For this reason it has been necessary to inject only fresh water into the Pittsburg sand. The salt water, therefore, has been diverted to the lower pressure systems serving the Bacon and Hill reservoirs, and the resulting performance has been much more satisfactory. With existing equipment, the injection of fresh water is limited mainly by the ability of the overburden to withstand the pressure imposed. For this reason, Pittsburg well head injection pressures are kept below 4,000 psig. Fig. 2 shows how the various field lines, pumping stations and water supply wells are located with respect to the water injection wells. These systems are tied in with one another so that it is possible to deliver salt water or fresh water to the injection wells as needed.

CONCLUSION

The project, while still in its preliminary stage, has demonstrated the feasibility of controlling reservoir pressures by the injection of water even under difficult conditions. From an operating viewpoint, the maintenance of pressure alone has been worthwhile by sustaining flowing production from all except a few wells. Indications had already become apparent that it would be difficult to produce the wells by artificial lift with low fluid levels, particularly with gas coming out of solution in the immediate vicinity of the producing wells.

We believe that the project is a step forward in the practical application of sound engineering principles in the control of reservoir performance for the purpose of increasing ultimate recovery, and perhaps most important of all for the prevention of reservoir waste and the conservation of natural resources.

ACKNOWLEDGMENT

Appreciation is expressed to the respective managements of Tide Water Associated Oil Co. and Seaboard Oil Co. of Delaware for permission to publish this report.

Special acknowledgment is given E. B. Miller, Jr., for his helpful suggestions in preparing the paper. Special acknowledgment is also expressed to the New Hope Field production personnel, and especially to R. H. Coe, H. P. Shackleford, H. D. Spires, and J. L. Grolemund, who have been largely responsible for carrying on the field operations since discovery.

REFERENCES

1. E. C. Babson: *Trans.* AIME (1944), 155, 120.
2. P. D. Torrey: *Trans.* AIME (1930), 86, 259.

★ ★ ★

T.P. 2937

PERFORMANCE OF THE LOWER PAWELEK RESERVOIR, FALLS CITY FIELD, KARNES COUNTY, TEXAS

JOHN W. CRUTCHFIELD, CRUTCHFIELD AND PRUETT, CORPUS CHRISTI, TEX., AND **EMIL F. BOWERS,** SOUTHERN MINERALS CORP., CORPUS CHRISTI, TEX., MEMBERS AIME

ABSTRACT

This paper presents the initial results of a pressure maintenance by water return project in the Lower Pawelek reservoir of the Falls City Field, Karnes County, Southwest Texas. Production is from the Lower Wilcox section at an average depth of 6,030 ft on the downthrown side of a "down to the coast" fault. Of particular interest is that the reservoir oil is high gravity and low viscosity but far undersaturated with gas at the original reservoir pressure and temperature. The early pressure and production history indicated only a partial or limited water drive, and this fact, coupled with the characteristics of the reservoir fluid and artificial lifting problems, made advisable the water injection program to maintain reservoir pressure.

The paper includes a description of the reservoir and reservoir fluids, the pressure and production history, a description of the water injection facilities, and the results of reservoir calculations involving Hurst's unsteady state flow and the material balance equations for calculation of water influx and prediction of the pressure-production relationship at various rates of withdrawal.

The reservoir calculations and initial field results indicate that reservoir pressures in excess of 85 per cent of original pressure can be maintained by control of water injection even at very high rates of production.

INTRODUCTION

The purpose of this paper is to report the initial results of a pressure maintenance by water return program in the Lower Pawelek reservoir, Falls City Field, Karnes County, Texas, and to calculate an empirical relationship between pressure and production in this limited or partial water drive reservoir.

DISCUSSION

Location

The Falls City Field (Fig. 1) is located two miles north of the town of Falls City in Karnes County, Texas, and is approximately 50 miles south-southeast of San Antonio on U. S. Highway 181.

Discovery and Development

The initial block of leases was taken after a surface geological survey identified a major east-west fault and closure on the south or downthrown section. The discovery well, Southern Minerals Corporation's Joe F. Bartosch 1, was completed at 4,650 ft in the Lower Bartosch sand in December, 1944. Drilling was continuous until December, 1946, and resulted in the discovery of 12 oil reservoirs between 4,600 and 6,050 ft in the Middle and Lower Wilcox formations. These are shown on the cross-section (Fig. 2). As of the current date there are 64 oil wells completed as follows:

Reservoir	Southern Minerals Corp.	Gulfshore Oil Co.	Magnolia Petroleum Corp.	Total
Upper Bartosch	0	0	0	0
Lower Bartosch	16	0	0	16
Shulze	7	0	1	8
Upper Faires	2	0	0	2
Lower Faires	4	0	0	4
Upper Moczygemba	0	0	0	0
Lower Moczygemba	2	0	0	2
Olinick	2	0	0	2
Upper Martinez	0	0	0	0
Lower Martinez	5	0	0	5
Upper Pawelek	0	1	0	1
Lower Pawelek	27	1	3	31
	—	—	—	—
Total	65	2	4	71

---

[1] References are given at end of paper.

Manuscript received at office of the Petroleum Branch December 5, 1949. Paper presented at a meeting of the Southwest Texas Section of the Branch in Corpus Christi, Tex., November 16, 1949.

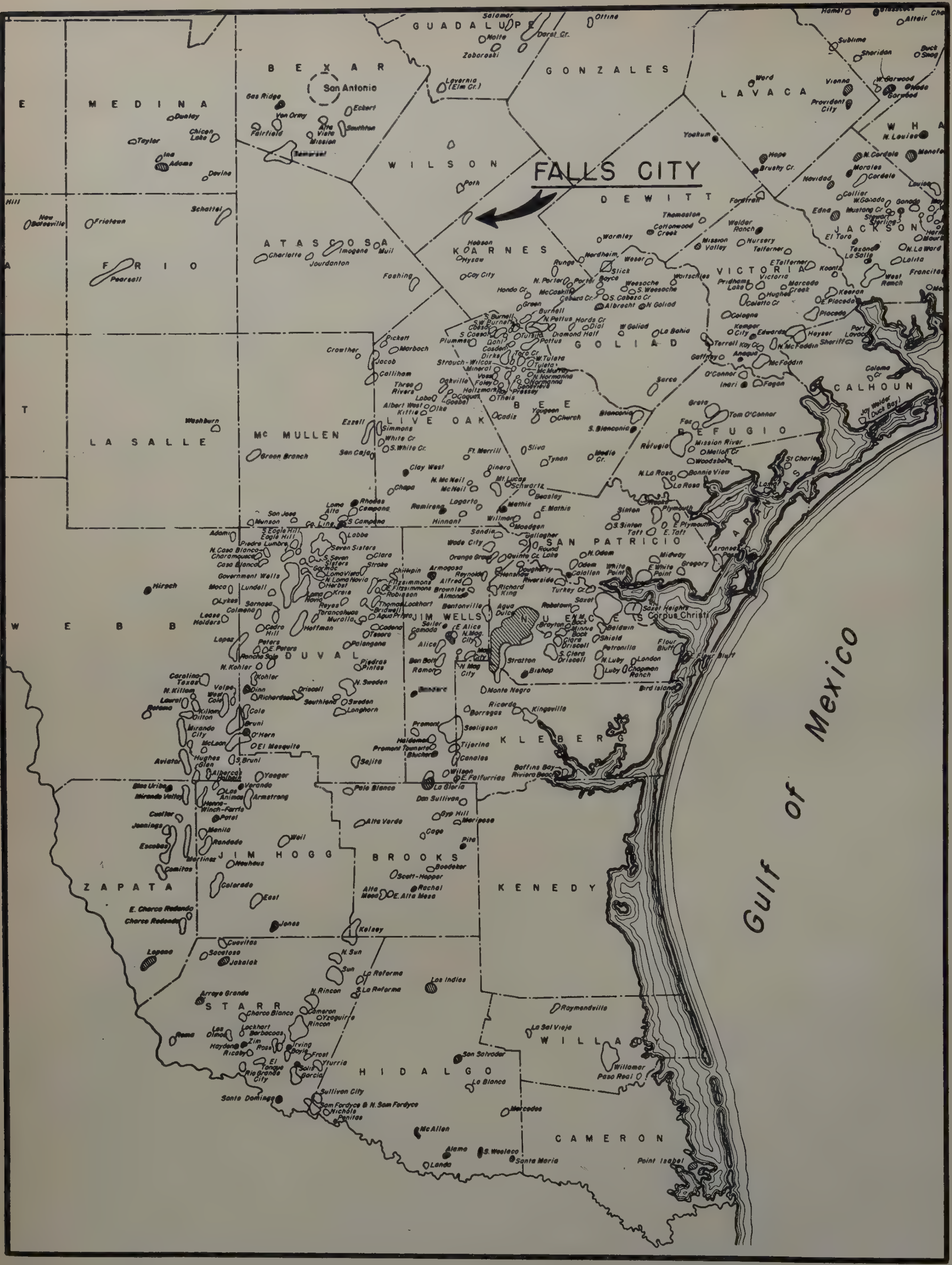

FIG. 1 — OIL AND GAS FIELDS OF SOUTHWEST TEXAS.

A deep test well was drilled in 1949 to 10,235 ft which penetrated the Edwards formation and a portion of the Glenrose formation. No commercial oil or gas production was indicated below the Lower Wilcox.

LOWER PAWELEK RESERVOIR

Geological Data

The Lower Pawelek reservoir is an elliptical, low relief structure with sand thicknesses ranging from 25 to 40 ft. The producing formation (Fig. 3) has been encountered as high as 5,663 ft subsea, and original water table has been established by drill stem tests at 5,716 ft subsea, indicating a maximum oil column of 53 ft. No gas cap has been encountered.

The average net effective oil sand thickness (Fig. 4) is 16 ft and the producing area includes 919 acres. The producing formation can be described as medium grained, gray, calcareous sand sometimes being interbedded with shale. Analyses of 47 core samples from two wells indicate an average porosity of 24.5 per cent and average permeabilities parallel and perpendicular to the bedding plane of 311 and 121 md, respectively. Connate water saturations by restored state or capillary tests were measured in three cores, and are calculated to average 37 per cent of pore space corresponding to the average permeability and to the average height of sand above water. A summary of reservoir data is presented in Table I.

Engineering Data

Because of the multiplicity of producing sands and the desire to complete some wells in each of the productive reservoirs, it was not possible to uniformly pattern the producing wells over the Lower Pawelek reservoir. The average well density is 34 acres per well; however, the minimum distance between offsetting wells is 660 ft.

Completion practice was to core into the Lower Pawelek sand, bottom the hole approximately five ft above the water level, set 5½-in. casing to bottom, and gun perforate the lower five to ten ft of sand. An effort was made to select completion intervals between impermeable barriers and breaks. The latter one-half of the wells were completed with multi-stage cementing devices set at approximately 5,600 ft for added protection against migration of reservoir fluids in upper sands.

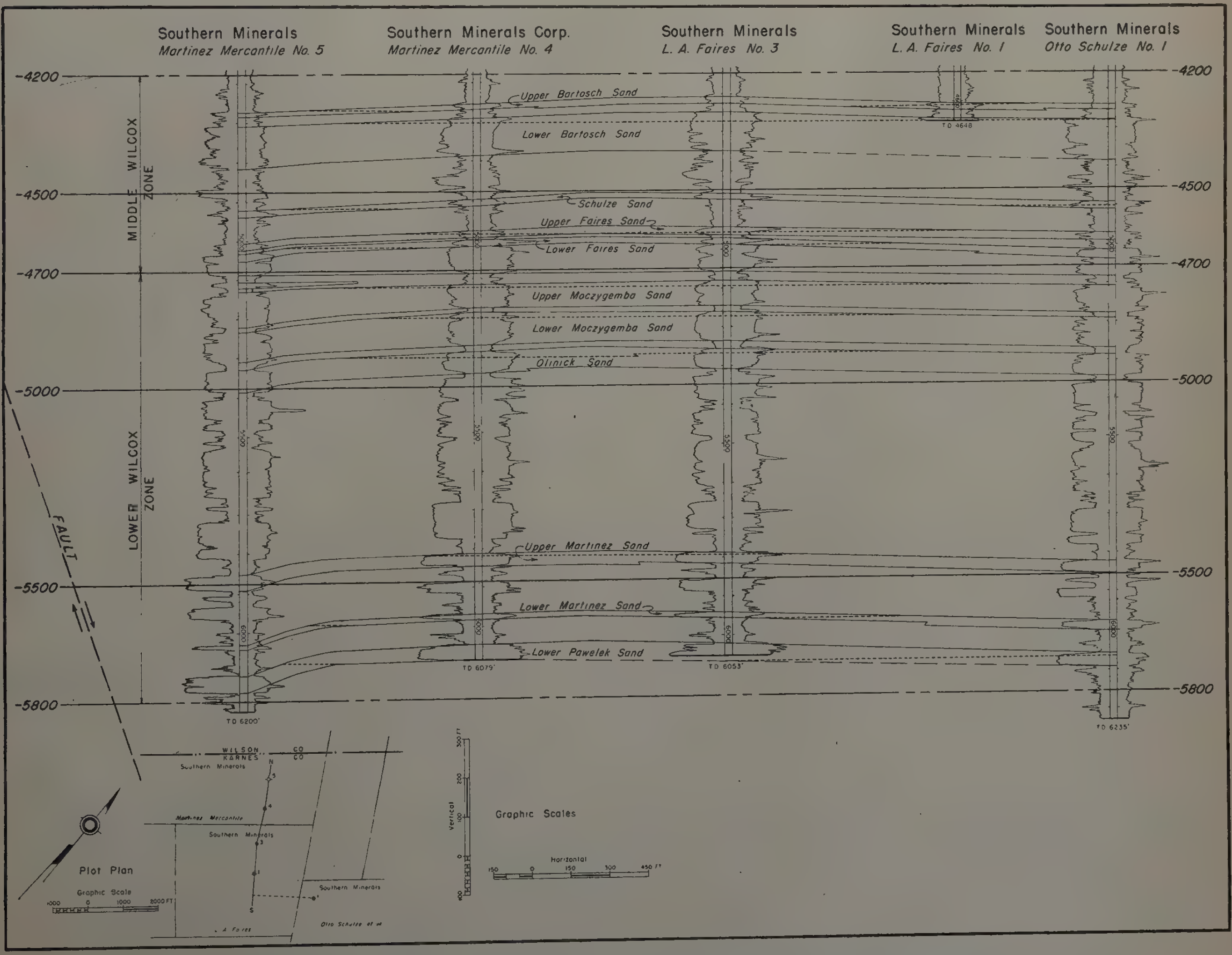

FIG. 2 — NORTH-SOUTH CROSS SECTION, FALLS CITY FIELD, KARNES COUNTY, TEXAS.

The first Lower Pawelek reservoir pressure measured was 2,583 psi in Bartosch 1-A in November, 1945, at which time the cumulative production was 23,132 bbl of oil. Pressures as high as 2,611 psi (Olinick 6, March, 1946) have been measured, and the original reservoir pressure has been assumed to be 2,625 psi. The subsurface pressure datum plane is 5,685 ft subsea, midway between the crest of the structure and the original water level.

A subsurface sample of Lower Pawelek reservoir oil and gas was taken in November, 1945. Flash liberation, differential liberation, and viscosity data are shown in Figs. 5, 6, and 7. Briefly, the sample showed a saturation pressure of 797 psi at the reservoir temperature of 190°F. The stock tank gas-oil ratio at zero lb separator pressure was 167 cu ft per bbl with an API gravity of 39.2 degrees and a shrinkage factor of 0.847. The oil viscosity was 1.03 centipoises at original reservoir conditions, and 1.64 centipoises at atmospheric pressure and reservoir temperature.

An analysis of bottom water from the reservoir indicated a salinity of 18,691 ppm chloride. It is of interest to note that five of the upper reservoirs in the Falls City Field are underlain with water having chloride contents of less than 5,000 ppm.

Table I — Reservoir Data

Falls City Field — Lower Pawelek Sand

Original Oil-Water Contact, Ft SS	5,716
Average Porosity, Per Cent	24.5
Permeability, Millidarcys*	
Parallel to Bedding Plane	311
Perpendicular to Bedding Plane	121
Connate Water, Per Cent of Pore Space	37
Average Net Pay Section, Ft	16.1
Productive Area, Acres	919
Estimated Oil in Place, MM Reservoir Bbl	17.70
Original Reservoir Pressure, psig at 5,685 Ft SS	2,625
Reservoir Temperature, F	190
Characteristics of Produced Oil**	
Dissolved Gas-Oil Ratio	167
Shrinkage Factor, Bbl Stock-Tank Oil Per Reservoir Bbl	0.847
Oil Gravity, API	39.2
Sodium Chloride Content of Connate Water, PPM	18,690
Viscosity of Original Reservoir Oil Centipoises	1.03

*Average of approximately 47 determinations on cores from two wells.
**Original reservoir oil produced under separator conditions of 0 psi and 70°F.

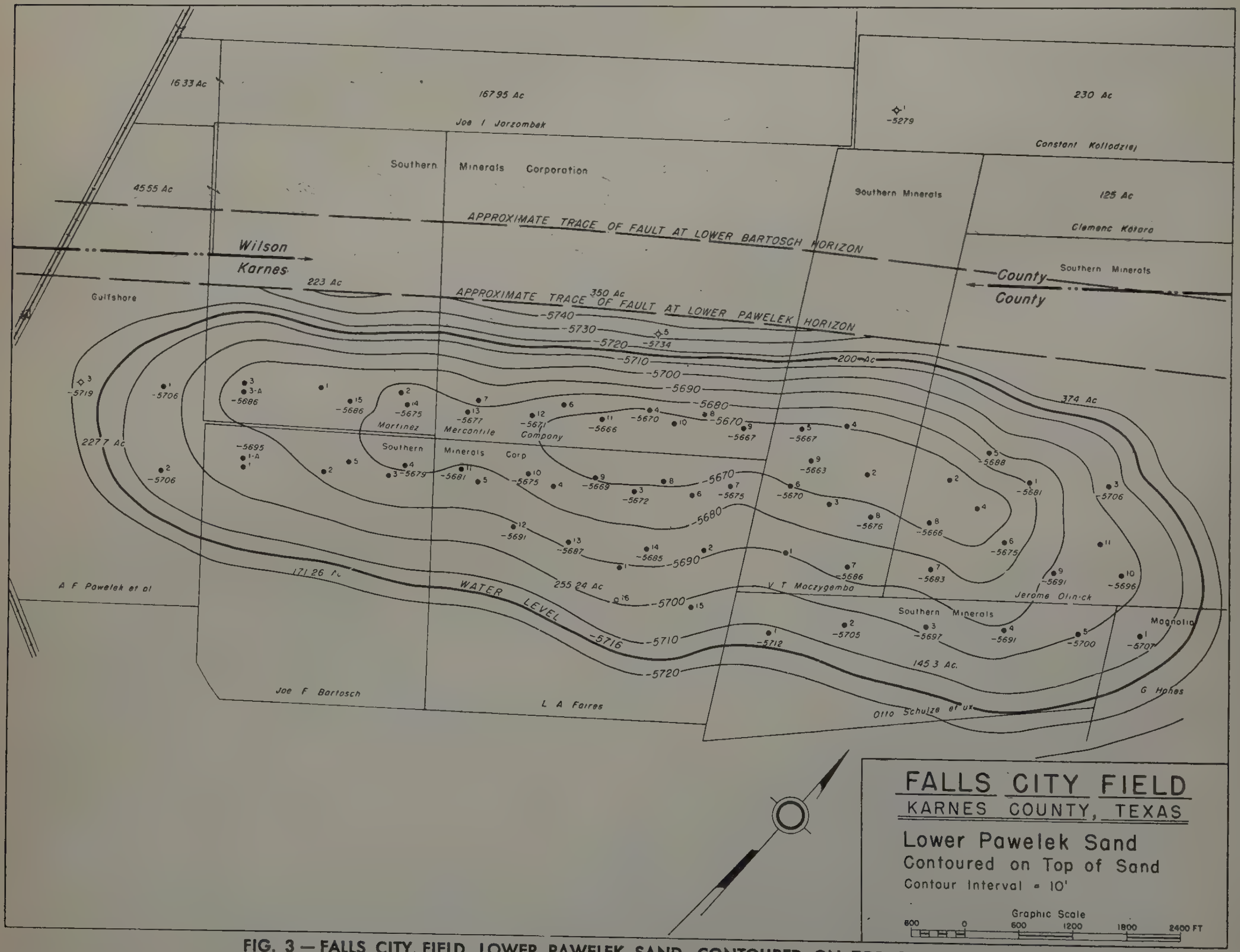

FIG. 3 — FALLS CITY FIELD, LOWER PAWELEK SAND, CONTOURED ON TOP OF SAND.

Pressure-Production History

A total of eight shut-in subsurface pressure surveys (Fig. 8) had been made in key wells up to March 1, 1948, with a maximum of six months between any two surveys. Reservoir pressures have been determined by area-weighting the entire reservoir. Cumulative production on that date was 694,281 bbl. Many of the structurally low wells produced water which averaged 20 per cent of total fluid during the latter part of 1947. Following development, oil production ranged from approximately 1,000 to 1,250 B/D.

As late as March, 1947, it was believed that the reservoir pressure would stabilize at a high level although no reservoir calculations had been made by that date. It appeared that the water influx was approaching reservoir withdrawals in magnitude since any large difference would result in a major pressure decline because of the extremely low compressibility of the undersaturated reservoir oil. It soon became apparent, however, that the aquifer was limited in extent and that the drive would not support the desired rate of oil production with increasing volumes of saltwater at reservoir pressures which would sustain natural flow.

By March 1, 1948, the reservoir pressure had declined to 2,281 psi, or 344 lb less than the original pressure. Five wells had been placed on artificial lift and a majority of the remaining wells had declined in tubing pressure to the critical point required to maintain natural flow.

It should be pointed out that this field is located in an area almost devoid of natural gas reserves which might be utilized for gas lift. Installation of convential pumping or hydraulic pumping equipment appeared inadvisable because of limited fluid capacity available for depletion of water drive reservoirs and also because of the high initial investment required. Limited quantities of natural gas were obtained by laying eight miles of transmission line and installing compressor facilities to pick up casinghead gas.

A second production problem became apparent during this period when surface evaporation was no longer adequate for disposing of the increasing volumes of salt-water. These two problems strongly indicated the desirability of a pressure maintenance program by returning produced water to the Lower Pawelek reservoir.

Prediction of Pressure-Production Relationship

To fully evaluate the effect of water injection on reservoir pressure, a series of reservoir calculations was made involving the volumetric balance equation[1] and Hurst's[2] unsteady state

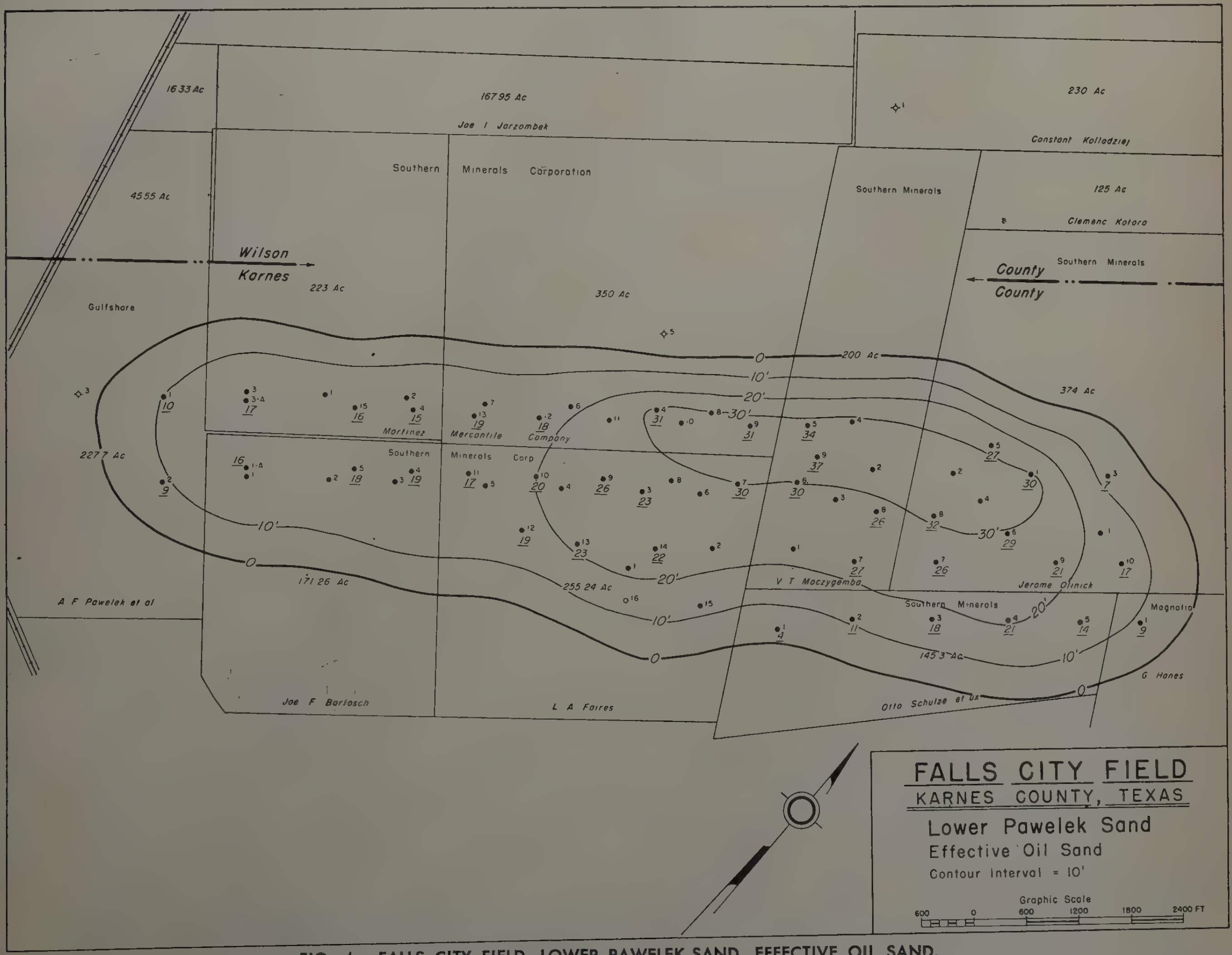

FIG. 4—FALLS CITY FIELD, LOWER PAWELEK SAND, EFFECTIVE OIL SAND.

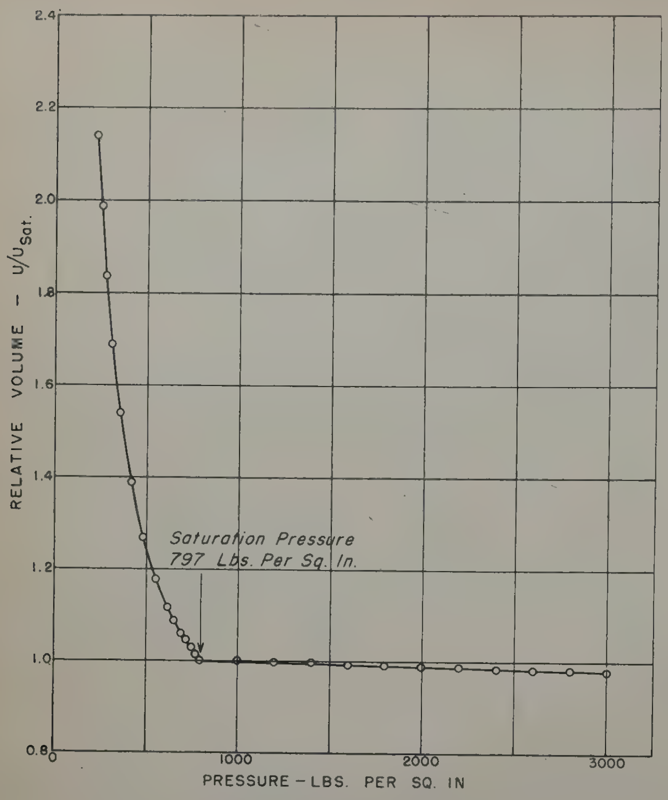

FIG. 5 — PRESSURE-VOLUME RELATIONS AT 190°F.

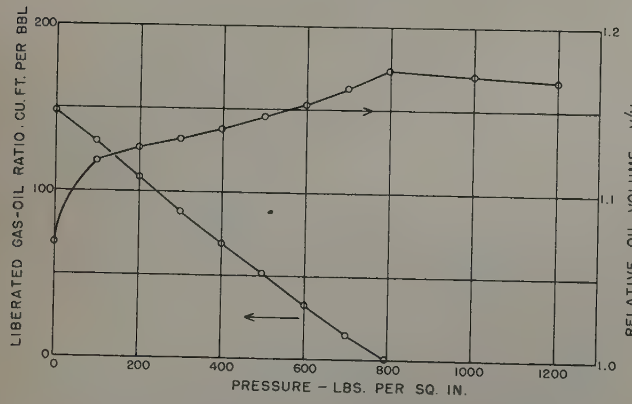

FIG. 6 — DIFFERENTIAL GAS LIBERATION AT 190°F.

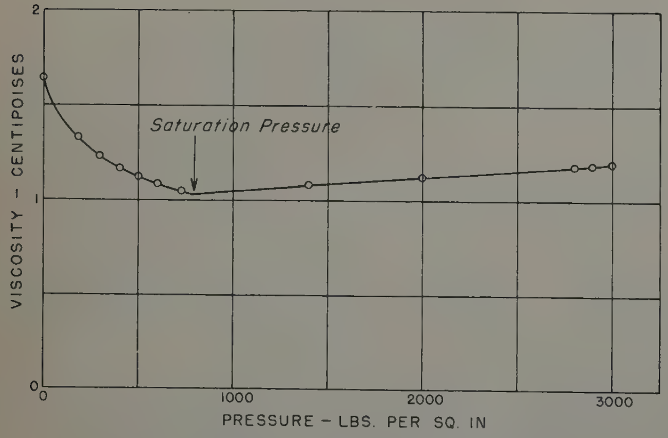

FIG. 7 — VISCOSITY OF RESERVOIR OIL AT 190°F.

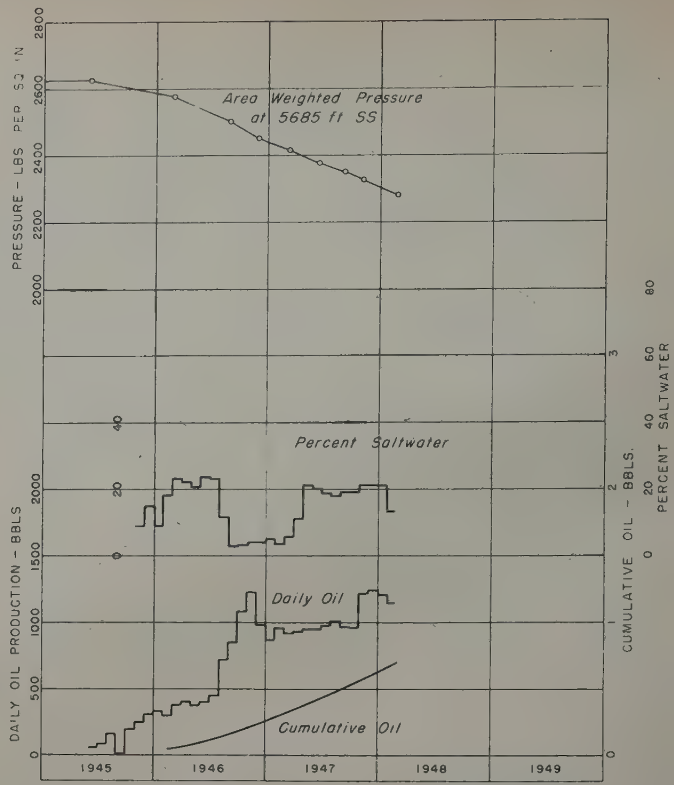

FIG. 8 — PRESSURE AND PRODUCTION DATA, LOWER PAWELEK SAND.

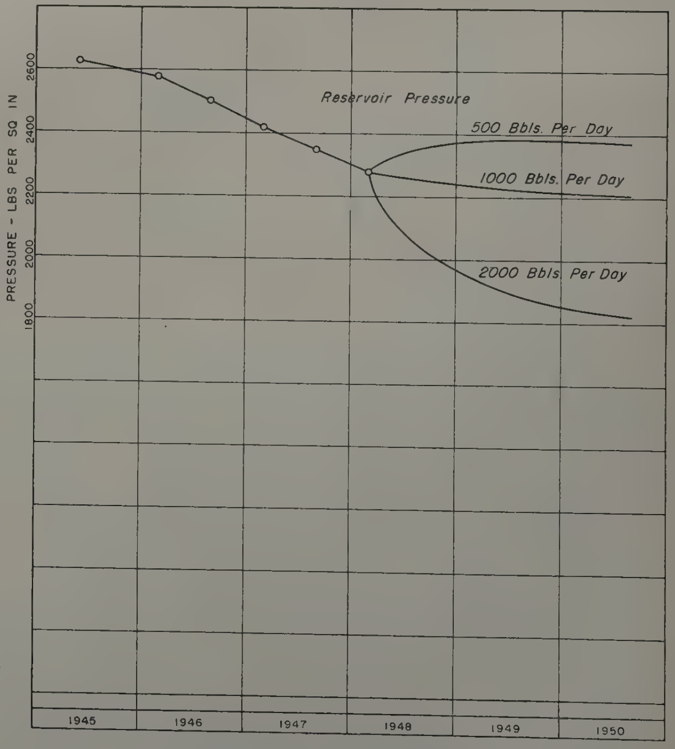

FIG. 9 — CALCULATED RESERVOIR PRESSURES AT VARIOUS RATES OF WITHDRAWAL.

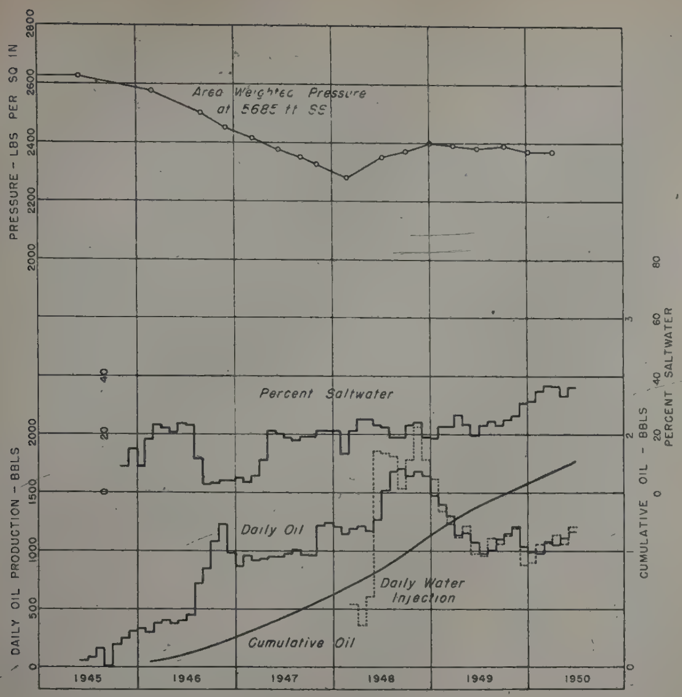

FIG. 10 — PRESSURE AND PRODUCTION DATA, LOWER PAWELEK SAND.

flow equation for calculating water influx and predicting reservoir pressures at various rates of oil and water production and water injection. The equations, adapted to the Lower Pawelek reservoir, are as follows:

$$\underset{\text{Total Water Influx}}{Z} = \underset{\text{Oil and Water Withdrawals}}{[\Delta n\ \mu + z]} - \underset{\text{Water Injection}}{z'} - \underset{\text{Expansion of Oil Remaining}}{[n(\mu - \mu_o)]}$$

where

$Z =$ Total water influx, bbl

$\Delta n =$ Cumulative oil produced, stock tank bbl

$n =$ Original oil in place, stock tank bbl

$\mu_o =$ Bbl of oil under original reservoir conditions which yield on bbl of stock tank oil

$\mu =$ Bbl of oil, and gas released from solution, at pressure P resulting from μ_o bbl of original reservoir oil

$z =$ Cumulative water production, bbl

$z' =$ Cumulative water injection, bbl

$Z =$ Cumulative total water influx, bbl

and Hurst's formula for radial water influx,

$$Z = \frac{161 K H \sigma R^2}{\propto^2 \mu} \sum_{i=0}^{i=n-1} (P_i - P_{i+1})\ f \left[(\theta_n - \theta_i)\ \frac{K}{\mu \phi c}\ \frac{1}{R^2} \right]$$

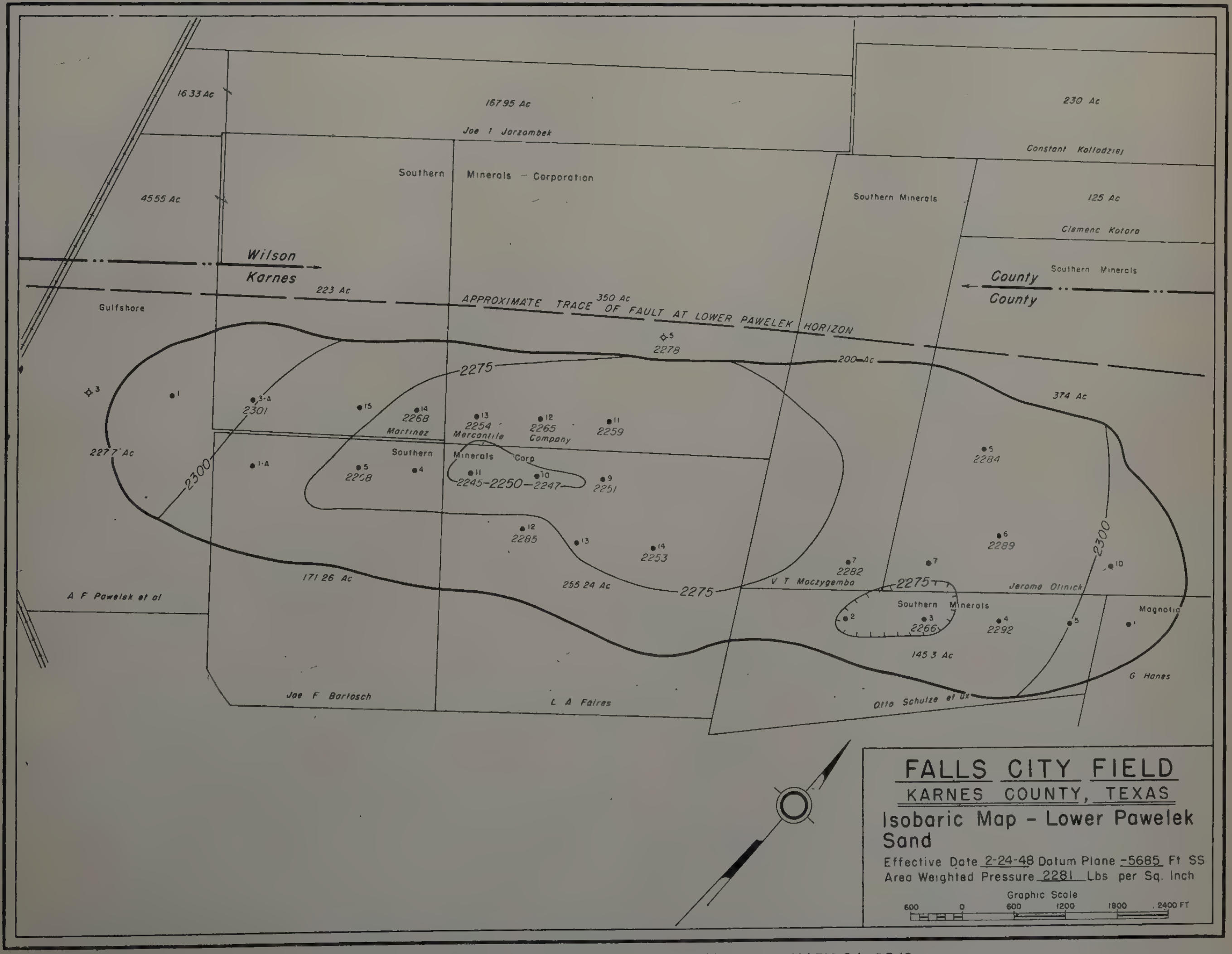

FIG. 11 — ISOBARIC MAP, LOWER PAWELEK SAND, FEBRUARY 24, 1948.

where

P = Reservoir pressure, lb psi
K = Permeability, cu ft/day/sq ft/lb/sq ft/ft
μ = Water viscosity, centipoises
c = Apparent compressibility, cu ft/cu ft/lb/sq ft
ϕ = Porosity, fractional
$\propto^2 = \frac{K}{\mu \phi c}$, diffusivity
R = Effective radius of reservoir, ft
H = Thickness of producing formation, ft
σ = Fraction of perimeter through which water can enter
θ = Time, days
Z = Cumulative water influx, bbl

The above equation can be simplified by letting

$$\overline{K} = f\left[(\theta_n - \theta_1) \frac{\propto^2}{R^2} \right]$$

and the final equation becomes

$$Z = 161\, \phi\, c\, H\, \sigma\, R^2 \int_{\overline{K}\theta_o}^{K\theta_n} (P_o - P)\, d\overline{K}$$

The procedure used in the calculations was to solve the volumetric balance at each of the survey dates over the life of the field to determine the total water influx. These data were then substituted in the unsteady state equation and various values were assumed for $\propto^2/R^2$ until a more or less constant value was found for the term $161\, \phi\, c\, H\, \sigma\, R^2$ involving the physical constants of the reservoir. An assumed value of $\propto^2/R^2$ equal to .01 gave the best series of values for the physical constant which varied a maximum of four per cent from the arithmetic average over six pressure surveys.

With the above assigned values, the unsteady state equation and volumetric balance were solved simultaneously for the prediction of reservoir pressures at various rates of oil and water withdrawals and water injection. The results of these calculations are shown in Fig. 9. By this method it was calculated that a reservoir pressure of approximately 2,400 psi could be maintained at a fluid production rate of 2,000 B/D with the injection of 1,500 B/D of water. In a similar manner it was calculated that the reservoir pressure would have declined to 2,077 psi by January 1, 1949, in the absence of pressure maintenance.

Water Injection Facilities

A closed, gravity type, saltwater gathering system having a total capacity of 7,800 B/D was installed to collect the water

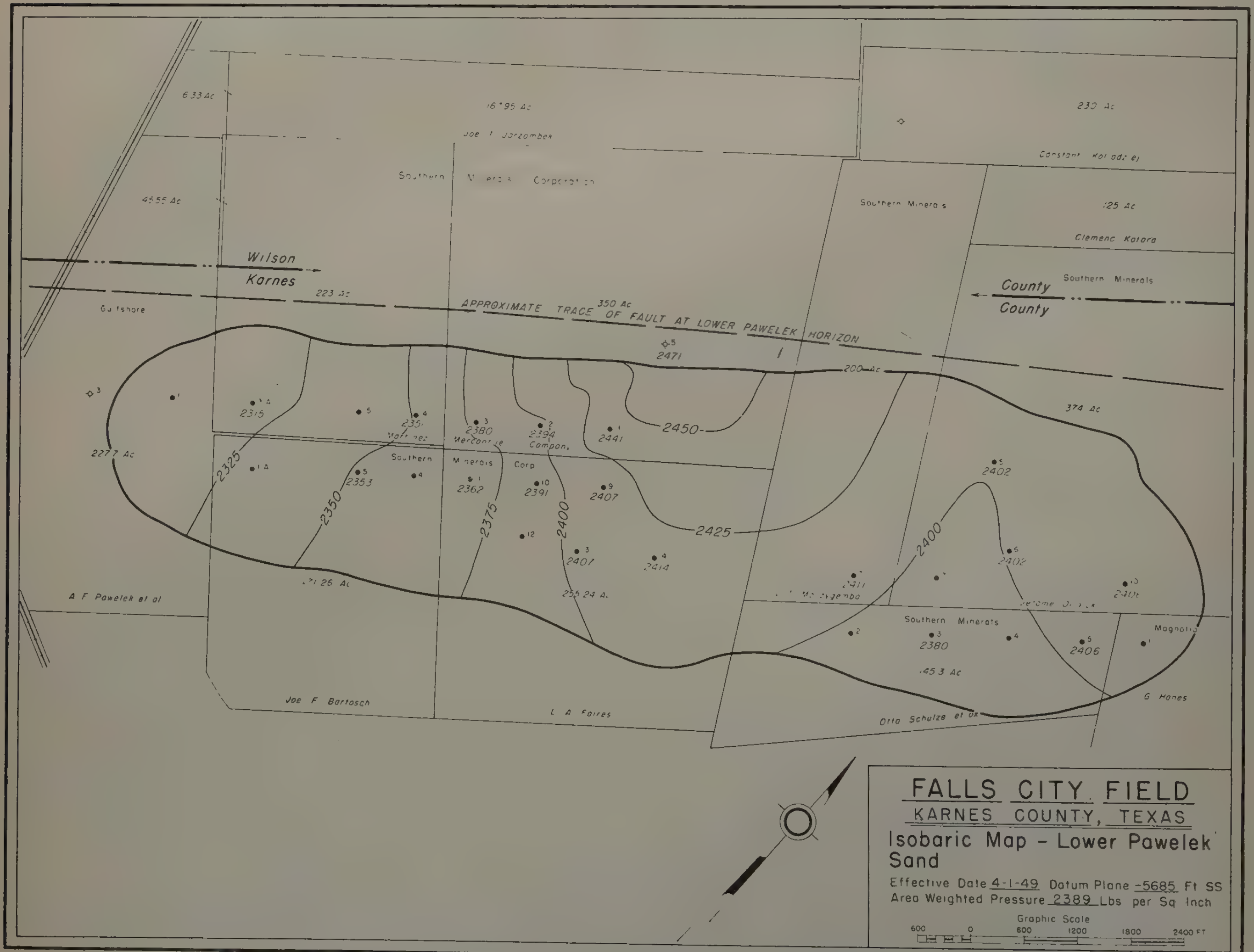

FIG. 12 — ISOBARIC MAP, LOWER PAWELEK SAND, APRIL 1, 1949.

at a central point for settling and pumping into the injection well. The system consists of 8,600 ft of 4½-in. O.D. fibre and steel lines with steel pipe installed at road and creek crossings. Water from the gathering system is discharged into a 500-bbl settling tank where the water surface is covered with a 12-in. blanket of crude oil to prevent exposure to air and light. A reciprocating pump, rated at 4,800 B/D at 250 psi pressure and equipped with a torsion-tube liquid level speed control, picks up the water after it has been measured through a recording orifice meter. The water is then delivered through a high pressure steel line to the injection well.

The water injection well (Martinez 5) was completed by washing down a previously abandoned dry hole located midway the long axis of the reservoir and between the water level and the major fault. Top of the Lower Pawelek sand in the well is 18 ft below the original water table. Location of the well is particularly advantageous since it is located in the area most remote from the natural water drive. The well was completed with 5½-in. casing with 40 ft of slotted pipe below the cementing assembly which consisted of a solid bottom cement whirler float collar and metal petal basket. The total initial investment for the gathering system and injection well was $21,351 and $17,789, respectively.

Results of Water Injection

The first water was injected on March 3, 1948, at the rate of 500 B/D which was increased to 1,800 B/D in June (Fig. 10). Injection well surface pressures ranged from 400 to 600 lb. The area-weighted pressure measured immediately prior to water injection was 2,281 psi (Fig. 10). On July 1, 1948, after the injection of 100,000 bbl of water, the pressure had increased 64 lb to 2,345 psi. Approximately 213,000 bbl of reservoir fluids had been withdrawn during the same period. As may be noted from the pressure-production curve, the net rate of withdrawals was maintained at approximately 500 reservoir B/D and the pressure increased to 2,400 psi as anticipated by the reservoir calculations. This relative rate of withdrawals and injection has been maintained as closely as possible up to the present time and the last measured pressure was 2,369 lb on April 6, 1950.

Inspection of the isobaric maps (Figs. 11, 12, and 13) gives a graphic picture of the change in the pressure pattern resulting from the injection program.

It may be noted from the pressure-production curve (Fig. 10) that the increase in saltwater production has been moderate since the start of water injection. One well located 1,140

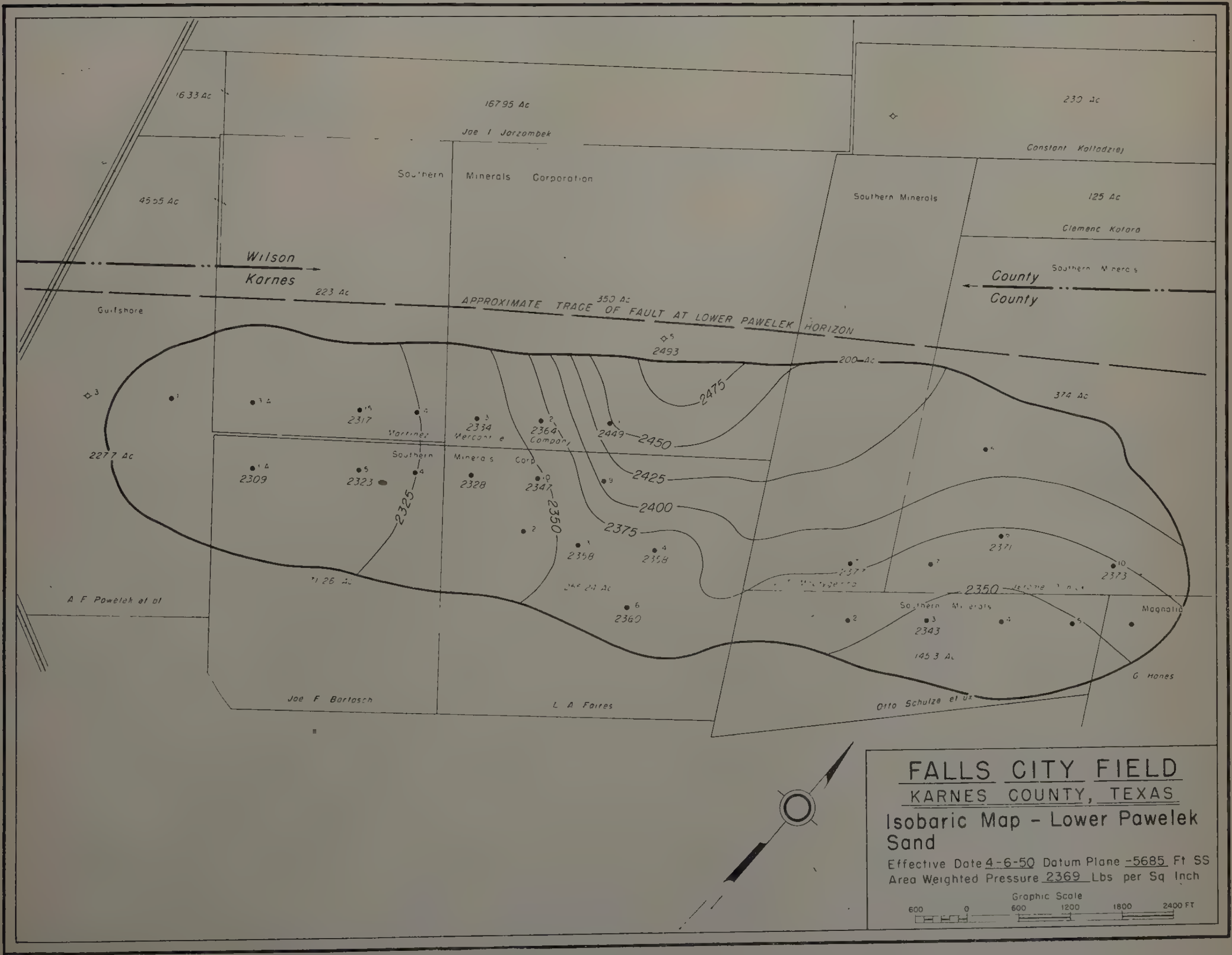

FIG. 13 — ISOBARIC MAP, LOWER PAWELEK SAND, APRIL 6, 1950.

ft from the injection well showed an abrupt increase in water percentage and was recompleted higher in the same sand. No significant changes in water production in other wells have been recorded. The downward trend in flowing tubing pressures has been arrested and in some wells the tubing pressures have been increased as much as 100 psi.

Because of the limited amount of water which can be used in the pressure maintenance program, additional saltwater disposal wells in other sands will be necessary to handle all of the produced water. Also, in the later stages of depletion of the Lower Pawelek reservoir, additional injection wells will be required to provide the necessary injection capacity and to distribute properly the injected water.

ACKNOWLEDGMENT

The writers wish to express their thanks to Maston Nixon, executive vice-president for the Southern Minerals Corporation, for permission to publish this paper, and to others of the company for their assistance in its preparation.

REFERENCES

1. R. J. Schilthuis: Active Oil and Reservoir Energy. *Trans.* AIME (1936), 33.
2. W. Hurst: Water Influx into a Reservoir and Its Application to the Equation of Volumetric Balance. *Trans.* AIME (1942), 57.

★ ★ ★

CORRELATION OF BOTTOM HOLE SAMPLE DATA

GUY BORDEN, JR. AND **MICHAEL J. RZASA,** STANOLIND OIL AND GAS CO., TULSA, OKLA., MEMBERS AIME

ABSTRACT

Laboratory data on bubble point pressures and reservoir volume factors have been correlated as functions of solution gas-oil ratio, calculated gas gravity of the pentanes-and-lighter fraction of the entire fluid, differential residual oil gravity, and reservoir temperatures.

INTRODUCTION

Several correlations of crude oil properties have appeared in the literature.

D. L. Katz[4] in 1942 presented five methods of predicting oil shrinkage, these being of decreasing accuracy for decreasing amounts of information available.

M. B. Standing[6] in 1947 published three correlations of laboratory flash vaporization data of California crudes. From values of GOR (gas-oil ratio), gas gravity, liquid gravity, and temperature, his correlations will predict bubble point pressure, formation volumes of bubble point liquids, and two-phase formation volumes.

Curtis and Brinkley[2] in 1949 presented several correlations. From the gas-oil ratio, an approximation of reservoir volume factor and barrels of condensate recoverable per barrel of reservoir space may be obtained; along with liquid gravity and reservoir temperature, the GOR will allow prediction of bubble point pressure. These last correlations seem to be more qualitative than quantitative.

Generally, laboratory bottom hole sample tests furnish information on solution gas-oil ratios, residual oil gravities, bubble point pressures, viscosities of oils, liquid shrinkages, and occasionally gas gravities. Each of these data has its own applications and use in reservoir engineering calculations. The particular uses of correlated bottom hole sample data are found in

(1) Providing a basis for obtaining estimates of formation crude properties in fields where bottom hole sampling is impractical or impossible.

(2) Greatly reducing the time in obtaining the desired information.

(3) Determining the applicability of the results from various bottom hole samples to particular field problems.

(4) Avoiding, in many cases, the uncertainties of sampling by replacing it with an element over which greater control can be exercised.

(5) Permitting use of preliminary field data in application of production procedures before a bottom hole sample can be obtained and analyzed in the laboratory.

(6) Serving as a check on data which may appear out of line.

(7) Estimating for a particular type crude the appropriate equilibrium constants by working backward from the bubble point pressure.

(8) Estimating original or other past history properties of reservoirs that were not sampled in the past.

PROCEDURE

Application of the published correlations[4,6] to Stanolind laboratory data indicated that the general scheme presented by Standing[6] could give desirable results if changes were made in parameter positions and scales. The correlation curves were drawn with all the variables having consistent gradations except the temperature increments which were drawn in to best fit the data.

The variables from available Stanolind laboratory data are defined below:

(1) Gas-oil Ratio: Gas is liberated at reservoir temperature by differential vaporization (or rather by a series of flashes, approaching differential vaporization) and measured at atmospheric pressure and temperature, at which the compressibility factor is assumed to be unity. The oil is the residual liquid remaining after the pressure has been reduced to atmospheric. For the gas-oil ratio both volumes are corrected to standard conditions of 14.7 psia and 60°F.

(2) Gas Gravity: It was decided to arbitrarily divide the hydrocarbons of the entire bottom hole sample into pentanes-and-lighter and hexanes-and-heavier, and use a calculated gas gravity of the pentanes-and-lighter for a correlating variable. (Sample calculation is shown in Table III.)

(3) Liquid Gravity: This is the API gravity of the residual liquid from the differential vaporization. The gravity is measured at room temperature and corrected to 60°F.

---

[1] References given at end of paper.

Manuscript received in the office of the Petroleum Branch May 29, 1950. Paper presented at the Mid-Continent Joint Meeting in Tulsa, Okla., May 12-13, 1950.

(4) Temperature: This is the temperature at which the differential vaporization and bubble point pressure determinations are carried out, and is usually the bottom hole (reservoir) temperature.

(5) Bubble Point Pressure: This is the pressure at which there is a break in slope of the pressure-volume curve; that is, the pressure at which gas starts to evolve as pressure is decreased. This bubble point pressure is at the test temperature.

(6) Reservoir Volume Factor: This is the barrels of bubble point oil per barrel of residual oil at 60°F and atmospheric pressure. Separation of gas is by differential vaporization at reservoir temperature.

USE OF CORRELATION CHARTS

Prediction of Bubble Point Pressure and Reservoir Volume Factor

Published data of three samples were used to test the correlations. Table II shows the properties of these crudes and the comparisons of predicted and experimental bubble point pressures and reservoir volume factors.

Example uses of the correlation charts are shown in Figs. 1 and 2.

The method of calculating gas gravity is shown in Table III.

Use of Bubble Point Pressure Correlation Chart to Predict Saturation of Reservoir

Crude "A"[3] was sampled at 3,600 psia and 218°F. The tank oil gravity was 27.4°API. Calculated gravity of pentanes-and-lighter is 0.79.

By entering Fig. 1 at 3,600 psia for bubble point pressure and ending up with gas-oil ratio, while using the above quantities for the variables, a gas-oil ratio of 615 cu ft/bbl is predicted. This means that Crude "A" can hold in solution approximately 615 cu ft/bbl of .79 gravity pentanes-and-lighter gas at 3,600 psia and 218°F and be at its bubble point. Comparing 615 with 525 cu ft/bbl shows that the oil is undersaturated at the sampling conditions. Extrapolating experimental data on Crude "A" shows that 575 cu ft/bbl could be in solution at the sampling conditions. Thus, the undersaturation of the oil is correctly predicted.

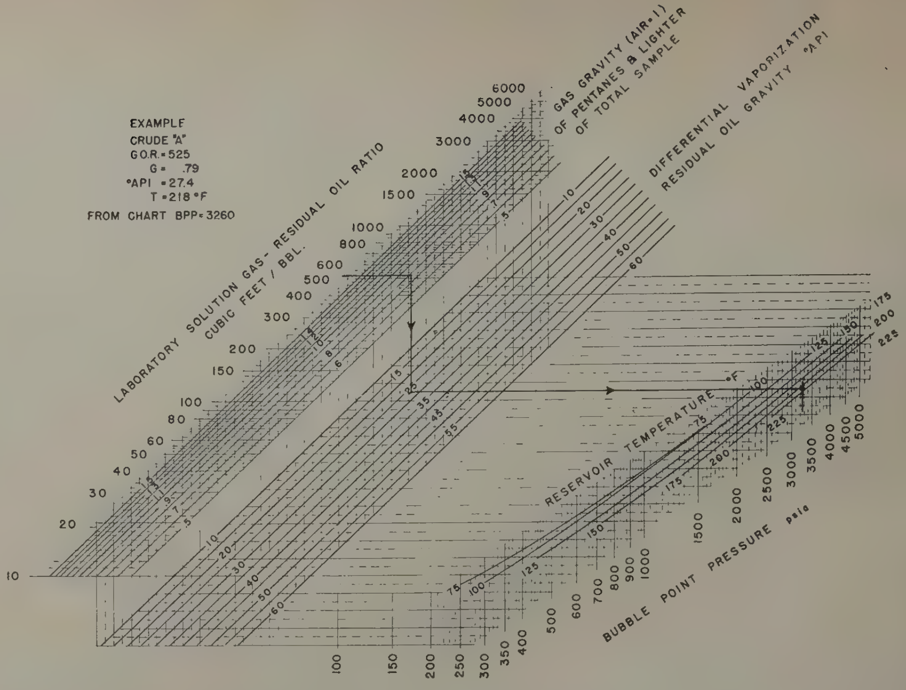

FIG. 1 — BUBBLE POINT PRESSURE CORRELATION.

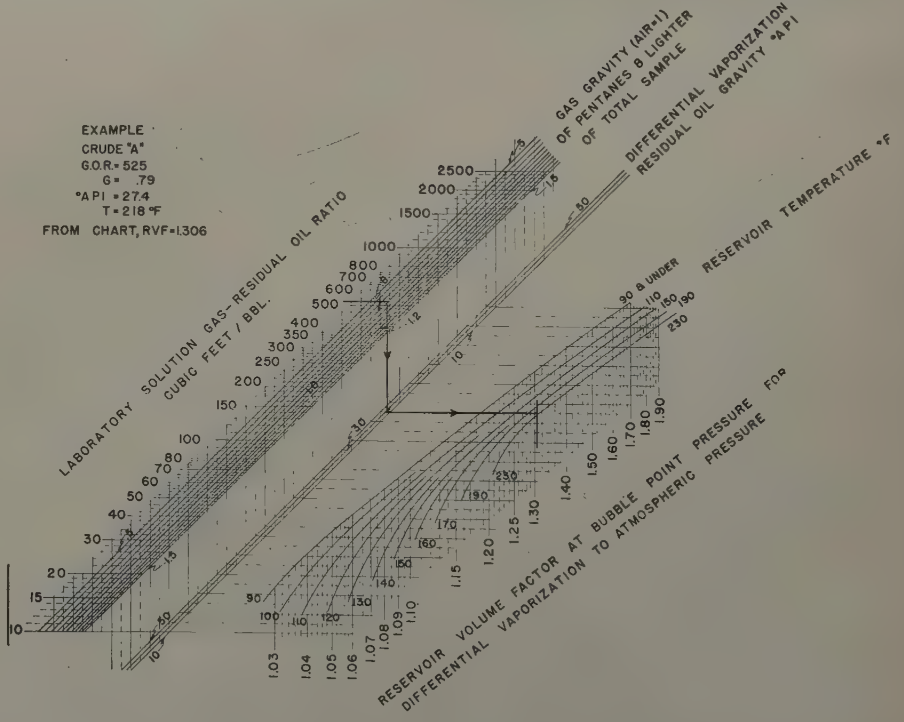

FIG. 2 — RESERVOIR VOLUME FACTOR CORRELATION.

Table I — Range of Data on Bottom Hole Samples from Which Correlations Were Made

	Company Operating Divisions							
	Division 1		Division 2		Division 3		Division 4	
	Min.	Max.	Min.	Max.	Min.	Max.	Min.	Max.
Bubble Point Pressure psia	1187	4650	246	3625	514	3551	292	1239
Reservoir Vol. Factor, bbl/bbl*	1.082	1.745	1.054	1.610	1.098	1.678	1.037	1.217
Gas-Oil Ratio, cu ft/bbl*	156	1165	94	1383	151	1246	50	318
Oil Gravity, °API*	23.8	49.6	29.1	42.6	22.7	49.9	24.8	31.5
Calculated Gas Grav. (Air = 1)	.56	1.21	.92	1.66	.837	1.30	1.09	1.36
Reservoir Temp., °F**	126	236	82	159	101	236	122	156

*From laboratory differential vaporization.

**Division 2 data dominated the temperature range up to 105°F; Division 3, the range 105° to 125° F; Division 4, the range 125° to 145°F; and Division 1, the range from 145°F, up.

Table II — Properties of the Crudes

Component	Analysis, Mol Fractions		
	Crude "A"[3]	Crude "B"[3]	Crude "W"[1]
Methane	.4404	.5345	.4573
Ethane	.0432	.0636	.1032
Propane	.0405	.0466	.0665
Butanes	.0284	.0379	.0417
Pentanes	.0174	.0274	.0297
Hexanes	.0290	.0341	
Heavier	.4011	.2559	.3016

	Crude "A"[3]	Crude "B"[3]	Crude "W"[1]		
			Flash Data	Differential Data	Field Data
Reservoir Temperature, °F	218	243	145	145	145
Lab. Flash GOR, cu ft/bbl*	525	1078	959		921
Differential Vaporization GOR				1065	
Residual Oil Gravity, °API	27.4	34.5	42.0	40.3	42.4
Calculated Gas Gravity of C_{5-}	.790	.812	.886	.886	.797
Experimental Bubble Pt Pr, psia	3305	4470	2952	2952	2952
Correlated Bubble Pt Pr, psia (Fig. 1)	3260	4620	2640	2960	2730
Experimental Res Vol Fac, bbl/bbl	1.305	1.64	1.477	1.550	1.477
Correlated Res Vol Fac (Fig. 2)	1.306	1.700	1.490	1.541	1.450
Differences: BPP psi	45	–150	–312	–8	–222
RVF bbl/bbl	–.001	–.060	–.013	.009	.027
Per Cent Difference: BPP	1.4	3.2	11.8	.3	8.1
RVF	.1	3.7	.9	.6	1.9

*Standard conditions for volumes are 14.7 psia, 60°F

Table III — Calculation for Gas Gravity of Pentanes-and-Lighter (Crude "A"[3])

Component	Mol Fraction	Molecular Weight	Mol Fr x M W
Methane	.4404	16.04	7.064
Ethane	.0432	30.07	1.299
Propane	.0405	44.09	1.786
Butanes	.0284	58.12	1.651
Pentanes	.0174	72.15	1.255
SUMS	.5699		13.055

$$\text{Molecular weight } C_{5-} = \frac{13.055}{.5699} = 22.91$$

Molecular weight of air = 29

$$\text{Gas Gravity } C_{5-} = \frac{22.91}{29} = .790$$

DISCUSSION

Accurate predictions of reservoir fluid properties are of great importance in reservoir engineering studies. It was for this purpose that this investigation was begun and correlations determined. Published correlations[4,6] aided the course of action and suggested the forms of the correlations.

Laboratory data for correlation purposes were obtained from bottom hole sample reports filed at the Stanolind Oil and Gas Co. Research Laboratory. These data are from samples from the company's wells extending from the Gulf Coast to the Rocky Mountains. Standing used California oils and gases for his correlations[6] which may account for the differences in the correlations.

Table IV shows the precision of the correlations with the data from which they were made.

The samples of Table II were chosen to show the use of the correlations because their data have been published.[1,3] The correlations were made from differential vaporization data only. It is realized, however, that the usefulness of this type of correlation would be greatly increased if crude properties and conditions as determined from flash vaporization and field data might also be correlated by the same charts. Flash vaporization data of Crudes "A" and "B" are fairly well correlated by Figs. 1 and 2. The flash and field data of Crude "W" are not as well fitted to the correlations as are the differential vaporization data.

Normally, flash vaporization will show greater gas release than differential if both are conducted at the same temperature. The reason for the lower gas-oil ratio in Crude "W," Table II, is because the flash was conducted in two stages and the second stage temperature was 60°F, which allowed less gas evolution than the higher temperature. These differences in the types of vaporization and the temperatures will necessitate judgment in the use of flash data with the presented correlations.

The use of these correlations with field data may be hazardous, inasmuch as laboratory data were used to develop the charts. However, a rough estimate of bubble point pressure and relative volume factor using field data with these correlations may be of some usefulness.

It was found that the geographical location of the Stanolind wells sampled made little difference in the prediction of bubble point pressures and reservoir volume factors. Recombination samples were not well predicted by the correlation for bubble point pressure. Four samples at lower temperatures (95°F to 127°F) had bubble point pressures predicted from 12 per cent to 53 per cent low; two at higher temperatures (208°F and 230°F), 10.8 per cent and 18.37 per cent high.

Differences in reservoir volume factors for samples at bubble point pressures and at pressures higher than the bubble point are due to the liquid compressibility. Compressibilities range from 5×10^{-6} to 18×10^{-6} bbl/bbl/psi for Stanolind samples with most falling in the 7×10^{-6} to 11×10^{-6} bbl/bbl/psi limits. Therefore, the reservoir volume factor will decrease by approximately 0.001 for every hundred psi above the bubble point pressure.

CONCLUSIONS

Figs. 1 and 2 will permit estimation of bubble point pressures and reservoir volume factors from laboratory solution gas-oil ratios, calculated specific gravities of the pentanes-and-lighter fraction of the entire fluid, residual oil gravities, and reservoir temperatures. It should be possible, in many instances, to determine if a reservoir is saturated or undersaturated.

ACKNOWLEDGMENT

The authors wish to express their appreciation to the management of the Stanolind Oil and Gas Co. for permission to present and publish this paper.

Table IV — Precision of Correlated Data

Bubble Point Correlation, Fig. 1		
Total Points from Bottom Hole Sample Data		188
Total Points from Recombination Sample Data		6
Average Per Cent Prediction High		8.16%
Average Per Cent Prediction Low		10.50%
Average Per Cent Prediction Total		1.84% Low
Per Cent of Data Points Within 10% of Predicted BPP		65.5%
Per Cent of Data Points Within 15% of Predicted BPP		84.5%
Maximum % Deviation (True Value 1437, Predicted 863)		66.5%
Maximum psia Deviation (True Value 3760, Predicted 4600)		840 psia
Division	Total Samples	Within 15% Predicted
Division 1	77	72
Division 2	81	61
Division 3	19	15
Division 4	17	16
No. of Samples with Predicted BPP More than 200 psi High		23
No. of Samples with Predicted BPP More than 200 psi Low		30
Reservoir Volume Factor Correlation, Fig. 2		
Total Points from Bottom Hole Sample Data		172
Total Points from Recombination Sample Data		6
Average Total Deviation		1.0%
Per Cent of Points within 2.6% of Predicted Value		95.5%
Average Deviation High (bbl/bbl)		.015
Average Deviation Low (bbl/bbl)		.014
Maximum % Deviation (True Value 1.445, Predicted 1.605)		10%
Maximum Deviation bbl/bbl (True Value 1.445, Predicted 1.605)		.160

REFERENCES

1. A. B. Cook, E. J. Dewees and H. M. Harris: "Bureau of Mines Analysis of Subsurface Oil Samples," *Petroleum Engineer,* (May, 1945) 85.
2. R. C. Curtis and T. W. Brinkley: "Calculation of Natural Condensate Recovery," Presented API Div. of Prod., Tulsa, Okla., March 23-25, 1949.
3. C. R. Dodson and M. B. Standing: "Prediction of Volumetric and Phase Behavior of Naturally Occurring Hydrocarbon Systems," *API Drill. and Prod. Prac.,* (1941) 326-340.
4. D. L. Katz: "Prediction of Shrinkage of Crude Oils," *API Drill. and Prod. Prac.,* (1942) 137-147.
5. B. H. Sage and H. Reamer: *Trans.* AIME, (1941) **170,** 179.
6. M. B. Standing: "A Pressure-Volume-Temperature Correlation for Mixtures of California Oil and Gases," *API Drill. and Prod. Prac.,* (1947) 275-287.

★ ★ ★

T.P. 2894

THE EFFECT OF PERMEABILITY STRATIFICATION IN COMPLETE WATER-DRIVE SYSTEMS

MORRIS MUSKAT, GULF OIL CORP., PITTSBURGH, PA., MEMBER AIME

ABSTRACT

A theory is presented for calculating the performance history of complete water-drive systems producing from idealized stratified formations. The general equations are applied to systems where the permeability stratification is either of the exponential or linear type. Calculations were carried through for different degrees of permeability stratification, but with special emphasis on the effect of the mobility ratio between the produced oil and the invading water on the resultant performance. These results are also expressed graphically as curves for the initial water breakthrough recovery, for the different degrees of stratification, as a function of the mobility ratio, and of the composition of the produced fluid stream as a function of the cumulative oil recovery. For several typical cases the latter has also been plotted as a function of the cumulative oil and water throughflow. The general result is that when the mobility of the oil is lower than that of the invading water the channelling tendency resulting from the permeability stratification becomes aggravated as the higher permeability zones become flooded out. Situations of this type would obtain when producing low gravity or highly viscous oils. Conversely, if the mobility of the oil is high compared to that of the invading water, the flooding of the high permeability zones will lead to a retarding and choking effect, and the gross bypassing phenomena will be partially suppressed. These conditions would correspond to those of flooding high gravity or low viscosity oils. A discussion is given of the various basic assumptions made in the analysis, including that of ignoring the stripping phase of the production history as implied by relative permeability concepts.

INTRODUCTION

The physical ultimate recoveries from oil reservoirs are basically determined and limited by the physical oil displacement processes associated with the reservoir producing mechanism. In practice, however, the economic ultimate recoveries are further limited by the mobility of the reservoir fluids and the uniformity and continuity of the producing formation. In fact, it is the differential depletion between the component parts of the composite reservoir which ultimately determines the total recovery at the time of field abandonment. While this observation applies to both the solution gas drive and gravity drainage mechanisms, in which use is made only of the energy contained within the original oil-bearing reservoir, it is of even more paramount importance under operations wherein the energy associated with extraneous fluids provides the ultimate oil expulsion mechanism. Whether the invading fluid is the water from an edgewater drive, water injected for pressure maintenance, gas injected for pressure maintenance, or gas returned to the formation in a cycling program, it is often the continuity and uniformity of the producing section which will control the economic efficiency of the operations.

The importance of the problem of reservoir non-uniformity does not, of course, lessen its complexity or the difficulties of its solution. In fact, these are inherently such that the concept of a "general" solution is virtually meaningless. About all that can be reasonably hoped for is the analysis of specific and well-defined types of non-uniformity which may give some degree of approximation to actual reservoir conditions. Since variations in the nature of the reservoir which depend only on the position along the streamlines will not lead directly to major differential depletion development within the reservoir, the types of non-uniformity considered thus far have involved stratification assumptions. That is, the producing section has been replaced by a multi-layer "sandwich," each uniform areally, and differing from the others only in its basic physical constants as to thickness, porosity and permeability. The fluid motion in the composite system is thus approximated by a parallel superposition of the independent fluid movements in the individual strata.

For the specific application to cycling operations the theory of the effect of permeability stratification has been developed for both discontinuous[1] and continuous types of permeability stratification. Among the latter, treatments have been given of systems in which permeability distributions are governed by exponential, linear[2] or probability[3] functions. In all these studies complete dynamical equivalence was assumed between the injected dry gas and the displaced wet gas. The overall effective permeability of each stratum was therefore considered as constant and independent of the degree of invasion of the injected fluid.

In the case of the displacement of oil by water, the assumption of dynamical equivalence between the water and oil will be strictly valid only by accident. Even if the oil viscosity should be the same as that of the water, the effective permeability to the oil in the presence of the connate water will in general be quite different from that of the water behind the water-oil interface flowing past the trapped residual oil. As a result the effective permeability for the stratum as a whole and rate of water invasion will change with time as the intrusion continues. The differential fluid motion in the individual strata will thus also vary with time. Qualitatively, it is easy to predict the resultant effects. If the permeability to viscosity ratio of the invading fluid exceeds that of the fluid displaced, the stratification and bypassing effect of the perme-

---

[1] References given at end of paper.

Manuscript received in the office of the Petroleum Branch December 27, 1949.

ability variation itself will be accentuated. Conversely, if the permeability to viscosity ratio of the invading fluid is less than that of the fluid displaced, the rate of fluid advance in the more permeable strata will become increasingly retarded as the invasion continues, and the channelling tendency will be reduced. It is the quantitative aspects of these phenomena which require detailed analytical treatment and will be the subject of the following sections.

GENERAL THEORY

A little consideration will show that even for a single uniform stratum the history of the fluid motion when the invading and displaced fluids are not dynamically identical will be extremely difficult to determine. In fact, thus far only the cases of simplest geometry, namely linear, radial and spherical, have been quantitatively treated.[4] General well pattern effects are necessarily ignored in such simplified approximations, and the produced fluid is assumed to change suddenly and completely to the invading fluid when the latter first reaches the producing wells. The effect of incomplete pattern sweep efficiency has been taken into account in the study of cycling operations in formations with exponential permeability distributions.[4] It can also be formally included in a general theory of the composition history of the production from stratified formations even when the invading and displaced fluids are not assumed to be dynamically equivalent. From a practical standpoint, however, the resulting analysis is virtually intractable.

The only theoretical treatment thus far reported on the recovery of oil by invading water in undepleted stratified formations without ignoring the differences in mobility between the oil and water is that of Dykstra and Parsons.[5] A discrete layer analysis was used in this study, and a probability permeability distribution was simulated by proper choices of the individual permeabilities of a 50-layer subdivision of the composite section. In this paper will be given the general formulation of the problem for continuous permeability distributions, and this will be applied specifically to the exponential and linear distributions.

If it is assumed that the permeability-saturation characteristics of all the strata in the composite section are the same and that the residual oil saturations behind the water-oil interfaces are the same, as well as the oil saturations in the uninvaded areas,* the rate of water invasion or oil production, in reservoir volume, for any unit thickness lamina at depth z, of homogeneous permeability k, will be expressible as:

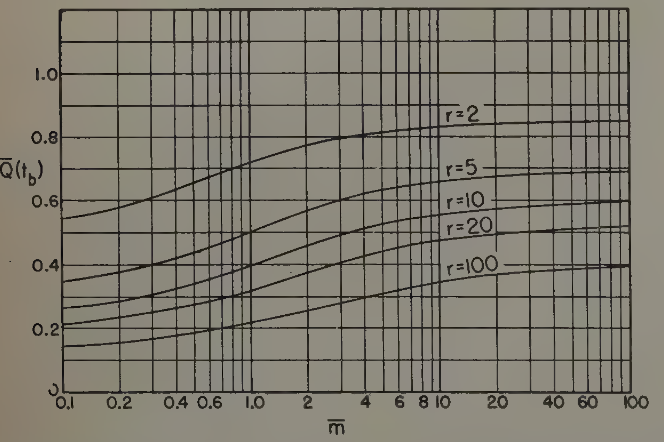

FIG. 1 — THE VARIATION OF THE INITIAL BREAKTHROUGH RECOVERY IN EXPONENTIALLY STRATIFIED SYSTEMS WITH THE MOBILITY RATIO OF THE INVADING AND DISPLACED FLUIDS. $\overline{Q}(t_b)$ = FRACTION OF TOTAL DISPLACEABLE OIL RECOVERED AT THE TIME OF INITIAL BREAKTHROUGH, t_b. $\overline{m}$ = (MOBILITY OF DISPLACED OIL)/(MOBILITY OF INVADING WATER); r = STRATIFICATION RATIO OF ASSUMED EXPONENTIAL PERMEABILITY DISTRIBUTION.

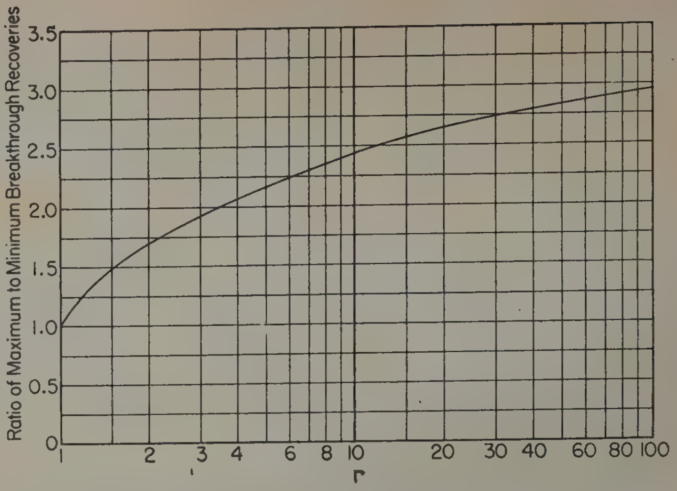

FIG. 2 — THE VARIATION OF THE RATIO OF MAXIMUM TO MINIMUM WATER BREAKTHROUGH RECOVERIES IN EXPONENTIALLY STRATIFIED MEDIA WITH THE STRATIFICATION RATIO, r, FOR THE LIMITS OF INFINITE AND VANISHING MOBILITY RATIOS.

$$Q(t,z) = k\ F(kt) \quad . \ . \ . \ . \ . \ . \ . \ . \quad (1)^{**}$$

where the function $F(kt)$ expresses the effect of the displacing fluid invasion on the overall resultant permeability, and the factor k accounts for the absolute permeability of the lamina. The cumulative throughflow to the time t will then be:

$$\overline{Q}(t,z) = k \int_0^t F(kt)\ dt \quad . \ . \ . \ . \ . \quad (2)$$

Initial water breakthrough will develop when the total throughflow equals the volume of clean recoverable oil in the lamina, i.e., when:

$$\overline{Q}(t,z) = AS\overline{f} = k \int_0^t F(kt)\ dt \quad . \ . \ . \ . \ . \quad (3)$$

where A is the initial oil productive area, S the areal sweep efficiency, and $\overline{f}$ the net displacement porosity, i.e., the product of the porosity and the increase in local water saturation in the water invaded area or decrease in oil saturation. Since by Equation (3), $AS\overline{f}$ is evidently a function only of kt, it may be formally inverted so as to give:

$$t(breakthrough) = \frac{\Psi(AS\overline{f})}{k} \quad . \ . \ . \ . \quad (4)$$

where Ψ is the inverse of the integral of Equation (3). Equation (4) shows that the breakthrough times will in general be inversely proportional to k, as in the case of cycling operations where the differences between the invading and displaced fluids are neglected.

The cumulative recovery from the whole section of thickness

---

*These assumptions of uniformity, together with that for f below, are made both for reasons of simplicity and the lack of any well established alternative assumptions. Actually, however, the method of analysis given here could also be applied if these parameters were taken as variable with depth or k, although the formal analysis would become considerably more complicated.

**While the product kt is indicated in Equation (1) as the basic element of the argument F to emphasize the role played by a potentially varying permeability, it is the ratio of k to the viscosity which is actually the important dynamical variable.

H, at a time t before breakthrough, will then be, as a fraction of the recoverable oil in the reservoir,

$$\bar{Q}(t) = \int_0^H k\,dz \int_0^t F(kt)\,dt \Big/ A \int_0^H \bar{f}\,dz \quad . \quad . \quad (5)$$

and that at initial water breakthrough will be:

$$\bar{Q}(t_b) = \int_0^H dz \int_0^{kt_b} F(\tau)\,d\tau \Big/ A \int_0^H \bar{f}\,dz \quad . \quad . \quad . \quad (6)$$

where t_b is the breakthrough time in the highest permeability layer, as defined by Equation (4) for $k = k(z = H)$. It is assumed in Equations (5) and (6), and in all the subsequent analyses, that the various permeability strata have been rearranged in increasing sequence from $z = 0$ to $z = H$.

After the first water breakthrough in any individual stratum there will be a gradual rise in water-oil ratio as the initial water cusps expand and ultimately completely envelop the producing wells. The history of this latter phase of the oil production will evidently depend on the well pattern, field geometry, and relative producing rates of the wells. While its effect could be formally introduced into the general theory, there is little point in such a generalization, since the assumed functional form for this phase of the history would necessarily have to be quite specific and arbitrary and would not warrant the additional laborious computations required for its numerical evaluation. Accordingly, it will be assumed hereafter that the production in any layer is converted to 100 per cent water as soon as there is any breakthrough at all.* This is equivalent to setting the pattern sweep efficiency, $S = 1$ in Equation (3), etc.

Proceeding to the period after breakthrough in the most permeable layer, i.e., for $t > t_b$, the fractional oil content in the total fluid production will then be:

$$R_o(t) = \frac{\int_0^{z_0} k(z)F(kt)\,dz}{\int_0^H k(z)F(kt)\,dz} \quad . \quad . \quad . \quad . \quad . \quad . \quad (7)$$

where z_o is determined by the condition:

$$k(z_o) = \frac{\Psi(A\bar{f})}{t} \quad . \quad . \quad . \quad . \quad . \quad . \quad . \quad . \quad . \quad . \quad (8)$$

and represents the depth to which breakthrough has already occurred.

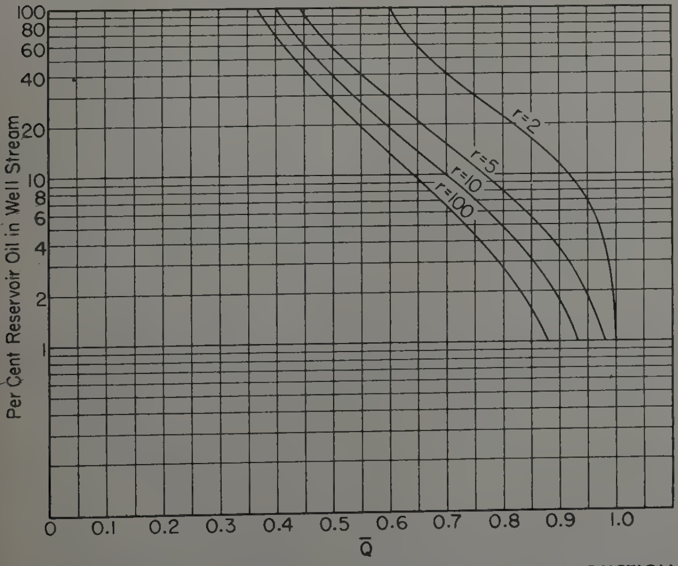

FIG. 3 — THE VARIATION OF THE OIL CONTENT IN THE PRODUCTION FROM EXPONENTIALLY STRATIFIED WATER-DRIVE RESERVOIRS WITH THE CUMULATIVE RECOVERY, FOR $\bar{m} = 0.1$; $\bar{Q}$ = CUMULATIVE RECOVERY, AS A FRACTION OF THE TOTAL RESERVOIR DISPLACEABLE RECOVERY. r = STRATIFICATION RATIO; $\bar{m}$ = (MOBILITY OF DISPLACED OIL)/(MOBILITY OF INVADING WATER).

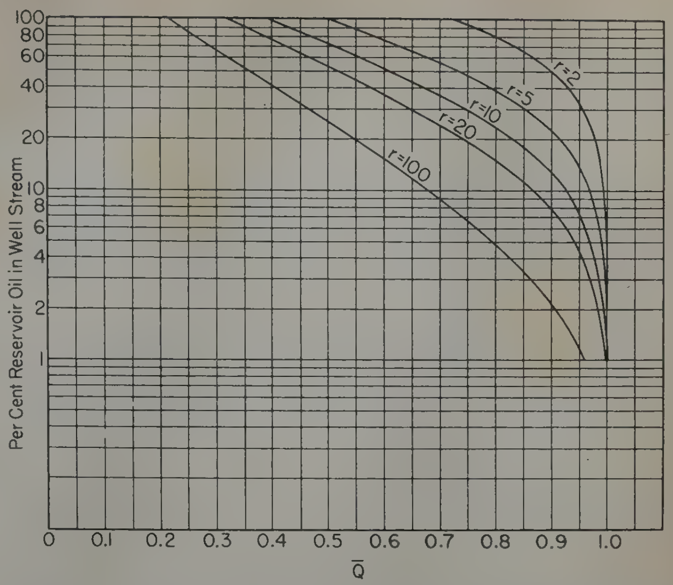

FIG. 4 — THE VARIATION OF THE OIL CONTENT IN THE PRODUCTION FROM EXPONENTIALLY STRATIFIED WATER-DRIVE RESERVOIRS WITH THE CUMULATIVE RECOVERY, FOR $\bar{m}$ = 1; $\bar{Q}$ = CUMULATIVE RECOVERY, AS A FRACTION OF THE TOTAL RESERVOIR DISPLACEABLE RECOVERY. r = STRATIFICATION RATIO; $\bar{m}$ = (MOBILITY OF DISPLACED OIL)/(MOBILITY OF INVADING WATER).

The cumulative oil production as a fraction of the total recoverable oil in the reservoir will then be:

$$\bar{Q}(t) = \left[A \int_{z_0}^H \bar{f}\,dz + \int_0^{z_0} k(z)\,dz \int_0^t F(kt)\,dt\right] \Big/ A \int_0^H \bar{f}\,dz \quad . \quad . \quad . \quad . \quad . \quad . \quad . \quad . \quad . \quad (9)$$

If the permeability included in the net productive section has a non-vanishing lower limit, the production phase governed by Equations (7) and (8) will terminate after breakthrough in the tightest layer, as determined by Equation (4). Under the assumption of 100 per cent pattern efficiency, i.e., $S = 1$, this will necessarily terminate the whole oil production history, although in practice a limiting value of R_o will generally control the state of abandonment.

The Function *F* for Linear Flow

As a practical matter drastic simplifications must be made in applying the general equations developed above. As a first step a functional form must be derived for the function F. For this purpose the case of an ideal linear system will be assumed here as was done by Dykstra and Parsons,[5] since anything more complex which might be of practical significance would be virtually intractable from a strictly analytical standpoint.

It may be shown that the rate of throughflow per unit cross section at any time t in a linear system in which a liquid (w) is displacing another (o), may be expressed as:

$$Q = \frac{m_w \bar{f} a L/2}{\sqrt{1-(1-\bar{m})a m_w t}}; \quad \bar{m} = m_o/m_w; \quad a = \frac{2\bar{m}\Delta p}{\bar{f}L^2} \quad . \quad (10)*$$

---

*This simplification involves the further assumption that there is no "subordinate phase" or stripping of the residual oil behind the advancing water-oil interface. This will be further discussed later.

*Equation (10) can be derived by applying the analysis given in "Flow of Homogeneous Fluids Through Porous Media," §8.3, for two-fluid linear encroachment systems.

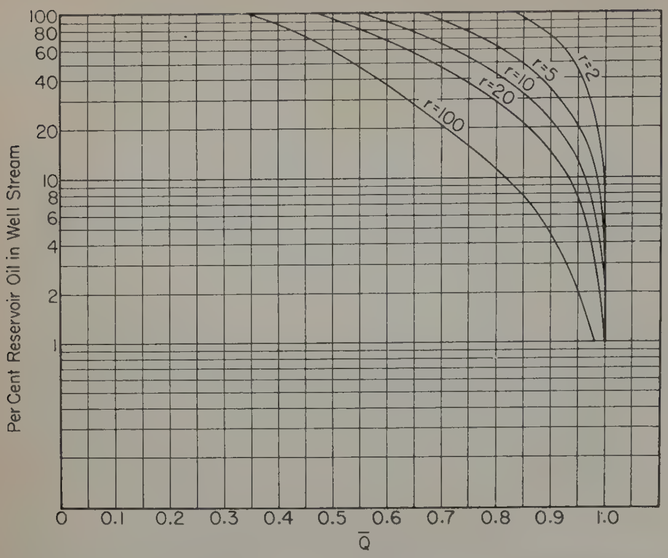

FIG. 5 — THE VARIATION OF THE OIL CONTENT IN THE PRODUCTION FROM EXPONENTIALLY STRATIFIED WATER-DRIVE RESERVOIRS WITH THE CUMULATIVE RECOVERY, FOR $\bar{m} = 10$; $\bar{Q}$ = CUMULATIVE RECOVERY. AS A FRACTION OF THE TOTAL RESERVOIR DISPLACEABLE RECOVERY. r = STRATIFICATION RATIO; $\bar{m}$ = (MOBILITY OF DISPLACED OIL)/MOBILITY OF INVADING WATER).

where m_w, m_o are the "mobilities" for the displacing and displaced fluids, L the total length of the system, Δp is the driving pressure differential, which is assumed to be constant,* and $\bar{f}$ is the net displacement porosity. The mobility is defined as the ratio of the effective permeability to the viscosity. By reference to Equation (1) it follows that the function F is given by:

$$F(kt) = \frac{\bar{f}aL/2\mu_w}{\sqrt{1-(1-\bar{m})am_wt}} \quad . \; . \; . \; . \; . \; . \quad (11)$$

The cumulative throughflow per unit cross section to the time t will be, on integrating Equation (10):

$$\bar{Q}(t.z) = \frac{\bar{f}L}{1-\bar{m}}\left[1-\sqrt{1-(1-\bar{m})am_wt}\right] . \quad (12)$$

The time for breakthrough is obtained by setting $\bar{Q}(t,z)$ equal to $\bar{f}L$, and is found to be:

$$t_b = \frac{1+\bar{m}}{am_w} \quad . \; . \; . \; . \; . \; . \; . \; . \; . \; . \quad (13)$$

To proceed further it is necessary to specify the nature of the permeability, k or m_w, distribution.** Here, too, one must make, as a matter of practical necessity, a further simplification in considering that the mobility ratio $\bar{m}$ is a constant, independent of the absolute permeability. As to the permeability distributions themselves, the exponential and linear distributions will be analyzed in detail.

EXPONENTIAL PERMEABILITY DISTRIBUTION

As in the case of the previous[4] study of cycling operations ($\bar{m} = 1$), the exponential permeability distribution will be taken in the form:

$$k = k_{min}\, e^{bz/H};\; b = \log r \quad . \; . \; . \; . \; . \quad (14)$$

where k_{min} is the minimum permeability, at $z = 0$, rk_{min} is the maximum permeability at $z = H$, H is the net thickness of the section and, as already indicated, the various strata are considered to be rearranged in a monotonic sequence increasing with depth. The parameter r defines the particular exponential distribution of interest, and will be termed the stratification ratio. It will also be assumed that there is no cross flow between the strata, which will not be strictly true unless the vertical permeability is zero, and that the net displacement porosity $\bar{f}$ is independent of k, which also will represent an approximation assumption.

Under these assumptions the total throughflow from the whole section at a time t before any breakthrough has developed, as a fraction of the total recoverable oil, will then be given essentially by integrating Equation (12), as:

$$\bar{Q}(t) = \frac{1}{(1-\bar{m})H}\int_0^H \left[1-\sqrt{1-(1-\bar{m})am_wt}\,\right] dz$$

$$= \frac{1}{1-\bar{m}}\Bigg[\;1-\frac{2}{b}\left\{\sqrt{1-(1-\bar{m}^2)t/t_b}-\sqrt{1-(1-\bar{m}^2)t/rt_b}\right\}$$

$$-\frac{1}{b}\log\frac{\sqrt{1-(1-\bar{m}^2)t/t_b}-1}{\sqrt{1-(1-\bar{m}^2)t/t_b}+1}+\frac{1}{b}\log\frac{\sqrt{1-(1-\bar{m}^2)t/rt_b}-1}{\sqrt{1-(1-\bar{m}^2)t/rt_b}+1}\Bigg]$$

$$. \; . \; . \; . \; . \; . \; . \; . \quad (15)$$

where t_h is the time of initial breakthrough, as given by:

$$t_b = \frac{(1+\bar{m})}{ar\; m_{w\,min}} \quad . \; . \; . \; . \; . \; . \; . \; . \; . \quad (16)$$

$m_{w\,min}$ corresponding to k_{min}.

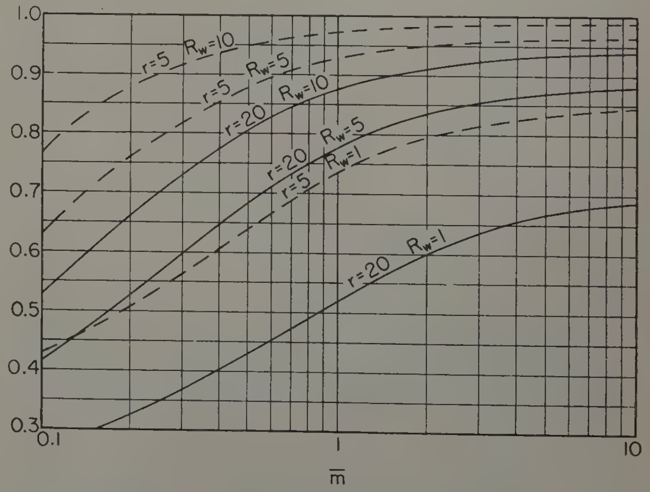

FIG. 6 — THE VARIATION OF THE CUMULATIVE RECOVERY, $\bar{Q}$, IN EXPONENTIALLY STRATIFIED WATER-DRIVE RESERVOIRS WITH THE MOBILITY RATIO $\bar{m}$, TO FIXED VALUES OF THE WATER-OIL RATIO R_w, AND FOR FIXED VALUES OF THE STRATIFICATION RATIO r. $\bar{Q}$ = CUMULATIVE RECOVERY AS A FRACTION OF THE TOTAL RESERVOIR DISPLACEABLE RECOVERY. $\bar{m}$ = (MOBILITY OF DISPLACED OIL)/(MOBILITY OF INVADING WATER).

---

*It is also tacitly assumed throughout this work that at all times the pressures are above the bubble point, corresponding to a complete water drive operation of an undersaturated reservoir.

**Under the assumption that the relative permeabilities both ahead and behind the water-oil interfaces are independent of the homogeneous fluid permeabilities, the distributions of the latter, as given by Equation (14) or (21), will apply also to the effective permeabilities and mobilities which enter directly in the analysis.

At this time $\bar{Q}$ will have the value:

$$\bar{Q}(t_b) = \frac{1}{1-\bar{m}}\Big[\ 1-\frac{2}{b}\Big\{\ m-\sqrt{1-(1-\bar{m}^2)/r}\ \Big\} -\frac{1}{b}\log\frac{m-1}{m+1}+\frac{1}{b}\log\frac{\sqrt{1-(1-\bar{m}^2)/r}-1}{\sqrt{1-(1-\bar{m}^2)/r}+1}\ \Big] \quad \text{. . . . . (17)}$$

After the initial breakthrough the cumulative fractional recovery will be, on applying Equations (10) and (14) to Equation (9):

$$\begin{aligned}\bar{Q}(t) &= 1-\frac{z_o}{H}+\frac{1}{(1-\bar{m})H}\int_0^{z_o}\Big[1-\sqrt{1-(1-\bar{m})am_w t}\ \Big]\,dz \\ &= 1+\frac{\bar{m}}{(1-\bar{m})b}\log\frac{r}{\bar{t}}-\frac{1}{(1-\bar{m})b}\Big[\ 2\Big\{\bar{m}-\sqrt{1-(1-\bar{m}^2)t/r}\ \Big\} \\ &\quad +\log\frac{\bar{m}-1}{\bar{m}+1}-\log\frac{\sqrt{1-(1-\bar{m}^2)\bar{t}/r}-1}{\sqrt{1-(1-\bar{m}^2)\bar{t}/r}+1}\ \Big]\end{aligned} \quad \text{. . . . . (18)}$$

where z_o is the value of z above which there has been water breakthrough at the time t, and $\bar{t} = t/t_b$. The water-oil ratio will be:

$$R_w = \frac{Q_w}{Q_o} = \frac{\int_0^{z_o} k(z)F(kt)dz}{\int_{z_o}^{H} k(z)F(kt)dz} = \frac{(1-\bar{m}^2)(\bar{t}-1)}{2\bar{m}\Big\{\sqrt{1-(1-\bar{m}^2)t/r}-\bar{m}\ \Big\}} \text{. (19)}$$

It will be readily verified that for $\bar{m} = 1$, as may be assumed for the case of cycling operations, Equations (17)-(19) reduce to:

$$\begin{aligned}\bar{Q}(t_b) &= \frac{1}{rb}(r-1);\ t_b = \frac{\mu_w \bar{f} L^2}{r\Delta p k_{min}(eff)}, \\ \bar{Q}(t>t_b) &= \frac{1}{b}\Big[\ 1-\frac{\bar{t}}{r}+\log \bar{t}\ \Big] \\ R_w &= \frac{\bar{t}-1}{1-\bar{t}/r}\end{aligned} \quad \text{. . . . . (20)}$$

which agree with those derived for this case previously.

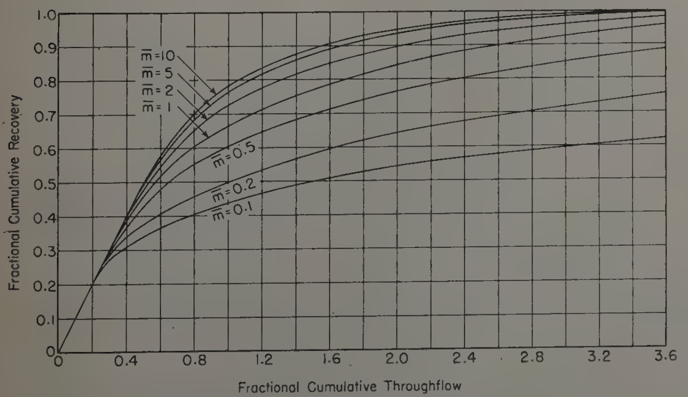

FIG. 7 — THE CUMULATIVE OIL RECOVERY HISTORY VS. THE TOTAL FRACTIONAL CUMULATIVE WATER AND OIL THROUGHFLOW IN EXPONENTIALLY STRATIFIED WATER-DRIVE RESERVOIRS FOR DIFFERENT VALUES OF THE MOBILITY RATIO, $\bar{m}$ = (MOBILITY OF DISPLACED OIL)/(MOBILITY OF INVADING WATER). IN ALL CASES THE STRATIFICATION RATIO = 20.

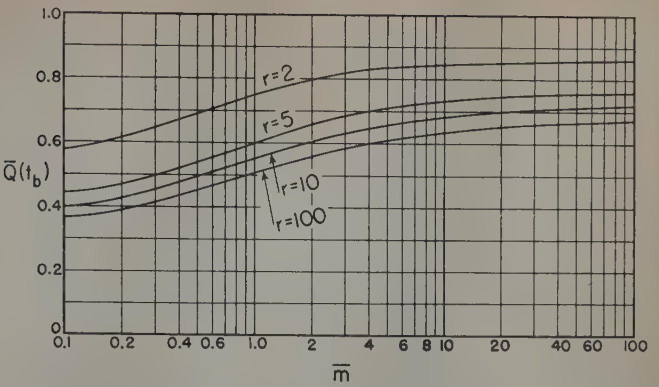

FIG. 8 — THE VARIATION OF THE INITIAL BREAKTHROUGH RECOVERY IN LINEARLY STRATIFIED SYSTEMS WITH THE MOBILITY RATIO OF THE INVADING AND DISPLACED FLUIDS. $\bar{Q}(t_b)$ = FRACTION OF TOTAL DISPLACEABLE OIL RECOVERED AT TIME OF INITIAL BREAKTHROUGH, t_b. $\bar{m}$ = (MOBILITY OF DISPLACED OIL)/(MOBILITY OF INVADING WATER); r = STRATIFICATION RATIO OF ASSUMED LINEAR PERMEABILITY DISTRIBUTION.

On the other hand, in the limit of $\bar{m}\rightarrow\infty$, in which the invading fluid (water, m_w) has a negligible mobility as compared to that displaced (oil, m_o), Equations (17)-(19) reduce to:

$$\begin{aligned}\bar{Q}(t_b) &= \frac{2}{b}\Big(1-\frac{1}{\sqrt{\bar{r}}}\Big);\ t_b = \frac{\mu_w \bar{f} L^2}{2r\Delta p k_{min}(eff)}, \\ \bar{Q}(t>t_o) &= 1-\frac{1}{b}\log\frac{r}{\bar{t}}+\frac{2}{b}\Big(1-\sqrt{\bar{t}/r}\Big), \\ R_w &= \frac{(\bar{t}-1)}{2(1-\sqrt{\bar{t}/r})}\end{aligned} \quad \text{. . . . . (21)}$$

And in the converse limit of $\bar{m}\rightarrow 0$, where the resistance to the invading fluid is negligible as compared to that displaced, the water-oil ratio will rise precipitously to infinite values immediately after initial breakthrough, and the total fractional recovery $\bar{Q}$ will be essentially that at t_b, as given by Equation (17) for $\bar{m} = 0$.

The values of the fractional flooding recovery at the time of first water breakthrough, $\bar{Q}(t_b)$, as given by Equation (17), are plotted vs. the mobility ratio $\bar{m}$ in Fig. 1 for fixed values of stratification ratio r. As previously anticipated, for $\bar{m}<1$, i.e., when the mobility of the displacing fluid (water) exceeds that of the fluid displaced (oil) the bypassing tendency is accentuated and the breakthrough recovery is reduced. Conversely, when the mobility of the displacing fluid is lower than that displaced, $\bar{m}>1$, the continued entry of the former in the higher permeability strata will automatically retard itself and the breakthrough recovery will be increased. These effects increase with increasing stratification ratios r. The ratio of maximum breakthrough recovery, for $\bar{m} = \infty$, to the minimum at $\bar{m} = 0$, is plotted vs. r in Fig. 2. The total maximum range of the effect of the mobility contrast is 3.26, for $r = \infty$.

Because of the rapid buildup of the water production after initial breakthrough, especially for $\bar{m}<1$, it is difficult to devise a satisfactory graphical representation of this later phase of the production history in terms of the water-oil ratio R_w. It has been found preferable to use as an index the percentage of oil in the composite fluid stream, in reservoir measure. This quantity, denoted by R_o, will be given simply by $1/(1+R_w)$, and is plotted vs. the cumulative fractional displaceable oil recovery, for fixed values of stratification ratio r and several values of mobility ratio $\bar{m}$ in Figs. 3-5.

The starting points of the curves of these figures represent the initial breakthrough recoveries. The general shifts of the curves, for mixed $\overline{m}$, to the right as r decreases, are of course to be expected apriori. It is of interest to note, however, that whereas for $\overline{m}<1$, Fig. 3, the systems with lowest breakthrough recoveries, greatest values of r, have the steepest initial rates of fall in oil content of the flow stream, the converse is true for $\overline{m}>1$, Fig. 5. Moreover, whereas for $\overline{m}<1$, the curves tend to be initially concave upward, they ultimately develop steep slopes, for all mobility ratios m, as the oil content of the flow stream becomes small and complete flooding develops throughout the reservoir.

Figs. 3-5 show that the differences in ultimate oil recoveries for reservoirs with different stratification and fluid characteristics will be considerably lower if the operations are continued to low oil contents than at initial water breakthrough. Thus, for $\overline{m}=0.1$ the recovery at one per cent oil content in the well stream will be only 30 per cent greater for $r=2$ than for $r=100$, whereas the breakthrough recovery for $r=2$ will be 3.7 times as great as for $r=100$. For $\overline{m}=10$, the recovery at one per cent oil content for $r=2$ will exceed that for $r=100$ by only about two per cent, as compared to a ratio of 2.4 at initial breakthrough. Similarly for r fixed at 20, the breakthrough recoveries for $\overline{m}=10$ and 0.1 are in the ratio of 2.2, whereas the recoveries at one per cent oil content are in the ratio of only 1.06.

The variation of the recoveries to fixed water-oil ratio, R_w, with the value of $\overline{m}$, for several values of r, is plotted in Fig. 6. Here again will be seen the effect of increasing mobility ratio $\overline{m}$ in improving the resultant recoveries. It will be noted, too, that the recoveries are more sensitive to $\overline{m}$ in the range $\overline{m}<1$ than for $\overline{m}>1$. The gross comparative positions of the curves reflect the degree of reservoir stratification and the limiting water-oil ratios to which the production is continued.

The oil recovery vs. total throughflow or production history can be calculated from the relation (valid for $1 \leqslant \bar{t} \leqslant r$):

$$\overline{V}(\bar{t}) = \overline{Q}(\bar{t}) + \frac{1+\overline{m}}{2\overline{m}b}\left[\bar{t}-1-\log \bar{t}\right] \quad . \quad . \quad . \quad (22)$$

where $\overline{V}(\bar{t})$ is the cumulative total liquid production, in reservoir volume, expressed in units of the total displaceable reservoir liquid content. $\overline{Q}(\bar{t})$ is the cumulative fractional oil recovery given by Equation (18). A typical set of production history curves calculated by Equations (22) and (18) are those plotted in Fig. 7 for a stratification ratio $r=20$. The effect of the mobility ratio $\overline{m}$ is here strikingly shown by comparative values of the cumulative throughflow, $\overline{V}$, for equal total recoveries, and especially at high values of the latter. Thus, at a total fractional recovery of 35 per cent the total fractional throughflow would be 0.35, 0.36, and 0.55 for $\overline{m}=10$, 1, 0.1; at a recovery of 50 per cent these would be 0.51, 0.57 and 1.5 respectively; and for 80 per cent cumulative recovery the corresponding fractional throughflows or total reservoir fluid production would be 1.06, 1.68 and 8.0 for $\overline{m}=10$, 1 and 0.1 respectively.

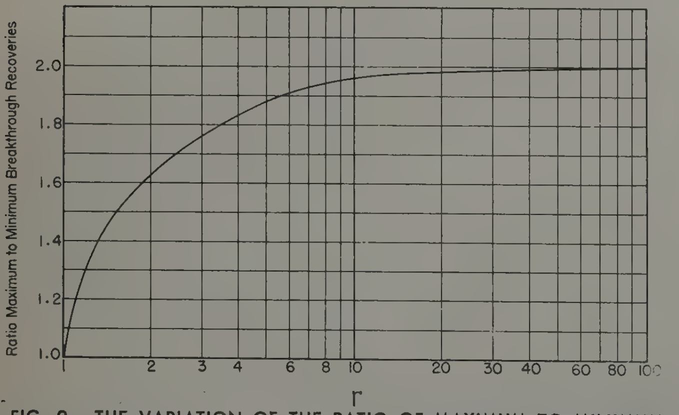

FIG. 9 — THE VARIATION OF THE RATIO OF MAXIMUM TO MINIMUM WATER BREAKTHROUGH RECOVERIES IN LINEARLY STRATIFIED MEDIA WITH THE STRATIFICATION RATIO r, FOR THE LIMITS OF INFINITE AND VANISHING MOBILITY RATIOS.

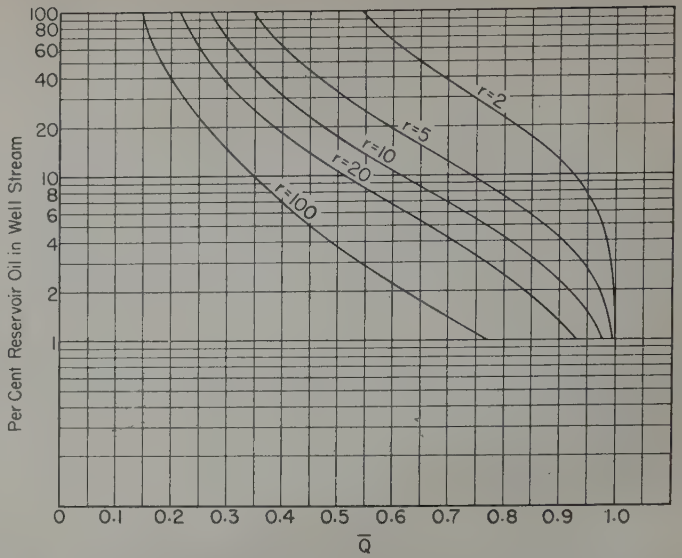

FIG. 10 — THE VARIATION OF THE OIL CONTENT IN THE PRODUCTION FROM LINEARLY STRATIFIED WATER-DRIVE RESERVOIRS WITH THE CUMULATIVE RECOVERY, FOR $\overline{m}=0.1$; $\overline{Q}$ = CUMULATIVE RECOVERY, AS A FRACTION OF THE TOTAL RESERVOIR DISPLACEABLE RECOVERY. r = STRATIFICATION RATIO; $\overline{m}$ = (MOBILITY OF DISPLACED OIL)/(MOBILITY OF INVADING WATER).

LINEAR PERMEABILITY DISTRIBUTION

The linear permeability distribution may be defined by:

$$k(z) = k_{\min}\left[1+(r-1)z/H\right] \quad . \quad . \quad . \quad (23)$$

where here, too, the stratification ratio r is the ratio of the maximum permeability $rk_{\min}$, at $z=H$, to the minimum $k_{\min}$, at $z=0$. The total throughflow at a time t before breakthrough has developed, as a fraction of the total recoverable oil, will be, analogous to Equation (15):

$$\overline{Q}(t) = \frac{1}{(1-\overline{m})H}\int_0^H \left[1-\sqrt{1-(1-\overline{m})am_w t}\right]dz$$

$$= \frac{1}{1-\overline{m}}\left[1+\frac{2}{3b}\left\{(a-b)^{3/2}-a^{3/2}\right\}\right] \quad . \quad (24)$$

where:

$$a = 1-(1-\overline{m}^2)\bar{t}/r; \quad b = (1-\overline{m}^2)(r-1)\bar{t}/r;$$

$$\bar{t} = t/t_b; \quad t_b = \frac{(1+\overline{m})\mu_w}{ar\ k_{\min}} \quad . \quad . \quad . \quad . \quad . \quad . \quad (24a)$$

The fractional recovery at first water breakthrough, i.e., $\bar{t}=1$, will then be:

$$\overline{Q}(t_b) = \frac{1}{1-\overline{m}}\left[1+\frac{2r}{3(r-1)(1-\overline{m}^2)}\left\{\overline{m}^3-(1-(1-\overline{m}^2)/r)^{3/2}\right\}\right.$$

$$. \quad . \quad . \quad . \quad . \quad . \quad . \quad . \quad . \quad (25)$$

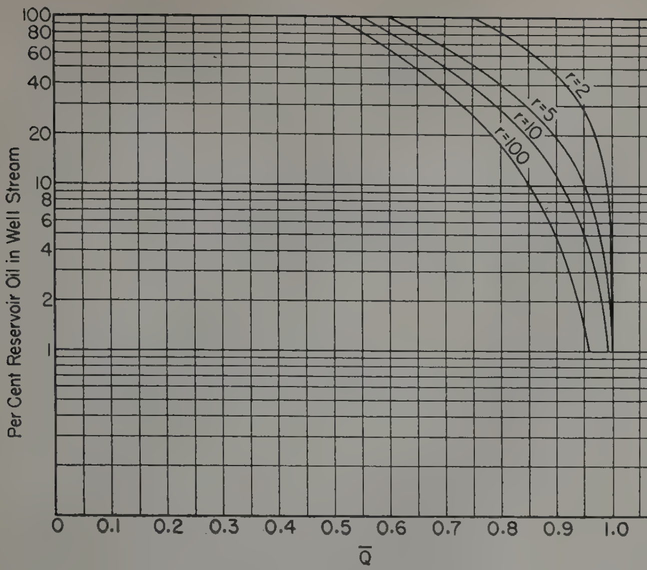

FIG. 11 — THE VARIATION OF THE OIL CONTENT IN THE PRODUCTION FROM LINEARLY STRATIFIED WATER-DRIVE RESERVOIRS WITH THE CUMULATIVE RECOVERY, FOR $\overline{m} = 1$; Q = CUMULATIVE RECOVERY, AS A FRACTION OF THE TOTAL RESERVOIR DISPLACEABLE RECOVERY. r = STRATIFICATION RATIO; $\overline{m}$ = (MOBILITY OF DISPLACED OIL)/(MOBILITY OF INVADING WATER).

After the initial water breakthrough, $\bar{t} > 1$, the cumulative recovery will be:

$$\overline{Q}(\bar{t}) = 1 - \frac{z_o}{H} + \frac{1}{(1-\overline{m})H}\int_o^{z_o}\left[1 - \sqrt{1-(1-\overline{m})am_w t}\,\right]dz$$
$$= 1 + \frac{\overline{m}}{1-\overline{m}}\,\frac{(r/\bar{t}-1)}{r-1} + \frac{2r/\bar{t}}{3(1-\overline{m})(1-\overline{m}^2)(r-1)}\left\{\overline{m}^3 - a^{3/2}\right\} \quad . \; . \; . \; . \; . \; . \; . \; . \; . \quad (26)$$

where z_o is the value of z above which there has been water breakthrough. It will be noted that at $\bar{t} = 1$, Equation (26) becomes equivalent to Equation (25). And at the time of breakthrough in the tightest layer, $\bar{t} = r$, $\overline{Q}$ becomes unity, as it should under the assumed conditions.

The water-oil ratio during this period is given by:

$$R_w = \frac{Q_w}{Q_o} = \frac{3(1-\overline{m}^2)^2(\bar{t}^2-1)}{4\overline{m}} \bigg/ \left[\left\{2+(1-\overline{m}^2)\frac{\bar{t}}{r}\right\}\sqrt{1-(1-\overline{m}^2)\bar{t}/r} - \overline{m}\,(3-\overline{m}^2)\right] \quad . \; . \quad (27)$$

In the limit of $\overline{m} = 1$, corresponding to cycling operations, R_w reduces, as it should, to:

$$R_w = \frac{\bar{t}^2 - 1}{1 - \bar{t}^2/r^2} \quad . \; . \; . \; . \; . \; . \; . \; . \quad (28)$$

It will be noted, too, that at $\bar{t} = 1$, $R_w = 0$, and that it becomes indefinitely large as $\bar{t}$ approaches r.

The total reservoir fluid throughflow, in units of the total displaceable reservoir content volume, may be shown to be given by:

$$\text{Throughflow} = \overline{Q}(\bar{t}): \quad 0 \leqslant \bar{t} \leqslant 1$$
$$= \overline{Q}(\bar{t}) - \frac{r(1+\overline{m})}{2\overline{m}(r-1)}\left[1 - \frac{1}{2}\left(\bar{t} + \frac{1}{\bar{t}}\right)\right]: \quad 1 \leqslant \bar{t} \leqslant r \; . \quad (29)$$

The variation of the initial breakthrough recoveries with the mobility ratio $\overline{m}$, as given by Equation (25), for fixed values of r is plotted in Fig. 8. The general shapes of these curves, reflecting the effect of the mobility ratio on the breakthrough recovery, is similar to that shown in Fig. 1 for the exponential permeability distribution. As a whole the curves of Fig. 8 lie higher than those of Fig. 1, showing that for the same stratification constant and mobility parameter the linear permeability distribution represents a type of reservoir non-uniformity which is not as serious as the exponential distribution. This is further indicated by the closer grouping of the curves of Fig. 8 than the corresponding ones for Fig. 1, which again shows that the effects of the permeability variation will be much more limited when distributed linearly than when it varies exponentially. In fact, whereas the breakthrough and subsequent recoveries become vanishingly small as r approaches infinity for the exponential distribution, the breakthrough recovery approaches the non-vanishing limit $(2\overline{m}+1)/3(1+\overline{m})$ as r becomes infinitely large in the linear permeability distribution.

The gross overall effect of the mobility ratio in the linearly stratified formations, as expressed by the ratio of the maximum to minimum water breakthrough recoveries, is plotted vs. the stratification ratio r in Fig. 9. These represent the ratios $\overline{Q}(t_b)$ for $\overline{m} = \infty$ to that for $\overline{m} = 0$. The curve of Fig. 9 is of the same general shape as that of Fig. 2 for the exponentially stratified system, except that the maximum asymptotic limit has here the value 2.0, as compared to 3.26 in Fig. 2. This once more reflects the smaller total effect of permeability non-uniformity when distributed according to a linear stratification as compared to that when it follows an exponential distribution.

The resultant production histories after first water breakthrough in the linearly stratified systems are plotted in Figs. 10-12. Here, as in the case of the exponential distributions, the ordinates represent the per cent reservoir oil in the composite well stream, and the abscissas are the cumulative fractional oil recoveries. The uppermost points of the various curves give the breakthrough recoveries. The general characteristics of this set of curves are similar to those for the exponential distributions plotted in Figs. 3 to 5. Once again the

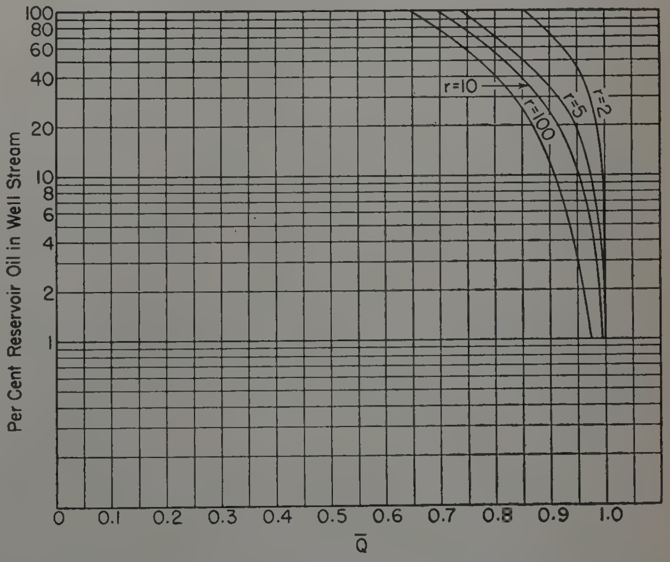

FIG. 12 — THE VARIATION OF THE OIL CONTENT IN THE PRODUCTION FROM LINEARLY STRATIFIED WATER-DRIVE RESERVOIRS WITH THE CUMULATIVE RECOVERY, FOR $\overline{m} = 10$; $\overline{Q}$ = CUMULATIVE RECOVERY, AS A FRACTION OF THE TOTAL RESERVOIR DISPLACEABLE RECOVERY. r = STRATIFICATION RATIO; $\overline{m}$ = (MOBILITY OF DISPLACED OIL)/(MOBILITY OF INVADING WATER).

more limited effects of the differential mobility in the linearly stratified system are exhibited by the closer grouping of the curves for different stratification constants and their general shift toward the region of higher recoveries. It is for the former reason that in Figs. 10-12 the curves for $r = 20$ have been omitted, because of the small separation between the curves for $r = 10$ and $r = 100$. It will be noted, too, on comparison of the corresponding figures for the linearly and exponentially stratified systems, that while as a group the curves for the former are shifted toward the right, those for the same values of r for the two types of stratification ultimately cross, so as to result in somewhat lower cumulative oil recoveries at very low oil contents in the linearly stratified formations. The general effect of the mobility ratio $\bar{m}$ is again the same for the linear case as it is for the exponential case. That is, the curves shift toward increasing recoveries as $\bar{m}$ is increased, and they become grouped more closely for the different values of the stratification constant. This implies that the effect of the permeability variation will be less serious the higher the value of the mobility ratio $\bar{m}$.

The variation of the recoveries to fixed water-oil ratios R_w with the mobility ratio m, for the two values of r, is plotted in Fig. 13. The similarities and differences between the curves of Fig. 13 and the corresponding ones in Fig. 6 for the exponential distribution are quite apparent, and of the same character as discussed with respect to the composition history curves of Figs. 10-12.

A set of curves, similar to those of Fig. 7, illustrating the cumulative oil recovery vs. the total reservoir fluid production histories is given in Fig. 14 for $r = 20$ in the linear permeability distribution. The implications of these curves are similar to those noted with respect to Fig. 7, and need no further specific discussion.

For the sake of completeness the results analogous to those of Figs. 6 and 13 for the probability distribution have been replotted in Fig. 15 from graphs of Dykstra and Parsons.[5] The parameter characterizing the probability distribution is here the "variation," V, which is related to the standard deviation σ of the probability distribution by:

$$V = 1 - 2^{-\sigma} \quad . \quad . \quad . \quad . \quad . \quad . \quad . \quad . \quad . \quad . \quad (30)$$

V ranges between 0 and 1 as the corresponding formation changes from one of complete uniformity to infinite variability. It will be seen that the general features of the curves in Fig. 15 are similar to those of Figs. 6 and 13, although the quantitative effect of the mobility ratio $\bar{m}$ seems to be somewhat less in the case of the probability distribution than in either of the other distributions.

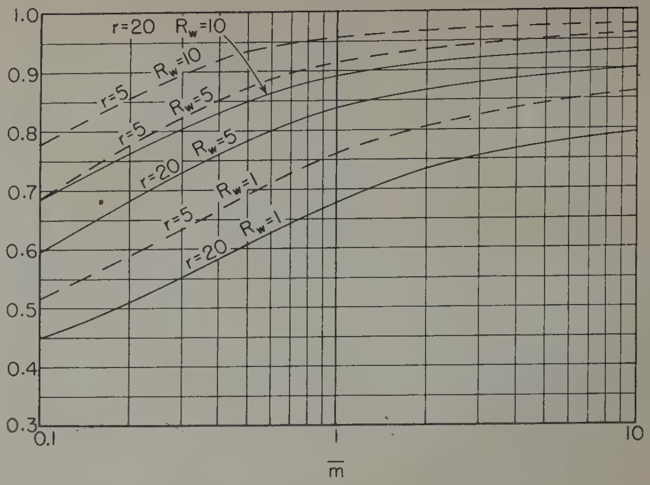

FIG. 13 — THE VARIATION OF THE CUMULATIVE RECOVERY, $\bar{Q}$, IN LINEARLY STRATIFIED WATER-DRIVE RESERVOIRS WITH THE MOBILITY RATIO $\bar{m}$, TO FIXED VALUES OF THE WATER-OIL RATIO R_w, AND FOR FIXED VALUES OF THE STRATIFICATION RATIO r. $\bar{Q}$ = CUMULATIVE RECOVERY AS A FRACTION OF THE TOTAL RESERVOIR DISPLACEABLE RECOVERY. $\bar{m}$ = (MOBILITY OF DISPLACED OIL)/(MOBILITY OF INVADING WATER).

DISCUSSION

While the general features of the implications of the theory of the performance of stratified water drive reservoirs have been discussed above, it must be understood that the basic theory involves three fundamental assumptions.

These are: (1) idealized stratification, (2) 100 per cent areal or pattern sweep efficiency, and (3) the absence of stripping action behind the water-oil interface. It is virtually necessary to make each of these assumptions in order to develop a tractable formulation of the theory. However, it is well to understand what their physical implications are and the possible effect they may have on the final numerical results which are calculated by the simplified theoretical analysis.

The assumption of idealized stratification will certainly never be satisfied in practice. Its significance lies only in the concept that it may provide a statistical equivalence to the actual non-uniformity in permeability which does obtain in the producing formation. Such equivalence may be valid, at least in an approximate degree, under conditions where the invading and displaced fluids have the same mobilities, as is generally assumed in the case of cycling operations and which is represented by the special case of $\bar{m} = 1$ in the generalized analytical theory. The steady state pressure and flow distributions under such conditions may then be represented by a steady state type of streamline distribution, which automatically provides a type of stratification which is at least analogous to that assumed in the analytical treatment. The assumption of vanishing cross-flow, which is an integral part of the idealized stratification concept, is then also automatically satisfied in the actual steady state streamline system, although microscopically the resultant streamline stratification will in no sense be coincident with the strictly parallel stratification assumed in the theory.

However, when the mobilities of the displaced and invading fluids are different, the instantaneous steady state representations will continually change as the water invasion proceeds, and with such changes will be associated new streamline distributions. The assumption of vanishing cross-flow will then no longer be valid unless by accident the cross-bedding permeability happens to be strictly zero. It is clear, therefore, that the concept of idealized stratification can at best represent only an extreme simplification. On the other hand, aside from the realistic necessity of making such an assumption in order to arrive at a tractable analysis, it does have the further justification that it probably represents the least favorable type of permeability non-uniformity, as compared to those which actually occur, from the point of view of the initial breakthrough recovery. That is, the simplified theory should at least give minimum values of the breakthrough recoveries. It also seems probable that the recovery history after breakthrough will also be inherently less favorable under idealized stratification and vanishing cross-flow than under actual conditions where there are both two and three dimensional variations of permeability. From this point of view the theory has value in providing at least lower limits for the recovery possibilities in non-uniform water-drive systems, thus giving the least favorable expectations for the performance of such reservoirs. Since it is not feasible to treat arbitrary types of reservoir non-uniformity, it is felt that means for fixing at least the poorest recovery potentialities of the actual reservoir systems does represent a constructive contribution to their analysis.

The assumption of perfect areal or pattern sweep efficiency will also never be valid in practice. It may be recalled, however, that in the earlier study of cycling operations in exponentially stratified reservoirs it was found that the effect of imperfect areal sweep efficiency was rather minor compared to the direct effect of the stratification, except in reservoirs of a very high degree of uniformity. It seems likely, therefore, that in actual producing formations the simplification made in assuming perfect areal pattern sweep efficiency will not in itself cast serious doubt on the significance of the results.

The final major assumption made in the theory developed here lies in assuming that there is no oil stripping in the flooded part of the formation and behind the advancing water-oil interface. This may be expressed by the assumption that the permeability to the oil behind the water-oil interface[*] is 0. A theory was developed some time ago[6] in which the advance of water in an oil bearing system was analyzed under the more general assumption that the permeability to the oil remained non-vanishing even after passage of the water front. This led to a separation of the composite well producing history into a primary phase corresponding to the displacement of the oil bank ahead of the water-oil interface and a subsequent subordinate phase giving the history of the continued stripping of the oil beind the water-oil front. This latter phase is determined primarily by the relative permeabilities and viscosities to the water and oil behind the water front.

This theory is based on a simple and straightforward application of relative permeability concepts. For the linear[**] water-flooding system it leads to an equation for the saturation distribution at any time t which may be expressed as:

$$x = \frac{Qt}{f}\,\frac{dF_w}{d\rho_w} + \Phi(\rho_w) \qquad \ldots\ldots \quad (31)$$

where Q is the constant rate of throughflow, f the porosity, F_w the water fraction of the local flow-stream, and $\Phi(\rho_w)$ defines the initial saturation distribution. F_w is given explicitly by:

$$F_w = \frac{m_w}{m_o + m_w} \qquad \ldots\ldots\ldots \quad (32)$$

where m_w, m_o are the mobilities of the water and oil respectively. While Equation (31) apparently involves no basic physical approximations except for the neglect of capillary pressure effects, it leads to the curious and physically meaningless result that the saturation distribution ahead of the initial interface will be multiple-valued.[*] As noted by Buckley and Leverett,[6,7][**] this difficulty may be circumvented when applying the theory by arbitrarily imposing a sharp single valued front at the advanced interface, on requiring that the total increase in water content of the flooded area equal the total volume of invading water. From a physical standpoint, however, it is far from satisfying to have to resort to such an artifice, and the fundamental significance of the whole procedure still remains obscure. Moreover, question may be raised if the relative permeability concepts, as derived from multiphase systems in which two or more phases are continually supplied for flow across each internal cross section, are inherently applicable to displacement processes occurring at the advancing front of an identifiable wetting phase displacing liquid. Intuitively, at least, it is conceivable that under the latter conditions the non-wetting phase would be stripped locally to a discontinuous distribution of vanishing permeability as soon as it has been invaded and passed by the wetting phase "front."

Finally, it may be noted that because of the approximate symmetry of F_w and F_w' for unconsolidated sands about the saturation for maximum slope, when the oil and water viscosities are equal, Equation (31) when applied[†] to "oil flooding" of a water sand would give essentially the same type of invasion history as for water flooding. This, however, is hardly to be expected in view of the differential wettability between oil and water, and even though the relative permeabilities themselves presumably reflect these wettability differences.

In spite of these theoretical questions regarding the validity of Equation (31), it has apparently served to give a correlation of laboratory water-flooding data.[8] The effect of the water-oil viscosity ratio on the breakthrough recoveries appears to be subject to at least semi-quantitative description by Equation (31). Especially in the range of low invading fluid mobilities, as compared to that of the displaced fluid, the breakthrough recoveries are particularly low, and the corresponding subordinate phase recoveries become of comparable magnitude. While the permeability stratification theory would qualitatively give similar effects, it is admittedly doubtful if in these particular experiments permeability non-uniformity was the controlling factor. If these experimental results and the other implications of Equation (31) should be extended and confirmed for other systems, it will, of course, be neces-

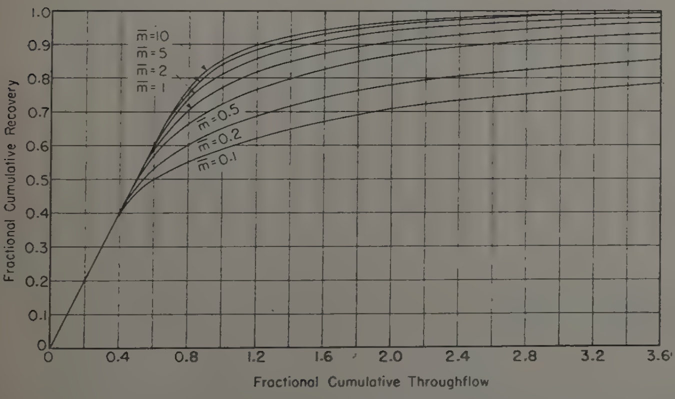

FIG. 14 — THE CUMULATIVE OIL RECOVERY HISTORY VS. THE TOTAL FRACTIONAL CUMULATIVE WATER AND OIL THROUGHFLOW IN LINEARLY STRATIFIED WATER-DRIVE RESERVOIRS FOR DIFFERENT VALUES OF THE MOBILITY RATIO, $\bar{m}$ = (MOBILITY OF DISPLACED OIL)/(MOBILITY OF INVADING WATER). IN ALL CASES THE STRATIFICATION RATIO = 20.

---

[*] As previously noted, it has been further assumed that the amount of this residual oil is independent of the absolute permeability, since satisfactory data are not available on the relationship, if any, between these parameters.

[**] It may be readily shown that in the similar case of perfect radial systems, Equation (31) will still apply provided x is replaced by πr^2.

[*] This ambiguity does not arise when F_w is a linear function of ρ_w or increases monotonically with ρ_w. In the former case, which implies linear k_w and k_o curves, the original water-oil boundary will advance without distortion, and in the latter initial distributions in which ρ_w decreases with x will continually become more stretched out.

[**] Although the inclusion of the capillary pressure term may formally resolve this ambiguity, the quantitative features of the distributions would then also be modified.

[†] For oil flooding, Equation (31) retains its general form with ρ_w replaced by ρ_o and F_w by $F_o = 1 - F_w$. When F_w and F_o are not symmetrical for equal viscosities, it may be possible to make them symmetrical by choosing a suitable viscosity ratio.

sary to accept its basic validity even though it has not been fully clarified in all respects.

While these considerations cast doubt on the predominating importance of the permeability non-uniformity in controlling actual water-drive recoveries, the stratification theory presented here should give the implications of at least one major factor in the recovery processes. If the validity of Equation (31) and its underlying concepts should become definitely established, it will be appropriate to consider the composite effect of these two factors. In principle, it should be possible to develop a superposition treatment, analogous to the manner in which the incompleteness of the pattern efficiency was incorporated in the theory of cycling in exponentially stratified media.[9] While it would be hazardous to predict the resultant production histories without making quantitative calculations, it seems reasonable to anticipate that the composite effect would correspond to surprisingly low breakthrough and subsequent recoveries under conditions which could occur in practice. Thus for $r = 20$ in the exponentially stratified distribution, the breakthrough recovery would be only 23 per cent for $\overline{m} = 0.2$ even for sharp water-oil interfaces. And in a uniform stratum the breakthrough recovery for a water-oil viscosity ratio of 0.2 would probably be about 50 per cent or less according to Equation (31). Although the superimposed resultant will not be the simple product of these two factors, the net theoretical effect will undoubtedly indicate discouragingly low breakthrough and overall recoveries. It is evident that this whole subject warrants a great deal of further experimental and theoretical study.

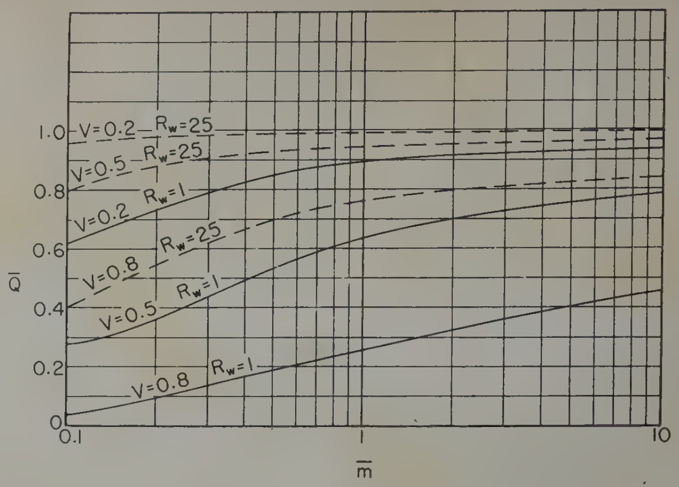

FIG. 15—THE VARIATION OF THE CUMULATIVE RECOVERY, $\overline{Q}$, IN STRATIFIED WATER-DRIVE RESERVOIRS WITH PROBABILITY PERMEABILITY DISTRIBUTIONS, WITH THE MOBILITY RATIO $\overline{m}$, TO FIXED VALUES OF THE WATER-OIL RATIO R_w, AND FOR FIXED VALUES OF THE "VARIATION" PARAMETER V. $\overline{Q}$ = CUMULATIVE RECOVERY AS A FRACTION OF THE TOTAL RESERVOIR DISPLACEABLE RECOVERY. $\overline{m}$ = (MOBILITY OF DISPLACED OIL)/(MOBILITY OF INVADING WATER).

ACKNOWLEDGMENTS

The author is indebted to Miss M. O. Taylor for carrying through the numerical calculations reported here, and to P. D. Foote, executive vice-president of Gulf Research and Development Co., for permission to publish this paper.

REFERENCES

1. W. Hurst and A. F. Van Everdingen: *Trans.* AIME (1946), **165**, 35.
2. M. Muskat: *Trans.* AIME (1949), **179**, 313.
2. M. B. Standing, E. W. Lindblad, R. L. Parsons: *Trans.* AIME (1948), **174**, 165.
4. M. Muskat: *Physics* (1934), **5**, 250.
5. H. Dykstra and R. L. Parsons: API meetings, Los Angeles, May, 1948.
6. S. E. Buckley and M. C. Leverett: *Trans.* AIME (1942), **146**, 107.
7. H. C. Brinkman: *App. Sci. Res.* (1949), **1**, 333.
8. J. P. Everett, F. W. Gooch, Jr., and J. C. Calhoun, Jr.: AIME meetings, San Antonio, Texas, Oct., 1949.
9. M. Muskat: *Trans.* AIME (1948), **179**, 216.

★ ★ ★

Technical Note 55

ATTAINMENT OF CONNATE WATER IN LONG CORES BY DYNAMIC DISPLACEMENT

ROBERT L. SLOBOD, MEMBER AIME, THE ATLANTIC REFINING CO., DALLAS

ABSTRACT

In much of the work reported in the literature on long cores, true connate water values probably have not been obtained because of insufficient flow of oil to attain equilibrium. A satisfactory method for establishing connate water in long cores has been developed in which oil flow is maintained until *no* additional water is displaced.

INTRODUCTION

Long cores have been used by severals investigators in an effort to evaluate the efficiency of oil recovery for various producing schemes. The effects of many variables such as rate of displacement, pressure drop, volume of displacing medium, gas-oil ratio, interfacial tension, and others have been investigated, and the merits of gas drive have been compared with water drive. In the older experiments no connate water was used, but in the more recent studies the philosophy of the experiment calls for a core containing oil and connate water (irreducible water) as the starting point of the experiment. The method generally used to establish this condition in long cores involves dynamic[1] displacement wherein one or more phases are forced through the core, flow being maintained at a constant rate or at a constant pressure until a steady state is reached wherein there is no change of saturation with time. It is one purpose of this paper to point out that in much of the work reported in the literature true connate water values probably have not been obtained. The reason for this failure is pointed out, and a method for obtaining more reliable connate water values on long cores is presented. It is impossible at this time to completely evaluate the effect on the conclusions in the earlier papers resulting from the failure to obtain true connate water in the long cores, but some data are presented which indicate that serious errors may be present in many cases.

MATERIALS AND APPARATUS

Cores cut from outcrop sandstones (Strawn, Torpedo, and Elgin sandstones) with permeabilities of the order of 300 md were used. The major experiments were made with a core 18-in. long and 2-in. in diameter. Cores of the same diameter but only 12-in. long were used in a few tests, and in some work a core 1-in. in diameter and 11-in. long was used. These materials were all somewhat bentonitic. To reduce the effect of such constituents, one of the cores (Torpedo No. 10) on which the most work was performed was acid extracted at the start of the experiment.

Brine containing 50,000 ppm chloride and naphtha (Stoddard's Solvent) were used as the water and oil phases, respectively.

The core was mounted in a rubber sleeve which forms the inner lining of a brass cylinder. In this arrangement[2] the rubber sleeve is forced against the core by applying pressure to water in the annular space between the rubber sleeve and the brass cylinder wall. The core is therefore sealed in rubber so that all fluids introduced at the input end of the core flow through the core. With this equipment the core may be easily removed for inspection and analysis. Also, other cores may be introduced for study with no extra time for preparation such as is required when plastic mounting is used.

When pressure or conductivity measurements are desired at intermediate points along the length of the core, the brass cylinder comprising the outer jacket of the core holder is cut into sections of the desired length. Each section is then made up as an individual unit with its own rubber sleeve (see Fig. 1). The individual units are then butted up against a ring of plastic or other insulating material which carries an electrical contact for resistivity measurements and an opening which can be used for the measurements of fluid pressures. The individual units are forced tightly against the plastic ring separators and held in place with several tie rods. Inlet and outlet end butts of the same diameter as the core and several inches in length are provided to control the introduction and withdrawal of fluids and to complete the arrangement for sealing the core within the rubber sleeve. Fluid flow is maintained either by applying pressure to the liquid confined in a reservoir or by the use of a gear pump. The latter is preferable where continuous flow at a moderate rate over a long time interval is desired since a small volume of liquid can be readily recirculated using filters to prevent plugging of the core.

EXPERIMENTAL

The oven-dried core is weighed and is then completely saturated with brine

---

[1] References are given at end of paper.

Manuscript received at office of Petroleum Branch August 18, 1949. Presented at Branch Fall Meeting, San Antonio, Texas, October 5-7, 1949.

by evacuating the dry core in an appropriate chamber at a total pressure of less than 1 mm of Hg for several hours. Previously evacuated brine is then added to cover the core and time allowed for the brine to saturate the core. The saturated core is weighed and then placed in the core holder where it is driven down to connate water by flowing naphtha through the core until no more water is produced. Small amounts of water discharged from the core are measured accurately by means of inserting the outlet tube from the core into a small graduated cylinder, allowing the water to settle to the bottom of the graduate and the oil to overflow and return to the reservoir. This procedure insures accurate measurements of the cumulative water production over a long period of time. The total volume of oil forced through the core is calculated from periodic measurements of the flow rate. The displacing oil phase is completely saturated with water to avoid dissolving water from the core in the flowing oil. Saturation changes are followed both by resistivity measurements and material balance. The displacing oil phase is carefully filtered to avoid plugging of the core. The change in the residual water content of the core with time is followed by plotting the water content of the core against the log of time. Compressing of the time scale in the plot is necessary to show the continuous but slow displacement of water by oil. The use of a linear time scale leads to the erroneous conclusion that equilibrium is essentially obtained after relatively few pore volumes have passed through the core.

RESULTS

Whenever oil is used to displace water from a core, almost all of the displaceable water *appears* to be recovered ahead of the oil interface. After the oil phase breaks through, a high oil-water ratio is observed which reaches such a large value after several pore volumes that it is common practice to assume that only an insignificant amount of displaceable water remains. Consequently, the water saturation of the core, after perhaps as few as 3 pore volumes of oil have passed through the core, is assumed to be a reliable measure of the connate (irreducible) water. That this procedure is erroneous and can result in serious error is shown by the data in Table I and Fig. 2.

From these data on the water saturation of an acid extracted Torpedo sandstone outcrop core (Table I) it is obvious that not 3 pore volumes but more nearly 3000 pore volumes are necessary to reduce the water saturation to a point where water no longer flows. The water content of the core at this point represents the true connate water value (irreducible water value). In this particular study water was observed to be displaced from the core for 37 days, during which time 2452 pore volumes of oil were forced through the 18-in. core under a pressure head of 20 psi (equivalent to 13.3 psi/ft). For the subsequent 5 days 448 additional pore volumes of oil were driven through the core with no additional displacement of water. Consequently, the experiment was concluded after 42 days with a connate water of 15.0 per cent obtained and with oil-water ratios exceeding 20,000,000 observed in the latter stages of the oil drive.

Additional confirmation of the correctness of the connate water value in the vicinity of 15 per cent was provided by a capillary pressure connate water determination on a portion of the same core material which yielded a value of 18 per cent for the "irreducible water."

Similar results have been observed on other cores, the pertinent data being shown in Table II. All of the cores used were cut parallel to the bedding plane of the outcrop sandstone indicated. The residual water content remaining in the various cores after a stated number of pore volumes of oil had been forced through the core, originally saturated 100 per cent with brine, are also given in this table. From these data it is obvious that in all cases relatively high interstitial water values were observed after the use of only several volumes of displacing oil. Increasing the number of pore volumes through the core resulted in lower water values. In Table II the data on core No. 6, a Torpedo outcrop core which was not acid extracted, show that the water saturation was reduced to 34 per cent with 6 pore volumes of oil, 23.5 per cent with 395 pore volumes of oil, and finally 22.2 per cent with 1,165 pore volumes. The experiment was terminated at this point after a flow of 39 days because of apparatus failure. It is assumed that more water would have been produced with continued oil flow until the residual water content was reduced to approximately 17 per cent, in agreement with that observed in capillary pressure measurements on a representative core specimen. The above data confirm the previously discussed results obtained on Torpedo core No. 10 (Table I). A portion of these earlier data on core No. 10 is also included in Table II.

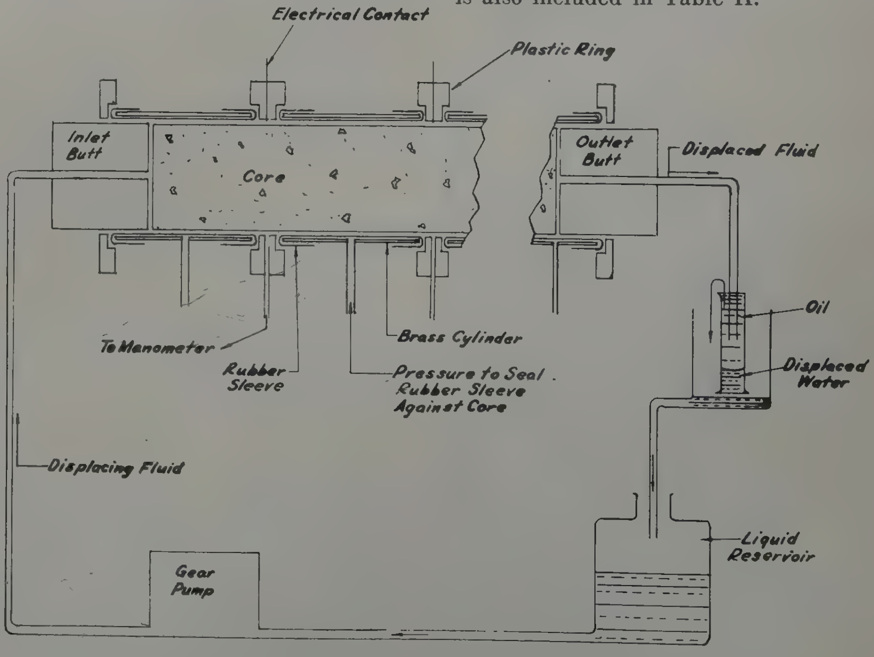

FIG. 1 — SCHEMATIC DIAGRAM OF APPARATUS FOR OBTAINING CONNATE WATER IN LONG CORES.

DISCUSSION

In long core experiments it is common practice to assume that connate water has been established using oil as the displacing medium after several pore volumes of oil have passed through the core.[3] This criterion has been accepted because most of the water appears to be displaced ahead of the water-oil interface, and very little additional water is observed in the effluent as the flow of displacing oil is continued. This conclusion is erroneous since a considerable amount of water in excess of connate water may remain in the core, but because relative permeability to water is extremely low, an almost inappreciable flow of water is observed. From the results presented in the preceding section it is obvious that this very small flow rate can bring about a significant change in the water saturation if the flow of the displacing oil phase is continued for a sufficient time. Thus, in the experiment cited the connate water value was reduced from 32 per cent to 15 per cent over a period of approximately 40 days as a result of flowing about 2300 additional pore volumes of oil which displaced an additional 37 cc of water from the core.

These results are obviously of importance in evaluating the use of the dynamic method of establishing connate water. Previously the method was not considered reliable by some investigators because of the high connate water value observed. End effects and other extraneous factors were offered as a partial explanation for the observed high values of water saturation. Now it appears that these results were in error because of failure to drive the core for a sufficient time to reach true equilibrium. The long times (many pore volumes) required to bring a long core to equilibrium are obviously not practical for routine determinations, but the possibility of using the dynamic method for producing connate water in small core plugs offers interesting practical possibilities since much shorter displacing times are required. It is important to note that the use of higher pressure gradients in the long core studies will undoubtedly shorten the time required for establishing irreducible water saturation.

Many variables such as rate of water flooding, pressure gradient, interfacial tension between liquids used, nature of the porous system, temperature, viscosity, and others should be considered in evaluating oil recoveries by water flooding, but the results of the present study are interpreted as indicating that time may be the single most important variable in laboratory studies. Failure to operate for a time interval sufficient for the system to reach equilibrium will undoubtedly result in obtaining meaningless data. Attempts to interpret such data with reference to the part played by the variable in question may result in unfortunate interpretations.

The relation between the pressure used in driving a water saturated core with oil and the connate water value obtained is important. In such flow experiments pressure differences between the phases are generated which desaturate the core in much the same manner as in the capillary pressure method where the core is mounted in a semipermeable disc. Some data have been obtained which indicate that if a very small pressure is applied to the flowing oil phase, only a portion of the displaceable water is removed as predicted by the data from capillary pressure studies. Consequently, in long core experiments a pressure gradient somewhat in excess of the pressure required to desaturate the core to connate water in a capillary pressure apparatus should be used. To minimize end effects high pressure gradients should be used and an end butt of similar core material on the output end of the core may be introduced. High pressure gradients may also lead to a more rapid establishment of connate water.

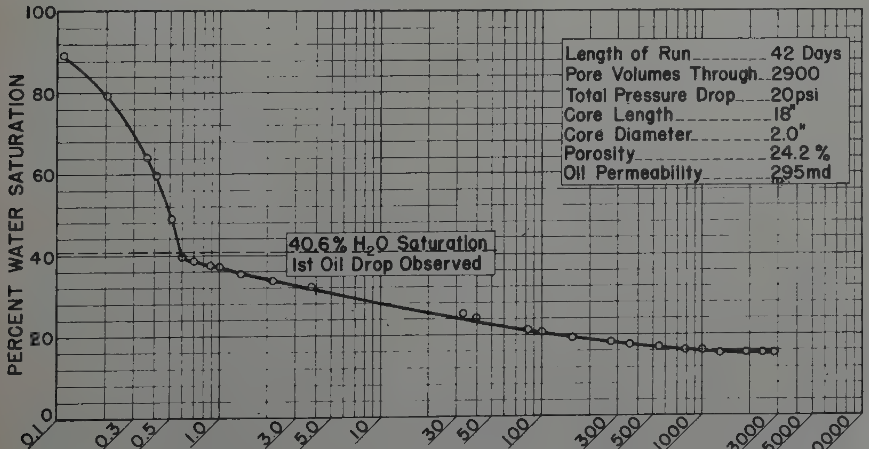

FIG. 2 — INTERSTITIAL WATER SATURATION IN LONG CORE AS A FUNCTION OF PORE VOLUMES OF DISPLACING NAPHTHA.

EFFECT OF ERRONEOUS CONNATE WATER VALUES ON RESIDUAL OIL DETERMINATIONS

The effect of erroneously high connate water values in cores used to evaluate the efficiency of various means of production on the per cent of oil recovered is difficult to estimate at this time. It is likely, however, that all of the information in the literature on recovery of oil by flooding which is based on cores with erroneous connate water values is unreliable. Furthermore, these data cannot be simply corrected at present, for there are no accepted generalizations which relate the amount of recoverable oil with the amount of in place oil or the effect of connate water on residual oil. In this connection it is interesting to note that the residual oil for the Torpedo sandstone discussed above was found to be 18 per cent of the pore space for the core containing 15 per cent connate water and 85 per cent oil (see Table III) when driven by water until no more oil was recoverable (water/oil ratio greater than 100,000:1), while the same core with an initial water saturation of 33 per cent (67 per cent oil) was observed to have a residual oil saturation of 30 per cent (when driven until the water-oil ratio reached a value of 600:1). The recoverable oil in the former case amounts to 79 per cent of the in place oil, while only 55 per cent of the in place oil was recoverable in the latter case with the erroneously high connate water value. These differences are of obvious importance and demonstrate the magnitude of the error possible in interpreting experimental data obtained from long cores with improper connate water saturations.

CONCLUSIONS

The establishment of connate water (irreducible water) in long cores is difficult. The passage of only a few pore volumes of displacing oil through the core does not reduce the water saturation to the irreducible value. On the contrary, apparently several thousand pore volumes are necessary. The effect of rate on the time required to obtain connate water may be important, but has not yet been established. Preliminary data indicate that flooding experiments to determine recoverable oil using long cores with incorrect connate water values are not reliable.

ACKNOWLEDGMENTS

The author gratefully acknowledges the cooperation of Miss E. A. Chambers and Raymond R. Hawthorne in carrying out the experimental portion of this study.

REFERENCES

1. E. R. Brownscombe and R. L. Slobod, *Petr Tech*, September, 1948, Discussion of T.P. 2433, p. 10.
2. Hassler, U. S. Patent No. 2,345,935, April 4, 1944.
3. J. N. Breston and R. V. Hughes, *Jnl. of Petr. Tech.*, 1, No. 4, 100 1949.
4. *Producers Monthly*, 13, No. 2, 14 (1948).

★ ★ ★

DISCUSSION

By Martin Felsenthal, Production Laboratory, Continental Oil Co.

It is most interesting to note the great number of pore volumes of oil required in the attainment of true irreducible water saturation by dynamic displacement as described in Slobod's note. The displacing fluid used in these tests was naphtha. It is believed that less pore volumes of displacing fluid would have been required had a more viscous displacing fluid been chosen. This belief is based on observations which were made during a recent series of tests on the effect of viscosities on water flooding. Preceding each water flood of this series, an attempt was made to reach a uniform initial water saturation in a long core by dynamic displacement of brine by oil. It was found that the water saturations at oil break-through decreased with increasing oil viscosities. Thus, at oil break-through, only 0.65 pore volumes of a 30 centipoise oil (a 91-9 per cent mixture of mineral oil and naphtha) was able to effect a lower water saturation by dynamic displacement than did 54 pore volumes of a 0.44 centipoise oil (naphtha). The flow rate at a given pressure drop immediately following oil break-through was not as unfavorable for the more viscous oil as might have been supposed from a consideration of the viscosity ratio alone, since effective permeability to oil was considerably higher for the more viscous oil due to the higher oil saturation. In order to speed up the process of reaching irreducible water saturation by dynamic displacement, it may perhaps be feasible to remove the bulk of the displaceable water with about one pore volume of a high viscosity oil (e.g.;

Table I

Effect of Volume of Displacing Oil on Residual Water in Long Cores

No. of Pore Volumes of Displacing Oil	Water Content of Core % of Pore Space	Oil/Water Ratio
0.0	100	—
0.6	40	0*
1.0	37	28/1
3.0	32	106/1
10	28	—
30	24	415/1
100	20	4,650/1
300	18	8,300/1
1000	16	200,000/1
2300	15.03	1,030,000/1
2452	15.00	>10,000,000/1
2900	15.00	>>20,000,000/1

Core Description: Torpedo Sandstone—Oklahoma Outcrop Acid Extracted
Core #10
Porosity 222.7 cc (24.2%)
Oil Permeability = 295 md
Length = 18″ Diameter = 2″
$\Delta P = 20$ psi $\equiv$ 13.3 psi/ft

*First drop of oil produced at output end of core.

Table II

Displacement of Water by Oil in Long Cores

Type of Sandstone Used	Core No.	No. of Pore Volumes of Flooding Oil	Time of Flood	ΔP/ft.	Water Saturation
Torpedo..........	8	2.5	1050 min		44 %
Torpedo..........	8	7.5	1400 "	10	39
Elgin............	7	1.0	500 "		44
Elgin............	7	6.5	1360 "	20	33
Elgin............	5	1.5	63 "	13.3	46
Elgin............	5	4.5	1175 "	20	35
Torpedo..........	6	0.67	75 "	16.6	45
Torpedo..........	6	1.0	90 "	20	45
Torpedo..........	6	6.0	300 "	13.3	34
Torpedo..........	6	395	215 hr	13.3	23.5
Torpedo..........	6	1000	540 "	13.3	22
Torpedo (acid extracted).......	10	0.6	23 min	13.3	40
Torpedo..........	10	1.0	40 "	13.3	37
Torpedo..........	10	6.0	310 "	13.3	30
Torpedo..........	10	1000	390 hr	13.3	16
Strawn..........	5	2.5	103 min	25	58
Strawn..........	5	3.5	165 "	32	56
Strawn..........	5	20	200 "	25	51

CORE DESCRIPTION

Torpedo # 8	Length=12″	Dia.=2″	Pore Space=175 cc	Porosity=28.4%
Torpedo # 6	" =18″	" =2″	" =220 cc	" =23.9
Torpedo #10	" =18″	" =2″	" =223 cc	" =24.2
Elgin # 5	" =18″	" =2″	" =203 cc	" =22.0
Elgin # 7	" =12″	" =2″	" =163 cc	" =26.4
Strawn # 5	" =11″	" =1″	" =122 cc	" =19.1

Permeability of above cores 200—600 md

Table III

Effect of Original Saturation on Oil Recovery

Run No.	Original Saturation		Content after Water Flood		Water/Oil Ratio at Termination	% of Original Oil Recovered
	Water	Oil	Water	Oil		
A........	15%	85%	82%	18%	100,000/1	79%
B........	33%	67%	70%	30%	600/1	55%*

*On the basis of run A, only a negligible increase in recovered oil would be expected after reaching a 600/1 water/oil ratio.

mineral oil) and then complete the process with the aid of naphtha.

Results cited in Slobod's note for Runs No. A and B tend to refute the general accepted theory that residual oil saturation attainable by water flooding is independent of initial oil saturation provided the initial oil saturation is above a certain limiting value. It would be interesting to obtain a few more data on the two water floods, especially the oil saturation at the time of water break-through.

Author's Reply to Martin Felsenthal

The comments of Felsenthal on the use of high viscosity oils to displace water from porous systems are pertinent. We have observed similar beneficial action. The displacing efficiency obviously increases with increase in the viscosity ratio expressed as $\frac{\text{viscosity of oil}}{\text{viscosity of water}}$. At the highest ratio in our experimental work to date (approximately 100), however, displaceable water was still present in the core after flooding with 10 pore volumes. In a typical experiment on a small core plug (1-in. long) 20 per cent of the water remained in the core at oil breakthrough. Nine additional pore volumes of this high viscosity oil reduced the water saturation to 15 per cent of the pore space. (Irreducible water in this plug is 10 per cent.) In the same core, using a low viscosity oil (viscosity oil/viscosity water=1.4), the water saturation at oil breakthrough was approximately 35 per cent of the pore space, and, after 10 pore volumes of displacing oil had flowed through the core, the water saturation was 23 per cent. Thus, 10 pore volumes of low viscosity oil (viscosity ratio 1.4) are not as effective as one pore volume of high viscosity oil (viscosity ratio 100), but even with the high ratio oil (100) apparently a considerable number of pore volumes will be required to establish "irreducible water." ★

Technical Note 56

STAINLESS STEEL CONTAINERS FOR LABORATORY DRILLING MUD TEST WORK

W. B. LILIENTHAL, MAGNOLIA PETROLEUM CO., DALLAS, TEXAS

A considerable saving in time and money has been effected by use of a specially designed stainless steel container for laboratory drilling mud test work. This container involves use of a standard tall-form stainless steel beaker for service in which the mud sample is heated to an elevated temperature and maintained there for protracted periods of time, while undergoing agitation to facilitate mixing of mud components. Agitation is accomplished by rotating the filled containers on motor-driven rollers within an oven. Several porcelain balls are generally placed in the containers to further improve agitation.

Soft glass containers (Mason jars) were used in this service in early work, and were found to be unsuitable for the following reasons:

1. Poor resistance to thermal shock.
2. Containers could withstand only relatively low pressures.
3. Accidental breakage in handling.
4. Chemical deterioration and subsequent mud contamination from reaction of high pH muds with the glass at elevated temperatures.

Pyrex containers were also considered, but, inasmuch as they provided improvement only in items 1 and 4 listed above the additional cost was not believed to be justified.

A scale drawing of the container is shown in the figure illustrating details in cross-section. A pressed stainless steel lid was fabricated to match the rolled edge of the beaker

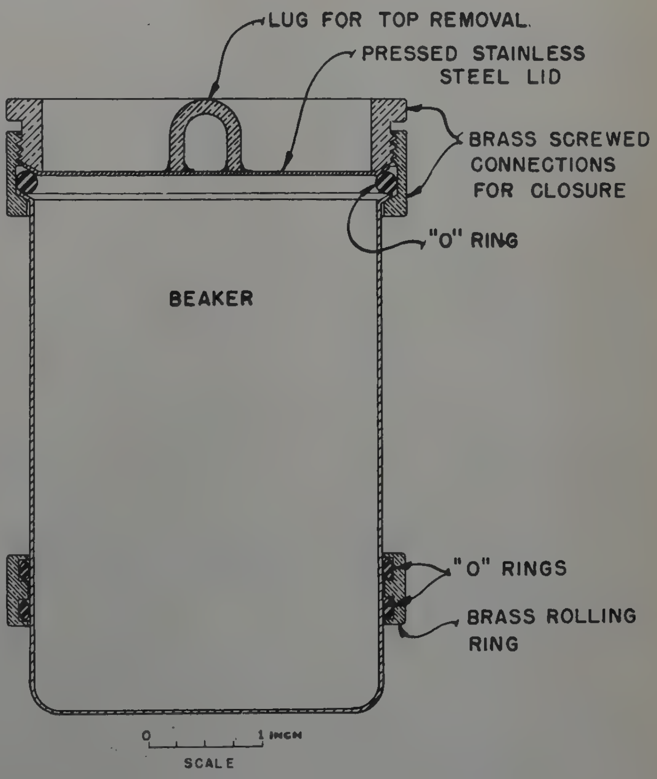

Fig. 1 — Stainless steel mud container.

top, and male and female screwed connections external to the container were made up to complete the closure with the O-ring used as a gasket between the lid and beaker. The brass screwed connections were made from extra heavy brass pipe, and were knurled on their periphery for ease of handling. In order to insure sealing, it was necessary to make certain that the beaker top was perfectly round in cross-section. After this condition was checked and corrected on a lathe if required, the container was ready for assembly. With the closure made up "hand-tight" the container was tested pneumatically at 20 psig. This container was made up with a 500 ml beaker to facilitate handling of customary 350 ml pilot samples, but almost any standard-sized beaker with a rolled lip may be used equally well, since O-rings are available in a large variety of sizes. The lower ring on the container was added so that the unit would ride evenly on the motor-driven rollers in the oven.

These containers have given highly satisfactory service over the past six months in that no samples have been lost due to faulty closures, and no unusual difficulties in reassembly or in failure of parts have been involved. Although the initial cost of these containers is relatively high by comparison with costs for conventional soft glass and Pyrex containers of similar size, it is believed that the savings in time and samples and the additional safety of the metal containers more than justify such costs. ★ ★ ★

Technical Note 57

ANOMALIES IN THE MEASUREMENT OF WETTING LIQUID PRESSURE GRADIENTS

WALTER ROSE, MEMBER AIME, AND **BERNARD GREIFER,** GULF RESEARCH AND DEVELOPMENT CO.,
PITTSBURGH, PENNSYLVANIA

The purpose of this note is to call attention to a source of difficulty which can be responsible for inaccurate estimates of wetting liquid pressure gradients in mixture flow experiments of the Hassler[1] type. It has been our experience occasionally to observe what were indicated to be negative pressure gradients, and these were regarded as anomalous in the sense that physically they seemed to contradict the requirement that the flux be in the direction of the potential field.

At first it was thought that our scheme of assembling barriers and core sample led to such asymmetry in the distribution of isobars that the manometric leads at each end of the core were responding to internal pressures (within the core sample) which could be either positive or negative with respect to each other, and which in fact might tend to reflect on different effective core lengths in an unpredictable fashion as the wetting liquid saturation was changed. However, no compelling evidence of this possibility has been established. In addition, we were cognizant of the requirements to be satisfied in selecting manometric instrumentation to minimize the delay in response of the manometer to the differential pressures being measured, and were thus assured that our observations of anomalous pressure gradients could not be explained by faulty instrumentation.

What we suggest is that if a leak sink occurs in the fluid lines connecting the core to either side of the differential manometer, errors exceeding 100 per cent may result in the estimation of wetting liquid pressure gradient, even though the leak is of such small magnitude that its existence would tend to be obscured by evaporation effects. This is because in a system with leaks at the specified places, the manometer records at steady state the pressure drop across the manometer barrier elements in addition to the pressure drop across the core sample.

This possibility will be illustrated below analytically and by numerical example for the special case where the leak occurs on the high presure side of the core, since we are especially desirous to explain the significance of our observations of the so-called negative pressure gradients. It will be indicated, however, that leak sinks on the low pressure side of the core can account for observations of anomalously high values of pressure gradient, and that multiple leaks on both sides of the core can provide for some compensation so that the errors in pressure estimation are reduced. However, the major point to be emphasized is the fact that the impracticality of detecting the small leak sinks which give rise to the difficulties makes it a complicated task for the experimenter in a particular case to know with certainty that his estimation of pressure gradient lies within the limits of error which can be tolerated.

Fig. 1 shows the electrical analog of the flow system we have employed in our studies. The inflow and outflow barriers, R_{b1} and R_{b2}, the manometer barriers, R_{m1} and R_{m2}, and the core sample, R_c — for a particular fluid saturation and distribution — are all designated as resistance elements; the flowmeter is designated by an ammeter, A; the pressure source is designated by E; and the manometric device is designated by the voltmeter, V. Included in the circuit are the variable resistances, R_x and R_y, which may be regarded as the leak sinks, and which, in general, can vary in magnitude from zero (i.e., a large hole or shunt in the system) to infinity (i.e., no leak). Upon application of Ohm's and Kirchoff's laws to the circuit of Fig. 1, one obtains the following expressions of interest which hold when $R_x \geqslant 0$ and $R_y = \infty$:

$$Q_x = \frac{E(R_c + R_{b2})}{\Delta} \quad . \; . \; . \; . \; . \; . \; . \; . \quad (1)$$

where Q_x is the rate of flow through the leak, and where the denominator, Δ, is defined by:

$$\Delta = (R_cR_x + R_cR_{m1} + R_cR_{b1} + R_xR_{b1} + R_xR_{b2} + R_{m1}R_{b1} + R_{m1}R_{b2} + R_{b1}R_{b2})$$

The pressure drop across the core, P_c, is given by:

$$P_c = \frac{E\,R_c\,(R_{m1} + R_x)}{\Delta} \quad . \; . \; . \; . \; . \; . \quad (2)$$

whereas the pressure, V, as read by the manometer is:

$$V = \frac{E(R_cR_x - R_{b2}R_{m1})}{\Delta} \quad . \; . \; . \; . \; . \; . \; . \quad (3)$$

Thus, one can express the per cent error in pressure estimation as:

$$\%\ \text{error} = 100\left(\frac{P_c - V}{P_c}\right) = 100\left[\frac{R_{m1}\ (R_c + R_{b2})}{R_c\ (R_x + R_{m1})}\right] \quad . \; . \; . \; . \quad (4)$$

In the above equations when the pressures, E, V, and P_c, are expressed in atmospheres and the flow rates in cubic centimeters per second, the resistance parameters, R, will be in units of (atm.sec./cc.), and will be defined by Posseuille's or Darcy's law depending on whether the flow is directed through a hole as in the case of a leak, or through porous media as in the case of the barriers and core.

Eq. (1) shows that the rate of flow through the leak, Q_x, is zero when R_x is infinite, but of finite magnitude (proportional to the various resistance elements of the system) when R_x is finite or zero. On the other hand, Eq. (4), in expressing the difference between P_c and V in terms of R_x and the other resistance elements of the system, shows that when:

$$R_x < \frac{R_{m1}\ R_{b2}}{R_c}$$

V will be negative, although the true pressure drop across the core, P_c, is always positive. When R_x is equal to or greater than $\frac{R_{m1}\ R_{b2}}{R_c}$, V will be positive, although it may still be in error. It should be noted that positive, albeit false values of V, exceeding P_c in magnitude, are obtained when the leak is at Y instead of X.

A numerical examination of the equations given above emphasizes the difficulty of obtaining reliable estimates of P_c from a measurement of V when R_x is finite and R_y is infinite. For example, if R_c is assumed to be 10 atm.sec./cc. (equivalent to a 100 md. core, L = 5 cm., A = 5 cm², μ = 1 c.p.), and if R_{m1}, R_{b1}, R_{m2}, R_{b2} are assumed to be 500 atm.sec./cc. (equivalent to 1 md. barriers of usual dimensions), then the error in pressure measurement will be about 10 per cent when $R_x = 2.55 \times 10^5$ atm.sec./cc., and Q_x is about 10^{-6} cc./sec.* On the other hand, decreasing R_x by a factor of 10 increases the error to 100 per cent (while increasing Q_x to only 4×10^{-5} cc./sec.), and further decreases in R_x result in the observation

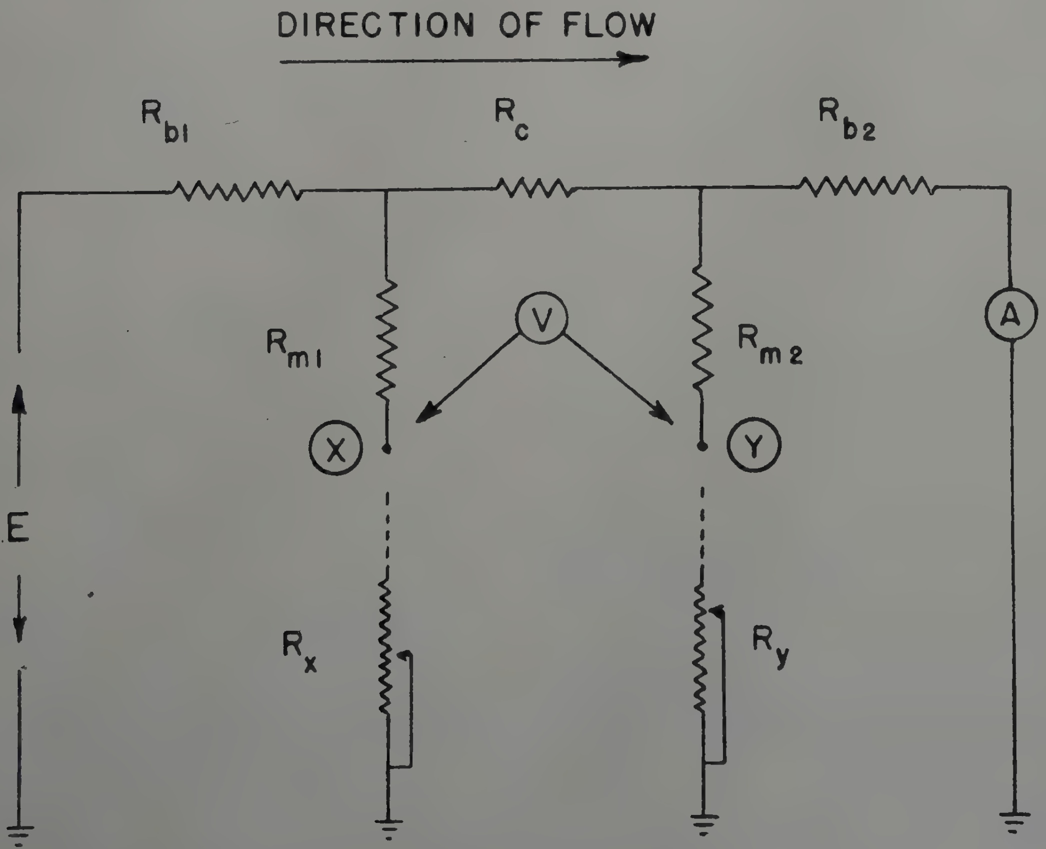

FIG. 1 — ELECTRICAL ANALOG OF FLOW SYSTEM.

---

* In the numerical example, E is chosen as two atmospheres. Note that a flow rate of 10^{-6} cc/sec. is approximately equivalent to 14 hours per drop (~ 0.05 cc).

of the so-called negative pressures at V. It is thus seen that leaks of such small magnitude that evaporation effects would tend to conceal their existence, nonetheless are sufficient in certain cases to introduce pressure anomalies in the Hassler scheme of pressure gradient determination.

We do not presume to offer a general solution for the problem of leak control as discussed in this note, it being realized that precautions to avoid detectable leaks are followed as common practice. However, the fact that leaks might escape detection nonetheless cause difficulty, suggests the use of barriers having permeabilities as high as will be compatible with the desired barrier displacement pressure properties. In any event, it is our recommendation that a numerical check be made, according to the method outlined in this note, to investigate the possibility of encountering the leak-caused pressure anomaly in each particular system which is being investigated.

Such a check involves postulating the minimum value of Q_x which sufficiently exceeds evaporation rates so that it can be detected, and using Eq. (1) to calculate the values of R_x which when substituted in Eq. (4) give the error in measurement. Alternately, if the leak occurs at the point Y or simultaneously at the points X and Y, other more general equations for the per cent error can be derived in the manner indicated above, to test the probability of encountering errors in pressure estimation.

REFERENCE

1. G. L. Hassler. U. S. Patent 2,345,935, April 4, 1944. ★ ★ ★

Technical Note 58

LIME CONTENT OF DRILLING MUD—CALCULATION METHOD

M. D. NELSON AND **T. E. WATKINS,** MAGNOLIA PETROLEUM CO., DALLAS, TEXAS

A method of determining the lime content of drilling muds proposed by Battle and Chaney* has been examined both in the Field Research Laboratories of Magnolia Petroleum Co. and in field drilling operations. This proposed analytical method is condensed as follows: Titrate one ml of mud and one ml of mud filtrate, each with 0.02 N H_2SO_4, to the end point with phenolphthalein. The volume of acid in ml required for the mud titration is recorded as P_m and that of the mud filtrate titration as P_f. Calculation of the lb lime/bbl mud is accomplished by use of the formula,

$$\text{lb lime/bbl mud} = 0.6\ (P_m - 1.3P_f) - 0.6$$

The analytical procedure outlined by Battle and Chaney was found to be quite satisfactory when reasonable precautions are used in mud sampling technique. Calculation of lime concentration by the method proposed in the above publication, however, has given values that varied as much as 100 per cent from the known lime content, for muds of either high or low solids concentration.

By use of a formula, lb lime/bbl mud = $0.26\ (P_m - F_L P_f)$, based on chemical equivalents† of acid required for titration, both laboratory and field data have been satisfactorily correlated with the known amounts of lime present in the muds. In this formula a correction, F_L, or volume fraction of liquid in the mud, is made for the solid content of the mud. P_m and P_f have the same significance as in the Battle and Chaney equation. Table I shows typical data employing both formulas in calculating the lime content of various lime muds.

This suggested procedure ignores lime which is in solution in the mud. The solubility of lime in water, normally about 0.5 lb per bbl, is greatly decreased by the addition of caustic soda, and, in a lime mud, it is probable that the concentration of dissolved lime is of the order of 0.1 lb per bbl. Such an amount of lime can be ignored, since it is within the range of accuracy of the method.

Table I
Calculation of the Lime Content of Various Muds Using Two Formulae

Mud	Total Lime #/bbl	P_m Ml	P_f Ml	# Lime /bbl Mud $0.6(P_m - 1.3P_f) - 0.6$	Error #/bbl	# Lime /bbl Mud $0.26(P_m - F_L P_f)$	Error #/bbl	Mud Composition
A	1	10.65	6.10	1.04	+0.04	1.18	+0.18	Non Bentonite Lime
A	4	20.75	5.15	3.65	−0.35	4.04	+0.04	“ “ “
A	8	35.60	6.00	16.10	+8.10	7.66	−0.34	“ “ “
B	6.25	20.75	4.61	8.25	+2.0	4.26	−1.99*	Bentonite–Lime
B	10.25	34.36	4.73	13.32	+3.07	7.75	−2.50*	“ “
B	12.25	41.68	4.91	20.58	+8.33	9.60	−2.65*	“ “
C	4.25	17.53	6.67	4.71	+0.46	2.91	−1.34*	“ “
C	6.25	24.45	6.72	8.83	+2.58	4.69	−1.56*	“ “

* Error is partially due to the lime assimilated by base exchange.

---

* Paper on “Lime Base Muds,” presented by J. L. Battle (Humble Oil and Refining Co., Houston, Tex., and P. E. Chaney (Sun Oil Co., Beaumont, Tex.), at the 1949 Spring Meeting of the Southwestern District API Division of Production, Dallas, Tex. The analytical procedure has also had wide distribution in a trade journal, *Kembreak*, published by the Accuracy Rig and Tool Co., Houston, Tex.

†Derivation of equation

lb/bbl = grams/350 ml

1 ml 0.02 N acid = 0.000741 grams of lime

1 ml 0.02 N acid/ml lime suspension = 0.26 lb of lime bbl

lb of lime/bbl = $0.26\ (P_m - F_L P_f)$

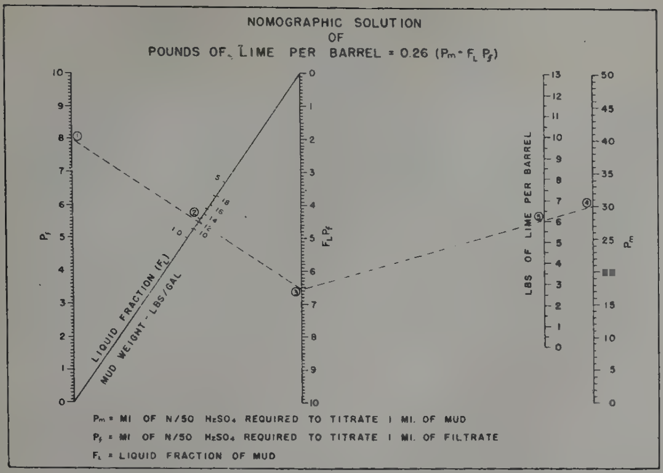

Fig. 1 — Nomographic Solution of pounds of lime per bbl. = 0.26 (P_m - F_LP_f)

A nomograph for the graphical determination of lime content by this method is shown in Fig. 1. In the construction of this nomograph, it was assumed that weighted muds contain 8 volume per cent of light solids. This value was based on the average composition of a number of lime muds. Using a value of 4.30 for the specific gravity of barite, total liquid fractions (F_L) were calculated for weighted muds up to 18 lb/gal (135 lb/ft^3)

Employing this nomograph, results on the analysis of five muds were determined independently by five separate operators. In the 25 indicated operations, results showed a maximum deviation of 0.1 lb of lime per bbl from the value calculated by means of the equation. This degree of accuracy and reproducibility was attained by plotting the P_f and P_m titration values to the nearest 0.05 and 0.5 ml, respectively, and the mud weight to the nearest 0.5 lb/gal.

A limited number of copies of this nomograph are available and may be secured from the authors. ★ ★ ★

Technical Note 59

INFLUENCE OF DIFFERENT TYPES OF FORMATION WATERS ON DISINTEGRATION OF CEMENTS

ROSCOE C. CLARK, JR., STANOLIND OIL AND GAS COMPANY, TULSA, OKLAHOMA

ABSTRACT

A study of the effect of various corrosive waters on five different types of cements indicated that those cements containing less than 5 per cent tricalcium aluminate were the most resistant to corrosion.

INTRODUCTION

Oil field experience indicates that some formation waters are excessively corrosive to some cements. A study has been made to determine the most corrosive waters and the relative resistance of various types of cement to these corrosive waters.

PROCEDURE

This study of the corrosion of cement was limited to an evaluation of the effect of various corrosive waters on five different types of cements. A determination was made of the types of cements which offer the greatest resistance to corrosion and of the chemical contents of waters found to be the most destructive to cements.

The laboratory tests were conducted by immersing small cylinders of 20 samples of set cement in various corrosive waters. The initial mixing of most of the cement slurries was done using Tulsa tap water as the mixing water; however, a few of the slurries were mixed using a sulfate water as the mixing water. When the 20 samples had been immersed for a period of nine months, they were removed from their corrosive baths, inspected and photographed.

The field tests were conducted by placing ten cement specimens, each contained in a screen wire thimble, in the gas anchors of insert pumps in wells in six different fields. The specimens were observed whenever it was necessary to pull the pumps and were returned to the laboratory when deterioration had reached a serious state.

EXPERIMENTAL RESULTS

In both the field and laboratory tests the resistance of the different cements to corrosion was determined by the condition of the samples and the number of samples of each that were in good condition at the end of the immersion period. Table I lists the various cements tested in the order of their resistance to corrosion with the most resistant at the top and the least resistance at the bottom.

An analysis of Table I reveals that the upper half of the table predominates in slow set and sulphate resisting cements (low $3CAO.Al_2O_3$ content) while in the lower half the portland and high early strength cements are in the majority. Of the last two the high early strength cements appear to offer less resistance to sulfate water corrosion.

An investigation of the composition of the cements listed in Table I indicated that as a general rule the cements containing less than five per cent tricalcium aluminate will exhibit the greatest resistance to corrosion.

The destructive action of various corrosive waters was compared by listing the waters in the order of those containing the largest number of samples that failed completely. These ratings are presented in Table II with the most corrosive waters listed first and the least corrosive last.

Figs. 1 and 2 show the end views of cement samples which had been immersed in the baths of five per cent $MgSO_4$ water and the five per cent Na_2SO_4 water respectively in the laboratory. These pictures are representative of the results obtained and present a pictorial evaluation of the corrosive resistance of various types of cements.

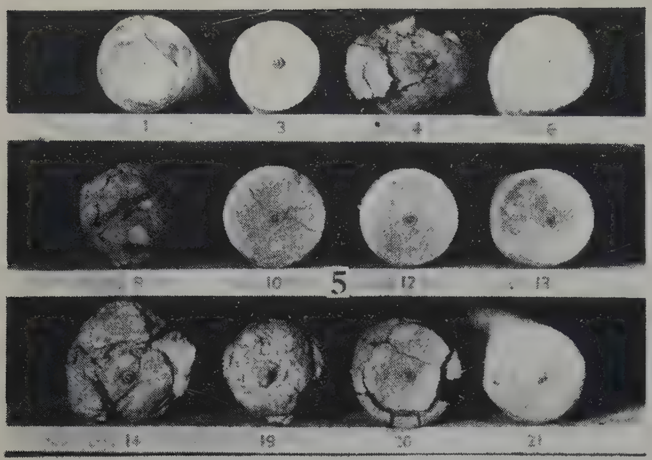

FIG. 1 — SLOW SET CEMENTS — 6, 12, 13; STANDARD PORTLAND CEMENTS — 1, 10, 20, 21; HIGH EARLY STRENGTH CEMENTS — 3, 4, 9, 14, 19; SAMPLES OF CEMENTS IMMERSED IN THE FIVE PER CENT $MgSO_4$ BATH FOR NINE MONTHS.

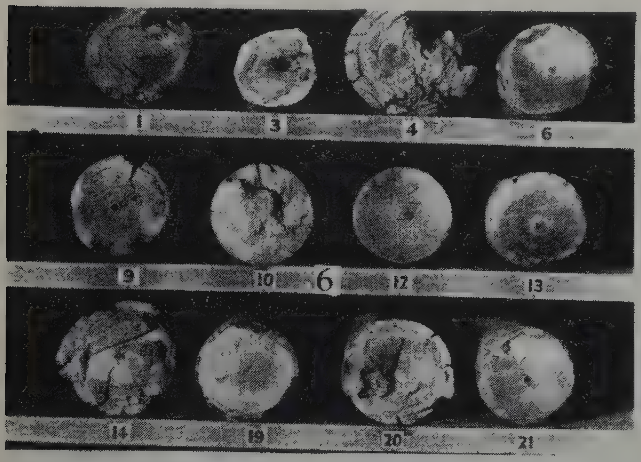

FIG. 2 — SLOW SET CEMENTS — 6, 12, 13; STANDARD PORTLAND CEMENTS — 1, 10, 20, 21; HIGH EARLY STRENGTH CEMENTS — 3, 4, 9, 14, 19; SAMPLES OF CEMENTS IMMERSED IN THE FIVE PER CENT $NaSO_4$ BATH FOR NINE MONTHS.

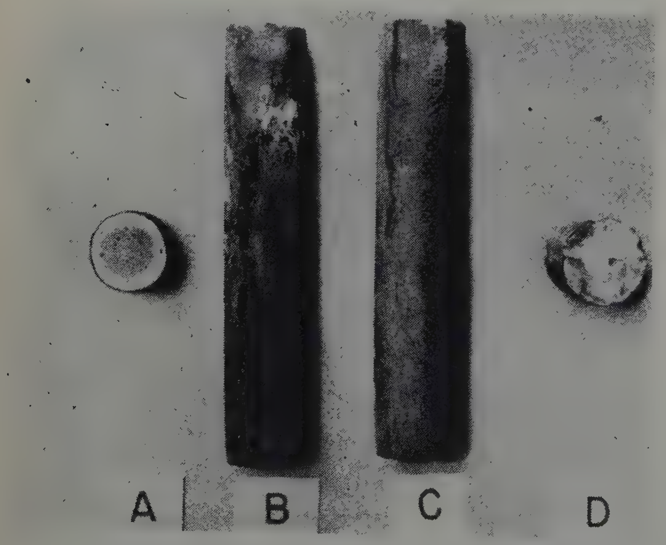

FIG. 3 — RESULTS OF FIELD TESTS. SAMPLE A, TYPE II CEMENT; SAMPLE B, SLOW SET CEMENT; SAMPLE C, MISCELLANEOUS CEMENT; SAMPLE D, HIGH EARLY STRENGTH CEMENT.

Table I

Resistance of Cements to Corrosion

	Number of Sound Samples		
Cement	Out of 17 Lab. Tests Each with a Different Corrosive Water	Out of 6 Field Tests	Per Cent Tricalcium Aluminate
A-1	17	4	4.1
B-1	15	3	------
A-2	15	3	.23
A-3	14	3	2.0
C-1	13	3	------
C-2	13	2	------
A-4	12	--	------
C-3	12	--	9.5
A-5	11	--	3.5
A-6	11	--	------
C-4	11	--	------
C-5	7	--	------
D-1	6	2	10.95
C-6	6	2	13.69
C-7	6	--	10.10
D-2	5	--	------
D-3	5	--	12.20
C-8	5	--	------
D-4	5	1	12.4
D-5	0	0	------

Key: A — Slow Set Cements
B — Sulphate Resisting Cements
C — Standard Portland Cements
D — High Early Strength Cements

Table II

Order of Corrosive Effects on Cement

Rating	
1	Two per cent $MgSO_4$ two per cent Na_2SO_4 $CaSO_4$ (Sat. Soln) charged with H_2S gas
2	Five per cent $MgSO_4$
3	Five per cent Na_2SO_4
4	Tulsa city water (cement mixed with water containing 0.1 per cent $MgSO_4$)
5	Saturated solution of $CaSO_4$
6	Tulsa city water (cement mixed with water containing 0.5 per cent $MgSO_4$)
7	Tulsa city water (cement mixed with water containing 0.05 per cent $MgSO_4$)
8	Formation water from Salt Creek, Wyoming Field, Sulphates 1,619 PPM
9	Tulsa city water charged with H_2S gas
10	Two per cent $MgSO_4$ two per cent Na_2SO_4 $CaSO_4$ (Sat. Soln)
11	Formation water from Goldsmith, Texas, Field, Sulphates 5,434 PPM
12	Formation water from Hobbs, New Mexico, Field, Sulphates 1,590 PPM
13	Formation water from Abell, Texas, Field, Sulphates 3,896 PPM
14	Formation water from E. Hackberry, Louisiana, Field, Sulphates 121 PPM
15	Formation water from Polo Field, Sulphates 9,713 PPM
16	Formation water from Hastings, Texas, Field, Sulphates 70 PPM

Figs. 3 and 4 are representative of the results obtained from the field tests. In evaluating the effects of these formation waters on cement samples it should be noted that the specimens were placed in the well in such a position that they were exposed to extremely large volumes of formation water. Cements exposed to smaller quantities of water in relation to the cement volume under less violent agitation should withstand corrosive waters much longer than the time indicated by these tests. It is believed, therefore, that cement placed in a well should probably not corrode rapidly until a channel is developed through which formation waters can pass. After a channel has been developed, however, the rate of cement corrosion may be expected to be on the order of that shown in Figs. 3 and 4.

SUMMARY

In summation, it is evident from both laboratory and field tests that cement corrosion is a real problem in areas where the formation waters to which cement will be exposed contain any appreciable quantities of sulfates or sulfides, but that the corrosion will probably not be prohibitive if low tricalcium aluminate content cements are used.

★ ★ ★

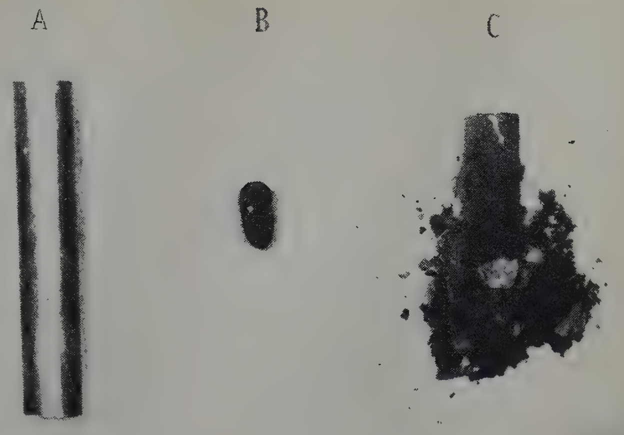

FIG. 4 — RESULTS OF FIELD TESTS. SAMPLE A, METALLIC CYLINDER STOCK REPRESENTING THE ORIGINAL SIZE OF THE TEST SAMPLES; SAMPLE B, SLOW SET CEMENT; SAMPLE C, TYPE II CEMENT. CUTLINES—WATER FLOOD ARTICLE

Technical Note 60

INTERPRETATION OF CAPILLARY PRESSURE DATA

W. R. PURCELL, SHELL OIL CO., HOUSTON, TEX., MEMBER AIME

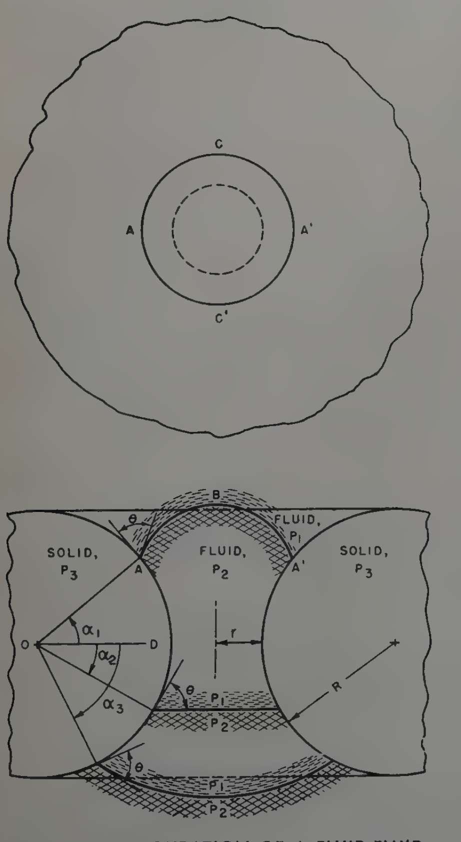

FIG. 1 — CONFIGURATION OF A FLUID-FLUID INTERFACE AT VARIOUS POSITIONS WITHIN A "DOUGHNUT-SHAPED" PORE.

In a previous technical note[1] by Walter Rose, evidence is offered in support of the contention that "the possibility of describing oil recovery features in terms of capillary pressure phenomena has not been established entirely." It is not the purpose of this note to present further discussion of this possibility but rather to point out that the argument presented there does not appear to be generally valid.

In the cited note[1] reference is made to the experiments of Welge[2] wherein it was shown that when water was displaced by oil from a core the pressure in the water phase was less than in the oil phase but that when this oil was then produced by water drive the pressure in the water phase was greater than in the oil phase. Rose has concluded from these observations that conditions of static equilibrium did not obtain since the fluid saturations were such that phase discontinuities seemed unlikely. The argument from which this conclusion was drawn is based on the contention that "the pressure is *always* greatest in the non-wetting phase at each static interstitial interface of contact with the wetting phase." This premise appears to have been reached from a consideration of capillary phenomena in cylindrical tubes, although it may also hold for other types of pore geometry, but as will be shown below it does not hold for *all* pore shapes and hence is not generally applicable.

Since the pore structure of porous media such as reservoir rocks is in general so complex as to defy exact description, it is undoubtedly of great value to establish a model in terms of pore shapes of known geometry, provided of course that the limitations of the model are recognized. That the limitations of the capillary, or cylindrical, tube model have not always been fully recognized will be evident from the following discussion of a pore of different shape but one which may as logically be considered as the capillary tube.

The pore space to be considered is that shown in Fig. 1, which may be thought of as the "hole in a doughnut."* Consider the interface, *A-B-A'*, between two immiscible fluids, P_1 and P_2, which interface meets the solid along a line, *A-C-A'-C'*. The interface *A-B-A'* is the surface of a spherical segment† while the line of mutual contact between the three phases (A-C-A'-C') is a circle. The contact angle, θ, will be determined by the relative magnitudes of the interfacial tensions between the solid, P_3, and fluid, P_1, and fluid, P_1, between the solid and fluid, P_2, and between the two fluids. If the contact angle as measured through fluid P_1 is less than 90° (as in Fig. 1) then P_1 is said to be the wetting phase; if the contact angle with respect to P_1 is greater than 90° it is said to be the non-wetting phase. The sign of the difference in pressures of the fluids, P_1 and P_2, at equilibrium will not be determined solely, however, by the wetting characteristics of the solid, as would be the case in a cylindrical tube, but will depend also on the position of the interface within the pore. For example, when the interface is in the position A-B-A', determined by the angle, α_1, (see Fig. 1), it will be convex with respect to fluid P_1 and the pressure in this phase will be less than that in fluid P_2. If the interface is in a position represented by α_2, however, it will be flat and no pressure difference will exist between the two fluid phases. Finally, if the position of the interface is defined by α_3, it will be concave with respect to P_1 and the pressure in this phase will be greater than in fluid P_2.

---

*For the treatment of a similar pore in a study of textiles, see References 3 and 4.

†In this discussion, the effect of gravity on the shape of the interface is considered to be negligible.

The above considerations have shown, then that there are equilibrium positions within the theoretical pore of Fig. 1 for which the pressure in one fluid phase may be greater than, equal to, or less than the pressure in the other fluid phase although the wetting properties and contact angle are everywhere the same.

From geometrical considerations, it can be shown[5] that for the pore under discussion,

$$\frac{P_cR}{2\sigma} = \frac{\cos\,(\theta - \alpha)}{1 + R/r\ (1 - \cos\alpha)},\ ‡$$

where P_c (the capillary pressure) is the pressure difference between the two fluids, P_1 and P_2, σ is the interfacial tension, R the radius of curvature of the solid, r the minimum radius of the pore and θ and α are angles as defined above. Fig. 2 shows the dimensionless quantity $\frac{P_cr}{2\sigma}$ plotted as a function of α for various values of contact angle, θ, as measured through fluid P_1 and for an arbitrary R/r spacing of 4. From this plot it is seen that for a given contact angle (0° and 180° excepted), the capillary pressure, P_c, exhibits both positive and negative values for positions of the interface within the pore, since r and σ are always positive. Positive values of P_c indicate that the pressure in fluid P_2 is greater than that in P_1; negative values indicate the converse situation.

We consider now the capillary behavior in a three dimensional array of pores similar to that shown in Fig. 1. The pore spaces are originally filled with water (P_1) which is to be displaced with oil (P_2) by the standard porous plate capillary pressure technique. Let us say the solid is preferentially water wet and that the contact angle of oil and water against the solid is 30° as measured through the water phase. As oil is brought into contact with the water saturated specimen, the pressure in the two liquid phases being the same, there will a slight spontaneous displacement of the water until the oil-water interface

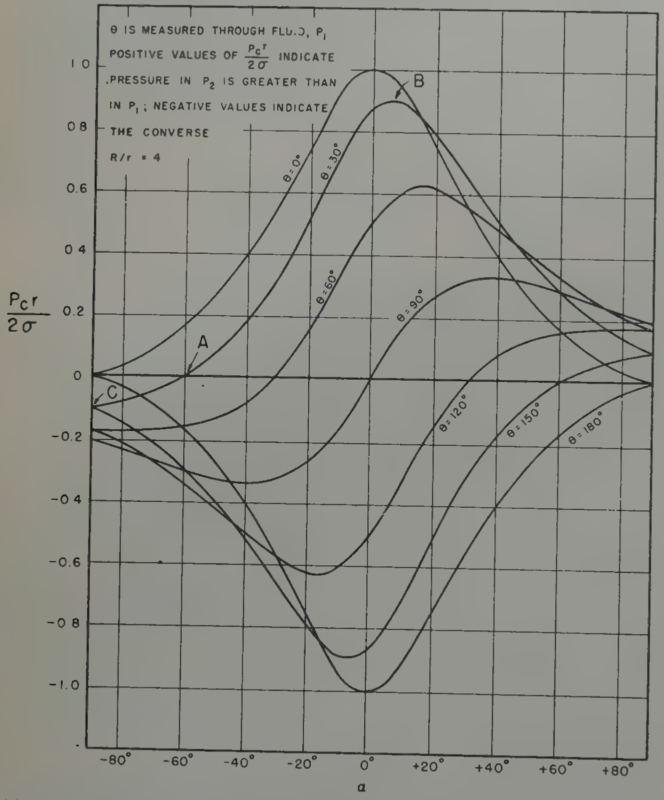

FIG. 2 — PLOT SHOWING THE DEPENDENCE OF CAPILLARY PRESSURE ON THE POSITION OF A FLUID-FLUID INTERFACE WITHIN THE PORE OF FIG. 1.

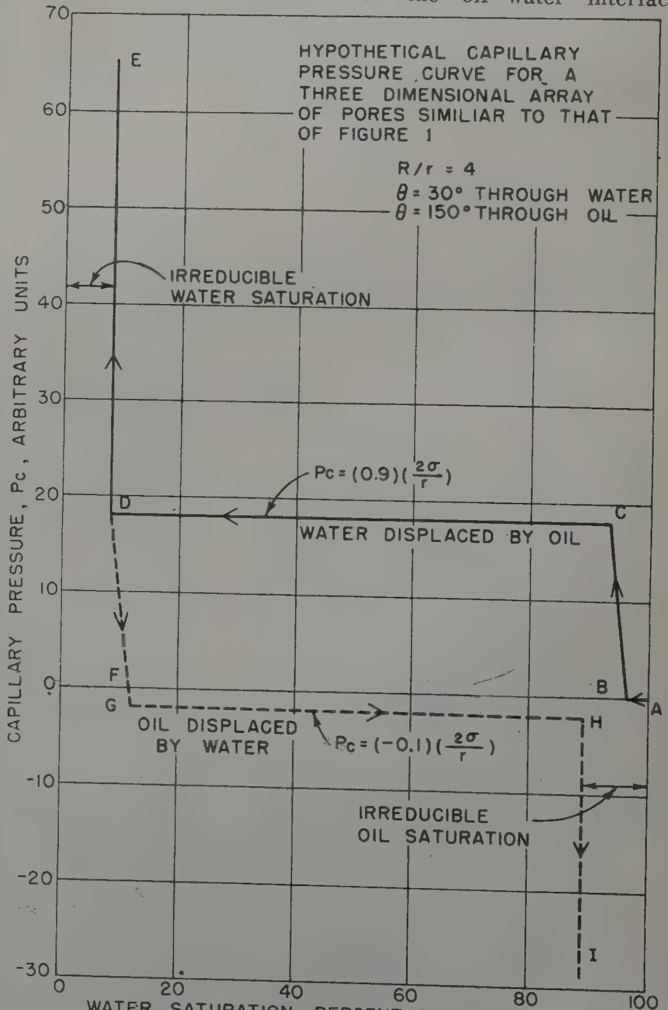

FIG. 3 — HYPOTHETICAL CAPILLARY PRESSURE CURVE FOR A THREE DIMENSIONAL ARRAY OF PORES SIMILAR TO THAT OF FIG. 1.

‡Compare this equation with that for a capillary tube, $\frac{P_cr'}{2\sigma} = \cos\theta$, where r' is the internal radius of the tube

reaches a position described by $\propto = -60°$ (Point *A*, Fig. 2) in the pores exposed at the surface. If the number of surface pores is small, compared to the total number of pores, the volume of water displaced, in terms of total pore space, will be relatively small. This initial displacement is represented by a portion, *A-B*, of a hypothetical capillary pressure curve shown in Fig. 3. Pressure in excess of that of the water phase is now applied gradually to the oil resulting in a further small displacement of water corresponding to movement of the interface in the surface pores from $\propto = -60°$ to $\propto = +7°$ (Point *B*, Fig. 2) and represented by the line *B-C* of the capillary pressure curve. At point *B* a sufficiently high pressure differential, corresponding to a value of $\frac{P_c r}{2\sigma} = 0.9$, is reached to cause most of the water, including that in the interior pores, to be displaced (*C-D*, Fig. 3), since this value represents the maximum stable capillary pressure that can be realized in any of the pores. Some water may be trapped in corners of the pores because of bridging of the oil-water interface as it moves from one pore to the next in the displacement of water from the interior pores and this results in an irreducible minimum as shown in Fig. 3.

If the pressure difference between the oil and water is now reduced to zero a slight amount of oil may be displaced by imbibition of water in the surface pores as from *D* to *F* in Fig. 3. The bulk of oil will be displaced, however, only if the pressure in the water is made greater than that in the oil. All of the oil, except that trapped by bridging, will be displaced when the pressure excess in the water phase corresponds to a value of $\frac{P_c r}{2\sigma} = -0.1$ (*G* to *H*, Fig. 3; point *C*, Fig. 2).

If one adopts the capillary tube model, then it may be necessary to postulate that Welge's experiments showed lack of equilibrium conditions, as suggested by Rose. It is possible, however, to assume that the experiments were carried out under equilibrium conditions and explain the results on the basis of the pore geometry illustrated by Fig. 1. It is believed that the pore herein considered may be more nearly descriptive than the capillary tube of the pores actually existing in reservoir rocks.

REFERENCES

1. Walter Rose, "A Note on the Application of the Capillary Pressure Method for the Determination of Oil Recovery," *Petr. Tech.*, Section 1, p. 30, (March, 1949).
2. H. J. Welge, "Displacement of Oil from Porous Media by Water or Gas," AIME *Trans.*, Vol. **179** (1948).
3. A. B. D. Cassie and S. Baxter, "Wettability of Porous Surfaces," *Trans. of the Faraday Soc.*, **40**, 546 (1944).
4. A. B. D. Cassie, "Permeability to Water and Water Vapor of Textiles and Other Fibrous Materials," *Discussions of the Faraday Society*, No. **3**, p. 239, (1948).
5. D. J. Crisp and W. H Thorpe, "The Water-Protecting Properties of Insect Hairs," *Ibid.*, p. 210.

★ ★ ★

Technical Note 61

PRESSURE DISTRIBUTION IN UNSATURATED OIL RESERVOIRS

E. R. BROWNSCOMBE AND **FRANCIS COLLINS,** THE ATLANTIC REFINING CO., DALLAS, TEX., MEMBERS AIME

The pressure distribution in a reservoir producing an incompressible fluid by radial flow in a horizontal structure is a simple logarithmic function[1] used daily by reservoir engineers. The assumption of an incompressible liquid is equivalent to assuming that pressure is maintained constant at the well radius and at some external "radius of drainage," or, in other words, that the entire flow into the well passes across the external radius. In most cases a well is surrounded by other wells draining adjoining areas so that the "radius of drainage" is not a line of constant pressure with flow equal to the flow into the well but rather a contour of zero pressure gradient across which no flow occurs, production being due to the expansion of the liquid within the area.

The radial flow steady state pressure distribution for this case does not seem to be extensively used despite the fact that the mathematical analysis has been given in detail[2] and the results are simple and generally applicable. The object of this discussion is to develop this result from a physical rather than a mathematical viewpoint, thereby aiding intuition in judging circumstances to which it may be applicable.

If the production rate at a well in an unsaturated reservoir is maintained constant while no flow occurs across the outer radius a steady state will soon be reached in which the flow rate or pressure gradient is constant with time at all points in the reservoir. To preserve such a condition it is necessary that the pressure decline at the same rate at all points in the reservoir, that is, the curves of pressure versus radial distance at successive times are all parallel. Then each unit volume of oil is expanding at the same rate and contributing an equal share to the production. The rate of flow q across any circle r is thus proportional to the volume of the reservoir between r and the external radius r_e, or

$$q = q_w \left(1 - \frac{r^2}{r_e^2}\right) \quad . \; . \; . \; . \; . \; . \quad (1)$$

where q_w is the production from the well and it is assumed that r_w is very small compared with r_e.

This equation can be combined with the differential form of Darcy's law for radial flow,

$$q = \frac{2\pi hkr}{\alpha\mu\beta}\frac{dp}{dr} \quad . \; . \; . \; . \; . \; . \; . \; . \quad (2)$$

where q is not a constant as in the incompressible flow case but is a function of r given by Equation (1). If Equation (1) is substituted in Equation (2) the variables p and r can be separated and the result integrated to obtain the pressure distribution

$$p = p_w + \frac{\alpha\mu q_w\beta}{2\pi kh}\left[\ln\frac{r}{r_w} - \frac{r^2}{2r_e^2}\right] \quad . \; . \; . \; . \; . \; . \quad (3)$$

This equation differs from the incompressible case only in the addition of the term proportional to the square of the radius which causes the logarithmic distribution to flatten out to zero pressure gradient as the external radius is approached. For comparison this distribution is plotted in the accompanying figure along with the distribution for an incompressible fluid.

The concept leading to the flow rate distribution of Equation (1) may be extended to include the case of a fixed flow across the external boundary which is an arbitrary fraction of the constant production rate from the well. This result is useful for example in connection with the estimation of oil migration in the interpretation of bottom-hole pressure build-up curves,[3] and as an initial condition for an unsteady-state two-phase flow calculation.[4]

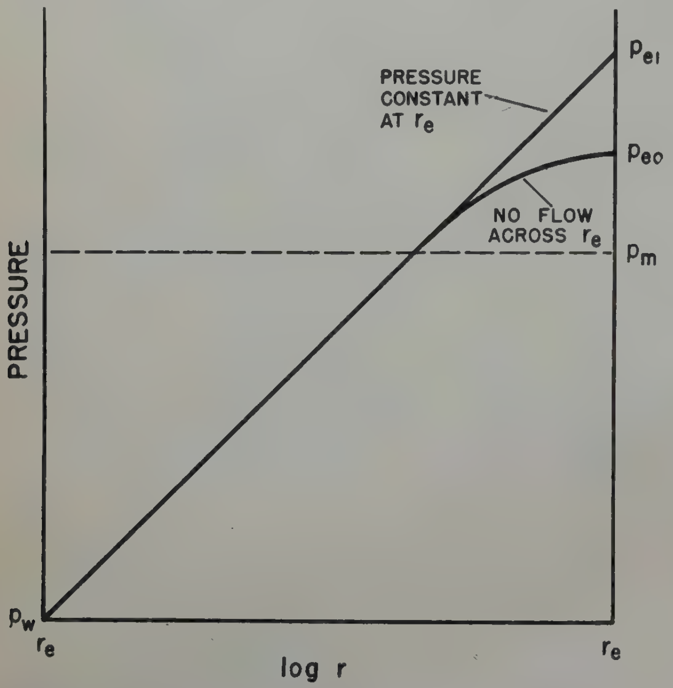

PRESSURE DISTRIBUTION IN STEADY STATE RADIAL LIQUID FLOW. LINE MARKED "PRESSURE CONSTANT AT r_e" CORRESPONDS TO INCOMPRESSIBLE LIQUID WITH FLOW ACROSS r_e EQUAL TO WELL FLOW AT r_w. CURVE MARKED "NO FLOW ACROSS r_e" IMPLIES ZERO PRESSURE GRADIENT AT r_e AND PRODUCTION BY EXPANSION OF LIQUID INSIDE r_e.

NOMENCLATURE

r = radial distance from center of well
r_w = well radius
r_e = external radius of area drained by well
p = pressure at radius r, psia
p_w = pressure at well radius, psia
p_{e1} = pressure at external radius for case of constant pressure maintained at r_e, psia
p_{eo} = pressure at external radius for closed reservoir (no flow across r_e), psia
p_m = average pressure in closed reservoir

$$= p_{e1} - \frac{3\alpha\mu q_w\beta}{8\pi kh} = p_{eo} - \frac{\alpha\mu q_w\beta}{8\pi kh}$$

$$= p_w + \frac{\alpha\mu q_w\beta}{2\pi kh}\left(\ln\frac{r_e}{r_w} - \frac{3}{4}\right)$$

k = permeability, millidarcies
h = net pay thickness, feet
μ = oil viscosity, centipoise
β = formation volume factor, reservoir bbl per stock tank bbl
q = rate of flow across radius r, stock tank bbl per day
q_w = production rate at well, stock tank bbl per day
α = constant required to make equations homogeneous in above dimensions = 887.

REFERENCES

1. M. Muskat: *Flow of Homogeneous Fluids Through Porous Media,* J. W. Edwards, Inc., Ann Arbor, Mich., (1946), 150-56.
2. *Ibid.,* 657-61.
3. C. C. Miller, A. B. Dyes, and C. A. Hutchinson, Jr.: "The Estimation of Permeability and Reservoir Pressure from Bottom Hole Pressure Build-up Characteristics," *Trans.,* AIME, (1950), **189,** 91.
4. C. C. Miller, E. R. Brownscombe, and W. F. Kieschnick, Jr.: *Trans.* AIME, (1949), **186,** 235.

★ ★ ★

Technical Note 62

HIGH PRESSURE MERCURY PUMP

J. R. SPENCER, TEXAS PETROLEUM RESEARCH COMMITTEE, UNIVERSITY OF TEXAS, AUSTIN, TEX., MEMBER AIME

When supplies of high pressure mercury or other liquids are required in analytical work, it is convenient to have the source of supply at a relatively constant pressure and available in sufficient volume to satisfy the requirements of the apparatus in use. It is also desirable that the pressuring device be as simple and as inexpensive as possible and convenient to operate. This pump combined with a small storage reservoir containing gas under pressure has the attributes of (1) positive control of the maximum output pressure through the use of a regulator in the low pressure air supply; (2) an increasing capacity as the rate of withdrawal of mercury from the pressured system is increased; and (3) simplicity, requiring only the use of a lathe, drill press, and welding unit in its construction.

DESCRIPTION

Essential parts of the pump are shown in Fig. 1. In appearance the unit is similar to the usual steam pump in common use in industrial applications although considerably smaller in size. The main differences lie in the area ratio of the air and mercury pistons and in the design of the air valve mechanism. Approximate diameters of these pistons are 4.25 in. to 0.375 in. respectively, giving an area ratio of about 130 to 1. The air piston (2) is attached to the end of shaft (4), with the mercury piston being merely a reduced extension of the shaft. Mercury intake and discharge to the pump are controlled by high pressure check valves that screw into the ports indicated at (6). Air supply is controlled by the valve assembly mounted on top of the

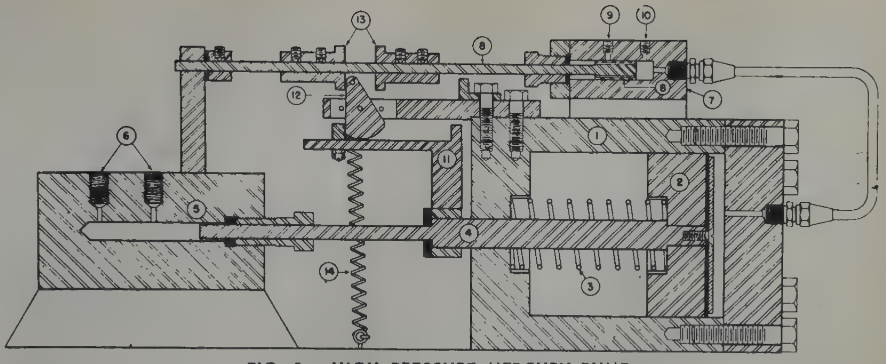

FIG. 1 — HIGH PRESSURE MERCURY PUMP.

main cylinder (1). The valve is of the sliding piston type, the piston (8) being perforated longitudinally to allow free passage to both ends of the cylinder (7).

A packing assembly was provided on the valve shaft to reduce air leakage to a minimum even though the resultant extra friction in the mechanism was not advantageous. Mounted on the valve shaft are two cam riders (13) and a stop, the latter stopping movement to the left when it strikes the post supporting the outer end of the shaft. Excessive movement to the right is avoided by the fixed stop on the cam support which acts against the back side of the right cam rider. The cam (12) pivots on a fixed beam and is actuated by fingers on the valve trip (11) which is rigidly attached to the main shaft of the pump. Tension springs (14), attached to the upper lobe of the cam, provide positive action to the valve which minimizes stalling under normal operating conditions.

OPERATION

Air enters the pump through the inlet port (10) into the valve cylinder (7), passes through the connecting tubing and main cylinder head and acts on the piston (2). Pressure in the air cylinder (1) increases until the pressure in the mercury end is sufficient to open the discharge check valve, one of the ports indicated at (6). When this critical pressure is reached the piston moves forward and the mercury end of the shaft (4) displaces mercury through the check valve. The end of the stroke is high when the finger on the valve trip (11) hits the cam (12) and rotates it past center. Just past center the tension spring (14) pulls the cam abruptly against the right hand cam rider (13) forcing the valve piston (8) to the right, simultaneously closing the intake port (10) and opening the exhaust port (9).

Pressure in the main cylinder decreases until the total pressure against the piston (2) is less than the tension in the return spring (3); the piston then returns to the original position drawing mercury from the supply reservoir through the intake check valve. As the original position is approached the opposing finger on the trip (11) strikes the cam which is brought sharply against the left hand cam riger (13), forcing the valve piston to the left and returning it to the intake position. The snap nature of the valve action will cause the cycle to be repeated indefinitely as long as the mercury discharge pressure is less than the maximum discharge pressure dictated by the pressure of the air supply.

Although the pump as installed is used intermittantly by hand control of the air supply it could easily be made automatic by the installation of a variable pressure regulator in the air supply line. The internal friction resulting from inaccurate machining and alignment of the component parts sometimes causes the pump to stall during slow operation at maximum discharge pressures above 5,000 psi. At lower pressures than this, the pump works satisfactorily and has done so during approximately six months of operation. Although the pump as designed is fully capable of producing pressures between 5,000 and 10,000 psi, it is believed that operation in this range would be greatly facilitated by altering the valve and cylinder to provide air powered return rather than the spring return now used.

ACKNOWLEDGMENT

The author wishes to express appreciation to the Texas Petroleum Research Committee and to G. H. Fancher, its director, for permission to publish this paper and to William E. Fickert for preparing the sectional drawing.

★ ★ ★

Technical Note 63

CARTER RESERVOIR ANALYZER TIMING CIRCUIT

W. F. BALDWIN, MAGNOLIA PETROLEUM CO., DALLAS, TEX.

The timing circuit generally employed in Carter Reservoir Behavior Analyzers consists of a synchronous motor driven cam which actuates a microswitch. A mechanically actuated timer of this type has several inherent disadvantages, among which are the following:

1. The first time interval may not be of uniform length, depending on the exact position of the cam at the conclusion of a previous run.
2. The positioning adjustments on the microswitch lever arms are critical and require periodic readjustment.
3. The mechanical system is subject to wear which will ultimately impair its accuracy.

It was therefore considered desirable to devise an alternate method which would eliminate these difficulties without introducing others that would be equally troublesome. This note describes the design of an electronic timing device which has been incorporated in the analyzer constructed by the Field Research Laboratories of Magnolia Petroleum Co.

The electronic timer circuit is built around a simple neon glow tube relaxation oscillator, the complete circuit diagram of which is shown in Fig. 1. The operation of the circuit is as follows: Condenser C_1 is charged to the critical firing voltage of the neon glow tube VR-75 by battery B_1 through resistors R_1 and R_2. When the neon glow tube fires, the condenser C_1 is discharged. The charging cycle then repeats itself,

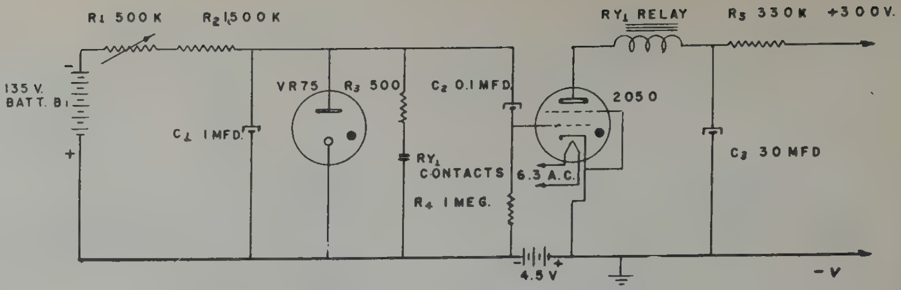

FIG. 1 — CARTER ANALYZER ELECTRONIC TIMER.

the repetition rate being determined by the values chosen for resistors R_1 and R_2, condenser C_1, and battery B_1. The transient developed at the instant the neon glow tube fires triggers the 2050 thyratron which in turn pulses the relay feeding the rotary relay ratchet circuits.

In practice, the following precautions should be observed:

1. Battery B_1 should be at least 135 volts, so that the firing voltage of the VR-75 occurs on the steep portion of the RC charging curve. This results in a more constant recurrent oscillation rate.

2. Resistors R_1 and R_2 should be wire wound. Resistor R_1 is variable to permit changing the time constant of the charging circuit and thereby the oscillation recurrence rate. In the circuit constructed, this was adjusted to 2.500 ± 0.003 seconds.

3. Condenser C_1 should be a good can-enclosed oil-filled type.

4. Stability of the oscillator can be improved by surrounding the neon glow tube VR-75 with a shield opaque to light.

In operation, the pulse generated by the relaxation oscillator triggers the grid of the 2050 thyratron. The current generated in the plate circuit of the thyratron actuates Relay Ry 1. The RC network in the plate supply of the thyratron is required to reduce the plate voltage of the thyratron to a value which will permit the grid to regain control. Condenser C_3 holds enough charge to keep relay Ry 1 closed for approximately 0.4 seconds after which time the voltage on condenser C_3 falls low enough to cut off the thyratron and permit the grid to regain control, which allows condenser C_3 to recharge through R_5. Relay Ry 1 has several sets of contacts, one set of which delivers the 2.5 second timing pulse. The contacts shown in Fig. 1 are used to discharge the condenser C_1 in the relaxation oscillator. This permits the use of small values of R and C in the oscillator circuit, thus improving stability. In actual installation of the circuit in the analyzer a locking circuit was provided through an additional relay. The locking circuit delays the actuation of the rotary switches in the analyzer until one pulse is generated in the timer circuit. This guarantees that the first period is always of proper length. Since the pulses recur every 2.5 seconds, the delay involved is negligible.

The circuit has been rigorously checked and found to have an inherent accuracy of one part in 1,000 under conditions of reasonably constant temperature and humidity. The circuit has none of the disadvantages of the mechanical system, but is influenced by ambient conditions involving high humidity. The circuit has been in operation for eight months and has required only a minimum amount of attention, largely associated with the aging of battery B_1. It is believed that the circuit possesses reliability and durability greater than that of the mechanical timer.

ACKNOWLEDGMENT

Acknowledgment is made to the management of Magnolia Petroleum Co. for permission to publish this note. ★

Technical Note 64

SOME CONTROLLING FACTORS REGARDING VARIABLE WEIGHTING OF CEMENT SLURRIES

M. A. MALLINGER, STANOLIND OIL AND GAS CO., TULSA, OKLA.

ABSTRACT

A series of laboratory tests was conducted to determine the limits of practicability in regulating the weights of various cement slurries. It was found that slurry weights of 12 to 19 lb per gallon could be obtained by adding bentonite to decrease the weight and barytes ore to increase the weight. It was also found that barytes ore was not usable in all cements.

LIGHTWEIGHT CEMENT SLURRIES
INTRODUCTION

During the drilling and completion of oil wells the magnitude of the hydraulic pressures exerted on certain formations is critical. In many cases considerable care must be exercised to prevent drilling mud weights from becoming too high, and in those wells where loss of circulation is a problem, the use of normal weight cement slurries will generally result in lost returns during casing cementing operations. While mud weights can easily be controlled, it is necessary to exercise care in the selection of weight reducing additives for cement slurries in order that slurry weights may be reduced sufficiently to prevent the loss of a large portion of the cement to the thief formations without seriously affecting the setting properties of the cement.

EXPERIMENTAL RESULTS

An extensive search revealed that a large number of materials that might have been otherwise practicable as a weight reducing additive were not acceptable for use with oil well cements because the imposition of pressure on the slurries caused the additive being tested to be compressed or to absorb water from the slurries, resulting in negligible decrease in the slurry weight.

This search for lightweight additives disclosed that bentonite, a material very commonly used for reducing the weight of drilling muds and cements, produced the best results without undue harmful effects on the properties of oil well cements. It was found that there was a limit to the amount of benton-

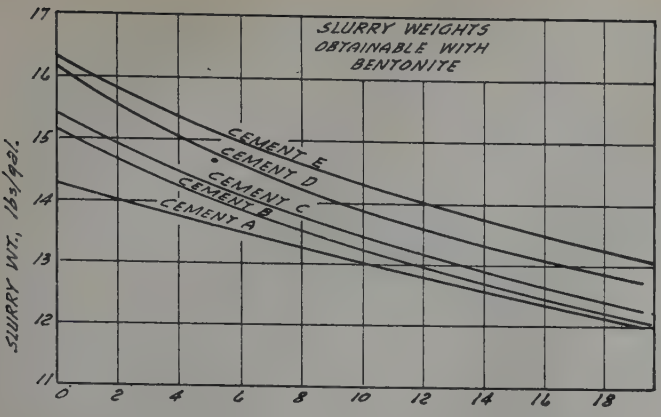

FIG. 1 — PER CENT BENTONITE BY WEIGHT OF CEMENT.

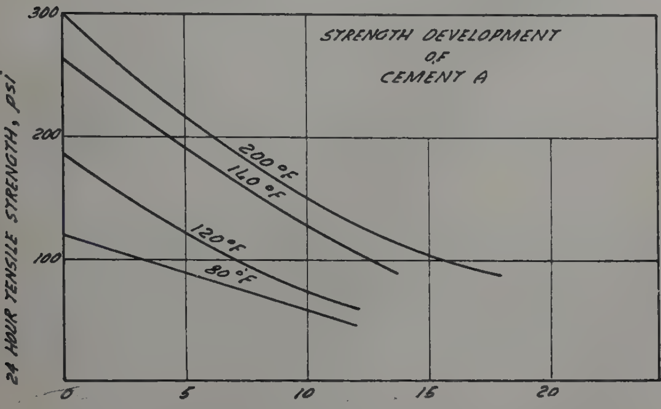

FIG. 2 — PER CENT BENTONITE BY WEIGHT OF CEMENT.

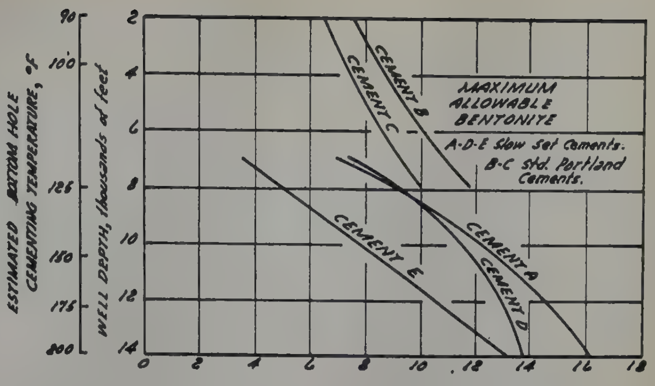

FIG. 3 — MAXIMUM ALLOWABLE PER CENT BENTONITE.

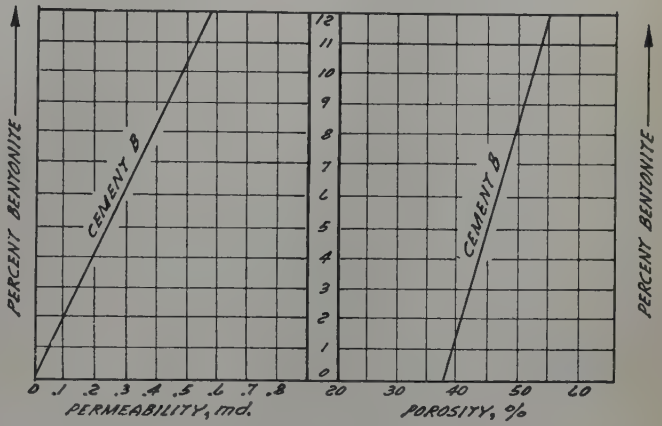

FIG. 4 — EFFECT OF BENTONITE ON THE POROSITY AND PERMEABILITY OF SET CEMENT.

ite that could be used, but that this limit was, in many cases, considerably higher than is generally believed practicable.

In the evaluation of bentonite as a slurry weight reducing additive, the following characteristics were analyzed: Effect on slurry weight; effect on strength; effect on pumping time; effect on porosity and permeability.

(1) *Slurry Weight* — The slurry weights of all brands of cements were proportionally decreased by the addition of bentonite. Fig. 1 illustrates the weight reductions that can be accomplished in five different cements by adding increasing amounts of bentonite. These slurry weights could not be altered by the imposition of 10,000 psi pressure on the slurry.

(2) *Strength* — In the determination of the maximum allowable per cent bentonite that can be added to cement, a tensile strength development of 100 psi in 24 hours was selected as the minimum strength acceptable.

Strength tests at curing temperatures from 80°F to 200°F were conducted on all of the cement-bentonite mixtures shown in Fig. 1. Fig. 2 is a plot of the data obtained on one cement and is typical of the curves plotted for each cement evaluated. These curves serve as an indication of the maximum amount of bentonite that can be safely used at various curing temperatures. The maximum usable per cent bentonite for each curing temperature can be determined in Fig. 2 by reading the abscissa at the intersection of each temperature curve and the 100 psi ordinate. By the use of this type of plot and by substituting well depth for temperature, it was possible to determine the maximum allowable per cent bentonite that could be used in any cement at any depth. Fig. 3 is a geographical presentation of these data.

(3) *Pumping Time* — Stirring time tests conducted on the high pressure Stanolind Pressure Thickening Time Tester (API Code 32, Tentative), a machine which measures the consistency and pumping time of cement slurries at pressures and temperatures comparable to those encountered at any well depth, indicated that the pumping time of cement slurries was neither increased nor decreased by the addition of any operable amount (see Fig. 3) of bentonite, if the initial consistency of the slurry containing bentonite was the same as a slurry of the same cement with no bentonite. This indicates that the bentonite, when used as recommended, has little or no retarding or accelerating effect on the pumping time of cement slurries.

(4) *Porosity and Permeability* — The effect of the addition of bentonite to cement slurries on the porosity and permeability of the set cement was determined by adding various quantities of bentonite to several cement slurries, allowing the samples to cure and measuring the porosity and permeability of the set cement-bentonite samples. It was found that both the porosity and permeability of the set cement did increase with the addition of bentonite, however, the permeabilities, even with the highest percentages of bentonite, were less than one millidarcy. The permeability measurements were all made with air as the flowing medium in order to evaluate the most severe conditions. It is believed that the permeability of this cement to water would be even lower. The porosities reached a figure as high as 55 per cent; however, it is believed that this factor has no detrimental effect on set cement other than to result in a reduction in strength, which characteristic was thoroughly investigated. Fig. 4 illustrates the porosity and permeability values of a typical bentonite cement.

With the specific gravity of dry bentonite approximately 2.7, it is believed that its lightweight producing qualities are a result of the ability of the bentonite to absorb large quantities of water, and it is the addition of this extra water which

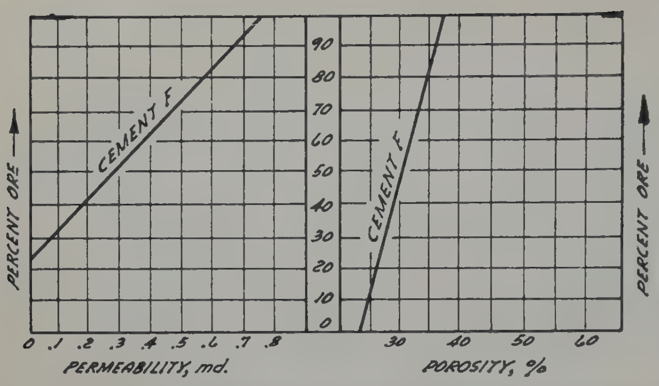

FIG. 5 — EFFECT OF BARYTES ORE ON THE POROSITY AND PERMEABILITY OF SET CEMENT.

is directly responsible for reducing slurry weights. The amount of water, over and above the volume normally used for mixing cement, that should be added to the slurry for the purpose of wetting the bentonite is .34 gal per sack of cement per per cent bentonite. For example, when using 3 per cent bentonite the water-cement ratio should be increased 1.02 gal per sack over that normally used for the neat cement. With water-cement ratios increased by this factor the lightweight slurries should have consistencies approximately equal to the consistency of the neat cement slurry.

SUMMARY

Lightweight bentonite-cement slurries containing up to 12 per cent bentonite have been tested successfully in the field. There have been no unsuccessful jobs contributable to the cement and, in some areas, tests indicate that the use of a high bentonite-cement is the only method that can be used which will insure returns throughout the cementing operation.

HEAVYWEIGHT CEMENT SLURRIES

INTRODUCTION

Recently deeper wells have been requiring heavier muds and, consequently, a need is anticipated for heavier cement slurries. At present there is only a limited demand for slurries heavier than can be obtained with neat cement. The greatest application is anticipated in plug back jobs in which 17 lb per gallon or heavier mud must be used. In these plug back jobs a cement as heavy as mud is desirable in order to eliminate the tendency of the cement to float in the mud. It is visualized that, as wells are drilled deeper and deeper, the higher formation pressures encountered will require that heavier slurries than are obtainable with neat cement be required in casing cementing operations in order to eliminate the hazard of a blowout during the operation.

EXPERIMENTAL RESULTS

The most practicable additive found to date for increasing cement slurry weights is barytes ore; however, care must be exercised in the selection of the cement to be used with this ore because the setting characteristics of many cements are unfavorably affected by the addition of large quantities of this ore. A study of Table I will reveal that slurry weights and strength development vary widely with different brands of cement. It is pointed out that this wide variation is caused by the large quantities of ore that are needed, as compared with the relatively small quantities of bentonite used in lightweight slurries, therefore, the effect of the additive on different cements is greatly magnified. Cement "F," for example, in Table I is usable at any depth with 100 per cent ore, while Cement "G" can only be used at much greater depths. Cement "H," on the other hand, illustrates a cement to which can be added additional weighting material with increasing depth at which it is used.

Pressure has no effect on the weight of this type of heavy slurry; furthermore, the pumping time of these slurries is not appreciably affected by the addition of the amounts of barytes ore shown in Table I.

The effect of this additive on the porosity and permeability of the set cement was determined by the same procedure as was used for the bentonite. Again, there was little appreciable effect on permeability. The porosity was not as greatly affected by the heavyweight additive as it was by the addition of bentonite. Fig. 5 illustrates the porosity and permeability results of a typical cement. The other brands of cement tested produced similar results and it was concluded that the addition of barytes ore up to 100 per cent of the weight of the cement would not cause excessive porosity and permeability.

There have been no field tests with this additive; however, a number of experimental plug back tests are planned for the future with heavyweight slurries.

SUMMARY

In summation, when slurries heavier than a neat cement slurry are desired, the weight can be increased to as much as 19 lb per gallon by adding up to 100 per cent barytes ore, but pilot strength tests should be conducted with the ore and brand of cement to be used prior to the job in order to insure that the set cement will develop adequate strength. ★ ★ ★

Table I — Maximum Slurry Weights

Cement	Depth, ft	Max. Slurry Weight, lb/gal	% Barytes Ore by Vol
Cement "F"	2,000	18.1	100
"	6,000	18.1	100
"	10,000	18.1	100
"	14,000	18.1	100
Cement "G"	2,000	*	*
"	6,000	*	*
"	10,000	*	*
"	14,000	17.4	100
Cement "H"	2,000	*	*
"	6,000	17.3	25
"	10,000	18.5	75
"	14,000	19.0	100

*Cannot be used because of inadequate strength development.

INDEX TO TRANSACTIONS, VOLUME 189

(Plus Reference to Articles and Technical Notes Published in Journal of Petroleum Technology in 1950)

A

Allen, F. H., et al.: *Performance Characteristics of a Volumetric Condensate Reservoir*, 83

B

Baldwin, W. F.: *Carter Reservoir Analyzer Timing Circuit* (Tech. Note), Nov. JPT

Beeson, Carroll M.: *The Kobe Porosimeter and the Oilwell Research Porosimeter*, 313

Berlin, E. W., et al.: *1949 — A Year of World-Wide Production Growth* (Art.), May JPT

Borden, Granville S.: Taxation Vs. Mineral Resources (Art.), Apr. JPT

Borden, Guy, Jr., et al.: *Correlation of Bottom Hole Sample Data*, 345

Bowers, Emil F., et al.: *Performance of the Lower Pawelek Reservoir, Falls City Field, Karnes County, Texas*, 335

Boyd, William L., et al.: *The Water Vapor Content of Essentially Nitrogen-Free Natural Gas Saturated at Various Conditions of Temperature and Pressure*, 241

Brownscombe, E. R., et al.: *Pressure Distribution in Unsaturated Oil Reserves* (Tech. Note), Oct. JPT

Bubb, F. W., et al.: *An Electronic Analog Computer for Solving the Flash Vaporization Equilibrium Equation*, 143

Burdine, N. T., et al.: *Pore Size Distribution of Petroleum Reservoir Rocks*, 195

Bush, Robert E., et al.: *Some Preliminary Investigations of Quantitative Interpretations of Radioactivity Logs*, 19

C

Calhoun, John C., Jr., et al.: *Liquid-Liquid Displacement in Porous Media As Affected by the Liquid-Liquid Viscosity Ratio and Liquid-Liquid Miscibility*, 215

Callaway, F. H., et al.: *Critical Analysis of the Effect of Well Density on Recovery Efficiency*, 269

Carpenter, P. G., et al.: *An Electronic Analog Computer for Solving the Flash Vaporization Equilibrium Equation*, 143

Casing: Relative productivity of perforated casing, 179, 323
  Effect on well productivity of penetration beyond perforated casing, 309

Cement: Squeeze cementing operations, 53
  Variable weighting of cement slurries (Tech. Note), Dec. JPT

Clark, Roscoe E., Jr.: *Influence of Different Types of Formation Waters on Disintegration of Cements* (Tech. Note), Aug. JPT

Collins, Francis, et al.: *Pressure Distribution in Unsaturated Oil Reserves* (Tech. Note), Oct. JPT

Coqueron, Frederick G., et al.: *Financing Transactions of the Petroleum Industry in 1949* (Art.), Feb. JPT

Cores: Analysis of fractured limestone cores, 225
  Mounting cores in thermoplastics (Art.), Dec. JPT

Corrosion: Within dehydrating tanks, 175

Craze, R. C.: *Performance of Limestone Reservoirs*, 287

Crutchfield, John W., et al.: *Performance of the Lower Pawelek Reservoir, Falls City Field, Karnes County, Texas*, 335

Culberson, O. L., et al.: *Phase Equilibria in Hydrocarbon-Water Systems I*, 1

Culberson, O. L., et al.: *Phase Equilibria in Hydrocarbon-Water Systems* II, 319

Cycling operations: In the La Gloria Field, 281

D

Dehydrating tanks: Corrosion mitigation, 175

DeWitt, Sam N., et al.: *High Pressure Water Injection for Maintaining Reservoir Pressures, New Hope Field, Franklin County, Texas*, 325

Doll, H. G.: *Selective SP Logging*, 129

Doll, H. G.: *The MicroLog — A New Electrical Logging Method for Detailed Determination of Permeable Beds*, 155

Doll, H. G.: *The SP Log in Shaly Sands*, 205

Doty, E. C., et al.: *Improvements in the X-Ray Saturation Technique of Studying Fluid Flow*, 183

Drilling mud: Ability to lift bit cuttings, 35

Duce, James T., et al.: *1949 — A Year of World-Wide Production Growth* (Art.), May JPT

Dyes, A. B., et al.: *The Estimation of Permeability and Reservoir Pressure from Bottom Hole Pressure Build-up Characteristics*, 91

Dynamometer charts and well weighing, 165

E

Electric logs: The presence of conductive solids in reservoir rocks as a factor in interpretation, 47
  Quantitative evaluation of the physical characteristics of reservoir rock, 105
  Selective SP logging, 129
  MicroLog, 155
  SP log in shaly sands, 205
  Estimation of interstitial water from electric logs, 295

Ellenberger, Richard A.: *Methods of Treating Water for Flooding Purposes* (Art.), Aug. JPT

Everett, J. P., et al.: *Liquid-Liquid Displacement in Porous Media As Affected by the Liquid-Liquid Viscosity Ratio and Liquid-Liquid Miscibility*, 215

F

Fagg, L. W.: *Dynamometer Charts and Well Weighing*, 165

Fairlie, John F.: *The Significance of Recent Canadian Oil Developments* (Art.), Nov. JPT

Fast, C. R., et al.: *Squeeze Cementing Operations*, 53

Field histories: Volumetric Behavior of Oil and Gas from a Louisiana Field, 261
- Study of reservoir performance of the First Grubb Pool, San Miguelito Field, 243
- Review of cycling operations in the La Gloria Field, 281
- High pressure water injection for maintaining pressures, New Hope Field, 325
- Performance of Lower Pawelek Reservoir, Falls City Field, 335

Flash vaporization: Electronic analog computer for solving flash vaporization equilibrium equation, 143

Fluid flow: X-ray saturation technique, 183

Frailing, W. G., et al.: *Lakeview Pool, Midway-Sunset Field*, 7

G

Gas: Relative permeability, 65
- Determining friction factors for measuring productivity of gas wells, 73

Gas wells: Determining friction factors for measuring productivity, 73

Gilmore, Robert B., et al.: *1949 — A Year of World-Wide Production Growth* (Art.), May JPT

Glenn, Wayne E.: *A Study of Reservoir Performance of the First Grubb Pool, San Miguelito Field, Ventura County, Calif.*, 243

Gooch, F. W., Jr., et al.: *Liquid-Liquid Displacement in Porous Media As Affected by the Liquid-Liquid Viscosity Ratio and Liquid-Liquid Miscibility*, 215

Gournay, L. S., et al.: *Pore Size Distribution of Petroleum Reservoir Rocks*, 195

Greifer, Bernard, et al.: *Anomalies in the Measurement of Wetting Liquid Pressure Gradients* (Tech. Note), June JPT

Grove, B. H., et al.: *1949 — A Year of World-Wide Production Growth* (Art.), May JPT

H

Hall, H. N., et al.: *Ability of Drilling Mud to Lift Bit Cuttings*, 35

Hopkins, George R.: *A Projection of Oil Discovery from 1949 to 1965* (Art.), June JPT

Horn, Albert B., et al.: *Phase Equilibria in Hydrocarbon-Water Systems*, 1

Howard, George C., et al.: *Squeeze Cementing Operations*, 53

Howard, Robert A., et al.: *Relative Productivity of Perforated Casing — I*, 179

Howard, Robert A., et al.: *Relative Productivity of Perforated Casing — II*, 323

Hutchinson, C. A., Jr., et al.: *The Estimation of Permeability and Reservoir Pressure from Bottom Hole Pressure Build-up Characteristics*, 91

Hydrocarbon-water systems — phase equilibria, 1, 319

I

Injection: High pressure water injection for maintaining reservoir pressures, 325

Interstitial water: Estimation from electric logs, 295

J

Jenks, L. H., et al.: *Relative Permeability to Gas*, 65

Johnson, J. W., et al.: *The Force Exerted by Surface Waves on Piles*, 149

Justice, W. H.: *Review of Cycling Operations in the La Gloria Field*, 281

K

Kartinen, Ernest O.: *Corrosion Mitigation within Dehydrating Tanks*, 175

Katz, Donald L., et al.: *The Coexistence of Liquid and Vapor Phases at Pressure above 10,000 PSI*, 119

Kaufman, Godfrey F., et al.: *1949 — A Year of World-Wide Production Growth* (Art.), May JPT.

Keller, W. O., et al.: *Critical Analysis of the Effect of Well Density on Recovery Efficiency*, 269

Kelton, Frank C.: *Analysis of Fractured Limestone Cores*, 225

L

Lakeview Pool, Midway-Sunset Field, 7

Leas, W. J., et al.: *Relative Permeability to Gas*, 65

Lilienthal, W. B.: *Stainless Steel Containers for Laboratory Drilling Mud Test Work* (Tech. Note), Apr. JPT

Mc

McCarthy, Eugene L., et al.: *The Water Vapor Content of Essentially Nitrogen-Free Natural Gas Saturated at Various Conditions of Temperature and Pressure*, 241

McDowell, J. M., et al.: *Improvements in the X-Ray Saturation Technique of Studying Fluid Flow*, 183

McDowell, J. M., et al.: *The Effect on Well Productivity of Formation Penetration Beyond Perforated Casing*, 309

McKetta, J. J., Jr., et al.: *Phase Equilibria in Hydrocarbon-Water Systems - I*, 1

McKetta, J. J., Jr., et al.: *Phase Equilibria in Hydrocarbon-Water Systems - II*, 319

M

Mallinger, M. A.: *Some Controlling Factors Regarding Variable Weighting of Cement Slurries* (Tech. Note), Dec. JPT

Mardock, E. S., et al.: *Some Preliminary Investigations of Quantitative Interpretations of Radioactivity Logs*, 19

MicroLog: Electrical logging method for detailed determination of permeable beds, 155

Miller, C. C., et al.: *The Estimation of Permeability and Reservoir Pressure from Bottom Hole Pressure Build-up Characteristics*, 91

Morgan, F., et al.: *Improvements in the X-Ray Saturation Technique of Studying Fluid Flow*, 183

Morison, J. R., et al.: *The Force Exerted by Surface Waves on Piles*, 149
Morrison, Paul W.: *Acidizing Fundamentals* (Art.), Sept. JPT.
Mull, J. B.: *American Oil-Shale Developments* (Art.), May JPT
Muskat, Morris: *The Effect of Permeability Stratification in Complete Water-Drive Systems*, 349
Muskat, Morris, et al.: *The Effect on Well Productivity of Formation Penetration Beyond Perforated Casing*, 309

N

Nelson, M. D., et al.: *Lime Content of Drilling Mud - Calculation Method* (Tech. Note), July JPT
Nigra, John O.: *Associate in Arts in Petroleum Technology: A New Approach to Formalized Training for the Petroleum Industry* (Art.), Jan. JPT
Nisle, R. G., et al.: *An Electronic Analog Computer for Solving the Flash Vaporization Equilibrium Equation*, 143
Nuss, Frank, et al.: *Ability of Drilling Mud to Lift Bit Cuttings*, 35

O

O'Brien, M. P., et al.: *The Force Exerted by Surface Waves on Piles*, 149
Offshore operations: Force exerted by surface waves on piles, 149

P

Patnode, H. W., et al.: *The Presence of Conductive Solids in Reservoir Rocks As a Factor in Electric Log Interpretation*, 47
Perforation: Effect on well productivity of formation penetration, 309
    Relative productivity of perforated casing, 323
Permeability: Estimation of permeability and reservoir pressure, 91
    Effect of permeability stratification in complete water drive systems, 349
Piles: Force exerted by surface waves, 149
Pogue, Joseph E., et al.: *Financing Transactions of the Petroleum Industry in 1949* (Art.), Feb. JPT
Pores: Distribution in reservoir rocks, 195
    Liquid-liquid displacement as affected by liquid-liquid viscosity ratio and miscibility, 215
    Kobe porosimeter and the Oilwell Research porosimeter, 313
Porosity: The Kobe porosimeter and the Oilwell Research porosimeter, 313
Porter, Joe A., et al.: *Vapor-Liquid Equilibrium Data on the System Natural Gas-Water-Triethylene Glycol at Various Temperatures and Pressures*, 235
Pressure: Estimation of permeability and reservoir pressure from bottom hole pressure build-up characteristics, 91
    Coexistence of liquid and vapor phases at pressure above 10,000 psi, 119
    Water vapor content of nitrogen-free natural gas saturated at various conditions of temperature and pressure, 241
    Vapor-liquid equilibrium data, 235
    High pressure water injection, New Hope Field, 325
    Bubble point pressures and reservoir volume factors, 345
Purcell, W. R.: *Interpretation of Capillary Pressure Data* (Tech. Note), Aug. JPT

R

Radioactivity: Some preliminary investigations of quantitative interpretations, 19
Reamer, H. H., et al.: *Volumetric Behavior of Oil and Gas from a Louisiana Field I*, 261
Recovery efficiency: Critical analysis of the effect of well density, 269
Reichertz, P. P., et al.: *Pore Size Distribution of Petroleum Reservoir Rocks*, 195
Reid, Laurance S., et al.: *Vapor-Liquid Equilibrium Data on the System Natural Gas-Water-Triethylene Glycol at Various Temperatures and Pressures*, 235
Reid, Laurance S., et al.: *The Water Vapor Content of Essentially Nitrogen-Free Natural Gas Saturated at Various Conditions of Temperature and Pressure*, 241
Reservoirs: Performance characteristics of a volumetric condensate reservoir, 83
    Study of reservoir performance of the First Grubb Pool, San Miguelito Field, 243
    Volumetric Behavior of oil and gas from a Louisiana Field, 261
    Performance of limestone reservoirs, 287
    Performance of Lower Pawelek Reservoir, Falls City Field, 335
Rocks: Quantitative evaluation of the physical characteristics of reservoir rock from electric log data, 105
    Pore size distribution, 195
    Analysis of fractured limestone cores, 225
    Performance of limestone reservoirs, 287
Roe, R. P., et al.: *Performance Characteristics of a Volumetric Condensate Reservoir*, 83
Rose, Walter D., et al: *Anomalies in the Measurement of Wetting Liquid Pressure Gradients* (Tech. Note), June JPT
Rose, Walter D., et al.: *Some Theoretical Considerations Related to the Quantitative Evaluation of the Physical Characteristics of Reservoir Rock from Electrical Log Data*, 105
Russell, Charles D., et al.: *Relative Permeability to Gas*, 65
Rzasa, Michael J., et al.: *Correlation of Bottom Hole Sample Data*, 345
Rzasa, Michael J., et al.: *The Coexistence of Liquid and Vapor Phases at Pressure above 10,000 PSI*, 119

S

SP Log: Selective SP logging, 129
    The SP log in shaly sands, 205
Sage, B. H., et al.: *Volumetric Behavior of Oil and Gas from a Louisiana Field I*, 261
San Miguelito Field: Study of reservoir performance of the First Grubb Pool, 243
Schaaf, S. A., et al.: *The Force Exerted by Surface Waves on Piles*, 149
Showalter, W. E.: *Mounting Core Analysis Specimens in Thermoplastics* (Art.) Dec. JPT
Sims, W. P., et al.: *Lakeview Pool, Midway-Sunset Field*, 7
Slobod, Robert L.: *Attainment of Connate Water in Long Cores by Dynamic Displacement* (Tech. Note), Mar. JPT
Smith, R. V.: *Determining Friction Factors for Measuring Productivity of Gas Wells*, 73
Spacing: Critical analysis of the effect of well density on recovery efficiency, 269

SPENCER, J. R.: *High Pressure Mercury Pump* (Tech. Note), Nov. JPT

T

TAYLOR, VERNON, et al.: *1949 — A Year of World-Wide Production Growth* (Art.), May JPT

THOMAS, H. R., et al.: *The Present and Potential LP-Gas Market* (Art.), Oct. JPT

THOMPSON, E. O.: *The Application of the Market Demand Statute to Oil Production in Texas* (Art.), Mar. JPT

THOMPSON, HOWARD, et al.: *Ability of Drilling Mud to Lift Bit Cuttings*, 35

THORNE, W. R., et al.: *The Present and Potential LP-Gas Market* (Art.), Oct. JPT

TRUBE, ALBERT S., JR., et al.: *High Pressure Water Injection for Maintaining Reservoir Pressures, New Hope Field, Franklin County, Texas*, 325

V

Viscosity: Liquid-liquid displacement in porous media, 215

W

Water drive: Effect of permeability stratification in complete water drive systems, 349

Water vapor content: Of nitrogen-free natural gas saturated at various conditions of temperature and pressure, 241

WATKINS, T. E., et al.: *Lime Content of Drilling Mud - Calculation Method* (Tech. Note), July JPT

WATSON, MARSH S., JR., et al.: *Relative Productivity of Perforated Casing - I*, 179

WATSON, MARSH S., JR., et al.: *Relative Productivity of Perforated Casing - II*, 323

WESTMAN, BURTON J.: *Mud Flow Through Oil Field Diamond Core Bits* (Art.), July JPT

WICKENDEN, WILLIAM E.: *The Second Mile* (Art.), Feb. JPT

WILLIAMS, MILTON: *Estimation of Interstitial Water from the Electric Log*, 295

WOODWARD, LOUIS A.: *Aerial Photogrammetry As Applied to the Petroleum Industry* (Art.), Jan. JPT

WYLLIE, M. R. J., et al.: *Some Theoretical Considerations Related to the Quantitative Evaluation of the Physical Characteristics of Reservoir Rock from Electrical Log Data*, 105

WYLLIE, M. R. J., et al.: *The Presence of Conductive Solids in Reservoir Rocks As a Factor in Electric Log Interpretation*, 47